NUCLEAR PHYSICS

JOURNAL DEVOTED TO THE EXPERIMENTAL AND THEORETICAL STUDY OF THE FUNDAMENTAL CONSTITUENTS OF MATTER AND THEIR INTERACTIONS

EDITOR: L. ROSENFELD - COPENHAGEN
ASSOCIATE EDITOR: O. NATHAN - COPENHAGEN

VOLUME XV

NORTH-HOLLAND PUBLISHING COMPANY - AMSTERDAM

NUCLEAR PHYSICS

EDTIORIAL BOARD

AUSTRALIA & NEW ZEALAND: H. Messel (Sydney), M. L. Oliphant (Canberra)

AUSTRIA: B. Karlik, (Vienna), H. Thirring (Vienna)

BELGIUM: M. de Hemptinne (Louvain), J. Verhaeghe (Ghent)

CANADA: G. Volkoff (Vancouver)

DENMARK: C. Møller (Copenhagen), S. Rozental (Copenhagen)

FINLAND: L. Simons (Helsinki)

FRANCE: A. Berthelot (Saclay), S. Gorodetzky (Strasbourg)

GERMANY (DEM. REP.): G. Hertz (Leipzig)

GERMANY (FED. REP.): W. Gentner (Freiburg i. B.), J. H. D. Jensen (Heidelberg)

GREAT BRITAIN: S. Devons (Manchester), T. H. R. Skyrme (Harwell)

HUNGARY: L. Janossy (Budapest)

INDIA: H. Bhabha (Bombay), R. Ramanna (Trombay)

IRISH REPUBLIC: J. McConnell (Maynooth)

ISRAEL: G. Racah (Jerusalem)

ITALY: E. Amaldi (Rome)

JAPAN: S. Kikuchi (Tokyo), S. Tomonaga (Tokyo)

MEXICO: M. Moshinsky (Mexico)

NETHERLANDS: H. Brinkman (Groningen), S. R. de Groot (Leiden)

NORWAY: E. Hylleraas (Oslo), A. Lundby (Oslo), H. Wergeland (Trondheim)

POLAND: L. Infeld (Warsaw)

PORTUGAL: J. M. Araújo (Porto), J. R. de Almeida Santos (Coimbra)

SOUTH AMERICA: G. Beck (Saõ Paulo), J. Leite Lopes (Rio de Janeiro)

SPAIN: J. M. Otero (Madrid), C. Sanchez del Rio (Madrid)

SWEDEN: O. Klein (Stockholm), K. Siegbahn (Uppsala), I. Waller (Uppsala)

SWITZERLAND: P. Huber (Basel), P. Scherrer (Zürich)

U.A.R. & ARAB COUNTRIES: F. El Bedewi (Alexandria), M. G. Nooh (Cairo)

U.S.A. H. H. Barschall (Madison, Wisconsin), V. Weisskopf (Cambridge, Mass.)

U.S.S.R.: M. A. Markov (Moscow), I. S. Shapiro (Moscow), D. V. Skobeltzyn (Moscow)

YUGOSLAVIA: I. Supek (Zagreb)

NUCLEAR PHYSICS

JOURNAL DEVOTED TO THE EXPERIMENTAL AND THEORETICAL STUDY OF THE FUNDAMENTAL CONSTITUENTS OF MATTER AND THEIR INTERACTIONS

EDITOR: L. ROSENFELD - COPENHAGEN

VOLUME XV

FEBRUARY 1960—MARCH 1960

NORTH-HOLLAND PUBLISHING COMPANY-AMSTERDAM

PRINTED IN THE NETHERLANDS

8.B

Nuclear Physics **15** (1960) 1—12; © *North-Holland Publishing Co., Amsterdam*

Not to be reproduced by photoprint or microfilm without written permission from the publisher

SPACE AND TIME REFLECTIONS IN RELATIVISTIC THEORY

Yu. M. SHIROKOV

P. N. Lebedev Physical Institute, Moscow

Received 22 June 1959

Abstract: A complete classification of representations of the inhomogeneous Lorentz group is obtained including space reflections and time reflections of the Wigner type. The problem of the squares of various reflection operations for particles of semi-integer spin is investigated in detail. The general results thus obtained are compared with those obtained when superimposing additional requirements on the theory, notably, the requirements of the locality of the field operators.

1. Introduction

The purpose of the paper is to obtain all the laws of transformations for the wave functions (the state vectors) for space and time reflections using only requirements of the relativistic invariance without resorting to the properties of the locality of the field operators.

The following propositions are taken as a starting point.

a) *Relativistic invariance.* The mathematical formulation of these requirements consists [1]) in that the theory should contain the operators $M_{\mu\nu}$, p_λ, satisfying the commutation relations

$$\begin{aligned} [M_{\mu\nu}, M_{\lambda\sigma}] &= i(\delta_{\mu\sigma}M_{\lambda\nu}+\delta_{\mu\lambda}M_{\nu\sigma}+\delta_{\nu\sigma}M_{\mu\lambda}+\delta_{\lambda\nu}M_{\sigma\mu}), \\ [M_{\mu\nu}, p_\lambda] &= i(p_\nu\delta_{\mu\lambda}-p_\mu\delta_{\nu\lambda}), \quad [p_\mu, p_\nu] = 0. \end{aligned} \tag{1}$$

b) *The Wigner formulation of the law of time reflection* [2]) is accepted, according to which the transformation of the state vector

$$\Psi = \mathscr{I}_t \Psi' \tag{2}$$

corresponds to the operation $t = -t'$, where $\mathscr{I}_t$ is a certain linear operator and K is the non-linear operation of complex conjugation

$$K\Psi' = \Psi'^*. \tag{3}$$

The Schwinger rule of transpositon of matrix elements [3]) may be obtained from the Wigner formulation by substituting (3) in (2). The formulation in the framework of the conventional theory of representations is considered in ref. [4]).

c) *The operations of reflections are not assigned explicitly and are determined by their geometrical properties.* Thus, the inversion $\mathcal{I}_s$ is determined as an operator transforming the state vector in reflecting the space coordinates $\mathbf{x} = -\mathbf{x}$:

$$\Psi = \mathcal{I}_s \Psi'. \tag{4}$$

The operator of time reflection is determined in (2). It is convenient to introduce another operator $\mathcal{I}_{st}K$ corresponding to the reflection of all four axes

$$x_\mu = -x'_\mu, \quad \Psi = \mathcal{I}_{st} K \Psi'. \tag{5}$$

It is obvious that

$$\mathcal{I}_s \mathcal{I}_t = \mathcal{I}_{st}. \tag{6}$$

Speaking figuratively the inversion is defined as an operator connecting the state vector with that of the same physical system observed through a mirror.

From the above definitions and from the fact that the sequences of coordinate transformations

$$\begin{aligned} &x_\mu = x'_\mu + \xi_\mu + \varepsilon_{\mu\nu} x'_\nu, \quad x'_\mu = -x''_\mu \\ &x_\mu = -x'''_\mu, \quad x'''_\mu = x''_\mu - \xi_\mu + \varepsilon_{\mu\nu} x''_\nu \end{aligned} \tag{7}$$

and

lead to the same resulting system one may obtain the commutation relations for the operator $\mathcal{I}_{st}$

$$p_\mu \mathcal{I}_{st} - \mathcal{I}_{st} p_\mu^* = 0, \tag{8}$$

$$M_{\mu\nu} \mathcal{I}_{st} + \mathcal{I}_{st} M_{\mu\nu}^* = 0. \tag{9}$$

Here the star designates complex (not hermitian) conjugation †. Similarly for $\mathcal{I}_s$ the following relations may be obtained:

$$[\mathcal{I}_s, \mathbf{M}] = 0, \quad [\mathcal{I}_s, p_0] = 0, \quad \mathcal{I}_s \mathbf{p} + \mathbf{p} \mathcal{I}_s = 0, \quad \mathcal{I}_s \mathbf{N} + \mathbf{N} \mathcal{I}_s = 0, \tag{10}$$

where

$$N_i = -iM_{i4}. \tag{11}$$

It is important to emphasise that each of the operations of reflection determined by relations (2)—(5) may or may not contain charge conjugation. According to (8) and (10), on the other hand, these operations should be invariant for all interactions.

d) *For particles of integer spin the squares of all reflections are equal to unity. For particles of half integer spin the squares of each of the reflections $\mathcal{I}_s$, $\mathcal{I}_t K$, $\mathcal{I}_{st} K$ may be equal to unity or minus unity, but must be the same for all particles with half integer spins.* In other words the squares of reflections determine the properties of space-time itself and not a property of individual particles. There-

† The operation of complex conjugation does not affect the imaginary unity in the fourth components of vectors and tensors, so that $p_4^* = ip_0^*$, for example. This fact is not essential since the use of contravariant vectors with the conventional definition of conjugation leads to the same results.

fore particles with different squares of reflection cannot exist simultaneously[5]) since that would lead to the existence of systems with an integer angular momentum and a negative square of reflection.

As was indicated in refs.[4,6]), the above considerations may be given a geometric interpretation if a group of rotations is changed so that the element $\mathscr{I}_{2\pi}$ of a rotation of angle 2π around an arbitrary axis is introduced into this group. (This extension naturally arises in considering the topological properties of parameter space of a rotation group.) The square of each reflection may be then equal either unity or a rotation of angle 2π, which leads to the following eight groups:

TABLE 1

$\mathscr{I}^2$	G_1	G_2	G_3	G_4	G_5	G_6	G_7	G_8
$\mathscr{I}_0^2$	1	1	$\mathscr{I}_{2\pi}$	$\mathscr{I}_{2\pi}$	$\mathscr{I}_{2\pi}$	$\mathscr{I}_{2\pi}$	1	1
$(\mathscr{I}_1 K)^2 = \mathscr{I}_1 \mathscr{I}_1^*$	1	$\mathscr{I}_{2\pi}$	1	$\mathscr{I}_{2\pi}$	$\mathscr{I}_{2\pi}$	1	$\mathscr{I}_{2\pi}$	1
$(\mathscr{I}_{01} K)^2 = \mathscr{I}_{01} \mathscr{I}_{01}^*$	1	$\mathscr{I}_{2\pi}$	$\mathscr{I}_{2\pi}$	1	$\mathscr{I}_{2\pi}$	1	1	$\mathscr{I}_{2\pi}$

Table 1 holds both for integer ($\mathscr{I}_{2\pi} = 1$) and half integer ($\mathscr{I}_{2\pi} = -1$) spins. Real space-time is transformed according to one of these eight groups, which fixes the squares of reflections for all particles at once. Thus there are eight structures of space-time non-equivalent to each other.

Below it will be shown that the difference between these structures is in principle accessible to experimental check.

e) *No assumptions are made as to the locality of the field operators and the kind of equations of motion in general.*

The above-listed basic propositions have a number of features different from those accepted in the investigations of this kind (see, for example, ref. [7]) which as a review contains references to the principal previous papers).

The adoption of a) and e) allows for an extensive generalization and makes it possible to obtain a number of transformations of reflection which satisfy the requirements of relativistic invariance and yet cannot be reduced to local transformations of the Dirac field operators. Point (c) is in fact not new but rather imparts to the operations of reflection their original geometrical meaning. This point, however, involves a certain change of the very ideology of research of the reflection operations. Usually (as in ref. [7])) certain operators (P, PC, T, CT, etc.) are assigned to act upon the field operators and a study is made of their conservation properties. The present author, on the other hand, assigns the requirement of the existence of conserved operators connected with certain coordinate transformations and satisfying relations (6), (8), (9), (10) and one

of the columns of table 1. (The non-fulfilment of this requirement is tantamount to the rejection of Euclidian space-time.) The task of the present investigation is to find the explicit form of these operators. The requirements of d) are not new [8]. (though they contain a somewhat unusual geometric interpretation), but are investigated in detail for the first time. These requirements impose rather rigid limitations (different for each of the eight groups) on the possible form of the reflection operators.

2. Particles with Non-Zero Rest Mass

The methods of the field theory are unsuitable for research which is not based on the locality of the theory. Therefore we shall make use of the mathematical technique employed in ref. [8]) for obtaining an explicit form of the representations of the inhomogeneous Lorentz group. These representations were first obtained by Wigner[9]). According to ref. [8]), the state vector of the free relativistic particle of mass κ and spin s may always be reduced to the form

$$\Psi^{\kappa s\alpha}_{m_s}(\mathbf{p}) \tag{12}$$

where the kinematic variables are the three-dimensional momentum $\mathbf{p}$ and the projection of the spin m_s. Apart from mass and spin, the particle may possess other variables (such as charge) invariant with respect to the non-dimensional rotations and translations; to designate these the index α is introduced. The relativistic invariance is here ensured by the fact that for the state vector (12) the operators $M_{\mu\nu}$, p_λ satisfying relations (1) may be determined [8]) as follows:

$$\hat{\mathbf{p}} = p, \quad p_0 = e_p \equiv \sqrt{p^2+\kappa^2},$$
$$\mathbf{M} = -i\mathbf{p}\times\frac{\partial}{\partial\mathbf{p}} + \mathbf{S}, \quad \mathbf{N} \equiv ie_p\frac{\partial}{\partial\mathbf{p}} - \frac{\mathbf{S}\times\mathbf{p}}{e_p+\kappa}, \tag{13}$$

$$[S_1, S_2] = S_3, \ldots \mathbf{S}^2 = s(s+1). \tag{14}$$

The argument is complete because only one irreducible representation of the inhomogeneous Lorentz group corresponds to the given values of mass and spin, which may always be reduced to the form (13).

Now we have to find for the state vector (12) operators $\mathscr{I}_s$, $\mathscr{I}_t$, $\mathscr{I}_{st}$ satisfying (6), (8), (9), (10) and one of the columns of table 1. Let us represent these operators in the form

$$\mathscr{I}_s = \lambda_s P, \quad \mathscr{I}_t = \lambda_t T, \quad \mathscr{I}_{st} = \lambda_{st} PT, \tag{15}$$

where P is an operator acting only on the variable $\mathbf{p}$ and changing the sign of the momentum:

$$P\Psi^{\kappa s\alpha}_{m_s}(\mathbf{p}) = i^{2s}\Psi^{\kappa s\alpha}_{m_s}(-\mathbf{p}), \tag{16}$$

and T is an operator acting on $\mathbf{p}$, m_s (but not on α) and changing the sign of the momentum and the spin projection:

$$T\Psi^{\kappa s\alpha}_{m_s}(\mathbf{p}) = (-1)^{s-m_s}\Psi^{\kappa s\alpha}_{-m_s}(-\mathbf{p}). \tag{17}$$

From (16), (17) it follows that

$$P^{-1}\mathbf{p}P = -\mathbf{p}, \quad P^{-1}\mathbf{S}P = \mathbf{S}, \tag{18}$$

$$T^{-1}\mathbf{p}T = -\mathbf{p}, \quad T^{-1}\mathbf{S}T = -\mathbf{S}^*, \tag{19}$$

$$P^2 = T^2 = \mathscr{S}_{2\pi} = \begin{cases} 1 \text{ (integer spin)} \\ -1 \text{ (half integer spin).} \end{cases} \tag{20}$$

Determined through (16) and (17), the operations P, T are a natural generalization, for arbitrary spin, of the quantities used in the spinor field theory. Substituting (13) and (15) in (6), (8), (9) and (10) and using (18) and (19) we obtain

$$\lambda_s\lambda_t = \lambda_{st}, \tag{21}$$

$$[\lambda_s, \hat{p}_\mu] = 0, \quad [\lambda_s, M_{\mu\nu}] = 0, \quad [\lambda_{st}, \hat{p}_\mu] = 0, \quad [\lambda_{st}, M_{\mu\nu}] = 0. \tag{22}$$

According to (22) the operators λ_s, λ_t, λ_{st} do not act on the kinematic variables $\mathbf{p}$, m_s since they are either numbers or matrices with respect to the invariant variable α. For single-valued representations, according to (11) and (20),

$$\lambda_s^2 = \lambda_t\lambda_t^* = \lambda_{st}\lambda_{st}^* = 1 \quad \text{(integer spin)} \tag{23}$$

and all factors λ may be numbers. Two non-equivalent representations differentiated by parity correspond here to every value of mass and spin:

$$\begin{array}{l} 1)\ \lambda_s = \ \ 1, \quad \lambda_t = 1 \\ 2)\ \lambda_s = -1, \quad \lambda_t = 1 \end{array} \text{(integer spin).} \tag{24}$$

(The representations distinguished by a phase factor for λ_t are not different, since this factor, according to (2) and (3), may be eliminated by multiplying by the corresponding phase factor of the state vector.) To obtain double-valued representations the formulae (15) and (20) should be substituted in (2) and $\mathscr{S}_{2\pi}$ put equal to -1. As a result we obtain

λ^2	G_1	G_2	G_3	G_4	G_5	G_6	G_7	G_8
λ_s^2	-1	-1	1	1	1	1	-1	-1
$\lambda_t\lambda_t^*$	-1	1	-1	1	1	-1	1	-1
$\lambda_{st}\lambda_{st}^*$	-1	1	1	-1	1	-1	-1	1

(25)

If λ_t (λ_{st}) is a number, the quantity $\lambda_t\lambda_t^*$ ($\lambda_{st}\lambda_{st}^*$) is necessarily positive definite.

Therefore the factors λ may be numbers only in the groups G_2, G_5. In the remaining six groups these factors must be two-row matrices acting on the additional independent variable so that the dimension of their reducible representation is double that of the corresponding representation of the proper group. It may be directly verified that the following irreducible sets of factors satisfy relations (21) and (25):

λ	G_1		G_2		G_3	G_4	G_5		G_6		G_7	G_8
λ_s	i	$-i$	i	$-i$	ρ_1	ρ_1	1	-1	1	-1	$i\rho_1$	$i\rho_1$
λ_t	ρ_2	ρ_2	1	1	ρ_3	ρ_3	1	1	ρ_2	ρ_2	ρ_3	ρ_3
λ_{st}	$i\rho_2$	$-i\rho_2$	i	$-i$	$i\rho_3$	$-i\rho_3$	1	-1	ρ_2	$-\rho_2$	ρ_3	$-\rho_3$

(26)

In (26) the matrices ρ_1, ρ_2, ρ_3 have the form of the corresponding Pauli matrices and act upon an additional variable (of the charge type) of the state vector. The matrices ρ_1, ρ_2 correspond to an operation of the type of charge conjugation. As a result of a presence of the operation of complex conjugation in (2) and (5) the matrices ρ_1, ρ_2 cannot be transformed into each other through the transformation of equivalence if they enter in λ_t or λ_{st}. Table (26) exhausts the irreducible representations for each of the groups G_1—G_8 for a half integer spin.

3. Particles with Zero Rest Mass

For zero rest mass two irreducible representations of the proper group, one-dimensional with respect to the spin variables and different by the sign of the spin projection on the momentum (spirality), correspond to each absolute value of the spin [9]).

The change of sign of the momentum changes the sign of spirality so that the representations of the group containing space reflections should be two-row with respect to the spin variable of the sign of spirality. The operators p_μ, $M_{\mu\nu}$ for these representations may be written in the form

$$\hat{\mathbf{p}} = \mathbf{p}, \quad p_0 = |\mathbf{p}|,$$

$$M_1 = -i\left(p_2\frac{\partial}{\partial p_3} - p_3\frac{\partial}{\partial p_2}\right) + s\sigma_3\frac{\cos\varphi}{\sin\vartheta},$$

$$M_2 = -i\left(p_3\frac{\partial}{\partial p_1} - p_1\frac{\partial}{\partial p_3}\right) + s\sigma_3\frac{\sin\varphi}{\sin\vartheta}, \qquad M_3 = -i\left(p_1\frac{\partial}{\partial p_2} - p_2\frac{\partial}{\partial p_1}\right), \tag{27}$$

$$N_1 = ip\frac{\partial}{\partial p_1} - s\sigma_3\sin\varphi\operatorname{ctg}\vartheta, \quad N_2 = ip\frac{\partial}{\partial p_2} + s\sigma_3\cos\varphi\operatorname{ctg}\vartheta, \quad N_3 = ip\frac{\partial}{\partial p_3}.$$

Here σ_3 is the Pauli matrix acting on the variable of the sign of spirality, φ and ϑ are the polar angles of the momentum vector. For integer spin the operators $\mathscr{I}_s$, $\mathscr{I}_t$, $\mathscr{I}_{st}$ satisfying (6), (8), (9), (10) and (11) are equal to

$$\mathscr{I}_s = \sigma_1 P, \quad \mathscr{I}_t = P, \quad \mathscr{I}_{st} = \sigma_1 \quad \text{(integer spin)}. \tag{28}$$

Only one irreducible representation here corresponds to each absolute value of the spin. For half integer spin we shall seek the operators $\mathscr{I}_s$, $\mathscr{I}_t$ and $\mathscr{I}_{st}$ in the form

$$\mathscr{I}_s = \lambda'_s P', \quad \mathscr{I}_t = \lambda'_t P', \quad \mathscr{I}_{st} = -\lambda'_{st}. \tag{28a}$$

The operation P' acts on the wave function as P, i.e. changes the momentum sign and its square is also equal to -1:

$$P'\Psi(\mathbf{p}) = \Psi(-\mathbf{p}), \quad (P')^2 = -1, \tag{29}$$

since the eigenfunctions of the operators (27) contain a factor $\exp(\pm\frac{1}{2}i\varphi)$, multiplied by i if φ replaced by $\varphi+\pi$. Substituting (28) in (6), (8), (9) and (10) we shall obtain

$$\lambda'_s\lambda'_t = \lambda'_{st}, \tag{30}$$

$$\lambda'_s\sigma_3+\sigma_3\lambda'_s = 0, \tag{31}$$

$$\lambda'_t\sigma_3-\sigma_3\lambda'_t = 0, \tag{32}$$

$$\lambda'_{st}\sigma_3+\sigma_3\lambda'_{st} = 0. \tag{33}$$

Relations (31)—(33) express the fact that the spin projection on the momentum does not change under time reflection and changes sign under inversion. Substituting (28) in (11) and using (29) we obtain the following table for the squares of λ':

$(\lambda')^2$	G_1	G_2	G_3	G_4	G_5	G_6	G_7	G_8
$(\lambda'_s)^2$	-1	-1	1	1	1	1	-1	-1
$\lambda'_t\,\lambda'^*_t$	-1	1	-1	1	1	-1	1	-1
$\lambda'_{st}\lambda'^*_{st}$	1	-1	-1	1	-1	1	1	-1

(34)

According to (32) the factor λ'_t with respect to the spin variable is either unity or proportional to σ_3. Therefore, in the groups G_1, G_3, G_6, G_8, where the values $(\lambda'_t\lambda'^*_t)$ are negative another discrete variable has to be introduced so that the

state vector of the representation must consist of four rows. In the remaining groups this doubling is not needed. Relations (30)—(34) are satisfied by the following sets of the factors exhausting the irreducible representations of the state vectors of the particles with zero rest mass and half integer spin:

λ'	G_1	G_2	G_3	G_4	G_5	G_6	G_7	G_8
λ'_s	$i\sigma_1\rho_2$	$i\sigma_1$	σ_1	σ_1	σ_1	$\sigma_1\rho_3$	$i\sigma_1$	$i\sigma_1$
λ'_t	ρ_2	σ_3	ρ_2	1	σ_3	ρ_2	1	ρ_2
λ'_{st}	$\rho_1\sigma_1$	σ_2	$\sigma_1\rho_2$	σ_1	$-i\sigma_2$	$-i\rho_1\sigma_1$	$i\sigma_1$	$i\sigma_1\rho_2$

(35)

4. Dirac Equation

The requirement of the locality of the field operators imposed on the theory leads to an essential change of the final results which may be traced on the example of a Dirac spinor field. These differences arise from three reasons. First, the Dirac equation is always a four-component one, while two-component spinors are possible in the above discussion for the groups G_2 and G_5 (see eq. (26)). Second, certain representations in the local formulation prove forbidden. Third, certain representations equivalent within the framework of the general theory of representations may prove to be non-equivalent with respect to local transformations. Before proceeding to the investigation of the Dirac equation let us enumerate all physically non-equivalent four-component representations allowed by table (26) for the particles of a spin $\frac{1}{2}$:

No.	G	λ_s	λ_t	λ_{st}
1	G_1	i	ρ_2	$i\rho_2$
2		$-i$	ρ_2	$-i\rho_2$
3	G_2	i	1	i
4		$-i$	1	$-i$
5		i	ρ_1	$i\rho_1$
6		$-i$	ρ_1	$-i\rho_1$
7		$i\rho_3$	ρ_2	i
8		$i\rho_1$	1	$i\rho_1$
9		$i\rho_1$	ρ_1	i
10	G_3	ρ_1	ρ_2	$i\rho_3$
11		ρ_3	ρ_2	$-i\rho_1$
12	G_4	ρ_1	ρ_3	$-i\rho_2$
13		ρ_3	ρ_1	$i\rho_2$

(36)

No.	G	λ_s	λ_t	λ_{st}
14	G_5	1	1	1
15		-1	1	-1
16		ρ_1	ρ_1	1
17		1	ρ_1	ρ_1
18		-1	ρ_1	$-\rho_1$
19		ρ_1	ρ_1	1
20		ρ_1	1	ρ_1
21	G_6	1	ρ_2	ρ_2
22		-1	ρ_2	$-\rho_2$
23	G_7	$i\rho_1$	ρ_3	ρ_3
24		$i\rho_3$	ρ_1	$-\rho_2$
25	G_8	$i\rho_1$	ρ_2	$-\rho_3$
26		$i\rho_3$	ρ_2	ρ_1

(36)

We call representations such as No. 7 and No. 8 "physically" non-equivalent if they are mathematically equivalent but correspond to different physical conceptions: in No. 7) the particle transforms into itself under inversion (parity conservation), in No. 8 it turns into the antiparticle under inversion (conservation of combined inversion).

Now let us consider the possible transformations for the operators of the Dirac field which will correspond to the addition of the requirement of locality to the invariance conditions of (1), (8), (9) and (10). In the local formulation the following requirements are equivalent to these conditions:

1. Invariance of equations for the field operators.
2. Invariance of commutation relations.
3. Invariance of definition of the vacuum.

Taking into account these requirements it may be established that only the following non-equivalent sets of transformations of the Dirac field operators $\psi(x, t)$ may correspond to the coordinate transformations of reflections:

group	No.	operators corresponding to coordinate reflection			number of corresponding representations in (36)
		$\mathbf{x} = -\mathbf{x}'$	$t = -t'$	$x_\mu = -x'_\mu$	
G_1	—	—	—	—	—
G_2	1	iP	T	iPT	7
G_3	2	PC	iCT	iPT	10
G_4	3	PC	iT	$-iPCT$	12
	4	PC	$-iT$	$iPCT$	12

(37)

group	No.	operators corresponding to coordinate reflection			number of corresponding representations in (36)
		$\mathbf{x} = -\mathbf{x}'$	$t = -t'$	$x_\mu = -x'_\mu$	
G_5	5	P	T	PT	14
	6	$-P$	T	$-PT$	15
	7	P	CT	PCT	17
	8	P	$-CT$	$-PCT$	17
	9	$-P$	CT	$-PCT$	18
	10	$-P$	$-CT$	PCT	18
	11	PC	CT	PT	19
	12	PC	T	PCT	20
	13	PC	$-T$	$-PCT$	20
G_6	14	P	iCT	$iPCT$	21
	15	$-P$	iCT	$-iPCT$	22
G_7	16	iP	CT	$iPCT$	24
	17	iP	$-CT$	$-iPCT$	24
G_8	18	iP	iCT	$-PCT$	26
	19	iP	$-iCT$	PCT	26

(37) (continued)

In (37) the operations P, T and C may be determined in the standard manner (with the assigned phase factors):

$$P\psi(\mathbf{x}, t) = i\gamma_4\psi(-\mathbf{x}, t), \tag{38}$$

$$T\psi(\mathbf{x}, t) = \gamma_1\gamma_3\gamma_4\bar{\psi}(\mathbf{x}, -t), \tag{39}$$

$$C\psi(\mathbf{x}, t) = \gamma_2\gamma_4\bar{\psi}(\mathbf{x}, t). \tag{40}$$

It may be shown that with the above choice of the phase factors, transformation (38) and (39) upon the operators of the Dirac field are equivalent to transformations (16) and (17) upon the corresponding state vector. These operations are therefore designated by the same letters. This equivalence may be established with the aid of a Foldy-Wouthuysen's transformation [10]) of the solution of the Dirac equation for the field operators and further transition to the configuration representation according to ref. [11]).

Table (37) exhausts all possible laws of local transformation of reflections for Dirac particles. It will be remembered that here only those particles may exist simultaneously whose operators are transformed by the representations entering the same group, and that all operators of reflection should be conserved.

5. Discussion

The above study shows that the known properties of space-time should be fully determined in accordance with one of the rows of table 1, so that the question arises according to which group G_i real space time is transformed. To solve this problem the following differences between representations of these groups may be used:

a) *Pseudoscalarity of the ground state of positonium.* This argument does not depend on whether parity or combined parity is conserved, since the system of two photons has even charge parity. This requirement excludes from table (36), representations 1—6, 8, 9, 11, 13, 16, 23 and 25 which are just the same representations which are absent in the local variants (37). Thus, the requirements of pseudoscalarity of positonium eliminates the possibility of group G_1 in which the squares of all reflections are equal to unity.

b) *A two-component neutrino.* If the neutrino is two-component, the groups G_1, G_3, G_6, G_8 become impossible according to (35).

c) *Four components for all known spinor particles with non-zero rest mass.* This argument, taken together with the previous one, makes especially probable such representations in which the wave function of the particle of spin $\frac{1}{2}$ may be two-component for zero mass but is necessarily four-component for particles of finite mass. This condition is satisfied in the groups G_4, G_7.

The next set of arguments is connected with non-conservation of the operation of charge conjugation $C(\rho_1, \rho_2)$. It stands to reason that what is meant here is the conservation in all interactions, since the problem as it is discussed involves the geometrical properties of space-time. The non-conservation of C leads to the fact that if, for example, the quantity PC corresponds to the transformation $\mathbf{x} = -\mathbf{x}'$ and consequently is conserved, the quantity P will not conserve. On the basis of this remark the following additional restrictions on the representations may be considered:

d) *Conservation of PCT.* This requirement is hypothetical if the condition of locality is not imposed on the theory. The conservation of PCT leads to the non-conservation of PT, whereby representations 3, 4, 7, 9, 10, 14—16 and 19 in (36) are excluded. Taken together with a) this requirement leads to the exclusion of the groups G_2 and G_3.

e) *The hypothesis of conservation of combined parity* [5, 12]. The conservation of PC eliminates representations 1—7, 11, 13, 14—18, 21, 22, 24 and 26 from (36). Taken jointly with a) this point excludes all representations of the groups G_1, G_2, G_6, G_7 and G_8.

f) *The hypothesis of the conservation of T.* It excludes representations 1, 2, 5, 6, 9—11, 13, 17—19, 21, 22, 24—26, i.e., jointly with a) it excludes all representations of the groups G_1, G_3, G_6, G_7 and G_8. The requirement of locality is equivalent to the combination of conditions a) and d). Only representation 12 from (36) satisfies all the above-enumerated requirements. This representation

belongs to the group G_4. In (37) two locally non-equivalent representations 3 and 4 correspond to it. If requirement c) is rejected, the remaining requirements will also be satisfied by representation 20 of the group G_5 from (36). In (37) two locally non-equivalent representations, 12 and 13, will correspond to it. In this case, however, the particles whose wave-functions transform according to other various representations of the group G_5 become possible in principle, as a result of which the laws of conservation of d), e) and f) will lose their universal character.

Thus, the presently available experimental data lead us to the conclusion that real space-time transforms either according to the group G_4 or according to the group G_5, the group G_4, in which the squares of inversion and reflection of all four axes are equal to unity being more probable. (It will be noted that if the reflection is interpreted as a rotation at an angle π around a certain additional coordinate axis the square of reflection will be reduced to a rotation at 2π).

It is noteworthy that such a subtle property of space-time connected with the topology of the parameter space of the rotation groups turns out to be accessible to experimental determination.

In the group G_4 all particles should transform according to representation 12 from (36). In the transition to the local formulation two representations, 3 and 4, non-equivalent with respect to local transformations, will correspond in (37) to this representation. A characteristic of these representations is that while the transformation properties of the state vectors of the particles described by them are perfectly indentical, the field operators are transformed differently on reflecting all four axes. The difference between these particles therefore will have no effect on the conditions of invariance of the S matrix, determined, for example, according to ref. [13]), but will have a marked effect in deriving the interaction Lagrangian converting one particle into another †.

† Prof. A. S. Wightman informed me that some of the questions considered in this paper have also been investigated by Prof. E. P. Wigner (unpublished).

References

1) P. A. M. Dirac, Revs. Mod. Phys. **21** (1949) 392
2) E. P. Wigner, Nachr. Acad. Wiss. Gött. (1932) 546
3) I. Schwinger, Phys. Rev. **82** (1951) 914
4) Yu. M. Shirokov, JETP **36** (1959) 879
5) E. P. Wigner, C. G. Wick and A. S. Wightman, Phys. Rev. **88** (1952) 101
6) Yu. M. Shirokov, JETP **34** (1958) 717
7) T. D. Lee and C. N. Yang, Elementary Particles and Weak Interaction. Brookhaven, 1957
8) Yu. M. Shirokov, JETP **33** (1957) 861, 1196, 1208
9) E. P. Wigner, Ann. of Math. **40** (1939) 149
10) L. L. Foldy and S. A. Wouthuysen, Phys. Rev. **78** (1950) 29
11) Yu. M. Shirokov, JETP **24** (1953) 129, 135
12) T. D. Lee and C. N. Yang, Phys. Rev. **105** (1957) 1672;
L. D. Landau, JETP **32** (1957) 405;
V. G. Solovyev, Nuclear Physics **6** (1958) 618
13) Yu. M. Shirokov, JETP **35** (1958) 1005

8.B

Nuclear Physics **15** (1960) 13—15; © *North-Holland Publishing Co., Amsterdam*

Not to be reproduced by photoprint or microfilm without written permission from the publisher

TYPES OF SYMMETRY OF ELEMENTARY PARTICLES

Yu. M. SHIROKOV

Scientific Research Institute of Nuclear Physics, Moscow University, USSR

Received 20 June 1959

Abstract: It is shown that five different types of symmetry relative to space-time reflections are possible for elementary particles. The treatment is based only on properties of relativistic invariance and does not depend on locality or any other specific properties of the equations of motion. It is shown that only two types of symmetry are possible for particles with a zero rest mass and a non-zero spin.

1. Classification of Types of Symmetry

All the laws of transformations of state vectors under space and time reflections, satisfying the requirements of relativistic invariance, were obtained in ref. [1]). As applied to elementary particles this analysis can be supplemented by considering possible types of symmetry of elementary particles, which constitutes the purpose of the present article. The treatment is based on the macroscopically evident fact that each particle both can and cannot possess a symmetry relative to each of the reflections $\mathbf{x} \to -\mathbf{x}, t \to -t, x_\mu \to -x_\mu$. In the case of symmetry the particle, when reflected, transforms into itself, while in case of asymmetry it goes over into another state with the same mass and spin, i.e., into an antiparticle. In the latter case, the transformation of the state vector relevant to the corresponding reflection should involve an operation C of the charge conjugation type which transforms the particle into an antiparticle.

Altogether the following five types of symmetry are possible for particles with a finite mass:

1. *Total symmetry.* The particle transforms into itself in all reflections. In this case the conserving operations are P (change of the momentum signs), T (change of the spin and momentum signs). There are no antiparticles.

2. *T-symmetry.* The particle transforms into itself under time reflection and transforms into an antiparticle under space reflection. The conserving transformations are PC (called a combined inversion in ref. [2]), T, PCT. The nonconserving transformations are P, PT. A rotating nut can be given as an example of macroscopic bodies possessing this type of symmetry.

3. *P-symmetry.* The particle transforms into an antiparticle under time reflection and does not change under inversion. The conserving transformations

are P, CT, the non-conserving ones T, PT. This type of symmetry is inherent, for instance, to a revolving anemometer.

4. *PT-symmetry.* The particle transforms into an antiparticle under inversion and does not change under reflection of all four coordinates. The conserving transformations PC, CT, PT the non-conserving ones are P, T, PCT. In this case there is a conservation of combined inversion, but the PCT-theorem of Lüders-Pauli (see, for instance, ref.[3])) is not fulfilled. This type of symmetry is inherent to a rotating conical rackwheel.

5. *Total asymmetry.* The particle does not transform into itself under any of the reflections and, consequently, possesses four different states with the same mass and spin. In this case one can introduce two independent operations C_1 and C_2 of the charge conjugation type. The conserving transformations will be PC_1, C_2T, $PC_3T(C_3 = C_1C_2)$. The hypothesis of right and left protons (p_R and p_L) mentioned by Lee and Yang in one of their first papers [4]) on non-conservation of parity would correspond to this case.

For zero rest mass the states of particles should be defined as states with a definite projection of spin on momentum (i.e., spirality), since such definition is invariant with respect to the proper four-dimensional rotations and displacements. The sign of spirality changes under space inversion and does not change under time reflection. Therefore only *T-symmetry* (type 2) and *total asymmetry* (type 5) are found to be possible for particles with zero rest mass (the spin being non-zero).

Operation C which transforms the states with the same mass and spin into one another has been called above not a charge conjugation but an operation of the charge conjugation type since in some cases it may not change the sign of any charge (for photons, for example).

It is to be observed that different restrictions of the S-matrix will correspond to different types of symmetry of particles. So, for instance, in types 3 and 4 the S-matrix will not be symmetrical but will be connected with the transposed matrix S^T by the relation

$$S^T = C^{-1}SC.$$

The foregoing considerations can be given a somewhat different interpretation based on the transformation properties of physical quantities which characterize the particle. It follows from group-theory considerations [5]) that the free particle states are described by mass, spin, momentum, spin projection, and also by other possible variables which are necessarily invariant with respect to four-dimensional rotations and displacements. However, these additional variables can be either scalar or pseudoscalar with respect to reflections. If all additional variables are scalar, the particle belongs to the first type (total symmetry). If an additional variable (as, for instance, spirality) is pseudoscalar relative to space reflection and scalar relative to time reflection, the particle belongs to

the second type (T-symmetry) etc. Thus, the study of symmetry types can be reduced to investigating the behaviour relatively to reflections of the quantities which characterize the particles (for instance, the various charges).

2. Conclusion and Further Remarks

The work reported here is a direct continuation of ref. [1]). The purpose of both papers has been to investigate such properties of reflections, as like the law of conservation of momentum — can be determined irrespective of the specific type of equations.

Summarizing the results obtained, one may say that investigation of the reflection operations reduces to answering the following three questions:

1. To which group G_1—G_8 [1]) does the transformation of the real space-time belong?

2. According to which representation (formulae (24), (26), (28) and (35) in ref. [1])) does each particle transform?

3. To which type of symmetry does each particle belong?

All other tasks that might arise in studying relections either reduce to the above-mentioned or essentially depend on the specific choice of the equations of motion.

Of some interest will be an analysis of the available experimental data along the lines of the methods developed above. Wu's experiment, from this point of view, would only indicate that at least one of the particles participating in the process (for instance, the neutrino) does not transform into itself under inversion.

It is also interesting to determine the sum total of experiments required for furnishing exhaustive answers to the above set questions. Thus, in order to find the asymmetry types of the proton, it is necessary to investigate the conservation transformations P, T, PT in different processes with protons involved. If, for instance, it turns out that none of the three transformations is conserved this will imply that the proton possesses four different states (with the same mass) in accordance with the Lee and Yang [4]) hypothesis.

References

1) Yu. M. Shirokov, Nuclear Physics **14** (1959)
2) L. Landau, JETP **32** (1957) 405
3) W. Pauli, in Niels Bohr and the Development of Physics (London, 1955)
4) T. Lee and C. Yang, Phys. Rev. **104** (1956) 254
5) Yu. M. Shirokov, JETP **33** (1957) 1197

2.E

Nuclear Physics **15** (1960) 16—32; © *North-Holland Publishing Co., Amsterdam*

Not to be reproduced by photoprint or microfilm without written permission from the publisher

MANY-BODY BASIS FOR THE OPTICAL MODEL

LEE M. FRANTZ † and ROBERT L. MILLS

The Ohio State University, Columbus, Ohio ††

Received 1 October 1959

Abstract: A formal expression is derived for an optical model potential based on an assumed two-body interaction between nucleons, which provides an exact description of the elastic scattering of a single nucleon by a closed shell (or closed shell ± 1) nucleus. A second-quantized description is used for the many-fermion system, the true state vector being expanded in terms of a complete set of single-particle model wave functions. Elimination of the variables of all but the scattered nucleon yields a weighting function which satisfies a one-body Schrödinger equation, whose S-matrix elements are identical with those of the true S-matrix between states corresponding to elastic scattering. The effective optical model potential is identified from this Schrödinger equation, and is found, of course, to be complex and non-local. It contains all the effects of the exclusion principle, and is in the form of a linked-cluster perturbation expansion, so that the spurious divergence of Brillouin-Wigner perturbation theory for a large number of nucleons is absent.

1. Introduction

In this paper a derivation of the optical-model potential will be presented starting from the Brueckner-Bethe-Goldstone treatment [1, 2, 3]) of the nuclear many-body problem. The rigorous equivalence of the optical-model and many-body descriptions of elastic scattering of a nucleon by a nucleus has previously been shown by others [4]). A different approach is adopted here, which results in an explicit prescription for calculating the optical potential by the use of Goldstone diagrams. This prescription involves a linked-cluster (Rayleigh-Schrödinger) expansion similar to that used by Brueckner *et al.* in calculating properties of static nuclei [1]). The exclusion principle is taken fully into account, and it will be seen that one of its effects on the qualitative nature of the optical potential is immediately evident from the formal expression for the potential. Specifically, the optical potential contains a projection operator which makes the optical wave function orthogonal to the occupied states of the nucleus, as described by a suitably chosen independent-particle model. On the basis of this property of the optical potential it has already been suggested that a modification be made in the usual scattering analysis by means of phenomenological optical-model potentials [5]).

† Now at the Ramo-Wooldridge Corporation, Los Angeles, California.

†† Supported by the National Science Foundation.

The basic idea of the present approach is the following. First we exhibit the many-body state vector of the system in a representation constructed from the eigenstates of an independent-particle model. Then we examine the projection of this state vector on the subspace in which the nuclear particles occupy the unexcited model states. Now, at sufficiently large distances the portion of the state vector describing the elastic scattering contains essentially the product of one wave function for the unexcited nucleus, and another for the scattered nucleon; this is because these two bodies cease to influence each other at large distances. Thus any projection of this state vector on a subspace for which the nucleus is in a given bound model state will show the same asymptotic behaviour for the scattered nucleon as the state vector itself. The sub-space we have chosen is clearly of the required form and therefore provides us with a complete description of the elastic scattering. Moreover, as we shall demonstrate, the weighting function for the state of the incident nucleon within this subspace satisfies a Schrödinger equation from which we can identify the optical-model potential. We now proceed to carry out this program.

In the remainder of this section the notation is introduced and the linked cluster expansion for the scattering state vector is displayed. In sections 2 and 3 the validity of this expression is proven directly without recourse to an adiabatic hypothesis.

Section 4 contains the derivation of the effective optical potential by means of the projection procedure described above, while section 5 contains the proof of the equivalence of the optical wave function to the true state vector for elastic scattering, and a discussion of the role played by inelastic scattering in this theory. In section 6, some conclusions are presented.

We wish to describe the elastic scattering of a single nucleon from a nucleus containing A particles, assuming that we know the two-body potential $v(1,2) = v(2, 1)$. We start by choosing a single-particle model potential U, which approximately describes the nucleus, e.g., a shell-model potential. U must be hermitian in order to provide a complete set of model states, but it may be non-local, i.e. velocity-dependent or angular-momentum-dependent. In the present treatment we shall neglect the recoil of the nucleus: it will be consistent with this approximation to keep U fixed in space. The eigenstates of the single-particle model Hamiltonian are defined by

$$(T+U)\chi_\nu = \omega_\nu \chi_\nu; \tag{1}$$

the subscript ν designates all coordinates necessary for identification of the state, including spin and isobaric spin, and in the continuum it includes the asymptotic momentum. For convenience in describing the many-body system, especially with regard to the exclusion principle, we shall use a second-quantized formalism. The creation and annihilation operators $a_\nu^\dagger$ and a_ν for the single-particle model states of eq. (1) satisfy the usual anticommutation relations

appropriate to a system of fermions. The total many-body Hamiltonian H is split into an unperturbed part H_0, and a perturbation H_1, given in the above representation by [6]) †

$$\begin{aligned} H_0 &= \sum_{\mu,\nu} a_\mu^\dagger(\mu|T+U|\nu)a_\nu = \sum_\mu \omega_\mu a_\mu^\dagger a_\mu, \\ H_1 &= \tfrac{1}{2}\sum_{\mu\nu\rho\sigma} a_\mu^\dagger a_\nu^\dagger(\mu\nu|v|\rho\sigma)a_\sigma a_\rho - \sum_{\mu\nu} a_\mu^\dagger(\mu|U|\nu)a_\nu \\ &\equiv H_1^{(1)} - H_1^{(2)}, \end{aligned} \tag{2}$$

where

$$(\mu\nu|v|\rho\sigma) = (\chi_\mu(1)\chi_\nu(2)|v(1,2)|\chi_\rho(1)\chi_\sigma(2)).$$

We denote the model ground state of the nucleus by the state vector $\Phi_0 \equiv a_A^\dagger \ldots a_1^\dagger \Phi_{\text{vac}}$. Goldstone [3]), using the results of Gell-Mann and Low [7]) for the vacuum-state vector, has shown that the state vector for the unexcited nucleus is given by

$$\Phi_A = \frac{U(0,-\infty)\Phi_0}{\langle\Phi_0|U(0,-\infty)|\Phi_0\rangle}, \tag{3}$$

where $U(0,-\infty)$ is the Møller wave matrix. This reduces to the more explicit expression

$$\Phi_A = \sum_{n=0}^{\infty}{}^{\text{L}} (\mathscr{E}_A{}^{-1}H_1)^n \Phi_0, \tag{4}$$

$\mathscr{E}_A = E_A - H_0$, E_A being the model energy of the nucleus. The symbol $\sum^{\text{L}}$ means a sum over all linked diagrams, ignoring the exclusion principle in intermediate states. We shall use the diagram convention of ref. [3]), which relates excited states to the nuclear model ground state: a line directed upward represents a particle present in an excited model state, while a line directed downward represents a hole, that is, the absence of a particle from a normally occupied state. In this context a diagram is defined to be unlinked if it contains an isolated subdiagram having no external nucleon or hole lines. If we invoke the adiabatic hypothesis, as is frequently done in field theory [8]), the state vector Ψ_k for a nucleon having the asymptotic momentum of model state k impinging on a nucleus of mass number A is given, in an expression analogous to (3), by

$$\Psi_k = \frac{U(0,-\infty)a_k^\dagger\Phi_0}{\langle\Phi_0|U(0,-\infty)|\Phi_0\rangle}, \tag{5}$$

which reduces to

$$\Psi_k = \sum_{n=0}^{\infty}{}^{\text{L}} (\mathscr{E}_k{}^{-1}H_1)^n a_k^\dagger\Phi_0. \tag{6}$$

The energy denominator in (6) is defined by $\mathscr{E}_k = E_A + \omega_k - H_0 + i\varepsilon$, where $i\varepsilon$

† Summation signs and integration symbols both have the same meaning when used with reference to the model states: namely sum over the discrete states and integrate over the continuum. The choice of symbol made in a particular case is based only on convenience or aesthetics.

is an imaginary infinitesimal whose purpose is to define the contour of integration over the continuum states in such a way as to give Ψ_k an asymptotically outgoing scattered part. The terms in the expansion of Ψ_k will have poles at those values of ω_k corresponding to discrete intermediate model states of the $(A+1)$-nucleon system. These of course are shifted, when the series is summed, to the energies of the true $A+1$ nucleon system, and give resonances in the elastic scattering.

It is possible to show without recourse to the adiabatic hypothesis that (6) gives the proper expression for Ψ_k. This will be done in section 3 by using a theorem on factorization in the linked cluster expansion, which we prove next.

2. Factorization Theorem

Let us now define a disconnected diagram as one (like those shown in figs. 1 and 2) consisting of two isolated subdiagrams, which may or may not themselves

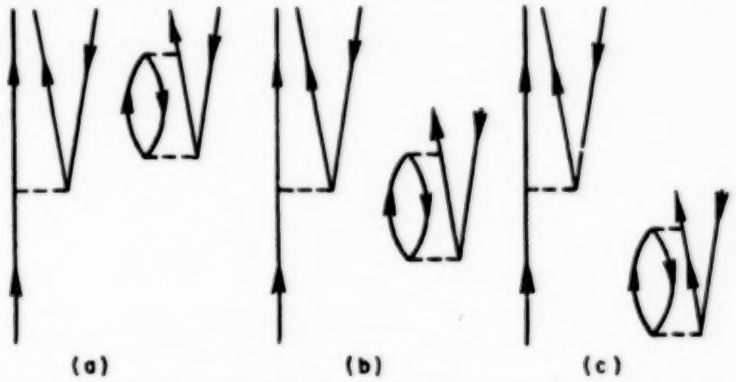

Fig. 1. Example of a class of disconnected diagrams differing only in the relative ordering of the vertices.

be disconnected, and which may or may not have external lines. (An unlinked diagram is thus a special case of a disconnected diagram). The disconnected diagrams contributing to a state vector such as Φ_A or Ψ_k fall into classes with all the members of a given class involving the same particle and hole states and the same interactions in the same way in each subdiagram, and differing only in the relative ordering of the vertices between the different subdiagrams. The diagrams of fig. 1 constitute such a class.

Now the contribution associated with any diagram can be written as the product of a state vector and a c-number. The state vector is a product of particle and hole creation operators acting on the model ground state, while the c-number factor is a product of interaction matrix elements and energy denominators. All the members of a given class of diagrams correspond to the same state vector part; we shall now prove that the sum of c-number factors over all the members of a class is simply the product of the c-number factors which would be associated with the separate sub-diagrams, if they were themselves regarded as diagrams. The product of matrix elements is the same for each

member of the class, and has already the desired property, so it remains only to give a proof for the energy denominator parts. There is of course no change in sign among the members of a given class, since they differ only in the interchange of even numbers of creation and annihilation operators.

The final step can be accomplished as follows. Consider a set of energy denominators corresponding to two disconnected subgraphs, a and b. Let the denominators corresponding to diagram a taken alone be $\mathscr{E}_1{}^a, \ldots, \mathscr{E}_m{}^a$, and similarly, $\mathscr{E}_1{}^b, \ldots, \mathscr{E}_n{}^b$ for diagram b, where $\mathscr{E}_l{}^a$ is the appropriate energy plus the imaginary infinitesimal $i\varepsilon$. Then take the sum over all possible permutations of the order in which a and b energies change relative to each other. This corresponds to summing over diagrams having all possible relative orders of the vertices in the a and b subdiagrams. We define this sum to be Δ_{mn}, which may be written

$$\Delta_{mn} = \sum_{\{\alpha,\beta\}} \prod_{p=1}^{m+n} (\mathscr{E}^a_{\alpha(p)} + \mathscr{E}^b_{\beta(p)})^{-1}, \tag{7}$$

where the summation is over all sets of $m+n$ integer pairs $\alpha(p), \beta(p)$ satisfying

(i) either $\alpha(1) = 1, \ \beta(1) = 0,$

or $\alpha(1) = 0, \ \beta(1) = 1;$

(ii) either $\alpha(p+1) = \alpha(p)+1, \ \beta(p+1) = \beta(p)$

(corresponding to a vertex in the a subdiagram),

or $\alpha(p+1) = \alpha(p), \ \beta(p+1) = \beta(p)+1$ (a b-vertex);

(iii) $\alpha(m+n) = m, \ \beta(m+n) = n$ (corresponding to the fact that there are a total of m a-vertices, and n b-vertices); and where we understand

$$\mathscr{E}_0{}^a = \mathscr{E}_0{}^b = 0. \tag{8}$$

The product of energy denominators for diagram a taken alone, which we denote by $\Delta_m{}^a$, is seen to be identical to Δ_{m0}:

$$\Delta_m{}^a = \Delta_{m0} = \prod_{p=1}^{m} (\mathscr{E}_p{}^a)^{-1}; \tag{9}$$

while similarly, $\Delta_n{}^b = \Delta_{0n}$. We define

$$\Delta_0{}^a = \Delta_0{}^b = \Delta_{00} = 1. \tag{10}$$

It is now possible to prove the algebraic identity †

$$\Delta_{mn} = \Delta_m{}^a \Delta_n{}^b, \tag{11}$$

as follows: clearly the terms of Δ_{mn}, as it is written in eq. (7), can be divided into two classes, according to whether the last two factors in each product are of the form

$$(\mathscr{E}^a_{m-1} + \mathscr{E}_n{}^b)^{-1}(\mathscr{E}_m{}^a + \mathscr{E}_n{}^b)^{-1},$$

† The identity, which corresponds to the natural factorization in a time-dependent theory, was pointed out to the authors independently by J. Goldstone.

or of the form

$$(\mathscr{E}_m{}^a+\mathscr{E}_{n-1}^b)^{-1}(\mathscr{E}_m{}^a+\mathscr{E}_n{}^b)^{-1}.$$

Apart from the last factor, which is common to both classes, the terms in these two classes are just the terms comprising $\Delta_{m-1,n}$ and $\Delta_{m,n-1}$, respectively, so that

$$\Delta_{mn} = (\Delta_{m-1,n}+\Delta_{m,n-1})(\mathscr{E}_m{}^a+\mathscr{E}_n{}^b)^{-1}.$$

This equation will be seen by inspection to be valid even if m or n is equal to 1. Now suppose that eq. (11) holds for $\Delta_{m-1,n}$ and $\Delta_{m,n-1}$. Then

$$\begin{aligned}\Delta_{mn} &= (\Delta_{m-1}^a\Delta_n{}^b+\Delta_m{}^a\Delta_{n-1}^b)(\mathscr{E}_m{}^a+\mathscr{E}_n{}^b)^{-1}\\ &= \Delta_m{}^a\Delta_n{}^b(\mathscr{E}_m{}^a+\mathscr{E}_n{}^b)(\mathscr{E}_m{}^a+\mathscr{E}_n{}^b)^{-1} \qquad (12)\\ &= \Delta_m{}^a\Delta_n{}^b,\end{aligned}$$

using the simple product character of $\Delta_m{}^a$ and $\Delta_n{}^b$. Since (11) holds for m or n equal to zero (eqs. 9 and 10), the identity is valid, by induction, for all m and n.

In view of the fact that $i\varepsilon$ is an infinitesimal whose only purpose is to define the singularities in the energy denominators, we can replace a positive multiple of $i\varepsilon$ by $i\varepsilon$ itself, wherever necessary in (11). With this in mind we can see that (11), combined with the preceding considerations of this section, constitutes the proof that it is possible to factorize a sum of state vectors corresponding to disconnected subdiagrams having all possible relative orderings, but individually maintaining the same internal ordering. This result will be referred to as the factorization theorem.

3. The State Vectors

We are now in a position to prove (6). We start by operating on both sides with $E_k-H_0+i\varepsilon$, where $E_k = E_A+\omega_k$. Remembering that ε is an infinitesimal, and that $H_0a_k{}^\dagger\Phi_0 = E_ka_k{}^\dagger\Phi_0$, we find

$$(E_k-H_0)\Psi_k = \sum_n{}^{\mathrm{L}} H_1(\mathscr{E}_k{}^{-1}H_1)^n a_k{}^\dagger\Phi_0. \qquad (13)$$

A diagram which has at any point become unlinked cannot be linked again, so the last H_1 on the right-hand side of (13) can be taken out of the summation sign without affecting the linked quality of those portions which precede it. However, a previously linked diagram can be unlinked by the last H_1, so if we take it outside $\sum^{\mathrm{L}}$ we must write (13) as

$$(E_k-H_0)\Psi_k = H_1\sum_n{}^{\mathrm{L}}(\mathscr{E}_k{}^{-1}H_1)^n a_k{}^\dagger\Phi_0-[H_1\textstyle\sum^{\mathrm{L}}(\mathscr{E}_k{}^{-1}H_1)^n a_k{}^\dagger\Phi_0]_{\mathrm{UL}} \qquad (14)$$

where the subscript UL means take only unlinked diagrams. The first term on the right-hand side of (14) is simply $H_1\Psi_k$. The second term consists of diagrams which are linked before the application of the last H_1, but unlinked after. Such diagrams are typified by that shown in fig. 2. The circles represent linked

subgraphs of arbitrary complexity with the restriction that the only external nucleon lines are those explicitly shown. In order that the diagram be linked before the last H_1, subdiagrams A and B must each be internally linked, although they may contain disconnected subgraphs. Also, A may have any number of open pair lines leaving it. Since all possible diagrams of the type shown in fig. 2 are included in the second term of (14), the subgraphs of type A are the same as the graphs in Ψ_k. (Note that in order for this statement to be true, the rule that we ignore the exclusion principle in intermediate states is essential.) Since the last vertex in subgraph B must follow all the vertices of A, we can only apply the factorization theorem to the portion of the graph preceding the last vertex. The matrix elements for the whole graph factorize as usual, and the energy denominator part is $\Delta_m{}^A \Delta_n{}^B$. Here $\Delta_m{}^A$ is the proper factor for A taken alone, so that this term in (14) may be written $\Delta E_A \Psi_k$, where ΔE_A is

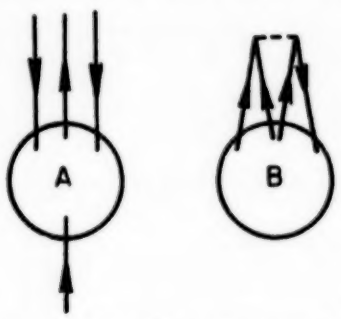

Fig. 2. Typical diagram contributing to $\Delta E_A \Psi_k$; it is linked before the last vertex, but unlinked after.

the c-number factor associated with the diagrams of type B, including the matrix element from the last H_1. It is equivalent to write

$$\Delta E_A = \langle \Phi_0 | H_1 \sum_n^L (\mathscr{E}_A{}^{-1} H_1)^n | \Phi_0 \rangle. \tag{15}$$

We may now write (14) as

$$H\Psi_k = (E_k + \Delta E_A)\Psi_k. \tag{16}$$

To identify ΔE_A, we perform analogous manipulations on Φ_A, eq. (4), with the result

$$H\Phi_A = (E_A + \Delta E_A)\Phi_A. \tag{17}$$

It follows from (4) that in the limit as the perturbation H_1 vanishes, $\Phi_A \to \Phi_0$, the model ground-state vector of the nucleus. This fact, coupled with (17), shows that Φ_A is indeed the state vector for the unexcited nucleus, and identifies ΔE_A as the difference between the true energy and the model energy for this nucleus †. It then follows from (6) and (16) that Ψ_k is the state vector describing a nucleon of energy ω_k bombarding a nucleus of A particles. Letting $H_1 \to 0$ again, we see that $\Psi_k \to a_k{}^\dagger \Phi_0$. This completes the identification of the state as

† The algebraic method used to obtain this result was briefly outlined in ref. [3]).

that in which the incident nucleon has the asymptotic momentum of state k. Finally, we note that the imaginary infinitesimal in the energy denominators has a + sign, giving the wave an outgoing scattered part, as is necessary to be consistent with the use of $a_k^\dagger$ as the creation operator for a single-particle model state with outgoing scattered part.

4. Reduction to the Single-Particle Equation

In discussing the $(A+1)$ nucleon system we shall refer to a model subspace analogous to the model ground state of the A nucleon system. In this case it is defined to be the subspace spanned by those $(A+1)$ particle states for which the A lowest single-particle model states are occupied, the state of the $(A+1)^{st}$ particle being arbitrary. We define, also, the projection operator Λ_0 on the model subspace, and the projection operator off the model subspace †, $\Lambda = I - \Lambda_0$. Now consider the diagrams comprising the state vector (6). Each diagram can be broken into a succession of one or more subgraphs connected each to the next by a single line, that is, by an intermediate state lying in the model subspace. This can be interpreted as the iteration of an effective interaction operator, which operates on the model subspace, and which we shall now single out and identify. The first stage is most readily carried out without the restriction to linked diagrams, the restriction being imposed later. Thus,

$$\Psi'_k \equiv \sum_n (\mathscr{E}_k^{-1} H_1)^n a_k^\dagger \Phi_0 = \Lambda_0 \sum_n (\mathscr{E}_k^{-1} H_1)^n a_k^\dagger \Phi_0 + \mathscr{E}_k^{-1} \Lambda H_1 \Psi'_k. \quad (18)$$

Rearranging terms yields

$$(1 - \mathscr{E}_k^{-1} \Lambda H_1) \Psi'_k = \Lambda_0 \sum_n (\mathscr{E}_k^{-1} H_1)^n a_k^\dagger \Phi_0,$$

and hence

$$\begin{aligned} \Psi'_k &= (1 - \mathscr{E}_k^{-1} \Lambda H_1)^{-1} \Lambda_0 \sum_n (\mathscr{E}_k^{-1} H_1)^n a_k^\dagger \Phi_0 \\ &= \sum_m (\mathscr{E}_k^{-1} \Lambda H_1)^m \Lambda_0 \sum_n (\mathscr{E}_k^{-1} H_1)^n a_k^\dagger \Phi_0. \end{aligned} \quad (19)$$

This relation may be substituted into the Schrödinger equation satisfied by Ψ_k, in the modified form (13), with the result

$$\begin{aligned} (E_k - H_0) \Psi_k &= \Big[\sum_{m,n} H_1 (\mathscr{E}_k^{-1} \Lambda H_1)^m \Lambda_0 (\mathscr{E}_k^{-1} H_1)^n a_k^\dagger \Phi_0 \Big]_L \\ &= \sum_m{}^L H_1 (\mathscr{E}_k^{-1} \Lambda H_1)^m \Lambda_0 \sum_n{}^L (\mathscr{E}_k^{-1} H_1)^n a_k^\dagger \Phi_0, \end{aligned} \quad (20)$$

where it is clear that the portions of each diagram preceding and following the single line represented by Λ_0 must separately be linked in order for the whole

† This projection operator should not be confused with the one assigned the same symbol in ref. [5]).

diagram to be linked. We can identify the factor $\Lambda_0\sum_n^L(\mathscr{E}_k^{-1}H_1)^n a_k^\dagger\Phi_0$ as simply the model subspace projection Ψ_{0k} of Ψ_k:

$$\Psi_{0k} = \Lambda_0\Psi_k = \Lambda_0\sum_n^L(\mathscr{E}_k^{-1}H_1)^n a_k^\dagger\Phi_0. \tag{21}$$

Operating on eq. (20) with Λ_0, we obtain an equation for Ψ_{0k} alone,

$$(E_k-H_0)\Psi_{0k} = \sum_m^L \Lambda_0 H_1(\mathscr{E}_k^{-1}\Lambda H_1)^m\Psi_{0k}, \tag{22}$$

which has the form of a Schrödinger equation. The trivial manipulations below now reduce the factor of Ψ_{0k} on the right to an expression for an effective nonlocal potential W_k.

The state vector Ψ_{0k} may be expressed as a sum over all the basis vectors spanning the model subspace as follows †:

$$\Psi_{0k} = \int \mathrm{d}s\varphi_k(s)a_s^\dagger\Phi_0, \tag{23}$$

where $\varphi_k(s)$ is a c-number weighting factor, which we shall show to be a representation of an optical model wave function. If we next take the scalar product of (22) with $a_t^\dagger\Phi_0$, and substitute the expression in (23) for Ψ_{0k}, we find

$$\omega_t\varphi_k(t)+\int \mathrm{d}sW_k(t,s)\varphi_k(s) = \omega_k\varphi_k(t), \tag{24}$$

where

$$W_k(t,s) = \langle\Phi_0|a_t\sum_m^L H_1(\mathscr{E}_k^{-1}\Lambda H_1)^m a_s^\dagger|\Phi_0\rangle. \tag{25}$$

Equation (25) is the desired result in an unfamiliar representation. To put it in more recognizable form we first define φ_k to be the single-particle state vector having $\varphi_k(s)$ as its representative with respect to χ_s:

$$\varphi_k = \int \mathrm{d}s\varphi_k(s)\chi_s. \tag{26}$$

Note the distinction between the state vector φ_k and the wave function (c-number weighting factor) $\varphi_k(s)$. With the aid of (1) it can now be seen that (24) is just the representative with respect to χ_t of the state vector equation

$$(T+U+W_k)\varphi_k = \omega_k\varphi_k, \tag{27}$$

where the potential operator W_k is given in terms of its χ-representation $W_k(t,s)$ by

$$W_k = \int\int \mathrm{d}t\mathrm{d}s|\chi_t)W_k(t,s)(\chi_s|. \tag{28}$$

Equation (27) is the desired single-particle Schrödinger equation from which we identify the optical-model potential $V_k = U+W_k$. It might be expected

† See footnote p. 18.

intuitively that if, as can be done by means of (27), we are able to calculate the ground state projection of Ψ_k, we are then in a position to obtain a reasonable approximation to the elastic scattering. However, as we asserted in the introduction, the description of the elastic scattering given by (27) is actually exact. In the next section, where we analyze the behaviour of the model wave function and derive the S-matrix, we shall exhibit the necessary analytical support of the verbal arguments in section 1.

5. Scattering Formalism

As a preliminary to a detailed derivation of the S-matrix we examine here the asymptotic behaviour of the model scattering wave function, as compared to that of the true scattering state; it is most concise to follow a procedure due to Bell and Squires †. Expressing the annihilation operator in configuration space,

$$\psi(\mathbf{x}) = \sum_{\mu} a_{\mu}\chi_{\mu}(\mathbf{x}), \tag{29}$$

we see that the model wave function is given, according to (23), by

$$\varphi_k(\mathbf{x}) = \langle \Phi_0|\psi(\mathbf{x})|\Psi_k\rangle. \tag{30}$$

Apart from contributions due to production processes, which are more complicated, but may be treated similarly, the asymptotic form of Ψ_k itself is described by the quantities

$$\langle \Phi_N|\psi(\mathbf{x})|\Psi_k\rangle \sim f_N r^{-1} e^{ik_N r} + \delta_{N,A} e^{i\mathbf{k}\cdot\mathbf{x}}, \tag{31}$$

where Φ_N is one of the true state vectors for the bound states of the A-nucleon system, and k_N is the appropriate wave number for the outgoing particle in this possibly inelastic process $[k_N = \sqrt{k^2 - (2m/\hbar^2)(E_N - E_A)}]$. For large $\mathbf{x}$, the function $\varphi_k(\mathbf{x})$ is given by

$$\begin{aligned} \varphi_k(\mathbf{x}) &= \sum_N \langle \Phi_0|\Phi_N\rangle\langle \Phi_N|\psi(\mathbf{x})|\Psi_k\rangle \\ &\sim \sum_N \langle \Phi_0|\Phi_N\rangle f_N r^{-1} e^{ik_N r} + \langle \Phi_0|\Phi_A\rangle e^{i\mathbf{k}\cdot\mathbf{x}}. \end{aligned} \tag{32}$$

Thus $\varphi_k(\mathbf{x})$ contains outgoing waves corresponding to both elastic and inelastic processes; the incoming plane wave and the outgoing elastically scattered wave have of course the same normalization, while the normalization of the outgoing inelastically scattered wave is different.

Since $\varphi_k(\mathbf{x})$ satisfies a Schrödinger equation, with the effective potential $V_k(\mathbf{x}, \mathbf{x}')$, it is clear that above the threshold for inelastic processes $V_k(\mathbf{x}, \mathbf{x}')$ must have non-vanishing parts even for arbitrarily large $\mathbf{x}$, in order to accommodate the inelastic parts of $\varphi_k(\mathbf{x})$. Nonetheless, the wave function does include the elastic parts correctly, and indeed includes in principle the energy and

† We are indebted for this to J. S. Bell and E. J. Squires (see ref. [9])) and, more importantly, for pointing out the presence of inelastic scattering parts in $\varphi_k(\mathbf{x})$ itself.

angular dependence of the cross sections associated with those excited states which have the same spin and parity as the ground state and which are energetically allowed.

In spite of the presence of inelastic parts in $\varphi_k(\mathbf{x})$ it is not necessary to single out the elastic portions in order to calculate the elastic scattering. This can in fact be done by evaluating the transition amplitudes in terms of $V_k(\mathbf{x}, \mathbf{x}')$ and $\varphi_k(\mathbf{x})$ as though they were an ordinary elastic potential and wave function. To prove this we shall now compare the S-matrices which follow from the many-body and single-particle descriptions corresponding, respectively, to (16) and (27).

In the following we shall use $+$ and $-$ signs to distinguish states having, respectively, incoming and outgoing plane wave parts. The state vector for a nucleus of A particles being bombarded by a nucleon having the asymptotic momentum of model state m is given by

$$\Psi_m^{(\pm)} = a^\dagger_{m(\pm)}\Phi_A + R_m^{(\pm)}, \tag{33}$$

where $R_m^{(\pm)}$ is the scattered portion of the wave resulting from H_1, i.e., from the interaction of the incident nucleon with the particles in the nucleus. The first term $a^\dagger_{m(\pm)}\Phi_A$ contains the incoming (or outgoing) plane wave part as well as the scattering due to the model potential; it contains no scattering due to direct interaction with the nuclear particles through the perturbation Hamiltonian. Both Φ_A and the model state vector $\chi_m^{(\pm)}$ represented by $a^\dagger_{m(\pm)}$ are taken to be normalized to unity. This means that $\Psi_m^{(\pm)}$ is normalized to unit incoming (or outgoing) flux, and, consequently, the state vector as a whole is normalized to unity. To find $R_m^{(\pm)}$ we shall need the commutation relations

$$\begin{aligned} H_1 a^\dagger_{m(\pm)} &= a^\dagger_{m(\pm)} H_1 + Q^\dagger_{m(\pm)}, \\ H_0 a^\dagger_{m(\pm)} &= a^\dagger_{m(\pm)}(H_0+\omega_m). \end{aligned} \tag{34}$$

The operator $Q_m^{(\pm)}$, which we shall later use explicitly, is

$$\begin{aligned} Q_{m(\pm)} = \tfrac{1}{2}\sum_{\mu\nu\rho} a^\dagger_{\rho(\pm)}[&(\chi_\rho^{(\pm)}\chi_m^{(\pm)}|v|\chi_\mu^{(\pm)}\chi_\nu^{(\pm)}) \\ &-(\chi_m^{(\pm)}\chi_\rho^{(\pm)}|v|\chi_\mu^{(\pm)}\chi_\nu^{(\pm)})]a_{\nu(\pm)}a_{\mu(\pm)} \\ &-\sum_\mu (\chi_m^{(\pm)}|U|\chi_\mu^{(\pm)})a_{\mu(\pm)}. \end{aligned} \tag{35}$$

Since $\Psi_m^{(\pm)}$ is an eigenstate of H corresponding to eigenvalue $E_m = \Delta E_A + E_A + \omega_m$, we have, with the aid of (34),

$$(E_m - H)\Psi_m^{(\pm)} = 0 = -Q^\dagger_{m(\pm)}\Phi_A + (E_m - H)R_m^{(\pm)}, \tag{36}$$

from which it follows that

$$R_m^{(\pm)} = (E_m - H \pm i\varepsilon)^{-1} Q^\dagger_{m(\pm)}\Phi_A; \tag{37}$$

the $\pm i\varepsilon$ has been inserted in the denominator of (37) to comply with the boundary condition that the scattered part of the wave be (outgoing, incoming). That $R_m^{(\pm)}$ contains no further term satisfying the homogeneous equation $(E_m-H)\Psi=0$ is clear from the fact that $R_m^{(\pm)}$ may contain only (outgoing, incoming) waves, while any solution of the homogeneous equation contains both. We now have

$$\begin{aligned}\Psi_m^{(\pm)} &= a^\dagger_{m(\pm)}\Phi_A+(E_m-H\pm i\varepsilon)^{-1}Q^\dagger_{m(\pm)}\Phi_A\\ &= a^\dagger_{m(\pm)}\Phi_A+(E_m-H\mp i\varepsilon)^{-1}Q^\dagger_{m(\pm)}\Phi_A\\ &\quad+[(E_m-H\pm i\varepsilon)^{-1}-(E_m-H\mp i\varepsilon)^{-1}]Q^\dagger_{m(\pm)}\Phi_A,\end{aligned} \tag{38}$$

$$\begin{aligned}\Psi_m^{(\pm)} &= a^\dagger_{m(\pm)}\Phi_A+(E_m-H\mp i\varepsilon)^{-1}Q^\dagger_{m(\pm)}\Phi_A\\ &\quad\mp 2\pi i\delta(E_m-H)Q^\dagger_{m(\pm)}\Phi_A,\end{aligned} \tag{39}$$

where we have used the fact that the Dirac delta function can be represented formally by

$$\delta(x)=\lim_{\varepsilon\to 0}\frac{1}{\pi}\,\frac{\varepsilon}{x^2+\varepsilon^2}. \tag{40}$$

Since creation operators transform in the same way as the state vectors to which they correspond [6]), and since (34) shows that $Q^\dagger_{m(\pm)}$ transforms in the same way as $a^\dagger_{m(\pm)}$, (41b) and (41c) below follow from (41a):

$$\chi_m^{(\pm)}=\sum_n \chi_n^{(\mp)}(\chi_n^{(\mp)}|\chi_m^{(\pm)}), \tag{41a}$$

$$a^\dagger_{m(\pm)}=\sum_n a^\dagger_{n(\mp)}(\chi_n^{(\mp)}|\chi_m^{(\pm)}), \tag{41b}$$

$$Q^\dagger_{m(\pm)}=\sum_n Q^\dagger_{n(\mp)}(\chi_n^{(\mp)}|\chi_m^{(\pm)}). \tag{41c}$$

Applying (41b, c) to (39) yields

$$\begin{aligned}\Psi_m^{(\pm)} &= \sum_n (\chi_n^{(\mp)}|\chi_m^{(\pm)})[a^\dagger_{n(\mp)}\Phi_A+(E_m-H\mp i\varepsilon)^{-1}Q^\dagger_{n(\mp)}\Phi_A\\ &\quad\mp 2\pi i\delta(E_m-H)Q^\dagger_{n(\mp)}\Phi_A]\\ &= \sum_n (\chi_n^{(\mp)}|\chi_m^{(\pm)})[\Psi_n^{(\mp)}\mp 2\pi i\delta(E_m-H)Q^\dagger_{n(\mp)}\Phi_A].\end{aligned} \tag{42}$$

The probability amplitude, or S-matrix element, for scattering from an initial state l with incoming plane wave to a final state k with outgoing plane wave is given by the projection of one onto the other, $S_{kl}=\langle\Psi_k^{(-)}|\Psi_l^{(+)}\rangle$. Thus, we find from (42),

$$\begin{aligned}S_{kl} &= (\chi_k^{(-)}|\chi_l^{(+)})\\ &\quad-2\pi i\delta(E_k-E_l)\sum_n(\chi_k^{(-)}|\chi_n^{(+)})\langle\Phi_A|Q_{n(+)}|\Psi_l^{(+)}\rangle.\end{aligned} \tag{43}$$

Since we have assumed Φ_A and $\Psi_l^{(+)}$ to be normalized to unity, if we are to

use (4) and (6) they must be modified by the insertion of a normalization constant $Z^{\frac{1}{2}}$, where

$$Z^{-1} = [\langle \Phi_0 | \sum_n (H_1 \mathscr{E}_A^{-1})^n]_L [\sum_m (\mathscr{E}_A^{-1} H_1)^m | \Phi_0 \rangle]_L. \tag{44}$$

The rectangular brackets with subscript L are reminders that it is the diagrams pertaining to the individual state vectors in the inner product which must be linked, not necessarily the overall diagrams. $\Psi_l^{(+)}$ has been given the same normalization constant as Φ_A, since in the asymptotic region, where the normalization to unit flux is made, the interactions of the incident nucleon with the nucleus do not appear. Using the normalized versions of (4) and (6) we find

$$Z^{-1}\langle Q \rangle = [\langle \Phi_0 | \sum_p (H_1 \mathscr{E}_A^{-1})^p]_L Q_{n(+)} [\sum_q (\mathscr{E}_l^{-1} H_1)^q a_{l(+)}^\dagger | \Phi_0 \rangle]_L, \tag{45}$$

where for the sake of brevity in succeeding equations we have introduced the symbol $\langle Q \rangle = \langle \Phi_A | Q_{n(+)} | \Psi_l^{(+)} \rangle$. We see from (35) that $Q_{n(+)}$ destroys a particle and provides an ordinary vertex operator for the transition of this particle into state n. Diagramatically, $Q_{n(+)}$ causes the final interaction of some nucleon line. Since in (45) all other particles eventually return to the model ground state of the nucleus, this line is the continuation of the bombarding nucleon line. Now, because we are neglecting the recoil of the nucleus we can replace $\delta(E_k - E_l)$ by $\delta(\omega_k - \omega_l)$ in (43). The resulting equality of ω_k and ω_l, together with the fact that $(\chi_k^{(-)} | \chi_n^{(+)})$ vanishes unless states k and n are degenerate in energy, quarantees that the energy denominators to the left of $Q_{n(+)}$ in (45) are appropriate to a system of $(A+1)$ particles in which the $(A+1)^{st}$ or bombarding nucleon has settled permanently into a state with its original energy $\omega_n = \omega_l$. The diagrams in fig. 3 are typical of those comprising (45); the encircled Q represents the vertex due to the $Q_{n(+)}$. As required by (45) the subdiagrams before and after the $Q_{n(+)}$ (below and above the dashed line) are individually linked. Notice, however, that the diagram as a whole may be unlinked. The expression in (45) indicates that every possible diagram appears in which the bombarding nucleon starts in state l and ends in state n after having gone through at least one interaction, and in which the subdiagrams before and after the $Q_{n(+)}$ are individually linked. This means that every possible linked subgraph appears in a diagram with every possible unlinked subgraph with the restriction that the upper and lower portions (above and below the dashed line) of the unlinked subgraph are individually linked. In addition the upper portions of the linked and unlinked subgraphs appear in all relative orderings, and the same is true of the lower portions. Consequently, we can apply the factorization theorem to the state vectors represented by the upper and lower subdiagrams, and thereby separate the linked and unlinked parts. The factor resulting from the sum of linked diagrams is

$$\langle \Phi_0 | \sum_{p,q}^{L} (H_1 \mathscr{E}_A^{-1})^p Q_{n(+)} (\mathscr{E}_l^{-1} H_1)^q a_{l(+)}^\dagger | \Phi_0 \rangle. \tag{46}$$

In writing down the expression for the sum of the unlinked diagrams we must notice that the $Q_{n(+)}$ does not appear in them (otherwise they would be connected to the bombarding nucleon line, and, hence, linked), so that at the dashed line in fig. 3 we have two successive energy denominators with no vertex operator in between. The sum of the unlinked diagrams, then, is given by the expression in (44); it is just $1/Z$. Therefore $\langle Q\rangle$ is given by (46). Combining (19) with (46) now yields

$$\langle Q\rangle = \langle \Phi_0| \sum_{p,q}^{L} (H_1 \mathscr{E}_A^{-1})^p Q_{n(+)} (\mathscr{E}_i^{-1} \Lambda H_1)^q \times \Lambda_0 \sum_{r}^{L} (\mathscr{E}_i^{-1} H_1)^r a^{\dagger}_{i(+)} |\Phi_0\rangle. \tag{47}$$

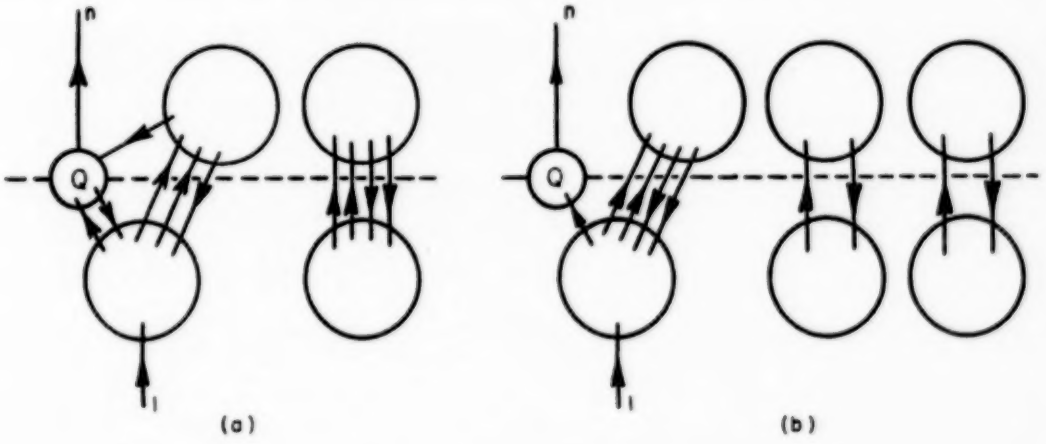

Fig. 3. Typical diagrams contributing to $Z^{-1}\langle Q\rangle$. The linked portions are associated with $\langle Q\rangle$, without the factor Z^{-1}, and hence, with the S-matrix element.

As in (20) the superscript L has been appended to the right-hand summation sign as a reminder that the diagram as a whole cannot be linked unless it is linked at all intermediate points. Using (21) and then (23) we now find

$$\begin{aligned}\langle Q\rangle &= \langle \Phi_0| \sum_{p,q}^{L} (H_1 \mathscr{E}_A^{-1})^p Q_{n(+)} (\mathscr{E}_i^{-1} \Lambda H_1)^q |\Psi^{(+)}_{0i}\rangle \\ &= \int ds W'_i(n, s) \varphi_i^{(+)}(s),\end{aligned} \tag{48}$$

where

$$W'_i(n, s) = \langle \Phi_0| \sum_{p,q}^{L} (H_1 \mathscr{E}_A^{-1})^p Q_{n(+)} (\mathscr{E}_i^{-1} \Lambda H_1)^q a^{\dagger}_{s(+)} |\Phi_0\rangle. \tag{49}$$

Note that $W'_i(n, s)$ contains exactly the same diagrams as $W_i(n, s)$. The expressions are merely written differently in that $W'_i(n, s)$ has the final interaction of the incident nucleon explicitly indicated. Thus $W'_i(n, s)$ is identical with $W_i(n, s)$ and we may rewrite (43) as

$$S_{ki} = (\chi_k^{(-)}|\chi_i^{(+)}) - 2\pi i \delta(\omega_k - \omega_i) \times (\chi_k^{(-)}| \{ \sum_n |\chi_n^{(+)}) \int ds W_i(n, s) \varphi_i^{(+)}(s) \}, \tag{50}$$

or with the aid of (26) and (28) as

$$S_{kl} = (\chi_k^{(-)}|\chi_l^{(+)}) - 2\pi i\delta(\omega_k - \omega_l)(\chi_k^{(-)}|W_l|\varphi_l^{(+)}). \tag{51}$$

We shall now put (51) into a more recognizable form by using the scattering state solutions [11]) of (1) and (27):

$$\chi_m^{(\pm)} = \xi_m + (\omega_m - T \pm i\varepsilon)^{-1} U \chi_m^{(\pm)} \tag{52a}$$

$$\chi_m^{(\pm)} = \xi_m + (\omega_m - T - U \pm i\varepsilon)^{-1} U \xi_m, \tag{52b}$$

$$\varphi_m^{(\pm)} = \xi_m + (\omega_m - T \pm i\varepsilon)^{-1}(U + W_m)\varphi_m^{(\pm)}, \tag{53}$$

where ξ_m is the free particle state vector defined by $T\xi_m = \omega_m \xi_m$. It follows from (52b) and (40) that

$$\begin{aligned}\chi_m^{(\pm)} &= \xi_m + (\omega_m - T - U \mp i\varepsilon)^{-1} U \xi_m \\ &\quad + [(\omega_m - T - U \pm i\varepsilon)^{-1} - (\omega_m - T - U \mp i\varepsilon)^{-1}] U \xi_m \\ &= \chi_m^{(\mp)} \mp 2\pi i\delta(\omega_m - T - U) U \xi_m,\end{aligned}$$

so that

$$(\chi_k^{(-)}|\chi_l^{(+)}) = \delta_{kl} - 2\pi i\delta(\omega_k - \omega_l)(\chi_k^{(-)}|U|\xi_l). \tag{54}$$

Substituting (54) into (51) results in

$$S_{kl} = \delta_{kl} - 2\pi i\delta(\omega_k - \omega_l)[(\chi_k^{(-)}|U|\xi_l) + (\chi_k^{(-)}|W_l|\varphi_l^{(+)})]. \tag{55}$$

Now using (53) to find $\xi_l - \varphi_l^{(+)}$, we have

$$\begin{aligned}&(\chi_k^{(-)}|U|\xi_l) + (\chi_k^{(-)}|W_l|\varphi_l^{(+)}) = (\chi_k^{(-)}|U + W_l|\varphi_l^{(+)}) + (\chi_k^{(-)}|U|\xi_l - \varphi_l^{(+)}) \\ &= (\chi_k^{(-)}|U + W_l|\varphi_l^{(+)}) - (\chi_k^{(-)}|U(\omega_l - T + i\varepsilon)^{-1}(U + W_l)|\varphi_l^{(+)}) \\ &= [(\chi_k^{(-)}| - (\chi_k^{(-)}|U(\omega_l - T + i\varepsilon)^{-1}](U + W_l)|\varphi_l^{(+)}) \\ &= (\xi_k|(U + W_l)|\varphi_l^{(+)}) = (\xi_k|V_l|\varphi_l^{(+)}).\end{aligned}$$

In obtaining the third equality we used (52a) and the fact that $\omega_k = \omega_l$, as required by the $\delta(\omega_k - \omega_l)$ in (55). We now have the desired result:

$$S_{kl} = \delta_{kl} - 2\pi i\delta(\omega_k - \omega_l)(\xi_k|V_l|\varphi_l^{(+)}). \tag{56}$$

Equation (56) is the standard expression [11]) for the scattering in a single-particle potential V_l. This constitutes the proof that the elastic scattering of a nucleon by a large nucleus is described exactly by a single-particle Schrödinger equation (27) containing the optical-model potential V_l.

6. Conclusions

The expression (25) for $W_k(t, s)$ is effectively a rule for writing down a perturbation expansion of the optical model potential. The essence of this rule is that we must enumerate all linked diagrams, disregarding the exclusion

principle in intermediate states, and then calculate the matrix elements corresponding to these diagrams. It should be noted that the exclusion principle, in spite of being ignored in intermediate states, continues to be effective. In general an exclusion-principle-violating diagram will be cancelled by its exchange diagram, which also violates the exclusion principle; it is only in the case of linked diagrams whose exchange diagrams are unlinked that this cancellation fails to occur. In addition the convention of starting all diagrams from the nuclear model ground state, or "model vacuum" [3]), (except for the bombarding nucleon line) prevents particles from scattering into occupied unexcited states of the model nucleus.

Certain qualitative features of the optical potential are evident from (25). First it is dependent on the energy of the incident nucleon, as we have emphasized with the subscript in $V_k = U+W_k$. Also, the presence of the $i\varepsilon$ in the energy denominators makes it complex; this is necessary to provide a sink in the probability conservation equation and thereby account for the effects of energetically possible inelastic processes [10]). In addition the optical potential is nonlocal. This characteristic, unlike the first two, has not been taken into account in most phenomenological treatments. Most aspects of this nonlocality are too complicated to be considered in any generality; one of its facets, however, is quite clear from (25), viz., that the optical potential contains a projection operator off the occupied model states (the eigenstates $1, \ldots, A$ of $T+U$, which comprise the model ground state of the nucleus). Specifically,

$$W_k(t, s) = 0, \quad \text{if } s \text{ or } t = 1, \ldots, A. \tag{57}$$

This is a consequence of the anticommutation relations satisfied by the creation operators, i.e., $a_s^\dagger \Phi_0 = 0$ if s designates an unexcited state. Let us define the projection operator P off the set of occupied states,

$$P = I - \sum_{\mu=1}^{A} |\chi_\mu)(\chi_\mu|. \tag{58}$$

Then (57) implies that we may rewrite (27) in either of the two equivalent forms:

$$(T+U+PW_k)\varphi_k = \omega_k \varphi_k; \tag{59}$$

$$(T+U+PW_kP)\varphi_k = \omega_k \varphi_k. \tag{60}$$

The P's are, of course, superfluous, since they are already built into W_k. They are explicitly indicated here to emphasize that in a phenomenological treatment a local optical potential V ought to be replaced by one of the forms $U+P(V-U)$ or $U+P(V-U)P$. The use of (59) for phenomenological analyses was proposed in ref. [5]).

The two equations (59) and (60) are easily seen to be equivalent for scattering states, yielding solutions which are automatically orthogonal to the occupied

states χ_ν. Eq. (60) has the slight aesthetic advantage that it is also satisfied by the occupied state vectors χ_ν themselves, the third term on the left vanishing identically in that case.

Bell and Squires [9]) have observed that the elastic scattering may be described by a different non-local potential from this one, and indeed there exists a wide range of non-local, energy-dependent potentials which will describe the elastic scattering equally accurately, even though the corresponding wave functions differ at small distances (and even asymptotically, with respect to inelastic parts). The exclusion principle is nonetheless valid, and it is physically reasonable that to the extent that the bound nucleons behave as independent particles, the scattering wave function should be orthogonal to the occupied bound states. If the scattered particle sees the same effective single particle potential as the bound nucleons, this is of course automatic (as in the trivial case mentioned by Bell and Squires) while if the model potential U is not the effective potential seen by the bound nucleons it is unreasonable to require that the scattered nucleon be in a state orthogonal to the occupied levels of $T+U$. But if the effective potentials U and V actually seen by the bound and scattered nucleons, respectively, are different, then the orthogonality condition is meaningful and non-trivial, so that the best way in which to introduce a local potential as an approximation would still seem to be in conjunction with the exclusion principle.

The authors would like to express their gratitude to Dr. Andrew M. Sessler for the aid and advice which he provided during the course of this investigation.

References

1) K. A. Brueckner and J. L. Gammel, Phys. Rev. **109** (1958) 1023 (this paper contains a more complete list of references);
Brueckner, Gammel and Weitzner, Phys. Rev. **110** (1958) 431
2) H. A. Bethe, Phys. Rev. **103** (1956) 1353;
H. A. Bethe and J. Goldstone, Proc. Roy. Soc. A **238** (1957) 551
3) J. Goldstone, Proc. Roy. Soc. A **239** (1957) 267
4) N. C. Francis and K. M. Watson, Phys. Rev. **92** (1953) 291
5) Frantz, Mills, Newton and Sessler, Phys. Rev. Letters **1** (1958) 340
6) P. A. M. Dirac, The Principles of Quantum Mechanics (Oxford University Press, London, 1947) Chapter X
7) M. Gell-Mann and F. Low, Phys. Rev. **84** (1951) 350
8) F. J. Dyson, Phys. Rev. **82** (1951) 428
9) J. S. Bell and E. J. Squires, Private communication; Phys. Rev. Letters **3** (1959) 96
10) H. A. Bethe, Phys. Rev. **57** (1940) 1125
11) M. Gell-Mann and M. L. Goldberger, Phys. Rev. **91** (1953) 398

1.C

Nuclear Physics **15** (1960) 33—38; © *North-Holland Publishing Co., Amsterdam*

Not to be reproduced by photoprint or microfilm without written permission from the publisher

A DERIVATION OF THE PAIRING-CORRELATION METHOD

B. F. BAYMAN

Institute for Theoretical Physics, University of Copenhagen, Denmark

Received 13 October 1959

Abstract: A discussion is given of the problem of a system of fermions moving in a set of single-particle orbits, and interacting by means of a pairing force. The Bardeen-Cooper-Schrieffer equations are derived by a method which exhibits their approximation as that inherent in the saddle-point method, and without the introduction of fluctuations in the number of particles.

The behaviour of a system of fermions moving in a set of single-particle orbits and interacting by means of a 'pairing force' has recently been discussed in connection with superconductivity [1]) and nuclear structure [1, 3, 4]). Using the formalism of second quantization, the hamiltonian can be written

$$H = \sum_{\alpha>0} 2\varepsilon_\alpha b_\alpha^\dagger b_\alpha - G \sum_{\alpha,\beta>0} b_\alpha^\dagger b_{-\alpha}^\dagger b_{-\beta} b_\beta, \tag{1}$$

where the creation and annihilation operators obey the usual anti-commutation rules

$$\begin{aligned} \{b_\alpha^\dagger, b_\beta^\dagger\} = \{b_\alpha, b_\beta\} &= 0 \\ \{b_\alpha^\dagger, b_\beta\} &= \delta_{\alpha,\beta}. \end{aligned} \tag{2}$$

The labelling is such that $b_\alpha^\dagger$ and $b_{-\alpha}^\dagger$ create time-reversed states. If the single-particle energies ε_α are independent of α (the 'degenerate model'), the ground state of H for an even number of particles is

$$\psi_{\mathrm{deg}} = \sqrt{\frac{(\Omega-p)!}{p!\,\Omega!}} \left(\sum_{\alpha>0} b_\alpha^\dagger b_{-\alpha}^\dagger\right)^p |0\rangle \tag{3a}$$

with the energy

$$E_{\mathrm{deg}} = 2p\varepsilon - Gp(\Omega-p+1). \tag{3b}$$

Here Ω is the number of $(\alpha, -\alpha)$ pairs of states. This was shown by Racah [5]), who first considered the pairing force and the 'seniority' coupling scheme defined by it. Eqs. (3a) and (3b) can also be derived [3]) as a consequence of the commutation relation

$$[H_{\mathrm{deg}}, \sum_{\alpha>0} b_\alpha^\dagger b_{-\alpha}^\dagger] = (2\varepsilon - G(\Omega+2-N)) \sum_{\alpha>0} b_\alpha^\dagger b_{-\alpha}^\dagger; \tag{4}$$

$N \equiv \sum_\alpha b_\alpha^\dagger b_\alpha$ is the number operator.

If we now admit splittings between the ε_α which are small compared to $G\Omega$, first-order perturbation theory gives

$$\psi \approx \Big(\sum_{\alpha>0} b_\alpha^\dagger b_{-\alpha}^\dagger\Big)^p|0\rangle - \frac{2}{G\Omega}\Big(\sum_{\beta>0}(\varepsilon_\beta-\varepsilon)b_\beta^\dagger b_\beta\Big)\Big(\sum_{\alpha>0} b_\alpha^\dagger b_{-\alpha}^\dagger\Big)|0\rangle$$
$$= \Big(\sum_{\alpha>0}\Big[1-\frac{2(\varepsilon_\alpha-\varepsilon)}{G\Omega}\Big] b_\alpha^\dagger b_{-\alpha}^\dagger\Big)^p|0\rangle, \tag{5a}$$

$$E \approx 2p\varepsilon - Gp(\Omega-p+1) - \frac{4p(\Omega-p)}{G\Omega^2(\Omega-1)}\sum_{\alpha>0}(\varepsilon_\alpha-\varepsilon)^2, \tag{5b}$$

where ε is taken at the barycentre of the spectrum ε_α (cf. ref. [4]) eq. (68)).

For larger single-particle splittings a variational approach has been used [1, 3]; (3a) and (5a) suggest a trial wave function of the form

$$\psi = \Big(\sum_{\alpha>0} c_\alpha b_\alpha^\dagger b_{-\alpha}^\dagger\Big)^p|0\rangle, \tag{6}$$

where the c_α are to be determined by minimizing the expectation value of H.

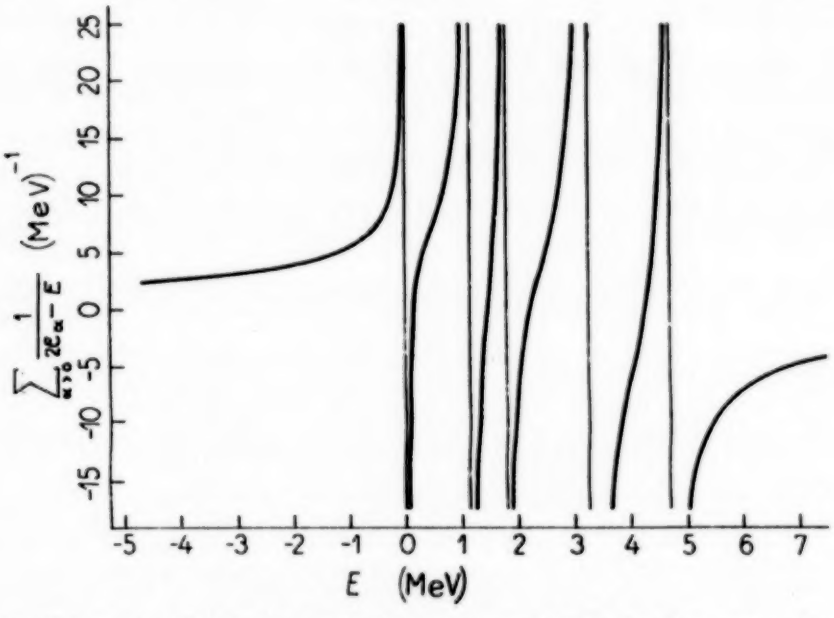

Fig 1. Illustration of eq. (8) for the single-hole states available to the neutron holes in Pb^{206}. $p_{\frac{1}{2}}(0)$, $f_{\frac{1}{2}}(0.57)$, $p_{\frac{3}{2}}(0.89)$, $i_{\frac{13}{2}}(1.63)$, $f_{\frac{5}{2}}(2.34)$.

Moreover, if we set all the c_α equal to zero, except $c_{\alpha_1}, \ldots, c_{\alpha_p}$, then (6) becomes the single product

$$p!\, c_{\alpha_1}\ldots c_{\alpha_p} b_{\alpha_1}^\dagger b_{-\alpha_1}^\dagger \ldots b_{\alpha_p}^\dagger b_{-\alpha_p}^\dagger|0\rangle$$

which is an eigenvector of H in the opposite limit at which G is negligibly small compared to the single-particle splittings. If G and these splittings are comparable, we shall generally be unable to attain the true eigenvector using (6), but the fact that (6) is exact at both limits suggests that it may be a good approximation between them.

If $p = 1$, some of the true eigenvectors will be of the form (6) for any G. To determine the c_α in this case, we can minimize

$$\langle\psi|H|\psi\rangle - E\langle\psi|\psi\rangle = \sum_{\alpha>0}(2\varepsilon_\alpha - E) - G(\sum_{\alpha>0} c_\alpha)^2 \tag{7}$$

leading to

$$(2\varepsilon_\alpha - E)c_\alpha = G\sum_{\alpha>0} c_\alpha$$

and the eigenvalue equation

$$\frac{1}{G} = \sum_{\alpha>0}\frac{1}{2\varepsilon_\alpha - E}. \tag{8}$$

The nature of the solutions of (8) is illustrated in fig. 1, where one sees the transition from the free-particle spectrum at $G = 0$ to the characteristic depression of the ground state (energy gap) as G becomes large.

For $p > 1$ the sums corresponding to (7) become very complicated, and are most conveniently handled by means of generating functions. The coefficient of $z^{\frac{1}{2}p}$ in the function

$$\Psi(z) \equiv \prod_{\alpha>0}(U_\alpha + z^{\frac{1}{2}}V_\alpha b_\alpha b^\dagger_{-\alpha})|0\rangle = \sum_p \frac{z^{\frac{1}{2}p}}{p!}\prod_{\beta>0}U_\beta\left(\sum_{\alpha>0}\frac{V_\alpha}{U_\alpha}b_\alpha{}^\dagger b^\dagger_{-\alpha}\right)^p|0\rangle \tag{9}$$

is an un-normalized trial function of the form (6). Then

$$\langle\Psi(z)|\Psi(z)\rangle = \prod_{\alpha>0}(U_\alpha{}^2 + zV_\alpha{}^2) \tag{10a}$$

or

$$\frac{1}{2p}\langle\Psi(z)|N|\Psi(z)\rangle = \frac{1}{p}\prod_{\alpha>0}(U_\alpha{}^2 + zV_\alpha{}^2)\sum_{\beta>0}\frac{zV_\beta{}^2}{U_\beta{}^2 + zV_\beta{}^2} \tag{10b}$$

are generating functions for the normalization integral of this trial function, and

$$\langle\Psi(z)|H|\Psi(z)\rangle \tag{11}$$
$$= \prod_{\alpha>0}(U_\alpha{}^2 + zV_\alpha{}^2)\left[\sum_{\beta>0}\frac{2\varepsilon_\beta zV_\beta{}^2}{U_\beta{}^2 + zV_\beta{}^2} - G\left(\sum_{\beta>0}\frac{z^{\frac{1}{2}}U_\beta V_\beta}{U_\beta{}^2 + zV_\beta{}^2}\right)^2 - G\sum_{\beta>0}\left(\frac{zV_\beta{}^2}{U_\beta{}^2 + zV_\beta{}^2}\right)^2\right]$$

is a generating function for the expectation value of H. Then for p pairs we must minimize

$$E = \frac{\oint z^{-p-1}\langle\Psi(z)|H\Psi|(z)\rangle dz}{\frac{1}{2p}\oint z^{-p-1}\langle\Psi(z)|N|\Psi(z)\rangle dz} \tag{12}$$

with respect to U_α and V_α. The contours in (12) encircle the origin.

Eq. (12) is exact, but we now wish to approximate the integrals there by means of the saddle-point method [6]). If the function $e^{g(z)}$ has a strong maximum at some point on the real axis, then

$$\oint e^{g(z)}\,dz \approx \frac{1}{\sqrt{2\pi g''(z_0)}}e^{g(z_0)}, \tag{13}$$

where z_0 is the saddle-point, determined by the condition

$$g'(z_0) = 0.$$

For the four integrals we need in (12), the saddle-point conditions are

$$\frac{1}{p}\int z^{-p-1}\prod_{\alpha>0}(U_\alpha^2+zV_\alpha^2)\sum_{\beta>0}\frac{zV_\beta^2}{U_\beta^2+zV_\beta^2}\,dz: \quad p=\sum_{\beta>0}\frac{z_0V_\beta^2}{U_\beta^2+z_0V_\beta^2}-\frac{\sum_{\beta>0}\left[\frac{z_0V_\beta^2}{U_\beta^2+z_0V_\beta^2}\right]^2}{\sum_{\beta>0}\frac{z_0V_\beta^2}{U_\beta^2+z_0V_\beta^2}}, \tag{14a}$$

$$\int z^{-p-1}\prod_{\alpha>0}(U_\alpha^2+zV_\alpha^2)\sum_{\beta>0}\frac{2\varepsilon_\beta zV_\beta^2}{U_\beta^2+zV_\beta^2}\,dz: \quad p=\sum_{\beta>0}\frac{z_0V_\beta^2}{U_\beta^2+z_0V_\beta^2}-\frac{\sum_{\beta>0}2\varepsilon_\beta\left[\frac{z_0V_\beta^2}{U_\beta^2+z_0V_\beta^2}\right]^2}{\sum_{\beta>0}2\varepsilon_\beta\frac{z_0V_\beta^2}{U_\beta^2+z_0V_\beta^2}}, \tag{14b}$$

$$\int z^{-p-1}\prod_{\alpha>0}(U_\alpha^2+zV_\alpha^2)\left(\sum_{\beta>0}\frac{z^{\frac{1}{2}}U_\beta V_\beta}{U_\beta^2+zV_\beta^2}\right)^2 dz: \quad p=\sum_{\beta>0}\frac{z_0V_\beta^2}{U_\beta^2+z_0V_\beta^2}-2\frac{\sum_{\beta>0}\frac{z_0^{\frac{1}{2}}U_\beta V_\beta^3}{(U_\beta^2+z_0V_\beta^2)^2}}{\sum_{\beta>0}\frac{z_0^{\frac{1}{2}}U_\beta V_\beta}{U_\beta^2+z_0V_\beta^2}}, \tag{14c}$$

$$\int z^{-p-1}\prod_{\alpha>0}(U_\alpha^2+zV_\alpha^2)\sum_{\beta>0}\left(\frac{zV_\beta^2}{U_\beta^2+zV_\beta^2}\right)^2 dz: \; p-1=\sum_{\beta>0}\frac{z_0V_\beta^2}{U_\beta^2+z_0V_\beta^2}-2\frac{\sum_{\beta>0}\left(\frac{z_0V_\beta^2}{U_\beta^2+z_0V_\beta^2}\right)^3}{\sum_{\beta>0}\left(\frac{z_0V_\beta^2}{U_\beta^2+z_0V_\beta^2}\right)^2}. \tag{14d}$$

We first consider situations in which G is large compared to the single-particle level spacing. The transition from the occupied to unoccupied states thus takes place gradually, and Ω_{eff}, the number of pairs of states for which $1>V_\beta^2/(U_\beta^2+V_\beta^2)>0$, is large. In this case, the z_0-dependent part of the first sum in (14a–d) is greater than the z_0-dependent part of each of the second sums by a factor of order† Ω_{eff}. Moreover, the contribution to the pairing energy by (14c) is greater by a similar factor than that by (14d). Thus the saddle-point for each of the integrals (14a–d) is approximately given by the single equation

$$p=\sum_{\beta>0}\frac{z_0V_\beta^2}{U_\beta^2+z_0V_\beta^2}. \tag{15}$$

Moreover, it is easy to show that under these circumstances $g''(z_0)$ is also the same for each of the integrals (14). Thus the ratio (12) is approximately equal to

† These order-of-magnitude estimates are based on a continuous constant level density, and a Fermi distribution given, in the region $(\varepsilon_1, \varepsilon_2)$ of transition from occupied to unoccupied states, by

$$\frac{V_\beta^2}{U_\beta^2+V_\beta^2}=\frac{1}{2}\left[1-\cos\left(\pi\frac{\varepsilon_\beta-\varepsilon_2}{\varepsilon_1-\varepsilon_2}\right)\right], \quad \frac{U_\beta^2}{U_\beta^2+V_\beta^2}=\frac{1}{2}\left[1+\cos\left(\pi\frac{\varepsilon_\beta-\varepsilon_2}{\varepsilon_1-\varepsilon_2}\right)\right].$$

$$\frac{\langle\Psi(z_0)|H|\Psi(z_0)\rangle}{\frac{1}{2p}\langle\Psi(z_0)|N|\Psi(z_0)\rangle}=\sum_{\beta>0}\frac{2\varepsilon_\beta z_0 V_\beta^2}{U_\beta^2+z_0V_\beta^2}-G\left(\sum_{\beta>0}\frac{z_0^{\frac{1}{2}}U_\beta V_\beta}{U_\beta^2+z_0V_\beta^2}\right)^2-G\sum_{\beta>0}\left(\frac{z_0V_\beta^2}{U_\beta^2+z_0V_\beta^2}\right)^2. \quad (16)$$

where z_0 is determined from (15).

Our procedure could now be to choose a set of U_β, V_β, solve (15) for z_0 as a function of them, substitute this function into (16), and then minimize with respect to U_β and V_β. However, it is more convenient to regard z_0 as an independent variable on the same footing as the U_β and V_β, and to look for the unconditional minimum of the quantity

$$E-\lambda p=\sum_{\beta>0}\frac{(2\varepsilon_\beta-\lambda)z_0V_\beta^2}{U_\beta^2+z_0V_\beta^2}-G\left(\sum_{\beta>0}\frac{z_0^{\frac{1}{2}}U_\beta V_\beta}{U_\beta^2+z_0V_\beta^2}\right)^2-G\sum_{\beta>0}\left(\frac{z_0V_\beta^2}{U_\beta^2+z_0V_\beta^2}\right)^2, \quad (17)$$

where λ is a Lagrange multiplier whose value is afterwards determined from (15). Since z_0 and V_β always enter (15) and (17) in the combination $z_0^{\frac{1}{2}}V_\beta$, and since (15) and (17) remain unchanged if U_β and V_β are both multiplied by the same factor, it is sufficient to set $z_0=1$ and restrict U_β and V_β by the condition $U_\beta^2+V_\beta^2=1$. Thus we must minimize

$$\sum_{\beta>0}(2\varepsilon_\beta-\lambda)V_\beta^2-G(\sum_{\beta>0}U_\beta V_\beta)^2-G\sum_{\beta>0}V_\beta^4 \quad (17')$$

under the restriction $U_\beta^2+V_\beta^2=1$, and determine λ from the equation

$$p=\sum_{\beta>0}V_\beta^2. \quad (15')$$

Eqs. (15′) and (17′) were first given by Bardeen, Cooper and Schrieffer [1]). They regard $\Psi(z)$ of (9) as the wave function of a system of particles whose number is subject to fluctuations. Our derivation deals with systems with definite particle number, but exhibits the error in (15′) and (17′) as that involved in replacing the ratio of the two contour integrals (12) by the ratio of their integrands at the saddle-point.

This error will be small if a) the dominant contributions to the integrals (12) come from the immediate vicinity of the saddle-point, or b) the integrands are approximately proportional over the entire contour. Condition a) is roughly equivalent to the requirement that the width of the maximum at the saddle-point be small compared to the length of the contour:

$$\frac{1}{\sqrt{g''(z_0)}}\ll\pi z_0. \quad (18)$$

For the integrals (14),

$$z_0^2g''(z_0)\approx p-\sum_{\beta>0}V_\beta^4=\sum_{\beta>0}V_\beta^2(1-V_\beta^2)\approx\tfrac{1}{4}\Omega_{\text{eff}}.$$

Hence the condition of validity of our saddle-point derivation of the pairing correlation method is

$$\frac{1}{\sqrt{\Omega_{\text{eff}}}} \ll \tfrac{1}{2}\pi. \tag{19}$$

On the other hand, condition b) holds in the free-particle limit ($V_{\alpha_1} = \ldots = V_{\alpha_p} = 1$; $V_{\alpha_{p+1}} = \ldots = V_{\alpha_\Omega} = 0$), since in this case the integrals in (12) are essentially

$$\oint \frac{1}{z}\,\mathrm{d}z = i\int_0^{2\pi} \mathrm{d}\varphi.$$

It was pointed out by Kisslinger (private communication) that (15′) and (17′) do in fact yield the exact wave functions and energies in the free-particle limit. It thus appears that these equations have a rather wide domain of validity.

In the degenerate model the first excited states for even particle number are those of seniority 2. They can also be written [3]) in the form (6):

$$\begin{aligned}\psi_\alpha &= \Big(\sum_{\beta>0} b_\beta^\dagger b_{-\beta}^\dagger - \frac{\Omega}{p}\, b_\alpha^\dagger b_{-\alpha}^\dagger\Big)^p |0\rangle \\ &= \Big(\sum_{\beta=0} b^\dagger{}_\beta b_{-\beta}^\dagger\Big)^p |0\rangle - \Omega\Big(\sum_{\beta>0} b_\beta^\dagger b_{-\beta}^\dagger\Big)^{p-1} b_\alpha^\dagger b_{-\alpha}^\dagger |0\rangle \\ &= \Big(\sum_{\beta>0} b_\beta^\dagger b_{-\beta}^\dagger\Big)^{p-1}\Big(\sum_{\beta>0} b_\beta^\dagger b_{-\beta}^\dagger - \Omega b_\alpha^\dagger b_{-\alpha}^\dagger\Big)|0\rangle.\end{aligned} \tag{20}$$

If we want to use (6) as a trial function for the excited states when there are single-particle splittings, we must supplement (15′) and (17′) by the condition that each new state be orthogonal to those already determined. However, for large Ω_{eff} the different solutions of the variational problem based on (15′) and (17′) alone are already nearly orthogonal and have been used for a discussion of the excited states of H. The principal effect of the remaining non-orthogonality is the introduction of a spurious state.

The author is indebted to Professor Aage Bohr for several illuminating discussions.

References

1) Bardeen, Cooper and Schrieffer, Phys. Rev. **108** (1957) 1175
2) A. Bohr, Proceedings of the Paris Conference on Nuclear Physics 1958 (Paris 1959) p. 203
3) B. R. Mottelson, Lectures at the Summer School in Theoretical Physics at Les Houches (1958) p. 383
4) S. T. Belyaev, Mat. Fys. Medd. Dan. Vid. Selsk. **31** No. 11 (1959)
5) G. Racah, Phys. Rev. **63** (1943) 367
6) E. Schrödinger, Statistical Mechanics (Cambridge University Press 1946), Chap. VI

1.D.2

Nuclear Physics **15** (1960) 39—55; © *North-Holland Publishing Co., Amsterdam*

Not to be reproduced by photoprint or microfilm without written permission from the publisher

ON THE EXISTENCE OF OCTUPOLE VIBRATIONS IN NUCLEI

A. M. LANE

Atomic Energy Research Establishment, Harwell, Didcot, Berks.

and

E. D. PENDLEBURY

Atomic Weapons Research Establishment, Aldermaston, Berks.

Received 16 September 1959

Abstract: It is shown that several different kinds of experimental data point to the existence of octupole vibrations in nuclei. These occur at an excitation energy of about 2.5 to 3 MeV in most nuclei, and rather higher in the light nuclei. Some detailed theoretical interpretation is made of (1) the observed E3 lifetimes, which are interpreted in terms of sum-rules, and (2) the constancy of the octupole excitation energy which is in marked contrast to the well-known peaking in the quadrupole energy near closed shells. Attention is drawn to several kinds of experiment that may give useful further evidence.

1. Introduction

The first excited states of many even nuclei are found to be systematically ordered in a manner suggestive of collective motion. Nuclei in the mass-ranges $152 < A < 190$ and $A > 226$ have spectra of the kind expected from rotation of a deformed nucleus with axial symmetry [1]). Many nuclei outside these ranges have spectra of a vibrational kind [2]). These spectra have been interpreted in various ways [3, 4]), but the most widely-held view is that they are due to quadrupole surface vibrations about a spherical equilibrium shape [1]). Successive bands of levels in the spectrum correspond to the excitation of 0, 1, 2, 3 . . . quadrupole vibration quanta, each quantum carrying angular momentum 2^+. Accepting this picture, one may enquire about the existence of any other modes of collective vibration. From a theoretical view, collective excitations carrying 0^+ or 1^- are not likely to occur at low energies. Such modes cannot be simple surface vibrations, but must involve changes in the internal composition or density of the nucleus. Nuclear matter appears to be nearly incompressible, and strongly resistent to composition changes, so this requires large energy. To support this view, the present data give no obvious hints that these modes exist (except, of course, the 1^- photonuclear vibration at 15 MeV).

The theoretical situation for the existence of a low-lying 3^- "octupole" mode is more favourable, because octupole surface vibration is possible. According to estimates based on the hydrodynamical model [1]), the energy should be

about 2 to 3 times that of the quadrupole mode, which is usually found to be between 0.5 and 1 MeV. Thus we may expect a 3^- vibration at an excitation of no more than a few MeV.

In section 2, various kinds of data are shown to suggest the existence of a nuclear octupole vibration at a few MeV excitation. E3 lifetime data gives particularly valuable evidence. These data are analysed in section 3. A feature of the octupole vibrations is the constancy of their excitation energy. Since quadrupole excitations fluctuate with mass number, this needs explanation. We discuss this matter and other theoretical points in section 4, and summarise the situation in section 5.

2. Experimental Evidence for Nuclear Octupole Vibrations

2.1. SYSTEMATICS OF THE FIRST EXCITED NEGATIVE PARITY STATES IN EVEN NUCLEI FROM RADIOACTIVITY DATA

The systematics of the lowest odd parity states in even nuclei was studied by Morinaga [5]). Most of the data were obtained from beta or gamma ray decay schemes and the main feature is that the angular momentum, where the

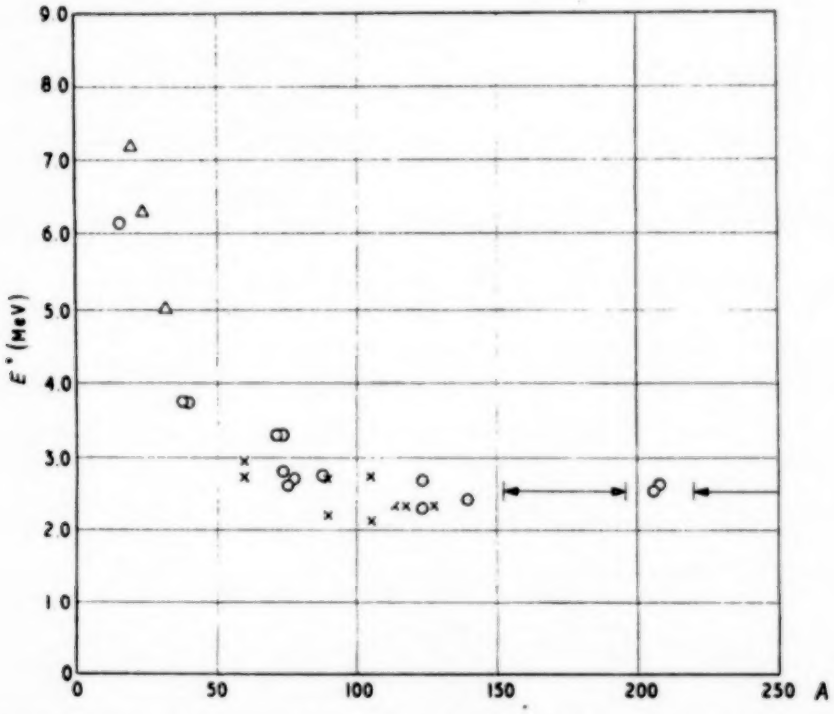

Fig. 1. Energies E^* of known or proposed 3^- states in even nuclei as a function of mass number A:
o levels established as 3^- from decay and other data,
△ levels from (α, α') data [18]),
× levels from Cohen's [9,10]) (pp') spectra;
|←→| regions of strong nuclear deformation.

angular momentum is certain, is predominantly 3^-. With only a few exceptions, mainly for very light elements and for very heavy elements the 3^- states lie in the range 2 to 3 MeV. From published decay schemes, notably those of Dželepov and Peker [6]) and of Strominger *et al.* [7]), we have identified most of the points plotted by Morinaga along with a few others. Van Lieshout [8]) has assembled evidence for a 3^- state at 2 to 3 MeV excitation in a few elements with mass numbers in the region of 70. Furthermore the E3 decay of the 3^- state to the 0^+ ground state is sometimes observed [8]) to compete with the E1 decay to the 2^+ first excited state. This suggests strong E3 enhancement.

The excitation energies of the 3^- states obtained mainly from the above sources are plotted in fig. 1 as a function of mass number. It will be seen that the excitation energy of these states varies in a regular way with increasing mass number and, for intermediate mass nuclei, lies in the range 2 to 3 MeV.

2.2. INELASTIC SCATTERING OF PROTONS, DEUTERONS AND ALPHA PARTICLES

We now turn to consider the spectra of protons obtained by Cohen [9, 10]) from the inelastic scattering of 23 MeV protons by quite a wide range of elements, in particular say those with mass numbers between about 60 and 120. Cohen's earlier results [9]) with 0.5 MeV resolution show a pronounced peak — which is sometimes a double peak — in the region of energy loss $-Q = 2$ to 3 MeV for almost all elements considered, whether even- or odd-mass. This is the highest Q value peak in these early results apart from the peak due to elastic scattering. Later results [10]) with improved (120 keV) resolution show much more structure. The double peaks are better resolved and there are now several other peaks between $Q = 0$ and $Q = -2$ MeV the main one occurring at around $-Q = 0.5$ to 1.0 MeV. These general features hold for almost all elements considered. The strongest peak occurring in the $-Q = 0.5$ to 1 MeV region can usually be identified with the excitation of a known 2^+ level of the collective type studied by Goldhaber and Weneser [2]). The structure occurring in the region of $-Q = 2$ to 3 MeV has roughly the same strength as the peak due to the excitation of the 2^+ collective level. It therefore seems a reasonable hypothesis that most of this structure is due to the excitation of a collective octupole vibration †. The fact that the vibration does not appear as a single sharp peak is of little consequence. In many nuclei, there will be several states

† For some time, we seriously considered the possibility that the group at $-Q = 2$ to 3 MeV was due to favoured particle excitations (for instance, those of the kind $j = l+\frac{1}{2} \rightarrow j = l-\frac{1}{2}$ where the radial state is unchanged). We finally discarded this model because it seemed to be impossible to reproduce the systematic nature of the observed group. Not only is the energy of the group remarkably constant, even across closed shells, but the cross-section for exciting it is also much more constant than the particle model would allow. Other workers [11]) have suggested that particular results near Pb^{208} can be interpreted as single particle excitations, but we are reluctant to accept this in view of the strong E3 transition that is reported in Pb^{208} (see sec. 2.3). The possibility of a collective octupole interpretation was suggested by Professor N. Levinson in a discussion with one of us (A. M. L.).

in the vicinity of 3 MeV having the same spins and parity as the octupole vibration. Inevitably these states will mix with the vibration so that no single state can be referred to as "the octupole vibration". Our interpretation is not disturbed by the fact that the vibration is shared by several states, provided that these are confined to a limited energy region.

Excitation energies obtained from Cohen's curves are plotted in fig. 1 where they fit in quite well with the general distribution of known 3^- levels.

Further support to the hypothesis of collective octupole oscillation is given by the angular distribution of the protons which contribute to the peak. On the collective model of octupole excitation the angular distribution of the inelastically scattered protons is given, in the Born approximation, by $|j_3(\Delta kR)|^2$, where j_3 is the spherical Bessel function, R is the nuclear radius and Δk is the change in the proton momentum which determines the angle of scatter for a given Q value. The angular distributions calculated from the above expression are in good agreement with angular distributions measured by Cohen [9] — generally there are the correct number of peaks and they occur at the required angles. Also the relative intensities of the peaks in the calculated angular distributions are about the same as in the measured ones.

Cohen has not studied nuclei with $A < 50$, but Hornyak and Sherr [12] have studied O^{16} with 19 MeV protons and found that the strongest group corresponds in energy to the doublet at $Q = -6.1$ MeV, one of which is known to be a 3^- state. The 3^- state in Ca^{40} at 3.73 MeV is strongly excited by 6 and 8 MeV protons [13]. Experiments [14] repeating some of Cohen's measurements near 10 MeV incident energy found little trace of the group at $-Q = 2$ to 3 MeV, but this can be plausibly attributed to the fact that at lower energies the direct reaction cross-section is dominated by the compound nucleus cross-section which is not expected to select the octupole vibration.

An interesting feature of Cohen's results is that the group at $-Q = 2$ to 3 MeV tends to disappear in nuclei like W and U which have rotational spectra i.e. have non-spherical equilibrium shape. This is in accord with the interpretation in terms of an octupole vibration because such a vibration will be split into four component vibrations by the deformation, and the corresponding proton group will be smeared out.

Similar structure to that found by Cohen in the inelastic proton spectra has been found by Yntema and Zeidman [15] in the spectra of inelastically scattered deuterons from elements ranging from Nickel to Gold with incident deuterons of 21.6 MeV. Roughly similar structure has also been found by Sweetman and Wall [16] in the spectra of inelastically scattered 30 MeV alpha particles.

Yavin and Farwell [17] have excited the O^{16} doublet at 6.1 MeV with 40 MeV alpha particles. Robison and Farwell [18] have excited states in Ne^{20}, Mg^{24} and S^{32} with the same beam and the theory of Blair [19] identifies one state in each nucleus as 3^-. These states are included in fig. 1.

2.3. INELASTIC ELECTRON SCATTERING AND LIFETIME MEASUREMENTS

Inelastic high energy electron scattering is perhaps the ideal method for examining nuclear collective oscillations. The advantage over inelastic heavy particle scattering is that the transition is not caused by nuclear forces but by the better understood Coulomb forces. The angular distribution of scattering distinguishes the multipole order of the excitation and the absolute cross-section gives the electric multipole matrix element. Helm [20]) has exposed 3^- levels in Ca^{40} and Sr^{88}, and lately Helm, Oeser and Yearian [21]) have examined Pb^{208} and Bi^{208}. They have found in preliminary results that the known 3^- level at 2.6 MeV in Pb^{208} is excited. Also a level at 2.6 MeV in Bi^{209} and levels at 4.3 MeV in Pb^{208} and Bi^{209} are excited. All have the same angular distribution (and so may all be 3^-) and the levels at 4.3 MeV are more strongly excited than the others.

The lifetimes of E3 transitions in O^{16} and Pb^{208} have been measured directly. Those in Ca^{40} and Sr^{88} can be deduced from inelastic electron scattering data. The values are given in table 1.

TABLE 1

Observed E3 transitions and comparison of the reduced transition probability $B(3 \to 0)$ with the single particle values $B_{sp}(3 \to 0)$ (see eq. (3))

Nucleus	Energy E of 3^- state (MeV)	Mean lifetime τ (sec)	Reference	$\frac{B(3 \to 0)}{e^2}$ in $(10^{-13}\,\mathrm{cm})^6$	$\frac{B_{obs}(3 \to 0)}{B_{sp}(3 \to 0)}$
O^{16}	6.13	$1.2(\pm 0.6) \times 10^{-11}$	[22])	4.8×10^2	7
Ca^{40}	3.73	0.71×10^{-10}	[20])	2.2×10^3	11
Sr^{88}	2.76	1.08×10^{-10}	[20])	1.3×10^4	26
Pb^{208}	2.61	$4(\pm 2) \times 10^{-11}$	[23])	5.0×10^4	22

From the relation

$$\frac{\hbar}{\tau} = 4.4 \times 10^{-4} \left(\frac{E}{19.7}\right)^7 \frac{B(3 \to 0)}{e^2}\ \mathrm{eV}$$

we have extracted values of the "reduced transition probability" $B(3 \to 0)$, which, for general multipole order λ, is defined by

$$\frac{B(\lambda \to 0)}{e^2} = |\langle 0(0)|Q_{\lambda 0}|\lambda(0)\rangle|^2, \tag{1}$$

where the numbers in brackets are magnetic quantum numbers and the λ-pole electric operator $Q_{\lambda 0}$ is defined by

$$Q_{\lambda 0} = \sum_{\text{protons}} r_i^{\lambda} Y_{\lambda 0}(\Omega_i). \tag{2}$$

3. Analysis of Lifetime Data in Terms of Models and Sum Rules

3.1. ANALYSIS WITH SINGLE PARTICLE MODEL

The reduced Eλ transition probability for a single proton jumping from a state of spin λ to one of spin 0 is

$$\frac{B_{\mathrm{SP}}(\lambda \to 0)}{e^2} = \frac{\langle \mathrm{f}|r^\lambda|\mathrm{i}\rangle^2}{4\pi}, \tag{3}$$

where $\langle \mathrm{f}|r^\lambda|\mathrm{i}\rangle$ is the matrix element of r^λ taken between the initial and final radial wave-functions. For a rough estimate of this, we set $\langle \mathrm{f}|r^\lambda|\mathrm{i}\rangle$ equal to the λ^{th} moment of the proton density distribution in the nucleus:

$$\langle r^\lambda \rangle \equiv \int r^\lambda \rho(\mathbf{r})\mathrm{d}\mathbf{r} \Big/ \int \rho(\mathbf{r})\mathrm{d}\mathbf{r}, \tag{4}$$

where $\rho(\mathbf{r})$ is the proton density distribution normalised by

$$\int \rho(\mathbf{r})\mathrm{d}\mathbf{r} = Z \tag{5}$$

We have used the densities determined by electron scattering [24]) to compute various moments of the density. Densities and moments are given in table 2.

TABLE 2

Proton density distributions for various nuclei

Nucleus	R (10^{-13} cm)	z (10^{-13} cm)	$\langle r^2 \rangle$ (10^{-13} cm)^2	$\langle r^3 \rangle$ (10^{-13} cm)^3	$\langle r^4 \rangle$ (10^{-13} cm)^4	$\langle r^6 \rangle$ (10^{-13} cm)^6
O^{16}	2.70	0.55	8.48	29.7	116	2330
Ca^{40}	3.66	0.55	12.2	49.3	217	5260
Sr^{88}	4.76	0.55	17.4	82.7	418	12700
Pb^{208}	6.33	0.55	28.7	170	1060	46000

R and z are the half value radius and surface thickness parameter occurring in the form

$$\rho(r) = \rho_0\left[1 + \exp\left(\frac{r-R}{z}\right)\right]^{-1}.$$

The values quoted are determined from electron scattering [24]).

We include in table 1 the ratios of the observed transition probability to the single particle one, which has been computed by inserting the third moments of table 2 in the above formulae.

It can be seen that the observed transition probabilities are always much stronger (by about an order of magnitude) than the single particle values. This is fairly clear evidence of a collective interpretation of the 3^- states in table 1.

3.2. ANALYSIS WITH COLLECTIVE MODEL

The collective Hamiltonian has the form [1])

$$H(\alpha_{\lambda\mu}) = \tfrac{1}{2}B_\lambda \dot{\alpha}^2_{\lambda\mu} + \tfrac{1}{2}C_\lambda \alpha^2_{\lambda\mu}. \tag{6}$$

for deformations of multipole order λ, component μ. The deformation parameter $\alpha_{\lambda\mu}$ is defined below. We will drop the subscript μ in the following.

The frequency of the quantised vibration is

$$E_\lambda = \hbar\sqrt{\frac{C_\lambda}{B_\lambda}} \tag{7}$$

and, for a uniform density distribution of radius R the transition probability is [1])

$$\frac{B_{\mathrm{coll}}(\lambda \to 0)}{e^2} = \left(\frac{3ZR^\lambda}{4\pi}\right)^2 \frac{1}{2[B_\lambda C_\lambda/\hbar^2]^{\frac{1}{2}}}. \tag{8}$$

For a non-uniform distribution $\rho(\mathbf{r})$, it is easy to generalise this result [25]). The deformation parameter α_λ for volume preserving deformations is such that the deformed density distribution is

$$\rho(\mathbf{r}, \alpha_\lambda) = \exp\left[\frac{\alpha_\lambda}{\lambda R^{\lambda-2}} \nabla(r^\lambda Y_\lambda) \cdot \nabla\right]\rho(\mathbf{r}). \tag{9}$$

In order to make α_λ dimensionless, we have inserted the factor $R^{\lambda-2}$, where R is the half-value radius. The deformation corresponds to the spherical surface $r = r_0$ being changed to the surface

$$r = r_0\left(1+\alpha\left(\frac{r_0}{R}\right)^{\lambda-2} Y_\lambda\right) \tag{10}$$

to first order in α_λ. The Eλ operator (see (2))

$$Q_\lambda = e\int r^\lambda Y_\lambda \rho(\mathbf{r}, \alpha_\lambda)\mathrm{d}\mathbf{r} \tag{11}$$

is easily seen to reduce to

$$\frac{e\alpha_\lambda}{R^{\lambda-2}}\int r^{2\lambda+1}\frac{\mathrm{d}\rho}{\mathrm{d}r}\mathrm{d}\mathbf{r} = \frac{e\alpha_\lambda(2\lambda+1)}{R^{\lambda-2}}\int r^{2\lambda}\rho(\mathbf{r})\mathrm{d}\mathbf{r} = \frac{Ze\alpha_\lambda(2\lambda+1)}{4\pi}\frac{\langle r^{2\lambda-2}\rangle}{R^{\lambda-2}}. \tag{12}$$

The form of $B_{\mathrm{coll}}(\lambda \to 0)$ generalised to non-uniform density is then

$$\frac{B_{\mathrm{coll}}(\lambda \to 0)}{e^2} = \left(\frac{Z(2\lambda+1)\langle r^{2\lambda-2}\rangle}{4\pi R^{\lambda-2}}\right)^2 \frac{1}{2[B_\lambda C_\lambda/\hbar^2]^{\frac{1}{2}}}. \tag{13}$$

Using the fourth moments of table 2, the observed data on E3 transitions can be analysed in terms of the collective model parameters B_λ and C_λ (table 3). For comparison, table 3 includes theoretical values of these parameters which have been computed with the "hydrodynamical model". In this model the collective motion is the irrotational flow of an incompressible liquid drop, and B_λ is given by [25])

$$(B_\lambda)_{\mathrm{hyd}} = \frac{2\lambda+1}{\lambda}\frac{AM}{4\pi}\frac{\langle r^{2\lambda-2}\rangle}{R^{2\lambda-4}}. \tag{14}$$

For the surface tension parameter C_λ Bohr and Mottelson [1]) give, for the case of uniform density inside radius R,

$$C_\lambda = (\lambda-1)(\lambda+2)R^2S - \frac{3}{2\pi}\frac{\lambda-1}{2\lambda+1}\frac{Z^2e^2}{R}, \tag{15}$$

where S is the observed surface energy: $4\pi R^2 S = 15.4A^{\frac{2}{3}}$ MeV. In order to generalise this to the case of non-uniform density, one must go into some detail about the nature of the nuclear surface and surface energy. For the present purpose, such effort is unwarranted; the above formula is a reasonable representation of the hydrodynamical model and the entries in table 3 are based on it.

TABLE 3

Observed values of B_3 and C_3, and comparison with Hydrodynamical Model estimates

Nucleus	Observed values				Hydrodynamical Model	
	$\sqrt{\frac{B_3C_3}{\hbar^2}}$	$\hbar\sqrt{\frac{C_3}{B_3}}$	$\frac{B_3}{\hbar^2}$ (MeV)$^{-1}$	C_3(MeV)	$\frac{B_3}{\hbar^2}$ (MeV)$^{-1}$	C_3(MeV)
O^{16}	40 ± 20	6.13	6 ± 3	240±120	1.17	78
Ca^{40}	99.3	3.73	26.6	370	2.98	140
Sr^{88}	133	2.76	48.2	367	7.46	240
Pb^{208}	600 ±300	2.61	220 ±110	1500±750	24.9	430

From the table it can be seen that the mass parameter B_3 is on average about 7 times the hydrodynamic value. The restoring force parameter C_3 is always greater than and fluctuates more relative to the hydrodynamic value. The size of the errors and the limited number of nuclei make it difficult to make any detailed comparison. (It should be noted that there is a difference between our value of C_3 for O^{16} and the value of 650 MeV derived by Blair [18]) from his analysis of (α, α') reactions, but we are not sure what accounts for this difference.)

3.3. ANALYSIS WITH SUM RULES

From the definition (1) of $B_n(\lambda \to 0)$ where n is any state of spin λ, we have the sum-rule

$$\sum_n \frac{B_n(\lambda \to 0)}{e^2} = \langle 0|Q^2_{\lambda 0}|0\rangle. \tag{16}$$

For an estimate of the sum, we may assume that the shell-model gives a good approximation to the ground state wave-function ref. [26]), (p. 643). Ignoring anti-symmetrisation, this means that cross-terms from the squaring of the

operator $Q_{\lambda 0}$ do not contribute to the sum which may be written

$$\sum_n \frac{B_n(\lambda \to 0)}{e^2} = \frac{Z}{4\pi} \langle r^{2\lambda} \rangle. \tag{17}$$

In table 4, the observed values of $B(3 \to 0)$ are compared with the limits imposed by this sum-rule.

TABLE 4

Comparison with approximate limits imposed by the first sum-rule

Nucleus	Sum in $(10^{-13}\,\mathrm{cm})^6$	$\frac{B_{obs}}{e^2} \Big/$ Sum
O^{16}	1.5×10^3 (7.4×10^2)	0.32 (0.64)
Ca^{40}	$8.5\times10^3\,z$ $(4.2\times10^3\,z)$	$0.26/z$ $(0.52/z)$
Sr^{88}	$3.9\times10^4\,z$	$0.33/z$
Pb^{208}	$3.0\times10^5\,z$	$0.17/z$

z is an anti-symmetrisation factor and is < 1 (see text). The bracketed numbers are for transitions with $\Delta T = 0$.

In the table, z is a factor < 1 to account for the anti-symmetrisation correction. It decreases from unity for O^{16} (i.e. no correction) to a value of rather more than $\frac{1}{2}$ for Pb^{208}. For O^{16} and Ca^{40} we can obtain a stronger (but equally valid) sum rule limit by exploiting the fact that the states involved are such that the transitions involve no change of isobaric spin i.e. $\Delta T = 0$. The sum-rule can be broken into two equal parts, one for $\Delta T = 0$, and one for $\Delta T = 1$ transitions.

One sees from table 4 that the observed transitions account for about 50 % of the sum-rule. This strongly suggests that the transitions involve collective effects.

For the transitions in O^{16} and Ca^{40} with $\Delta T = 0$, an alternative sum-rule limit which is essentially exact can be imposed. This is the energy-weighted sum used by Gellmann and Telegdi [17]) for E2 transitions. For E3 transitions, one easily finds that

$$\sum_{n(\Delta T=0)} (E_n - E_0) \frac{B_n(3 \to 0)}{e^2} = \frac{21}{32\pi} \frac{\hbar^2}{M} A \langle r^4 \rangle, \tag{18}$$

where $A (= 2Z)$ is the mass-number and M the nucleon mass. In table 5, the data are compared with the limits from this rule which are obtained by use of table 2 for the fourth moments.

It will be seen that the observed values are less than the sum rule limit by factors of about 5 and 10. These are larger than the corresponding factors of about 2 to 3 applying to the first sum-rule. This may be due in part to the approx-

imate nature of the latter sum rule, but also to the energy weighting in the former sum rule. (A state n with an arbitrary small E3 matrix element will give a large effect if its energy E_n is high enough.)

TABLE 5

Comparison with limits imposed by the second sum-rule

Nucleus	Sum in MeV · $(10^{-13}\text{cm})^6$	$(E_n - E_0)\frac{B_{obs}(3\to 0)}{e^2} \Big/$ Sum
O^{16}	1.6×10^4	0.18
Ca^{40}	7.5×10^4	0.11

It is appropriate to discuss here the kind of deductions one can make from sum-rule studies about the "collectiveness" of nuclear motion. The first thing to recognise is that the fact that a certain fraction of a sum-rule is used by a transition from a given excited state does not mean that the state has only that fraction of collective state in it. There are several prescriptions that one can think of for collective excited states. The simplest is perhaps $Q_3^{(1)}\psi_0$ where $Q_3^{(1)}=\sum_i r_i^3 Y_3(\Omega_i)$ (the sum being over *all* particles) and ψ_0 is the ground state. Such a "state" automatically exhausts the $\Delta T = 0$ sum-rules, and is the only state to do so. Unfortunately it has never been suggested on any physical grounds. Another prescription is $Q_3^{(2)}\psi_0$, where

$$Q_3^{(2)} = \sum_i \nabla_i(r_i^3 Y_3(\Omega_i)) \cdot \nabla_i.$$

This kind of state corresponds to a hydrodynamical oscillation. [It is a special case of the general form [28]) $\int f(\alpha)\exp[i\alpha Q_3^{(2)}]\psi_0 d\alpha$ obtained by setting $f(\alpha) = = \delta'(\alpha)$. The choice $f(\alpha) = \delta(\alpha)$ gives the ground state ψ_0]. In order to study to what extent this kind of collective state exhausts the sum-rules, it is necessary to assume some specific model for ψ_0. As an example we have considered the harmonic oscillator shell model applied to O^{16} (without centre-of-mass corrections). For the general collective state

$$\left(\frac{x}{b^2}Q_3^{(1)}+Q_3^{(2)}\right)\psi_0,$$

where x is a free parameter, and b is the size parameter of the oscillator potential, the wave-functions of which contain the factor $\exp(-r^2/2b^2)$. The transition probability from this state (when normalised) to the ground state is

$$\frac{B(3\to 0)}{e^2} = \frac{105}{16\pi}\frac{(5x-12)^2}{(5x^2-24x+33)}b^6. \qquad (19)$$

[In deriving (19), the following general relation was useful:

$$\langle 0|Q_3^{(1)}Q_3^{(2)}|0\rangle = -\frac{21}{8\pi}A\langle r^4\rangle.]$$

The maximum value achieved by (19) is at $x = \pm\infty$ and is just that expected from the first sum-rule: $B(3 \to 0)/e^2 = 525b^6/16\pi$. Other choices of x give values from zero up to this value. In particular, at $x = 0$, $B(3 \to 0)$ exhausts about 90 % of the sum-rule. At $x = 3$, the excited state consists of pure one-quantum excitation $(1s)^4(1p)^{12} \to (1s)^4(1p)^{11}(1d)$ and $B(3 \to 0)$ exhausts 30 % of the sum-rule. [For general x, the excited state is a mixture of one and three quantum excitation.]

It is interesting to compute the quantity $(E_n - E_0)B_n(3 \to 0)$ using the collective model. From (7) and (13) we see that this product depends only on B_3, not on C_3. Furthermore, on comparing with the sum-rule (18), the condition that the sum-rule be exhausted is that B_3 be equal to (14), which is just the hydrodynamical value. In other words, for a pure hydrodynamical oscillation, the sum-rule is just exhausted. It would appear that for any other oscillation, only the fraction $(B_3)_{\text{hyd}}/B_3$ of the sum-rule is exhausted. However, the assumption of incompressible irrotational flow has been assumed in deriving (14) (through (9)). Probably this assumption does not affect (14) critically, so this last assertion is essentially correct. If so, one sees that it implies that B_3 can never be smaller than $(B_3)_{\text{hyd}}$ and, physically this is very reasonable. (We are indebted to Prof. D. H. Wilkinson for some discussion on this matter.)

4. Some Theoretical Considerations of Octupole Vibrations

4.1. GENERAL

Most of the work to date on collective vibrations has been concerned with quadruple modes. Much information regarding the variation with mass number of the quadrupole mass and surface tension parameters has been obtained from studies of energy levels and their lifetimes. A list of parameters determined in this way is given by Alder *et al.*[29]) and more recently by Stelson and McGowan[30]).

The quadrupole mass parameter B_2 is remarkably constant at about 10 times the hydrodynamic value (14) for most nuclei. Values of B_2 different from this by more than a factor 2 are rare and occur randomly (e.g. Se^{82}, Nd^{146} with $B_2 \approx 30\times$ hydrodynamic value). In contrast, the quadrupole surface tension parameter C_2 oscillates systematically about the hydrodynamic value (15) when plotted as a function of mass number. It varies between about 10 times and 0.1 times the hydrodynamic value and achieves its largest values in the neighbourhood of closed major shells. There is little evidence for any similar fluctuations in the value of B_2 in the neighbourhood of closed shells. The explanation of the behaviour of the quadrupole surface tension parameters has been

the object of theoretical papers by Marumori *et al.* [31]) and the increases in the region of closed shells has been reproduced qualitatively by them.

It appears from the study of the systematics of 3^- states in even nuclei (see section 2.1 of the present paper) that the energies of these states fluctuate very little with mass number, in sharp contrast to the fluctuations in the energies of the 2^+ states. If the 3^- states are collective, like the 2^+ states, this difference needs explanation, and we now discuss the two kinds of vibration in parallel.

4.2. MASS PARAMETER B_λ

On rather general grounds one can argue that the equilibrium shape of nuclei near closed shells, with interactions between particles, is spherical with respect to both quadrupole and octupole deformations [1]). According to the cranking model approach (Inglis [32])) the mass parameter B_λ for vibrations of multipole order λ is

$$B_\lambda = 2\hbar^2 \sum_K \frac{\langle K(\alpha_\lambda) \left| \frac{\partial}{\partial \alpha_\lambda} \right| L(\alpha_\lambda) \rangle^2_{\alpha_\lambda = 0}}{(E_K - E_L)} \tag{20}$$

where $|K(\alpha_\lambda)\rangle$, $|L(\alpha_\lambda)\rangle$ are wave functions for deformation α_λ and E_K, E_L are the energies corresponding to $|K(0)\rangle$, $|L(0)\rangle$; $|L(0)\rangle$ is the ground state wave function of the stationary system when the deformation is zero. According to the common prescription $|K(\alpha_\lambda)\rangle$ is obtained from $|K(0)\rangle$ by making the volume preserving transformation

$$|K(\alpha_\lambda)\rangle = \exp\left[i \frac{\alpha_\lambda Q_\lambda^{(2)}}{\lambda R^{\lambda-2}} \right] |K(0)\rangle, \tag{21}$$

where $Q_\lambda^{(2)}$ is the operator $\nabla(r^\lambda Y_\lambda) \cdot \nabla$ summed over all particles (cf. (9)).

For quadrupole vibrations ($\lambda = 2$), the value of B_2 in the absence of interactions can be evaluated for the harmonic oscillator using the fact that $\langle K(0)|Q_2^{(2)}|L(0)\rangle = 0$ unless $E_K - E_L = \pm 2\hbar\omega$. The result is that $B_2 \approx (B_2)_{\text{hyd}}$, the hydrodynamic value. The case of no interactions is artificial since the equilibrium shape is non-spherical (except at closed shell nuclei). The inclusion of interactions, which give rise to spherical equilibrium in nuclei near closed shells, causes configuration mixing in $|K\rangle$ and $|L\rangle$, with the result that there are contributions to B_2 from terms with $|E_K - E_L| \ll 2\hbar\omega$. Consequently B_2 is increased strongly by the presence of interactions, a prediction that agrees with the observed fact that $B_2 \approx 10(B_2)_{\text{hyd}}$. The presence of spin orbit forces and anharmonicity in the potential will also give effects in this direction. Another point of agreement with experiment comes from the expectation that B_2 should not change much across a shell closure for neutrons or protons since the non-magic particles always provide small energy spacings $(E_K - E_L)$.

At doubly closed shell nuclei (O^{16}, Ca^{40}, Pb^{208}) one can expect a stronger change. Significantly no collective 2^+ states have been found in these nuclei.

For octupole vibrations, oscillator wave functions have the property that $\langle K|Q_3^{(2)}|L\rangle = 0$ unless $E_K - E_L = \pm\hbar\omega$ or $\pm 3\hbar\omega$. (When $E_K = E_L$, the matrix elements are trivially zero as a result of parity.) As in the quadrupole case $B_3 \approx (B_3)_{\text{hyd}}$ for the oscillator without perturbations, but may be considerably larger when perturbations are included. In the octupole case, spin-orbit and anharmonicity effects are expected to be more important relative to interaction effects than in the quadrupole case. This is because the latter effects in themselves do not give rise to terms with $|E_K - E_L| \ll \hbar\omega$, whereas the former can do this by bringing states of opposite parity close together in energy. This difference from the quadrupole case may be responsible for the observed fact that $B/(B)_{\text{hyd}}$ is rather different in the two cases (≈ 10 for quadrupole, ≈ 7 for octupole; table 3). The fact that $B_3/(B_3)_{\text{hyd}}$ is > 1 is in agreement with the predictions. Of course, observed values of $B_3/(B_3)_{\text{hyd}}$ are for nuclei near or at double closed shells, so these values may be rather special. In this connection one notes that some increase in B_3 can be expected when the highest occupied orbit occurs near an orbit of opposite parity that is mixed in by the octupole operator $Q_3^{(2)}$.

4.3. RESTORING FORCE PARAMETER C_λ

When a nucleus has spherical equilibrium against deformation of multipole order λ, the energy as a function of deformation parameter α_λ is

$$E(\alpha_\lambda) = E(0) + \tfrac{1}{2}C_\lambda \alpha_\lambda^2 \tag{22}$$

to order α_λ^2. For our qualitative purposes, C_λ can be calculated by identifying E with the energy of a shell system of particles moving in a potential of deformation β_λ:

$$V(\beta_\lambda) = \tfrac{1}{2}M\omega^2\left[r^2 + \beta_\lambda r^\lambda Y_\lambda + \beta_\lambda^2 \frac{r^{2\lambda-2}}{4}(2\lambda+1)(Y_0)^2\right] + a(\mathbf{l}\cdot\mathbf{s}), \tag{23}$$

and then relating the potential deformation β_λ to the density deformation α_λ. The term in β_λ^2 is inserted to preserve the volume inside equipotentials [33]) to order β_λ^2 thereby simulating the effects of nuclear cohesion. It is not determined uniquely by this condition. For instance the factor $(Y_0)^2$ could be replaced by $(Y_\lambda)^2$ without affecting the volume condition.

The term $\bar{C}_\lambda$ in the expression $E(\beta_\lambda) = E(0) + \frac{1}{2}\bar{C}_\lambda\beta_\lambda^2$ is found by applying second order perturbation theory to the β dependent terms in the potential V. Thus,

$$\tfrac{1}{2}\bar{C}_\lambda = \langle L|\tfrac{1}{2}M\omega^2\frac{r^{2\lambda-2}}{4}(2\lambda+1)(Y_0)^2|L\rangle + \sum_K \frac{|\langle K(0)|\frac{1}{2}M\omega^2 r^\lambda Y_\lambda|L(0)\rangle|^2}{(E_K - E_L)}. \tag{24}$$

Here we assume that the *change* in the energy of the system due to the *change*

in the potential arising from the terms in β_λ and β_λ^2 is equal to the sum of the changes in the single particle energies †.

The second term in the expression for $\bar{C}_\lambda$ is negative, whereas $\bar{C}_\lambda$ must be positive for stable spherical equilibrium so we see that the presence of the volume preserving term in V is essential. Whilst the first term in $\bar{C}_\lambda$ varies smoothly with mass number the second fluctuates because the spin-orbit force in V causes fluctuations in the spacings of the particle levels. The presence of such a force in the $\lambda = 2$ case is vital to get meaningful results since otherwise the second term in $\bar{C}_2$ will contain terms with $E_K = E_L$. Clearly $\bar{C}_2$ is expected to fluctuate much more than $\bar{C}_3$ since the former contains contributions from terms with $E_K - E_L$ small even in the absence of a spin-orbit force whereas terms in the latter have $|E_K - E_L| \approx \hbar\omega$ except for an occasional term with $|E_K - E_L| \ll \hbar\omega$ due to the effect of the spin-orbit force.

We have calculated $\bar{C}_3$ as a function of particle number using oscillator shell model wave functions for matrix elements [35]) together with realistic energy spacings taken from the work of Ross, Mark and Lawson [36]). The energy spacings we used were based mainly on the neutron energy level scheme for gold given in fig. 5 of ref. [36]), together with the results the authors give for the higher levels in lead. We performed the calculation in non-dimensional form, and to convert from the absolute energies for gold to suitable non-dimensional energies, the size parameter b of the oscillator potential was taken to be 2.5×10^{-13} cm. The uncertainty in the absolute value of $\bar{C}_3$ increases as the particle number becomes large due to the greater uncertainty in the location of the higher energy levels. Even so the results are still expected to be qualitatively correct. In fig. 2 the calculated values of the non-dimensional quantity $4\pi M \bar{C}_3/\hbar^2$ are plotted as a function of particle number.

It is gratifying to see that Suekane [37]) has arrived at similar results using an infinite square well potential and following the method used by Marumori *et al.* [31]) for the quadrupole case.

When comparison is made between the octupole surface tension parameter in fig. 2 of the present paper and the quadrupole parameter given in fig. III of the paper by Marumori *et al.* [31]) one sees that the fluctuations in the octupole parameter are an order of magnitude less than the fluctuations in the quadrupole parameter. This is therefore in keeping with apparent fact that energies of 3^- states as a function of particle number fluctuate less than the energies of the collective 2^+ states. This consequently supports the theory that the 3^- states are in fact collective.

† It may be argued that it is preferable to take a factor $\frac{1}{2}$ in the potential term before summing over all single particle energies in order to allow for the two-body nature of the forces giving rise to the potential (which of course would lead to a different result for $\bar{C}_\lambda$ to that quoted above). Although this is more correct for the total energy of the system one can argue (cf. Moszkowski [34]), p. 511) that for changes in energy with deformation (i.e. the value of $\bar{C}_\lambda$) one should not do this. In fact neither recipe is reliable quantitatively, and qualitatively they give much the same results.

In order to extract values of the usual restoring force parameter C_3 from $\bar{C}_3$, we must use $C_3\alpha_3^2 \equiv \bar{C}_3\beta_3^2$ in conjunction with a relation between α_3 and β_3. From (24) the equipotential surface $V = \frac{1}{2}M\omega^2 r_0^2$ for $\lambda = 3$ is

$$r = r_0(1-\tfrac{1}{2}\beta_3 r_0 Y_3) \tag{25}$$

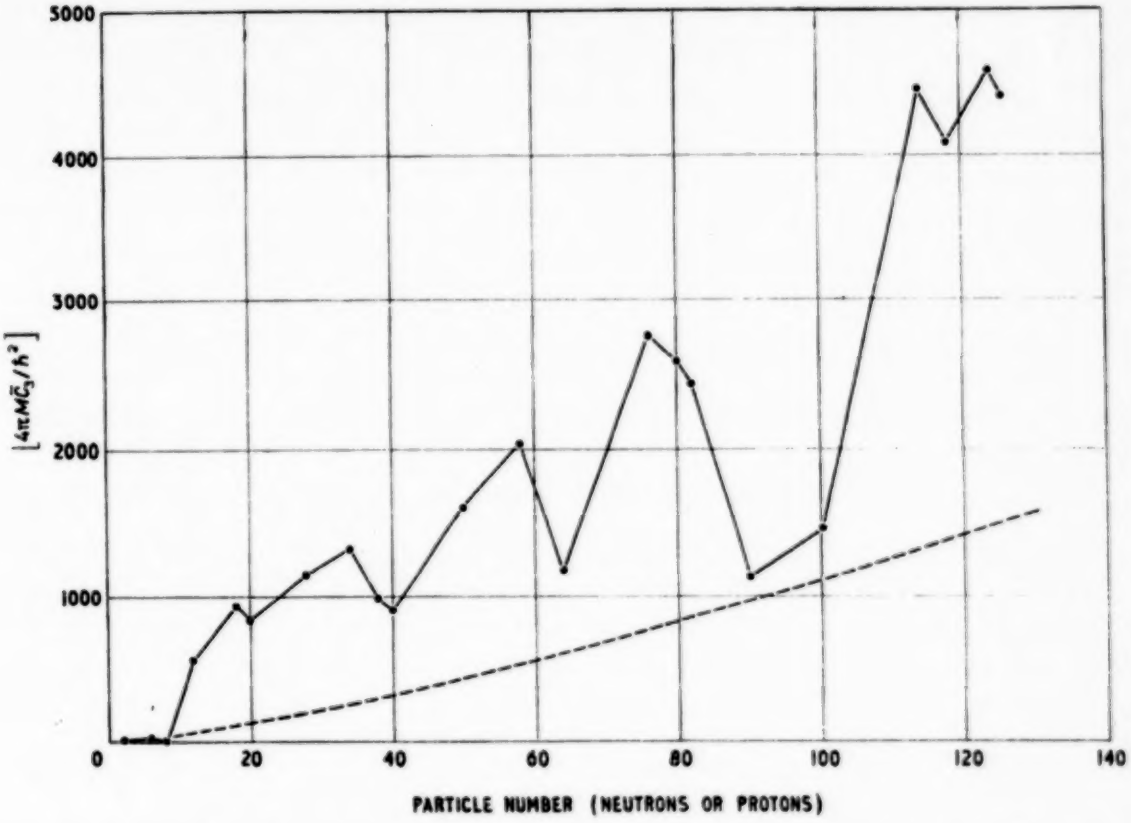

Fig. 2. Restoring force parameter $\bar{C}_3$ (times $4\pi M/\hbar^2$) as a function of particle number. The graph gives $\bar{C}_3$ for one species of particle (neutrons or protons). The total $\bar{C}_3$ for a given nucleus is obtained by adding the two contributions. The value of the conventional parameter C_3 can be obtained from $\bar{C}_3$ by using the relation $C_3 = 4\bar{C}_3/R^2$ (see text) where R is the nuclear radius. The broken curve represents half the predicted hydrodynamic value (eq. (15)) as a function of $\frac{1}{2}A$.

to first order in β_3. If our treatments were self-consistent in the sence discussed by Moszkowski [38]), the density and potential deformations would always be approximately equal. Comparing (10) and (25) then gives the condition

$$\frac{\beta_3}{2} = -\frac{\alpha_3}{R}, \tag{26}$$

so that C_3 is given by

$$C_3 = \bar{C}_3\left(\frac{4}{R^2}\right). \tag{27}$$

The proportionality constants in these relations do not have any quantitative significance because we have not made our treatment self-consistent. As

Moszkowski has pointed out, for quadrupole deformations the density deformation of an oscillator potential system is only a half of the potential deformation if no "configuration spilling" is allowed (i.e. when energy levels cross as the deformation increases, particles are not allowed to switch to the lowest level). Approximate self-consistency is attained if spilling is allowed. If internuclear forces are introduced, this will be done automatically. In our present treatment, no such forces are introduced, and no spilling effects have been allowed for. This means that α_3 is rather less than the value given by (26) and C_3 is correspondingly greater than the value given by (27). It must be emphasised that the absence of self-consistency means that, not only are relations (26) and (27) subject to corrections, but the meaning of the calculation of $\bar{C}_3$ is thrown into doubt. The only significance that we attach to the present calculation is that it gives a qualitative idea of the fluctuations with changing mass number in the magnitude of C_3, especially relative to those in C_2. Such fluctuations are due to fluctuation in the spacing of single particle energy levels (as represented in the energy denominators of (24)), and the effects of this are expected to persist qualitatively in a more correct (i.e. more self-consistent) calculation.

The value of C_3 following from fig. 2 and eq. (27) is about 1000 MeV for medium masses. (For given nucleus $A(N, Z)$, $\bar{C}_3 = (\bar{C}_3)_N + (\bar{C}_3)_Z$ where $(\bar{C}_3)_N$ and $(\bar{C}_3)_Z$ can be read from fig. 2.) If it is assumed that $B_3/(B_3)_{\text{hyd}}$ is about 7, the predicted energy of the octupole oscillations is about 3 MeV, the observed value. In view of the above discussion, little significance can be attached to this agreement.

5. Conclusions

In this paper we have made some speculations on the existence of nuclear octupole oscillations. As has been shown in section 2, there are several strong hints from various kinds of data that such oscillations do indeed occur. However, the amount of detailed information on the 3^- states constituting the oscillations is still meagre. Only four E3 lifetimes of 3^- states are reported and those have considerable uncertainties. We have analysed them in terms of sum-rules in section 3, and have made some general theoretical remarks on the octupole collective parameters in section 4.

We hope that the present work will stimulate further experiments, especially those giving detailed information. High energy inelastic electron scattering appears especially useful for reasons discussed in 2.3, and experimental work of this kind is being done [21]) at present. The recent successful applications of Blair's theory [19]) of diffraction inelastic scattering of alphas and deuterons suggests that this type of experimental result will also be useful for quantitative studies. An essential feature of the theory is that incident particles crossing the nuclear boundary should be strongly absorbed. This condition is not very well

satisfied by nucleons, and the evidence on octupole modes from nucleon scattering may thus be of mainly qualitative value. Nevertheless extension of the work of Cohen [9, 10]) perhaps with better energy resolution, will certainly be instructive. Coulomb excitation does not appear to be very useful, unfortunately (for Pb^{208}, the predicted cross section for 7 MeV protons is ≈ 1 μb).

We are grateful to Profs. A. Bohr, J. S. Blair, R. A. Ferrell and S. Moszkowski for discussions and correspondence, and to Profs. R. Hofstadter, A. W. Sunyar and R. van Lieshout for experimental information.

References

1) A. Bohr and B. R. Mottelson, Mat. fys. Medd. Dan. Vid. Selsk., **27** No. 16 (1953)
2) G. Scharf-Goldhaber and J. Weneser, Phys. Rev. **98** (1955) 212
3) A. S. Davidov and G. F. Fillipov, Nuclear Physics **8** (1958) 237;
C. Marty, Nuclear Physics **1** (1956) 85; ibid **3** (1957) 193
4) L. Wilets and M. Jean, Phys. Rev. **102** (1956) 788
5) H. Morinaga, Phys. Rev. **103** (1956) 503
6) V. S. Dželepov and L. K. Peker, Report A.E.C.L. 457 (1957)
7) D. Strominger, J. M. Hollander and G. T. Seaborg, Revs. Mod. Phys. **30** (1958) 585
8) R. van Lieshout, private communication; Also Ythier *et al.*, Physica (to be published)
9) B. L. Cohen, Phys. Rev. **105** (1957) 1549
10) B. L. Cohen and A. G. Rubin, Phys. Rev. **111** (1958) 1568
11) T. Tamura and D. C. Choudhury, Phys. Rev. **113** (1959) 552
12) W. F. Hornyak and R. Sherr, Phys. Rev. **100** (1955) 1409
13) C. M. Braams, Phys. Rev. **107** (1956) 1764
14) G. W. Greenlees, J. Lowe, A. B. Robbins and P. M. Rolph, Proc. Phys. Soc. **71** (1958) 904
15) J. L. Yntema and B. Zeidman Phys. Rev. to be published
16) D. R. Sweetman and N. S. Wall, Comptes Rendus du Congrès International de Physique Nucléaire (1958) (Dunod, Paris 1959) p. 547
17) A. I. Yavin and G. W. Farwell, Nuclear Physics **12** (1959) 1
18) P. C. Robison and G. W. Farwell, unpublished work quoted by J. S. Blair, Proceedings of the International Conference on the Optical Model (Florida State University, Tallahassee (1959))
19) J. S. Blair, Phys. Rev. to be published
20) R. H. Helm, Phys. Rev. **104** (1956) 1466
21) R. H. Helm, J. Oeser and M. R. Yearian, private communication (1959)
22) D. Kohler and H. H. Hilton, Phys. Rev. **110** (1958) 1094
23) A. W. Sunyar, private communication (1959)
24) R. Hofstadter, Ann. Rev. Nucl. Sci. **7** (1957) 231
25) L. J. Tassie, Aust. Journ. Phys. **9** (1956) 407
26) J. M. Blatt and V. F. Weisskopf, Nuclear Physics (John Wiley & Sons, New York 1952)
27) M. Gell-Mann and V. L. Telegdi, Phys. Rev. **99** (1953) 169
28) R. A. Ferrell and W. M. Visscher, Phys. Rev. **102** (1956) 450
29) K. Alder, A. Bohr, T. Huus, B. R. Mottelson and A. Winther, Revs. Mod. Phys. **28** (1956) 432
30) P. H. Stelson and F. K. Mc Gowan, Phys. Rev. **110** (1958) 489
31) T. Marumori, S. Suekane and A. Yamamoto, Prog. Theor. Phys. **16** (1956) 320
32) D. R. Inglis, Phys. Rev. **97** (1955) 701
33) K. Lee and D. R. Inglis, Phys. Rev. **108** (1957) 774
34) S. A. Moszkowski, Handbuch der Physik **39** (1957) 411 (Springer Verlag, Berlin, 1957)
35) W. H. Shaffer, Revs. Mod. Phys. **16** (1944) 245
36) A. A. Ross, H. Mark and R. D. Lawson, Phys. Rev. **102** (1956) 1613
37) S. Suekane, Prog. Theor. Phys. **21** (1959) 74
38) S. A. Moszkowski, Phys. Rev. **103** (1956) 1328

8.B

Nuclear Physics **15** (1960) 56—59; ©*North-Holland Publishing Co., Amsterdam*

Not to be reproduced by photoprint or microfilm without written permission from the publisher

ON THE SPIN OF THE Σ-HYPERON

SHOICHI HORI

Institut for Teoretisk Fysik, Copenhagen, Denmark †

Received 9 October 1959

Abstract: The large asymmetry factor observed in the decay of the Σ^+-hyperon indicates that the spin J of the hyperon is either $\frac{1}{2}$ or $\frac{3}{2}$, when an inequality eq. ((1)) derived by Lee and Yang is taken into consideration. Nevertheless, the distribution function in the case of $J = \frac{3}{2}$ manifests a quite different behaviour from that for $J = \frac{1}{2}$ when it is calculated taking into account the observed large value of the asymmetry factor. Thus, if the corresponding distribution curve could be measured experimentally, it would not be difficult to determine the spin of the Σ-hyperon.

Recently, J. Leiter *et al.* [1]) have obtained strong evidence in favour of $J = \frac{1}{2}$ for the Σ-hyperon. They had, however, to make certain assumptions to obtain this result. Though the assumptions seem to be well grounded, the author feels that it would not be without interest to confirm this result by a different and more direct method which is free from additional assumptions.

T. D. Lee and C. N. Yang pointed out that the measurement of the asymmetry in hyperon decay would be a good tool for determining the spin of the hyperon [2]). They derived two inequalities

$$|\langle\xi\rangle| \leqq \frac{1}{2J+2} \tag{1}$$

and

$$|\langle\xi\rangle| \leqq \frac{1}{6J}\,; \tag{2}$$

here J is the spin of the hyperon, and $\xi = \cos\theta$, where θ is the angle between the normal of the production plane and the direction of the relative momentum of the two decay secondaries.

The relation (2), however, would not give a useful criterion in general, because the inequality was derived under the assumption that the distribution function $w(\xi)$ is linear with respect to ξ. This already corresponds to the assumption of $J = \frac{1}{2}$, as we shall see below.

We shall take the normal of the production plane as the polar axis. If we do not consider the azimuthal distribution of the decay proton, the initial state of the decaying hyperon can be regarded as an incoherent mixture of states,

† On leave of absence from Kanazawa University, Kanazawa, Japan.

each with a definite angular momentum m along the z-axis †. Then, the observed distribution would be expressed as $w(\xi) = \sum_m p(m) w_m(\xi)$, where $p(m)$ is the probability of finding the hyperon in a state m, and $w_m(\xi)$ is the distribution function for the hyperon in a pure state m. The distribution function $w_m(\xi)$ has also been calculated by the author [3]), taking into consideration the four-dimensional invariance; as the published result was erroneous, we shall present here the correct expression:

$$w_m(\xi) = (-)^{J-\frac{1}{2}}(2K+1)[(2J+1)/4\pi]^{\frac{1}{2}} \sum_L [(KK00|KKL0)W(KKJJ; L\tfrac{1}{2}) + \lambda[(2K+3)/(2K+1)]^{\frac{1}{2}}(KK+100|KK+1L0)W(KK+1JJ; L\tfrac{1}{2})] \times (JLm0|JLJm)Y_L^0(\xi), \quad (3)$$

where $K = J-\frac{1}{2}$, m is the z-component of the spin, and λ is a parameter which depends on the detailed structure of the decay interaction ($\lambda \leqq 1$).

Let us define the degree of polarization as

$$P = \langle m \rangle / J, \quad (4)$$

where

$$\langle m \rangle = \sum_m m p(m). \quad (5)$$

If the polarization is complete ($P = 1$), the distribution function is equal to $w_{\frac{1}{2}}(\xi)$. Otherwise, the function $w(\xi)$ will be expressed in terms of three parameters $\langle |m| \rangle$, a and b:

$$w(\xi) = \frac{1}{4\pi}[3\xi^2 + \langle |m| \rangle (1-3\xi^2) + \lambda\{\tfrac{3}{2}a\xi(1-\xi^2) + \tfrac{1}{2}b(9\xi^3-5\xi)\}], \quad (6)$$

where the parameters $\langle |m| \rangle = \sum |m| p(m)$, $a = p(\frac{3}{2}) - p(-\frac{3}{2})$, and $b = p(\frac{1}{2}) - -p(-\frac{1}{2})$ are confined to the regions

$$\tfrac{3}{2}|a| + \tfrac{1}{2}|b| \leqq \langle |m| \rangle \leqq \tfrac{3}{2}, \quad |a| \leqq 1, \quad |b| \leqq 1, \quad |a+b| \leqq 1.$$

One has

$$\langle \xi \rangle = \tfrac{1}{5}\lambda P, \quad P = a + \tfrac{1}{3}b.$$

There is some ambiguity in the definition of the asymmetry factor in the case of $J = \frac{3}{2}$. In the case of $J = \frac{1}{2}$, this factor α may be defined either by the equation

$$\alpha = 3\langle \xi \rangle / P \quad (7)$$

or by

$$\alpha = 4\pi \left[\int_0^1 w(\xi) \mathrm{d}\xi - \int_{-1}^0 w(\xi) \mathrm{d}\xi \right] P, \quad (8)$$

and we have the same result $\alpha = \lambda$ in each case. On the other hand, in the case

† See the footnote of ref. [1]), p. 1755.

of $J = \frac{3}{2}$. we have

$$|\alpha| = \tfrac{3}{5}|\lambda| \leqq \tfrac{3}{5} \tag{9}$$

and

$$|\alpha| = \tfrac{3}{4}|\lambda| \leqq \tfrac{3}{4}, \tag{10}$$

respectively, corresponding to the definitions (7) and (8).

Recently, F. S. Crawford, Jr. *et al.* [4]), using the method suggested by Lee and Yang, have determined the spin of the Λ-hyperon to be $\frac{1}{2}$. In this case, the measured value of $\alpha\bar{P}$ is 0.57 ± 0.066. Although this value, if it corresponds to the definition (7), would not be inconsistent with $J = \frac{3}{2}$ so far as the inequality (1) is concerned, the observed linearity of the distribution is sufficient to exclude $J = \frac{3}{2}$.

R. L. Cool *et al.* [5]) have obtained the result

$$\alpha\bar{P} = 0.70\pm0.30 \tag{11}$$

for the decay $\Sigma^+ \to \mathrm{p}+\pi^0$. Their instrumentation corresponds to the definition (8). Since the average polarization $\bar{P}$ should be less than unity, we have

$$\alpha \geqq 0.70\pm0.30. \tag{12}$$

This value is not inconsistent with the inequality (10) within the experimental error. Therefore, we must refer to the distribution function $w(\xi)$ to determine the spin of the Σ-hyperon.

Let us consider the case in which the decay products p and π are emitted in the direction of the z-axis ($\theta = 0$ or π). Then, the z-component of the orbital angular momenta of the secondaries is zero, so that the hyperon in the state $m = \frac{3}{2}$ cannot disintegrate in this direction owing to the conservation of the z-component of the total angular momentum. In addition, we see that if the spin of the hyperon is $\frac{3}{2}$, the hyperon should be almost exclusively in the state $m = \frac{3}{2}$ (or $m = -\frac{3}{2}$) in order to satisfy the observed relation (8), i.e., $b \approx 0$. Therefore, the distribution function should fall off to zero at both ends ($\theta = 0$ or π). The situation is quite different from that for $J = \frac{1}{2}$. In fig. 1, we

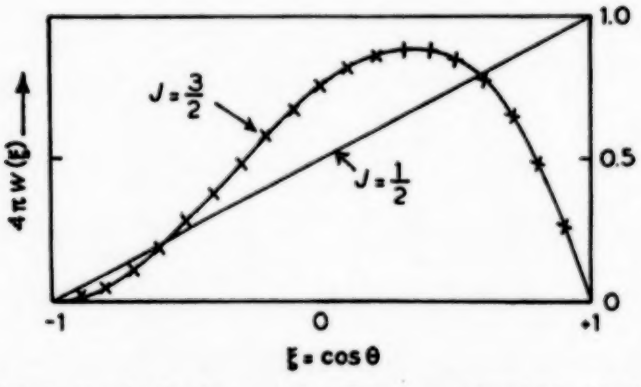

Fig. 1. Calculated distribution in the decay of the Σ-hyperon, in which J is the spin of the hyperon and we put $a = 1$, $b = 0$ and $\lambda = 1$.

have plotted the calculated distribution curve with $a = 1$, $b = 0$, and $\lambda = 1$, together with the corresponding curve for $J = \frac{1}{2}$. The author believes that it is not too difficult at the present stage of experimental technique to determine the spin of the Σ-hyperon by this method.

The author wishes to express his gratitude to Professors Niels Bohr and Aage Bohr for their kind hospitality, and he is also indebted to Professor L. Rosenfeld for valuable discussions.

References

1) J. Leiter *et al.*, Phys. Rev. Lett. **3** (1959) 238
2) T. D. Lee and C. N. Yang, Phys. Rev. **109** (1958) 1755
3) S. Hori, Progr. Theor. Phys. **21** (1959) 613
4) F. S. Crawford, Jr., M. Cresti, M. L. Good, M. L. Stevenson and H. K. Ticho, Phys. Rev. Lett. **2** (1959) 114
5) R. L. Cool, B. Cork, J. W. Cronin and W. A. Wenzel, Phys. Rev. **114** (1959) 912

1.B

Nuclear Physics **15** (1960) 60—71;©*North-Holland Publishing Co., Amsterdam*

Not to be reproduced by photoprint or microfilm without written permission from the publisher

DEUTERON PHOTODISINTEGRATION AND P-WAVE PHASE SHIFTS IN THE MEDIUM ENERGY RANGE

GUSTAV KRAMER

Institut für theoretische Physik der Universität Heidelberg

Received 8 October 1959

Abstract: The angular distribution and the parameter of the polarization of nucleons produced in deuteron photodisintegration are calculated for different phase shift sets which fit n—p scattering data corresponding to 40 MeV, 100 MeV and 150 MeV in the laboratory system. It is found that all the sets which are characterized by positive $^3P_0$ and negative $^3P_1$ phase shifts give similar results for the angular distribution. A small polarization results from sets with a large $^3P_0$ phase shift. For all of the sets which are characterized by a negative $^3P_0$ and a positive $^3P_1$ phase shift we obtain angular distributions which are outside the experimental errors, if one assumes that the D-state probability of the ground state is not extremely large.

1. Introduction

The investigation of deuteron photodisintegration can give one or the other of two kinds of information about the neutron-proton system. If the radiative interaction is known, it may give useful information about the wave functions in the initial and final states. If, on the other hand, the wave functions are known, one can learn something about the radiative interaction. In the medium energy range (20—100 MeV) the deuteron photoeffect is mostly an electric dipole and electric quadrupole process. Therefore, the interaction with the electromagnetic field is well known if the Siegert theorem is applied. The wave function of the ground state is fairly well known through studies of low energy phenomena. Because of this, photodisintegration would provide useful information about the nuclear force in the ^{3}P-state if we restrict ourselves to the electric dipole process. This can be done because the electric dipole transitions are the important ones in the medium energy range.

Another kind of information about nuclear forces can be obtained by the analysis of nucleon-nucleon scattering experiments, especially those with polarized beams. This has been done in the last few years. Several investigations of these experiments in terms of potentials have shown, however, that their interpretation is not unique [1–4]). It has also become clear that phase shift analyses of the experimental data give many different solutions [5–11]). It is well known that it would be possible to distinguish between the various sets of phase shifts by performing triple scattering experiments. These triple scattering experiments have been done only for high energies (310 MeV) [12]). For 150 MeV several authors have reported contradictory experimental results [13]).

Considering only single and double nucleon-nucleon scattering experiments, all the phase shift solutions [5–11]) and the phase shifts calculated from potentials [1–4]) are equivalent. The various sets of phase shifts reported differ in many respects from one another. The question arises whether experimental data aside from triple scattering data are useful in excluding some of these sets. For this purpose, measurements of angular distributions of the deuteron photodisintegration are available. Recent calculations of De Swart and Marshak [14]) are in excellent agreement with the experimental data. In these calculations, which are based on the Signell-Marshak potential [4]), the Gartenhaus wave function is used for the ground state. This wave function contains a D-state admixture of 6.7 %. Other calculations, done by Banerjee, Kramer and Krüger [15]) with Hulthén wave functions and 4 % D-state admixture for the ground state agree only within the rather large experimental errors. These authors describe the final state wave function in terms of phase shifts given by Marshak [16]), which are almost identical to the phase shifts calculated from the Signell-Marshak potential. The quantitative disagreement of the angular distribution parameter between these two calculations is, in the energy range considered, of the order of 20—30 percent. Since the phase shifts are almost the same in the two analyses and the isotropic term varies with the D-state probability, we conclude that the differences have their origin mainly in the different D-state probabilities assumed in the two calculations. It would be interesting, however, to know whether these differences are independent of the assumed phase shifts. It may be possible to obtain a larger isotropic term with the low D-state admixture of 4 %, if one uses other phase shifts which also fit the nucleon-nucleon scattering data and which are different from those of Signell and Marshak.

Another experimental quantity which gives information about deuteron photodisintegration is the polarization of the outgoing nucleons. Formulas for the polarization parameters have been developed by Czyż and Sawicki [17]), by Kawaguchi [18]) and by De Swart [19]). Predictions based on the Signell-Marshak potential and the Gartenhaus wave function for the ground state have been obtained by Czyż, Sawicki and De Swart [20]). Although there are at present no measurements of the polarization it would be worthwhile to investigate the dependence of the polarization parameters on the phase shifts as well. Several authors discuss nucleon-nucleon phase shifts in connection with deuteron photodisintegration [21, 22]). But in these investigations some or all of the D-state contributions to electric dipole transitions are neglected. It has become obvious in recent calculations that these contributions are important for the angular distribution [14, 15, 23]).

In section 2 we discuss briefly the various phase shift sets. The parameters of the angular distribution and the one parameter of the polarization which is most dependent on the electric dipole transitions, are calculated approximately

in section 3. The approximations used are discussed. Section 4 contains a summary and conclusions.

2. P-Wave Phase Shifts

In order to calculate angular distribution and polarization parameters of deuteron photodisintegration one needs the phase shifts for the final state which is a scattering state of the n—p system. Such phase shifts can be obtained by phase shift analyses of the experimental n—p scattering data or can be calculated from potentials. Clementel and Villi [6]) develop from the experimental angular distribution of n—p scattering four sets of P-wave shape shifts. They assume charge independence and obtain therefore similar sets from the analysis of p—p-scattering [5]). To restrict the number of possible solutions they take into account continuity of the phase shifts versus neutron energy. They ignore coupling and partial waves of angular momentum higher than 2. Their sets (A) and (C) are characterized by positive $^3P_0$, negative $^3P_1$ and positive $^3P_2$ phase shifts ($\delta_{10} > 0$, $\delta_{11} < 0$, $\delta_{12} > 0$), while sets (B) and (D) have $\delta_{10} < 0$ and $\delta_{11} > 0$. Only the sets (A) and (D) can fit p—p-polarization at 170 MeV. In spite of this we also discuss sets (B) and (C) in connection with deuteron photodisintegration because we are interested in the results for the lower energies. Set (A) of Clementel and Villi is very similar to the set of phase shifts obtained by Signell and Marshak [4, 16]), who analysed p—p- and n—p-scattering data with the help of a potential which is characterized by a strong spin orbit coupling term. The effect of this term on the Signell-Marshak phase shifts (as well as on the phase shifts calculated by Gammel and Thaler [3])) is to yield smaller δ_{10} and larger $|\delta_{11}|$ than those of set (C) of Clementel and Villi, which can be obtained from central and tensor forces alone †. Although one cannot fit p—p polarization with this set (C), Otsuki [9]), Watari [10]) and Tamagaki [11]) are able to fit all the p—p and n—p data at 90 MeV and 150 MeV (in the laboratory system) with phase shifts which are characterized by large $^3P_0$ phase shifts similar to set (C). These authors have taken coupling fully into account and claim that these phase shifts can be calculated from static potentials, derived from meson theory, which have a positive tensor force in the odd state. The four sets, namely the phase shifts reported by Marshak [16]) for 40 MeV, 100 MeV and 150 MeV, the set reported by Gammel and Thaler [3]) for 40 MeV, 100 MeV and 150 MeV, the set consisting of the phase shifts developed by Noyes and Mac Gregor [7]) (40 MeV), Watari [10]) (100 MeV) and Tamagaki [11]) (150 MeV) and set (C) of Clementel and Villi are collected in table 1. We denote them by (1), (2), (3) and (4). All these phase shifts have the characteristics of phase shifts that can be calculated from a form of positive tensor potential (namely $\delta_{10} > 0$, $\delta_{11} < 0$ and $\delta_{12} > 0$) which is suggested by a

† We conclude this from the comparison of set (C) with the phase shifts calculated by Gammel, Christian and Thaler [24]).

meson theory of nuclear forces. Although it has become clear that the P-wave phase shifts are determined by the positive one-pion exchange potential for lower energies one cannot conclude anything from current pion theory about their behaviour at higher energies. Therefore, we also discuss phase shifts that do not have this behaviour (but have $\delta_{10} < 0$ and $\delta_{11} > 0$) and are fitted to nucleon-nucleon scattering data. Such phase shifts are sets (B) and (D) of

TABLE 1

P-phase shifts in degrees (E = laboratory energy)

	(1)					(2)				
E	δ_{10}	δ_{11}	δ_{12}	δ_{32}	ε_2	δ_{10}	δ_{11}	δ_{12}	δ_{32}	ε_2
40	8.5	−6.3	4.6	0	—	12.9	− 8.5	5.4	−0.3	−21.8
100	15.8	−14.0	9.8	−1.5	—	8.8	−14.4	11.2	0.1	−16.6
150	15.6	−17.2	11.5	−1.6	—	3.3	−17.8	13.9	1.0	−12.2
	(3)					(4)				
E	δ_{10}	δ_{11}	δ_{12}	δ_{32}	ε_2	δ_{10}	δ_{11}	δ_{12}	δ_{32}	ε_2
40	16.9	−6.9	3.0	0	−2.2	21.5	−3.0	2.5	—	—
100	29.8	−14.9	4.6	−2.3	−10.3	33.2	−6.9	2.5	—	—
150	28.6	−17.2	7.5	−4.6	−14.9	45.5	−9.0	2.5	—	—

Clementel and Villi and the phase shifts developed by Feshbach and Lomon [1]) and Saperstein and Durand III [2]). The latter two sets are calculated from energy-independent boundary conditions and are characterized by negative $^3P_0$ phase shifts with a very large absolute value. These sets are here denoted by (5) (set (B) of Clementel and Villi), (6) (their (set (D)), (7) (Feshbach-Lomon set) and (8) (Saperstein-Durand III set) and are given in table 2.

TABLE 2

P-phase shifts in degrees (E = laboratory energy)

	(5)				(6)			
E	δ_{10}	δ_{11}	δ_{12}	δ_{32}	δ_{10}	δ_{11}	δ_{12}	δ_{32}
40	− 8.0	11.5	−1.5	—	−16.0	8.0	2.5	—
100	−17.0	16.0	−2.5	—	−24.0	12.0	2.5	—
150	−18.0	22.5	−6.5	—	−42.0	13.0	2.5	—
	(7)				(8)			
E	δ_{10}	δ_{11}	δ_{12}	δ_{32}	δ_{10}	δ_{11}	δ_{12}	δ_{32}
40	−12.0	0	2.0	0	—	—	—	—
100	−31.0	2.2	6.0	−1.0	−17.0	2.1	8.9	−0.3
150	−47.0	2.3	8.0	−1.6	—	—	—	—

3. Results of the Calculation

3.1. ANGULAR DISTRIBUTION

The angular distribution of protons or neutrons produced in the photodisintegration of the deuteron has the general form

$$\frac{\mathrm{d}\sigma}{\mathrm{d}\Omega} = a+b\sin^2\Theta+c\cos\Theta+d\sin^2\Theta\cos\Theta+f\sin^4\Theta. \tag{1}$$

As is well known, the photodisintegration is a dipole transition in the medium energy range, as a consequence of the high relative momentum of the outgoing nucleons. Quadrupole disintegration is responsible for the interference terms proportional to c and d, which cause the protons to go preferentially into the forward direction [25, 20]). It also makes a contribution to the parameters a and b, the contribution to a being negligible. The contribution to b from the electric quadrupole transition, which gives the largest effect of all of the quadrupole contributions, is mostly compensated by the $\sin^4\Theta$ term which is usually disregarded in the experimental analyses. At medium energy the contribution of the magnetic dipole processes to a and b is only a few percent of that of the E1 transitions. Therefore it is sufficient to consider the E1 contribution to the angular distribution parameters alone.

In this approximation the parameters a and b of the electric dipole photodisintegration are given by the formulas [19])

$$\begin{aligned} a = \tfrac{1}{36}\mathscr{B}(k)\{&4L_{10}^2+9L_{11}^2+(9\xi_2^{\,2}+4\eta_2^{\,2})L_{12}^2+(9\xi_2^{\,2}+9\eta_2^{\,2})L_{32}^2 \\ &-18L_{11}L_{12}\xi_2\cos(\delta_{11}-\delta_{12})-8L_{10}L_{12}\eta_2\cos(\delta_{10}-\delta_{12}) \\ &+18L_{11}L_{32}\eta_2\cos(\delta_{11}-\delta_{32})-12L_{10}L_{32}\xi_2\cos(\delta_{10}-\delta_{32}) \\ &-6L_{11}L_{32}\eta_2\xi_2\cos(\delta_{12}-\delta_{32})\}, \end{aligned} \tag{2}$$

$$\begin{aligned} b = \tfrac{1}{24}\mathscr{B}(k)\{&3L_{11}^2+(3\xi_2^{\,2}+4\eta_2^{\,2})L_{12}^2+(9\xi_2^{\,2}+3\eta_2^{\,2})L_{32}^2 \\ &+8L_{10}L_{12}\eta_2\cos(\delta_{10}-\delta_{12})+18L_{11}L_{12}\xi_2\cos(\delta_{11}-\delta_{12})+12L_{10}L_{32}\xi_2\cos(\delta_{10}-\delta_{32}) \\ &+6L_{12}L_{32}\eta_2\xi_2\cos(\delta_{12}-\delta_{32})-18L_{11}L_{32}\eta_2\cos(\delta_{11}-\delta_{32})\}; \end{aligned} \tag{3}$$

the $L_{\lambda j}$'s are the amplitudes of the outgoing waves with quantum number λ and total angular momentum j. By application of the Siegert theorem they are given by [19])

$$\begin{aligned} L_{10} &= \int_0^\infty \alpha r(u(r)-\sqrt{2}w(r))v_{10}(kr)\mathrm{d}r, \\ L_{11} &= \int_0^\infty \alpha r\left(u(r)+\tfrac{1}{\sqrt{2}}w(r)\right)v_{11}(kr)\mathrm{d}r, \\ L_{12} &= \cos\varepsilon_2\left\{\int_0^\infty \alpha r\left(u(r)-\tfrac{\sqrt{2}}{10}w(r)\right)v_{12}^1(kr)\mathrm{d}r\right\} \\ &\qquad +\sqrt{\tfrac{3}{2}}\sin\varepsilon_2\left\{\tfrac{3}{5}\sqrt{2}\int_0^\infty \alpha r w(r)v_{32}^1(kr)\mathrm{d}r\right\}, \end{aligned} \tag{4}$$

$$L_{32} = \cos\varepsilon_2 \left\{\tfrac{3}{5}\sqrt{2}\int_0^\infty \alpha r w(r) v_{32}^3(kr)\mathrm{d}r\right\} - \sqrt{\tfrac{2}{3}}\sin\varepsilon_2 \left\{\int_0^\infty \alpha r[u(r) - \tfrac{\sqrt{2}}{10} w(r)] v_{12}^3(kr)\mathrm{d}r\right\}.$$

Further,

$$\mathscr{B}(k) = \frac{1}{12}\,\frac{e^2}{\hbar c}\,\frac{M\omega}{\hbar k}\,\frac{N^2}{\alpha^2},$$

where M is the nucleon mass, $\hbar\omega$ the energy of the γ-quantum, k the relative wave number of the outgoing nucleons, $1/\alpha$ the radius of the deuteron and N the normalization constant of the ground state wave function

$$\Psi_1 = N\left\{\frac{u(r)}{r} Y_{011} + \frac{w(r)}{r} Y_{211}\right\}:$$

N is chosen to give the standard effective range normalization

$$\lim_{r\to\infty} u(r) = \mathrm{e}^{-\alpha r}. \tag{6}$$

Because of the tensor force there is a coupling of states with different orbital angular momenta $l = j \pm 1$. In this case there exists a quantum number $\lambda(\lambda = j-1,\ j,\ j+1)$, which becomes equal to l if the coupling goes to zero. In the final state of the E1 photodisintegration process we have mixing between the $^3P_2$ and $^3F_2$ waves; ε_2 is the mixing parameter and ξ_2 and η_2 are connected with ε_2 by

$$\xi_2 = \cos\varepsilon_2 - \sqrt{\tfrac{2}{3}}\sin\varepsilon_2, \quad \eta_2 = \cos\varepsilon_2 + \sqrt{\tfrac{3}{2}}\sin\varepsilon_2.$$

The radial wave functions for a scattering state are v_{lj}^λ, which are normalized to

$$\lim_{r\to\infty} v_{lj}^\lambda(kr) = \sin(kr - \tfrac{1}{2}l\pi + \delta_{\lambda j}), \tag{8}$$

where the $\delta_{\lambda j}$ are the scattering phase shifts. If ε_2 is set equal to zero the formulas (2), (3) and (4) are identical with the formulas for a and b first given by Austern [26]) (see also refs. [14]) and [15])).

The total disintegration cross section σ is related to a and b by

$$\sigma = 4\pi(a + \tfrac{2}{3}b). \tag{9}$$

In order to calculate a and b, the phase shifts and the amplitudes are needed. The $L_{\lambda j}$ depend on the radial wave function of the ground state and on the radial wave function of the final state which is a scattering state. For $u(r)$ and $w(r)$ we use the phenomenological deuteron wave functions of Hulthén and Sugawara [27]), which are fitted to given values of binding energy, quadrupole moment, deuteron effective range and D-state probability, assumming a definite value for the hard core radius in the n–p potential. For the binding energy and the quadrupole moment, experimental values are taken. For the

deuteron effective range we have assumed the experimental value of the triplet effective range corresponding to the shape-independent approximation. The D-state probability p_D is not known. Neglecting the influence of exchange current effects, relativistic effects and effects of energy-dependent potentials in the n–p interaction (for example spin orbit couplings) on the deuteron magnetic moment μ_D, one obtains from the experimental value of μ_D the value $p_D = 0.04$. We assume this value, considering, however, p_D as a parameter which is kept fixed. For the hard core radius we take the value $r_c = 1/10\alpha = 0.4316 \times 10^{-13}$ cm.

The functions v_{ij}^{λ} for the final state have to be calculated from potentials which give the scattering parameters $\delta_{\lambda j}$ and ε_2 collected in tables 1 and 2. These potentials are known for sets (1) and (2) only. The integrals do not depend strongly on the shape of the function $v_{ij}^{\lambda}(kr)$ for small r. Firstly, there occurs a factor r in the integrals, and secondly $u(r)$ and $w(r)$ vanish at the hard core radius r_c. The maxima of $u(r)$ and $w(r)$ lie near $r = 1.5 \times 10^{-13}$ cm. Beyond the range R of the nuclear potential the function $v_{ij}^{\lambda}(kr)$ takes the form

$$v_{ij}^{\lambda}(kr) = kr\{\cos\delta_{\lambda j} j_l(kr) - \sin\delta_{\lambda j} n_l(kr)\}, \tag{10}$$

where j_l and n_l are, respectively, the spherical Bessel and Neumann functions. If we approximate v_{ij}^{λ} by expression (10) for all distances we get a first approximation to the amplitudes $L_{\lambda j}$. This approximation has already been used by several authors [21, 22]). The main differences between the exact expression for v_{ij}^{λ} and the expression (10) in the region $r_c \leqq r < R$ are that the latter does not vanish for $r = r_c$ and that the asymptotic form (10) becomes large for small r because of the presence of the Neumann function $n_l(kr)$. This function is negative in the region $r_c \leqq r < R$ for k-values corresponding to medium energies: therefore, the amplitudes $L_{\lambda j}$, calculated from the v_{ij}^{λ} as given by (10) are larger than the exact ones for positive phase shifts $\delta_{\lambda j}$, and smaller for negative $\delta_{\lambda j}$. A different approximation for the v_{ij}^{λ} is the following [14]):

$$v_{ij}^{\lambda}(kr) = \begin{cases} kr\{\cos\delta_{\lambda j} j_l(kr) - \sin\delta_{\lambda j} n_l(kr)\} & \text{for } r \geqq R \\ kr\cos\delta_{\lambda j} j_l(kr) & \text{for } r_c \leqq r < R. \end{cases} \tag{11}$$

In this approximation the wave function goes nearly to zero for $r = r_c$, if the energy is not too large. But the wave function (11) is no longer continuous for $r = R$. With this approximation for v_{ij}^{λ} the contribution of the Neumann function is reduced and therefore the amplitudes $L_{\lambda j}$ are smaller than in the approximation based on (10). In ref. [15]) we have calculated the amplitudes $L_{\lambda j}$ assuming square well potentials with a hard core which are fitted to the Marshak phase shifts (1). We have compared these $L_{\lambda j}$ with those for the two approximations: (I) substituting expression (10) for v_{ij}^{λ} and (II) using (11) for v_{ij}^{λ}. We find that the $L_{\lambda j}$ calculated in ref. [15]) lie between the $L_{\lambda j}$ obtained with the approximations (I) and (II). Thus, if we call the values obtained in ref. [15])

the "exact" ones, we have

$$L_{10}^{\mathrm{II}} < L_{10}^{\mathrm{ex}} < L_{10}^{\mathrm{I}}, \quad L_{11}^{\mathrm{I}} < L_{11}^{\mathrm{ex}} < L_{11}^{\mathrm{II}}, \quad L_{12}^{\mathrm{II}} < L_{12}^{\mathrm{ex}} < L_{12}^{\mathrm{I}}, \tag{12}$$

and

$$L_{10} < L_{12} < L_{11}$$

for all three approximations. Taking $R = 1.55 \times 10^{-13}$ cm we find that $L_{\lambda j}^{\mathrm{ex}}$ is closer to the $L_{\lambda j}$ calculated with approximation (I).

For the Marshak phase shifts we also have

$$\begin{aligned} L_{11}^{\mathrm{I}} - L_{12}^{\mathrm{I}} &< L_{11}^{\mathrm{ex}} - L_{12}^{\mathrm{ex}} < L_{11}^{\mathrm{II}} - L_{12}^{\mathrm{II}}, \\ L_{12}^{\mathrm{I}} - L_{10}^{\mathrm{I}} &< L_{12}^{\mathrm{ex}} - L_{10}^{\mathrm{ex}} < L_{12}^{\mathrm{II}} - L_{10}^{\mathrm{II}}. \end{aligned} \tag{13}$$

Setting the cosines of the phase shift differences equal to 1 we get for a and b:

$$\begin{aligned} a &= \tfrac{1}{36}\mathscr{B}(k)\{4(L_{12} - L_{10} + \tfrac{3}{2}L_{32})^2 + 9(L_{11} - L_{12} + L_{32})^2\}, \\ b &= \tfrac{1}{24}\mathscr{B}(k)\{4L_{10}^2 + 12L_{11}^2 + 20L_{12}^2 + 30L_{32}^2\} - \tfrac{3}{2}a. \end{aligned} \tag{14}$$

Because of (13) we have therefore

$$a^{\mathrm{I}} < a^{\mathrm{ex}} < a^{\mathrm{II}}, \quad b^{\mathrm{II}} < b^{\mathrm{ex}} < b^{\mathrm{I}}, \tag{15}$$

where the indices I and II, as before, refer to the approximations used. The relations (13) between the two approximations are valid for all sets which are characterized by $\delta_{10} > 0$, $\delta_{11} < 0$ and $\delta_{12} > 0$. If $\delta_{10} < 0$, $\delta_{11} > 0$ and $\delta_{12} < 0$, the indices I and II have to be interchanged.

It seems reasonable to suppose that the two approximations give upper and lower bounds, respectively, to a and b for the phase shift sets (1), (2), (3), (4) and (5). Also for the sets (6), (7) and (8) we have $\delta_{10} < 0$ and $\delta_{11} > 0$, but $\delta_{12} > 0$. Therefore, instead of (12) one has the relations

$$L_{10}^{\mathrm{I}} < L_{10}^{\mathrm{II}}, \quad L_{11}^{\mathrm{II}} < L_{11}^{\mathrm{I}}, \quad L_{12}^{\mathrm{II}} < L_{12}^{\mathrm{I}}$$

and

$$L_{10} < L_{12} < L_{11}.$$

For set (6) we establish that the following relations hold, just as for set (5):

$$L_{11}^{\mathrm{II}} - L_{12}^{\mathrm{II}} < L_{11}^{\mathrm{I}} - L_{12}^{\mathrm{I}}, \quad L_{12}^{\mathrm{II}} - L_{10}^{\mathrm{II}} < L_{12}^{\mathrm{I}} - L_{10}^{\mathrm{I}}. \tag{16}$$

But for (7) and (8) we only have

$$L_{12}^{\mathrm{II}} - L_{10}^{\mathrm{II}} < L_{12}^{\mathrm{I}} - L_{10}^{\mathrm{I}}. \tag{17}$$

For the difference $L_{11} - L_{12}$, we obtain

$$L_{11}^{\mathrm{I}} - L_{12}^{\mathrm{I}} < L_{11}^{\mathrm{II}} - L_{12}^{\mathrm{II}}. \tag{18}$$

Both approximations give, however, nearly the same values for $L_{11}-L_{12}$. Therefore, we conclude that in this case the two approximations give approximate results for a and b.

Calculations have been performed for energies corresponding to n—p scattering at 40 MeV, 100 MeV and 150 MeV in the laboratory system and, therefore, for γ-ray energies of 22.5 MeV, 53.7 MeV and 80.5 MeV, respectively. The results for a and b for the sets (1) to (4), which are similar to the Marshak phase shifts, are collected in table 3, together with the so-called "exact" calculations of ref. [15]) †.

TABLE 3

The parameters a and b in μb for phase shift sets (1), (2), (3) and (4)

	(1)			(2)		(3)		(4)	
E_γ	a^{I}	a^{ex}	a^{II}	a^{I}	a^{II}	a^{I}	a^{II}	a^{I}	a^{II}
22.5	3.3	3.4	3.8	3.2	3.8	3.3	4.1	3.6	4.3
53.7	3.3	3.5	4.3	3.3	3.9	3.5	4.5	3.2	4.1
80.5	2.7	2.9	3.7	2.5	3.5	3.0	4.1	2.7	3.5
E_γ	b^{I}	b^{ex}	b^{II}	b^{I}	b^{II}	b^{I}	b^{II}	b^{I}	b^{II}
22.5	54.6	55.0	54.0	58.7	54.7	54.3	53.6	54.0	53.0
53.7	12.1	11.7	11.0	14.1	13.1	12.6	11.8	12.5	11.9
80.5	5.1	4.7	4.1	6.3	5.5	5.6	2.9	5.2	4.5

We see from table 3 that for all the phase shifts (1), (2), (3) and (4) we get similar results for a and b. Comparing them with the values obtained from the Signell-Marshak phase shifts we have the result that, for $E_\gamma = 22.5$ MeV, a and b are almost equal for each of the 4 sets. For the two larger γ-ray energies a is reduced for set (2), increased for set (3), and b is increased for set (2). For set (4) a and b have nearly the same values as for set (1).

TABLE 4

The parameters a and b in μb for phase shift sets (5), (6), (7), (8)

	(5)		(6)		(7)		(8)	
E_γ	a^{I}	a^{II}	a^{I}	a^{II}	a^{I}	a^{II}	a^{I}	a^{II}
22.5	3.8	3.1	3.8	3.2	3.4	3.2	—	—
53.7	2.1	1.5	2.2	1.6	2.7	2.4	2.5	2.4
80.5	1.3	1.0	1.8	1.8	2.2	2.1	—	—
E_γ	b^{I}	b^{II}	b^{I}	b^{II}	b^{I}	b^{II}	b^{I}	b^{II}
22.5	54.8	53.6	55.1	53.7	55.2	55.2	—	—
53.7	12.6	12.7	12.6	12.3	12.5	11.9	12.4	11.7
80.5	5.8	6.2	5.4	4.8	5.0	5.0	—	—

† A refined calculation has led to slightly modified values of a^{ex} and b^{ex}.

We now discuss the results for the phase shift sets with negative $^3P_0$ phase shift and positive $^3P_1$ phase shift. They are collected in table 4. For these sets the parameters a and b, for $E_\gamma = 22.5$ MeV, are also similar to the values given for set (1). Thus, although the differences between the phase shift sets are as large as 30°, we cannot reach any conclusion about these differences from the values of a and b. For the two larger γ-ray energies we have the result that a falls outside the experimental errors. Including the experimental errors the experimental data are [28, 29, 30]) (in μb)

$E_\gamma = 22.5$ MeV: $a = 3.3$ to 12.1, $b = 40$ to 68, $\sigma = 500$ to 660;

$E_\gamma = 54$ MeV: $a = 3.1$ to 5.7, $b = 6.9$ to 10.2, $\sigma = 125$ to 155;

$E_\gamma = 80.5$ MeV: $a = 3.4$ to 5.5, $b = 2.9$ to 5.6, $\sigma = 78$ to 98.

Our calculations are based on a D-state probability $p_D = 0.04$. Of course, it is possible to get larger values for a if one increases p_D. A rough estimate for the phase shifts (8) ($E_\gamma = 53.7$ MeV) indicates that p_D must be increased up to 10 % to get nearly the same values as for the Signell-Marshak phase shifts. For cases (5) and (6) p_D must be of the order of magnitude of 15 %. Such large D-state probabilities seem to be unreasonable. Very large mesonic corrections and contributions from a spin orbit potential [31, 32]) would be necessary to bring this D-state admixture into agreement with the experimental value of the magnetic moment of the deuteron.

3.2. POLARIZATION

The polarization $P(\mathrm{p})$ in the direction $\mathbf{n}_\mathrm{p} = \mathbf{k}_\gamma \times \mathbf{k}/|\mathbf{k}_\gamma \times \mathbf{k}|$, produced in the photodisintegration of the deuteron by unpolarized γ-rays, has the form [17, 19])

$$\frac{\mathrm{d}\sigma}{\mathrm{d}\Omega} P(\mathrm{p}) = \sin\Theta\{\gamma_0(\mathrm{p}) + \gamma_1(\mathrm{p})\cos\Theta + \gamma_2(\mathrm{p})\cos^2\Theta\}. \tag{19}$$

The polarization of the neutron $P(\mathrm{n})$ is different from the proton polarization but has the same form (19) [17, 19]), with other parameters $\gamma_0(\mathrm{n})$, $\gamma_1(\mathrm{n})$ and $\gamma_2(\mathrm{n})$. The parameters $\gamma_2(\mathrm{p})$, $\gamma_2(\mathrm{n})$ and the differences between proton and neutron polarization come from the interference between dipole and quadrupole transitions. The parameters $\gamma_0(\mathrm{p})$ and $\gamma_0(\mathrm{n})$ are contributed by the M1—E1 interference, and are independent of the transition to the $^3P_0$-state. The phase shift sets (1) to (4) differ significantly only in the $^3P_0$ phase shift. Further we are only interested in pure dipole effects. Therefore we discuss only the parameter

$$\gamma_1 = \tfrac{1}{2}(\gamma_1(\mathrm{p}) + \gamma_1(\mathrm{n}))$$

which can be obtained from the analysis of the angular dependence of the sum of the proton and neutron polarizations. If we add these two polarizations the interference terms between dipole and quadrupole transitions cancel [17]).

The formula for γ_1, taken from ref. [19]), is

$$\gamma_1 = \tfrac{1}{12}\mathscr{B}(k)\{6\eta_2 L_1 L_2 \sin(\delta_2-\delta_1)-4\xi_2 L_0 L_2 \sin(\delta_0-\delta_2) \\ +9\xi_2 L_1 L_3 \sin(\delta_3-\delta_1)+(2\eta_2{}^2+3\xi_2{}^2)L_2 L_3 \sin(\delta_2-\delta_3) \\ +4\eta_2 L_0 L_3 \sin(\delta_0-\delta_3)\}. \quad (20)$$

The calculated γ_1 for the phase shift sets (1) to (4) are given in table 5.

TABLE 5

γ_1 in μb for phase shift sets (1) to (4)

	(1)			(2)		(3)		(4)	
E_γ	$\gamma_1{}^{\mathrm{I}}$	$\gamma_1{}^{\mathrm{ex}}$	$\gamma_1{}^{\mathrm{II}}$	$\gamma_1{}^{\mathrm{I}}$	$\gamma_1{}^{\mathrm{II}}$	$\gamma_1{}^{\mathrm{I}}$	$\gamma_1{}^{\mathrm{II}}$	$\gamma_1{}^{\mathrm{I}}$	$\gamma_1{}^{\mathrm{II}}$
22.5	4.6	4.7	4.7	4.8	5.0	3.1	3.3	0.6	0.8
53.7	3.4	3.5	3.5	3.6	3.6	2.6	2.9	1.8	2.0
80.5	1.9	2.3	2.4	2.6	2.7	0.2	1.5	1.0	1.1

As we can see from table 5 there are no striking differences between the results for the different phase shift sets. For (1) and (2) we have very similar values. In comparison with (1) and (2) set (3) is connected with somewhat smaller polarization. Set (4) is distinguished from the other in that it gives small polarization for the two lower γ-energies. For the Marshak phase shifts we have

$$\gamma_1{}^{\mathrm{I}} < \gamma_1{}^{\mathrm{ex}} < \gamma_1{}^{\mathrm{II}}. \quad (21)$$

We suppose that (21) is true for the other sets also.

4. Summary and Conclusions

We have calculated the angular distribution parameters a and b in deuteron photodisintegration for different P-wave phase shifts fitted to n—p scattering data in the medium energy range (40 MeV, 100 MeV and 150 MeV in the laboratory system). For all the phase shift sets corresponding to positive tensor force (which are characterized by $\delta_{10} > 0$ and $\delta_{11} < 0$) we obtain similar results for a and b, which can account for the experimental data. But for all sets corresponding to negative tensor force (which are characterized by $\delta_{10} < 0$ and $\delta_{11} > 0$) the calculated values for a are outside the experimental errors, if we make the reasonable assumption that the D-state probability is not extremely large. Therefore only potentials with a positive tensor part in the triplet odd state, as suggested by a pion theory of nuclear forces, can account for deuteron photodisintegration data.

The term proportional to $\sin^2\Theta$ in the polarization of the nucleons produced in deuteron photodisintegration varies somewhat more for the different phase shift sets (with $\delta_{10} > 0$, $\delta_{11} < 0$) than the parameters a and b. For sets with a large $^3P_0$ phase shift we get small polarization.

References

1) H. Feshbach and E. Lomon, Phys. Rev. **102** (1956) 891
2) A. M. Saperstein and L. Durand III; Phys. Rev. **104** (1956) 1102
3) J. Gammel and R. Thaler, Phys. Rev. **107** (1957) 291, 1337
4) P. S. Signell and R. E. Marshak, Phys. Rev. **109** (1958) 1229
5) E. Clementel, C. Villi and L. Jess, Nuovo Cimento **5** (1957) 907
6) E. Clementel and C. Villi, Nuovo Cimento **5** (1957) 1166
7) H. P. Noyes and M. H. MacGregor, Phys. Rev. **111** (1958) 223
8) M. H. MacGregor, Phys. Rev. **113** (1959) 1559
9) S. Otsuki, Prog. Theor. Phys. **20** (1958) 171
10) W. Watari, Prog. Theor. Phys. **20** (1958) 181
11) R. Tamagaki, Prog. Theor. Phys. **20** (1958) 505
12) O. Chamberlain, E. Segrè, R. D. Tripp, C. Wiegand and T. Ypsilantis, Phys. Rev. **105** (1957) 288
13) C. F. Hwang, T. R. Ophel, E. H. Thorndike, R. Wilson and N. F. Ramsey: Phys. Rev. Lett. **2** (1959) 310
14) J. J. De Swart and R. E. Marshak, Phys. Rev. **111** (1958) 272
15) B. Banerjee, G. Kramer and L. Krüger, Zeitschr. f. Phys. **153** (1959) 630
16) R. E. Marshak, Proc. of Seventh Rochester Conference on High Energy Physics (New York, Interscience Publishers Inc., 1957) Ch. III
17) W. Czyż and J. Sawicki, Nuovo Cimento **5** (1957) 45; Phys. Rev. **110** (1958) 900; Nuclear Physics **8** (1958) 621
18) M. Kawaguchi, Phys. Rev. **111** (1958) 1314
19) J. J. De Swart, Physica **25** (1959) 233
20) W. Czyż, J. Sawicki and J. J. de Swart, Phys. Rev. Lett. **2** (1959) 51
21) S. H. Hsieh, Nuovo Cimento **4** (1956) 138; Prog. Theor. Phys. **16** (1956) 68; **18** (1957) 637; **21** (1959) 185; **21** (1959) 211
22) B. Banerjee, unpublished (1957)
23) A. F. Nicholson and G. E. Brown, Proc. Phys. Soc. **73** (1959) 221
24) J. L. Gammel, R. S. Christian and R. M. Thaler, Phys. Rev. **105** (1957) 311
25) B. Banerjee and G. Kramer, Zeitschr. f. Phys. **154** (1959) 513
26) N. Austern, Phys. Rev. **108** (1958) 973
27) L. Hulthén and M. Sugawara, Handbuch der Physik Bd. **39** (Berlin-Göttingen-Heidelberg, Springer, 1957) p. 99 ff
28) L. Allen Jr., Phys. Rev. **98** (1955) 705
29) E. A. Whalin, B. D. Schriever and A. O. Hanson, Phys. Rev. **101** (1956) 377
30) U. A. Aleksandrov, N. B. Delone, L. I. Slovokhotov, G. A. Sokol and L. B. Shtarkov, Soviet Physics (JETP) **6** (1958) 472
31) H. Feshbach, Phys. Rev. **107** (1957) 1626
32) J. J. De Swart, R. E. Marshak and P. S. Signell, Nuovo Cimento **6** (1957) 1189

Editor's note: See also J. Iwadare, S. Otsuki, M. Sano, S. Takagi, and W. Watari, Progr. Theor. Phys. **16** (1956) 658. The calculations in this paper, based on a meson theory of nuclear interaction, are in agreement with Dr. Kramer's results. See further a forthcoming paper by J. Iwadare and M. Matsumoto in Progr. Theor. Phys.

2.B:2.E

Nuclear Physics **15** (1959) 72—78; © *North-Holland Publishing Co., Amsterdam*

Not to be reproduced by photoprint or microfilm without written permission from the publisher

RELATION BETWEEN ANGULAR DISTRIBUTION AND POLARIZATION IN THE OPTICAL MODEL

LEONARD S. RODBERG †

Los Alamos Scientific Laboratory, University of California, Los Alamos, New Mexico ††

Received 11 September 1959

Abstract: The relation between the angular dependence of the cross section and the polarization is discussed. A formula is derived for estimating the depth of the spin-orbit potential from the observed polarization. Sufficient conditions for the validity of these results are derived. In the course of this discussion a useful approximate formula is derived which relates the depth of the central potential, the size of the target, and the positions of the minima in the angular distribution.

1. Introduction

The optical model has been very successful in describing the elastic scattering of nucleons by nuclei, as well as in problems in pion and K-meson scattering [1]). The characteristic features of the results, such as the regular dependence of the angular distribution on the size of the target, the close relation between the target radius and potential depth (the "VR^2 rule"), and the close correspondence between the angular dependence of the cross section and the polarization (in the case of nucleons), would suggest that the important properties of this model have an essentially simple foundation.

In this report we wish to give a simple heuristic discussion of the relation between the cross section and the polarization †††. The result will be a formula from which the shape of the polarization can be predicted from the experimental angular distribution, and the depth of the spin-orbit potential can be estimated if the magnitude of the polarization is known.

In section 2 the relation between the angular dependence of the cross section and the polarization is derived and discussed. In section 3 we derive an approximate relation between the real part of the central potential, the radius of the target, and the positions of the minima in the angular distribution. This connection between well depth and angle is then used to relate the magnitude of the polarization to the depth of the spin-orbit potential. In section 4 the scattering amplitude is calculated to first order in the spin-orbit potential, and

† Permanent address: Physics Department, University of Maryland, College Park, Maryland.

†† Work performed under the auspices of the U. S. Atomic Energy Commission.

††† The general result derived here is known to many people and has been discussed by N. M. Hintz [2]).

sufficient conditions for the validity of the earlier results are discussed. It appears that these conditions are general properties of the nuclear optical model.

The type of discussion involved here appears useful in estimating radii and well depths from observed scattering data. It cannot replace a detailed calculation since, for instance, the precise shape of the angular distribution appears to involve a complicated interplay of all the parameters involved.

2. Relation Between Angular Distribution and Polarization

Let us consider incident particles with a given spin-projection m_s along the normal to the scattering plane (defined by $\mathbf{k}_i \times \mathbf{k}_f$). We conjecture that, to first approximation, the only effect of a real spin-orbit potential is to shift the angular distribution for particles of this spin through an angle $\delta\theta$, leaving the shape unchanged.

This simple dependence on the spin-orbit potential seems reasonable, since optical model calculations [3]) show that the most important effect of a small change in the real part of the central potential is to produce such a bodily shift. If the addition of a weak spin-orbit potential is equivalent to such a change, the conjectured modification will occur.

The shift in angle depends on the presence of a central potential. A spin-orbit potential of the form $V_{so}(r)\boldsymbol{\sigma} \cdot \mathbf{l}$ will appear either attractive or repulsive, depending on whether the orbital angular momentum $\mathbf{l}$ of the incident particle with respect to the centre of the target is positive or negative. If the particles which are observed at a given angle θ have come in equal amounts from the two sides of the target, the net effect of the spin-orbit potential will tend to cancel out. If there is a central potential, the contributions from the left-right hemispheres of the target will be unequal. The refraction produced by the real part, and the absorption produced by the imaginary part, will both lead to this inequality. (In Born approximation [4]) the refraction is neglected and the two contributions are equal unless the central potential has an imaginary part.)

Let us then consider a situation in which both a central potential and a spin-orbit potential are present, and for which the scattering amplitude with no spin-orbit potential is $M(\theta)$. Our conjecture is that, with the spin-orbit potential turned on, the scattering amplitude for a spin-up particle is

$$M_{\uparrow}(\theta) = M(\theta+\delta\theta) \approx M(\theta)+\delta\theta \frac{\partial M(\theta)}{\partial \theta}. \tag{1}$$

For a spin-down particle it is

$$M_{\downarrow}(\theta) = M(\theta-\delta\theta) \approx M(\theta)-\delta\theta \frac{\partial M(\theta)}{\partial \theta}. \tag{2}$$

The polarization is defined as

$$P(\theta) = \frac{N_\uparrow(\theta) - N_\downarrow(\theta)}{N_\uparrow(\theta) + N_\downarrow(\theta)}$$

where $N_\uparrow(\theta)$ and $N_\downarrow(\theta)$ are the number of particles of the given spin observed at an angle θ. In our case we have

$$P(\theta) = \frac{|M_\uparrow(\theta)|^2 - |M_\downarrow(\theta)|^2}{|M_\uparrow(\theta)|^2 + |M_\downarrow(\theta)|^2} \approx \frac{2\,\mathrm{Re}\, M(\theta)^* \dfrac{\partial M(\theta)}{\partial\theta}}{|M(\theta)|^2}\,\delta\theta. \tag{4}$$

To order $(\delta\theta)^2$, $\sigma(\theta) = |M(\theta)|^2$ so that

$$\frac{\partial\sigma(\theta)}{\partial\theta} = 2\,\mathrm{Re}\, M(\theta)^* \frac{\partial M(\theta)}{\partial\theta} \tag{5}$$

and

$$P(\theta) \approx \frac{\dfrac{\partial\sigma(\theta)}{\partial\theta}}{\sigma(\theta)}\,\delta\theta. \tag{6}$$

The polarization is proportional to the derivative of the angular distribution; it is zero at the maxima and minima and is a maximum in between. This result is characteristic both of optical model calculations [5]) and of experiments with medium-energy protons [6]). It is a reflection of the fact that the equal and opposite shifts in the angular distribution lead to equal numbers of spin-up and spin-down particles at the positions of the original maxima and minima, and give a maximum difference in between. If the angular distribution had a simple sinusoidal shape (a fairly good approximation if the dependence on momentum transfer rather than angle is considered), the "phase" of the polarization is shifted by 90° relative to the angular distribution.

3. Positions of Minima in the Angular Distribution; Magnitude of Spin-Orbit Potential

Equation (6) will be useful in estimating the magnitude of the spin-orbit potential if we can determine the relation between $\delta\theta$ and $V_{so}(r)$.

To do this, let us first obtain an approximate expression for the positions of the maxima and the minima in the angular distribution. We assume that the central potential is a square well and is real, since optical model calculations [3, 7]) show that the dependence on the potential shape is weak except near $\theta = 180°$, and that the imaginary potential does not affect the positions of the minima.

In general, the scattering amplitude has the form

$$M(\theta) = \frac{-2m}{4\pi\hbar^2}\int \mathrm{d}^3 r \mathrm{e}^{-i\mathbf{k}_f\cdot\mathbf{r}} V(r)\psi_1(r) \tag{7}$$

where, asymptotically,

$$\psi_1(r) \underset{r\to\infty}{\to} \mathrm{e}^{i\mathbf{k}_1\cdot\mathbf{r}} + M(\theta)\frac{\mathrm{e}^{ikr}}{r}$$

and $|k_1| = k = \sqrt{2mE/\hbar^2}$. We approximate $\psi_1(r)$ by $\mathrm{e}^{i\mathbf{K}_1\cdot\mathbf{r}}$, where $|K_1| = K = \sqrt{2m(E-V)/\hbar^2}$ is the wave number in the well. We then find

$$M(\theta) \approx \frac{2mV_0R^2}{\hbar^2 q} j_1(qR) \tag{8}$$

with

$$V(r) = \begin{cases} -V_0 & r < R \\ 0 & r > R, \end{cases}$$

$$q = |\mathbf{k}_f - \mathbf{K}_1| = \sqrt{k^2 + K^2 - 2Kk\cos\theta},$$

and where $j_1(qR)$ is the spherical Bessel function of order 1 [8]). The minima in the angular distribution are then given approximately by the zeroes of $j_1(qR)$. The positions of these zeroes are given quite accurately (within 5 % except for the zero at $qR = 0$) by the zeroes of $\cos qR$ i.e., at $qR = \frac{1}{2}(2n+1)\pi$ ($n = 1, 2, \ldots$). (This is because $j_1(qR) \to -\cos qR/qR$ for large qR.)

One can gain additional confidence in this use of eq. (8) from the fact that a variational principle for $M(\theta)$ can be written as the ratio of two terms [8]), with the numerator equal to the square of $M(\theta)$. Therefore, while we expect the shape of the angular distribution to deviate markedly from eq. (8), the error in the positions of the minima (at which $M(\theta) \approx 0$) will be only of *second* order in the difference between $\psi_1(r)$ and our trial function $\mathrm{e}^{i\mathbf{K}_1\cdot\mathbf{r}}$.

As an example of the use of our result, the minima in the observed angular distribution for 14-MeV neutrons on Pb imply, with eq. (8), an optical well of 47 MeV. Alternatively, if we use the well depth of 44 MeV found by Bjorklund and Fernbach [9]), our rule predicts minima at 31°, 62°, 93° and 135°; the actual calculated minima are at 26°, 58°, 88°, 125° and 152°. The rule appears to be unreliable for scattering angles greater than about 130 degrees.

To return to our original problem, we want to find the shift in angle $\delta\theta$ when the potential is changed by an amount δV. Our rule fixes the minima at angles satisfying

$$qR = \tfrac{1}{2}(2n+1)\pi \text{ with } q = \sqrt{k^2 + K^2 - 2kK\cos\theta}. \tag{9}$$

For fixed n and radius R, q is fixed by this equation. Then

$$\delta\theta = -\frac{K-k\cos\theta}{Kk\sin\theta}\delta K = -\frac{K-k\cos\theta}{K^2k\sin\theta}\frac{m\delta V}{\hbar^2}. \tag{10}$$

For $\theta \approx 90°$,

$$\delta\theta \approx -\frac{m\delta V}{\hbar^2 Kk}.$$

The spin-orbit potential $V_{so}(r)\boldsymbol{\sigma}\cdot\mathbf{l}$ is most important for particles with large orbital angular momentum, i.e., near the surface of the target. Then $l \approx kR$, and

$$\delta V \approx kRV_{so}(R). \tag{11}$$

Finally we have, near $\theta = 90°$,

$$P(\theta) \approx -\frac{1}{\sigma(\theta)}\frac{\partial\sigma(\theta)}{\partial\theta}\frac{mR}{\hbar^2 K}V_{so}(R). \tag{12}$$

To illustrate the use of eq. (12), we graphically differentiate the theoretical angular distribution for 14-MeV neutrons on Pb given by Bjorklund and Fernbach and use their form $V_{so}(R) = V_{SR}(\hbar/\mu c)^2 1/4aR$, with $V_{SR} = 8.3$ MeV and $a = 0.65\times10^{-13}$ cm. We find, for instance, polarizations of $+61$ %, -75 % and $+82$ % at $\theta = 64°$, 79° and 92° respectively. The calculations of ref. [9]) give $+50$ %, -55 % and $+77$ % at $\theta = 61°$, 86° and 95°.

4. Conditions for Validity of eq. (6)

We would like to see what conditions are required for the simple derivative relation between angular distribution and polarization to be correct. To do this we examine the scattering amplitude to first order in the spin-orbit potential.

Consider a problem in which the interaction Hamiltonian consists of two parts, a central potential V_c and a weak spin-orbit potential V_{so}. Gell-Mann and Goldberger [10]) have shown that the matrix element for such a problem can be written

$$T_{fi} = \langle\phi_f|V_c|\chi_i^{(+)}\rangle + \langle\psi_f^{(-)}|V_{so}|\chi_i^{(+)}\rangle \tag{13}$$

where $\chi_i^{(+)}$ is the wave function describing scattering in the potential V_c:

$$\chi_i^{(+)} = \phi_i + \frac{1}{E-H_0+i\varepsilon}V_c\chi_i^{(+)}; \tag{14}$$

$\psi_f^{(-)}$ is the exact wave function including both potentials and can be written

$$\psi_f^{(-)} = \chi_f^{(-)} + \frac{1}{E-H_0-V_c-i\varepsilon}V_{so}\psi_f^{(-)}. \tag{15}$$

The first term in (13) is simply the matrix element for scattering in the central potential and is related to the scattering amplitude $M(\theta)$ discussed earlier by

$$M(\theta) = \frac{-2m}{4\pi\hbar^2} \langle \phi_f | V_c | \chi_1^{(+)} \rangle. \tag{16}$$

The first-order correction to $M(\theta)$ due to the spin-orbit potential is then, using (13) and (15),

$$\delta M(\theta) = -\frac{2m}{4\pi\hbar^2} \langle \chi_f^{(-)} | V_{so} | \chi_1^{(+)} \rangle. \tag{17}$$

Since $\chi_1^{(+)}$ and $\chi_f^{(-)}$ do not depend on the spin of the scattering particle, we can write [8])

$$\chi_1^{(+)} = \sum_{l=0}^{\infty} (2l+1) i^l \frac{u_l^+(r)}{kr} P_l(\cos\theta) \tag{18}$$

with $\cos\vartheta = \mathbf{k}_1 \cdot \mathbf{r}/kr$, and similarly for $\chi_f^{(-)}$. We can also expand $M(\theta)$ as

$$M(\theta) = \sum_{l=0}^{\infty} (2l+1) \frac{e^{(2i\delta_l)} - 1}{2ik} P_l(\cos\theta). \tag{19}$$

If we use (18) and the fact that

$$(\boldsymbol{\sigma} \cdot \mathbf{l}) P_l(\cos\vartheta) = i(\boldsymbol{\sigma} \cdot \mathbf{n}_r) \frac{\mathrm{d}}{\mathrm{d}\vartheta} P_l(\cos\vartheta) \qquad \text{where } \mathbf{n}_r = \frac{\mathbf{k}_1 \times \mathbf{r}}{kr \sin\vartheta},$$

we find that we can write

$$\delta M(\theta) = \sum_{l=0}^{\infty} (2l+1) \frac{e^{2i\delta_l}}{2ik} \beta_l \frac{\mathrm{d}}{\mathrm{d}\theta} P_l(\cos\theta). \tag{20}$$

We have taken out a phase factor for convenience, so that

$$\beta_l = -\frac{2}{k} e^{-2i\delta_l} \int_0^{\infty} \mathrm{d}r \, u_l^{(-)*}(r) V_{so}(r) u_l^{(+)}(r), \tag{21}$$

using $V_{so} = V_{so}(r)\boldsymbol{\sigma} \cdot \mathbf{l}$. If V_c is real, $u_l^{(-)*}(r) = u_l^{(+)}(r)$, and the phase of $u_l^{(+)}(r)$ is simply δ_l. (This follows from the fact that the asymptotic phase of $u_l^{(+)}(r)$ is δ_l, and the presence of a real potential for finite r cannot alter this.) Then, if $V_c(r)$ and $V_{so}(r)$ are real, β_l is a real number.

Now note that [11]) $\sum_{l=0}^{\infty}(2l+1)P_l(\cos\theta) = 2\delta(1-\cos\theta)$, so that, except at $\theta = 0$,

$$M(\theta) = \sum_{l=0}^{\infty} (2l+1) \frac{e^{2i\delta_l}}{2ik} P_l(\cos\theta). \tag{22}$$

Therefore, if β_l were a constant $\bar{\beta}$ independent of l, we would have

$$\delta M(\theta) = \bar{\beta} \frac{\partial}{\partial \theta} M(\theta). \tag{23}$$

This is the condition we require for our earlier results.

We see that a sufficient condition for the validity of our earlier conjecture is that β_l be nearly independent of l over the range of l's that make a significant contribution. This is a reasonable requirement on a potential model, which favours no particular state and implies smooth variations with orbital angular momentum. The fact that the derivative relation between the angular distribution and polarization is a general feature of medium-energy nucleon-nucleus scattering would suggest that this condition is indeed fulfilled. Calculations [5]) show that the shape of $V_{so}(r)$ is not important for this result.

I would like to acknowledge a fruitful discussion with Dr. R. M. Thaler.

References

1) See, for instance, Proceedings of the International Conference on the Nuclear Optical Model, Florida State University, Tallahassee, Florida (1959)
2) N. M. Hintz,Proceedings of the Pittsburgh Conference on Nuclear Structure, University of Pittsburgh, Pittsburgh, Pennsylvania (1957)
3) A. E. Glassgold *et al.*, Phys. Rev. **106** (1957) 1207
4) E. Fermi, Nuovo Cimento **10** Supp. 2 (1955) 84
5) G. W. Erickson and W. B. Cheston, Phys. Rev. **111** (1958) 891
6) L. Rosen and J. E. Brolley, Jr., Proceedings of the Second United Nations International Conference on the Peaceful Uses of Atomic Energy, Vol. 14 (United Nations, Geneva, 1958)
7) A. E. Glassgold and P. J. Kellogg, Phys. Rev. **107** (1957) 1372
8) P. M. Morse and H. Feshbach, Methods of Theoretical Physics (McGraw-Hill Book Company, Inc., New York, 1953)
9) F. Bjorklund and S. Fernbach, Phys. Rev. **109** (1958) 1295
10) M. Gell-Mann and M. L. Goldberger, Phys. Rev. **91** (1953) 398
11) L. D. Landau and E. M. Lifshitz, Quantum Mechanics (Pergamon Press, Ltd., London, 1958)

4.A

Nuclear Physics **15** (1960) 79—88; © *North-Holland Publishing Co., Amsterdam*

Not to be reproduced by photoprint or microfilm without written permission from the publisher

SEARCH FOR PSEUDOSCALAR INTERACTION IN BETA-DECAY

S. G. COHEN and R. WIENER

Department of Physics, The Hebrew University, Jerusalem, Israel

Received 5 October 1959

Abstract: The degrees of longitudinal polarization of high energy monoenergetic electrons from Pr^{144} and Rh^{106} were compared by measuring the circular polarization of external bremsstrahlung produced by these electrons when stopped in lead.

By using conventional β-decay theory the upper limit for $|X| = |C_T \int \beta\gamma_5 / C_A \int \sigma_r|$ of the Pr^{144} $0^- \rightarrow 0^+$ transition was determined to be 0.08. Making special assumptions regarding the pseudoscalar matrix element, this leads to $|C_P/C_A| \leqq 20$.

1. Introduction

Recent experiments [1, 2, 3]) on β-decay have shown that the β-interaction is of the V—A type. This conclusion is in agreement with the theoretical ideas put forward in the last two years in connection with a universal weak interaction [4, 5]). However, the experimental results do not exclude the possibility of a pseudoscalar contribution to the β-interaction. Since such a contribution (unless very small) would be inconsistent with these theoretical ideas †, it would be a matter of some interest to obtain as good a limit as possible to the contribution of pseudoscalar interaction to the total interaction. This is not easy since the pseudoscalar interaction would only be displayed in a relativistic type of transition, and even then only if the value of the coupling constant for the pseudoscalar transition is relatively large. Previous estimates of the amount of pseudoscalar interaction [7, 8]) have been mainly based on measurements of the shape of β-spectra in favourable types of transition. Apart from the earlier confusion in interpretating such results due to the fact that the main interaction was thought to be S—T instead of V—A, there are further theoretical difficulties in interpretating such results, as discussed later in this article.

The discovery of the longitudinal polarization of negatons and positons emitted in β-decay [9–12]) provided a new and somewhat more reliable tool in looking for P-interaction. The polarization of electrons emitted in ordinary (non-relativistic) transitions is known to be very near to $-v/c$. Now these transitions are known to be produced essentially by the V—A type of interaction. According to the two-component theory [13]), a pure pseudoscalar interaction would give, then, a polarization of $+v/c$ and for P, A, V mixtures, a

† An "induced" pseudoscalar interaction is predicted by these theories [6]), but is only significan t for high momentum transfers.

polarization between $-v/c$ and $+v/c$ might be expected, the departure from $-v/c$ depending on the extent of the pseudoscalar contribution.

Transitions of the $0^- \rightarrow 0^+$ type are particularly favourable for this type of investigation, since there the vector interaction is excluded by selection rules and only A and P interactions are possible. Furthermore, the nuclear matrix elements, though complicated, have a simpler structure than would occur in more complicated types of transitions. Graham, Geiger and Eastwood [8]) examined the exact shape of the $0^- \rightarrow 0^+$ transition of Pr^{144} and compared it to the theoretical ones for different A—P mixtures. They hereby obtained an upper limit for C_P/C_A.

In the present experiment the degrees of polarization of monoenergetic electrons from the $Pr^{144} \rightarrow Nd^{144}$ $(0^- \rightarrow 0^+)$ [7, 14]) and the allowed $Rh^{106} \rightarrow Pd^{106}(1+ \rightarrow 0+, 2+)$ [15]) transitions were compared. From the ratio of the measured polarization degrees an estimate of the pseudoscalar contribution to the former transition was made.

2. Experimental

The electron polarization was obtained by measuring the circular polarization of the external bremsstrahlung [10]) produced when the β-particles were stopped in lead. This circular polarization (which is the same in sense as the longitudinal electron polarization, for high energy electrons [16]) was determined by measuring the change in transmitted intensity of the bremsstrahlung through longitudinally magnetized iron upon reversing the direction of magnetization[17]). Since for high energy electrons the bremsstrahlung is emitted within a narrow forward cone, a magnetic lens spectrometer could be used in order to select electrons of a well-defined given energy and help minimize disturbing effects of nuclear γ-rays on the measurements.

The experimental arrangement is shown in fig. 1. The sources used were Ce^{144} and Ru^{106} in equilibrium with their daughters Pr^{144} and Rh^{106} respectively. In both cases the strength was about 10 mc. They were prepared on 4 mg/cm² nylon foils and were covered by 2 mg/cm² foils. The sources were about 1 cm in diameter and not more than 10 mg/cm² in thickness. Electrons of 2.56 MeV energy from these sources were focused by a thin lens spectrometer onto a lead absorber, 1 mm thick and 2 cm in diameter. The spectrometer was operated at a momentum resolution of 6 % and a transmission of 0.5 %. The effective length of the saturated iron of the analyzing magnet was about 4.7 cm. A $2'' \times 1\frac{3}{4}''$ NaI scintillator was used as a detector for the transmitted bremsstrahlung, and was situated at the end of a 10″ light pipe. It was shielded against background radiation. The photomultiplier of the scintillation counter was screened magnetically by various mu-metal and iron shields. A hollow lead cylindrical shield was placed around the electron focus in order to minimize the amount of

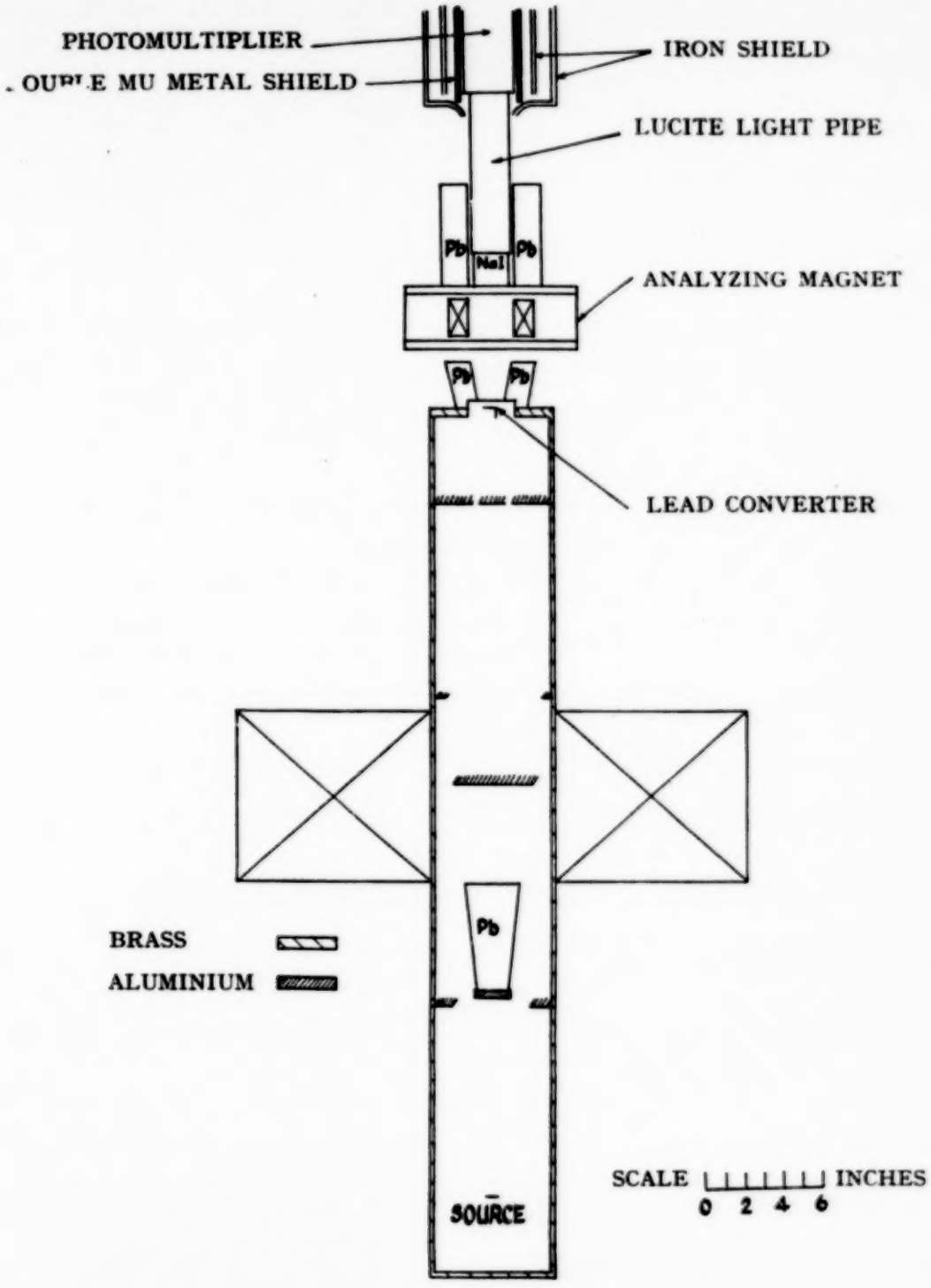

Fig. 1. Experimental arrangement for measuring longitudinal polarization of monoenergetic electrons.

electromagnetic radiation coming from the spectrometer walls (scattered nuclear γ-rays or possibly bremsstrahlung) and reaching the scintillation crystal. Pulses from the scintillation counter were recorded within a channel corresponding to γ-ray energies between 1.5 and 2.0 MeV. This interval was chosen as an optimal compromise between intensity and asymmetry. For Rh^{106} as well as for Pr^{144}, the counting rate obtained in this way was about 24 counts per minute, of which 11 counts per minute were due to external background.

Since the bremsstrahlung produced in the lead absorber is responsible for only part of the γ-ray intensity recorded by the crystal, the experimentally measured asymmetry must be corrected for the rather large effect of dilution of the polarization by the presence of the presumably non-polarized background radiations. The extent to which the polarization ought to be diluted because of this was determined in the following two independent ways:

1) If the current through the spectrometer coil is reduced so as to focus 1.26 MeV electrons then, of course, β-particles of this energy cannot produce bremsstrahlung in the energy interval 1.5—2.0 MeV. The counting rates obtained in the NaI crystal, when 2.56 and 1.26 MeV β-particles were respectively focused, were therefore compared (with the analyzing magnet in the same state), the spectrometer current being switched between the two values every five minutes, in order to minimize drift in the scintillation detection set-up. If $N(E_1)$ and $N(E_2)$ are the counting rates at the two energies E_1 and E_2 (2.56 and 1.26 MeV respectively), the dilution factors f is given by $f = N(E_1)/[N(E_1)-N(E_2)]$, if one assumes that no polarized radiation is detected other than bremsstrahlung produced in the lead absorber.

2) The lead absorber could be replaced by a lucite absorber and then the intensity of bremsstrahlung produced in the absorber is reduced by about a factor of ten. Again the counting rates obtained with the lead and lucite converters could be compared, at a spectrometer current focusing 2.56 MeV electrons. If the counting rates are N and n respectively, the dilution factors are given by $f = 0.9\,N/(N-n)$. The values for f obtained by using the mentioned methods are given in table 1.

TABLE 1

Dilution factors

Isotope	f (%)	
	measured by changing current	measured by changing absorber
Rh^{106}	3.47±0.05	3.2±0.2
Pr^{144}	6.61±0.22	7.2±1.5

From the agreement, within the experimental error, of the values of f obtained by the two methods for each isotope, one may conclude that the inten-

sity of any bremsstrahlung coming from different parts of the spectrometer, other than the lead absorber, is small in comparison with that produced in the lead converter. The unpolarized background is thus presumably made up of the source independent external background and of γ-rays from the source, transmitted by the spectrometer or scattered from its walls and parts. (γ-rays of energies larger than 1.5 MeV are present in Rh^{106} and Pr^{144} with intensities of 0.6 [15]) and 1.3 % [7]) respectively).

Furthermore it is not difficult to see that by using the dilution factors f obtained by changing the spectrometer current, the upper limit for the ratio of the Pr^{144} and Rh^{106} electron polarization obtained in the present experiments can only be smaller than the real one. Here the following facts are taken into account:

a) The detected amount of bremsstrahlung coming from various parts of the spectrometer would become larger when the current through the spectrometer coil is lowered, more high-energy electrons then being able to reach the upper parts of the spectrometer.

b) Relatively more high-energy electrons are present in the case of Rh^{106} than in that of Pr^{144}, the corresponding endpoints of their spectra being 3.5 and 3.0 MeV respectively.

The slight dependence of the photomultiplier amplification on the direction of magnetization of the analyzing magnet was determined with aid of unpolarized nuclear γ-rays from Co^{60}. It was found that the change in counting rate on reversing the direction was $+0.09\pm0.01$ % for a measurement where $dN/dE = 3.8$ ($N =$ counting rate, $E =$ pulse height).

Although this seemed very unlikely, a possible influence of reversal of direction of magnetization of the analyzing magnet on the number of electrons reaching the lead absorber was investigated. For this purpose a 0.1 mc Ce^{141} source with a diameter of 0.5 cm was placed into the spectrometer and 1.5 MeV electrons were focused into a Geiger counter whose window was situated where normally the lead bremsstrahlung converter was placed and had a diameter of 0.8 cm. No change in the counting rate recorded by the Geiger counter could be detected upon reversing the direction of magnetization, and it was concluded that the assumed effect had a negligible influence on the results.

In the polarization measurements the polarity of the analyzing magnet was automatically reversed every five minutes and the counting rate recorded until a total of a million counts were obtained for each isotope.

3. Results

The observed asymmetries are shown in the table 2.

Taking into account the dilution factors, whose measurements has already been discussed, and making a slight correction for the influence of the direction

of magnetization on the pulse size (the values of dN/dE were 3.3 and 2.5 respectively for Rh^{106} and Pr^{144}), the final asymmetries were calculated and are also shown in table 2. (The expected asymmetry for full polarization is -3.5 %.)

TABLE 2

Observed asymmetries

Isotope	Measured asymmetry (%)	Undiluted asymmetry (%)
Rh^{106}	-0.87 ± 0.13	-3.29 ± 0.45
Pr^{144}	-0.63 ± 0.13	-4.56 ± 1.08

From here one gets

$$\left[\frac{\langle\sigma_P\rangle_{Pr^{144}}}{\langle\sigma_P\rangle_{Rh^{106}}}\right]_{E=2,56\ MeV} = 1^{-0.13}_{+0}$$

in agreement with previous polarization results, obtained by Møller scattering for non-monoenergetic electrons from Pr^{144} [18]).

4. Theory and Conclusions

The theoretical expression for $\langle\sigma_P\rangle$ in a $0^- \to 0^+$ transition, assuming A−P mixture, is given by [19])

$$\langle\sigma_P\rangle = \frac{N(\sigma_P=+1)-N(\sigma_P=-1)}{N(\sigma_P=+1)+N(\sigma_P=-1)}$$

$$= \frac{\begin{array}{r}(C_P C_P'^* + C_P' C_P')|\int\beta\gamma_5|^2 i(e^{i\eta}f_{+1}^* g_{-1} - e^{-i\eta}g_{-1}^* f_{+1}) - (C_A C_A'^* + C_A' C_A')|\int\sigma_r|^2 i(e^{-i\eta}f_{-1}^* g_{+1} - e^{i\eta}g_{+1}^* f_{-1}) \\ +[(C_P C_P'^* + C_P' C_P')(\int\sigma_r)(\int\beta\gamma_5)^* + \text{c.c.}](e^{i\eta}f_{+1}^* f_{-1} - e^{-i\eta}g_{-1}^* g_{+1})\end{array}}{\begin{array}{r}(C_P C_P'^* + C_P' C_P'^*)|\int\beta\gamma_5|^2(f_{+1}^* f_{+1} + g_{-1}^* g_{-1}) + (C_P C_P^* + C_A' C_A'^*)|\sigma_r|^2(f_{-1}^* f_{-1} + g_{+1}^* g_{+1}) \\ +[(C_A C_P^* + C_A' C_P'^*)(\int\sigma_r)(\int\beta\gamma_5)^* - \text{c.c.}]i(f_{+1}^* g_{+1} + g_{-1}^* f_{-1})\end{array}}$$

$f_{+1}, f_{-1}, g_{+1}, g_{-1}$ appear as the radial parts of the solutions of the Dirac equation in a central field, which according to Rose [20]) can be written

$$\psi_{kjm} = \begin{pmatrix} i\chi^{ljm} f_\kappa(r) \\ -\chi^{ljm} g_\kappa(r)\end{pmatrix} \quad \text{with} \quad \kappa = \begin{cases} +(j+\frac{1}{2}) & l' = l+1 = \kappa \\ -(j+\frac{1}{2}) & l' = l-1 = |\kappa|\end{cases};$$

χ^{ljm} is the spin-angular part of the usual two-component wave function of a Pauli-electron in a central field:

$$\chi^{ljm} = \sum_\alpha (lm-\alpha;\ \tfrac{1}{2}\alpha|jm) Y_{l(m-\alpha)}\chi_\alpha,$$

$$\chi_{+\frac{1}{2}} = \begin{pmatrix}1\\0\end{pmatrix}, \quad \chi_{-\frac{1}{2}} = \begin{pmatrix}0\\1\end{pmatrix};$$

η is defined by $\eta = \eta_{+\kappa} - \eta_{-\kappa}$,

where

$$e^{+2i\eta_\kappa} = -\left(\frac{K-i\dfrac{y}{w}}{\gamma+iy}\right),$$

$$\gamma = [(j+\tfrac{1}{2})^2-(\alpha Z)^2]^{\frac{1}{2}}, \quad y = \frac{\alpha Z w}{p}$$

(p is the momentum of the electron, w its energy and Z is the charge of the residual nuclei).

In evaluating the above expression the relativistic part of the axial vector interaction was neglected. The non-relativistic part, appearing in a $0^- \to 0^+$ transition is of order of αZ times the allowed G.T. matrix element. On the other hand, the ratio of relativistic to allowed matrix elements is about T/M where T is the kinetic energy and M the mass energy of the decaying nucleon. Assuming $T = 30$ MeV, $(T/M)/\alpha Z \approx \frac{1}{20}$ for Pr^{144}. Furthermore, only the dominating term of the non-relativistic axial vector interaction has been taken into account.

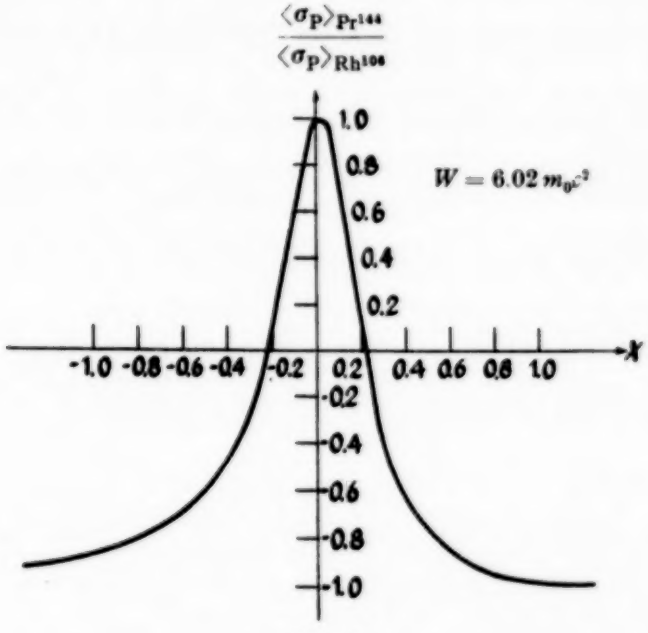

Fig. 2.

Theoretically predicted dependence of $\langle\sigma_P\rangle_{Pr^{144}}/\langle\sigma_P\rangle_{Rh^{106}}$ on the parameter $X = -iC_P\int\beta\gamma_5/C_A\int\sigma_r$ for the Pr^{144} transition ($W = 6.02\, m_0c^2$).

Making the approximation $(\alpha Z)^2 \ll 1$ in the expressions for f, g and η, one gets

$$\langle\sigma_P\rangle = \frac{\left\{(C_PC_P'^*+C_P'C_P^*)|\int\beta\gamma_5|^2\,4-(C_AC_A'^*+C_A'C_A^*)|\int\sigma_r|^2(\alpha Z)^2 + [(C_AC_P'^*+C_A'C_P^*)(\int\sigma_r)(\int\beta\gamma_5)^*+\text{c.c.}]2(\alpha Z)^2\frac{1}{p}\right\}\frac{v}{c}}{(C_PC_P^*+C_P'C_P'^*)|\int\beta\gamma_5|^2\,4+(C_AC_A'^*+C_A'C_A^*)|\int\sigma_r|^2(\alpha Z)^2 - [(C_AC_P^*+C_A'C_P'^*)(\int\sigma_r)(\int\beta\gamma_5)^*-\text{c.c.}]2\alpha Z\frac{1}{w}}.$$

Assuming time reversal invariance, two-component theory [13]) and a left-handed neutrino [1]), the following relations hold:

$$C_i = C'_i = C_i^*.$$

Defining $X = -iC_P \int \beta\gamma_5 / C_A \int \sigma_r$, $\langle \sigma_P \rangle$ is then given by

$$\langle \sigma_P \rangle = \frac{[4|X|^2 - (\alpha Z)^2]\,\frac{v}{c}}{4|X|^2 - 4X\alpha Z\,\frac{1}{w} + (\alpha Z)^2}.$$

In fig. 2, $\langle \sigma_P \rangle_{0^- \to 0^+} / \langle \sigma_P \rangle_{\text{allowed}}$ is shown as a function of X, when $Z = 60$ and $W = 6.02\ m_0c^2$, corresponding to the conditions of the experiment described above. A polarization of $-v/c$ is assumed for the allowed transition of Rh^{106}.

From the experimental result obtained for $[\langle \sigma_P \rangle_{Pr^{144}} / \langle \sigma_P \rangle_{Rh^{106}}]_{E=2.56\ \text{MeV}}$ and from fig. 2, one obtains the limitation

$$|X| \leqq 0.08.$$

5. Discussion

Graham, Geiger and Eastwood [8]) obtained from shape measurements the limit $C_P/C_A < 15$. This result was based on Rose and Osborns [21]) considerations, which yield the theoretical shape factor of an A—P transition. The treatment of pseudoscalar interaction has been modified by the above mentioned authors for the following reason.

On evaluating the pseudoscalar matrix element $\int \beta\gamma_5 L$ (L is the lepton covariant) in the non-relativistic approximation of the nucleon and thus expressing the small Dirac components v of its wave function by the large ones u:

$$v = \frac{f(\boldsymbol{\sigma} \cdot \mathbf{p})}{2M}\,u, \quad f = \left(1 + \frac{T-V}{2M}\right)^{-1}$$

(T is the kinetic energy of the nucleon, M its rest mass and V the nuclear potential), then $\int \beta\gamma_5 L$ vanishes in the zero order approximation and one gets [21])

$$\int \beta\gamma_5 L = \frac{1}{2M} \int u_f^* \sigma (L\nabla f + f \nabla L) u_i$$

(∇ denotes differentiation with respect to the coordinates of the decaying nucleon). This means that, without making any further approximations, one has to consider the variations of f as well as L over the nucleus.

Rose and Osborn [21]) neglected the variation of the nuclear potential over the nucleus ($\nabla f = 0$), but did take into account the variations of the lepton waves over the same region ($\nabla L \neq 0$). The latter assumption is in contrary to the conventional theory of β-decay, which implies that the nuclear matrix elements are regarded as numbers independent of the parameters describing the lepton fields.

However, on calculating the theoretical polarization in the present work, the following approximation was made: $\nabla f \neq 0$, $\nabla L = 0$. This was suggested by Konopinsky and is in agreement with conventional theory. With these assumptions Alaga, Kofoed-Hanson and Winther [23]) got $\int\beta\gamma_5/\int\sigma_r \approx T^2R/6M$ (R is the radius of the decaying nucleus). If one assumes $T = 30$ MeV, this leads to $\int\beta\gamma_5/\int\sigma_r \approx \frac{1}{270}$ for Pr^{144}. Together with the experimental result $|X| \leqq 0.08$ one then obtains

$$\left|\frac{C_P}{C_A}\right| \leqq 20.$$

The theory of Rose and Osborn[21]) predicts that a pure pseudoscalar transition has a spectrum whose shape is very different from that of an allowed transition. According to the conventional theory of β-decay, however, the former transition has an allowed spectrum. Therefore, results regarding the pseudoscalar contribution to a β-transition are very sensitive to theoretical assumptions when they are obtained by shape measurements. This is not the case when the same results are reached by polarization measurements. Here theory unambiguously predicts opposite polarizations for pure A and P extreme relativistic β-rays, because of the fact that the pseudoscalar operator anticommutes with γ_5 but the axial operator commutes with it. Thus conclusions concerning the pseudoscalar contributions drawn from polarization experiments seem to be somewhat more certain then those obtained by shape measurements.

The authors would like to thank Dr. J. Burde for helpful discussions and for kindly placing at their disposal the lens spectrometer. They also are greatly indebted to Dr. G. Rakavy for his help in the theoretical part of this work, and to Dr. G. Goldring for advice.

References

1) M. Goldhaber, L. Grodzins and W. Sunyar, Phys. Rev. **109** (1958) 1015
2) F. Boehm and A. H. Wapstra, Phys. Rev. **109** (1958) 456
3) W. B. Herrmansfeldt, D. R. Maxson, P. Stahelin and J. S. Allen, Phys. Rev. **107** (1957) 641
4) R. P. Feynman, and M. Gellman, Phys. Rev. **109** (1958) 193
5) F. C. G. Sudarshan and R. E. Marshall, Phys. Rev. **109** (1958) 1960
6) M. Goldberger and S. Treiman, Phys. Rev. **110** (1958) 1478
7) M. J. Laubitz, Proc. Phys. Soc. A **69** (1956) 789
8) R. L. Graham, J. S. Geiger and T. A. Eastwood, Can. J. Phys. **36** (1958) 1084
9) H. Fraunfelder, R. Bobone, E. von Goeler, N. Levine, H. R. Lewis, R. N. Peacock, A. Rossi and G. de Pasquali, Phys. Rev. **106** (1957) 386
10) M. Goldhaber, L. Grodzins and W. Sunyar, Phys. Rev. **106** (1957) 826
11) De Waard and Poppema, Physica **23** (1957) 597
12) N. Benczer-Koller, A. Schwarzschild, I. B. Vise and C. S. Wu, Phys. Rev. **109** (1958) 85
13) T. D. Lee and L. N. Yang, Phys. Rev. **105** (1957) 1671
14) Ketelle and Brosi, (see ref. [10]))
15) D. E. Alburger, Phys. Rev. **88** (1952) 339

16) K. W. Mc Voy, Phys. Rev. **106** (1957) 828
17) S. B. Gunst and C. A. Page, Phys. Rev. **92** (1953) 790
18) I. S. Geiger, G. I. Ewan, R. L. Graham and D. R. MacKenzie, Phys. Rev. **112** (1958) 1684
19) G. Rakavy, Private communication
20) M. E. Rose, Phys. Rev. **51** (1937) 484
21) M. E. Rose and K. Osborn, Phys. Rev. **93** (1954) 1315
22) E. J. Konopinsky, Phys. Rev. **74** (1954) 492
23) G. Alaga, O. Kofoed-Hansen and A. Winther, Mat. Phys. Med. Dan. Vid. Selsk., No. 28 (1953)

1.C

Nuclear Physics **15** (1960) 89—91; © *North-Holland Publishing Co., Amsterdam*

Not to be reproduced by photoprint or microfilm without written permission from the publisher

UNE DÉMONSTRATION SIMPLIFIÉE DU THÉORÈME DE WICK EN MÉCANIQUE STATISTIQUE

MICHEL GAUDIN

Département de Recherche Physique, Centre d'Etudes Nucléaires de Saclay, Gif-sur Yvette (S. &. O)

Reçu le 9 Septembre 1959

Abstract: Wick's theorem in statistical mechanics is proved directly by using the commutation rules.

Nous proposons une démonstration du théorème de Wick généralisé [1]) concernant la valeur moyenne, au sens de la mécanique statistique, d'un produit d'opérateurs de création et d'annihilation de bosons ou de fermions. Ce théorème est à la base d'un développement du potentiel de Gibbs en termes de diagrammes, analogue à celui de Goldstone pour l'énergie de l'état fondamental.

L'opérateur statistique ρ du système non perturbé est un produit d'opérateurs ρ_k, relatifs à chaque état k, commutant les uns avec les autres:

$$\rho_k = \frac{e^{-\beta E_k n_k}}{\mathrm{Tr}\, e^{-\beta E_k n_k}},$$

où

$$n_k = \eta_k^\dagger \eta_k,$$

et

$$E_k = \varepsilon_k - \lambda,$$

ε_k étant l'énergie de l'état k et λ le potentiel chimique. Les opérateurs η et $\eta^\dagger$ suivent les règles de commutation habituelles. Nous poserons

$$[\eta\eta^\dagger] = \eta\eta^\dagger - \varepsilon\eta^\dagger\eta,$$

où ε est égal à $+1$ ou à -1 suivant que η est un opérateur de boson ou de fermion.

Il s'agit de calculer $\mathrm{Tr}\{abcd \ldots ef\rho\}$, où $abcd \ldots ef$ est un produit quelconque de $2n$ opérateurs de création ou d'annihilation. Un tel produit n'a d'éléments diagonaux dans le nombre total de particules que s'il contient autant d'opérateurs de création que d'annihilation. Pour un nombre impair d'opérateurs la trace considérée est donc nulle. Nous allons montrer que si le théorème est vrai pour tout produit de $2(n-1)$ opérateurs, il est vrai aussi pour $2n$ opérateurs.

En commutant successivement a avec les opérateurs $b, c, \ldots f$, nous obtenons

$$\begin{aligned}
&\mathrm{Tr}\{abcd\ldots ef\rho\}\\
&= \mathrm{Tr}\{[ab]cd\ldots ef\rho\}+\varepsilon\,\mathrm{Tr}\,\{b[ac]d\ldots ef\rho\}\\
&+ \mathrm{Tr}\{bc[ad]\ldots ef\rho\}+\ldots+\mathrm{Tr}\{bcd\ldots e[af]\rho\}\\
&+\varepsilon\,\mathrm{Tr}\{bcd\ldots efa\rho\}.
\end{aligned}\tag{1}$$

Les crochets du type $[ab]$ sont des nombres purs égaux à 1, -1 ou 0, que l'on peut faire sortir des traces. D'autre part, il est aisé de démontrer les égalités suivantes:

$$\begin{aligned}
e^{-\beta E_k n_k}\eta_k^{\dagger} &= e^{-\beta E_k}\eta_k^{\dagger}e^{-\beta E_k n_k},\\
e^{-\beta E_k n_k}\eta_k &= e^{+\beta E_k}\eta_k\ e^{-\beta E_k n_k};
\end{aligned}$$

d'où l'on déduit

$$\begin{aligned}
\rho\eta_k^{\dagger} &= e^{-\beta E_k}\eta_k^{\dagger}\rho,\\
\rho\eta_k &= e^{+\beta E_k}\eta_k\ \rho.
\end{aligned}$$

Dans la dernière trace du second membre de l'égalité (1), nous pouvons donc remplacer $a\rho$ par $\rho a e^{\pm\beta E}$, en choisissant $e^{\beta E}$ ou $e^{-\beta E}$ suivant que a est un opérateur de création ou d'annihilation; E est l'énergie relative à l'opérateur a. Nous avons donc

$$\mathrm{Tr}\{bcd\ldots efa\rho\} = e^{\pm\beta E}\,\mathrm{Tr}\{abcd\ldots ef\rho\}.$$

Portons ce résultat dans l'égalité (1), faisons passer au premier membre le dernier terme du second membre et divisions par $1-\varepsilon e^{\pm\beta E}$. Nous obtenons

$$\begin{aligned}
&\mathrm{Tr}\{abcd\ldots ef\rho\}\\
&= \frac{[ab]}{1-\varepsilon e^{\pm\beta E}}\,\mathrm{Tr}\{cd\ldots ef\rho\}\\
&+\varepsilon\,\frac{[ac]}{1-\varepsilon e^{\pm\beta E}}\,\mathrm{Tr}\{bd\ldots ef\rho\}\\
&+\ldots\\
&+\frac{[af]}{1-\varepsilon e^{\pm\beta E}}\,\mathrm{Tr}\{bcd\ldots e\rho\}.
\end{aligned}\tag{2}$$

Nous définissons maintenant la contraction de deux opérateurs a et b par l'égalité

$$\overset{\cdot}{a}\overset{\cdot}{b} = \frac{[ab]}{1-\varepsilon e^{\pm\beta E}},$$

où E est l'énergie relative à l'opérateur a. Cette contraction n'est différente de zéro que dans les deux cas suivants:

1°) a est un opérateur de création, soit $\eta_k^\dagger$:

$$\eta_k^{\dagger\cdot}\eta_k^{\cdot} = \frac{[\eta_k^\dagger \eta_k]}{1-\varepsilon e^{-\beta E_k}} = \frac{-\varepsilon}{1-\varepsilon e^{-\beta E_k}} = \frac{1}{e^{\beta E_k}-\varepsilon}.$$

2°) a est un opérateur d'annnihilation, soit η_k:

$$\eta_k^{\cdot}\eta_k^{\dagger\cdot} = \frac{[\eta_k \eta_k^\dagger]}{1-\varepsilon e^{\beta E_k}} = \frac{1}{1-\varepsilon e^{\beta E_k}}.$$

L'égalité (2) s'écrit alors sous la forme

$$\begin{aligned} &\mathrm{Tr}\{abcd \ldots ef\rho\} \\ &= a^{\cdot}b^{\cdot}\,\mathrm{Tr}\{cd \ldots ef\rho\} + \varepsilon a^{\cdot}c^{\cdot}\,\mathrm{Tr}\{bd \ldots ef\rho\} \\ &+ a^{\cdot}d^{\cdot}\,\mathrm{Tr}\{bc \ldots ef\rho\} + \ldots \\ &+ a^{\cdot}f^{\cdot}\,\mathrm{Tr}\,\{bcd \ldots e\rho\}. \end{aligned} \tag{3}$$

Les traces du deuxième membre de cette égalité contiennent $2(n-1)$ opérateurs; si le théorème de Wick est supposé vrai jusqu'à cet ordre, nous reconnaissons au second membre les systèmes de contractions du produit de $2n$ opérateurs a, b, c, d, ... e, f, qui contiennent successivement $a^{\cdot}b^{\cdot}$, $a^{\cdot}c^{\cdot}$, ..., $a^{\cdot}f^{\cdot}$.

Bibliographie

1) T. Matsubara, Progr. Theor. Phys. **14** (1955) 351;
T. Thouless, Phys. Rev. **107** (1957) 1162:
C. Bloch et C. De Dominicis, Nuclear Physics **7** (1958) 459

1.E.5:
2.L

Nuclear Physics **15** (1960) 92—101; © *North-Holland Publishing Co., Amsterdam*
Not to be reproduced by photoprint or microfilm without written permission from the publisher

DISPERSIVE EFFECTS IN ELASTIC ELECTRON SCATTERING BY COMPLEX NUCLEI

K. GOTTFRIED †

Universitetets Institut for Teoretisk Fysik, Copenhagen

Received 17 October 1959

Abstract: A Z-independent estimate of the validity of the conventional analysis of elastic electron scattering is made with the help of an optical potential. It is concluded that the dispersive corrections are always of order 1/137.

1. Introduction

The analysis of elastic electron scattering data †† in terms of a nuclear charge distribution is based on a number of assumptions, the most important of which are:

(I) simplification in the interaction Hamiltonian which describes the coupling of the electron to the nuclear system (e.g. deletion of scattering by anomolous magnetic moments and mesic currents);

(II) neglect of the dynamics of the target, that is to say, neglect of virtual nuclear excitation.

As is well known, (I) and (II) *together* imply that the electron only experiences the average Coulomb field of the nuclear protons, and that the scattering therefore gives direct access to the charge distribution $\rho(\mathbf{x})$. If assumption (II) *alone* is made, the corrections arising from (I) should be quite easy to evaluate and are expected to be very small for the momentum transfers at present observed in scattering by complex nuclei. In this paper we shall assume (I) and confine our attention tρ (II). Corrections arising from virtual meson production are not taken into account.

If the scattering amplitude is computed with the Born series, the dispersive effects begin to appear in second order. Schiff [3]), Downs [4]) and Lewis [5]) have reported such second order Born calculations and concluded that the dispersive effects are negligible, except possibly at diffraction minima. Unfortunately the Born series is not reliable for heavier nuclei ($Z \gtrsim 8$), and their work does not, therefore, lead to unambiguous conclusions for the majority of elements. Schiff [6]) has also studied the scattering amplitude with the high energy approximation. His derivations are valid for all Z, but the resulting expressions are

† Present Address: Physics Department Harvard, University, Cambridge, Mass.

†† For recent resumés of this work the reader is referred to the articles by Hofstadter [1, 2]).

rather complicated, and consequently no estimate of dispersive corrections is given.

As the electron scattering data are already very precise, it would be desirable to have a reliable estimate of the validity of the conventional analysis in terms of a static charge distribution which is not limited to small Z. In this note we wish merely to point out that a simple estimate valid for large Z can be made with the general theory of the optical model due to Watson [7]) (see also ref. [8])). *The advantage of this procedure is that the optical potential possesses an expansion in powers of e^2, whereas the scattering amplitude is a complicated function of Ze^2.* In the next section we shall estimate this potential seen by the incident electron; the elastic scattering is thereby reduced to a one-body problem, and can therefore be solved exactly, or if warranted, some further approximation scheme can be employed.

2. The Optical Potential

Let v_α be the Coulomb field of the α^{th} proton. Then the Coulomb field of the ground state charge distribution is

$$V_0 = \sum_{\alpha=1}^{Z} \langle v_\alpha \rangle_0, \tag{1}$$

where $\langle \ldots \rangle_0$ designates the ground state expectation value. The field actually experienced by the electron, the "optical" potential, is then

$$V = V_0 + \delta V; \tag{2}$$

according to Watson [7]) (cf. also ref. [8]), especially (eq. 16)) the correction term is

$$\delta V \approx \sum_{\alpha,\beta} \left\langle v_\alpha \frac{1-\Lambda_0}{p_0+E_0-h-H_N-V_0+i\varepsilon} v_\beta \right\rangle_0. \tag{3}$$

Here p_0 and E_0 are the energies of the incident electron and target ground state respectively, $h = \boldsymbol{\alpha} \cdot \mathbf{p}_{\text{op}}$ and H_N the free electron and nuclear Hamiltonians respectively, and Λ_0 the projection operator onto the target's ground state †. Eq. (3) is not quite an exact expression for δV since the electron-nucleus interaction appearing in the exact propagator is replaced by V_0 itself. Since, however, the charge distribution is fairly independent of excitation energy, (3) is expected to give an accurate representation of δV ††.

We shall estimate (3) by further approximating the propagator. The operator $H_N - E_0$ will be replaced by an average virtual excitation energy $\bar{E}_{\text{exc}}$, which

† $\hbar = c = 1$, and the electron mass is put equal to zero.

†† V_0 and δV are still operators in the electron's Hilbert space; the electron's momentum space wave function $\chi(\mathbf{p})$ satisfies

$$(\boldsymbol{\alpha} \cdot \mathbf{p} - p_0)\chi(\mathbf{p}) + \int (\mathbf{p}|V|\mathbf{p}')\chi(\mathbf{p}')\mathrm{d}^3\mathbf{p}' = 0.$$

we may expect to depend somewhat on the momentum transfer $\mathbf{q} = \mathbf{p}-\mathbf{p}'$ appropriate to the matrix element $(\mathbf{p}|V|\mathbf{p}')$ in question. This replacement is justified if $\bar{E}_{\text{exc}} \ll p_0$; Schiff [6]) has given quite convincing arguments to show that this condition is actually satisfied for the q's of interest to us. Clearly this approximation is only admissible if the final answer is insensitive to reasonable variations of $\bar{E}_{\text{exc}}$, and as we shall see, this is actually the case. Furthermore we shall replace V_0 by $\bar{V}_0 = \int \rho(\mathbf{x}) V_0(\mathbf{x}) \mathrm{d}^3\mathbf{x}$, the average potential strength † seen by the electron in the nucleus, $\rho(\mathbf{x})$ being the charge distribution normalized to unity. This latter approximation is based on the observation that $V_0(\mathbf{x})$ is very slowly varying inside the nucleus and therefore leads predominantly to forward scattering. Of the two replacements $H_N - E_0 \to \bar{E}_{\text{exc}}$ and $V_0 \to \bar{V}_0$, the former is much more open to question.

Calling

$$E = p_0 - \bar{V}_0 - \bar{E}_{\text{exc}},$$

we have

$$(\mathbf{p}|\delta V|\mathbf{p}') = \int \mathrm{d}^3\mathbf{k} \, \frac{(\mathbf{p}|M_\mathbf{k}|\mathbf{p}')}{E - \boldsymbol{\alpha}\cdot\mathbf{k} + i\varepsilon}, \tag{4}$$

with

$$(\mathbf{p}|M_\mathbf{k}|\mathbf{p}') = \sum_{\alpha,\beta} (\mathbf{p}|\{\langle v_\alpha \lambda_\mathbf{k} v_\beta\rangle_0 - \langle v_\alpha\rangle_0 \lambda_\mathbf{k} \langle v_\beta\rangle_0\}|\mathbf{p}'), \tag{5}$$

$\lambda_\mathbf{k}$ being the projection operator onto the free electron state with momentum $\mathbf{k}$. Now define the correlation function

$$C(\mathbf{x}_1|\mathbf{x}_2) = \rho(\mathbf{x}_1|\mathbf{x}_2) - \rho(\mathbf{x}_1)\rho(\mathbf{x}_2), \tag{6}$$

where

$$\rho(\mathbf{x}_1|\mathbf{x}_2) = \sum_{\text{spin}} \int \mathrm{d}^3\mathbf{x}_3 \ldots \mathrm{d}^3\mathbf{x}_Z \mathrm{d}^3\mathbf{y}_1 \ldots \mathrm{d}^3\mathbf{y}_{Z-A} \cdot |\Psi_0(\mathbf{x}_1 \ldots \mathbf{y}_{Z-A})|^2, \tag{7}$$

$$\rho(\mathbf{x}) = \int \mathrm{d}^3\mathbf{x}' \rho(\mathbf{x}|\mathbf{x}'), \tag{8}$$

Ψ_0 being the nuclear ground state wave function, the $\mathbf{x}$'s and $\mathbf{y}$'s proton and neutron coordinates respectively, and $\sum_{\text{spin}}$ indicating a sum over *all* nucleon spin variables. Eq. (5) now reads

$$(\mathbf{p}|M_\mathbf{k}|\mathbf{p}') = (\mathbf{p}|M_\mathbf{k}^{(1)}|\mathbf{p}') + (\mathbf{p}|M_\mathbf{k}^{(2)}|\mathbf{p}'), \tag{9}$$

$$(\mathbf{p}|M_\mathbf{k}^{(1)}|\mathbf{p}') = Z(2\pi^3) v(K_1)[f(q) - (2\pi)^3 f(K_1) f(K_2)] v(K_2), \tag{9a}$$

$$(\mathbf{p}|M_\mathbf{k}^{(2)}|\mathbf{p}') = Z(Z-1)(2\pi)^6 v(K_1) D(\mathbf{K}_1|\mathbf{K}_2) v(K_2), \tag{9b}$$

with

$$v(k) = \frac{e^2}{2\pi^2} \frac{F(k)}{k^2}, \tag{10}$$

† $\bar{V}_0 \approx 10$ MeV for $Z = 20$, $\bar{V}_0 \approx 20$ MeV for $Z = 90$.

$F(k)$ being the proton's electric form factor [1, 2]), while

$$D(\mathbf{K}_1|\mathbf{K}_2) = (2\pi)^{-6}\int d^3\mathbf{x}_1 d^3\mathbf{x}_2 e^{-i(\mathbf{K}_1\cdot\mathbf{x}_1+\mathbf{K}_2\cdot\mathbf{x}_2)} C(\mathbf{x}_1|\mathbf{x}_2), \quad (\mathbf{K}_1 = \mathbf{p}-\mathbf{k},\quad \mathbf{K}_2 = \mathbf{k}-\mathbf{p}',\quad \mathbf{q} = \mathbf{K}_1+\mathbf{K}_2), \tag{11a}$$

and

$$f(k) = (2\pi)^{-3}\int d^3\mathbf{x} e^{-i\mathbf{k}\cdot\mathbf{x}}\rho(\mathbf{x}) \tag{11b}$$

is the ordinary elastic form factor.

According to these definitions

$$D(\mathbf{K}|0) = 0, \tag{12a}$$

or equivalently

$$\int d^3\mathbf{x}_1 C(\mathbf{x}_1|\mathbf{x}_2) = 0. \tag{12b}$$

Moreover

$$\lim_{\substack{\mathbf{k}\to\mathbf{p}\\ \text{or}\\ \mathbf{k}\to\mathbf{p}'}} [f(\mathbf{p}-\mathbf{p}') - (2\pi)^3 f(\mathbf{p}-\mathbf{k}) f(\mathbf{k}-\mathbf{p}')] = 0. \tag{12c}$$

As one can see from (3) or (9), eqs. (12a, c) are simply a concise form of the trivial statement that it is not possible to excite a system by applying to it a spatially constant potential (i.e. supplying zero momentum transfer).

We first consider $M^{(2)}$ (cf. (9b)) which arises from those terms of (5) for which $\alpha \neq \beta$. Here the electron excites the target by striking proton α, and then deexcites by collision with a *different* proton β, something which can only occur if α and β are correlated. It is frequently stated that the quantity which describes this correlation, the function $C(\mathbf{x}_1|\mathbf{x}_2)$, tends to zero rapidly as $|\mathbf{x}_1-\mathbf{x}_2|$ increases beyond the mean inter-nucleon separation. This statement is almost correct, but the slight error it contains is just sufficient to violate condition (12a, b) †. This point can be understood by examining the independent particle model (with Pauli principle, of course). In this case

$$\rho(\mathbf{x}) = \frac{2}{N}\sum_{n=1}^{\frac{1}{2}N} |\varphi_n(\mathbf{x})|^2,$$

$$C(\mathbf{x}_1|\mathbf{x}_2) = \frac{1}{N-1}\rho(\mathbf{x}_1)\rho(\mathbf{x}_2) - \Gamma(\mathbf{x}_1|\mathbf{x}_2), \tag{13}$$

with

$$\Gamma(\mathbf{x}_1|\mathbf{x}_2) = \frac{2}{N(N-1)}\left|\sum_{n=1}^{\frac{1}{2}N} \varphi_n(\mathbf{x}_1)\varphi_n^*(\mathbf{x}_2)\right|^2,$$

the $\varphi_n(\mathbf{x})$ being the single-particle orbitals. One easily verifies that $(N-1)\int d^3\mathbf{x}_1 \Gamma(\mathbf{x}_1|\mathbf{x}_2) = \rho(\mathbf{x}_2)$ i.e. (12b) is satisfied. The character of the two

† See Lewis [4]), footnote 8, for a related observation.

terms of (13) is greatly clarified if one considers a large system of N particles contained in a volume Ω. Then $\rho(\mathbf{x}) = 1/\Omega$, and

$$\Gamma(\mathbf{x}_1|\mathbf{x}_2) = \tfrac{9}{2}\Omega^{-2}\left(\frac{\sin k_F r - k_F r \cos k_F r}{(k_F r)^3}\right)^2 \equiv \Gamma(r),$$

where k_F is the Fermi momentum and $r = |\mathbf{x}_1 - \mathbf{x}_2|$. Thus at $r = 0$ the first term of (13) equals $1/\Omega^2 N$ while $\Gamma(0)$ is larger than this factor $\frac{1}{2}N$. For $k_F r \gg 1$, $\Gamma(r)$ falls off as $(k_F r)^{-4}$, and thus, for most values of r, $C(r)$ can be said to have a range of the order of the interparticle spacing. Nevertheless, for $r > r_c$, with

$$r_c = \frac{0.76}{N^{1/3}} R, \qquad R = \text{radius of system},$$

$C(r)$ approaches the exceedingly small constant value $(\Omega^2 N)^{-1}$ †. From these observations we conclude that

$$D(\mathbf{K}_1|\mathbf{K}_2) = (2\pi)^{-6}\int d^3\mathbf{x}_1 d^3\mathbf{x}_2 e^{-i(\mathbf{K}_1\cdot\mathbf{x}_1 + \mathbf{K}_2\cdot\mathbf{x}_2)}\Gamma(\mathbf{x}_1|\mathbf{x}_2), \tag{14}$$

unless $K_1 R$ and/or $K_2 R$ are less than one. Thus the usual assumption concerning $C(\mathbf{x}_1|\mathbf{x}_2)$, which in effect ignores the first term of (13), leads to a $D(\mathbf{K}_1|\mathbf{K}_2)$, which in effect ignores the first term of (13), leads to a $D(\mathbf{K}_1|\mathbf{K}_2)$ correct everywhere except in very small neighbourhoods surrounding $\mathbf{K}_1 = 0$ and $\mathbf{K}_2 = 0$. At these points the approximate form (14) fails to satisfy (12a). In problems involving forces of finite range such an approximation to $D(\mathbf{K}_1|\mathbf{K}_2)$ does not lead to any serious consequences because $v(k)$ is well behaved at $k = 0$. In the Coulomb case, however, the small momentum transfers are greatly favoured, and a $D(\mathbf{K}_1|\mathbf{K}_2)$ finite at $\mathbf{K}_1$ (or $\mathbf{K}_2$)$=0$ leads to a divergence in the imaginary part of δV ††.

Unfortunately it is quite difficult to work with a correlation function which satisfies (12a, b), and we have been forced to employ a device which simulates the essential consequences of this condition. This device is based on the fact that for $K_1 R \ll 1$, $D(\mathbf{K}_1|\mathbf{K}_2)$ is proportional to K_1 (dipole transitions only!), which means that

$$v(K_1)D(\mathbf{K}_1|\mathbf{K}_2)v(K_2) \xrightarrow[K_1 R \ll 1]{} \frac{2\pi^2 K_1}{e^2}\left[\hat{\mathbf{K}}_1 \cdot \frac{\partial}{\partial \mathbf{K}_1} D(\mathbf{K}_1|\mathbf{K}_2)\right]_{\mathbf{K}_1=0} \cdot v(K_2).$$

We therefore claim that if the replacement

$$v(k) \to u(k) = \frac{e^2}{2\pi^2}\frac{F(k)}{k^2+\gamma k} \qquad (\gamma \approx 1/R) \tag{15}$$

† Note that for reasonable values of N, r_c is a considerable fraction of R; thus for $N = 200$, $r_c \approx \frac{1}{2}R$.

†† In the second order calculations of refs. [3-5]) only the real part of δV enters. A third order Born calculation using the correlation functions assumed by these authors leads to the divergence.

is made, one can also approximate $C(\mathbf{x}_1|\mathbf{x}_2)$ by a short range pair correlation function. In fact we shall now put

$$C(\mathbf{x}_1|\mathbf{x}_2) = -\rho(\mathbf{x}_1)\rho(\mathbf{x}_2)\Delta(|\mathbf{x}_1-\mathbf{x}_2|), \tag{16}$$

with $\Delta(r)$ tending to zero rapidly for $k_F r \gtrsim 1$. Taking advantage of the slowly varying nature of $\rho(\mathbf{x})$ we have

$$D(\mathbf{K}_1|\mathbf{K}_2) \approx -\tfrac{1}{2}G(q)[\tilde{\Delta}(K_1)+\tilde{\Delta}(K_2)], \tag{17}$$

where

$$\tilde{\Delta}(k) = (2\pi)^{-3}\int e^{i\mathbf{k}\cdot\mathbf{r}}\Delta(r)d^3\mathbf{r}, \tag{18}$$

and

$$G(k) = (2\pi)^{-3}\int e^{-\mathbf{k}\cdot\mathbf{x}}|\rho(\mathbf{x})|^2 d^3\mathbf{x}. \tag{19}$$

Now the quantity of central interest is the ratio $\delta V/V_0$, or more precisely,

$$\frac{(\mathbf{p}|\delta V|\mathbf{p})}{(\mathbf{p}|V_0|\mathbf{p})} = U^{(1)}(\mathbf{p}|\mathbf{p}')+U^{(2)}(\mathbf{p}|\mathbf{p}') + \boldsymbol{\alpha}\cdot[\mathbf{W}^{(1)}(\mathbf{p}|\mathbf{p}')+\mathbf{W}^{(2)}(\mathbf{p}|\mathbf{p}')], \tag{20}$$

with

$$(\mathbf{p}|V_0|\mathbf{p}') \equiv V_0(q) = 4\pi Ze^2 f(q)/q^2.$$

The superscripts on U and $\mathbf{W}$ indicate whether they arise from $M^{(1)}$ or $M^{(2)}$ (cf. eq. (9)).

At the high energies we are concerned with, the scattered wave tends to stay in the vicinity of the energy shell, and so we shall confine our attention to the matrix elements having $p \approx p' \approx p_0(\approx E)$. Consider first the imaginary part of $U^{(2)}$. Combining (4), (9b), (15) and (17) we have †

$$\operatorname{Im} U^{(2)}(\mathbf{p}|\mathbf{p}') = 2\pi^2(Z-1)e^2\frac{G(q)}{f(q)}Eq^2 I^{(2)}(\mathbf{p}|\mathbf{p}'), \tag{21}$$

with

$$I^{(2)}(\mathbf{p}|\mathbf{p}') = \int\frac{\delta(E^2-k^2)F(K_1)[\tilde{\Delta}(K_1)+\tilde{\Delta}(K_2)]}{(K_1^2+\gamma K_1)(K_2^2+\gamma K_2)}d^3\mathbf{k}. \tag{22}$$

In the independent particle model $\tilde{\Delta}(k)$ is positive definite and attains its maximum value at $k = 0$; we shall assume this also to be true of the actual correlation function. We also recall that $0 \leqq F(k) \leqq 1$. Therefore,

$$\begin{aligned} I^{(2)}_{\max}(\mathbf{p}|\mathbf{p}') &= 2\tilde{\Delta}(0)\int\frac{\delta(E^2-k^2)d^3\mathbf{k}}{(K_1^2+\gamma K_1)(K_2^2+\gamma K_2)} \\ &= E\tilde{\Delta}(0)\int\frac{d\hat{\mathbf{k}}}{[(\mathbf{p}-E\hat{\mathbf{k}})^2+\gamma|\mathbf{p}-E\hat{\mathbf{k}}|]\,[(\mathbf{p}'-E\hat{\mathbf{k}})^2+\gamma|\mathbf{p}'-E\hat{\mathbf{k}}|]} \end{aligned} \tag{23}$$

† The fact that $\operatorname{Im} U^{(2)}(\mathbf{p}|\mathbf{p})$ is positive does not contradict the requirement that the optical potential be absorptive. It is sufficient for $\operatorname{Im}[U^{(1)}(\mathbf{p}|\mathbf{p})+U^{(2)}(\mathbf{p}|\mathbf{p})]$ to be negative, which will be seen to be the case.

provides a rigorous upper bound to Im $U^{(2)}(\mathbf{p}|\mathbf{p}')$. We have not succeeded in integrating (23) analytically, and are only able to give an asymptotic evaluation valid for $\gamma \to 0$ (i.e. for very heavy nuclei). In this limit, and provided $q > \gamma$, the integrand of (23) has two sharp maxima at $\hat{\mathbf{k}} \approx \hat{\mathbf{p}}$ and $\hat{\mathbf{k}} \approx \hat{\mathbf{p}}'$, and we can replace $\hat{\mathbf{k}}$ by $\hat{\mathbf{p}}$ in $[(\mathbf{p}'-E\hat{\mathbf{k}})^2+\gamma|\mathbf{p}'-E\hat{\mathbf{k}}|]$ when $\hat{\mathbf{k}} \approx \hat{\mathbf{p}}$, and vice versa. Therefore

$$\begin{aligned} I^{(2)}_{\max} &\underset{\gamma\to 0}{\approx} \frac{E\tilde{\Delta}(0)}{q^2}\int \mathrm{d}\hat{\mathbf{k}}\left(\frac{1}{K_1^2+\gamma K_1}+\frac{1}{K_2^2+\gamma K_2}\right) \\ &\approx \frac{\tilde{\Delta}(0)}{q^2}\left\{\frac{1}{p}\ln\left(\frac{p+E}{|p-E|+\gamma}\right)+\frac{1}{p'}\ln\left(\frac{p'+E}{|p'-E|+\gamma}\right)\right\}. \end{aligned} \tag{24}$$

Furthermore $q^2 I^{(2)}_{\max} \to 0$ for $q \to 0$ for all $\gamma \neq 0$, i.e. for any finite Z. We note that (24) is largest when $p = p' = E$, and we have, therefore,

$$\begin{aligned} \operatorname{Im} U^2(\mathbf{p}|\mathbf{p}') &< 2\pi^2 Ze^2 \frac{G(q)}{f(q)}\,\tilde{\Delta}(0)\,\ln 2pR \\ &\qquad \text{if } qR > 1, \\ &= 0 \quad \text{if} \quad q = 0. \end{aligned} \tag{25}$$

The functions $\rho(\mathbf{x})$ and $|\rho(\mathbf{x})|^2$ having nearly the same dependence on $\mathbf{x}$, comparison of (11b) and (19) yields

$$G(q)/f(q) \approx 1/\Omega. \tag{26}$$

An extreme upper bound to $\tilde{\Delta}(0)$ is obtained by assuming $C(\mathbf{x}_1|\mathbf{x}_2)$ to *vanish* identically for $|\mathbf{x}_1-\mathbf{x}_2|$ smaller than the average inter-particle distance, i.e.

$$\tilde{\Delta}(0) < \frac{1}{(2\pi)^3}\int_{|\mathbf{x}|<\omega^{\frac{1}{3}}} \mathrm{d}^3\mathbf{x} = \frac{\omega}{6\pi^2}, \tag{27}$$

where ω is the volume per particle ($A\omega = \Omega$). Thus we finally have †

$$\operatorname{Im} U^{(2)}(\mathbf{p}|\mathbf{p}') < \tfrac{1}{3}\frac{Z}{A}e^2 \ln 2pR. \tag{28}$$

It should be stressed that (28) represents a gross overestimate of Im $U^{(2)}$ since $\tilde{\Delta}(0)$ is certainly much smaller than $\omega/6\pi^2$: the success of the shell model precludes such monstrous correlations. Nevertheless the right hand side of (28) is only $0.64\,e^2$ for uranium with $p = 1$ GeV/c.

Next consider

$$\operatorname{Re} U^{(2)}(\mathbf{p}|\mathbf{p}') = -2\pi(Z-1)e^2\frac{G(q)}{f(q)}\,Eq^2 R^{(2)}(\mathbf{p}|\mathbf{p}'), \tag{29}$$

† We should point out that the divergence of eq. (28) as $R \to \infty$ is spurious. In a really large medium the electron's Coulomb field is screened, and the imaginary part of the refractive index is therefore always of order e^4.

with

$$R^{(2)}(\mathbf{p}|\mathbf{p}') = \mathrm{P}\int \frac{F(K_1)[\tilde{\Delta}(K_1)+\tilde{\Delta}(K_2)]F(K_2)}{(K_1^2+\gamma K_1^2)(E^2-k^2)(K_2^2+\gamma K^2)}\,\mathrm{d}^3\mathbf{k}. \tag{30}$$

It is important to retain the proton form factors when evaluating (30). This is because the proton's charge radius is of the same magnitude as the correlation length, and consequently the correlation scattering is somewhat washed out in comparison to that of a system composed of point protons. On the other hand the integral in (30) is well behaved at $\gamma = 0$, and one can revert to the unmodified Coulomb denominators here.

For the form factor we take $F(k) = b^2(b^2+k^2)^{-1}$, with $b^2 = 8.0\times 10^{26}$ cm^{-2}; this corresponds to a Yukawa charge distribution which fits the data (fig. 8 of ref. [2])) quite well up to momentum transfers of 650 MeV/c, and is therefore adequate for our purpose. The choice of $\tilde{\Delta}(k)$ is far more arbitrary, of course. We first define a correlation length r_{corr} by

$$(2\pi)^3\tilde{\Delta}(0) = \tfrac{4}{3}\pi r_{\mathrm{corr}}^3 = \int \Delta(r)\mathrm{d}^3\mathbf{r}; \tag{31}$$

we may expect r_{corr} to lie between 0.5 and 1.0×10^{-13} cm. A simple correlation function is then †

$$\tilde{\Delta}(k) = \frac{r_{\mathrm{corr}}^3}{6\pi^2}\left(\frac{a^2}{a^2+k^2}\right)^2, \quad a^2 r_{\mathrm{corr}}^2 = 12, \tag{32}$$

which corresponds to an exponential $\Delta(r)$ with r.m.s. radius $\sqrt{\frac{3}{5}}\times r_{\mathrm{corr}}$. With this choice of $\tilde{\Delta}(k)$ and $F(k)$ we can reduce (30) to integrals already evaluated by Lewis [9]), and we then find that for $0.5 \leqq r_{\mathrm{corr}} \leqq 1.0\times 10^{-13}$ cm, 200 MeV/c $\leqq p_0 \leqq$ 1 GeV/c, Re $U^{(2)}$ is *always considerably smaller than* e^2, and varies slowly as p, p' and E are varied about the energy shell p_0.

We now turn to $U^{(1)}$ which arises from processes where the same proton is excited and subsequently de-excited. Here the finer details of the charge distribution are of no importance, and so we put $F(k) = 1$. From (4) and (9a) we then have

$$U^{(1)}(\mathbf{p}|\mathbf{p}') = \frac{e^2}{2\pi^2}q^2 E\int \frac{[1-(2\pi)^3 f(K_1)f(K_2)/f(q)]}{K_1^2(E^2-k^2+i\varepsilon)K_2^2}\,\mathrm{d}^3\mathbf{k}. \tag{33}$$

Re $U^{(1)}$ has been evaluated by Lewis [5]) for an exponential model of $f(K)$, and we shall confine ourselves to recalling that he finds corrections of order 3 %

† In Lewis' article [5]) the correlation function is always normalized so that $\int\Delta(r)\mathrm{d}^3\mathbf{r} = \omega$ (in his notation $\int g(r)\mathrm{d}^3\mathbf{r} = 1$). We are of the opinion that *if* the correlation distance is smaller than the inter-particle spacing, there is no normalization requirement at all on $\Delta(r)$, because the normalization of $C(\mathbf{x}_1|\mathbf{x}_2) = \rho(\mathbf{x}_1)\rho(\mathbf{x}_2)[1-\Delta(r)]$ is then independent of $\Delta(r)$ to order $1/N$. The only requirement is that $\Delta(r) \geqq -1$, which is violated with Lewis' normalization when the correlation length is small. Because of this difference in normalization we find considerably smaller values of Re $U^{(2)}$ than Lewis did.

at most. In order to have an order of magnitude estimate of Im $U^{(1)}$ we shall put

$$f(K) = \left(\frac{1}{2\pi}\right)^3 \frac{c^2}{c^2+K^2},$$

with $c^2 = 6.95\, A^{-\frac{2}{3}} \times 10^{26}\ \mathrm{cm}^{-2}$, which corresponds to an r.m.s. radius of $\sqrt{\frac{3}{5}} \times 1.20\, A^{\frac{1}{3}} \times 10^{-13}$ cm. Again using Lewis' [9]) integrals we find ($p = p' = p_0 = E$)

$$\mathrm{Im}\, U^{(1)}(\mathbf{p}|\mathbf{p}') = \tfrac{1}{2}e^2 \left\{ \frac{q^2}{c^2} \ln \left[\frac{q^2(4p_0^2+c^2)c^2}{4p_0^2(q^2+c^2)^2} \right] + \frac{qp_0}{Y} \frac{q^2+c^2}{c^2} \ln \left(\frac{Y+qp_0}{Y-qp_0} \right) \right\}, \quad (34)$$

with $Y^2 = (p_0^2q^2+4c^2p_0^2+c^4)$. The limiting behaviour of (34) is given by

$$\mathrm{Im}\, U^{(1)} \sim \begin{cases} -\frac{3}{8}e^2 & \text{for } q \gg c,\ p_0 \gg c, \quad (35a) \\ -\frac{1}{2}e^2 \left(\frac{q}{c}\right)^2 \left[\ln \left(\frac{c^2}{q^2}\right) - 2 \right] & \text{for } q \ll c,\ p_0 \gg c. \quad (35b) \end{cases}$$

The terms proportional to α may be computed by the well known method of Dalitz [10]); they lead to contributions of the same size as those discussed above.

3. Conclusions

1) The scattering of electrons by complex nuclei can be conveniently described by an optical potential, the leading term of which is the Coulomb field of the ground state charge distribution. The correction terms are of order e^2, i.e. essentially *independent of* Z.

2) The corrections arising from virtual correlation scattering are considerably smaller than e^2 and therefore completely negligible.

3) Those corrections which are due to virtual excitation of single protons are probably slightly larger than e^2. Extensive calculations with realistic elastic form factors $f(k)$ should be made in order to substantiate or invalidate this *very* tentative conclusion.

The author takes great pleasure in thanking Prof. N. Bohr, Prof. A. Bohr, and the members of the Institute for the kind hospitality extended to him. This work was initiated while the author was a Junior Fellow in the Society of Fellows, Harvard University, and a guest of the Theoretical Group, CERN, Geneva; the support and hospitality of these institutions is gratefully acknowledged.

References

1) R. Hofstadter, Revs. Mod. Phys. **28** (1956) 214
2) R. Hofstadter, Ann. Rev. Nuclear Science **7** (1957) 213
3) L. I. Schiff, Phys. Rev. **98** (1955) 756
4) B. W. Downs, Phys. Rev. **101** (1956) 820
5) R. R. Lewis, Phys. Rev. **102** (1956) 544
6) L. I. Schiff,Nuovo Cimento **5** (1957) 1223
7) K. M. Watson, Phys. Rev. **105** (1957) 1388
8) H. Feshbach, Ann. Rev. Nuclear Science **8** (1958) 49
9) R. R. Lewis, Phys. Rev. **102** (1956) 537
10) R. H. Dalitz, Proc. Roy. Soc. A **206** (1951) 509

7.A:8.B

Nuclear Physics **15** (1960) 102—107; © *North-Holland Publishing Co., Amsterdam*

Not to be reproduced by photoprint or microfilm without written permission from the publisher

PROOF OF DISPERSION RELATIONS FOR PION-HYPERON SCATTERING

Y. S. JIN †

Office of Atomic Energy, Seoul, Korea

Received 18 September 1959

Abstract: Proof of dispersion relations for elastic and inelastic pion-hyperon scattering $Y_1+\pi_1 \to Y_2+\pi_2$ (where Y is Λ- or Σ-hyperon) is presented. Though the mass-difference $M_\Sigma - M_\Lambda$ gives rise to a small unphysical region which survives even for the forward scattering, the method of Lehmann and Oehme and Taylor allows us to derive dispersion relations for these processes up to a momentum-transfer $2\mu^2$ or $3\mu^2$.

1. Introduction

Recently, H. Lehmann [1]) and R. Oehme and J. G. Taylor [2]) succeeded to prove dispersion relations in a rigorous way for (N, π), (π, π) and (Ξ, π) scattering and pion photoproduction in the lowest order in the electromagnetic interaction, by making use of the Dyson-Jost-Lehmann [3]) integral representation of the causal commutator.

In this paper, we present the proof of the dispersion relations for the pion-hyperon scattering $Y_1+\pi_1 \to Y_2+\pi_2$, where Y is $\Lambda-$ or $\sum$-hyperon. Though we are rather far from being able to use these processes for practical purposes, it might not be of mere academic interest to consider them, since these processes appear already as intermediate transitions in some processes of immediate physical interest, e.g., $\overline{K}+N \to \overline{K}+N$ or $\overline{K}+N \to Y+\pi$, so that the result could perhaps be useful in a future proof of dispersion relations for such processes, while the failure so far to prove them seems to be caused by the inability to take into account the information about the intermediate states [4]). Besides, it could also in the future be applied to the analysis of the relevant processes themselves, e.g., for the determination of the coupling constants, as soon as these processes are accessible in a laboratory.

We proceed along the line of refs. [1]) and [2]). There exists in fact a competing channel $Y+\pi \to N+\overline{K}$; however, it does not matter at all, because its threshold is higher than that for the scattering processes under consideration. The mass-difference $(M_\Sigma - M_\Lambda)$, which we do not neglect in our treatment, gives rise to a small unphysical region which even survives for the forward scattering of

† This work has been done during the author's stay at the Swiss Federal Institute of Technology, Zürich.

$\Sigma+\pi \to \Sigma+\pi$ and $\Lambda+\pi \to \Sigma+\pi$, but our method covers this small unphysical region, provided the momentum-transfer is smaller than $2\mu^2$ or $3\mu^2$, respectively.

2. Integral Representation of Absorptive Part

We consider the scattering process $Y_1+\pi_1 \to Y_2+\pi_2$. Let the four-momenta of Y_i be p_i, and those of π_i be $k_i (i = 1, 2)$. Now we introduce the following kinematical variables:

$$\omega = \frac{(p_1+p_2)(k_1+k_2)}{2\sqrt{(p_1+p_2)^2}}, \quad 4\Delta^2 = -(k_1-k_2)^2, \quad k_1^2 = k_2^2 = \zeta. \tag{1}$$

The additional variable ζ ($\zeta = \mu^2$ for the physical pion) is introduced as usual for the purpose of the analytic continuation. Then, in the Breit frame ($\mathbf{p}_1+\mathbf{p}_2 = 0$), we obtain

$$\pi_x^2 = \frac{\Delta^2}{\Delta^2+\varepsilon^2}\omega^2-\Delta^2-\zeta, \quad \pi_y = 0, \quad \pi_z = \frac{\varepsilon\omega}{\sqrt{\Delta^2+\varepsilon^2}}, \tag{2}$$

with

$$(\omega, \boldsymbol{\pi}) = \tfrac{1}{2}(k_1+k_2), \quad \varepsilon = \tfrac{1}{2}(p_{10}-p_{20}), \quad p_i^2 = M_i^2.$$

It is obvious that we can derive dispersion relations for the virtual pion off the mass-shell with mass $\zeta < -\Delta^2$, since then $\boldsymbol{\pi}$ is real for any real $\omega \geqq 0$; besides we need not care about the crossing process, since it is identical with the relevant process. Now the kinematical variables in the c.m.s. turn out to be

$$\begin{aligned} K_i^2(\zeta) = k_i^2 = p_i^2 &= \frac{(W^2+M_i^2-\zeta)^2-4M_i^2W^2}{4W^2}, \\ \cos\theta &= \frac{K_1^2(\zeta)+K_2^2(\zeta)-4\Delta^2-(2W)^{-2}(M_2^2-M_1^2)^2}{2K_1(\zeta)K_2(\zeta)}; \end{aligned} \tag{3}$$

W is the total energy in the c.m.s.

According to Lehmann [1]), the absorptive part of the causal amplitude regarded as a function of W and Δ^2 turns out to be

$$2\,\mathrm{Im}\,T(W, \Delta^2) = [M(W, \zeta, \Delta^2)]_{\zeta=\mu^2}, \tag{4}$$

where

$$\begin{aligned} M(W, \zeta, \Delta^2) = \frac{1}{8\pi K_1(\zeta)K_2(\zeta)} &\int \mathrm{d}u_{i0} \int |\mathbf{u}_i|\mathrm{d}|\mathbf{u}_i| \int_0^\infty \mathrm{d}\sigma_i^2 \int_0^{2\pi} \mathrm{d}\alpha \int_0^\pi \mathrm{d}\beta_i \\ &\int_0^{2\pi} \mathrm{d}\chi \, \frac{\Psi(u_{i0}, \mathbf{u}_i^2, \sigma_i^2, \cos\alpha\sin\beta_1\sin\beta_2+\cos\beta_1\cos\beta_2, W)}{[x_1(\zeta)-\cos(\theta-\chi)][x_2(\zeta)-\cos(\chi-\alpha)]}, \end{aligned} \tag{5}$$

with $\mathrm{d}u_i = \mathrm{d}u_1\mathrm{d}u_2$, etc., and

$$x_i(\zeta) = \frac{K_i^2(\zeta)+\mathbf{u}_i^2+\sigma_i^2-\left(\frac{M_i^2-\zeta}{2W}+u_{i0}\right)^2}{2K_i(\zeta)|\mathbf{u}_i|\sin\beta_i}. \tag{6}$$

The support of the weight function Ψ is given by

$$\Psi = 0, \text{ unless}$$
$$W > c \text{ and } \tfrac{1}{2}W > |\mathbf{u}_i| > 0 \text{ and } \tfrac{1}{2}W-|\mathbf{u}_i| > u_{i0} > -\tfrac{1}{2}W+|\mathbf{u}_i|, \text{ and} \tag{7}$$
$$\sigma_i > \text{Max}\,\{0,\ a_i-\sqrt{(\tfrac{1}{2}W+u_{i0})^2-\mathbf{u}_i^2},\quad b_i-\sqrt{(\tfrac{1}{2}W-u_{i0})^2-\mathbf{u}_i^2}\}.$$

The mass parameters a_i, b_i and c are determined by the selection rules, and in the cases under consideration one has $a_1 = a_2$ and $b_1 = b_2$. In fact, the spectral conditions read

$$\begin{aligned}
&\langle 0|j|n\rangle = 0 \quad \text{unless} \quad p_n^2 > a^2 = (3\mu)^2,\\
&\langle 0|f_i|n\rangle = 0 \quad \text{unless} \quad p_n^2 > b^2 = (M_\Lambda+\mu)^2,\\
&\langle p_i, k_i|n\rangle = 0 \quad \text{unless} \quad p_n^2 > c^2 = (M_\Lambda+\mu)^2,
\end{aligned} \tag{8}$$

where j and f_i denote the interaction currents of the pion and the hyperon, respectively.

Performing the integration over χ, eq. (5) now reads

$$M(W, \zeta, \Delta^2) = \int_0^{2\pi} \mathrm{d}\alpha \frac{\tilde{\Psi}(\alpha)}{y(\zeta)-\cos(\theta-\alpha)}, \tag{5'}$$

with

$$y(\zeta) = x_1(\zeta)x_2(\zeta)+(x_1^2(\zeta)-1)^{\frac{1}{2}}(x_2^2(\zeta)-1)^{\frac{1}{2}}.$$

Consequently we know that the singularities of $M(W, \zeta, \Delta^2)$ regarded as a function of ζ occur only at the points where

$$\cos\theta = y(\zeta)\cos\alpha \pm i\sqrt{y^2(\zeta)-1}\sin\alpha. \tag{10}$$

Substituting eq. (3) into (10), we conclude that M is an analytic function of ζ for $-\infty < \mathrm{Re}\,\zeta < \mu^2$ in the neighbourhood of the real axis, provided

$$0 < \Delta^2 < \phi(W, \zeta, u_i, \sigma_i) \text{ for all } W, \zeta, u_i, \sigma_i \tag{11}$$

with

$$\phi(W, \zeta, u_i, \sigma_i) = \tfrac{1}{2}K_1(\zeta)K_2(\zeta)y(\zeta)+\tfrac{1}{4}(K_1^2(\zeta)+K_2^2(\zeta))-\left(\frac{M_2^2-M_1^2}{4W}\right)^2.$$

It should be noted here that eq. (11) is justified also for $K_i^2(\zeta) < 0$. In fact, if $K_1^2(\zeta)K_2^2(\zeta) < 0$, both $\cos\theta$ and $y(\zeta)$ become imaginary so that the condition for analyticity turns out to be $|\cos\theta| < |y|$. For $K_1^2(\zeta) < 0$ and $K_2^2(\zeta) < 0$, the condition is the same. This condition leads us to eq. (11) regardless of the sign of $K_i^2(\zeta)$.

Now we are to find the minimum value of ϕ with respect to u_i, σ_i, ζ and W in the regions given by (7) and by $-\infty < \mathrm{Re}\,\zeta \leqq \mu^2$. First of all, we minimize y with respect to u and σ. The results of refs. [1]) and [2]) show that

$$\underset{(u,\sigma)}{\mathrm{Min}}\, y(\zeta) = \tilde{y}(\zeta) = \tilde{x}_1(\zeta)\tilde{x}_2(\zeta) + \sqrt{\tilde{x}_1^2(\zeta)-1}\sqrt{\tilde{x}_2^2(\zeta)-1}, \tag{12}$$

with †

$$\tilde{x}_i(\zeta) = \left[1 + \frac{(a^2-\zeta)(b^2-M_i^2)}{K_i^2(\zeta)\{W^2-(a-b)^2\}}\right]^{\frac{1}{2}}. \tag{13}$$

Substituting (12) into (11), we get

$$\begin{aligned}\tilde{\phi}(W,\zeta) = \underset{(u,\sigma)}{\mathrm{Min}}\, \phi(W,\zeta,u_i,\sigma_i) &= \frac{1}{2}\prod_{i=1}^{2}\left[K_i^2(\zeta) + \frac{(a^2-\zeta)(b^2-M_i^2)}{W^2-(a-b)^2}\right]^{\frac{1}{2}} \\ &+ \frac{1}{2}\prod_{i=1}^{2}\left[\frac{(a^2-\zeta)(b^2-M_i^2)}{W^2-(a-b)^2}\right]^{\frac{1}{2}} + \tfrac{1}{4}(K_1^2(\zeta)+K_2^2(\zeta)) - \left(\frac{M_2^2-M_1^2}{4W}\right)^2.\end{aligned} \tag{14}$$

It is obvious that $\tilde{\phi}(W,\zeta)$ regarded as a function ζ for $-\infty < \zeta \leqq \mu^2$ is a monotone-decreasing, so that we may now put $\zeta = \mu^2$. The remaining problem is to find the minimum of $\tilde{\phi}$ with respect to W.

One point to be noted here is that $\tilde{x}_i(\zeta)$ may in fact become *imaginary* for certain small values of W, viz. $M_i+\mu \geq W > c$; however, this does not cause any trouble, because the $\tilde{x}_i$ occur in $\tilde{\phi}$ exclusively in the form $K_i\tilde{x}_i$ which is always *real*, since K_i becomes also imaginary whenever $\tilde{x}_i$ is imaginary. Therefore, the important point is that $K_i\tilde{x}_i$ does not vanish, i.e. the first term of eq. (14) is positive definite. This will be shown in the next section.

3. Estimate of Δ^2_{max}

To find the maximum values of momentum-transfer for which the derivation of dispersion relations can be justified, it suffices to evaluate the minimum values of $\phi_0(W) = \tilde{\phi}(W,\mu^2)$ with respect to W for each process.

i) $\Lambda+\pi \to \Lambda+\pi$

In this case, there is no unphysical region in the forward scattering, so we can make use of the result for pion-nucleon scattering [1]), viz.

$$\Delta^2_{\mathrm{max}} = \mathrm{Min}\,\phi_0(W) = \frac{8}{3}\frac{2M_\Lambda+\mu}{2M_\Lambda-\mu}\mu^2 \equiv \Delta_\Lambda^2 \approx 3\mu^2. \tag{15}$$

ii) $\Sigma+\pi \to \Sigma+\pi$

For $M_i = M_\Sigma$, eq. (14) now reads

† It can be easily seen that the second minimum given by eq. (4.17a) of ref. [2]) does not affect us here. This was pointed out to the author by Dr. J. G. Taylor.

$$\phi_0(W) = K_\Sigma{}^2(W) + \frac{(a^2-\mu^2)(b^2-M_\Sigma{}^2)}{W^2-(a-b)^2}. \tag{14'}$$

For the region $W > M_\Sigma+\mu$, i.e., where $K_\Sigma{}^2(W) > 0$, we can immediately find the minimum value of ϕ_0, namely

$$\underset{W>M\Sigma+\mu}{\text{Min}}\ \phi_0(W) = \frac{8\mu^2\{(M_\Lambda+\mu)^2-M_\Sigma{}^2\}}{(M_\Sigma+\mu)^2-(M_\Lambda-2\mu)^2} \equiv \Delta_0{}^2 \approx 3\mu^2. \tag{16}$$

As to the region $M_\Sigma+\mu > W > M_\Lambda+\mu = c$, a lower bound to the minimum value of ϕ_0 can be obtained through minimizing each term of the right-hand side of (14') separately: $K_\Sigma{}^2(W)$ takes its minimum value at $W=M_\Lambda+\mu$ and its minimum value turns out to be $\approx -\mu^2$, while the second term takes its minimum value $\Delta_0{}^2$ at $W = M_\Sigma+\mu$, when $K_\Sigma{}^2(W) = 0$. Thus we obtain

$$\underset{W>c}{\text{Min}}\ \phi_0(W) > \Delta_0{}^2 + [K_\Sigma]_{W=M_\Lambda+\mu} \equiv \Delta_\Sigma{}^2 \approx 2\mu^2. \tag{17}$$

iii) $\Lambda+\pi \to \Sigma+\pi$

For the inelastic nature of the process (viz., $M_1 = M_\Lambda$, $M_2 = M_\Sigma$ and therefore $K_1 \neq K_2$), we cannot rationalize the terms in (14), so we rewrite (14) in the following form, in order to find a lower bound to Min $\phi_0(W)$:

$$\begin{aligned}\phi_0(W) = \tfrac{1}{4}\left\{\left[K_\Lambda{}^2 + \frac{(a^2-\mu^2)(b^2-M_\Lambda{}^2)}{W^2-(a-b)^2}\right]^{\frac{1}{2}} + \left[K_\Sigma{}^2 + \frac{(a^2-\mu^2)(b^2-M_\Sigma{}^2)}{W^2-(a-b)^2}\right]^{\frac{1}{2}}\right\}^2 \\ -\tfrac{1}{4}\left(\frac{a^2-\mu^2}{W^2-(a-b)^2}\right)\{(b^2-M_\Lambda{}^2)^{\frac{1}{2}} - (b^2-M_\Sigma{}^2)^{\frac{1}{2}}\}^2 - \left(\frac{M_\Sigma{}^2-M_\Lambda{}^2}{4W}\right)^2.\end{aligned} \tag{14''}$$

From (15) and (17), the lower bound to the first term of (14'') appears to be $\frac{1}{4}(\Delta_\Lambda+\Delta_\Sigma)^2$, while the second and third terms give only very small contributions to $\phi_0(W)$ in comparison with the first term. Actually, the contribution from them amounts only to $\approx -\frac{1}{2}\mu^2$ even at $W = c = M_\Lambda+\mu$. Thus, we may now conclude that dispersion relations can be derived also for the inelastic scattering $\Lambda+\pi \to \Sigma+\pi$, provided

$$0 < \Delta^2 < \Delta^2_{\text{max}} \approx 2\mu^2. \tag{18}$$

As a matter of fact, our discussion so far is still incomplete, since $M(W, \zeta, \Delta^2)$ will have contributions from the single-baryon states (in our case, single Λ- and Σ-hyperon states, i.e., for $W = M_\Lambda$ and $W = M_\Sigma$) which we have not yet considered. However, they give no trouble, since the situation is exactly same as in the case of the single-nucleon term in the (N, π)-scattering discussed by H. Lehmann [5]).

We have so far proved dispersion relations for pion-hyperon scattering up to the momentum-transfer given by (15), (17) and (18), respectively, for the *realistic masses* of the relevant particles, but not for the *model masses* [4]). Together

with the (N, π) and (Ξ, π) scattering[6]), *dispersion relations have now been proved for every pion-baryon scattering up to the momentum-transfer* $2\mu^2$ or $3\mu^2$ *by the present method*, but this method fails for (K, N) scattering, etc.

The author would like to thank Prof. R. Jost for valuable instruction on the integral representation. He is also very grateful to Dr. J. G. Taylor for reading the manuscript and making helpful comments.

References

1) H. Lehmann, Nuovo Cimento **10** (1958) 579
2) R. Oehme and J. G. Taylor, Phys. Rev. **113** (1959) 371
3) F. J. Dyson, Phys. Rev. **110** (1958) 1460
4) R. F. Streater, Nuovo Cimento **13** (1959) 57
5) H. Lehmann, Course on Mathematical Problems of Quantum Theory of Particles and Fields, Varenna, 1958 (to be published in Nuovo Cimento Suppl.)
6) J. G. Taylor, Proof of Certain Dispersion Relations in Quantized Field Theories, Institute for Advanced Study, preprint (1958)

1.E.1:
4.E

Nuclear Physics **15** (1960) 108—124; © *North-Holland Publishing Co., Amsterdam*
Not to be reproduced by photoprint or microfilm without written permission from the publisher

LOW MASS ODD-ODD ISOMERS OF THALLIUM

B. JUNG and G. ANDERSSON

The Gustaf Werner Institute for Nuclear Chemistry, University of Uppsala

Received 11 September 1959

Abstract: β-spectrometer measurements on mass separated sources from synchrocyclotron bombardments of Hg and Tl with protons have yielded information about some previously unknown nucleides: (1.41 ± 0.02)h Tl^{196m}, (11 ± 2)min Pb^{194}, (32.8 ± 0.2)min Tl^{194m}, and (33.0 ± 0.5)min Tl^{194}. Reinvestigation of the internal branch of (1.87 ± 0.03)h Tl^{198m} has shown that it is more complex than assumed earlier, suggesting the following level sequence: 7+ (544 keV), 3− (283 keV), 2− (260 keV), and 2− (ground state). In Tl^{196} an analogous pattern is indicated: 7+ (395 keV), 3− (275 keV), 2− (241 keV), and 2− (ground state). No internal branch has been found from Tl^{194m}, while about 4 % I.T. can be calculated for Tl^{196m} and about 55 % I.T. for Tl^{198m}. Some systematic energy level trends are discussed.

1. Introduction

The present knowledge of energy levels in odd-odd nuclei is strikingly poor. One reason undoubtedly is that their neighbouring isobars often are stable in the region where disintegration studies otherwise are most feasible. Further away from the stability line, the experimental difficulties have been discouraging, the more so because of the lack of a general theoretical approach that can cope with the complexities which occur with odd numbers of both neutrons and protons.

In the vicinity of a double shell closure, however, as in the lead region, the situation should be rather favourable for an attempt to correlate the behaviour of levels in odd-odd nuclei with single-particle shell model features. An indication of how this might be done was given in a survey by Bergström and Andersson[1]), where a similarity in energy systematics between $\frac{13}{2}+$ states in odd mass Pb isotopes and 7+ states in even mass Tl isotopes was pointed out and tentatively explained from assumptions about nucleon configurations. The meager data on other Tl levels further seemed to give some support to the theoretical prediction of a linear variation with nucleon number of the energy difference between low-lying levels with the same configuration, as discussed by Zeldes [2]).

Recent nuclear spectroscopy at this Institute has aimed at extending the energy level systematics of the odd-odd Tl isotopes towards lower mass numbers. One aspect of this work concerns the decay of even mass Pb isotopes. In this way, Tl^{198} [3]) and Tl^{196} [4]) levels have been studied. The present paper deals

with another aspect of the problem; namely, the existence of isomeric states in the Tl isotopes of interest. It may be useful to review briefly the earlier situation in this field.

Tl^{198} is known to have an 1.9 h 7+ state decaying to the 5.3 h 2− ground state by an M4—M1 cascade and thus via an intermediate 3− level [5]). Atomic beam resonance measurements have confirmed the spins 7 [6]) and 2 [7]). In Tl^{202} the corresponding 7+ level has a much shorter half-life, 475 μs, which is ascribed to a level crossing that makes the intermediate level 4− and the internal cascade E3—E2 [8]). A 65 μs activity, also accompanied by two γ-rays[9]), has analogously been assigned to Tl^{204} [8]). The ground state spin 2 is experimentally verified in both these nuclei [6,10]) as well as in Tl^{200} [11]), where, however, the 7+ state has not yet been observed.

Level systematics based on these data seemed to indicate the possibility of fairly long-lived M4 isomers in odd-odd Tl isotopes with $A < 198$. Of these nucleides only the 1.8 h ground state of Tl^{196} [12]) was known previous to this investigation, the primary purpose of which was the search for isomeric states of Tl^{196} and Tl^{194}. It also proved necessary to reinvestigate the decay of Tl^{198m}, which had in fact to be used as a basis for the interpretation of data on the lower mass nucleides.

2. Experimental Procedures

The main part of the measurements was made in the two-directional focusing β-spectrometer of the institute [13]). Conversion electron spectra normally were studied at a momentum resolution of about 0.35 % and with a 0.9 mg/cm² Mylar film as the G. M. counter window. In some special runs a thinner window ($\approx$ 0.05 mg/cm² VYNS film) and somewhat better resolution ($\approx$ 0.25 %) were used.

In view of the short half-lives involved, a general survey of the spectra would have been tedious indeed without the automatic scanning device of the spectrometer [13]). The bulk of the data reported in this paper, however, has been obtained by subsequent manual measurements.

$B\rho$ values were calculated from magnet current readings by means of a calibration curve, based on ThB lines (cf. ref. [14])). A semi-logarithmic plot of the calibration constant $B\rho/I$ against I is linear enough to allow in most cases an unambiguous determination of the conversion element (see table 1), although the method does not ensure the highest precision in absolute energy values. In this respect the very accurately measured 412 keV transition in Hg^{198} was useful as a calibration standard.

Half-life determinations were carried out by following the decay of suitable conversion lines in the β-spectrometer. The constancy of the magnetic field, the relative purity of the sources, and the use of a crystal controlled counter with

automatic recording led to rather accurate decay curves (cf. fig. 4). In table 1, only standard errors from (in general) least squares treatment of the data are given, while error limits of half-lives in the text are meant to include also other sources of uncertainty.

An electron-gamma coincidence setup at the Physics Department of this University[15]) was used † for complementary measurements on Tl^{196m}. Resolution and transmission of the electron channel were 2 % and 0.7 %, respectively.

All spectrometer sources were prepared by the method of direct deposition in our electromagnetic mass separator [16, 17]). The activities were collected on 2 mg/cm² Al foils, forming carrier-free sources of the approximate dimensions 1.5 mm × 15 mm, which could be used in the β-spectrometer without further procedures. The purity of the sources as well as the overall efficiency of the separation process have recently been discussed in some detail in connection with the decay of Pb^{198} [3]). It may be remarked that the effective width is less than 1.5 mm due to the non-homogeneous distribution of the ion intensity across a mass line, its half-width being about 1 mm. For use in the coincidence spectrometer the collector strips were cut into pieces and pasted together to about square shape (5 mm × 5 mm).

The activities were produced by (p, xn) reactions in the Werner synchrocyclotron. In order to get both the 2−Tl ground states and the 7+ states, Hg_2Cl_2 was bombarded with protons of 80—90 MeV maximum energy. Tl was isolated chemically and brought to mass separation as TlCl. Sources prepared in this way will be referred to as *type A sources*.

The investigations were much facilitated, however, by the fact that the 7+ states of interest are not fed to any detectable degree from Pb activities prepared by irradiation of Tl. (This indicates that possible high spin states of the low mass even Pb isotopes are too short-lived to survive the chemical separation of Pb from Tl.) Thus two other source types were obtained by Tl(p, xn)Pb reactions:

Type B. Chemical isolation of Pb and mass separation with $PbCl_2$ as the charge material.

Type C. Chemical isolation of Pb and subsequent "milking" of Tl, mass separated as TlCl.

The chemical procedures were mainly those described in refs. [5, 18]) and [19]).

3. Results

3.1. THE INTERNAL BRANCH OF 1.9 h Tl^{198m}

Early investigators of this activity [20, 21]) found it to be accompanied by three γ-rays, which for intensity reasons were supposed to cascade to the 5.3 h ground state. However, the conversion element could not be established with

† We are grateful to Prof. K. Siegbahn and his coworkers for the use of this instrument.

TABLE 1

Transitions in the decays of Tl^{198m}, Tl^{196m}, Tl^{195}, Pb^{194}, Tl^{194m}, and Tl^{194}

Mass number	Electron energy (keV)	Apparent half-life with standard error	Relative electron intensity	Calculated transition energy (keV)			Adopted conversion element and transition energy (keV)
				Conv. shell	Conv. element Hg	Conv. element Tl	
198	7.76 [a]	≈2 h (A)		L_I	22.60	23.11	Tl 23.1 ± 0.1
	19.43	2.1 h (A)	3.4 ± 0.3 (A)	M_I	22.99	23.14	
	19.75			M_{II}	23.03	23.17	
	22.28	1.7 h (A)		N_I	23.09	23.13	
	33.55		71 ± 6 (A)	L_{II}	47.76		Hg 47.8 ± 0.2
	174.1 [b]	1.9 ± 0.3 h (A)	9 ± 1 (A)	K		259.6	Tl 259.6 ± 0.8
	175.34	1.9 ± 0.1 h (A)	100 (A)	K	258.46	260.87	Tl 260.9 ± 0.5
	245.50			L_I	260.34	260.85	
	248.23			L_{III}	260.52	260.89	
	257.47			M_{II}	260.75	260.89	
	260.12			N_{II}	260.80	260.85	
	197.51	1.87 ± 0.01 h (A)	60 ± 4 (A)	K	280.63	283.04	Tl 283.0 ± 0.6
	267.65			L_I	282.49	283.00	
	279.11			M_I	282.67	282.82	
196	18.43		25 ± 10 (A)	L_I	33.27	33.77	Tl [c] 33.7 ± 0.3
	29.84			M_I	33.40	33.54	
	70.12			L_{II}	84.33	84.82	Hg 84.4 ± 0.3
	72.07	1.41 ± 0.01 h (A)	1690 ± 170 (A)	L_{III}	84.36	84.73	
	81.12			M_{II}	84.40	84.54	
	81.50			M_{III}	84.35	84.46	
	83.71			N_{II}	84.39	84.44	
	84.32			O_{II}	84.41	84.42	
	34.52			K	117.64	120.05	Tl 120.1 ± 0.3
	104.78	1.3 h (A)		L_I	119.62	120.13	
	105.43	1.5 h (A)		L_{II}	119.64	120.13	
	107.42	1.4 h (A)	100 (A)	L_{III}	119.71	120.08	
	117.09	1.4 h (A)		M_{III}	119.94	120.05	
	119.57			N_{III}	120.15	120.18	
	155.18 [d]	1.5 h (A)	≤23 (A)	K	238.30	240.71	Tl 240.7 ± 0.6
	225.35	1.4 h (A)		L_I	240.19	240.70	
	189.09 [e]	1.4 h (A)	50 ± 10 (A)	K	272.21	274.62	Tl 274.6 ± 0.6
	259.9			L_I	274.7	275.2	
	342.72	1.53 ± 0.02 h (A) 1.84 ± 0.03 h (B)		K	425.84		Hg 425.8 ± 0.4
194	82.95	32.8 ± 0.1 min (A)	250 ± 50 (A) < 15 (B)	L_{II}	97.16	97.65	Hg 97.2 ± 0.3
	84.88			L_{III}	97.17	97.54	
	93.86			M_{II}	97.14	97.28	
	94.23			M_{III}	97.08	97.19	
	96.56			N_{II}	97.24	97.29	
	118.7	11 ± 1 min (B)	100 (A, B)	K		204.2	Tl 204 ± 2 [f]
	344.40	33.0 ± 0.2 min (A) 33.4 ± 0.4 min (B) 32.6 ± 1.0 min (C)		K	427.52	429.93	Hg 427.5 ± 1.5
	413.37			L_{II}	427.58	428.07	
	415.68 [g]			L_{III}	427.97	428.34	
	424.71 [h]			M_{II}	427.99	428.13	
	427.11 [h]			N_{II}	427.79	427.84	

Capital within parenthesis denotes the source type used; see section 2.

[a] Not resolved from L Auger lines.
[b] Not resolved from K 261.
[c] Cf. the text (3.3).
[d] Complex line.
[e] Badly superimposed.
[f] Automatically recorded only.
[g] Poor statistics; not resolved from L_{II}.
[h] Poor statistics.

TABLE 2

Conversion ratios

Nucleus	Transition energy (keV)	Adopted multipole order	Conversion ratio	Experimental value	Theoretical value † according to	
					Rose [22])	Sliv [23])
Tl^{198}	23.1	M1	M_I/M_{II}	≈ 6	9.5 ††	—
			M/N	3.2 ±0.6	—	—
			N/O	>2	—	—
	260.9	M4	K/L	0.89±0.06	0.99	0.98
			L_I+L_{II}/L_{III}	1.38±0.07	1.40	1.35
			L/M	3.6 ±0.4	—	—
			M/N	3.6 ±0.4	—	—
	283.0	M1	K/L	5.9 ±0.3	6.4	5.7
			L_I/L_{III}	>20	—	—
			L/M	4.6 ±0.9	—	—
Tl^{196}	120.1	M4	K/L	0.14±0.07	≈ 0.1	≈ 0.1
			L_I/L_{III}	0.36±0.07	0.39	0.36
			L_{II}/L_{III}	0.14±0.05	0.08	0.08
			L_I+L_{II}/L_{III}	0.48±0.04	0.46	0.44
			L/M	3.0 ±0.3	—	—
			M/N	2.6 ±0.5	—	—
Hg^{196}	84.4	E2	L_I/L_{II}	<0.07	0.04	0.04
			L_{II}/L_{III}	1.03±0.05	1.10	1.15
			M_I/M_{II}	<0.3	0.04	—
			M_{II}/M_{III}	1.04±0.10	1.05	—
			$M_{II}+M_{III}/M_{IV}+M_V$	70 ±40	70	—
			L/M	4.0 ± 0.4	—	—
			M/N	3.4 ± 0.4	—	—
			N/O	7 ± 4	—	—
Hg^{194}	97.2	E2	L_I+L_{II}/L_{III}	1.24± 0.05	1.20	1.26
			L/M	3.6 ± 0.4	—	—
			M/N+O	2.7 ± 0.3	—	—
	427.5	E2	K/L	3.0 ± 0.6	2.85	2.85
			L_I+L_{II}/L_{III}	5.1 ± 1.0	4.8	4.8
			L/M	1.3 ± 0.5	—	—

† Interpolation uncertainties estimated as about ±3 %.
†† By extrapolation.

certainty for the lowest energy transition (48 keV) and this was indeed later shown to convert in Hg [5]) (see further 3.2.).

The conversion electron intensities of the remaining two transitions indicated an M4 assignment for one of them (261 keV), which was further supported by transition probability considerations, and M1 for the other (283 keV) [21]). A fulfilment of the assumed cascade relation, however, required the latter to have an E2 admixture of the order of 50 %. The discrepancy was thought to be

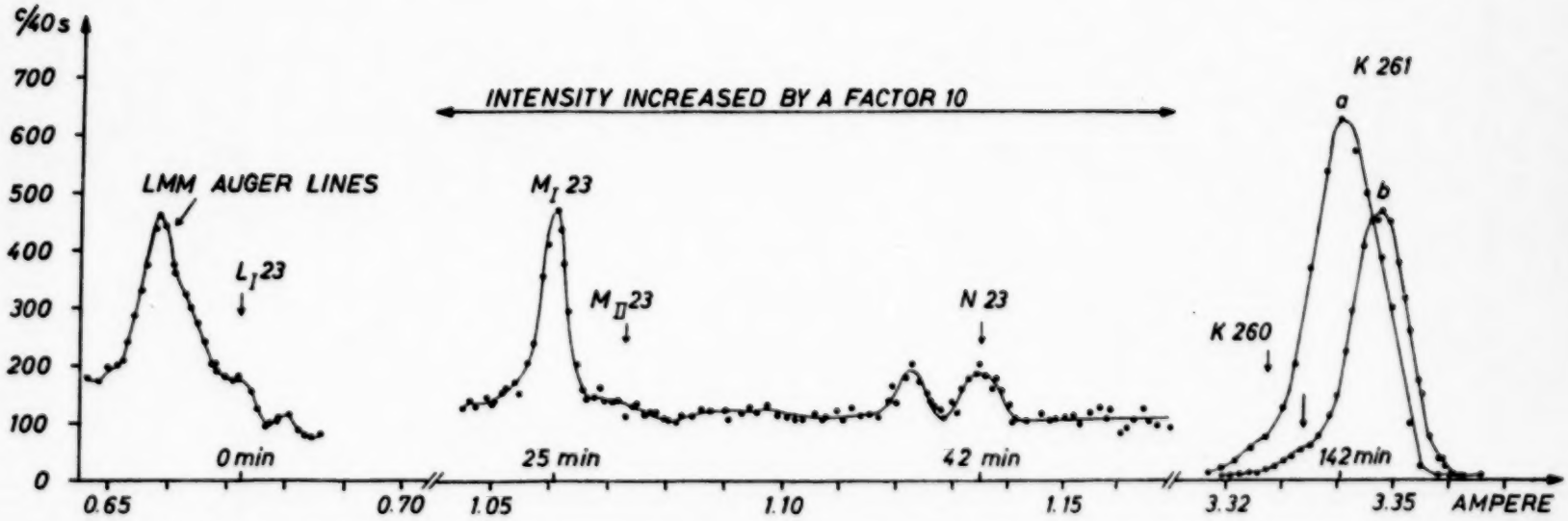

Fig. 1. Parts of the conversion electron spectrum from the decay of 1.9 h Tl^{188m}. For K 261, peak *a* gives the intensity relative to the rest of the spectrum, while peak *b* has been included to illustrate the more clear appearance of K 260 at better resolution. Counting time per point = 40 s.

due to inaccurate intensity measurements and/or errors in the theoretical conversion coefficients.

In order to settle this question, we remeasured the conversion lines of the 261 keV and 283 keV transitions. It then turned out that the K line of the former had a weak parasite on its low energy side (see fig. 1), which was confirmed in additional runs with better resolution. The energy was found to coincide within the limits of error with that of the K line of an M1 transition (with possible E2 admixture) in the decay of 2.4 h Pb^{198}, which de-excites a 260 keV level in Tl^{198} according to the proposed level scheme [3]). This made apparent another explanation of the above-mentioned intensity discrepancy, namely the existence of a rather weak stop-over branch from the intermediate 3— level. Because of the strong L complex of the M4 transition, no L line corresponding to the K 261 parasite was seen in the decay of Tl^{198m}, thus leaving the question of conversion element open.

Assuming the 260 keV level to be fed from the 283 keV 3— level, however, one could postulate a 23 keV γ-ray in the Tl^{198m} decay. With a thin window in the G.M. tube of the β-spectrometer it was in fact possible to demonstrate the presence of L, M, and N lines of such a transition (fig. 1). Even though, unfortunately, the L line was not resolved from an Auger line group, conversion in Tl seems quite strongly indicated (table 1). From the M_I/M_{II} ratio ≈ 6 (table 2) the multipolarity must be mainly M1; all other multipolarities give theoretical ratios $M_I/M_{II} \lesssim 1$ [22]).

A check of the intensity relations, using the data given in table 1 together with theoretical conversion coefficients [22, 23]), shows that the sum of the 283 keV and 260 keV transitions (both assumed to be pure M1) equals the M4 intensity rather convincingly:

$$\frac{I(283+260)}{I(261)} = 1.04 \pm 0.08.$$

As to the 23 keV transition, the M_I intensity (table 1), the experimental conversion ratios (table 2), and the empirical rule $L/M+N+\ldots \approx 3$, make possible an estimate of the total intensity, leading to

$$\frac{I(23)}{I(260)} = 0.9 \pm 0.3.$$

These intensity ratios seem to justify the interpretation of the internal decay of Tl^{198m} expressed in fig. 5. (It must be especially pointed out that the level schemes include only those transitions which are relevant to the discussions in this paper.) The combined information from the present investigation and from the decay of Pb^{198} [3]) suggests a 2— assignment for the 260 keV level in Tl^{198}.

The branching from the 3— state is given by

$$\frac{I(283)}{I(260)} = 7.7 \pm 1.2.$$

3.2. THE I.T./E.C. BRANCHING OF Tl^{198m}

The E.C. branch of Tl^{198m} is still incompletely known. In order to determine the branching ratio of the isomeric state, however, it has been assumed that the 48 keV transition represents the whole E.C. intensity and that its multipolarity is E2. The validity of these assumptions may need some discussion.

A more detailed study of the decay schemes of both Tl^{198} and Tl^{198m} has been started in connection with the present investigation and has revealed a large number of γ-transitions in Hg^{198}. From type A sources they all show apparent half-lives longer than 1.9 h (with the upper limit 5.3 h, the ground state half-life) with the prominent exception of the 48 keV transition, which goes with a pure 1.9 h period. This indication that the other γ-rays are more or less strongly fed from the ground state is further supported by their presence in type B spectra. Direct branches from Tl^{198m} to Hg levels that are also reached in the ground state decay are improbable for spin reasons. This leads to the conclusion that the part of the E.C. intensity from Tl^{198m} that can possibly bypass the 48 keV transition must be quite small.

The experimental L shell internal conversion ratios as well as the M_{II}/M_{III} ratio of the 48 keV transition [5]) were found to agree satisfactorily with those derived from the point charge computations by Rose *et al.* [24]) for the multipolarity E2. However, the agreement with E3 was about as good, while M_{II}/M_{III} seemed to exclude E4. A reexamination of the data in view of the now available nuclear size corrected L coefficients [22, 23]) does not alter the situation in any decisive way. A strong argument against E3, however, is the experimental M_{IV+V} intensity, which is compatible with the theoretical ratio $M_{IV+V}/M_{III} \approx 0.035$ for E2 [22]) but definitely too weak for the corresponding E3 ratio ≈ 0.2.

It may be remarked that the multipolarity probably could be more firmly established by a lifetime measurement of the level where the 48 keV transition originates. Earlier attempts [25, 26]), covering the region 5 ns to 100 μs, failed to give any result, but this hardly excludes either multipolarity. As long as the theoretical M shell conversion ratios have not been disproved, however, we feel confident in assigning the 48 keV transition an E2 multipolarity.

Under the assumptions discussed above and with the intensities given in table 1, the branching of Tl^{198m} is calculated as

$$\frac{\text{I.T.}}{\text{E.C.}} = \frac{I(261)}{I(48)} = 1.2 \pm 0.1.$$

The isomeric half-life has been redetermined as (1.87±0.03)h, which leads to a deviation factor F(M4), as defined by Bergström and Andersson [1]), of

$(2.9\pm0.3)\times10^{-1}$ for the M4 transition probability, in agreement with the earlier value 3.0×10^{-1} [1]).

3.3. THE DECAY OF 1.4 h Tl^{196m}

With a type A sample of mass 196 the K line of the earlier known 426 keV $2+\rightarrow0+$ transition in Hg^{196} showed an apparent half-life of about 1.5 h, which already indicated the existence of an isomeric state in Tl^{196}, shorter-lived than the 1.8 h ground state. More direct evidence was obtained by the presence of several 1.4 h conversion lines, notably those of an 120 keV M4 transition converting in Tl (tables 1 and 2, fig. 2). By far the strongest lines in the spectrum, however, were found to belong to an 84 keV E2 transition in Hg, for intensity reasons most probably analogous to the 48 keV γ-ray in the decay of Tl^{198m}. As in that case, the multipolarity assignment is supported in particular by the internal M shell conversion ratios (table 2).

In measuring the energy of the 426 keV transition (table 1) a special technique for source preparation was used: after collection of mass 196 on an Al strip in the mass separator, the mass spectrum was moved and mass 198, containing the calibration lines from the 412 keV transition in Hg^{198}, was collected on the same strip.

If we assume again (cf. 3.2) that the whole E.C. intensity from the isomeric state goes via the low energy E2 transition, we obtain for Tl^{196m}

$$\frac{\text{I.T.}}{\text{E.C.}}=\frac{I(260)}{I(84)}=0.041\pm0.005.$$

The half-life was measured over 6 periods as (1.41 ± 0.02) h and the deviation factor [1]) of the M4 transition probability calculated as $F(\text{M4})=(4.6\pm0.5)\times\times10^{-1}$.

The search for additional lines in the internal branch of Tl^{196m} met with considerable difficulties because of the complexity of the conversion spectrum and the dominance of the E.C. branch. Quite a number of line combinations in reasonable energy and intensity regions for the postulated transitions from the excited 3— and 2— levels to the 2— ground state were carefully measured, but in most cases conversion in Hg was clearly indicated.

The level scheme proposed in fig. 5 is based on the following arguments (cf. table 1). A 241 keV γ-ray in the decay of Pb^{196} (B source) showed up with much lower relative intensity with an A source. This transition is interpreted as analogous to the 260 keV M1 γ-ray in Tl^{198}. Type A, but not type B spectra, were found to contain what may be the K line of a 275 keV transition converting in Tl. The L line could not be satisfactorily resolved from a much stronger neighbour, but a tentative analysis seems to support conversion in Tl and the multipolarity $\text{M1}(\text{K/L}\gtrapprox6)$.

The energy difference between these two γ-rays is very nicely bridged by a

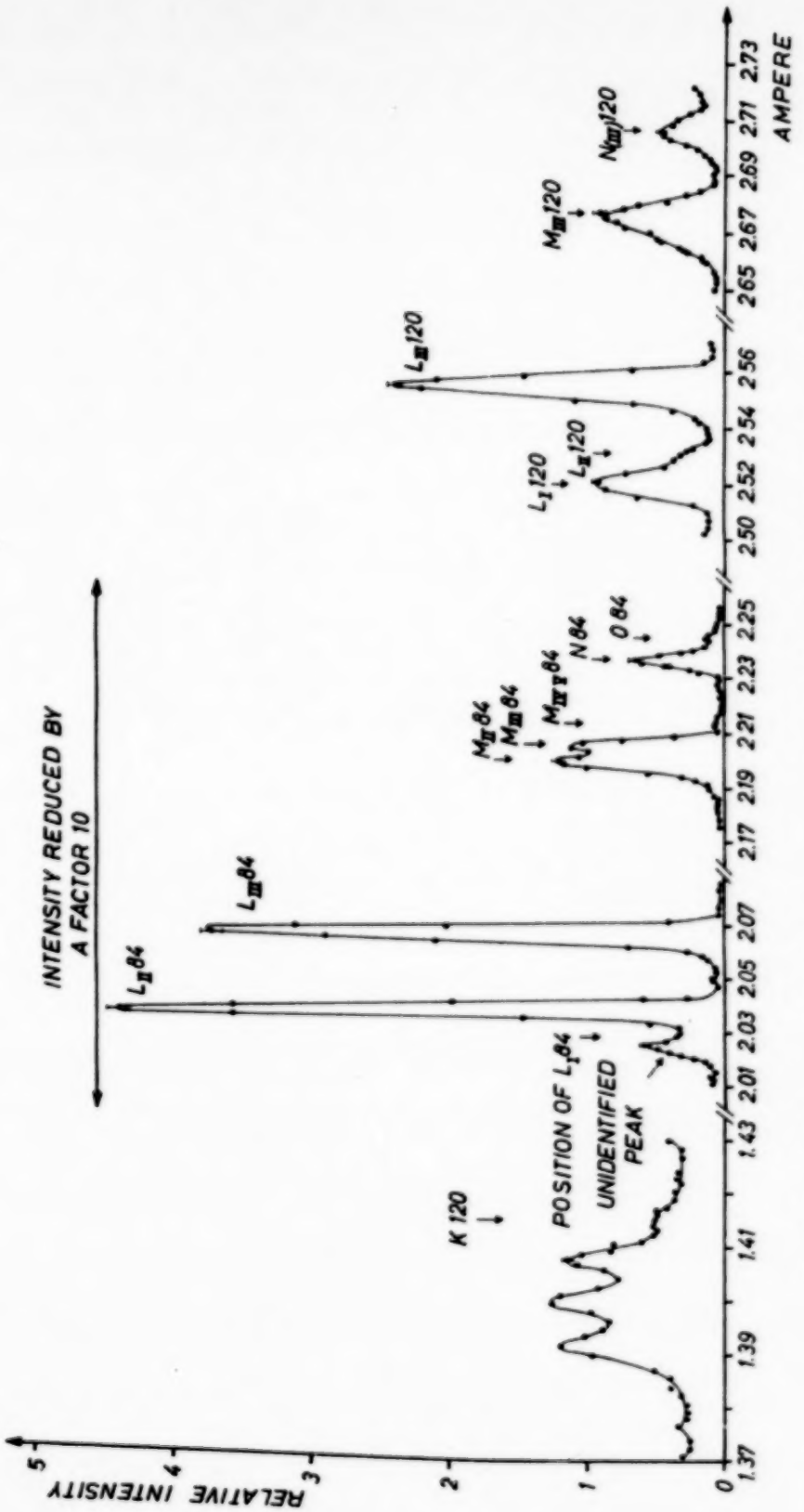

Fig. 2. Parts of the conversion electron spectrum from the decay of 1.4 h Tl^{196m}. As not all lines were measured in the same run and varying counting times were used, the decay corrected intensities have been normalized and the statistics shown by error limits at the top of the peaks.

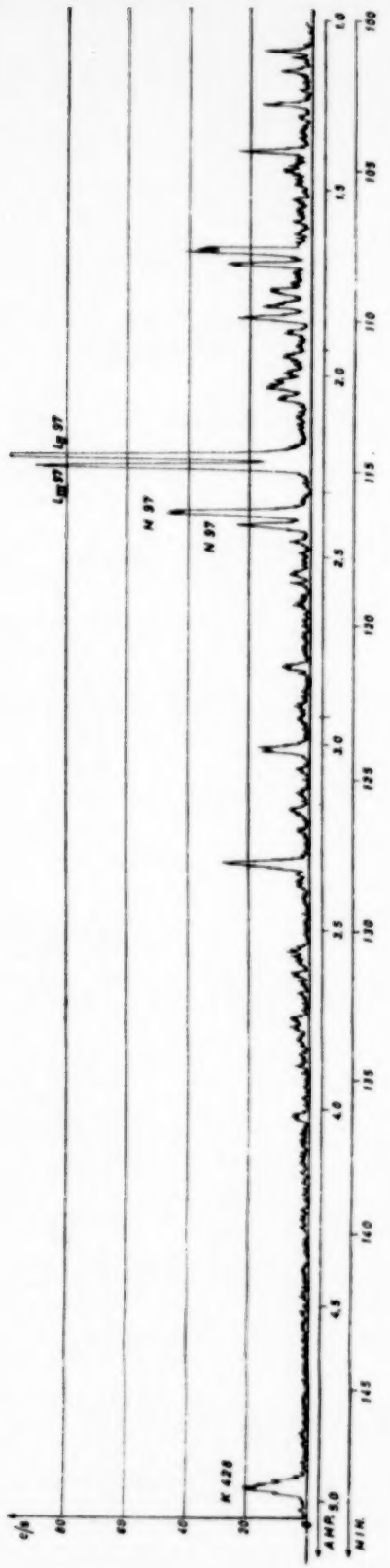

Fig. 3. Automatically recorded conversion electron spectrum in the energy region 20—350 keV from the decay of 33 min ^{194m}Tl.

34 keV γ-ray, most probably M1, since only L_I and M_I were seen. It should be remarked, though, that the line energies rather seem to favour conversion in Hg.

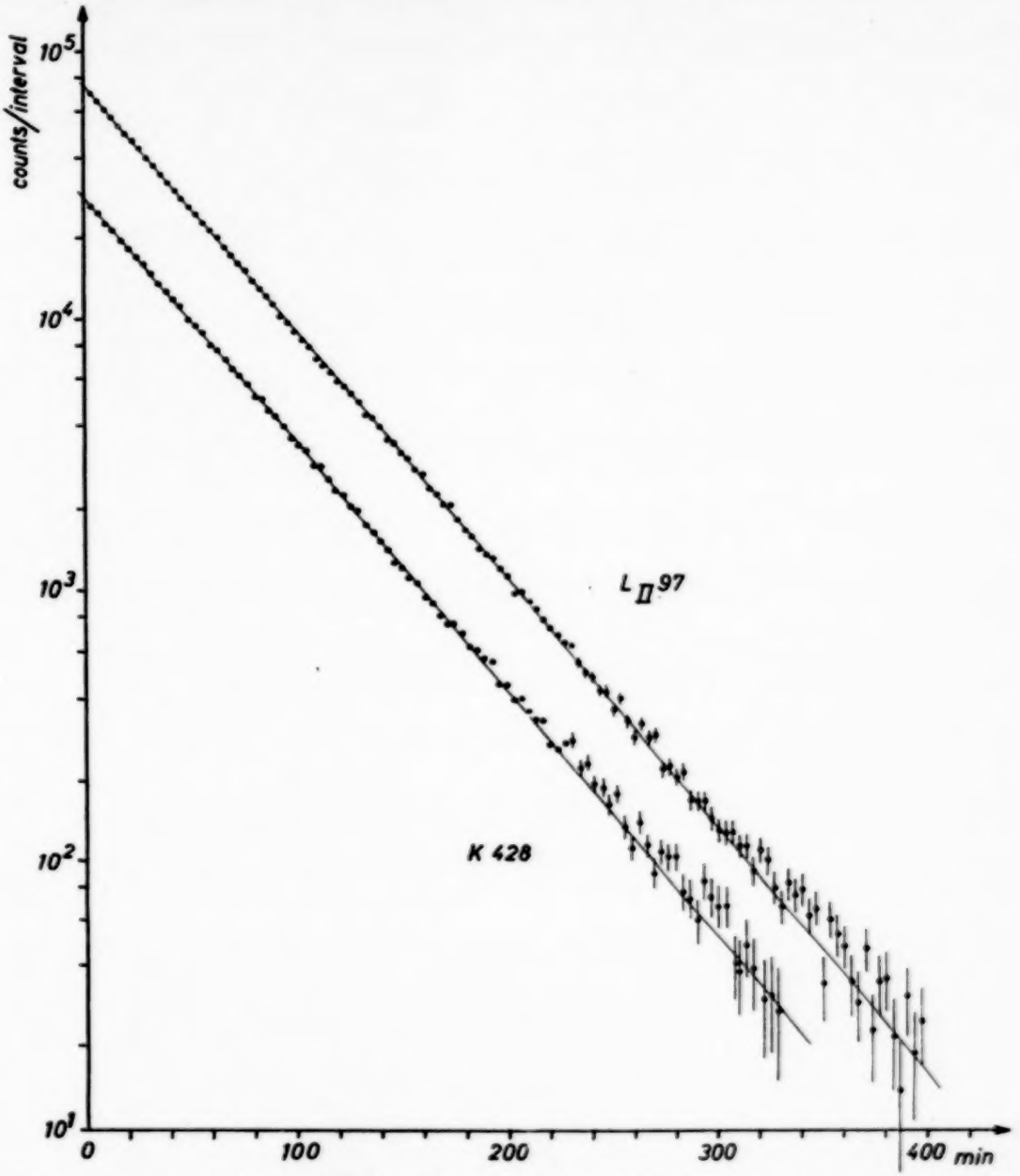

Fig. 4. Decay curves of electron lines in the decay of 33 min Tl^{194m}. Counting time per point = 190s for L_{II} 97 and 200s for K 428.

Within the wide limits of error, however, the total intensity of the 34 keV transition fits well into the picture:

$$\frac{I(275+34)}{I(120)} = 1.04 \pm 0.30, \qquad \frac{I(275)}{I(34)} = 4.7 \pm 2.2.$$

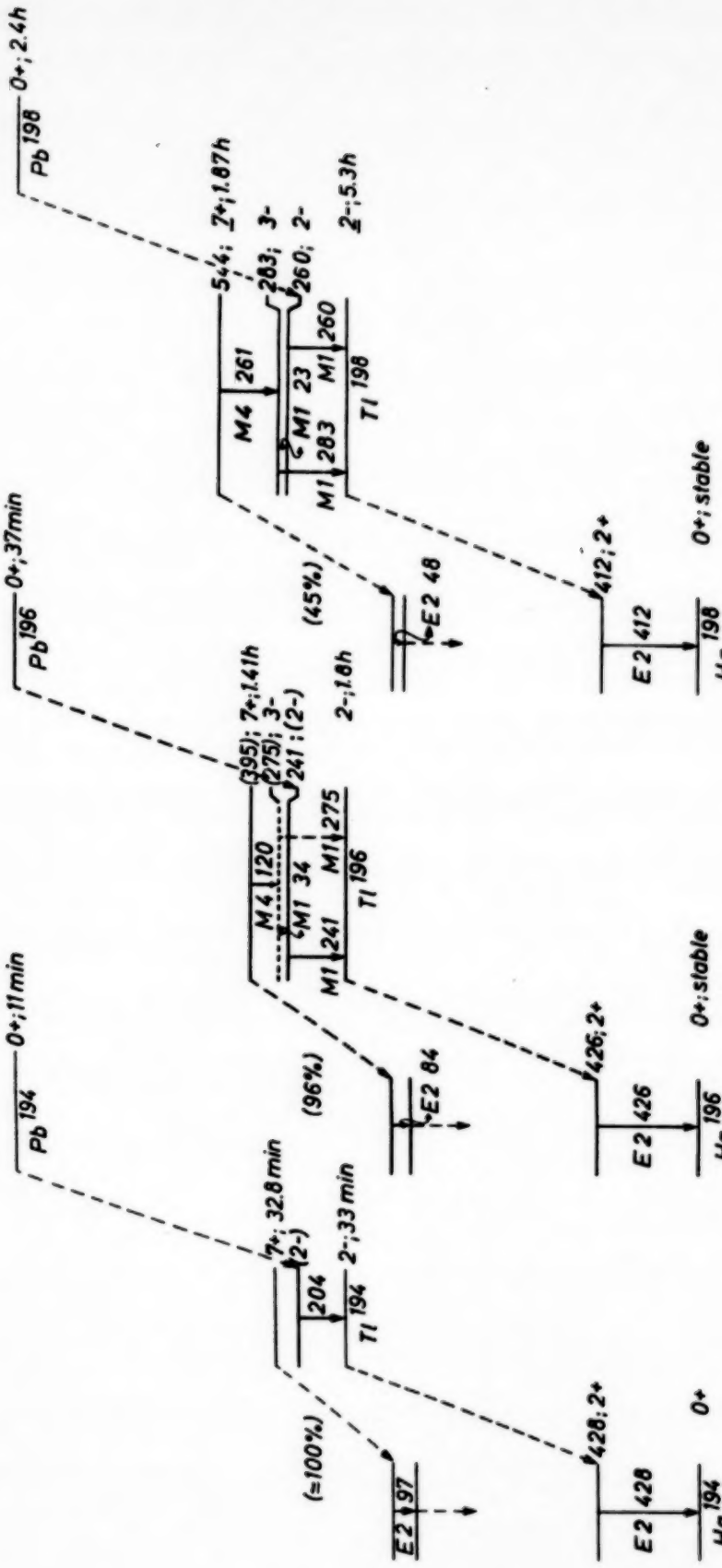

Fig. 5. Proposed level schemes of Tl^{198}, Tl^{196} and Tl^{194}. *Note that only levels of interest in the present connection are included.*

Because the K line of the 241 keV γ-ray is not pure in type A spectra, the total intensity cannot be calculated in this case. However, the upper limit obtained is not incompatible with a 34 keV—241 keV cascade.

Finally, the level scheme receives some support from the $e^- - \gamma$ coincidence measurements. With the L complex of the 120 keV M4 transition in the electron channel, a broad peak at a γ energy of about 250 keV appeared in the coincidence spectrum.

3.4. ACTIVITIES OF MASS NUMBER 194

The dominating lines in a type A conversion electron spectrum of mass 194 (fig. 3) were those of a 97 keV E2 transition, converting in Hg and apparently a member of the same series as the 48 keV γ-ray in Hg^{198} and the 84 keV γ-ray in Hg^{196}. Thus it should belong to the E.C. branch of a 7+ state in Tl^{194}. No lines that could be ascribed to an M4 transition were found, but this is well understood from the increasing relative probability of β-decay through Tl^{198m} and Tl^{196m}. More puzzling was the fact that a 428 keV E2 γ-ray, obviously $2+ \rightarrow 0+$ in Hg^{194}, showed the same half-life, 33 min, as the 97 keV transition over about 10 periods (fig. 4).

In order to look for the ground state of Tl^{194}, a B sample was prepared. The earlier unknown Pb^{194} turned out to have an 11 min half-life, measured on the K line of a 204 keV γ-ray converting in Tl and tentatively identified as the $2- \rightarrow 2-$ transition ($K/L > 4$). As expected, the 97 keV lines were absent; the weak activities found near their positions (table 1) can be explained by a minor contamination of 17 min Pb^{195}, which has a strongly converted 99 keV E3 transition in its decay [27]). The K line of the 428 keV γ-ray was present, however, still with the 33 min half-life. The same result was obtained with a source of type C, which was used in order to avoid the possible influence from the mother-daughter relationship between 11 min Pb^{194} and Tl^{194} in a type B source. Thus the only conclusion we can draw is that, within the limits of error, the ground state and the 7+ isomeric state of Tl^{194} have the same half-life, (33.0 ± 0.5) min and (32.8 ± 0.2) min, respectively. This leads to the level scheme shown in fig. 5.

4. Discussion of the Results

Fig. 6 illustrates the striking similarity in behaviour between the level spacings 7+ to 2− (g.s.) in even mass Tl isotopes and $\frac{13}{2}+$ to $\frac{5}{2}-$ in odd mass Pb isotopes (cf. ref. [1])). The contribution to the systematics made by the present investigation, however, seems to cause a slight deviation from the parallelism of the curves. For this reason a comparison with the $\frac{13}{2}+$ to $\frac{5}{2}-$ level distances in odd mass Hg isotopes is of a certain interest. While the sparse data indicate a steep rise towards higher mass numbers as in Pb and Tl, a definite

flattening out occurs at the lower ones. In this respect the Tl curve represents an intermediate situation, which may be significant.

Attention should be drawn further to the relative constancy of the 3— level above the ground state in Tl^{198} and Tl^{196} (fig. 7). Thus the energy difference between the isomeric state and this level also varies as the $\frac{13}{2}+$ to $\frac{5}{2}-$ spacing. This at least does not contradict the tentative explanation [1]) that the 7+ level

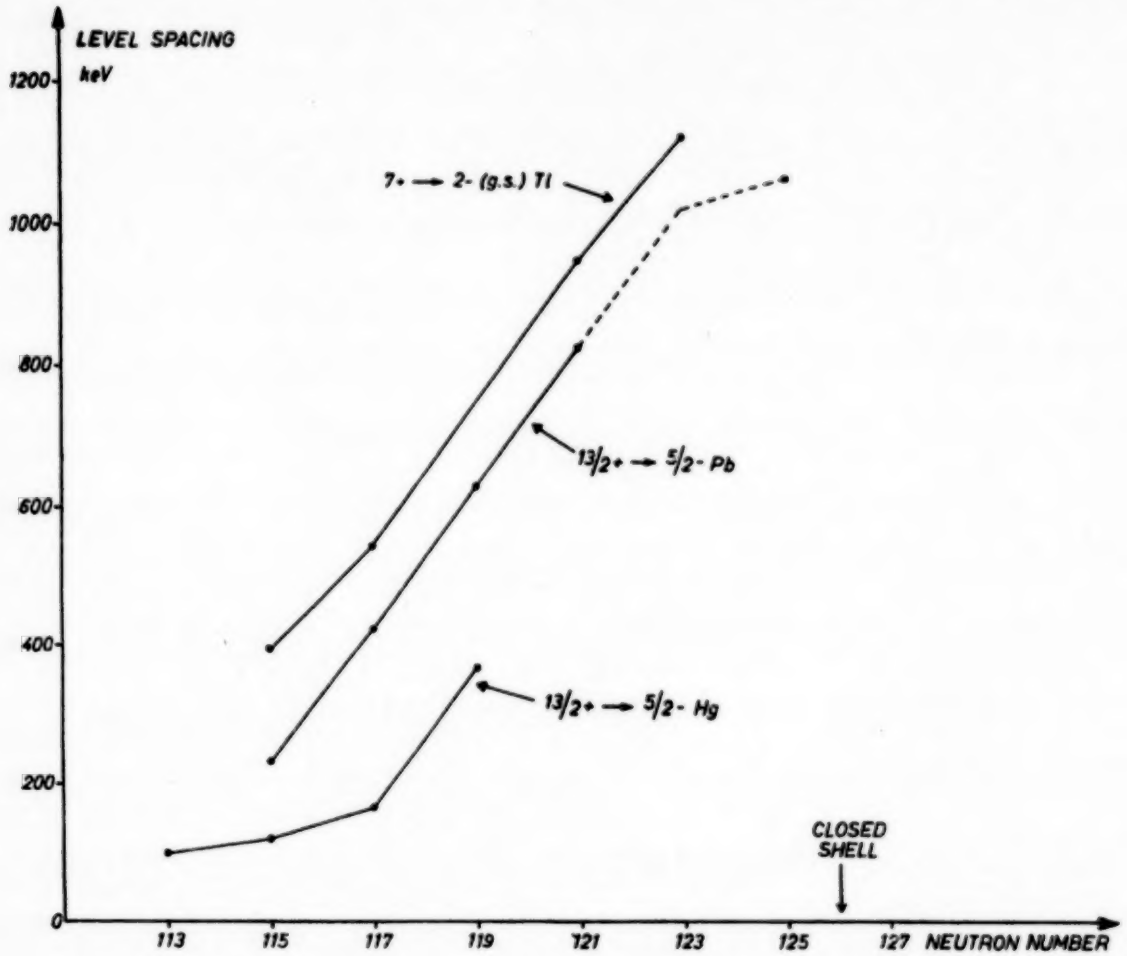

Fig. 6. Level spacing versus neutron number for $7+ \rightarrow 2-$ (ground state) in odd-odd Tl isotopes $\frac{13}{2}+ \rightarrow \frac{5}{2}-$ in odd-neutron Pb and Hg isotopes. Additional references: see ref. [1]).

has the odd neutron in the single particle state $i_{\frac{13}{2}}$, while the ground state and the 3— level both have the same configuration, characterized by an $f_{\frac{5}{2}}$ neutron. The odd proton is assumed to remain in the $s_{\frac{1}{2}}$ state throughout.

If the 2— ground state and the 3— excited state have the same configuration, their constant energy spacing also follows from the theoretical considerations by Zeldes [2]), provided that the neutron pairs add to even shells. The configuration discussed above, however, is not consistent with Zeldes' assumption that the 0— level (fig. 7) should belong to the same configuration as the ground

state in order to explain the linear relationship with neutron number of its excitation energy. It may be pointed out further that this assumption is in conflict with the strong Nordheim rule, which predicts the 0− level to be the lower for all 2−, 0− combinations that can be obtained with the odd proton in an $s_{\frac{1}{2}}$, $d_{\frac{3}{2}}$, $d_{\frac{5}{2}}$ or $h_{\frac{11}{2}}$ state and the odd neutron in a $p_{\frac{1}{2}}$, $p_{\frac{3}{2}}$, $f_{\frac{5}{2}}$ or $i_{\frac{13}{2}}$ state. From this point of view the excited 2− level is of a certain interest, although it may as well have a different configuration from that of the 0−level.

It is very unfortunate that the internal branches of Tl^{194m} and Pb^{195m} [27]) are

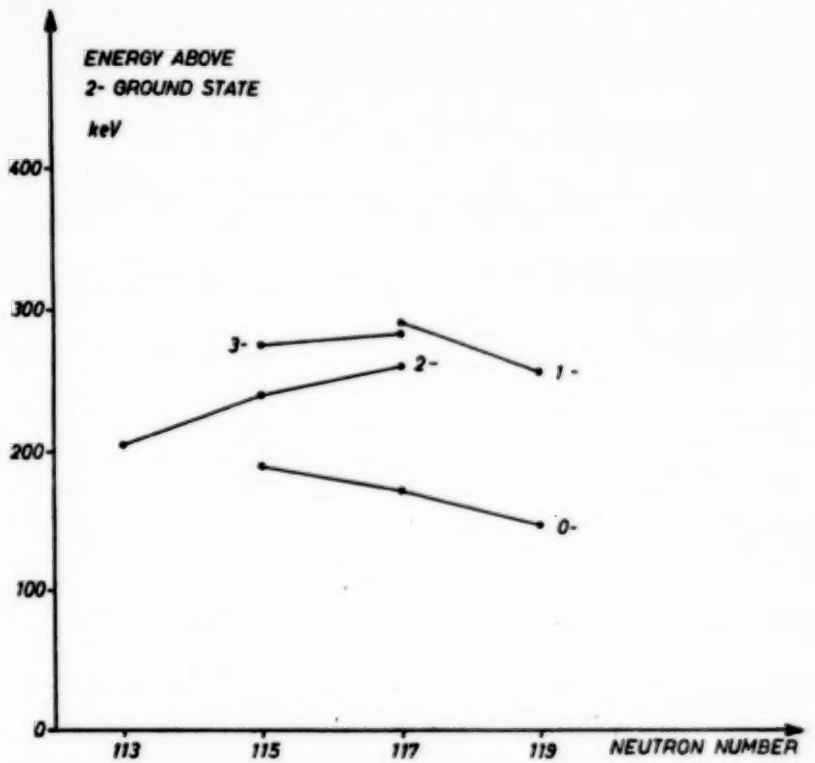

Fig. 7. Energy systematics of low-lying levels in odd-odd Tl isotopes.

not subject to study with now excisting experimental methods. Some other "missing points" give more hope. This is true in particular of the $\frac{13}{2}+$ state of Pb^{205}; the isomeric half-life has been reported [28, 29]), and the search for a half-life-determining transition is in progress [29]). It should be possible to reach the 7+ state of Tl^{200} by direct excitation in the beam of an accelerator. This may apply also to $\frac{13}{2}+$ levels in Hg^{201} and Hg^{203}.

Under the assumption that the M4 transitions in Tl^{198} and Tl^{196} are of the same type ($i_{\frac{13}{2}} \rightarrow f_{\frac{5}{2}}$), the difference between their deviation factors is remarkably large. If this is due to experimental errors, one suspects most likely the branching ratios, in particular that of Tl^{196m}. While in the case of Tl^{198m} the assumption that the whole E.C. intensity passes through the 48 keV transition seems reasonable, the greater complexity of the Tl^{196m} conversion spectrum

may have left undiscovered a sufficiently strong branch which by-passes the 84 keV transition. On the other hand, a similar difference between M4 matrix elements is indicated for Hg^{193} and Hg^{195} [1]). It may be remarked that a very detailed knowledge of the decay modes of isomeric states is needed in order to make conclusive studies of such "fine structure effects" in transition probabilities.

We are indebted to Professor The Svedberg for stimulating working conditions, to Fil. Mag. I. B. Svensson for chemical separations, to Ing. R. Ringh for mass separations, and to Ing. Å. Svanheden and his synchrocyclotron crew for irradiations. The work has been financially supported by the Swedish Atomic Energy Commission.

References

1) I. Bergström and G. Andersson, Arkiv Fysik **12** (1957) 415
2) N. Zeldes, Nuclear Physics **7** (1958) 27
3) B. Jung, Nuclear Physics **10** (1959) 440
4) B. Jung, work in progress
5) G. Andersson and I. Bergström, Nuclear Physics **3** (1957) 506
6) G. O. Brink, J. C. Hubbs, W.A. Nierenberg and J. L. Worcester, Phys. Rev. **107** (1957) 189
7) I. Lindgren, C. M. Johansson and S. Axensten, Phys. Rev. Letters **1** (1958) 473
8) J. A. McDonell, R. Stockendal, C. J. Herrlander and I. Bergström, Nuclear Physics **3** (1957) 513
9) S. H. Vegors Jr. and P. Axel, Phys. Rev. **101** (1956) 1067
10) L. L. Marino, W. B. Ewbank, H. A. Shugart and H. B. Silsbee, Bull. Am. Phys. Soc. **3** (1958) 319
11) L. L. Marino, G. O. Brink, W. B. Ewbank, H. A. Shugart and H. B. Silsbee, Bull. Am. Phys. Soc. **3** (1958) 186
12) G. Andersson, J. O. Burgman and B. Jung, Phil. Mag. **3** (1958) 105
13) E. Arbman and N. Svartholm, Arkiv Fysik **10** (1956) 1
14) E. Arbman, Thesis, Univ. of Uppsala 1958
15) T. R. Gerholm and B.-G. Petterson, Nuclear Instruments **4** (1959) 107
16) G. Andersson, Arkiv Fysik **12** (1957) 331
17) J. O. Burgman and G. Andersson, Nuclear Instruments **3** (1958) 33
18) A. H. Wapstra, D. Maeder, G. J. Nijgh and L. T. M. Ornstein, Physica **20** (1954) 169
19) G. Andersson, P. A. Tove, B. Jung and I. B. Svensson, Nuclear Physics **3** (1957) 493
20) I. Bergström, R. D. Hill and G. de Pasquali, Phys. Rev. **92** (1953) 918
21) T. O. Passell, M. C. Michel and I. Bergström, Phys. Rev. **95** (1954) 999
22) M. E. Rose, Internal Conversion Coefficients (North-Holland Publishing Company, Amsterdam, 1958)
23) L. A. Sliv and I. M. Band, Coefficients of Internal Conversion of Gamma Radiation (U.S.S.R. Academy of Sciences, Moscow-Leningrad, 1956 and 1958)
24) M. E. Rose *et al.*, privately distributed tables (1954–1956)
25) B. Åström, B. Johansson and I. Bergström, Arkiv Fysik **12** (1957) 205
26) G. Andersson, E. Arbman, J. O. Burgman and P. A. Tove, quoted by G. Andersson, Arkiv Fysik **12** (1957) 331
27) G. Andersson, E. Arbman and B. Jung, Arkiv Fysik **11** (1957) 297
28) S. H. Vegors Jr. and R. L. Heath, Bull. Am. Phys. Soc. **3** (1958) 209; Phys. Rev., in press
29) I. Bergström, E. Bonacalza and P. Thieberger, private communication (1959)

1.D.2:
1.E.1:
3.A

Nuclear Physics **15** (1960) 125—133; © *North-Holland Publishing Co., Amsterdam*
Not to be reproduced by photoprint or microfilm without written permission from the publisher

DDECAY OF Re^{188}

R. G. ARNS, R. D. RIGGS † and M. L. WIEDENBECK

Harrison M. Randall Laboratory of Physics, The University of Michigan, Ann Arbor, Michigan ††

Received 8 October 1959

Abstract: The gamma rays in Os^{188} following beta decay of 18-h Re^{188} have been studied using coincidence and directional correlation techniques. The results agree with the principal features of the decay scheme proposed by Johns *et al.* [1]). A number of new, weak transitions are observed and an additional level is proposed at 1.750 MeV. Directional correlation measurements were made on six cascades. From the directional correlation measurements, spins 2, 2, 0, 2, 0, 2 are assigned to the levels at 0.155 MeV, 0.633 MeV, 1.086 MeV, 1.461 MeV, 1.765 MeV and 1.941 MeV, respectively. The 0.478-MeV gamma ray is a dipole-quadrupole mixture with $Q \leqq 99\ \%$. The 0.828-MeV and 1.308-MeV gamma rays are pure dipole.

1. Introduction

The decay of 18-h Re^{188} to levels in Os^{188} has been studied by a number of investigators [1–7]) †††. Johns *et al.* [1]) have proposed a decay scheme on the basis of external conversion and coincidence measurements. Os^{188} is on the edge of a region in which the nuclei exhibit a well-defined rotational structure ($155 \leqq A \leqq 185$). A 4+ state has recently been found at 0.479 MeV in Os^{188} fed by the decay of Ir^{188} [8, 9]). It appears that this nucleus does exhibit some rotational structure, and it is hoped that some of the higher excited levels can be related through the unified model.

2. Experimental Procedure

Samples of spectroscopically pure rhenium metal were irradiated at a flux of 2×10^{12} neutrons/cm^2 · sec for periods of 2 to 6 hours in the Ford Nuclear Reactor. The sources used in the coincidence and directional correlation measurements consisted of irradiated rhenium powder dissolved in nitric acid and diluted. The only observed impurity was the 91-h Re^{186}. Data for the 0.478-MeV—0.155-MeV directional correlation were taken during the first few hours after irradiation in order to minimize possible interference from the very

† National Science Foundation Research Participant. Permanent address: Jackson Junior College, Jackson, Michigan.

†† Supported in part by the Michigan Memorial-Phoenix Project and United States Atomic Energy Commission.

††† Since completion of the present research, a report has appeared [13]) which describes directional correlation measurements leading to spin assignments in agreement with the present work.

weak 0.631-MeV—0.137-MeV cascade in Re^{186}. The 91-hour activity did not interfere with any of the other measurements.

The coincidence measurements employed a fast-slow coincidence circuit with a resolving time of 30 ns. Pulses coincident with a selected energy range were fed through a linear gate and recorded on a 256-channel analyzer.

A fast-slow coincidence circuit with a resolving time of 18 ns was used in the directional correlation measurements. The detectors in all cases consisted of 2-in. by 2-in. NaI(Tl) crystals mounted on RCA 6342 or 6342A phototubes. Differential analyzers provided energy selection in the directional correlation measurements. Lateral lead shield was used to prevent counter-to-counter scattering. Data were taken in a double-quadrant sequence at seven angles (i.e., every 15°) in each quadrant. The real coincidence rate was corrected for source decay and electronic drift. After making a least squares fit [10]), the expansion coefficients were normalized and corrected for finite resolution [11]).

3. Results

3.1. COINCIDENCE MEASUREMENTS

Fig. 1 shows the gamma ray spectrum of Re^{188} as recorded on the multichannel analyzer. The observed width of the 1.610-MeV and 1.79-MeV photopeaks indicates that these transitions are complex.

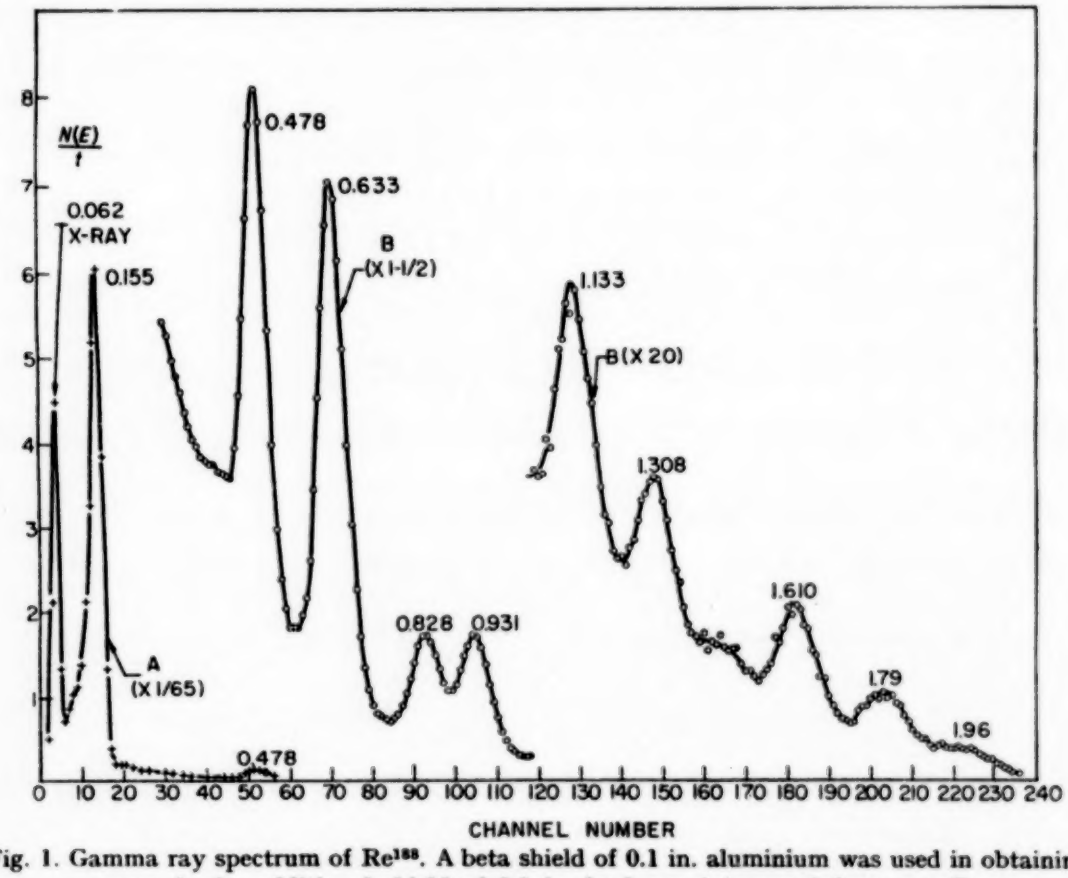

Fig. 1. Gamma ray spectrum of Re^{188}. A beta shield of 0.1 in. aluminium was used in obtaining curve A. An additional shield of 0.1 in. lead was interposed for curve B.

Measurements were made of the spectrum of gamma rays in coincidence with the 0.155-MeV, 0.478-MeV, 0.633-MeV and 0.828-MeV photopeaks. Fig. 2 shows the spectrum of gamma rays coincident with the 0.155-MeV photopeak. A complex peak is found which is made up of the 0.633-MeV and 0.673-MeV transitions. The weak 0.633-MeV and 0.155-MeV peaks are due to the presence of the Compton distribution of higher-energy gamma rays beneath the 0.155-MeV photopeak in the range-selecting channel. The observed complexity of the 1.133-MeV photopeak is attributed to the presence of a weak 1.151-MeV

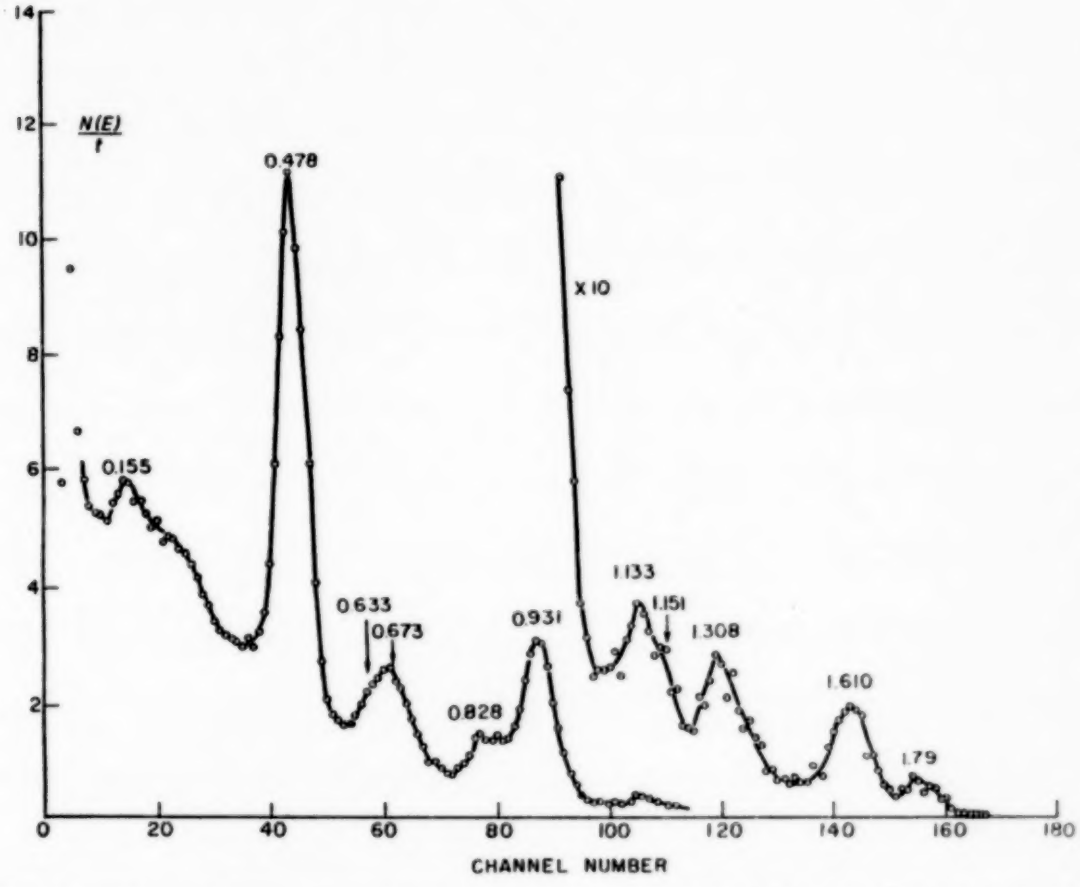

Fig. 2. Spectrum of gamma rays coincident with the 0.155-MeV photopeak. The detector which selected the 0.155-MeV gamma ray was shielded with aluminium to eliminate beta particles. An additional shield of 0.1 in. lead was used for the analyzed detector.

transition between the 1.306-MeV level and the 0.155-MeV level. The 1.609-MeV photopeak also appears to be complex. This is probably due to weakly-fed level ≈ 0.015 MeV below the 1.765-MeV level. Additional evidence for a second level will be discussed in regard to the 1.133-MeV $-$0.633-MeV directional correlation measurement and as a result of the 0.828-MeV coincidence spectrum. The complexity of the peak at 1.79 MeV has been explained by Johns *et al.* [1]). Two gamma rays are present with energies of 1.783 MeV and 1.803 MeV.

Fig. 3 illustrates the spectrum of gamma rays coincident with a narrow range of the 0.633-MeV photopeak. Curve B is the observed coincidence spectrum after subtraction of interference due to the Compton distribution of higher-energy gamma rays beneath the 0.633 MeV peak. The 0.673-MeV photopeak is clearly resolved. The photopeak at 0.480 MeV suggests a weak transition of this energy (in addition to the 0.478-MeV gamma ray), probably between the 1.941-MeV and 1.461-MeV levels. The 1.133-MeV photopeak is wider than would be expected for a single gamma ray.

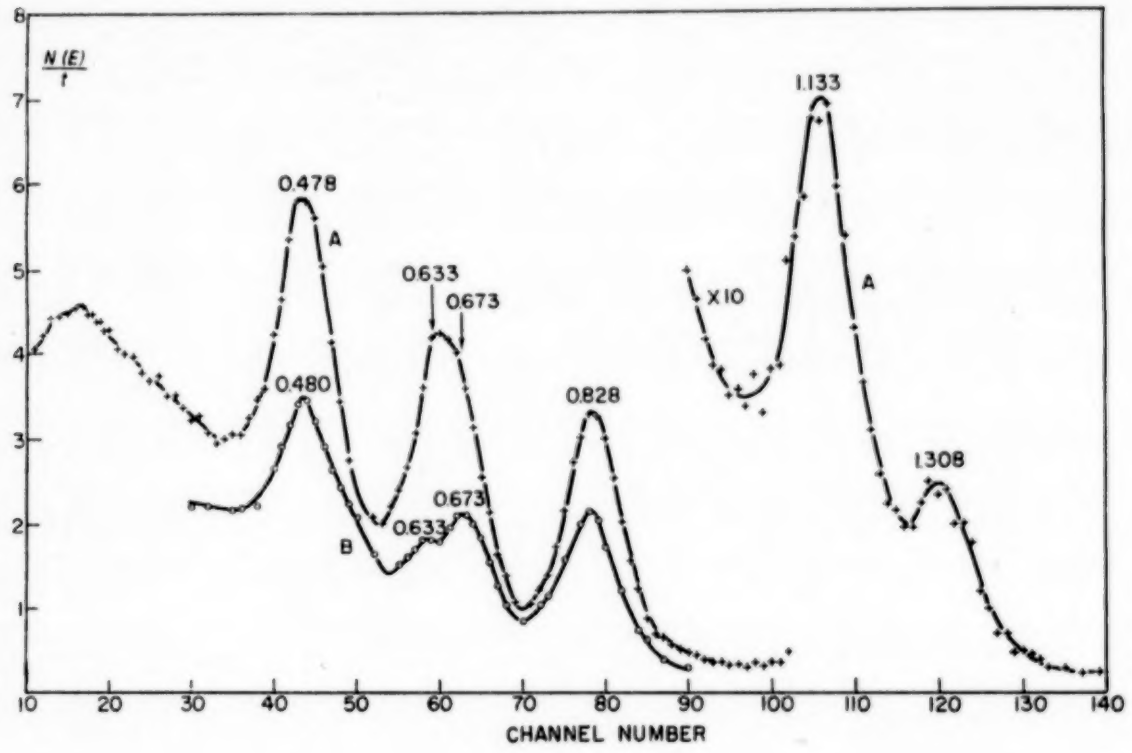

Fig. 3. Spectrum of gamma rays coincident with the 0.633-MeV photopeak. Both detectors were shielded with 0.1 in. each of aluminium and lead. Curve A is the observed coincidence spectrum. Curve B is a similar spectrum after subtraction of interference due to Compton distributions from higher-energy gamma rays beneath the 0.633-MeV photopeak.

The spectrum of gamma rays in coincidence with the 0.828-MeV photopeak is shown in fig. 4. Curve A shows a portion of this coincidence spectrum obtained with detectors shielded to eliminate beta particles. Two new gamma rays are observed at 0.209 MeV and 0.288 MeV. The 0.209-MeV transition is interpreted as a transition from the 1.958-MeV level to a new level at 1.750 MeV. The 0.288-MeV gamma ray is a transition from the 1.750-MeV level to the 1.461-MeV level. These transitions were also observed in a spectrum of gamma rays coincident with the 0.633-MeV photopeak. Curve B was obtained with 0.1 in. lead shielding in addition to the beta shield. The peak at 0.478 MeV is relatively stronger in this spectrum than in the single spectrum when compared with the

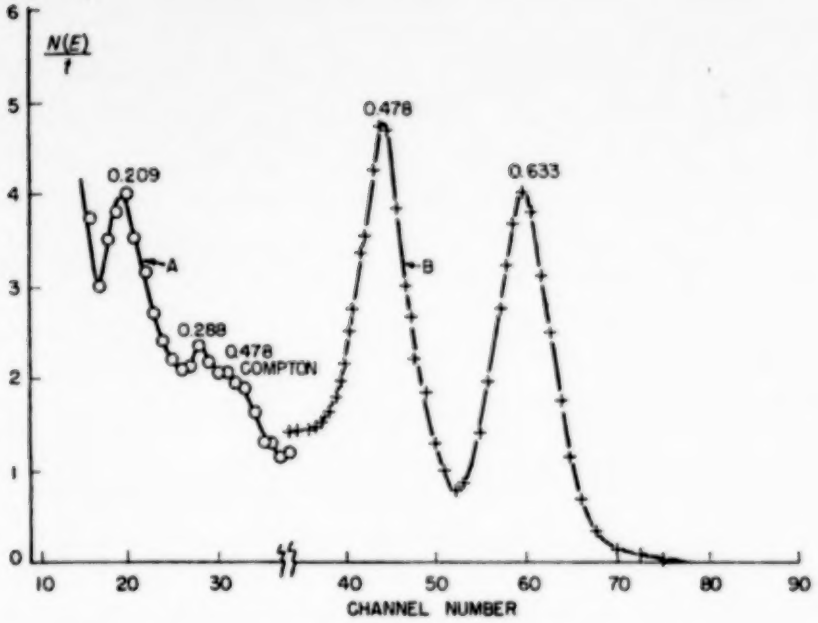

Fig. 4. Spectrum of gamma rays coincident with the 0.828-MeV photopeak. Curve A was recorded with 0.1 in. of aluminium on the detectors to absorb beta particles. For curve B an additional 0.1 in. of lead was added to the shielding. The curves are not drawn to the same scale.

TABLE 1

Relative intensities of the gamma rays of Re^{188}

E (MeV)	Intensity
0.155	7.2 [a]
0.209	0.03
0.288	0.008
0.454	0.02
0.478 [b]	0.62
0.633	1.00
0.673	0.14
0.828	0.35
0.931	0.46
1.133 [b]	0.086
1.151	0.003
1.306	0.007
1.308	0.040
1.610 [b]	0.046
1.783	0.024
1.805	
1.959	0.022

[a] Unconverted gamma ray intensity.
[b] Complex.

The intensities have been normalized to the 0.633-MeV transition. An accuracy of ± 10 % is expected for the strong transitions. The uncertainty may be considerably larger for the weak gamma rays.

0.633-MeV peak. This attests to the relative weakness of the 0.454-MeV transition compared to the 0.673-MeV transition.

The spectrum of coincidences with the 0.478-MeV peak (not shown) indicates the presence of a weak peak at 0.454 MeV as proposed by Johns *et al.* in addition to the other gamma rays expected.

The results of the coincidence measurements are summarized in table 1. The proposed relative intensities were measured from the scintillation spectrometer curves and have been corrected for efficiency and correlation effects.

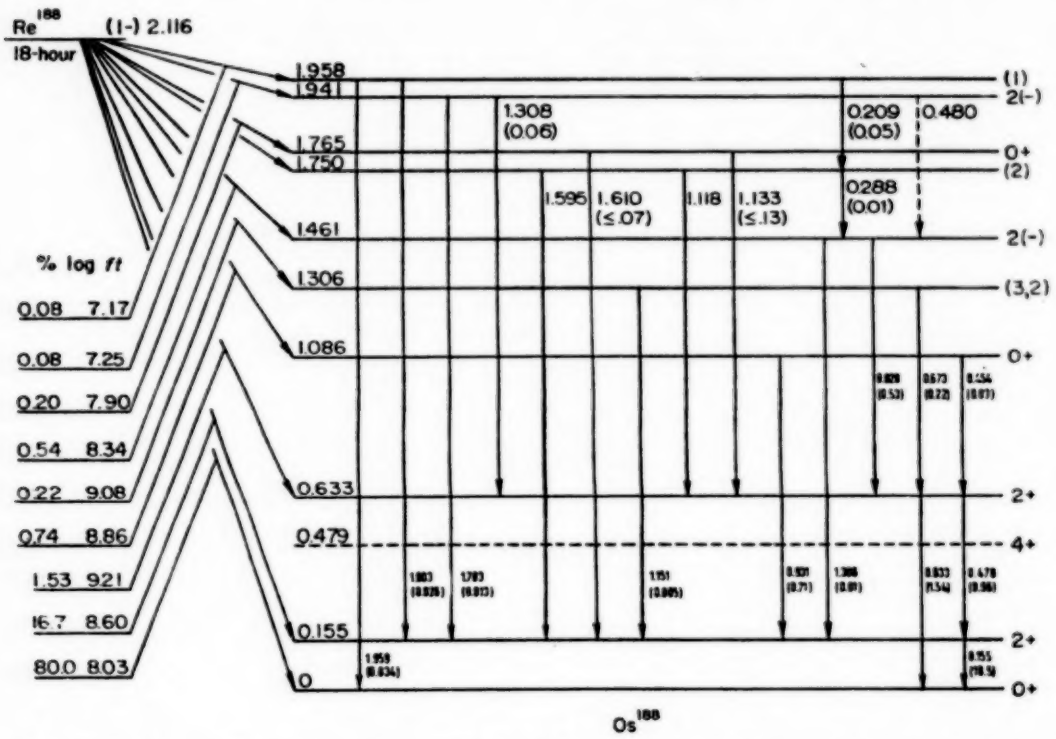

Fig. 5. Decay scheme of Re^{188}. The energies (in MeV) are taken from Johns *et al.* [1]). The relative intensities (in percent) are the result of the present measurements.

The proposed decay scheme is shown in fig. 5. It agrees with the scheme of Johns *et al.* with the exception of some possible weak transitions and an additional level at 1.750 MeV. The log *ft* values quoted have been calculated from the observed gamma-ray branching, making use of the known ground-state beta intensity and conversion coefficients for the 0.155-MeV gamma ray [1]).

3.2. DIRECTIONAL CORRELATION MEASUREMENTS

0.828-MeV — 0.633-MeV CASCADE

This directional correlation was measured by accepting a narrow range of pulses on the 0.828-MeV photopeak in one differential analyzer and the full photopeak of the 0.633-MeV gamma ray in the other differential analyzer.

With this arrangement, about 14.5 ± 1.5 % of the real coincidences observed result from the 1.133-MeV — 0.633-MeV and 1.308-MeV — 0.633-MeV cascades. The interference was measured and subtracted from the observed correlation function. The resultant expansion coefficients, after correction for finite angular resolution, were found to be $A_2 = +0.245\pm0.016$, $A_4 = 0$.

Assuming that the 0.633-MeV gamma ray is pure 2(Q)0, these coefficients are in good agreement with the theoretical coefficients of a pure 2(D)2(Q)0 sequence, $A_2 = +0.250$, $A_4 = 0$. The error limits will allow a quadrupole content of no more than $Q = 0.001$ in the 0.828-MeV gamma ray. The coefficients will not fit sequences of the form 3(D, Q)2(Q)0 or 1(D, Q)2(Q)0.

1.308-MeV — 0.633-MeV and 1.133-MeV — 0.633-MeV CASCADES

Although the 1.308-MeV and the 1.133-MeV photopeaks were easily resolved by the scintillation counters, there remained a slight overlap of these lines which was considered in analyzing the directional correlation data. Two directional correlation measurements were made. In both cases one differential analyzer was set to accept the full photopeak of the 0.633-MeV gamma ray. In one case the second differential analyzer was set on the 1.308-MeV photopeak and in the other case it was set on the 1.133-MeV photopeak.

Using the relative intensities measured in the coincidence experiments, the pair of peaks was constructed from known shapes of single gamma rays in this region. The contribution of both gamma rays to each correlation function was then determined. The two correlation functions were combined with special attention to the errors in the relative intensities, and channel settings. In this manner the 1.133-MeV—0.633-MeV cascade yielded corrected expansion coefficients of $A_2 = +0.150\pm0.046$, $A_4 = +0.702\pm0.060$. The observed A_4 coefficient is too large to allow a spin assignment of 2 to the 1.765 level. Thus the spin of this level must be zero, although the observed coefficients do not agree well with the theoretical coefficients for a 0(Q)2(Q)0 sequence, i.e., $A_2 = +0.3571$, $A_4 = +1.143$. The source was in solution and no attenuation is expected to be present. Potnis *et al.* [4]) observed the full correlation for the 0.478-MeV—0.155-MeV cascade using a metallic source. The lifetime of the 0.633-MeV level is expected to be shorter than that of the 0.155-MeV level and this, together with the fact that the full correlation is observed for other cascades involving the 0.633-MeV level, tends to rule out a perturbation due to extranuclear fields. The present discrepancy can be explained if it is assumed that another level lies close to the 1.765-MeV level and decays via an unresolved gamma ray with energy near 1.133 MeV. This lends strong support to the existence of the level proposed at 1.750 MeV as a result of the coincidence measurements. The presence of the new level does not change the fact that the 1.765-MeV level must be assigned a spin of zero.

In the manner described above, the corrected expansion coefficients for the

1.308-MeV—0.633-MeV cascade were found to be $A_2 = +0.309 \pm 0.065$, $A_4 = +0.044 \pm 0.089$. These coefficients agree well with the theoretical coefficients for a 2(D)2(Q)0 cascade, namely $A_2 = +0.25$, $A_4 = 0$. If this sequence is of the form 2(D, Q)2(Q)0, the coefficients limit the quadrupole content of the 1.308-MeV transition to $Q \leqq 0.035$. The experimental coefficients will also fit a 3(D, Q)2(Q)0 sequence if the quadrupole content is in the range $Q = 0.42 \pm 0.13$. This degree of mixing is highly improbable and therefore the 1.941-MeV level is assigned a spin 2.

0.931-MeV — 0.155-MeV CASCADE

In this directional correlation the window of one differential analyzer was set to accept the 0.155-MeV photopeak. The second analyzer was set to accept a narrow range of pulses on the upper portion of the 0.931-MeV photopeak. With this arrangement a small fraction of the real coincidences accepted were due to 0.828-MeV—0.155-MeV cascade and an additional small interference resulted from coincidences of the 0.155-MeV gamma ray with the Compton distributions of higher-energy gamma rays beneath the 0.931-MeV gamma ray. The interfering correlations were measured and subtracted from the observed coefficients. After correction for finite angular resolution, the expansion coefficients were found to be $A_2 = 0.35 \pm 0.05$, and $A_4 = +1.06 \pm 0.17$. These are in good agreement with the theoretical coefficients for a 0(Q)2(Q)0 sequence, i.e., $A_2 = +0.3571$ and $A_4 = +1.143$. The observed coefficients will not fit any other spin sequence.

0.478-MeV—0.155 MeV CASCADE

For this cascade, each of the differential analyzers was allowed to accept the full-energy peak of one of the gamma rays. Due to the complexity of the decay, a significant portion of the real coincidences accepted were due to other cascades which were measured and subtracted from the basic correlation function. This yielded corrected expansion coefficients of $A_2 = -0.079 \pm 0.054$ and $A_4 = = +0.402 \pm 0.083$. These coefficients will fit a 2(D, Q)2(Q)0 sequence with a large ($Q \geqq 0.99$) quadrupole content in the first transition.There appears to be good evidence for other gamma rays at energies near 0.478 MeV in coincidence with the 0.155-MeV transition. Hence, the quadrupole content derived above may be somewhat in error, although the spins of the 0.633-MeV and 0.155-MeV levels are certainly 2. Neither of the previous directional correlation measurements on this cascade [4, 7]) took the interference into consideration.

0.673-MeV — 0.633-MeV CASCADE

A directional correlation measurement was attempted on the weak 0.673-MeV—0.633-MeV cascade. However, the interference from other cascades is quite large as can be seen from fig. 3, curve B. This results in large errors on the

expansion coefficients. Within these limits, the expansion coefficients were consistent with a spin 3 or 2 for the 1.306-MeV level in agreement with the observed gamma ray branching.

4. Summary and Discussion

As a result of directional correlation measurements, spins 2, 2, 0, 2, 0 and 2 have been assigned to the levels at 0.155 MeV, 0.633 MeV, 1.086 MeV, 1.461 MeV, 1.765 MeV and 1.941 MeV, respectively. The transition from the second 2+ state to the first excited state (spin = 2+) has been shown to be mostly E2 with a small M1 admixture. A 4+ state has recently been found at 0.479 MeV (fed from Ir^{188} [8, 9]). This state and the first excited state are interpreted as members of the ground-state rotational band.

As a result of the directional correlation measurements, it has been shown that the 1.308-MeV and 0.828-MeV gamma rays are nearly pure dipole transitions from spin 2 states to the 2+ level at 0.633 MeV. If the de-excited levels have positive parity, the resultant gamma rays must be M1 in character, which is contrary to the interpretation of these levels as collective excitations. If negative parity is assumed, the calculated log *ft* values for beta decay to the 1.941-MeV and 1.461-MeV levels, viz., 7.25 and 8.34, are larger than would be expected.

The second 2+ state at 0.633 MeV may be considered as a member of the ground-state rotational band in terms of the interpretation of the unified model due to Davydov and Filippov [12]). Many of the high-energy gamma rays observed following the decay of Ir^{188} do not occur in the decay of Re^{188}. This indicates that a different set of levels are fed by the two decays. An attempt to interpret the higher excited states of Os^{188} may be more reasonable when more is known concerning the levels fed from Ir^{188}.

The authors wish to acknowledge the aid of R. E. Sund in recording some of the data.

References

1) Johns, McMullen, Williams and Nablo, Can. J. Phys. **34** (1956) 69
2) C. C. McMullen and M. W. Johns, Phys. Rev. **91** (1953) 418
3) Richmond, Grant, and Rose, Proc. Phys. Soc. A **65** (1952) 484
4) Potnis, Dubey and Mandeville, Phys. Rev. **102** (1956) 459
5) V. R. Potnis, Phys. Rev. **104** (1956) 722
6) K. O. Nielsen and O. B. Nielsen, Nuclear Physics **5** (1958) 519
7) T. Wiedling, Directional Correlation Measurements and Some Other Related Investigations of Excited Nuclei (Almquist and Wiksells Boktryckeri AB, Uppsala, 1956)
8) R. M. Diamond and J. M. Hollander, Nuclear Physics **8** (1958) 143
9) P. S. Fisher and R. A. Naumann, Phys. Rev. **112** (1958) 1717
10) M. E. Rose, Phys. Rev. **91** (1953) 610
11) Arns, Sund and Wiedenbeck, Univ. of Mich. Res. Inst. Report 2375-4-T, February, 1959
12) A. S. Davydov and G. F. Filippov, Nuclear Physics **8** (1958) 237
13) W. J. King and M. W. Johns, Can. J. Phys. **37** (1959) 755

1.D.2:1.
E.4:2.H

Nuclear Physics **15** (1960) 134—142; © *North-Holland Publishing Co., Amsterdam*
Not to be reproduced by photoprint or microfilm without written permission from the publisher

INELASTIC SCATTERING FROM ODD-MASS RARE EARTHS

M. C. OLESEN and B. ELBEK

Institute for Theoretical Physics, University of Copenhagen, Denmark

Received 13 October 1959

Abstract: The reduced electric quadrupole transition probabilities and excitation energies of the accessible low lying states in Eu^{151}, Eu^{153}, Tb^{159}, Ho^{165}, Er^{167} and Tm^{169} have been measured by Coulomb excitation with protons or deuterons having an initial energy of about 4.5 MeV. The measurements were performed on the groups of inelastically scattered particles by means of a magnetic spectrograph, a method particularly suited for the determination of the absolute transition probability. The results are discussed in terms of the rotational model.

1. Introduction

The work reported in this paper is part of a systematic survey of the E2-transition probabilities for low lying rotational states of nuclei in the region of the rare earths by means of Coulomb excitation. The cross section is determined by measuring the number of inelastically scattered particles relative to the number of elastically scattered particles. The absolute inelastic cross section is obtained by assuming that the Rutherford scattering law is valid for the elastic scattering.

2. Experimental Arrangement

The apparatus and the experimental procedure are the same as described in earlier papers [1, 2, 3]). Protons or deuterons were accelerated in a 5 MeV electrostatic generator and passed a 90° analyzing magnet before they hit the target placed at the source position of a heavy-particle spectrograph. The particles scattered through 145° into the spectrometer were recorded after energy analysis on 25 or 50 μ C-2 Ilford nuclear research plates.

3. Targets

Separated targets of Er^{167} were prepared in the electromagnetic isotope separator of this Institute. The separated isotopes of Eu were obtained in the form of oxides from Oak Ridge National Laboratory. Tb, Ho, and Tm have only one stable isotope each. We are greatly indebted to Professor Spedding, Iowa State College, for supplying us with samples of pure oxides of these elements.

From the oxides the targets were prepared by evaporation in vacuo. In order to obtain a convenient rate of evaporation it is necessary to use temperatures between 2000 and 3000° C. We found that the most suitable way of obtaining these high temperatures was to use a small crucible heated by electron bombardment. The apparatus used is shown in fig. 1. The cylindrical 2×5 mm crucibles were made from spectroscopically pure carbon rods, and were normally loaded with 1—5 mg of the oxide together with a drop of pure nitric acid. By subsequent heating the nitrate formed was again transformed into the oxide, but now the material had less tendency to "jump" off the crucible during the first stages of evaporation. An electron current of 100 mA accelerated through

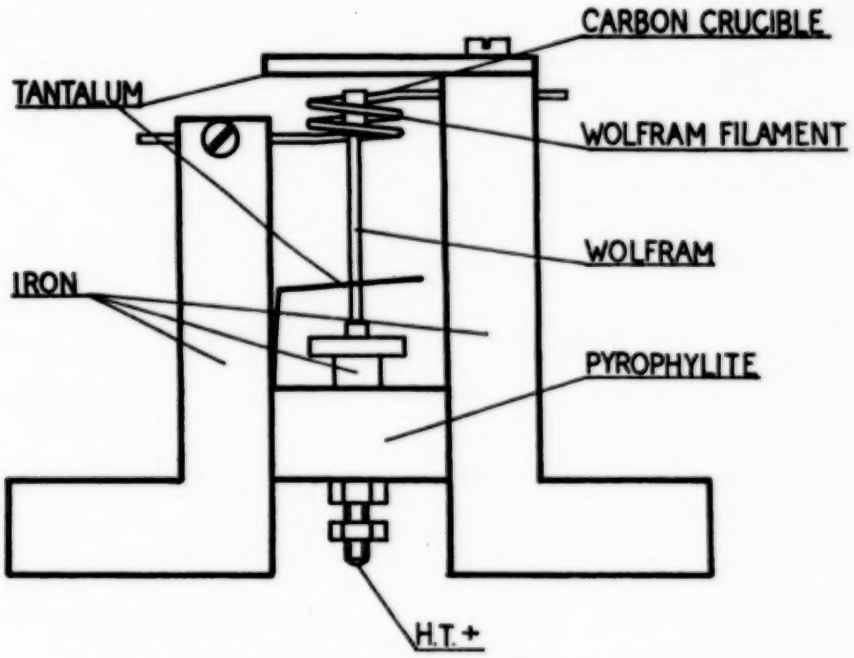

Fig. 1. Arrangement for heating the small crucible by electron bombardment.

1 kV would raise the temperature of the crucible to about 3000° C. It was interesting to note how the presence of several of the rare earths gave a considerable increase in the electron emission from the tungsten filament.

The use of carbon crucibles has a serious disadvantage: it appeared that the oxides were often reduced to carbides of very low vapour pressure. Therefore, we also tried to use crucibles of tantalum; but it turned out that the targets then became contaminated with tantalum, which was very inconvenient for our purpose. Furthermore, the tantalum available contained a small amount of a lighter element, probably tin, also giving rise to target contamination.

The target backings were mostly aluminium-coated formvar, but also pure carbon foils have been used. The latter have some advantages compared to the aluminium-formvar foils. Especially they are more heat-resistant, a property of

great importance here, where the evaporation temperature is so high. In the deuteron exposures one also avoids the often troublesome protons from (d, p) reactions in aluminium.

The carbon foils, which normally had a thickness of 50—100 μg per cm^2, were prepared by evaporation in vacuo onto glass slides. The evaporation took place from an arc between two spectroscopically pure carbon rods in a way similar to that described by Sarma [4]). To avoid target contamination we found it advantageous to replace the NaCl-layer used by Sarma by a thin layer of sugar, which was obtained by dipping the carefully cleaned slide into a glucose solution. The excess sugar was removed by rubbing to dryness with a clean piece of cotton. After evaporation the foils were floated off the plate on the surface of distilled water, and could then be "fished" on an aluminium target frame.

4. Results

With the exception of Eu^{151} all the nuclei investigated are strongly deformed. Under the experimental conditions employed, the Coulomb excitation of an odd-mass deformed nucleus appreciably populates only the two lowest excited states of the ground-state rotational band. This experiment directly measures the differential cross section for excitation of these states. From the measured cross section for inelastic scattering the reduced electric quadrupole transition probability was determined by means of the formula for the differential cross section of electric quadrupole excitation [5]). In this calculation we have made use of the classically evaluated function $f(\xi, \theta)$ (table 2, 8 of ref. [5])) since for the cases considered this function does not deviate markedly from the exact,

TABLE 1

Measured excitation energies, electric quadrupole transition probabilities, and intrinsic quadrupole moments

Nucleus	I_0	E_1	E_2	E_2/E_1	B_1(E2)	B_2(E2)	B_2/B_1	Q_0
Eu^{151}	$\frac{5}{2}$	195	306	—	0.09 ± 0.01	0.46 ± 0.04	—	—
Eu^{153}	$\frac{5}{2}$	83	194	2.34	2.28 ± 0.10	0.70 ± 0.04	0.307	6.94
Tb^{159}	$\frac{3}{2}$	59	138	2.34	2.81 ± 0.08	1.45 ± 0.06	0.516	7.41
Ho^{165}	$\frac{7}{2}$	94	206	2.22	2.41 ± 0.07	0.63 ± 0.04	0.261	7.56
Er^{167}	$\frac{7}{2}$	80	178	2.23	2.57 ± 0.08	0.60 ± 0.04	0.233	7.80
Tm^{169}	$\frac{1}{2}$	—	117	—	—	3.37 ± 0.07	—	7.52

I_0 is the ground state spin, E_1 and E_2 are the energies of the first and second excited states, respectively, in keV. B_1(E2) and B_2(E2) are the corresponding reduced transition probabilities in units of $e^2\times10^{-48}$ cm^4. Q_0 is the intrinsic nuclear quadrupole moment derived from the B_1(E2) (except in the case of Tm^{169} where only the B_2(E2) could be measured) by use of the formulae of the rotational model [5]). The unit is here 10^{-24} cm^2. The errors given on the B(E2)-values are standard deviations on the mean. The errors on the excitation energies are estimated to be 1—2 keV.

quantally evaluated function [6]). The excitation energies, which in most cases were known with a good accuracy from other experiments, were — as a check on the bombarding conditions and isotopic assignment — determined from the position of the inelastic groups on the photographic plate.

The results of our measurements are shown in table 1. The table also lists the ratio of the excitation energies and the ratio of the transition probabilities for the observed rotational states in each nucleus. The transition probabilities are directly related to the intrinsic nuclear quadrupole moment Q_0. Furthermore the table lists the Q_0 for the deformed nuclei obtained from the formulae of the rotational theory [5]).

A few remarks concerning the individual nuclei are given below.

Eu^{151}. The spectrum of Eu^{151} is not of the rotational type [7]). The exposures were performed on targets containing 95 % Eu^{151} and 5% Eu^{153}. The presence of Eu^{153} in the target was troublesome in view of the fact that the first excited state in Eu^{151} has almost the same energy as the second excited state in Eu^{153}. The corresponding groups would therefore coincide on the photographic plate. The cross section for the second excited state in Eu^{153} is about seven times larger than the cross section for excitation of the first state in Eu^{151}. Furthermore, the Eu^{151} cross section is so small that the intensity of the inelastically scattered particles is of the same order of magnitude as the intensity of accidentally scattered particles. The uncertainty on the B_1(E2)-value might therefore be somewhat higher than the standard deviation stated in table 1. Nevertheless, the measured transition probabilities are in good agreement with earlier measurements by Class and Meyer-Berkhout [7]).

Tb^{159}. Out of nine exposures on Tb three were made on targets containing 10 % Dy. The correction for the Dy content was obtained from the intensity of the inelastically scattered groups belonging to the first rotational states in Dy^{162} and Dy^{164} by using the recently determined reduced transition probabilities for these states [8]).

The other measurements were made on targets prepared from 99 % pure Tb.

Ho^{165}. The measured excitation energies and transition probabilities are in agreement with earlier Coulomb excitation measurements in which γ-ray or conversion electron detection has been used and they are in agreement with the rotational theory for a spin $\frac{7}{2}$ nucleus.

Recently, the excitation energies for Coulomb excited levels of several of the rare earth nuclei have been accurately measured with a curved crystal spectrometer [9]). Generally, the excitation energies we determine from inelastic scattering are in agreement with the accurately determined ones within a kilovolt or so, i.e., within our stated error. In the case of the second excited state in Ho, however, we find an energy of 209 ∓ 2 keV in agreement with the average value of other determinations [10, 11, 12, 13]) whereas the energy given in ref. [9]) is 204.63 keV.

We mention this discrepancy because it is the only case in which the energy ratios determined in ref. [9]) deviate considerably from the rotational prediction. An energy of 209 keV for the state in question would be in excellent agreement with the theory.

A spectrum of inelastically scattered deuterons from Ho is shown in fig. 2.

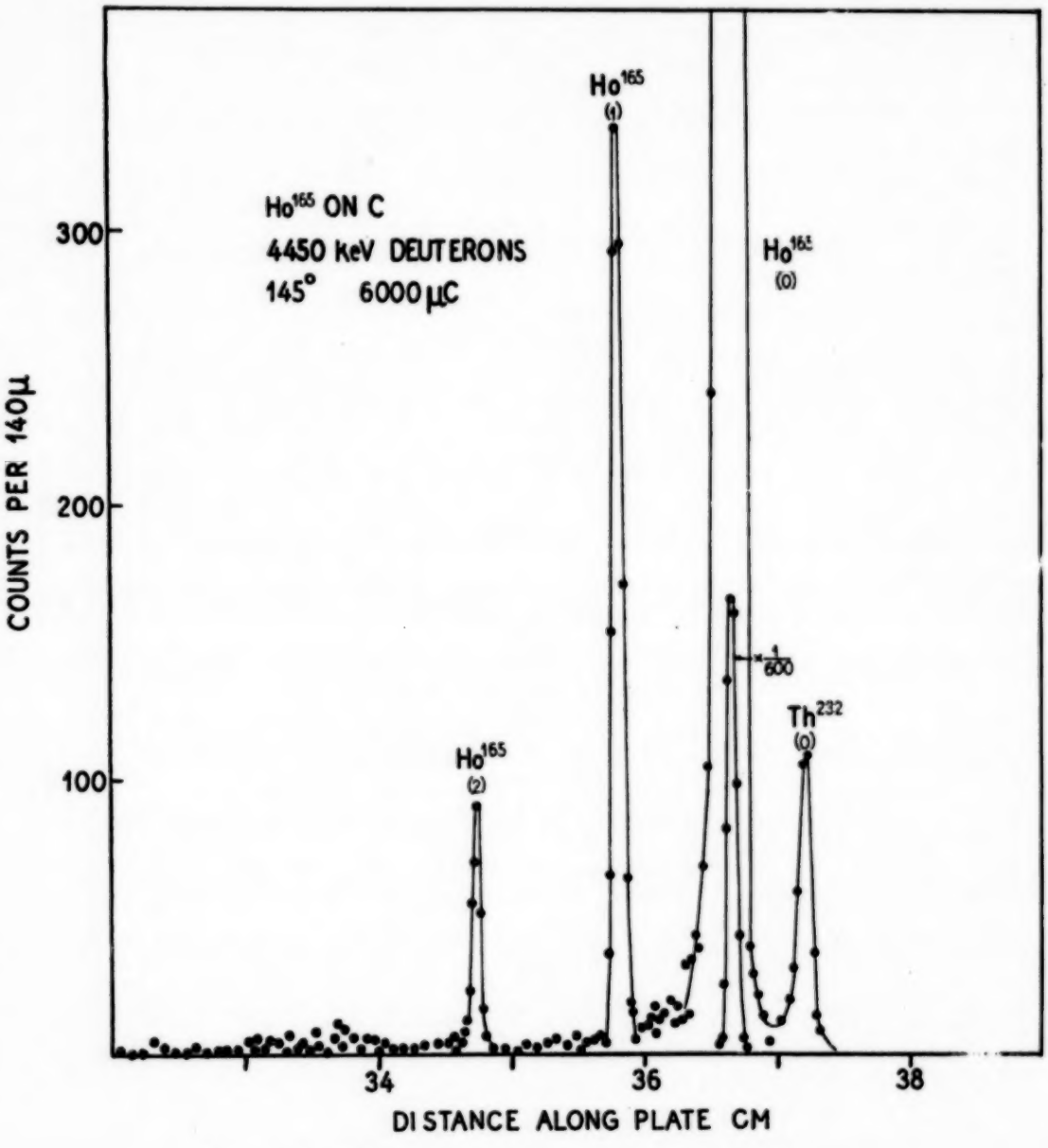

Fig. 2. Spectrum of deuterons scattered from a Ho-target.

Er^{167}. The Er^{167} targets were all prepared in the electromagnetic isotope separator. The collecting system was changed somewhat from that described earlier [1,3]), the ions now being sputtered from a piece of graphite onto carbon foils. The method will be described in more detail in a forthcoming paper [8]).

The measured energies and transition probabilities fit the rotational model for a nucleus with ground state spin $\frac{7}{2}$.

Tm^{169} is known to have ground state spin $\frac{1}{2}$. According to the rotational theory it has an "anomalous" spectrum, the first excited state being at 8 keV [13]). Due to the intense elastic group this state could not be observed. We found only one group ascribed to inelastic scattering from Tm, corresponding to an excitation energy of 117 keV, in agreement with earlier measurements [13]). It is reasonable to assume that the 117 keV level has spin $\frac{5}{2}$ [14]). The rotational theory then yields the intrinsic quadrupole moment given in table 1.

5. Discussion

According to the rotational theory the ratio of the E2-transition probabilities from the ground state to the two rotational states observed should be dependent on the ground state spin only [5]). This is also the case for the ratio of the excitation energies of these states. For convenience, we have collected the theoretical ratios in table 2. In fig. 3 the measured ratios B_2/B_1 are compared

TABLE 2

Theoretical ratio of the energies and of the reduced electric quadrupole transition probabilities for the two first excited rotational states in an odd-mass nucleus

Ground state spin I_0	E_2/E_1	B_2/B_1
$\frac{1}{2}$	—	1.500
$\frac{3}{2}$	2.40	0.556
$\frac{5}{2}$	2.29	0.350
$\frac{7}{2}$	2.22	0.257
$\frac{9}{2}$	2.18	0.204

with the ratios predicted from the rotational theory. The figure also includes the results of our earlier measurements on odd-mass nuclei [1, 2, 3]). In most cases the measured ratios are in reasonable agreement with the theoretical predictions although on the average, they are somewhat smaller than expected (about 8 %). This deviation might partly be real, partly due to experimental errors. It is worth noting that the largest discrepancies are found in cases when the experimental technique was not yet fully developed (Dy^{161} and Dy^{163}). On the other hand it is interesting to compare our ratios with those measured by Goldring and Paulissen [12]) who used a coincidence technique. For nuclei in about the same region as considered here their average ratio is about 7 % lower than expected from theory.

Various perturbations could cause deviations from the simple rotational description of the levels [5]). Actually it is known that such perturbations are responsible for the increase in the nuclear moment of inertia of odd nuclei

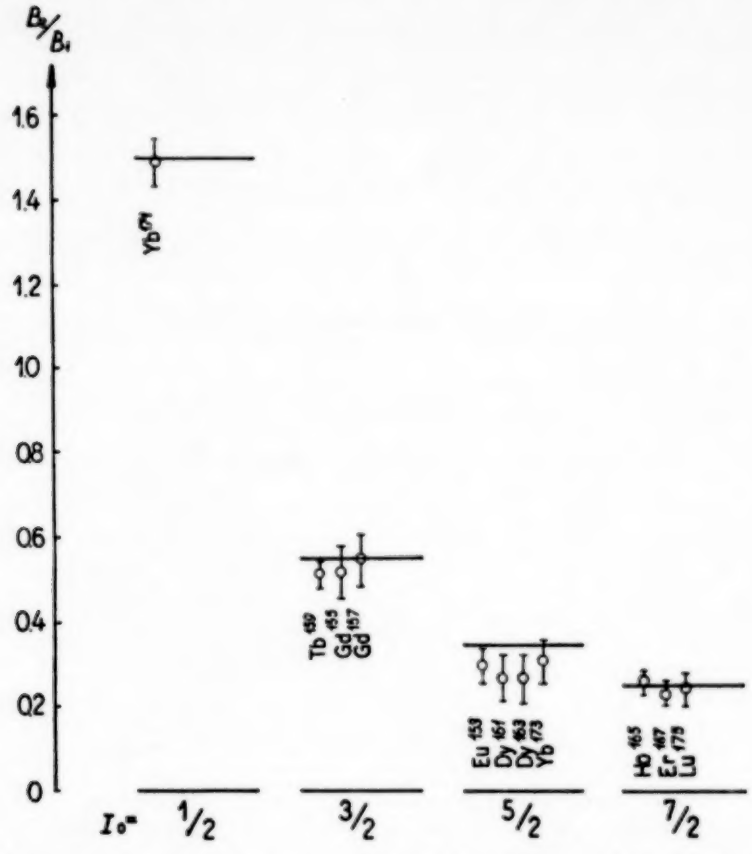

Fig. 3. Ratios between the transition probabilities for the second and the first excited state compared with the rotational prediction.

relative to even nuclei for rotational levels. In the same way the transition probabilities will be somewhat affected. However, theoretical estimates indicate that the perturbations so far considered should modify the ratio of the B(E2)-values by a few percent only [15]).

6. Nuclear Deformation

By assuming the nucleus to be an uniformly charged spheroid the intrinsic quadrupole moment Q_0 can be related to a deformation parameter for the nucleus. We have chosen to express the nuclear deformation by the parameter β connected with Q_0 through the equation [5])

$$Q_0 = \frac{3}{\sqrt{5\pi}} Z R_0^2 \beta (1+0.16\beta).$$

The values of β for the nuclei investigated are tabulated in table 3. In fig. 4 our experimental deformations are compared with those calculated by Mottelson and Nilsson [14]) by minimizing the total nuclear energy when the particles are

TABLE 3

Nuclear deformation parameter derived from the observed E2 transition probabilities to the first excited rotational state

Nucleus	Eu^{153}	Gd^{155}	Gd^{157}	Tb^{159}	Dy^{161}	Dy^{163}	Ho^{165}	Er^{167}	Tm^{169}	Yb^{171}	Yb^{173}	Lu^{175}	Lu^{176}
β	0.338	0.308	0.308	0.336	0.326	0.321	0.327	0.330	0.310	0.319	0.311	0.292	0.289

filled pairwise into Nilsson orbits. The experimental deformations appear to be somewhat smaller than the calculated ones, although there is some similarity between the two curves.

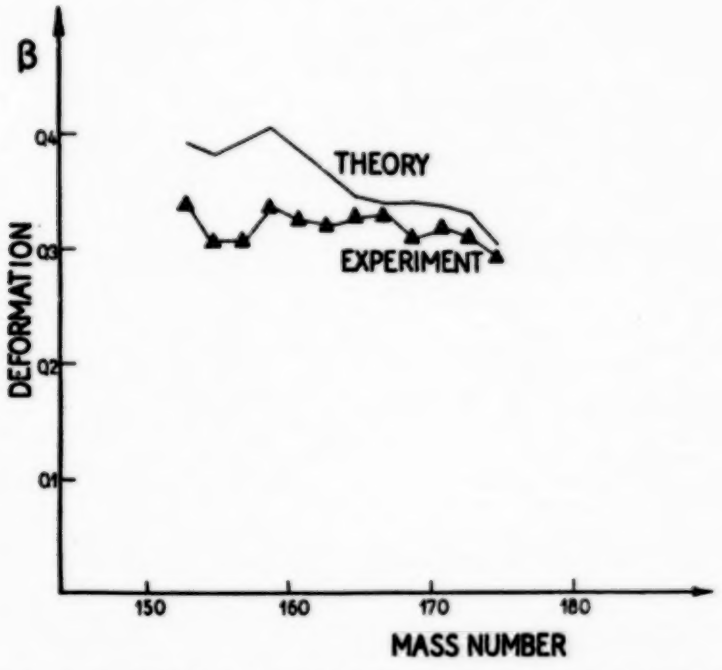

Fig. 4. Deformation parameter β for ellipsoidal shapes obtained from the measured Q_0-values. The solid line shows the β-values calculated by Nilsson and Mottelson.

We wish to thank Professor Niels Bohr for the excellent working conditions at his Institute and Professor Aage Bohr for enlightening discussions. We are indebted to Mr. O. Skilbreid for preparing the Er-targets in the isotope separator and to Mr. P. Ambrosius-Olesen for his invaluable help in the experiments. We also wish to thank Mrs. Ruth Hansen and Miss Helle Hansen for scanning the plates.

References

1) B. Elbek, K. O. Nielsen and M. C. Olesen, Phys. Rev. **108** (1957) 406
2) V. Ramsak, M. C. Olesen and B. Elbek, Nuclear Physics **6** (1958) 451
3) B. Elbek, M. C. Olesen and O. Skilbreid, Nuclear Physics **10** (1959) 294
4) N. Sarma, Nuclear Instruments **2** (1958) 361
5) K. Alder, A. Bohr, T. Huus, B. Mottelson and A. Winther, Revs. Mod. Phys. **28** (1956) 432
6) J. Bang, private communication
7) C. M. Class and U. Meyer-Berkhout, Nuclear Physics **3** (1957) 656
8) B. Elbek, M. C. Olesen and O. Skilbreid, to be published in Nuclear Physics
9) E. L. Chupp, J. W. M. DuMond, F. J. Gordon, R. C. Jobson and Hans Mark, Phys. Rev. **112** (1958) 518
10) N. P. Heydenburg and G. M. Temmer, Phys. Rev. **105** (1957) 1524
11) E. M. Bernstein and H. W. Levis, Phys. Rev. **104** (1956) 981
12) G. Goldring and G. T. Paulissen, Phys. Rev. **103** (1956) 1314
13) T. Huus, J. H. Bjerregård and B. Elbek, Mat. Fys. Medd. Dan. Vid. Selsk. **30**, No. 17 (1956)
14) B. R. Mottelson and S. G. Nilsson, Mat. Fys. Skr. Dan. Vid. Selsk. **1**. No. 8 (1959)
15) P. C. Hemmer, private communication

1.D.3:
2.F

Nuclear Physics **15** (1960) 143—145; © *North-Holland Publishing Co., Amsterdam*

Not to be reproduced by photoprint or microfilm without written permission from the publisher

EINE KERNREAKTION VOM TYP (α, α+3n)

WOLFGANG RIEZLER

Institut für Strahlen- und Kernphysik der Universität Bonn

Eingegangen am 27. September 1959

Abstract: If cesium is irradiated with alpha-particles, at energies higher than about 55 MeV Cs^{130} is formed. From a calculation of the reaction energies involved it follows that the reaction is (α, α+3n). It is suggested that the alpha-particle behaves inside the struck nucleus as a cluster, which is emitted again, before all his kinetic energy is distributed to form a compound nucleus.

Bei der Bestrahlung von Rhodium mit Alphateilchen von etwa 60 MeV [1]) hatte sich gezeigt, daß mit verhältnismäßig großer Häufigkeit neutronenarme Isotope des bestrahlten Elements auftreten. Nun überwiegt in der Mitte des periodischen Systems auch bei der hier in Frage kommenden Anregungsenergie die Wahrscheinlichkeit für die Aussendung eines Neutrons aus einem Zwischenkern, die jenige für die Aussendung eines Protons so erheblich, daß Prozesse vom Typ (α, 2p+xn) sehr selten sein sollten. Auch erschien es zweifelhaft, ob die verfügbare Energie überhaupt für die Aussendung der erforderlichen Zahl von einzelnen Nukleonen ausreichend war, so daß auch die Entstehung der beobachteten Nukleide über einen (α, xn)-Prozeß und zwei anschließende β^+- oder K-Umwandlungen nicht sehr wahrscheinlich war. Es lag vielmehr der Verdacht nahe, daß hier (α, α+xn)-Prozesse vorlagen, die bisher an schweren Elementen nicht beobachtet worden sind.

Um festzustellen, ob derartige Prozesse vorkommen, wurde Caesium 133 mit Alphateilchen des Bonner Synchro-Zyklotrons bestrahlt. Die Energietönung der Reaktion Cs^{133} (α, 2p+5n) wäre 55 MeV; der Schwellenwert für die Reaktion müsste aber um mehr als 10 MeV höher liegen, da die austretenden Nukleonen, insbesondere die Protonen, noch einen erheblichen Betrag an kinetischer Energie mitnehmen müssten. Der Prozess Cs^{133}(α, 2p+5n) kann daher auch bei der höchsten von uns angewandten Einschussenergie von 64 MeV noch nicht mit beobachtbarer Intensität auftreten. Die Bildung von Cs^{130} durch radioaktive Umwandlung einer Muttersubstanz ist nicht möglich, da das infrage kommende Mutternukleid Ba^{130} stabil ist; ein Teil des Cs^{130} geht durch β^--Umwandlung mit einer Umwandlungsenergie von 0.44 MeV in dieses über.

Wenn also Cs^{130} bei der Bestrahlung von Caesium mit Alphateilchen auftritt, so kann es nur durch die Reaktion Cs^{133}(α, α+3n) entstanden sein. Die Energietönung für diese Reaktion ist 29 MeV, es stehen schon bei 54 MeV Einfalls-

energie 25 MeV als kinetische Energie für die austretenden Teilchen zur Verfügung, wovon der grösste Teil auf den wieder austretenden Heliumkern entfallen dürfte.

Das Caesium wurde in Form von Caesiumchlorid als Pulver in einer Schichtdicke von ca. 0.2 mm im Inneren des Zyklotrons bestrahlt. Die Bestrahlungsdauer war jeweils 3 bis 5 Minuten, die Stromstärke 0.1 bis 0.25 μA. Das bestrahlte CsCl wurde in destilliertem Wasser gelöst. Dieser Lösung wurde etwas $La_2(NO_3)_3$-Lösung zugesetzt und daraus das Lanthan mit Oxalsäure gefällt. Dann wurde dem Filtrat Bariumchlorid-Lösung zugesetzt und das Barium als Sulfat gefällt. Schließlich wurde noch durch Zusatz von Silbernitratlösung das Chlor aus dem Filtrat entfernt. Alle Niederschläge und das Endfiltrat, welches das gesamte Caesium enthält, wurden mit Szintillationsspektrometern untersucht.

In allen Fällen war die stärkste Aktivität in der Lanthan-Fraktion. Hier wurden bei allen Versuchen Halbwertszeiten von 4 Stunden, 6.5 Minuten und 9 Minuten nachgewiesen, bei denen überall eine starke Vernichtungsstrahlung von 0.51 MeV auftrat. Bei der 4-Stunden-Aktivität handelt es sich um die Isotope 132 oder 133 ((α, 5n) und (α, 4n)), bei der 6.5-Minuten-Aktivität um das Isotop 134 (α, 3n), bei der 9-Minuten-Aktivität um das Isotop 136 (α, n). Das Isotop La^{135} konnte wegen seiner verhältnismäßig langen Halbwertszeit nicht beobachtet werden.

Die Barium-Fraktion zeigte nur eine verhältnismäßig geringe Aktivität, die nicht näher untersucht wurde.

Auch in der Chlor-Fraktion zeigte sich eine Vernichtungsstrahlung mit einer Halbwertszeit von etwa 30 min, da sich in dem bestrahlten Chlorid Cl^{34} gebildet hatte. Ob dieses Isotop durch (α, α+xn) oder durch Cl^{35}(α, 5n) und nachfolgende Umwandlung eines kurzlebigen Kalium- und Argon-Isotops gebildet wird, wurde durch den vorliegenden Versuch nicht sicher entschieden. Da Chlor 34 starke energiereiche Gamma-Linien zeigt, die beim Caesium 130 fehlen, konnte es leicht von dem letzteren unterschieden werden.

Im Cäesium-Filtrat zeigten die mit den höchsten Energien bestrahlten Proben eine Vernichtungsstrahlung mit 0.51 MeV, die mit einer Halbwertszeit von 30 Minuten abfiel. Durch das Fehlen von Gamma-Linien höherer Energie war eindeutig bewiesen, daß diese Strahlung nicht durch etwa nicht mit ausgefällte Cl^{34} hervorgerufen war.

Es wurden im ganzen vier Versuchsreihen durchgeführt mit einer Maximalenergie der Alphastrahlung von 64, 60, 54 und 47 MeV. Dabei ist zu berücksichtigen, daß die Energie-Inhomogenität der Alphateilchen im inneren Strahl unseres Zyklotrons einige MeV beträgt. Sie ist bei den einzelnen Versuchen nicht sehr genau bekannt, da sie erheblich von den jeweiligen Betriebsbedingungen der Maschine abhängt. Ebenso bedingt die endliche Dicke der Caesium-Chlorid-Schicht eine Energieunschärfe von einigen MeV. Auf Sättigungsaktivität

umgerechnet verhielt sich die Intensität der 0.51 MeV-Linie von Cs^{130} zu der von $La^{132+133}$ bei der höchsten Bestrahlungsenergie von 64 MeV etwa wie 1 : 30. Bei 60 MeV-Energie der Alphateilchen war die Aktivität des Cs^{130} auf gleiche Ionenzahl im Strahl umgerechnet auf etwa die Hälfte zurückgegangen. Bei 54 MeV war die 30-Minuten-Aktivität des Cs^{130} nicht mehr sicher nachzuweisen. Bei 47 MeV war sie sicher nicht mehr vorhanden. Die Versuche zeigen, daß die Reaktion $Cs^{133}(\alpha, \alpha+3n)Cs^{130}$ ihren Schwellenwert in der Gegend von 55 MeV hat. Oberhalb dieser Energie nimmt ihr Wirkungsquerschnitt schnell zu.

Über den Ablauf eines (α, α+3n)-Prozesses muß man sich wohl folgendes Bild machen: Wenn ein Alphateilchen mit hinreichender Energie in einen Kern eindringt, so wird es nicht sofort einen Zwischenkern bilden, der das „Gedächtnis" an seine Entstehung verloren hat, sondern es wird zunächst als "Cluster" im Sinne der Cluster-Theorie [2]) erhalten bleiben, aber beim Durchlaufen des Kerns Energie an die einzelnen Nukleonen im Kern abgeben. Ist die Energie des Alphateilchens groß genug, so besteht eine endliche Wahrscheinlichkeit dafür, daß es mit verringerter Energie den getroffenen Kern wieder verläßt und ihm einen bestimmten Energiebetrag als Anregungsenergie übertragen hat, der ausreicht um mehrere Neutronen abdampfen zu lassen. Man kann die getroffene Kernmaterie also als ein Bremsmedium auffassen, in dem das Alphateilchen einen bestimmten Energieverlust erleidet. Wenn diese Auffassung richtig ist, muß dieser Energieverlust in schweren Kernen etwas größer sein als in leichteren. Der Schwellenwert für den (α, α+xn)-Prozeß müßte also mit zunehmender Kernladung etwas ansteigen und die Zahl x sollte bei schweren Kernen im Durchschnitt größer sein als bei leichteren. Versuche, um diese Gesetzmäßigkeiten nachzuweisen, sind im Gange.

Literatur

1) R. Boom und H. Brückmann, unveröffentlicht
2) z. B. K. Wildermuth, CERN report 59—23

3.C

Nuclear Physics **15** (1960) 146—151; © *North-Holland Publishing Co., Amsterdam*

Not to be reproduced by photoprint or microfilm without written permission from the publisher

MEASUREMENTS OF THE FLUORESCENT YIELD OF THE K-SHELL WITH A PROPORTIONAL COUNTER

H. L. HAGEDOORN and A. H. WAPSTRA

Laboratorium voor Technische Fysika der Technische Hogeschool, Delft, Holland

Received 8 October 1959

Abstract: Using a proportional counter in coincidence with a scintillation spectrometer, fluorescent yields in the K-shell were determined from measurements on nuclei decaying by electron capture.

The following results were obtained:

ω_K(Ti) = 0.18±0.01; ω_K(Cr) = 0.219±0.012;

ω_K(Co) = 0.31±0.01; ω_K(Zn) = 0.43±0.02; ω_K(Sr) = 0.64±0.03.

A new set of constants in the semi-empirical formula giving the relation between ω_K and Z was derived from these results in combination with earlier data.

1. Introduction

The values of the fluorescent yields of the K-shell can be computed from a semi-empirical formula [1,2])

$$\left(\frac{\omega_K}{1-\omega_K}\right)^{\frac{1}{4}} = A+BZ+CZ^3.$$

Values of the three constants given by Burhop [1]) are

$$A = -0.044, \quad B = +0.0346, \quad C = -1.35\times10^{-6}.$$

More recent values are given by Laberrigue-Frolow [2]):

$$A = -0.0217, \quad B = +0.03318, \quad C = -1.14\times10^{-6}.$$

The newest and most exact experimental data for the fluorescent yields in the K-shell are shown in table 1.

2. Measuring Method

Consider a nucleide decaying to an excited level for a fraction $P_{\beta+}$ (which may be zero) by positon emission and for a fraction $(1-P_{\beta+})$ by electron capture. The positons and the Röntgen-peak are measured in a proportional counter, in coincidence with the gamma rays de-exciting the level mentioned, which are counted in a scintillation spectrometer. The ratio of the coincidences

TABLE 1

Data of the fluorescent yields

Element	Z	$\omega_K \times 10^3$	$\omega_K^{\dagger} \times 10^3$
A	18	129 ± 11 [a] [††]	95
		81 ± 6 [b]	
Fe	26	308 ± 15 [c]	310
		340 ± 30 [c]	
Ni	28	330 ± 20 [d]	380
		366 ± 11 [e]	
Cu	29	390 ± 20 [d]	410
		410 ± 12 [e]	
		390 ± 20 [b]	
Zn	30	440 ± 20 [d]	450
		446 ± 12 [e]	
Kr	36	660 ± 20 [a]	660
		620 ± 30 [e]	
Zr	40	700 ± 20 [e]	700
Nb	41	730 ± 20 [e]	720
Mo	42	730 ± 20 [e]	740
Tc	43	700 ± 30 [f]	750
Rh	45	786 ± 15 [e]	780
Pd	46	790 ± 15 [e]	800
Ag	47	821 ± 19 [e]	810
		830 ± 30 [g]	
Cd	48	827 ± 15 [e]	820
		830 ± 30 [g]	
In	49	820 ± 20 [b]	830
		870 ± 30 [f]	
Sn	50	840 ± 10 [h]	840
		846 ± 12 [e]	
Xe	54	880 ± 30 [a]	870
Ba	56	850 ± 30 [h]	880
La	57	940 ± 20 [i]	890
Yb	70	936 ± 10 [k]	930
Pt	78	940 ± 15 [l]	940
Bi	83	960 ± 15 [m]	950
Po	84	942 ± 5 [k]	950
U	92	967 ± 10 [k]	950

† Values computed from the semi-empirical formula, with the constants of Laberrigue-Frolow.
†† Adopted value 100 ± 20.

[a] J. Heintze, Z. Phys. **143** (1955) 153
[b] G. R. Harrison, R. C. Crawford, J. I. Hopkins, Phys. Rev. **100** (1955) 841
[c] C. E. Roos, Phys. Rev. **100** (1955) 1267; Phys. Rev. **105** (1957) 931
[d] E. T. Patronis Jr., C. H. Braden and L. D. Wyly, Phys. Rev. **105** (1957) 681
[e] J. P. Welker, M. L. Perlman, Phys. Rev. **100** (1955) 74
[f] J. Laberrigue-Frolow, P. Radvanyi, J. Phys. Rad. **17** (1956) 944
[g] O. Huber, F. Humbel, H. Schneider and A. de Shalit, Helv. Physica Acta **24** (1951) 627
[h] T. Azume, J. Phys. Soc. Japan **9** (1954) 443
[i] Charles, H. Pruett, Roger G. Wilkinson, Phys. Rev. **96** (1954) 1340
[k] P. R. Gray, Phys. Rev. **101** (1956) 1306
[l] R. M. Steffens, O. Huber and F. Humbel, Helv. Phys. Acta **22** (1949) 167
[m] M. Mladjenovic, H. Slatis, Ark. Fys. **9** (1955) 41

to the number of gamma quanta counted is

1) for the positons:

$$\frac{N_e}{N_\gamma} = \varepsilon_{\beta^+} P_{\beta^+},$$

2) for the K-Röntgen rays:

$$\frac{N_e}{N_\gamma} = \varepsilon_K \omega_K k(1-P_{\beta^+}),$$

k being the fraction of capture transitions occurring by K-capture, ω_K the fluorescent yield of the K-shell, ε_K the efficiency for detecting the K-Röntgen rays and ε_{β^+} that for positons. The quantity k can be computed accurately from theory [5, 6]); in our experimental set up, where the source was mounted on a thin film at the wall of the proportional counter, ε_{β^+} is very nearly equal to 0.5, as was checked by measurements on ^{198}Au. We can, therefore, determine P_{β^+} accurately, as described elsewhere [3, 4, 7]); if ε_K can be determined we may also obtain precise values of ω_K.

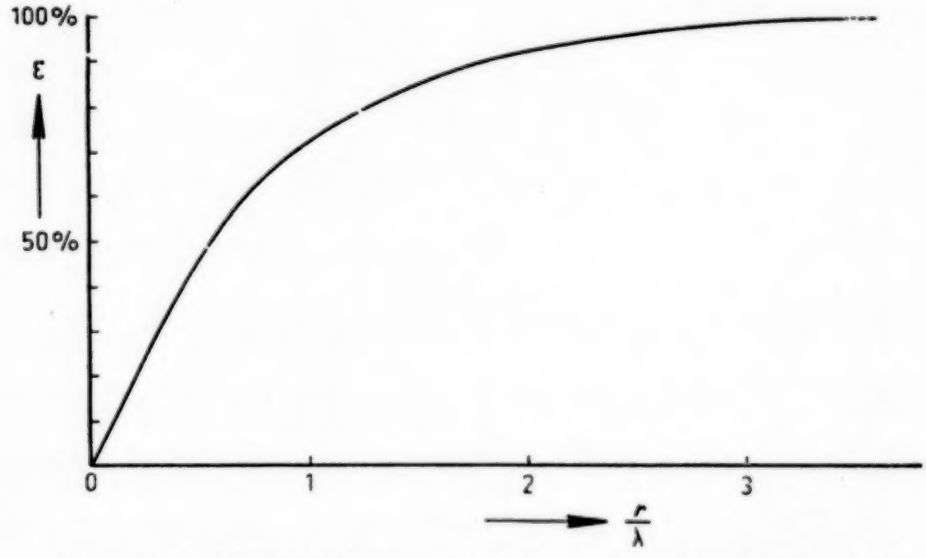

Fig. 1. The efficiency of the proportional counter as a function of r/λ.

The efficiency ε_K of the proportional counter for the X-rays is determined by measurements with a source emitting soft X-rays, at different pressures in the counter. Since the efficiency is a function of r/λ alone (see fig. 1) (r being the radius of the cylindrical counter and λ the mean free path of the X-rays), varying the pressure is equivalent with varying the energy of the γ-rays so long as the absorption occurs predominantly by photoeffect. For high values of r/λ, ε_K is evidently nearly equal to 1. The relation between λ and the X-ray energy was obtained from the known [8]) behaviour of the mass absorption coefficient as a function of energy (fig. 2).

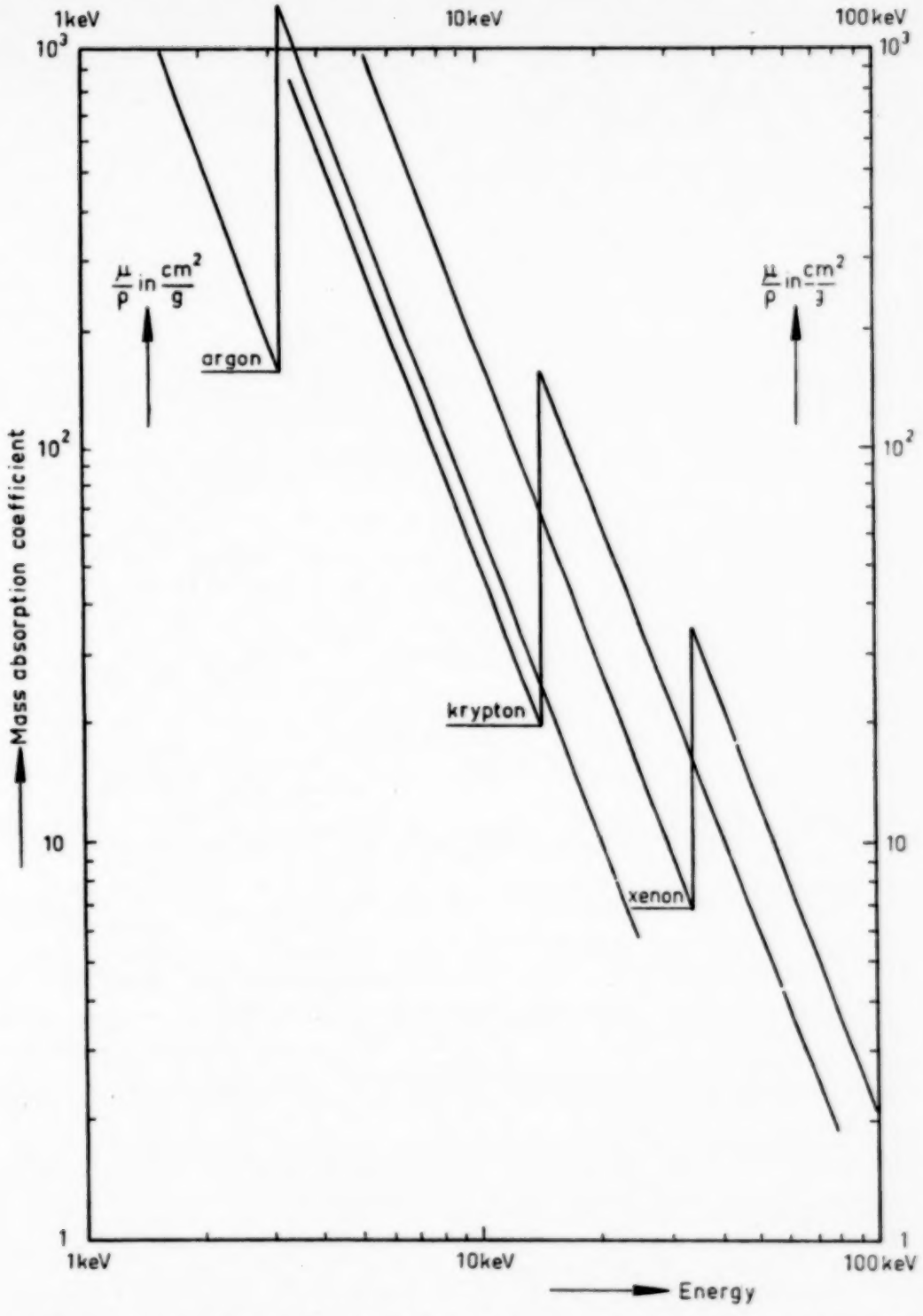

Fig. 2. The mass absorption coefficient μ/ρ ($\mu = 1/\lambda$, ρ = density) as a function of energy for A, Kr and Xe.

3. Experimental Results

The pulses of the scintillation spectrometer were delayed by 1μ sec in order to compensate for the time delay in the proportional counter. The resolving time of the coincidence circuit was 2.0μ sec. In all cases the ratio of true to accidental coincidences was at least 20.

^{67}Ga decays by electron capture only to several excited levels in ^{67}Zn [9]. By measurements in coincidence with the 180 keV gamma quanta we found $\omega_K = 0.43 \pm 0.02$.

Measuring coincidences between all γ-rays and X-rays in ^{88}Y we find $\omega_K(\mathrm{Sr}) = 0.64 \pm 0.03$.

Results on the K-fluorescent yield of Ti, Cr, and Co measured on ^{48}V, ^{52}Mn and ^{57}Ni by the above method have already been published. The results are collected in table 2 [3, 4, 10, 11, 12]).

TABLE 2

Results on the K-fluorescent yield, derived by the experimental method described in this paper

Element	Z	$\omega_K(\mathrm{exp}) \times 10^3$	ω_K† $\times 10^3$
Ti	22	180±10	190
Cr	24	219±12	240
Co	27	310±10	340
Zn	30	430±20	450
Sr	38	640±30	650

† See table 1.

As shown in table 2, the results are not inconsiderably lower than those derived from the semi-empirical formula given by Laberrigue-Frolow [2]).

Recent measurements by Roos [13]) agree with this formula but other measurements (table 1) also indicate that the values derived from it are somewhat high. For this reason we made a least square analysis using our data together with all the data given in table 1. The following values were obtained for the three constants in the semi-empirical formula:

$$A = -0.064 \pm 0.021, \quad B = +0.0340 \pm 0.0008, \quad C = (-1.03 \pm 0.14) \times 10^{-6}$$

(The ratio of external to internal errors is 1.2; the errors given above have not been multiplied by this factor.)

In table 3 we have given values of ω_K, derived from the semi-empirical formula with our new constants, together with their statistic errors.

TABLE 3

Values of the K-fluorescent yield, computed with the new constants A, B and C. The error is about 0.006 in all cases

Z	ω_K	Z	ω_K	Z	ω_K	Z	ω_K
10	0.0058	32	0.4896	48	0.8172	70	0.9369
12	0.0135	34	0.5500	49	0.8278	72	0.9412
14	0.0273	36	0.6045	50	0.8377	74	0.9449
16	0.0486	38	0.6532	52	0.8553	76	0.9481
18	0.0814	40	0.6960	54	0.8704	78	0.9523
20	0.1202	41	0.7153	56	0.8834	80	0.9536
22	0.1702	42	0.7333	58	0.8948	82	0.9558
24	0.2286	43	0.7500	60	0.9044	84	0.9577
26	0.2925	44	0.7656	62	0.9128	86	0.9594
27	0.3265	45	0.7800	64	0.9201	88	0.9609
28	0.3593	46	0.7933	66	0.9262	90	0.9621
29	0.3929	47	0.8057	68	0.9320	92	0.9630
30	0.4260						

References

1) E. H. S. Burhop, J. Phys. Rad. **16** (1955) 625
2) J. Laberrigue-Frolow and P. Radvanyi, J. Phys. Rad. **17** (1956) 944
3) H. L. Hagedoorn, Thesis, Technische Hogeschool Delft (1958)
4) J. Konijn, Thesis, Technische Hogeschool Delft (1958)
5) A. H. Wapstra, G. J. Nijgh and R. van Lieshout, Nuclear spectroscopy tables (North Holland Publishing Company, Amsterdam, 1959)
6) M. E. Rose and J. L. Jackson, Phys. Rev. **76** (1949) 1540
7) J. Konijn, B. van Nooyen, H. L. Hagedoorn and A. H. Wapstra, Nuclear Physics **9** (1959) 296
8) Handbook of Chemistry and Physics (Chemical Rubber Publishing Company, 1953)
9) K. Way, *et al.*, Nuclear Data Sheets
10) H. L. Hagedoorn and J. Konijn, Physica **23** (1957) 1069
11) J. Konijn, H. L. Hagedoorn and B. van Nooyen, Physica **24** (1958) 129
12) J. Konijn, B. van Nooyen and H. L. Hagedoorn, Physica **24** (1958) 377
13) C. E. Roos, Phys. Rev. **105** (1957) 931

2.J

Nuclear Physics **15** (1960) 152—154; © *North-Holland Publishing Co., Amsterdam*

Not to be reproduced by photoprint or microfilm without written permission from the publisher

ANGULAR DISTRIBUTION OF FRAGMENTS FROM FISSION OF URANIUM INDUCED BY 185-MeV PROTONS

U. L. VALLINDER and H. TYRÉN

The Gustaf Werner Institute for Nuclear Chemistry, University of Uppsala

Received 10 September 1959

Abstract: Protons of 185 MeV were used to study the angular distribution of the total fission products from natural uranium. The distribution is found to have an anisotropy of -0.09 ± 0.05.

1. Introduction

In recent years the angular distribution of fragments from fission of uranium has been studied at several energies and with different bombarding charged particles [1,2]), and with neutrons and photons. When this experiment was initiated, the only charged particles used previously were protons of 22 and 660 MeV [3,4]). At 22 MeV the anisotropy, defined as $[\sigma(0°)/\sigma(90°)]_{c.m.}-1$, where 0° and 90° refer to the incident beam direction, was found to be positive, and at 660 MeV it has a large negative value.

Preliminary results obtained with the internal circulating proton beam at (170 ± 15) MeV made it clear that the anisotropy of the total fission fragments is small. To avoid difficulties due to the magnetic field in the cyclotron, the experiments were continued with the external proton beam at (185 ± 1) MeV.

2. Experimental Procedure

The experimental arrangement is shown in fig. 1. The set-up was constructed to give a geometrical accuracy of about 1%. The target, a uranium filament with a diameter of 0.13 mm, was adjusted by optical means at the centre of a cylinder ($r = 65$ mm). The target can be moved in two perpendicular directions at the two points where it was fastened to the cylinder. The direction of the beam was perpendicular to the cylinder axis. The position of the target in the beam was controlled by photographic film. To get the target uniformly irradiated, the beam was swept horizontally by an electromagnet during the whole bombardment. The cylinder was rotated from one experiment to the other to average out geometrical errors. The fragments emitted from the target were collected in ten polyethylene foils mounted around the cylinder. Each of the foils covered 24° with one foil at every 30° from 30° to 150°, and 210° to 330°. The thickness

of the catcher foils was 9.2 mg/cm², that is a few times the maximum range of fission fragments. By adding a second foil behind each catcher foil, it was checked that the only activity produced in the plastic foils is C^{11}. Therefore, after bombardment, any C^{11} formed was allowed to decay before the foils were counted by an end-window Geiger-counter. This gave a background of about 25 counts/min in four experiments and 1.7 counts/min in one. However, the measured activities were rather low; so even with several hours bombardment the counting statistics were not better than 2—5 %. All activities were followed at least for 20 hours. The first of the bombardments with the external beam was carried out with a uranium foil, 0.5 mil thick and about 0.2 inch broad. The set-up was in this case somewhat simpler than the one just described which has been used in all the other bombardments. With the foil target the geometrical errors are larger, but the activity in the catcher foils was enough to give about 1 % counting statistics versus 2—5 % in the other experiments. The normal of the plane of the target foil was at 60° to the beam direction so that for other angles one must apply a correction for "effective depth" in the target. Since the anisotropy is a rather small effect, it is very sensitive to this correction. Fragments emitted isotropically would emerge from a thick foil in a cosine distribution with respect to the foil normal, as has been checked experimentally to about 10 % by Winhold *et al.* [5]).

3. Results

To get the angular distribution in the centre-of-mass system of the fissioning nucleus, one has to correct for centre-of-mass motion. This is characterized by the quantity η, which is the ratio of the velocity of centre-of-mass to the velocity of the fission fragment in the centre-of-mass system. It is assumed that the preferred direction of the centre-of-mass motion is in the direction of the incident protons and further that the angular distribution is symmetric about 90° in the centre-of-mass system.

An approximate value of η was chosen and the measured activities were corrected to correspond to the approximate centre-of-mass angles. These data were then used to determine a new value of η on the assumption that the ratio of the ranges of fragments in two opposite directions is proportional to the ratio of the initial fragment velocities in these directions. That this is a reasonable approximation, especially for absorption in the heavier elements, can be seen from range-energy measurements on the light and heavy fission fragment groups in various solid materials carried out by Fulmer [6]). This new value of η was used for a new geometrical correction of the activities, etc. Successive approximations give a value of $\eta = 0.048 \pm 0.005$. This value, when used for range corrections, gives the same anisotropy in the forward and backward directions. By assuming the anisotropy to be of the form $\sigma(\theta) = a + b \cos^2\theta$,

weighted mean values of b/a were calculated from σ values for angles corresponding to 30° and 60° (150° and 120°). The anisotropy at three different times (5, 10, 15 hours after the end of bombardment) shows no significant variation with time. The mean value of b/a from the five experiments is -0.09 ± 0.05 where the error is the mean deviation. The considerable spread of values is due to the poor counting statistics and probably also to the very different duration of bombardments, from about 2 to 13 hours, which gives different composition of the activity. However, it is not possible to see any systematic variation in b/a.

Meadows [1]) has recently shown that the gross fission fragments from fission of U^{238} with 155-MeV protons have $b/a = -0.036$. He also has estimated from chemical separations the anisotropy of fission fragments representing symmetric and asymmetric fission. Symmetric fragments give positive anisotropy whereas asymmetric fragments give negative anisotropy. Lozhkin *et al.* [4]) report a large negative anisotropy for the total fission fragments from fission of uranium with 660 MeV protons. Fission of bismuth with 450-MeV protons has a positive anisotropy [7]).

A proposed explanation of the negative anisotropy has recently been given by Halpern [8]). He has shown how "transverse collisions" between bombarding protons and nucleons in the nuclei can give rise to angular distributions peaking at right angles to the original beam. These transverse collisions corresponding to glancing or nearly head-on collisions are favoured at high energies. Our results are therefore in good agreement both with previous measurements and with Halpern's theory for the anisotropy at high bombarding energy.

We are grateful to Prof. T. Svedberg for his interest and encouragement. The work has been supported by the Swedish Atomic Energy Commission.

References

1) J. W. Meadows, Phys. Rev. **110** (1958) 1109
2) C. T. Coffin and I. Halpern, Phys. Rev. **112** (1958) 536
3) B. L. Cohen, B. L. Ferrel-Bryan, D. J. Coombe and M. K. Hullings, Phys. Rev. **98** (1955) 685
4) O. V. Lozhkin, N. A. Perfilov and V. P. Shamov, JETP. **29** (1955) 292 (transl. Soviet Phys. JETP **2** (1956) 116)
5) E. J. Winhold, P. T. Demos and I. Halpern, Phys. Rev. **87** (1952) 1139
6) C. B. Fulmer, Phys. Rev. **108** (1957) 1113
7) R. L. Wolke and J. R. Gutmann, Phys. Rev. **107** (1957) 850
8) I. Halpern, Nuclear Physics **11** (1959) 522

2.E: 2.L

Nuclear Physics **15** (1960) 155—165; © *North-Holland Publishing Co., Amsterdam*

Not to be reproduced by photoprint or microfilm without written permission from the publisher

SCATTERING OF 14.6 MeV NEUTRONS BY Mg, Ca, Cd, Ta AND Bi

W. G. CROSS and R. G. JARVIS

Chalk River Laboratory, Atomic Energy of Canada Limited, Chalk River, Ontario, Canada †

Received 26 October 1959

Abstract: Differential cross-sections for 14.6-MeV neutrons scattered elastically from Mg, Ca, Cd and Bi have been measured at 25 angles between 8° and 130° and from Ta at angles out to 80°. A neutron beam was defined by counting only neutrons in delayed coincidence with a collimated beam of alpha particles from the T(d, n)He^4 reaction. The neutron detector bias was set to reject neutrons below 10.5 MeV. The results are corrected for angular resolution (±3°) and for absorption and multiple scattering in the thin (0.05 to 0.1 MFP) cylindrical scatterer. The results have been compared by several authors with optical model calculations.

1. Introduction

A considerable number of measurements have been made recently on the angular distribution of neutrons scattered elastically from nuclei [1–4]). The primary interest lies in the comparison of these results with the predictions of the optical model [5, 6]) and in determining the parameters of this model. To determine the variation of these parameters it is necessary to obtain scattering distributions for a wide variety of nuclei and over a range of neutron energies.

Most of the angular distributions at 14 MeV have been measured using ring-shaped scatterers [2, 3]). This geometrical arrangement gives a much higher ratio of scattered neutrons to background than does a "point" scatterer. On the other hand it is impracticable to make the necessarily large rings of more than a limited number of elements. The present experiment employs a small scatterer and what is in effect a collimated incident beam of neutrons. Measurements have been made on neutrons scattered elastically by Mg, Ca, Cd and Bi from 8° to 130° and by Ta out to 80°. Comparison of these results with theoretical predictions have been made by several authors [5]). These, along with similar comparisons with other results, suggest that while the main features of the experimental distributions are well matched by the optical model predictions there is still room for refinement of both the experimental results and the theory.

2. Experimental Arrangement

The experimental arrangement used for the measurement of angular distributions is shown in fig. 1. Neutrons are produced by the T(d, n)He^4 reaction,

† A preliminary report of this experiment has been given previously [4]).

using 140-keV deuterons, and a target of tritium in Zr. These neutrons are effectively collimated in the following way. A narrow beam of alpha particles from the reaction is detected in one counter, and only neutrons emitted in delayed coincidence with these alpha particles are recorded by the neutron counter. These coincident neutrons, emitted at about 177° to the alpha-particle beam and at 35° to the incident deuteron beam, have an energy of 14.6 ± 0.1 MeV. This neutron "beam" passes through the target backing, through a 0.7 mm thick Al window and through the centre of a thin disc-shaped scatterer, about 15 cm from the target. Measurement of the angular distribution of the scattered neutrons consists essentially of counting delayed coincidences between the

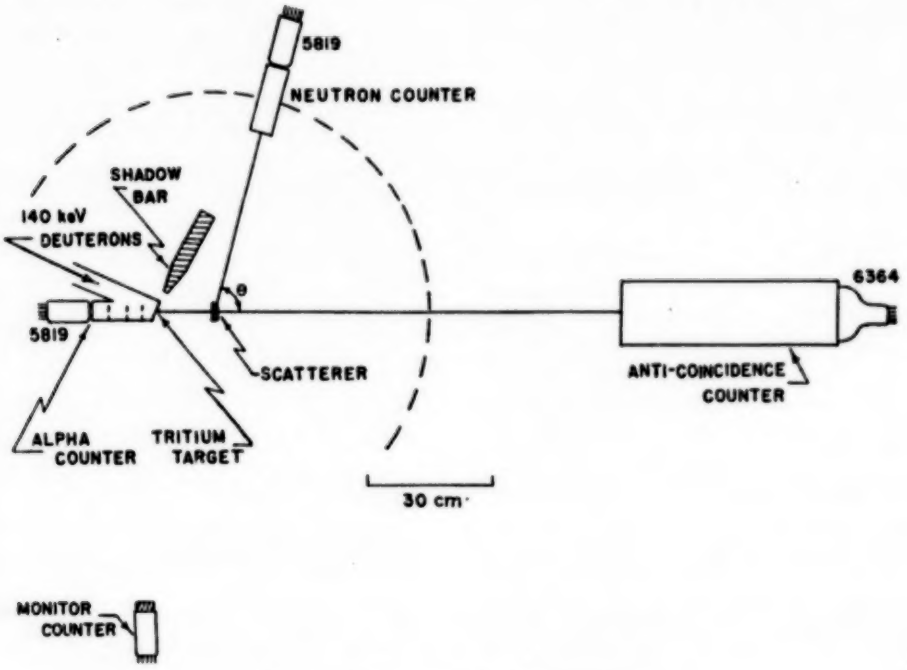

Fig. 1. Experimental arrangement.

alpha and neutron counters as the neutron counter is rotated in a circular arc around the scatterer.

The scatterers were circular discs 3.6 cm in diameter, this being sufficient to more than cover the defined neutron beam, and between 2 and 9.6 g/cm² thick. In most cases two thicknesses were used, the thinner one for measurements at scattering angles up to about 60° and the thicker one mainly for larger angles. These ranges of angles overlapped and no difference in measured cross section in the overlapping region was found for the different thicknesses of scatterer. The thinner ones scattered elastically up to 4 % of the incident neutrons and the thicker ones up to 8 %. The Mg, Ca and Ta scatterers were of solid metal. For Cd and Bi both solid and powdered samples were used, the latter being held in a light Al can which was shown to give a negligible contribution to the background. For the thicknesses used (in g/cm²) in the direction of the beam,

a powdered sample of given linear diameter has a smaller effective thickness at right angles to the beam than a solid sample and therefore gives smaller absorption and multiple scattering in that direction. The purity of all scatterers was greater than 99 %.

Mg and Ca were chosen in preference to other neighbouring elements because of their small number of low-lying levels. In the case of Ca^{40} the bias on the neutron detector was almost high enough to eliminate inelastic scattering.

The alpha detector was a disc of scintillating plastic 1.3 cm in diameter and 0.025 cm thick. The neutron detector was a cylinder of the same plastic, 15 cm long and 5 cm in diameter, at about 60 cm from the scatterer. Both detectors were viewed by RCA 5819 photomultipliers operated at 1400 volts.

The electronic circuits of the coincidence system are conventional, using a fast coincidence circuit, slow side channels for pulse-height analysis, and requiring a slow triple coincidence among the outputs of the side-channel discriminators and the fast coincidence circuit. A distributed amplifier was used between each photomultiplier and the fast coincidence circuit. The coincidence resolution curve had a full width at half maximum of 4 ns.

A differential discriminator was used to separate the alpha pulses from the protons, tritons and He^3 ions which were produced in unavoidable D-D reactions in the target. The energy of the elastically scattered neutrons varies slightly with scattering angle, affecting both the efficiency of detection in the neutron counter and their flight time. The latter, in turn, affects the efficiency for detecting coincidences. The neutron counter was biased to reject neutrons below 10.5 MeV and its efficiency for neutrons of varying energy was calculated to increase roughly linearly with energy from 11 to 14.6 MeV. The variation with neutron energy of the overall efficiency for detecting coincidences, including the effect of flight time, is shown in fig. 2.

The neutron output from the target was monitored by a fixed anthracene scintillation counter in the position shown in fig. 1. Its bias was set low to reduce the effect of changes in gain on its efficiency but high enough to reject D-D neutrons.

The angular resolution of the whole system was measured by moving the neutron counter through the neutron "beam". The resulting angular distribution had approximately a Gaussian shape with a full width at half maximum of 6°. For measurements of scattering angles below 15°. this width was reduced to 3° by increasing the distance to the neutron counter. Any much narrower resolution is limited by scattering of the alpha particles in the target.

The background coincidence counting rate, measured with no scatterer present, consisted mainly of accidental coincidences between alpha particles and neutrons which went directly from the target to the neutron counter. A copper bar placed between the source and the neutron counter reduced the counting rate in the neutron counter by a factor of about 20. To reduce the

accidental coincidence rate further, a second counter shown in fig. 1, was set to detect neutrons remaining in the main straight-through 'beam' which had not been scattered in the scatterer. Pulses from this counter were used to cancel the corresponding alpha pulses, thus effectively reducing the counting rate in the alpha counter and hence the accidental coincidence counting rate by about 40 %. This detector consisted of a glass tank of liquid scintillator 10 cm in diameter and 50 cm in length. It was viewed by a single Dumont 6364 5-inch photomultiplier and was surrounded by lead.

At large scattering angles where the true coincidence rate was low the accidental coincidence counting rate set a limit of 10^4 neutrons/sec to the

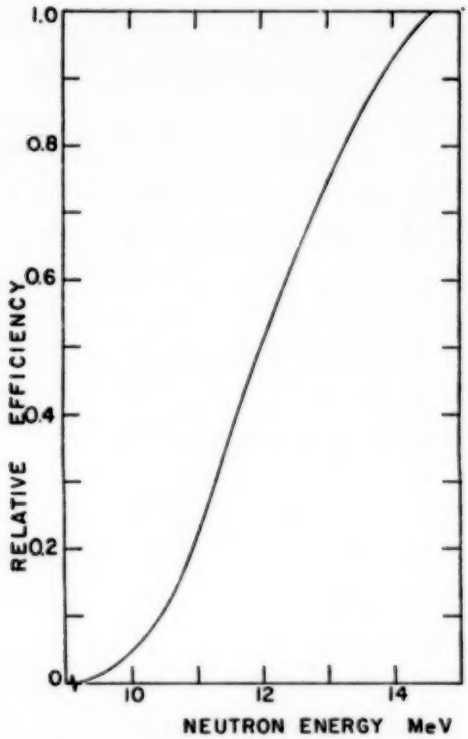

Fig. 2. Calculated variation with neutron energy of the overall efficiency of neutron counter and coincidence system. The nominal bias on the neutron counter is 10.5 MeV.

usable neutron 'beam' through the target. This gave approximately equal numbers of true and accidental coincidences.

3. Experimental Procedure

The experiment consisted of counting coincidences at each of 25 angles between 8° and 130° with the scatterer alternately in and out. Several runs were made at each angle and the total counting time for each point varied from a few minutes for small angles to 20 hours at backward angles. Measurements at different angles were normalized by comparing them with repeated measurements made at 15°.

The constancy of the ratios of the counting rates in the alpha counter and the neutron monitor served as a check on their correct operation, while the behaviour of the neutron counter was checked by the reproducibility of the neutron counting rate in repeated runs at the same angle.

Accidental coincidence rates, calculated from the rates in the alpha and neutron counters and the measured resolving time, were equal to the 'background' coincidence rates measured with the scatterer out. This indicates that the coincidence counting rate produced by neutrons scattered in the end of the target chamber or in the air was not significant, as was expected.

To convert the relative angular distribution measurements to differential cross sections, the neutron counter was moved to the position usually occupied by the scatterer, and the coincidence rate was measured. Like the scatterer, the neutron counter completely covered the "beam". The rate R measured in this position is the product $S\varepsilon_0$ of the intensity of the neutron beam and the efficiency of the neutron counter for 14.7-MeV neutrons. The relation between coincidence counting rate C (background subtracted) in the angular distribution experiment and the differential cross section $\sigma(\theta)$ in the laboratory system is then

$$\sigma(\theta) = \frac{C\varepsilon_0}{RNt\Omega\varepsilon},$$

where Ω is the effective solid angle which the neutron counter subtends at the scatterer during angular distribution measurements, Nt is the number of nuclei/cm^2 in the scatterer and ε is the efficiency of the neutron counter for scattered neutrons. The ratio $\varepsilon/\varepsilon_0$ is given in fig. 2. The uncertainty in the resulting absolute differential cross section at 15° was estimated to be ± 7 %.

4. Results

The differential cross sections which were obtained are shown in figs. 3 to 7. Angles are in the centre-of-mass system. The experimental points shown are corrected for (a) absorption and multiple scattering of the neutrons in the scatterer, (b) the angular resolution of the system, and (c) the variation with neutron energy of the efficiency of the neutron counter and the coincidence system. In the case of Mg the points are also corrected for inelastic scattering. The solid curve is drawn to fit the corrected points. At backward angles the large errors on the points make the position of this curve somewhat subjective. The dashed line in figs. 4, 5 and 7 is the experimental curve before the corrections for angular resolution and multiple scattering were made. The errors shown on the points are only the statistical errors and apply to the relative angular distribution. They do not include the additional error in the absolute normalization to differential cross section (± 7 %) or uncertainties in the corrections given above.

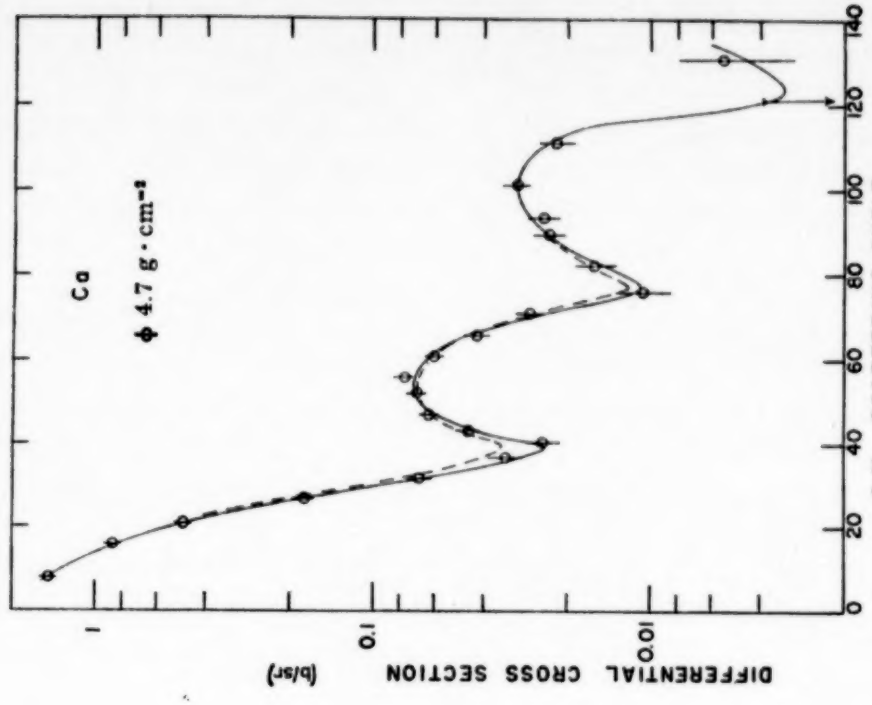

Fig. 4. Differential cross section for elastic scattering from Ca. The experimental points are corrected as described in text. The dashed curve is a smooth curve through the experimental points uncorrected for multiple scattering and angular resolution.

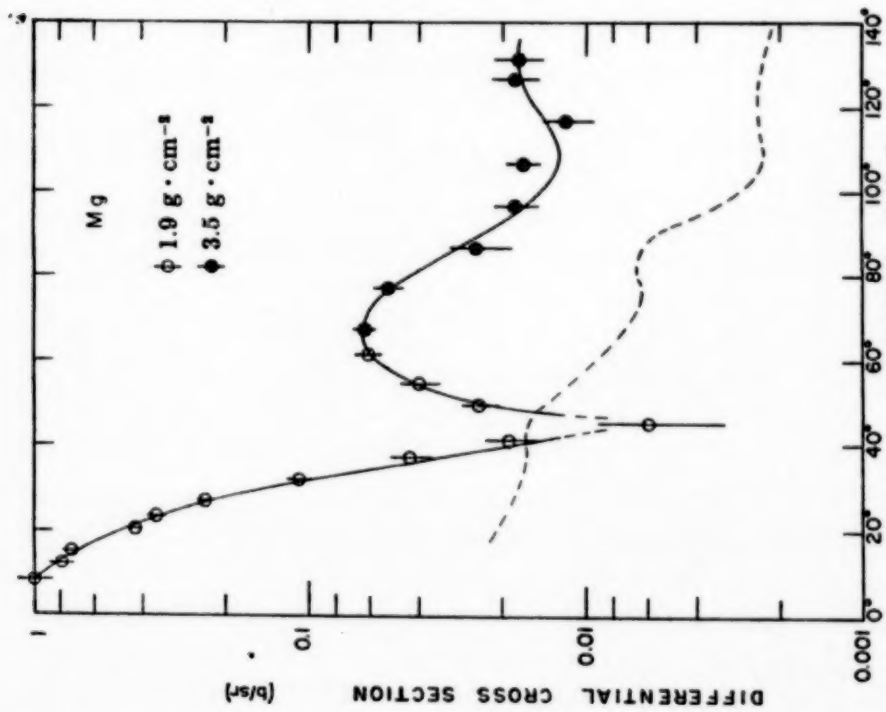

Fig. 3. Differential cross section for elastic scattering from Mg. The dashed curve indicates the estimated contribution of inelastic scattering for which the experimental points have been corrected.

The correction for angular resolution was made using the expression given by Eckart [7]). The correction for double scattering was made using the distribution of polar angles of twice-scattered particles given by Blok and Jonker [8]). While this distribution was derived for an infinite medium, the distribution for double scattering will apply also to a finite medium if the probability of the second scattering is independent of the polar scattering angle of the first scattering, i.e.,

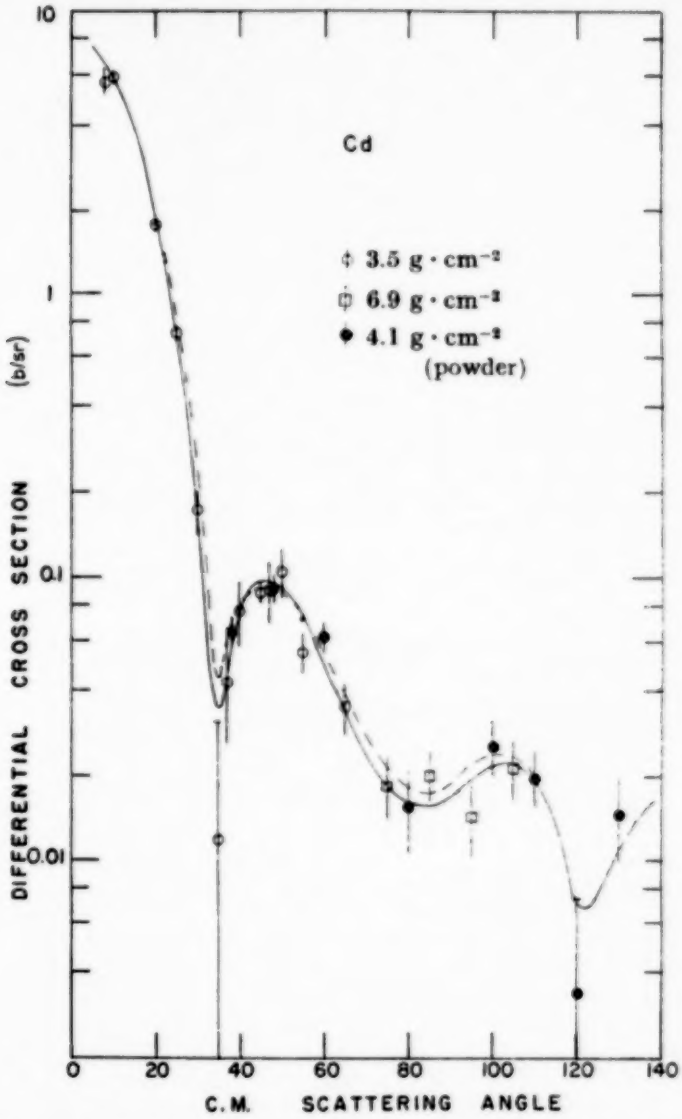

Fig. 5. Differential cross section for elastic scattering from Cd. The dashed curve gives the results uncorrected for multiple scattering and angular resolution.

if the mean distance which the once-scattered particle must travel to escape from the medium (averaged over all points of the medium) is independent of the first scattering angle. This would be true for a spherical scatterer and only slightly in error for any scatterer of which the dimensions are all nearly equal. For 14-MeV neutrons scattered by heavy elements, the restrictions on the shape

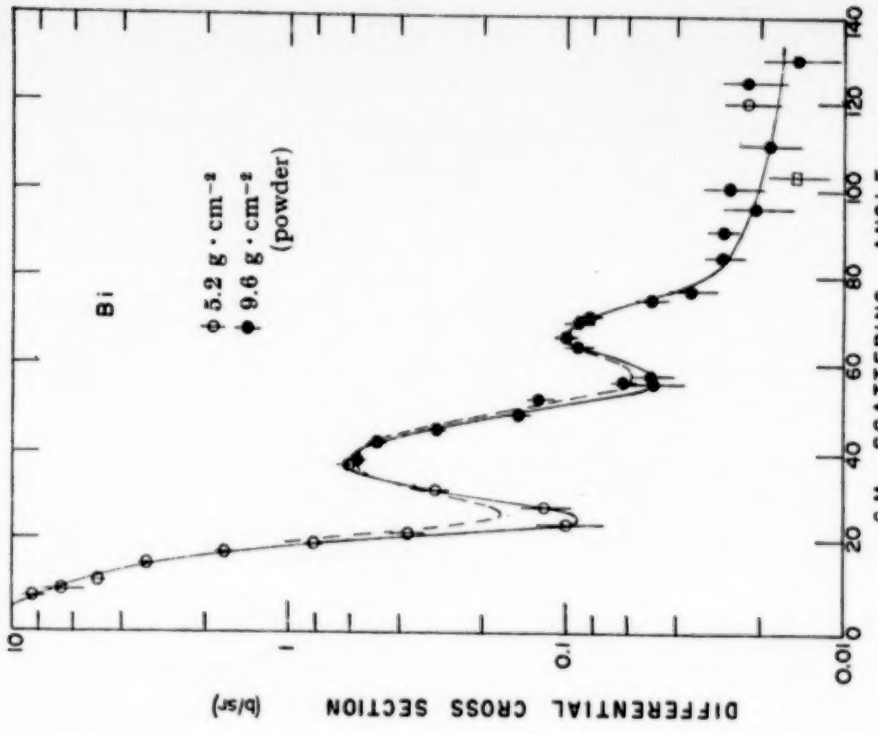

Fig. 7. Differential cross section for elastic scattering from Bi. The dashed curve gives the results uncorrected for multiple scattering and angular resolution.

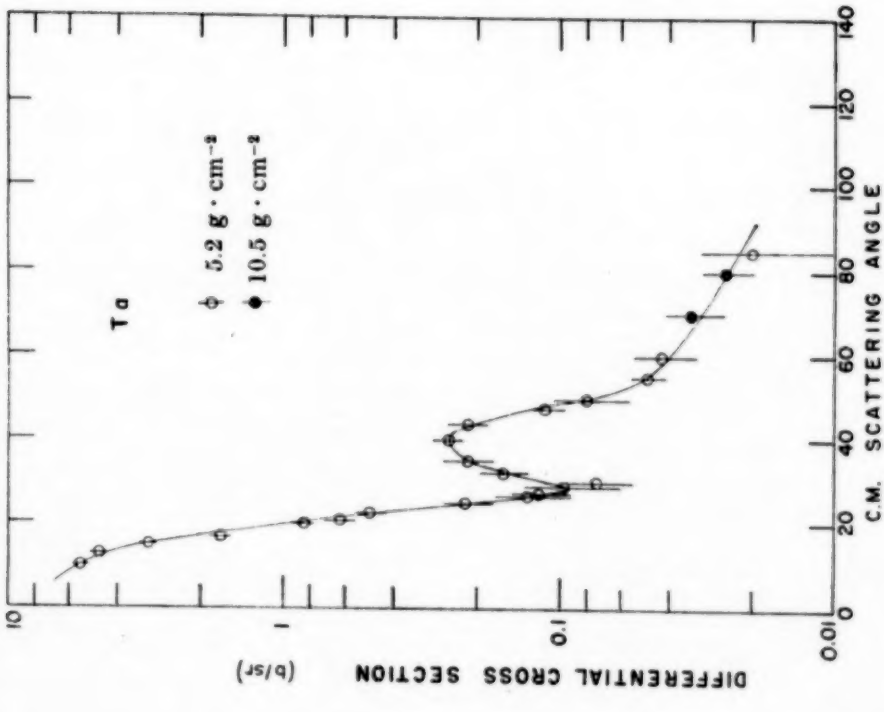

Fig. 6. Differential cross section for elastic scattering from Ta.

of the scatterer are less important because scattering is concentrated in the forward directions.

Because of the small size of the scatterer, further scatterings in it will not alter the distribution significantly. As can be seen in figs. 4, 5 and 7 these corrections are most important at the minima of the distribution. Unfolding the experimental curve with the angular resolution function will of course not reveal any features of the true distribution which are appreciably narrower than the resolution function. For this reason the first minimum of the Bi distribution may be appreciably deeper than is shown.

5. Discussion

In this section the accuracy of the results will be considered. The main result of multiple scattering and of limited angular resolution is to fill in the minima of the angular distributions obtained. Angular resolution has an important effect only at the first minimum, which may be so sharp that the method used to correct for finite angular resolution breaks down. If theory predicted unambiguous values one could correct the theoretical curves for angular resolution (rather than correcting the experimental results), but the theoretical curves are sufficiently uncertain that this is not practicable. A similar uncertainty exists for multiple scattering corrections; it is at the minima that the approximate expression for $\sigma(\theta)$ used in the multiple scattering corrections is least accurate. At these points, the magnitude of the corrections, shown by the difference between the dashed and full curves in figs. 4 and 5, serves only as an indication of the importance of these corrections.

A more serious uncertainty, also most important where the elastic differential cross section is small, is the detection of neutrons which have been scattered inelastically from low-lying levels. Neutrons scattered from levels less than 4 MeV above the ground state can be detected in this experiment, although, as shown in fig. 2, the detection efficiency for 11-MeV neutrons would be only 10 per cent of that for elastically-scattered neutrons. For Ca, inelastic scattering is considered to be unimportant. For Mg^{24}, only the 1.37-MeV level is important. An estimate of the contribution of this level can be obtained from measurements of the inelastic differential cross section for this level [9]) and the calculated efficiency of the neutron counter given in fig. 2. This contribution is shown by the dashed curve in fig. 3 and has been subtracted from the observed "elastic" distribution. Cd, Ta and Bi have several sufficiently low-lying levels that inelastically-scattered neutrons will be detected, but no experimental results are yet available from which to estimate accurately the importance of inelastic scattering to the present experiment. From the measurements of Coon *et al.* [2]) on the differential cross sections of Sn and Pb for all neutrons emitted with energies between 9 and 14 MeV, it appears likely that, for angles greater than

90°, inelastically scattered neutrons will contribute to our observed cross sections amounts comparable to the statistical errors shown.

Uncertainty in the variation of the overall efficiency of the coincidence system with neutron energy is important only for Mg, for which the energy of measured elastically scattered neutrons varied from 14.6 to 12.7 MeV.

A check of the accuracy of the absolute values of the cross sections which have been obtained is given by integrating the elastic differential cross sections over all angles and comparing the results, σ_e, with the difference of the total and non-elastic cross sections. This comparison is shown in columns 4 and 5 of table 1. All values are in units of 10^{-24} cm^2. Total cross sections are taken from the combined results of ref. [10]) and non-elastic cross sections from ref. [11]).

TABLE 1

Comparison of σ_e and $\sigma_t - \sigma_{ne}$

Element	σ_t	σ_{ne}	$\sigma_t - \sigma_{ne}$	σ_e
Mg	1.77±0.02	0.97±0.02	0.80±0.03	0.75±0.09
Ca	2.21±0.03	1.36±0.02	0.85±0.05	0.82±0.07
Cd	4.42±0.05	1.92±0.03	2.50±0.06	2.37±0.21
Bi	5.44±0.05	2.56±0.04	2.88±0.07	2.71±0.24

Unless the differential cross sections become unexpectedly large between 130° and 180°, less than 2 per cent of the total elastic cross section is contributed by this angular region (except for Mg where the contribution is 9 per cent). The accuracy of the cross section assumed for this region is, therefore, not important. There is agreement between σ_e and $\sigma_t - \sigma_{ne}$ within the errors of the measurements.

In summary, there are several uncertainties which may increase the value of the differential cross section by considerably more than the statistical errors shown, wherever the cross section is low, and particularly at the minima. Where the experimental cross section is low it should therefore be regarded as an upper limit to the true elastic cross section. These uncertainties may be the origin of the lack of agreement obtained by different experimenters at angles greater than 90°. (For instance the present results for Cd and Bi at backward angles are consistently higher than those of Anderson *et al.*[3]), and of Coon *et al.*[2]) for Sn and Pb.)

6. Conclusions

These differential cross sections, along with those obtained elsewhere, have been compared by several authors [5]) with theoretical calculations. For neutrons of 14 to 15 MeV the most notable general difference between theory and experiment is the prediction of deeper minima than are observed, particularly at angles greater than 90°. While much of this discrepancy may be the result of

the experimental errors described, the similar situation which exists in the elastic scattering of 14—30 MeV protons, for which the angular and energy resolution are much better than in neutron experiments, suggests that the whole of the discrepancies cannot be explained in this way. Significant filling-in of the minima of the theoretical distributions has been obtained by the introduction of spin-orbit potentials [6]).

Scattering distributions for a wide range of energies have been fitted fairly well by a remarkably small range of the four or five theoretical parameters specifying the nuclear potential [5, 6]). However the remaining uncertainty in these parameters, particularly in the strength and shape of the imaginary well and in the width of the diffuse edge, indicates that more experimental results are required at several energies. The relatively large cross-section found [9]) at 14 MeV for inelastic scattering to the lowest excited state of Mg^{24} emphasizes the importance of completely excluding inelastic scattering from such results.

References

1) J. P. Conner, Phys. Rev. **89** (1953) 712;
J. R. Smith, Phys. Rev. **95** (1954) 730;
D. F. Shaw, Proc. Phys. Soc. A **68** (1955) 43
2) Coon, Davis, Felthauser and Nicodemus, Phys. Rev. **111** (1958) 250
3) J. O. Elliot, Phys. Rev. **101** (1956) 684;
H. Nauta, Nuclear Physics **2** (1956) 124;
Nakada, Anderson, Gardner and Wong, Phys. Rev. **110** (1958) 1439;
Anderson, Gardner, Nakada and Wong, Phys. Rev. **110** (1958) 160
4) W. G. Cross and R. G. Jarvis, Phys. Rev. **99** (1955) 621A;
Dolan, Fincher, Kenny, Berko and Whitehead, Bull. Am. Phys. Soc. **1** (1956) 339;
L. A. Rayburn, Bull. Am. Phys. Soc. **2** (1957) 233 and U.S.A.E.C. Document TID 7547 (unpublished);
Berko, Groseclose, Stetson and Walker, Bull. Am. Phys. Soc. **4** (1959) 257;
Berko, Whitehead and Groseclose, Nuclear Physics, **6** (1958) 210
5) Bjorklund, Fernbach and Sherman, Phys. Rev. **101** (1956) 1832;
H. McManus, Bull. Am. Phys. Soc. **1** (1956) 56;
Beyster, Walt and Salmi, Phys. Rev. **104** (1956) 1319;
W. S. Emmerich and R. M. Sinclair, Phys. Rev. **104** (1956) 1399;
W. S. Emmerich and H. J. Amster, Bull. Am. Phys. Soc. **2** (1957) 71;
Lukyanov, Orlov and Turovtsev, Nuclear Physics **8** (1958) 325
6) Culler, Fernbach and Sherman, Phys. Rev. **101** (1956) 1047;
F. E. Bjorklund and S. Fernbach, Phys. Rev. **109** (1958) 1295
7) C. Eckart, Phys. Rev. **51** (1937) 735
8) J. Blok and C. C. Jonker, Physica **18** (1952) 809
9) W. G. Cross and R. L. Clarke, Bull. Am. Phys. Soc. **4** (1959) 258
10) E. R. Graves and R. W. Davis, Phys. Rev. **97** (1955) 1205;
M. H. MacGregor, W. P. Ball and R. Booth, Phys. Rev. **108** (1957) 726;
N. N. Flerov and V. M. Talyzin, Jour. Nuc. Energy **4** (1957) 529
11) J. H. Coon, E. R. Graves and H. H. Barschall, Phys. Rev. **88** (1952) 562;
A. Bratenahl, J. M. Peterson and J. P. Stoering, Phys. Rev. **110** (1958) 927;
J. P. Conner, Phys. Rev. **109** (1958) 1268

1.D.2:
1.E.3

Nuclear Physics **15** (1960) 166—186; © *North-Holland Publishing Co., Amsterdam*

Not to be reproduced by photoprint or microfilm without written permission from the publisher

MEASUREMENT OF *g*-FACTORS OF SEVERAL SHORT LIVED NUCLEAR STATES IN ODD-MASS NUCLEI

G. MANNING † and J. D. ROGERS

California Institute of Technology, Pasadena, California ††

Received 11 September 1959

Abstract: The *g*-factors of several excited states have been measured by observing the rotation of the angular correlation of $\gamma-\gamma$ cascades by an applied magnetic field. The results are: 280-keV state of As^{75}($\tau = 3.4\times10^{-10}$ sec) $g = 0.42\pm0.13$, 114-keV state of Lu^{175} ($\tau = 9.4\times10^{-11}$ sec) $g = 0.5\pm0.2$ and 113-keV state of Hf^{177} ($\tau = 6\times10^{-10}$ sec) $g = 0.22\pm0.06$. These results are compared with the theoretical predictions of the Nilsson model and are in good agreement. For the case of As^{75} other relevant properties are also compared with the model predictions. The results indicate that the model can be usefully applied to As^{75} and that the nucleus has a prolate deformation ($\eta \approx 2.5$). The *g*-factor of the 91-keV level of Pm^{147} has also been studied, a definite rotation of the angular correlation being observed. Computation of the *g*-factor from the observed data is uncertain because the time dependent attenuation of the $\gamma-\gamma$ correlation is not known. The results are $g = (0.9\pm0.2)/G_2$. The effect of the paramagnetic nature of the rare earth ions on such measurements on this group of nuclei is discussed as an appendix. Other assumptions made in deducing the *g*-factors from the observed rotations of the angular correlations are also discussed in the paper.

1. Introduction

The experiments to be described use a well known method for determining *g*-factors of short lived nuclear states. The method is applicable when an anisotropic gamma-gamma angular correlation exists with the level to be studied as the intermediate state. The angular correlation can be measured with a magnetic field applied to the source in a direction perpendicular to the plane of the correlation measurement. The field interacts with the nuclear magnetic moment while the nucleus is in its intermediate state and results in a rotation, and attenuation, of the angular correlation pattern. This method has been used by many authors [1]) to measure the *g*-factors of several nuclear states. The mean lifetime of the measured nuclear states range from few $\times10^{-7}$ to $\approx 10^{-9}$ sec. The general idea of the method, viz. the observation of the effect of an applied magnetic field on an angular distribution, is applicable in cases other than $\gamma-\gamma$ cascades. Measurements have been made using Coulomb excitation to excite the levels to be studied (see Goldring and Scharenberg [2])) for measurements on Nd^{150}, Sm^{152} and Sm^{154} and the compilation of Strominger *et al.* [3]) for a list of

† Present address: United Kingdom Atomic Energy Research Establishment, Harwell, Didcot, Berkshire, England.

†† Work performed under the auspicies of the U. S. Atomic Energy Commission.

authors who have measured the g-factor of the 197-keV level of F^{19}). The 0.060-keV level of Np^{237} has been studied using an $\alpha-\gamma$ cascade [3]). All these states have mean lifetimes of 2×10^{-9} sec or longer.

The measurements described below were made using $\gamma-\gamma$ cascades. The states studied have lifetimes in the range $\approx 10^{-9}$ to $\approx 10^{-10}$ sec. The extension of the usable lifetime range from $\approx 10^{-9}$ sec to shorter than 10^{-10} sec is not the result of any fundamental change, but is achieved by measuring smaller rotations of the angular correlation patterns than has previously been measured. (The smallest rotation observed in the experiments below is $-(0.17\pm0.06)$ degree.) The applicability of the method to states with lifetimes in the region of 10^{-9} to 10^{-10} sec considerably broadens the scope of such experiments. This is particularly true because many of the lower excited states of nuclei in the region of large nuclear deformation have lifetimes in the range 10^{-9} to 10^{-11} sec. Measurements of nuclear g-factors often provide a sensitive test of the predictions of nuclear models and the results described below are compared with theoretical estimates.

2. Experimental Method

The theoretical angular correlation pattern for a $\gamma-\gamma$ cascade between nuclear states of definite parity can be written as a sum of even Legendre polynomials, as a sum of even powers of $\cos\theta$, or as a sum of the form

$$W(\theta) = \sum_k C_k \cos k\theta \tag{1}$$

where the sum is over even k, including zero, up to a certain value determined by details of the decay. In practice for $\gamma-\gamma$ cascades k greater than 4 is never required. The form of eq. (1) is the most convenient for application here. A magnetic field is applied to the source material which results in a field H_{eff} at the nuclei during the lifetime of the intermediate states †, with a direction perpendicular to the plane of the correlation measurement. The nuclei precess, while in their intermediate state, with a frequency given by

$$\omega = -\frac{\mu\mu_0 H_{eff}}{I\hbar} = -\frac{g\mu_0 H_{eff}}{\hbar}$$

where μ is the nuclear magnetic moment in the intermediate state in units μ_0 (the nuclear magneton) and I is the spin of the intermediate state. The nuclear g-factor, $g = \mu/I$, can be measured even if the nuclear spin is not known. Assume the angular correlation is measured in the presence of the magnetic

† The relationship between H_{eff} and the applied field (H_{app}) is assumed to be of the form $H_{eff} = \beta H_{app}$. The value of β depends upon the properties of the ions that contain the nuclei while in their intermediate states. Estimation of β is in many cases a complex problem. The appendix contains a discussion of the relevant factors and estimates the parameter for certain reasonable assumptions.

field with equipment having a resolving time large compared to the lifetime of the nuclear intermediate state. If the nuclei react only with H_{eff} we can write the observed correlation pattern as

$$\overline{W(\theta, H)} = \tau^{-1} \int_0^\infty \sum_k C_k \cos k(\theta+\omega t) \exp(-t/\tau) \mathrm{d}t;$$

τ is the mean lifetime of the intermediate state. Integration gives

$$\begin{aligned} \overline{W(\theta, H)} &= \sum_k C_k [1+(k\omega\tau)^2]^{-\frac{1}{2}} \cos k(\theta+\Delta\theta_k), \\ \Delta\theta_k &= \frac{1}{k} \tan^{-1}(k\omega\tau). \end{aligned} \tag{2}$$

It can be seen that the angular correlation pattern is attenuated and rotated. In the limit $\omega\tau \ll 1$, eq. (2) reduces to

$$\overline{W(\theta, H)} = \sum_k C_k \cos k(\theta+\omega\tau), \tag{3}$$

which is the angular correlation pattern for zero field rotated by $\omega\tau$.

In practice the nuclei in their intermediate state often interact with local electric and magnetic fields arising in the source. These interactions can be reduced by using dilute liquid sources but are often still significant. Abragam and Pound [4]) have considered the effects of these interactions on angular correlations and they show that in general they can be represented as a time dependent attenuation of the anisotropy. For a theoretical correlation pattern $W(\theta) = \sum_k A_k P_k(\cos\theta)$ the pattern observed with a resolving time long compared to the nuclear intermediate lifetime is

$$\begin{aligned} \overline{W(\theta)} &= \tau^{-1} \int_0^\infty \sum_k A_k P_k(\cos\theta) \exp(-t/\tau) \exp(-\lambda_k t) \mathrm{d}t \\ &= \sum_k G_k A_k P_k(\cos\theta), \quad \text{where} \quad G_k = (1+\lambda_k\tau)^{-1}. \end{aligned}$$

For this type of attenuation the angular correlation measured in the presence of a magnetic field H_{eff} is, for a correlation including no terms higher than $P_4(\cos\theta)$,

$$\begin{aligned} \overline{W(\theta, H)} = 1 &+ \tfrac{1}{4} G_2 A_2 \left[1 + \frac{3\cos 2(\theta+\Delta\theta_{22})}{[1+(2G_2\omega\tau)^2]^{\frac{1}{2}}}\right] \\ &+ \tfrac{1}{64} G_4 A_4 \left[9 + \frac{20\cos 2(\theta+\Delta\theta_{24})}{[1+(2G_4\omega\tau)^2]^{\frac{1}{2}}} + \frac{35\cos 4(\theta+\Delta\theta_{44})}{[1+(4G_4\omega\tau)^2]^{\frac{1}{2}}}\right] \end{aligned} \tag{4}$$

where

$$\Delta\theta_{22} = \tfrac{1}{2}\tan^{-1}(2G_2\omega\tau), \quad \Delta\theta_{24} = \tfrac{1}{2}\tan^{-1}(2G_2\omega\tau), \quad \Delta\theta_{44} = \tfrac{1}{4}\tan^{-1}(4G_4\omega\tau).$$

For the case $kG_k\omega\tau \ll 1$ the general expression for all k is

$$\overline{W(\theta, H)} = \sum_k G_k A_k P_k[\cos(\theta + G_k\omega\tau)]. \tag{5}$$

It can be seen that the time dependent attenuation of the angular correlation also results in a corresponding reduction in the rotation of the angular correlation from the nuclear precession in the field H_{eff}. To determine the nuclear g-factor from the observed rotation it is necessary to know the values of G_k.

Abragam and Pound [4]) show that it is possible in solids to obtain a fixed, or "hard core" attenuation. If such an attenuation existed in a source used for a g-factor measurement, eq. (4) would no longer hold. Abragam and Pound show that if "hard core" attenuation is to exist in liquid sources it is necessary for the correlation time τ_c for the ion † to be very much longer than the nuclear lifetime. This implies that $\tau \ll 10^{-11}$ sec. In this case the attenuation effects are small and it does not constitute a large error to take $G_k = 1$. Hence, for the liquid sources used, all observed attenuations are taken as time dependent ††.

In the experiments reported below the rotation of the angular correlation pattern was determined by observing the change in coincidence counting rate at a fixed value of θ when the applied field was reversed. To obtain the maximum sensitivity the value of θ was chosen to maximize $\mathrm{d}\overline{W(\theta)}/\mathrm{d}\theta$. For an angular correlation of the form $\overline{W(\theta)} = 1 + C_2 \cos 2\theta$ (i.e. no $\cos 4\theta$ or higher terms) the optimum angles are $\theta = \frac{1}{4}\pi, \frac{3}{4}\pi, \frac{5}{4}\pi$ or $\frac{7}{4}\pi$. For $\omega\tau G_2 \ll 1$, using eq. (5) we can write

$$R = \frac{\overline{W(\theta, H)} - \overline{W(\theta, -H)}}{0.5[\overline{W(\theta, H)} + \overline{W(\theta, -H)}]} = \mp 4C_2\omega\tau G_2,$$

$$\omega\tau = \mp \frac{R}{4C_2G_2}, \tag{6}$$

$$g = \pm \frac{\hbar}{\mu_0} \frac{R}{4C_2G_2\tau H_{eff}}.$$

In each case the top sign is for $\theta = \frac{1}{4}\pi$ or $\frac{5}{4}\pi$ and the bottom sign is for θ $\frac{3}{4}\pi$ or $\frac{7}{4}\pi$. If $\omega\tau G_2 \gtrsim 1$ no simple expression can be given for determination of g from R, but it can be simply computed by using eq. (4). Similar expressions can be written for correlations containing $\cos 4\theta$ terms. In this case the optimum angle depends upon the relative size of C_2 and C_4.

† The time τ_c is defined by Abragam and Pound and is related to the mean time between collisions in the liquid. A value of 10^{-11} sec is quoted as a typical value.

†† In some cases hyperfine interactions result in attenuation of angular correlations even in liquid sources. If such attenuations exist they would require a change in eq. (4).

3. Experimental Details

A g-factor determination consisted of two parts; measurement of the angular correlation for the cascade of interest, and measurement of the change in counting rate at one fixed angle for a reversal of the applied field (i.e. measurement of R). The electronic equipment used for both parts was the same. It consisted of a conventional fast-slow coincidence arrangement with a resolving time of $\approx 2\times10^{-8}$ sec. The NaI(Tl) crystals used were $1\frac{1}{2}$ inches in diameter. One was 2 inches long and the other $1\frac{1}{2}$ inches. They were mounted directly on RCA 6655 A photomultiplier tubes without the use of light pipes. The photomultipliers were shielded from magnetic fields by two layers of Netic and Co-Netic shielding †.

The system used for taking data was that the spectrum from one counter in coincidence with a narrow range of pulse heights from the other counter was recorded in a PENCO PA-4 pulse height analyzer ††. The instrument was used as a 50 channel analyzer with two sets of storage. For the angular correlation measurements two angles were studied alternately, the spectrum at one angle being stored in one memory array and the spectrum at the other angle being stored in the second memory array. (If more than two angles were studied separate runs were made for pairs of angles.) The equipment was run automatically with alternate short counting periods at each of the two angles. A pair of scalers was also switched automatically to sum separately, at each angle, the total counts in the narrow pulse height range accepted from one of the counters. The counting time at each angle was also automatically summed. The same arrangement was used for the g-factor measurement, one set of storage being used for the field up, and the second for the field down. The use of automatic interchange between two counting arrangements enabled a single measurement to be broken down into many hundreds of alternate counting periods and hence effectively eliminated errors due to small changes in gain or efficiency of parts of the system.

The philosophy for the g-factor measurements was to design a magnet to minimize the leakage fields and then to run it at a sufficiently low field to ensure that all of its iron was in a region of high permeability. Fig. 1 shows a sketch of the magnet and one of the counters. Fig. 2 is a photograph of the apparatus with one counter pulled back from the source. The flux return path for the magnet was a hollow cylinder around the coils and poles. A slot was cut in the cylinder to accept the conical lead shields for the scintillation counters. With this arrangement, and a field of 13 000 gauss in the $\frac{1}{8}''$ gap between the poles, the largest leakage field just outside the magnet was kept to a small fraction of a gauss. It was not necessary to use light pipes to remove the photomultiplier tubes from the vicinity of the magnet. The counters were set at the

† Made by Perfection Mica Co., Illinois.

†† Made by Pacific Electro-Nuclear Co., Californa.

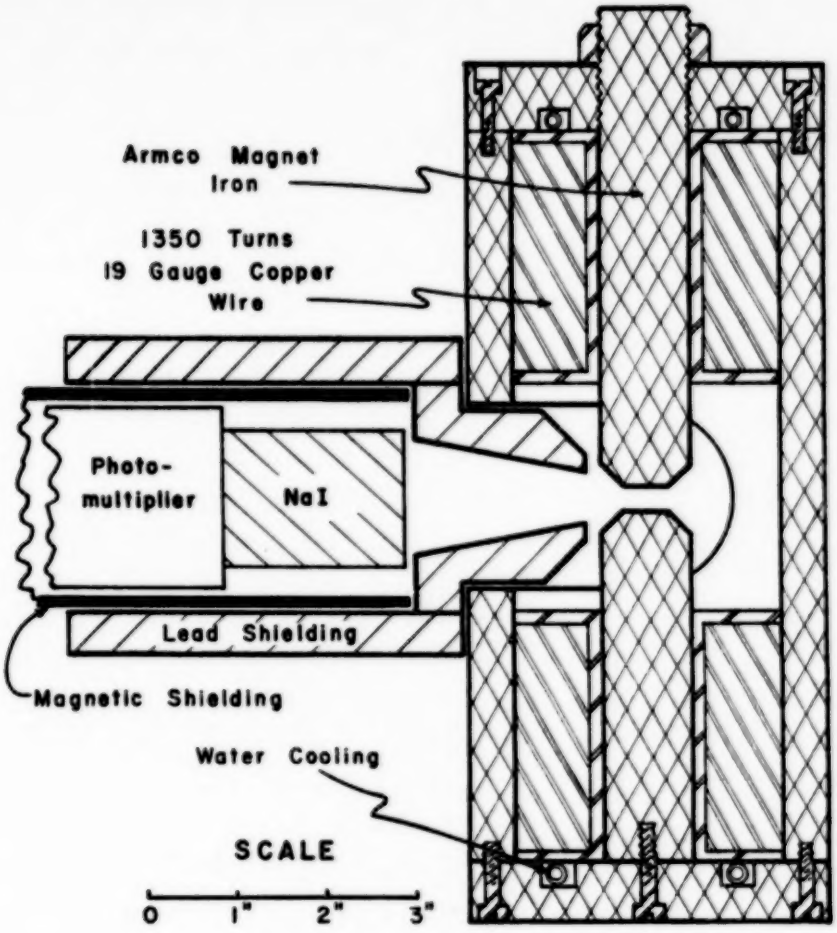

Fig. 1. Section through the magnet and one of the counters.

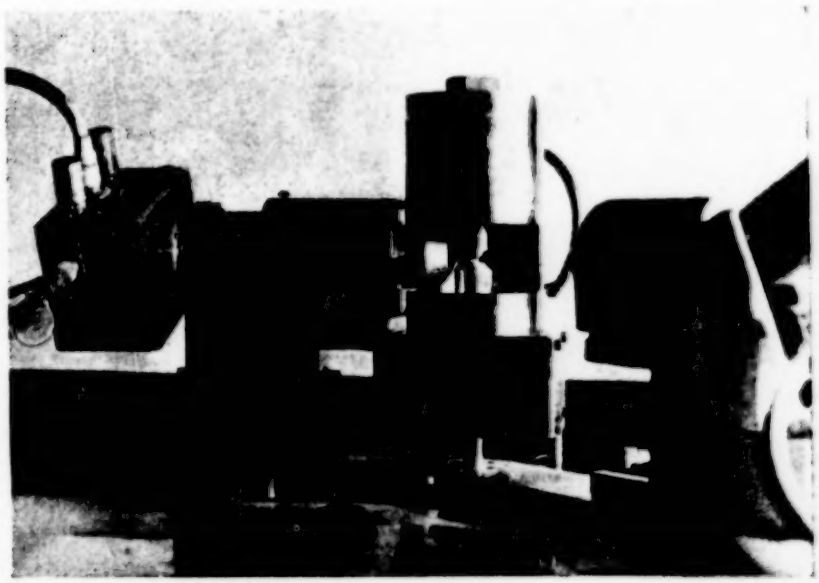

Fig. 2. Photograph of the magnet and counter assembly. One counter was pulled away from the magnet while taking the photograph.

value of θ required and their change in gain, when the magnet was reversed, was measured. This was repeated for several rotations of the counters about their own axis. A position was found for each counter at which the gain change reversed sign. The counters were thus set to minimize the effects of the magnetic field. The maximum gain change for either counter was less than 1 %, and at the rotation used was less than 0.05 %. This procedure could be adopted for any angle θ between the two counters. It was essential to reduce systematic effects resulting from reversal of the magnetic field as the rotations of the angular correlation patterns to be measured were extremely small. A continual check on these systematic magnetic field effects was maintained throughout the experiment. For each direction of the field the coincidence spectra from one counter were recorded, together with the summed counts within the small range of pulse heights accepted from the other counter.

In such experiments two checks on the results are sometimes possible. If the angle between the counters is changed from θ to $(2\pi-\theta)$ the value of R should be reversed in sign. If the settings of the electronics are reset so that the γ-rays accepted by the two counters are interchanged, θ is changed to $(2\pi-\theta)$ without moving the counters. The systematic field effects are not reversed and hence their presence can be detected. The second check can be used when one of the γ-rays has a significant K-conversion coefficient. These γ-rays, together with the KX-rays which are in coincidence with the other γ-ray of the cascade, are recorded in the pulse height analyzer. The angular correlation of the X-rays is isotropic and hence R for the γ-ray—X-ray coincidences should be zero. This in some cases provided a second check on absence of systematic effects.

The counters used had lead collimators to reduce spurious effects due to γ-ray scattering between the crystals. These collimators allowed a $1\frac{1}{4}$ inch diameter entrance aperture to the crystals at a distance of $2\frac{1}{2}$ inches from the source. With this arrangement the finite solid angle correction for the counters required that the observed $P_2(\cos\theta)$ and $P_4(\cos\theta)$ coefficients, after correction for randoms, be multiplied by 1.10 ± 0.01 and 1.34 ± 0.04 respectively. As the effects to be measured were small a large number of coincidence counts were necessary in order to obtain the required accuracy. It was reasonable in general, to run with a significant proportion of random coincidences, as the effect of these was easily calculated, and the increased statistical accuracy obtained in a given counting time more then compensated for slight uncertainties so introduced. The random coincidences were easily measured by adding a delay of $\approx 10^{-7}$ sec in one of the signal leads to the fast coincidence unit.

4. Experimental Results

4.1. 280-keV STATE OF As^{75}

The cascade used to measure the g-factor of the 280-keV state of As^{75} was the 121—280 keV cascade from the 401-keV level to the ground state. The 401-keV

level was populated by electron capture from Se^{75}. Relevant parts of the decay scheme are shown in fig. 3.

The angular correlation for the 121—280 keV cascade has been measured by Schardt and Welker [5]) who used a solid source and obtained †

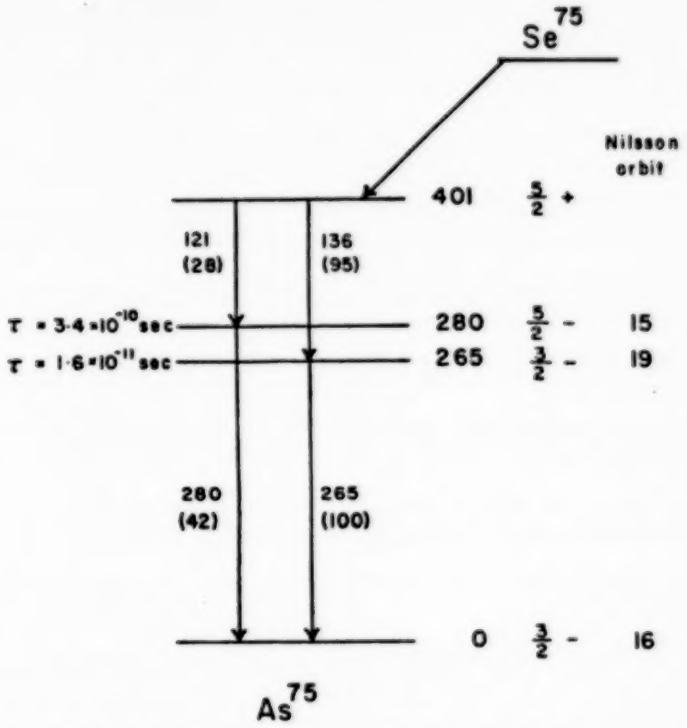

Fig. 3. Relevant parts of the Se^{75} decay scheme. Level and γ-ray energies are shown in keV. The relative γ-ray intensities are shown in brackets. These values are taken from Edwards and Gallagher [11]). Spins and parities, and the Nilsson orbits we have assigned to the levels, are shown to the right of the diagram. Relevant mean lifetimes are shown to the left.

$\overline{W(\theta)} = 1-(0.42\pm0.03)P_2(\cos\theta)$, by Kelly and Wiedenbeck [6]) who do not state the form of their source and obtained $\overline{W(\theta)} = 1-(0.41\pm0.03)P_2(\cos\theta)$, and by van den Bold *et al.* [7]) who used dilute selenic acid, obtaining $\overline{W(\theta)} = 1-(0.466\pm0.02)P_2(\cos\theta)$. The difference between the results may be in part due to the use of solid sources, but may also be due to the difficulty that the 401-keV state also decays by a 136—265 keV cascade which was not completely resolved from the 121—280 keV cascade in any of the above experiments. All three authors also determined the angular correlation for the 136—265 keV cascade. Their results are $\overline{W(\theta)} = 1-(0.019^{+0.01}_{-0.02})P_2(\cos\theta)$, $\overline{W(\theta)} = 1+(0.016\pm0.03)P_2(\cos\theta)$, and $\overline{W(\theta)} = 1-(0.011\pm0.009)P_2(\cos\theta)$, respectively.

The conversion coefficients of the γ-rays following the decay of Se^{75} have been measured by several authors [5, 8, 9, 10, 11]). They all conclude that the 121-keV

† Here and below we have omitted small insignificant $P_4(\cos\theta)$ terms.

transition is pure electric dipole and that the 280-keV transition is a mixture of E2 and M1. Metzger and Todd [19]) conclude from their conversion coefficient measurements that the absolute value of the E2/M1 mixture parameter (δ) for the 280-keV transition lies between 0.33 and 0.44. Edwards and Gallagher [11]) from their conversion coefficient measurements, obtain $|\delta| = 0.52 \pm 0.14$. Van den Bold *et al.* [7]) from their angular correlation results conclude that $\delta = -(0.75 \pm 0.1)$. There appears to be a significant difference between the mixture parameter obtained from angular correlation measurements and that obtained from conversion coefficient measurements. The value of δ^2 is needed in order to compute the lifetime of the 280-keV state from the observed Coulomb excitation cross section. We therefore use an average value, $\delta^2 = 0.40 \pm 0.15$. This value, together with the conversion coefficient for the 280-keV γ-ray and the reduced E2 transition probability obtained from Coulomb excitation, yields a mean lifetime of $(3.4 \pm 1.1) \times 10^{-10}$ sec for the 280-keV level. Metzger and Todd [10]) also compute the lifetime of the 280-keV state in a similar manner and obtain 2.4×10^{-10} sec. The value quoted in the nuclear data sheets [12]), which was obtained by a similar analysis, is 5.5×10^{-10} sec. Our value, $(3.4 \pm 1.1) \times 10^{-10}$ sec, lies between the other computed values.

Our source was prepared by dissolving neutron irradiated Se^{74} in nitric acid. As the 121—280 keV cascade could not be resolved from the 136—265 keV cascade our measurements were made including the whole of both of the composite peaks. This reduces the observed anisotropy, but is of no real trouble in the g-factor measurement as the 136—265 keV cascade is nearly isotropic and the lifetime of the 265-keV level (1.6×10^{-11} sec) is considerably shorter than that of the 280-keV level. Our observed angular correlation for the composite cascade was $\overline{W(\theta)} = 1 - (0.056 \pm 0.003) \cos 2\theta$. This after correction for random coincidences and the finite solid angles of the counters gave $\overline{W(\theta)} = 1 - (0.10 \pm 0.01) P_2(\cos\theta)$. This value is in agreement within the quoted errors with other measurements [5, 6, 7]) if one takes the relative strengths of the 121—280 keV and 136—265 keV cascades as 28 : 95 as indicated by the γ-ray intensities of Edwards and Gallagher [11]). The coincidence counting rate used in the angular correlation measurements and the g-factor determination was ≈ 100 per sec.

The g-factor measurements were made at angles of 135° and 225° with a field of 13 000 gauss. A total of $\approx 8 \times 10^{+6}$ counts were obtained in the coincidence peak for each direction of the field at each of the angles. The values of R obtained were (0.0023 ± 0.0005) and $-(0.0017 \pm 0.0006)$ for $\theta = 135°$ and 225° respectively. These averaged together give $G_2\omega\tau = -(1.72 \pm 0.34) \times 10^{-2}$ radians or $-(0.99 \pm 0.19)$ degrees. Using eq. (6) this gives

$$g = \frac{(0.42 \pm 0.13)}{G_2\beta}.$$

Arsenic is not paramagnetic and hence $\beta = 1$. The fact that the angular correlation results for the 121—280 keV cascade do not differ strongly for liquid and solid sources [$-(0.466\pm0.02)$ compared to $-(0.42\pm0.03)$] indicate that $G_2 \approx 1$ for liquid sources. This is to be expected theoretically as the 280-keV state has a mean lifetime of $\approx 3.4\times10^{-10}$ sec and the quadrupole and magnetic moments of As^{75} are not large. We therefore conclude that the g-factor for the 280-keV level of As^{75} is $+(0.42\pm0.13)$.

4.2. 91-keV LEVEL OF Pm^{147}

The g-factor of the 91-keV level of Pm^{147} has been the subject of two previous investigations. Lindqvist and Karlsson [13]) obtained an upper limit, $|g| \leqq 1$. Bodenstedt *et al.* [14]) obtained a preliminary value, $g = (0.43\pm0.15)$. Both previous investigations were made using the 321—91 keV cascade from the 412-keV state to the ground state. The 412-keV state was populated following the β-decay of Nd^{147}. Lindqvist and Karlsson obtained an angular correlation $\overline{W(\theta)} = 1-(0.097\pm0.007)P_2(\cos\theta)+(0.023\pm0.018)P_4(\cos\theta)$ using a source made by disolving Nd_2O_3 in alcohol. They remeasured the angular correlation with the source in a magnetic field of 25 000 gauss and were only able to place a limit on the g-factor. Bodenstedt *et al.* used a saturated aqueous solution of $NdCl_3$ as a source, but do not quote the anisotropy they observed. They used a magnetic field of 37 200 gauss and observed a rotation of the angular correlation for each direction of the magnetic field from which they obtained the preliminary value quoted above. They do not mention that they have applied a correction for the expected paramagnetism of the Pm^{3+} ion. They made delayed coincidence measurements of the anisotropy and concluded that there is no serious attenuation of the angular correlation. They state that their measurements were somewhat hampered by poor energy resolution of their counters. Our measurements were also made using the 321—91 keV cascade following the β decay of Nd^{147}. We used sources of Nd_2O_3 dissolved in alcohol. Our observed angular correlation was $\overline{W(\theta)} = 1-(0.025\pm0.003)\cos 2\theta$ which after correction for random coincidences and the finite solid angles of the counters gave $\overline{W(\theta)} = 1-(0.038\pm0.005)P_2(\cos\theta)$. This value is significantly smaller than that quoted by Lindqvist and Karlsson [13]) but a careful repetition of the measurements failed to change the results significantly. The measurements were made at 5 angles between 90° and 180° and showed no significant $P_4(\cos\theta)$ term.

The g-factor measurements were made at $\theta = 135°$ with a field of 13 000 gauss. The 91-keV γ-ray is K-converted and the resulting X-ray in coincidence with the 321-keV γ-ray was used as a check on the measurement. The observed value of R for the 321—91 keV cascade was (0.031 ± 0.004) while that for the 321—X-ray cascade was (0.002 ± 0.005). Eq. (4) was used to evaluate $G_2\omega\tau$ and the value obtained was $G_2\omega\tau = -(0.38\pm0.09)$ radians $= -(22\pm5)$

degrees. The lifetime of the 91-keV state has been measured to be 3.4×10^{-9} sec. The value of the g-factor is given by

$$g = \frac{(1.8\pm0.4)}{\beta G_2}.$$

The value of β is estimated as 2.1 in the appendix. Bodenstedt *et al.* [14]) conclude that $G_2 \approx 1$ but do not give their observed anisotropy. As our observed anisotropy is considerably smaller than that quoted by Lindqvist and Karlsson [13]) it is difficult to feel confident that $G_2 = 1$. We therefore conclude that the g-factor of the 91-keV state of Pm^{147} is $(0.9\pm0.2)/G_2$, where G_2 is probably between 0.5 and 1.0.

4.3. 114-keV LEVEL OF Lu^{175}

The cascade used to measure the g-factor of the 114-keV level of Lu^{175} was the 282—114 keV cascade from the 396-keV level to the ground state following the β decay of Yb^{175}. The source was made by neutron irradiation of Yb^{174} oxide. The active material was dissolved in dilute nitric acid.

The angular correlation of the 282—114 keV cascade has been studied by Klema [15]) and by Wiedling [16]). Klema obtained $\overline{W(\theta)} = 1+(0.221\pm0.004)P_2(\cos\theta)$ for a liquid source and $\overline{W(\theta)} = 1+(0.210\pm0.003)P_2(\cos\theta)$ for a solid source. Wiedling measured the anisotropy for aqueous solutions of $Yb(NO_3)_3$ with and without glycerine added and observed no change. His value for the angular correlation was $\overline{W(\theta)} = 1+(0.227\pm0.004)P_2(\cos\theta)$. These results indicate that for liquid sources $G_2 \approx 1$. The angular correlation observed by us after correction for random coincidences and the finite solid angles of the counters were in agreement with the above values. The angular correlation and g-factor measurements were made with sources that gave coincidence counting rates of between 20 and 90 counts per sec. The g-factor measurements were made at an angle of 135° with a field of 13 000 gauss. A total of $\approx 1.7\times10^7$ coincidence counts were observed in the 114-keV peak. The average value of R observed was $-(0.0019\pm0.0006)$. The 114-keV γ-ray is K-converted and the spectra taken included a peak corresponding to the KX-ray in coincidence with the 282-keV γ-ray. The value of R was $-(0.0002\pm0.0005)$. The quantity $G_2\omega\tau$ obtained for the 282—114 keV cascade using eq. (6) was

$$G_2\omega\tau = -(3.0\pm1.0)\times10^{-3} \text{ radians} = -(0.17\pm0.06) \text{ degrees}.$$

The lifetime of the 114-keV level has not been directly measured but its Coulomb excitation cross section has been measured. The E2/M1 mixture parameter for the 114-keV transition can be estimated by comparing the observed K, L_I, L_{II} and L_{III} conversion coefficients with the theoretical values of Rose [17]). The value thus deduced is in agreement with that reported by Martin *et al.*[18]), viz. $\delta^2 = 0.22$. This value, together with the total conversion

coefficient of the 114-keV transition, and the reduced E2 transition probability quoted in the compilation of Alder *et al.*[19]) gives a mean lifetime for the 114-keV level of 9.4×10^{-11} sec.

Eq. (6) gives

$$g = \frac{0.51\pm0.17}{\beta G_2};$$

$\beta = 1$ (see appendix), and $G_2 \approx 1$, and hence we conclude that the g-factor of the 114-keV state of Lu^{175} is 0.5 ± 0.2.

4.4. 113-keV STATE OF Hf^{177}

The β decay of 6.8 d Lu^{177} feeds the first three excited states of Hf^{177}. The two strongest γ-rays in the decay are 208 and 113 keV. These form a cascade between the 321-keV state and the ground state via the 113-keV level. The 208—113 keV angular correlation has been measured by several authors. Wiedling [16]) measured the correlation for liquid sources of different viscosity and concluded that the unperturbed correlation is $\overline{W(\theta)} = 1-(0.163\pm0.002)P_2(\cos\theta)$. For dilute aqueous sources he obtained $\overline{W(\theta)} = 1-0.160P_2(\cos\theta)$. Ofer [20]) obtained a result of $\overline{W(\theta)} = 1-(0.13\pm0.01)P_2(\cos\theta)$ for aqueous sources. Klema [15]) measured the correlation for both solid, and dilute aqueous sources and obtained $\overline{W(\theta)} = 1-(0.149\pm0.002)P_2(\cos\theta)$ and $\overline{W(\theta)} = 1-(0.1614\pm0.0015)P_2(\cos\theta)$ respectively. Behrend [21]) measured the correlation for $LuCl_3$ in aqueous solution, with glycerine added to increase viscosity, and for polycrystalline $LuCl_3$ and obtained $P_2(\cos\theta)$ coefficients of $-(0.1627\pm0.0032)$, $-(0.1511\pm0.0027)$ and $-(0.1311\pm0.0023)$ respectively. Our results obtained with sources made by dissolving neutron irradiated Lu_2O_3 in dilute nitric acid were in agreement with the value obtained by Wiedling, Klema and Behrend for aqueous solutions. The measurements of these authors indicate that $G_2 \approx 1$ for such solutions.

Measurements of the g-factor were made at $\theta = 135°$ and $\theta = 225°$ with a field of 13 000 gauss. In order to obtain a high coincidence counting rate a strong source was used which resulted in a random to true coincidence ratio of between 10 and 20 % (it decreased as the source decayed). The total coincidence rate was in the range 100—200 per second. This rate included both the X-ray, following the K-conversion of the 113-keV γ-ray, and the general background due to random coincidences. In 6 days of continual counting a total of $\approx 1.2\times10^7$ counts was observed in the peak corresponding to the 113-keV γ-rays for each direction of the magnetic field. Table 1 summarizes the results. The average value found for $G_2\omega\tau$ was $-(0.0091\pm0.0014)$ radians or $-(0.52\pm0.08)$ degrees. The X-ray data shows no significant systematic effects.

The lifetime of the 113-keV level has been measured by Berlovich [22]) who obtained $\tau = 6\times10^{-10}$ sec. This value is in good agreement with that calculated

TABLE 1

Results for measurements on the 113-keV state of Hf^{177}

θ	R for 208 keV X-ray coincidences	R for 113–208 keV coincidences	average value of C_2 for 208–113 keV cascades	$G_2\omega\tau$
135°	$-(0.0002\pm0.0007)$	$+(0.0024\pm0.0006)$	-0.070	$-(0.0086\pm0.0021)$
225°	$-(0.0005\pm0.0007)$	$-(0.0031\pm0.0006)$	-0.081	$-(0.0095\pm0.0019)$
			average value	$-(0.0091\pm0.0014)$

R is the observed fractional difference in coincidence counting rate for field up and field down. C_2 is the observed coefficient of cos 2θ for the 208–113 keV angular correlation. The value of R for the 208 keV—X-ray cascade is not significantly different from zero indicating that there is no systematic magnetic field effect. This is further supported by the fact that $\omega\tau$ observed at both the angles are the same within the quoted errors.

from the measured Coulomb excitation cross section, $\tau = 5\times10^{-10}$. Taking $\beta = 1$ (see appendix), $G_2 = 1$ and $\tau = 6\times10^{-10}$ sec we obtain $g = 0.22\pm0.06$ for the g-factor of the 113-keV level of Hf^{177}.

5. Comparison of Results with Theoretical Estimates

Measurements of magnetic moments of the ground states of odd-mass nuclei have proved to be a fruitful source of data for checking the predictions of nuclear models. The models most commonly used are the shell model [23]), and the unified model in which the odd nucleon is assumed to move in an ellipsoidal potential [24]). In the shell model the magnetic moment is, in the first approximation, taken to be due to the single odd nucleon. In the unified model a contribution is added to that of the odd nucleon because of collective motion of the nucleus as a whole. The unified model in particular has enjoyed considerable success in quantitatively explaining the properties of the lower excited states of many nuclei. It is therefore of interest to compare the results obtained from our measurements with predictions of these models.

The shell model first order calculation predicts for an odd proton

$$\mu = (2.79+I-\tfrac{1}{2})\mu_0 \qquad \text{for} \quad I = l+\tfrac{1}{2},$$

$$\mu = \frac{I}{I+1}\,(-2.79+I+\tfrac{3}{2})\mu_0 \qquad \text{for} \quad I = l-\tfrac{1}{2};$$

for an odd neutron

$$\mu = -1.91\mu_0 \qquad \text{for} \quad I = l+\tfrac{1}{2},$$

$$\mu = \frac{1.91\,I\mu_0}{I+1} \qquad \text{for} \quad I = l-\tfrac{1}{2};$$

μ_0 is the nuclear magneton, $I\hbar$ is the total angular momentum of the state and $l\hbar$ is the orbital angular momentum.

The magnetic moment predicted by the unified model is given, for $\Omega \neq \frac{1}{2}$, by

$$\mu = \frac{1}{I+1}[\tfrac{1}{2}(g_s-g_l)K\sum_l (a^2_{l,\Omega-\frac{1}{2}}-a^2_{l,\Omega+\frac{1}{2}})+(g_l-g_R)K\Omega+g_R I(I+1)];$$

the symbols used in this expression are the standard ones for this model and are fully defined in the article by Nilsson [24]). The values of a^2_{lA} are given in that article and a later one by Mottelson and Nilsson [25]). The value of g_R, the g-factor associated with the collective motion of the nucleus, is estimated on the assumption of flow of uniformly charged nuclear matter to be $\approx Z/A$. The limited experimental evidence available to date seems to indicate that its actual value is of the order of one half of this estimate.

In the discussion below an attempt has been made to correlate our measured values with some of the other measured nuclear properties using the predictions of the models.

5.1. As^{75}

Our measured value for the g-factor of the 280-keV $\frac{5}{2}-$ level is 0.42 ± 0.13. This gives a magnetic moment of $(1.0\pm0.3)\mu_0$. The magnetic moment of the ground state is $1.43\mu_0$ [3]) and the quadrupole moment for the ground state is 0.27 ± 0.04 [33]). The other fact of interest is that the 280-keV transition is observed to be a 30 % E2, 70 % M1 mixture. The ground state spin and parity is $\frac{3}{2}-$. If we interpret the ground state and the 280-keV state as single particle shell model states for the odd proton the predicted magnetic moments would be $3.75\mu_0$ and $0.87\mu_0$. The single particle estimate for the E2 mixture in the 280-keV transition is 0.014 %. It is clear that the first order shell model calculations are far from agreement with the data available.

The unified model has not yet been applied to As^{75}. The positive ground state quadrupole moment of As^{75} indicates that the distortion of the As^{75} nucleus is positive (prolate shape). The intrinsic quadrupole moment can be computed from the observed quadrupole moment using

$$Q = \frac{Q_0 I(2I-1)}{(I+1)(2I+3)}.$$

From this we obtain $Q_0 = 1.3\pm0.2$. The Nilsson model predicts that $Q_0 \approx 0.8ZR_Z^2\delta(1+\frac{2}{3}\delta)$. This estimate of Q_0 is plotted against δ (and η) in fig. 4. The experimental value indicates η of 3.4 ± 0.6. The lowest level predicted by the Nilsson model for a nucleus with this distortion and 33 protons is orbit 16 with spin and parity $\frac{3}{2}-$. The observed 199-keV level, with a possible spin of $\frac{1}{2}$ and negative parity may be a hole excitation of orbit 20. The $\frac{3}{2}-$ level at 265-

keV and the $\frac{5}{2}-$ level at 280-keV agree well with the levels next predicted by the model viz. orbits 19 and 15 respectively.

The magnetic moments of orbits 16 (corresponding to the ground state) and 15 (corresponding to the 280-keV state) have been computed from the formula given (taking $g_R = Z/A = 0.44$) and are shown in fig. 4. The E2/M1 intensity ratio for the 280-keV transition can also be computed using the model. The results are also shown in fig. 4. The M1 matrix element vanishes due to a

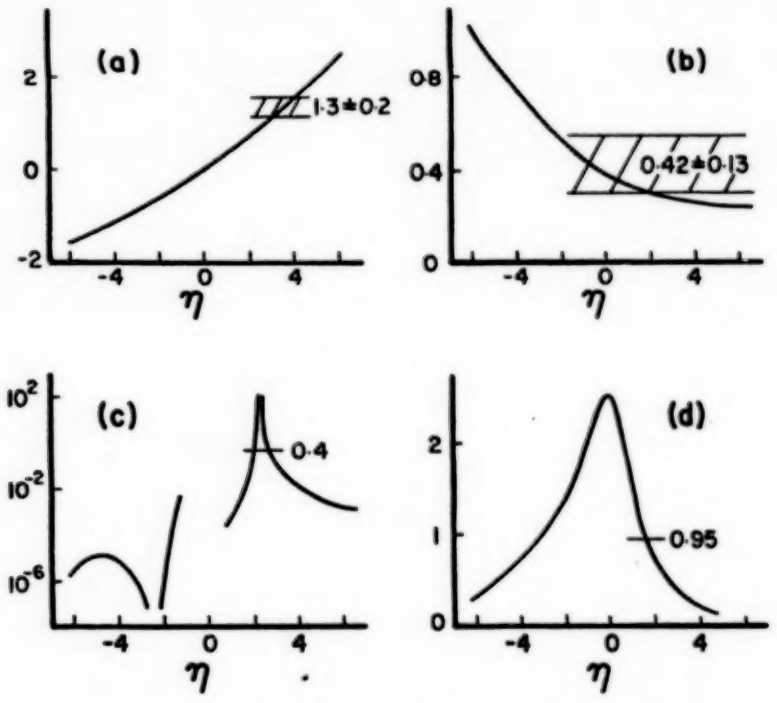

Fig. 4. Comparison of experimental and theoretical values of several properties of As^{75} levels. The theoretical values are computed using the equations and wave functions given by Nilsson [24]). The ground and 280-keV states are taken as orbits 16 and 15 respectively. The agreement with the model predictions is reasonable and indicates that the deformation of As^{75} is prolate ($\eta \approx 2.5$, $\delta \approx 0.12$).

a) shows the ground state quadrupole moment.
b) is the 280-keV state g-factor.
c) shows the E2/M1 intensity ratio for the 280-keV transition.
d) is the ground state g-factor.

cancellation for a distortion $\eta \approx 2.4$. The distortion at which this vanishing occurs depends upon the value taken for g_R. For g_R smaller than Z/A the matrix element vanishes at a smaller distortion. All the results computed indicate that the distortion of As^{75} is prolate and that the model predictions are well borne out by the data considered. It therefore seems worthwhile to extend the analysis of the properties of As^{75} (and possibly neighbouring nuclei) using the Nilsson Model.

5.2. Pm^{147}

Pm^{147} is not a stable nucleus and the ground state magnetic and quadrupole moments have not been measured. The decay scheme is not completely worked out and the spins of the ground state and the 91-keV state are not definitely assigned. The data available at the moment are therefore not sufficient to provide a critical test of the model predictions.

5.3. Lu^{175}

Lu^{175} is a strongly deformed nucleus and the unified model has been used to explain some of the properties of its low levels Mottelson and Nilsson [25]), in a recent compilation list the $\frac{9}{2}+$ 114-keV level as being the first rotational level based on the $\frac{7}{2}+$ ground state. The ground state is interpreted as corresponding to the [404 $\frac{7}{2}$] orbital. The nuclear deformation is taken as $\delta = 0.28$. The ground state magnetic moment is in reasonable agreement with the value deduced from the theory on these assumptions. The g-factor (or magnetic moment) of the 114-keV state can also be evaluated using the same model and assumptions. The value we obtain is $g = 0.41$ which is in good agreement with our measured value of 0.5 ± 0.2.

The shell model is not believed to be applicable in this region of the periodic table but it is true to say that it has enjoyed some small success in approximately predicting the ground state magnetic moments in many regions of the periodic table. The first order calculation for a $\frac{7}{2}+$ state in an odd-Z nucleus is $g = 0.49$, which is in reasonable agreement with the observed value $+0.57$. The value expected for a $\frac{9}{2}+$ shell model state in an odd-Z nucleus is 1.51, which is markedly different from our observed value of 0.5 ± 0.2.

Our measurement is a further verification of the predictions of the unified model and is direct evidence in agreement with the conclusion that the 114.-keV state is the first rotational state based on the ground state.

5.4. Hf^{177}

The unified model has been used with reasonable success in interpreting the properties of the lower levels of Hf^{177}. Mottelson and Nilsson [25]) interpret the 113-keV $\frac{9}{2}-$ level as being the first rotational state based on the $\frac{7}{2}-$ ground state. They assign the ground state to the [514 $\frac{7}{2}$] orbital and conclude that the nuclear deformation is $\delta = 0.27$. The observed magnetic moment of the ground state, $0.6\mu_0$ [26]) is somewhat lower than the value predicted by the theory, $1.4\mu_0$. The magnetic moment predicted by the theory for the 113-keV state on the above assumptions can be evaluated from the expression given. We obtain $\mu = 1.85\mu_0$ for $g_R = Z/A$. Our observed value is $(1.0 \pm 0.2)\mu_0$. This can be taken as an indication that g_R should be less than Z/A. (The contribution from g_R is positive.) The assumption of $g_R = Z/A$ is not believed to be an

accurate estimate. Measurements that have been made to date indicate a value somewhat less than Z/A.

6. Conclusions

The above experiments demonstrate that it is quite feasible to measure rotations of $\gamma-\gamma$ angular correlation patterns as small as a fraction of a degree for reasonable cascades. This enables one to make g-factor measurements on states whose lifetimes are $\approx 10^{-10}$ sec. The deduction of the g-factor from the observed rotations necessitates in certain cases that assumptions be made concerning the form of attenuation of the angular correlation and the effective field produced at the nucleus. The former becomes less important for short lifetimes.

We have analyzed our data on what we feel are reasonable assumptions about the corrections but as there is little conclusive experimental evidence the final g-factors must be taken as reasonable estimates whereas the observed values of R are definite.

It is a pleasure to aknowledge the assistance of Mr. H. E. Henrikson in the construction of the equipment used in this experiment and to other members of the group for their continued support. The separated isotopes used in preparing the sources were obtained from Oak Ridge National Laboratory.

Appendix

Goldring and Scharenberg [2]) have pointed out the existence of effects due to paramagnetism in experiments such as ours. Paramagnetism contributes an effective field at the nucleus greater than the applied field, thereby leading to an erroneously large value of g. This effect can be described in terms of the parameter β where

$$H_{\text{eff}} = \beta H_{\text{app}};$$

the calculation of β for elements in the rare earth region, under certain assumptions, is described below.

The problem of calculating the effective field during the lifetime of the intermediate state is complicated by the fact that one is not certain of the electronic configuration. A typical case we encounter is that of a β-decay followed by a γ-ray cascade. At the beginning of this event the ionic structure is that of the $3+$ ion of the parent rare earth element. Sometime during or after the event the ion reaches the stable $3+$ configuration of the daughter element. The times for the reorganization of the electron configuration must be very short or very long compared to the nuclear lifetime, for the calculation of the effect to be feasible.

Some relevant times for such reorientation to occur may be inferred from various sources. The time for de-excitation of holes in the inner electron shells is known from X-ray work to be very short compared to the times of interest here, viz. 10^{-10} sec. Abragam and Pound [4]) state that the correlation time τ_c, which is essentially the time during which the molecule or ion retains an orientation in the liquid, is of the order 10^{-11} sec for water molecules in water, and should be approximately the same for ions. Goldring and Scharenberg [2]) show that a paramagnetic relaxation time $\tau_s \leqq 10^{-12}$ sec is required to explain their results for Nd^{3+} ions and Sm^{3+} ions in solution. This time is again the time that the ions in question remain in a stable electronic state. It can be expected that such times are those which are relevant in the reorientation of the outer electron shells from parent to daughter ions, and are therefore truly short compared to the nuclear lifetime.

In the case of β^- decay it is also necessary for the ion to pick up an extra electron, while for K-capture it may be necessary for the ion to obtain as many as 5 or 6 electrons due to the loss of Auger electrons in the de-excitation of the inner electron shells. A crude order of magnitude calculation shows that the density of electrons from ionization due to the electron emitted is high enough that the time necessary to pick up an electron is of the order of 10^{-10} sec †. No experimental evidence is available. It is also possible in most cases to discuss the situation in which the electron is not picked up and the configuration reaches an otherwise stable state.

Goldring and Scharenberg [2]) have given formulae for the calculation of the effective field under the consideration that the ion is in thermal equilibrium with the surroundings in the configuration of the daughter element, and the paramagnetic relaxation time is short. They obtain (in our notation)

$$H_{\mathrm{eff}} = \beta H_{\mathrm{app}} = H_{\mathrm{app}} \left[1 + \frac{\mu_e}{\mu_0} \left(\frac{A}{g_{\parallel} g_n} \right) \frac{\mu_{\mathrm{eff}}^2}{3kT} \right].$$

The value of μ_{eff}, the effective magneton number of the ion, is given for the rare earths by Van Vleck [27]); μ_e and μ_0 are the Bohr and nuclear magneton respectively, and the value of $(A/g_{\parallel} g_n)$ can be evaluated from the articles of Elliott and Stevens [28, 29]). Elliott and Stevens demonstrate that if the ground state of the ion is made up by mixing states of the same J, one may write

$$\frac{A}{g_{\parallel} g_n} = 2\mu_e \mu_0 \left(\overline{\frac{1}{r^3}} \right) \frac{\langle J \| N \| J \rangle}{\langle J \| A \| J \rangle}.$$

The values of $\langle J \| A \| J \rangle$ (the Landé g-factor) and the matrix elements $\langle J \| N \| J \rangle$ are given in this work [28]). The value of $\overline{(1/r^3)}$ for the electron has been estimated by Baker and Bleaney [30]) for rare earth elements. The validity of the approxi-

† In the case of β^+ decay the ion has to lose an electron and it seems reasonable that the time taken for this is of the order of the collision time.

mation that the ground state is made up from states of the same J depends on details of the electric fields on the ion, and on the magnitude of the spin-orbit coupling. For ions between Tb and Lu the first excited electronic state is known to be well above the ground state and this mixing should be insignificant. Between Ce and Eu the splitting decreases as one proceeds along the periodic table, and the value of $(A/g_{\|}g_n)$ is more strongly affected. For Sm the effect is known to be sizable in ethyl sulphate crystals, while for Nd it is already small. If one assumes that the environment of the ion in solution is on the average spherically symmetric, and that the deviations from this symmetry are small, the theory would be valid for all the rare earth ions. The factor $A/g_{\|}g_n$ is a

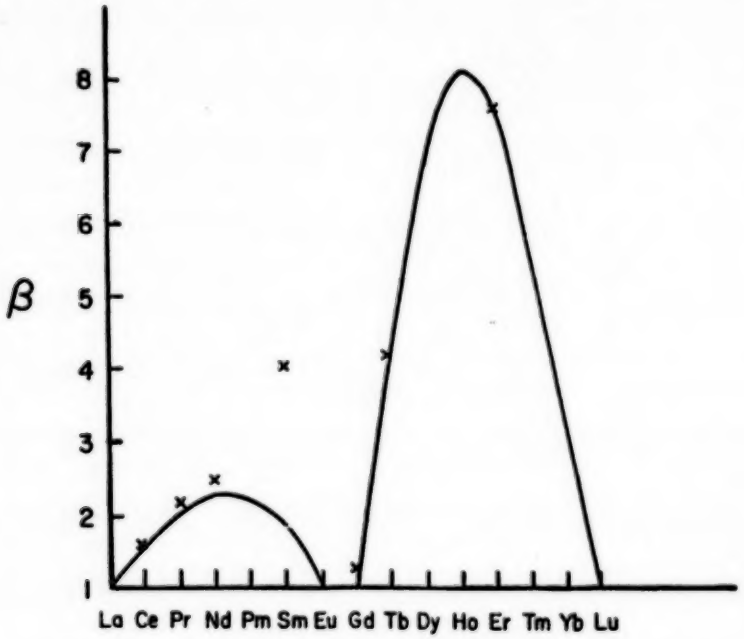

Fig. 5. The effective field correction for rare earth 3^+ ions.

constant for all levels of the same nucleus and hence the ground state experimental values can be applied to the excited states.

Fig. 5 shows the curve for β calculated from the above formula with experimental values for ethyl sulphate crystals, using paramagnetic resonance data [31, 32]) where they are known, indicated by crosses. Table 2 is a summary of the data. The curve is normalized on erbium since this theory is the basis for one calculation of its magnetic moment [29]). The agreement between theory and experiment is seen to be good except for the case of Sm. The experimental value for Sm^{3+} is shown by Elliott and Stevens [29]) to be the result of electronic configurational mixing resulting from the crystalline fields. In a liquid the theoretical value corresponding to a pure J state is perhaps more probable.

Of the nuclei we treat only Pm^{3+} is paramagnetic and from fig. 5 the value of $\beta = 2.1 \pm 0.2$ is seen to be reasonable. With this value the possibility that the

ion does not capture an electron but comes to a stable 4^+ configuration which is electronically the same as Nd^{3+} is also included in the limits.

For the case of Lu^{175} β should be unity as the 3^+ ion is not paramagnetic. If the 4^+ state of Lu were present the error would be large since the β would then be 2.7 instead of 1.

TABLE 2

Calculated and experimental values for the effective field correction for rare earth 3^+ ions

Z	Element	$\beta_{\text{theo.}}$	$\beta_{\text{exp.}}$
58	Ce	1.4	1.5
59	Pr	2.0	2.2
60	Nd	2.3	2.5
61	Pm	2.1	—
62	Sm	1.9	4.1
63	Eu	1	1
64	Gd	1	1.2
65	Tb	4.0	4.2
66	Dy	6.7	—
67	Ho	8.1	—
68	Er	7.7	7.7
69	Tm	5.6	—
70	Yb	2.7	—

The experimental results are calculated from paramagnetic resonance and cryogenic data in ethyl sulphate crystals except for Gd where the data was obtained in cerium magnesium nitrate crystals.

For Hf^{177} both parent and daughter nuclei are not paramagnetic and $\beta = 1$ seems quite certain.

For As^{75} both the parent and the daughter are not paramagnetic and for this reason $\beta = 1$ is expected. It is not likely that the K-capture will change the electron configuration significantly enough to cause paramagnetism to occur.

References

1) H. Frauenfelder, Beta- and Gamma-ray Spectroscopy (North-Holland Publ. Co., Amsterdam, 1955)
2) G. Goldring and R. P. Scharenberg, Phys. Rev. **110** (1958) 701
3) D. Strominger, J. M. Hollander and G. T. Seaborg, Revs. Mod. Phys. **30** (1958) 585
4) A. Abragam and R. V. Pound, Phys. Rev. **92** (1953) 943
5) A. W. Schardt and J. P. Welker, Phys. Rev. **99** (1955) 810
6) W. H. Kelly and M. L. Wiedenbeck, Phys. Rev. **102** (1956) 1130
7) H. C. van den Bold, J. van de Geijn and P. M. Endt, Physica **24** (1958) 23
8) A. A. Bashilov and V. V. Il'in, Izvestia AN SSSR, ser. fiz. **23** (1959) 154
9) E. P. Grigor'ev, A. V. Zolotavin, V. I. Klement'ev and R. V. Sinitzyn, Izvestia AN SSSR, ser. fiz. **23** (1959) 159
10) F. R. Metzger and W. B. Todd, Nuclear Physics **10** (1959) 220

11) W. F. Edwards and C. J. Gallagher, Jr., Bull. Am. Phys. Soc. **4** (1959) 279; and private communication
12) Nuclear data sheets (National Academy of Sciences — National Research Council, 1958)
13) T. Lindqvist and E. Karlsson, Ark. Fys. **12** (1957) 519
14) E. Bodenstedt, E. Matthias, H. J. Körner and R. H. Siemssen, Z. Naturforschg. **13a** (1958) 425
15) E. D. Klema, Phys. Rev. **109** (1958) 1652
16) Tor Wiedling, Thesis (University of Stockholm, 1956)
17) M. E. Rose, Internal Conversion Coefficients (North-Holland Publ. Co., Amsterdam, 1958)
18) M. Martin, P. Marmeir and J. de Boer, Helv. Phys. Acta **31** (1958) 435
19) K. Alder, A. Bohr, T. Huus, B. Mottelson and A. Winther, Revs. Mod. Phys. **28** (1956) 432
20) S. Ofer, Nuclear Physics **3** (1957) 479
21) H. J. Berend, Z. Naturforschg. **13a** (1958) 211
22) S. E. Berlovich, Izvestia AN SSSR, ser. fiz. **20** (1956) 1438
23) M. G. Mayer and J. H. D. Jensen, Elementary theory of Nuclear Shell Structure (Chapman and Hall, London, 1955)
24) S. G. Nilsson, Mat. Fys. Medd. Dan. Vid. Selsk. **29**, no. 16 (1955)
25) B. R. Mottelson and S. G. Nilsson, Mat. Fys. Skr. Dan. Vid. Selsk. **1**, No. 8 (1959)
26) D. R. Speck, Bull. Am. Phys. Soc. **1** (1956) 282
27) J. H. Van Vleck, The theory of Electric and Magnetic Susceptibilities (Clarendon Press, Oxford, 1932)
28) R. J. Elliott and K. W. H. Stevens, Proc. Roy. Soc. A **218** (1953) 553
29) R. J. Elliott and K. W. H. Stevens, Proc. Roy. Soc. A **219** (1953) 387
30) J. M. Baker and B. Bleaney, Proc. Phys. Soc. A **68** (1955) 936
31) K. D. Bowers and J. Owen, Reports on Progress in Physics **18** (1955) 304
32) C. F. M. Cacho, M. A. Grace, C. E. Johnson, A. C. Knipper, R. G. Scurlock and R. T. Taylor, Phil. Mag. **46** (1955) 1287
33) K. Murakawa, Phys. Rev. **110** (1958) 393

Nuclear Physics **15** (1960) 187; © *North-Holland Publishing Co., Amsterdam*

10.A

NEWS ITEM

CERN BUDGET FOR 1960

At its Fourteenth Session, held in Geneva on December 2nd 1959, the Council of CERN, European Organization for Nuclear Research, approved contributions from the 13 Member States totalling 65 000 000 Swiss francs for 1960. This compares with a budget of 55 000 000 Swiss francs for 1959.

Of the 1960 expenditure, 38 500 000 Swiss francs are earmarked for capital expenses, of which 15 000 000 Swiss francs for new buildings and general site facilities, and 18 000 000 Swiss francs for auxiliary experimental equipment. The remaining 26 500 000 Swiss francs will cover general staff and operating expenditure.

With the commissioning of CERN's 25 GeV proton synchrotron, attainment of whose full energy was announced on 25 November, 1959, CERN enters into a new era of research activity. The proton synchrotron will require elaborate and costly auxiliary experimental equipment, as well as certain ancillary buildings if it is to be used to its full advantage. Thus, CERN now enters into a second stage of capital investment.

10.E

ERRATA

A. Bisi and L. Zappa, Relation between circular polarization and energy for external bremsstrahlung from beta-rays (Nuclear Physics **10** (1959) 331).

On fig. 4, page 340, instead of 100Δ, read 10Δ.

N. Nath, M. A. Rothman, D. M. van Patter and C. E. Mandeville, Inelastic scattering in Mn^{55} (Nuclear Physics **13** (1959) 74).

On p. 86, the text should start at line 22, and lines 1—21 should follow lines 22—42.

10.D *Nuclear Physics* **15** (1960) 188; © *North-Holland Publishing Co., Amsterdam*

BOOK REVIEW

S. FLÜGGE (Editor), *Handbuch der Physik, Encyclopedia of physics:* Vol. 41/1, *Nuclear reactions II: Theory* (vii—580 pages. Dm 116); Vol. 44, *Nuclear instrumentation I* (vii—473 pages. DM 125); Vol. 38/2. *Neutrons and related gamma ray problems* (vi—868 pages. DM 178) (Springer-Verlag, Berlin, 1959)

The nuclear physics section of the Encyclopedia has now been enriched by three new volumes, in which a formidable amount of material is collected and systematically surveyed. Although these three volumes are more uniform in their respective scopes than the others of the group, they are nevertheless neither intended nor suited as textbooks in the subjects they cover: their main function is analytic, not synthetic, and it would be unfair to criticize them from the point of view of the non-specialist curious of gaining some insight into these matters; this kind of idler must seek satisfaction elsewhere. Thus, the volume on nuclear instrumentation, devoted to accelerators of every description, is packed with minute detail about each of them, but has no chapter discussing the problem in general terms and presenting a rational classification of the various principles involved in the design and construction of these apparatus.

The volume on the theory of nuclear reactions (which is devoted to resonance reactions in general, including polarization effects, and to Coulomb excitation) is entirely the work of Professor Breit and his distinguished associates. This does not, unfortunately, give it the unity of treatment which it would have had if the authors had felt free to be more selective of their material; in spite of his supreme mastery of the subject, which is everywhere noticeable, the senior author could not hold the encyclopedic overgrowth in check and prevent it from concealing the features of the edifice. It is, however, a welcome compensation for this well-nigh inevitable drawback to find here a really *critical* analysis of the chaotic mass of theoretical work published in this field; and this all too rare quality gives the volume a clearly defined and very valuable place beside the textbooks and survey articles treating the same subjects.

The volume on neutrons and "related" X-ray problems brings under the same cover two topics whose "relationship" is a rather distant one: neutrons and X-rays are both susceptible to absorption and diffusion when they penetrate into matter. I should not like to harp on the same point too much; but with each new volume of this Encyclopedia one cannot help noticing the glaring inadequacy of a plan which reflects the state of nuclear physics fifteen years ago, and wondering why the Editors persist in upholding it, while they keep finished articles for years in their drawers before being able to issue them in volume form. Professor Amaldi was asked to treat the "production and slowing down of neutrons", and he has most brilliantly performed this enormous task, which includes on the one hand the discussion of those reactions in which neutrons appear as single end products, and on the other the theory of slowing down and diffusion of neutrons of various energies. The chief application of the latter theory is to provide the basis of reactor design: but in his introduction the author has to refer the reader to vol. 41 for fission and to vol. 44 for pile technique. He has also to point out that "other information about neutrons" is dispersed in all the volumes of the nuclear physics series, as well as in vol. 32, which does not even belong to this group. He is certainly the last person to blame for the heterogeneous character of his article; the general introduction is a splendid presentation of the essential aspects, and the successive parts, taken separately, are likewise distinguished by elegance and clarity. The article on X-ray penetration and diffusion, due to U. Fano, L. V. Spencer and M. J. Berger, is also of high quality. We must just reconcile ourselves to the idea that with this Encyclopedia we are given (if this is the right word) a collection of monographs, bound together in a haphazard way in bulky and expensive volumes; then, we must at any rate be grateful to the authors, who have not shunned the not always inspiring task of preparing for the practical guidance of their fellow-workers encyclopedic monographs of such excellence.

L. R.

10.C

Nuclear Physics **15** (1960) 189—198; © *North-Holland Publishing Co., Amsterdam*

Not to be reproduced by photoprint or microfilm without written permission from the publisher

SALOMON ROSENBLUM
(1896—1959)

M. VALADARES

Laboratoire de l'Aimant permanent du CNRS, *Orsay*

Reçu le 25 janvier 1960

Salomon Rosenblum naquit en 1896 à Ciechanowiec, aux environs de Minsk, dans une famille aisée. Ses premières études furent très irrégulières, parfois même décevantes; plus tard, il aimait raconter que devant ces difficultés, son père essayait de l'encourager en lui disant qu'il serait toute sa vie suffisamment riche pour se permettre de ne faire que ce qu'il lui plairait. Comme c'était l'usage dans certaines familles russes, ses parents l'envoyèrent en Allemagne pour faire ses études secondaires; cependant, au début de la première guerre mondiale il fut obligé de se réfugier au Danemark et c'est à Copenhague qu'il passa, en 1915, son baccalauréat. Passant ensuite en Suède il poursuivit ses études universitaires de lettres à Lund où il commença à rédiger une thèse sur les langues orientales comparées. Pourtant, par un pur hasard, sa vie intellectuelle allait être orientée vers une branche toute différente.

En effet, un jour, Rosenblum rencontra, dans un café de Copenhague, un assistant de Niels Bohr qui lui raconta comment celui-ci avait pu arriver à concevoir la distribution des électrons autour du noyau atomique. L'image planétaire de l'atome enthousiasma tellement Rosenblum qu'il prit sur le champ la décision d'abandonner la rédaction de sa thèse pour entreprendre des études de physique. Ce „coup de tête" avait d'autant plus de mérite qu'entre temps les conditions économiques avaient complètement changé la situation de la famille de Rosenblum et qu'il ne pouvait plus compter sur l'aide de ses parents; pourtant sa passion pour la physique était devenue telle qu'il abandonna la carrière qui s'ouvrait devant lui pour aller, avec une bourse très modeste, apprendre la physique.

Après ces années en Suède, Rosenblum vint à Paris, pour étudier l'optique, muni d'une lettre d'introduction pour un physicien français connu. Avec cette franchise naturelle qui était un des traits de son caractère, Rosenblum n'hésita pas à raconter comment il était passé de l'étude des langues orientales à son intérêt pour la physique; or, le professeur auquel il s'adressait n'avait pas la tournure d'esprit propre à accepter ces changements brusques de vocation et il l'éconduisit poliment tout en lui suggérant que, peut-être, il pourrait trouver une place au Laboratoire Curie. Madame Pierre Curie, qui avait comme prin-

cipe de ne jamais refuser sa chance à un jeune qui frappait à la porte du Laboratoire, accepta que Rosenblum s'initiât aux recherches de radioactivité. C'est en 1923 que Rosenblum est entré au Laboratoire Curie quelques mois après la publication en langue allemande d'un recueil de poèmes qu'il avait écrit, de 1916 à 1923. On trouve déjà dans ces poèmes de jeunesse cette grande tristesse, parfois même cette hantise du néant, qui devait tellement assombrir les dernières années de sa vie.

Après une prise de contact avec les différentes techniques employées en radioactivité, Rosenblum entreprit sa première recherche; il se proposait d'effectuer une nouvelle détermination du rapport des vitesses des deux groupes de rayons α émis par le dépôt actif du thoron. Pour cette détermination il utilisa un petit électro-aimant en employant la méthode de déviation directe; c'est alors qu'il crut s'apercevoir visuellement que la raie du thorium C avait un aspect différent de celle du thorium C′ et il pressentit comme explication une structure complexe pour le premier de ces émetteurs, alors que tous ceux qui travaillaient la radioactivité admettaient qu'à un émetteur α correspondait un groupe monocinétique de rayons. Malheureusement, les faibles dimensions des pièces polaires de l'électro-aimant ne permettaient pas d'augmenter la dispersion spectrale et Rosenblum dût se résigner à ne pas éclaircir cette impression visuelle. Il prépara alors sa thèse de doctorat (Recherches expérimentales sur le passage des rayons α à travers la matière) qu'il soutint en 1928.

Mais toujours préoccupé de lever le doute qui lui restait de sa première recherche, il pensa que le grand électro-aimant de l'Académie des Sciences de Paris, qui venait d'être installé à Bellevue par A. Cotton et G. Mabboux, devrait lui permettre d'appliquer, pour la première fois aux spectres α, la méthode spectrographique de focalisation à 180° qui avait déjà fait ses preuves dans l'étude des spectres β.

Dans la première série d'expériences que Rosenblum réalisa en 1929, à Bellevue, le pouvoir séparateur de son nouveau spectrographe était 22 fois plus grand que celui du spectrographe utilisé précédemment au Laboratoire Curie. Dès la prise du premier spectre, ce qui était une hypothèse de travail se transforma immédiatement en une vérité éclatante: tandis que le spectre α du thorium C′ était constitué par une seule raie, le spectre du thorium C était formé par quatre raies, c'est-à-dire que les rayons α du thorium C étaient émis avec quatre vitesses différentes. Bien que la vérité fût éclatante personne — surtout parmi ceux qui connaissaient le mieux la radioactivité — ne voulait le croire. En effet, dans tous les esprits était ancrée l'idée qu'à chaque émetteur α correspondait un seul groupe monocinétique de particules α. Ce préjugé explique d'ailleurs pourquoi les chercheurs qui avaient trouvé auparavant des anomalies dans la distribution des parcours des particules α de certains émetteurs avaient toujours essayé de les interpréter comme étant dues à la présence de radioéléments inconnus.

C'est à cette complexité spectrale des rayons α émis par le thorium C que Rosenblum a donné le nom de „structure fine du spectre magnétique des rayons α" (1929). Le qualificatif de „magnétique" peut paraître aujourd'hui superflu, mais il avait dans l'esprit de Rosenblum une raison d'être: il ne voulait pas fermer la porte à l'hypothèse que le champ magnétique fût responsable de cette complexité. C'est d'ailleurs cette même idée qui conduisit Rutherford à refaire l'expérience de Rosenblum en l'absence de champ magnétique; en employant un compteur différentiel, il put confirmer, en collaboration avec Ward et Wynn-Williams, l'existence de la structure fine du thorium C et la découvrir dans l'actinium C et le radium C. Dans les années qui suivirent, Rosenblum allait montrer que le phénomène de structure fine du spectre α était un phénomène très général. Je garde de cette époque un souvenir tel que je m'en voudrais de ne pas le raconter.

En 1932 Madame Pierre Curie et Rosenblum voulaient étudier le spectre magnétique des rayons α émis par le radioactinium; quelques mois auparavant, Madame Irène Joliot-Curie avait montré, à l'aide de la chambre de Wilson, que ce rayonnement α comportait deux groupes d'intensité comparable. Madame Pierre Curie se chargeait au Laboratoire Curie de la préparation chimique des sources et lorsque la première fut préparée, nous sommes partis, Rosenblum et moi-même, à Bellevue pour faire un premier essai, tandis que Madame Curie restait à Paris pour préparer une deuxième source. Après une heure de pose nous avons enlevé la plaque et pendant que j'allais la développer, Rosenblum faisait un nouvel essai. Un quart d'heure après je suis venu dire à Rosenblum que le spectre α du radioactinium présentait six raies; Rosenblum s'est précipité dans la chambre noire, a vu les six raies du spectre et s'est mis à exécuter une danse russe endiablée, ce qui était sa manière très caractéristique d'extérioriser sa joie. Je suis parti à Paris chercher la nouvelle source et, en route, j'ai dessiné sur un papier le spectre du radioactinium, où les groupes observés par Madame Joliot correspondaient en fait à un doublet et à un triplet de raies très rapprochées et où on observait encore, au milieu de ces deux groupes, une raie plus faible. Arrivé rue Pierre Curie, je suis allé directement au petit pavillon dans la cour du laboratoire, j'ai frappé à la porte de la pièce où Madame Curie préparait la nouvelle source et de l'entrée de la pièce je lui ai annoncé que le spectre avait six raies. Madame Curie s'est retournée d'un seul bloc, de sa main gauche a enlevé ses lunettes, m'a regardé avec un sourire qu'à cette époque il était déjà très rare de voir sur sa figure et elle m'a dit: „Six raies?!... Ce n'est pas possible!... Vous blaguez, Monsieur!... Six raies?!... Ah, je vais tâcher de faire une source encore plus belle!...".

Je n'ai jamais eu de toute ma vie une sensation aussi nette de la joie profonde que la recherche fondamentale peut apporter à certains êtres que ce jour-là où j'ai assisté, à une heure d'intervalle, aux réactions d'un homme qui commen-

çait sa vie scientifique et d'une vieille dame qui, déjà couverte de gloire, s'approchait de la fin.

Pendant cette période de 1929—1932, Rosenblum non seulement découvrit plusieurs structures fines, mais il put encore prouver expérimentalement qu'il y avait une relation numérique simple entre l'énergie des quanta γ émis au cours de la transmutation et les intervalles énergétiques des raies de structure fine. C'est d'ailleurs ce résultat expérimental qui donna à la découverte de la structure fine toute son importance, parce qu'il mit en évidence le fait que le spectre α fournissait une image directe du schéma des niveaux nucléaires.

Peut-être sera-t-il difficile pour les jeunes physiciens, habitués dès leurs études universitaires à entendre parler de schémas de niveaux nucléaires, de se rendre compte de l'importance de cette découverte à une époque où d'ailleurs l'expression „schéma de niveaux" n'était même pas encore introduite dans le vocabulaire du physicien nucléaire. Il convient, à ce propos, de reproduire quelques unes des phrases que Louis de Broglie a écrites, précisément en 1932, pour la préface du fascicule consacré à la structure fine dans la Collection des Actualités Scientifiques: „De ces résultats expérimentaux, Monsieur Rosenblum est parvenu à dégager une relation entre le quantum d'un grand nombre de rayons γ et les différences d'énergie dans le spectre des rayons α. Ainsi se trouve établie sur une base solide l'idée plus d'une fois suggérée que la loi des fréquences de Bohr est applicable au noyau. La loi des fréquences, mise par Bohr à la base de ses raisonnements dans sa théorie de l'atome, est la traduction dans le cadre des conceptions quantiques du principe de combinaison de Ritz, principe qui avait été tiré d'abord de l'étude purement empirique des spectres optiques. On peut dire que la loi de Bohr a été la clef qui nous a ouvert les portes du monde atomique. Que cette même loi soit encore valable, au moins dans certains cas, pour les phénomènes nucléaires, c'est un fait encourageant permettant d'espérer que les méthodes dont le succès nous a conduits à un schéma cohérent pour la périphérie de l'atome, ne perdront pas toute leur valeur quand on sera en mesure d'aborder l'étude théorique du noyau."

Il est d'ailleurs intéressant du point de vue historique de rappeler que, déjà en 1922, Smekal avait proposé de considérer le rayonnement γ émis au cours d'une transmutation α comme étant dû à une hétérogénéité dans le spectre α, mais cette hypothèse de Smekal n'avait eu aucun écho, tout le monde étant fermement convaincu du monocinetisme des particules α émises par chaque radioélément.

Toutes ces recherches de structure fine étaient effectuées avec l'électroaimant de Bellevue, ce qui impliquait une surveillance constante du courant et empêchait, pratiquement, l'étude des radioéléments à vie longue. C'est pour cette raison que Rosenblum avait envisagé, dès 1938, la construction d'un grand aimant permanent avec lequel il pourrait poursuivre ses recherches sur la déviation des rayons α; le projet de cet aimant était terminé lorsque pendant

la guerre, à la fin de 1941, il fut contraint d'abandonner la France. Néanmoins, le Professeur Aimé Cotton réussit à obtenir les crédits nécessaires à sa construction et lorsque Rosenblum rentra en France, en 1945, l'aimant était déjà en voie d'achèvement. La construction de cet appareil, alors unique au monde, fut à l'origine de la création d'un nouveau laboratoire du Centre National de la Recherche Scientifique, dirigé par Rosenblum.

Avec ce nouvel instrument de travail, Rosenblum s'attacha non seulement à chercher d'autres structures fines parmi les émetteurs naturels à longue période et les radioéléments transuraniens, mais encore à déterminer avec une précision accrue les intensités des différentes raies spectrales, ce qui présentait un intérêt certain pour comparer les théories d'émission α à l'expérience. Pour la détermination des intensités on employa des plaques nucléaires permettant l'observation de chaque trajectoire α; ainsi les rapports d'intensité entre les différentes raies, qui auparavant étaient très grossiers, furent connus avec une bonne précision.

C'est dans ce laboratoire que Rosenblum a donné toute la mesure de ses qualités d'animateur. Il savait si bien faire partager sa passion et son enthousiasme pour la recherche que pour tous ses collaborateurs la vie du laboratoire passait avant toute autre chose.

Si la structure fine fournit une image indiscutable du schéma de niveaux, elle ne permet pas de mesurer les intervalles énergétiques avec une précision suffisante; c'est pour cette raison que Rosenblum a élargi le domaine de recherches du laboratoire à l'étude des rayonnements γ, par leurs électrons de conversion, en connexion avec la structure fine. Comme parmi ces rayonnements il s'en trouve beaucoup de très faible énergie, la détection des électrons de conversion correspondants par plaque photographique était difficile; Rosenblum a pensé à accélérer ces électrons de façon à leur fournir une énergie suffisante pour leur permettre d'impressionner la plaque. Ici encore se manifesta une des caractéristiques fondamentales de toute son oeuvre scientifique: l'amour de la simplicité, cette simplicité qui étonne ceux qui regardent son premier spectrographe ou son compteur à étincelles. Parmi les différents procédés qu'on pouvait imaginer pour accélérer ces électrons il défendit âprement, dans toutes les discussions avec ses collaborateurs, l'emploi d'un dispositif très simple, si simple que ses collaborateurs étaient assez sceptiques sur les résultats qu'on pourrait obtenir; mais encore une fois Rosenblum avait vu juste: le très simple a donné d'excellents résultats.

Désirant améliorer encore le pouvoir séparateur en spectrographie α et refaire toutes ses anciennes mesures absolues de vitesses, Rosenblum envisagea vers 1954 la construction d'un nouvel aimant permanent, dont la surface des pièces polaires serait de 100×160 cm et l'entrefer variable de 2 à 10 cm. Cet aimant fut installé en 1958 dans les nouveaux locaux du Laboratoire à Orsay et il a commencé à fonctionner il y a quelques mois.

Si l'oeuvre scientifique d'un savant peut permettre parfois, à ceux qui ne l'ont pas connu, de se faire une image assez juste de sa personnalité, une telle déduction dans le cas de Rosenblum resterait nécessairement très incomplète. En effet, tous ceux qui l'approchaient, qui travaillaient avec lui, se rendaient compte qu'il avait une personnalité hors série. Si ces poèmes de jeunesse sont empreints d'une profonde mélancolie, parfois même d'un attrait maladif pour l'au-delà, on dirait que son passage à la recherche scientifique avait effacé ce penchant et à l'époque où il travaillait au Laboratoire Curie il était le plus gai de nous tous, le plus gai et — certainement — le plus généreux. Nous tous, ses anciens camarades de travail du Laboratoire Curie, nous nous rappelons l'avoir vu sortir du laboratoire, s'arrêter rue Pierre Curie et donner à un clochard l'argent qu'il avait en poche. Après, on allait déjeûner et c'était seulement au moment de l'addition qu'il constatait avoir donné au clochard tout l'argent qui lui restait jusqu'à la fin du mois. Pendant quelques jours il devait vivre dans des conditions encore plus modestes et pourtant, jamais aucun de nous, ses camarades de travail — incapables naturellement d'un pareil geste — n'a osé lui faire aucune remarque. On n'osait pas, parce qu'on le sentait extrêmement heureux, parce qu'on devenait timide devant une telle générosité.

Il est évident qu'un pareil homme devait souffrir terriblement de tous les événements qui se sont déroulés dans le monde pendant le dernier quart de siécle, d'autant plus qu'après son mariage et la venue au monde de deux enfants les soucis quotidiens lui avaient ôté la belle insouciance que nous lui avions connue. La montée du nazisme, la disparition dans des conditions tragiques de quelques membres de sa famille et de ses amis, l'emploi d'armes nucléaires, la crainte — très vivace en lui — d'un renouveau possible du racisme, lui avaient imprimé un sceau de tristesse, d'angoisse, voire de dégoût. Aussi, malgré la chaude atmosphère familiale dans laquelle il vivait, malgré les succès remportés par ses filles au cours de leurs études, son climat spirituel est-il peu à peu redevenu celui qui lui avait dicté ses poèmes de jeunesse et peu à peu la vie de tous les jours lui apparut-elle insupportable. C'est sans doute dans cette évolution spirituelle qu'on trouve la clef de sa fin tragique.

Liste des publications Scientifiques †

Sur une nouvelle détermination du rapport des vitesses des deux groupes de rayons α émis par le dépôt actif du Thorium C (C.R. **180** (1925) 1332).

Sur le ralentissement des rayons α par la matière (C.R. **183** (1926) 198; C.R. **185** (1927) 851).

Sur les pouvoirs de ralentissement par atome relatifs aux rayons α (C.R. **185** (1927) 1275).

† Les publications principales sont marquées d'un astérisque.

*Recherches expérimentales sur le passage des rayons α à travers la matière, Thèses de la Faculté des Sciences de l'Université de Paris (Masson et Cie) (Voir aussi Annales de Physique **10** (1928) 408).

Geschwindigkeitsverluste der α-Strahlem beim Durchgang durch Metallfolien (Physikalische Zeitschrift **29** (1928) 737).

*Structure fine du spectre magnétique des rayons α du Thorium C (C.R. **188** (1929) 1401).

Structure fine du spectre magnétique des rayons α (C.R. **190** (1930) 1124).

Nouveau spectrographe magnétique à rayons α (C.R. **191** (1930) 1004).

Progrès récents dans l'étude du spectre magnétique des rayons α (Journal de Physique et le Radium **1** (1930) 438).

Figures de distribution du dépôt actif sur les électrodes [S. Rosenblum et M. Valadares]. (C.R. **192** (1931) 939).

Spectre magnétique des rayons α du dépôt actif de l'actinon [S. Rosenblum et Mme Pierre Curie] (C.R. **193** (1931) 33).

Sur les rayons α de long parcours émis par le Th C+C' et quelques déterminations de vitesses de rayons α (C.R. **193** (1931) 848).

*Spectre magnétique des rayons α du dépôt actif de l'Actinium [Mme Pierre Curie et S. Rosenblum] (Journal de Physique et le Radium **2** (1931) 309).

Spectre magnétique des rayons α du dépôt actif de l'Actinon [Mme Pierre Curie et S. Rosenblum] (Journal de Physique et le Radium **2** (1931) 781).

*Sur la structure fine des rayons α du Th C [S. Rosenblum et M. Valadares] (C.R. **194** (1932) 967).

*Sur la structure fine du spectre magnétique des rayons α du R Ac [Mme Pierre Curie et S. Rosenblum] (C.R. **194** (1932) 1232).

Mesures absolues des vitesses des principaux groupes des rayons α [S. Rosenblum et G. Dupouy] (C.R. **194** (1932) 1919).

*Origine des rayons γ — Structure fine du spectre magnétique des rayons α (Hermann et Cie, Paris, 1932).

Structure fine du spectre magnétique des rayons α du Ra (C.R. **195** (1932) 317).

*Mesure absolue des vitesses des principaux groupes de rayons α [S. Rosenblum et G. Dupouy] (Journal de Physique et le Radium **4** (1933) 262).

Mesure directe des intensités de la structure fine des rayons α [S. Rosenblum et P. Chevallier] (C.R. **196** (1933) 1484).

Sur la structure fine du spectre magnétique des rayons α du R Ac et de ses dérivés [Mme Pierre Curie et S. Rosenblum] (C. R. **196** (1933) 1598).

Sur le rayonnement α du R Th et de ses dérivés [S. Rosenblum et C. Chamié] (C.R. **196** (1933) 1663).

*Sur les diamètres effectifs des noyaux radioactifs [G. Gamow et S. Rosenblum (C.R. **197** (1933) 1620).

Discussions, Conseil de Physique Solvay (1934) 231.

Sur l'existence de la raie α_5 et la décomposition du spectre magnétique du Th C en deux séries (C.R. **202** (1936) 943).

*Sur l'intensité des groupes de structure fine du spectre magnétique du R Ac et de ses descendants [S. Rosenblum, M. Guillot et M. Perey] (C.R. **202** (1936) 1274).

Sur les spectres dans la famille de l'Ac X [S. Rosenblum, M. Guillot et M. Perey] (C.R. **204** (1937) 175).

Sur la possibilité de l'existence de niveaux énergétiques équidistants dans les noyaux des corps radioactifs [S. Rosenblum et M. Guillot] (C.R. **204** (1937) 345).

Sur certaines régularités dans les niveaux nucléaires des atomes radioactifs [S. Rosenblum et M. Guillot] (C.R. **204** (1937) 975).

Sur le spectre γ du Ra B et du R Ac [S. Rosenblum et M. Guillot] (C.R. **204** (1937) 1727).

*A simple counting system for Alpha-Ray Spectra [S. Rosenblum et W. Y. Chang] (Physical Review **67** (1945) 265).

Fernand Holweck (Renaissance **2** (1944—1945) 225).

Making very thin glass-windows [S. Rosenblum et R. J. Walen] (Journal of Scientific Instruments **22** (1945) 197).

Récents progrès de la spectrométrie des rayons α (Grand Aimant Permanent de Bellevue) in Transactions of Instruments and Measurements (Conférence Stockholm (1947)).

Le Grand Aimant Permanent de Bellevue [S. Rosenblum et B. Tsaï] (C.R. **224** (1947) 1278).

Complexité du rayonnement α du protactinium [S. Rosenblum et E. Cotton] (C.R. **224** (1948) 171).

A new method for the determination of the mass of mesons [C.F. Powell et S. Rosenblum] (Nature **161** (1948) 473).

Os espectros magnéticos dos raios alfa (Gazeta de Fisica **1** (1948) 263).

Structure fine du spectre magnétique des rayons α de l'Ionium [S. Rosenblum, M. Valadares et J. Vial] (C.R. **227** (1948) 1088).

Le spectre du rayonnement α émis par R Th+Th X [S. Rosenblum, M. Valadares et M. Perey] (C.R. **228** (1949) 385).

*Recent progress in alpha-ray spectroscopy (Nucleonics **4** (1949) 38).

Nouvelle détermination de la structure fine du spectre α du Radium [S. Rosenblum, M. Guillot et G. Bastin-Scoffier] (C.R. **229** (1949) 108).

Complexité du rayonnement α du protactinium [S. Rosenblum, E. Cotton et G. Bouissières] (C.R. **229** (1949) 825).

Structure fine du spectre magnétique α du Th X [S. Rosenblum, M. Valadares M. Perey et J. Vial] (C.R. **229** (1949) 1009).

On the spectrum of light particles produced in cosmic ray desintegration [C. Franzinetti et S. Rosenblum] (Nuovo Cimento Suppl. **6** (1949) 349).

Nouvelle détermination de quelques rayons des noyaux radioactifs lourds [S. Rosenblum et M. Valadares] (C.R. **230** (1950) 384).

*Structure fine du spectre magnétique α du Plutonium 239 [S. Rosenblum, M. Valadares et B. Goldschmidt] (C.R. **230** (1950) 638).

Sur le renforcement radioactif des raies spectrales (C.R. **230** (1950) 1766).

Le spectre béta de conversion interne émis dans la transmutation Ionium → Radium [S. Rosenblum et M. Valadares] (C.R. **232** (1951) 501).

Sur le schéma nucléaire du Th C' (C.R. **234** (1952) 202).

Spectre β de conversion interne émis dans la transmutation Th X → Thoron [S. Rosenblum, M. Valadares et M. Guillot] (C.R. **234** (1952) 1767).

Les spins des niveaux des noyaux pairs-pairs et la théorie de l'émission α [S. Rosenblum et M. Valadares] (C.R. **234** (1952) 2359).

Spectre d'électrons de conversion interne émis dans la transmutation R Th→Th X [S. Rosenblum, M. Valadares et M. Guillot] (C.R. **235** (1952) 238).

Sur les niveaux nucléaires A (premiers états excités) [S. Rosenblum et M. Valadares] (C.R. **235** (1952) 711).

The Nuclear A Levels (Conférence Didcot (1952)).

Classification des „rayons" des noyaux émetteurs α en fonction de l'excès neutronique (I) [S. Rosenblum et M. Valadares] (C.R. **236** (1953) 196).

Sur les travaux du magnétisme en U.R.S.S. (Nuovo Cimento Suppl. **10** (1953) 441).

Sur les rayonnements émis au cours de la transmutation R Ac→Ac X (1ère partie) [M. Frilley, S. Rosenblum, M. Valadares et G. Bouissières] (Journal de Physique et le Radium **15** (1954) 129).

Sur la structure fine α de l'Ionium [S. Rosenblum, M. Valadares, J. Blandin-Vial et R. Bernas] (C.R. **238** (1954) 1496).

Sur le spectre d'électrons de conversion émis par $^{241}Am \xrightarrow{\alpha} {}^{237}Np$ [J. Milsted, S. Rosenblum et M. Valadares] (C.R. **239** (1954) 259).

Sur le schéma de niveaux du ^{237}*Np [J. Milsted, S. Rosenblum et M. Valadares] (C.R. **239** (1954) 700).

Le spectre d'électrons de conversion émis dans la transmutation Ionium → Radium [S. Rosenblum, M. Valadares et R. Bernas] (C.R. **239** (1954) 759).

*Le spectre de vitesses α des isotopes du Polonium [S. Rosenblum et H. Tyrén] (C.R. **239** (1954) 1205).

Spectres de rayons α (Conférence faite le 4 Mai 1954 au cours des réunions sur les Propriétés et la structure des noyaux, sous la présidence de Monsieur Louis de Broglie) (Cah. Phys. **53** (1955) 38).

A propos du compteur à étincelles (Journal de Physique et le Radium **16** (1955) 159).

Sur les rayonnements émis au cours de la transmutation R Ac → Ac X (2ème partie) [M. Frilley, S. Rosenblum, M. Valadares et G. Bouissières] (Journal de Physique et le Radium **16** (1955) 378).

L'aspect historique de la découverte de la Radioactivité artificielle (Journal de Physique et le Radium **16** (1955) 743).

*Spectrographe magnétique avec pré-accélération pour l'étude d'électrons de faible énergie [S. Rosenblum, J. Sant'Ana Dionisio et M. Valadares] (Journal de Physique et le Radium **17** (1956) 112).

*Études sur la transmutation $^{241}Am \xrightarrow{\alpha} {}^{237}Np$ (S. Rosenblum, M. Valadares et J. Milsted] (Journal de Physique et le Radium **18** (1957) 609).

Spectres magnétiques des particules alpha et Épilogue (Volume du 80ème anniversaire de Lise Meitner, Otto Hahn et Max von Laue (1959)).

1.D.2:
1.E.1:
3.B

Nuclear Physics **15** (1960) 199—215 © *North-Holland Publishing Co., Amsterdam*

Not to be reproduced by photoprint or microfilm without written permission from the publisher

0+ STATES OF Sm^{152} AND Gd^{152}

I. MARKLUND

Institute of Physics, Uppsala†

and

O. NATHAN and O. B. NIELSEN

Institute for Theoretical Physics, University of Copenhagen

Received 12 October 1959

Abstract: The decay of Eu^{152m} (9.2 h) is studied by means of internal and external conversion and $e^- - \gamma$ coincidence measurements with particular interest focused on the possible low-lying 0+ levels in the transition region between spherical and non-spherical nuclei. Such levels are now found at 615.3 keV in the near-spherical nucleus Gd^{152} and at 685.0 keV in the strongly deformed nucleus Sm^{152}. The experimental K-conversion coefficients for the $0+ \rightarrow 0+$ transitions are $\geqq 0.770$ and $\geqq 0.250$, respectively. The e_K^-/γ branching ratios μ from the 0+ levels to the ground states and to the first excited 2+ states are compared with the theoretical values:

$$Gd^{152}: \mu_{exp} = 0.10 \pm 0.03, \quad \mu_{theory} = 0.085;$$
$$Sm^{152}: \mu_{exp} = 0.013 \pm 0.001, \quad \mu_{theory} = 0.13.$$

1. Introduction

Most of the present knowledge about the spectra of Sm^{152} and Gd^{152} is due to studies of the β-decay and electron capture decay of Eu^{152} ($T_{\frac{1}{2}} = 12.2$ y) and of Eu^{152m} ($T_{\frac{1}{2}} = 9.2$ h). Considerable experimental attention has been given to these decays in the past years and a large amount of information is now available on both decay schemes (see, e.g., refs.[1–7]). Part of this interest is motivated by the fact that Eu^{152m} happens to be a suitable source for neutrino helicity experiments which involve nuclear resonance fluorescence. In this investigation, however, we shall emphasize another interesting feature of the Eu^{152} and Eu^{152m} decays, which is associated with the particular position of the Eu^{152} nucleus between the group of vibrational nuclei with neutron numbers $N \leqq 88$ and the group of strongly deformed nuclei with $N \geqq 90$. Thus, one can study the spectrum of a vibrational nucleus (Gd^{152}; $N = 88$) and that of a strongly deformed nucleus (Sm^{152}; $N = 90$) at the same time, and it is hoped that these studies will provide useful information on the properties of collective nuclear modes of excitation and on the mutual relationship between such modes in the two different types of nuclei.

† This work is in part supported by the U. S. Air Research and Development Command.

This investigation is particularly concerned with a search for low lying 0+ levels in Sm^{152} and Gd^{152}, whose existence is predicted by the unified model, but for which no experimental evidence has been presented so far. In the case of the spheroidal nucleus Sm^{152}, the theory predicts the presence of a one-phonon quadrupole vibrational state of the 0+ type (β-vibration), while in the case of a spherical nucleus such as Gd^{152} a 0+ state is expected to occur in a two-phonon quadrupole vibration which splits up into a 0+, 2+, 4+ triplet. A general description of nuclear shape vibrations within the framework of the unified model may be found, for instance, in the review article by Alder *et al.* [8]) and need not be repeated here.

The possible existence of β-vibrations in Sm^{152} was recently discussed by Nathan and Hultberg [3]) on the basis of γ-ray measurements on Eu^{152}. These authors proposed a level at 811 keV in Sm^{152} which was assigned as a 2+ rotational state associated with a postulated, but not observed 0+ β-vibrational excitation. The existence of the 811 keV state has since then been confirmed by Coulomb excitation experiments [9]). The 0+-2+ separation in the ground-state rotational band of Sm^{152} is 122 keV and, keeping in mind the expected near-equality of the moments of inertia for different rotational bands within the same nucleus, it follows that the 0+ β-vibrational state should occur about 122 keV below the 811 keV state, i.e., around 690 keV. In Gd^{152}, the 0+ state would be expected in the same energy region, since a 756 keV level which is populated in the 12.2 year decay probably can be interpreted as the 2+ or 4+ member of the two-phonon triplet.

On the basis of these considerations, it was decided to reinvestigate the spectra of internal conversion electrons and γ-rays from Eu^{152m} and in particular to look for strongly converted transitions in the region 0.5—1.0 MeV. The spin and parity of Eu^{152m} being 0− [7]), it seemed that the conditions would be quite favourable for the observation of conjectured 0+ states in the daughter nuclei, considering the high sensitivity which is obtained in β-ray spectrometers with good resolution for the detection of the fully converted 0+ →0+ transitions.

2. Experimental Procedure and Results

Two β-ray spectrometers were employed in this investigation, *viz.*, a double-focusing iron yoke spectrometer with $\rho = 50$ cm [10]) in which an accurate field measurement relative to an iron-free Helmholtz coil is performed by the rotating coil method [11]), and a six-gap spectrometer [12]) which can be used for electron-gamma coincidence experiments. The former instrument has been adapted especially to precise energy determination of electron lines, and it is also well suited for measurements of γ-ray spectra by means of photoelectric conversion. On the other hand, the six-gap instrument with its high transmission

is a very efficient coincidence spectrometer, and in this work it was used mainly for the study of internal conversion electron-gamma coincidences in which coincident γ-rays were recorded on a 100 channel kicksorter. The measurements were initially confined to an energy region above 600 keV, but were later on extended to somewhat lower energies in an attempt to detect transitions from the tentatively established 0+ states of Sm^{152} and Gd^{152} to the first excited states of these nuclei.

2.1. MEASUREMENTS WITH THE DOUBLE-FOCUSING SPECTROMETER

The sources for these measurements were produced by reactor irradiation of Eu_2O_3 or $EuCl_3$ † at AB Atomenergi, Stockholm. For the internal conversion

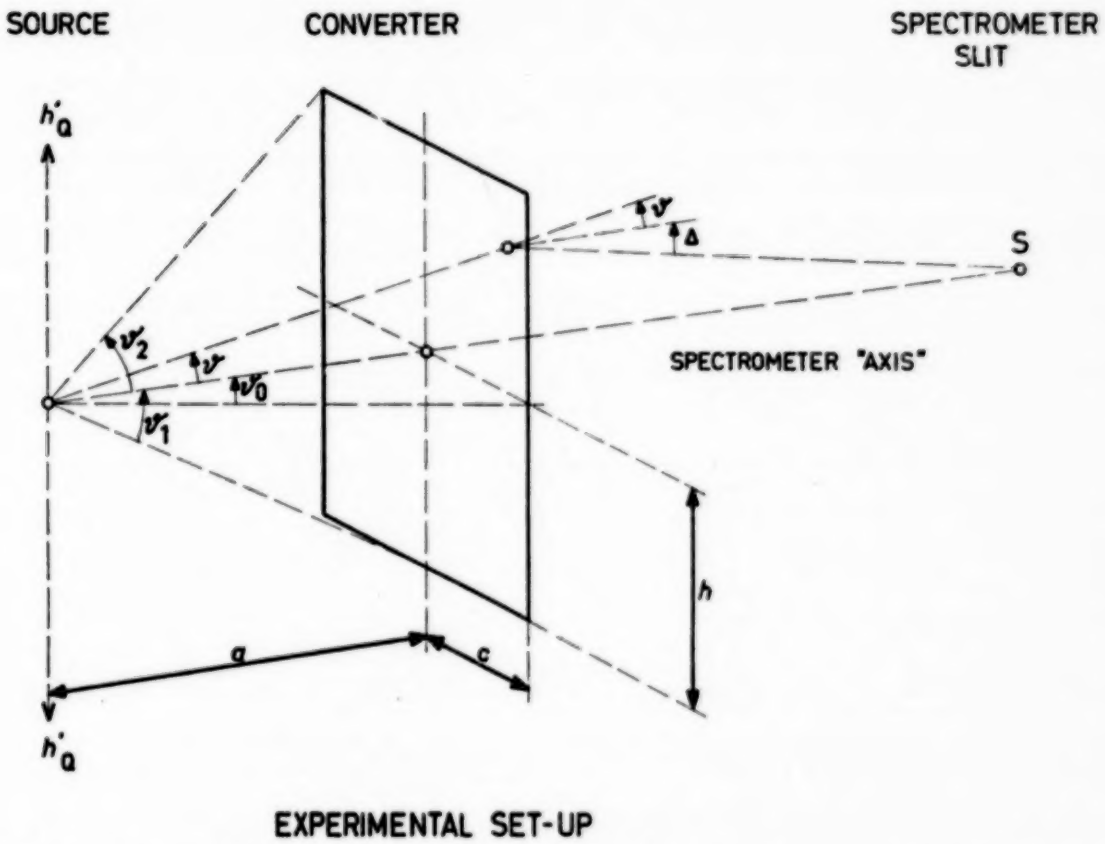

Fig. 1. Scheme of the experimental arrangement for external conversion measurements. The point and line sources Q were placed at a distance $a = 2.0$ mm from the rectangular converters $2c \times 2h$ (2×20 mm, 4×20 mm, 8×20 mm) of thickness 0.9—3.3 mg U_3O_8/cm^2. S is the first spectrometer slit.

part the sources were produced by vacuum evaporation on 0.2—0.8 mg/cm² Al-backing. An estimated source thickness of 0.1—0.5 mg/cm² and a source size of 2×20 and 4×20 mm resulted in a momentum resolution of 0.2—0.3 %. For the external conversion part, the sources had an initial strength of about

† Supplied in part by Johnson, Mattey and Co. Ltd, London, and in part by Oak Ridge Nat. Lab., Tenn. The latter material was enriched in Eu^{151}.

500 mc and were enclosed in a copper cylinder for absorption of the β-rays. The rectangular converters were 2×20 mm, 4×20 mm, and 8×20 mm and their thickness 0.9—3.3 mg U_2O_3/cm^2. The momentum resolution here was 0.3—0.5 %. The electron energies were measured against the earlier determined

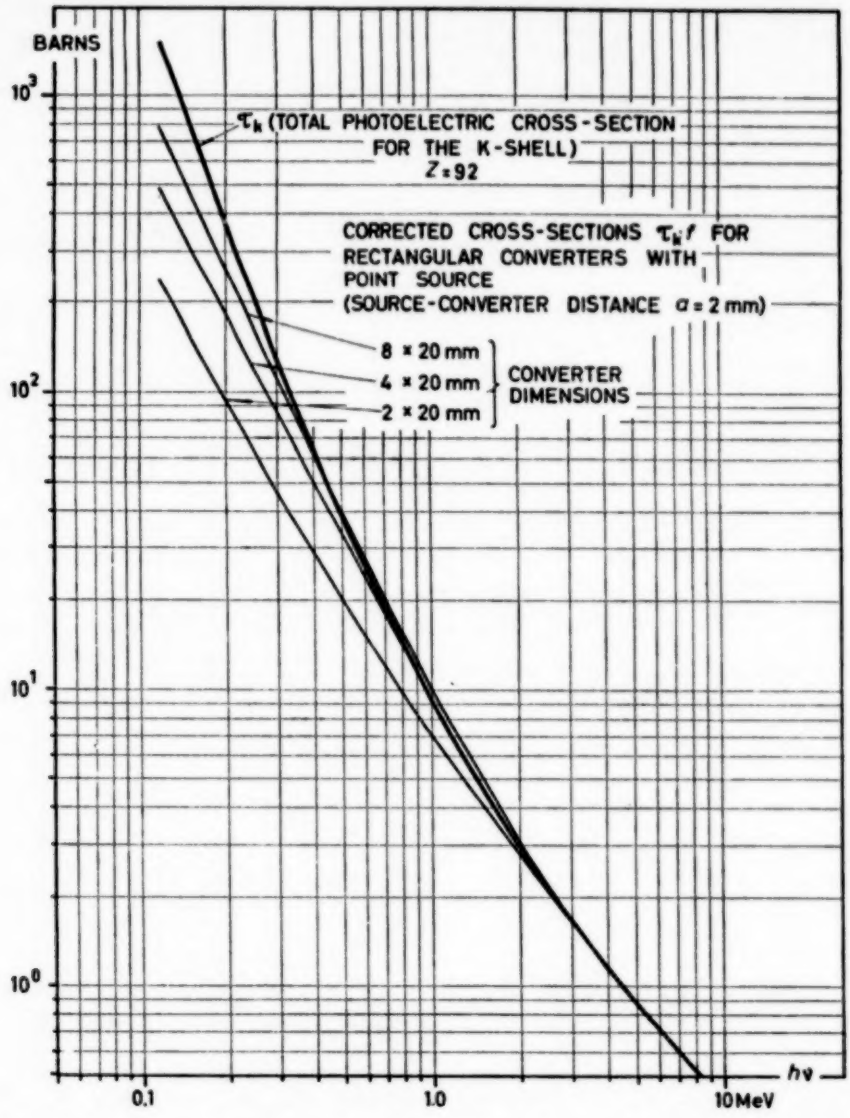

Fig. 2. Photoelectric cross-section τ_K for the K-shell ($Z = 92$) and the effect of converter extension as a function of gamma ray energy.

121.78 keV γ-ray energy in Eu^{152m} [5]) and the reference lines from Cs^{137} and Co^{60}.

In order to determine the relative γ-ray intensities accurately we have made use of the method of Hultberg [13]) and of his tabulated photoelectric distribution curves $J(\vartheta)$. [14]) However, for optimum resolution, rectangular converters and long cylindrical sources were chosen, and Hultberg's method was applied to this type of converters †.

† Discussions with Dr. S. Hultberg during this phase of the work are much appreciated.

The experimental arrangement is drawn schematically in fig. 1 for a point source Q at a distance a from a rectangular converter $2c \times 2h$. The relative intensities are found from

$$I_\gamma = \text{const.} \frac{A_\gamma}{\tau_K f g_{ls}}, \tag{1}$$

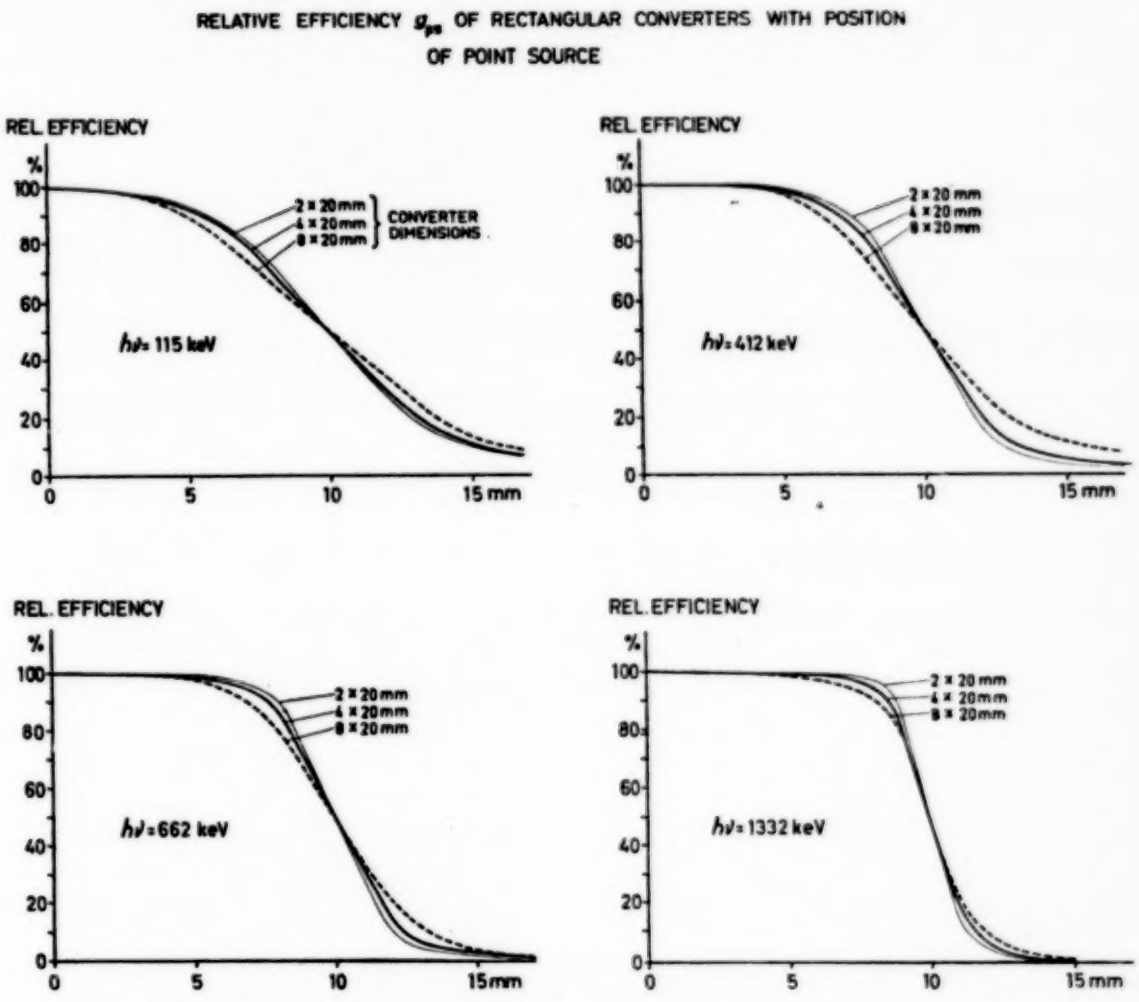

Fig. 3. Relative efficiency of rectangular converters at four gamma ray energies as a function of the distance h'_Q from the symmetric position of a point source (fig. 1) outwards parallel to the converter length h.

where

A_γ = recorded intensity of photoelectrons (area of line profile divided by $B\rho$),
τ_K = total photoelectric cross section for the K shell,
f = correction factor for photoelectric angular distribution and converter dimensions,
g_{ls} = correction factor for extension of the line source.

The photoelectric cross section τ_K as a function of energy is shown in fig. 2 together with three curves $\tau_K f$ corresponding to the three different converter

dimensions. The f values of $\tau_K f$ in fig. 2 are calculated at four energies (115, 412, 662 and 1332 keV) by a normalized integration over the tabulated photoelectric distribution function $J(\vartheta)$ times an expression for the rectangular converter area:

$$f = \frac{(2/\pi)\int_0^{\vartheta} J(\vartheta+\Delta)\ \mathrm{tg}\ \vartheta \arcsin\left(\frac{c}{a\ \mathrm{tg}\ \vartheta}\right) \mathrm{d}\vartheta}{\int_0^{\pi} J(\theta)\ \sin\theta\ \mathrm{d}\theta}, \qquad (2)$$

where arcsin x is replaced by $\frac{1}{2}\pi$ when $x \geqq 1$. The other quantities are defined in fig. 1. For details of such calculations the reader is referred to the paper by Hultberg [14]).

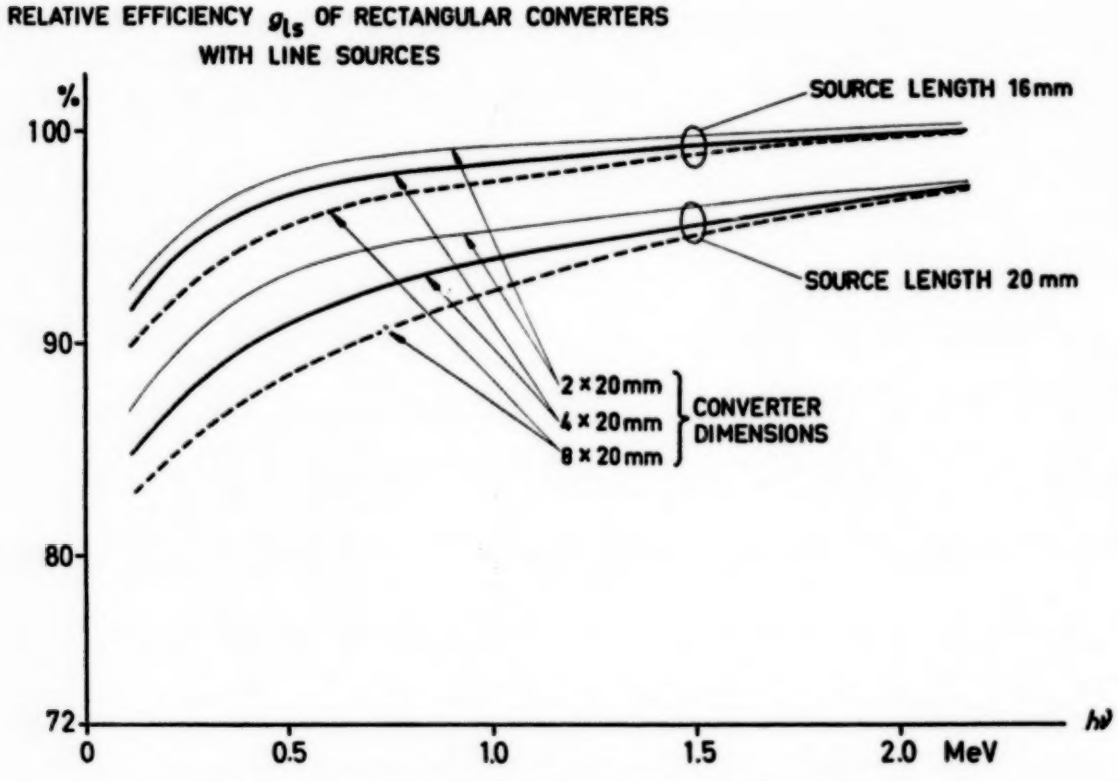

Fig. 4. Effect of source extension as a function of gamma ray energy.

In order to correct for source extension, calculations were carried out on the relative efficiency g_{ps} of rectangular converters for different positions of a point source. The result is seen in fig. 3, in which the efficiency is plotted as a function of the distance h'_Q from the symmetric position of the source outwards parallel to the converter length (fig. 1). An inflexion point appears at the edge of the converters, 20 mm in length ($h'_Q = 10$ mm). The efficiency at this point is somewhat higher than 50 per cent. The relative efficiency g_{ls} of a rectangular converter with line source is found by integration under the curves in fig. 3. The result is presented in fig. 4 for two line sources, 16 and 20 mm long, and

20 mm long converters. As expected, source extension has its largest influence on the γ-ray intensities in the low-energy region.

The results of the measurements in the double-focusing spectrometer are listed in table 1 and parts of the internal and external conversion spectra are shown in fig. 5. In order to get sufficiently small statistical errors ($\approx$ the diameter of the rings in fig. 5) some parts of the spectra have been run with a total measuring time of half an hour or more on each point. Of the twelve transitions listed in the table, the 563, 615 and 685 keV radiations have not been observed previously. The existence of a 260 and a 725 keV γ-ray was reported by Grodzins and Kendall [15]), but these quanta were only seen in γ—γ coincidence spectra and their place in the decay scheme could not be unambiguously determined. The remaining seven transitions are well known from earlier studies of Eu^{152m}, and the positions of these radiations are uniquely established by various coincidence measurements and by energy fits. Our results on these transitions are in good agreement with the earlier data.

2.2. MEASUREMENTS WITH THE SIX-GAP SPECTROMETER

Internal conversion lines in the 250—700 keV region were measured in this spectrometer at a momentum resolution of 0.4—0.5 %. The sources were prepared from Eu_2O_3 (enriched in Eu^{151} — see footnote p. 197) which was dissolved in HCl, evaporated to dryness on 2 mg/cm² plastic foil, and finally irradiated in the Kjeller reactor. The source thickness was estimated to about 0.75 mg/cm². The internal conversion data listed in table 2 agree excellently with the results quoted in table 1.

The coincidence between the 344 and 271 as well as between the 615 and 700 keV transitions was established in e—γ coincidence experiments. The arrangement used in these measurements has been described in detail elsewhere [22]); in the actual case, a $1.5'' \times 1.5''$ NaI-crystal was employed. The β-ray spectrometer was selecting the lines K_{344} and K_{615}, respectively, and quantitative estimate of the intensities of the 271 and 700 keV γ-rays could be obtained from the efficiency with which the two γ-ray peaks were recorded in the coincident spectra. The results, which are given in column 3 of table 2,

TABLE 2

Results of e_K—γ coincidence measurements

E (keV)	$I_{e_K} \times 10^5$	I_γ %
271	3.9±0.5	0.09±0.02
344	(77)	(2.5)
563	3.1±0.5	
615	9.9±1.2	
685	4.9±0.8	
700		0.05±0.01

See table 1 for normalization.

TABLE 1

Results of internal and external conversion measurements on the decay of Eu^{152m}(9.2 h) (only about one per cent around the expected lines is scanned)

Z	E_γ (keV)	$I_{e_K} \times 10^5$ [b]	I_γ(%) [a]	$\varepsilon_K \times 10^3$	$\varepsilon_K \times 10^3$ Sliv and Band [21])	Multipole assignment	Remarks
62	121.78±0.05	5400 ±250		$L_I : L_{II} : L_{III}$ 1.0 : 2.6 : 2.5	$L_I : L_{II} : L_{III}$ E1 1 : 0.17 : 0.22 E2 1 : 2.5 : 2.4 M1 1 : 0.07 : 0.02 M2 1 : 0.11 : 0.15	E2	$(K/L)_{exp} = 1.8$ $(K/L)_{theor} = \begin{cases} E1\ 7.34 \\ E2\ 1.81 \\ M1\ 7.98 \\ M2\ 4.34 \end{cases}$
64	271.0 ±0.2	4.0 ± 0.3	0.08 ±0.02	50 ±20	E1 17.5 E2 62 M1 107 M2 463	E2	
64	344.3 ±0.2	77	2.50	30.9	E2 30.9	E2	normalized
62	563.2 ±0.3	2.9 ± 0.2	0.31 ±0.05	9 ± 2	E1 2.8 E2 7.8 M1 13.6 M2 41.1	E2	
64	615.3 ±0.4	8.1 ± 0.4	≦0.010	≧770	E1 2.6 E2 6.9 M1 12.8 M2 36.7	E0	
62	685.0 ±0.4	4.1 ± 0.3	≦0.015	≧250	E1 1.9 E2 4.8 M1 8.3 M2 23.3	E0	

64	700.2 ±0.7	0.20± 0.06	0.05 ±0.02	4 ± 2	E1 2.0 E2 5.1 M1 9.4 M2 25.6	E1	
62	841.6 ±0.3	16.7 ± 0.4	13.2 ±0.8	1.3± 0.1	E1 1.3 E2 3.1 M1 5.1 M2 13.3	E1	
62	963.3 ±0.3	10.8 ± 0.3	11.5 ±0.8	0.9± 0.1	E1 1.0 E2 2.3 M1 3.6 M2 9.1	E1	
64	970.3 ±0.5	0.5 ± 0.2	0.5 ±0.1	1.0± 0.5	E1 0.9 E2 2.2 M1 3.6 M2 9.1	E1	
64	1315.0 ±0.5	0.6 ± 0.2	1.2 ±0.3	0.5± 0.2	E1 0.6 E2 1.4 M1 2.1 M2 4.8	E1	
62	1389.3 ±0.5	0.5 ± 0.2	1.1 ±0.3	0.4± 0.2	E1 0.5 E2 1.1 M1 1.6 M2 3.6	E1	

[a]) The relative gamma intensities are normalized to a mean of the strong beta branches reported in refs. [1]) and [6]).

[b]) The c_K-intensities are normalized to give an experimental conversion coefficient ε_K^{exp} for the known E2 344.2 keV transition equal to the coefficient ε_K tabulated by Sliv and Band. [21])

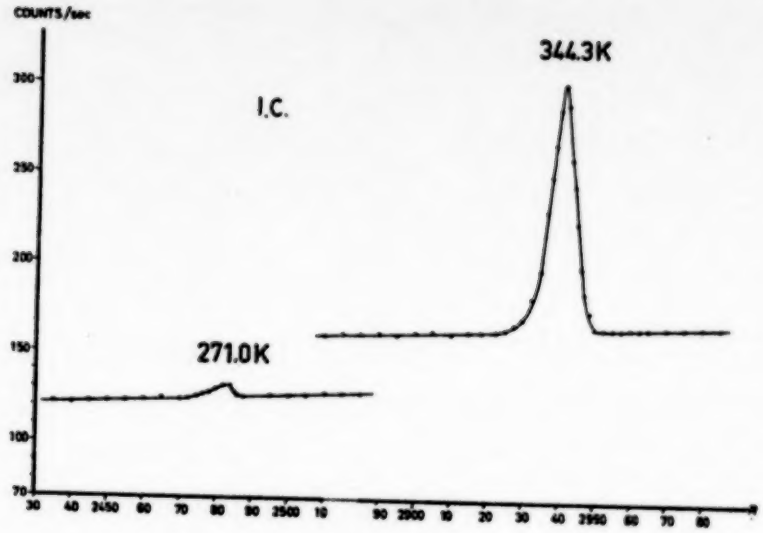

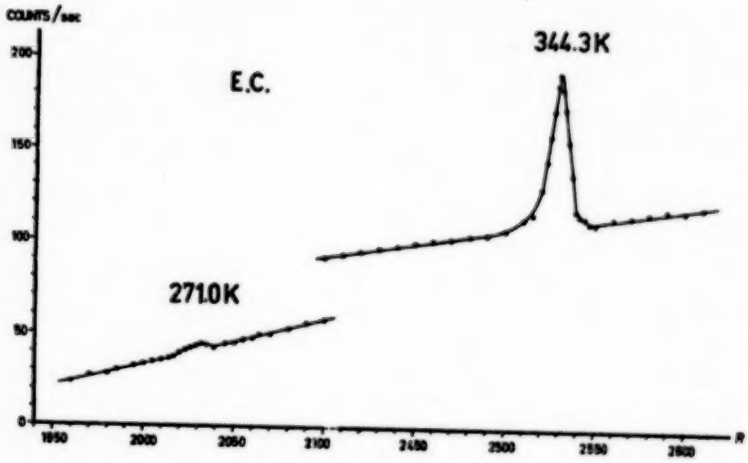

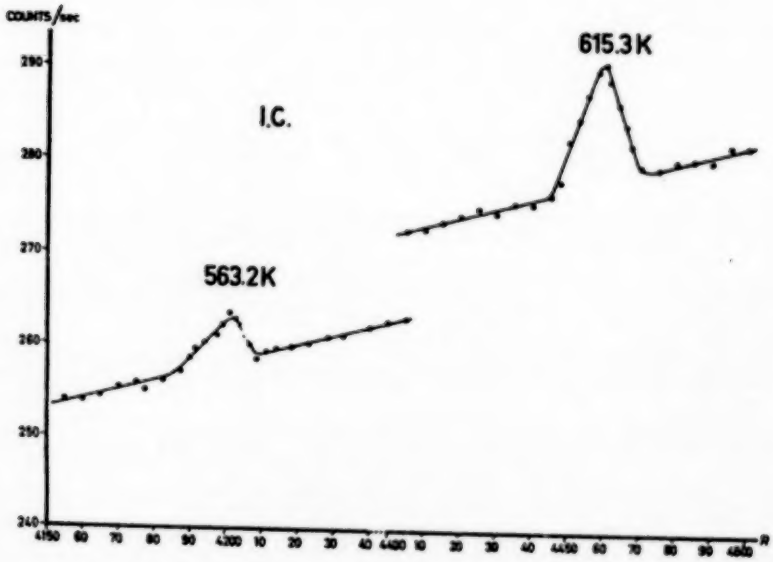

Fig. 5. See also p. 209

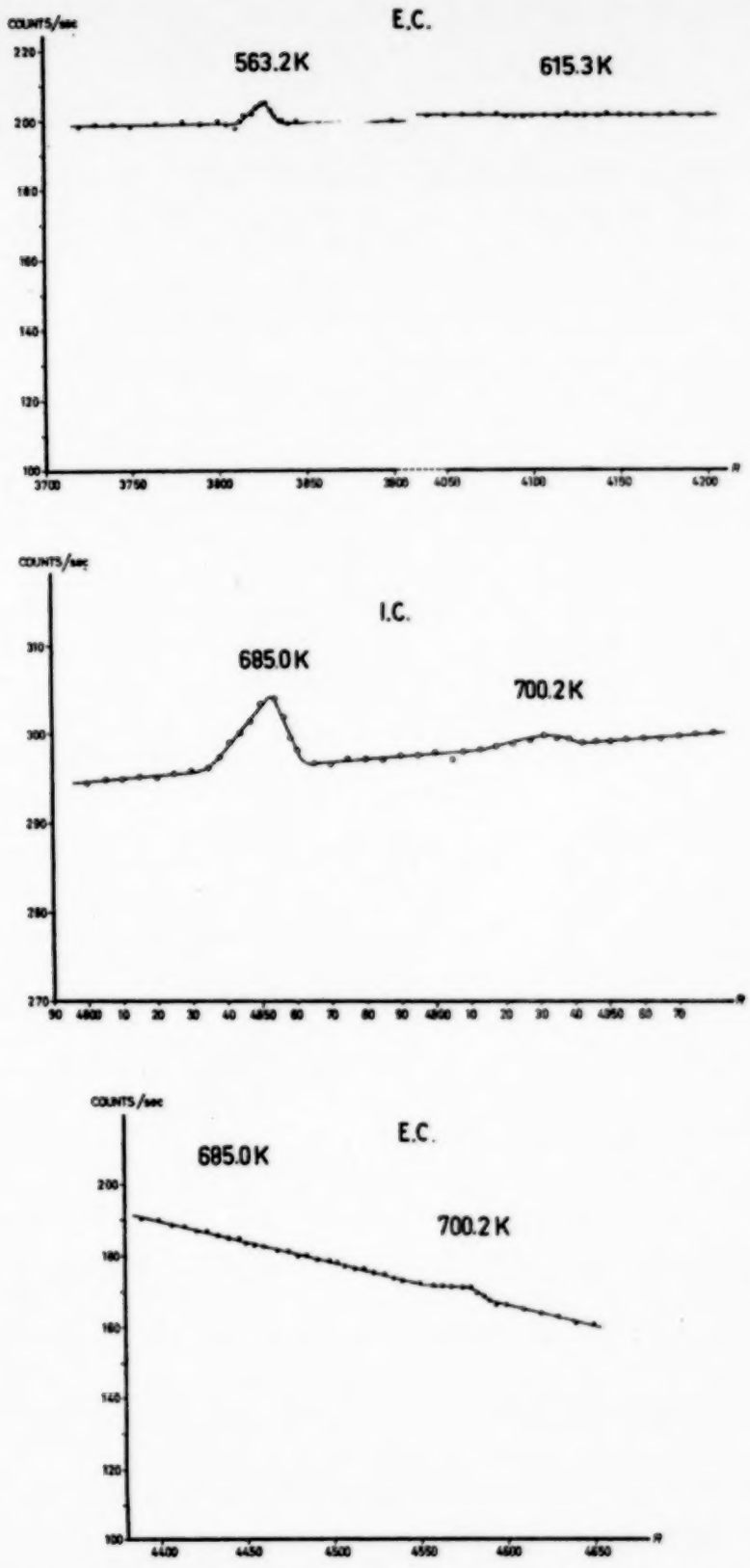

Fig. 5. Parts of internal (I.C.) and external (E. C.) conversion spectra. Most of the lines are situated on a high background, causing time consuming measurements to reach statistical errors ≈ the diameters of the rings. The ratios between I.C. and E.C. line areas give relative conversion coefficients. These are very high for the 615.3 keV and 685.0 keV transitions.

agree with the figures in table 1. The appearance of the 700 keV γ-ray peak in the spectrum coincident with K_{615} is shown in fig. 6.

3. Decay Scheme

The experimental evidence presented in the preceding paragraph clearly establishes the existence of two new levels in Sm^{152} and Gd^{152}: a 0+ state of Sm^{152} at 685 keV and a 0+ state at 615 keV in Gd^{152}. These levels are included in the decay scheme of fig. 7 which is otherwise based on the information contained in the papers on Eu^{152m} by Alburger *et al.* [2]), Marklund [5]), and Wood [16]).

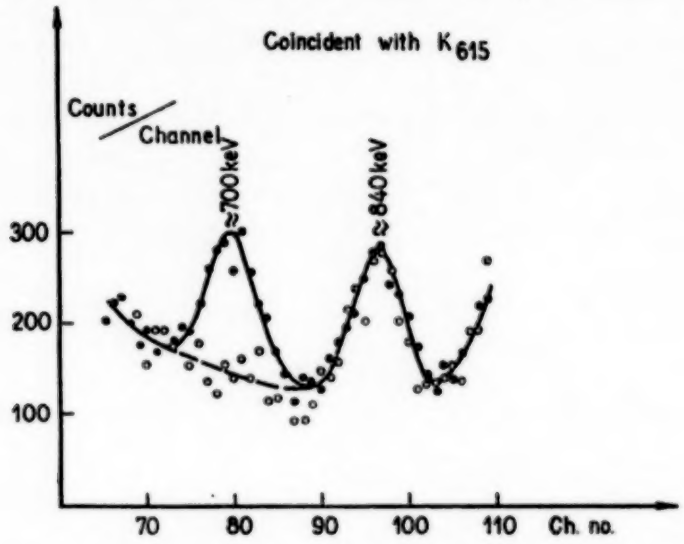

Fig. 6. Representative spectrum from the $e_K^- - \gamma$ coincidence measurements. Filled points are coincidences with the 615 keV K-conversion line in Gd^{152}, open points are coincidences with the β-ray continuum immediately above the line. The different coincidence behaviour of the two lines in the spectrum is obvious from inspection of fig. 7.

Both 0+ states decay by a transition to the ground state and another transition to the first excited state. This is supported by the excellent energy fits $563.2+121.8 = 685.0\pm0.3$ keV and $344.3+271.0 = 615.3\pm0.3$ keV compared to the cross-over transitions 685.0 ± 0.4 keV and 615.3 ± 0.4 keV and also by the $e-\gamma$ coincidence measurements. The 0+ character of the two states is unambiguously established by the extremely high lower limit which, according to table 1, can be put on the internal conversion coefficients of the 615 and 685 keV transitions, together with the observed E2 character of the 271 and 563 keV transitions to the first excited 2+ states.

The 700 keV radiation is found to be coincident with the 615 keV K-conversion line, fig. 6, and this fact together with the energy sum $700.2+615.3 = 1315.5\pm0.7$ keV (cross-over transition energy 1315.0 ± 0.5 keV) allows us to conclude that this radiation proceeds between the previously established 1− level at 1315 keV in Gd^{152} [16]) and the 615 keV level. We therefore expect E1 multipolarity for the 700 keV photon, which is consistent with the rather

uncertain data given in table 1 for this weak radiation. The E1 character of the 970, 1315 and 1389 keV transitions which is expected from the results of Wood's polarization-correlation measurements[16]) is also borne out by the data of table 1.

On the basis of the total transition intensities within Sm^{152} and Gd^{152}, which are indicated on the decay scheme fig. 7, we can estimate the *ft*-values for the first forbidden decays from the Eu^{152m} 0− state to the two excited 0+ states. In this way we arrive at the values log *ft* = 8.0 for the electron capture decay to Sm^{152} and log *ft* = 10 for the β-decay to Gd^{152}. It is interesting to note that the latter decay is considerably more retarded than the other first forbidden transitions between Eu^{152m} and Gd^{152} and Sm^{152}.

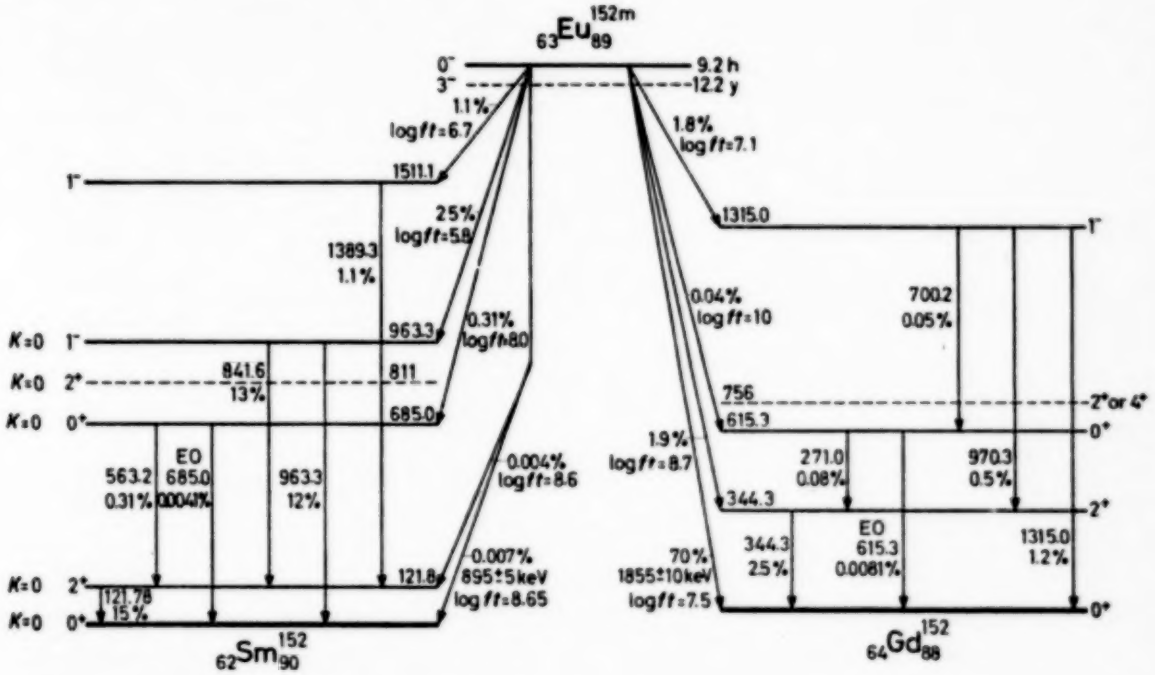

Fig. 7. Decay scheme of Eu^{152m} (9.2 h). The dashed levels are excited from Eu^{152} (12.2 y).

4. Discussion

Let us first consider the 685 keV, 0+ level in Sm^{152}. The position of this state 126 keV below the 811 keV 2+, $K = 0$ state observed in the Eu^{152} ground state decay [3]) and in Coulomb excitation [9]) makes it very likely that we are dealing with two members of the same rotational band. It seems most likely that this band is associated with the predicted β-vibrational motion, although it is still conceivable that other mechanisms such as pair excitation could be responsible for the existence of the 0+ state. The moment of inertia associated with the band is seen to deviate only 3 % from the moment of inertia of the ground-state band, in contrast to the γ-vibrational band in Sm^{152} whose moment is about 20 % smaller [3]).

Only a few examples of 0+ β-vibrational states have been reported. In the rare-earth region, a 1460.4 keV state of Er^{166} [1]) † may be an example of such a vibration, and among the heavy deformed nuclei two 0+ levels have been observed which probably can be identified as β-vibrations, *viz.*, the 803 keV, 0+ state of U^{234} and the 940 keV, 0+ state of Pu^{238} [1]). In the two latter cases, experimental data are available on the e_K/γ branching ratio μ, i.e., the ratio between the intensity of the K-conversion electrons emitted in the $0+ \rightarrow 0+$ transition and the intensity of the E2 γ-rays emitted in the $0+ \rightarrow 2+$ transitions to the first excited state. The measured values are $\mu = 1.0$ for U^{234} and $\mu = 0.5$ for Pu^{238} [17]). In a recent work by A. Reiner [18]) on structure effects in the interaction between nuclei and atomic electrons, a theoretical expression for μ has been derived for the case of vibrations of strongly deformed nuclei. It appears that μ depends on the nuclear equilibrium quadrupole deformation β_0, whose magnitude can be obtained from a measurement of the cross section for Coulomb excitation of the first rotational state, whereas the nuclear vibrational parameters cancel out. In the notation of Reiner [ref. [18]), p. 94, eq. (5.57)], μ is given by

$$\mu = \frac{W^{E0,e_K}}{W^{E2,\gamma}} = S^{-1}\,\frac{147}{\pi\alpha}\,\frac{\Omega}{R^4}\,\frac{\beta_0^2}{k_\gamma^5}, \qquad (3)$$

$$\Omega = B(Z)F(Z, E_{k_e}, R)[1-\tfrac{27}{98}(Z\alpha)^2]\,R^4,$$

where Ω is the electronic factor defined by Church and Weneser [19]), which contains the electronic matrix element for E0 transitions. R is the nuclear radius, S is a geometrical factor equal to 1 for the decay of a 0+ state to a 2+ state and k_γ is the γ-ray energy in units of mc^2.

For U^{234} and Pu^{238} Reiner obtains the values $\mu = 0.9$ and 0.63, respectively, in agreement with the findings of the Berkeley group. In the case of Sm^{152}, however, we are faced with a serious discrepancy between theory and experiment. The experimental value obtained from table 1 is 0.013 ± 0.001 in contrast to the theoretical value †† 0.13.

In discussing these numbers, two comments should be made, one concerning the model upon which Reiner's calculations are based, and one concerning the peculiar properties of Sm^{152}.

To evaluate the collective E0 matrix elements Reiner makes the rather arbitrary assumption of a homogeneous nuclear charge distribution. In actual nuclei, however, the deformation and the charge distribution for a given state may depend critically on the properties of the particular configuration involved,

† A search for low-lying 0+ levels in the rare-earth region was reported at the Stockholm Conference, June 1959, by Marklund *et al.* [23]), who also reported 0+ states in Os^{188} at 1086 keV and at 1766 keV and in Pt^{194} at 1267 keV.

†† The theoretical values quoted for Sm, U, and Pu have been communicated to the authors by Reiner and deviate somewhat from the earlier values given in ref. [18]). The differences are apparently due to interpolation errors in the evaluation of the F-functions.

and the collective E0 matrix element may consequently deviate from Reiners' values in some cases.

Furthermore, it should be kept in mind that Sm^{152} is a limiting case of a deformed nucleus and has a strong rotation-vibration interaction, reflected in the energies of the ground state band which deviate strongly from the simple rotational formula. The effect of a coupling between the ground state band and the $K = 0$ β-vibrational band is to increase the E2 transition probabilities somewhat while leaving the $0+ \rightarrow 0+$ transition rate unaffected. A calculation for Sm^{152} based on a first-order perturbation treatment indicates an E2 enhancement factor of about 2†. This effect might therefore be responsible for part of the observed Sm^{152} discrepancy. Also, it seems possible that the structure of the β-vibrational mode could be more complicated for nuclei in a transition region, in which case the present calculations of the E0 matrix element would be much in doubt.

On these grounds it is not too surprising that Reiner's calculations fall short by a factor of ten for Sm^{152}, and a much more detailed theoretical calculation of the collective matrix elements seems required to explain the observations.

Let us next consider the 0+ excited state of Gd^{152}. This level is situated at an excitation energy 1.8 times that of the first excited state, compared to 2.2 for the 756 keV, 2+ or 4+ state. These figures are close enough to the energy ratio 2 expected for a harmonic oscillator to make it reasonable to suggest that we are in fact dealing with members of a 0+, 2+, 4+ two-phonon triplet. The position of the 0+ level below the 754 keV state is contrary to the general predictions of the weak coupling model regarding the level sequence in the triplet. However, it has been pointed out by Goldhaber [20]) that the triplet levels may cross over if strong anharmonic terms are present in the collective Hamiltonian. In the following we shall explore the implications of a two-phonon interpretation of the 0+ state of Gd^{152}, although the possibilities of other mechanisms such as pair excitation certainly cannot be rejected on the basis of the present data.

A theoretical prediction of the e_K/γ branching ratio in the decay of a two-phonon 0+ state can be derived from Reiner's work. Using equations (5.45)—(5.49) of ref. [18]) we obtain, in analogy with (3),

$$\mu = \frac{147}{8\pi\alpha} \frac{\Omega}{R^4} \frac{\hbar}{2\sqrt{BC}} \frac{1}{k_\gamma{}^5}. \tag{4}$$

Note that, in this case, μ depends on the vibrational parameters B and C which represent the mass transport associated with the vibration and the effective surface tension, respectively. However, since the first excited state of these nuclei is the one-phonon state, the vibrational parameters can be obtained from a measurement of the cross section for Coulomb excitation of this state.

† We are indebted to Dr. A. Bohr for working out this calculation.

The relation between the product BC and the reduced E2 transition probability which is provided by the Coulomb excitation experiment is [8])

$$B(\mathrm{E2}) = 5\left(\frac{3}{4\pi} ZeR_0^2\right)^2 \frac{\hbar}{2\sqrt{BC}}. \tag{5}$$

No Coulomb excitation has been reported for Gd^{152}, but a good estimate of the $B(\mathrm{E2})$ value may, nevertheless, be obtained by considering the neighbouring nucleus Sm^{150}. This nucleus has the same neutron number as Gd^{152} and its first excited state occurs at 337 keV compared to 344 keV in Gd^{152}. The $B(\mathrm{E2})$ value observed in the Coulomb excitation of the 337 keV state of Sm^{150} is $B(\mathrm{E2}) = 0.98\, e^2 \times 10^{-48}\ \mathrm{cm}^4$, which yields the following value for the product of the vibrational parameters:

$$\frac{\hbar}{2\sqrt{BC}} = 5.45 \times 10^{-3}.$$

If we assume that Sm^{150} and Gd^{152} have approximately the same vibrational parameters, we obtain for the $0+$ state of Gd^{152} $\mu_{\mathrm{theor}} = 0.085$. The experimental value which we deduce from table 1 is $\mu_{\mathrm{exp}} = 0.10 \pm 0.03$. At this point it may be noted that, although some two-phonon $0+$ states have been observed previously in vibrational nuclei (Pd^{106}, Cd^{114}, Po^{214}), the available experimental data in these cases do not allow a similar quantitative comparison with the theoretically expected branching ratios.

In view of the remarks made previously about Reiner's model, the agreement between the observed e/γ branching in Gd^{152} and the theoretical value is rather surprising and can probably be regarded as somewhat accidental. Furthermore, Reiner's calculations for collective transitions in vibrational nuclei do not include the effect of anharmonic terms in the vibrational motion. However, the observed spectrum of Gd^{152} seems to indicate that such terms are, indeed, present in this nucleus and we would expect the transition rates between the vibrational states to be affected significantly by this fact. Just as was the case for Sm^{152}, the present experimental evidence on Gd^{152} therefore calls for a more refined theoretical calculation of the e/γ branching ratio which is based on a more detailed description of the collective motion. Experimentally, it would seem important for future work to establish such branching ratios for a wider range of nuclei within the group of vibrational and strongly deformed nuclei.

The authors like to express their sincere gratitude to Professor Aage Bohr for enlightening discussions and to Professor Kai Siegbahn for his stimulating interest in this work. We are grateful to Dr. J. M. Hollander for several discussions and to Dr. A. Reiner for his critical reading of the manuscript. Our

thanks are also due Dr. G. Bäckström for the loan of the double-focusing spectrometer, to Mr. S. Gustafsson for many spectrometer runs, and to Dr. G. T. Wood for valuable assistance in the initial phase of the experiment.

References

1) Strominger, Hollander and Seaborg, Table of isotopes, Revs. Mod. Phys. **30** (1958) 585
2) Alburger, Ofer and Goldhaber, Phys. Rev. **112** (1958) 1998
3) O. Nathan and S. Hultberg, Nuclear Physics **10** (1959) 118
4) R. W. Lide and M. L. Wiedenbeck, Phys. Rev. **113** (1959) 840
5) I. Marklund, Nuclear Physics **9** (1958/59) 83
6) G. T. Wood and O. Nathan, Congrès International de Physique nucléaire (Paris 1958) p. 864
7) L. Grodzins and A. W. Sunyar, Phys. Rev. Letters **2** (1959) 307
8) Alder, Bohr, Huus, Mottelson and Winther, Revs. Mod. Phys. **28** (1956) 432
9) Sheline, Nielsen, Skilbreid and Sperduto, to be published
10) G. Bäckström, Ark. f. Fysik **10** (1956) 387
11) G. Bäckström, Nuclear Instruments **1** (1957) 253
12) O. B. Nielsen, to be published
13) S. Hultberg and R. Stockendal, Ark. f. Fysik **14** (1959) 565
14) S. Hultberg, Ark. f. Fysik **15** (1959) 307
15) L. Grodzins, Bull. Am. Phys. Soc. **1** (1956) 163
16) G. T. Wood, to be published
17) I. Perlman, private communication
18) A. Reiner, Structure Effects in the Interaction Between Nuclei and Atomic Electrons, Thesis, University of Amsterdam (1958)
19) E. L. Church and J. Weneser, Phys. Rev. **103** (1957) 1035
20) G. S. Goldhaber, Nuclear Structure, Proc. of the University of Pittsburg Conference June 1957, p. 454
21) L. A. Sliv and I. M. Band, Tables of Internal Conversion Coefficients, Part II (Izdat. Akad. Nauk SSSR., Moscow-Leningrad 1958)
22) Gregers Hansen, Nielsen and Sheline, Nuclear Physics **12** (1959) 389
23) I. Marklund and Z. Grabowski, B. van Nooyen and I. Marklund, Ark. f. Fysik **16** (1960)

1.B:7.C

Nuclear Physics **15** (1960) 216—230; © *North-Holland Publishing Co., Amsterdam*

Not to be reproduced by photoprint or microfilm without written permission from the publisher

NOTE ON ONE PION EXCHANGE POTENTIAL

G. BREIT and M. H. HULL Jr.

Yale University, New Haven, Connecticut †

Received 5 November 1959

Abstract: The phase-parameters of nucleon-nucleon scattering are worked out for the one-pion exchange potential in a way allowing localization of effects in space for each parameter. Success of phenomenologic phase-parameter fits making use of one-pion exchange values for the higher L and J is discussed in terms of the localization. It is shown that the one-pion exchange potential is probably the main interaction at distances greater than 2.9×10^{-13} cm. With somewhat less certainty it is concluded that it is the major interaction for $r > 1.6\times10^{-13}$, cm and evidence is presented for believing that some other interaction is the principal one for $r < 1.6\times10^{-13}$ cm.

1. Introduction

The possible importance of the potential derived from meson theory in the treatment of the nucleon-nucleon system for large internucleon distances r has been emphasized by Iwadare *et al.* [1]). It has been found by Moravcsik, Cziffra, Mac Gregor and Stapp [2]) that the analysis of Stapp, Ypsilantis and Metropolis [3]) of p—p scattering data at 310 MeV can be appreciably improved by including the contributions to the scattering amplitudes arising from the higher orbital angular momenta L. Such an analysis is referred to by Moravcsik *et al.* [2]) as the modified phase shift analysis. The viewpoint of these authors is related to that of Chew who employs a representation of the scattering amplitudes in terms of poles in a complex plane. The derivation of the formulas for the phase shifts and coupling parameters as conducted by Cziffra, Mac Gregor, Moravcsik and Stapp [2]) has been arranged, therefore, in terms of relativistic values which would apply in the first Born approximation for the amplitudes as a whole and are then analyzed in terms of partial wave substates. It may be that the interaction of nucleons will eventually be understood in terms of some such representation as used by Chew [2]). On the other hand, the simple potential description may be expected to apply at the larger r and, therefore, in a sense at the higher L. It appears desirable therefore to examine the localization in space of the effects of the one-pion exchange potential so as to be able to draw conclusions from the empirical applicability of one-pion exchange formulae regarding the absence of more complicated interactions in specified regions of space. For this reason the

† This research was supported by the U. S. Atomic Energy Commission under Contract AT (30-1)—1807 and by the Office of Ordnance Research, U. S. Army.

way in which the one-pion contributions arise from the elementary viewpoint of localized potentials will be described. In this way there will also be available the subdivision of effects according to their spin-spin and tensor force contributions.

NOTATION

E = non relativsistic energy of incident nucleon in the laboratory system,
E' = non relativistic energy of relative motion in the centre of mass system,
m_π = meson mass,
m = electron mass,
M = nucleon mass,
r = internucleon distance,
g = pion-nucleon coupling constant,
σ = Pauli spin vector for a particle,
τ = isobaric spin vector for a nucleon,
μ = reciprocal length defined in eq. (1.1); $2\pi/\mu$ = Compton wavelength of pion,
k = wave number of relative motion times 2π,
$F_L(kr)$ = regular solution of the radial equation for $r \times$ radial function normalized so that $F_L > 0$ at $r \to 0$ and asymptotic to sine function of unit amplitude at $r = \infty$,
ρ = kr,
F'_L = $\mathrm{d}F_L(\rho)/\mathrm{d}\rho$,
Q_L = Legendre function of the second kind and order L,
$L\hbar$, $J\hbar$ = orbital and total angular momenta of relative motion,
$\hat{a}$ = coefficient of $(-\rho)$ in exponent of e^{-x}.

2. Calculations

The one-pion exchange interaction following from the pseudoscalar theory with pseudoscalar coupling is

$$V^{(2)} = \tfrac{1}{3}g^2\left(\frac{\hbar\mu}{2Mc}\right)^2(\tau_1\cdot\tau_2)\left[(\sigma_1\cdot\sigma_2)+S_{12}\left(1+\frac{3}{x}+\frac{3}{x^2}\right)\right]\frac{\mathrm{e}^{-\mu r}}{r}, \qquad (1)$$

$$\mu = \frac{m_\pi c}{\hbar}, \quad x = \mu r, \qquad (1.1)$$

and g is the unrenormalized coupling constant used in the same convention as the letter f was used in a related connection [4]). The calculation of phase shifts to the first order in the perturbing potential can be performed employing a formula due to H. M. Taylor, *viz.*,

$$K_L = -\int (\delta V)F_L{}^2(\rho)\,\frac{\mathrm{d}\rho}{E'}, \qquad (1.2)$$

where $F_L(\rho)$ is the regular function of the central field to which the phase shift is referred, $\rho = kr$, $k/2\pi$ is the wave number and E' is the energy in the centre of mass system. This formula provides a unique meaning to the localization of the effect of the potential δV on the phase shift provided δV is small enough to make first order perturbation theory applicable. If the effects of δV have to be calculated in higher orders the same type of localization of the effects can be formally introduced by employing the well known relation between $\sin K_L$ and the integral involving in place of $F_L{}^2$ the product $F_L\mathcal{F}_L$, with $\mathcal{F}_L$ standing for the regular function in the presence of δV. In this case the localization of effects involves the knowledge of $\mathcal{F}_L$ and is more cumbersome than in the case of small δV. Other localizations can be devised. Thus for finite δV if one chooses a set of N functions $f_i(\mathbf{r})$ subject to $\sum_1^N f_i(\mathbf{r}) = \delta V(r)$ and instead of applying δV in one step applies changes in the potential $\sum_1^N \lambda_i f_i(r)$ with the λ_i finally attaining values 1. The sum of first order effects arising from a narrow range of $\mathbf{r}$ depends in a complicated way on the way in which the λ_i are made to approach their final values. In spite of the arbitrariness of the recipe for localization in terms of eq. (1.2) and its generalization for $\sin K_L$ involving $F_L\mathcal{F}_L$ it will be used throughout below. In terms of it a narrow range of $\mathbf{r}$ makes a contribution to the integral which determines the portion of K_L or more generally of $\sin K_L$ which arose from the range of values of $\mathbf{r}$. Eq. (1.2) holds for cases of no spin but it is clearly applicable also to the interaction energy in eq. (1) provided the values of $(\boldsymbol{\tau}_1 \cdot \boldsymbol{\tau}_2)$, $(\boldsymbol{\sigma}_1 \cdot \boldsymbol{\sigma}_2)$ and S_{12} are inserted for the states with sharp total angular momenta $J\hbar$ arising from orbital angular momenta $L\hbar$. That this is the case is seen directly from the connection between the phase shift and the change in energy of a system in a large quantizing volume [5]). Employment of (1.2) implies smallness of distortions of the wave function by the perturbing potential δV and this presupposes the smallness of the phase shift produced. A brief discussion of the degree to which these assumptions are satisfied in some of the applications will be given presently. The first order phase shifts corresponding to triplet states according to (1) and (1.1) are

$$\delta_J^L = -\frac{g^2\hbar^2\mu^2 k}{12M^2c^2E'}(\boldsymbol{\tau}_1 \cdot \boldsymbol{\tau}_2)\int_0^\infty \left[1+\left(1+\frac{3}{x}+\frac{3}{x^2}\right)S_{12,J}\right] e^{-x} F_L{}^2(kr)\,\frac{dx}{x}. \quad (1.3)$$

Here

$$S_{12,J} = \left(-\frac{2L+1}{2L+3}, 2, -\frac{2(L+1)}{2L-1}\right) \quad (1.4)$$

for

$$J = (L+1, L, L-1) \quad (1.5)$$

respectively. Approximating the regular Coulomb function $F_L(kr)$ by its field free ($\eta = 0$) value the radial integrals occurring in (1.2) can be evaluated in closed form. The replacement of $F_L(kr)$ by its field free approximation is very

well justified for laboratory energies above $\approx$ 18 MeV and the Coulomb corrections are not serious even at much lower energies. It is shown in Appendix A that

$$\int_0^\infty e^{-\mu r}[F_L^2(kr)/r]dr = \tfrac{1}{2}Q_L(1+\tfrac{1}{2}\hat{a}^2) \tag{2}$$

with

$$\hat{a} = \mu/k. \tag{2.1}$$

Here Q_L is the Legendre function of the second kind and of order L. It is also seen in Appendix A that

$$\int_0^\infty \left(1+\frac{3}{x}+\frac{3}{x^2}\right) e^{-x} F_L^2(kr)\,\frac{dr}{r} = \frac{1}{2}Q_L + \frac{3/(2\hat{a}^2)}{2L+1}\,(Q_{L-1}-Q_{L+1}) \tag{2.2}$$

with the same argument of the Q_L as in eq. (2) from here on. The phase shifts for triplets are therefore

$$\delta_J^{\,L} = -\frac{g^2\hbar^2\mu^2 k}{24M^2c^2E'}\,(\tau_1\cdot\tau_2)\left\{Q_L+S_{12,J}\left[Q_L+\frac{(3/\hat{a}^2)}{2L+1}\,(Q_{L-1}-Q_{L+1})\right]\right\}. \tag{2.3}$$

Substituting by means of (1.3) and making use of recurrence relations for the Q_L to eliminate $\hat{a}^2$ one finds

$$\delta_{L+1}^{L} = -\frac{g^2k/(4Mc^2)}{2L+3}\,(\tau_1\cdot\tau_2)(Q_{L+1}-Q_L), \tag{2.4}$$

$$\delta_L^{\,L} = -\frac{g^2k/(4Mc^2)}{2L+1}\,(\tau_1\cdot\tau_2)[LQ_{L+1}+(L+1)Q_{L-1}-(2L+1)Q_L], \tag{2.5}$$

$$\delta_{L-1}^{L} = -\frac{g^2k/(4Mc^2)}{2L-1}\,(\tau_1\cdot\tau_2)(Q_L-Q_{L-1}). \tag{2.6}$$

According to eq. (17.6) of [6]) the replacement

$$F_\Lambda \mathcal{Y}_\mu^{\Lambda J} \to F_\Lambda \mathcal{Y}_\mu^{\Lambda J} + \sum_L h'_{L\Lambda} H_L \mathcal{Y}_\mu^{LJ}$$

represents the effect of a perturbation energy which when expressed in a suitable normalization is denoted by h'. Here the $\mathcal{Y}_\mu^{LJ}$ are the angular spin functions [7]) and the replacement takes place in representing the effect of switching on h' on the outgoing wave modification of a plane wave. The $H_L = G_L + iF_L$ furnish here the outgoing waves. Accordingly the effect of $V^{(2)}$ is to produce coupling of states with different J and the same L in such a way that in the matrix T of ref. [8]) the off-diagonal elements are obtainable from the perturbing energy by the same formula as the diagonal elements, the only difference being that, instead of $F_L\mathcal{Y}_\mu^{LJ}$ used for both functions of the inner product giving the matrix element, two different such functions with different

L and the same J have to be used. Since for small phase shifts the diagonal elements of T are $2i\delta_J{}^L$ it is convenient to denote the off-diagonal elements by $2i(\delta^{L-1,\,L+1})_J$. The symmetry of the forms used for T makes the order of $L-1$, $L+1$ immaterial. The necessary integral is discussed in the Appendix and is

$$\int_0^\infty \left(1+\frac{3}{x}+\frac{3}{x^2}\right) e^{-x} F_{n-1}(kr) F_{n+1}(kr)\,\frac{dr}{r} = \frac{Q_{n+1}+Q_{n-1}-2Q_n}{2\hat{a}^2}. \tag{3}$$

On insertion of the value of the off-diagonal element of S_{12}:

$$(L-1|S_{12}|L+1) = \frac{2[L(L+1)]^{\frac{1}{2}}}{2L+1}, \tag{3.1}$$

there results, similarly to (2.3),

$$(\delta^{L-1,\,L+1})_{J=L} = -[L(L+1)]^{\frac{1}{2}}\frac{g^2k/(4Mc^2)}{2L+1}(\tau_1\cdot\tau_2)[Q_{L+1}+Q_{L-1}-2Q_L]. \tag{3.2}$$

Finally for singlet states, $(\tau_1\cdot\tau_2) = -3$. The integral of eq. (2) suffices for the evaluation of the singlet phase shift which is readily found to be

$$K_L = \frac{g^2k\hat{a}^2}{8Mc^2}(\tau_1\cdot\tau_2)Q_L. \tag{3.3}$$

Introducing a dimensionless coupling constant by means of

$$g_0{}^2 = \frac{g^2}{\hbar c}, \quad g^2 = 137.0\,e^2g_0{}^2, \tag{4}$$

one has, employing somewhat arbitrarily the mass of the charged pion $139.63\ \mathrm{MeV}/c^2 = 273.3\,m$, the following values of the combinations of constants occurring in the formulae

$$\begin{gathered}\tfrac{1}{3}g^2\left(\frac{\hbar\mu}{2Mc}\right)^2\mu = 3.61(g_0{}^2/14)\mathrm{MeV}, \quad \frac{g^2\hbar^2\mu^2k}{24M^2c^2E'} = \frac{0.559(g_0{}^2/14)}{\sqrt{E_{\mathrm{MeV}}}}, \\ \frac{g^2k}{4Mc^2} = 0.0807(g_0{}^2/14)\sqrt{E_{\mathrm{MeV}}}, \quad \frac{g^2k\hat{a}^2}{8Mc^2} = \frac{1.681(g_0{}^2/14)}{\sqrt{E_{\mathrm{MeV}}}}; \\ \hat{a} = \frac{6.45}{\sqrt{E_{\mathrm{MeV}}}}.\end{gathered} \tag{4.1}$$

The values of $g_0{}^2 = 14$ and of the mass of m_π just mentioned correspond to the value of the "renormalized coupling constant" $g_0{}^2(m_\pi/2M)^2 = 0.0775$. The numbers are expressed in terms of $g_0{}^2 = 14$ because this is believed to be the approximate value of the constant. The first of the parameters in (4.1) enters eq. (1) with $1/r$ replaced by μ/x; the second enters (2.3) and is $\frac{1}{2}$ of the coefficient

in front of $(\tau_1 \cdot \tau_2)$ and the integral in (1.3); the third is for use in (2.4), (2.5), (2.6), the fourth is for (3.3) and the last enters the arguments of the Q_L in several of the equations. The adjustments in the numbers entering (4.1) caused by the use of a different pion mass are obvious from the entrance of μ. Thus the first is proportional to $m_\pi{}^3$, the second and third to $m_\pi{}^2$. Employment of relativistic effects in the calculation of one pion phase shifts is not clearly justifiable because of the difficulty [9]) in making relativistic corrections to the parts of the interaction which arise from the smaller distances. From this viewpoint it is self-consistent to use the non relativistic formulae derived so far. On the other hand, if a phase-parameter is caused entirely by the region in which the one-pion potential is dominant its value is determined by the relativistic forms of formulae analogous to (2.4), (2.5), (2.6), (3.1), (3.3). Such formulae have been obtained first in a different notation by Cziffra, Mac Gregor, Moravcsik and Stapp [2]). Their treatment being arranged in terms of one-pion scattering amplitudes does not bring out the localization of effects. It is appropriate therefore to describe the way in which the relativistic modification can be obtained without losing the spatial localization of effects.

From eqs. (5) and (5.3) of ref. [4]) one obtains on neglecting effects quadratic in $g^2 e^{-x}/x$

$$\left\{\hat{E}^2 - 4M^2c - 4c^2p^2 - 2\frac{c^2\hbar^2}{\hat{E}}\left[\left[(\sigma_1 \cdot \sigma_2) + (\sigma_1 \cdot \mathbf{r})(\sigma_2 \cdot \mathbf{r})\frac{\mathrm{d}}{r\mathrm{d}r}\right]\frac{\mathrm{d}F}{r\mathrm{d}r}\right]\right\}\Psi = 0,$$
$$F = \frac{g^2}{r}(\tau_1 \cdot \tau_2)e^{-\mu r}. \tag{4.3}$$

Here $\hat{E}$ is the sum of relativistic energies of both nucleons in the centre of mass system while p is the absolute value of the relative momentum in the same frame. Evaluation of the last term in (4.2) gives

$$\left\{\hat{E}^2 - 4M^2c^4 - 4c^2p^2 - \frac{2g^2\mu^2}{3\hat{E}}c^2\hbar^2(\tau_1 \cdot \tau_2)\left[(\sigma_1 \cdot \sigma_2) + S_{12}\left(1 + \frac{3}{x} + \frac{3}{x^2}\right)\right]e^{-x}/r\right\}\Psi = 0. \tag{4.4}$$

Here there appears essentially $V^{(2)}$ of eq. (1) which will now be written for emphasis $V^{(2)}_{\mathrm{NR}}$. For sharp L and J, on introducting $\mathscr{F} = r\Psi$ one has therefore

$$\left\{\frac{\mathrm{d}^2}{\mathrm{d}r^2} - \frac{L(L+1)}{r^2} + \frac{\hat{E}^2 - 4M^2c^4}{4c^2\hbar^2} - \frac{2M^2c^2}{\hbar^2\hat{E}} - V^{(2)}_{\mathrm{NR}}\right\}\mathscr{F} = 0. \tag{4.5}$$

Comparing this form with the corresponding one in the absence of $V^{(2)}_{\mathrm{NR}}$, multiplying the first by $-F$ and the second by $\mathscr{F}$, adding and integrating, a formula for the sine of a $\delta_J{}^L$ or a K_L is obtained. Only the structure of the formula need be considered, *viz.*

$$k \sin \delta = -\frac{2M^2c^2}{\hbar^2\hat{E}}\int V^{(2)}_{\mathrm{NR}}\mathscr{F}F\mathrm{d}r. \tag{4.6}$$

This formula differs from the non relativistic one through the presence of an extra factor $2Mc^2/\hat{E}$ on the right hand side. This relativistic correction factor has to be used jointly with the relativistic value of k in the centre of mass system. Its inclusion corresponds to the change of the factor

$$\frac{g^2k}{4Mc^2} \to \frac{g^2k}{4E_{1\,\mathrm{cm}}} \tag{4.7}$$

where

$$E_{1\,\mathrm{cm}} = \tfrac{1}{2}\hat{E} \tag{4.7'}$$

is the relativistic kinetic energy of a single nucleon in the centre of mass system. The relativistic

$$k = \frac{[\frac{1}{2}M(E_{r,\,\mathrm{lab}} - Mc^2)]^{\frac{1}{2}}}{\hbar} \tag{4.8}$$

where $E_{r,\,\mathrm{lab}}$ is the relativistic kinetic energy, including the rest mass energy, of the incident proton in the laboratory system. Since

$$E_{r,\,\mathrm{lab}} - Mc^2 = Ve \tag{4.9}$$

where V is the effective accelerating potential for the nucleon eq. (4.8) means that k is the same as calculated non relativistically. This coincidence has already been used [10]) in another connection but is explicitly set down for the sake of definiteness.

3. Localization of Contributions

In fig. 1 there are shown graphs of μ/k times the integrands of the integral in eq. (1.3) for $L = 5$, $\hat{a} = 0.39$. With the value of m_π used the value of $\hat{a}$ corresponds to $E = 274$ MeV. The factor $S_{12,\,J}$ entering the second part of the integral is not included and the oscillatory contributions for the larger ρ are not shown because they are relatively not important. It is seen that the contributions to the integral drop off steeply at small x. The vertical lines in the figure give the values of $\rho = [L(L+1)]^{\frac{1}{2}}$ and $\rho = L$ respectively. The first of these gives the point of inflection of the F_L versus ρ plot, the second the value of ρ corresponding to the literally interpreted classical turning point of radial motion for angular momentum $L\hbar$, *i.e.* for $\rho = L\hbar$. The main contributions lie above these values of x and especially so for the classical turning point. Empirical applicability of phase-parameters for $L \geqq 5$ may be interpreted therefore as indicating that the one-pion potential is the main interaction for $x > 1.95$ or $x > 2.14$ which corresponds to $r > 2.7(5)\times 10^{-13}$ cm or $r > 3.0(2)\times 10^{-13}$ cm. Taking into account the relationship between this distance and L and employing the smaller number for the distance, it is seen that applicability of one-pion exchange phase shifts for $L \geqq 3$ at 275 MeV is an indication of the dominance of $V^{(2)}$ at

$r > 1.6(5) \times 10^{-13}$ cm or $x > 1.1(7)$. Some of the phase shift analyses performed at Yale indicate that one-pion exchange phase-parameters are reasonably applicable to p—p scattering data for 300 MeV $> E >$ 200 MeV and it appears therefore that empirically there is evidence for the dominance of $V^{(2)}$ at $x > 1.2$, although the exact value of x is still subject to question since the average E is 10 % lower than corresponds to $\hat{a} = 0.39$, and therefore a 5 % larger x. The results concerning the fits have been recently reported [11]). The value of r

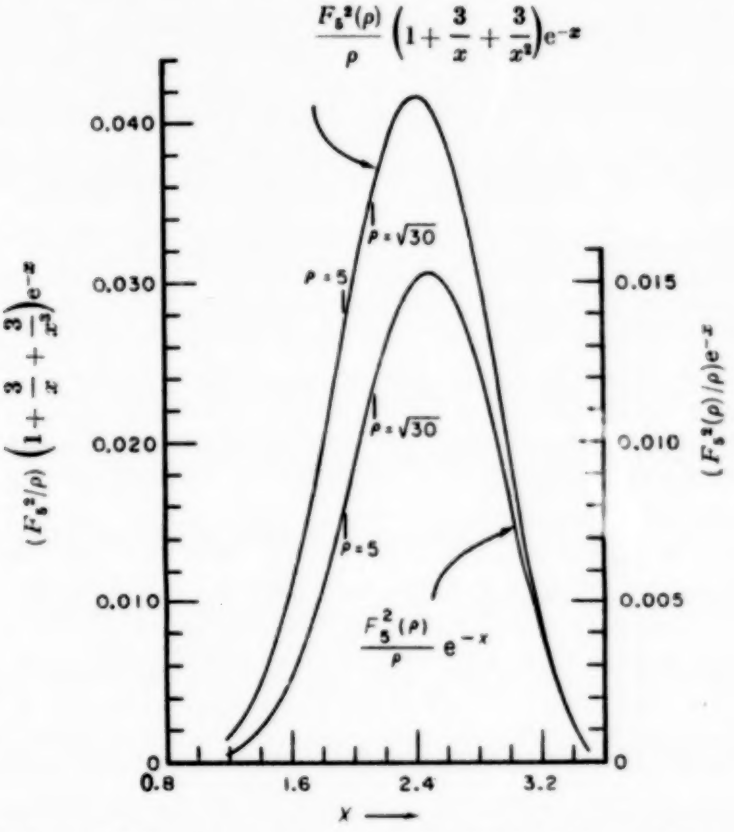

Fig. 1. Integrands for eq. (1.3) or eqs. (2) and (2.2), for 274 MeV, $L = 5$. The vertical lines mark the point of inflection for $F_5(\rho)$ (at $\rho = \sqrt{30}$) and the classical turning point (at $\rho = 5$).

beyond which $V^{(2)}$ dominates stated in the report there presented was based on the applicability of $L \geqq 5$ phase-parameters and was therefore more conservatively stated as 2.9×10^{-13} cm even though smaller values were already likely in view of the successful use of the "3—4 group" of phase-parameters, *i.e.*, the phase shifts for $^3F_3$, $^3F_4$, the $^3F_4$, $^3H_4$ coupling constant and the phase shift K_4 for $^1G_4$.

It is realized that first order calculations employing $V^{(2)}$ are inapplicable if the interaction at the smaller distances is large enough. It is possible to conceive of a potential at small r which causes approximate resonance and in such a case the estimates of phase-parameters caused by $V^{(2)}$ would be seriously in error. However such a situation is unlikely and for ordinary small changes in phase

shifts the following argument indicates that there exist circumstances for which the first order estimates of $V^{(2)}$ are applicable. Denoting the potential at distances smaller than a certain critical distance r_{cr} by V_1 and the potential for $r > r_{cr}$ by V_e, the effect of V_1 in the absence of V_e is to produce a phase shift K_L. The effect of K_L is to change F_L in $r > r_{cr}$ into $F_L \cos K_L + G_L \sin K_L$, the factor $\exp(iK_L)$ being dropped here since it does not affect first order phase shift estimates. In estimating K_L as a first order effect of V_1 it is convenient to express the integral in a form showing the essential quantities as follows

$$\int_0^{r_{cr}} \frac{V_1}{E'} F_L^2(kr)\mathrm{d}r = \tfrac{1}{2}C \frac{V_1(r_{cr})}{E'} F_L^2(kr_{cr})r_{cr}. \tag{5}$$

Here C is a dimensionless number which may be thought of as twice the ratio of the effective distance through which the integrand should be continued to the left of the right boundary with the value it has at the boundary to r_{cr}. In this notation

$$\mathscr{F}_L(kr) \approx F_L(kr) - Ck[V_1(r_{cr})/E]r_{cr} F_L^2(kr_{cr})G_L(kr) \tag{5.1}$$

and

$$\mathscr{F}_L(kr_{cr})/F_L(kr_{cr}) \approx 1 - C(kr_{cr})^2[V_1(r_{cr})/E](F_L G_L/kr)_{r=r_{cr}}. \tag{5.2}$$

The number C may be expected to be of order 1 or less provided V_1 does not increase so fast at small r that the main contributions come from that region. Assuming that this is not the case and remembering that $F_L(\rho)G_L(\rho)/\rho$ does not depend critically on barrier penetration effects and is a moderate number the main requirement for the validity of the first order approximation in the calculation of $V^{(2)}$ is that $V_1(r_{cr})/E$ be reasonably small. In the $(L+\frac{1}{2})^2$ modification of the JWKB approximation eq. (5.2) becomes

$$[\mathscr{F}_L(kr_{cr})/F_L(kr_{cr})] - 1 = -\frac{6.0\times 10^{23}\ \mathrm{cm}^{-2} r_{cr}^2 (V_1)_{\mathrm{Mev}} C}{[(L+\frac{1}{2})^2 + 0.035 - (1.097\times 10^{12}\,\mathrm{cm}^{-1} r_{cr})^2 E_{\mathrm{Mev}}]^{\frac{1}{2}}}. \tag{5.3}$$

For $E = 274$ MeV, $V_1(r_{cr}) = 1.4$ MeV, $r_{cr} = 1.65\times 10^{-13}$ cm ($x \approx 1.2$), the right hand side of the above formula is $\approx C/78$ for $L = 3$ and $C/200$ for $L = 5$. For a 10 percent accuracy of the first order one-pion exchange determination $\mathscr{F}/F$ has to be within ≈ 5 percent of unity. Therefore for $L = 5$ one may increase V_1 by a factor 10 up to 14 MeV but for $L = 3$ by a smaller factor up to 5.5 MeV. These numbers make no allowance for C which depends on the shape of V_1 and depends besides on the shape of the $F_L^2(\rho)$ plot against ρ. A steep fall-off of $F_L^2(\rho)$ as ρ decreases to the left of the turning point $\rho = \rho_L$ gives a small value of C.

For small L the fall-off of $F_L^2(\rho)$ with ρ to the left of ρ_L is less pronounced than for the larger L. In fig. 2 there are shown graphs of $F_L^2(\rho)/\rho$ against ρ for $L = 1$ and 5 plotted with such scales for ρ as to make the classical turning

points appear at the same position on the paper. The vertical scales have been adjusted to make the maxima of the graphs have approximately the same height. The factor $1/\rho$ has been included in order to make the left part of the graphs appear on a larger scale. To the left of the literally taken classical turning point, with $\rho = [L(L+1)]^{\frac{1}{2}}$, the sensitivity measure $F_L^2(\rho)$ is seen to be much the larger for $L = 1$ at $\rho(L = 5) = 3$. Accordingly the parts of V_1 which lie appreci-

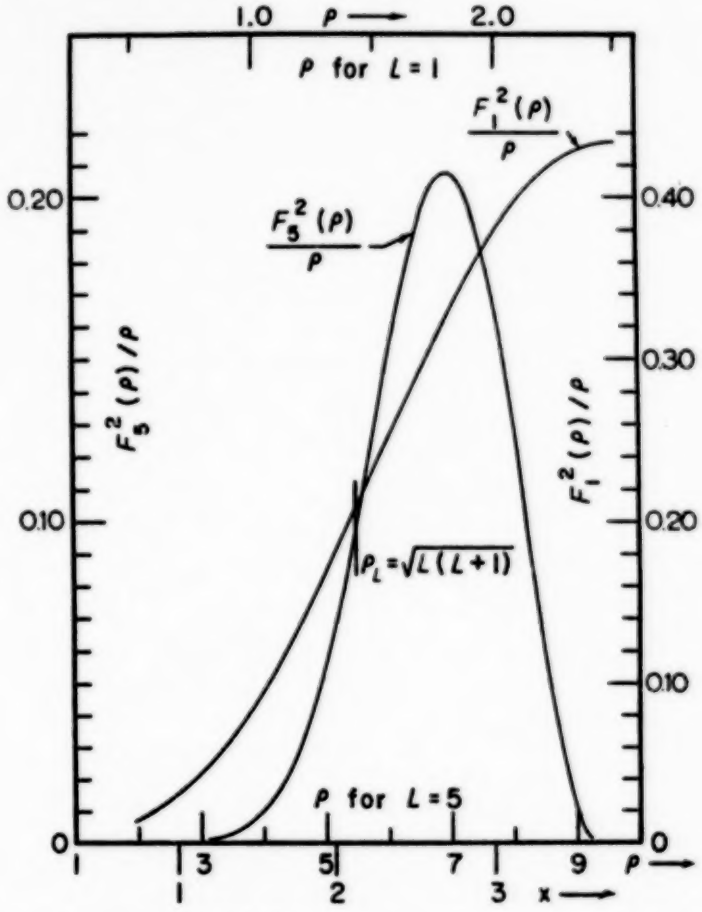

Fig. 2. The square of r times the radial wave function divided by ρ for $L = 1,5$. The point of inflection is marked ($\rho = \rho_L$), and the abscissa scales are adjusted to have it fall at the same distance to the right for $L = 1$ and $L = 5$. The ordinate scales are adjusted so that the maxima of the two curves are at about the same level. The scale of x refers to the graph for $L = 5$ and corresponds to 274 MeV.

ably to the left of the classical turning point may be expected to have a much larger effect for $L = 1$ than for $L = 5$. It is to be expected therefore that at low energies and small L adjusted to correspond to high energies and large L on the basis of the same x for the classical turning point, the one-pion approximation will be relatively poorer than at high energies. For example the value of r corresponding to the classical turning point at $E = 300$ MeV and $L = 5$ is reproduced for $L = 1$ at $E = (2/30)300 = 20$ MeV but one would not expect the one-pion approximation to be as good for $L = 1$ at 20 MeV as for $L = 5$

at 300 MeV. Another view of the same matter is obtained by seeing to what distance to the left of the turning point one must go in order to decrease F^2 to some assigned fraction of the value it has at the turning point. For $L = 1$ a decrease to 50 % takes place in roughly twice the distance required for $L = 5$. It is understandable therefore † that the one-pion exchange potential does not work very well for P states in p−p scattering as reported by Mac Gregor, Moravcsik and Noyes [2]). They are concerned with data from 1.397 to 39.4 MeV. At the lowest energies the considerations of experimental accuracy and of applying all corrections for spurious effects are important. At energies such as 18.2 MeV where the p-waves become more pronounced the considerations illustrated by fig. 2 apply. Assuming the correctness of the phenomenologic inapplicability of the one-pion exchange potential one has to conclude that to the left of the turning point of $L = 1$ at ≈ 20 MeV which corresponds to $\approx 2.9\times 10^{-13}$ cm there is a region of interactions much stronger than the one pion interaction. According to fig. 2 this region could well be to the left of distances corresponding to $\rho = 3$ on the lower scale in the figure, the sensitivity for $L = 5$ being small at such distances while the sensitivity for $L = 1$ is still appreciable. Comparing this ρ with $\rho = 5.47$ for the turning point the value of r below which the additional interaction sets in is $(3/5.47)2.88\times 10^{-13}$ cm $= 1.5(8)\times 10^{-13}$ cm. This distance is just below the region $r > 1.6(5)\times 10^{-13}$ cm in which it was tentatively concluded on the basis of $L \geqq 3$ trials that the one-pion interaction applied. The close joining of the two regions is doubtless accidental but it appears nevertheless likely that $r = 1.6\times 10^{-13}$ cm is the approximate lower limit of the region of applicability of the one-pion exchange potential.

The considerations made above are crude in several respects already described. In addition it may be mentioned that deviations from the one-pion exchange potential are not likely to have the same fractional value as compared with the one-pion potential for different combinations of quantum numbers S, J, T. Therefore the applicability of the one-pion potential on a relative basis is likely to differ for different sets of the quantum numbers.

The qualitative aspects of indications in the phase shift analysis of the validity of the one-pion exchange potential at the larger distances and of its failure at the smaller ones have been known [11]) for some time. Additional stimulus for setting the arguments down in a definite form has resulted from the receipt of a preprint of a paper by Sugawara and Okubo who in making calculations on the pseudoscalar theory with pseudoscalar coupling find in a non-renormalized form of the theory that the large fourth order potential is expected to be largely cancelled at the larger distances as a result of a redefini-

† This point, and the possibility of analyzing the problem by the sensitivity curves has been mentioned at the London conference [11]) in the report on "Two Nucleon-Phenomenologic Phase Shift Analysis" made by G. Breit, and again in connection with a discussion of the Berkeley analysis of low energy p−p data.

tion of the wave function by means of a unitary transformation. They obtain similar results in a modification of the ps—pv theory adjusted to be in agreement with low energy pion-nucleon s-wave scattering. The writers are very grateful to Professor Sugawara for the communication of the results of these calculations.

It should be emphasized that the considerations of the present paper presuppose that the radial wave functions are not strongly distorted by the interactions taking place at distances well inside the classical turning point. It has not been proved that this is the case for the values of L used and therefore the conclusions are not completely established. A partial justification may be found in the fact that the one-pion exchange phase shifts are small indicating the smallness of wave function distortion. This justification is only partial because higher order potentials such as the two-pion exchange may conceivably cause larger distortions than the one-pion exchange potential.

The agreement with a meson theory calculation regarding the apparent sufficiency of the one-pion potential for $r > 1.6\times 10^{-13}$ cm has also to be considered with some reservations because of the variety of answers available in meson theories. The partial cancellation of the outlying part of the fourth order potential took place in a calculation which omitted charge and mass renormalization and stopped at the g^4 terms of the final potential. In spite of these and other reservations the empirical evidence appeared to be definite enough to be justifiably mentioned in the present work.

Appendix

EVALUATION OF THE INTEGRALS

On p. 389 of G. N. Watson's book [12]) there is available a formula for the definite integral over a variable t of the product of an exponential and two Bessel functions of the same order and of arguments bt, ct. A special case of this formula for $b = c$ and the order of the Bessel function $\nu = L+\frac{1}{2}$ gives eq. (2) of the text. The same integral can be obtained in a variety of ways. One of them is related to familiar physical problems and consists in employing the expansion of $\sin kR/R$, $R = (a^2+r^2-2ar\mu)^{\frac{1}{2}}$ in $J_{n+\frac{1}{2}}(ka)J_{n+\frac{1}{2}}(kr)P_n(\mu)$ as on p. 366 of ref. [12]) which for $r = a$ on multiplication by $P_n(\mu)$ and integration furnishes the formula.

To obtain eq. (2.2) of the text one may conveniently employ the identity

$$\int_0^\infty [F_{n-1}^2(\rho) - F_{n+1}^2(\rho)]\frac{e^{-4\rho}}{\rho}\,d\rho = (2n+1)\int_0^\infty \frac{F_n}{\rho}\left(2F'_n - \frac{F_n}{\rho}\right)\frac{e^{-4\rho}}{\rho}\,d\rho$$
$$= (2n+1)\hat{a}^2\int_0^\infty \left(\frac{1}{x}+\frac{1}{x^2}\right)e^{-x}F_n^2(\rho)\frac{d\rho}{\rho}. \qquad \text{(A1)}$$

Here use is made of the recurrence relations

$$F_{n+1}+F_{n-1}=(2n+1)F_n/\rho,\quad F_{n-1}-F_{n+1}=2F'_n-F_n/\rho$$

and an obvious transformation of the integrand followed by a partial integration gives the third form of the integral in eq. (A1). The argument of F_n is throughout $\rho = kr$. Combining (A1) with eq. (2) one obtains eq. (2.2) of text by addition. To obtain the off-diagonal matrix element it is convenient to employ the recurrence relations satisfied by the F_n to obtain

$$\rho\frac{\mathrm{d}}{\mathrm{d}\rho}\left(\frac{F_n^2}{\rho}\right)=\frac{\mathrm{d}}{\rho\mathrm{d}\rho}(\rho F_{n-1}F_{n+1}). \tag{A2}$$

This formula follows for instance if one expresses $\mathrm{d}(F_{n-1}F_{n+1})/\mathrm{d}\rho$ in terms of F_n, F_{n-1}, F_{n+1} giving $-(F_{n-1}F_{n+1}/\rho)+F_n(F_{n-1}-F_{n+1})$ and then on replacing $F_{n-1}-F_{n+1}$ by $2F'_n-F_n/\rho$ one obtains

$$\frac{\mathrm{d}}{\mathrm{d}\rho}(F_{n-1}F_{n+1})=\frac{-F_{n-1}F_{n+1}}{\rho}+\rho\frac{\mathrm{d}}{\mathrm{d}\rho}\left(\frac{F_n^2}{\rho}\right) \tag{A2'}$$

which is equivalent to (A2). Since the off-diagonal element can be produced only by the part containing S_{12} the identity

$$\int_0^\infty \mathrm{e}^{-\alpha x}\left(1+\frac{3}{x}+\frac{3}{x^2}\right)F_{n-1}F_{n+1}\frac{\mathrm{d}x}{x}=\int_0^\infty \mathrm{e}^{-\alpha x}\left(1+\frac{1}{x}+\frac{1}{x^2}\right)F_n^2\frac{\mathrm{d}x}{x} \tag{A3}$$

together with eqs. (A1), (2) furnish the answer. The validity of eq. (A3) may be seen as follows. Employing the identity

$$\hat{a}^2\frac{\mathrm{e}^{-\hat{a}\rho}}{\rho}\left(1+\frac{3}{x}+\frac{3}{x^2}\right)=\rho\frac{\mathrm{d}}{\mathrm{d}\rho}\left(\frac{\mathrm{d}}{\rho\mathrm{d}\rho}\frac{\mathrm{e}^{-\hat{a}\rho}}{\rho}\right) \tag{A4}$$

one sees that

$$\begin{aligned}\int_0^\infty \frac{\mathrm{e}^{-\hat{a}\rho}}{\rho}\left(1+\frac{3}{x}+\frac{3}{x^2}\right)F_{n-1}F_{n+1}\mathrm{d}\rho&=\frac{1}{\hat{a}^2}\int_0^\infty F_{n-1}F_{n+1}\left[\frac{\rho\mathrm{d}}{\mathrm{d}\rho}\left(\frac{\mathrm{d}}{\rho\mathrm{d}\rho}\frac{\mathrm{e}^{-\hat{a}\rho}}{\rho}\right)\right]\mathrm{d}\rho\\&=-\frac{1}{\hat{a}^2}\int_0^\infty F_n^2\left[\frac{\mathrm{d}}{\rho\mathrm{d}\rho}\left(\frac{\rho\mathrm{d}}{\mathrm{d}\rho}\frac{\mathrm{e}^{-\hat{a}\rho}}{\rho}\right)\right]\mathrm{d}\rho.\end{aligned} \tag{A5}$$

Carrying out the differentiations in the last form there results eq. (A3). In obtaining the third from the second form in (A5) two integrations by parts give a form in which the product $F_{n-1}F_{n+1}$ can be replaced by combinations in terms of F_n^2 making use of (A2). Two further integrations by parts remove differentiation from F_n^2 and give the final form in (A5). The parts outside the integral which have been dropped in the integrations by parts vanish at both limits for $n > 0$ and since in the application $n = L$ dropping these parts is justifiable.

While the evaluations of the integrals as conducted here makes use of special simplifying circumstances a more systematic procedure can be used employing the known expressions as on p. 389 of ref. [13]) for

$$\int_0^\infty e^{-at} J_\nu(bt) J_\nu(ct) t^{\mu-1} dt$$

in terms of a definite integral involving the hypergeometric function, integrating term by term and then applying standard relations between hypergeometric functions.

When the one-pion phase parameters are needed for a large number of angular momenta and energies, the required values of $Q_L(1+\frac{1}{2}\hat{a}^2)$ may be conveniently obtained with the aid of recurrence relations. If only a few values are needed, or if qualitative considerations such as estimates of convergence for large L are needed approximate formulae which are given below are useful. They are readily obtainable [13]) from the Laplacian integral for $Q_n(z)$:

$$Q_n(z) = \int_0^\infty \{z+(z^2-1)^{\frac{1}{2}} \cosh\theta\}^{-(n+1)} d\theta. \tag{A6}$$

For $z > 1$ real, the principal contribution to the integral comes from small values of θ especially for n large. Expansion of $\cosh\theta$ about $\theta = 0$ and retention of only the first term allows the integral to be carried out in closed form. There results

$$Q_n(\cosh\beta) \approx \frac{\pi \exp[-(n+1)\beta]}{[1-\exp(-2\beta)]^{\frac{1}{2}}} \frac{n(2n-1)!}{2^{2n-1}(n!)^2}, \tag{A7}$$

where

$$\cosh\beta = 1+\tfrac{1}{2}\hat{a}^2.$$

The phase parameters themselves may be approximated by

$$\delta_{L+1}^{L} = \frac{\pi L(2L-1)![g^2k/(4Mc^2)]}{2^{2L-1}(L!)^2(2L+3)} (\boldsymbol{\tau}_1\cdot\boldsymbol{\tau}_2) \frac{e^{-(L+1)\beta}}{(1-e^{-2\beta})^{\frac{1}{2}}} \left[1-\frac{2L+1}{2(L+1)} e^{-\beta}\right],$$

$$\delta_{L}^{L} = -\frac{\pi(L^2-1)(2L-3)![g^2k/(4Mc^2)]}{2^{2L-3}(2L+1)[(L-1)!]^2} (\boldsymbol{\tau}_1\cdot\boldsymbol{\tau}_2) \frac{e^{-L\beta}}{(1-e^{-2\beta})^{\frac{1}{2}}} \left[1+\frac{4L^2-1}{4(L+1)^2} e^{-2\beta} - \frac{4L^2-1}{2L(L+1)} e^{-\beta}\right],$$

$$\delta_{L-1}^{L} = \frac{\pi(L-1)(2L-3)![g^2k/(4Mc^2)]}{2^{2L-3}[(L-1)!]^2(2L-1)} (\boldsymbol{\tau}_1\cdot\boldsymbol{\tau}_2) \frac{e^{-L\beta}}{(1-e^{-2\beta})^{\frac{1}{2}}} \left[1-\frac{2L-1}{2L} e^{-\beta}\right]. \tag{A8}$$

The coupling parameter may be conveniently calculated from

$$(\delta^{L-1,\,L+1})_{J=L} = [L(L+1)]^{\frac{1}{2}}(\delta_L^{L+1}-\delta_L^{L-1}). \tag{A9}$$

For $L = 5$ at 300 MeV and at 40 MeV, the expressions in eqs. (A8) have a 10 % accuracy. The exponential dependence on β is related to the value of $e^{-\pi}$ at the first maximum of F_L^2.

References

1) Iwadare, Otsuki, Tamagaki and Watari, Prog. Theor. Phys. **16** (1956) 455; Suppl. to Prog. Theor. Phys. No. **3** (1956) Part II;
S. Otsuki, Prog. Theor. Phys. **20** (1958) 171;
R. Tamagaki, Prog. Theor. Phys. **20** (1958) 505
2) G. F. Chew, Phys. Rev. **112** (1958) 1380; Proc. Ann. Int. Conf. on High Energy Physics at CERN (CERN, Geneva, 1958) p. 96;
Moravcsik, Cziffra, Mac Gregor and Stapp, Bull. Am. Phys. Soc. **4** (1959) 49;
M. J. Moravcsik, UCRL-5317-T, Aug (1958) (unpublished);
M. H. Mac Gregor, UCRL 5348, Phys. Rev. **113** (1959) 559;
Mac Gregor, Moravcsik and Noyes, UCRL-5582-T (unpublished);
P. Cziffra and M. J. Moravcsik, UCRL-8707 (unpublished);
Cziffra, Mac Gregor, Moravcsik and Stapp, UCRL-8510, Phys. Rev. **114** (1959) 880
3) Stapp, Ypsilantis and Metropolis, Phys. Rev. **105** (1957) 302
4) G. Breit, Phys. Rev. **111** (1958) 652
5) G. Breit, Revs. Mod. Phys. **23** (1951) 238
6) G. Breit, Phys. Rev. **99** (1955) 1581
7) G. Breit and M. H. Hull, Jr., Phys. Rev. **97** (1955) 1047
8) Breit, Ehrman and Hull, Phys. Rev. **97** (1955) 1051
9) G. Breit, Phys. Rev. **106** (1957) 314
10) G. Breit, Phys. Rev. **99** (1955) 1581;
L. Durand, Phys. Rev. **108** (1957) 1597
11) International Conference on Nuclear Forces and the Few-Nucleon Problem, held 8—11 July, 1959 at University College, London
12) G. N. Watson, A Treatise on the Theory of Bessel Functions (Cambridge University Press, 1922)
13) E. T. Whittaker and G. N. Watson, Modern Analysis (Cambridge University Press, 1927)

3.C

Nuclear Physics **15** (1960) 231—238; © *North-Holland Publishing Co., Amsterdam*

Not to be reproduced by photoprint or microfilm without written permission from the publisher

CIRCULAR POLARIZATION OF EXTERNAL BREMSSTRAHLUNG FROM β-RAYS IN MAGNETIZED TARGETS

A. BISI, A. FASANA and L. ZAPPA

Istituto di Fisica del Politecnico, Milano

Received 16 November 1959

Abstract: The degree of circular polarization of the external bremsstrahlung, produced by β-rays from ^{90}Y in magnetized targets of silver and annealed Armco iron was investigated. It was found that the polarization is greater when the momentum of the radiating electron is backward with respect to the target magnetization.

The ratio of the polarizations corresponding to backward and forward momenta is nearly independent of the quantum energy and equal to 1.33 ± 0.09 ($B = 4400$ gauss) and 1.53 ± 0.09 ($B = 7000$ gauss) respectively for Ag and Fe targets. A small effect was also detected by measuring the polarization of the external bremsstrahlung produced in a weakly magnetized iron target, relative to that produced in a highly magnetized target, when the magnetization was perpendicular to the electron momentum. The ratio of the polarizations, not greater than 1.17 and also independent of the quantum energy, appears to be a complicated function of the magnetization. No such effect was detected when silver targets were used under the latter conditions.

1. Introduction

In the course of an investigation on the degree of circular polarization of the external bremsstrahlung (EB) excited by β-rays from ^{90}Y in various absorbers, some of us [1]) observed a magnetic perturbation in the polarization when a magnetized iron target was used as β absorber. More specifically, by magnetizing the target perpendicularly to the polarimeter axis ($B = 16000$ gauss), a decrease of polarization, nearly constant with respect to the quantum energy and equal to about 10 %, was noticed.

Further research was carried out to collect more experimental data and understand the origin of the perturbation. Some interesting results were obtained, which are reported in the present paper; in particular the following points stand out: a) dependence on the magnetic induction of the perturbation observed with targets magnetized perpendicularly to the polarimeter axis; b) dependence on the direction of magnetization of the polarization observed with targets magnetized parallel to the polarimeter axis. In both cases targets of annealed Armco iron or silver were used.

As concerns the understanding of the observed effect, no progress was made by us until now.

2. Experimental Apparatus

The circular polarization of the EB quanta was analyzed through Compton scattering with polarized electrons available in magnetized iron; the experimental apparatus, sketched in fig. 1, and the experimental procedure used to measure quantum polarization were the same as described in a previous work [2]).

The following paragraphs are limited to the description and discussion of the experimental features of the sample and magnetized target arrangement.

The source of β-rays was a disc of silver 0.05 mm thick, of 1 cm diameter, containing uniformly dispersed 40 mc of ^{90}Sr-carbonate, backed by 0.8 mm of

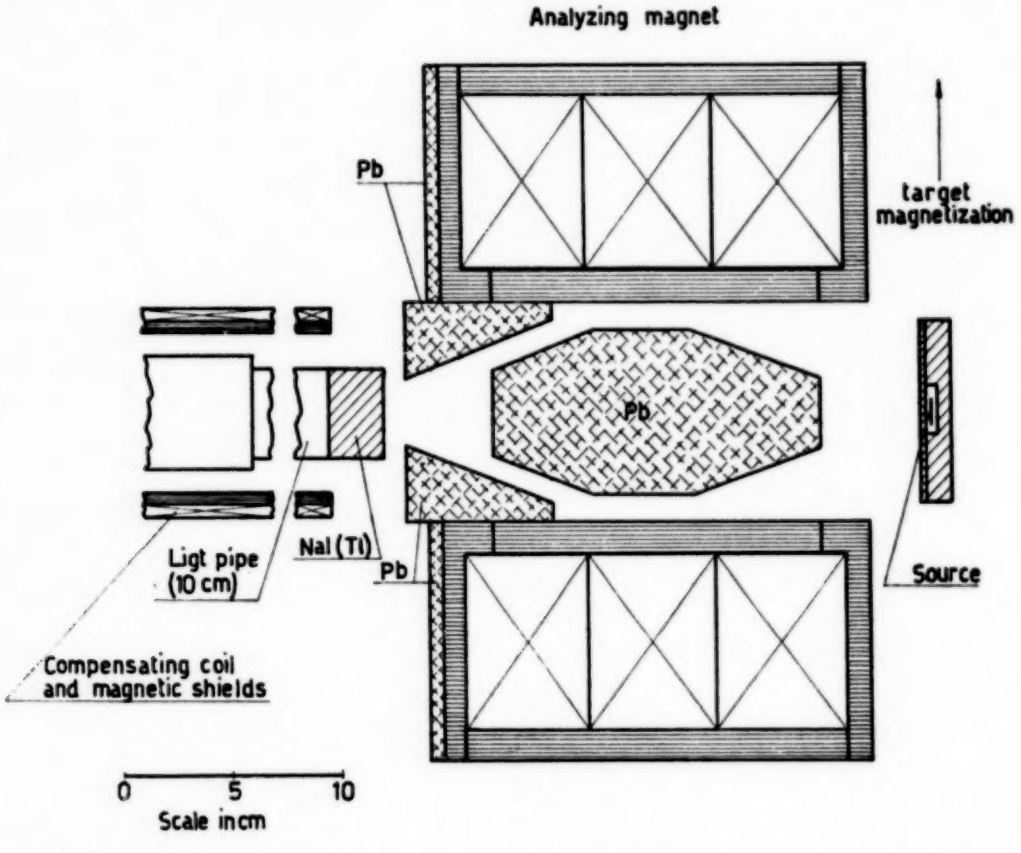

Fig. 1. Gamma polarimeter with target magnetized in "perpendicular" set-up.

silver and covered by a 0.1 mm layer of silver; the ^{90}Sr is in equilibrium with its daughter ^{90}Y ($E_{max} = 2.26$ MeV).

Targets of silver and annealed Armco iron, of about 900 mg/cm^2 thickness and placed just over the active sample, were used to produce EB. When other thicknesses were used, a mention of it will be made in the text. In order to magnetize the target, perpendicularly or parallely to the polarimeter axis, two different magnets were employed, for convenience of construction.

The principal features of the two different arrangements of housing the sample are as follows:

a) *Perpendicular magnetic field.* The sample and the target are placed between the cores of a Weiss type magnet and the circuit is closed (no air gap) by an iron slab. The arrangement offers the advantage of very low stray fields and also of very low fields in the container housing the sample. The measurements of the polarization of the EB produced in iron were made with and without the iron slab; when the Ag target substituted the Fe target the iron slab was obviously removed (air gap), other conditions being unchanged;

b) *Parallel magnetic field.* A horseshoe magnet was used, with a keeper separated from one of the poles, by an air gap in which the sample was located. In order to minimize the absorption and the scattering of the γ-rays the keeper is hollow just above the active area of the sample, and a cylindrical iron plug, as thin as possible (≈ 0.5 cm), is inserted in the hole and used as target when analyzing EB in iron. The target was magnetized along the polarimeter axis and the direction of magnetization could be reversed by reversing the current in the magnetizing coils.

As regards the direction of the β-ray momentum with respect to the direction of the target magnetization, the following comment can be made. An uncollimated beam was used so that the angle between the initial β-momentum and the target magnetization varied over all permissible values. However, because hard bremsstrahlung quanta are emitted prevailingly forward, the γ-rays impinging on the polarimeter, arises from radiating electrons with their momentum about perpendicular, parallel or antiparallel to the target magnetization respectively in the set-up a) and b).

3. Measuring Techniques

The measurements consisted of several 6-minute counting runs, one for each opposite polarimeter field direction, made alternatively with highly and weakly magnetized targets in "perpendicular" set-up and with backward and forward magnetized targets in "parallel" one. In all cases the percentage difference of counting rates for opposite directions of the polarimeter magnetization represents the degree of circular polarization of the γ-rays.

No correction factor of any instrumental effect [2]), not even the polarimeter efficiency, was taken into account, because we were interested in the relative variation of polarization and because the spectral distributions of the γ-rays scattered off by the polarimeter had an identical shape for the two magnetization states of the target.

Obviously this is right if no source of systematic errors is present in the experimental apparatus.

In practice it is difficult to ensure that this situation holds; the care taken in the course of our investigation to minimize these sources of errors can be summarized as follows:

a) *Influence of the polarimeter magnetic stray field on the photomultiplier.* The NaI(Tl) crystal ($1\frac{1}{2}''$ diam $\times$ $1''$ thick) was coupled through a 10 cm lucite light pipe to an EMI 9514 photomultiplier, surrounded by three magnetic shields and a compensating coil. Other conditions remaining unchanged, the scintillator was radiated with EB quanta from ^{90}Y emerging from an unmagnetized scatterer identical to that contained in the polarimeter. As a result the direction of the polarimeter magnetic field showed no sensible influences on the single counting rates. A typical result of the percentage differences of the counting rates, obtained by reversing the polarimeter magnetization, is $(4\pm8)\times10^{-4}$.

b) *Magnetic coupling of polarimeter and target magnet.* In view of the fact that the magnetomotance of the polarimeter prevailed and that the iron scatterer was magnetized to saturation, no trouble could arise from the target magnet. This situation was checked and the result was quite satisfactory. On the contrary, the magnetization of the target, especially in "parallel field" condition, is sensitive to the reversing of the polarimeter magnetization; the effect, though not too serious, amounts to about ±10 % at 4400 gauss.

c) *Variable transmission of the whole apparatus.* As seen in b) the target magnetization is slightly altered by reversing the polarimeter field. In order to establish whether the transmission of the whole apparatus is a function of the magnetization state of the target, several counting runs were repeated alternatively with unmagnetized and magnetized target, without magnetizing the polarimeter and leaving "in situ" the β source. Typical results of the transmission ratio in this condition are: $T_{\mathrm{unm}}/T_{\mathrm{m}} = 1.0007\pm0.0013$, so that it can be concluded that the transmission is independent of the magnetization state of the target.

4. Results

For the two experimental set-ups mentioned in section 2 the dependence of the magnetic perturbation of the EB circular polarization on the target magnetization and quantum energy was investigated with different sets of measurements, whose results are described as follows:

4.1. PERPENDICULAR FIELD

a) *Iron target.* Six sets of polarization measurements were made by magnetizing the iron target alternatively to saturation and to a magnetization state corresponding to $B = 15\,200$, 6100, 2100, 1300, 280, < 100 gauss. After each set the iron target was demagnetized.

By assuming the polarization of the EB in saturated iron target to be equal to 1, we obtain the EB polarization in the whole analyzed spectral region (from 0.50 MeV to 1.53 MeV) for the six magnetization states, hereafter called relative polarization, as listed in table 1 and reported in fig. 2. The states of magnetization indicated by sets 2, 3, 4, 5 were obtained by magnetizing to

saturation and following the descending part of the hysteresis loop, whereas the first state is obtained by demagnetizing the target. For that reason it is doubtful if the first point in the graphs ($B < 100$ gauss) can be connected with the others by the same curve.

TABLE 1

Measurement set	Target	Target induction (gauss)	polarization	Remarks
1 (perpendicular field)	Fe	100	0.89 ± 0.05	Relative to saturation
2 (perpendicular field)	Fe	280	1.11 ± 0.09	Relative to saturation
3 (perpendicular field)	Fe	1 300	1.16 ± 0.08	Relative to saturation
4 (perpendicular field)	Fe	2 100	1.12 ± 0.04	Relative to saturation
5 (perpendicular field	Fe	6 100	1.00 ± 0.02	Relative to saturation
6 (perpendicular field)	Fe	15 200	1.00 ± 0.02	Relative to saturation
7 (perpendicular field)	Ag	100	1.01 ± 0.08	Relative to $B = 9000$ gauss
8 (parallel field)	Fe	7 000	1.53 ± 0.09	Backward relative to forward
9 (parallel field)	Ag	4 400	1.33 ± 0.09	Backward relative to forward

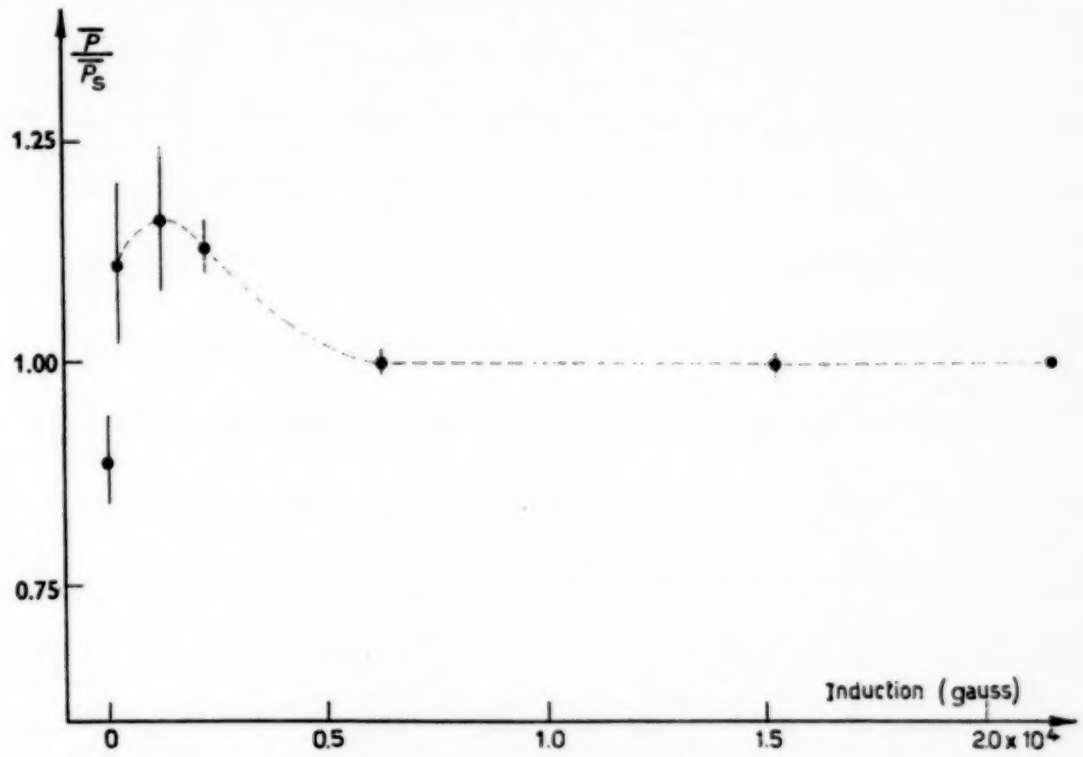

Fig. 2. Relative polarization as a function of the magnetic induction of Fe target (perpendicular set-up).

As regards the energy dependence of the observed effect, we report in fig. 3 the relative polarizations for set 4 as function of the energy. This curve is a typical one: the same trend is obtained with the other values of the target magnetization.

In order to ascertain that the observed effect did not depend on the target thickness, the set 4 of measurements was repeated by using a target of 1 cm thickness. The obtained value of the relative polarizations in the whole spectral region was the same as for the thin target; moreover the relative polarization appear to be still independent of energy.

Finally, as a further check, set 4 of measurements was repeated by inserting a layer of Ag sufficiently thick to stop all β particles, between the source and the iron target. In this way the EB was produced in Ag, where the value of the magnetic induction with saturated iron target, was not larger than 100 gauss. The obtained relative polarization was 0.98 ± 0.05.

b) *Silver target.* One set of measurement was made by magnetizing the target alternatively to $B = 9000$ gauss and to $B \approx 100$ gauss (residual induction). Taking the EB polarization at $B = 9000$ gauss as equal to 1, the relative polarization, constant in the whole spectral region, was 1.01 ± 0.08.

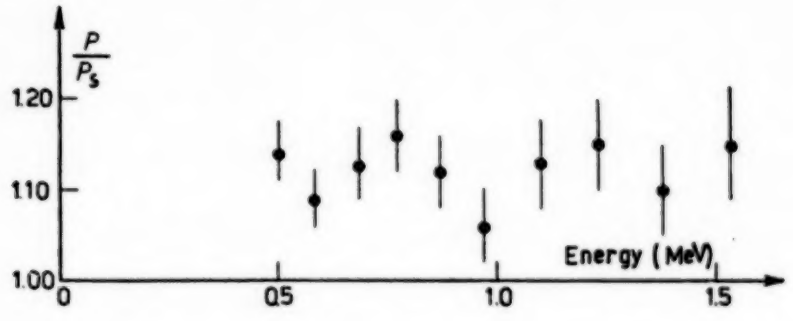

Fig. 3. Relative polarization as a function of the quantum energy for Fe target ($B = 2000$ gauss; perpendicular set-up).

4.2. PARALLEL FIELD

a) *Iron target.* As mentioned in section 3, the measurements of EB circular polarization were made in this case by magnetizing the target alternatively forward and backward with respect to the β momentum ($B = 7000$ gauss).

The relative polarization, defined now as the ratio P_b/P_f and plotted in fig. 4,

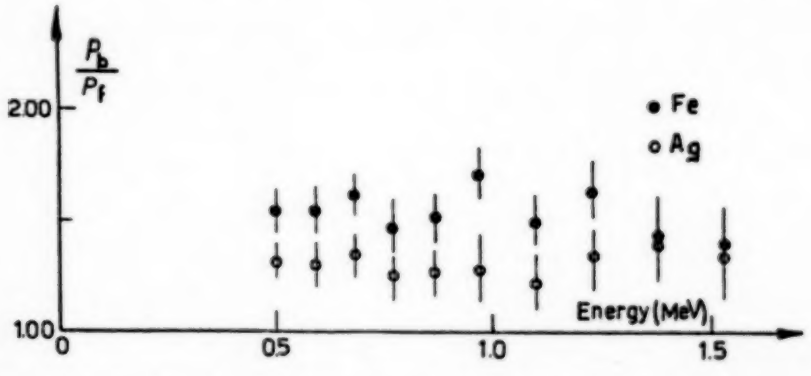

Fig. 4. Relative polarization as a function of the quantum energy for Fe ($B = 7000$ gauss) and Ag ($B = 4400$ gauss) targets (parallel set-up).

was found to be in the whole considered spectral region

$$\frac{P_b}{P_t} = 1.53 \pm 0.09. \tag{1}$$

The observed perturbation is now much higher than in the case of a perpendicular field. Owing to the fact that the spin of a β^- particle points opposite to its momentum, eq. (1) means that the EB polarization is higher when the magnetic induction in the target is in the same direction as the β^- spins.

The relative polarization measurements were not repeated with different values of magnetic induction, as they are very troublesome.

On the basis of the results reported in sections 4.1 and 4.2 a), one can be led to the assumption that the observed effect is due to a depolarization of β^- particles resulting from the interaction between their spin and the spin of the oriented electrons in magnetized iron. This interpretation, which at first glance appears reasonable, cannot be upheld, both for theoretical reasons † and because of the results of the following sub-section b.

b) *Silver target.* The EB circular polarization measurements were made by magnetizing the target in the same way as described in a). The magnetic induction was however lower and equal to 4400 gauss. The relative polarization, plotted in fig. 4 was found to be

$$\frac{P_b}{P_t} = 1.33 \pm 0.09$$

in the whole spectral region.

Finally, we wish to emphasize that the total cross section for EB production in the magnetized target in the two experimental set-ups was found to be independent from the magnetization state of the target within $(2 \pm 2) \times 10^{-3}$.

As regards the accuracy of all previous measurements, the quoted errors represent the standard deviation of the mean value. In this connection it must be pointed out that a statistical discussion of the polarization data has been made and the standard deviations are found quite consistent with what is to be expected on the basis of both the counting rates and the drifts of the whole electronic equipment.

In particular, if the standard deviations are correlated both to the observed pulse height distribution and only to fast fluctuations in the supply voltage of the photomultiplier, we found that they are consistent with fluctuations not exceeding 0.008 percent. This value is quite reasonable if the matter is considered from an electronic point of view.

† G. Morpurgo: private communication.

5. Discussion

The change of EB polarization observed in a magnetic field with the experimental apparatus described in the previous sections, does not seem to be interpretable as an effect instrumental in origin. We are, then, led to assume that the magnetic field is responsible for the strong perturbation observed on the circular polarization of EB produced by β-rays, and that it does not affect the total EB cross section. The present results, however, cannot establish the origin of the perturbation; for instance, they cannot establish if the effect is to be attributable to a depolarization of β-rays when traversing magnetized matter, as could appear at first glance, or to some other phenomena. Consequently, and in view of the fact that it is not easy to find an explanation of the effect, which appears surprisingly large, further theoretical and experimental work should be attempted. In particular, other experiments with different apparatus and measuring techniques are necessary.

Note added in proof: Any attempt at explaining the dependence of the electron depolarization on the magnetic field would face the serious difficulty that the spin precession period in the magnetic field is many times larger than the time spent by the electrons in the target before radiating.

References

1) A. Bisi and L. Zappa, Phys. Rev. Letters **2** (1959) 348
2) A. Bisi and L. Zappa, Nuclear Physics **10** (1959) 331

1.D.2:
1.E.3:
1.E.4

Nuclear Physics **15** (1960) 239—253; © *North-Holland Publishing Co., Amsterdam*
Not to be reproduced by photoprint or microfilm without written permission from the publisher

THE NUCLEAR *g*-FACTOR OF THE 111 keV ROTATIONAL LEVEL AND OTHER ANGULAR CORRELATION MEASUREMENTS ON W^{184}

E. BODENSTEDT, E. MATTHIAS, H. J. KÖRNER, E. GERDAU, F. FRISIUS and D. HOVESTADT

II. Institut für Experimentalphysik, Physikalisches Staatsinstitut Hamburg

Received 19 October 1959

Abstract: The angular correlations of the 793 keV—111 keV cascade and the 895 keV—111 keV cascade of W^{184} have been measured as

$$W(\theta) = 1-(0.036\pm0.004)\cdot P_2(\cos\theta)+(0.219\pm0.006)\cdot P_4(\cos\theta),$$
$$W(\theta) = 1-(0.177\pm0.013)\cdot P_2(\cos\theta)-(0.043\pm0.024)\cdot P_4(\cos\theta),$$

respectively. The source was prepared as $KReO_4$ in a liquid solution. It was shown that the coefficients are attenuated by internal fields. We determined the attenuation factors as

$$G_2 = 0.54 \quad \text{and} \quad G_4 = 0.67.$$

These angular correlation results confirm the proposed spin values $I = 2$ for the 904 keV level and $I = 3$ for the 1006 keV level and identify the 793 keV and the 895 keV transitions as pure E2. A reinvestigation of the half life of the 111 keV state gave

$$T_{\frac{1}{2}} = (1.28\pm0.08)\times10^{-9}\ \text{sec}.$$

The half life of the mother isotope Re^{184} was found to be

$$T_{\frac{1}{2}} = 38\pm1\ \text{d},$$

in disagreement with the earlier value of 50 ± 2d.

The nuclear *g*-factor of the 111 keV rotational level was obtained by determining the rotation of the 793 keV—111 keV angular correlation in an external magnetic field of 36040 gauss. The result,

$$g = +0.38\pm0.05,$$

is in agreement with the prediction of the collective model $g_R = Z/A$.

1. Introduction

The rotational *g*-factor g_R is predicted by the collective model as Z/A [1]. A direct experimental determination of g_R is possible for rotational levels of strongly deformed even nuclei by the method of disturbing angular correlations by external magnetic fields [2].

Recently measurements of this kind have been performed by G. Goldring and R. P. Scharenberg [3] on the nuclei Nd^{150}, Sm^{152} and Sm^{154}, by K. Sugimoto [4] on Sm^{152}, and by P. Debrunner *et al.* [5] on Dy^{160}. All these nuclei have paramagnetic atomic shells and thus corrections are necessary for the effective

magnetic field at the position of the nucleus [3]). The exact value of these corrections is difficult to evaluate.

In the case of W^{184} there are no paramagnetic perturbations and therefore an accurate determination of the g-factor of the 111 keV rotational level should be possible.

2. Preparation of the Source

We obtained Re^{184} sources by deuteron bombardments of ordinary tungsten in the Heidelberg cyclotron and the synchrocyclotron at Bonn. Re^{184} decays by electron capture into excited states of W^{184}.

In addition to Re^{184} the isotope Re^{183} is produced in comparable activity [6]).

The chemical separation of the rhenium activity from the inactive tungsten was done in the following way [6]):

The tungsten foil was dissolved in a mixture of 90 % HNO_3 conc. and 10 % HF conc. A few tenths of a milligram of inactive $KReO_4$ were added as a carrier. Then the solution was digested for several hours in a steam bath. The tungsten precipitates quantitatively as WO_3. The solution was finally evaporated to dryness and again taken up by a very dilute solution of HNO_3. After filtration the supernatant liquid containing the activity as ReO_4^- was concentrated to a volume of about 0.02 cm^3 and filled into a lucite container.

3. Decay Scheme of Re^{184}

The disintegration of Re^{184} has recently been studied by C. J. Gallagher *et al.* [6]) who proposed the decay scheme of fig. 1. The 364 keV and 111 keV

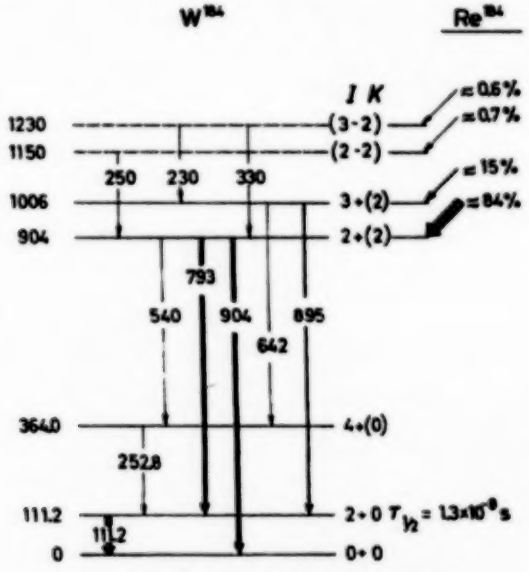

Fig. 1. Decay scheme of Re^{184}.

levels together with the ground state level form a rotational band with the spin sequence 4+, 2+, 0+. Probably there are no electron transitions directly to these rotational levels. 84 % of the EC decay go to the 904 keV level, 15 % to the 1006 keV level, and about 1 % to levels around 1.2 MeV. C. J. Gallagher *et al.* [6]) give arguments for the spin assignments 3+ and 2+ for the 1006 keV

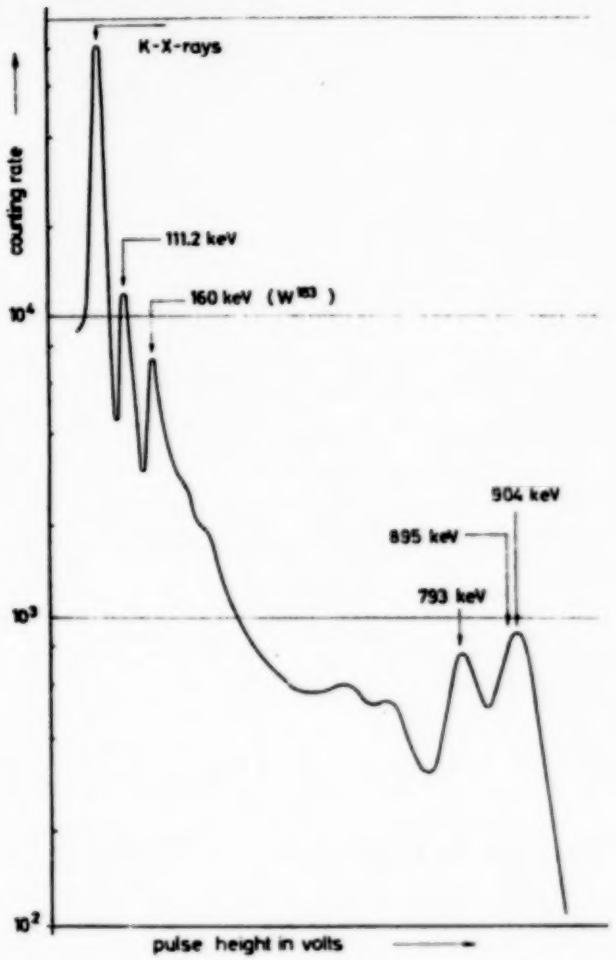

Fig. 2. Pulse height spectrum of Re^{184}.

and 904 keV levels respectively. The half life of the 111 keV level was determined by the same authors as

$$T_{\frac{1}{2}} = (1.3 \pm 0.4) \times 10^{-9} \text{ sec.}$$

They used the method of delayed coincidences and central shift analysis. F. K. McGowan and P. H. Stelson [7]) calculated the half life from Coulomb excitation data and got

$$T_{\frac{1}{2}} = 1.02 \times 10^{-9} \text{ sec.}$$

The pulse height spectrum of fig. 2 was obtained by use of a 1.5″ × 1″ NaI(Tl) scintillation crystal. It contains intense photopeaks at 900 keV, 793 keV, 160 keV, 111 keV, and the K X-ray peak at 70 keV. The 160 keV gamma ray belongs to the decay of Re^{183} as pointed out by C. J. Gallagher *et al.* [6]). The peak at 900 keV consists of the two lines 895 and 904 keV.

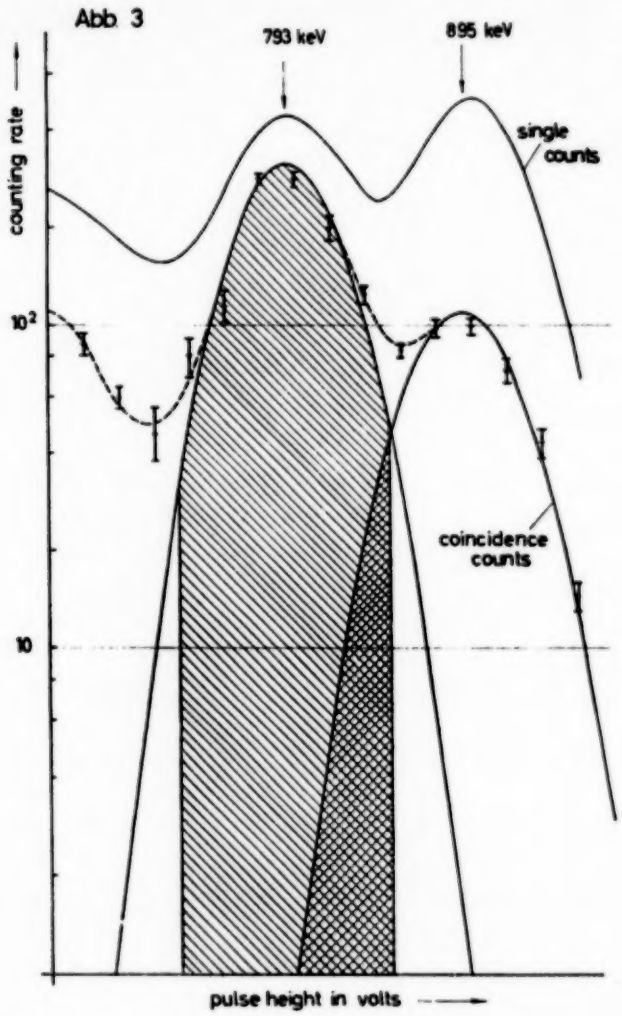

Fig. 3. Coincidences between the 111 keV line and the high energy transitions. The setting of the single channel analyser for the measurement of the 793 keV–111 keV angular correlation is marked.

The coincidence spectrum (fig. 3) shows the coincidences between the 111 keV line and the high energy transitions at 793 keV and 895 keV, thus confirming the proposed decay scheme.

The coincidences between the 793 keV line and the low energy part of the spectrum are shown in fig. 4. Besides the intense peaks of the K X-rays and the 111 keV line only two very weak peaks are observed which probably have to be assigned to the 250 keV and 330 keV transitions.

In the decay of Re^{183} there are no high energy gamma lines but many lines up to 350 keV which contribute to the single counts but not to the coincidences.

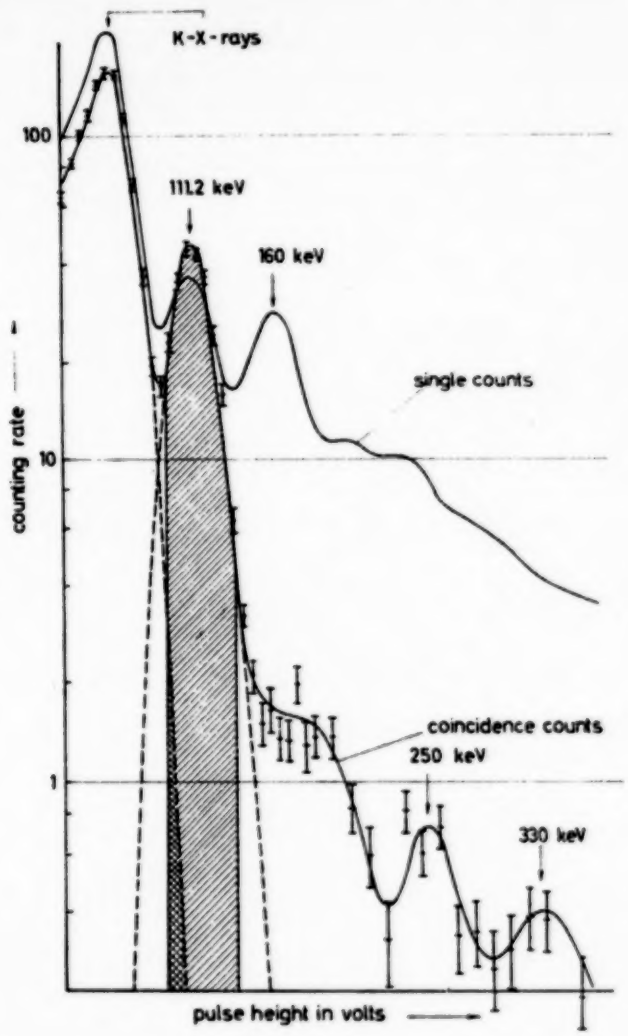

Fig. 4. Coincidences between the 793 keV line and the low energy part of the spectrum. The setting of the single channel analyser for both angular correlation measurements is drawn in.

4. Angular Correlation Measurements on the 793 keV—111 keV Cascade and the 895 keV—111 keV Cascade

For the measurement of the nuclear g-factor of the 111 keV level this level must be the intermediate state of a gamma-gamma-cascade. The 252 keV—111 keV cascade is not suitable because of the complex background of many other Re^{183} and Re^{184} gamma-transitions. However, the 793 keV—111 keV and the 895 keV—111 keV cascades can be measured without any appreciable admixtures of other gamma-lines. Furthermore, the determination of the absolute coefficients of these two angular correlations gives additional informa-

tion concerning the spin assignments of the 904 keV and the 1006 keV levels and the multipolarity of the different gamma-lines involved.

The angular correlation measurements have been performed by using a conventional fast-slow-coincidence circuit. Fig. 3 and fig. 4 show the settings of the single channel analysers for the measurements of the 793 keV—111 keV cascade. A correction for 3.4 % admixture of the 895 keV—111 keV cascade is necessary. In the case of the 895 keV—111 keV cascade the single channel analyser for the 985 keV line was set on the right side of the peak thus making admixtures of the 793 keV line negligible. The setting of the 111 keV single channel analyser (fig. 4) has been the same in both measurements. The back-

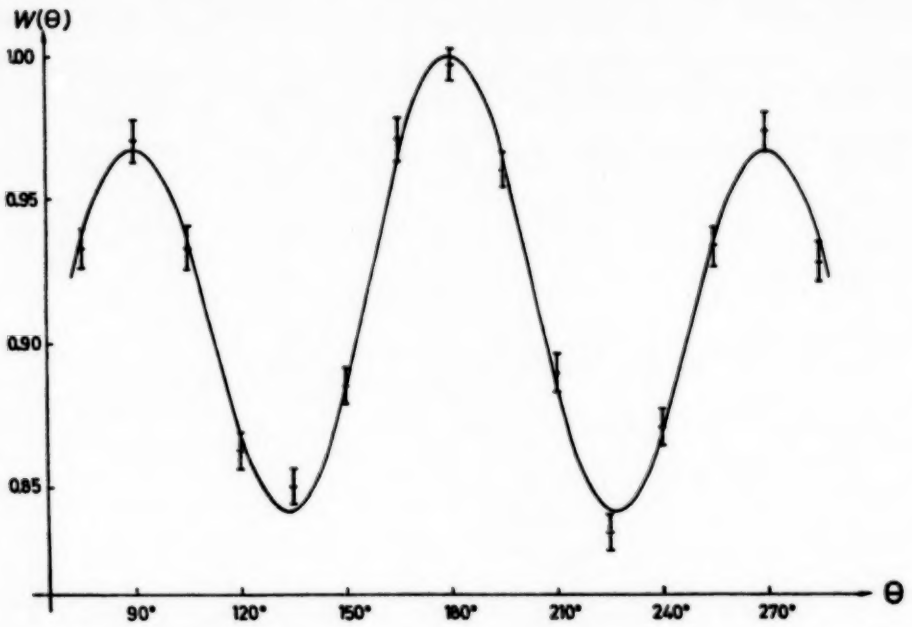

Fig. 5. Angular correlation of the 793 keV—111 keV cascade.

ground of the K X-rays was about 0.7 % and has been taken into account. There is an additional admixture by the low energy gamma-transitions which lead to the 1006 keV and the 904 keV levels. A correction for this contribution has not been applied. C. J. Gallagher *et al.* [6]) have estimated the intensities of these transitions. They are in the order of magnitude of only 1 % as compared to the K X-ray line. To stabilize the settings of the single channel analysers during the periods of measurements an electronic device described by H. de Waard [8]) has been used. The distance between the crystals (1.5″ × 1″ NaI(Tl)) and the source was 70 mm for the 793 keV—111 keV cascade and 52 mm for the 895 keV—111 keV cascade.

The measured angular correlations are plotted in fig. 5 and fig. 6. After correction for the admixtures and the finite solid angles of the detectors the results are

$$W(\theta) = 1-(0.036\pm0.004)\cdot P_2(\cos\theta)+(0.219\pm0.006)\cdot P_4(\cos\theta)$$

for the 793 keV—111 keV cascade and

$$W(\theta) = 1-(0.177\pm0.013)\cdot P_2(\cos\theta)-(0.043\pm0.024)\cdot P_4(\cos\theta)$$

for the 895 keV—111 keV cascade. These functions do not contain corrections for an attenuation by internal fields. A small attenuation might be expected for a half life of 1.3×10^{-9} sec because of the large quadrupole moment of the W^{184} nucleus.

A comparison of the result for the 793 keV—111 keV angular corelation with the theoretical function was done under the assumptions that the ground state

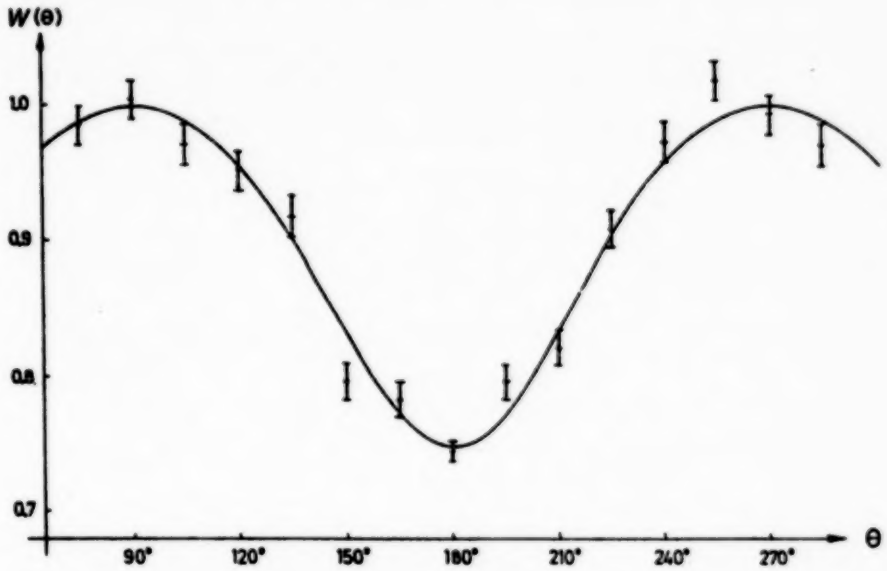

Fig. 6. Angular correlation of the 895 keV—111 keV cascade.

spin is 0^+ and the spin of the 111 keV level is 2^+. For the 904 keV level all spin values between 0 and 5 have been discussed. As shown in table 1 the only

TABLE 1

Comparison of the experimental result for the 793—111 keV angular correlation with the theoretical coefficients

Spin of the 904 keV level	Multipolarity of the 793 keV transition	solution	arguments
0	quadrupole	no	$A_2 > 0$
1	dipole+quadrupole	no	$A_4 < 0$
2	dipole+quadrupole	yes	The multipolarity of the 793 keV line must be pure E2 (see fig. 7)
3	dipole+quadrupole	no	$A_4 < 0$
4	quadrupole	no	$A_2 > 0$
5	octupole	no	$A_2 > 0$; $A_4 < 0$

possible solution is $I = 2$ for the 904 keV level in agreement with the proposed assignment of C. J. Gallagher *et al.*[6]). The analysis of the M1—E2 mixing ratio for the 793 keV line was carried out by the method of R. G. Arns and M. L. Wiedenbeck [9]). Fig. 7 shows that agreement with the theoretical values can be

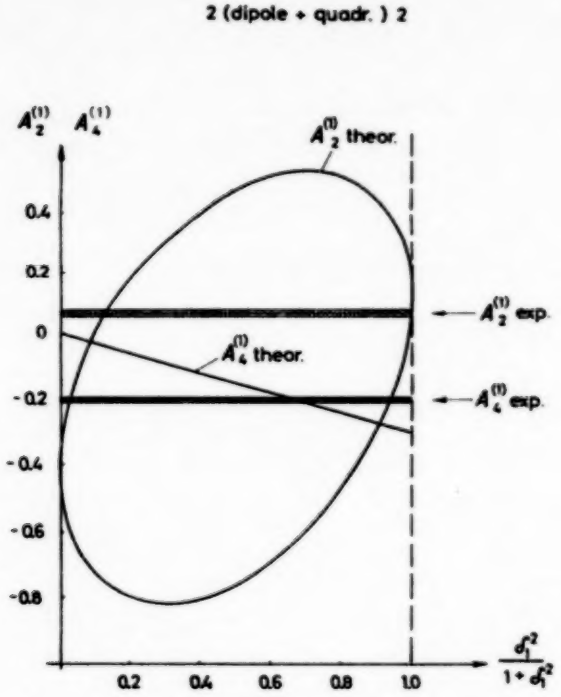

Fig. 7. Analysis of the dipole-quadrupole mixing of the 793 keV transition according to R. G. Arns and M. L. Wiedenbeck [9]).

achieved only under the assumption of attenuation factors for A_2 and A_4. The 793 keV transition is approximately pure E2, the M1 admixture must be less than 0.5 %. There is some discrepancy between this result and the measured conversion coefficient of the 793 keV radiation [6]) which predicts a larger M1 mixing. The attenuation factor of A_4 is

$$G_4 = 0.673 \pm 0.020.$$

The attenuation factor G_2 was calculated under the assumption of pure electric quadrupole interactions using the theory of A. Abragam and R. V. Pound [10]). This gave

$$G_2 = 0.54.$$

This value is compatible with the mixing ratio analysis.

The result for the 895 keV—111 keV angular correlation was compared with the theoretical coefficients admitting all spin values between 0 and 5 for the 1006 keV level. Again there is only one solution: $I = 3$ (table 2). The mixing

TABLE 2

Comparison of the experimental result for the 895h keV—111 keV angular correlation with the theoretical coefficients

Spin of the 1006 keV level	Multipolarity of the 895 keV transition	solution	arguments
0	quadrupole	no	$A_2 > 0$
1	dipole+quadrupole	no	$A_4 \approx 0$
2	dipole+quadrupole	no	$A_2 > 0$
3	dipole+quadrupole	yes	The multipolarity of the 895 keV line must be appr. E2 (see fig. 8)
4	quadrupole	no	$A_2 > 0$; $A_2 > 0$
5	octupole	no	$A_2 > 0$

ratio analysis proves that the 895 keV transition is approximately pure E2 (fig. 8) and in agreement with the assumption of the same attenuation factors as derived for the 793 keV—111 keV cascade. The results for the

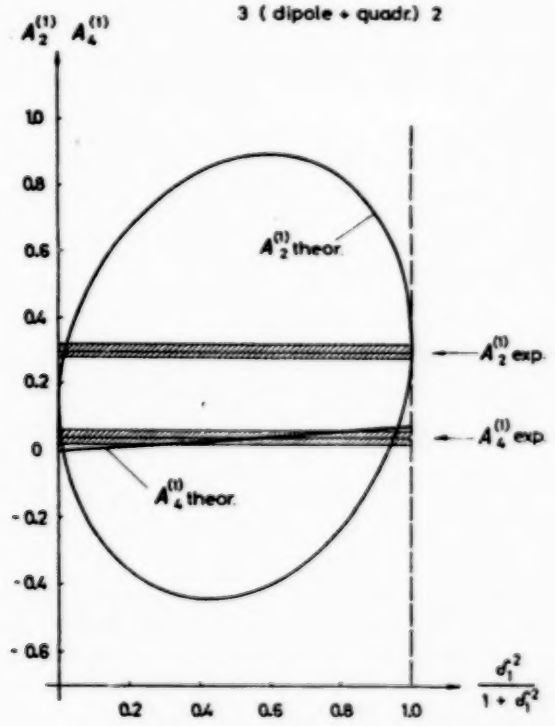

Fig. 8. Analysis of the dipole-quadrupole mixing of the 895 keV transition according to R. G. Arns and M. L. Wiedenbeck [9]).

multipolarity of the 793 keV and 895 keV gamma transitions can be understood from the K-selection rule [11]), as follows.

As C. J. Gallagher *et al.* derived from the branching ratios of the different gamma transitions the levels at 904 keV and 1006 keV belong to a second rotational band with an intrinsic configuration characterized by $K = 2$. The K-selection rule

$$|K_i - K_f| \leqq \lambda$$

(λ = multipolarity of the gamma transition) thus forbids the multipolarity M1 for the 793 keV and 895 keV gamma transitions.

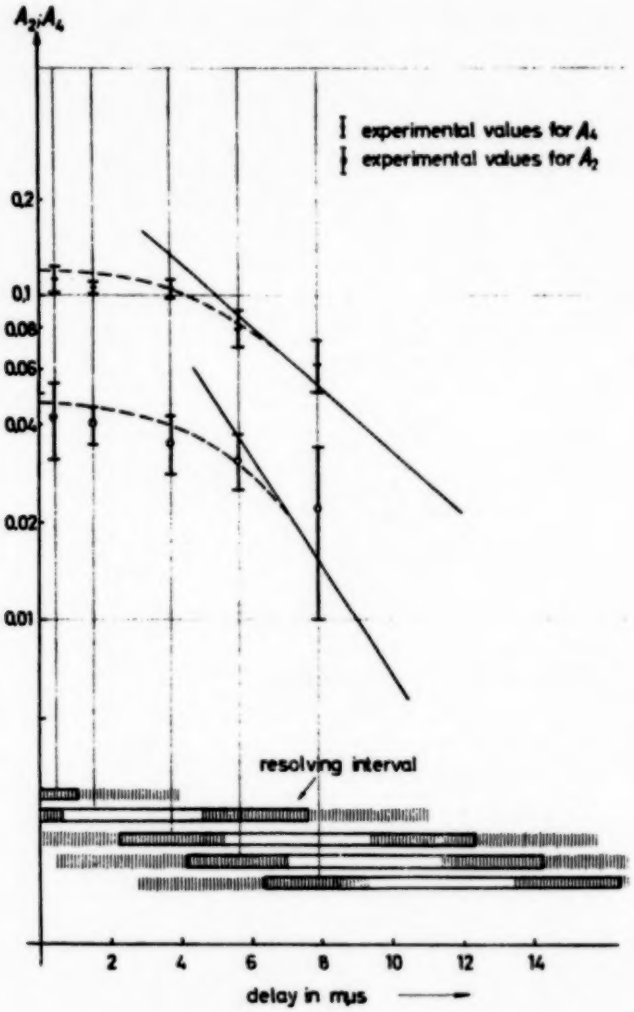

Fig. 9. Measurement of the coefficients A_2 and A_4 of the 793 keV $-$ 111keV angular correlation for different time delays. The resolving intervals for the different delays are drawn in. The shadowed areas indicate the not well defined edges. The experimental points are plotted at the weighted centers of the resolving intervals.

The direct experimental determination of the attenuation factors by measuring the differential angular correlation as a function of the time delay between

the two gamma-rays is difficult because of the short half life of the intermediate state. We performed a delay experiment by using a resolving time of $2\tau = 10$ ns. The result (fig. 9) shows the very existence of an attenuation. However, it is impossible to derive values for G_2 and G_4 from this measurement because the edges of the resolving interval are not well defined. The two straight lines in fig. 9 correspond to an exponential attenuation computed for the above determined integral attenuation factors G_2 and G_4 [12]). It was not possible to measure the angular correlation at even larger time delays ($> 6T_{\frac{1}{2}}$) for intensity reasons.

5. Half Life of the 111 keV State

For the investigation of the nuclear g-factor the half life of the level must be known exactly. Since the limits of error of previous measurements [6, 7]) were rather large we tried a new determination by the method of delayed coincidences. The result is plotted in fig. 10. The slope on the right side corresponds to a

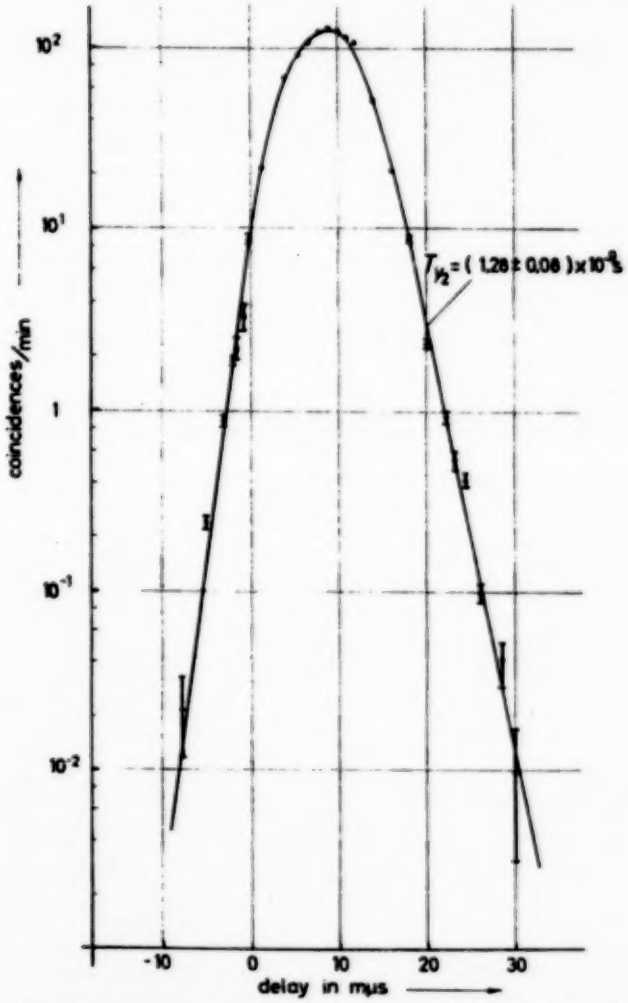

Fig. 10. Measurement of the half life of the 111 keV level.

half life of

$$T_{\frac{1}{2}} = (1.28 \pm 0.08) \times 10^{-9} \text{ sec.}$$

This value was obtained by a least square fit which employed only the points with a delay corresponding to more than 6 $T_{\frac{1}{2}}$. In this way additional errors due to the smeared out edges of the resolving intervals were eliminated.

6. The Nuclear *g*-Factor of the 111 keV Level

The experimental set up for the measurement of angular correlations in an external magnetic field has been described previously [12]). The 793 keV—111

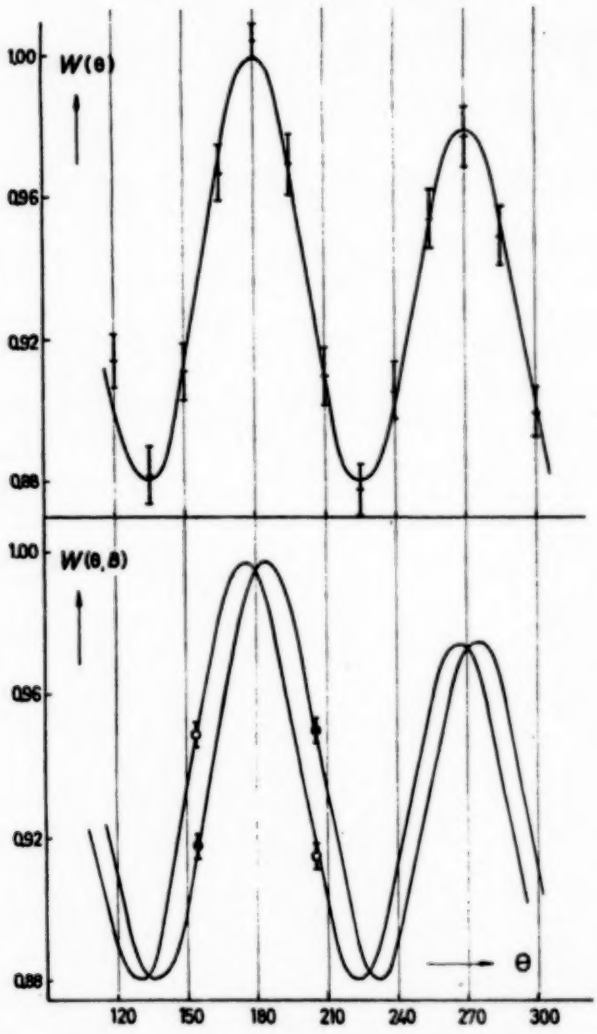

Fig. 11. Measurement of the *g*-factor of the 111 keV level.
I angular correlation of the 793 keV – 111 keV cascade without magnetic field.
I, I angular correlation of the same cascade in an external magnetic field of 36 040 gauss with field direction up and down respectively.

keV cascade was used for the determination of the nuclear g-factor because it has a higher intensity than the 895 keV—111 keV cascade. The distance between the source and the crystals was 50 mm. A magnetic field of 36 040 gauss has been applied. The field strength was determined by means of a coil and a flux-meter which had been calibrated by the proton resonance method.

As the expected rotation of the angular correlation pattern was only a few degrees even at this rather large magnetic field, this measurement has been restricted to the two angles 155 and 205 degrees, where the counting rate is most sensitive to small shifts of the correlation curve.

In fig. 11 the upper diagram shows the zero field angular correlation. Below this curve the experimental points for both field directions are plotted. The two lines represent the least square fit for the function $W(\theta, B)$. In this calculation the attenuation factors G_2 and G_4 have been taken into account [12]).

The resulting value for the nuclear g-factor is

$$g = +0.38 \pm 0.05.$$

The sign follows from the direction of the rotation of the correlation pattern. As the measurement of the g-factor was done in a continuous run of 30 days a precise value of the half life of the Re^{184} isotope could be derived from the single counting rates. Contributions of the 71 day Re^{183} radiations were eliminated by using the 793 keV channel.

The result,

$$T_{\frac{1}{2}}(Re^{184}) = 38 \pm 1\text{d},$$

is in disagreement with the earlier value of 50 ± 2d reported by G. Wilkinson and H. G. Hicks [13]).

7. Conclusions

The collective model predicts that the rotational g-factor is described by the ratio of charge to mass in the nuclear rotational motion. Under the assumption of an equal radial distribution of neutrons and protons in the nucleus the rotational g-factor should be Z/A [1]).

The results of the measurements of G. Goldring and R. P. Scharenberg [3]) of the first excited levels of three even-even rare earth isotopes were:

$$g_R(Nd^{150}) = +0.22 \pm 0.04,$$
$$g_R(Sm^{152}) = +0.21 \pm 0.04,$$
$$g_R(Sm^{154}) = +0.21 \pm 0.04.$$

Paramagnetic correction factors of about 2 had been applied. These g-factors are in disagreement with the theoretical prediction $Z/A = +0.41$.

The isotope Sm^{152} has been investigated by K. Sugimoto [4]) too. He reported

$$g_R(Sm^{152}) = +0.36 \pm 0.16.$$

This value has not yet been corrected for paramagnetic effects and perturbations by internal fields †.

P. Debrunner *et al.* [5]) recently studied the even nucleus Dy^{160}. In order to avoid the difficult calculation of the paramagnetic correction factor these authors measured the g-factor as a function of the temperature. They extrapolated the results to the temperature infinite, where the paramagnetic perturbations should vanish. They found

$$g_R(Dy^{160}) = +0.18 \pm 0.08.$$

The applicability of this method is limited by attenuations of the directional correlation due to internal fields. Especially if solid sources have to be used one has to expect strong attenuations which might be sensitive functions of the temperature. In the case of Dy^{160}, P. Debrunner *et al.* [5]) found that strong perturbations existed.

In contrast to these previous measurements our result for the first excited level of W^{184},

$$g_R = +0.38 \pm 0.05,$$

agrees with the theoretical prediction for this nucleus $Z/A = +0.40$. It is not yet understood whether this deviation between our value and the results on the rare earth isotopes is still due to experimental inadequacies †, but there might be also a systematic deviation from Z/A for the different nuclei.

The authors would like to thank Prof. W. Jentschke and Prof. H. Neuert for their interest in this work and stimulating discussions. Mr. H. Schaarschmidt and Miss H. Wulff assisted in taking the data and helped to perform the numerical calculations. The irradiations done by the cyclotron groups at Heidelberg and Bonn are gratefully acknowledged. The Bundesministerium für Atomkernenergie und Wasserwirtschaft supported this investigation by financial funds.

† *Note added in proof:* K. Sugimoto recently published [14]) a calculation of the paramagnetic correction factor in which he concluded that the correction is only about 15 %. This is in contrast to the estimation of G. Goldring and R. P. Scharenberg [3]). If the calculation of K. Sugimoto is correct, his measurement for g_R as well as the measurement of G. Goldring and R. P. Scharenberg would yield values compatible with Z/A.

References

1) A. Bohr and B. R. Mottelson, in Beta- and Gamma-Ray-Spectroscopy, Ed. K. Siegbahn (North-Holland Publishing Co., Amsterdam 1955) Ch. XVII
2) H. Frauenfelder, in Beta- and Gamma-Ray-Spectroscopy, Ed. K. Siegbahn (North-Holland Publishing Co., Amsterdam 1955) Ch. XIX (I)

3) G. Goldring and R. P. Scharenberg, Phys. Rev. **110** (1958) 701
4) K. Sugimoto, Journ. of Phys. Soc. Japan **13** (1958) 240
5) P. Debrunner, W. Kündig, J. Sunier and P. Scherrer, Helv. Phys. Acta **31** (1958) 326
6) C. J. Gallagher, D. Strominger and J. P. Unik, Phys. Rev. **110** (1958) 725
7) F. K. McGowan and P. H. Stelson, Phys. Rev. **109** (1958) 901
8) H. de Waard, Nucleonics **13** (July 1955) 36
9) R. G. Arns and M. L. Wiedenbeck, Phys. Rev. **111** (1958) 1631
10) A. Abragam and R. V. Pound, Phys. Rev. **92** (1953) 943
11) B. R. Mottelson and S. G. Nilsson, Dan. Vid. Selsk. Mat. Fys. Skr. **1**, No. 8 (1959) 9
12) E. Bodenstedt, E. Matthias and H. J. Körner, Zs. f. Phys. **153** (1959) 423
13) G. Wilkinson and H. G. Hicks, Phys. Rev. **77** (1950) 314
14) J. Kanamori and K. Sugimoto, J. Phys. Soc. Japan **13** (1958) 754

1.E.1:
2.G:3.A

Nuclear Physics **15** (1960) 254—260; © *North-Holland Publishing Co., Amsterdam*
Not to be reproduced by photoprint or microfilm without written permission from the publisher

SPIN OF THE FIRST EXCITED STATE OF B^{12}

E. KONDAIAH and C. BADRINATHAN

Tata Institute of Fundamental Research, Colaba, Bombay-5

Received 22 October 1959

Abstract: Angular distribution of gamma rays arising from the 0.95 MeV level of B^{12} in the reaction B^{11}(d, p)B^{12} has been studied at a deuteron energy of 0.8 MeV. It has been found that the gamma angular distribution is definitely non-isotoropic and has a minimum at an angle of 45° to the incident deuteron beam. This leads to the exclusion of $0^{\pm}$, 1^- and 2^- assignments to the 0.95 MeV level in B^{12} leaving the possible assignments 2^+ or 3^+.

1. Introduction

The B^{11}(d, p)B^{12} reaction is known to lead to the ground state as well as excited states in B^{12} [1]. The ground state Q-value for this reaction is 1.136 MeV and accordingly, at a deuteron energy of 0.8 MeV, only the ground state and the first excited state of B^{12} are reached favourably. Holt and Marsham [2]) studied the angular distribution of protons in this reaction using 8 MeV deuterons. The observed angular distributions of protons leading to ground and first excited states of B^{12} fitted very well with $l_n = 1$ curves based on stripping theory. The ground state of B^{11} is known to be a $\frac{3}{2}^-$ state. Hence, the ground state as well as the first excited state of B^{12} should have even parity and a spin of 0, 1, 2 or 3. The ground state of B^{12} is known to be a 1^+ state.

2. Theoretical gamma Angular Distributions

According to Satchler [3]), the angular distribution of a gamma ray observed in coincidence with the outgoing nucleon in a (d, p) or (d, n) reaction can be calculated from

$$W(\theta) = \sum_{\nu jj' L' L} B(j)B(j')\, C(L)\, C(L')\, \eta_\nu(jj' J_i J_e)\lambda_\nu(LL' J_f J_e)\, P_\nu(\cos\theta),$$

where θ is the angle that the gamma ray makes with the recoil axis (see fig. 1), $B(j)$ and $C(L)$ are proportional to the (real) reduced matrix elements for the capture of the nucleon and the emission of the gamma ray respectively so that $b^2(j)$ is the fraction captured with j, and so on; J_i is the spin of the target nucleus, J_e the spin of the excited state emitting the gamma ray, J_f the spin of the final state to which the gamma ray is emitted; j is the total angular momentum of the captured nucleon; L is the multipole order of the gamma ray.

j takes values consistent with J_1 and J_e, whereas L takes values consistent with J_f and J_e. One has to sum over all values of j and L consistent with J_1, J_e and J_f. Values of the reduced matrix elements $B(j)$ and $C(L)$ are not actually known and are taken out as constants which may be evaluated by fitting the theoretical distribution to the experimentally observed distribution in suitable cases. The function $P_\nu(\cos\theta)$ is the Legendre polynomial of ν th order; ν takes all even values consistent with j, L and J_e with the condition that

$$\nu \leqq (j+j'), \quad (L+L'), \text{ or } 2J_e.$$

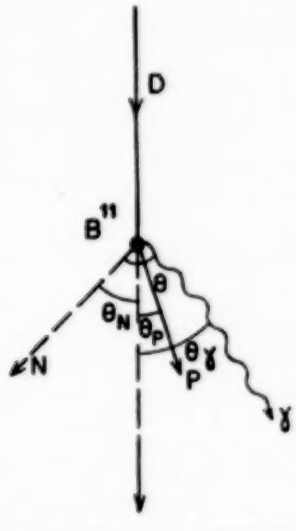

Fig. 1. Schematic diagram of B^{11}(d, p)B^{12} reaction.
D = Deuteron beam, N = Recoiling nucleus, P = Proton, γ = Gamma-ray.

Satchler [3]) has tabulated values of η_ν and λ_ν for certain values and has given methods of calculating these factors for other values. Using these methods, the gamma angular distribution has been evaluated for the B^{11}(d, pγ)B^{12} reaction for $J = 0^\pm$, $1^\pm$, $2^\pm$ and 3^+ for both electric and magnetic multipole order gamma rays. Table 1 gives these theoretical gamma ray angular distributions.

For $l_n = 1$, the value $J_e = 0^\pm$ gives uniform angular distribution, as $J_e = 0$ and $P_0(\cos\theta) = 1$. The values $J_e = 1-$ or $2-$ also give uniform angular distribution if one considers only $l_n = 0$ (that is s-wave neutron capture), as $\nu \leqq (j+j')$ i.e. 0.

The value $J_e = 1^+$ gives a distribution peaked at $\theta = 90°$ (see fig. 3 (ii)), as the constants b and β in the expression for $W(\theta)$ happen to be both positive †. For this case, $b = \gamma_{11}(A+0.112\,B+B^2/A)$ and $\beta = \gamma_{11}(0.335\,B+0.3B^2/A)$, where $\gamma_{11} = C(1)C(1)$, $A = B^2(\frac{1}{2})$, $B = B(\frac{1}{2})B(\frac{3}{2})$ and $B^2/A = B^2(\frac{3}{2})$; as all these are positive, the constants b and β are positive. If only p-wave ($l_n = 1$) neutron absorption is considered, $J_e = 3^+$ gives an angular distribution

† The same is true for $J_e = 2^+$ if only M1 gammas are considered; in this case, $b = \gamma_{11}(A+0.35\,B+B^2/A)$ and $\beta = 1.05\,B\gamma_{11}$.

$W(\theta) = k(0.8167+0.5499\ \cos^2\theta)$, where $k = \gamma_{22}B^2(\frac{3}{2})$, γ_{22} standing for $C(2)C(2)$. If this is the case actually holding, one can obtain the value of k and thereby the value of reduced matrix elements by fitting the theoretical angular distribution to the observed distribution.

TABLE 1

Theoretical angular distributions of $B^{11}(d, p\gamma)B^{12}$ reaction

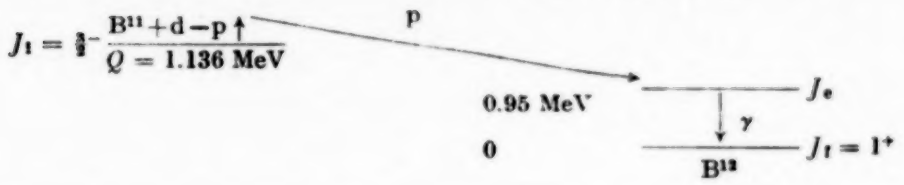

J_e	l_n	j or j'	L or L'	ν	$W(\theta)$
$0\pm$				0	constant
$1^-, 2^-$	0	$\frac{1}{2}$		0	constant
1^+	1	$\frac{1}{2}, \frac{3}{2}$	1	0, 2	$(b-\beta\cos^2\theta)$
$1^-, 2^-$	2	$\frac{1}{2}, \frac{3}{2}, \frac{5}{2}$	1	0, 2	$(b+\beta\cos^2\theta)$
1^+	1, 3	$\frac{1}{2}, \frac{3}{2}, \frac{5}{2}$	1	0, 2	$(b+\beta\cos^2\theta)$
2^+	1	$\frac{1}{2}, \frac{3}{2}$	1, 2	0, 2	$(b+\beta\cos^2\theta)$ †
2^+	1, 3	$\frac{1}{2}, \frac{3}{2}, \frac{5}{2}, \frac{7}{2}$	1, 2	0, 2, 4	$(b+\beta\cos^2\theta+\rho\cos^4\theta)$
3^+	1	$\frac{3}{2}$	2	0, 2, 4	$k(0.8167+0.5499\cos^2\theta)$
3^+	1, 3	$\frac{3}{2}, \frac{5}{2}, \frac{7}{2}$	2	0, 2, 4	$(b+\beta\cos^2\theta+\rho\cos^4\theta)$

† For this case, if pure M1 gammas are considered we get $W(\theta) = k'-1.05\,k''\cos^2\theta$, where k' and k'' are both positive and hence a peak at $\theta = 90°$ will be obtained as shown in fig. 3 (ii).

For the other cases which take into account higher order orbital angular momenta of the captured neutron, the forms of gamma angular distribution are given under $W(\theta)$ in the last column of table 1. The values of b, β and ρ occurring in the expressions for $W(\theta)$ given in the last column of table 1 differ from case to case and they can in general be positive or negative independently.

Fig. 3 gives the shapes of gamma angular distributions to be expected in the $B^{11}(d, p\gamma)B^{12}$ reaction considering only the lowest possible orbital angular momentum of captured neutron consistent with parity.

3. Experiment and Results

An isotopically separated B^{11} target was obtained from A.E.R.E. Harwell. The thickness of the target was 100 μg/cm^2. The gamma detector was a 2″ diameter, 2″ long NaI(Tl) crystal. A 800 keV deuteron beam was obtained from

the 1 MeV cascade accelerator of this Institute. A typical gamma spectrum taken at 0° to the incident deuteron beam is given in fig. 2. The 511 keV peak is due to the $C^{12}(d, n)N^{13}(\beta^+)$ reaction; C^{12} contamination arose from the oil diffusion pump of the accelerator. The 661 keV peak is due to a Cs^{137} gamma source purposely kept for calibration. The peak at (900 ± 50) keV agrees with the energy of the gamma ray expected from the 0.95 MeV level in B^{12} due to the $B^{11}(d, p)B^{12}$ reaction.

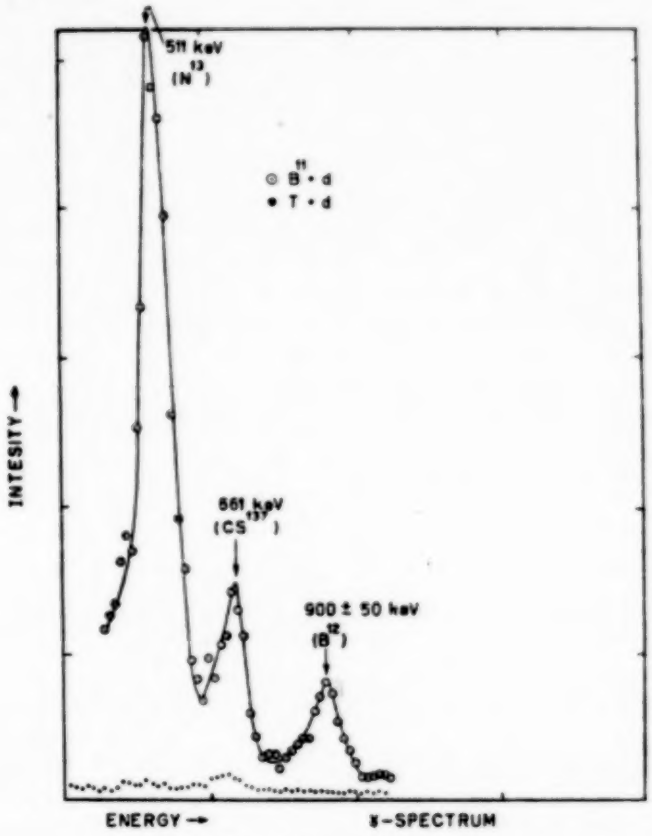

Fig. 2. γ-spectrum.

The $B^{11}(d, n)C^{12}$ reaction which occurs simultaneously with the $B^{11}(d, p)B^{12}$ reaction, may also give rise to gamma rays around 900 keV due to neutron interactions with the gamma detector as well as surrounding materials like the target tube etc. $B^{11}(d, n)C^{12}$ neutrons are polyergic with a maximum energy up to 13.4 MeV at 800 keV incident deuteron energy. Accordingly, a study of the gamma spectrum was undertaken using a T(d, n) source giving fast neutrons. The T(d, n) source was operated to give the same number of neutrons as the $B^{11}(d, n)$ source using a neutron monitor. This gamma spectrum is also given in fig. 2. It can be seen that there is no peak around 900 keV gamma energy in the T(d, n) case at the same level of neutron intensity as for $B^{11}(d, n)$. The general counting rate in this region of the gamma spectrum is about 10 to 15 times less in the case of T(d, n) source than in the case of the $(B^{11}+d)$ source. Hence,

the peak at 900 keV in fig. 2 can safely be taken as due to the $B^{11}(d, p)B^{12}$ reaction and not to any second order effects of neutrons arising from the $B^{11}(d, n)C^{12}$ reaction.

While studying the angular distribution of these gamma rays, the 900 keV

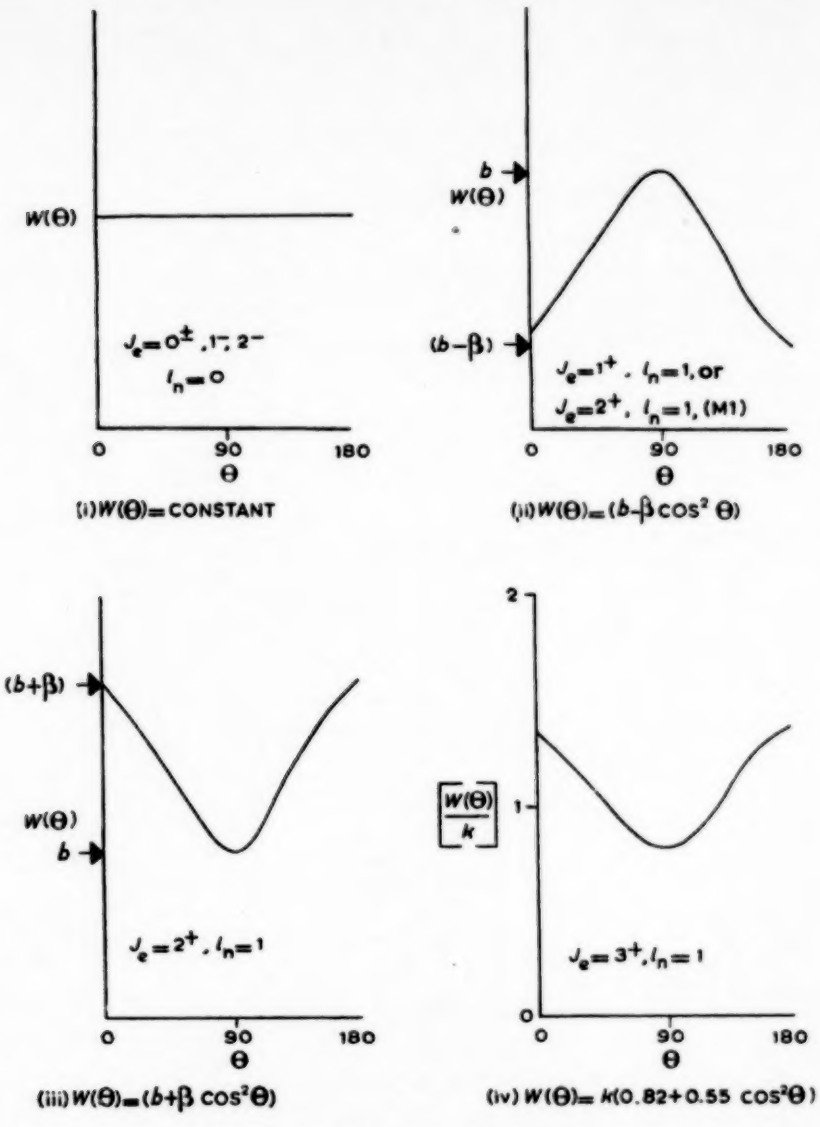

Fig. 3. Theoretical gamma angular distributions.

gamma rays emitted at 0° to the deuteron beam were used as monitor, whereas the movable gamma detector was moved around the target as centre. Each of the points in the gamma spectra recorded by the movable detector was calculated for a fixed number of counts in the monitor. Statistical acuracy of each of the points in all the spectra taken at different angles is better than 2 %. The angular aperture of the movable gamma detector was 10° at all the angles.

Gamma spectra were recorded at 15° intervals in the region 0° to 135° with respect to the incident deuteron beam. Observations at each angle were repeated at least twice and intensities of the 900 keV gamma rays at each angle agree within the errors shown in fig. 4 which gives the observed angular distribution.

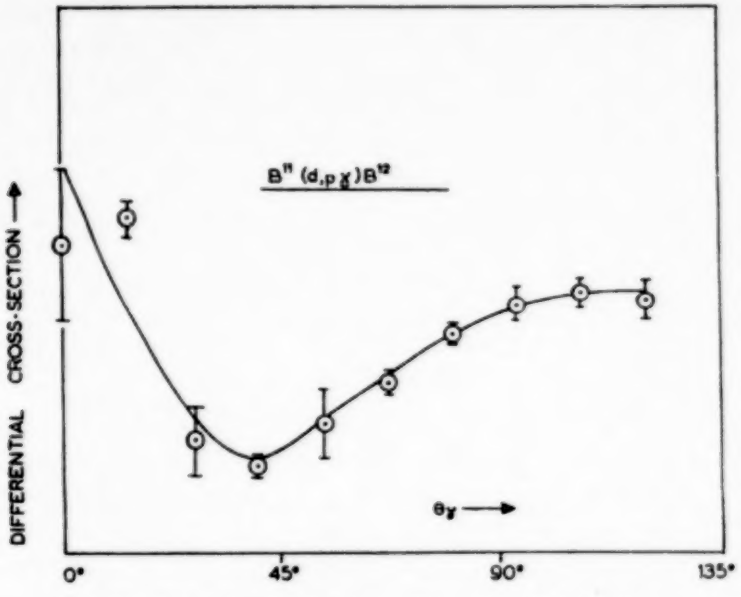

Fig. 4. Experimental gamma angular distribution.

The errors given in fig. 4 refer to self consistency of the intensities observed in different runs at each angle. The gamma angular distribution is definitely nonisotropic and has a minimum at an angle of 45° to the incident deuteron beam.

4. Discussion

The theoretical angular distributions given in table 1 and fig. 3 are for p—γ coincidence distributions whereas the observed gamma angular distribution given in fig. 4 is for gamma rays only. Observation of p—γ coincidences fixing the proton detector enables one to locate the axis of recoil and hence the actual position of maxima or minima in the angular distribution. From mere observation of gamma angular distributions in a (d,p) or (d, n) reaction, it is not possible to locate the angular positions of the maxima or minima with respect to the recoil axis since the direction of the captured nucleon is no longer fixed. However, the gamma angular distribution should have the same general shape as the (p—γ) coincidence angular distribution irrespective of the angular positions of the maxima and minima. Thus, for different values of J_e, the general shape of gamma angular distributions should be similar to the ones shown in fig. 3.

As the observed gamma angular distribution is definitely non-uniform (see fig. 4), $J_e = 0^{\pm}$ as well as $J_e = 1^-, 2^-$ (if s-wave neutron absorption only is considered) can be ruled out. As $J_e = 1^+$ ($l_n = 1$) should give a peak (see fig. 3 (ii)) and not a trough as seen in fig. 4, it can also be ruled out, on the assumption that only p-wave neutrons take part, which is found to be true even at 8 MeV deuteron energy [2]).

Thus, the 0.95 MeV level of B^{12} is most probably a 2^+ or 3^+ state. The (p—γ) coincidence angular distribution in this reaction, which may throw further light on the spin of this level, is at present under study in our laboratory.

Messrs M. D. Deshpande and M. S. Kamath have given technical assistance during the course of this work.

References

1) F. Ajzenberg and T. Laurtisen, Nuclear Physics **11** (1959) 1
2) J. R. Holt and T. N. Marsham, Proc. Phy. Soc. A **66** (1953) 1032
3) G. R. Satchler, Proc. Phys. Soc. A **66** (1953) 1081

7.A

Nuclear Physics **14** (1960) 261 – 288; © *North-Holland Publishing Co., Amsterdam*

Not to be reproduced by photoprint or microfilm without written permission from the publisher

ON A METHOD OF FINDING SINGULARITIES OF FEYNMAN GRAPHS

L. B. OKUN and A. P. RUDIK

Institute of Theoretical and Experimental Physics of the USSR Academy of Sciences, Moscow

Received 30 June 1959

Abstract: The method of finding the singularities of Feynman graphs suggested by Landau is investigated. Techniques are evolved to establish whether any Feynman graph has a singularity. If it has, the method under discussion makes it possible easily to determine its location. To illustrate possibilities of the method the singularities of baryon form-factors and the nearest singularities of some simple scattering amplitudes are determined.

1. Introduction

1.1. SINGULARITIES AND FEYNMAN GRAPHS

As is well known, one of the principal tasks of the quantum field theory is the calculation of the amplitudes describing interaction among elementary particles. These amplitudes are analytic functions of the invariants characterizing the process, such as total energy, momentum transfer, and so on. In investigating the analytic properties of amplitudes it is essential to determine the location of singularities, i.e. the points at which either the amplitude or its derivatives go to infinity.

It is necessary to know singularities to evolve and study the dispersion relations [1, 2, 3]), which are in fact a corollary of the analyticity of the amplitudes. The location of singular points is essential in deriving spectral representations of Green's functions [4]) and vertex parts. Of especial importance is the "geography" of singularities in an analysis of spectral representation proposed by Mandelstamm [16, 17, 18]). Recently the singularities have been found to be of importance in studies of the peripheral interactions of elementary particles [6, 7, 8]), the electromagnetic form-factors of strongly interacting particles [9, 10]) and certain decays of strange particles [11]). A number of papers have been concerned with the analysis of singularities in the amplitude of one process near the threshold of another competing with the former [12–15]).

Recently, Karplus, Sommerfield and Wichmann [19, 20]), and Landau [21]) used the technique of the Feynman graphs for locating singularities. In ref. [19, 20]) the two simplest Feynman graphs were considered, one corresponding to the vertex part and the other to the scattering amplitude. In ref. [21]) the same graphs were analysed by a simpler and more elegant method, and it was shown that

this method may be applied to any Feynman graph. The present paper is an attempt to develop Landau's method.

It is common knowledge that the technique of the Feynman graphs directly involves the perturbation theory. It should be noted, however, that in the present paper the perturbation theory is applied not to the conventional meson-theory Lagrangian but to the phenomenological Lagrangian which contains arbitrarily complex vertex parts corresponding to the interaction of three, four and more fields. It may be hoped that despite the well-known inadequacy of the perturbation theory in considering strong interactions the results obtained below are correct. This hope stems from the fact that close to singularities the virtual particles are quasi-free ($q^2 \approx m^2$) and therefore we do not expect to come across the usual difficulties arising when receding from the energy surface (the divergences caused by interactions at small distances).

It should, however, be emphasized that within the limits of the method under consideration it is impossible to obtain such singularities as would correspond not to one graph but a sum of graphs (the pole in nucleon-nucleon scattering corresponding to the deuteron, for example). Within the method under consideration, therefore, the deuteron should be regarded as an elementary particle.

1.2. POSING THE PROBLEM

Consider the integral

$$F(p) = \int \delta(\sum_{(1)} q) \ldots \delta(\sum_{(v-n)} q) \cdot \delta(\sum^{(1)} q - p_1) \ldots \delta(\sum^{(n)} q - p_n)(q_1^2 - m_1^2)^{-1} \ldots (q_l^2 - m_l^2)^{-1} \, dq_1 \ldots dq_l \tag{1}$$

which corresponds to the Feynman graph with l inner lines, $v-n$ inner vertices and n vertices reached by external lines. In eq. (1) the sum of the $\sum_{(i)} q$ type denotes a sum of 4-momenta reaching the i-th inner vertex, while the sum $\sum^{(i)} q$ is a sum of inner 4-momenta reaching the i-th external vertex. We shall call the external vertices *poles* † and consequently call the graphs with $n = 2$ *two-poles*, with $n = 3$ *three-poles*, and with $n = 4$ *four-poles*. Let us make a substitution in integral (1):

$$(q_1^2 - m_1^2)^{-1} \ldots (q_l^2 - m_l^2)^{-1} = (l-1)! \int f^{-l} \delta(\alpha_1 + \ldots + \alpha_l - 1) d\alpha_1 \ldots d\alpha_l, \tag{2}$$

where

$$f = \alpha_1(q_1^2 - m_1^2) + \ldots + \alpha_l(q_l^2 - m_l^2).$$

According to Landau, the singularity of the function $F(p)$ corresponds to such values $p_i^0 (i = 1, \ldots, n)$ as would be solutions of the following set of equations:

† This term is not misleading since all the singularities considered below are branching points and not poles.

$$\sum_{(i)} q = 0 \quad (i = 1, \ldots, v-n), \tag{A.1}$$

$$\sum_{(i)} q = p_i \quad (i = 1, \ldots, n), \tag{A.2}$$

$$\sum \alpha = 1, \tag{A.3}$$

$$q_i^2 = m_i^2 \quad (i = 1, \ldots, l), \tag{A.4}$$

$$\sum_{\langle i \rangle} \alpha q = 0 \quad (i = 1, \ldots, k). \tag{A.5}$$

The singularity of the function F_p has the form

$$[(p/p_0)^2-1]^\kappa \quad \text{for semi-integer } \kappa,$$

$$[(p/p_0)^2-1]^\kappa \ln [(p/p_0)^2-1] \quad \text{for integer } \kappa,$$

where

$$\kappa = \tfrac{3}{2}(l+1)-2v.$$

Eqs. (A.1) and (A.2) correspond to δ-functions in the numerator of eq. (1) and express the conservation of 4-momentum. The number of the vector equations (A.1) is equal to $v-n$, the number of the vector equations (A.2) is equal to n. Yet one of the equations is trivial, since it expresses the law of conservation of external 4-momenta. Eq. (A.3) corresponds to the δ function in the numerator of eq. (2). As is known, the Feynman parameters α satisfy the condition $\alpha \geqq 0$. Yet in the future we shall be interested only in the solutions of set (A) for which all $\alpha > 0$: we shall correlate the singular point corresponding to the solution with one of the α's equal to 0 ($\alpha_i = 0$) not with the given graph but with the reduced one which is obtained from the given graph by contracting the i-th line to a zero length.

Eqs. (A.4) and (A.5) are conditions for the quantity f in eq. (2) having an extremum with respect to all variables α and q. Indeed, eq. (A.4) follows from the requirement $\partial f/\partial \alpha_i = 0$, while eq. (A.5) follows from the requirement $\partial f/\partial q_m = 0$, if (A.1) and (A.2) are taken into account. In eq. (A.5) $\sum_{\langle i \rangle}$ denotes the summation over the graph lines forming the i-th closed contour. The number of these vector equations is equal to k, the number of independent contours of the graph or, which amounts to the same, the number of independent integrations in integral (1). Taking into account that l variables of the integration q satisfy $v-1$ conditions (one δ-function being responsible for the conservation of external 4-momenta) we shall have

$$k = l-v+1. \tag{3}$$

This formula is closely connected with the well-known Euler formula expressing the number of the faces of the polyhedron by the number of its edges and vertices.

Below, we investigate the set (A) to find when the set has a solution and how it can be obtained. In sections 2, 3 and 4, we shall consider the graphs with $n = 2$, $n = 3$ and $n = 4$, respectively. Sect. 5 will be concerned with the problems connected with the pseudo-euclidian nature of the 4-vector of energy-momentum and the positiveness of the Feynman parameters α. In the appendices the singularities of the vertex parts and of the simplest four-poles are investigated.

2. Two Poles

CONDITION OF SOLUBILITY OF SET (A) FOR TWO-POLES

Two-poles may represent the singularities of the Green's function (in this case one external line reaches each pole), of the vertex part (two external lines reach one pole and one the other), of the scattering amplitude (two external lines reaching each pole) and so on. Yet in all these cases only the sum of external four-momenta reaching the given pole is of significance. In the following, therefore, we shall consider the two-poles corresponding to Green's functions (as in fig. 1). Let us designate the external 4-momentum reaching pole 1 as p_1

Fig. 1.

and the 4-momentum reaching pole 2 as p_2. The conservation law gives

$$p_1+p_2 = 0 \tag{4}$$

and consequently both 4-vectors lie in one line. Selecting a coordinate system such that the direction of this line coincides with one of the coordinate axes, we see that the two-pole is described by one external parameter, p_1^2, for example.

The number of vector equations (A.1), (A.2) and (A.5) is equal to l, i.e. the number of the unknown vectors q. Therefore, these equations uniquely determine q through p (and scalar quantities α), whence it follows that q should lie in the same line as vectors p_1 and p_2. This fact greatly simplifies an analysis of set (A).

The total number of unknowns (p, q and α) in set (A) is equal to $2l+1$, since the vectors p and q are one-dimensional. The complete number of equations of set (A) is also equal to $2l+1$. Thus, the complete number of equations is equal to the number of unknowns, and set (A) may in general be solved. Yet the unknowns q and α are not equivalent: the former enter all equations except (A.3), while the latter enter only equations (A.3) and (A.5). It may thus turn

out that the number of the unknowns α exceeds the number of the equations from which these α may be determined, and the number of equations for q and p exceeds the number of these vectors. This will lead to the occurrence, among the masses of intermediate particles entering eq. (A.4), of relations contradicting in general the condition of stability of the intermediate particles.

Let us determine the conditions under which set (A) may be solved with respect to p and q as well as α.

The number of equations (A.3) and (A.5) for α is equal to $k+1 = l-v+2$, while the number of α is equal to l. Hence it follows that the number of α which remain indeterminate is equal to

$$\Delta = v-2. \tag{5}$$

The number of equations of (A.1), (A.2) and (A.4) for q and p is equal to $l+v-1$, while the number of vectors of q and p is equal to $l+1$. The number of vectors q and p which remain indeterminate is equal

$$s = 2-v. \tag{6}$$

From the definition of the two-pole it follows that $v \geqq n = 2$. If $v = 2$, $\Delta = s = 0$ and the set has always a solution. If $v > 2$, $\Delta = -s > 0$, and we cannot determine all unknown α from set (A). We are able, therefore, to put some of these α equal to zero, thus reducing the graph. Therefore, the only category of two-poles which have singularities corresponds to the graphs

Fig. 2.

with $v = 2$ and an arbitrary l (as in fig. 2). The graphs with $v > 2$ (as in fig. 3a, for example) contain no singularities.

The two-poles of the 3b type should be singled out as an exception. For these

Fig. 3a.

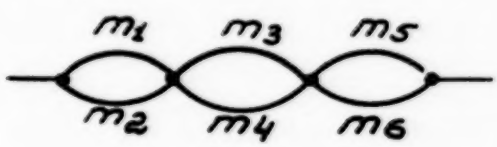

Fig. 3b.

two-poles $v > 2$. Yet no relations contradicting the stability of virtual particles arise if such a two-pole describes, for example, a succession of scattering processes of two particles on each other ($m_1 = m_3 = m_5$, $m_2 = m_4 = m_6$). It is evident, however, that the singular points of graph 3b and of the arbitrary loop of this graph coincide.

The location of the singularity of the two-pole with $v = 2$ is easily determined if one takes into account that all vectors p and q are one-dimensional; the singularity corresponds to the value p^2 equal to $p_0^2 = (\sum_{i=1}^{l} m_i)^2$ where summation is carried out with respect to all virtual particles.

3. Three Poles

3.1. CONDITION OF SOLUBILITY OF SET (A) FOR THREE-POLES

Three-poles may contain singularities of both vertex parts and more complex amplitudes when more than one external line reaches some of the poles. Yet only the total external 4-momentum reaching the pole is of significance, just as for two-poles. Therefore we shall consider the three-poles corresponding

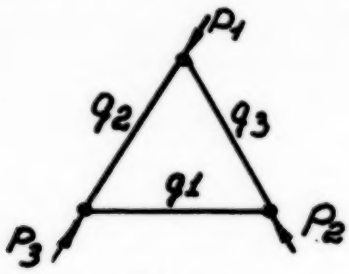

Fig. 4a.

to the vertex parts (as in fig. 4a). The external 4-momenta satisfy the conservation law

$$p_1+p_2+p_3 = 0 \tag{7}$$

and consequently lie in one plane. It is easy to see that this system of vectors is described by three parameters. We select p_1^2, p_2^2, p_3^2 as such external parameters describing the three-pole.

Expressing the vectors q through p with the aid of eqs. (A.1), (A.2) and (A.5) we come to the conclusion that all vectors q lie in the same plane as the vectors p and consequently are two-dimensional.

Let us determine the conditions under which set (A) may be solved for a three-pole with respect to p and q as well as α. In virtue of the vectors q being two-dimensional the complete number of equations (A.3) and (A.5) is equal to $2k+1 = 2l-2v+3$. The number of the unknowns α is equal to l. Hence the number of α which remain indeterminate is equal to

$$\Delta = -l+2v-3. \tag{8}$$

The number of eqs. (A.1), (A.2) and (A.4) for q and p is equal to $2(v-1)+l$. The number of external parameters and components of the vectors q is equal to $2l+3$. The number of them remaining indeterminate is equal to

$$s = l-2v+5. \tag{9}$$

Since $\Delta+s=2$ for a three-pole, at least two quantities remain indeterminate in the solution of set (A). We shall call the set (A) *normal* if two external parameters may be selected for these arbitrary quantities. This means that the conditions $s \geqq 2$ and $\Delta \leqq 0$ should be fulfilled. Below we shall see that these conditions are necessary yet not sufficient to solve set (A).

3.2. SCHEMES OF THREE-POLES

Let us make a more detailed analysis of set (A.1), (A.2) and (A.4) serving to determine q and p only. It is convenient to make this analysis by using the graphic method proposed by Karplus, Sommerfield and Wichman [20]) and by Landau [21]). Let us correlate each vertex of the Feynman graph with a closed contour consisting of the vectors q and p, in accordance with eqs. (A.1) and (A.2), the length of the i-th line corresponding to the vector q_i being selected equal to m_i, according to (A.4). Following Landau we shall call the figure thus obtained a scheme. The scheme corresponding to the graph of fig. 4a is represented in fig. 4b. It is clear from this scheme that assigning p_2^2 and p_3^2 with

Fig. 4b.

given m_1, m_2 and m_3 we uniquely obtain the value p_1^2 corresponding to the singularity. This corresponds to the value s for the three pole of fig. 4a being equal to 2, according to eq. (9). The presence of two arbitrary external parameters corresponds to the fact that if no external momenta are represented in the scheme, the figure thus obtained (which we shall also call a scheme) will

Fig. 4c.

have two degrees of freedom (the angles φ_1 and φ_2 in fig. 4c). Thus the simplest example shows that the quantity s coincides with the number of degrees of freedom of the scheme †.

† K. A. Ter-Martirosyan drew the authors' attention to the significance of the concept of degrees of freedom of a scheme.

3.3. MORE COMPLEX GRAPHS AND THE METHOD OF DRAWING UP SCHEMES

Let us see how the number of degrees of freedom changes when the Feynman graph becomes more complex. This complication may be achieved if an internal line is added to the given graph. The added line may link a) two lines, b) a line and a vertex, and c) two vertices. It is easy to see that these possibilities correspond to a) $\Delta l = 3$, $\Delta v = 2$, b) $\Delta l = 2$, $\Delta v = 1$, and c) $\Delta l = 1$, $\Delta v = 0$. According to eq. (9) the quantity s changes in the following way: a) $\Delta s = -1$, b) $\Delta s = 0$, and c) $\Delta s = +1$. By way of illustration let us take a sequential complication of the simplest three-pole (figs. 5, 6 and 7). It can easily be seen

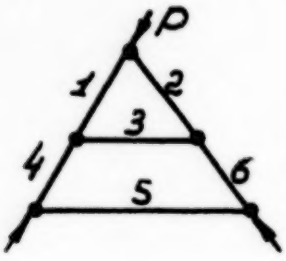

Fig. 5a.

Fig. 5b.

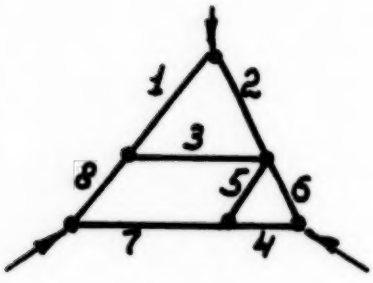

Fig. 6a.

Fig. 6b.

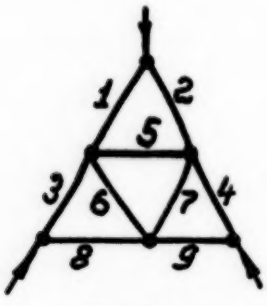

Fig. 7a.

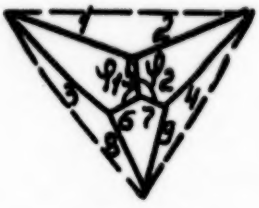

Fig. 7b.

that scheme 5b corresponding to graph 5a has one degree of freedom (the angle φ). Scheme 6b corresponding to graph 6a has also one degree of freedom. Scheme 7b corresponding to graph 7a has two degrees of freedom (the angles φ_1 and φ_2, for example).

It is obvious that it is easy to obtain a graph with any s by complicating a simple graph.

In drawing the schemes for complex graphs it is convenient to employ a method suggested by Smorodinsky †. According to this method we put a point inside each external and internal region of the Feynman graph. (The three-pole has three external regions separated by external lines.) Let us connect these points by lines, each of which crosses only one internal line of the Feynman graph and has a length equal to the mass of the line it crosses. It is easy to see (see figs. 4—7) that thereby we shall obtain the scheme corresponding to the graph in question.

This method, however, cannot be directly applied to the graphs that contain superposed lines having no common vertices. Let us consider, for example, graph 8a. If we correlate each vertex of this graph with the triangle describing the conservation of 4-momentum (eqs. (A.1) and (A.2)) it will turn out that lines 5 and 6 repeat themselves twice on scheme 8b thus obtained. It can easily

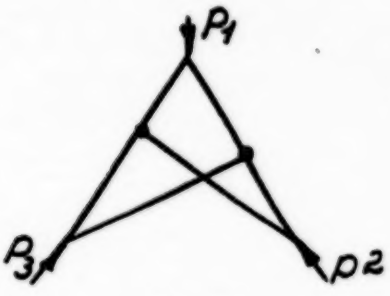

Fig. 8a.

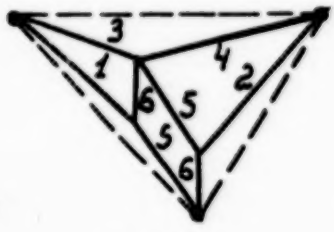

Fig. 8b.

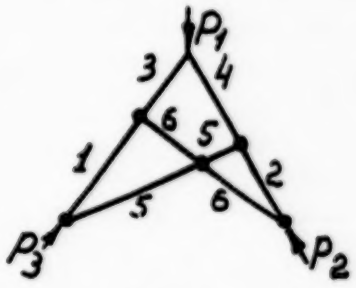

Fig. 8c.

be seen that scheme 8b coincides with the scheme for graph 8c which contains scattering of particle 5 on particle 6 ††. This agrees with the fact that if the superposition of two lines in the graph is replaced by their crossing the number of degrees of freedom of the scheme will not change. Indeed, $\Delta l = 2$, $\Delta v = 1$ and $\Delta s = 0$, according to eq. (9).

The following rule may be formulated for the general case: to determine the location of the singularity corresponding to the Feynman three-pole graph with superposition of lines, this graph should be replaced by the one with the crossing of lines and a scheme should be drawn for the latter.

3.4. SYMMETRICAL THREE-POLES

Hitherto we have been considering the three-poles which have no symmetry. Now let us consider the three-poles whose squares of two external 4-momenta are equal ($p_2^2 = p_3^2$) and the masses of virtual particles situated symmetrically with respect to the momentum p_1 are equal in pairs. These three-poles are symmetrical with respect to the axis passing through p_1.

The expression for the degree of freedom of the scheme corresponding to the symmetrical three-pole differs from eq. (9).

† Y. A. Smorodinsky, private communication.

†† It will be noted that graph 8c is a particular case of graph 6a if in the latter $m_2 = m_5$ and $m_3 = m_6$.

Let us designate the number of the graph vertices lying on the axis of symmetry by v_0 and the number of lines lying on the axis of symmetry or crossing it by l_0. The total number of the unknown projections of the vectors q is equal to $l_0+l-l_0 = l$, since the vectors corresponding to the lines lying on the axis of symmetry or crossing it have only one projection. The number of external parameters is equal to 2. Similarly, the number of eqs. (A.1) and (A.2) is equal to $v_0+v-v_0-1 = v-1$. The number of equations (A.4) is equal to $l_0+\frac{1}{2}(l-l_0) = \frac{1}{2}(l+l_0)$. Hence the number of degrees of freedom of the symmetrical scheme is equal to

$$s_0 = l+2-(v-1)-\tfrac{1}{2}(l+l_0) = \tfrac{1}{2}(s+1-l_0), \tag{10}$$

where s is the number of degrees of freedom of the relevant non-symmetrical scheme. From eq. (10) it follows that $s_0 = 0$ for symmetrized scheme 5b and $s_0 = 1$ for symmetrized schemes 4b, 6b, 7b, 8b.

It is important to stress that the existence of a singularity of a graph does not depend on its symmetry but is determined by the quantities Δ and s (and not s_0): if a symmetrical graph has $s<2(\Delta>0)$, some af the α could be put equal to zero and such a graph has no singularity.

3.5. REDUCTION OF GRAPHS WITH $s < 2$

Let us correlate the three-pole described by the external parameters p_1^2, p_2^2 and p_3^2 with the space of these parameters $\mathscr{P}$. Then the three-pole with $s = 2$ (see, for example, fig. 4a or 7a) corresponds in general to a certain surface in this space: assigning p_2^2 and p_3^2 we uniquely obtain p_1^2. The three-pole with $s = 1$ corresponds to a certain line in the space $\mathscr{P}$. This line may be flat, as for graph 5a, in which the value p_1^2 does not depend on the values p_2^2 and p_3^2, or skew as for graph 6a. In both cases this line belongs to a certain surface corresponding to the graph with $s = 2$, which is obtained from the given graph with $s = 1$ through reduction. Thus, as a result of the reduction of

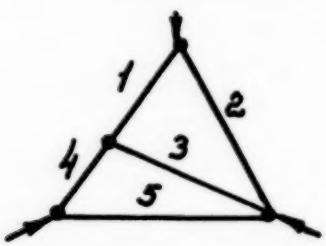

Fig. 9a.

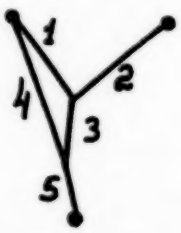

Fig. 9b.

graph 5a, graph 9a is obtained corresponding to scheme 9b having two degrees of freedom and differing from scheme 5b by the absence of line 6 †.

† Graph 5a may be reduced in two ways: contracting either line 6 or line 4. Thus, the line corresponding to graph 5a in the space $\mathscr{P}$ lies at the crossing of the surfaces corresponding to the two reduced graphs. Yet in virtue of the Feynman parameters being positive (see below) only one of the two kinds of reduction mentioned above is possible for the given external parameters p.

Similarly graph 6a is reduced to graph 10a with scheme 10b.

Let us consider graph 11a with $s = 0$ which corresponds to scheme 11b. This graph corresponds to a point in the space $\mathscr{P}$. It is easy to see that by contracting line 9 in the graph 11a we arrive at the graph 6a, the reduction of which has been considered above.

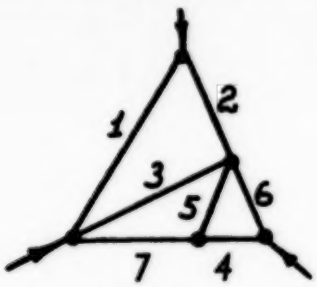

Fig. 10a.

Fig. 10b.

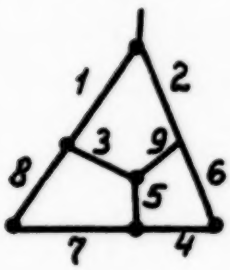

Fig. 11a.

Fig. 11b.

The above-mentioned examples of graphs with $s < 2$ were characterized by the values of their external parameters being fixed. Yet there are graphs with $s < 2$ which in the space $\mathscr{P}$ correspond to surfaces just as graphs with $s = 2$ do. An example of such a graph with $s = 1$ is three-pole 13a. Scheme 13b which

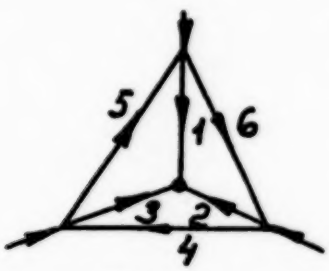

Fig. 12a.

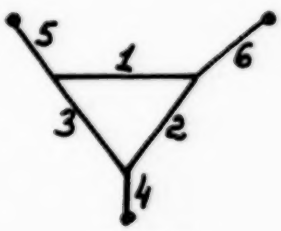

Fig. 12b.

corresponds to it possesses two degrees of freedom (the angles φ_1 and φ_2), yet its internal part is overdeterminate, as is clear from the figure. This means that there is a rigid relation between the masses of virtual particles forming the three central triangles in the scheme. The singularities corresponding to graph 13 belong to a multitude of singularities of the reduced graphs with $s = 2$, which are obtained from graph 13a by contracting one of the lines 1, 2 or 3, or by contracting lines 4, 5 and 6.

Thus we came to the conclusion that to find the location of singularities the graphs with $s < 2$ should not be considered, since their singularities belong to a multitude of singularities corresponding to the reduced graphs with $s = 2$.

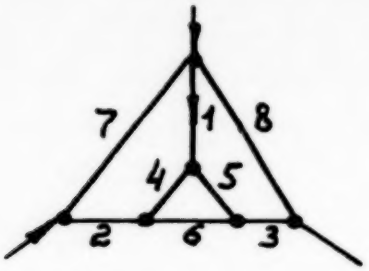

Fig. 13a.

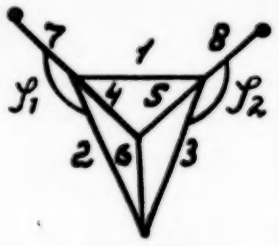

Fig. 13b.

3.6. TAUTENING SCHEMES WITH $s > 2$

Let us consider the graphs whose schemes have $s > 2$. To determine the relation between external parameters in this case it is insufficient to have eqs. (A.1), (A.2) and (A.4) determining the scheme and it is necessary to use eq. (A.5). Since $\Delta + s = 2$ for the three-pole, the condition $s > 2$ means that set of equations (A.5) and (A.3) is overdeterminate with respect to the variables α, precisely to the degree to which the system of equations (A.1), (A.2) and (A.4) is underdeterminate with respect to the variables q and p. This makes it possible to use set (A.5) for obtaining the deficient equations for q and p †.

To make this point clear let us give an example of the simplest graph with $s = 3$ (fig. 12a). The set of equations (A.5) corresponding to this graph has the form

$$\begin{aligned} \alpha_1 q_1 &= \alpha_3 q_3 - \alpha_5 q_5, \\ \alpha_2 q_2 &= \alpha_1 q_1 - \alpha_6 q_6, \\ \alpha_3 q_3 &= \alpha_2 q_2 - \alpha_4 q_4. \end{aligned} \tag{11}$$

Vectorially multiplying the first of these equations by q_5, the second by q_6 and the third by q_4 and multiplying the left and right parts we shall obtain

$$[q_1 q_5][q_2 q_6][q_3 q_4] = [q_3 q_5][q_1 q_6][q_2 q_4]. \tag{12}$$

It is easy to see that condition (12) demands that the continuations of lines 4, 5 and 6 in scheme 12a cross at one point. Taking account of this condition, the number of degrees of freedom of scheme 12b decreases from $s = 3$ to $s = 2$. This decrease of the number of degrees of freedom of a scheme with the aid of eqs. (A.5) will be called the *tautening* of the scheme. By tautening, any scheme with $s > 2$ may be reduced to a scheme with $s \leqq 2$.

† The authors are indebted to L. D. Landau for a discussion contributing to the elucidation of this point.

3.7. AN EXAMPLE OF TAUTENING A SCHEME WITH $s = 2$. ADDITIONAL REMARKS ON INTERNAL OVERDETERMINATENESS

Let us consider graph 14a which corresponds to scheme 14b. It may easily be seen that this scheme for which $s = 2$ is partially overdeterminate, on the one side, and underdeterminate, on the other. Underdeterminateness calls for the tautening of a scheme, i.e., the establishment of the relation among the angles

Fig. 14a.

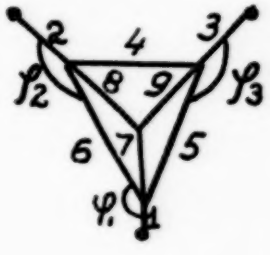

Fig. 14b.

φ_1, φ_2 and φ_3. At first glance it seems impossible to obtain this relation from set (A), since the number of unknowns α is equal to the number of eqs. (A.5) and (A.3), which corresponds to $s = 2$. We shall show, however, that in virtue of the inner overdeterminateness of the scheme eqs. (A.5) for α degenerate and one of α cannot be determined, which gives rise to an additional condition with respect to the vectors q.

Set (A.5) for the graph 14a has the form

$$\begin{aligned} &\alpha_1 q_1 + \alpha_2 q_2 + \alpha_3 q_3 = 0, \\ &\alpha_7 q_7 + \alpha_3 q_3 + \alpha_9 q_9 = 0; \end{aligned} \tag{13}$$

$$\begin{aligned} &\alpha_4 q_4 + \alpha_8 q_8 - \alpha_5 q_5 - \alpha_9 q_9 = 0, \\ &\alpha_4 q_4 - \alpha_2 q_2 - \alpha_6 q_6 + \alpha_8 q_8 = 0. \end{aligned} \tag{14}$$

From eqs. (13) it follows that

$$\begin{aligned} &\alpha_2 = -\alpha_1 \frac{[q_1 q_3]}{[q_2 q_3]}, \quad \alpha_3 = -\alpha_1 \frac{[q_1 q_2]}{[q_3 q_2]}, \\ &\alpha_8 = -\alpha_7 \frac{[q_7 q_9]}{[q_8 q_9]}, \quad \alpha_9 = -\alpha_7 \frac{[q_7 q_8]}{[q_9 q_8]}. \end{aligned} \tag{15}$$

Solving each of eqs. (14) with respect to α_4 and equalizing the solutions thus obtained we have

$$\alpha_2 \frac{[q_2 q_6]}{[q_4 q_6]} - \alpha_8 \frac{[q_8 q_6]}{[q_4 q_6]} = -\alpha_3 \frac{[q_3 q_5]}{[q_4 q_5]} + \alpha_9 \frac{[q_9 q_5]}{[q_4 q_5]}. \tag{16}$$

Substituting the expressions for α from (15) into (16) we obtain

$$\alpha_1\left\{\frac{[q_1q_3]}{[q_2q_3]}\frac{[q_2q_6]}{[q_4q_6]}+\frac{[q_1q_2]}{[q_3q_2]}\frac{[q_3q_5]}{[q_4q_5]}\right\}=\alpha_7\left\{\frac{[q_7q_9]}{[q_8q_9]}\frac{[q_8q_6]}{[q_4q_6]}+\frac{[q_7q_8]}{[q_9q_8]}\frac{[q_9q_5]}{[q_4q_5]}\right\}. \quad (17)$$

It will be noted that the denominators of the two addends in brackets for α_7 are equal to each other in virtue of the condition $q_4+q_5+q_6=0$. Considering the numerator in the coefficient of α_7 it is easy to see that it is equal to 0, since lines 7, 8 and 9 in the scheme 14b cross at one point and pass through the vertices of the triangle formed by lines 4, 5 and 6. Since $\alpha_1 \neq 0$ we obtain the following condition:

$$[q_1q_3][q_2q_6]+[q_1q_2][q_3q_5]=0. \quad (18)$$

This condition requires that the continuation of lines 1, 2 and 3 in the scheme cross at one point and be the wanted condition for the tautening of the scheme 14^b.

The above-mentioned examples have shown that the quantity s is insufficient for a complete description of a graph since inner overdeterminateness is highly essential. Being a local property of the graph the latter cannot be detected with the aid of computation of the number of lines and vertices of the graph. From the above-mentioned examples it follows that the simplest method of detecting inner overdeterminateness is an analysis of the scheme in question.

Fig. 15a.

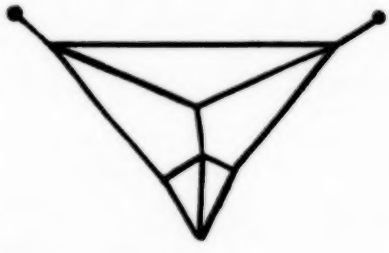

Fig. 15b.

It will be noted that in this analysis the internally overdeterminate schemes should not be confused with the schemes that cannot be drawn only with a rule and compasses. An example of such a scheme and a graph corresponding to it are given in fig. 15b and 15a.

3.8. TWO-POLES IN THREE-POLES

Let us apply the above-considered concepts of tautening and overdeterminateness to the three-pole graphs containing two-poles. These graphs may be divided into three categories.

1. A two-pole is obtained through the insertion into a graph of a line connecting two extreme points of a line (as in fig. 16a). Scheme 16b has $s=3$ (the

angles φ_1, φ_2 and φ_3). Its tautening is trivial if one considers that lines 1 and 2 forming two sides of the two-pole should lie in one straight line (fig. 16c).

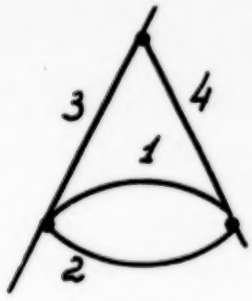

Fig. 16a.

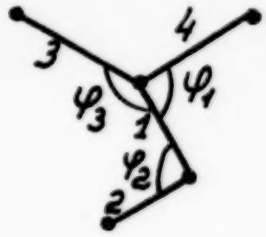

Fig. 16b.

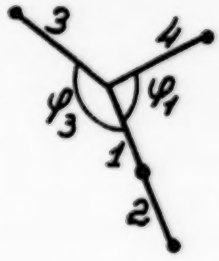

Fig. 16c.

2. A two-pole is obtained through the insertion into a graph of a line connecting the extreme point of a line with its internal point (as in fig. 17a). The graph thus obtained formally has $s = 2$. Yet after the tautening of the corre-

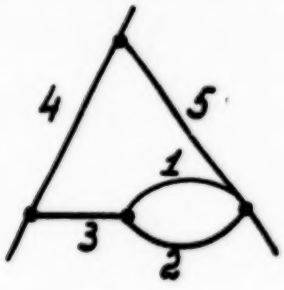

Fig. 17a.

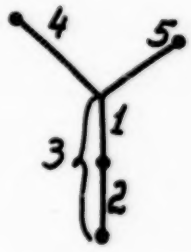

Fig. 17b.

sponding scheme we may see that the graph is internally overdeterminate, the additional relation among the masses of virtual particles 1, 2 and 3 leading to the instability of particle 3 (see fig. 17b).

3. A two-pole is obtained through the insertion into a graph of a line connecting two internal points of a line (as in fig. 18a). The graph thus obtained for-

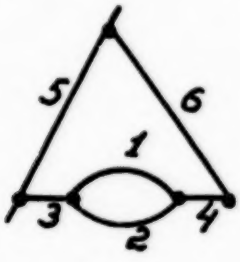

Fig. 18a.

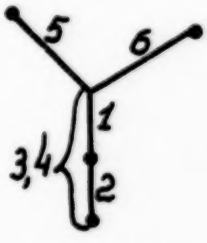

Fig. 18b.

mally has $s = 1$. After the tautening of the relevant scheme we can see that it is twice internally overdeterminate, this overdeterminateness leading to the instability of particles 3 and 4.

Thus, when determining the singular points we should exclude the graphs of category 2 and 3, because they are overdetermined.

4. Four-Poles

4.1. CONDITION OF SOLUBILITY OF SET (A)

Four-poles are characterized by four external 4-momenta. In virtue of the conservation law,

$$p_1+p_2+p_3+p_4 = 0. \tag{19}$$

Hence it follows that the momenta p_1, p_2, p_3, p_4 lie in a space of three dimensions and may be characterized by six parameters. In virtue of this and taking into account that the vectors q are also three-dimensional it is easy to obtain the expression for the number of degrees of freedom of the four-pole scheme, just as was done for two-poles and three-poles:

$$s = 2l-3v+9. \tag{20}$$

The number of the parameters α which are not determined by eqs. (A.3) and (A.5) is given by the relation

$$s+\Delta = 5. \tag{21}$$

Hence it follows that the condition $s \geqq 5$ should hold if eqs. (A.3) and (A.5) are to be solved with respect to α. We shall call a four-pole normal if five external parameters can be chosen as five independent parameters (the sixth external parameter being uniquely determined by set (A)). Usually we shall select quantities p_1^2, p_2^2, p_3^2, p_4^2 and the quantity of $(p_1+p_2)^2$ type as given external parameters.

4.2. COMPLICATION OF FOUR-POLES AND CONSTRUCTION OF SCHEMES

It can easily be seen that the simplest four-pole graph (fig. 19a) has $s = 5$. Let us see how s will change when the graph is complicated by adding new lines.

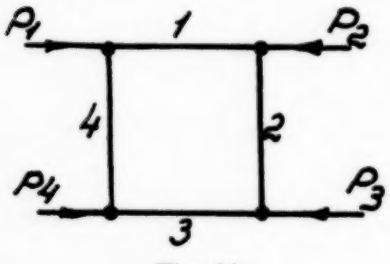

Fig. 19a.

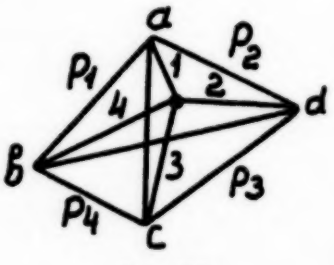

Fig. 19b.

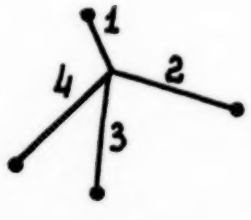

Fig. 19c.

From eq. (20) it follows that if the added line connects two lines, $\Delta s = 0$. If it connects a line and a vertex $\Delta s = 1$. And if it connects two vertices, $\Delta s = 2$. Thus we see that unlike three-poles, the complication of four-poles may only increase s, the number of degrees of freedom of the scheme.

In the case of four-poles the vectors q have three dimensions and therefore the schemes of four-poles are not two-dimensional but three-dimensional. It is

conventient to draw these schemes in the following manner. First a point is put inside each region of the Feynman graph. Then all points are connected, as was done for three-poles. The "hinged lattice" thus obtained, however, is not in general flat, unlike the three-pole schemes. In drawing the scheme we have used the values of four external parameters out of the six: the squares of external 4-momenta. If we now assign the fifth external parameter, $(p_1+p_2)^2$, for example, the value of the sixth external parameter $(p_1+p_4)^2$ is determined uniquely. In scheme 19b of graph 19a this will correspond to the assignment of the length bd, the length ac being determined uniquely.

To determine the number of degrees of freedom of the scheme it is convenient to represent the scheme without the lines corresponding to the external parameters. For graph 19a such a scheme will have the form of 19c. In scheme 19c the relative location of lines 1 and 2 is described by one angle, while the location of each of lines 3 and 4 with respect to plane 1, 2 by two angles. Thus scheme 19c has five degrees of freedom which agree with eq. (20).

4.3. TAUTENING FOUR-POLES

For the four-pole with $s > 5$ eqs. (A.5) make it possible to decrease the real number of degrees of freedom to 5. As in the case of three poles this corresponds to the tautening of the scheme. Let us show how the tautening is done taking

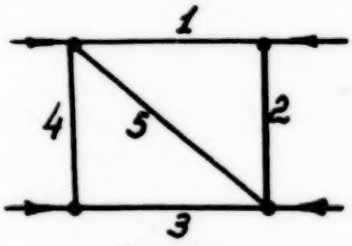

Fig. 20a.

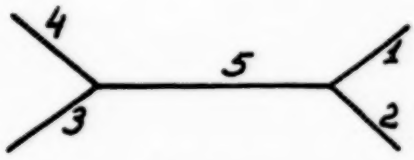

Fig. 20b.

scheme 20b corresponding to graph 20a which has seven degrees of freedom. From eqs. $\sum \alpha q = 0$ written for each of the two internal contours of graph 20a it follows that in scheme 20b vector 5 should lie in the plane of vectors 1 and 2, on the one side, and in the plane of vectors 3 and 4, on the other. As may easily be checked these two conditions decrease the number of degrees of freedom of scheme 20b to five.

4.4. PARTIAL OVERDETERMINATENESS OF FOUR-POLES

It has been established above that $s \geqq 5$ for four-poles. Yet four-poles, just as three-poles, may contain partial overdeterminateness which leads to the real number of degrees of freedom of the four-pole scheme being less than five. This partial overdeterminateness stems from some part of the four-pole graph being a two-pole or a three-pole. The first of these possibilities will not be considered, since it does not practically differ from the above-discussed case of three-poles containing two-poles. An example of partial overdeterminateness

caused by a three-pole is graph 21a. For this graph the value p_1^2 cannot be assigned arbitrarily, since this value is uniquely determined by the masses of virtual particles 1, 2, 3, 4 and 5. This can easily be seen from scheme 21b in which triangles 243 and 135 lie in the same plane. (The fact that lines 1, 2

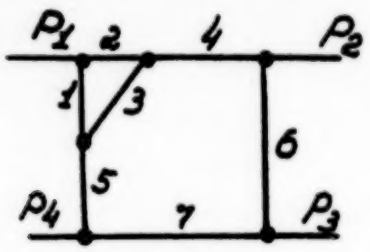

Fig. 21a.

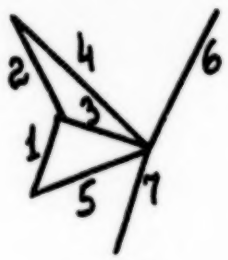

Fig. 21b.

and 3 lie in the same plane follows from the equation $\sum \alpha q = 0$ for triangle contour 1, 2, 3 in the graph.) The latter also shows that the number of degrees of freedom of scheme 21b is equal to four.

5. Using Schemes for Calculating the Location of Singularities

5.1. SCHEME METRICS †

To investigate the general properties of a scheme (the number of degrees of freedom, the presence of local overdeterminateness, etc.) it was sufficient to consider it without the lines corresponding to external momenta. Yet to locate a singularity with the aid of a scheme it is necessary to draw it with these lines. Let us analyse when such a scheme may be drawn on a euclidian plane and in euclidian space.

For two-poles the problem of scheme metrics does not arise, for all vectors p and q are one-dimensional in virtue of condition (4) and set of equations (A).

The situation is more complex for three-poles. The vectors p and q lie in a plane, one axis of which is the axis of energy (p_0, q_0) and the other is the axis of spacial momentum (p_x and q_x, for example). We shall consider that the squares of external 4-momenta p are real and positive, and we shall confine ourselves to the case of real energy E. Then from the definitions $p_1^2 = E_1^2 - \vec{p}_1^2$, $p_2^2 = E_2^2 - \vec{p}_2^2$, $p_3^2 = E_2^2 - \vec{p}_3^2$ it follows that none of the values p and E can be complex: each of them is either real or purely imaginary. Introduce the notations $\sqrt{p_1^2} = M_1$, $\sqrt{p_2^2} = M_2$, $\sqrt{p_3^2} = M_3$ and call M_1, M_2 and M_3 the "masses" of the external particles.

Then two cases are possible:

Case I: *Euclidian scheme.* Let a spatial component of an external momentum be purely imaginary. In virtue of condition (7) the spatial components of the two other external momenta are purely imaginary as well. Yet the pseudo-

† The authors are indebted to V. N. Gribov for discussion which contributed to the elucidation of a number of problems touched upon in the present section.

euclidian vectors p_1, p_2 and p_3, each with one purely imaginary spatial component, are in fact euclidian vectors with real components. It follows from condition (7) that

$$M_1 \leqq M_2+M_3, \quad M_2 \leqq M_1+M_3, \quad M_3 \leqq M_1+M_2. \tag{22}$$

These inequalities physically denote the "stability" of external particles. From set (A) it follows that the spatial components of the vectors q are purely imaginary as well. Thus, in this case, it is possible in principle to draw a scheme on an Euclidian plane, made up of the vectors p and q with purely real components. With the aid of this scheme it is possible to determine directly the location of a singularity if it exists.

Case II: *Pseudo-euclidian scheme.* Let the spatial components of an external momentum be real. Then the spatial components of all other momenta p and q are real as well. This means, however, that p and q are truly pseudo-euclidian vectors. Hence it follows that it is impossible to represent directly such a scheme on an euclidian plane. Yet, though purely symbolical the scheme turns out to be rather useful in an analytic solution of set (A).

Let us see what type of a three-pole may correspond to the case of the pseudo-euclidian scheme. We shall confine ourselves to the case of stable intermediate particles. First consider the three-pole which contains at least one internal vertex which is reached by only three lines. If the spatial components of the vectors p and q are real in this case, it is obvious that for any three vectors conforming to the condition of type (7) inequalities (22) do not hold, i.e., one of the three particles in (7) is unstable. Proceeding from the condition of the stability of virtual particles we come to the conclusion that such three-poles cannot possess pseudo-euclidian metrics.

It can easily be seen that if the three-pole has not a single internal vertex reached by only three lines, this three-pole may possess both euclidian and non-euclidian metrics (see fig. 4a, for example). It should be emphasized that the scheme of any given three-pole should be either completely pseudo-euclidian or completely euclidian.

In the case of a four-pole the situation becomes still more complex. As a rule the schemes of four-poles have parts with pseudo-euclidian metrics and those with euclidian metrics. In Appendix 2 we shall give several examples to illustrate how the schemes of four-poles may be used to simplify the finding of the location of singularities.

5.2. ACCOUNT OF THE POSITIVENESS OF PARAMETERS α

By their definition the Feynman parameters α are positive. Taking into account that α is positive decreases the number of the graphs having singularities. The reason is that, as can easily be seen from eqs. (A.5), the positiveness of α imposes additional limitations on the scalar products $q_i q_j$.

For a two-angle contour we have from (A.5)

$$q_1\alpha_1+q_2\alpha_2 = 0. \tag{23}$$

Hence we obtain

$$\begin{aligned} m_1^2\alpha_1+q_1q_2\alpha_1 &= 0, \\ q_1q_2\alpha_1+m_2^2\alpha_2 &= 0. \end{aligned} \tag{24}$$

From α being positive the condition follows

$$q_1q_2 < 0. \tag{25}$$

In fact we have used this condition in tautening the two poles. It means that the vectors q_1 and q_2 in the scheme should be antiparallel.

For the triangular contour,

$$q_1\alpha_1+q_2\alpha_2+q_3\alpha_3 = 0. \tag{26}$$

Hence it follows that

$$\begin{aligned} m_1^2\alpha_1+q_1q_2\alpha_2+q_1q_3\alpha_3 &= 0, \\ q_2q_1\alpha_1+m_2^2\alpha_2+q_2q_3\alpha_3 &= 0, \\ q_3q_1\alpha_1+q_3q_2\alpha_2+m_3^2\alpha_3 &= 0. \end{aligned} \tag{27}$$

It can easily be seen that for this system to have solutions at $\alpha > 0$, it is necessary for at least two of the three scalar products (q_1q_2, q_2q_3, q_3q_1) to be negative. This condition acquires an especially simple interpretation when the given triangular contour enters a three-pole graph which corresponds to the scheme with euclidian metrics. In this case none of the angles between q_1 and q_2, q_2 and q_3, or q_3 and q_1 in the scheme should exceed π.

In the case of a four-angular contour which corresponds to four vectors originating in one point in the scheme, arguments similar to these above should be evolved for the set of equations

$$\begin{aligned} m_1^2\alpha_1+q_1q_2\alpha_2+q_1q_3\alpha_3+q_1q_4\alpha_4 &= 0, \\ q_2q_1\alpha_1+m_2^2\alpha_2+q_2q_3\alpha_3+q_2q_4\alpha_4 &= 0, \\ q_3q_1\alpha_1+q_3q_2\alpha_2+m_3^2\alpha_3+q_3q_4\alpha_4 &= 0, \\ q_4q_1\alpha_1+q_4q_2\alpha_2+q_4q_3\alpha_3+m_4^2\alpha_4 &= 0, \end{aligned} \tag{28}$$

proceeding from the equation

$$q_1\alpha_1+q_2\alpha_2+q_3\alpha_3+q_4\alpha_4 = 0. \tag{29}$$

6. Conclusions

To determine whether the given graph has a singularity it is necessary first of all to establish the number of external vertices (poles) of the graph.

If the number of poles is equal to two, the graph has a singularity only if it has no internal vertices.

If the number of poles is equal to three or four, it is necessary to draw the scheme corresponding to the graph and tauten the scheme if possible. As a result one of two possibilities may occur:

1. The scheme has no overdeterminateness. In this case a singularity may correspond to the graph.

2. The scheme has overdeterminateness. In this case no new singularity corresponds to the graph. All singularities belong to a set of singularities of reduced graphs which have no overdeterminateness. An overdetermined graph of this kind should not, therefore, be considered.

If the above-mentioned analysis discovers that the given graph may have a singularity, the positiveness of the α's should be checked.

If all α are positive, the graph has a singularity and the calculation of its location reduces itself to a purely trigonometrical problem.

The authors are indebted to L. D. Landau for useful discussions and opportunity to see ref. [21]) before it was published, as well as to V. N. Gribov and I. Ya. Pomeranchuk for numerous comments. They are indebted also to R. Karplus, C. Sommerfield and E. Wichmann for sending the preprint of ref. [20]).

Appendix 1

SINGULARITIES OF VERTEX PARTS

Let us consider the vertex parts whose two external particles are free baryons (N, Λ, Σ, Ξ), while the virtual particles are baryons, π-mesons, and K-mesons. Let us confine ourselves to the three-pole graphs which contain no two-poles. We shall consider the four types of three-poles represented in figs. I.1—I.4.

The schemes represented in fig. I.1b—I.4b are formed by the following "elementary" triangles whose sides are equal to the masses of elementary particles:

$$(\pi\mathrm{NN}),\ (\pi\Sigma\Lambda),\ (\pi\Sigma\Sigma),\ (\pi\Xi\Xi),\ (\mathrm{K}\mathrm{N}\Lambda),\ (\mathrm{K}\mathrm{N}\Sigma),\ (\mathrm{K}\Lambda\Xi),\ (\mathrm{K}\Sigma\Xi).$$

It is convenient to write these "elementary" triangles in the following sequence: (123) (345) for scheme I.1b; (123) (345) (567) for scheme I.2b; (123) (345) (567) (789) for scheme I.3b; (123) (345) (567) (789) (9 10 11) for scheme I.4b.

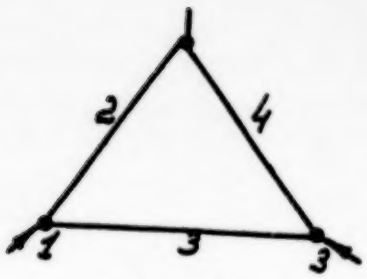

Fig. I. 1a.

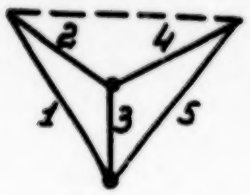

Fig. I. 1b.

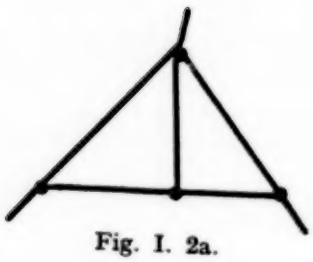

Fig. I. 2a.

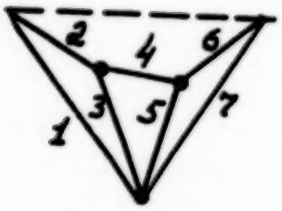

Fig. I. 2b.

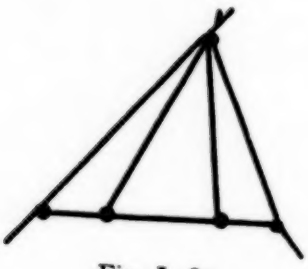

Fig. I. 3a.

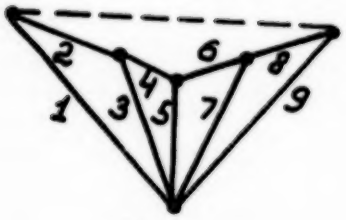

Fig. I. 3b.

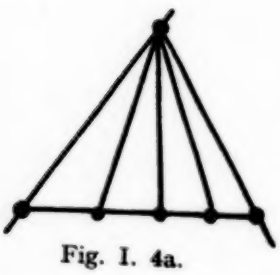

Fig. I. 4a.

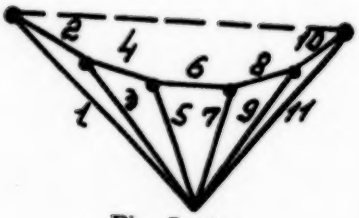

Fig. I. 4b.

The following schemes may exist:

Schemes I.1b

Ten symmetrical schemes (corresponding to electromagnetic baryon form factor): $(\Lambda NK)(KN\Lambda)$, $(\Sigma NK)(KN\Sigma)$, $(\Xi\Lambda K)(K\Lambda\Xi)$, $(\Xi\Sigma K)(K\Sigma\Xi)$, $(\Sigma\pi\Lambda)(\Lambda\pi\Sigma)$, $(\Sigma\Lambda\pi)(\pi\Lambda\Sigma)$, $(\Lambda KN)(NK\Lambda)$, $(\Sigma KN)(NK\Sigma)$, $(\Xi K\Lambda)(\Lambda K\Xi)$, $(\Xi K\Sigma)(\Sigma K\Xi)$.

Twelve asymmetrical schemes: $(\Lambda NK)(KN\Sigma)$, $(\Lambda NK)(K\Lambda\Xi)$ $(\Lambda NK)(K\Sigma\Xi)$, $(\Lambda KN)(NK\Sigma)$, $(\Sigma NK)(K\Lambda\Xi)$; $(\Sigma NK)(K\Sigma\Xi)$, $(\Xi\Lambda K)(K\Sigma\Xi)$, $(\Sigma\pi\Lambda)(\Lambda K\Xi)$, $(\Sigma\Lambda\pi)(\pi NN)$, $(\Sigma\pi\Lambda)(\Lambda KN)$, $(N\pi N)(N\Lambda K)$, $(\Xi K\Sigma)(\Sigma\pi\Sigma)$.

Schemes I.2b

Three symmetrical schemes (corresponding to electromagnetic baryon-form factor):

$$(\Sigma KN)(N\pi N)(NK\Sigma),\ (\Lambda KN)(N\pi N)(NK\Lambda),\ (\Xi K\Sigma)(\Sigma\pi\Sigma)(\Sigma K\Xi).$$

Four asymmetrical schemes: $(\Sigma KN)(N\pi N)(NK\Lambda)$, $(\Sigma\pi\Lambda)(\Lambda KN)(N\pi N)$, $(\Sigma\pi\Lambda)(\Lambda KN)(NK\Lambda)$, $(\Sigma\pi\Lambda)(\Lambda KN)(NK\Sigma)$.

Schemes I.3b

One symmetrical scheme (electromagnetic form-factor of Σ^- particle):

$$(\Sigma\pi\Lambda)(\Lambda KN)(NK\Lambda)(\Lambda\pi\Sigma).$$

Two asymmetrical schemes:

$$(\Lambda KN)(N\pi N)(NK\Lambda)(\Lambda\pi\Sigma),\ (\Sigma KN)(N\pi N)(NK\Lambda)(\Lambda\pi\Sigma).$$

Schemes I.4b

There is only one symmetrical scheme:

$$(\Sigma\pi\Lambda)(\Lambda KN)(N\pi N)(NK\Lambda)(\Lambda\pi\Sigma).$$

The schemes of these three-poles have been found with a set of "elementary" triangles made of plexiglass. Table 1† shows the magnitudes of the angles in the "elementary" triangles forming schemes I.1b—I.4b. The following values of the masses of elementary particles (in MeV) are used:

$m_{\pi^\pm} = 139.63 \pm 0.06$, $m_{\pi^0} = 135.04 \pm 0.16$;
$m_{K^\pm} = 494.0 \pm 0.20$, $m_{K^0} = 498 \pm 1$;
$m_p = 938.213 \pm 0.01$, $m_n = 939.506 \pm 0.01$;
$m_\Lambda = 115.2 \pm 0.13$;
$m_{\Sigma^+} = 1189.3 \pm 0.35$, $m_{\Sigma^-} = 1196.4 \pm 0.5$, $m_{\Sigma^0} = 1190^{+0.9}_{-1.9}$;
$m_{\bar{\Xi}^0} = 1321 \pm 3.5$.

† The authors are indebted to S. A. Nemirovskaya for preparing this table.

TABLE 1

Triangle			Angle φ_{12}			Angle φ_{23}			Angle φ_{31}		
1	2	3	max	optim	min	max	optim	min	max	optim	min
p	p	π^0	8°15′49″	8°15′14″	8°14′39″	85°53′11″	85°52′24″	85°51′36″	85°53′11″	85°52′21″	85°51′36″
p	n	π^+	8 31 57	8 31 42	8 31 1	85 13 58	85 12 31	85 11 50	86 16 29	86 15 52	86 15 17
n	n	π^0	8 15 07	8 14 33	8 13 57	85 53 30	85 53 09	85 51 55	85 53 30	85 52 42	85 51 55
Σ^+	Σ^+	π^0	6 31 07	6 30 33	6 29 38	87 02 46	86 44 43	86 26 42	87 02 46	86 44 43	86 26 42
Σ^+	Σ^0	π^+	6 44 15	6 43 44	6 43 79	87 16 12	86 20 56	85 50 11	87 26 15	86 55 20	85 59 51
Σ^-	Σ^0	π^-	6 42 28	6 42 04	6 41 44	90 15 37	89 16 17	88 42 03	84 36 00	84 01 50	83 02 36
Σ^-	Σ^-	π^0	6 28 47	6 28 14	6 27 37	87 11 34	86 45 53	86 20 16	87 11 34	86 45 53	86 20 16
Σ^0	Σ^0	π^0	6 31 25	6 30 21	6 29 34	87 56 15	86 44 49	85 33 29	87 56 15	86 44 19	85 33 29
Ξ^-	Ξ^-	π^0	5 52 55	5 52 35	5 50 14	90 02 54	87 04 12	84 06 22	90 02 54	87 04 12	84 06 22
Ξ^-	Ξ^0	π^-	6 04 41	6 03 31	6 02 26	89 50 46	86 58 13	84 06 16	89 50 48	86 58 13	84 06 16
Ξ^0	Ξ^0	π^0	5 52 55	5 51 35	5 50 14	90 02 44	87 04 12	84 06 22	90 02 54	87 06 45	84 06 22
Σ^0	Λ^0	π^0	5 39 58	5 35 40	5 33 21	121 23 19	120 47 36	119 40 56	54 33 59	53 36 45	53 08 15
Σ^+	Λ^0	π^+	5 54 05	5 53 34	5 52 43	119 19 00	119 03 34	118 48 10	55 15 39	55 03 01	54 50 21
Σ^-	Λ^0	π^-	5 39 11	5 38 12	5 37 06	123 02 25	122 41 27	122 20 35	51 57 43	51 40 21	51 22 54
p	k^+	Λ^0	97 26 07	97 23 60	97 21 56	56 33 13	56 32 31	56 31 48	26 04 28	26 03 29	26 02 29
n	k^0	Λ^0	97 02 47	97 01 47	96 50 33	56 45 04	56 45 02	56 44 59	26 22 47	26 18 50	26 14 53
p	Σ^+	k^0	23 34 12	23 29 30	23 24 46	48 40 01	48 40 29	48 40 18	107 59 26	107 50 01	107 40 40
n	Σ^-	k^+	22 59 27	22 57 23	22 55 19	47 55 57	47 52 58	47 49 59	109 15 41	109 09 38	109 03 37
n	Σ^0	k^0	23 37 51	23 29 14	23 23 07	48 55 42	48 45 12	48 41 21	108 00 01	107 45 33	107 22 04
p	Σ^0	k^+	23 17 53	23 12 47	23 09 13	48 39 08	48 26 44	48 21 03	108 30 11	108 20 59	108 02 01
Λ^0	Ξ^0	k^0	21 41 22	21 32 01	21 22 36	55 39 16	55 19 23	54 54 29	103 46 29	103 11 08	102 36 05
Λ^0	Ξ^-	k^+	21 26 12	21 19 21	21 12 26	55 34 11	55 10 16	54 46 19	104 02 07	103 30 21	102 58 48
Σ^+	Ξ^0	k^+	21 58 47	21 53 50	21 48 50	64 17 40	63 52 38	63 27 38	94 43 54	94 13 31	93 43 14
Σ^-	Ξ^0	k^-	21 59 58	21 55 11	21 50 23	65 08 14	64 42 11	64 16 09	93 53 51	93 22 38	92 51 31
Σ^0	Ξ^-	k^+	21 58 37	21 53 59	21 49 08	64 26 22	63 57 33	63 21 44	94 50 02	94 08 28	93 34 17
Σ^0	Ξ^0	k^0	22 12 32	22 05 34	21 58 24	64 27 44	63 59 29	63 24 27	94 38 55	193 54 55	93 18 24

Using the values of the angles adduced in table 1 it is easy to obtain the location of the singularity for any concrete graph of type I.1a—I.4a.

In conclusion it will be noted that in the combinations (NKΛ) ($\Lambda\pi\Sigma$), (NπN)(NKΛ) and ($\Sigma\pi\Sigma$)(ΣKΞ) the lines π and K are almost parallel to each other. Hence it follows that the singular points of these three-poles practically coincide with the singular point of the two-pole with K and π mesons as virtual particles. This coincidence is noteworthy in itself.

Appendix 2

SINGULARITIES OF FOUR-POLES

As an example let us show how the location of the singularity is found for the simplest four-pole corresponding to nucleon-nucleon scattering (fig. II.1). The scheme corresponding to it is given in fig. II.2. Here the length DE is equal to

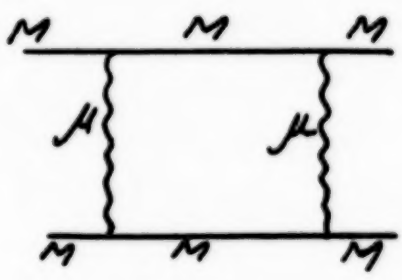

Fig. II, 1.

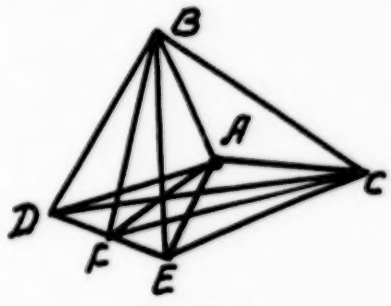

Fig. II, 2.

W, the total energy of two nucleons in the system of their centre of mass, the length BC is equal to the momentum transfer q; the lengths AB and AC are equal to the mass μ of π-meson, and the lengths BD, BE, AD, AE, CD, CE are equal to the mass of the nucleon M. It can easily be seen that the scheme of fig. II.2 for $W > 2M$ is purely conventional since the triangles DBE, DAE and DCE are pseudo-euclidian, and the angles BFA and CFA which we shall designate as φ in the following are purely imaginary. If r denotes the length of BF, AF and CF, it is evident that $r^2 = M^2 - \frac{1}{4}W^2 = M^2 - E_N^2 = -\mathbf{p}^2 < 0$; where $\mathbf{p}$ is the three-dimensional momentum of a nucleon in the centre-of-mass system. It is easy to obtain from the scheme that the value of the momentum transfer corresponding to the singularity † is equal to

$$q^2 = 2\mathbf{p}^2(\mathrm{ch}\, 2\varphi - 1), \quad \text{where} \quad \mathrm{ch}\, \varphi = 1 + \frac{\mu^2}{2\mathbf{p}^2}, \tag{II.1}$$

i.e.

$$q^2 = 4\mu^2 + \frac{\mu^4}{\mathbf{p}^2}. \tag{II.2}$$

† This singularity proves to be highly essential in an analysis of peripheral nucleon interaction [8])

It is easy to check that the condition $\alpha > 0$ leads to graph II.1 having no singularities when $W < 2M$ (which corresponds to $\mathbf{p}^2 < 0$).

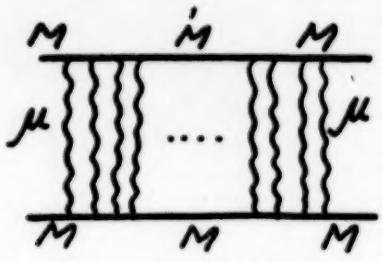

Fig. II, 3.

Similarly for the graph with n virtual π-mesons (fig. II.3) it is easy to obtain

$$q^2 = 2\mathbf{p}^2(\mathrm{ch}\, n\varphi - 1) \tag{II.3}$$

where $\mathrm{ch}\, \varphi = 1+(\mu^2/2\mathbf{p}^2)$ as before.

It is not difficult to calculate the location of the singularity for the graph of type II.4 as well, where every nucleon line is "dressed" with π-meson lines. As

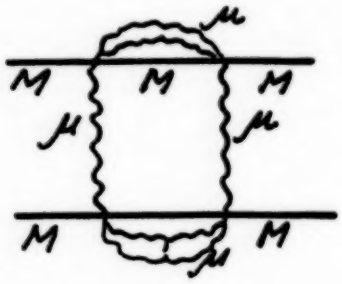

Fig. II, 4.

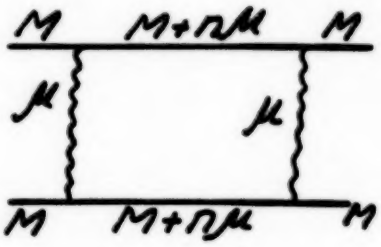

Fig. II, 5.

shown above, graph II.4 reduces to graph II.5 in which the masses $M+n\mu$ correspond to two lines. The scheme corresponding to this graph differs from scheme II.2 only in that in it the lengths of AD and AE are equal to $M+n\mu$. Taking this into account we obtain

$$q^2 = 2\mathbf{p}^2(\mathrm{ch}\, 2\varphi - 1) \tag{II.4}$$

where

$$\mathrm{ch}\, \varphi = \frac{M^2 - \frac{1}{4}W^2 + (M+n\mu)^2 - \frac{1}{4}W^2 - \mu^2}{2\sqrt{(M^2-\frac{1}{4}W^2)\,((M+n\mu)^2-\frac{1}{4}W^2)}}. \tag{II.5}$$

When $W \gg n\mu > M > \mu$, we have

$$q^2 \approx 4\mu^2 + \frac{4\mu^4 n^4}{W^2}. \tag{II.6}$$

Let us now consider π—π scattering. In this process the simplest four-pole graphs have the form of II.6 and II.7 and are equivalent to graphs II.8 and

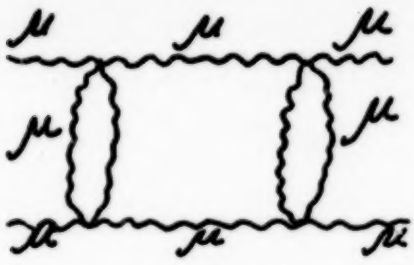

Fig. II, 6.

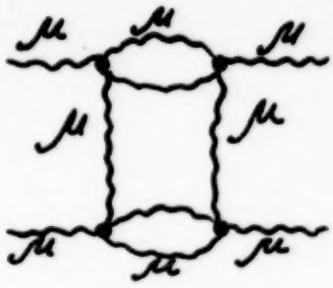

Fig. II, 7.

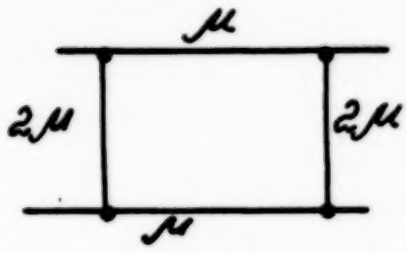

Fig. II, 8.

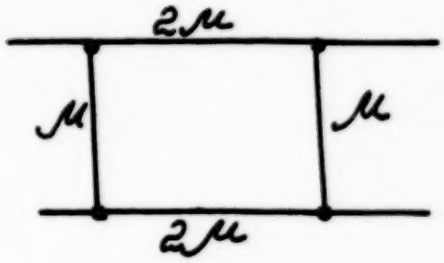

Fig. II, 9.

II.9 respectively. Considering the respective schemes we obtain

$$q^2 = \frac{4\mu^2 W^2}{\frac{1}{4}W^2 - \mu^2} \quad \text{for graph II.6,} \tag{II.7}$$

$$q^2 = \frac{\mu^2 W^2}{\frac{1}{4}W^2 - 4\mu^2} \quad \text{for graph II.7.} \tag{II.8}$$

From these formulas it is clear that for graph II.6 $q^2 \to \infty$ at $W^2 \to 4\mu^2$ and $q^2 \to 16\mu^2$ at $W^2 \to \infty$ and for graph II.7 $q^2 \to \infty$ at $W^2 \to 16\mu^2$ and $q^2 \to 4\mu^2$ at $W^2 \to \infty$. Eqs. (II.7) and (II.8) were first obtained by Mandelstamm [17]. (See also ref. [18]).)

References

1) M. Gell-Mann, M. L. Goldberger and W. Thirring, Phys. Rev. **95** (1954) 1612
2) M. L. Goldberger, Phys. Rev. **97** (1955) 508; **99** (1955) 99
3) N. N. Bogoliubov, B. V. Medvedev and M. K. Polivanov, Problems of the Theory of Dispersional Relations (GIFM, Moscow 1959).
4) H. Lehmann, Nuovo Cimento **11** (1954) 342
5) V. N. Gribov, JETP **34** (1958) 1310
6) G. F. Chew, Phys. Rev. **112** (1958) 1380

7) L. B. Okun and I. Ya. Pomeranchuk, JETP **36** (1959) 30; Nuclear Physics **10** (1959) **492**
8) A. D. Galanin, A. F. Grashin, B. L. Ioffe and I. Ya. Pomeranchuk, JETP (in print)
9) G. F. Chew, R. Karplus, S. Gasiorowicz and F. Zachariasen, Phys. Rev. **110** (1958) **265**
10) F. Federbush, M. L. Goldberger and S. B. Treiman, Phys. Rev. **112** (1258) **648**
11) R. E. Behrends, Phys. Rev. **111** (1958) 1691
12) E. P. Wigner, Phys. Rev. **73** (1948) 1002
13) A. I. Baz, JETP **33** (1957) 923
14) A. I. Baz and L. B. Okun, JETP **35** (1958) 757
15) R. X. Adair, Phys. Rev. **111** (1958) 632
16) S. Mandelstamm, Phys. Rev. **112** (1958) 1344
17) S. Mandelstamm, preprints
18) G. F. Chew and S. Mandelstamm, preprint
19) R. Karplus, C. Sommerfield and E. Wichmann, Phys. Rev. **111** (1958) 1187
20) R. Karplus, C. Sommerfield and E. Wichmann, preprint
21) L. D. Landau, Nuclear Physics **13** (1959) 181

2.C

Nuclear Physics **15** (1960) 289—315; © *North-Holland Publishing Co., Amsterdam*

Not to be reproduced by photoprint or microfilm without written permission from the publisher

PROTON CAPTURE BY N^{15}

D. F. HEBBARD

Kellogg Radiation Laboratory, California Institute of Technology, Pasadena, California †

Received 22 October 1959

Abstract: The cross section for the reaction $N^{15}(p, \gamma_0)$ at proton energies below 700 keV has been measured. The results fit well an analysis in terms of two interfering 1^- resonances at 338 and 1010 keV (12.43 MeV and 13.09 MeV respectively in O^{16*}), with destructive interference in the energy region between the resonances. The $N^{15}(p, \alpha_0)$ cross section has been analysed using the same parameters, with constructive interference between the resonances, and a good fit to the experimental cross section is obtained. The values of S obtained by extrapolation to a proton energy of 25 keV (laboratory system) are 32 keV-barn and 7.2×10^4 keV-barn respectively for the $N^{15}(p, \gamma_0)$ and $N^{15}(p, \alpha_0)$ reactions. The angular distributions of the $N^{15}(p, \alpha_0)$ reaction have been analysed. The presence of a 0^+ resonance near 500-keV proton energy, and a 2^+ resonance near 1000-keV proton energy, is indicated.

1. Introduction

The reactions occurring when N^{15} is bombarded by protons have been studied by many workers [1]), and have often been classified as follows:

$$N^{15}+p \rightarrow C^{12} + \alpha_0 \qquad \text{Reaction I}$$
$$N^{15}+p \rightarrow C^{12*} + \alpha_1 \qquad \text{Reaction II}$$
$$N^{15}+p \rightarrow O^{16} + \gamma \qquad \text{Reaction III.}$$

The study of these reactions, and especially the extrapolation of the cross sections to stellar energies, is of interest, since Reactions I and II are part of the carbon-nitrogen cycle of energy generation, while Reaction III allows a leakage of material from the C-N cycle. Attention will be confined in this report to the cross sections below a proton energy of 1300 keV.

1.1. REACTION I

Of the more recent experiments, Schardt, Fowler and Lauritsen [2]) (abbreviated to SFL) have studied the yield of $N^{15}(p, \alpha_0)C^{12}$ as a function of energy from 100 keV to 1600-keV proton energy at two fixed angles of observation. Cohen and French [3]) and Neilson *et al.* [4]) have measured the angular distribution of long range alpha particles from this reaction over the energy range from 230 to 960 keV. Angular distributions and the yield curve have been measured by Hagedorn and Marion [5]) from 900 keV to 1300-keV proton energy, and simi-

† Supported in part by the joint program of the Office of Naval Research and the U. S. Atomic Energy Commission.

lar work has been done by Bashkin *et al.* [6]) over the energy range from 950 keV to 4 MeV. The angular distributions measured by the different groups of workers [3–6]) agree well in the energy ranges where comparison is possible.

On the other hand, some inconsistencies are present when the yield curves are compared. The low energy data of SFL was taken with a proportional counter at 90° to the beam, while the high energy data was measured with a magnetic spectrometer at 137.8° to the beam. For the high energy measure-

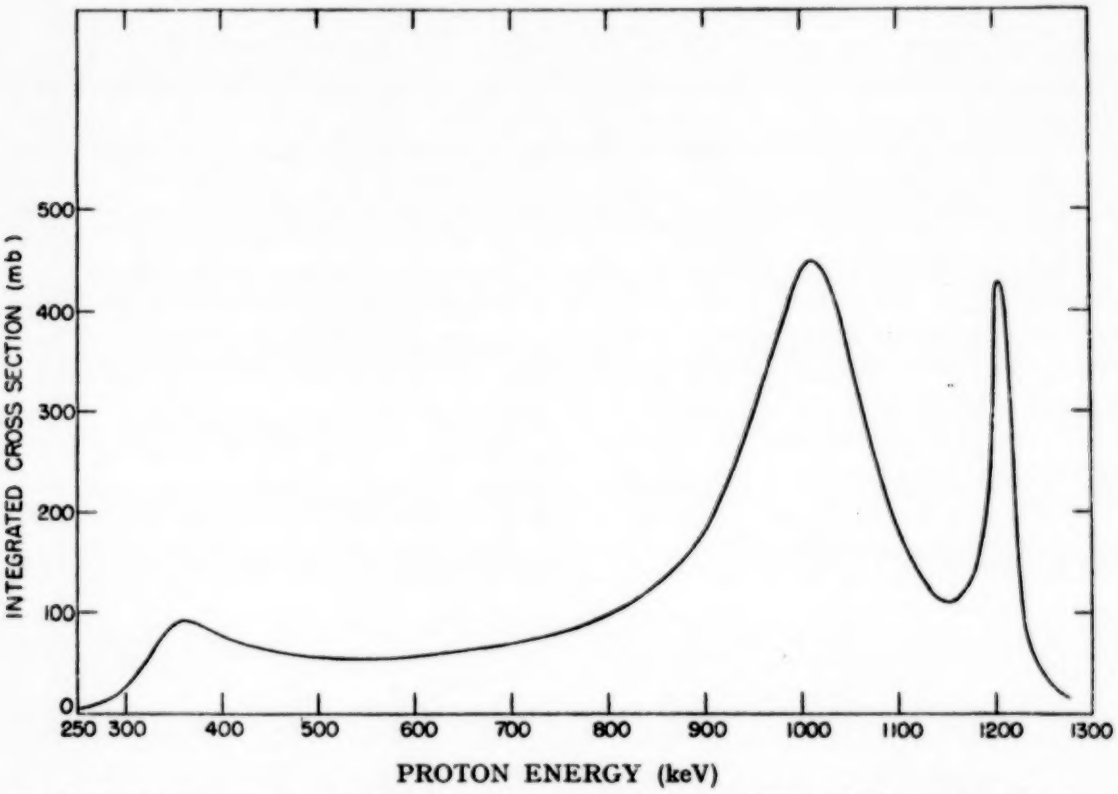

Fig. 1. The integrated cross section (over 4π steradian) for the $N^{15}(p, \alpha_0)C^{12}$ reaction. The high energy data of Schardt, Fowler and Lauritsen has been renormalized to make it fit smoothly onto the low energy data.

ments, the long range alpha particles were degraded in energy from 5 to 1.5 MeV before entering the magnetic spectrometer and no correction was made for loss of particles. When the known angular distributions are introduced, the two sets of data from SFL no longer fit smoothly together but they may be made to do so by scaling down the low energy data by a factor of 0.75. The single-level parameters for the 338-keV resonance in $N^{15}(p, \alpha_0)$ quoted in table 16.5 of ref. [1]) are based on this alteration of the low energy data to fit the high energy data of SFL.

However, Bashkin *et al.* [6]) have recently remeasured the $N^{15}(p, \alpha_0)$ cross section at energies near 1 MeV, and consistently find cross sections higher than those of SFL (high energy data) by a factor of approximately 1.3. It therefore

now appears preferable to scale up the high energy data of SFL by a factor of 1.33, making it consistent with the SFL low energy data, and simultaneously making it consistent with the work of Bashkin *et al.* [6]).

For the purposes of this report, the integrated cross section for Reaction I has been computed over the energy range from 200-keV to 1300-keV proton energy. The resultant mean integrated cross section is shown in fig. 1, with the high energy data of SFL increased by the factor 1.33. The single-level Breit-Wigner parameters for best fit to the integrated cross section of fig. 1 are displayed in table 1, assuming energy levels at proton energies of 338 keV, 1010 keV, and 1210 keV.

TABLE 1

The single-level parameters for three $N^{15}(p, \alpha_0)C^{12}$ resonances

E_R (keV)	O^{16*} (MeV)	Γ_p (keV)	Γ_{α_0} (keV)	Γ_{α_1} (keV)	Γ (keV)
338	12.43	1.1	93		94
1010	13.09	100	40	≈ 1	140
1210	13.25	4.5	10.5	7.5	22.5

1.2. REACTION II

The $N^{15}(p, \alpha_1)C^{12*}$ reaction exhibits resonances that do not occur for Reaction I. Resonances have been found at energies of 429 keV, 898 keV, 1040 keV and 1210 keV. The first two of these resonances are given the spin and parity assignment 2^-, an assignment that satisfactorily explains the absence of long range alpha particles to the ground state of C^{12}. The higher resonances are believed to be the same levels as those participating in Reaction I, with a displacement of the 1010-keV resonance because of its width and the penetration factor for the short range alpha particles of Reaction II.

The absolute cross sections at these four resonances in Reaction II have been measured by SFL, by detecting the short range alpha particles, or by detecting the 4.43-MeV gamma rays from the de-excitation of the C^{12*}, or both. Fixed angles of observation were used. The angular distributions of α_1 of or the 4.43-MeV gamma rays have been measured by Barnes *et al.*[7]), by Kraus *et al.* [8]), by Hagedorn [9]), by Bashkin and Carlson [10]), and more recently by Bashkin *et al.* [6]). The angular distributions obtained by the different workers agree well in general, but there is disagreement on the magnitude of the cross section. The absolute cross-section measurements of Bashkin *et al.* [6]) are smaller than those of SFL, to which all the other workers have normalized their results. In addition, the integrated cross sections which may be deduced for short range alpha particles and for 4.43-MeV gamma rays do not agree. The data of SFL for the 898-keV resonance gives enough information to allow a

correction factor to be established, eliminating the disagreement mentioned above.

The ratio of alpha particles (observed at 58°) to 4.43-MeV gamma rays (observed at 90°) was found by SFL at the 898-keV resonance to be 0.85. The angular distributions of Kraus *et al.*[8]) show that the ratio that should have been observed was 1.20 (allowing for the smearing effect on the angular distributions of the apparatus used by SFL). This is a discrepancy by a factor of 1.42, which must be adjusted to make SFL internally consistent. The alpha-particle measurements were made with a magnetic spectrometer, and the gamma-ray measurements were made with a Geiger counter. The efficiency and solid angle of a Geiger counter for detecting gamma rays is difficult to calculate, so that it appears to be preferable to ascribe the discrepancy of a factor 1.42 to the Geiger counter overall detection efficiency, which was given too small a value by SFL. When this adjustment is made to the gamma-ray data of SFL, it is found that the integrated cross section at the 1210-keV resonance given by SFL is conistent with the measurements of Bashkin *et al.* [6]). The latter workers find an integrated cross section of 250 ± 35 mb if the short range alpha particles are measured and an integrated cross section of 290 ± 60 mb if the 4.43-MeV gamma rays are measured. The data of SFL, corrected for the angular distribution of 4.43 MeV gamma rays at the 1210-keV resonance, and also corrected in the opposite direction by the factor 1.42, for the gamma ray detector efficiency, gives an integrated cross section of 285 mb. This result is in good agreement with the measurements by Bashkin *et al.* [6]).

1.3. REACTION III

The $N^{15}(p, \gamma)$ reaction shows the presence of a level at a proton energy of 710 keV that does not take part in either of Recactions I or II. The spin and parity of this level are known to be 0^-, from measurements of the elastic scattering of protons on N^{15} by Hagedorn [9]). This spin and parity assignment satisfactorily explain the forbidden nature of the break-up into C^{12} or C^{12*} plus an alpha particle. The ground state gamma-ray decay is also forbidden, and what is observed by Hagedorn [9]) is a cascade through the 6 and 7-MeV levels in O^{16}. The ground state gamma-ray decay of the 1010-keV resonance is not forbidden, and an extremely strong E1 transition has been observed by SFL and by Hagedorn [9]), with a maximum cross section of 1 mb. The angular distribution of the 13-MeV gamma rays has been found by Kraus [11]) to be isotropic at the 1010-keV resonance.

The remaining resonances have not previously been investigated with sufficient sensitivity to detect gamma rays from Reaction III. An upper limit has been placed by Kraus [11]) on the cross section for $N^{15}(p, \gamma_0)O^{16}$ at the 338-keV resonance. This upper limit corresponds to a cross section of 10 μb.

1.4. ELASTIC SCATTERING OF PROTONS

The elastic scattering of protons [6, 9]) by N^{15} has confirmed the spin and parity assignments [1]) of the levels occuring as resonances at proton energies of 710, 898, 1010 and 1210 keV. No observations have been reported for the 338 or 429-keV resonances. The anomalies expected for the latter resonances are extremely small, because of the small ratios Γ_p/Γ. Although Γ_p is not found experimentally for either the 338 or the 429-keV resonance but only the product $\Gamma_p\Gamma_\alpha/\Gamma$ is known, in both cases the Wigner limit to the reduced proton width indicates that the smaller possible value of the proton width should be chosen.

1.5. ANGULAR DISTRIBUTIONS

There is good agreement among all workers on the angular distributions of the long range alpha particles from Reaction I. The angular distribution is isotropic below 400-keV proton energy, but above this energy a gradually increasing $\cos\theta$ term appears. This was interpreted by Cohen and French [3]) as the interference of a 0^+ level at 338 keV and a 1^- level at 1010 keV. The extension of the angular distribution measurements by Hagedorn and Marion [5]) to energies above 950 keV has forced the abandonment or modification of this interpretation. The term in $\cos\theta$ becomes extremely large even at the 1010-keV resonance, and additional terms in $\cos^2\theta$, $\cos^3\theta$ and $\cos^4\theta$ appear. Interference of 0^+ and a 1^- level cannot lead to terms in $\cos^3\theta$. The magnitudes of the coefficients involved can be explained if we assume that the resonance at 1010 keV (known to be 1^- from the large radiative width) is suffering interference from both a 0^+ and a 2^+ level, and that the 2^+ level is located close to the 1010-keV resonance. In this regard it is interesting to note that the elastic scattering of alpha particles by C^{12}, investigated by Bittner and Moffat [12]), shows evidence that the s and d-wave resonant alpha-particle phase shifts are both passing through 90° in the energy region around an alpha-particle energy of 7 MeV. This is the same excitation region in O^{16} as that reached by the $N^{15}+p$ reaction at proton energies below 1 MeV.

It therefore appears likely that there are two undiscovered levels in O^{16}. In order to explain why their presence is felt only through the angular distributions of Reaction I, and through the elastic scattering of alpha particles from C^{12}, one must postulate large alpha-particle widths and small proton widths. Under these circumstances, the cross sections for Reactions II and III and the proton elastic scattering anomalies for the undiscovered levels may be made small. The alpha particles of Reaction I from the 338-keV and 1010-keV resonances will mask the yield from the undiscovered levels.

1.6. SPIN AND PARITY ASSIGNMENTS

There is general agreement on the spin and parity assignments of the 429, 710, 898, and 1010-keV resonances. The situation for the 1210-keV resonance is not so satisfactory. The possible spin and parity assignments for the 1210-keV

resonance are limited to 3^- or 4^+. The former assignment is indicated by measurements of the $N^{15}(p, p)$ reaction [9]), and by measurements of the angular correlation of short range alpha particles and 4.43-MeV gamma rays [9]). The angular distribution of long range alpha particles [5, 6]) favors the assignment 3^- but cannot exclude 4^+, and the distribution of 4.43-MeV gamma rays [7, 8, 10]) is consistent with either 3^- or 4^+. The angular distribution of short range alpha particles, measured by Kraus *et al.* [8]) and by Hagedorn [9]) is inconsistent with 3^-, and favors 4^+. On the other hand, the short range alpha-particle angular distributions measurements of Bashkin *et al.* [6]), while in general agreement with Kraus *et al.* and with Hagedorn over most of the angular range, differ significantly from these workers at backward angles greater than 150°. It is just in this range of angles that the angular distributions of short range alpha particles expected for the assignments 3^- and 4^+ differ most markedly, and the results of Bashkin *et al.* [6]) definitely favor the 3^- assignment. Bashkin *et al.* [6]) observe an energy shift of the peak yield with angle for Reaction I at the 1210-keV resonance, but the energy of the peak yield of Reactions II and III stays constant to within 2 keV. This indicates that the angular distribution of Reaction II is probably not changing rapidly with energy, so that there is a real disagreement between the angular distributions of short range alpha particles measured at the 1210-keV resonance by the workers of refs. [6]) and [9]).

The 338-keV resonance has at various times been labelled 0^+ or 1^-. Either assignment is consistent with the isotropic angular distribution of long range alpha particles at this resonance. An argument in favour of 0^+ has been the ability of a 0^+ level of the observed width to explain [3]) the $\cos\theta$ terms in the long range alpha-particle angular distribution up to a proton energy of 950 keV. The argument against 0^+ is the fact that such a level must be formed by p-wave protons, and the proton reduced width required [5, 13]) is slightly in excess of the Wigner limit. An anomaly exists in the elastic scattering cross section for 7.05-MeV alpha-particles on C^{12}. This anomaly has been analyzed [12]), and it is found that a 1^- level at an excitation of 12.43 MeV in O^{16} is needed to fit the data. This is the same excitation energy as the 338-keV resonance for $N^{15}+p$, but the width measured in $C^{12}(\alpha, \alpha)$ is approximately twice that measured in $N^{15}(p, \alpha_0)$. The diffference is many times the claimed energy resolution for both experiments. Thus, the identity of the 12.43-MeV level in $C^{12}(\alpha, \alpha)$ and $N^{15}(p, \alpha_0)$ is in doubt, so that the spin and parity assignment for the 12.43-MeV level in $C^{12}(\alpha, \alpha)$ cannot necessarily be taken as valid for the 12.43-MeV level in $N^{15}(p, \alpha_0)$.

The experimental work described in this report was undertaken with the purpose of distinguishing between the possible spin assignments 0^+ and 1^- for the 338-keV resonance in $N^{15}+p$, and with the purpose of providing an estimate of the cross section for proton capture at stellar energies. A study of the $N^{15}(p, \gamma_0)$ reaction at low energies provides the necessary information.

2. Method

2.1. TARGET PREPARATION

The targets used for the $N^{15}(p, \gamma)$ measurements were of nitrided titanium, which has been found to be stable under bombardment. Several different types of target were employed. For the initial runs, a thick target was used, in order to maximize the gamma-ray yield. Later targets used were a thin layer of nitrided titanium on a thick backing of platinum or nickel. The latter targets were satisfactory where energy resolution in the kilovolt region was desirable. Neither the titanium nor the nickel on proton bombardment gives gamma rays above about 7 MeV.

The titanium was evaporated onto the metal backing, and the resultant layer was nitrided by induction heating to a red-heat for a short time in an atmosphere of dry ammonia at approximately 5 cm pressure. The ammonia, during the nitriding process, is contained in a pyrex glass vessel. Neither the pressure, temperature, nor time of heating of the target blank has been found to be critical. The amount of ammonia available for the reaction is quite limited, and the reaction may be monitored by the change in pressure as the reaction proceeds. A fifty per cent increase in pressure indicates that all the ammonia is decomposed. Too high a temperature in the induction furnace will allow the titanium layer to diffuse into the backing, taking nitrogen with it. Too low a temperature does not allow the nitriding reaction to proceed rapidly. The backing material is chosen because it does not nitride easily.

The thick nitrided titanium target was prepared in a manner similar to that used for the thin targets, by induction heating a piece of titanium, 0.020 inches thick, in an atmosphere of dry ammonia, and repeating the process several times with fresh ammonia.

The amount of oxygen on the targets is reduced by previous outgassing of the apparatus, prior to the evaporation of titanium, and the evaporation of considerable titanium before deposition on the target blank. The drying of the ammonia also appears to effect a significant reduction in the amount of oxide formed on the targets.

The ammonia is prepared from ammonium nitrate, supplied by the Eastman Kodak Company, with the ammonium radical enriched in N^{15} to 67 per cent. The ammonia is released from the nitrate by gentle warming with calcium oxide. The chemical reaction releases water, and more is given off by the calcium oxide. This water is removed by drying the ammonia over potassium hydroxide. Any remaining water is eliminated by freezing the ammonia with liquid nitrogen, and taking only the fraction that evaporates first.

2.2. GAMMA RAY DETECTION

The gamma-ray detector was a 4×4-inch NaI(Tl) crystal, mounted on a Dumont 6364 photomultiplier. The crystal was shielded, except from the front,

with several inches of lead, and was mounted so that it could approach the target to a distance of 0.3 inches. The entire experimental area of the 600-keV electrostatic accelerator was enclosed within concrete walls with a thickness of six inches, and this helped materially in reducing the unwanted background radiations. The electronics was conventional, and spectra from the 4-inch crystal were displayed on a 100-channel analyzer.

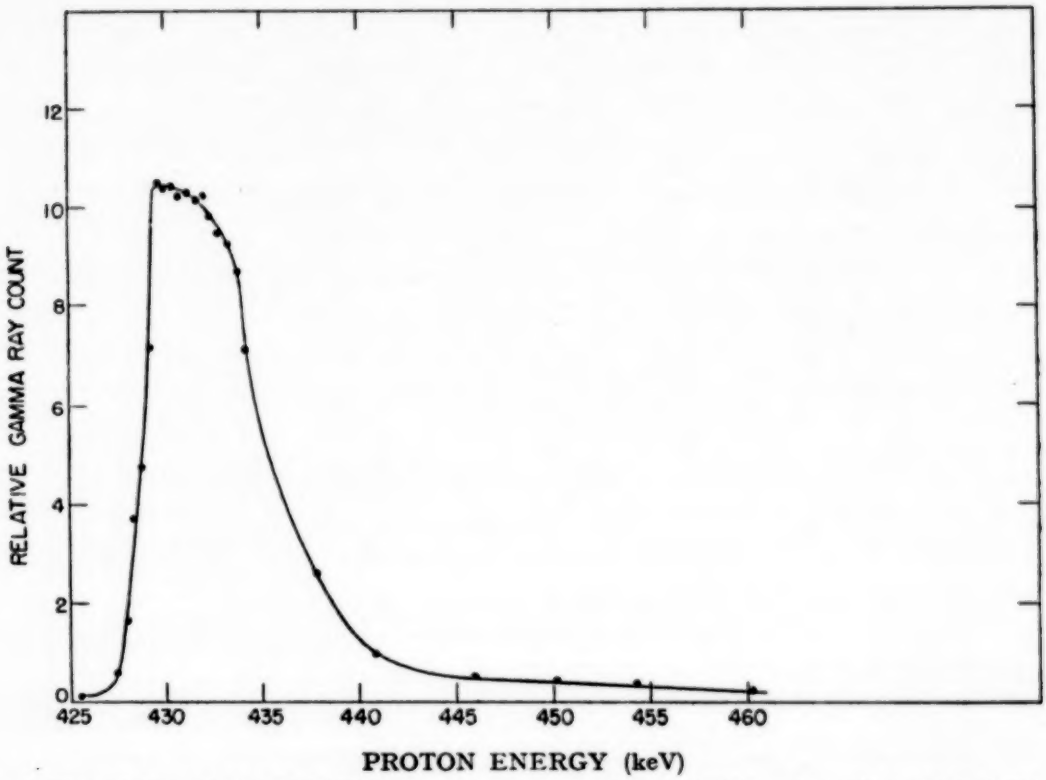

Fig. 2. The relative yield of 4.43-MeV gamma rays following the $N^{15}(p, \alpha_1)$ reaction at the 429-keV resonance. The yield is plotted as a function of proton energy, revealing the distribution of N^{15} within the target. The target was a layer of nitrided titanium (67 per cent N^{15}) on a thick nickel backing.

The thickness and composition of the nitrided titanium targets were investigated by measuring the yield of 4.43-MeV gamma rays as a function of proton energy near the 429-keV resonance of $N^{15}(p, \alpha_1\gamma)$. Fig. 2 shows the yield obtained from one of the targets on a thick nickel backing. All targets made were thick compared to the width of the 429-keV resonance. It was noticed that, for each target, the maximum yield of 4.43-MeV radiation occurred when the protons passed through the resonance energy immediately below the surface. The maximum yield obtained was the same for all targets.

The amount of N^{15} in the targets was first estimated by assuming that the maximum yield was obtained from the chemical compound TiN, known to be formed by heating titanium in ammonia. Using the yield of 4.43-MeV gamma rays as a function of proton energy and hence of depth in the target, the amount

of N^{15} present was calculated. For the data shown in fig. 2, the amount of N^{15} present was 1.8×10^{17} atom · cm^{-2}. The assumption that the surface of the target corresponds to TiN may be checked from the data of SFL [2]) and of Kraus *et al.* [8]). The targets used by SFL were KNO_3 enriched to 61 per cent of N^{15}, and the 4.43-MeV gamma rays were measured with a Geiger counter at 90° to the beam. Correction must be made for the angular distribution and the smoothing factor for the finite size and position of the Geiger counter. An additional correction must be made for the Geiger counter efficiency. As explained in the introduction, an increase by a factor 1.42 in the counter efficiency estimated by SFL leads to internal consistency in the α_1 and γ measurements by SFL at the 898-keV resonance, and leads to agreement at the 1210-keV resonance with the absolute cross-section data of Bashkin *et al.* [6]). The resultant corrected thick target yield of 4.43-MeV gamma rays from the 429-keV resonance is $2.92 \times 10^{-9} \gamma$/p for a thick target of KNO_3 with 61 per cent N^{15}. Therefore, the thick target yield from a TiN target with 67 per cent N^{15} is $6.74 \times 10^{-9} \gamma$/p. The assumed stopping cross sections for 429-keV protons are shown in table 2. The observed maximum yield of 4.43-MeV gamma rays from

TABLE 2

Proton stopping cross sections for K, Ti, N and O, at 429 keV

	$\times 10^{-15}$ eV · cm^2		$\times 10^{-15}$ eV · cm^2
K	15.9	Ti	16.9
N	8.9	N	8.9
O_3	29.4		
	54.2		25.8
61 % N^{15}	89.0	67 % N^{15}	38.5

the nitrided titanium targets is $7.3 \times 10^{-9} \gamma$/p, correcting for the angular distribution and the smoothing factor for the 4-inch sodium iodide crystal at a distance of 6.5 inches and at 0° to the beam. The gamma-ray detector efficiency for a 4-inch crystal has been computed [14]) at the California Institute of Technology. The agreement between the observed and expected gamma-ray yields is good, and justifies confidence in the assumption that the surface layer of the target is TiN.

A further check on the target composition comes from the yield of elastically scattered protons from the thick nitrided titanium target compared with the yield from a titanium target. The ratio of the yields of elastically scattered protons agrees with the ratio of stopping cross sections per titanium atom for a pure titanium and a TiN target.

3. Experimental Results

The pulse height spectrum observed at a proton bombarding energy of 370 keV on a nitrided titanium target with a nickel backing is shown in fig. 3. The cross section as a function of energy for the 12-MeV gamma ray is displayed in fig. 4. These gamma rays are of the correct energy for the ground state

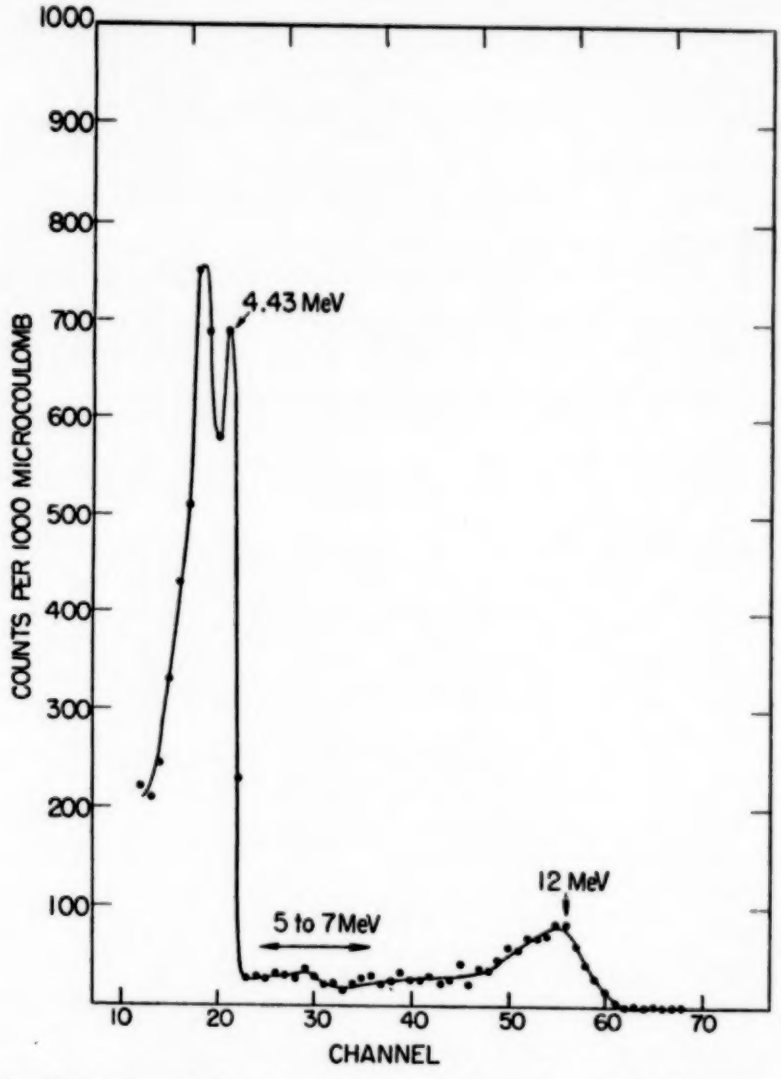

Fig. 3. The pulse-height spectrum from a nitrided titanium target (10 keV, 67 per cent N^{15}) on a thick nickel backing. The proton energy is 370 keV, close to the energy at which all the gamma rays marked had a broad resonance, attributed to $N^{15}+p$.

transition of the $N^{15}(p, \gamma_0)O^{16}$ reaction. In addition, there is a resonance in the cross section for the production of these gamma rays at the same energy and with the same width as the resonance already observed in the reaction $N^{15}(p, \alpha_0)C^{12}$. The maximum cross section for production of 12-MeV gamma rays occurs at a proton energy of 345 keV, instead of 360 keV, which is the energy

for the maximum of the $N^{15}(p, \alpha_0)C^{12}$ cross section. The difference of energy can, however, be explained satisfactorily, and will be treated in more detail later. The maximum cross section, which can now be attributed to the $N^{15}(p, \gamma_0)O^{16}$ reaction, is 6.5 μb. This result is just lower than the upper limit to the cross section set by Kraus [11]). The different targets used gave peak cross sections consistent within 5 per cent with the mean value quoted above.

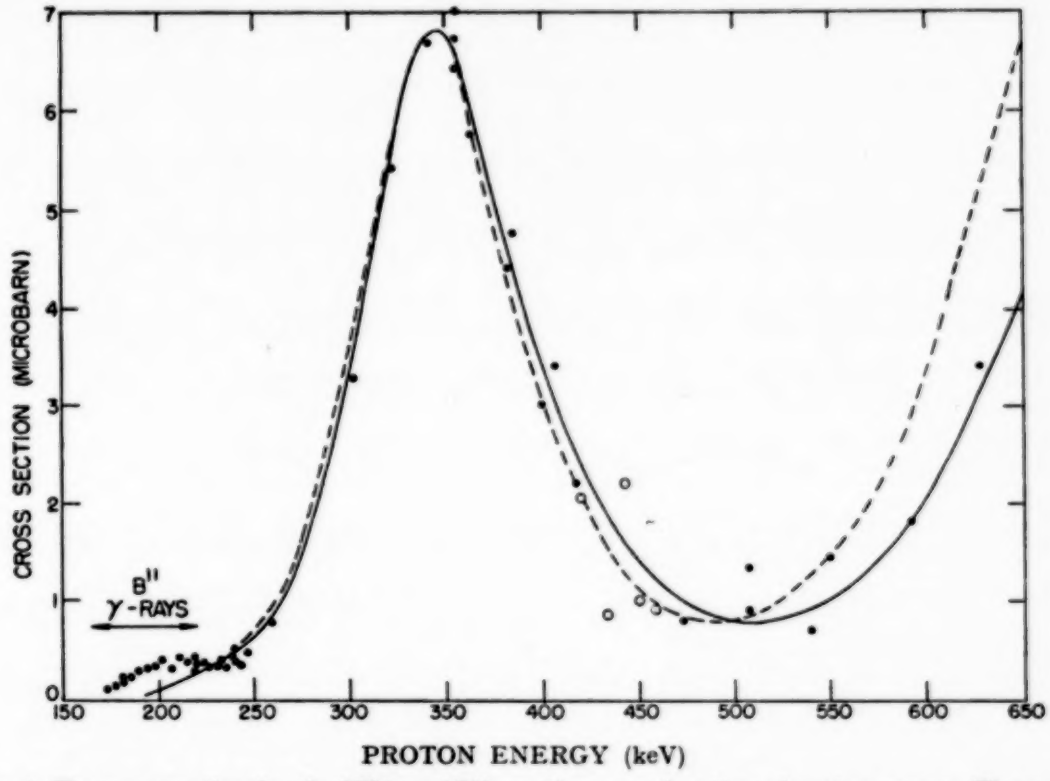

Fig. 4. The cross section for the $N^{15}(p, \gamma_0)O^{16}$ reaction, as a function of proton energy. The open circles are measurements that required correction for the simultaneous detection of both members of a cascade from the 429-keV resonance through the 6 and 7-MeV states in O^{16}. The dashed curve is the theoretical curve for destructive interference between two 1^- resonances at 338 keV and 1010 keV, with the 1010-keV resonance having a peak cross section of 1000 μb. The full curve shows the improved agreement when the 1010-keV resonance peak cross section is reduced by the factor 1.42. Both theoretical curves are normalized to match the peak height of the 338-keV resonance. More weight should be attached to the points at 592 keV and 627 keV than to the scattered points between 425 keV and 550 keV.

The spectrum of fig. 3 shows a strong 4.4-MeV gamma ray from the $N^{15}(p, \alpha_1\gamma)$ reaction. The excitation function of this gamma ray is shown in fig. 5. The yield of 4.4-MeV gamma rays shows a distinct step in the tail of the 429-keV resonance, which is shown by the dashed line in fig. 5. When this tail is subtracted, a peak is left in the cross section for production of 4.43-MeV gamma rays. This peak has a width consistent with the width of the 338-keV resonance in $N^{15}(p, \alpha_0)C^{12}$. The maximum cross section occurs at a proton energy of 375 keV. When this is corrected for the short range alpha-particle

barrier penetrability, the peak position is also consitent with that of the 338-keV resonance in $N^{15}(p, \alpha_0)C^{12}$.

The spectrum of fig. 3 also shows the presence of low intensity gamma rays with energies of 5 to 7 MeV. These gamma rays are attributed to cascade transitions through the 6 and 7-MeV levels in O^{16} but it has not been possible to determine which levels are involved in the cascades. The cascades are weakly

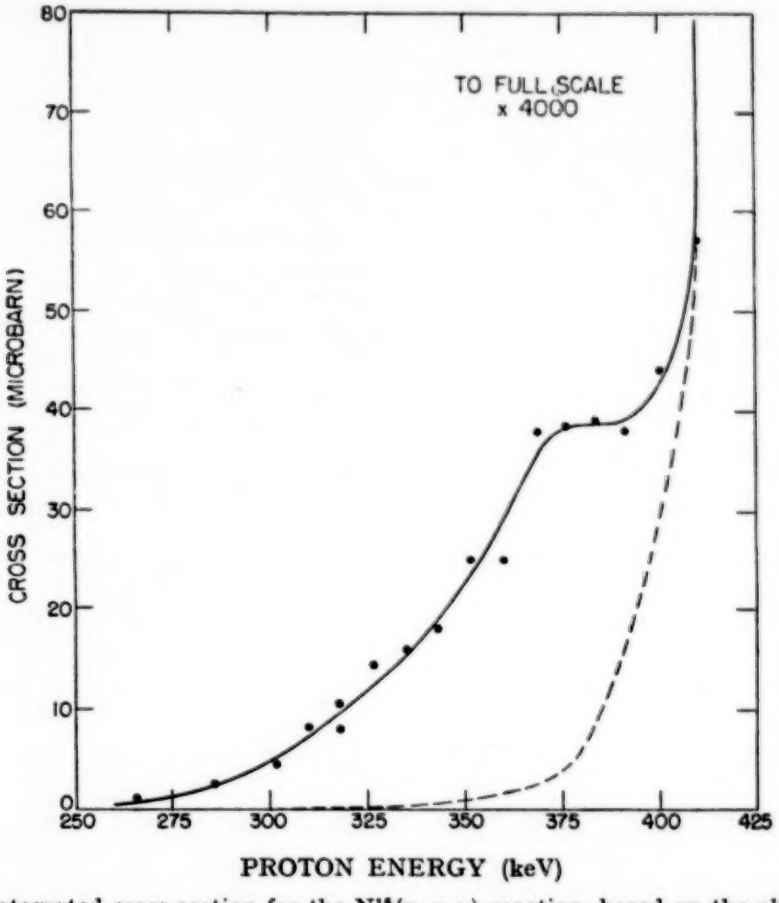

Fig. 5. The integrated cross section for the $N^{15}(p, \alpha_1\gamma)$ reaction, based on the observed yield of 4.43-MeV gamma rays from a 10-keV thick nitrided taitanium target, is shown. The dashed curve represents the expected shape of the tail of the 429-keV resonance, assuming a width of 900 eV.

resonant at 350-keV proton energy, having an excitation function similar to the excitation function of the ground state radiation. The cascade transitions are quite strongly resonant at the 429-keV resonance. In addition, some 12-MeV pulses were observed, but these could all be explained as simultaneous detection of both members of a cascade. The ratio of the number of 12-MeV pulses to the observed number of 5 to 7-MeV pulses decreased as the detector was withdrawn from the vicinity of the target. This behaviour is consistent with the expected behaviour for double pulse detection. At the 429-keV resonance, with the 4-inch sodium iodide crystal close to the target, the number of double pulses observed was much greater than the number of pulses caused by 12-MeV gamma rays.

A correction was made for this effect and the open circles of fig. 4 indicate the points that have been corrected. The correction was taken to be proportional to the observed yield of 4.43-MeV radiation, and the constant of proportionality was chosen so that the lowest energy corrected point fell on a smooth interpolation between the results below and above the 429-keV resonance. The magnitude of the correction ranges from 85 per cent of the observed yield of 12-MeV pulses down to 20 per cent.

Down to a proton bombarding energy of 220 keV, the gamma-ray spectrum remains similar to that shown in fig. 3. However, below 220 keV, the spectrum changes, and at a proton energy of 200 keV, the high energy gamma-ray peak has shifted down slightly in energy. In an attempt to trace the source of the contaminant responsible for the gamma-ray yield at low proton energies, targets were partially prepared, and the introduction of the contaminant was found to occur during the final nitriding process. A target was nitrided with natural nitrogen in the form of ammonia using identical techniques, and the contaminant was identified as B^{11}, coming from the pyrex glass vessel in which the nitriding took place. An estimate of the amount of B^{11} in the nitrided titanium targets was made. It was found that 1.1×10^{15} atoms $\cdot$ cm^{-2} or 2×10^{-8} g $\cdot$ cm^{-2} of B^{11} spread through approximately 40 keV of target thickness (for 200 keV protons) below the nitrided titanium layer was sufficient to explain the observed yield. This amount of B^{11} makes a negligible contribution to the yield of 12-MeV gamma rays plotted in fig. 4. At the minimum in the cross section near 500-keV proton energy, the contribution to the observed yield from the $B^{11}(p, \gamma)$ reaction is of the order of 5 per cent.

Because of the presence of the boron contamination, the measurements taken below a proton energy of 220 keV have been rejected in the calculation of the $N^{15}(p, \gamma_0)O^{16}$ cross section. The proton energy of 220 keV is the lowest energy at which it is known that the gamma-ray spectrum is consistent with the $N^{15}(p, \gamma_0)O^{16}$ reaction. Below this energy, the target behaves as a thick target for the 163-keV $B^{11}(p, \gamma)$ resonance. Before the recognition of the contamination, the yield curve at low energies was interpreted by the author as possible evidence for a resonance at 190 keV [1]), but this interpretation can no longer be supported.

TABLE 3

Single-level parameters for the 338 and 429 keV resonances

O^{16*} (MeV)	E_R (keV)	Γ_p (keV)	Γ_{α_0} (keV)	Γ_{α_1} (keV)	Γ_{γ_0} (eV)	$\Gamma_{\gamma\text{cascade}}$ (eV)
12.43	338	1.1	93	0.025	8	0.4
12.52	429	0.020	forbidden	0.90	—	0.006

Table 3 gives the relevant single-level parameters for the 338-keV and 429-keV resonances that best fit the observed cross sections for gamma ray or

short range alpha-particle emission. The cross sections are based on the assumption of the isotropy of the gamma radiation for the 338-keV resonance Because of the low yield of radiation, it was not possible to check this assumption. The detector crystal was very close to the target, so that any anisotropy would be greatly reduced. In addition, it can be shown that the presence of 12-MeV gamma radiation implies formation of the compound nucleus by s-wave protons, and hence isotropy would be expected.

4. Discussion

4.1. INTERFERENCE

The observation of ground state gamma radiation from the 338-keV resonance in $N^{15}+p$ shows that 0^+ is not the correct assignment for the O^{16} level involved. Since, from other evidence, the possibilities were limited to 0^+ or 1^-, the correct assignment 1^- is now unique and requires s-wave proton formation. This assignment raises the question of the interference of the 1^- levels at 12.43 MeV and 13.09 MeV (the 338 and 1010-keV resonances) in the integrated cross section. Fowler and Thomas [15]) have computed the interference between the two levels with constructive interference between the resonances, for the $N^{15}(p, \alpha_0)C^{12}$ reaction. This interference was suggested by SFL as the explanation of the high $N^{15}(p, \alpha_0)$ cross section between the resonances. The cross section was found to be adequately explained by the interference assumed. Since the work referred to [15]) has not been published and further measurements [5]) have since been made on Reaction I angular distributions, it was necessary to repeat these calculations. At the same time they were extended to the case of the $N^{15}(p, \gamma_0)O^{16}$ reaction.

The multi-channel two-level Breit-Wigner expression [16]) for the integrated cross section was used. The channels appearing explicitly were for O^{16} breakup into $N^{15}+p$, $C^{12}+\alpha_0$, $C^{12*}+\alpha_1$, and $O^{16}+\gamma$. The energy shifts for these channels were also introduced explicitly, as were the variations with energy of the partial widths. The calculations were performed on the Datatron 205 computer at the California Institute of Technology. The fits achieved are shown in fig. 6(a) and 6(b), while the two-level reduced widths found are displayed in table 4.

TABLE 4

Two-level parameters for the 338 and 1010-keV resonances

E_R (keV)	γ_p^2 (keV)	$\gamma^2_{\alpha_0}$ (keV)	$\gamma^2_{\alpha_1}$ (keV)	Γ_{γ_0} (eV)
338	354	19.8	76	12.8
1010	450	4.27	20.7	88

The $N^{15}(p, \alpha_0)C^{12}$ cross section is a reasonably good fit to the two-level formula with constructive interference between the resonances. However, the

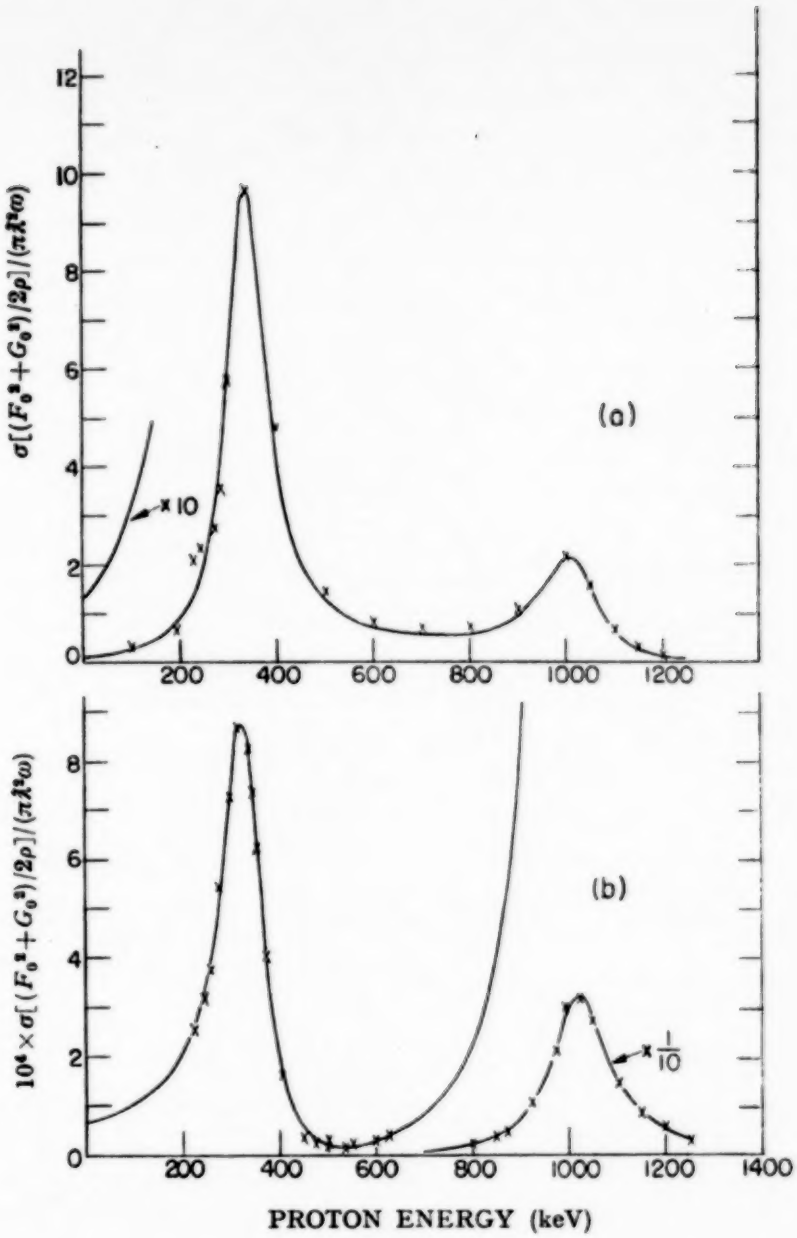

Fig. 6.

(a) The $N^{15}(p, \alpha_0)$ integrated cross section with the external energy-dependent factors removed. The full curve represents the calculated cross section for constructive interference between the two 1^- resonances at 338 keV and 1010 keV. The points are either experimental points (at low energies) or are selected at intervals from the smooth curve of fig. 1. The effects of the 1210-keV resonance have been supressed. The ordinate at low energies is directly proportional to S, the conversion being effected by multiplication of the ordinate by 4.41×10^6, to give S in b. keV.
(b) The $N^{15}(p, \gamma_0)$ integrated cross section with the external energy-dependent factors removed. The full curve represents the calculated cross section for destructive interference between the two 1^- resonances at 338 keV and 1010 keV. The points are all experimental, the ones for the 1010-keV resonance being obtained from the data of Hagedorn [9]) renormalized to a peak cross section of 700 μb.

computed cross section between the resonances consistently lies below the experimental cross section. It must be remembered that there are probably two levels in this energy region, manifesting themselves by their effects on the $N^{15}(p, \alpha_0)C^{12}$ angular distributions and the alpha-particle phase shifts for elastic scattering on C^{12}. Since the levels needed would add to the integrated cross section without interference terms, it is possible that the discrepancy between the calculated and experimental cross sections represents the effect of these levels. The behaviour of the computed cross section has been studied as the reduced width parameters were varied. The $N^{15}(p, \alpha_0)$ cross section in the constructive interference region is dependent only on the values of the cross sections at resonance, the resonance total widths, and the separation of the peaks. In order to fit the region between resonances, the good fit at both resonances for both the $N^{15}(p, \alpha_0)$ and the $N^{15}(p, \gamma_0)$ cross sections would have to be completely destroyed.

It is seen from fig. 6(b) that the $N^{15}(p, \gamma_0)$ cross section is extremely low in the energy range between the 1^- resonances. The γ_0 cross section near 500 keV is approximately one tenth of that expected from the sum of the tails of the two 1^- resonances without interference. The cross section, calculated for destructive interference between the resonances, does not pass through zero, because of the influence of the channels for break-up into $C^{12} + \alpha_0$ and $C^{12*} + \alpha_1$. Nevertheless, in spite of the gamma-ray de-excitation of the levels involved being of relatively minor importance compared with the proton and alpha-particle channels, there is only a small contribution to the γ_0 cross section from these channels. The 0^+ and 2^+ levels postulated in the region between the two 1^- levels will not contribute appreciably to the $N^{15}(p, \gamma_0)$ cross section. The small $N^{15}(p, \gamma_0)$ cross section between the 1^- resonances and the general agreement between the calculated and experimental values of this cross section over the whole energy range give strong support to the correctness of the analysis of the $N^{15}(p, \alpha_0)$ and $N^{15}(p, \gamma_0)$ cross sections in terms of interfering states of the same spin and parity.

As well as leading to agreement in the gross features of the $N^{15}(p, \alpha_0)$ and $N^{15}(p, \gamma_0)$ cross sections, the analysis in terms of states of the same J^π leads to agreement in less noticeable features of the cross section. In the case of constructive interference between two resonances of the same spin and parity, the resonance peaks tend to be drawn together, while for destructive interference between the resonances, the peaks tend to be pushed apart. These energy shifts of the peaks appear in the integrated cross section measurements. If, when barrier penetrability factors are taken out, one of the peaks is considerably larger than the other, then it is the smaller peak that will suffer the larger energy shift. Table 5 shows, for the $N^{15}(p, \alpha_0)$ and $N^{15}(p, \gamma_0)$ reactions, which resonance is dominant, and the energy shift observed experimentally. The calculated and experimental values of the energy shifts are in good agreement.

The calculations of the $N^{15}(p, \alpha_0)$ and $N^{15}(p, \gamma_0)$ cross sections were made both for the case of constructive and for the case of destructive interference between the 338-keV and 1010-keV resonances for short- range alpha-particle production. There are no significant differences in the computed γ_0 and α_0 cross sections for the two cases of interference in the $N^{15}(p, \alpha_1)$ cross section. There is some reason to believe that the interference in the $N^{15}(p, \alpha_1)$ cross section is destructive between resonances. The 338-keV resonance is dominant,

TABLE 5

Energy shifts in peak cross sections

E_R (keV)	$N^{15}(p, \alpha_0)$	$N^{15}(p, \gamma_0)$	$N^{15}(p, \alpha_1)$
338	dominant	shifted, -15 keV	dominant
1010	shifted, -10 keV	dominant	shifted, $\approx +20$ keV

and is therefore not shifted relative to the (p, α_0) resonance, except for the short-range alpha-particle barrier penetrability. The 1010-keV $N^{15}(p, \alpha_1)$ resonance is therefore the one that should suffer an energy shift relative to the position of the (p, γ_0) resonance. Bashkin *et al.* [6]) report a peak in the $N^{15}(p, \alpha_1)$ cross section at a proton energy of 1085 keV. The difference between 1085 keV and 1030 keV (where the maximum $N^{15}(p, \gamma_0)$ cross section occurs) is too large to be explained entirely by the short-range alpha-particle barrier penetrability, so that it is possible that an additional upward shift in energy is present, caused by destructive interference between the (p, α_1) resonances. The curves of fig. 6 have been computed, assuming this destructive interference between the 338-keV and 1010-keV $N^{15}(p, \alpha_1)$ resonances.

It has been possible to fit the $N^{15}(p, \gamma_0)$ cross section without the explicit consideration of the presence of more than two levels, and without the introduction of direct radiative capture. Although such effects must be present, it appears that the resonant cross sections are dominant in the ground state gamma ray transition.

4.2. ISOBARIC SPIN MIXING

The breakup of O^{16} into an alpha particle plus C^{12} in either its ground state or first excited state is allowed only for levels with isobaric spin $T = 0$. Electric dipole radiation from a self-conjugate nucleus is required to follow the selection rule that $T = 0$ to $T = 0$ transitions are forbidden. The extremely large electric dipole width of the 13.09-MeV level in O^{16} (the 1010-keV resonance) and its excitation energy suggest that it is the $T = 1$ level corresponding to the 392-keV 1^- level of N^{16}. The fact that it also decays by alpha-particle emission shows that there is an appreciable, though small, $T = 0$ component

to this level. The source of this $T = 0$ component is believed to be the 1^- level at 12.43 MeV (338-keV resonance), which is also a mixture of $T = 0$ and $T = 1$ states, but with the $T = 0$ component dominant. The two levels satisfy the static and dynamic criteria [16]) for mixing of isobaric spins. If this is the correct interpretation of the source of the mixture of $T = 0$ and $T = 1$ components in the two levels, the ratio of reduced widths for α_0 break-up of the two levels should equal the ratio of the reduced widths for α_1 break-up, and should also equal the inverse ratio of the γ_0 widths. There should be no significant difference in the proton reduced widths. Table 4, with the two level parameters, illustrates that the ratios are indeed approximately equal. The ratios of the α_0 and of the α_1 reduced widths are 4.6 : 1 and 3.7 : 1 respectively, while the ratio of the γ_0 widths is 1 : 6.9. The ratio of the proton reduced widths is 0.8 : 1. We may estimate, therefore, that the mixture in intensity of the isobaric spin states is close to 15 per cent of the minor component.

The question arises of the correct method of treatment of the interference of two levels of the same spin and parity under conditions ranging from no mixing of the isobaric spin states to complete mixing. The justification of the method adopted is confined to the appendix.

4.3. ANGULAR DISTRIBUTIONS

This section is concerned with the varying angular distributions of Reaction I, from the isotropic distribution at the 338-keV resonance to the strongly anisotropic and asymmetric distributions near the 1010-keV resonance. The initial assumptions are that there are known 1^- resonances at 338 and 1010 keV, and that the 1210-keV resonance has spin and parity 3^-. The aim is to extract the available information about the presence of any 0^+ and 2^+ levels influencing the angular distributions. No other levels are considered because there is no experimental evidence requiring their presence.

TABLE 6

Coefficients of $\cos^n\theta (= A_n)$ in the $N^{15}(p, \alpha_0)$ angular distributions

A_0	$a^2+b^2+c^2+d^2-2ab\cos(\beta-\alpha)-2cd\cos(\gamma-\delta)$
A_1	$4ad\cos(\delta-\alpha)+2ac\cos(\gamma-\alpha)-6bc\cos(\beta-\gamma)$
A_2	$-2b^2+3d^2+6ab\cos(\beta-\alpha)+6cd\cos(\gamma-\delta)$
A_3	$8bd\cos(\beta-\delta)+10bc\cos(\beta-\gamma)$
A_4	$5b^2$

The integrated cross section $\Sigma = a^2+\frac{5}{3}b^2+c^2+2d^2$.

The amplitudes and phases for the 1^-, 3^-, 0^+ and 2^+ levels are $a\exp(i\alpha)$, $b\exp(i\beta)$, $c\exp(i\gamma)$ and $d\exp(i\delta)$ respectively. Some numerical factors are absorbed into the amplitudes during the derivation, in order to simplify the coefficients.

The amplitude and phase of the outgoing alpha-particle waves from the 1^- levels are written $a\exp(i\alpha)$ and from the 3^- level, $b\exp(i\beta)$. Similarly, for the

0^+ level, $c\exp(i\gamma)$, and for the 2^+ level, $d\exp(i\delta)$ represent the amplitude and phase. Then the coefficients of the various powers of $\cos\theta$ may be written down. These are shown in table 6, and when integrated over all angles, the integrated cross section becomes $\Sigma = a^2+\frac{4}{3}b^2+c^2+2d^2$. The coefficients of the various powers of $\cos\theta$ (A_0 to A_4) are shown as a function of proton energy in fig. 7(a)

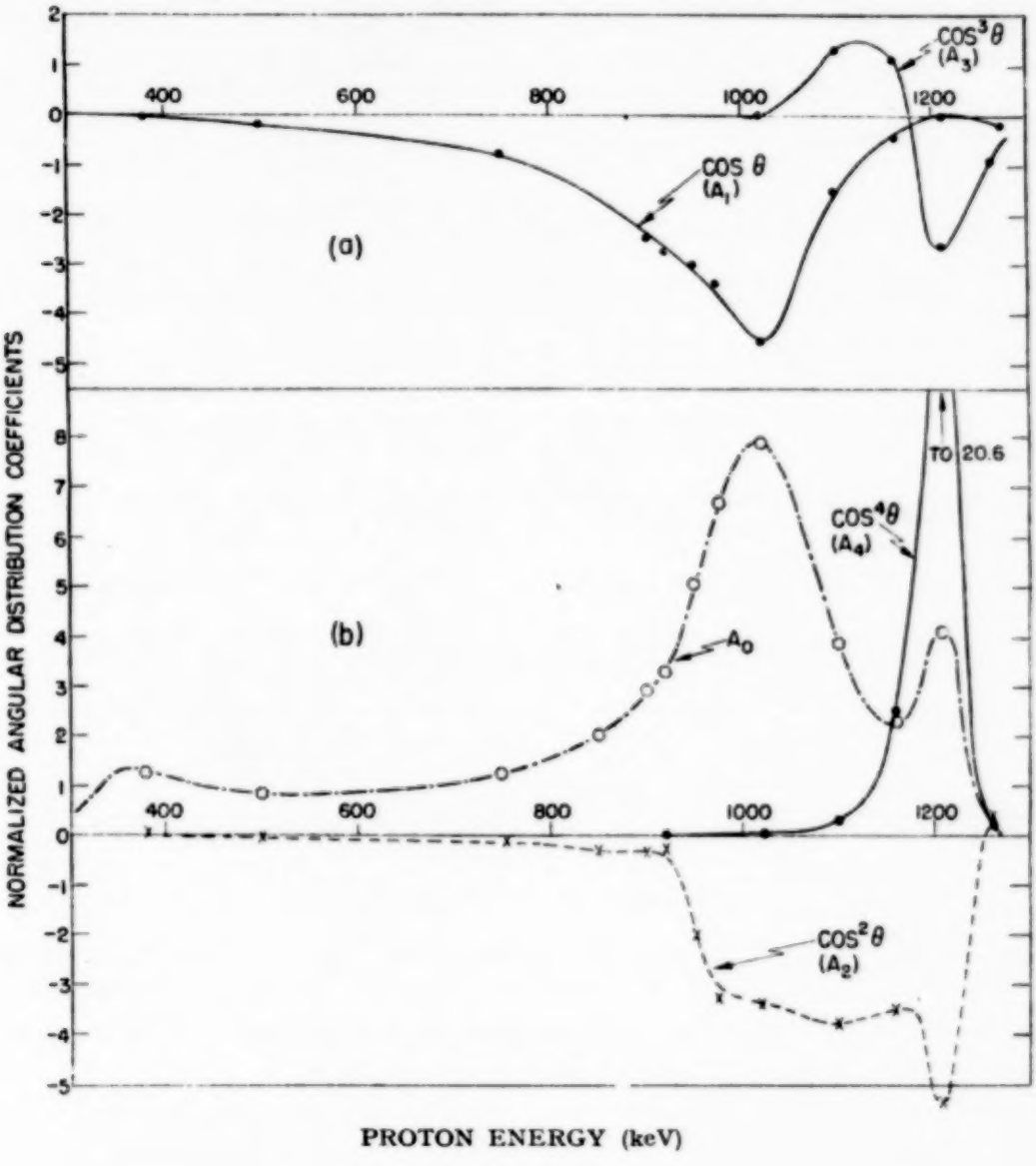

Fig. 7.

(a) The coefficients of $\cos^3\theta(A_3)$ and $\cos\theta(A_1)$, for the $N^{15}(p, \alpha_0)$ angular distributions are plotted as a function of the proton energy. The presence of an anomaly in A_3 at 1200 keV, and its absence in A_1, indicates the influence of a 2^+ level. From the form of variation of A_3 with energy, this 2^+ level is located near 1000 keV.

(b) The coefficients of $\cos^4\theta(A_4)$, $\cos^2\theta(A_2)$ and $1(A_0)$, for the $N^{15}(p, \alpha_0)$ angular distributions are plotted as a function of the proton energy. The function A_0 merely reproduces the main features of the integrated cross section, so is of little interest here. The normalization is such that 1 ordinate unit equals 66.7 mb.

and (b). These coefficients are normalized so that Σ is proportional to the actual integrated cross section.

It is of interest to compare the energy variation of the coefficients of $\cos\theta$ and $\cos^3\theta$. The latter term is produced by interference of the 3^- level with either a 0^+ or a 2^+ level. There is a large and rapid variation in A_3 close to 1200-keV proton energy. If interference with the 0^+ level were responsible, the term $10bc\cos(\beta-\gamma)$ would be large in this energy region. However, A_1 varies only slowly and smoothly in this energy region, in spite of having a term $6bc\cos(\beta-\gamma)$ in A_1. We must conclude, therefore, that the pronounced variation in the $\cos^3\theta$ coefficient near 1200 keV is associated with the term $8bd\cos(\beta-\delta)$, and is not associated with the term $10bc\cos(\beta-\gamma)$. Thus, a 2^+ level is required. The coefficient of $\cos^3\theta$ appears to pass through zero twice, once just below the 1210-keV resonance, and once near 1050 keV. This behaviour is usually caused by the factor $\cos(\beta-\delta)$ passing through zero near each of the resonances. Thus, it is probable that the 2^+ resonance required is at an energy close to 1000 keV. If the factor b is removed from the $\cos^3\theta$ term, the residual term, assumed to be $8d\cos(\beta-\delta)$, shows that $d \approx 1$ at its peak value, and indicates that this peak value should occur at a proton energy slightly below 1030 keV. With this value of d, the contribution to the integrated cross section would be approximately 20 per cent of the peak contribution of the 1^- levels. The location of the 2^+ level within the peak of the 1^- level would effectively hide the contribution of the 2^+ state.

The coefficient of $\cos^4\theta$ is always positive, with its sole source being the 3^- resonance at 1210 keV. The energy variation of A_4 is consistent with the published width of the 1210-keV resonance. The coefficient of $\cos^2\theta$ has several sources. The term $-2b^2$ may be calculated, and also the term $6ab$, but the factor $\cos(\beta-\alpha)$ for the latter term is more doubtful. The quantity A_2+2b^2+6ab may be calculated, as shown in fig. 8. This quantity is more positive than the quantity $3d^2+6cd\cos(\gamma-\delta)$ because $6ab$ is always more positive than $-6ab\cos(\beta-\alpha)$. Since $3d^2$ must be positive, and there are large energy regions in fig. 8 where A_2+2b^2+6ab is negative, it follows that in these energy regions, the term $6cd\cos(\gamma-\delta)$ must be dominant, as this is the only source of a sufficiently large negative term. The presence of this term requires the presence of both a 0^+ and a 2^+ level.

The energy variation of $6ab\cos(\beta-\alpha)$ may be estimated more accurately by requiring a slow, smooth variation with energy of the term $A_2+2b^2-6ab\cos(\beta-\alpha)$ near the 1210-keV resonance. This fixes the phase difference $(\beta-\alpha)$ at the 1210-keV resonance, and the resonant phase shifts can be used to extend the term to other energies where it has an appreciable effect. Because of the factor b, the effect of the term $6ab\cos(\beta-\alpha)$ drops off rapidly below 850-keV proton energy. Fig. 9 shows the estimated term $3d^2+6cd\cos(\gamma-\delta)$ as a function of energy. In this figure, the proton barrier

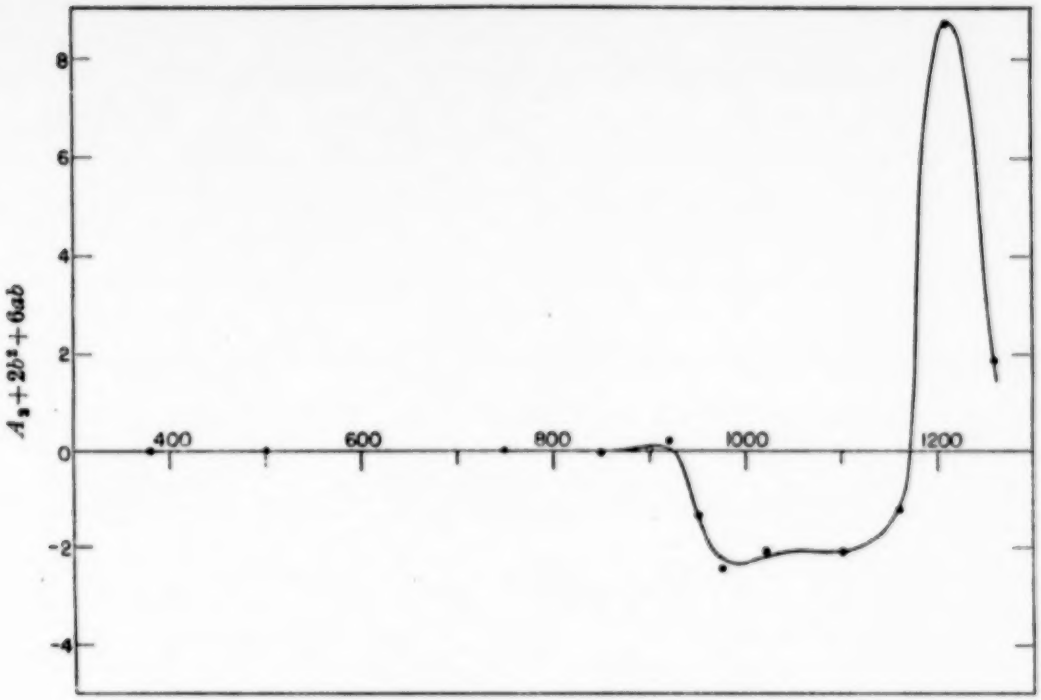

Fig. 8. The function A_2+2b^2+6ab is shown. The residual negative value of this function over a considerable energy range is attributed to interference between a 0^+ and 2^+ resonance.

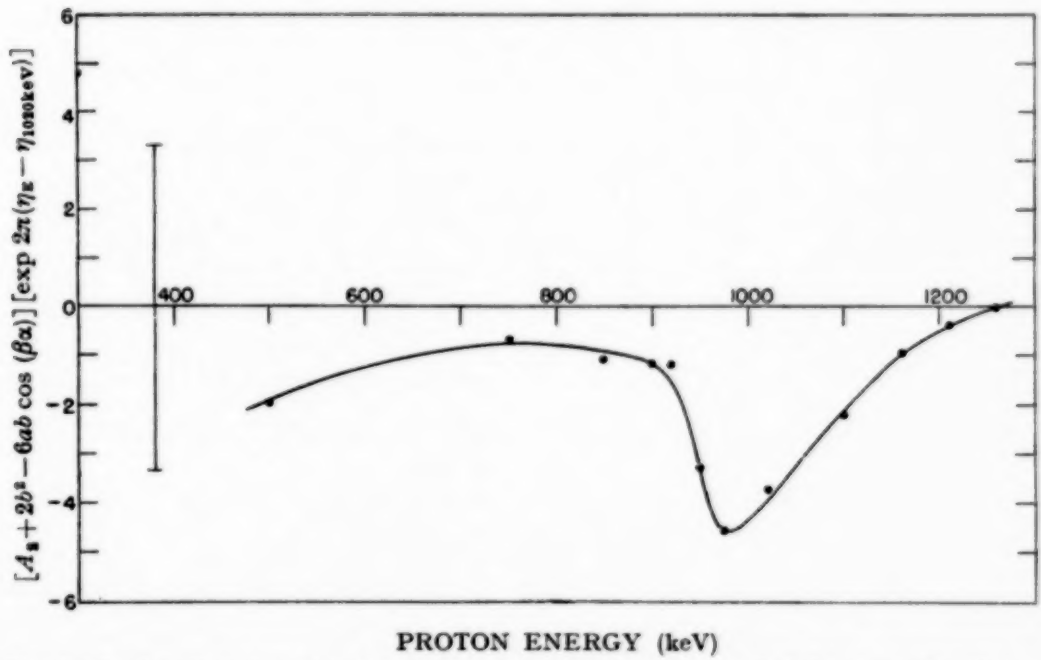

Fig. 9. The function $A_2+2b^2-6ab\cos(\beta-\alpha)$, modified by removal of the proton barrier penetrability (normalized to unity at 1020 keV), is shown. The inverted peak of this function near 1000 keV is attributed to the presence of a 2^+ level near this energy. An appreciable peak is possible near 500 keV, without introducing large $\cos\theta$ interference terms with the 338-keV resonance. This energy (500 keV) is the probable location of the 0^+ resonance shown to be required by fig. 8.

penetrability (normalized to unity at 1020 keV) has been removed. Below 500-keV proton energy, only limits to the term $3d^2+6cd\cos(\gamma-\delta)$ are available, but it is clear that around a proton energy of 400 to 500 keV, a significant value of $6cd$ is possible. There is a peak (inverted) at 975 keV, which should be associated with the 2^+ level near this energy. The experimental data are not sufficiently precise to limit the position of the 0^+ level very well. It would appear, from fig. 9, to be either below 600 keV or close to 1000 keV. The latter position is unlikely, as then the term $6bc\cos(\beta-\gamma)$ in A_1 and A_3 would not have been negligible.

The energy variation of A_1 may be used to support the assignment of the 0^+ level to an energy well below 1000 keV. Fig. 10 shows the energy variation

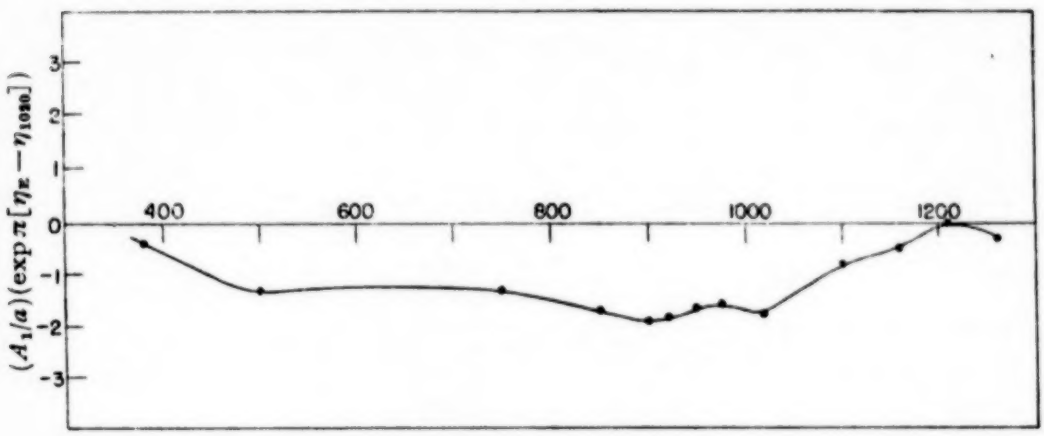

Fig. 10. The function A_1/a, modified by removal of the proton barrier penetrability (normalized to unity at 1020 keV), is shown. The broad spread of the appreciable negative value of this function can be achieved only by having two widely spaced positive parity levels, interfering with the 1^- levels.

of A_1/a with the penetrability factor, again normalized to unity at 1020 keV, removed. This is a plot of the function $4d\cos(\delta-\alpha)+2c\cos(\gamma-\alpha)-6(b/a)c\cos(\beta-\gamma)$. Below 1020 keV, the factor $6b/a$ is negligible compared with 2, so that the third term of this function may be neglected. The function has an appreciable negative value over the whole range from 350 keV up to 1200-keV proton energy. This is only possible if the 0^+ and 2^+ resonances are spaced well apart. Since the 2^+ level has been located near 1000 keV, this puts the 0^+ level close to 500 keV. The magnitude required for c^2 is of the order of 20 per cent to 25 per cent of the integrated cross section at 500 keV. It is therefore very likely that this is the cause of the discrepancy between the calculated and experimental values of the $N^{15}(p, \alpha_0)$ cross section in the region of 500 to 600-keV proton energy. A 0^+ level in this energy region was proposed by Neilson [17]), to explain the Reaction I angular distributions below 950-keV proton energy.

The 2^+ level underlying the 1010-keV 1^- resonance will not lead to important

changes in the fit of the two-level Breit-Wigner formula to the $N^{15}(p, \alpha_0)$ and $N^{15}(p, \gamma_0)$ cross sections. A slight reduction in $\gamma^2_{\alpha_0}$ for the 1010-keV resonance will be sufficient to reduce the 1^- cross section without altering the resonance width very much. This will then leave room for the addition of a 2^+ resonance to restore the integrated cross section to the experimental value.

The coefficients in table 6 are based on the assumption that only the lower of the two possible values of the proton orbital angular momentum forming each level is significant. The argument concerning the existence of a 2^+ resonance near 1000-keV proton energy is not dependent on this assumption, but is valid for all possible angular momenta. The argument concerning the concerning the existence of a 0^+ resonance, based on the negative value of the $\cos^2\theta$ term, is weakened somewhat because of the increased uncertainty in the terms it is necessary to calculate. However, inspection of the energy dependence of A_4, and the lack of need for terms in $\cos^5\theta$ and $\cos^6\theta$, show that the effect of higher order angular momenta must be small. The argument in favour of the wide separation of the 0^+ and 2^+ levels is more qualitative, and is not affected by the introduction of higher order angular momenta.

4.4. STELLAR ENERGIES

The good general agreement of the calculated and experimental integrated cross sections leads to confidence in the cross section extrapolated to stellar energies. The curves of fig. (6a) and (b) have ordinates that are directly proportional to $S = \sigma E \exp(2\pi\eta)$. The extrapolated values of S at 25-keV proton energy are 32 keV · b for $N^{15}(p, \gamma_0)$ and 7.2×10^4 keV · b for $N^{15}(p, \alpha_0)$. The value of S for the $N^{15}(p, \gamma_0)$ reaction depends on the normalization adopted for the 1010-keV γ_0 resonance. The dependence is not as marked as it might be because both the 338-keV resonance and the 1010-keV resonance contribute comparable amplitudes near 25 keV. Thus, the 42 per cent difference in the peak cross sections at 1010 keV for the different normalizations leads to an 18 per cent difference in S at 25-keV proton energy. For the $N^{15}(p, \alpha_0)$ reaction, the contribution from the 1010-keV resonance is small compared with the contribution of the 338-keV resonance. Therefore, the renormalization of the former has had little effect at stellar energies.

The ratio of the S-values for the $N^{15}(p, \alpha_0)$ and $N^{15}(p, \gamma_0)$ reactions is approximately 2200 : 1. The latter reaction represents a leakage from the carbon-nitrogen cycle of energy generation, but the O^{16} produced is returned to the carbon-nitrogen cycle mainly via the reactions $O^{16}(p, \gamma)F^{17}(\beta^+)$ $O^{17}(p, \alpha)N^{14}$. Of these, the $O^{16}(p, \gamma)$ reaction is the slowest, so that most of the matter circulating in this sub-cycle will be in the form of O^{16} while that in the main cycle will be in the form of N^{14}.

The ratio of the amount of nitrogen to the amount of oxygen in a star burning on the C-N cycle, should equal the product of the $N^{15}(p, \alpha)$ and

$O^{16}(p, \gamma)$ cross sections divided by the product of the $N^{15}(p, \gamma)$ and the $N^{14}(p, \gamma)$ cross sections. This ratio, from the estimated cross sections at 25-keV proton energy [18]), is 9 : 1, while the ratio observed [19]) is 14 : 1. The star HZ44, believed to contain material which has been in equilibrium under the C-N cycle [18]), has a very low carbon abundance and a relatively high abundance of nitrogen. It provides the quoted abundance ratio for nitrogen to oxygen.

5. Conclusion

The correction factor of 1.33 applied to the high energy $N^{15}(p, \alpha_0)$ data of SFL leads to internal consistency in the cross sections for Reaction I reported by these workers. Simultaneously it leads to agreement with the later absolute cross section measurements of Bashkin *et al.* All other recent workers have normalized to the data of SFL.

The correction factor of 1.42 applied to the Geiger counter gamma ray overall detection efficiency in the data of SFL leads to internal consistency in the cross sections for Reaction II, if applied to the 4.43-MeV gamma ray efficiency. It simultaneously leads to agreement within experimental error with the absolute measurements of Bashkin *et al.* at the 1210-keV resonance. Again, all other recent workers have normalized their results to the data of SFL. If the same correction factor is applied to the 13-MeV gamma ray efficiency, it leads to appreciably improved agreement between calculation and experiment for the $N^{15}(p, \gamma_0)$ cross section near 600-keV proton energy. The improved agreement is shown in detail in fig. 4. Only SFL have made an absolute cross section measurement for $N^{15}(p, \gamma_0)$ at the 1010-keV resonance.

A very satisfactory fit is obtained to both the $N^{15}(p, \alpha_0)$ and $N^{15}(p, \gamma_0)$ cross sections from the lowest energies at which measurements have been made up to above 1200 keV. The angular distributions measured by Hagedorn and Marion yield considerable information on the presence of a 0^+ level near 500-keV proton energy and a 2^+ level near 1000-keV proton energy. The extrapolation of the cross sections to stellar energies is not strongly dependent on the cross sections for the resonances at which the correction factors were applied, nor on the presence or absence of the 0^+ and 2^+ levels.

The discrepancy in the width of the 12.43-MeV level in O^{16} observed by $C^{12}(\alpha, \alpha)$ and By $N^{15}(p, \alpha_0)$, $N^{15}(p, \alpha_1)$ and $N^{15}(p, \gamma_0)$ has not been resolved. The two-level parameters obtained for the present fit to the $N^{15}+p$ cross sections do not lead to agreement with the measured width for $C^{12}+\alpha$.

The author is grateful to Professor C. A. Barnes, Professor R. F. Christy, Professor W. A. Fowler, and Professor T. Lauritsen for many helpful suggestions and discussions. The assistance of Dr. N. Tanner with the early experimental work is gratefully acknowledged. The critical reading of the manuscript by Professor S. Bashkin has been much appreciated.

Appendix

INTERFERENCE OF STATES OF MIXED ISOBARIC SPIN

Under conditions when J^π and T are good quantum numbers, the R-matrix of Wigner [20]) may be written as a number of sub-matrices along the main diagonal, with all remaining terms zero. Each sub-matrix is specified by particular values of J^π and T, and the channels labelling the sub-matrix elements are all those channels by which it is possible to form a state of the particular J^π and T. Then the sub-matrix elements themselves contain explicitly only the sum of terms $\gamma_{\lambda c}\gamma_{\lambda c'}/(E_\lambda - E)$, over all levels λ with the particular J^π and T. This point of view, and the distinction which is sometimes drawn between "internal interference" (between levels of the same J^π) and "external interference" (when either J or π is different for two levels) although correct, are not helpful in extending the analysis of interference to the case of levels of mixed J^π or T. Thus, it is not immediately clear that a mixed set of states should not be analyzed as "internal interference" between the amplitudes of the parts with the same sets of $J^\pi T$, followed by "external interference" between the resultant amplitudes for different sets of $J^\pi T$. This analysis can give results quite different from those of the correct method, which ignores the bad quantum number initially.

Assuming that we are still working with states of pure J^π and T, the grouping of sub-matrix elements that we have found requires that the channels are defined to produce states of pure J^π and T. An alternate definition of channels, one of more physical significance, is to require that they be polarized in isobaric spin space, with definite T_3 components. In order to construct such channels, linear combinations must be taken over levels with all the possible values of T, so that, in the transformed R-matrix, the elements now contain, explicitly, summations over all levels with the correct value of J^π, and all possible values of T. Nevertheless, certain relationships must hold between the various matrix elements in order that the new matrix may be able to be transformed back to the original one. The transition to the case of mixed quantum states and the violation of selection rules is made by relaxing the requirements of these special relationships between the matrix elements. The quantum states that become mixed need not necessarily be isobaric spin states, but the same analysis may also be applied to states of mixed J or π.

Whatever the quantum states that are mixed, the group of sub-matrices that correspond to the possible contributors to the mixture must now be treated as a unit in the R-matrix. In the case of no mixture, this procedure leads to results identical with those obtained by treating the sub-matrices separately (internal interference) and then combining the resultant amplitudes and phases in the collision matrix (external interference).

The R-matrix elements have been shown [20]) to be of the form

$R_{cc'} = \sum_\lambda \gamma_{\lambda c}\gamma_{\lambda c'}/(E_\lambda - E)$. It is interesting to consider what happens when attention is transferred from a sub-matrix specified by a particular $J^\pi T$ (say) to a group of such sub-matrices. Although within each sub-matrix, the summation could be confined to levels of the particular J^π and T, when a group of sub-matrices is taken together, the matrix elements are no longer of the form required unless the $\gamma_{\lambda c}$ for each level occurring anywhere in the group of sub-matrices appears explicitly in the sum for each matrix element. The $\gamma_{\lambda c}$ may be zero, as it would be if not allowed by a selection rule, but it must appear, or the form of the matrix elements, deduced from very general considerations, is not preserved. When the R-matrix is considered as a whole, all levels must appear explicitly in the summation for the matrix elements. The operation of selection rules is now transferred back to the stage of calculation of the individual $\gamma_{\lambda c}$, rather than by a selection of the terms occurring in the summation for a particular matrix element.

Thus, even in the case of levels of pure $J^\pi T$, no distinction need be made between levels in the summation to form the matrix element. The transition to the case of mixed J, π, or T, is made by continuing to ignore any distinction between levels. Certain $\gamma_{\lambda c}$ which were originally required, by selection rules, to be zero, are now found to be non-zero, and may be interpreted as giving the amplitude of admixture of the various mixing states in the level at energy E_λ. This concept retains the selection rules and explains their failure by introducing the mixing of states.

The analysis of $N^{15}(p, \alpha_0)$ and $N^{15}(p, \gamma_0)$ has followed this concept. No distinction is drawn between $T = 0$ and $T = 1$ levels in the R-matrix, but attention has been confined to the 1^- levels. The $\gamma^2_{\gamma c}$ found have been interpreted as percentage admixtures in intensity of the $T = 0$ and $T = 1$ components in the two 1^- levels. It is not known whether there should be any general relation between the signs of the $\gamma_{\lambda c}$ taking part in the mixture. As far as this analysis goes, the $\gamma_{\lambda c}$ may be of completely arbitrary sign.

References

1) F. Ajzenberg-Selove and T. Lauritsen, Nuclear Physics **11** (1959) 1
2) Schardt, Fowler and Lauritsen, Phys. Rev. **86** (1952) 527
3) A. V. Cohen and A. P. French, Phil. Mag. **44** (1953) 1259
4) Neilson, James and Barnes, Phys. Rev. **92** (1953) 1084 A
5) F. B. Hagedorn and J. B. Marion, Phys. Rev. **108** (1957) 1015
6) Bashkin, Carlson and Douglas, Phys. Rev. **114** (1959) 1543
7) Barnes, James and Neilson, Can. J. Phys. **30** (1952) 717
8) Kraus, French, Fowler and Lauritsen, Phys. Rev. **89** (1953) 299
9) F. B. Hagedorn, Phys. Rev. **108** (1957) 735
10) S. Bashkin and R. R. Carlson, Phys. Rev. **106** (1957) 261
11) A. A. Kraus, Phys. Rev. **94** (1954) 975
12) J. W. Bittner and R. D. Moffat, Phys. Rev. **96** (1954) 374
13) A. W. Schardt, Ph. D. Thesis, California Institute of Technology (1951)

14) R. W. Kavanagh, Ph. D. Thesis, California Institute of Technology (1956)
15) W. A. Fowler and R. G. Thomas, Phys. Rev. **91** (1953) 473
16) A. M. Lane and R. G. Thomas, Revs. Mod. Phys. **30** (1958) 257
17) G. C. Neilson, Ph. D. Thesis, University of British Columbia (1955)
18) Burbidge, Burbidge, Fowler and Hoyle, Revs. Mod. Phys. **29** (1957) 623
19) G. Münch, Astrophys. J. to be published
20) E. P. Wigner and L. Eisenbud, Phys. Rev. **72** (1947) 29

2.B:2.D

Nuclear Physics **15** (1960) 316—325; © *North-Holland Publishing Co., Amsterdam*

Not to be reproduced by photoprint or microfilm without written permission from the publisher

THE ANGULAR AND ENERGY DISTRIBUTION OF PROTONS FROM Ni^{58} REACTIONS INDUCED BY 14.8 MeV NEUTRONS

I. KUMABE † and R. W. FINK ††

Department of Chemistry, University of Arkansas, Fayetteville, Arkansas †††

Received 28 September 1959

Abstract: The angular and energy distributions of protons from the Ni^{58}(n, p)Co^{58} and Ni^{58}(n, np)Co^{57} reactions with 14.8 MeV neutrons were measured using a shielded multiplate camera. The results indicate that the Ni^{58}(n, p) and Ni^{58}(n, np) reactions occur predominantly through the formation and decay of the compound nucleus, with a small contribution from the direct interaction of the incident neutrons with protons. A semilog plot of the relative level densities calculated from the energy distribution of the protons fits two straight lines corresponding to Maxwellian distributions with temperatures of about 1.0 MeV for the Ni^{58}(n, p) reaction and about 0.5 MeV for the Ni^{58}(n, p) and Ni^{58}(n, np) reaction. The total cross section determined from this data is 440 mb $\pm$ 10 %.

1. Introduction

Activation cross sections have been measured for many elements for the case of 14.5 MeV neutrons by Paul and Clarke [1]). They have shown that the (n, p) and (n, α) reaction cross sections for large mass numbers are much larger than those predicted by the evaporation theory, while the (n, 2n) reaction cross sections are approximately in agreement with the theory, and suggested the existence of a direct process in the case of (n, p) and (n, α) reactions. Experimental data of the angular and energy distributions on (n, p) reactions is necessary to give reliable information on these problems.

In previous papers [2–4]), the angular and energy distributions of the alpha particles from the interaction of 14.8 MeV neutrons was reported for medium weight nuclei. It has been found that the angular distributions for the entire energy region of particles are concave upward and are approximately 90° symmetrical. Therefore, this process proceeds principally by way of the compound nucleus mechanism.

In the past few years several workers [5–19]) have measured the angular and energy distributions of the protons from the interaction of approximately 14 MeV neutrons with medium weight nuclei. They found that the angular

† Postdoctoral fellow, 1958—1959. Present address: Department of Physics, Kyoto University, Kyoto, Japan.

†† Present address: Gustaf Werner Institute for Nuclear Chemistry, University of Uppsala, Sweden.

††† Supported in part by the U. S. Atomic Energy Commission.

distributions for the high energy region of protons exhibited a forward asymmetry which increased with increasing proton energy, while the angular distributions of the low energy region was shown to be approximately isotropic or 90° symmetrical. These results were interpreted as evidence that these reactions included a contribution from the direct interaction of the incident neutrons with the protons in target nuclei, although a large part of the reactions probably occur through the formation of a compound nucleus.

Since most of earlier work was carried out under special experimental arrangements, the results might include some ambiguity. To obtain more information about the interaction mechanisms, a similar study for Ni^{58} was undertaken using a multiplate camera with a large iron and paraffin shield.

2. Experimental Procedure

The experimental arrangement, shown in fig. 1, was similar to that used by Frye [20]). The 14.8 MeV neutrons were produced by the T, (D, n)He^4 reaction initiated with 400 keV deuterons in the University of Arkansas Cockcroft-Walton accelerator [21]). The neutron flux was monitored by counting the accom-

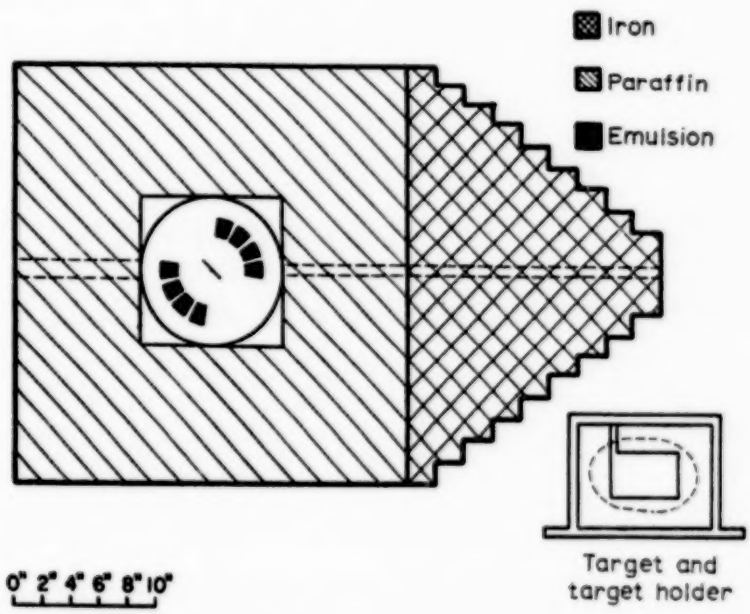

Fig. 1. Schematic of shielding and camera arrangement.

panying alpha particles from the D-T reaction. The camera plates were shielded from the neutron source with 18 inches of iron and 8 inches of paraffin forming a collimator of approximately pyramidal shape. A cylindrical channel in the iron, 0.75 inches in diameter, gave a neutron beam one inch in diameter at the target.

Proton tracks were recorded in Ilford C2 emulsion (1×1 inch), 400 microns thick, in a plane 0.75 inches below the axis of the beam. The inner edges of the emulsion plates were on a circle of radius 2.4 inches inside the camera. The

target was metallic Ni^{58} foil (99.6 %), obtained from Oak Ridge National Laboratory, which was placed in a target holder made of lead, as shown fig. 1, and placed at an angle of 45° to the incident beam. The target thickness was 17.3 mg/cm² and target size was 0.6×0.95 inches.

The plates and the Ni^{58} target were enclosed in an evacuated cylindrical aluminium chamber 10 inches in diameter and 3 inches high, lined with 1 mm of lead to minimize charged particle production in the wall. The total neutron flux at the target was 8.87×10^8 neutrons/cm².

Plates were developed by the temperature method [22]) and searched with a Leitz binocular microscope. Accepted tracks were required to originate at the emulsion surface and to travel in directions that assured their points of origin in the Ni^{58} foil. For each acceptable track, measurements were corrected using the edge and surface plane of the emulsion plate as the reference for range and angular components. Allowance was made for the loss of proton energy in passing through the target layer to the emulsion surface by adding to the observed energy of protons the energy it would have lost in traversing half the thickness of the target layer, taking account of its observed average angle of dip with respect to the emulsion surface. The shrinkage factor (1.8) was obtained by measuring the horizontal and vertical components of the lengths of ThC′ alpha tracks. From these data the energy of each accepted proton was determined using the range-energy relation of Rotblat [23]).

3. Results

The angular distribution of protons emitted from Ni^{58} for the entire energy region is shown in fig. 2. The total cross section for the emission of protons was found to be 440 mb $\pm$ 10 %. The angular distributions for three different ranges of proton energies are shown in fig. 3. The energy distributions of the emitted protons for four angular intervals are shown in fig. 4. Errors in figs. 2, 3 and 4 are the statistical errors derived from the track counts of target and background data.

Alpha particles are assumed not to affect interpretation of the data, since most of the anticipated alpha particles correspond to energies below 2 MeV on the abscissa in fig. 4 owing to the large absorption loss in the target and consideration of the energy distribution [2–4]) of the emitted alpha particles. The (n, pp) and (n, d) processes also are energetically possible, but they have been expected so far to make a negligible contribution to the observations because of the large negative Q-values and the Coulomb barrier. Recently, however, Colli and coworkers [24]) found that some (n, d) cross sections are of the same order of magnitude as the (n, p) values for medium weight nuclei.Consequently, the present results for the low energy region include some contribution from deuterons from the Ni^{58}(n, d) reaction, since deuteron tracks are not distinguished from proton tracks in the present work.

It is assumed that the relation between the measured proton energy distribution and the level density of the residual nucleus is given by the following formula [25]):

$$n(\varepsilon)\mathrm{d}\varepsilon = \text{const.}\ \varepsilon\sigma_c(\varepsilon)\omega(\varepsilon_\gamma)\mathrm{d}\varepsilon$$

where $n(\varepsilon)\mathrm{d}\varepsilon$ is the number of protons emitted with energy between ε and $\varepsilon+\mathrm{d}\varepsilon$, and $\sigma_c(\varepsilon)$ is the cross section, including the effects of barrier penetration for a nuclear radius of $1.3\times10^{-13}A^{\frac{1}{3}}$ cm, for the formation of the compound nucleus in the same state of excitation by the reverse reaction, in which protons

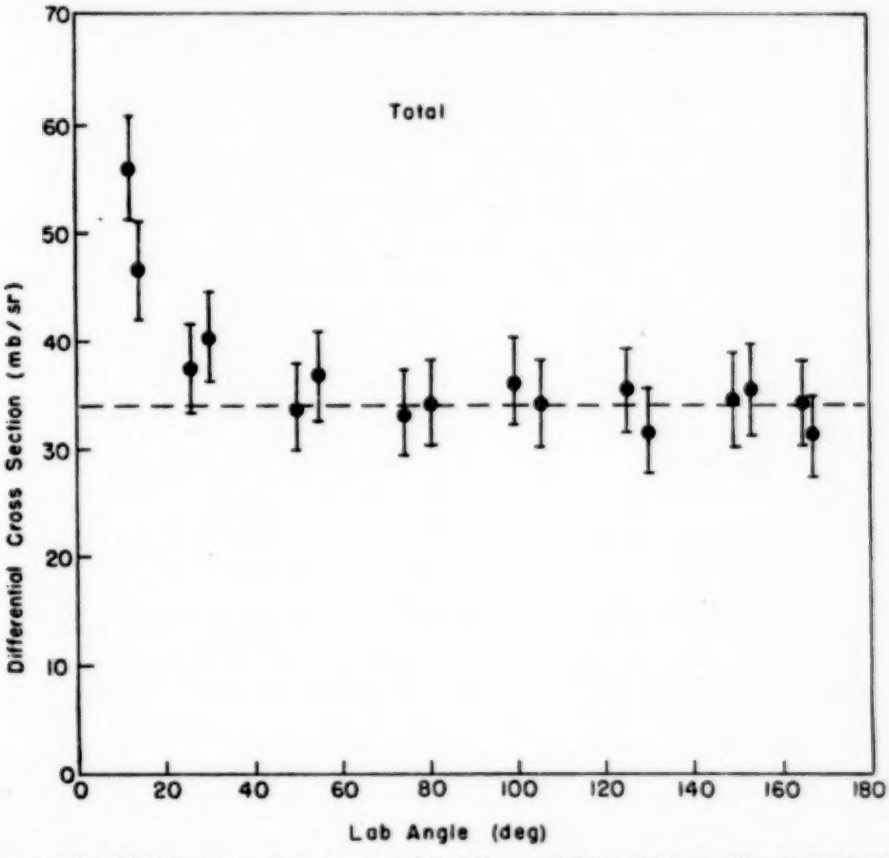

Fig. 2. The angular distribution of protons emitted from Ni^{58} irradiated with 14.8 MeV neutrons.

of energy strike the excited residual nucleus [26]). The factor $\omega(\varepsilon_\gamma)$ is the density of the energy levels of the residual nucleus at excitation $\varepsilon_\gamma = \varepsilon_{max}-\varepsilon$, where ε_{max} is the maximum energy which the emitted proton may have. Fig. 5 shows these results, represented by plotting the measured energy distribution in the angular range 90°—180°, divided by $\varepsilon\sigma_c(\varepsilon)$. The points lie on two straight lines corresponding to the † Ni^{58}(n, p)Co^{58} and Ni^{58}(n, p)Co^{58}+Ni^{58}(n, np)Co^{57} reactions. The slopes of the lines gives the temperature parameters, $T = 1.0$ MeV and $T = 0.5$ MeV, for the residual nuclei formed by these two reactions.

† The reaction denoted by (n, p) in this paper includes both the (n, pγ) and (n, pn) processes.

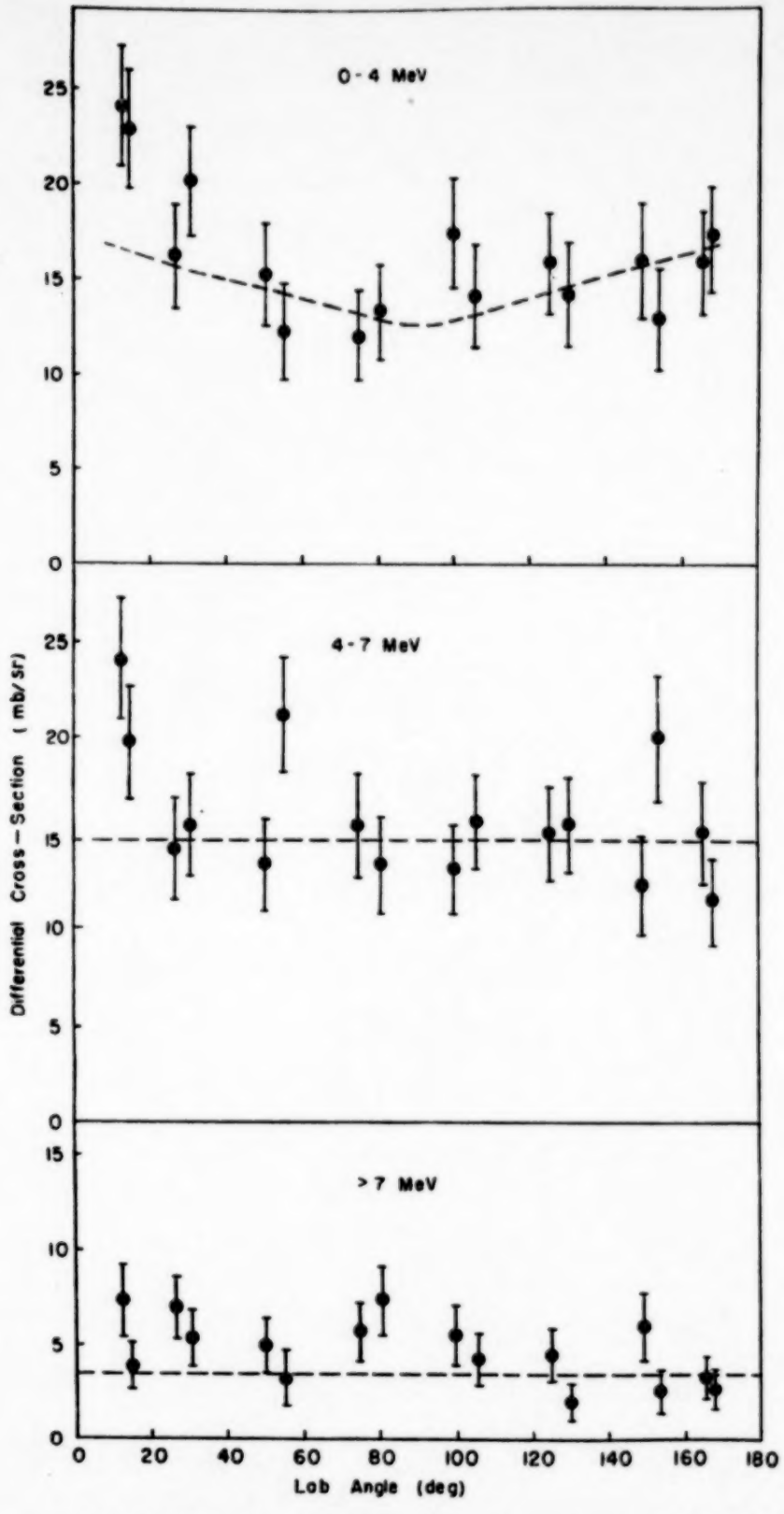

Fig. 3. The angular distribution of protons is shown in the energy ranges of from 0 to 4 MeV, 4 to 7 MeV, and greater than 7 MeV.

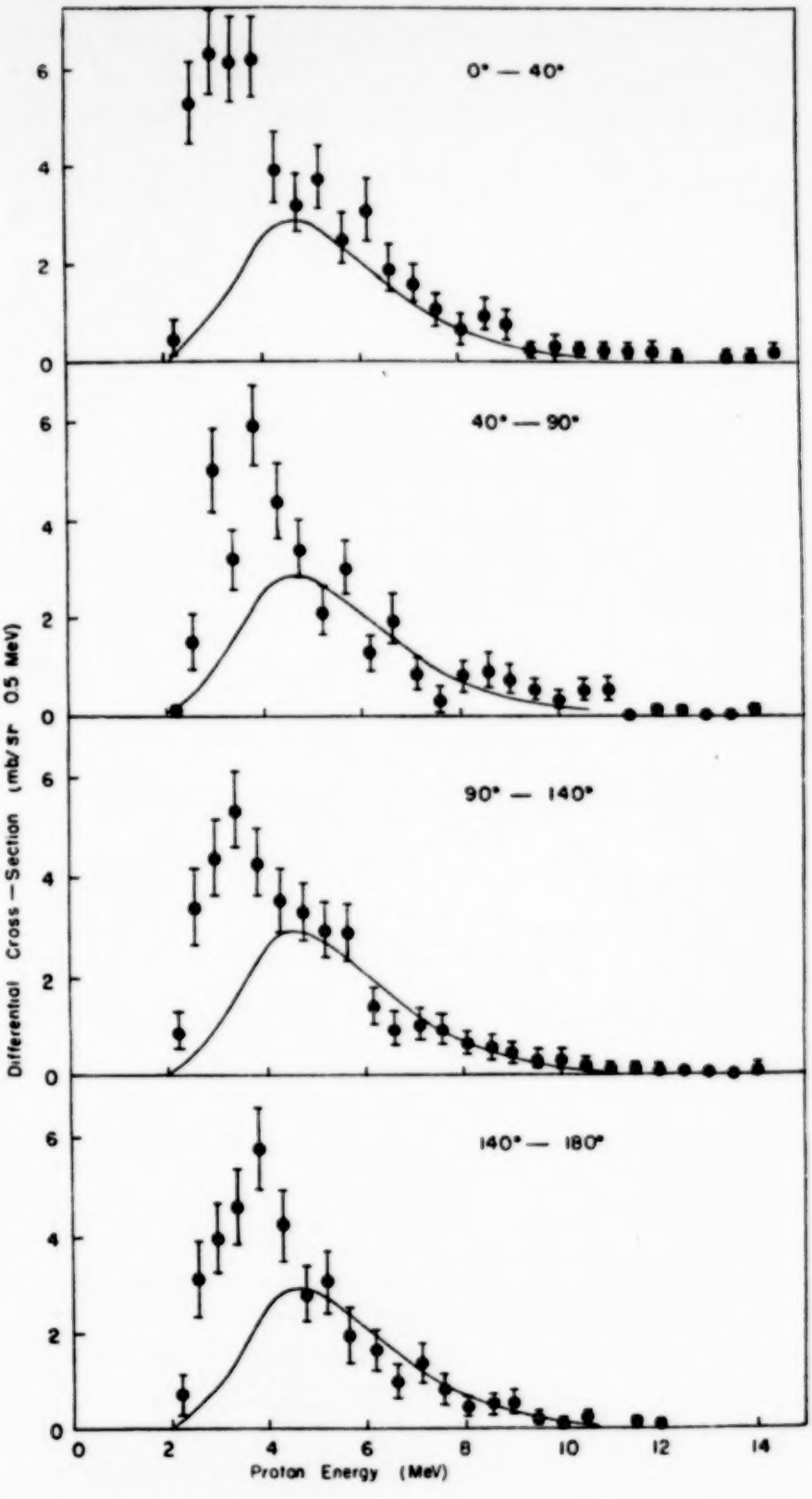

Fig. 4. The energy distribution of protons at angles from 0° to 40°, 40° to 90°, 90° to 140°, and 140° to 180°.

The curve represents the combined (n, p) and (n ,pp) spectrum predicted by the statistical theory on the basis of a Maxwellian proton energy distribution.

The solid lines in fig. 4 give the energy distribution for the (n ,p) reaction alone, derived from the line $T = 1.0$ MeV. The areas under the two spectra

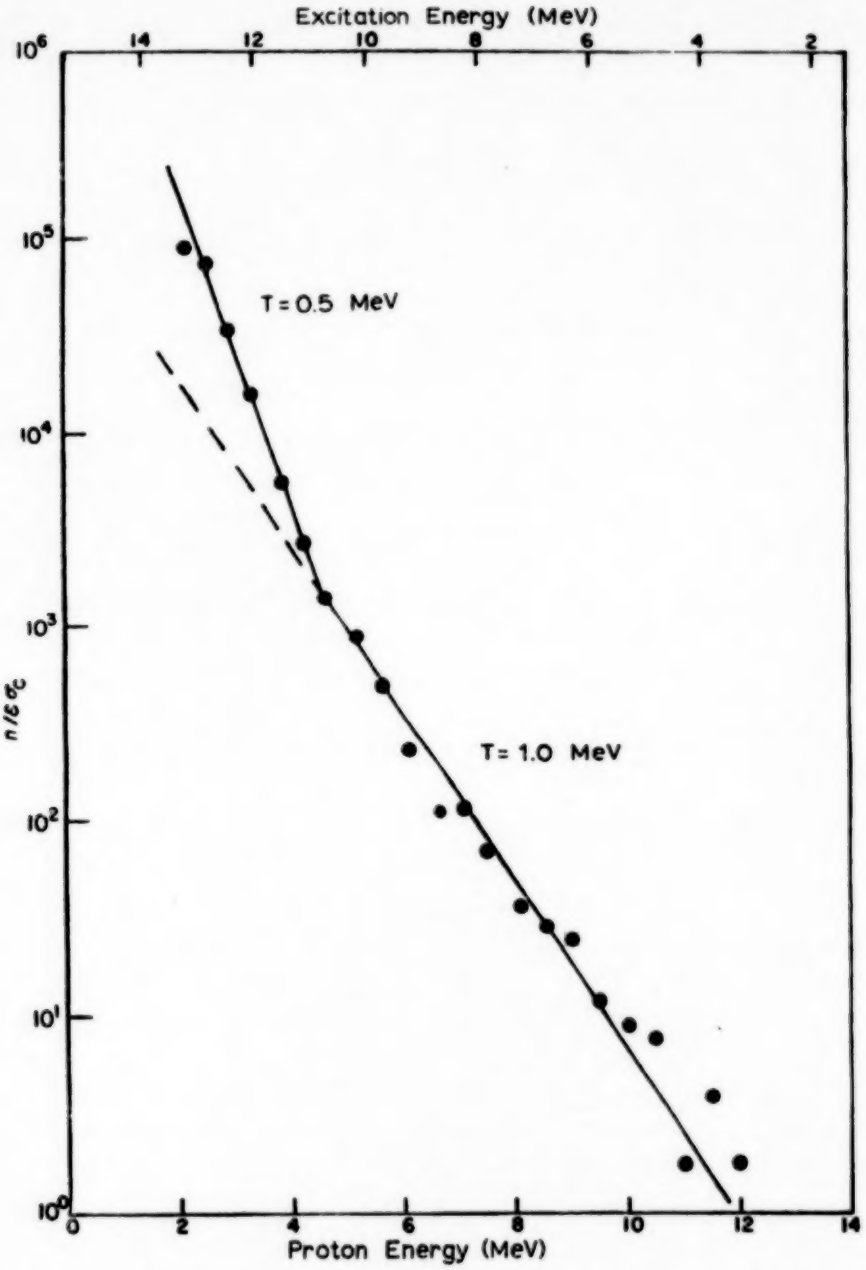

Fig. 5. The distribution of proton energy showing the nuclear temperatures for Ni^{58}(n, p) and (n, np) reactions.

give the relative contribution of the (n, p) and (n, np) reaction to the total proton emission cross section: they are 64 % and 36 % respectively. The total number of proton tracks observed was about 1500, with the number of background tracks being 44.

4. Discussion

All the energy distributions show similar shapes to each other within the statistical error and show a variation in the curve symmetry at about 5 MeV, which would correspond to a maxima of the energy distribution of the protons for the (n, p) reaction (fig. 4). Allan [5]) has observed a variation in the energy distribution of protons emitted from Ni^{58} at an angle $34\pm20°$ with respect to the incident neutrons.

The Q values for the (n, p), (n, np) and (n, 2n) reactions are $+0.6$, -7.7 and -11.7 MeV, respectively. Therefore the large number of protons with energies below 4 MeV emitted by Ni^{58} is probably due to the (n, np) reaction which is favoured to the (n, 2n) reaction due to the differences in Q values for the two reactions as pointed out by Allan [5]). Fig. 5 also illustrates the occurrence of the (n, np) reaction in Ni^{58} at energies below 4.5 MeV and the temperatures are in good agreement with those obtained by March *et al.* [9–11]) and Allan [6, 7]) for similar reactions induced by 13.5—14 MeV neutrons in Fe^{54}, Fe^{56}, Ni^{60}, and Cu.

Allan [7]) has pointed out that the angular distribution of the protons from a 14 MeV (n, np) reaction has a minimum at 90° and maxima at 0° and 180°, while that of the low energy (n, p) proton is more nearly isotropic. The broken lines on the angular distributions in figs. 2 and 3 were drawn through the mean experimental points at backward angles. It is seen that the angular distributions of the protons for the energy region 0—4 MeV and 4—7 MeV in fig. 3 are roughly 90° symmetrical and isotropic respectively, although there appears to be slight peaking in the forward direction. However, the angular distribution of the protons for the energy region greater than 7 MeV shows a large excess at the forward angles.

The forward peaking and excess in fig. 3 are probably due to the direct interaction [27, 28]) of the incident neutron with a proton of the target nucleus. If the 90° symmetrical or isotropic part of the proton distribution is attributed to the decay of a compound nucleus and the excess at forward angles to a direct interaction, then the maximum value for the compound nucleus cross section would be 420 mb (270 mb (n, p) and 150 mb (n, np)) and the direct interaction of the incident neutron with protons would have a minimum value of 17 mb. However, there is some ambiguity in assigning the protons from the (n, np) process to either compound nucleus formation or direct interaction of the incident neutron with a neutron in the nucleus, because of the over-lapping of the peaks in the energy distribution curves (fig. 4). If it is assumed that a second neutron is always emitted when the emission of a second neutron is energetically possible, the cross section for the (n, pγ) reaction only can be estimated to be $\approx$ 80 mb. It seems to be too small compared with an activation cross section (287 mb) obtained by Preiss and Fink [29]). It is difficult to explain

the difference between the present result and the activation result. There may be considerable contribution of the (n, pγ) reaction in the region where the emission of a second neutron is energetically possible.

Brown and Muirehead [28]) have calculated the contribution made by direct interactions assuming that nucleon-nucleon interactions can occur throughout the nuclear volume. The cross sections calculated by them for Ni^{58} are 470 mb for the compound nucleus and 60 mb for the direct interaction. The experimental cross section (17 mb) for the direct interaction is only about one third of the theoretical value, although that (420 mb) for the compound nucleus is in agreement with the theoretical value. Similar results have been obtained for Fe^{54} by Allan [7]). The experimental cross section for Fe^{54}(n, p) direct interaction at 14 MeV was found to be 20 mb while the theoretical value is 55 mb.

Allan [5]) has obtained the differential cross section of $530/4\pi$ mb/sr at an angle $34° \pm 20°$, which is in agreement with the value at an angle $34° \pm 20°$ obtained in this work of 41 mb/sr ($520/4\pi$ mb/sr).

Colli and coworkers [15]) measured the angular distribution of the protons emitted from natural nickel (67.4 % Ni^{58}, 26.7 % Ni^{60}) and found that the proton spectrum is more intense at forward than backward angles. The contribution from the direct interaction would be calculated from their data to be about 10 %. March and Morton [10]) have measured the angular and energy distribution of the protons emitted from Ni^{60} for bombardments with 13.5 MeV neutrons and found that about 30 % of the protons emitted can be attributed to the direct interaction processes. The value for Ni^{58} calculated from their results is not in disagreement with the present result (4 %). Considerable direct interaction effects have been observed for Al, Fe^{54}, Fe^{56}, Ni^{60} and Cu by March and Morton [9–11]), and Allan [5–7]). The main tendencies of their results are in general agreement with those reported in this work for Ni^{58}.

It may be concluded that the Ni^{58}(n, p)Co^{58} and Ni^{58}(n, np)Co^{57} reactions at 14.8 MeV occur predominantly through the formation and decay of the compound nucleus, although there is a contribution from the direct interaction of the incident neutrons with protons of the target nucleus amounting to at least 4 %.

The authors wish to thank Mr. F. L. Taylor, Mr. A. Poularikas, and Mr. G. Culp for their assistance throughout the course of the experiment, to Mr. J. M. Moring for help in calculations and to Mr. J. E. Wray of the Accelerator Laboratory for operation of the accelerator during bombardments.

References

1) E. B. Paul and R. L. Clarke, Can. J. Phys. **31** (1953) 267
2) Kumabe, Takekoshi, Ogata, Tsuneoka and Ōki, Phys. Rev. **106** (1957) 155
3) Kumabe, Takekoshi, Ogata, Tsuneoka and Ōki, J. Phys. Soc. Japan **13** (1958) 129

4) I. Kumabe, J. Phys. Soc. Japan **13** (1958) 325
5) D. L. Allan, Proc. Phys. Soc. A **70** (1957) 195
6) D. L. Allan, Nuclear Physics **6** (1958) 464
7) D. L. Allan, Nuclear Physics **10** (1959) 348
8) Brown, Morrison, Muirhead and Morton, Phil. Mag. **2** (1957) 785
9) P. V. March and W. T. Morton, Phil. Mag. **3** (1958) 143
10) P. V. March and W. T. Morton, Phil. Mag. **3** (1958) 577
11) P. V. March and W. T. Morton, Phil. Mag. **3** (1958) 1256
12) L. Colli and U. Facchini, Nuovo Cimento **4** (1956) 671
13) Badoni, Colli and Facchini, Nuovo Cimento **4** (1956) 1618
14) L. Colli and U. Facchini, Nuovo Cimento **5** (1957) 309
15) Colli, Facchini, Iori, Marcazzan and Sona, Nuovo Comento **7** (1958) 400; **13** (1959) 730
16) Colli, Pignanelli, Rytz and Zurmuehle, Nuovo Cimento **9** (1958) 280
17) Haling, Peck and Eubank, Phys. Rev. **106** (1957) 971
18) Verbinski, Hurliman, Stephans and Winhold, Phys. Rev. **108** (1957) 779
19) L. Rosen and A. H. Armstrong, Bull. Am. Phys. Soc. **1** (1956) 224
20) G. M. Frye, Jr., Phys. Rev. **93** (1954) 1086
21) Bronner, Ehlers, Eukel, Gordon, Marker, Voelker and Fink, Nucleonics **17** No. 1 (1959) 94
22) Dainton, Gaittiker and Lock, Phil. Mag. **42** (1951) 396
23) J. Rotblat, Nature **167** (1951) 550
24) L. Colli, F. Cvelbar, S. Micheletti and M. Pignanelli, Nuovo Cimento **13** (1959) 868
25) V. F. Weisskopf, Phys. Rev. **52** (1937) 295
26) J. M. Blatt and V. F. Weiskopf, Theoretical Nuclear Physics (John Wiley and Sons, Inc., New York, 1952) p. 353
27) Austern, Butler, and McManus, Phys. Rev. **92** (1953) 350
28) G. Brown and H. Muirehead, Phil. Mag. **2** (1957) 473
29) I. L. Preiss and R. W. Fink, Nuclear Physics **14** (1959/60)

2.A.1:
2.D:3.A

Nuclear Physics **15** (1960) 326—336; © *North-Holland Publishing Co., Amsterdam*

Not to be reproduced by photoprint or microfilm without written permission from the publisher

NEW ISOTOPES OF COBALT; ACTIVATION CROSS-SECTIONS OF NICKEL, COBALT, AND ZINC FOR 14.8 MeV NEUTRONS

I. L. PREISS † and R. W. FINK ††

Department of Chemistry, University of Arkansas, Fayetteville, Arkansas †††

Received 17 September 1959

Abstract: Absolute neutron activation cross-sections at 14.8 MeV have been measured for the five stable nickel isotopes, for cobalt, and for zinc, based on comparison with the $Cu^{63}(n, 2n)Cu^{62}$ reaction (556 mb), the $Cu^{65}(n, 2n)Cu^{64}$ cross-section (1000 mb), and the $Al^{27}(n, \alpha)Na^{24}$ reaction (115 mb). During the course of this investigation, three new cobalt activities have been identified as Co^{63}, 1.40 ± 0.05 h, and Co^{64} isomers: Co^{64m}, 2.0 ± 0.2 min, and Co^{64g}, 7.8 ± 0.2 min.

The reactions studied, measured half-lives, and activation cross-sections are listed in table 1. Comparison is made between the experimental cross-sections and the continuum model of the compound nucleus described by Blatt and Weisskopf. A discussion is presented concerning the possible reasons for the deviation of the experimental values from those calculated from theoretical considerations.

1. Introduction

Several groups have reported nuclear reactions on nickel isotopes such as (n, np) [1, 2, 3]), (α, αnp) and (α, α2p) [4, 5]), (p, np) [6]), (p, 2p) [7]), and (γ, pn) and (γ, p) [8]). The unusual feature of these is that those reactions involving proton emission predominate markedly over those involving neutron emission, e.g. $\sigma(p, 2p)/\sigma(p, pn) = 2.8$ [7]), $\sigma(\gamma, p)/\sigma(\gamma, n) = 2.35$ [8]), and $\sigma(n, p)/\sigma(n, 2n) = 5.5$ for Ni^{58} from values reported in this paper (table 1). Allan [1]) and March and Morton [2]), using emulsion techniques, and Colli and Co-workers [9]), utilizing a proportional coincidence scintillation counter method, found two groups of low energy protons in excess of that predicted by the continuum model of compound nucleus reactions. These observations lead to the conclusion that direct interaction processes contribute to proton emission to an appreciable extent.

Levkovskii [10]), in summarizing available yield data on (n, p) and (n, α) reactions, has noted sharply decreasing cross-sections with increasing neutron number at constant Z. The five stable nickel isotopes, ranging in N from 30 to

† Phillips Petroleum Company predoctoral fellow, 1957—1958. Present address: Heavy Ion Accelerator Laboratory, Yale University, New Haven 11, Conn.

†† Present address: Gustaf Werner Institute for Nuclear Chemistry, Univ. of Uppsala, Sweden.

††† Supported in part by the U. S. Atomic Energy Commission. A preliminary report of this work appeared in Bull. Am. Phys. Soc. **3** (1958) 322, H2. This work constitutes part of the PhD thesis of I. L. Preiss at the University of Arkansas.

TABLE 1

Absolute neutron activation cross-sections for nickel, cobalt and zinc reactions with 14.8 MeV neutrons and comparison with other work and theory

Reaction	Product	Measured half-life	Measured cross-section (mb)		Q-value (MeV)	a (MeV^{-1})	Calculated cross-section (mb)	Ratio $\sigma_{exp}/\sigma_{calc}$
			Present work	Other work				
$Ni^{64}(n, p)$	Co^{64m}	2.0 ±0.2 min	0.43± 0.02 †					
$Ni^{64}(n, p)$	Co^{64g}	7.8 ±0.2 min	4.1 ±0.05 ††		−5.08	1.8	6.7	0.68
$Ni^{64}(n, np)$	Co^{63}	1.40±0.05 h	0.93± 0.04		−10.86		0.0024	388
$Ni^{62}(n, p)$	Co^{62m}	1.9 ±0.3 min	2.0 ± 0.5 †					
$Ni^{62}(n, p)$	Co^{62g}	13.8 ±0.2 min	3.3 ± 0.02 ††		−3.14	1.7	17	0.31
$Ni^{62}(n, np)$	Co^{61}	1.70±0.05 h	0.65± 0.15		−9.70		0.008	81
$Ni^{61}(n, p)$	Co^{61}	1.7 ±0.05 h	22 ± 2	181 [a])	−0.63	1.6	30	0.27
$Ni^{61}(n, np)$	Co^{60m}	10.5 ±0.2 min	3.8 ± 1		−9.7		0.01	380
$Ni^{60}(n, p)$	Co^{60m}	10.5 ±0.2 min	9 ± 2	80 total [b])				
$Ni^{60}(n, p)$	Co^{60g}				1.06	1.6	120	0.65
$Ni^{60}(n, np)$	Co^{59}	Stable		68 [b])				
$Ni^{58}(n, p)$	Co^{58m}	9.0 ±0.2 h	40 ±15	310 [c])				
$Ni^{58}(n, p)$	Co^{58g}	72 d	237 ±20	560 [d])	1.61	1.5	462	0.61
$Ni^{58}(n, 2n)$	Ni^{57}	37 ± 1 h	52 ± 5	42 [a])	−12.1		320	0.16
				38 [d])				
$Co^{59}(n, 2n)$	Co^{58m}	9.0 ±0.2 h	4 ± 2					
$Co^{59}(n, 2n)$	Co^{58g}	72 d	145 ± 5		−10.5	1.5	365	0.412
$Co^{59}(n, p)$	Fe^{59}	45 d	82 ± 8		−0.6	1.5	145	0.57
$Co^{59}(n, \alpha)$	Mn^{56}	2.57±0.02 h	30 ± 3	39 [a])	+1.0	1.5	3.7	7.9
				25 [e])				
$Zn^{64}(n, p)$	Cu^{64}	13.0 ±0.2 h	284 ±20	216 [f])	−0.96	1.9	180	1.57
				386 [a])				
				590 [g])				
$Zn^{64}(n, 2n)$	Zn^{63}	36 ±2 min	254 ±20	224 [a])	−11.8		280	0.91
$Zn^{66}(n, p)$	Cu^{66}	5.2 ±0.3 min	77 ±10	100 [a])	−2.2	2.0	45	1.7
				80 [f])				
				110 [h])				
$Zn^{68}(n, p)$	Cu^{68}	36 ±5 sec	25 ±10		−4.42	2.2	5	5
$Zn^{68}(n, \alpha)$	Ni^{65}	2.25±0.02 h	51 ±10	7 [i])	1.1	2.2	5	10

† Lower limit for cross-section of upper state.

†† Upper limit for cross-section of lower state.

[a]) See ref. [18]).

[b]) See ref. [2]).

[c]) See ref. [1]).

[d]) K. M. Purser and E. W. Titterton, ANU/p-200 (1959)

[e]) I. Kumabe, J. Phys. Soc. Japan **13** (1958) 325.

[f]) Report to AEC, NCSAG Wash-191 (1956)

[g]) L. Rose and A. H. Armstrong, Bull. Am. Phys. Soc. **1** (1956) 224.

[h]) B. L. Cohen, Phys. Rev. **81** (1951) 184

[i]) M. G. Blosser, C. D. Goodman, T. H. Handley and M. L. Randolph, Phys. Rev. **100** (1955) 429.

36, afford an excellent opportunity to study the effect of increasing neutron number on (n, p) and (n, np) cross-sections.

Parmley and coworkers [11]) have reported a highly uncertain half-life of four to six minutes for the product of neutron irradiations of Ni^{64} enriched to about 83 %. Using the Arkansas 400 kV Cockcroft-Walton Accelerator, which provides total neutron fluxes ranging from 10^9 to over 10^{11} neutrons/sec, it was possible in the present study to resolve the uncertain 4—6 min half-life into two isomeric states of Co^{64}.

Cross-sections for (n, 2n), (n, p), and (n, α) reactions of Co^{59} and natural zinc also were investigated for comparison with those found for the nickel isotopes.

2. Experimental

2.1. SAMPLE IRRADIATION

Cross-sections in all cases were measured with 14.8 ± 0.9 MeV neutrons (10^9 to 10^{11} neutrons/sec) from the T(D, n)He^4 reaction at 0° to the incident deuteron beam on the Arkansas 400 kV Cockcroft-Walton accelerator for periods ranging from 30 sec to 8.9 h.

TABLE 2
Data for irradiated nickel isotopes

Isotope	Enrichment %	Major impurities %	Form
Ni^{64}	95.9	Ni^{58}, 2 Ni^{60}, 1.2 Ni^{62}, 0.77	NiO powder
Ni^{62}	97.8	Ni^{58}, 0.7 Ni^{60}, 1.1 Ni^{61}, 0.2 Ni^{64}, 0.2	NiO powder
Ni^{61}	83.1	Ni^{58}, 2.78 Ni^{60}, 10.4 Ni^{62}, 2.4 Ni^{64}, 1.4	NiO powder
Ni^{60}	99.1	Ni^{58}, 0.8 %	Ni metal powder
Ni^{58}	99.6	Ni^{60}, 0.3	Ni metal foil

Enriched nickel isotopes (table 2) either as metallic foils or powder or as NiO powder were irradiated. Flux monitoring was accomplished by utilizing the Cu^{63}(n, 2n) Cu^{62} (556 mb) cross-section reported by Yasumi [12]), the

$Cu^{65}(n, 2n)Cu^{64}$ (1000 mb) and $Al^{27}(n, \alpha)Na^{24}$ (115 mb) cross-section reported by Poularikas and Fink [13]). Sample and monitor thicknesses, in all cases, were approximately the same (3 to 35 mg/cm^2).

Foils of natural cobalt and zinc metals † were irradiated under similar conditions.

In the case of long-lived activities produced in Ni^{58} and Co^{59} irradiations, the cross-section reported in this paper (52 mb) for the $Ni^{58}(n, 2n)Ni^{57}$ (37 ± 1 h) reaction was employed as a flux monitor.

Cross-section determinations were based on at least three runs, and the reported experimental errors are estimated from the maximum deviation from average.

2.2. COUNTING TECHNIQUES

All beta counting was done with $2-\pi$ methane-flow proportional counters having 0.9 mg/cm^2 aluminized-mylar end-windows and/or $2-\pi$ windowless proportional counters. All samples were counted on saturation backscattering thicknesses of iron and corrected for geometry, self-adsorption, self-scattering, and back-scattering [14, 15]). Corrections for air absorption and scattering, window absorption, scattering from housing, and counting efficiency are assumed to be identical for samples and monitors.

In the case of electron capturing nuclei (Co^{58} and Ni^{57}) and for the highly converted isomeric transition in Co^{60m}, gross counting rates in end-window and windowless proportional counters were compared to the disintegration rates found by integrating under specific gamma peaks. For the case of $Zn^{64}(n, p)Cu^{64}$, efficiency corrections were computed similar to those estimated by Poularikas and Fink [13]).

Gamma counting was performed with a $1 \times 1\frac{1}{2}$ inch NaI(Tl) scintillation spectrometer with single-channel analyzer and manual scaler. The total disintegration rate found by integrating under a given gamma-ray peak, and corrected for the branching ratio were then corrected for geometry and for crystal efficiency [16]).

3. Results

3.1. BOMBARDMENTS OF ENRICHED Ni^{62} AND Ni^{64} SAMPLES

Enriched samples of $Ni^{64}O$ weighing about 10 mg were irradiated with 14.8 MeV neutrons, and gross beta decay was followed and is shown in fig. 1. Half-lives of 2.0 ± 0.2 min, 7.8 ± 0.2 min, and 1.40 ± 0.05 h were observed togehther with long-lived activities (attributed to an admixutre of 9 h Co^{56m}, 72 d Co^{58g}, and 36 h Ni^{57}, which are products of (n, p) and (n, 2n) reactions on Ni^{58}, respectively, (Ni^{58} being present in the enriched sample to the extent of

† Foils were obtained from A. D. Mackay, Inc., New York. Natural cobalt, 35 mg/cm^2, 100 %; natural zinc, 5 mg/cm^2, 100 %.

2 percent, table 2). The $Ni^{64}(n, \alpha)$ reaction, which produces 5.5 min Fe^{61}, can be ruled out because the threshold lies about 20 MeV [17]).

Samples of enriched Ni^{62} O(96 %), were bombarded under conditions similar to those in the Ni^{64} experiments. Half-lives of 1.9 ± 0.3 min, 13.8 ± 0.2 min, belonging to Co^{62m} and Co^{62g} isomers, respectively, and long-lived activities (9 h Co^{58m}, 72 d Co^{58g}, and 36 h Ni^{57} arising from Ni^{58}) were observed, but no 1.70 h Co^{61} was detected. However, under conditions of extremely high flux $(4-6) \times 10^8$ neutron/cm^2 · sec, the 1.70 h activity was observed.

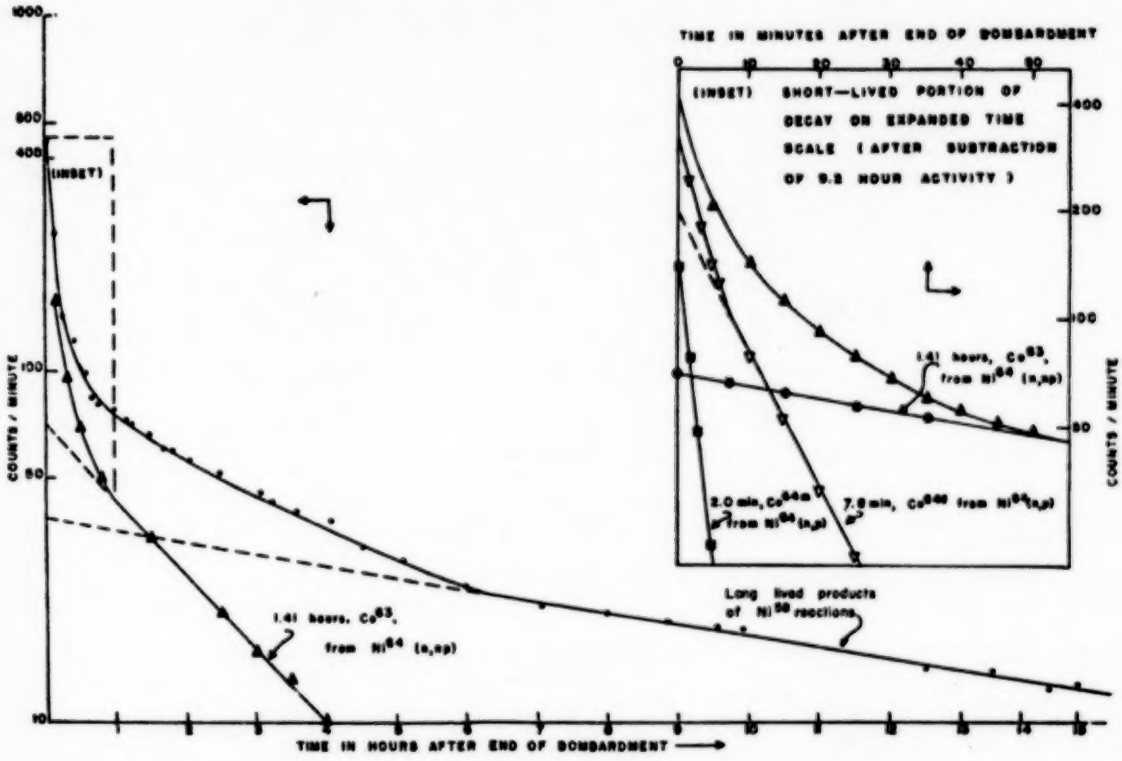
TIME IN MINUTES AFTER END OF BOMBARDMENT
(INSET) SHORT—LIVED PORTION OF DECAY ON EXPANDED TIME SCALE (AFTER SUBTRACTION OF 9.2 HOUR ACTIVITY)
COUNTS / MINUTE
1.41 hours, Co63, from Ni64 (n,np)
2.0 min, Co64m from Ni64 (n,p)
7.8 min, Co64g from Ni64 (n,p)
Long lived products of Ni58 reactions
TIME IN HOURS AFTER END OF BOMBARDMENT

Fig. 1
Typical gross beta decay from a 30-min irradiation of enriched (96 %) Ni^{64} with 14.8 MeV neutrons.

Samples of enriched $Ni^{61}O$ (83 %) were bombarded in an attempt to confirm the 187 mb cross-section value reported by Paul and Clarke [18]) for the $Ni^{61}(n,p)$ Co^{61} reaction. The cross-section obtained in the present work was found to be only 22 ± 2 mb (see section 3.2). However, even if the value of Paul and Clarke were correct, the amount of Ni^{61} present (0.17 %) in the enriched Ni^{64} sample would account for only 0.04 percent of the amount of 1.40 h activity observed from Ni^{64}, so that the 1.70 h activity observed in the high flux bombardment of Ni^{62} must be attributed to a $Ni^{62}(n, np)Co^{61}$ reaction (see table 1). The $Ni^{62}(n,p)$ Co^{62m} cross-section was found to be 2.0 ± 0.5 mb, again not large enough to be a contributing factor in the Ni^{64} bombardments.

Low energy neutrons (2.95 MeV) from the $D(d, n)He^3$ reaction at 400 kV

also were used to irradiate enriched Ni^{64} and Ni^{62}. With Ni^{64} a half-life of 3—6 minutes was found, together long-lived products ($\approx$ 6 h), but no other activity was observed, which establishes the fact that the 2.0 min activity from Ni^{64} is not identical with the 1.9 min half-life found from Ni^{62}.

Very short bombardments of enriched Ni^{64} also were carried out at 14.8 MeV

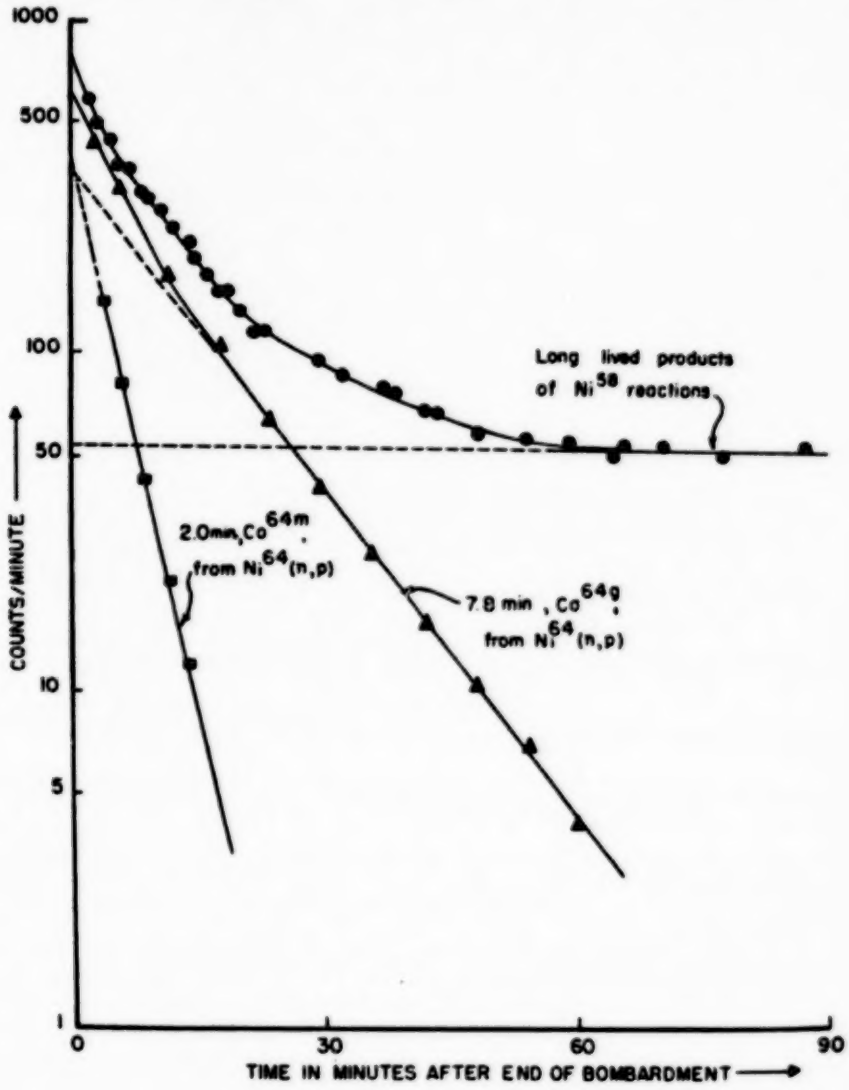

Fig. 2.
Typical gross beta decay from a 1.5 min irradiation of enriched Ni^{64} with 15.8 MeV neutrons.

for periods of 1.5 min and gross-decay curve shown in fig. 2. The 7.8 min activity was observed to grow in, but no 1.40 h activity was found even though enough of the 2.0 min and 7.8 min acitvities were formed so that an isomeric state with a half-life either of 2.0 min or 7.8 min which decays to a 1.40 h daughter would have been detected.

In other experiments, natural nickel foils were bombarded with 14.8 MeV

neutrons for durations of less than 1 minute, and no activity between about 1 second and 2 minutes was detected, which rules out the possibility of shorter-lived isomers.

The gamma-ray spectra of the new cobalt activities produced in the Ni^{64} irradiations were investigated with a 3×3-inch NaI(Tl) scintillation spectrometer with both a 50-channel analyzer and a greywedge analyzer. Because of the initial low intensity of the activity, it was not possible to follow the decay of the individual gamma-rays. However, all gamma-rays were found to exhibit half-lives of several minutes. No gamma-rays of energy above 100 keV were observed to be associated with 1.40 h Co^{63} also produced in these irradiations.

The observed gamma-ray energies from the Co^{64} isomers are as follows: 0.39 ± 0.1 MeV, 0.66 ± 0.1 MeV, 0.70 ± 0.18 MeV, 0.97 ± 0.14 MeV, 1.37 ± 0.27 MeV and 2.34 ± 0.6 MeV. The most intense gamma-rays appeared at energies of 0.66, 0.97 and 1.34 MeV. The 1.34 MeV gamma is in agreement with a known level in Ni^{64} found in the positon decay of Cu^{64} [19]), and so it serves as additional evidence for the mass assignment of the Co^{64} isomers.

3.2. BOMBARDMENTS OF ENRICHED Ni^{60} AND Ni^{61} SAMPLES

The cross-section for the Ni^{61}(n, p)Co^{61} (1.70 h) reaction was measured as described above. At relatively high neutron fluxes ($6—9\times10^8$ neutrons/cm$^2\cdot$sec). a 10.5 min activity was observed, possibly arising from the (n, np) reaction on Ni^{61}. To obtain an accurate value for this cross-section, it was necessary to obtain a value for the Ni^{61}(n, p)Co^{61m}(10.5 min) reaction.

Samples of enriched Ni^{60} metal were irradiated under similar conditions, and the decay of the 10.5 min Co^{60} isomer was followed by: (1) following the total decay with a beta proportional counter and (2) by following the decay of the 1.33 MeV gamma populated from β^--decay of the isomeric state. Since 0.3 % of all decay of the isomeric state proceed by β^- transitions, 100 % of which populate the 1.33 MeV level of Ni^{60} [20]), it was possible to determine the counting efficiency of the beta-proportional counter for gamma-rays and conversion electrons. This correction of approximately 3 % was applied to the gross-decay observed from Ni^{61} and the contribution of the Ni^{60}(n, p)Co^{60m} (10.5 min) (9 ± 2 mb) reaction subtracted. After making the counting efficiency and Ni^{60} contribution corrections, the Ni^{61}(n, np)Co^{60m}, (10.5 min), cross-section was found to be 4 ± 1 mb (see table 1).

3.3. BOMBARDMENTS OF ENRICHED Ni^{58}

Foils of enriched Ni^{58} metal, 13 mg/cm^2 thick, were irradiated, the gross beta-decay was followed, and the cross-section for the Ni^{58}(n, 2n)Ni^{57} (37 ± 1 h) reaction was measured.

Having determined an accurate value for the Ni^{58}(n, 2n)Ni^{57} cross-section (52 ± 5 mb, see table 1), it was feasible to attempt a measurement of the Ni^{58}(n, p) cross-section.

Twenty mg of enriched Ni^{58} foil were irradiated for 8.9 hours with a mean flux of 5×10^{10} neutrons/sec, and a 10 mg portion of the foil was counted for gross-decay with $2-\pi$ end-window and windowless proportional counters. The remaining 10 mg was treated chemically to separate Co^{58} and Ni^{57} reaction products.

The 10 mg sample selected for radio-chemical separation was dissolved in 10 ml of 7 *N* HCl, evaporated to 2 ml, and dropped onto a Dowex-1 anion exchange column, 10 cm $\times$ 1 cm dia. which had been previously washed with 7 *N* HCl. The column was eluted with 3.5 ml of 7 *N* HCl which removed the nickel fraction quantitatively. In the nickel fraction, decay of the 0.511 MeV annihilation gamma resulting from positon decay of Ni^{57} was followed with a NaI(Tl) scintillation spectrometer. The cobalt fraction was collected by further eluting the column with 8 ml of 3 *N* HCl, and its decay was studied with a manual single-channel scintillation spectrometer by following the decay of its well known 0.811 MeV gamma-ray [21]). Positive identification was made from the gamma spectrum of a standard Co^{58} sample obtained from Oak Ridge National Laboratory, and by comparison with standard spectra [22]).

Cross-section values obtained by integrating under the 0.811 MeV gamma peak and from following the gross-decay agreed with one another to within 3 % and are shown in table 1.

3.4. BOMBARDMENTS OF COBALT

In order to differentiate between Co^{59}(n, p)Fe^{59} (45 d) and Co^{59}(n, 2n)Co^{58g} (72 d) reactions, it was necessary to separate the products of the neutron irradiation of Co^{59} chemically. This was accomplished as follows: 40 mg of Co^{59} foil (35 mg/cm^2) was irradiated for 8.9 hours. A portion (20 mg) was dissolved in 4 *N* HCl and dropped onto an anion exchange column 10 cm $\times$ 1 cm diameter packed with Dowex-1 and previously made 4 *M* in HCl. The column was eluted with 9 ml of 3 *N* HCl and the Co-Mn fraction collected, evaporated, and counted in a $2-\pi$ windowless counter. Also the 0.81 MeV gamma of Fe^{58} [21]) was followed with a scintillation spectrometer. The decay of the remaining 20 mg of foil was followed on both windowless and end-window proportional counters. Cross-sections for 9 h Co^{58m} and 72 d Co^{58g}(n, 2n) products were determined as well as values for the Co^{59}(n, p)Fe^{59} (45 d), and Co^{59}(n, α)Mn^{56} (2.56 h) and are tabulated in table 1. The cross-sections found for Co^{59}(n, 2n)Co^{58m} (150$\pm$5 mb), and Co^{59}(n, α)Mn^{56} (30$\pm$2 mb), in the separated samples agreed to $\pm$5 % with those found in counting Co^{59} neutron irradiated foils in $2-\pi$ windowless counters.

3.5. BOMBARDMENTS OF NATURAL ZINC

Foils of natural zinc (5 mg/cm^2) were irradiated and gross-beta decay followed The gross decay curves resolved into the following half-lives: 13.0$\pm$0.2 h,

2.2 ± 0.2 h, 36 ± 2 min, 5.2 ± 0.3 min and 36 ± 5 sec, corresponding to the $Zn^{64}(n, p)Cu^{64}$, $Zn^{68}(n, \alpha)Ni^{65}$, $Zn^{64}(n, 2n)Zn^{63}$, $Zn^{66}(n, p)Cu^{66}$ and $Zn^{68}(n, p)Cu^{68}$ respectively. The cross-sections for these reactions are tabulated in table 1.

4. Discussion

On the basis of the Ni^{64} irradiations, the following mass assignments are proposed: $Ni^{64}(n, p)Co^{64m}$ (upper state), 2.0 ± 0.2 min; $Ni^{64}(n, p)Co^{64g}$ (lower state), 7.8 ± 0.2 min; $Ni^{64}(n, np)\ Co^{63}$, 1.40 ± 0.05 h (table 1).

A comparison of experimental with theoretical cross-sections based on the compound nucleus theory of Blatt and Weisskopf [23]) are shown in table 1. The calculations were based on the level density formula [23])

$$\omega(E) = C \exp(2\sqrt{aE}),$$

where C and a are empirical constants taken from NYO-636 [24]).

Variation of the level densities among even, odd-mass and odd-nuclei is generally expressed by means of C, the relation taken from Brown and Muirhead [25]) as

$$12\, C_{\text{even}} = 2.4\, C_{\text{odd-mass}} = C_{\text{odd}}.$$

Q-values were obtained from atomic mass tables based on experimental data [26]) and tables computed from a semi-empirical mass formula [27]).

Theoretical estimates of the (n, 2n) cross-sections were computed from the formula given by Blatt and Weisskopf [23]) with the threshold energies taken from Segrè [28]).

The (n, p) cross-sections calculated from compound nucleus theory [23]) follow a trend similar to that predicted by Levkovskii [10]). However, any theory having a large Q-value dependence will exhibit this property in the case of the nickel isotopes. The trend toward decreasing (n, p) cross-section with increasing neutron number is, evidently, an effect over and above the Q-value dependence as pointed out by Poularikas and Fink [13]).

Experimental results based on charged particle detection by nuclear emulsions [1–4]), indicate that direct interaction processes contribute to the observed (n, p), (n, np) and (n, pγ) reactions with Ni^{58} and Ni^{60}. Brown and Muirhead [29]) have proposed a direct interaction model based on the Fermi gas approximation i.e. an equal probability of direct interaction of the incident neutron with all nucleons. On the other hand, Wilkinson [30]) and Butler [31]) have pointed out that interactions of the incident neutron with nucleon "clusters" in the nuclear surface contribute significantly. Consequently, the anticipated shell structure effect might make the predictions of Brown and Muirhead too large in most cases.

One possible explanation of the relatively large (n, np) cross-sections (as compared to the compound nucleus prediction) as well as the three proton energy groups (approximately 4, 8 and greater than 10 MeV) found in emulsion work [1–4]) which exhibit a slightly anisotropic distribution is a direct interaction of the incident neutron with a proton, followed by a subsequent deexcitation by the emission of a neutron or gamma-ray. This approach is analagous to the (n, 2n) process explanation offered by Remy and Winter [32]). If it is assumed that nucleons in the filled $f_{\frac{7}{2}}$ proton level of nickel lie near the surface, then these eight protons outside the 20 proton closed shell lend themselves to a direct interaction process resulting in (n, pn), (n, p) and (n, pγ) reactions. With increasing neutron number in excess of the 28-neutron closed shell, direct interactions leading to (n, 2n) processes will become increasingly more important. This aspect offers itself to a qualitative explanation of the near integral decrease in (n, p) cross-sections.

For the specific cases of Ni^{58} and Ni^{60} another factor must be considered; specifically, Jensen [33]) has predicted that the neutron coupling energy in the region of 28 neutrons amounts to some 3 MeV per neutron pair. If the (n, 2n) reaction is considered to proceed according to the above mechanism, it is clear that a direct interaction with the $f_{\frac{7}{2}}$ protons will predominate if only because they are more available for surface interactions, hence we can consider the (n, n'γ) and proton emitting processes as being more energetically favorable than an (n, 2n) reaction.

The level densities of the product nuclei also have an effect, in addition to the shell structure considerations of the target nucleus mentioned above.

The large (n, α) cross-sections of Co^{59} and Zn^{68}, as compared to the compound nucleus theory, lends support to the nuclear cluster idea. The possibility of a pseudo-deuteron cluster model for the isotopes of Ni may explain the relatively large (n, np) cross-sections [34, 35]).

A comparison of $\sigma_{exp}/\sigma_{calc}$ for the nickel and zinc isotopes shows an apparent overemphasis on compound nucleus formation for nickel and theoretical values which are too small to explain the experimental cross-sections of the zinc isotopes. A conclusion as to the relative competition between compound nucleus formation and direct interaction for Ni and Zn must be based on angular distribution data which are not yet available for the latter and limited to only Ni^{58} and Ni^{60}.

The authors wish to thank Dr. R. Scalan and Dr. R. G. Wille for assistance in bombardment procedures and for help in counting. We wish to acknowledge the help of Mr. A. Poularikas on theoretical computations and the assistance of Mr. J. E. Wray of the Accelerator Laboratory for operation of the accelerator during bombardments.

References

1) D. L. Allan, Proc. Phys. Soc. A **70** (1957) 145
2) P. V. March and W. T. Morton, Phil. Mag. **3** (1958) 577
3) I. Kumabe, private communication (1959)
4) H. M. Blaum, T. D. Thomas and G. T. Seaborg, Nuclear Chem. Symposium, Am. Chem. Soc. Meeting, San Francisco, April, 1958 (unpublished)
5) T. D. Thomas (priv. communication) (1958)
6) B. L. Cohen, Phys. Rev. **108** (1957) 768
7) B. L. Cohen, E. Newman and T. D. Handley, Phys. Rev. **99** (1955) 723
8) J. H. Carver and W. Turchinetz, Proc. Phys. Soc. **73** (1959) 585; ANU/P-193
9) L. Colli, M. Pignanelli, A. Rytz and R. Zurmükle, Nuovo Cimento **9** (1958) 280; L. Colli, V. Facchini, I. Iori, G. Marcazzan, A. Sona and M. Pignanelli, Nuovo Cimento **7** (1957) 400; **13** (1959) 730
10) V. N. Levkovskii, Sov. Phys. JETP **6** (1958) 1174; **4** (1957) 291
11) T. J. Parmley, B. J. Moyer and R. C. Lilly, Proc. Phys. Soc. **75** (1949) 619
12) S. Yasumi, J. Phys. Soc. Japan **12** (1957) 433
13) A. Poularikas and R. W. Fink, Phys. Rev. **115** (1959) 989
14) W. E. Nervik and P. C. Stevenson, Nucleonics **10** No. 3 (1952) 18; J. P. Roalsvig and R. N. H. Haslam, Can. J. Phys. **37** (1959)
15) R. G. Baker and L. Katz, Nucleonics **11** No. 2 (1953) 14
16) P. R. Bell, Beta and Gamma-Ray Spectroscopy (North-Holland Publishing Co., Amsterdam, 1955) Ch. 5
17) E. Ricci and Pahissa Campa, Z. Naturf. **10a** (1955) 654
18) E. B. Paul and R. L. Clarke, Can. J. Phys. **31** (1953) 267
19) B. S. Dzhelepov and J. V. Hol'nov, Nuovo Cimento **3** (1956) 49
20) M. Deutsch and A. Hedgran, Phys. Rev. **83** (1941) 1059
21) H. Frauenfelder, N. Levine, A. Rossi and S. Singer, Phys. Rev. **103** (1956) 352
22) R. L. Heath, AEC Report IDO-16408, 27-58-2 (1957)
23) J. M. Blatt and V. F. Weisskopf, Theoretical Nuclear Physics, (John Wiley and Sons, Inc., New York, 1952) Ch. IX.
24) Feshbach, Goldberger, Goldstein and Weisskopf, Final Report, Fast Neutron Data Project, NYO-636 (1951)
25) G. B. Brown and H. Muirhead, Phil. Mag. **3** (1957) 473
26) A. H. Wapstra, Physica **21** (1955) 367; A. G. W. Cameron CRP-690 (1957)
27) N. Metropolis and G. Reitwiesner, Table of Atomic Masses, NP-1980 (1950)
28) E. Segrè, Experimental Nuclear Physics, Vol. II, (John Wiley and Sons, Inc., New York, 1953) p. 350
29) G. Brown and H. Muirhead, Phil. Mag. **2** (1957) 473
30) D. H. Wilkinson, Phil. Mag. **4** (1959) 215
31) S. T. Butler, Phys. Rev. **106** (1957) 272; I. V. Austern, S. T. Butler and H. McManus, Phys. Rev. **92** (1953) 350
32) E. Remy and K. Winter, Nuovo Cimento **9** (1958) 664
33) J. H. D. Jensen, Beta and Gamma Ray Spectroscopy (North-Holland Publishing Co., Amsterdam, 1955). Ch. XV
34) E. B. Bazhanov, M. Vokov and L. A. Kul'chtskii, Sov. phys. JETP **35** (1959) 224
35) J. H. Smith (Priv. communication) (1958)

2.E

Nuclear Physics **15** (1960) 337—341; © *North-Holland Publishing Co., Amsterdam*

Not to be reproduced by photoprint or microfilm without written permission from the publisher

NEUTRON STRENGTH FUNCTIONS IN A SURFACE ABSORPTION OPTICAL MODEL †

F. C. KHANNA †† and Y. C. TANG

Department of Physics, Florida State University, Tallahassee, Florida, U.S.A.

Received 3 October 1959

Abstract: The effect of a surface-peaked imaginary optical potential on the S-wave neutron strength functions is investigated. Analyses have been carried out with both a local potential and a non-local potential of the form used recently by Green and Wyatt in an effort to unify the scattering and bound state problems. The results indicate that with a surface-peaked imaginary potential, the deep valley between the giant resonances ($90 < A < 130$) may be fairly well accounted for.

The Nuclear Optical Model has been fairly successful in predicting the average ratio of neutron width to level spacing as a function of the mass number at low energies. By using a tapered well and a volume absorption term, one can produce a theoretical curve for the S-wave strength function which fits the observed values fairly well for most A [1]). There are, however, two major discrepancies. First, the peak at $A \approx 160$ seems to be broader and more irregular than the calculated curve. Second, the dip between the resonances ($A \approx 100$) is up to an order of magnitude deeper than what the theory predicts.

The first difficulty may be resolved by taking into account the spheroidal shape of the nuclei. This has been done by Chase, Wilets and Edmonds [2]). These authors showed that the aspherical nature of the nuclear shape serves to break the giant resonance into a number of resonances. By using experimentally determined values for the deformation parameter of the nuclei, they indeed successfully account for the qualitative features of near $A = 160$.

As to the second difficulty, Lane *et al.* [3]) have recently proposed a possible solution. They attribute the deep valley between the resonances ($90 < A < 130$) to two possible effects: (i) the imaginary part of the optical potential should be peaked near the nuclear surface [4]), and (ii) the value of the imaginary optical potential may be anomalously small when N and Z are near the magic number 50.

The purpose of this work is to investigate the effect of using a surface-peaked imaginary potential on the behaviour of the neutron S-wave strength function. In this study, we employ a local optical potential of the type

$$V = V_0\xi(r) + iW_0\eta(r), \tag{1}$$

† Work partially supported by the U. S. Atomic Energy Commission.

†† On leave from the Panjab University, Chandigarh, India.

where $\xi(r)$ is chosen to have the following form †:

$$\xi(r) = \begin{cases} 1, & r < a \\ \frac{1}{2} - \frac{15}{16}Z + \frac{10}{16}Z^3 - \frac{3}{16}Z^5, & a < r < b \\ 0, & r > b \end{cases} \tag{2}$$

where

$$Z = \frac{r - \frac{1}{2}(a+b)}{\frac{1}{2}(b-a)}.$$

For the sake of computational simplicity, $\eta(r)$ is taken simply as $-(\mathrm{d}/\mathrm{d}r)\xi(r)$. The surface limits a and b can be expressed in terms of more familiar constants, the surface thickness T and half fall-off radius R, by the simple relations

$$a = R - T, \quad b = R + T. \tag{3}$$

The work of Wyatt [5]) on nucleon-nuclear scattering and bound state phenomena indicated that if one takes $R = 1.20 \times A^{\frac{1}{3}}/(f = 10^{-13}\ \mathrm{cm})$, one has to give T a value around $2.85f$ in order to obtain good agreement with the nuclear last particle separation energies and the scattering data of neutrons at energies 4.1, 7 and 14 MeV. As to V_0 and W_0 at near-zero incident energy, we first tried to extrapolate from the values at 4.1, 7 and 14 MeV obtained, for instance, by Bjorklund and Fernbach [6]), but this procedure was soon found to be impractical. We, therefore, choose to vary V_0 to yield the positions of the giant resonances correctly, and then try out several values of W_0 to determine the variation of the strength function with respect to this parameter. Proceeding in this manner, V_0 is easily found to be -53 MeV. Now, if we designate by H_1 the value of $(\bar{\Gamma}_n^{(0)}/\bar{D}) \times 10^4$ at the resonance peak ($A \approx 54$) and by H_2 its value at the dip ($A \approx 100$), then for $W_0 = -2.5$, -5.0, -7.5 MeV, H_1 and H_2 are calculated to be 25.4, 13.3, 9.0 and 0.1, 0.2, 0.29 respectively. Experimentally, H_1 is found to lie within the range 8 to 15, and H_2 may be as small as 0.1. In order to be compatible with those values of W_0 obtained by Bjorklund and Fernbach at higher incident energies, we should probably let W_0 at near-zero energy equal -4 to -6 MeV. In fig. 1, the curve for the strength functions is plotted with $W_0 = -5.0$ MeV. As can be seen, the curve is still somewhat higher than the experimental points around $A = 100$. It should be remembered, however, that we have not considered the effect of shell closure which may further reduce the strength functions in this region. Therefore, with both absorption and shell closure taken into consideration, the deep valley between the resonance peaks may possibly be explained.

Owing to the extrapolation difficulty mentioned above, it is perhaps worthwhile to work with a non-local formulation of the optical model which was

† This form was used by Green and Wyatt in their studies on nucleon-nuclear scattering and bound state phenomena [5]). It was chosen in this particular form not because of theoretical inferences, but for ease of machine computations.

recently used by Green and Wyatt [5]) in an effort to unify the neutron scattering and bound state problems. In their formulation, it was assumed that the energy dependence of the nuclear optical potential arises primarily from its non-locality. They have not examined in great detail the theoretical justifica-

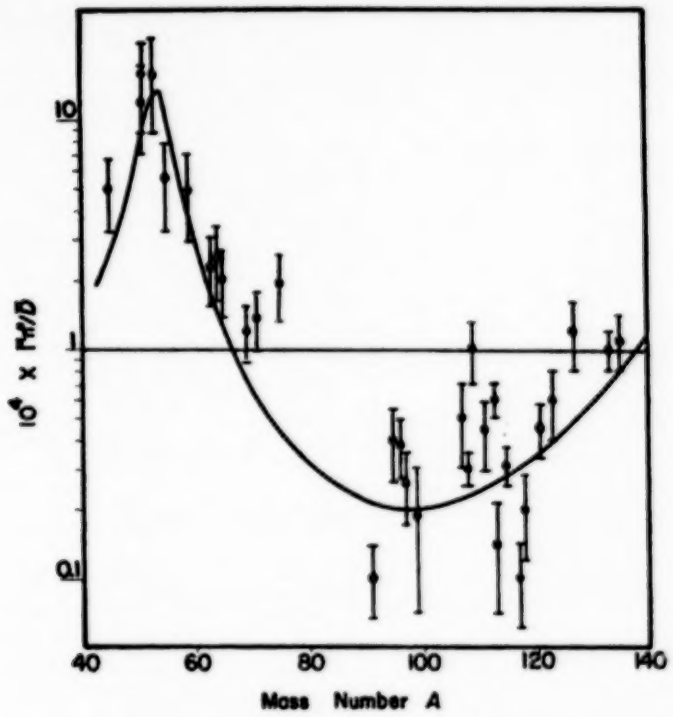

Fig. 1. Neutron S-wave strength functions as a function of the mass number. The references on the experimental data are quoted in ref. [3])

tion of this assumption. Rather, they have concentrated their main effort to prove the possibility of such an assumption in a phenomenological way; that is, to investigate whether it is possible under this assumption to unify the scattering and bound-state phenomena with a set of energy independent parameters. Essentially, what those authors did was to solve the equation

$$-\tfrac{1}{8}\hbar^2\left[\nabla^2\frac{1}{M(r)}+\nabla\frac{2}{M(r)}\nabla+\frac{1}{M(r)}\nabla^2\right]\psi(\mathbf{r}) \qquad (4)$$
$$+V^*[\xi(r)+i\rho_0\eta(r)]\psi(\mathbf{r})+\text{spin orbit term}=E\psi(\mathbf{r}),$$

where $M(r)$ is the effective mass and has the form

$$M(r)=\frac{\mu}{1+\dfrac{\mu V^* g^2}{2\hbar^2}[\xi(r)+i\rho_1\eta(r)]}. \qquad (5)$$

Eq. (4) may be shown to be simply the Frahn-Lemmer approximation [7]) at low energies of a Schrödinger equation with a non-local potential of more than one

complex kernel [8]). In these equations, μ is the reduced mass and g^2 is a quantity related to the ranges of the non-locality. In their study, V^* was written as $V_0+V_1(N-Z/A)$ to take into account neutron excess effect [9]). The quantities V_0, V_1, $r_0(R = r_0 A^{\frac{1}{3}})$, T, g^2, ρ_0 and ρ_1 are the parameters to be varied to obtain a best fit with the last particle separation energies and the data of neutron scattering at 4.1, 7 and 14 MeV. As their main purpose was to unify the bound state and scattering problems, V_0, V_1, r_0, T, g^2 were held to be strictly energy-independent and ρ_0, ρ_1 were allowed to have a step-function like dependence on energy, with the step occuring at zero incident energy. With this formulation, they were indeed able to find a set of values for those parameters which meet their purpose. Together with their probable variation, that set of values was

$$\begin{aligned} &V_0 = -75\pm 7 \text{ MeV}, \quad V_1 = 22\pm 6 \text{ MeV};\\ &r_0 = 1.20\pm 0.02f, \qquad T = 2.85\pm 0.40f;\\ &g^2 = 0.66\pm 0.03;\\ &\rho_0 = 0.2\pm 0.1, \qquad \rho_1 = -0.7\pm 0.3. \end{aligned} \tag{6}$$

It is interesting to note that in their study, they have not analyzed any scattering data with incident energy less than 4.1 MeV. If their formalism does unify the scattering and the bound state problems, the set of parameters in eq. (6) in conjunction with eq. (4) should yield the correct dependence of the strength functions as a function of the mass number. Using the values $V_0 = -80$ MeV, $V_1 = 22$ MeV, $r_0 = 1.20f$, $T = 2.85f$, $g^2 = 0.66$, $\rho_0 = 0.2$, $\rho_1 = -0.7$, it is indeed found that the positions of the giant resonances are reproduced correctly. However, H_1 and H_2 come out to be 3.9 and 0.7, in disagreement with experimental results. In fact, we found that if H_1 and H_2 are to be in the neighbourhood of 10 and 0.2, then $\rho_0 \approx 0.04$ and $\rho_1 \approx -0.2$, well beyond the probable ranges indicated by Wyatt. This finding is actually not surprising, but rather should be expected. According to Feshbach [10]), the generalized optical potential should be complex, non-local and energy-dependent. It is, therefore, not at all clear that one could make the assumption that the primary energy dependence of the nuclear potential arises from its non-locality alone.

In conclusion, the findings of this investigation are two-fold:

(i) By using an imaginary potential peaked at the surface, it is possible to explain the deep valley between the giant resonances, if shell-closure effects are also taken into consideration, and (ii) an energy-independent non-local optical model in the form used by Wyatt does not appear to be able to explain all the neutron scattering data in the range of incident energies from 0—25 MeV.

We wish to thank Dr. A. Green and Dr. P. J. Wyatt for the kind permission of using their neutron scattering code. Generous help by Mr. U. L. Stabler of the

U. S. Eglin Air Force Base in performing calculations on the I.B.M. 704 computer is also gratefully acknowledged.

References

1) H. Feshbach, Annual Review of Nuclear Science **8** (1958) 49
2) D. Chase, L. Wilets and A. Edmonds, Phys. Rev. **110** (1958) 1080
3) A. M. Lane, J. E. Lynn, E. Melkonian and E. R. Rae, Phys. Rev. Letters **2** (1959) 424
4) K. Harada and N. Oda, Prog. Theor. Phys. **21** (1959) 260
5) P. J. Wyatt, thesis (unpublished);
A. E. S. Green, Proceedings of the International Conference on the Optical Modal (1959) p. 44
6) F. E. Bjorklund and S. Fernbach, Phys. Rev. **109** (1958) 1295
7) W. E. Frahn and R. H. Lemmer, Nuovo Cimento **5** (1957) 1564
8) Y. C. Tang, R. H. Lemmer, P. J. Wyatt and A. E. S. Green (to be published)
9) A. E. S. Green and P. C. Sood, Phys. Rev. **111** (1958) 1147
10) H. Feshbach, Annals of Physics **45** (1958) 357

1.E.2:
6.D

Nuclear Physics **15** (1960) 342—355; © *North-Holland Publishing Co., Amsterdam*
Not to be reproduced by photoprint or microfilm without written permission from the publisher

ATOMIC MASSES OF NUCLIDES FOR $A \leqq 70$

F. EVERLING, L. A. KÖNIG and J. H. E. MATTAUCH
Max-Planck-Institut für Chemie (Otto-Hahn-Institut), Mainz
and
A. H. WAPSTRA
Instituut voor Kernphysisch Onderzoek, Amsterdam

Received 30 October 1959

Recently, the authors of this paper started a new computation of atomic masses of nuclides from all known experimental data. This was done partly as a result of the establishment of a Study Committee on Atomic (Nuclidic) Masses of the International Union of Pure and Applied Physics. Our undertaking was, in addition, encouraged by Dr. D. M. Van Patter in his function as Chairman of the Subcommittee on Nuclear Constants of the American Academy of Sciences. This paper presents the first results for masses up to $A = 70$ and is published in this way to make our results available and to invite criticism as soon as possible. Thus, the present results have not yet been approved by the commissions mentioned above; this may be the case in a later publication in which we will describe more in detail the selection of the data used in the present calculation and the different checks on these data before combining them in a least squares fit. We shall, however, mention some details of the computation in order to give the possibility for criticism.

Two kinds of data have been used: mass spectroscopic results [1, 2]) and nuclear reaction energies (including beta decay energies); the latter have mainly been taken from review articles by several authors in the Reviews of Modern Physics [3]) or from the Nuclear Data sheets [4]). If two experiments of the same kind yield results for the same mass (or the same combination of masses), but with errors which are at least different by a factor 3, only the most accurate result has been used in our computation. Thus, only mass spectroscopic results measured by the Minnesota and Brookhaven groups have been retained, and only nuclear reaction energy measurements measured by magnetic or electric spectroscopes, where available.

Uncertainties assigned by authors to their results are taken to be standard errors (i.e. estimates of the standard deviation). Yet, some errors have not

† Now with Nuclear Data Group, National Academy of Sciences — National Research Gouncil, Washington 25, D.C.

been accepted without change, especially those in three large and very important groups of data. The first are the Brookhaven mass doublets. These were analysed statistically by their author L. Smith [1]) who found consistency factors 3.58 and 2.35 for the two groups of data measured by him. We therefore multiplied his errors by these factors. The mean of them, namely a factor 2.97, was applied to the errors of the doublets measured by Friedman and Smith [1]).

A similar analysis of all interrelated Minnesota mass doublets in this region published since 1956 [2]) gave a consistency factor 2.65. Therefore, all uncertainties assigned by the Minnesota group to their mass doublets have been multiplied by this factor. As with the Brookhaven doublets, all reported doublets were included in computing the consistency factor, though some doublets later reported to be unreliable have been excluded from the definitive least squares fit.

Even more important corrections have been made to some nuclear reaction data. Most of these data have been obtained using an alpha particle energy of some naturally radioactive substance for calibration. We therefore introduced in our computation a calibration variable which takes care of the systematic error introduced by the common calibration. (An input value for this variable is obtained from various measurements which can be reduced to $B\rho$-values for the alpha particles of ^{210}Po, as discussed elsewhere [5])). As a result, however, the reported errors in the reaction energies may be decreased somewhat. Reaction energies reported by groups having measured a considerable number of reactions each have, therefore, been combined in a least squares computation which yielded a consistency factor 0.60. The uncertainties assigned by these groups have been multiplied by this factor before using them in our computation.

A value for the mass energy conversion factor is determined by the above data. Other measurements, however, yield the much more accurate value [6]) 1 MU(^{16}O = 16) = 931 145$\pm$10 keV; this result has therefore been included in our least squares adjustment as an input datum in addition to the mass spectroscopic doublets and reaction energies mentioned at the beginning.

The adjustment was made in three steps. There are only few and inaccurate connections between nuclei below and above $A = 46$, and a similar border is present at $A = 70$. In the group with $A \leq 46$ one half of the masses, and in the group $46 < A \leq 70$ about two thirds of them, are determined by essentially only one reaction energy; they were not included in the formal least squares adjustment but computed afterwards.

The least squares fit for the 358 equations in 68 masses in the first group gave a consistency factor 1.11 (compared with a theoretical value 1.00$\pm$0.04). It can therefore be said that, generally speaking, the mass spectroscopic results (after correction for internal consistency) are consistent with the nuclear reaction energy measurements. A nice result is obtained for the calibration

(*continued on p. 354*)

	N	Z	$N-Z$	A	Symb.	$^{12}C = 0$	
						M (keV)	s (keV)
1P	1	0	1	1	N	8071,3438	0,4075
2P	0	1	− 1	1	H	7288,7318	0,1050
3P	1	1	0	2	D	13135,3622	0,1682
4P	2	1	1	3	T	14949,0741	0,2574
5P	1	2	− 1	3	He	14930,9415	0,2582
6P	2	2	0	4	He	2425,1094	0,3477
6S	3	2	1	5	He	11453,4532	20,0080
7S	2	3	− 1	5	Li	11680,9160	37,0136
7S	4	2	2	6	He	17604,2598	17,0280
7P	3	3	0	6	Li	14089,2598	0,9755
8P	4	3	1	7	Li	14908,0042	1,0694
9P	3	4	− 1	7	Be	15768,6859	1,1420
8S	5	3	2	8	Li	20946,6346	1,4761
10P	4	4	0	8	Be	4944,3952	0,7152
7S	3	5	− 2	8	B	22924,3575	1,6061
11P	5	4	1	9	Be	11350,3134	0,8545
11S	4	5	− 1	9	B	12420,5014	1,8293
12P	6	4	2	10	Be	12607,3445	2,1358
13P	5	5	0	10	B	12051,8652	0,6565
13S	4	6	− 2	10	C	15674,2532	55,0056
14P	6	5	1	11	B	8667,1422	0,4108
14S	5	6	− 1	11	C	10649,5302	3,0534
15P	7	5	2	12	B	13368,9124	0,9647
12CP	6	6	0	12	C	0,0000	0,0000
12CS	5	7	− 2	12	N	17602,3880	90,0009
8S	8	5	3	13	B	16557,2766	50,0452
16P	7	6	1	13	C	3124,3125	0,6862
17P	6	7	− 1	13	N	5345,4653	1,3084
18P	8	6	2	14	C	3019,6658	0,3830
19P	7	7	0	14	N	2863,5993	0,1605
12CS	6	8	− 2	14	O	8011,5977	5,0195
18S	9	6	3	15	C	9873,2962	1,0788
20P	8	7	1	15	N	100,6651	0,8446
20S	7	8	− 1	15	O	2861,2531	1,7655
21P	9	7	2	16	N	5672,0080	5,6499
22P	8	8	0	16	O	−4736,4336	0,2619
23S	10	7	3	17	N	7992,8365	200,0018
23P	9	8	1	17	O	−807,1035	0,8601
24P	8	9	− 1	17	F	1954,5394	2,2805
25P	10	8	2	18	O	−782,5688	0,3212
25S	9	9	0	18	F	884,8192	4,0326

$^{12}C = 0$		$^{16}O = 0$			
M (μMU)	s (μMU)	M (μMU)	s (μMU)	B (keV)	b (keV)
8665,4363	0,4310	8986,1085	0,4295	0,0000	0,0000
7825,2201	0,0813	8145,6251	0,0691	0,0000	0,0000
14102,1927	0,1132	14742,5106	0,0891	2224,7134	0,4031
16049,4031	0,2253	17008,2573	0,2005	8482,3453	0,8116
16029,9358	0,2263	16988,7838	0,2007	7717,8659	0,4434
2603,6100	0,3723	3876,1068	0,3623	28295,0417	0,8964
12296,4881	21,4807	13889,9835	21,4872	27338,0418	20,0201
12540,6934	39,7380	14134,2664	39,7506	26327,9670	37,0308
18900,0267	18,2814	20813,5386	18,2869	29258,5790	17,0967
15126,3020	1,0366	17038,6145	1,0296	31990,9669	1,5101
16005,3102	1,1367	18235,8194	1,1347	39243,5663	1,8117
16929,3426	1,2147	19160,1455	1,2171	37600,2726	1,8109
22488,4181	1,5847	25038,9052	1,5853	41276,2798	2,3659
5308,3282	0,7660	7853,3539	0,7513	56495,9071	1,8170
24611,7119	1,7243	27162,8740	1,7174	37733,3329	2,2141
12185,7550	0,9093	15050,8844	0,8959	58161,3327	2,1449
13334,7162	1,9639	16200,2108	1,9593	56308,5328	2,6759
13535,3101	2,2887	16718,7859	2,2867	64975,6454	3,2045
12938,9446	0,6929	16122,2308	0,7071	64748,5127	2,2913
16827,9614	59,0543	20012,4838	59,0733	60343,5128	55,0477
9305,0886	0,4311	12805,1368	0,4719	76204,5795	2,6202
11433,3921	3,2781	14934,1169	3,2852	73439,5796	3,9832
14352,9333	1,0262	18172,5035	1,0255	79574,1531	2,9896
0,0000	0,0000	3815,0075	0,2110	92160,4536	2,6586
18898,0172	96,6254	22719,0322	96,6564	73775,4536	90,0393
17775,9800	53,7288	21914,5556	53,7461	84457,1328	50,1311
3354,2779	0,7359	7488,2688	0,7554	97107,4848	3,1112
5738,9191	1,4038	9873,6680	1,4150	94103,7200	3,1759
3241,9289	0,4101	7693,8012	0,4105	105283,4752	3,2849
3074,3750	0,1696	7526,1941	0,1696	104656,9298	3,0621
8601,2938	5,3890	13054,8702	5,3932	98726,3195	5,8653
10600,0232	1,1582	15372,1522	1,1585	106501,1888	3,7999
108,0746	0,9067	4876,8679	0,8953	115491,2077	3,5644
3071,8565	1,8955	7841,5924	1,8892	111948,0079	3,8672
6089,4970	6,0654	11178,1092	6,0639	117991,2086	6,8330
−5085,0596	0,2766	0,0000	0,0000	127617,0382	3,5086
8581,1517	214,7230	13988,4735	214,7911	123741,7241	200,0489
−866,5749	0,9234	4537,7431	0,8889	131759,1120	4,0652
2098,4036	2,4482	7503,6642	2,4297	128214,7971	4,4500
−840,1699	0,3448	4882,0738	0,2473	139805,8610	4,3040
949,9466	4,3294	6672,7599	4,3233	137355,8612	5,8757

	N	Z	N-Z	A	Symb.	$^{12}C = 0$	
						M (keV)	s (keV)
25S	8	10	- 2	18	Ne	5104,8192	200,0007
25S	11	8	3	19	O	3332,0616	4,0167
26P	10	9	1	19	F	-1486,0555	0,6812
26S	9	10	- 1	19	Ne	1762,3325	5,0624
27P	11	9	2	20	F	-13,4709	3,7595
28P	10	10	0	20	Ne	-7041,3018	0,4982
28S	9	11	- 2	20	Na	8276,0862	300,0007
26S	12	9	3	21	F	-25,7132	25,0107
29P	11	10	1	21	Ne	-5729,0678	1,5517
29S	10	11	- 1	21	Na	-2207,0678	30,0401
30P	12	10	2	22	Ne	-8024,8541	0,5527
31P	11	11	0	22	Na	-5183,3050	4,6487
30S	13	10	3	23	Ne	-5146,2237	5,0343
32P	12	11	1	23	Na	-9526,2312	1,5233
32S	11	12	- 1	23	Mg	-5466,8432	10,1229
33S	14	10	4	24	Ne	-5963,8171	40,0918
33P	13	11	2	24	Na	-8413,8171	2,7122
34P	12	12	0	24	Mg	-13930,0825	1,7937
34S	11	13	- 2	24	Al	87,3055	300,0057
35S	14	11	3	25	Na	-9389,4467	200,0090
35P	13	12	1	25	Mg	-13189,4467	1,8936
34S	12	13	- 1	25	Al	-8928,3507	6,2630
36P	14	12	2	26	Mg	-16215,5184	2,2125
37P	13	13	0	26	Al	-12201,4715	4,7328
38P	15	12	3	27	Mg	-14581,2319	3,6753
39P	14	13	1	27	Al	-17199,1668	1,9541
39S	13	14	- 1	27	Si	-12383,7788	11,1798
40S	16	12	4	28	Mg	-15014,5243	6,1810
40P	15	13	2	28	Al	-16851,5243	3,6338
41P	14	14	0	28	Si	-21491,0412	2,9341
41S	13	15	- 2	28	P	-7691,0412	300,0143
36S	16	13	3	29	Al	-18139,1408	50,0504
42P	15	14	1	29	Si	-21897,4179	3,3690
42S	14	15	- 1	29	P	-16937,4179	10,5523
43P	16	14	2	30	Si	-24440,3435	3,9979
47S	15	15	0	30	P	-20193,3973	10,0552
44P	17	14	3	31	Si	-22961,1390	4,6355
45P	16	15	1	31	P	-24437,8242	1,4550
45S	15	16	- 1	31	S	-19002,4362	17,0670
46S	18	14	4	32	Si	-24203,2428	50,0495
46P	17	15	2	32	P	-24303,2428	2,2255
47P	16	16	0	32	S	-26011,6501	1,0184
47S	15	17	- 2	32	Cl	-13011,6501	300,0017

$^{12}C = 0$		$^{16}O = 0$		B	b
M (μMU)	s (μMU)	M (μMU)	s (μMU)	(keV)	(keV)
5480,5610	214,7218	11204,8145	214,7899	132353,2492	200,0389
3577,3190	4,3124	9618,8848	4,3061	143762,5746	6,1622
-1595,4369	0,7312	4444,4839	0,6870	147798,0795	4,3750
1892,0495	5,4350	7933,0796	5,4302	143767,0797	6,6438
-14,4625	4,0363	6343,8782	4,0272	154396,8387	5,9879
-7559,5779	0,5295	-1203,6359	0,3747	160642,0576	4,3729
8885,2501	322,0823	15246,4205	322,1845	144542,0578	300,0319
-27,6058	26,8516	6648,6486	26,8584	162480,4250	25,5224
-6150,7567	1,6648	523,5504	1,6183	167401,1674	4,9888
-2369,5197	32,2512	4305,9903	32,2589	163096,5556	30,3583
-8615,5247	0,5870	-1624,0839	0,4237	177768,2974	5,1814
-5564,8231	4,9903	1427,5876	4,9786	174144,1363	6,6891
-5525,0131	5,4049	1785,3284	5,3889	182961,0111	7,4801
-10227,4110	1,6318	-2918,5654	1,5930	186558,4063	5,4153
-5869,2319	10,8680	1441,0002	10,8645	181716,4066	11,3721
-6402,7857	43,0428	1225,1940	43,0557	191849,9483	40,5377
-9033,1175	2,9096	-1405,9750	2,9019	193517,3360	6,2537
-14955,4084	1,9199	-7330,1486	1,9401	198250,9894	5,6512
93,7316	322,0877	7723,7765	322,1902	183450,9897	300,0532
-10080,5598	214,7307	-2135,8319	214,7991	202564,3097	200,1006
-14160,2580	2,0284	-6216,8282	2,0512	205581,6974	6,0050
-9585,5247	6,7240	-1640,6394	6,7277	200537,9897	8,2423
-17409,0642	2,3694	-9148,7500	2,3871	216679,1129	6,4873
-13099,5629	5,0791	-4837,8786	5,0765	211882,4540	7,5104
-15654,4857	3,9433	-7075,6964	3,9532	223116,1702	7,3902
-18465,1142	2,0897	-9887,2184	2,1080	224951,4931	6,4839
-13295,2906	12,0027	-4715,7501	12,0079	219353,4934	12,7688
-16119,6730	6,6360	-7223,1129	6,6370	231620,8067	9,1834
-18091,8834	3,8980	-9195,9517	3,9010	232675,1944	7,3900
-23072,8927	3,1410	-14178,5446	3,1299	236532,0993	6,9038
-8257,1426	322,0969	641,9168	322,1992	221949,4876	300,0724
-19474,2778	53,7344	-10260,8669	53,7519	242034,1550	50,5275
-23509,1808	3,6098	-14297,0541	3,6028	245009,8198	7,3760
-18184,1017	11,3290	-8970,2807	11,3281	239267,2081	12,2446
-26239,2788	4,2851	-16710,1028	4,2816	255624,0892	7,9806
-21679,7385	10,7953	-12149,1114	10,7929	250594,5313	12,0492
-24651,1972	4,9710	-14803,5991	4,9630	262216,2284	8,6605
-26236,5741	1,5397	-16389,4800	1,4741	262910,3016	7,1794
-20401,1163	18,3232	-10552,1655	18,3219	256692,3020	18,4538
-25984,7299	53,7334	-15819,6367	53,7490	271529,6764	50,6533
-26092,0869	2,3734	-15927,0295	2,3516	270847,0640	7,7662
-27926,2417	1,0572	-17761,7675	1,0173	271772,8594	7,1669
-13969,3766	322,0834	-3800,4638	322,1856	257990,2477	300,0776

	N	Z	N-Z	A	Symb.	$^{12}C = 0$	
						M (keV)	s (keV)
48S	18	15	3	33	P	-26333,8542	3,4128
48P	17	16	1	33	S	-26582,8542	2,7654
47S	16	17	- 1	33	Cl	-21007,9183	12,0437
49S	19	15	4	34	P	-24832,3541	200,0214
49P	18	16	2	34	S	-29932,3541	2,9252
49S	17	17	0	34	Cl	-24512,3541	30,1423
50P	19	16	3	35	S	-28842,8521	2,6146
51P	18	17	1	35	Cl	-29010,1954	2,6094
51S	17	18	- 1	35	A	-23030,1954	40,0850
22S	20	16	4	36	S	-30653,2392	3,2826
52P	19	17	2	36	Cl	-29515,5854	5,1363
53P	18	18	0	36	A	-30227,0371	3,1961
54S	21	16	5	37	S	-26975,9203	90,0235
54P	20	17	3	37	Cl	-31765,9203	2,0570
55P	19	18	1	37	A	-30949,9187	2,5330
55S	18	19	- 1	37	K	-24829,9187	100,0321
54S	22	16	6	38	S	-26804,2899	150,0140
54S	21	17	4	38	Cl	-29804,2899	8,2585
54S	20	18	2	38	A	-34719,8885	2,2525
59S	19	19	0	38	K	-28790,7416	10,5931
56S	22	17	5	39	Cl	-29803,3148	21,1875
56S	21	18	3	39	A	-33233,3148	5,7366
56P	20	19	1	39	K	-33798,3148	2,8123
56S	19	20	- 1	39	Ca	-27188,3148	40,0987
57S	23	17	6	40	Cl	-27537,2556	500,0007
57P	22	18	4	40	A	-35037,2556	0,8459
58P	21	19	2	40	K	-33524,5256	3,3420
59P	20	20	0	40	Ca	-34845,9944	3,4872
59S	19	21	- 2	40	Sc	-20945,9944	400,0152
60S	23	18	5	41	A	-33058,3355	10,8734
60P	22	19	3	41	K	-35548,3355	4,2696
61P	21	20	1	41	Ca	-35135,2550	8,2516
61S	20	21	- 1	41	Sc	-29185,2550	40,8422
62S	23	19	4	42	K	-35005,9043	20,4272
62P	22	20	2	42	Ca	-38535,9043	4,1557
62S	21	21	0	42	Sc	-32605,9043	550,0157
63S	24	19	5	43	K	-36577,0305	10,9702
63P	23	20	3	43	Ca	-38394,0305	4,5106
63S	22	21	1	43	Sc	-36174,0305	10,9702
64S	25	19	6	44	K	-35358,7468	200,0513
64P	24	20	4	44	Ca	-41458,7468	4,5290
64S	23	21	2	44	Sc	-37810,7468	6,7462
64S	22	22	0	44	Ti	-37655,7468	11,8959
65P	25	20	5	45	Ca	-40806,9649	4,2664
66P	24	21	3	45	Sc	-41058,9496	3,9515
66S	23	22	1	45	Ti	-39000,5616	5,6374

$^{12}C = 0$		$^{16}O = 0$		B	b
M (μMU)	s (μMU)	M (μMU)	s (μMU)	(keV)	(keV)
-28272,1656	3,6640	-17789,8822	3,6940	280949,0196	8,5977
-28539,4894	2,9556	-18057,2929	3,0021	280415,4073	8,0311
-22554,2126	12,9302	-12070,1115	12,9270	274057,8597	13,9773
-26660,1471	214,7440	-15859,4340	214,8131	287518,8633	200,1948
-32135,5298	3,1241	-21336,5592	3,1914	291836,2509	8,4981
-26316,5934	32,3609	-15515,7711	32,3766	285633,6393	31,0931
-30965,8348	2,7897	-19848,5752	2,7986	298818,0927	8,6981
-31145,4954	2,7841	-20028,2928	2,7930	298202,8240	8,3595
-24725,3400	43,0355	-13606,0945	43,0489	291440,2124	40,7977
-32909,4803	3,5242	-21474,9192	3,5967	308699,8240	9,1623
-31688,0848	5,5050	-20253,1375	5,5074	306779,5578	9,7837
-32451,9029	3,4159	-21017,1984	3,4164	306708,3975	8,5926
-28961,4912	96,6497	-17207,7578	96,6818	313093,8489	90,4878
-34104,0559	2,1819	-22351,9594	2,2597	317101,2364	9,0372
-33227,9923	2,6981	-21475,6173	2,7602	315502,6228	9,0390
-26657,5325	107,3950	-14903,0667	107,4303	308600,0113	100,3781
-28777,2279	161,0558	-16705,5186	161,1078	320993,5623	150,3166
-31998,0438	8,8664	-19927,3584	8,8839	323210,9503	12,3456
-37275,4565	2,4183	-25206,4487	2,4638	327343,9369	9,0850
-30909,8930	11,3728	-18838,8616	11,3782	320632,1780	13,5373
-31996,9969	22,7470	-19608,3939	22,7552	331281,3190	23,2561
-35679,4631	6,1588	-23292,0307	6,1643	333928,7070	10,8687
-36286,0452	2,9964	-23898,8079	3,0199	333711,0946	9,3128
-29189,5190	43,0502	-16800,0235	43,0644	326318,4830	40,9956
-29564,1437	536,8034	-16856,8500	536,9737	337086,6036	500,0983
-37616,1784	0,8264	-24911,4467	0,6275	343803,9911	9,5572
-35992,1036	3,5711	-23286,8555	3,5865	341508,6491	9,7444
-37410,8393	3,7254	-24706,0422	3,7441	342047,5059	9,5441
-22487,7307	429,4584	-9778,1875	429,5950	327364,8944	400,1063
-35491,6044	11,6737	-22468,2777	11,6746	349896,4153	14,7421
-38164,8764	4,5681	-25142,4018	4,5731	351603,8028	10,5046
-37721,3909	8,8520	-24698,7753	8,8602	350408,1103	12,3662
-31333,4446	43,8484	-18308,7961	43,8624	343675,4988	41,7924
-37582,5246	21,9308	-24241,9452	21,9361	359132,7159	22,7516
-41372,3457	4,4421	-28032,9735	4,4480	361880,1034	10,5185
-35005,8719	590,4998	-21664,4734	590,6874	355167,4919	550,0945
-39269,2940	11,7777	-25611,3336	11,7760	368775,1859	15,1001
-41220,0291	4,8253	-27562,6913	4,8252	369809,5734	10,9875
-38836,6311	11,7777	-25178,5331	11,7760	366806,9619	14,6204
-37961,3382	214,7761	-23985,0446	214,8438	375628,2460	200,3435
-44510,3245	4,8419	-30536,1155	4,8285	380945,6335	11,3971
-40593,8184	7,2428	-26618,3617	7,2264	376515,0220	12,1491
-40427,4096	12,7715	-26451,9000	12,7650	375577,4100	15,3825
-43810,5680	4,5589	-29518,2192	4,5528	388365,1953	11,6836
-44081,1001	4,2190	-29788,8373	4,2126	387834,5681	11,2397
-41871,2099	6,0523	-27578,2419	6,0370	384993,5686	11,9302

	N	Z	$N-Z$	A	Symb.	$^{12}C = 0$	
						M (keV)	s (keV)
47S	26	20	6	46	Ca	−43136,1865	3,7774
67P	25	21	4	46	Sc	−41753,9799	5,1553
68P	24	22	2	46	Ti	−44119,2134	3,4576
68S	23	23	0	46	V	−36819,2134	400,0149
1S	27	20	7	47	Ca	−42369,6304	21,3175
1S	26	21	5	47	Sc	−44334,6304	7,6443
1P	25	22	3	47	Ti	−44934,6304	7,3780
1S	24	23	1	47	V	−42022,6304	12,4272
34P	28	20	8	48	Ca	−44226,0354	13,5633
2S	27	21	6	48	Sc	−44493,5554	9,6128
2P	26	22	4	48	Ti	−48483,5554	3,3773
2S	25	23	2	48	V	−44466,5554	6,0337
2S	24	24	0	48	Cr	−43066,5554	200,0285
34S	29	20	9	49	Ca	−41298,4054	14,8312
3S	28	21	7	49	Sc	−46489,1410	90,0607
3P	27	22	5	49	Ti	−48559,1410	3,3058
3S	26	23	3	49	V	−47947,7530	6,0074
3S	25	24	1	49	Cr	−45387,7510	11,4956
35S	29	21	8	50	Sc	−45125,7275	500,0199
35P	28	22	6	50	Ti	−51425,7275	4,4570
36P	27	23	4	50	V	−49213,0476	3,7207
4P	26	24	2	50	Cr	−50250,5883	4,2085
4S	25	25	0	50	Mn	−42550,5883	500,0177
5S	29	22	7	51	Ti	−49716,3143	20,3826
5P	28	23	5	51	V	−52181,3143	3,9307
6P	27	24	3	51	Cr	−51428,6735	4,1488
6S	26	25	1	51	Mn	−48248,6735	50,1718
5S	29	23	6	52	V	−51413,9713	7,1838
7P	28	24	4	52	Cr	−55407,9375	3,3345
7S	27	25	2	52	Mn	−50704,9375	8,6671
7S	26	26	0	52	Fe	−48321,9375	17,3239
8S	30	23	7	53	V	−52749,9543	50,1177
8P	29	24	5	53	Cr	−55279,9543	3,4334
8S	28	25	3	53	Mn	−54682,5663	8,7148
11S	27	26	1	53	Fe	−50690,7923	40,3893
9P	30	24	6	54	Cr	−56930,2595	4,4561
10P	29	25	4	54	Mn	−55551,2560	6,1172
11P	28	26	2	54	Fe	−56239,4523	5,5942
11S	27	27	0	54	Co	−47439,4523	500,0313
12S	31	24	7	55	Cr	−54879,4346	140,0509
12P	30	25	5	55	Mn	−57699,4346	3,7761
13P	29	26	3	55	Fe	−57467,6851	4,2421
13S	28	27	1	55	Co	−54007,6851	10,8626
14P	31	25	6	56	Mn	−56898,3389	5,2655
15P	30	26	4	56	Fe	−60607,1877	5,3140
15S	29	27	2	56	Co	−56007,1877	15,9135

$^{12}C = 0$		$^{16}O = 0$		B	b
M (μMU)	s (μMU)	M (μMU)	s (μMU)	(keV)	(keV)
-46311.2387	4.0554	-31701.7649	4.0370	398765.7613	11.7973
-44827.2883	5.5154	-30217.3455	5.5075	396600.9422	12.0672
-47366.6150	3.6822	-32757.4795	3.6674	398183.5637	11.1102
-39529.3029	429.4581	-24917.6732	429.5943	390100.9522	400.1451
-45488.2600	22.8866	-30560.6092	22.9083	406070.5020	24.0633
-47597.8944	8.2070	-32670.9143	8.2497	407252.8900	13.2210
-48242.0576	7.9211	-33315.2823	8.3595	407070.2782	12.7617
-45115.7190	13.3419	-30187.9498	13.3709	403375.6660	15.9764
-47481.3063	14.5616	-32236.3719	14.8183	415998.2501	17.8217
-47768.5172	10.3204	-32523.6740	10.3569	415483.1578	14.7477
-52052.2023	3.6259	-36808.7210	4.5343	418690.5460	11.3247
-47739.5298	6.4778	-32494.6774	6.5328	413890.9338	12.0548
-46236.4824	214.7517	-30991.1522	214.8215	411708.3218	200.2816
-44338.1872	15.9229	-28774.3362	15.9504	421141.9626	19.0519
-49910.9885	96.6896	-34348.9090	96.7241	425550.0862	90.8023
-52133.3514	3.5491	-36571.9786	4.5078	426837.4745	11.6836
-51476.9620	6.4496	-35915.3804	6.5070	425443.4742	12.3864
-48728.5303	12.3417	-33166.0750	12.3747	422100.8602	15.5420
-48447.2205	536.8240	-32566.7586	536.9954	432258.0155	500.1633
-55210.9339	4.7850	-39332.6222	5.5629	437775.4038	12.4299
-52835.3890	3.9946	-36956.3222	4.8991	434780.1119	11.8290
-53949.2983	4.5183	-38070.5855	5.3350	435035.0406	11.6426
-45682.5374	536.8217	-29801.1966	536.9930	426552.4283	500.1276
-53375.6988	21.8829	-37178.8863	21.9076	444137.3331	23.6531
-56022.1359	4.2201	-39826.1648	5.1165	445819.7214	12.2719
-55214.0968	4.4541	-39017.8688	5.3114	444284.4686	11.9919
-51800.0319	53.8647	-35602.7185	53.8890	440321.8563	51.3378
-55198.3124	7.7126	-38684.1620	7.7672	453123.7209	14.0052
-59486.2557	3.5799	-42973.4686	4.6383	456335.0754	12.1157
-54437.0899	9.3050	-37922.6975	9.3513	450849.4631	14.2210
-51878.6885	18.5990	-35363.4828	18.6267	447683.8511	20.4695
-56632.6308	53.8066	-39801.0192	53.8315	462531.0467	51.6337
-59348.8522	3.6861	-42518.1041	4.7564	464278.4350	12.5243
-58707.4933	9.3563	-41876.5412	9.4040	462898.4347	14.5655
-54421.9036	43.3622	-37589.5892	43.3856	458124.0487	41.9398
-61120.6287	4.7840	-43972.5266	5.6809	474000.0830	13.2154
-59640.1233	6.5674	-42491.5505	7.2477	471838.4675	13.5289
-60378.9744	6.0059	-43230.6365	6.7428	471744.0518	12.9632
-50931.2477	536.8363	-33779.9064	537.0077	462161.4395	500.1595
-58918.8522	150.3594	-41452.1328	150.4102	480020.6006	140.6382
-61946.4191	4.0540	-44480.6623	5.1154	482057.9889	13.0231
-61697.6117	4.5544	-44231.7757	5.5206	481043.6274	12.8126
-57982.9373	11.6621	-40515.9204	11.7045	476801.0151	15.9782
-61086.3586	5.6530	-43302.4111	6.4850	489328.2360	13.8968
-65068.1983	5.7052	-47285.5166	6.5305	492254.4728	13.5700
-60129.6139	17.0848	-42345.3621	17.1177	486871.8605	19.9993

	N	Z	$N-Z$	A	Symb.	$^{12}C = 0$	
						M (keV)	s (keV)
16S	32	25	7	57	Mn	−57477,0803	300,0507
16P	31	26	5	57	Fe	−60177,0803	5,5153
16S	30	27	3	57	Co	−59607,0803	30,5028
16S	29	28	1	57	Ni	−56372,0903	34,4444
17P	32	26	6	58	Fe	−62153,3714	6,5777
17S	31	27	4	58	Co	−59841,3714	13,6845
18P	30	28	2	58	Ni	−60225,0874	5,9198
18S	29	29	0	58	Cu	−51708,6974	70,2499
38P	33	26	7	59	Fe	−60667,3612	6,3867
19P	32	27	5	59	Co	−62230,3970	4,2983
20P	31	28	3	59	Ni	−61154,5592	4,7548
18S	30	29	1	59	Cu	−56356,3574	20,8577
21P	33	27	6	60	Co	−61655,8570	5,3379
22P	32	28	4	60	Ni	−64471,9379	5,4218
22S	31	29	2	60	Cu	−58324,5479	40,3658
22S	34	27	7	61	Co	−62933,5979	40,3658
22S	33	28	5	61	Ni	−64223,5949	8,0964
22S	32	29	3	61	Cu	−61992,5979	9,6724
22S	31	30	1	61	Zn	−56192,5979	300,0490
23S	35	27	8	62	Co	−61522,1986	40,4984
23P	34	28	6	62	Ni	−66742,1986	6,3343
23S	33	29	4	62	Cu	−62812,1986	11,8374
23S	32	30	2	62	Zn	−61122,1986	14,4611
24P	35	28	7	63	Ni	−65512,3068	5,3855
25P	34	29	5	63	Cu	−65579,0717	5,3734
25S	33	30	3	63	Zn	−62212,6817	6,7107
26S	36	28	8	64	Ni	−67101,9082	5,5585
26P	35	29	6	64	Cu	−65423,9082	5,1862
27P	34	30	4	64	Zn	−65997,0881	5,1056
27S	33	31	2	64	Ga	−58979,6981	150,0869
28S	37	28	9	65	Ni	−65162,8802	200,0859
28P	36	29	7	65	Cu	−67262,8802	5,8619
29P	35	30	5	65	Zn	−65914,6115	5,8802
29S	34	31	3	65	Ga	−62655,6115	16,1114
30S	38	28	10	66	Ni	−66052,1325	31,1961
30P	37	29	8	66	Cu	−66252,1325	8,5556
31P	36	30	6	66	Zn	−68881,9480	9,3881
31S	35	31	4	66	Ga	−63711,9480	31,4346
32S	38	29	9	67	Cu	−67284,3288	13,0492
32P	37	30	7	67	Zn	−67856,3288	10,3093
32S	36	31	5	67	Ga	−66857,9408	11,0653
32S	35	32	3	67	Ge	−62457,9388	100,5300
33P	38	30	8	68	Zn	−69983,7285	8,7637
33S	37	31	6	68	Ga	−67066,3385	10,0976
33S	36	32	4	68	Ge	−66366,3385	600,0640

$^{12}C = 0$		$^{16}O = 0$		B	b
M (μMU)	s (μMU)	M (μMU)	s (μMU)	(keV)	(keV)
-61707,6984	322,1360	-43606,0310	322,2399	497978,3199	300,3435
-64606,4327	5,9212	-46505,6869	6,7472	499895,7082	14,0138
-63994,4777	32,7480	-45893,5372	32,7732	498543,0959	32,9682
-60521,3645	36,9797	-42419,3200	37,0046	494525,4839	36,5202
-66728,1893	7,0619	-48310,2008	7,7918	509943,3421	14,8195
-64246,0139	14,6918	-45827,2361	14,7306	506848,7298	18,8101
-64657,9734	6,3556	-46239,3267	7,1575	506449,8341	13,8605
-55514,7319	75,4207	-37093,1786	75,4513	497150,8318	71,2948
-65132,8009	6,8568	-46396,3879	7,6310	516528,6747	15,0946
-66810,8844	4,6147	-48075,0049	5,7005	517309,0985	13,9793
-65655,8593	5,1048	-46919,6126	6,1043	515450,6487	13,7752
-60504,4843	22,3929	-41766,5999	22,4233	509869,8346	24,3456
-66194,0552	5,7308	-47140,0624	6,6658	524805,9013	14,7022
-69217,4147	5,8208	-50164,3829	6,7434	526839,3702	14,3856
-62617,5441	43,3369	-43562,4141	43,3631	519909,3679	42,3928
-67565,8446	43,3369	-48194,3705	43,3635	534154,9847	42,7562
-68950,7923	8,6923	-49579,7584	8,7588	534662,3697	15,9319
-66555,5820	10,3843	-47183,7867	10,4410	531648,7607	16,4840
-60328,6713	322,1342	-40954,8965	322,2383	525066,1487	300,3294
-66050,5589	43,4793	-46360,6857	43,5063	540814,9282	43,0137
-71654,7786	6,8006	-51966,6872	7,6571	545252,3166	15,4740
-67435,5097	12,7087	-47746,0768	12,7579	540539,7042	18,1390
-65621,1167	15,5255	-45931,1071	15,5674	538067,0922	19,6956
-70334,3602	5,7819	-50327,9317	6,7975	552093,7675	15,4820
-70406,0394	5,7689	-50399,6337	6,7865	551377,9205	15,1270
-66791,8652	7,2046	-46784,3105	7,2888	547228,9181	15,3156
-72040,9647	5,9676	-51717,1613	6,0712	561754,7114	15,9146
-70239,4550	5,5679	-49915,0791	6,6471	559294,0997	15,4346
-70854,8240	5,4814	-50530,6438	6,5748	559084,6677	15,0554
-63320,9168	161,1341	-42994,3415	161,1891	551284,6653	150,7191
-69959,2139	214,8133	-49316,8315	214,8845	567887,0262	200,6708
-72213,7851	6,2934	-51572,1196	7,2945	569204,4146	16,0435
-70766,2766	6,3130	-50124,1510	7,3114	567073,5338	15,7023
-67267,3970	17,2973	-46624,1589	17,3392	563031,9215	21,4670
-70913,9199	33,4923	-49953,9238	33,5224	576847,6213	34,9274
-71128,6410	9,1853	-50168,7133	9,9208	576265,0097	17,5571
-73952,0249	10,0791	-52992,9947	10,7541	578112,2132	17,6587
-68401,4854	33,7484	-47440,6907	33,7784	572159,6008	34,6524
-72236,8124	14,0097	-50959,3195	14,0619	585368,5484	20,4372
-72850,9147	11,0681	-51573,6172	11,7050	585157,9368	18,4934
-71779,0400	11,8798	-50501,4016	11,9399	583376,9364	18,6228
-67055,1745	107,9295	-45776,0345	107,9701	578194,3224	101,5855
-75134,9022	9,4087	-53540,4136	10,1705	595356,6793	18,0244
-72002,7769	10,8408	-50407,2923	10,9078	591656,6769	18,3949
-71251,2532	644,2319	-49655,5297	644,4378	590174,0649	600,2515

	N	Z	N-Z	A	Symb.	$^{12}C = 0$	
						M (keV)	s (keV)
37S	39	30	9	69	Zn	-68318,0632	26,5968
37S	38	31	7	69	Ga	-69223,0682	25,7835
37S	37	32	5	69	Ge	-66986,0632	28,2742
37S	36	33	3	69	As	-63086,0632	300,3714
37P	40	30	10	70	Zn	-69534,1132	14,9315
37S	39	31	8	70	Ga	-68881,7252	15,7515
37S	38	32	6	70	Ge	-70531,7252	18,5518
37S	37	33	4	70	As	-63991,7232	101,1086

variable: the $B\rho$-value of ^{210}Po is found to be 331 715$\pm$13 G · cm in agreement with the average of all direct determinations, but more accurate. The importance of this result for alpha energy determinations is discussed somewhere else [5]). The mass energy conversion factor is not changed; in fact, it was introduced only to obtain correct adjusted standard deviations s for the adjusted mass excesses M in the energy scale, especially for those of ^{1}H, ^{2}D, ^{3}T and ^{3}He, which without this precaution would have been about one third lower.

The second adjustment for the 103 equations in 38 masses in the range $46 < A \leqq 70$ yielded a consistency factor 0.98, which is again quite satisfactory (theoretical value 1.00 ± 0.09).

The accompanying table † presents our results in various ways. The adjusted mass excesses M and their standard deviations s are given in the present physical scale, in which the exact number 16 is assigned to the relative mass of ^{16}O, and also in the newly proposed [7]) unified physical and chemical scale in which the exact number 12 is assigned to ^{12}C; the mass excesses M and their standard deviations s in the ^{12}C scale are given both in mass units and in energy units. The last columns give the binding energies B and their standard deviations b. The mass energy conversion factor becomes in the new scale

$$1\ \text{MU}(^{12}\text{C} = 12) = 931\ 441\ \text{keV}$$

with a precision of one part in 10^5. The scale conversion factor is

$$1\ \text{MU}(^{12}\text{C} = 12) = 1.000\ 317\ 917\ \text{MU}(^{16}\text{O} = 16)$$

with a precision of 17 parts in 10^9.

An important result not mentioned in the table is the difference in mass of the neutron and the hydrogen atom, which is found to be ^{1}n$-^1$H = 782.61$\pm$ 0.40 keV.

† In the interest of a fast and accurate publication, this table is reproduced as obtained from the computer. As a result, commas are used instead of decimal points, the values have not been suitably abbreviated and the neutron is indicated by a capital N.

$^{12}C = 0$		$^{16}O = 0$		B	b
M (μMU)	s (μMU)	M (μMU)	s (μMU)	(keV)	(keV)
-73346,6352	28,5545	-51433,6606	28,5884	601762,3564	31,1150
-74318,2533	27,6813	-52405,5876	27,7158	601884,7494	30,2252
-71916,5929	30,3553	-50003,1637	30,3884	598865,1324	32,1953
-67729,5322	322,4803	-45814,7720	322,5850	594182,5204	300,7469
-74652,1929	16,0306	-52421,7163	16,5194	611049,7496	22,2868
-73951,7857	16,9109	-51721,0862	16,9595	609614,7492	22,5736
-75723,2344	19,9173	-53493,0981	19,9604	610482,1372	24,3649
-68701,8536	108,5507	-46469,4852	108,5920	603159,5232	102,2779

The results of the present computation will be used to prepare a table of best values of linear combinations of masses, such as nuclear reaction energies, beta decay energies and pairing energies, which will be published in the near future.

The computations have been carried out on an IBM 705 electronic computer in the Farbwerke Hoechst, kindly put at our disposal by Professor K. Winnacker; we are very thankful to him and to Mr. D. Kobelt who prepared the program for the machine. The work of one of us (A.H.W.) is part of the research program of the "Stichting voor Fundamenteel Onderzoek der Materie (F.O.M.)", which is financially supported by the "Nederlandse Organisatie voor Zuiver Wetenschappelijk Onderzoek (Z.W.O.)".

References

1) L. G. Smith, Phys. Rev. **111** (1958) 1606;
L. Friedman and L. G. Smith, Phys. Rev. **109** (1958) 2214

2) K. S. Quisenberry, T. T. Scolman and A. O. Nier, Phys. Rev. **102** (1956) 1071; **102** (1956) 1076; **104** (1956) 461;
K. S. Quisenberry, C. F. Giese and J. L. Benson, Phys. Rev. **107** (1957) 1664;
C. F. Giese and J. L. Benson, Phys. Rev. **110** (1958) 712

3) D. M. Van Patter and W. Whaling, Revs. Mod. Phys. **26** (1954) 402; **29** (1957) 757;
R. W. King, Revs. Mod. Phys. **26** (1954) 327;
L. J. Lidofski, Revs. Mod. Phys. **29** (1957) 773

4) K. Way, G. Andersson, G. H. Fuller, N. B. Gove, D. N. Kundu, J. B. Marion, C. L. McGinnis, M. K. Ramaswamy and M. Yamada, Nuclear Data Cards and Sheets, National Academy of Sciences, Washington D.C. (1957, 1958)

5) A. H. Wapstra, Energies of Alpha Particles, to be published

6) E. R. Cohen, J. W. M. DuMond, T. W. Layton and J. S. Rollett, Revs. Mod. Phys. **27** (1955) 363;
E. R. Cohen and J. W. M. DuMond, Phys. Rev. Letters **1** (1958) 291;
E. R. Cohen, private communication

7) J. Mattauch, Addendum No. 2, Report for 1957, Commission on Atomic Weights, International Union of Pure and Applied Chemistry, Comptes Rendus de la Dix-Neuvième Conférence, Paris 16—25 Juillet 1957, p. 153; J. Am. Chem. Soc. **80** (1958) 4125;
T. P. Kohman, J. H. E. Mattauch and A. H. Wapstra, Naturwiss. **45** (1958) 174; J. de Chimie Physique **55** (1958) 393; Science **127** (1958) 1431; Physics Today **12** (1959) 30;
J. Mattauch, ZS. Naturforschg. **13a** (1958) 572

2.L

Nuclear Physics **15** (1960) 356—362; © *North-Holland Publishing Co., Amsterdam*

Not to be reproduced by photoprint or microfilm without written permission from the publisher

THE SCATTERING OF 38 MeV ALPHA PARTICLES BY C^{12}

I. J. VAN HEERDEN †

Nuclear Physics Division of the National Physical Research Laboratory, C.S.I.R., Pretoria, South Africa

and

D. J. PROWSE

Department of Physics, University of California, Los Angeles 24, California

Received 29 October 1959

Abstract: The differential cross sections for the elastic and inelastic scattering of 38 MeV alpha particles from C^{12} have been measured using a photographic technique. Comparisons with the work of other authors at slightly different energies indicate that the angular distributions vary rather strongly with beam energy. The variation of the elastic distribution is too great to be explained on the basis of the simple optical model.

1. Experimental Procedure

The gas scattering camera described by Gibson, Prowse and Rotblat [1]) has been used to study the scattering of the 38 MeV α-particles from the Birming-

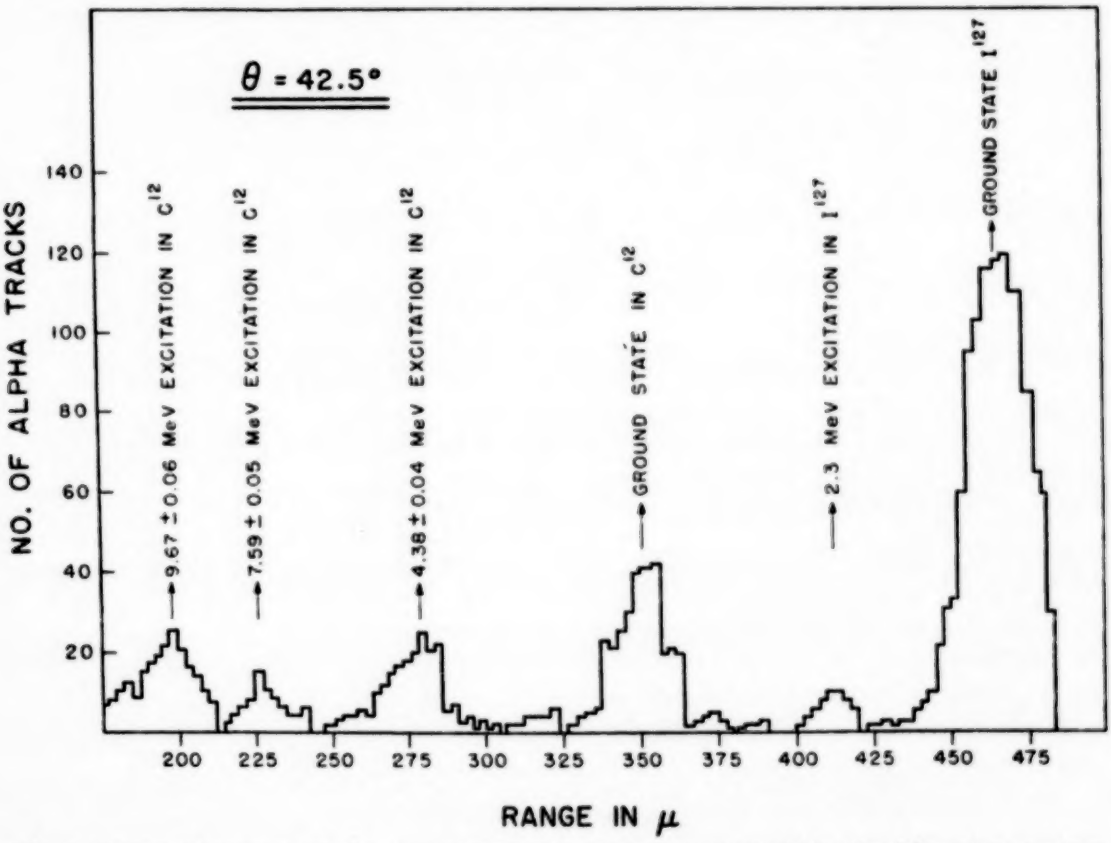

Fig. 1. Range histogram of the α-particle tracks measured at 42.5° in the laboratory system.

† Present address: National Research Council, Ottawa, Canada.

ham 60'' cyclotron. The gas used as a target was methyl-iodide vapour and groups of elastically scattered α-particles were observed from Carbon, Iodine and Hydrogen nuclei, as well as groups of inelastically scattered α-particles from Iodine and Carbon. The scattered particles were detected in Ilford C2 emulsions and at each angle of observation a range histogram of the particles observed in the emulsion was constructed. A typical example is shown in fig. 1 which refers to α-particles scattered through 42.5° in the laboratory system. After due correction for background tracks and range straggling, the numbers of particles in each group were determined. Discrimination against unwanted particles is good because the α-particles can be recognized at sight in the emulsion. The ranges of the elastically scattered particles from I^{127} and C^{12} provide, after correction for the loss in energy of the particles in travelling from the target gas to the detector, a determination of the incident beam energy via the range-energy tables derived from the proton data of Gibson, Prowse and Rotblat [2]). The result obtained is 38.09 ± 0.13 MeV.

2. Absolute Cross Section Measurements

A knowledge of the angle subtended by the detector together with values of the integrated current, gas pressure and size of the target is sufficient to

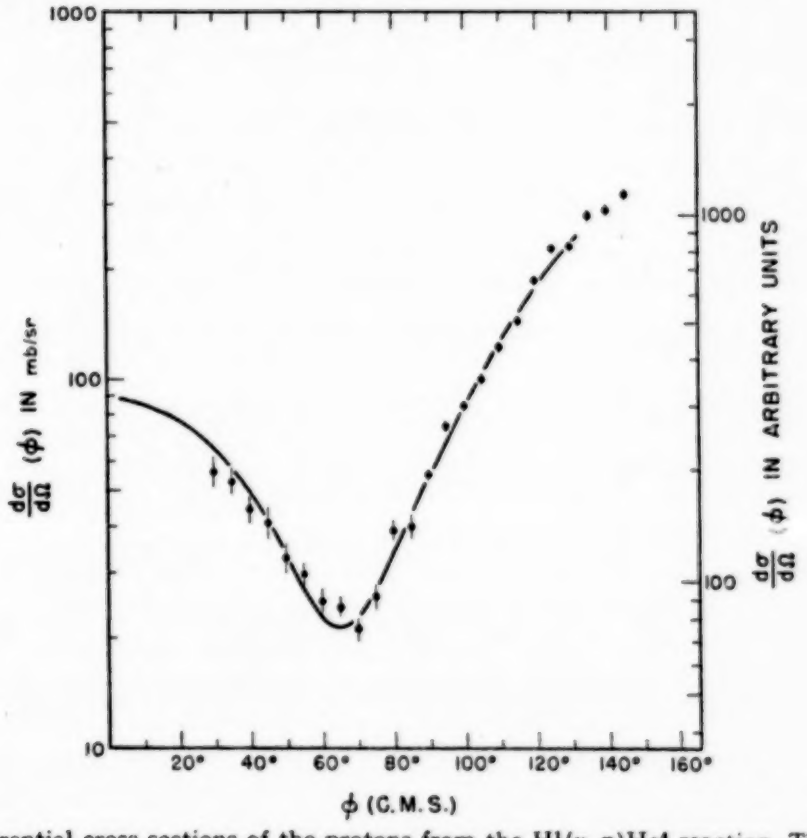

Fig. 2. Differential cross sections of the protons from the $H^1(\alpha, p)He^4$ reaction. The solid curve shows the angular distribution reflected about 90° of 9.76 MeV protons elastically scattered by He^4. This was obtained by Williams and Rasmussen [3]).

determine the absolute cross section. In this case, however, we are uncertain of the calibration of the integrator and so we chose to use as our standard the p—α scattering cross section. Another exposure was therefore made with hydrogen gas and the integrator was only used for a relative measurement of the integrated currents. The cross section for p—α scattering at 9.5 MeV is well known, many experiments having been performed at this energy [3–5]). In the centre-of-mass system this is of course equivalent to the scattering of 38 MeV α-particles from Hydrogen, of which the measured angular distribution is shown in arbitrary units in fig. 2. Also shown reflected about 90° is the distribution obtained by Williams and Rasmussen [3]) for the elastic scattering of 9.76 MeV protons from He^4. The agreement is very good and provides an excellent check of the correctness of the angular distribution. Using the absolute values of the cross section given by these authors we find that 1 arbitrary unit = 0.279 mb/sr. It is likely that the integrator gave relative values for the two exposures correct to at least 10 %, whereas Williams and Rasmussen quote a standard deviation of 5 %; our absolute differential cross sections are thus probably correct to 15 %.

3. Results and Discussion

The angular distribution for α-particles elastically scattered from C^{12} is shown in fig. 3. The experimental points start at 23° in the c.m. system; at more forward angles the two groups corresponding to elastic scattering from C^{12} and I^{127} were not resolved. At a number of angles there appeared a rather weak group of α-particles which corresponded to an excitation of about 2.3 MeV in I^{127}. Between 20° and 35° the presence of this group interfered with the elastic C^{12} group, so that values of the elastic C^{12} cross sections were somewhat difficult to estimate. Details of the elastic and inelastic scattering of α-particles from I^{127} are given in a separate publication [6]). The experimental values in fig. 3 were obtained by applying a suitable correction to the observed number of tracks, based on the assumption that the angular distribution for the 2.3 MeV inelastic Iodine group could be smoothly extrapolated to smaller angles from the values given in ref. [6]).

We have compared our results with those of Yavin and Farwell [7]) who have made similar measurements at 40 and 41 MeV. Their angular distributions are shown in fig. 3. There is a slight difference in absolute cross sections, but there also appears to be a marked energy dependence especially at backward angles. In addition to the results of Yavin and Farwell, there exists data at 40.2 MeV by Igo and Thaler [8]) and very recently at the same energy as that of the present results (38.1 MeV) by Aguilar *et al.* [9]). There appears to be a difference of a factor ten between our results and those shown in fig. 12 of Igo and Thaler. In addition to this difference, the positions of the maxima and minima do not

agree very well. This might be ascribed to the difference in beam energies. However, a comparison of our angular distribution of $(d\sigma/d\Omega)_{elastic}/(d\sigma/d\Omega)_{Coulomb}$ given in fig. 4 with a similar figure of Igo and Thaler, shows much better agreement. The results of Aguilar *et al.* are in fair agreement with ours except at

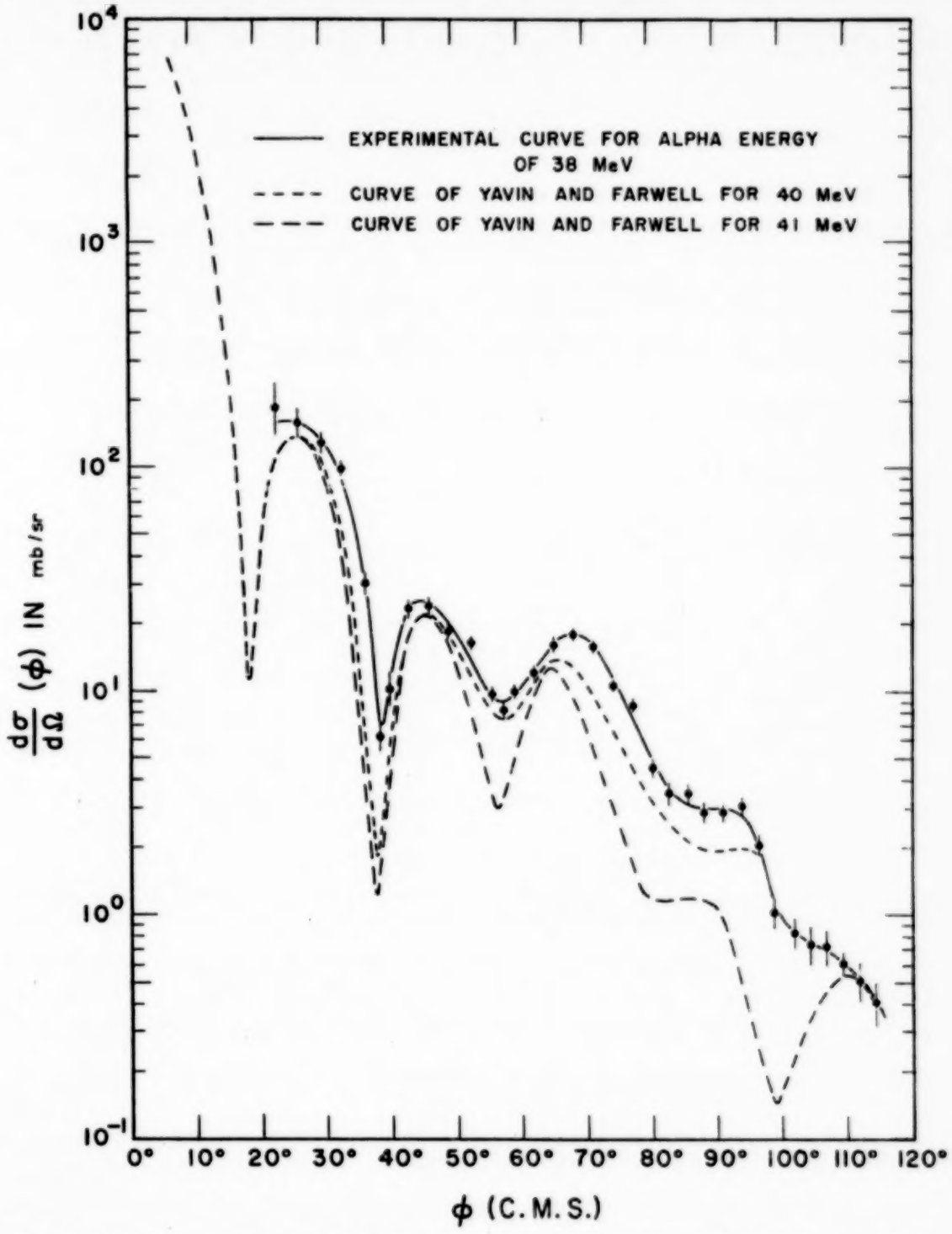
EXPERIMENTAL CURVE FOR ALPHA ENERGY OF 38 MeV
CURVE OF YAVIN AND FARWELL FOR 40 MeV
CURVE OF YAVIN AND FARWELL FOR 41 MeV
$\frac{d\sigma}{d\Omega}(\phi)$ IN mb/sr
10^4
10^3
10^2
10^1
10^0
10^{-1}
0° 10° 20° 30° 40° 50° 60° 70° 80° 90° 100° 110° 120°
ϕ (C.M.S.)

Fig. 3. Centre-of-mass angular distribution for the elastic scattering of 38.09 MeV α-particles by C^{12}. Also shown are similar results obtained by Yavin and Farwell [7]) at 40 and 41 MeV.

backward angles; this is demonstrated by fig. 4 in which the experimental points given by Aguilar *et al.* are directly compared with the present work. The apparent energy variation is more than can be explained on the basis of the simple diffuse surface optical model, and it may well be that the explanation lies in the direct interaction approach of Blair [10]).

The angular distribution of those α-particles inelastically scattered from C^{12} leading to the 4.4 MeV level is shown in fig. 5. Similar results by Yavin and Farwell at 40 MeV are also shown; although there is a general resemblance between the two sets of data, agreement in detail is not good. Again these

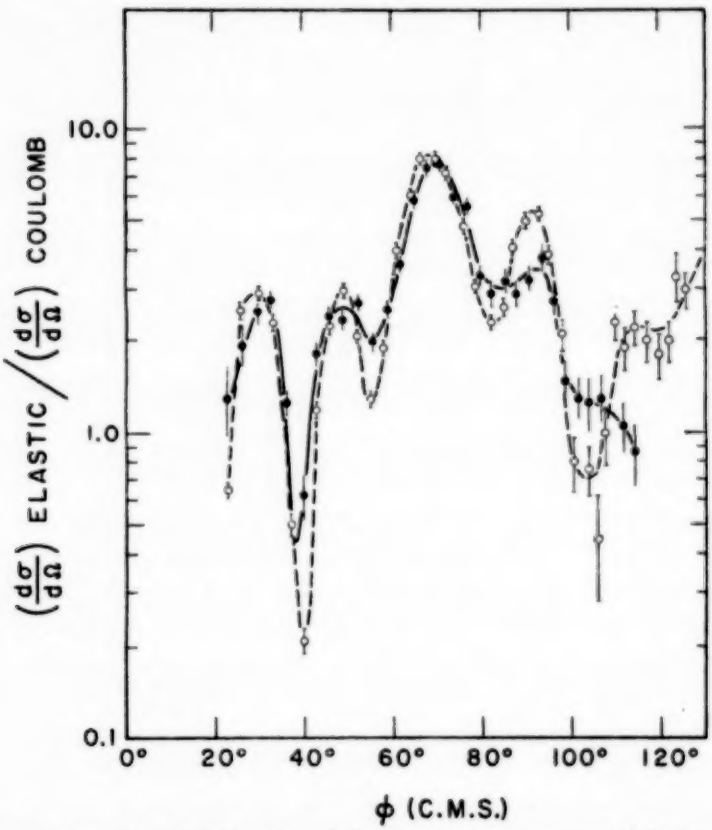

Fig. 4. Centre-of-mass angular distribution of the ratio of the measured differential cross section for elastic scattering of 38.09 MeV α-particles by C^{12} to the Coulomb value. Points shown as ϕ are from the work of Aguilar *et al.* [9]) and points shown as ϕ are the results of the present work.

differences may be ascribed to the different beam energies, especially as Yavin and Farwell also find considerable differences between their results at 40 and 41 MeV. The rapid fluctuation of the cross section with angle is strong evidence of a direct interaction type of process.

Groups of particles were observed at ranges corresponding to levels in C^{12} at 7.7 and 9.7 MeV at a number of angles, but they were not well enough resolved to enable angular distributions to be obtained. No groups corresponding to a higher excitation than 9.7 MeV could be resolved from a rather high background of very short tracks.

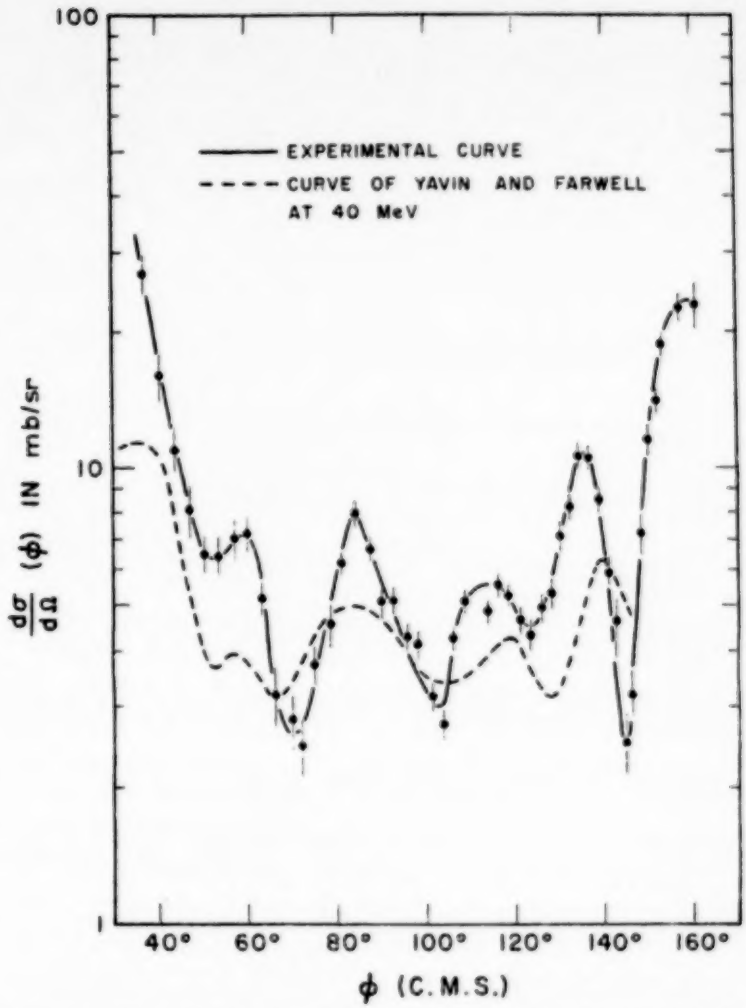

Fig. 5. Centre-of-mass angular distribution for the inelastic scattering of 38.09 MeV α-particles by C^{12} leading to the 4.4 MeV level. Also shown are the results obtained by Yavin and Farwell [7]) at 40 MeV.

The authors are deeply indebted to Professor W. E. Burcham and Dr. J. S. C. McKee at Birmingham for their help and interest in this work. We are also grateful to Professor W. E. Burcham for a preprint of the work of Aguilar *et al.* We also thank Dr. S. J. du Toit at Pretoria and Professor J. R. Richardson at Los Angeles for their encouragement. I. J. v. H. thanks the South African Council for Scientific and Industrial Research for the facilities provided in their laboratories. The scanners are also to be thanked for much of the microscope work.

References

1) W. M. Gibson, D. J. Prowse and J. Rotblat, Proc. Roy. Soc. A **209** (1951) 237
2) W. M. Gibson, D. J. Prowse and J. Rotblat, Nature **173** (1954) 1180
3) J. H. Williams and S. W. Rasmussen, Phys. Rev. **98** (1955) 56

4) R. G. Freemantle, T. Grotdal, W. M. Gibson, R. McKeague, D. J. Prowse and J. Rotblat, Phil. Mag. **45** (1954) 1090
5) R. M. Putnam, J. E. Brolley and L. Rosen, Phys. Rev. **104** (1956) 1303
6) I. J. van Heerden and D. J. Prowse, Nuclear Physics, in course of publication
7) A. I. Yavin and G. W. Farwell, Nuclear Physics **12** (1959) 1
8) G. Igo and R. M. Thaler, Phys. Rev. **106** (1957) 126
9) J. Aguilar, W. E. Burcham, J. Catala, J. B. A. England, J. S. C. McKee and J. Rotblat, Proc. Roy. Soc. A, to be published
10) J. S. Blair, private communication

2.1

Nuclear Physics **15** (1960) 363—372; © *North-Holland Publishing Co., Amsterdam*

Not to be reproduced by photoprint or microfilm without written permission from the publisher

EXCITATION OF THE NUCLEAR GIANT-DIPOLE RESONANCE BY INELASTIC ELECTRON SCATTERING

S. FALLIEROS †, R. A. FERRELL †† and M. K. PAL †††

University of Maryland, College Park, Maryland •

Received 19 October 1959

Abstract: The Goldhaber-Teller model of the giant dipole resonance of a nucleus has been cast in the language of the shell-collective model by using the generator coordinate method of Hill, Wheeler and Griffin. The wave function for the excited state found in this way has been used to evaluate explicitly the inelastic electron scattering form factor for excitation of the giant dipole resonance of the nucleus. The form factor is found to be proportional to the elastic form factor multiplied by the momentum transfer. From an estimate of the bremsstrahlung background extracted from Fregeaus's data it is concluded that experimental investigation of the giant dipole resonance by electron scattering is feasible at optimum momentum transfer.

1. Introduction

Goldhaber and Teller [1]) have noted that the electric dipole coupling of a nucleus with radiation is almost entirely accounted for by a collective oscillation of the nucleus, the so-called "giant-dipole resonance". They presented a simple intuitive picture of this resonance in terms of protons and neutrons surging in opposite directions back and forth through the nucleus. This hydrodynamical model has been carried further by Steinwedel and Jensen [2]), Danos [3]), and others. On the other hand, Wilkinson [4]) has attempted to account for the photonuclear effect entirely on the basis of single-particle excitations. Brink [5]) has pointed out that the collective and independent-particle models are actually not so far apart, as the wave function for the state of the nucleus which is excited by E1 radiation is the same in both models. It consists of a coherent sum of many single-particle excitations, thereby acquiring collective properties. But it is not only the wave function which exhibits special properties, but also the energy of excitation [6, 7]). The excitation energy is found to be relatively high, which can be attributed to the resonant interaction, by means of the internucleon force, between the different configurations which make up the superposition. A similar collective effect in the opposite direction, however, has been

† Present address: Bartol Research Foundation, Swarthmore, Pennsylvania.

†† Present address: CERN, Geneva, Switzerland (permanent address: University of Maryland).

††† On leave from Institute of Nuclear Physics, Calcutta.

• This investigation has been supported in part by the U. S. Atomic Energy Commission under contract AT(40-1) 2098 with the University of Maryland, and has been reported at the 1959 Washington meeting of the American Physical Society [12]).

exhibited by Ferrell and Visscher [8]) in connection with the breathing mode of excitation. In that case the isobaric spin is zero, corresponding to full symmetry of the excited state wave function. Because of Hund's rule there results a lowering in the energy. On the other hand, the giant dipole resonance has isobaric spin equal to one, corresponding to a break-up of the symmetry, with a consequent raising of the energy. This effect on the energy is exhibited explicitly by the detailed calculations for the special case of O^{16} by Elliott and Flowers [9]).

These authors have diagonalized the Hamiltonian matrix with the five $J = 1$, $T = 1$, odd parity states arising from the configurations $(1p)^{-1}$ (2s) and $(1p)^{-1}$ (1d) as basis. They find that the five resultant eigenstates lie in an energy range of 13.1 to 25.2 MeV. The highest state together with the next lower one at 22.6 MeV exhausts almost the entire electric dipole sum rule, the latter state having an E1 matrix element to the ground state which is about twice that of the former. Since two of the states are high up in energy, it is interesting to investigate [10]) the possibility of a high-energy spin-isobaric spin excitation of the collective type which can mix with the 'giant dipole' state (which involves isobaric spin excitation only) via the spin-orbit interaction. It should be noted that such a triplet spin-isobaric spin state has zero electric dipole matrix element to the ground state and, therefore, the result of Elliott and Flowers can be understood only if one considers its mixing with the giant dipole state through the spin-orbit coupling. It is tempting to identify this relatively high energy triplet excitation with a modification of the Goldhaber-Teller picture, in which instead of protons separating from neutrons, protons of one spin are grouped with neutrons of the opposite spin and together move in the opposite direction relative to neutrons of the same spin and protons of opposite spin orientation. Such an excitation has been discussed by Glassgold *et al.* [11]) for the case of infinite nuclear matter, and is one of the four possibilities for collective waves in the degenerate nucleon liquid (the other two being compressional and spin waves). To confirm this idea one needs to diagonalize the central part of the interaction Hamiltonian with the three triplet spin-isobaric spin states of angular momentum unity belonging to $(1p)^{-1}(2s)$ and $(1p)^{-1}(1d)$ as basis states and then verify if the highest eigenstate has a good overlap with the state obtained from the ground state by collective spin-isobaric spin excitation and if this has an energy close to that of the giant dipole state †. It should be emphasized that the splitting in the Elliott-Flowers calculation has a quite different origin from that which occurs in the heavier deformed nuclei. As Danos [13]) has pointed out, in the latter cases one may expect, on the basis of the hydrodynamical model, that the giant dipole will have a resonant frequency for vibrations along the semi-minor axes which is somewhat higher than that for vibrations in the direction of the semi-major axis.

† This question is presently being explored (see ref. [10])).

Because of the interesting splitting found by Elliott and Flowers for the giant dipole resonance, it would be highly desirable to be able to verify experimentally this feature of their calculation. The usual experimental study of photonuclear processes depends upon betatron techniques, using the continuous bremsstrahlung spectrum. With these techniques it is difficult to study in any detail the structure of the cross section as a function of energy, because of the necessity of differentiating the experimental data. Although some success has been reported along this line [14]), it is clearly desirable to have an alternative method. Inelastic electron scattering is one such possibility. Although it is difficult to make the energy resolution of a linear accelerator better than about one MeV, this might be sufficient for many purposes. The principal disadvantage of inelastic electron scattering as a tool for studying photo-nuclear processes, seems to be the fairly high background produced by the bremsstrahlung process. The cross section for the inelastic process under study needs to be sufficiently strong to show up above the background. The purpose of the present note is to compute this cross section, and thereby to reach a decision on the feasibility of using inelastic electron scattering for the purpose of investigating experimentally the giant dipole resonance. To accomplish this we do not need a detailed theory of the giant dipole, and can satisfy ourselves with calculating the cross section for the singlet state, ignoring the mixing with the nearby triplet state. If it is established that it is possible to detect the giant dipole resonance above the background, one may hope that with some refinement in the experimental techniques the splitting may also be detectable. In any case, the angular dependence of the differential cross section for the two separate members of the split giant dipole resonance is each given by the expression obtained below. The result of our investigation is that the giant dipole resonance possesses a cross section larger than background at the more favourable angles, and that its experimental detection should be feasible.

2. Cross-section for Electron Excitation

In order to calculate the cross section for giant dipole excitation, we need a specific wave function for the excited state. This is provided by the generator coordinate technique of Hill and Wheeler [15]) and Griffin [16]). As shown by Ferrell and Visscher [8]), this generator technique can be simplified, and its equivalence to the shell model can be exhibited explicitly. Following the Goldhaber-Teller [1]) picture, and introducing Cartesian coordinates, we consider the substate with zero z-component of angular momentum. Thus, the protons and neutrons are displaced through small distances a and $-a$, respectively, in the direction of the z-axis. If $\Phi_0(z_i, 0)$ is the normal shell model ground state of the nucleus, which we assume to possess equal numbers of protons and neutrons, the state of the deformed nucleus can be represented by the wave function

$$\Phi_0(z_i, a) = \Phi_0(z_i - \tau_3(i)a, 0); \tag{1}$$

z_i and $\tau_3(i)$ are the space and isobaric spin coordinates of the i^{th} nucleon. Using the generator coordinate technique and making an approximation which is appropriate for small amplitudes of vibration [8]), we find for the ground state

$$\Psi_0(z_i) = \Phi_0(z_i, 0) \tag{2}$$

and for the excited state

$$\Psi_1(z_i) = C \frac{\partial \Phi_0(z_i, a)}{\partial a}\bigg|_{a=0}. \tag{3}$$

This approximation neglects correlation in the ground state and the effect of backward going graphs in the excited states [17, 18]), but it corresponds to the standard shell model treatment, and to the extent that spin-orbit coupling can be neglected, is essentially equivalent to the calculation of Elliott and Flowers[9]). The approximation can be expected to be good enough for the present purposes. We further denote the partial derivative with respect to a by a prime. Introducing, for simplicity, oscillator wave functions with Gaussian factors $\exp(-\frac{1}{2}\gamma r^2)$, we have the identity

$$\Phi'_0(z_i, 0) = 2\gamma D \Psi_0, \tag{4}$$

where the dipole operator is

$$D = \tfrac{1}{2}\sum_i z_i \tau_3(i). \tag{5}$$

The normalization constant C can be evaluated by a simple device already employed in studying the collective enhancement of E2 transitions [19]). Consider the identity

$$\begin{aligned} &\frac{\partial}{\partial a}(\Phi_0(z_i, a), \quad D\Phi_0(z_i, a))|_{a=0} \\ &\quad = 2(\Phi'_0(z_i, 0), \quad D\Phi_0(z_i, 0)) \\ &\quad = 1/(\gamma C^2), \end{aligned} \tag{6}$$

where use has been made of eqs. (2)—(5). The quantity being differentiated can be reduced by a change of variable to

$$\tfrac{1}{2}\langle \sum_i [z_i + \tau_3(i)a]\tau_3(i)\rangle_0 = \tfrac{1}{2}Aa, \tag{7}$$

where A is the mass number. Thus we find

$$C = (2/\gamma A)^{\frac{1}{2}}. \tag{8}$$

Eqs. (3), (4) and (8) reproduce Brink's [5]) expression for the excited state.

We can now readily calculate the inelastic form factor F_1 for arbitrary momentum transfer $\hbar\mathbf{q}$. (The square of the form factor times the Mott elastic scattering cross section for a point charge nucleus gives the actual inelastic differential cross section.) We can first simplify the expression for the form factor by noting that only the $T = 1$ odd parity part of the recoil operator is effective in the transition between the ground state and the giant dipole state:

$$\begin{aligned} F_1 &= A^{-1}(\Psi_1, \sum_i e^{i\mathbf{q}\cdot\mathbf{r}_i}[1+\tau_3(i)]\Psi_0] \\ &= \frac{i}{A}(\Psi_1, \sum_i \sin(\mathbf{q}\cdot\mathbf{r}_i)\tau_3(i)\Psi_0). \end{aligned} \tag{9}$$

Inserting from eq. (3) and making a change of variable in the integrations for the scalar product, we find for the form factor

$$\begin{aligned} F_1 &= \frac{iC}{2A}\frac{\partial}{\partial a}(\Phi_0(z_i, a), \quad \sum_i \sin(\mathbf{q}\cdot\mathbf{r}_i)\tau_3(i)\Phi_0(z_i, a))|_{a=0} \\ &= \frac{iC}{2A}\frac{\partial}{\partial a}\langle\sum_i \sin(\mathbf{q}\cdot\mathbf{r}_i+\tau_3(i)qa)\tau_3(i)\rangle_0|_{a=0} \\ &= \frac{iqC}{2A}\langle\sum_i \cos(\mathbf{q}\cdot\mathbf{r}_i)\rangle_0 = \frac{iq}{(2\gamma A)^{\frac{1}{2}}}F_0, \end{aligned} \tag{10}$$

where the expectation value is taken with respect to the ground state. According to this very simple formula the inelastic form factor is proportional to the momentum transfer times the elastic form factor †. Because of the simplicity of this result it may be hoped that it is somewhat more general than the oscillator wave functions which went into its derivation. In any case, the oscillator wave functions are generally regarded as representing fairly well the Hartree-Fock single-nucleon wave functions, at least for the light nuclei. A further feature which may be noted is the factor of the square root of the mass number in the denominator. This is a manifestation of the collective nature of the giant dipole excitation. One would expect a factor A^{-1} for an ordinary single-nucleon transition. Thus the cross section is larger than that for a typical single-nucleon transition by a factor equal to the total number of nucleons. This is a result of the coherent participation of all of the nucleons in the nucleus in the giant dipole resonance.

3. Discussion

Because of the factor q in eq. (10) it would not be favourable to attempt to detect the giant dipole excitation at small angles. Because of the proportionality to F_0, large angles would also not be favourable. The form factor F_1 will have

† This result has already been reported (ref. [20]).

its maximum at about half way out to the first diffraction minimum of F_0. This might be considered as the optimum angle for attempting the detection, but a more relevant criterion would be to maximize the "signal-to-noise ratio" of the inelastic cross section relative to the bremsstrahlung background. We shall not, however, attempt to apply this criterion here. It is likely to yield an optimum angle somewhat closer to the diffraction minimum of the elastic scattering, since the bremsstrahlung cross section is expected to be proportional to the elastic scattering cross section [21]). In lieu of a calculation of the bremsstrahlung, which we have not undertaken, we can make use of the experimental data of Fregeau [22]), who studied the inelastic scattering of 187 MeV electrons from C^{12}. He gives us a plot of his data (fig. 2 of ref. [22])) up to energy losses of more than 30 MeV, for the case of $\Theta = 80°$. (This angle corre-

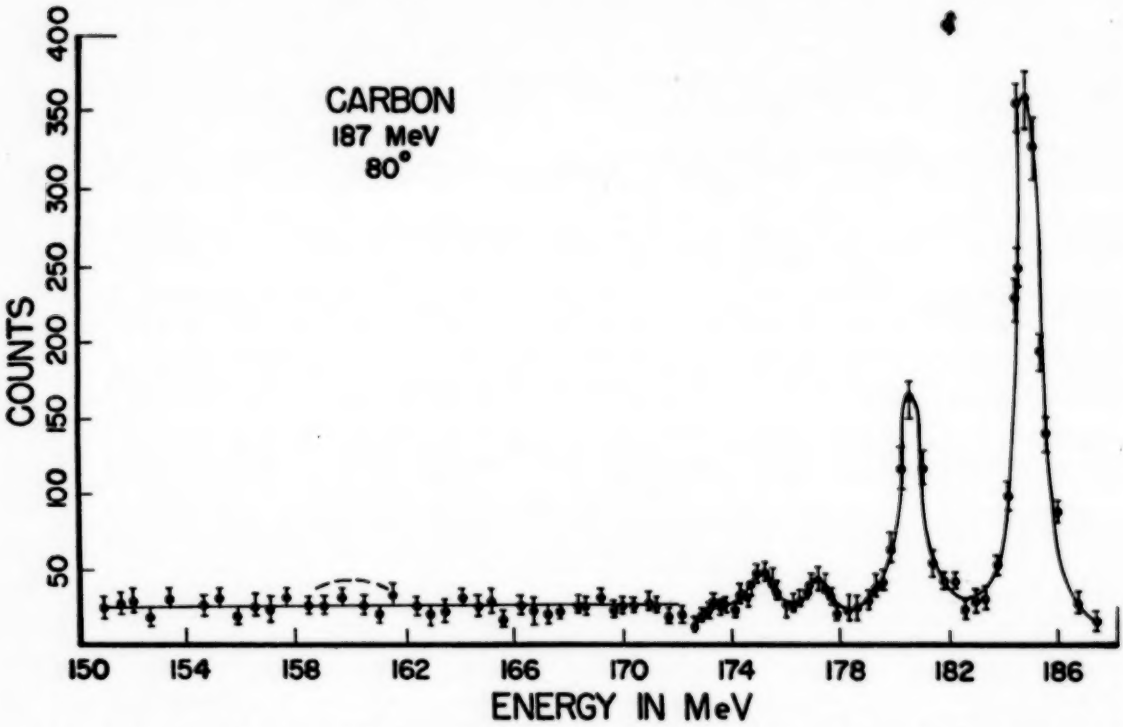

Fig. 1. Experimental curve of Fregeau [22]) for C^{12} showing number of counts against the energy of the scattered electrons at a scattering angle of 80°. The energy of incident electrons is 187 MeV. The dashed line shows a very rough theoretical estimate of the inelastic peak corresponding to the giant dipole state of the nucleus.

sponds to a momentum transfer of about two-thirds of that for the diffraction minimum, a fairly optimum choice for the purpose of detecting the giant dipole excitation.) From his plot, the background cross section can be estimated at roughly $5\times 10^{-32}\ \mathrm{cm^2 \cdot sr^{-1} \cdot MeV^{-1}}$. This may be compared with the value to obtained from eq. (10) by substituting $A = 12$ and $q\gamma^{-\frac{1}{2}} = 2$. Thus we find $|F_1|^2/|F_0|^2 = \frac{1}{6}$, so that multiplying by the observed elastic differential cross section of $7.5\times 10^{-31}\ \mathrm{cm^2 \cdot sr^{-1}}$, we obtain $1.2\times 10^{-31}\ \mathrm{cm^2 \cdot sr^{-1}}$ for the excita-

tion of the giant dipole. Dividing by the natural breadth, which may be estimated at 2 MeV, we find 6×10^{-32} cm$^2\cdot$sr$^{-1}\cdot$MeV^{-1} or a signal-to-noise ratio of only slightly more than unity. This is illustrated in fig. 1, where a flat line has been drawn through the points of Fregeau, indicating the background which is independent of energy loss. The dashed curve shows the bump on top of the background corresponding to the giant dipole excitation. Although there is no evidence of this bump in Freqeau's data, this absence may be ascribed to insufficient statics. It is evident that it ought to be possible to dectet the giant dipole resonance by accumulating enough counts in the relevant energy interval.

4. Case of O^{16}

O^{16} is another specific example where it would be especially desirable to have more experimental study of the giant dipole resonance. Here, because of the doubly closed shells, the theory is particularly straightforward and reliable. The calculations of Elliott and Flowers [9]) show that the dipole resonance may be expected to be split, and this qualitative feature of their calculation should be amenable to experimental verification. In our present simple treatment of the giant dipole resonance we neglect the influence of spin-orbit coupling, and therefore need consider only singlet states. It is instructive to analyze explicitly the excited state wave function Ψ_1 in the shell model. As basis functions we have the two odd parity $(J, T) = (1,1)$ singlet states, Ψ_s and Ψ_d, formed by the configurations $1p^{-1}2s$ and $1p^{-1}1d$, respectively. One finds

$$\Psi_1 = \sqrt{\tfrac{1}{6}}\Psi_s+\sqrt{\tfrac{5}{6}}\Psi_d. \tag{11}$$

It is of interest to evaluate the inelastic form factors for the s and d configurations separately. The calculation is not as transparent as that carried out in section 2, but it is straightforward and yields

$$F_s = \frac{i}{8\sqrt{3}}q'(1-\tfrac{1}{4}q'^2)e^{-\frac{1}{4}q'^2} \tag{12}$$

$$F_d = \frac{i\sqrt{5}}{8\sqrt{3}}q'(1-\tfrac{1}{10}q'^2)e^{-\frac{1}{4}q'^2}), \tag{13}$$

where we have introduced for convenience the abbreviation $q' = q\gamma^{-\frac{1}{2}}$. Taking the weighted sum gives

$$\begin{aligned} F_1 &= \sqrt{\tfrac{1}{6}}F_s+\sqrt{\tfrac{5}{6}}F_d \\ &= \frac{i}{4\sqrt{2}}q'(1-\tfrac{1}{8}q'^2)e^{-\frac{1}{4}q'^2}, \end{aligned} \tag{14}$$

which is identical to eq. (10) in this special case, for which the elastic form factor is given by

$$F_0 = (1-\tfrac{1}{8}q'^2)e^{-\frac{1}{4}q'^2}. \tag{15}$$

Both the elastic and the inelastic form factors for O^{16} are plotted in fig. 2. As already mentioned, it will be noted that the inelastic form factor has its maximum at about one-half of the momentum transfer corresponding to the diffraction minimum for the elastic scattering. It is further of interest to consider the other singlet state, which is orthogonal to the giant dipole resonance, This is an out-of-phase vibration of the two configurations, denoted by the superscript "out":

$$\Psi_1^{\text{out}} = -\sqrt{\tfrac{5}{6}}\Psi_s + \sqrt{\tfrac{1}{6}}\Psi_d. \tag{16}$$

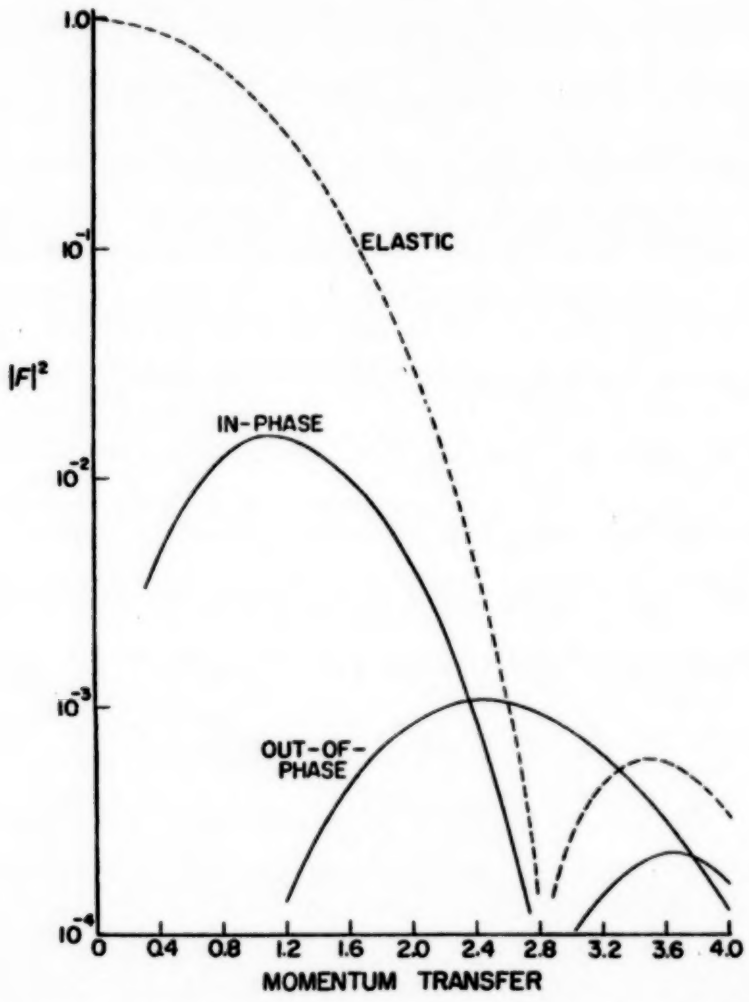

Fig. 2. Calculated square of the form factor for O^{16} plotted against the dimensionless momentum transfer $\gamma^{-1}q$. The curve marked "in-phase" corresponds to inelastic scattering for excitation of the giant dipole resonance state of the nucleus. The dashed curve, which corresponds to elastic scattering, has been drawn for the sake of comparison. Note that the giant dipole curve has a zero exactly at the zero of the elastic curve. The other solid curve labelled "out-of-phase" corresponds to inelastic scattering for excitation of the out-of-phase state defined in the text.

This out-of-phase combination of the two configurations possesses a vanishing E1 matrix element. Therefore the form factor approaches zero faster than q

at small angles. Substituting from eqs. (12) and (13) gives

$$F_1^{\text{out}} = -\sqrt{\tfrac{5}{6}}F_s + \sqrt{\tfrac{1}{6}}F_d = \frac{i\sqrt{10}}{320}q'^3 e^{-\frac{1}{4}q'^2}. \tag{17}$$

This form factor is too small to permit an experimental detection of the out-of-phase state by inelastic electron scattering, but it has been included in fig. 2 for the sake of completeness.

5. Summary

To summarize, we have given a survey of the status of the theory of the giant dipole oscillation from a unified collective-shell model point of view. By putting the Goldhaber-Teller model into shell model form we have arrived at an actual wave function for the excited state, which has made possible an explicit computation of the matrix element for the excitation process. The simple formula found for the form factor, proportional to the product of the momentum transfer times the elastic form factor, makes it especially easy to provide specific numerical predictions for the inelastic cross section for excitation of the giant dipole resonance. In this work we have assumed throughout the validity of the first Born approximation. We have also assumed that the incident electron energy is sufficiently high so that in the scattering kinematics one can neglect the energy loss of the scattered electron, compared to its initial energy. It is a straightforward matter to make the necessary kinematic corrections for cases in which this is not satisfied †. The result of the investigation has been to establish the feasibility of detecting experimentally the giant dipole resonance by inelastic electron scattering. This would be highly desirable as the structure of the giant dipole in the light nuclei has not been resolved by the betatron techniques. In particular, the splitting of the resonance, predicted by Elliott and Flowers for O^{16}, would be one of the first cases to investigate by inelastic electron scattering ††. In conclusion, we should like to observe that although we were able to circumvent an actual theoretical calculation of the bremsstrahlung background by using Fregeau's measurements, such a calculation would nevertheless be very useful in studying the "signal-to-noise" ratio for a wide variety of different angles.

† Such considerations are important for an experiment in progress at Stanford by F. Gudden and others, using 44 MeV electrons. We are indebted to Dr. Gudden for informing us of their preliminary results.

†† *Note added in proof:* The reality of the splitting has recently [23]) been established by measurements on the (p, γ) capture process in N^{15}.

References

1) M. Goldhaber and E. Teller, Phys. Rev. **74** (1948) 1046
2) H. Steinwedel and J. H. D. Jensen Z.f. Naturforsch **5a** (1950) 413
3) M. Danos, Ann. Phys. **10** (1952) 265
4) D. H. Wilkinson, Physica **22** (1956) 1039
5) D. M. Brink, Nuclear Physics **4** (1957) 215
6) R. A. Ferrell, Proceedings of the University of Pittsburgh Conference on Nuclear Structure (1957) p. 256, in particular see pages 265—267
7) R. A. Ferrell, Bull. Am. Phys. Soc. **3** (1958) 49
8) R. A. Ferrell and W. M. Visscher, Phys. Rev. **102** (1956) 450
9) J. P. Elliott and B. H. Flowers, Proc. Roy. Soc. **242** (1957) 57
10) Fallieros, Lee and Pal, to be published;
M. K. Pal and Y. C. Lee, Bull. Am. Phys. Soc. **4** (1959) 406
11) Glassgold, Heckrotte and Watson, Annals of Physics **6** (1959) 1
12) M. K. Pal, S. Fallieros and R. A. Ferrell, Bull. Am. Phys. Soc. **4** (1959) 229
13) M. Danos, Nuclear Physics **5** (1958) 23
14) E. G. Fuller and Evans Hayward, Phys. Rev. **101** (1956) 692;
A. S. Penfold and E. L. Garwin, Phys. Rev. **114** (1959) 1324;
A. S. Penfold and J. E. Leiss, Physs. Rev. **114** (1959) 1332;
S. Penner and J. E. Leiss, Phys. Rev. **114** (1959) 1101
15) D. L. Hill and J. A. Wheeler, Phys. Rev. **89** (1953) 1102
16) J. Griffin, Phys. Rev. **108** (1957) 328
17) R. A. Ferrell, Phys. Rev. **107** (1957) 1631; Bull. Am. Phys. Soc. **4** (1959) 59
18) S. Fallieros, Ph. D. Thesis, University of Maryland (1959) (unpublished)
19) R. A. Ferrell and W. M. Visscher, Phys. Rev. **104** (1956) 475
20) R. A. Ferrell, 1958 NBS Photonuclear Conference Proceedings (April 1958) p.50
21) M. Danos, private communication
22) J. Fregeau, Phys. Rev. **104** (1956) 225
23) Cohen, Fisher and Warburton, Phys. Rev. Letts. **3** (1959) 433

2.G

Nuclear Physics **15** (1960) 373—386; © *North-Holland Publishing Co., Amsterdam*

Not to be reproduced by photoprint or microfilm without written permission from the publisher

CROSS SECTION AND ASYMMETRY IN THE DEUTERON PICKUP REACTION $C^{12}(p, d)C^{11}$ AT 145 MeV

PAUL F. COOPER, Jr.† and RICHARD WILSON

Cyclotron Laboratory, Harvard Univerisity, Cambridge 38, *Massachusetts* ††

Received 22 October 1959

Abstract: A carbon target was bombarded with polarized protons of average energy 145 MeV and cross sections and asymmetries were measured for deuterons emerging at angles between 5° and 40° to the incident beam. The asymmetry is small at angles less than 15°, but rises rapidly to become nearly 100 % at 40°.

The results for the cross sections are in agreement with recent calculations including multiple scattering corrections to the impulse approximation. They show that multiple scattering effects dominate at large angles and prevent a search for high momentum components by this method.

1. Introduction

Several years ago Hadley and York [1]) found a large number of 80 MeV deuterons emerging in the forward direction from targets bombarded by 90 MeV neutrons. Soon thereafter, Chew and Goldberger [2]) explained these results as the high-energy "pickup" of a proton by the incoming neutron. Using the impulse approximation they related the probability of this process to that of finding a proton in the nucleus with the correct momentum to produce the observed deuteron. Thus they felt the process was suited to a direct study of momentum distributions.

Selove [3]) initiated such a study at Harvard several years ago. He used the 95 MeV external proton beam to study several reactions, principally $C^{12}(p, d)C^{11}$ and $Be^{9}(p, d)Be^{8}$. When he analysed his data, a puzzling feature appeared: there seemed to be a relatively high probability of finding a neutron with high momentum within the nucleus. This was considerably larger than had been expected on the basis of, or was consistent with, the independent particle model. He knew, of course, that Chew and Goldberger's theory must be corrected for multiple scattering since it is based on the impulse approximation; but he believed — as we can now show, erroneously — that these would only affect the observed momentum distribution through a normalizing factor.

† Now at Cambridge Electron Accelerator, Harvard University, Cambridge 38, Massachusetts.

†† Supported by the joint program of the Office of Naval Research and the U. S. Atomic Energy Commission.

Assuming, for the moment, that the theoretical arguments are correct, the momentum distribution as deduced from data on pickup experiments at two different energies should be the same. By comparing such results we have a check on the theory. This, in light of the results, became of high interest. Selove had planned such an extension of his work, but before this could be done, the Harvard cyclotron was converted to a higher energy [4]), and a polarized beam was extracted. It then seemed profitable not only to repeat the experiment at this higher energy of 149 MeV, but also to use this polarized proton beam. Since the momentum distribution is the same regardless of spin, there should be no asymmetry in the deuterons produced by such an initially polarized proton beam.

In performing the present experiment, therefore, we expected to check the validity of the existing theory in these two different ways. At the same time, we hoped that we would be able to obtain sufficient energy resolution to separate the pickup reactions leading to the formation of C^{11} in its various excited states.

2. Apparatus

In a study such as this the experimental problem is not only to measure the energy of the deuterons but also to separate them from the much more numerous protons and the less numerous tritons and heavier particles. Several ways of doing this are available. For example, Selove [3]) found the energy of the particles by measuring the range with a range telescope, while identifying the particles as deuterons by finding the specific ionization (dE/dx) in a thin scintillator in front of this telescope. Since the deuterons of a given range have a specific ionization 1.35 times that of a proton of the same range, such a crystal can produce pulses with adequate separation in heights for the two kinds of particles to distinguish between them by fairly crude means. It was necessary, however, to arrange the outputs of the range telescope and the pulse height analyser in coincidence on a 4 by 16 matrix of counters. Then the separation was done manually by comparing the results of a run containing both protons and deuterons with one in which sufficient absorber had been put in front of the telescope so that protons alone were present.

Since Selove performed his experiment there have been improvements in the precision of pulse height measurement which have enabled us to use a different method. Though we separated deuterons from protons, as before, by measuring the specific ionization of the particle, we substituted the total energy (less, of course, that lost in the counter measuring dE/dx) for the range. We inferred the energy from a measurement of the pulse height in a scintillator of 7″ length, sufficient to stop the particles. Since now we compare deuterons with protons of the same energy rather than the same range, the specific ionizations differ by a factor of 1.65. It therefore becomes feasible to discriminate against the proton

by electronic means and only display the deuterons, a considerable simplification. With a single setting of the discriminator on the output of the specific ionization counter, it was possible to separate protons from deuterons over a range of energies larger than 10 MeV. Actually, we used two specific ionization counters to render the particle identification more certain, while at the same time cutting down the accidental background.

The detecting equipment to do this consisted of two circular scintillators 0.2" thick, to measure dE/dx, followed by the 7" long scintillator to measure the total anergy. All these were made of Pilot Chemical Co. "Pilot B" scintillators. An RCA 6810 phototube viewed each of these scintillators. In the first two counters the tube saw the edge of the scintillator, while the third had a "head-on" mounting to collect the maximum light possible. Since the second

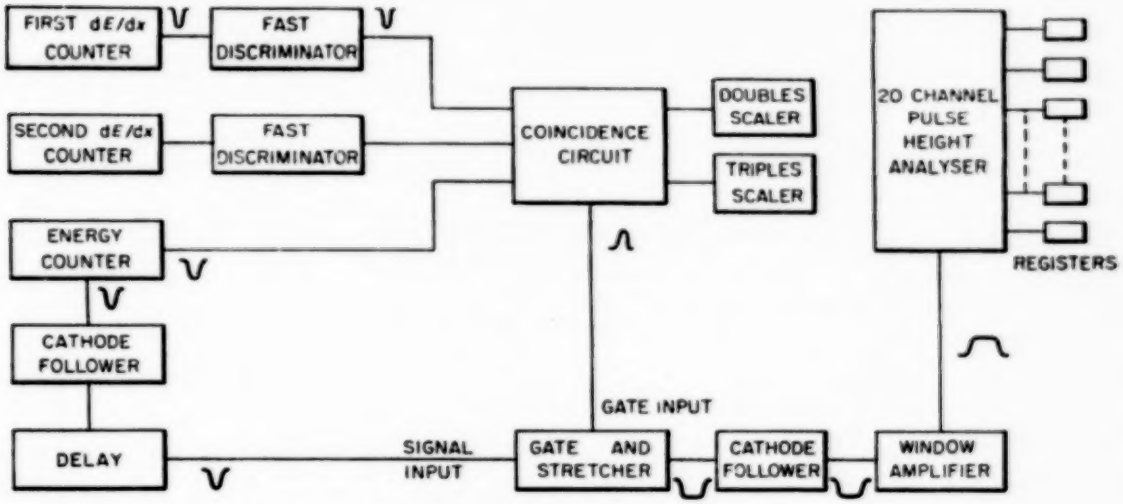

BLOCK DIAGRAM OF ELECTRONICS

Fig. 1. Block diagram of the electronic apparatus.

of the specific ionization counters (which was one inch in diameter) was smaller in diameter than either the first counter or the total energy counter, it was the defining counter.

A block diagram of the electronic equipment is shown in fig. 1. Since the desired deuterons appear in a large flux of protons, we tried to keep all pulses as short as possible. By the use of RCA 6810 photomultipliers we were able to obtain pulses 30 V high of 20 ns duration from the total energy counter; this made possible the use of particularly stable gate and stretcher circuits. The coincidence circuits are those of Garwin [5]); the gate is a simple diode circuit on the same principle; and the stretcher is that of Kelley [6]) inverted to use negative pulses. The fast discriminators are the EFP-60 circuits of Clark [7]) fed with 10 V negative pulses on the cathode. Various tests led us to believe that

this electronic equipment was not a limitation either on the available energy resolution nor on the available counting rate.

The Harvard polarized proton beam has already been described [4]). The "East Probe" was used as described therein to produce a beam of protons 72 ± 2 % polarized of energy 149 ± 1 MeV, with an energy spread of 2 MeV or less. About one million protons per second passed through a defining slit $\frac{3}{16}''$ wide and $1\frac{3}{4}''$ high. This beam then passed through the apparatus as drawn, to scale, in fig. 2.

As in other experiments in this laboratory, two beam monitors were used. An ionization chamber was used before the target as a relative monitor. At intervals, this was calibrated by a Faraday cup located after the scattering table.

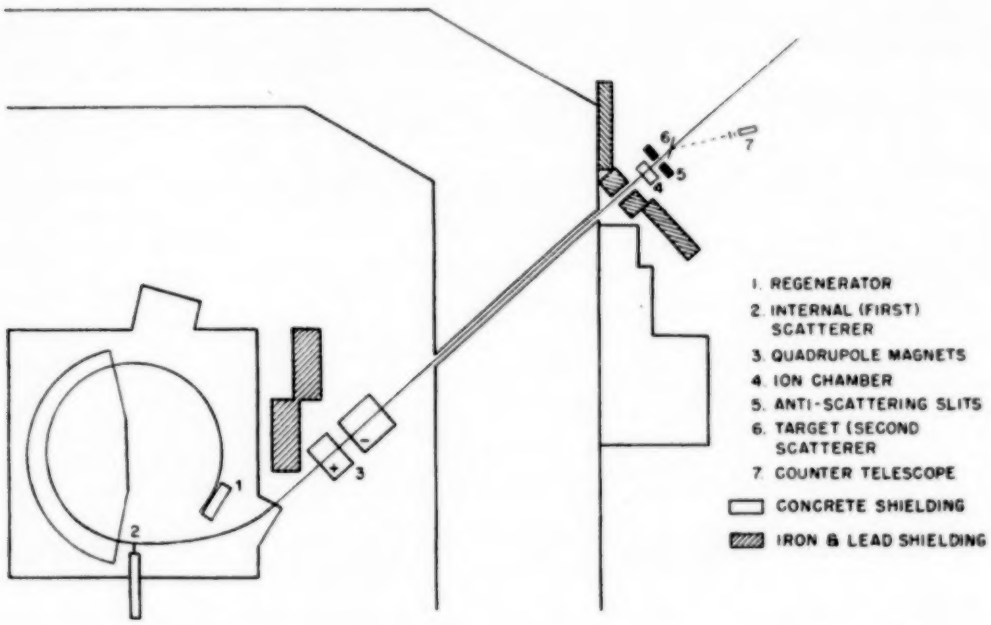

Fig. 2. Scale drawing of the apparatus layout.

It is obvious that in an experiment which measures polarization alignment is a critical factor. We therefore proceeded as follows. We defined the beam line by the defining slit and an X-ray photograph 6 ft. from the slit, and aligned a cathetometer on this line. The counter telescope was set on a rotating arm with its pivot on this beam line, and the centering was checked by a further photograph. To determine the angle for rotation of the telescope we constructed a beam profile by sweeping the telescope through the beam and observing the integrated current from the defining scintillator. Suitable fine adjustments were provided for bringing the nominal zero position of the counter telescope

into coincidence with the line defined by the pivot and by the "centre of gravity" of the beam at the defining counter as measured in this way. It is estimated that this could be done to with 2'30".

It is necessary to use targets of a few MeV thickness. To avoid smearing of the deuteron spectrum, in fact, we must use a target three to four times thinner han the desired thickness and to place it at a small angle to the beam. Then the scattered deuterons pass through less material than the protons, and by suitably choosing this target angle, the deuterons produced at the two sides of the target can emerge with the same energy. The necessary relation is [3])

$$\tan \phi = \sin \vartheta / [(\mathrm{d}E/\mathrm{d}x)_\mathrm{d}/(\mathrm{d}E/\mathrm{d}x)_\mathrm{p} - \cos \vartheta]$$

where ϕ is the angle of the target, as measured from the normal to the beam direction in the plane of scattering, ϑ is the scattering angle, and $(\mathrm{d}E/\mathrm{d}x)_\mathrm{p}$ and $(\mathrm{d}E/\mathrm{d}x)_\mathrm{d}$ are the rates of energy loss for protons and deuterons respectively. At small angles this leads to prohibitively thin targets placed almost parallel to the beam; as a reasonable minimum compromise no angle less than 15° was used.

As a result of this, if we use a target of thickness t, its effective thickness is $t \csc \vartheta$; if ϑ is 15°, to measure asymmetries to 0.01 we must know ϑ to within 2'30". In addition, it is necessary to change the orientation of the target when moving between a positive and a negative angle. Therefore we must be able to position the target accurately and reproducibly. This we achieved as follows. The target itself was mounted on a transit, which enabled it to be set at any desired angle with an accuracy of 0.5'. The zero angle was determined by using a mirror, whose parallelism to the target was independently checked, and making the mirror perpendicular to the beam line by use of the cathetometer described above together with a light source mounted directly above it. It is estimated that this process gave absolute knowledge of the target angle to within 3'30", which is seen to be barely adequate. This error is the largest single one in the measurement of the polarization, though it is seen to cancel out in obtaining the cross sections.

Two further matters about our experimental method deserve comment. First, anti-scattering slits play an important role. Low energy protons are readily scattered from the defining slit and enter the telescope. They have equal specific ionization to a high-energy deuteron and thus open the gate; random coincidences may then result which form an important contribution to the background. Fairly complex anti-scattering slits are needed to minimize this effect. With them, the target-out background was never more than 5 % of the target-in counting rate (in the region of the pickup peak), and could then be directly subtracted from the data. In view of its smallness, we made no attempt to correct for energy changes.

Finally, emphasis should be placed on the importance of testing the discri-

mination of the apparatus against protons. This was done every few hours in the course of a run as follows. First, enough absorber was placed in front of the telescope to slow elastically scattered protons down to an energy where they gave the same pulse height in the total energy scintillator as the deuterons under study. Various settings of the discriminators were then tested, and a graph of the percentage of protons excluded versus voltage level made for each. Then enough absorber was added to cause the elastic protons to give the same pulse height in the dE/dx scintillators as the desired deuterons, and voltage levels found which would cut out as many protons as possible but permit essentially all the deuterons to register counts. It was possible, in this way, to keep the residual proton counting rate always less than 0.1 % of the normal proton counting rate.

3. Results

Measurements were made with a 20-channel pulse height analyser of the deuteron spectrum from carbon at various angles from 5° lab to 40° lab. Half hour measurements at each positive angle alternated with similar ones at the same negative angle, and with measurements of elastically scattered protons for calibration purposes. The energy scale was derived from these calibrations, though it includes an arbitrary 1 MeV shift downwards to allow for non-linearity of the plastic scintillator used. This shift was determined by a comparison of the proton and deuteron spectra at 7° lab with calculated energies for this angle. This comparison assumed that, at this angle, there is no appreciable shifting of the observed deuteron peak by excitation of excited states of the residual nucleus.

Figs. 3 to 6 illustrate the results obtained. At small angles, the width of the deuteron peak is 3 MeV — the same as that of the proton calibration peaks. Of this, 2 MeV may be attributed to the energy spread in the beam, while the remaining 2 MeV seems to be due to the scintillator or the photomultiplier. There is no sign of deuterons from a pickup reaction which leaves the residual C^{11} nucleus in its 2.2 MeV excited state, though, owing to the arbitrary energy calibration discussed above, we can only infer this from the shape of the peaks and therefore cannot be as sure of it as Selove was in his work. The group of pulses below the peak can all be explained by small background effects.

At larger angles (above 15°), the peaks become much smaller compared to the general deuteron background, and their resolution is correspondingly more difficult. Thus there is a considerable uncertainty even in setting limits of the cross section for the pickup reaction which leads to the C^{11} ground state. We have therefore employed two extreme procedures in evaluating these cross sections. In the one, all pulses above a point 3 MeV below the peak have been considered to be true deuterons leaving the residual nucleus in its ground state;

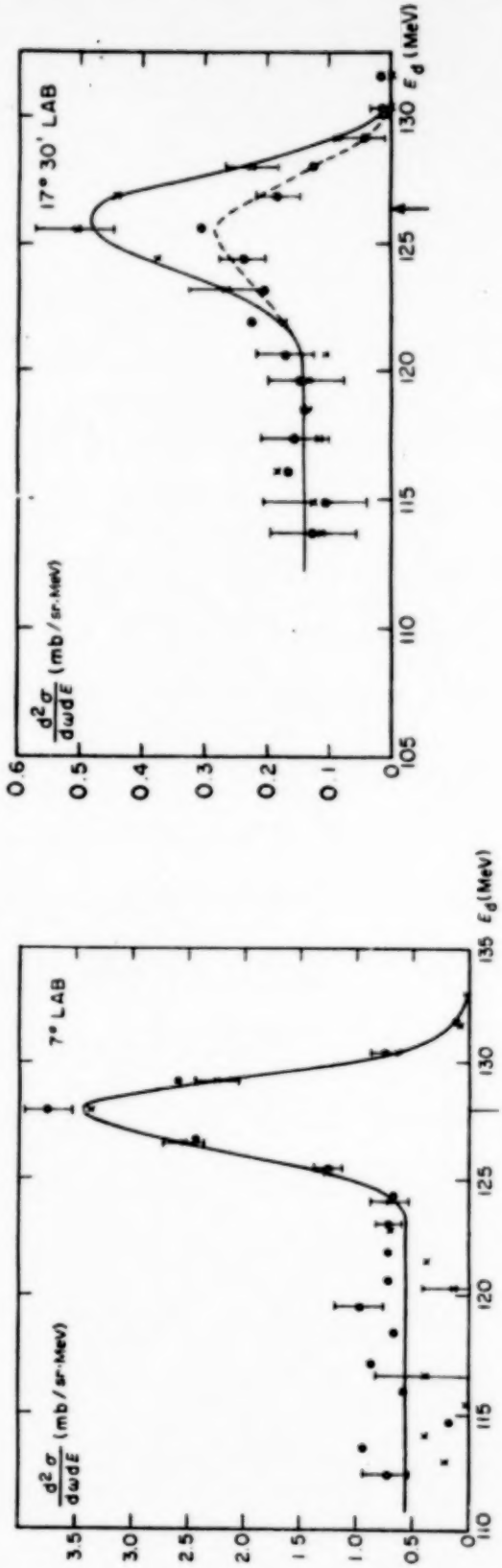

Fig. 3. Deuteron energy spectra at 7° and 15° lab.

Fig. 4. Deuteron energy spectra at 17½° and 20° lab.

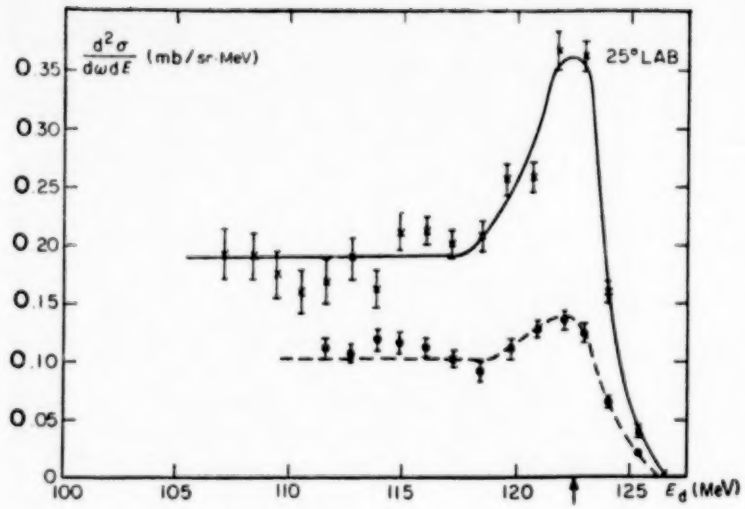

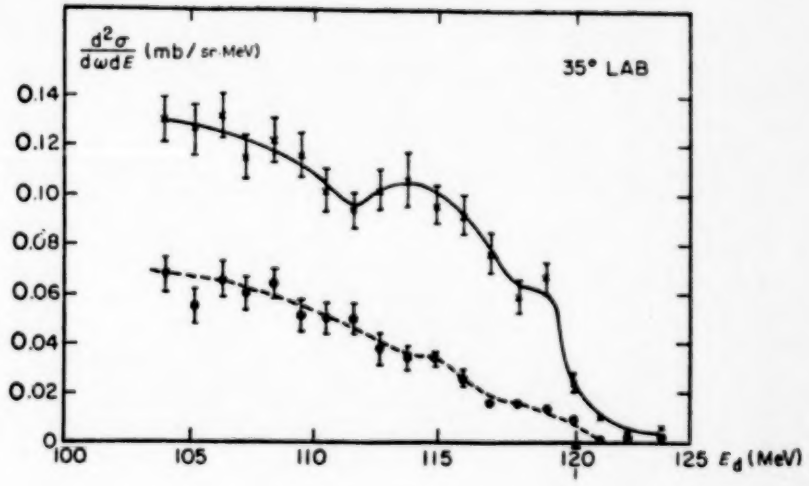

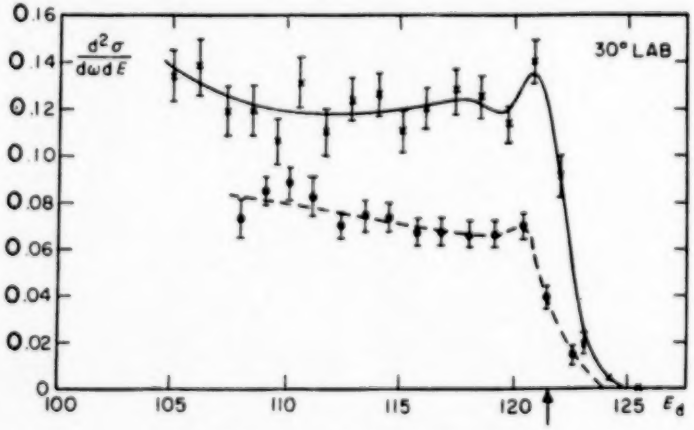

DEUTERON ENERGY SPECTRA

× POSITIVE ANGLES • NEGATIVE ANGLES

Fig. 5. Deuteron energy spectra at 25° and 30° lab.

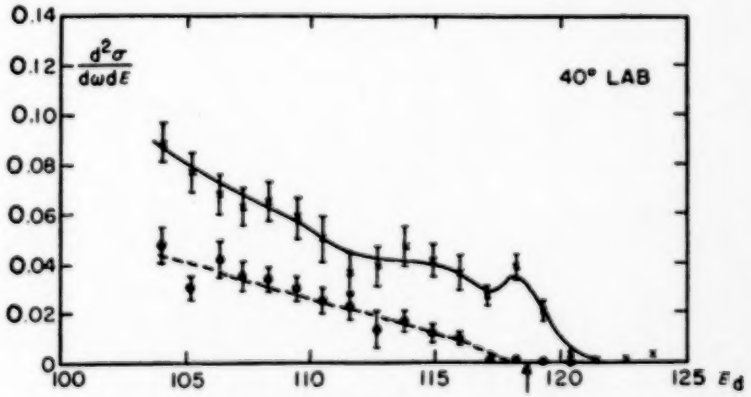

DEUTERON ENERGY SPECTRA

× POSITIVE ANGLES • NEGATIVE ANGLES

Fig. 6. Deuteron energy spectra at 35° and 40° lab.

the other is obtained by extrapolating the background measured below the peak region and subtracting it. The difference between these two procedures grows to a factor of 3 at 40°. The difference in the value of the asymmetry is

TABLE 1

Lab. angle	Cross-section (mb/sr) Cont. subtr.	Cont. not subtr.	Asymmetry Cont. subtr.	Cont. not subtr.
5°		17.83±0.44		−0.004±0.035
6°		15.45±0.41		−0.016±0.037
7°		13.87±0.36		−0.037±0.038
8° 30′		12.75±0.46		−0.006±0.061
10°		6.94±0.27		0.042±0.054
12° 30′		4.82±0.22		−0.008±0.062
15°	2.72±0.15	2.95±0.11	0.043±0.080	0.069±0.075
17° 30′	2.03±0.12	2.14±0.07	0.311±0.082	0.333±0.080
20°	1.51±0.05	1.64±0.04	0.424±0.050	0.355±0.035
25°	1.18±0.03	1.24±0.03	0.550±0.042	0.590±0.038
30°	0.37±0.02	0.61±0.02	0.548±0.065	0.542±0.049
35°	0.14±0.01	0.37±0.02	0.853±0.103	0.775±0.064
40°	0.06±0.007	0.17±0.01	0.990±0.198	0.858±0.177

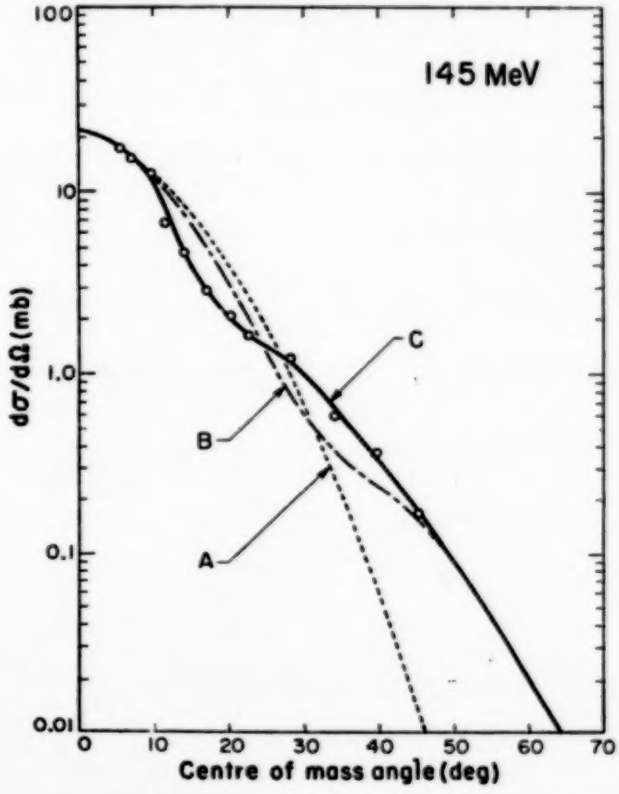

Fig. 7. Cross section as a function of angle for the reaction C^{12}(p, d)C^{11} at 145 MeV. Curve A shows the Chew-Goldberger theory for a distribution $e^{-\alpha^2/15}$; curve B includes the interaction of the incoming proton and curve C includes also the interaction of the outgoing deuteron.

less (having a maximum of 15 %), for the asymmetry of the background and that of the peak are almost proportional.

We may well ask whether this background of low energy deuterons is not due to some spurious effect. At the lowest energies shown in the spectra it is quite possible that some of these "deuterons" are given by pulses from inelastically scattered protons which have managed to escape being cut out by the dE/dx counters, but these should appear only in the lowest 20 % or so of the energy range shown. In our opinion, based on the measured cross sections for inelastic protons scattering at these energies [8]) and the measured rejection ratios, not more than 10 % of these counts are spurious. Predominantly they are, therefore, true deuterons which correspond to leaving the C^{11} nucleus in various excited states.

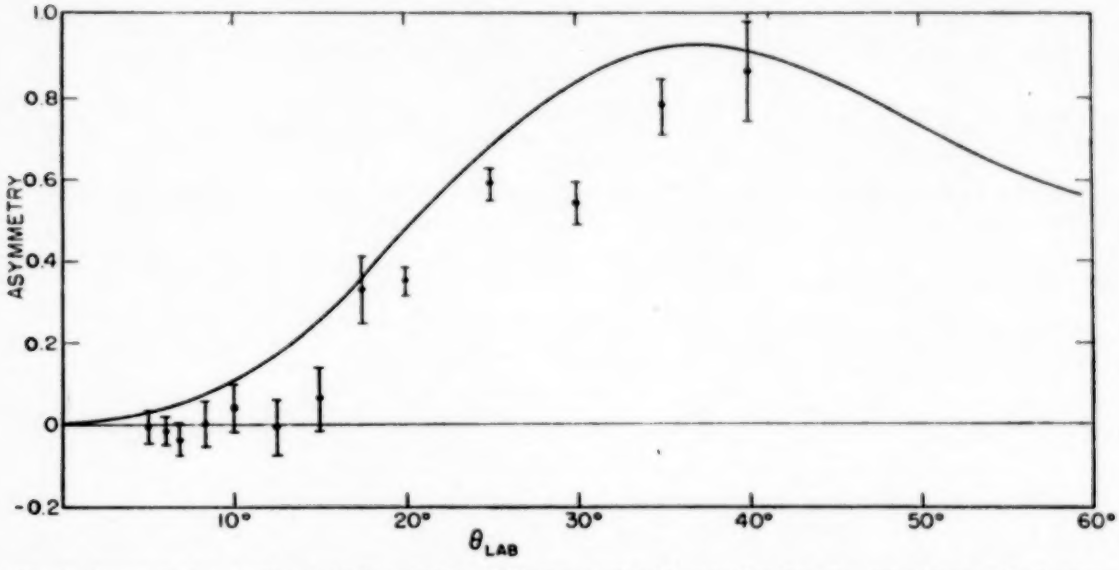

Fig. 8. Asymmetry in the reaction C^{12}(p, d)C^{11} by a 100 % polarized beam. The theoretical curve is a fit by Greider.

The cross section, as a function of angle, is given in table 1 and plotted in fig. 7 with values for both types of normalization included. The asymmetry is plotted in fig. 8.

4. Discussion

As a first step in discussing these data, we shall interpret them according to the theory of Chew and Goldberger [2]) with the refinements introduced by Selove [3]). We shall, however, define $N(\mathbf{n})$ — the probability of finding a neutron of momentum $\mathbf{n}$ within the nucleus — as the momentum distribution of the neutrons in the laboratory frame of reference, since this is the system in which the initial C^{12} nucleus is stationary. Following their method, we can use our

data to derive $N(\mathbf{n})/F^2$ (where F is the fractional parentage coefficient) as a function of $|\mathbf{n}|^2$. This has been done, and is plotted in fig. 9 for the data both of this experiment and that of Selove.

If this method of approach is meaningful, the results should agree. We see, however, that they do not; in particular, the large high momentum components found by Selove do not seem to be present in this experiment.

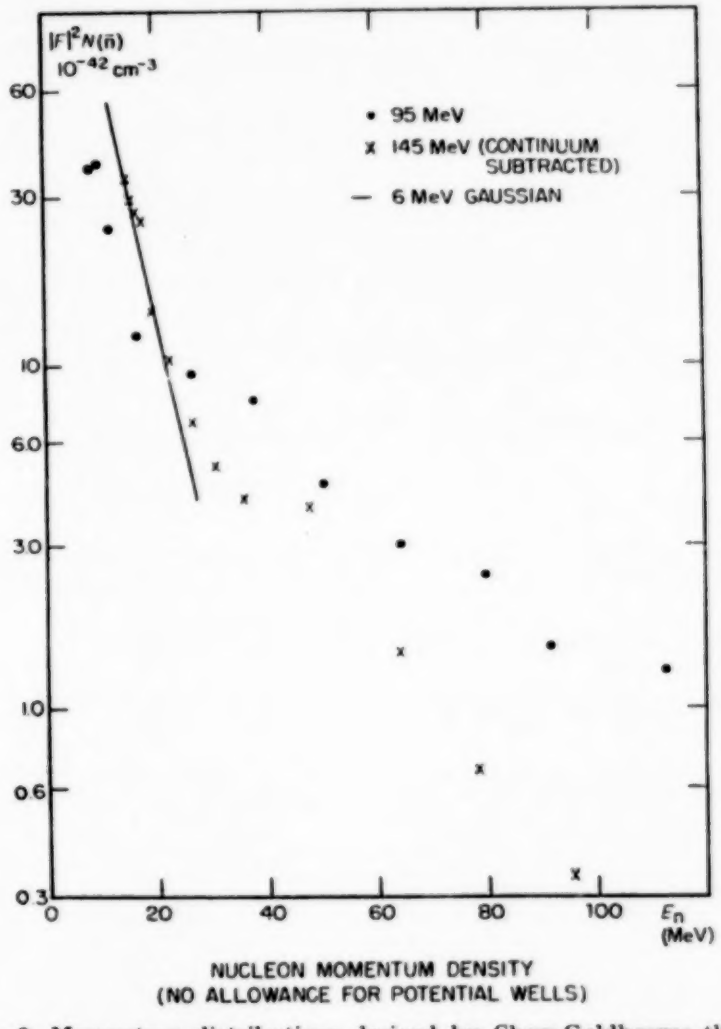

Fig. 9. Momentum distributions derived by Chew-Goldberger theory.

We then made a simple modification of the theory by considering the neutron pickup to take place after the incident proton had been accelerated in an attractive nuclear potential of 15 MeV at 145 MeV and 25 MeV at 95 MeV. This changes somewhat the relationship between the neutron momentum and the laboratory scattering angles. We then obtain the momentum distribution shown in fig. 10. We now see that the results of this experiment and of Selove's agree for small $\mathbf{n}$, but still not for large $\mathbf{n}$.

For these large angles and large values of **n**, we note that the simple theory of Chew and Goldberger cannot account for any asymmetry such as we observe in the picked-up deuterons. Though the measured asymmetry is indeed zero — as predicted by this theory — at small angles, it becomes large beyond 15° lab., and, at the largest angles measured is nearly 100 %. This suggests that at 15° lab. angle there is a change in mechanism. We feel that this is due

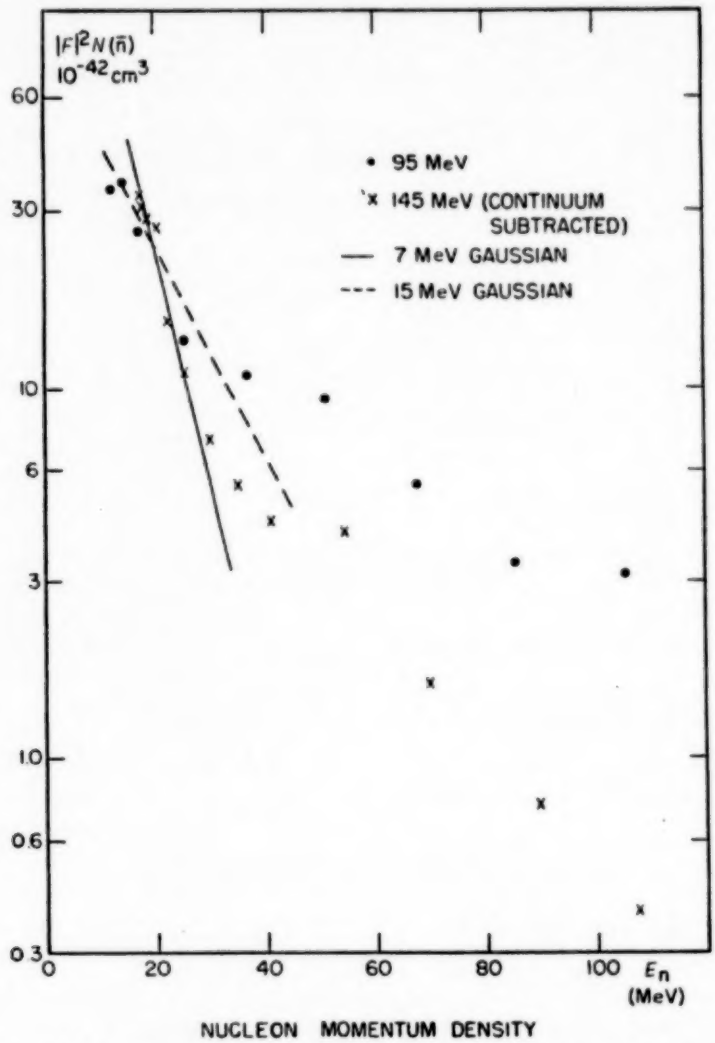

Fig. 10. Momentum distributions derived by Chew-Goldberger theory with kinematic modification.

to a change from a Chew-Goldberger type pickup at small angles to a two-stage process in which the incident proton first suffers an asymmetric scattering in the nuclear potential. This change may also be correlated with the kink in the plot of $N(\mathbf{n})$ vs $|\mathbf{n}|^2$ at the corresponding point.

This argument is given detailed support by the calculations of Greider [9]). who has extended the optical model so that he can use it to correct the Born approximation (in this case Chew-Goldberger theory) for inelastic processes.

As an example, he has calculated the pickup cross sections and asymmetries for carbon with an assumed momentum distribution $N(\mathbf{n}) = e^{-\mathbf{n}^2/20}$, a nuclear radius for C^{12} of 3.4×10^{-13} cm, and a "square well" potential for carbon of $-25-15i$ MeV at 95 MeV and $-13-18i$ MeV at 145 MeV. His results, in comparison with the experimental data, are shown in figs. 8 and 9. The agreement is not perfect, but Greider's assumed parameters are not necessarily the best.

At first we hoped that the elementary pickup theory might at least be used in the small angle ($< 15°$) region where the polarization is zero, and that information might be gained about the small momentum components. Greider has shown, however, that in this angular region the scattering is dominated by the interaction of the outgoing deuteron with the nucleus. This is also shown in fig. 8, curve C.

There are, of course, other direct means of finding the momentum distribution for carbon. These are the experiments which study the angular and energy correlation in the (p, 2p) reaction [10]) and the (γ, np) reaction [11]). These have been interpreted in terms of a momentum distribution $N(\mathbf{n}) = \exp(-|\mathbf{n}|^2/E_0)$ where E_0 is about 15 MeV. The interpretation of these experiments, however, is also affected by multiple scattering corrections to the impulse approximation. These corrections will also overestimate the higher momentum components.

As a more realistic basis for comparison we turn to evidence which, though indirect, is more certain. The charge distribution of the carbon nucleus may be inferred from electron scattering measurements [12]). The data from this experiment have been analysed as the sum of two distributions due to S and P nucleons moving in a harmonic oscillator well. The data are consistent with a theoretical charge distribution

$$\rho(r) = \rho(0)(1+\tfrac{4}{3}r^2/a^2)e^{-r^2/a^2}$$

where $a = 1.65\times10^{-13}$ cm. A correction for the proton charge distribution gives a similar shape for the nucleon density but with $a = 1.52\times10^{-13}$ cm.

The density is the sum of squares of the S and P wave functions $\psi_s^2(r)+\psi_p^2(r)$. The momentum wavefunctions $\phi(\mathbf{n})$ are given by the Fourier transforms of the spatial wave functions, and finally the momentum distribution $N(\mathbf{n})$ is given by the sum of squares of the momentum wave functions. Since harmonic oscillator functions transform into harmonic oscillator functions we obtain

$$N(\mathbf{n}) = a^3\pi^{-\frac{3}{2}}(2+\tfrac{8}{3}a^2n^2)e^{-a^2n^2}$$

as the momentum distribution of nucleons in the nucleus. The normalization is for 2 S neutrons and 4 P neutrons. If we wish to express n^2 in MeV instead of cm^{-2} we find $1/a^2 = 9.0$ MeV. Greider used a pure gaussian $e^{-n^2/20}$ but it is clear that these calculations are not sensitive to the momentum distribution

and no conclusions can be drawn as to the preference for the theoretical distribution.

In summary, then, we see that the results of this experiment for the small angle pickup process are in better agreement with theoretical expectations than the 13—20 MeV gaussian usually assumed. Furthermore, we find that it is impossible to affirm or deny the existence of high momentum components in $N(\mathbf{n})$ by such an experiment as this, for the wide angle process is dominated by multiple scattering effects. To study such high momentum components by this means, therefore, it would be necessary to study the reaction C^{12}(p, pd) B^{10} with coincidence techniques. Such an experiment, by comparison with known (p, d) elastic scattering, could yield information about the two nucleon correlation function and hence throw light on the high energy components of nucleons within the nucleus.

References

1) J. Hadley and H. York, Phys. Rev. **80** (1950) 345
2) G. Chew and M. Goldberger, Phys. Rev. **77** (1950) 470
3) W. Selove, Phys. Rev. **101** (1956) 231
4) G. Calame *et al.*, Nuclear Instruments **1** (1957) 169
5) R. L. Garwin, Rev. Sci. Inst. **24** (1953) 618
6) G. G. Kelley (private communication)
7) D. L. Clark, Thesis Rochester, 1952; described by J. J. Thresher, C. P. Van Zyl, R. G. P. Voss and R. Wilson, Rev. Sci. Inst. **26** (1955) 1186
8) P. Hillman, A. Johansson and G. Tibell, Nuclear Physics **648** (1957) 672
9) K. R. Greider, Phys. Rev. **114** (1959) 786
10) J. M. Wilcox and B. J. Moyer, Phys. Rev. **99** (1955) 875
11) A. Wattenberg, A. C. Odian, P. C. Stein, H. Wilson and R. Weinstein, Phys. Rev. **104** (1956) 1710
M. Q. Barton and J. H. Smith, Phys. Rev. **110** (1959) 1143
12) H. F. Ehrenberg, R. Hofstadter, U. Meyer-Berkhout, D. G. Ravenhall and S. E. Sobotka, Phys. Rev. **113** (1959) 666

10.A

Nuclear Physics **15** (1960) 387—389; © *North-Holland Publishing Co., Amsterdam*

Not to be reproduced by photoprint or microfilm without written permission from the publisher

THE NOBEL PRIZE IN PHYSICS FOR 1959

A. C. HELMHOLZ

Dept. of Physics, University of California, Berkeley

Received 30 November 1959

On October 26, the Swedish Academy of Science announced that it had awarded the Nobel Prize in physics for the year 1959 to Emilio Segrè and Owen Chamberlain for their discovery of the anti-proton. Both Segrè and Chamberlain are Professors of Physics at the University of California and their prize-winning discovery was made at the Lawrence Radiation Laboratory in Berkeley.

Although the positon or anti-electron had been discovered by Anderson in 1932 and its properties satisfactorily explained by the Dirac theory, there was doubt in the minds of some physicists as to the existence of the anti-proton. Hence the verification of its existence was an important achievement in physics and particularly in nuclear physics. The bevatron, constructed at the Lawrence Radiation Laboratory at the University of California in Berkeley, was designed to reach an adequately high proton energy so that anti-protons could be produced. The threshold for anti-proton production by a proton collision with a proton at rest is 5.6 GeV and because of Fermi momentum, is somewhat smaller for a collision with a bound nucleon. The identification of anti-protons was achieved [1]) by Segrè, Chamberlain, Wiegand and Ypsilantis on the basis of the negative charge, and protonic mass. The determination was made of the momentum p and the velocity v, thus excluding other particles, mainly π^- mesons which in the original experiments were present to numbers of 44000 for every one anti-proton. Negative particles produced by 6.2 GeV protons bombarding a copper target were deflected out of the bevatron field by the bevatron magnet. Those of momentum 1.19 GeV/c were selected by a magnet and their velocity measured by recording on an oscilloscope the time of flight between two scintillators, separated by 40 ft. An important element in the experiment was a pair of Čerenkov counters, one of which rejected the pions with $v/c = 0.99$ and one of which triggered the oscilloscope trace with particles of $0.75 < v/c < 0.79$ (anti-protons of $p = 1.19$ GeV/c have $v/c = 0.78$). For a pion the two pulses on the oscilloscope were separated by 40×10^{-9} sec while for the anti-proton the interval was 51×10^{-9} sec. Unstable particles of lifetimes shorter than about 10^{-8} sec were ruled out by the long length of path. These measurements showed the mass of the negatively charged particles to be 1840 ± 90 electron masses. Subsequent experiments using both counting and nuclear

emulsion techniques showed the characteristic annihilation with real protons, in which 1.88 MeV is released (mainly as pions). Experiments in 1956 by Cork, Lambertson, Piccioni and Wenzel [2]) showed that anti-protons in charge exchange reactions produced a neutral particle which, when annihilated, released about 1.9 GeV and hence could be identified as an anti-neutron.

Segrè and Chamberlain (along with Wiegand and Ypsilantis) are well-known for their experiments on high energy proton-proton and neutron-proton scattering (up to 345 MeV) and for their experiments on the polarization of protons and deuterons. These experiments have done much to determine the scattering phase shifts involved and also to elucidate the mechanism of polarization in proton scattering from complex nuclei. Difficult triple scattering experiments [3]) have been performed to measure depolarization and rotation in the proton-proton interaction.

Professor Segrè was born in Tivoli, Italy, on February 1, 1905; in 1944, he became an American citizen. He took his doctor's degree in physics at the University of Rome in 1928. After a year in the Italian army, he was appointed as instructor in physics at the University of Rome. In the next year he was promoted to Assistant Professor, and in 1932 to Associate Professor, which position he held until 1935. During this period he was active in many fields of physics, such as spectroscopy, Zeeman effect, and molecular beams. One of the most important influences in his career was his association at Rome with Enrico Fermi, who combined the abilities of a theorist and experimentalist. When Fermi became interested in nuclear physics and carried out his epoch-making researches on the production of artificial radioactivity by neutrons, Segrè was one of those who collaborated with him. In 1935 he was made Professor of Physics and chairman of the Department at the University of Palermo on the island of Sicily, where he continued his interest in nuclear physics. In 1936 with C. Perrier he discovered the first artificial element, element 43 or technetium, produced from bombardment of molybdenum in the Berkeley cyclotron. In 1938 he came to Berkely and in the years before the war he developed a chemical method of separating nuclear isomers (with Seaborg), discovered element 85, astatine (with Corson and Mackenzie), and performed a number of other notable experiments in the field of radioactivity. Following the discovery of Pu, he made several important investigations into the properties of Pu. In 1943 he moved to Los Alamos where he carried out important research on fission. In 1946 Segrè returned to Berkeley as Professor of Physics and has been engaged mainly in high energy nuclear physics since that time. In 1949, with Wiegand, he showed the influence of chemical binding on the K capture half-life of Be^7.

He is a Fellow of the American Physical Society and the Società Italiana di Fisica, and a member of the National Academy of Sciences and of the

Accademia Nazionale dei Lincei. He has been the Richtmyer Lecturer of the American Physical Society. He has been awarded the Hoffman Medal of the German Chemical Society and the Cannizzaro Medal of the Accademia Nazionale dei Lincei. Recently he was made a Commander of Merit of the Republic of Italy. He was married in 1936 to Elfriede Spiro. They have three children, Claudio 22, Amelia 16 and Fausta 13, and reside at 34 Crest Road, Lafayette, California.

Professor Chamberlain was born in San Francisco, California in 1920. He received the A. B. degree from Dartmouth College in 1941 and started graduate work in physics at the University of California in Berkeley in September 1941. His study was interrupted by World War II and he joined the group under Dr. Segrè in Berkeley and then in Los Alamos. At the completion of the war, he resumed his graduate studies under Fermi at the University of Chicago. He completed the work for the Ph. D. in 1948 when he became Instructor in Physics at the University of California. His thesis research was on neutron diffraction in liquid sulfur, lead and bismuth. On his return to Berkeley, he started work again with Segrè, and with Wiegand who had also been a member of the Los Alamos group, on the high energy nuclear physics experiments mentioned above. He advanced through the ranks of Assistant and Associate Professor and is now Professor of Physics. He is a Fellow of the American Physical Society and in 1957—58 was a Guggenheim Fellow.

Chamberlain was married in 1943 to Babette Copper. They have four children Karen 14, Darol 11, Lynn 9, Pia 2, and reside at 954 San Benito Road, Berkeley. During the fall semester of 1959, Chamberlain was the Loeb Lecturer at Harvard University.

References

1) Chamberlain, Segrè, Wiegand and Ypsilantis, Phys. Rev. **100** (1955) 947; Nature **177** (1956) 11
2) Cork, Lambertson, Piccioni and Wenzel, Phys. Rev. **104** (1956) 1193
3) For example, Chamberlain, Segrè, Tripp, Wiegand and Ypsilantis, Phys. Rev. **105** (1957) 288

10.A *Nuclear Physics* **15** (1960) 390—391; © *North-Holland Publishing Co., Amsterdam*

NEWS ITEMS

CONFERENCE ON SOLID STATE MICROWAVE AMPLIFIERS (6—8 April 1960)

The Institute of Physics announces that its Electronics Group in conjunction with the Radio Spectroscopy Group is arranging a Conference on *Solid state microwave amplifiers* to take place at the University of Nottingham from 6—8 April, 1960.

The subjects to be covered by the Conference include (a) masers, (b) parametric amplifiers, (c) related resonance studies.

Accommodation will be available in one of the University Halls of Residence.

Further particulars and application forms are available from The Secretary, The Institute of Physics, 47 Belgrave Square, London, S.W.1.

FIRST ANNUAL REPORT OF NORDITA (Nordisk Institut for teoretisk Atomfysik)

THE PURPOSE AND BASIS OF THE ORGANIZATION

The plan for an organization to intensify co-operation among the Nordic countries in the field of theoretical atomic physics was conceived in 1953 and discussed at a meeting held at Gothenburg on Swedish initiative. It was here decided to work for the establishment of a joint Nordic institute for theoretical atomic physics, to be situated in Copenhagen. That city already had, in the University Institute for Theoretical Physics (U.I.T.F.), a centre of research with a tradition of international co-operation, visited by many foreign physicists and thus offering good possibilities of contact.

The implementation of the plan was, however, deferred for various reasons, and the matter was taken up again in 1956. After a number of discussions the plan was submitted to Nordisk Råd (the Nordic Council), at whose meeting in Helsingfors on the 21st February, 1957, a recommendation to the Nordic Governments to establish the proposed institute was unanimously adopted.

It was realized, however, that if the desired results were to be achieved, the operation of a centre of research in Copenhagen would have to be supplemented by other functions in promotion of scientific co-operation in the North. Therefore, the plan agreed upon included additional activities such as interchange of physicists among the Nordic countries, invitation of foreign physicists to Nordic institutions, arrangement of symposia, etc. Great importance is attached to that part of the programme. The organization as a whole was given the name "Nordisk Organisation for Teoretisk Atomfysik".

"Nordisk Institut for Teoretisk Atomfysik" in Copenhagen — which thus forms a part of the Organization — is a centre of research, intended in particular to be a gathering place for Nordic physicists, who may there carry on research during visits of short or long duration and may utilize the existing possibilities of collaboration and contact with colleagues from other countries and keep informed of progress in the various branches of theoretical atomic physics. Moreover, provision is to be made for advanced training of young physicists from the Nordic countries admitted on fellowships to work at the Institute. For the sake of brevity the name of the Institute has been contracted into the word NORDITA, which is also used to designate the entire Organization.

The plan has been assented to by all the five Nordic states, and the Danish Government has promised to make available the premises necessary for the functioning of the Institute and to defray the expenses connected with their maintenance. Pending the completion of a building planned to be erected beside U.I.T.F., a number of premises of that institute are at the disposal of NORDITA.

The Organization will be formally founded on a convention between the five participating states. Until the instrument is signed and ratified, the Organization functions on an interim basis. It is managed by a Board composed of theoretical physicists appointed by the Governments of the five countries. The Institute is headed by a Director appointed by the Board.

ACTIVITIES DURING THE FIRST PERIOD

By decision of the Board the financial year of NORDITA runs from the 1st July to the 30th June. As functions were not commenced till the 1st October, 1957, the present report comprises only a nine months' period, from the 1st October, 1957, to the 30th June, 1958.

The activities in the period concerned were influenced by the provisional character of the Organization in that the majority of arrangements could be made only for shorter periods at a time (a few appointments of staff members required countracts for a longer term of years). While such a restriction must necessarily cause some inconvenience, at the same time it enables the Organization to feel its way in many practical questions without setting up precedents binding on it in future.

Both research and teaching activities were carried out on lines conforming to the purposes of NORDITA. Courses of lectures were given by physicists of the Institute as well as by invited scientists. Colloquia were held regularly by staff members and guests of NORDITA and U.I.T.F. These functions are specified in the lists of lectures and colloquia contained in the appendix to the report. Also the papers published in the period concerned are listed in the appendix. Offprints of the papers appear as numbers in a series entitled "NORDITA Publications" and are sent to institutions and scientists interested in them.

On invitations received, members of the staff of NORDITA attended congresses and gave lectures abroad. The Institute provides facilities, to a certain extent, for the research fellows to attend congresses outside Copenhagen as a useful supplement to their training.

While the functions of the Institute could largely be organized on the basis of experiences gathered from U.I.T.F. and the Theoretical Study Division of CERN, Nordic co-operation in atomic physics, whose promotion is one of the principal aims of the Organization, is a field that must be gradually developed.

So far, efforts in this direction have been concentrated on interchange of Nordic physicists and invitation to Nordic research centres of physicists from other countries. By way of experiment, on some occasions an outstanding foreign physicist has been invited to visit several institutions on a tour of the Nordic countries. Experience so far has shown that such arrangements meet with interest also on the part of those invited.

Facilities are provided for the research fellows to visit their home institutions once a year to report on the work going on at NORDITA. These visits take place on the initiative of the institutions concerned and seem to serve their purpose statisfactorily.

10.D *Nuclear Physics* **15** (1960) 392; © *North-Holland Publishing Co., Amsterdam*

BOOK REVIEWS

RICHARD FOSTER FLINT and EDWARD S. DEEVEY, JR. (Editors), *American Journal of Science, Radiocarbon Supplement*, Vol. 1 (Yale University, New Haven, Connecticut, 1959)

This is the first volume of a new annual series intended to be the "medium for primary publication of all radiocarbon measurements", and hence to include reports on the work of all laboratories engaged in C^{14} determinations.

The reports are given as far as possible according to a set form of presentation, which is concise and must contain all information relevant to the date published. This includes a full description of the samples and their archaeological or stratigraphical context, a statement of any treatment other than the routine C^{14} measurement and, where necessary, a brief comment on the date obtained.

The journal further includes reports of work on the underlying theories and techniques of radiocarbon dating. The inclusion of a bibliography dealing with the various aspects of radiocarbon work and the application of dates obtained is also very valuable.

Such a single series of publications in which all radiocarbon work is concentrated will be extremely useful to archaeologists and others interested in C^{14} dating. The full presentation of data concerning each sample is particularly welcome, as it is sometimes lacking in other reports quoting the results of C^{14} determinations.

A. R.

N. G. DE BRUIJN, *Asymptotic methods in analysis* (North-Holland Publishing Co., Amsterdam, 1958. xii + 200 pages. 20 fl.)

The Dutch mathematicians do not belong to that caricatural species of otherworldly individuals who affect to cultivate an exquisitely useless art; they are so anxious, on the contrary, to take an active part in the development of mathematical methods adapted to practical needs that they have for this purpose created an institution of their own, the Amsterdam "Mathematical Centre". In the different specialized sections of this well-equipped institute, all the aspects of applied mathematics are studied at the hand of problems, most of which are directly furnished by various "customers", ranging from academic research laboratories to industrial or commercial establishments. Moreover, the institute organizes courses of lectures on topical questions both in Amsterdam and at research centres all over the country.

The book under review is the text of one of these courses of lectures, and it affords an excellent example of the very high quality of the work done by the Mathematical Centre. There is here none of the attitude of esoteric aloofness too often adopted by contemporary mathematicians, and which makes their writings so unpalatable. Here, every step in the mathematical process is explained, its purpose and necessity made clear, with the result that the reader not only has no difficulty in following the rigorous proofs, but even turns to them with eager expectation. In achieving this remarkable effect, the author is well served by his sense of humour and a pleasant, straightforward style of exposition, occasionally even using the dramatic form of the dialogue. Above all, however, he is guided by a keen awareness of the concrete problems to which the mathematical techniques he analyses have to be applied; this gives his presentation of the subject its unique quality. The importance of asymptotic estimates in all branches of physics needs no emphasis; it is therefore a matter of special gratification for physicists to have now at their disposal a very complete survey of the relevant mathematical methods so well-adapted to their needs.

L. R.

1.D.1

Nuclear Physics **15** (1960) 393—410; © *North-Holland Publishing Co., Amsterdam*

Not to be reproduced by photoprint or microfilm without written permission from the publisher

SYMPLECTIC SYMMETRY IN THE NUCLEAR SHELL MODEL

J. B. FRENCH

Dept. of Physics and Astronomy, University of Rochester, Rochester, N.Y., U.S.A.

and

Fysisch Laboratorium der Rijksuniversiteit, Utrecht, the Netherlands †

Received 23 November 1959

Abstract: The nature of the general two-particle interaction which is compatible with symplectic symmetry in the jj coupling shell model is investigated. The essential result is that, to within an additive constant and an additive multiple of T^2, the interaction should have the form of a sum of scalar products of single-particle tensors which have odd rank in the single-particle j space. An example of an interaction satisfying these conditions is a central interaction with $\sigma_1 \cdot \sigma_2$ exchange nature. The condition for good symplectic symmetry is expressed also as a set of linear constraints on the two-particle energies, again as constraints on the particle-hole energies and finally in terms of the relationship between the particle-particle and particle-hole spectra. When we deal with identical particles only, the conditions for good symplectic symmetry (or seniority) are greatly relaxed and in particular are satisfied for a short-range (δ-function) interaction, as shown earlier by Racah and Talmi.

1. Introduction

The theory of seniority in many-particle spectroscopy which was invented by Racah [1]) in 1943 was later [2]) reformulated by him in terms of group theory. Racah's principal interest in these papers was in atomic spectroscopy in an LS representation (l^n) and the corresponding group was the orthogonal group in $(2l+1)$ dimensions. The later paper did point out however that the symplectic group would naturally enter in a jj representation.

For the more complicated nuclear case a classification of j^n according to symplectic symmetry was made by Flowers [3]), and in later papers Edmonds and Flowers [4]) calculated fractional parentage coefficients and applied their results to calculate spectra for a variety of cases. It was remarked by these authors that symplectic symmetry appeared to be rather "good" for the interactions and cases which they considered but little formal discussion was given about the conditions under which an interaction between nucleons is compatible with symplectic symmetry. Racah and Talmi [5]) investigated, for identical particles only, the closely related question of the pairing property of nuclear interactions and some of the results of the present paper represent an extension of theirs.

† Work at the University of Rochester was supported in part by the Atomic Energy Commission. Work at Utrecht was done while the author was Senior Post-Doctoral Fellow of the National Science Foundation on leave during 1959—60 from the University of Rochester.

The purpose of this paper is to investigate rather generally the conditions for good symplectic symmetry. The principal outcome will be that symplectic symmetry will be good if the two-particle interaction (apart from an interaction behaving like an additive arbitrary constant and arbitrary multiple of T^2) behaves in the combined orbital+spin space of one particle as a sum of tensors of odd rank only. This result, which is not surprising in view of some theorems of Racah [1]) concerning odd-rank tensors and the results of Racah and Talmi [5]), will be translated into a set of conditions on the two-particle energies and also into a relationship between the particle-particle and particle-hole spectra for equivalent particles. Our results for the most part will apply to configurations containing both neutrons and protons but we shall also pay special attention to the case of identical particles only. It will turn out that there are not enough experimental data to decide to what extent symplectic symmetry is actually good but we shall raise a few questions about spectra, the answers to which would be helpful.

The procedure which we shall use is quite elementary (and results quite simple) but we give them in some detail because they will later be found useful in dealing with inequivalent-nucleon configurations and for other purposes too. Before proceeding to this we remind the reader how the symplectic group enters into spectroscopy [3]).

A function in the vector space j^n may be taken to be a sum of products of n single-particle functions ψ_j^m each associated with a different particle number. The exclusion principle requirement (if the particles are identical, or if we use an isobaric-spin formalism for neutrons and protons) is that the function must be antisymmetric in all n particles. For mixed protons and neutrons, when we do not use a T-formalism (and we shall not), both one- and two-columned Young diagrams defining the representation of S_n are allowed, a single such diagram defining states of definite T. It is more useful not to consider the permutation group S_n explicitly but rather the group defined by unitary transformations in the $(2j+1)$-dimensional space of the single-particle functions ψ_j^m, the unitary group U_{2j+1}. It is well known that, for the product functions which we have, a function belonging to an irreducible representation of U_{2j+1} at the same time belongs to an irreducible representation of S_n and indeed the two representations may be labelled by the same Young diagram. A subset of the unitary transformations is of special interest, namely that subset which leaves invariant the $J = 0$ state of two particles; this subset is in fact the subgroup Sp_{2j+1} of the unitary group and since, in turn, the rotation group R_3 is a subgroup of the symplectic group we can classify states simultaneously by T (group U_{2j+1}), by symplectic symmetry† σ (group Sp_{2j+1}) and by J (group R_3).

† σ defines two parameters which we may take as the seniority (s) and reduced isobaric spin (l) of Edmonds and Flowers. For identical particles (or states with $T = \frac{1}{2}n$) there is only one significant parameter, the seniority.

In what follows we shall make very little use of group theory beyond indentifying certain operators as infinitesimal operators of the pertinent groups.

2. The Two-Body Interaction in Terms of Unit Tensors

Two-particle wave functions $\Psi_J(j^2)$ are not of course adequate to give a representation of an interaction operator H_{12} because in most cases H_{12} will connect states of different configurations. If we are resolved to consider only the states j^2 it is convenient to replace the physical interaction H_{12} by an interaction which gives the same results inside j^2 but which does not connect with other configurations. This is simply done by introducing Racah's unit tensor operators $u^r(i)$ [6]) which we may define by †

$$u_q^r(i)\psi_j^m = [j]^{-\frac{1}{2}} C_{m,q}^{jrj} \psi_j^{m+q}; \tag{1}$$

u^r operates on the angular and spin part of the function (not on the radial part) and, as shown by eq. (1), does not change the j value. The double-barred matrix element of Racah [6]) is then simply $\langle j||u^r||j\rangle = 1$ or more completely $\langle j'||u^r||j''\rangle = \delta_{jj}\,\delta_{jj''}$ (where the u^r are understood to affect only functions with angular momentum j and might be more completely labelled as ${}^{(j)}u^r$; for a quite complete notation we should specify also the orbital angular momentum). For $r = 0,\ 1$ we have simply

$$u^0 = [j]^{-\frac{1}{2}}, \quad u_q^1 = \{j(j+1)[j]\}^{-\frac{1}{2}}\mathbf{J}_q,$$

where $\mathbf{J}$ is the angular momentum operator. The higher-rank tensors could be constructed from $\mathbf{J}$; for example $u^2 \propto (\mathbf{J}\times\mathbf{J})^2$, $u^3 \propto ((\mathbf{J}\times\mathbf{J})^2\times\mathbf{J})^3$ and so on; but this representation is not very useful. From eq. (1) it also follows that $\big(u^r(i)\cdot u^r(i)\big) = [j]^{-1}$.

If now we are dealing with a j^2 configuration any two-particle interaction which conserves the total angular momentum can be written as [5])

$$H_{12} \equiv \sum_{r=0}^{2j} [r]\alpha_r\big(u^r(1)\cdot u^r(2)\big) = \sum_r H_{12}^r \tag{2}$$

provided we make an appropriate choice of the $(2j+1)$ interaction constants α_r. Questions which immediately come to mind now are:

(1) How are the α_r to be determined if we are given the 2-body energies $E_J^{(2)}$?

(2) What are the α_r for the interactions of common interest?

(3) What are the conditions on α_r and consequently on $E_J^{(2)}$ which will

† Notation: q is the "m" value and r the tensorial rank; C is a Clebsch-Gordan coefficient and $[j] = (2j+1)$. We shall also write $[ab\ldots] = (2a+1)(2b+1)\ldots$; $2\varepsilon_a = 1+(-1)^a$; $2\varepsilon_{ab\ldots} = \ldots = 1+(-1)^{a+b+\cdots}$. The scalar product of two tensor operators will be written as $(A^r\cdot B^r)$ and the general tensor product as $(A^r\times B^s)^t$; note then that $(A^r\cdot B^r) = (-1)^r[r]^{\frac{1}{2}}(A^r\times B^r)^0$.

ensure that the interaction is compatible with symplectic symmetry in the j^n case?

The first of these is trivial. Simply evaluating the matrix element of H_{12} in the j^2 states gives immediately

$$E_J^{(2)} = (-1)^{J+1} \sum_r [r] W(jjjj; rJ) \alpha_r, \tag{3}$$

and solving this backwards, using the unitarity condition on the Racah coefficients, we have for the constants

$$\alpha_r = \sum_J (-1)^{J+1} [J] W(jjjj; rJ) E_J^{(2)}. \tag{4}$$

We see that $(-1)^J E_J^{(2)}$ and the interaction constants α_r are in a sense simply Racah transforms † of each other.

The second question is somewhat outside the range of the present paper and it will be adequate for our present purposes to consider two special cases of a central interaction. Consider first a Wigner interaction $H_{12} = J(r_{12})$. We could apply eq. (4) to the calculated energies or could proceed directly as follows:

$$J(r_{12}) = \sum_k J_k(r_1, r_2)(C^k(1) \cdot C^k(2))$$

where $C_q^k = \{4\pi/[k]\}^{\frac{1}{2}} Y_k^q$, and, on evaluating the radial integral, $J_k(r_1, r_2)$ becomes $\varepsilon_k F^k$, the usual Slater integral. Since

$$\langle j||C^k||j\rangle = (-1)^{k+\frac{1}{2}-j}[j][k]^{-\frac{1}{2}} C^{jjk}_{\frac{1}{2},-\frac{1}{2}} \equiv (-1)^{k+\frac{1}{2}-j} D_{jjk},$$

we have

$$J(r_{12}) \equiv \sum_k \varepsilon_k (D_{jjk})^2 F^k (u^k(1) \cdot u^k(2))$$

and thus for the Wigner interaction

$$\alpha_r = \varepsilon_r [r]^{-1} (D_{jjr})^2 F^r. \tag{5}$$

We observe the important fact that a Wigner interaction involves only tensors of *even rank*. A minor point is that for interactions $V(r)$ which are everywhere positive (or negative) the α_r are all positive (or negative).

A little more effort will show that an interaction $\boldsymbol{\sigma}_1 \cdot \boldsymbol{\sigma}_2 J(r_{12})$ has tensors of *ocd rank only* [5]) and once again, if $J(r_{12}) \geqq 0$ for all r_{12}, then the α_r are all positive. We find in fact for the $\boldsymbol{\sigma}_1 \cdot \boldsymbol{\sigma}_2$ interaction

$$\alpha_r = 6[j]^2 \sum_k \varepsilon_k (D_{llk})^2 \begin{Bmatrix} l & \frac{1}{2} & j \\ l & \frac{1}{2} & j \\ k & 1 & r \end{Bmatrix}^2 F^k \tag{6}$$

† Many of the results of this paper could be derived most simply by using an explicit formalism for such transforms.

where $D_{llk} = [l][k]^{-\frac{1}{2}} C^{llk}_{0,0}$, the redundant ε_k is written for emphasis, and the vanishing of α_r for even r follows from the vanishing of the $9j$-symbol when $k+1+r$ is odd.

The other two central interactions, which we might write † as $J(r_{12})M_{12}$ and $\boldsymbol{\sigma}_1 \cdot \boldsymbol{\sigma}_2 J(r_{12})M_{12}$, where M_{12} is the space exchange operator, have more complicated forms, involving tensors of both even and odd orders, and it is not worth our while to write them here. The same is true of the two-body spin-orbit forces (vector forces) and the tensor forces whose forms have considerable complexity.

Before proceeding to the many-particle case we record the combination and commutation rules for the single-particle tensors. These results follow directly and easily from the defining eq. (1). We have

$$u_p^r(i) u_q^s(i) = (-1)^{r+s} \sum_t [t]^{\frac{1}{2}} Y_{rst} C^{rst}_{p,q} u^t_{p+q}(i), \tag{7}$$

$$(u^r(i) \times u^s(i)_{m'}) = (-1)^{r+s} [t]^{\frac{1}{2}} Y_{rst} u_{m'}{}^t(i), \tag{8}$$

$$[U_p^r, U_q^s] = 2(-1)^{r+s} \sum_t [t]^{\frac{1}{2}} \varepsilon_{rst1} C^{rst}_{p,q} Y_{rst} U^t_{p+q}, \tag{9}$$

$$(U^r \times U^s)_m{}^t - (-1)^{r+s-t} (U^s \times U^r)_m{}^t = 2(-1)^{r+s} [t]^{\frac{1}{2}} \varepsilon_{rst1} Y_{rst} U_m{}^t, \tag{10}$$

$$(u^r(i) \times u^s(i))_m{}^t - (u^s(i) \times u^r(i)_m{}^t = 0. \tag{11}$$

Here we have introduced the symbol

$$Y_{rst} = (-1)^t W(jsjr; jt), \tag{12}$$

which is completely symmetrical in all three indices. Eqs. (9), (10) are valid for the single-particle tensors $u^r(i)$ but, as we shall immediately see, for a more general case too, and we have indicated this by writing U^r instead of $u^r(i)$. Eqs. (8), (10) are entirely equivalent respectively to (7) and (9) and follow from them by introducing the definition of the tensor product of two tensor operators. The reader should note carefully that when a commutator is written in tensor-product form as in eq. (10) the phase factor enters automatically into the second term on the left-hand side. It comes from the fact that, in the Condon and Shortley [7]) phase convention which we use, the function describing the vector-coupling of angular momenta j_1, j_2 to a resultant J undergoes a phase change $(-1)^{j_1+j_2-J}$ when the ordering of the angular momenta is changed. Observe too that the commutator of two tensors U^r, U^s vanishes for arbitrary s if $r = 0, 1$ (as is *a priori* obvious); moreover the commutator of two odd-rank tensors is itself of odd rank. Note also that the expression occurring in eq. (11) is a commutator or anticommutator according as $r+s+t$ is even or odd.

† Remember that we do not have an explicit isobaric spin formalism and must therefore not introduce $\boldsymbol{\tau}_1 \cdot \boldsymbol{\tau}_2$.

3. Many-Particle Tensors

We introduce the symmetrical tensors which will be adequate to deal with any charge-independent † interaction

$$U^r = \sum_{i=1}^{n} u^r(i). \tag{13}$$

A bilinear form involving these tensors consists of both a one- (or zero) and a two-particle operator and the combination rule is not all identical with the $n = 1$ case. One result, important to us, is

$$A^t_{rs} = -A^t_{sr} \equiv (U^r \times U^s)^t - (U^s \times U^r)^t = 2\varepsilon_{rst1} \sum_{i,j(i\neq j)} \big(u^r(i) \times u^s(j)\big)^t. \tag{14}$$

From this one can see that for given t the quantities A^t_{rs} for different pairs of (r, s) values are linearly independent (consider each pair of particles (i, j) separately). The commutation rules on the other hand are the same for all n; i.e. eqs. (9) and (10) apply equally well to the single-particle and many-particle tensors.

Since a Hamiltonian involving only two-particle interactions is essentially equivalent to a bilinear form in the U's it is worthwhile investigating further commutators, namely certain of those involving triple and quadruple combinations of U's. For the first of these commutators which we evaluate in the usual way we find ††

$$[(U^r \cdot U^r), U^s] = 2(-1)^s[s]^{-\frac{1}{2}} \sum_t [t]\varepsilon_{rst1} Y_{rst} A^s_{rt}. \tag{15}$$

A significant question is now: *What is the general bilinear form* $\sum_r [r]\beta_r (U^r \cdot U^r)$ *which commutes with* U^s. Remembering that

$$(U^r \cdot U^r) = (-1)^r [r]^{\frac{1}{2}} (U^r \times U^r)^0,$$

we have for the commutator

$$[\sum_r [r]\beta_r (U^r \cdot U^r), U^s] = 2[s]^{-\frac{1}{2}} \sum_{t,r} (-1)^{t+r} [tr]\beta_r \varepsilon_{rst1} Y_{rst} A^s_{rt}. \tag{16}$$

This commutator will vanish for arbitrary s if β_r vanishes except for $r = 0$, 1 (and of course for all β_r if $s = 0, 1$). These results are trivial. It will vanish too if $\beta_r = 1$ since it is then a sum over two indices of a function antisymmetric in the indices. We shall see that this demonstrates only the charge-independence of the interaction operators constructed with symmetric tensors. For arbitrary s the linear independence of the A^t_{rs} ensures that there is no other solution. The

† For a charge-dependent interaction we would need as well the tensors which transform by a two-rowed Young diagram but it would in most cases then be simpler to introduce explicitly the isobaric spin.

†† Here and elsewhere (e.g. in eq. (13)) we do not write the "m" value which of course is the same for each term in the equation.

non-trivial case important for consideration of symplectic symmetry is the case s = odd; then noting that $(-1)^t \equiv (-1)^r$ so that $(-1)^r = \varepsilon_{rt}$ we see that $\beta_r = (-1)^r$ is also a solution (or of course $\beta_r = \varepsilon_r$ or ε_{r1}). In summary then we have

$$[\sum_r [r]\beta_r (U^r \cdot U^r), U^s] = 0 \quad \text{if} \begin{cases} s = 0,1; \\ \beta_r = 1; \\ s = \text{odd and} \\ \beta_r = (-1)^r, \text{ or } \varepsilon_r, \text{ or } \varepsilon_{r1}. \end{cases} \tag{17}$$

Next we evaluate the commutator for two scalar products. This follows easily from the preceding one and we find

$$[(U^r \cdot U^r), (U^s \cdot U^s)] = -2 \sum_t [t]\varepsilon_{rst1} Y_{rst}\{(rts)^0 - (trs)^0 + (srt)^0 - (str)^0\} \tag{18}$$

where

$$(rts)^0 = \big((U^r \times U^t)^s \times U^s\big)^0. \tag{19}$$

The quantity appearing inside {} in eq. (18) is antisymmetric in all three indices (r, s, t). Temporarily labelling it as A_{rst} we have, since the quantity on the left of eq. (18) is an (rs) commutator,

$$A_{rst} = -A_{srt}. \tag{20}$$

But interchanging (r, t) we have

$$A_{tsr} = (trs)^0 - (rts)^0 + (str)^0 - (srt)^0 = -A_{rst} \tag{21}$$

and these two equations demonstrate the complete antisymmetry. Besides this the distinct components A_{rst} are linearly independent; we see this as before by considering the three-body part of A_{rst} with definite particle numbers i, j, k.

We can now answer the following question: *What are the conditions on* α_r, β_s *so that*

$$[\tfrac{1}{2}\sum_r [r]\alpha_r (U^r \cdot U^r), \sum_s [s]\beta_s (U^s \cdot U^s)] = 0?$$

We have for this commutator the value

$$-\sum_{r,s,t} [rst]\alpha_r \beta_s \varepsilon_{rst1} Y_{rst} A_{rst}$$

and, remembering that Y_{rst} is symmetric while A_{rst} is antisymmetric and linearly independent, we have as the condition that $\alpha_r \beta_s$ must vanish when antisymmetrized with respect to the three indices r, s, t provided that $r+s+t$ = odd and (r, s, t) form a triangle. We may write this as

$$\Delta_{rst}\varepsilon_{rst1}\{\alpha_r(\beta_s - \beta_t) + \alpha_s(\beta_t - \beta_r) + \alpha_t(\beta_r - \beta_s)\} = 0 \tag{22}$$

where $\Delta_{rst} = 1$ if (rst) form a triangle, zero otherwise.

At this stage we should make some contact with the theory of symplectic symmetry. Directly from their definition (1) the single-particle unit tensors are seen to form a set of infinitesimal operators of the unitary group U_{2j+1} and since the many-particle tensors have the same commutation rules so also have they. The odd-rank tensors then, according to eq. (9), are the operators of a subgroup which is of course the symplectic group. The bilinear form $\sum[r](U^r \cdot U^r)$ which commutes with every U^s is the Casimir operator of the unitary group; it is related to the T^2 operator (in the configuration j^n) as follows [4]):

$$\sum[r](U^r \cdot U^r) \equiv -2T^2+\tfrac{1}{2}n(4j+6-n). \tag{23}$$

The bilinear form $2\sum_{r\ \mathrm{odd}}[r](U^r \cdot U^r)$ which commutes with odd rank tensors is the Casimir operator for the symplectic group; its eigenvalues, a general expression for which is given by Racah [8]), serve to label the various irreducible representations of this group or, as we shall say, serve to specify the symplectic symmetry. These facts are of course entirely well known; they are discussed quite throughly by Edmonds and Flowers [4]) and also by Racah [2, 8]).

Returning now to the commutator of two bilinear forms we may regard the α-form as defining an interaction † and the β-form as specifying an operator whose eigenvalues label the wave-functions. For the trivial cases $\beta_s = \delta_{s0}, \delta_{s1}, 1$ we derive from eq. (23) that the commutator vanishes for any α-form (the third of these demonstrates, via eq. (23), the charge independence to which we have earlier referred). The form $\beta_s = \varepsilon_{s1}$ will define the symplectic Casimir operator and the α-forms commuting with it are the interactions which allow symplectic symmetry. Since $\varepsilon_{s1}-\varepsilon_{r1} \equiv (-1)^s\varepsilon_r$, eq. (23) becomes (no summation being understood)

$$\Delta_{rst}\varepsilon_{rst1}\{(-1)^s\varepsilon_r\alpha_r+(-1)^t\varepsilon_s\alpha_s+(-1)^r\varepsilon_t\alpha_t\} = 0, \tag{24}$$

which is automatically satisfied unless two of the indices are even and the other odd. In the latter case, we must also exclude a zero value for the even index (since if one index is zero the other two must be equal). The equation now becomes

$$\alpha_r-\alpha_s = 0 \quad \text{for} \quad r, s \equiv \text{even}, \quad \neq 0. \tag{25}$$

The general bilinear operator then which preserves symplectic symmetry has the form

$$\alpha_0(U^0 \cdot U^0)+\alpha\sum_r[r](U^r \cdot U^r)+\tfrac{1}{2}\sum_{r\ \mathrm{odd}}[r]\alpha_r(U^r \cdot U^r) \tag{26}$$

which we might describe as *a constant+multiple of T^2+an operator with odd-*

† If the two-particle interaction is that of eq. (2) the interaction operator for n particles is

$$\tfrac{1}{2}\Sigma[r]\alpha_r(U^r \cdot U^r)-\tfrac{1}{2}n[j]^{-1}\Sigma[r]\alpha_r.$$

It is because of this that we have included the factor $\frac{1}{2}$ in defining the α-form. The last term (constant for given n) is of no interest to us at present and we shall usually ignore it.

rank scalar products only. The first two parts are trivial; the symplectic classification operates inside the classification by isobaric spin (the symplectic group is a subgroup of the other). It is the third term which is of real interest. We shall in fact often speak of the general symplectic-symmetry-preserving interaction as simply one which involves odd-rank scalars only, thereby ignoring the first two parts. We note incidentally the fact that no Wigner interaction can preserve symplectic symmetry while every $\sigma_1 \cdot \sigma_2$ interaction does so. In section 5 we shall comment on the relationship between these results and those of Racah and Talmi [5]) for identical particles.

4. Conditions on the Two-Body Energies

The conditions (25) impose $(j-\frac{3}{2})$ linear conditions on the two-body energies $E_J^{(2)}$. Thus symplectic symmetry is always good for $j = \frac{3}{2}$, we have one condition for $j = \frac{5}{2}$, and so on. From eq. (4) we see that the conditions are

$$\sum_J (-1)^J [J] W(jjjj; rJ) E_J^{(2)} = -\alpha \quad \text{for} \quad r \quad \text{even}, \quad \neq 0. \tag{27}$$

We may write these in homogeneous form as

$$\Delta^{(i)}(E_J) = 0 \quad (i = 1, \ldots, (j-\tfrac{3}{2})), \tag{28}$$

where the $\Delta^{(i)}$ are linearly independent † linear combination of $E_J^{(2)}$ *which do not involve* E_0 (formally because $W(jjjj : r0)$ is independent of r for even r, more fundamentally because the $J = 0$ two-particle state belongs by itself to an irreducible representation of $S\mathfrak{p}_{2j+1}$). Moreover if we write $\Delta^{(i)} = \sum_J \Delta_J^i E_J^{(2)}$ we have

$$\sum_J \Delta_J^i = \sum_{J \text{ even}} \Delta_J^i = \sum_{J \text{ odd}} \Delta_J^i = \sum_J \Delta_J^i J(J+1) = 0,$$

since $E_J^{(2)} =$ constant, and $E_J^{(2)} =$ constant for J even, $\neq 0$, and $E_J^{(2)} =$ a multiple of $J(J+1)$, all define interactions which preserve symplectic symmetry. Besides this we see at once that in a symplectic symmetry representation any off-diagonal matrix element of the Hamiltonian, expressed in terms of the two-body energies, must be a linear combination †† of the $\Delta^{(i)}$ (for it must vanish when $\Delta^{(i)} \to 0$). As a special case we see that for $j = \frac{5}{2}$ there is a fixed ratio, independent of the interaction, between any two off-diagonal matrix elements.

Eqs. (27) do not at all imply that if symplectic symmetry is good the states

† Linear independence follows from the fact that the equations

$$\sum_{r \text{ even} \neq 0} \beta_r W(jjjj; rJ) = 0 \text{ for all } J$$

implies $\beta_r = 0$ (multiply by $[J]W(jjjj; r'J)$ and sum over J).

†† This fact could be very helpful in evaluating fraction parentage coefficients.

with a definite T and σ are degenerate. An inverse statement is however true; separate degeneracy of the two-particle even $J(\neq 0)$ states and the odd J states would imply good symplectic symmetry, the interaction in this case being not only an operator which commutes with the symplectic Casimir operator but indeed a multiple of it.

To apply eq. (27) as they stand we should know all the two-particle (or two hole) energies both for $T = 0$ and $T = 1$. If we knew all but v of them, where $v < j-\frac{3}{2}$, we could eliminate the unknown energies and produce $j-\frac{3}{2}-v$ constraints involving the known energies which would be necessary but not sufficient for good symplectic symmetry. The only case where enough data are available and where there is at least some chance that jj coupling is respectable is Al^{26} ($j = \frac{5}{2}$). We have here only one $\Delta^{(1)} = \Delta$ say and (arbitrarily choosing the normalization)

$$\Delta = E_2-E_4+\tfrac{1}{45}(36E_1-91E_3+55E_5). \tag{29}$$

A reasonable identification of the $(d_{\frac{5}{2}})^2$ levels is [9]) (the energies are in MeV)

$$E_5 = 0, \quad E_0 = 0.23, \quad E_3 = 0.42, \quad E_2 \approx 2, \quad E_4 \geqq 5, \quad E_1 = ?$$

The lower limit for E_4 comes from the Mg^{26} spectrum; the uncertainty in E_2 reflects the fact that there are several 2^+ levels, without doubt belonging to rather mixed configurations; it appears that the first $J = 1$ level may be at ≈ 1.0 MeV. These numbers give

$$\Delta \approx -3.8+0.8E_1 \xrightarrow{E_1 \to 1\cdot 0} -3 \text{ MeV}. \tag{30}$$

Increasing E_4 enlarges Δ; to make $\Delta \approx 0$ we would need $E_1 \approx 5$ MeV. A 3 MeV Δ-value is not small compared with the energy spacings in the $d_{\frac{5}{2}}$ shell (our normalization of Δ has been reasonably chosen to make the energy coefficients around unity) and we can expect that it would not be compatible with good symplectic symmetry.

Consider the first two $J = \frac{5}{2}$ levels of Al^{25} at 0 and 1.81 MeV (there is probably no other below 4.5 MeV). There are two possible $(d_{\frac{5}{2}})^{-3}$ states which, in Flowers' classification [3]), have $(s, t) = (1, \frac{1}{2}), (3, \frac{1}{2})$. In this representation one finds (e.g. by using the c.f.p. tables) that the off-diagonal matrix element is $\frac{3}{28}\sqrt{10}\Delta$ and using the two-body energies above this has the value -1 MeV. The Hamiltonian matrix, in the symplectic symmetry representation, would have the form

$$H \approx \begin{pmatrix} 1 & -1 \\ -1 & 1 \end{pmatrix} \text{MeV}. \tag{31}$$

(since this has eigenvalues 0, 2.0 MeV). The eigenfunctions then would be eqaul mixtures of the two symplectic symmetries.

We tend to conclude from this that symplectic symmetry is quite probably

not good in the $d_{\frac{5}{2}}$ sheil. The conclusion is not certain, however; the same values of the two-body energies used above do not produce the degeneracy of eq. (31) between the two zero-order states. We have in fact for the zero-order energy difference

$$\langle H\rangle_{s=1}-\langle H\rangle_{s=3} = \tfrac{1}{1260}\{1470E_6-1065E_2-405E_4-162E_1-553E_3+715E_5\}, \tag{32}$$

and, for any reasonable value of E_1, this has a value ≈ -3.4 MeV instead of the zero value demanded by eq. (31). This large discrepancy indicates that jj coupling is a bad approximation or at the very least that the obvious identification of the $(d_{\frac{5}{2}})^{-2}$ levels is badly in error. So far as symplectic symmetry is concerned, there is still the possibility that the residual shell model interaction is of the odd-rank tensor type, the above disagreement then resulting from the departure from jj coupling.

For the higher shells, essentially nothing is known [10]) about the level structure of Sc^{42} or $Co^{51}(f_{\frac{7}{2}})^2$ while for the $g_{\frac{9}{2}}$ shell Nb^{82} is an altogether improbable nucleus. We turn therefore to a different method for testing the symplectic-symmetry hypothesis.

An essential feature which distinguishes between an even-rank and an odd-rank symmetrical tensor is the behaviour of its matrix elements when we proceed from particles to holes. Specifically we have Racah's theorem [6])

$$\langle (j^n)_\alpha||U^r||(j^n)_\beta\rangle = (-)^{r+1}\langle (j^{N-n})_{\alpha_c}||U^r||(j^{N-n})_{\beta_c}\rangle \tag{33}$$

where N is the number of particles in a closed shell and α_c, β_c describe the states which are complementary to α, β. In the present instance, since we do not use an isobaric-spin formalism, $N = (2j+1)$ = number of particles in a proton or neutron shell. To apply eq. (33) we must then consider neutrons and protons separately but we encounter here the difficulty that charge-independence will not in general permit the angular momenta of the separate groups to be specified (nor indeed can the separate seniorities usually be fixed even when the interaction preserves symplectic symmetry). These difficulties can be solved in may ways but at present we avoid them entirely by considering only the spectra for two particles, two holes, and a hole and a particle where, as is trivially obvious, the difficulties do not arise.

It will do us no good, except as a check, to compare spectra for two particles and two holes since these are identical (formally because the interaction is bilinear in the symmetrical tensors and the sign change of (33) is lost). For particle-hole system on the other hand it should be clear from eq. (33) (the reader can easily supply a formal proof or else see below) that for an odd-rank-tensor interaction the particle-particle and particle-hole spectra are identical while for an even-rank tensor interaction one is inverted with respect to the

other. Formally, if we write

$$E_J = E_J^{(\text{even})} + E_J^{(\text{odd})} \tag{34}$$

where $E_J^{(\text{even})}$ is that part of the energy due to the even-rank interaction, we have

$$E_J^{(\text{even})}(j^{-1}, j) = -E_J^{(\text{even})}(j^2), \quad E_J^{(\text{odd})}(j^{-1}, j) = +E_J^{(\text{odd})}(j^2). \tag{35}$$

Writing the energies in terms of the interaction constants by means of eq. (3) we have

$$E_J(j^{-1}, j) = (-1)^J \sum_r (-1)^r [r] W(jjjj; rJ) \alpha_r \tag{36}$$

and inversely

$$\alpha_r = (-1)^r \sum_J (-1)^J [J] W(jjjj; rJ) E_J(j^{-1}, j). \tag{37}$$

We observe parenthetically that writing the interaction constants of eq. (36) in terms of $E_J(j^2)$ by eq. (4) will give Pandya's result [11]) connecting the two energy-level systems, viz.

$$E_J(j^{-1}, j) = -\sum_{J'} [J'] W(jjjj; JJ') E_{J'}(j^2), \tag{38}$$

and conversely we could have derived eqs. (34)—(37) by starting with this.

We finally combine eqs. (4) and (37) to obtain

$$\alpha_r = -\sum_J (-1)^J [J] W(jjjj; rJ) \{E_J(j^2) - (-1)^r E_J(j^{-1}, j)\} \tag{39}$$

from which we see that identity of the spectra implies that the interaction constants vanish for even r. Thus the identity of the two spectra is both a necessary and a sufficient condition for the corresponding interaction to be of odd rank only.

Our general operator which preserves symplectic symmetry admits also an additive constant which we can obviously ignore and an additive multiple of T^2. Since the T values are not the same for the two systems [$J = 0$, even ($\neq 0$), odd, has $T = 1, 1, 0$, respectively, for j^2 and $T = \frac{1}{2}N, \frac{1}{2}N-1, \frac{1}{2}N-1$ for $j^{-1}j$] the effect of this operator will be to shift the three groups with respect to each other †. If it should turn out that the separate spectra for even $J(\neq 0)$ and for odd J are identical in the two systems the two separations between the groups are fixed by one parameter (the strength of the T^2 term). We can now state the symplectic symmetry condition in the following way: for the inter-

† Formally, by using

$$\sum_x [x] W(aaaa; xy) = 1, \quad \sum_x (-1)^x [x] W(aaaa; xy) = (-1)^{2a} [a] \delta_{y0}$$

and eq. (39), we can see that the shift of the even spectra with respect to the odd has the expected effect on α_r. Remember too (see the footnote between eqs. (23) and (24)) that our odd-rank interaction contains a constant term proportional to n, which we ignore.

action to produce good symplectic symmetry it is necessary and sufficient that the particle-particle and particle-hole spectra for the odd-J states be identical and similarly with the even $J(\neq 0)$ spectra.

Eq. (37) could be used in the same way as eq. (4) if the appropriate spectrum was available. For the $f_{\frac{7}{2}}$ and $g_{\frac{9}{2}}$ shells the nuclei would be Sc^{48} and Nb^{90} but little or no information is available. If we knew the spectra for both a particle-particle and the particle-hole system we would first check their relationship by eq. (38). If (38) were not satisfied we would be sure that either the coupling scheme was incorrect or that the effective interaction was not the same for both nuclei. If the equation were satisfied we would apply eq. (4) to the particle-particle system and settle things that way.

In a different manner however we can now use a small amount of data to investigate symplectic symmetry. For example consider Sc^{48}. The ground state [10]) has $J = 6$ or 7. The $J = 6$ value would require (if symplectic symmetry were good) that the lowest even J $(\neq 0)$ state of Sc^{42} be also $J = 6$ but this of course would be the analogue of the first excited state of Ca^{42}. It is in fact well known that the $J = 6$ state of Ca^{42} lies several MeV above the first-excited $J = 2$ state and so we can conclude immediately that a $J = 6$ value for Sc^{48} would imply a large breakdown of symplectic symmetry. A $J = 7$ value on the other hand would merely imply that, if symplectic symmetry is good, the lowest odd-J state of Sc^{42} would also be $J = 7$. For the $g_{\frac{9}{2}}$ shell the particle-hole nucleus is Nb^{90}. Nb^{82} for $(g_{\frac{9}{2}})^2$ is not accessible but the even J spectra could be compared with that of Mo^{92}. It is clear that in general we expect the lowest J even $(\neq 0)$ state for a particle and equivalent hole to be $J = 2$.

It is obvious that if some levels of the particle-particle system and some others of the particle-hole system were known the information could be combined by the proper use of eqs. (4) and (37). Also one is not restricted to comparison of simple spectra. But we give no results for more general cases because there seem once again to be few pertinent data.

Of considerably greater interest and with far more experimental possibilities is the comparison, for example, of the spectrum of a particle and an inequivalent group with that of the particle and the group complement. There are a great many different kinds of cases here (the particle and the group may be identical or not, if non-identical the subshell equivalent but non-identical with the particle may be filled or empty, and so on) and it seems better therefore to postpone discussion of the inequivalent case until a later paper.

5. The Identical-Particle Case

We have defined an interaction preserving symplectic symmetry as being one which commutes with the symplectic Casimir operator. We can be certain that an interaction which does not so commute will have *some* matrix elements

connecting different symplectic symmetries. We must notice, however, that only those states can physically occur whose permutation symmetry is described by one- or two-columned Young diagrams and therefore there emerges immediately the possibility that our definition of a "good" operator has been too demanding. Indeed if we deal only with identical nucleons (defined by one-columned diagrams) it is obvious that this is so, for in this case the conditions, expressed in terms of the two-body energies, cannot involve the odd-J states (only accessible for non-identical particles) while the conditions of constraint of eq. (27) involve both even-J and odd-J states. An immediate outcome of this consideration is that, as shown first by Racah and Talmi [5]), a delta-function force does give good seniority † even though no Wigner interaction preserves symplectic symmetry in general. For in the short range limit for identical particles we have $\delta(r_{ij}) \equiv -\frac{1}{3}\boldsymbol{\sigma}_i \cdot \boldsymbol{\sigma}_j \delta(r_{ij})$ and as shown above the $\boldsymbol{\sigma}_1 \cdot \boldsymbol{\sigma}_2$ interaction does preserve the seniority.

We must therefore find a modified set of conditions for dealing with the identical-particle case and indeed we must even reconsider the more general case of two-columned representations ($T < T_{\max}$). Let us first demonstrate that we have not made any very serious error in dealing with the latter case.

Consider the states of three particles (j^3) with $J = j$. Let the number of such states with $T = \frac{1}{2}, \frac{3}{2}$, be respectively $N_{\frac{1}{2}}$, $N_{\frac{3}{2}}$. We have ††

$$\begin{aligned} N_{\frac{1}{2}} &= \tfrac{1}{3}[j] - \frac{2}{3\sqrt{3}} \sin \tfrac{4}{3}\pi(j+\tfrac{1}{2}) \\ &= 1, 1, 2, 3, 3, 4, 5, 5, 6 \ldots \quad \text{for} \quad j = \tfrac{1}{2}, \tfrac{3}{2}, \tfrac{5}{2}, \ldots \\ N_{\frac{3}{2}} &= \tfrac{1}{2}[j] - N_{\frac{1}{2}} \\ &= 0, 1, 1, 1, 2, 2, 2, 3, 3, 3, 4 \ldots \quad \text{for} \quad j = \tfrac{1}{2}, \tfrac{3}{2}, \tfrac{5}{2}, \ldots \end{aligned} \tag{40}$$

For either T value there is a unique state with seniority 1 [Flowers' $(s, t) = (1, \frac{1}{2})$ state]. The $(N_T - 1)$ other states then have different symplectic symmetries than $(1, \frac{1}{2})$ and the requirement that the matrix element connecting each of these states with the seniority 1 state should vanish is a system of $(N_T - 1)$ linearly independent ††† linear constraints on the two-body energies. For $T = \frac{1}{2}$ we have $(N_{\frac{1}{2}} - 1) = 0, 0, 1, 2, 2, 3, \ldots$ for $j = \frac{1}{2}, \frac{3}{2}, \ldots$ while we have earlier imposed $0, 0, 1, 2, 3, 4, \ldots$ conditions. It follows then that for $j \leqq \frac{7}{2}$ the full set

† We shall speak of "seniority" instead of the more cumbersome "symplectic symmetry" when dealing with identical particles.

†† See for example ref. [12]), correcting there an obvious misprint.

††† The matrix element has the form

$$3 \sum_{J'} \langle J\sigma | J' \rangle \langle J\sigma' | J' \rangle E^{(2)}_{J'}$$

where $\langle J\sigma | J' \rangle$ is a fractional parentage coefficient, $J = j$, $\sigma \equiv (1, \frac{1}{2})$ and σ' describes the other state. The linear independence of the restraints for fixed σ, different σ', now follows from the linear independence of the c.f.p. considered as vectors, which in turn reflects the linear independence of the σ' states.

of eq. (28) is necessary; for $j = \frac{9}{2}, \frac{11}{2}$ there is a possibility that we have imposed one condition too many and for $j > \frac{11}{2}$ more than one condition. It scarely seems worthwhile now to investigate this further.

For identical particles we have $(N_{\frac{1}{2}}-1) = -1, 0, 0, 0, 1, 1, 1, 2, \ldots$ and there is thus the possibility that seniority is always good (for two-body interactions) if $j \leqq \frac{7}{2}$; in point of fact it is already well known that this is the case †. We will now show that the $(N_{\frac{1}{2}}-1)$ is for all j (except of course $j = \frac{1}{2}$) exactly the number of linearly independent conditions rather than the larger number implied by eq. (28) and we shall exhibit them explicitly. Our procedure will be as follows: we first find what conditions are imposed on the even-J two-body energies above by the set of equations (28). These conditions are then insufficient for good symplectic symmetry but they are sufficient for good seniority. Next by simple counting we establish that the number of such conditions is $N_{\frac{1}{2}}-1$. There are many ways of doing this: what follows is a particularly convenient one. We apply the identity

$$(-1)^{r+J} W(jjjj; rJ) = -\frac{\delta_{rJ}}{[r]} + 2 \sum_{J'} \varepsilon_{J'} [J'] W(jjjj; rJ') W(jjjj; JJ') \quad (41)$$

to eq. (36) and have then for the particle-hole energy (additive constants and multiples of T^2 are of course of no consequence here)

$$E_J(j^{-1}, j) = -\alpha_J + 2 \sum \varepsilon_{J'} [rJ'] W(jjjj; rJ') W(jjjj; JJ') \alpha_r, \quad (42)$$

and using eq. (3) we finally obtain the curious result

$$E_J(j^{-1}, j) = -\alpha_J - 2 \sum_{J' \text{ even}} [J'] W(jjjj; JJ') E_{J'}^{(2)}. \quad (43)$$

But if symplectic symmetry is good, then for even $J(\neq 0)$, $\alpha_J = \alpha$, $E_J(j^{-1}, j) = E_J{}^{(2)}$ and moreover the $J' = 0$ term on the right is independent of J. Thus we have as the conditions imposed on the even-J energies by the symplectic symmetry requirement

$$\sum_{J' \text{ even}, \neq 0} \{[J'] W(jjjj; JJ') + \tfrac{1}{2}\delta_{JJ'}\} E_{J'}^{(2)} = \text{constant for all even } J, \neq 0, \quad (44)$$

and writing this in terms of the interaction constants by eqs. (3) and (41) we find the completely parallel equation

$$\sum_{r' \text{ even}, \neq 0} \{[r'] W(jjjj; rr') + \tfrac{1}{2}\delta_{rr'}\} \alpha_{r'} = \text{constant} \quad \text{for all even } r, \neq 0. \quad (45)$$

In each case the restriction that the summation parameter must not equal zero is redundant. The remarkable correspondence between the two equations

† For $j \leqq \frac{5}{2}$ seniority must be good because the states are uniquely defined by their J value. For $j = \frac{7}{2}$ it has been noted by Schwartz and de Shalit [13]); in their consideration it arises from the fact that the only states not uniquely defined by J are certain states of the half-filled shell.

could in fact have been directly inferred from the properties of the Racah transforms mentioned above. The reader should remember that (44) and (45) are necessary but not sufficient for good symplectic symmetry; they are sufficient, but we have not yet proved that they are necessary, for good seniority.

The final step involves a problem of recognition. The $(j-\frac{3}{2})$ equations (44) are not linearly independent but they are closely related to the matrix element between the seniority 1 three-particle state with $J = j$ and the seniority 3 states, the form of which is given in the footnote following eq. (40). We have in fact [13]) for the unnormalized c.f.p. (J' of course being even)

$$\begin{aligned} \langle J = j, s = 1 | J' \rangle &= \delta_{J'0} - \frac{2[J']}{[j]}, \\ \langle J = j, s = 3 | J' \rangle &= (1-\delta_{J'0})[J']^{\frac{1}{2}} \left\{ W(jjjj;\, J'x) + \frac{\delta_{J'x}}{2[J']} - \frac{2}{(2j-1[j]} \right\}. \end{aligned} \tag{46}$$

In the $s = 3$ c.f.p., x is even $\neq 0$ and is otherwise arbitrary. We are free of course to take only $(N_{\frac{1}{2}}-1)$ values of x; the c.f.p. sets for other x depend linearly on these. For a given x the matrix element is, to within a multiplicative constant,

$$\sum_{J' \text{ even}, \neq 0} \{[J']W(jjjj; J'x) + \tfrac{1}{2}\delta_{J'x}\}E^{(2)}_{J'} - \frac{2}{(2j-1)[j]} \sum_{J' \text{ even}, \neq 0} [J']E^{(2)}_{J'},$$

and the condition for the vanishing of all the $\langle s = 3 | s = 1 \rangle$ matrix elements exactly reproduces eq. (44), since the last term in the above expression is x-independent. The constant on the right-hand side of eq. (44) is identified here. One could verify that the value is correct by multiplying (44) by $[J]$ and summing over even $J \neq 0$.

We have now shown quite directly that eqs. (44) or (45) form a set of necessary and sufficient conditions for good seniority. They imply no constraint for $j \leqq \frac{5}{2}$, are satisfied automatically for $j = \frac{7}{2}$ and imply one condition for $j = \frac{9}{2}, \frac{11}{2}, \frac{13}{2}$ and this condition is satisfied for short-range (δ-function) forces. For $j = \frac{9}{2}$ the explicit condition is

$$65E_2 - 315E_4 + 403E_6 - 153E_8 = 0 \tag{47}$$

and all interaction matrix elements in the $j = \frac{9}{2}$ shell which are non-diagonal in seniority are proportional to the expression occurring here.

An experimental check would be possible if the $(g_{\frac{9}{2}}^2)$ levels of Mo^{92} were available but of course they are not. Remembering that our method of deriving the constraint shows that if seniority is good for three particles it is good for the whole subshell, we see that we could investigate seniority via a three-particle system (or a more complicated one). One possibility here would be to

use the well-known rule of Racah [1]) that odd-rank tensors are diagonal in seniority (which follows from our eq. (17)); this would imply for example that, if seniority were good, the M1 or M3 electromagnetic transitions from $(g_{\frac{9}{2}})^3$ excited states of Tc^{93} to the ground state would be forbidden [14]).

We finally comment on the description of the general interaction which preserves good seniority. The interaction constants are as defined by eq. (45), one solution of which is simply the odd-rank interaction of eq. (25). Eq. (45) admits, however, a far wider class of solutions, as is physically obvious anyway, since good seniority imposes a restriction only on the like-particle forces. Let us remember, however, that, when dealing with identical particles only, we have more interaction constants than energy levels and thus the identical-particle wave functions and energies are invariant under a class of transformations of the α_r. The explicit transformations are (where A_x is arbitrary),

$$\alpha_r \to \alpha_r + \sum_{x \text{ odd}} A_x W(jjjj; rx), \tag{48}$$

since, from eq. (4), the A_x interaction gives zero energies for identical-particle states. Defining interactions which are connected by such a transformation as "equivalent interactions", we now observe that any seniority-preserving interaction is, to within an additive constant, equivalent to an odd-rank interaction; this follows from the fact that if we specify a set of even-J energies which satisfy the seniority conditions (44) we can always find a supplementary set of odd-J energies such that the total set satisfies the symplectic symmetry equations (27). One such set in fact will be

$$E_J^{(2)} = -\tfrac{3}{2} \sum_{J' \text{ even}} [J'] W(jjjj; JJ') E_{J'}^{(2)} \text{ for } J \text{ odd}, \tag{49}$$

as may be verified directly by insertion into eq. (27), making use of eq. (41). It is clear of course that this set is not unique (as shown for $j = \frac{5}{2}$ by inspection of eq. (29)) but this is of no present consequence. The point is that the symplectic symmetry equations (27) imply for the even-J energies the equations (44) and imply nothing else about them. We have indeed implicitly used this fact in deciding above that equations (44) were *sufficient* for good seniority.

The general interaction now which preserves the seniority is, apart of course from a constant and multiple of T^2, an odd-rank interaction plus an interaction which vanishes for identical-particle states. The result that odd-rank tensor interactions preserve the seniority is not at all new, since this was shown by Racah and Talmi [5]). They showed moreover that such interactions have the physically important pairing property defined by their eq. (4). We now see that *only* odd-rank interactions (or interactions equivalent to these) preserve the seniority and, from their work, that any seniority-preserving interaction has the pairing property.

A final word concerns the recent paper of Helmers [15]), who investigated, for identical particles and Wigner interactions only, the conditions under which there is "symplectic invariance" (which we would prefer to call "symplectic degeneracy") of the energy matrix. The result here of course is that, to within an additive constant, the interaction must be a multiple of the symplectic Casimir operator or equivalent to a multiple of it.

I am indebted to Mr. C. H. Kim for checking certain of the results in this paper and to Dr. K. Helmers for pointing out the existence of the paper by Racah and Talmi and for correspondence concerning his own paper.

References

1) G. Racah, Phys. Rev. **63** (1943) 367
2) G. Racah, Phys. Rev. **76** (1949) 1352
3) B. H. Flowers, Proc. Roy. Soc. A **106** (1952) 106
4) A. R. Edmonds and B. H. Flowers, Proc. Roy. Soc. A **214** (1952) 122; *ibid.* **215** (1952) 138; B. H. Flowers, *ibid.* **215** (1952) 398
5) G. Racah and I. Talmi, Physica **18** (1952) 1097
6) G. Racah, Phys. Rev. **62** (1942) 438
7) E. U. Condon and G. H. Shortley, Theory of Atomic Spectra (Cambridge, 1951)
8) G. Racah, Farkas Memorial Volume (Research Council of Israel, Jerusalem, 1952)
9) P. M. Endt and C. M. Braams, Revs. Mod. Phys. **29** (1957) 683
10) McGinnis, Anderson, Fuller, Marion and Yamada, Nuclear Data Sheets (National Research Council, Washington, D.C.)
11) S. P. Pandya, Phys. Rev. **103** (1956) 956
12) J. B. French, University of Pittsburgh Technical Report No. IX, Part 1 (1958)
13) C. Schwartz and A. de Shalit, Phys. Rev. **94** (1954) 1257
14) B. H. Flowers, Physica **18** (1952) 1101
15) K. Helmers, Nuclear Physics **12** (1959) 647

2.A.1

Nuclear Physics **15** (1960) 411—420; © *North-Holland Publishing Co., Amsterdam*

Not to be reproduced by photoprint or microfilm without written permission from the publisher

PROTON CAPTURE IN Be^7

RALPH W. KAVANAGH

Kellogg Radiation Laboratory, California Institute of Technology, Pasadena, California †

Received 2 November 1959

Abstract: Cross sections for proton capture by Be^7 measured at bombarding energies of 800 keV and 1400 keV are 0.48 ± 0.18 and 0.50 ± 0.20 μb, respectively, from which the corresponding cross section factors are $S = 0.027\pm0.010$ and 0.017 ± 0.007 keV · b. The reaction is therefore important in stellar energy production only in stars operating on the proton-proton chain at temperatures greater than about 2×10^7 degrees Kelvin.

1. Introduction

The conversion of hydrogen into helium in stellar interiors by means of the proton-proton chain has long been considered to have as a necessary link the reaction $He^3+He^3 \rightarrow He^4+2H$. However, the unexpectedly large non-resonant cross section recently reported by Holmgren and Johnston [1]) for the reaction $He^3+He^4 \rightarrow Be^7+\gamma$ indicates that this reaction may under certain conditions compete in consuming He^3. The chain is then completed by one (or both) of the following sequences

$$Be^7(e^-, \nu)Li^7(p, \alpha)He^4$$

or

$$Be^7(p, \gamma)B^8(\beta^+,\nu)Be^{8*}(\alpha)He^4.$$

The branching among the three possibilities can be computed if the nuclear cross sections and the stellar temperature and hydrogen-helium ratio are known. This computation has been done as a function of temperature by Fowler [2]) for conditions typical of the solar interior, using two assumed values differing by a factor of one hundred for the only unknown nuclear parameter, the cross section at stellar energies for the reaction $Be^7(p, \gamma)B^8$.

In any of these cases, the overall rate of production of He^4 in stellar interiors is determined primarily by the initial and by far the slowest process, $H^1+H^1 \rightarrow H^2+\beta^++\nu$, one such process being required to produce each He^3 atom. Therefore, in stars with high enough temperature and high enough He^4/H^1 ratio so that the $He^3(\alpha, \gamma)$ reaction predominates over $He^3(He^3, 2p)$, the He^4 production rate is doubled as compared to stars at the same temperature and density but

† Supported in part by the joint program of the Office of Naval Research and the U. S. Atomic Energy Commission.

lacking He^4. The rate of heat generation is not doubled, however, due to the neutrino energy loss in the two reactions given above. In the first case the low energy neutrino from Be^7 causes a reduction to 1.95 and in the second case the high energy neutrino from B^8 causes a reduction to 1.46. Thus, in stars proceeding via the $Be^7(p, \gamma)$ branch, since the useful energy released per He^4 produced is smaller, the nuclear fuel must be consumed at a higher rate (by 37 per cent) to maintain a given luminosity, and the time required for a main sequence star to evolve to the red-giant stage is proportionately reduced. These and other interesting aspects of the reactions in question are discussed in detail elsewhere [2, 3, 4]).

2. Experimental Arrangement

It is the purpose of the present experiment to measure the $Be^7(p, \gamma)B^8$ cross section at bombarding energies near 1 MeV to serve as a guide for extra-

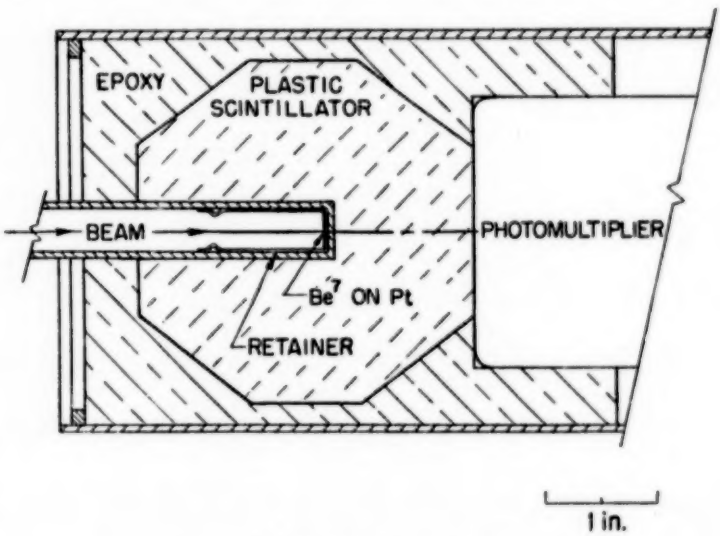

Fig. 1. Target and detector geometry.

polation to thermal energies. The required target material, Be^7, is radioactive, decaying with a half-life of 53 days by K-electron capture accompanied in 12 per cent of the cases by 478-keV gamma radiation [5]). Thus, a target having a surface density of 10^{17} atoms/cm^2 over an area of 0.1 cm^2 emits a gamma-ray flux of 2×10^8 per second; an optimistic estimate of the reaction yield from such a target bombarded with 1 μA of 1-MeV protons is 20 per second, the capture gamma rays having an energy of 1 MeV. Detection of the latter in the presence of the former is quite unfeasible with available techniques. However, the residual nucleus B^8 is also radioactive[5]), with 0.8-second half-life, the 14-MeV positon decay to the broad 3-MeV state of Be^8 being immediately followed by

two 1.5-MeV alpha particles. Of the various emanations, the high-energy positon appeared to offer the most promising detection possibility.

The detector and target arrangement are shown in fig. 1. The target consisted of a thin layer of Be^7O along with known impurities Li^7, Be^9, B, C, N, O and F, deposited over about a 5-mm diameter spot on a 0.005-inch thick platinum disk. The total thickness of the deposit was less than 4 keV for 1 MeV protons; the maximum surface density of Be^7 was about 10^{16} cm^{-2}, and the total activity was about 10 mc. The preparation of this target is described in the appendix.

The detector was a well-type plastic scintillator (Pilot "B"), painted white and cast in epoxy resin, viewed by an RCA C7245 photomultiplier. The scintillator size and shape were chosen to allow electrons having energies greater than about 7 MeV to escape through the scintillator, giving a pulse height corresponding to their energy loss of 6—7 MeV; a larger scintillator would unnecessarily increase the background counting rate. Into the scintillator well was inserted a thin-walled aluminium thimble containing the target at one end, and attached at the other to the vacuum system of the 2-MV electrostatic accelerator. The thimble was insulated to serve as a Faraday cup for beam current integration; to suppress secondary electrons from leaving or entering, the cup was maintained at +300 volts and was preceded by a negative ring around the collimated beam. The detector assembly was surrounded by a lead shield of 2-inch or greater thickness.

The detection efficiency for 478-keV gamma rays from the target was about 25 per cent, giving a pulse rate of about 10^7 per second. To avoid difficulties from such a high rate in the counting apparatus, the current pulses from the photomultiplier, having a decay constant of about 4×10^{-9} second, were amplified to a level of a few volts in Hewlett-Packard distributed amplifiers, following which pulses less than about 3 volts were rejected by a biased 1N34A diode, while those greater than the bias were stretched and further amplified for recording by scalers and a 100-channel pulse height analyzer. The somewhat non-linear gain above the bias was not troublesome. The system was adjusted so that pulses corresponding to 2- to 10-MeV energy loss in the crystal were displayed on the analyzer.

To take advantage of the radioactive delay for background reduction, the beam from the accelerator, after 90° magnetic analysis, was mechanically interrupted with a rotary shutter having a 0.8-second period, and the counters were gated off during the beam-on interval (0.3 cycle). The counting interval was about 0.6 cycle. The prompt count rate was about ten times the delayed rate, and was chiefly due to fluorine contamination.

3. Procedure

As is shown in the appendix, the last step of the target preparation left the target completely free of lithium, but thereafter Be^7 decayed to Li^7 with a

decay constant of 1.3 per cent per day. This fact provided a quite reliable method of measuring the target thickness, *averaged over the bombarded spot.* For this purpose, deuterium gas was introduced into the ion source of the accelerator, and the magnetic analyzer set to select the mass-two beam. Thus, Li^8 was produced in the target through the reaction Li^7(d, p)Li^8. Li^8 is the mirror of B^8 and has similar decay properties: its half-life is 0.85 second and the 13-MeV negative beta decay also proceeds to the 3-MeV excited state of Be^8. The cross section for Li^8 production in this way is, however, more than

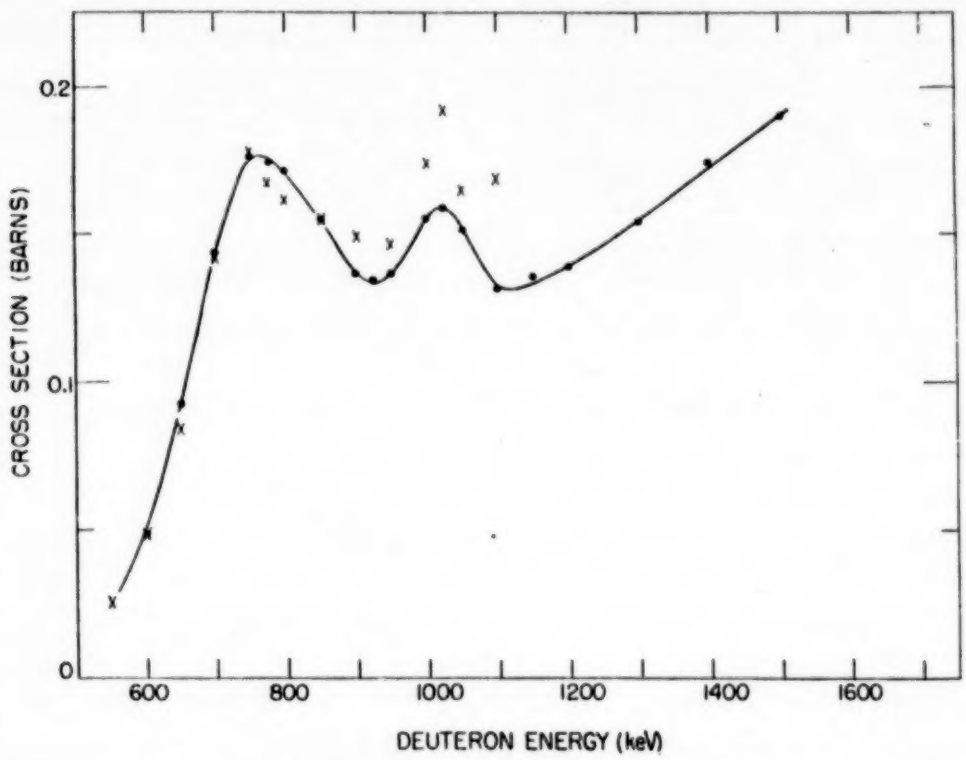

Fig. 2. The cross section as a function of energy for the reaction Li^7(d, p)Li^8 (circles), and the normalized yield from deuteron bombardment of the Be^7 target (crosses) taken at $\lambda t = 0.06$.

10^5 times greater than the cross section for B^8 production by proton capture in Be^7 at bombarding energies around 800 keV. The cross section for Li^7(d, p)Li^8 in the vicinity of the known [5]) resonances is shown in fig. 2 as the solid curve, taken using an evaporated lithium target and the detector of fig. 1. The absolute cross section was determined using a thin lithium target on 2500Å Ni foil, the Li^7 content having been measured by the yield of elastic scattered protons in a 10.5″ magnetic spectrometer. The elastic-scattering absolute cross section is known to 5 per cent from the work of Warters *et al.* [6]), who used the same spectrometer. The Li^8-production cross section at 750-keV bombarding energy was found to be $\sigma = 0.176 \pm 0.015$ b, which agrees with the value 0.150 b ($\pm$ 25 per cent) given by Bashkin [7]). The crosses in fig. 2 show the relative yields obtained from deuteron bombardment of the Be^7 target approximately

five days after preparation. The increasingly excessive yield with increasing energy is attributed to 20-msec B^{12} production from boron contamination in the target; the structure of the yield curve was almost entirely obliterated in the greater yield from this contaminant when a higher mechanical chopping frequency of 6 cycles per second was used.

The Li^8 yield was checked several times over a three-week period to monitor the growth of Li^7 in the target and to detect possible target loss. The yields are plotted in fig. 3 as a function of $1-e^{-\lambda t}$, where λ is the Be^7 decay constant.

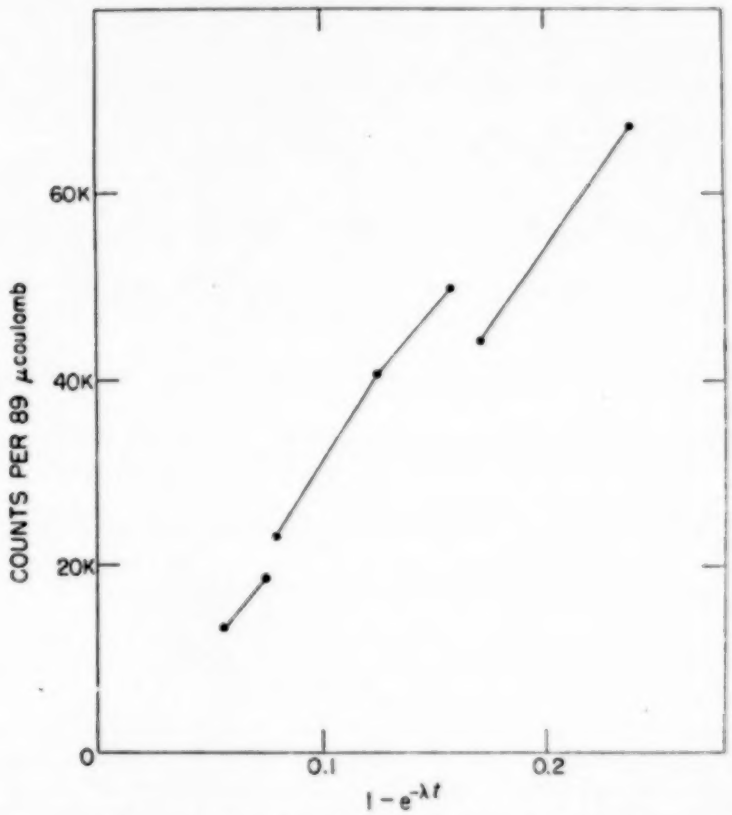

Fig. 3. The yield from 700-keV deuteron bombardment of the Be^7 target versus time after preparation expressed as a function of the Be^7 decay constant, showing the growth of Li^7 in the target. Unconnected points were taken under different detection conditions.

Connected points were taken under the same detection conditions; where breaks occur a change in target position or scaler bias and chopping cycle was made. The variations in slope and lack of zero intercept lead to an assignment of ± 15 per cent probable error to target thickness determinations.

Having found the $Li^7(d, p)Li^8$ yield, Y_{Li^8}, at times t_0 and t_1, to measure the cross section from the $Be^7(p, \gamma)B^8$ reaction it was only necessary to replace the ion source gas with normal hydrogen, select the mass-one beam, and measure the net yield Y_{B^8} of B^8 at time t_2, leaving the target geometry and counters unchanged. Then the cross section for B^8 production is given by

$$\sigma(B^8) = \sigma(Li^8)\,\frac{0.95\,Y_{B^8}(t_2)}{Y_{Li^8}(t_1)-Y_{Li^8}(t_0)} \times \frac{Q_d}{Q_p} \times \left[e^{\lambda(t_2-t_0)} - e^{\lambda(t_2-t_1)}\right],$$

where Q_d/Q_p is the ratio of integrated charges in the deuteron and proton runs. The cross section $\sigma(Li^8)$ at the appropriate energy was taken from fig. 2. The factor 0.95 is the correction for the difference in the spectrum fractions of Li^8 and B^8 below the effective bias. No gating-cycle correction is needed, since the half-lives are the same.

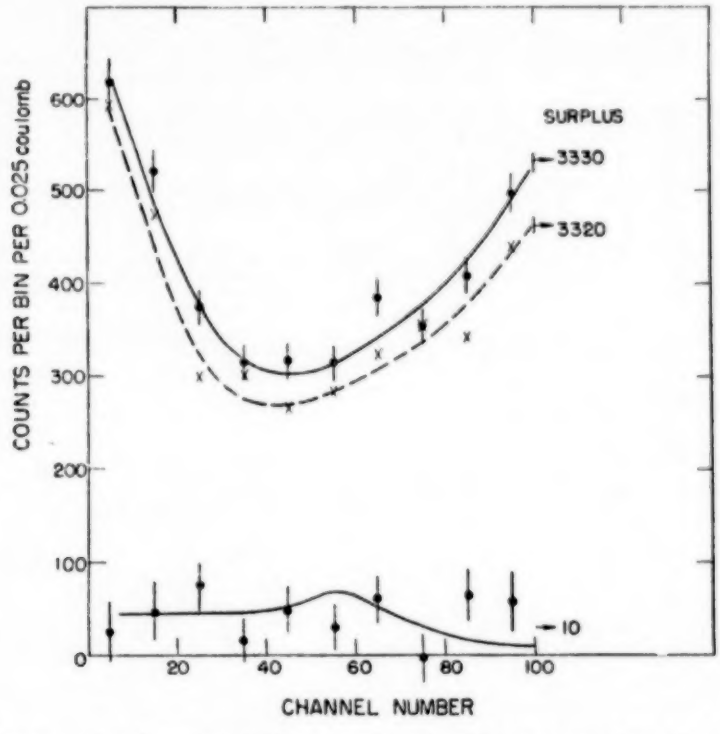

Fig. 4. Pulse-height spectra from (1) 800-keV proton bombardment of the Be^7 target (upper solid curve, circles); (2) proton bombardment of aluminium outside the detector for background (dashed curve, crosses); (3) the difference between the first two (lower circles), giving the net yield; and (4) 700-keV deuteron bombardment of the same target spot (lower solid curve), the vertical scale in this case not applying. Except for (4), the bin is ten channels. The amplifier bias was such that only the upper three-quarters of the spectra appear.

The uppermost curve of fig. 4 shows the pulse height distribution recorded from a total of 25 000 μC of 800-keV protons on the target; the next (dashed) curve is the background spectrum recorded with the same quantity of charge intercepted on an aluminium stopper about 15 cm from the target. Background and target runs were alternated with a period of 15 minutes in order to average out possible fluctuations in background or in the detection system during the two-day interval. Ninety per cent of the background was due to cosmic rays and therefore the background counts were simply increased by 3 per cent to correct for the difference of that amount in running times. Subtracting the background from the upper spectrum gives the net counts plotted below, the

sum of which between channels 30 and 100 being used for Y_{B^8}. The lower solid curve is the spectrum from Li^8; the channel 30 to 100 sums from this and a similar spectrum at a later date from the same target spot gives the Y_{Li^8} difference appearing in the expression for the cross section. The peak at about channel 57 is due to the roughly constant pulse height resulting from those electrons from the target having ranges greater than or equal to the crystal radius. It should be noted that a minimum-ionizing cosmic ray passing along a crystal diameter loses twice as much energy in the crystal as a high energy electron from the target, and the background spectrum should thus peak at twice the pulse height corresponding to the peak in the Li^8 spectrum, which accounts for the rise towards higher channels in the upper two curves.

Two separate scalers integral-biased at channels 40 and 100 permitted a check on the totals recorded by the analyzer and also a record of the surplus counts noted in fig. 4 above the last channel. The small net surplus is consistent with the expected spectrum shape from B^8.

To test the possibility that the proton beam might, in spite of magnetic analysis, be contaminated with deuterons, the Be^7 target was replaced with a thick target of Li_3N and bombarded with 1-MeV protons. The yield observed was such that less than 0.1 per cent of the net yield from the Be^7 target could be from Li+d. In view of this, and the fact that no other known nucleus bombarded with protons can result in residual radioactivity of sufficiently high decay energy to interfere, the net yield shown in fig. 4 is attributed entirely to $Be^7(p, \gamma)B^8$. The reaction cross section at 800 keV calculated as outlined above is $(0.48 \pm 0.18) \times 10^{-30}$ cm^2. From a similar run at 1400-keV proton energy, the value $\sigma = (0.50 \pm 0.20) \times 10^{-30}$ cm^2 was found.

4. Discussion

Recent investigations [8, 9]) of direct capture of protons by N^{14}, and by O^{16} and Ne^{20} have demonstrated that the cross sections for these reactions are quite well-described by [3]) expressions of the form

$$\sigma = SE^{-1} \exp(31.28\, Z_0 Z_1 A^{\frac{1}{2}} E^{-\frac{1}{2}})\ \text{b},$$

where Z_0, Z_1 and A are the atomic numbers and reduced mass of the particles interacting at centre-of-mass energy E (in keV), with the cross-section factor S (in keV · b) either constant or slowly varying with energy. Values of S calculated by Christy and Duck [10]) for proton capture by O^{16} and Ne^{20} have agreed [9]) with experiment to within a factor of two (being low in both cases), permitting extrapolation to stellar energies to be carried out with some confidence. For proton capture by Be^7, calculations by Christy [11]) at centre-of-mass energies of 25 and 1000 keV have given $S = 0.005$ keV · b in both cases. This is in disagreement with the value $S = 1.5$ keV · b in the vicinity of 25 keV calculated by Cameron [12]).

The level structure of Li^8 provides strong evidence that B^8 should have one (and only one) excited state in the vicinity of 1-MeV excitation, the mirror of the state in Li^8 at 0.97 MeV. The remaining member of the $T = 1$ triad is probably [5]) the $J = 1^+$, 17.64-MeV state of Be^8, supporting the shell model assignment of $J = 1^+$ to the triad. $Li^6(He^3, n)$ threshold measurements at two laboratories [13]) very probably locate the B^8 level at 0.79 ± 0.03 MeV; the level shift is not surprising in view of the open proton channel. Such a state would be resonant in the $Be^7(p, \gamma)$ reaction at a bombarding energy of 0.75 ± 0.03 MeV and thus might contribute to the cross section measured at 800 keV. For a crude estimate of this contribution, one may take the M1 gamma ray width to be 15 per cent of the Weisskopf limit (the average inhibition in Wilkinson's tabulation [14]) of M1 widths) or $\Gamma_\gamma \approx 0.002$ eV, and the total width to be 23 keV, calculated from the known reduced width $\gamma^2 = 0.064\ 3\hbar^2/2MR$ of the analogue level in Be^8. On this basis, the resonance contribution to the yield at 800 keV is somewhat less than 4 per cent; it could, of course, be much larger in view of the various uncertainties in this estimate.

From the cross sections measured at 800- and 1400-keV proton energy, one obtains the values $S = 0.027 \pm 0.010$ and 0.017 ± 0.007 keV · b, respectively. Considering the ratio (1.0) of the values of S calculated by Christy to be reliable to better than a factor of two, then based on the measured values the best estimate for the cross-section factor at 25 keV is taken to be $S_0 = 0.020 \pm 0.010$ keV · b. With this value, as pointed out by Fowler [15]), the proton-proton cycle will proceed through B^8 only in carbon-free stars having central temperatures $\geqq 20 \times 10^6$ degrees. For the conditions thought to exist in the solar interior, and from values and expressions given in refs. [2]) and [15]), it is readily shown that about 10^{-3} of the Be^7 formed in the sun is destroyed by proton capture. The decay of the B^8 then produces neutrinos having energies up to 14 MeV, with a flux at the earth's orbit of about 10^7 cm^{-2} · sec^{-1}.

It is a pleasure to thank Professors W. A. Fowler, R. F. Christy, and C. A. Barnes for their advice and assistance in many aspects of this experiment. The advice of Dr. C. J. Gallagher regarding chemical separation techniques was very helpful in target preparation.

Appendix on Target Preparation

The Be^7 used in this investigation was produced at the Crocker Cyclotron † by bombardment of thick metallic lithium with 24-MeV molecular-hydrogen ions. The lithium was wrapped in 0.5 mil stainless steel foil and the gas-cooled assembly withstood many-hour bombardments at currents of 25 μA. The ^{7}Beyield was about 0.25 mc/μA · h. The target assembly was shipped in oil to

† The help of Mr. William B. Jones of the Crocker Laboratory in supervising the bombardments is gratefully acknowledged.

minimize oxidation of the lithium. The radiation at this stage was mostly due to activity induced in the steel foil.

The material as received consisted of about 0.2 μg of Be^7 embedded in 1g of lithium. The bulk of the lithium was separated from the Be^7 and the steel by vacuum evaporation from a molybdenum crucible, with < 0.01 per cent loss of radioactivity. The residue was dissolved in HCl until the scintillation spectrum indicated that little Be^7 remained in the crucible. The solution, containing stable and radioactive isotopes of Fe, Mn, Co, Ni and other elements including aluminium from the target assembly, was dried, dissolved in water and precipitated with NH^4OH. The precipitate, dissolved in 10*N* HCl, was passed through a Dowex 1 ion-exchange column on which Fe, Co, Mn, Cr and many other metals, are adsorbed [16]) as chloride complexes, but not Ni nor elements of groups IA, IIA or IIIA. The radioactivity remaining in the eluant is now only Be^7. To eliminate the Al, Ni, and traces of other elements, the acetyl-acetonate of Be^7 was extracted with CCl_4 from slightly basic solution containing EDTA, after the method of Alimarin and Gibalo [17]) †, which is apparently specific for beryllium. After many cycles of precipitation (with Fe added as carrier), ion exchange, and solvent extraction, about 70 per cent of the Be^7 was finally obtained carrier-free except for impurities totalling about ten micrograms. The last cycle was carried out using quartz centrifuge tubes after it was found that boron from Pyrex vessels used during hot-drying operations was masking attempts to detect the Li^7(d, p)Li^8 yield in early trials because of the large yield of energetic electrons from B^{11}(d, p)B^{12}.

This small amount of material was then taken up in one drop of dilute HCl and deposited and dried with a heat lamp in a 2-mm diameter spot in the middle of a platinum strip. The strip was then heated to 1300°C in a vacuum, with a water-cooled foil placed immediately above the active spot to catch the volatiles. The beryllium, deposited on the strip as the oxychloride, forms the refractory BeO upon heating and remains on the strip, while other metals evaporate as chlorides. The foil with the impurities was then removed from above the strip and replaced with a platinum disk to be used as the target backing. One drop of HF was added to the Be^7 spot on the strip and dried in air, forming Be^7F_2. The evaporation process was repeated, depositing the Be^7 as the fluoride on the target disk; the evaporating geometry was such that about 50 per cent was deposited within a 4 mm circle. The disk was then exposed to the fumes from warm concentrated NH_4OH for several minutes, following which it was heated in air to red heat, driving off fluorides and forming the BeO target as finally used.

The total thickness of the deposit was determined to be less than 4 keV for 1 MeV protons by examining the excitation curve, with the apparatus of fig. 1, for the pairs from the reaction F^{19} (p, $\alpha\pi$)O^{16} around the well-known

† I am indebted to Dr. B. Povh for his translation of this paper.

780-keV resonance [5]), assuming the residual fluorine to be dispersed throughout the target deposit. The observed width was 4.6 keV. Other impurities of Be^9, B, and C, and N were observed using this target during a study of the Be^7(d, p)Be^8 reaction, which will be reported elsewhere.

References

1) H. D. Holmgren and R. L. Johnston, Phys. Rev. **113** (1959) 1556
2) W. A. Fowler, Ap. J. **127** (1958) 551
3) Burbidge, Burbidge, Fowler and Hoyle, Revs. Mod. Phys. **29** (1957) 547
4) A. G. W. Cameron, Ann. Rev. Nucl. Sci. **8** (1958) 299
5) F. Ajzenberg-Selove and T. Lauritsen, Nuclear Physics **11** (1959) 1
6) Warters, Fowler and Lauritsen, Phys. Rev. **91** (1953) 917
7) S. Bashkin, Phys. Rev. **95** (1954) 1012
8) R. E. Pixley, to be published
9) N. Tanner, Phys. Rev. **114** (1959) 1060
10) R. F. Christy and I. Duck, to be published
11) R. F. Christy, private communication
12) A. G. W. Cameron, Chalk River Report CRL-41, 2nd edition Jan. 1958 (unpublished)
13) B. J. Farmer and C. M. Class, Bull. Am. Phys. Soc. **4** (1959) 95;
Dunning, Butler and Bondelid, Phys. Rev. **110** (1958) 1076
14) D. H. Wilkinson, Phil. Mag. **1** (1956) 127
15) W. A. Fowler, Mémoires Soc. Roy. Sciences de Liège, to be published (1960)
16) K. A. Kraus and F. Nelson, Proc. Internat. Conf. on Peaceful Uses of Atomic Energy **7** (1955) 113
17) I. P. Alimarin and I. M. Gibalo, Zhur. Anal. Khim. **11** (1956) 389

2.L

Nuclear Physics **15** (1960) 421—435; © *North-Holland Publishing Co., Amsterdam*

Not to be reproduced by photoprint or microfilm without written permission from the publisher

SMALL ANGLE SCATTERING OF ELECTRONS

I. BERKES and I. DEMETER

Central Research Institute for Physics, Budapest

Received 13 November 1959

Abstract: The small angle scattering of 615 keV electrons has been studied on N, A, Kr and Xe gases. It has been found that if the electron cloud of atoms is considered in Hartree representation, for angles $\vartheta < 1.5\times10^{-3}$ radians, covered by our measurements, the differential cross sections for elastic and inelastic scattering are in agreement with the theory. The screening of elastic scattering being represented by an exponential factor $e^{-r/a}$, the screening parameters

$$a = (1.23\pm0.067)a_0 Z^{-\frac{1}{3}} \text{ and } a = (1.195\pm0.070)a_0 Z^{-\frac{1}{3}}\left(\frac{Z}{Z-1}\right)^{\frac{1}{3}},$$

respectively, give the best representation of the experimental results.

1. Introduction

Scattering experiments carried out on electrons with energies between a few hundred keV and a few MeV had the purpose of serving as experimental verification of the Dirac theory as well as of the general assumptions applied in the field theory. In view of this aim the measurements covered interactions occurring in the well known Coulomb field. These experiments led to the verification of the differential scattering cross section predicted by Mott's calculations [1]) and corrected subsequently by McKinley and Feshbach [2]) to give

$$\sigma(\vartheta) = \left(\frac{Ze^2}{2m_0c^2}\right)^2 \frac{1-\beta^2}{\beta^4} \frac{1}{\sin^4\frac{1}{2}\vartheta}\left[1-\beta^2\sin^2\tfrac{1}{2}\vartheta+\pi\alpha_f\sin\tfrac{1}{2}\vartheta(1-\sin\tfrac{1}{2}\vartheta)\right] \quad (1)$$

where

$$\alpha_f = \frac{Z}{137} \quad \text{and} \quad \beta = \frac{v}{c}.$$

Since the above expression holds for scattering which takes place in the unscreened Coulomb field, it only describes correctly scattering processes for which — in the classical sense — the impact parameter is much smaller than the size of the atom involved. Consequently, when dealing with problems in which the screening cannot be neglected, such as small angle, plural and multiple scattering, and computations of the total scattering cross section, we have to know the cross section for scattering in the screened field.

The purpose of our investigations is to determine from a direct single scattering experiment the angular dependence of the intensity of small angle scattering occurring in the atomic field.

2. Basic Considerations

An electron impinging on the atomic field may interact partly with the nuclear field screened by the electron cloud, partly with the electrons of the atom. In the following, our considerations will be restricted to small angle scattering so that by neglecting the spin term and other higher order approximations [3]) we have

$$\sigma(\vartheta) = \frac{\sigma_{\text{Ruth}}}{Z^2}\,[Z^2(1-F)^2+ZG], \tag{2}$$

where σ_{Ruth} is the Rutherford scattering cross section, F is the screening function and G is the contribution of inelastic scattering on electrons: F and G can be determined if the electron distribution is known.

2.1. THE SCREENED NUCLEAR FIELD

The elastic scattering cross section has been determined for elements ranging in atomic number from lithium to argon by Mott and Massey using the Hartree representation of the charge distribution in the electron cloud and covering the angular range in which the screening effect becomes appreciable [1]). The differential scattering cross section for mercury bombarded by 100 and 230 keV electrons has been tabulated by Bartlett and Welton [4]). Both the elastic and inelastic scattering cross sections for nitrogen have been computed by Moravcsik in the form of analytical series [5]).

In determining the screening function $\Phi(r)$ of the scattering potential

$$U(r) = -\frac{Ze}{r}\,\Phi(r)$$

we may use instead of the Hartree potential its expansion of the form [6])

$$\Phi(x) = \sum_i c_i e^{-k_i x}, \quad x = \frac{r}{\mu}, \quad \mu = 0.885\, a_0 Z^{-\frac{1}{3}},$$

and even limit ourselves to a single term exponential expression. For this case, the value of the constant k is given by Williams [7]) as 0.886, and by other authors, depending on the element in question, as 0.6—1.6. This potential yields for small angles in good approximation

$$\sigma(\vartheta) = \frac{\sigma_{\text{Ruth}}}{\left[1+\dfrac{\lambda}{(2a\sin\frac{1}{2}\vartheta)^2}\right]^2}. \tag{3}$$

Also higher order approximations to this potential were determined by Dalitz [9]).

The screening function $\Phi(r)$ may be obtained also by using the Thomas-Fermi representation instead of that of Hartree. The cross sections can be computed numerically or by making use of analytical approximations [9–13]).

2.2. THE INELASTIC SCATTERING

The inelastic scattering cannot be neglected in the angular range $\vartheta < (5\text{—}6)10^{-3}$ radians. With nitrogen, for instance, at angles smaller than $\vartheta = 2.5\times 10^{-3}$ radians, the cross section for inelastic scattering already exceeds that of the elastic one. An expression for the inelastic scattering cross section is given by Lenz [11]) as

$$G = 1 - \frac{1}{\left[1 + \frac{\vartheta^2}{\lambda^2}\,\frac{\theta}{6Z}\right]^2}$$

where $\theta = \int_0^\infty \rho(r) r^4 4\pi r^2 \mathrm{d}r$. Knowing the charge distribution $\rho(r)$ of the electron cloud, the integration can be carried out.

Since the values of θ reported by various authors are fairly different depending on the atomic model chosen and on the accuracy of numerical integration, only rather inaccurate values of G can be obtained from the above expression. The error is mainly due to the fact that the density distribution term in the integrand being multiplied by r^4, the outer part of the electron cloud, which in general is less accurately described, becomes preponderant in the calculations. Therefore, in our comparison with experimental results, instead of the above expression, we make use of the relation obtained for exponential screening with the screening parameter a,

$$G = 1 - \frac{1}{\left[1 + \left(\frac{\vartheta}{\lambda}\right)^2 a^2\right]^2}. \tag{4}$$

For $\vartheta = 2.5\times 10^{-3}$ radians, however, the former expression for a corresponds to the impact parameter $r \approx 8\times 10^{-9}$ cm for the electron wave-length $\lambda = 1.24\times 10^{-10}$ cm; thus, it seems advisable to determine a rather from the Hartree distribution, which for the outer parts of the atom gives certainly a more accurate description.

2.3. EXPERIMENTAL DETERMINATIONS

Owing to the large cross section for small angle scattering, the experimental conditions required to obtain pure single scattering are difficult to achieve. Therefore, instead of direct cross section measurements, multiple or plural scattering experiments were carried out and whenever possible, the screening was inferred from the distribution. In some of these experiments the results did not agree with the values expected theoretically [14]) and this was attributed to an inaccurate allowance for the screening effect. Other authors, however, verified multiple scattering distributions within the limit of experimental error [5, 15, 16, 17]).

Only few direct measurements are reported in connection with scattering

occurring in the atomic field. Scattering of 800 eV electrons on Ne, A, Kr and Xe was measured by Arnot; the deviations from the Thomas-Fermi distribution in the results were due to the error in the Born approximation when used for low energies [1]). Scattering experiments were performed by Simpson Craw and Marton with 20 keV electrons at angles of the order of 10^{-2} radians; their aim was to determine the characteristic energy loss of crystals [18]).

The most reliable measurements on small angle scattering were reported by Biberman and coworkers [19]), who determined the inelastic scattering distribution of 20, 40 and 60 keV electrons by a chromium foil target. For the small angle range of their measurements, not yet affected by the disturbing effect of coherent scattering, the measured distribution was found to be in agreement with that computed by Lenz from the Hartree potential.

Finally, we only want to mention that the screening functions and in this way the electron cloud distribution were extensively investigated in X-ray scattering experiments. The results thus obtained confirmed the quantal Hartree representation and are reported in various handbooks.

3. Experimental Apparatus

The experimental set up is sketched in fig. 1.

3.1. ELECTRON BEAM

The electron beam required for our experiments was produced by a free air type 1 MeV Van de Graaff generator [20]). In order to avoid beam straggling due to voltage fluctuations, the generator had to be stabilized. This is achieved by

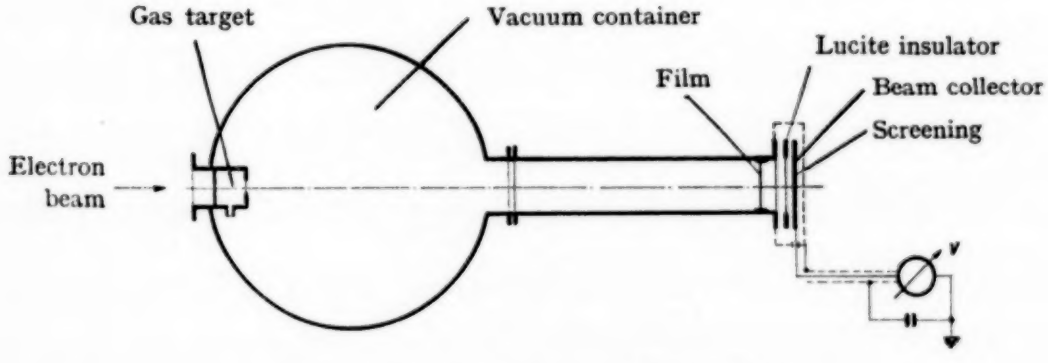

Fig. 1. Sketch of experimental apparatus.

varying the charging voltage by means of the high voltage measuring rotational field meter. The stability thus obtained is better than 1 %. The angular spread of the beam is about 5×10^{-4} radians.

3.2. GAS TARGET

The target has to be sufficiently thin so that no multiple scattering should occur. Evaluation is simpler and more accurate if the target consists of a single element; metal foils cannot be used on account of the disturbing effect of coherent scattering; therefore, a gas target seemed to be the most convenient (fig. 2). Continuously flowing gas was used since, owing to its thickness, (10 $\mu g/cm^2$) the mass of sealing foils could not be neglected.

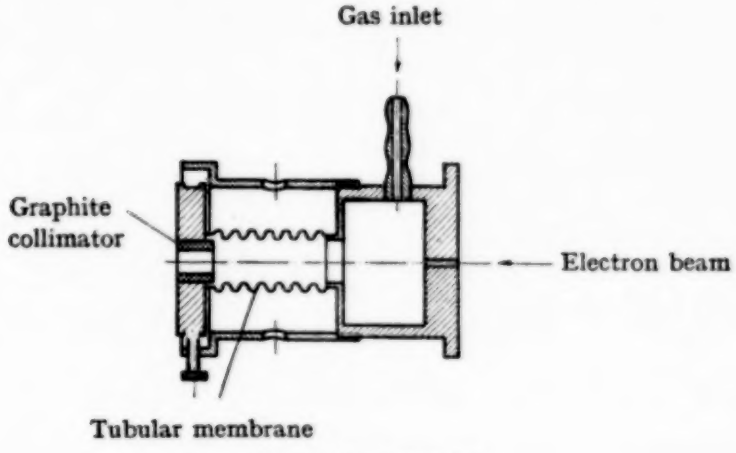

Fig. 2. Gas target.

At the inlet of the beam there is a circular aperture, 0.5 mm in diameter and at the outlet a 0.3×5 mm slit which serves for the detection of scattering. With the gas turned on, the pressure between target and detector is less than 1 μ. In order to reduce the scattering on the walls, the outlet slit of the target is made of graphite. For convenient adjustment to the beam it is possible to set separately both the position and the direction of the gas target.

3.3. DETECTION

Agfa Document films were used to detect scattering intensity. In irradiation experiments performed by using electrons of Cs^{137} ($W_{max} = 0.52$ MeV) and Y^{90}($W_{max} = 2.18$ MeV) the blackening in terms of exposure was found to be linear up to $D = 0.95$—1. The result was the same for the 615 keV electrons of the generator. For evaluation only the linear portion of the curve for blackening was used. Since the complete intensity range could not be covered by a single exposure, eight irradiation experiments were performed with exposures of various intensities and the curves thus obtained were subsequently fitted into a single plot. A micro-photometer was used to measure blackening. Stray background scattering due to the walls of the slit and the vacuum chamber was determined by measurements performed without gas with the same time of exposure. The charge proportional to the electron doses was measured by a static electrometer.

4. Experimental Corrections

4.1. LIMITATIONS OF EXPERIMENTAL ACCURACY

The accuracy of measurement is limited by the following errors:

1. Linearity of blackening may be affected by the non-uniformity of film material and development; this may cause a non-linearity of the order of ± 5—6 %. Since the curve was plotted by fitting the results of partial measurements, the overall error ($\Delta\sigma_1$) in the slope is about ± 2 %.

2. The spot produced by the primary beam is about 1.5 mm in diameter. The circular aperture is 0.5 mm in diameter; the evaluations within this range are not possible. This results in a goniometric error which will be denoted by $\Delta\vartheta$. The extension of the spot is due to the angular spread of the beam. Denoting the aperture of the incidence cone by τ and assuming all angles of incidence lying between $+\tau$ and $-\tau$ to be equally probable, we get instead of the true distribution

$$\mathcal{J}(\vartheta) = \frac{1}{2\tau}\int_{\psi=-\tau}^{+\tau} \sigma(\vartheta+\psi)\mathrm{d}\psi.$$

The correction, however, is only significant for low values of ϑ. The overall error $\Delta\sigma = \Delta\sigma_1 + (\mathrm{d}\sigma/\mathrm{d}\vartheta)\Delta\vartheta$ is shown on the experimental curve.

3. The experimental error in the determination of the inherent blackening of the film and of background effects may be included in the experimental error $\Delta\sigma_1$.

4.2. CORRECTION FOR THE FINITE LENGTH OF THE GAS TARGET

Since the gas target has a finite length we don not measure $\sigma(\vartheta)$ but its average along the target (see fig. 3)

Fig. 3. Effect of gas target length

$$\mathcal{J}(\vartheta) = \frac{1}{l}\int_{L-\frac{1}{2}l}^{L+\frac{1}{2}l} \frac{\sigma}{x^2}\,\mathrm{d}x = \frac{1}{l}\int_{L-\frac{1}{2}l}^{L+\frac{1}{2}l} \sigma(\vartheta)\mathrm{d}\vartheta.$$

The maximum deviation being 5 %, it is negigible as compared with other experimental errors.

4.3. SCATTERING OUTSIDE THE GAS TARGET

The pressure in the vacuum chamber between detector and target being lower at least by three orders of magnitude than in the target itself, scattering in the former cannot be more than 5 %. Nevertheless, near the primary beam

traces of scattering at higher angles may appear so that here an appreciable correction may be expected. For this reason the background was photographed by letting the same amount of gas flow into the vacuum chamber than used to escape into it through the slit of the gas target.

4.4. DOUBLE SCATTERING

If the collision probability $w = 1-\exp(-N\sigma_{\text{total}})$ is not much below unity (N is the number of scattering centers per cm^2) the probability for plural scattering increases. The probability for an electron having suffered double scattering to impinge on the detector is given by

$$p_2(\vartheta) = \int_{(\vartheta')} \int_{\varphi=0}^{2\pi} \Sigma(\vartheta')\Sigma(\vartheta, \vartheta', \varphi)\vartheta' \,\mathrm{d}\vartheta' \,\mathrm{d}\varphi$$

where $\Sigma = N\sigma$. The integration has to be extended over all values of ϑ' for which the distribution is appreciably affected by the integral.

Since the numerical integration is rather lengthy, it is more convenient to make the following assumptions. At a given gas pressure let Σ_1 and Σ_2 be the cross sections for double and single scattering, respectively. Now, if the pressure is increased a times, i.e. if there are a times as many scattering centres, then

$$\Sigma'_1 = a\Sigma_1, \quad \Sigma'_2 = a\Sigma_2$$

and consequently

$$\frac{w'}{a} - w = (a-1)(\Sigma_2 - \tfrac{1}{2}\Sigma_1^2).$$

In this expression $\Sigma_2 > \frac{1}{2}\Sigma_1^2$. With $a = 2.27$, the curves plotted for the two different pressures were of the same shape. The difference $(w'/a)-w$ could not be detected within the overall experimental error of about 20 %, owing to errors in the measurement of current and pressure. Thus, the distribution measured corresponds to the single scattering cross section.

5. Discussion

The experimental results have to be evaluated as follows:

1. Comparison of measured and calculated relative differential cross sections [1, 5, 12, 21].

2. Determination of screening parameter dependence on atomic number from scattering distributions obtained for various elements.

The magnitude of the differential cross section in general varies with the energy. The scattering amplitude computed by means of the Born approximation with small values for ϑ gives

$$|f(\vartheta)| = \frac{2m_0 Ze^2}{\hbar^2} \frac{\lambda}{\vartheta} \int_0^\infty \sin\left(\frac{\vartheta}{\lambda} r\right) \Phi(r)\mathrm{d}r = \frac{2m_0 Ze^2}{\hbar^2} \psi\left(\frac{\lambda}{\vartheta}\right);$$

hence the cross section is obtained as

$$\sigma(\vartheta) = \frac{1}{1-\beta^2} |f(\vartheta)|^2.$$

It is seen that if the abscissa is scaled by ϑ/λ, though the magnitude of the cross section depends on the energy, the distribution does not. On the other hand,

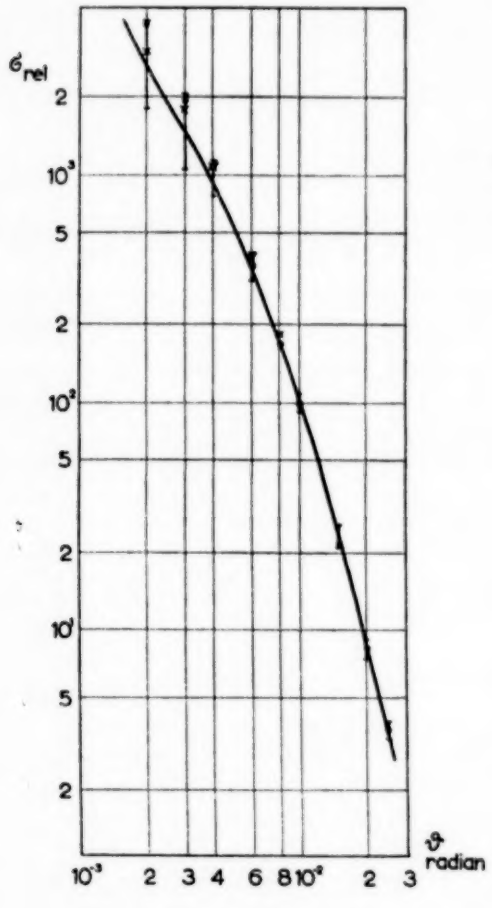

Fig. 4. Small angle scattering differential cross section for nitrogen.
Theoretical points denoted by • according to ref. [21]) calculated by the Hartree potential; theoretical points denoted by × according to eq. (2) and eq. (3) calculated with $a = 0.37 \times 10^{-8}$ cm.
The ordinate scale is arbitrary.

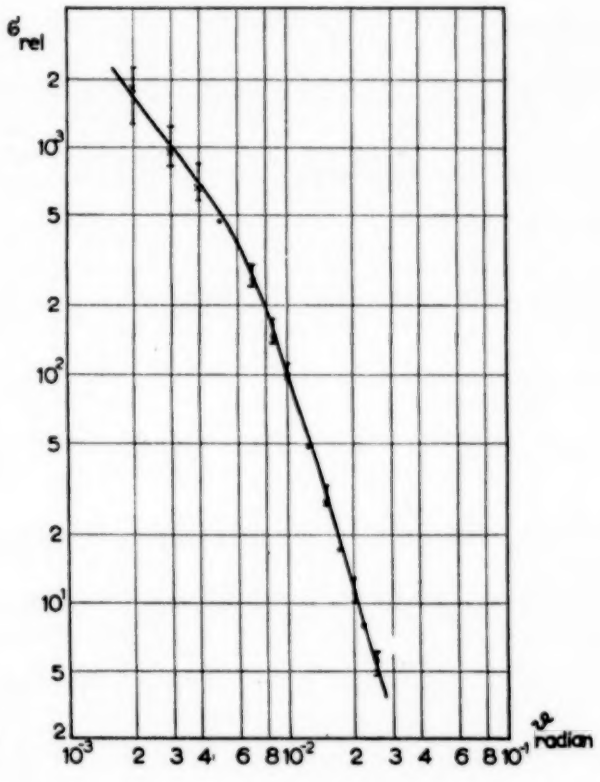

Fig. 5. Small angle scattering differential cross section for argon.
Theoretical points denoted by • according to ref. [1]) calculated by the Hartree potential (valid only for elastic scattering); theoretical points denoted by × according to eq. (2) and eq. (3) calculated with $a = 0.294 \times 10^{-8}$ cm.
The ordinate scale is arbitrary.

considering that these experiments yield only relative differential cross sections, the ordinate scale was chosen arbitrarily and the theoretical points were normalized to fit the experimental curves for 10^{-2} radians.

The elastic and inelastic contributions cannot be discriminated by detection,

so that the experimental curves represent the sum of both contributions. In figs. 4, 5, 6, 7 the results of our experiments on nitrogen, argon, krypton and xenon are shown. From fig. 4 it is seen that our experimental results are in good agreement with the differential cross sections predicted by the Hartree representation in the whole range covered by the measurements[21]). For nitrogen the scattering in the angular range $\vartheta > 2 \times 10^{-2}$ radians is already pure unscreened scattering. In fig. 5 the scattering cross section for argon is shown. The calcu-

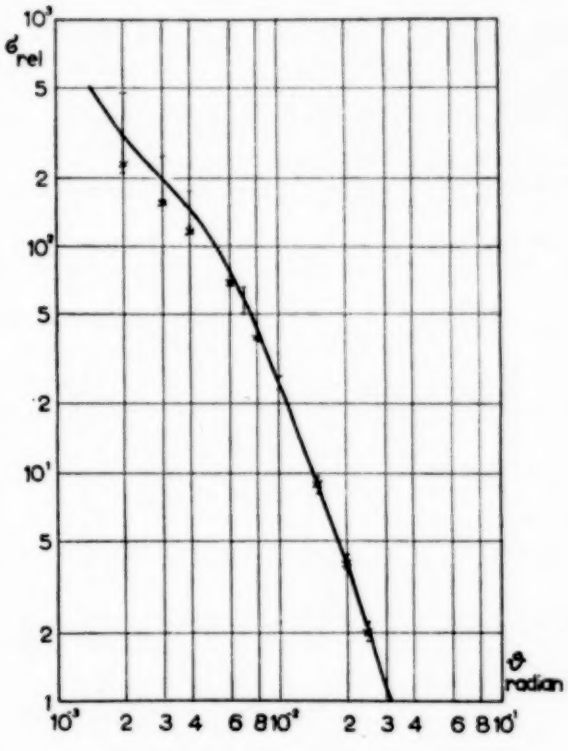

Fig. 6. Small angle scattering differential cross section for krypton.
Theoretical points denoted by × according to eq. (2) and eq. (3) calculated with $a = 0.180 \times 10^{-8}$ cm.
The ordinate scale is arbitrary.

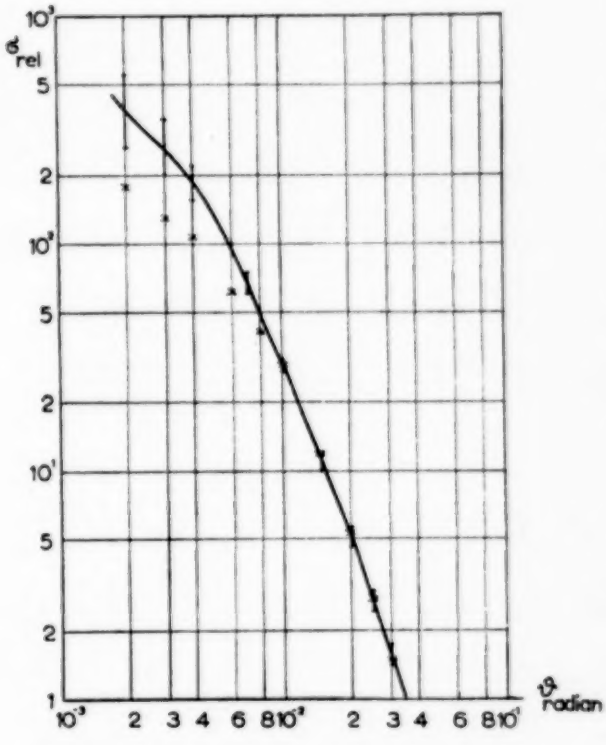

Fig. 7. Small angle scattering differential cross section for xenon.
Theoretical points denoted by × according to eq. (2) and eq. (3) calculated with $a = 0.165 \times 10^{-8}$ cm.
The ordinate scale is arbitrary.

lated points denoted by • represent only the elastic contribution computed from the Hartree potential [1, 12]).

It is more difficult to study the elastic scattering in terms of atomic number since in the ranges where the screening of elastic scattering becomes appreciable, the inelastic scattering cross section will be usually much higher than the elastic one.

In order to overcome this difficulty we shall use the following two approximations:

a) In calculating the elastic cross section, the screening effect will be

represented by a simple exponential. The constant in the exponential has to be determined in such a way that the true potential should differ least from the approximated one at about those values of r at which the interaction occurs.

Various electron distributions were considered in the range $0.15\times10^{-8} < r < 1.6\times10^{-8}$ cm with screening factor $\exp(-r/a)$. In fig. 8 we have shown in

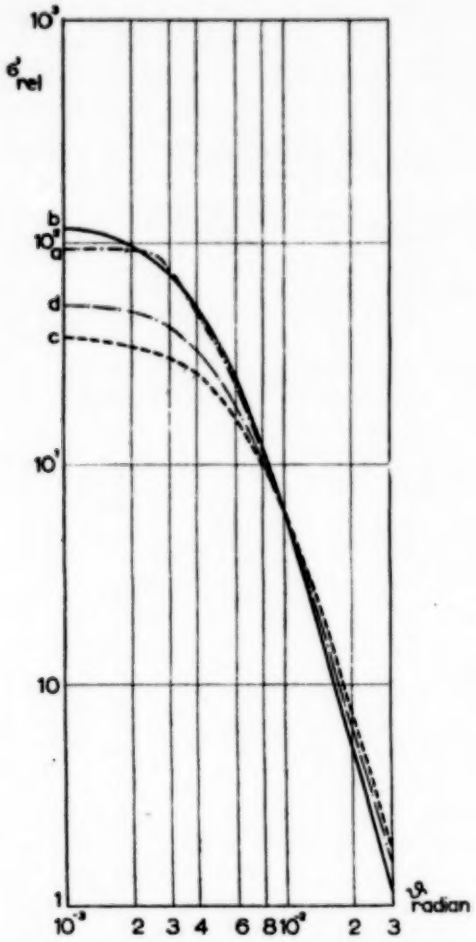

Fig. 8. Elastic scattering differential cross section for nitrogen,
a) calculated with the Hartree potential [21]),
b) with exponential screening $a = 0.37\times10^{-8}$ cm (measured value),
c) with exponential screening $a = 0.244\times10^{-8}$ cm,
d) with exponential screening $a = 0.275\times10^{-8}$ cm (according to ref. [7]).

addition to the elastic scattering curve computed by Moravcsik [curve a)] also the curves obtained by using the exponential screening, namely: curve c) for screening parameter $a = 0.244\times10^{-8}$ cm calculated from $a = 0.885\cdot a_0 Z^{-\frac{1}{3}}$, curve d) for $a = 0.275\times10^{-8}$ cm obtained by Williams, and curve b) for $a = 0.37\times10^{-8}$ cm, as measured in our experiment. It is seen that our result fairly approaches the exact scattering distribution.

TABLE 1

Screening functions $\Phi(x)$ for argon

x	0.2	0.4	0.6	0.8	1.0	1.2	1.4	1.6	1.8	2.0	2.3
Hartree-distribution, 3-term exponential approximation [6])	0.808	0.686	0.587	0.509	0.446	0.395	0.353	0.316	0.287	0.260	0.228
Thomas-Fermi model, Rozental approximation [22]) modified by Molière [10])	0.792	0.660	0.563	0.486	0.425	0.375	0.331	0.297	0.267	0.242	0.210
Thomas-Fermi model, Weizsäcker correction [23])	0.821	0.681	0.577	0.493	0.424	0.369	0.318	0.303	0.251	—	0.184
Thomas-Fermi model, Gombás correction [23])	0.807	0.640	0.536	0.451	0.383	0.327	0.278	0.249	0.215	—	0.152
Hartree distribution, single term exponential approximation with $a = 0.294 \times 10^{-8}$ cm	0.758	0.670	0.595	0.525	0.465	0.410	0.364	0.321	0.288	0.253	0.211

b) As long as the screening does not become markedly strong, the inelastic contribution, particularly for heavy elements, is very small compared with the elastic one. The shape of the curve representing elastic+inelastic scattering does not differ appreciably from the elastic scattering curve for angles $\vartheta > (5\text{—}6) \times 10^{-3}$ radians: thus it is possible to determine from our experimental results the screening parameter of the single term exponential screening potential even without knowing the cross section for inelastic scattering. The analysis of the curves gives

$$a = (0.37 \pm 0.03) \times 10^{-8} \text{ cm for nitrogen,}$$
$$a = (0.275 \pm 0.025) \times 10^{-8} \text{ cm for argon,}$$
$$a = (0.180 \pm 0.015) \times 10^{-8} \text{ cm for krypton,}$$
$$a = (0.165 \pm 0.015) \times 10^{-8} \text{ cm for xenon.}$$

In table 1 the screening potentials for argon are shown as computed by various approximations. Some theoretical results for a number of scattering cross sections are given in ref. [12]). It is seen that for the screening functions there is good agreement between the results obtained by different methods. The cross sections disagree appreciably only in the range of small angles where in any case the inelastic contribution is preponderant. From the single exponential approximation for the various screening potentials for argon, the following screening parameters are obtained:

Screening potential	a (10^{-8} cm)
Hartree distribution [1])	0.294
Thomas-Fermi model: Rozental approximation [22])	0.287
Thomas-Fermi model: Weizsäcker correction [23])	0.244
Thomas-Fermi model: Gombás correction [23])	0.227
Exponential approximation: of Williams [7])	0.202
Exponential approximation: of Molière [10])	0.171
Measured value	0.275 ± 0.025

In fig. 9 the screening parameters measured in the experiments are shown in terms of $Z^{-\frac{1}{3}}$.

The screening parameter

$$a = \frac{1}{k} \cdot 0.885 \cdot a_0 Z^{-\frac{1}{3}}$$

is obtained in our measurement as

$$a = (1.23 \pm 0.067) a_0 Z^{-\frac{1}{3}}.$$

If the scattering amplitude is obtained by series expansion from the Hartree potential, then, neglecting the term containing k^4, we have for nitrogen $a = 1.165 \cdot a_0 Z^{-\frac{1}{3}}$.

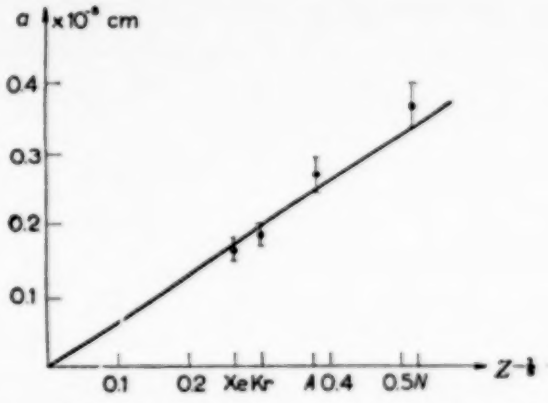

Fig. 9. Screening parameters of the exponential screening function calculated from our measurements.
Equation of the line $a = 1.23 \cdot a_0 Z^{-\frac{1}{3}}$.

According to the Fermi-Amaldi correction, known from the statistical theory which accounts for the self-interaction of electrons, we write

$$a = \frac{1}{k} \cdot 0.885 \cdot a_0 \left(\frac{Z}{Z-1}\right)^{\frac{2}{3}} Z^{-\frac{1}{3}}.$$

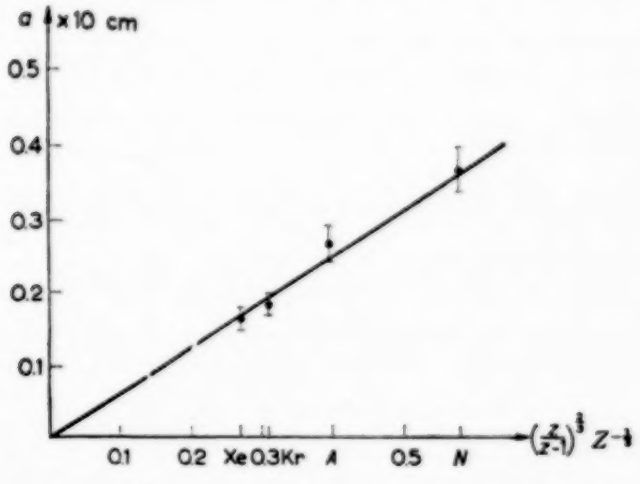

Fig. 10. Screening parameters of the exponential screening function calculated from our measurements, using the Fermi-Amaldi correction.
Equation of the line $a = 1.195 \cdot a_0 \left(\frac{Z}{Z-1}\right)^{\frac{2}{3}} Z^{-\frac{1}{3}}$.

In this case the expression

$$a = (1.195 \pm 0.070) a_0 \left(\frac{Z}{Z-1}\right)^{\frac{2}{3}} Z^{-\frac{1}{3}}$$

gives good agreement for nitrogen (fig. 10).

The inelastic scattering can be taken into account by expressions (2) and (4). The screening parameter of the single exponential screening function has to be determined from the Hartree distribution if the latter is known. Instead of the Hartree distribution we may also use the screening parameter given by the measured values. In figs. 4—7 the cross sections (denoted by $\times$) evaluated from expressions (2) and (4) are shown: for argon, calculated with the screening parameter $a = 0.294 \times 10^{-8}$ cm which is the best approximation of the Hartree distribution, and for N, Kr and Xe computed with the experimental values of a. It is seen that the measured distributions are in good agreement with the predicted ones with the exception of xenon; thus, the screening parameter determined from the screening of elastic scattering can be extrapolated — though with limited accuracy — to the outer periphery of the atom. (The deviation found for xenon may be partly attributed to the inaccuracy in the determination of a.)

6. Conclusion

Summarizing the above considerations it is found that:

1. The calculation of Moravcsik for nitrogen gives a true picture of the differential cross section for small angle scattering. The screening of elastic scattering is also correctly described by Mott, Tietz and other authors.

2. The resultant potential of the electron cloud and the atomic nucleus is of course not a Coulomb potential with simple exponential screening. The Hartree or the Thomas Fermi distribution, however, can be approximated in the range of interaction by such a potential. The screening of the elastic scattering can be represented by means of a suitably chosen screening parameter. The angular range of our experiments covers such values of the impact parameter at which the radial density of the electron cloud is relatively high so that our experiment yields information on this part of electron distribution.

3. In evaluating the small angle scattering distribution, the inelastic scattering on electrons may be neglected only if the angular range in question is higher than $(5—10) \times 10^{-3}$ radians. A less accurate approximation method, taking also into account the inelastic scattering, may lead to a better result than a calculation including higher order contributions restricted to elastic scattering.

References

1) N. F. Mott, Proc. Roy. Soc. A **124** (1929) 425
N. F. Mott and H. S. W. Massey, The Theory of Atomic Collisions, 2nd edition (Clarendon Press) p. 82
2) W. A. McKinley and H. Feshbach, Phys. Rev. **74** (1948) 1759
3) P. M. Morse, Phys. Zs. **33** (1932) 443
4) J. H. Bartlett and T. A. Welton, Phys. Rev. **57** (1940) 1063
5) M. J. Moravcsik, Phys. Rev. **100** (1955) 1009;
M. J. Moravcsik and I. M. Sellen, Rev. Sci. Instr. **26** (1955) 1159

6) W. J. Byatt, Phys. Rev. **104** (1956) 1298
7) E. G. Williams, Proc. Roy. Soc. A **169** (1939) 531; Revs. Mod. Phys. **17** (1945) 217
8) R. H. Dalitz, Proc. Roy. Soc. A **206** (1951) 509
9) M. Majewski and T. Tietz, Phys. Rev. **108** (1957) 193
10) G. Molière, Zs. f. Nat. f. **2a** (1947) 133
11) F. Lenz, Zs. f. Nat. f. **9a** (1954) 185
12) T. Tietz, Acta Phys. Hung. **10** (1959) 11
13) T. Gajewski, An. d. Phys. **456** (1958) 232; An. d. Phys. **456** (1958) 299
14) C. W. Sheppard and W. A. Fowler, Phys. Rev. **57** (1940) 273
15) C. W. Sheppard, Phys. Rev. **62** (1942) 313
16) B. C. Dees and B. Hammermash, Phys. Rev. **63** (1943) 297
17) S. Goudsmith and J. L. Saunderson, Phys. Rev. **57** (1940) 24
18) J. A. Simpson, T. F. Craw and L. Marton, Phys. Rev. **104** (1956) 64
19) L. M. Biberman, E. N. Vtorov *et al.*, Doklady **69** (1949) 519
20) I. Berkes, I. Demeter and P. Kostka, Magy. Fiz. Folyóirat **6** (1958) 209
21) M. J. Moravcsik, private communication and ref. [5])
22) S. Rozental, Zs. f. Phys. **98** (1935) 742
23) P. Gombás, Acta Phys. Hung. **5** (1955) 123

2.1

Nuclear Physics **15** (1960) 436—451; © *North-Holland Publishing Co., Amsterdam*

Not to be reproduced by photoprint or microfilm without written permission from the publisher

$(\gamma, {}^{np}_{d})$ REACTIONS IN S^{32}, Ca^{40}, Ge^{70}

F. FERRERO, S. FERRONI, R. MALVANO, S. MENARDI and E. SILVA †

Istituto di Fisica dell'Università, Torino

and

Istituto Nazionale di Fisica Nucleare, Sez. di Torino

Received 2 November 1959

Abstract: A detailed study, up to 31 MeV, of the (γ, np) and (γ, d) reactions in S^{32}, Ca^{40} and Ge^{7} has been carried out, together with the study of the other processes: (γ, n), (γ, Tn) $(\gamma, Tn)_{E_n \geq 5.5\ \mathrm{MeV}}$. A rather flat cross section is found for the $(\gamma, {}^{np}_{d})$ reaction, peaking presumably above 31 MeV. In the case of S and Ca it is found besides that the neutron spectrum associated with the above reaction is much more energetic than could be explained on the basis of a simple evaporation process. A discussion is given of the possible explanation of the above experimental evidence on the basis of some direct photonuclear process.

1. Introduction

In the investigation of photonuclear reactions the most interesting quantity to measure is the absorption cross section, that can be obtained either directly or by summing up the various partial cross sections (γ, n), (γ, p), etc.

The direct measurement is difficult because the nuclear photoeffect is responsible only for a small fraction of the total absorption. In various laboratories such measurements have been undertaken, specially in the low atomic number region where the electronic attenuation is small; but the experiments are still in a preliminary stage.

The second method, although strictly nuclear, presents some inconveniences: a) the cross sections are not directly measurable, but only their values averaged over the bremsstrahlung spectrum; b) an imperfect knowledge of the decay scheme of a residual radioactive nucleus can sometimes give rise to uncertainties in the evaluation of the absolute value of the cross section; c) in the case of total neutron detection the lack of knowledge of the neutron multiplicity prevents the precise evaluation of the absorption cross section.

The interest of the photonuclear reactions does not limit itself, however, to the study of the total absorption cross section; valuable information can also be obtained through the study of the different reaction cross sections. In particular, it is well known that the proton yield cannot be explained on the basis of a two-step reaction and the same is true also for other types of single

† On leave of Universitade de S. Paulo, Brazil. Fellow of the Conselho Nacional de Pesquisas, Brazil.

particle emission. On the contrary the multiple processes, such as $(\gamma, 2n)$, (γ, np), etc., have been considered so far to be quite in agreement with the statistical model, with the exception of the proton-neutron emission at extremely high energy. Our aim, in the particular case of the (γ, np) reactions, is to see if *the experimental results can be explained completely or not without introducing a particular direct interaction such as the one assumed in the high-energy quasi-deuteron model* [1]).

If one does not use a coincidence method to detect the (γ, np) events, as can be easily done above 100 MeV (where the n and p are strongly correlated in space) the only methods that can be used are the cloud chamber [2]) and the residual activity method. The latter, which is by far the most sensitive and the easiest to carry out, can unfortunately only be applied to a few cases among the light elements. On the other hand, the interest of the light elements lies principally in the fact that the theoretical value of the integrated cross section [3]) is much greater than the sum of the contributions from the (γ, n) and (γ, p) processes in the energy range up to 30 MeV: *a large contribution to the absorption cross section will be given, therefore, by other processes beyond the single particle emission.*

In the present research we have not confined ourselves to the study of the (γ, np) processes, but we have also investigated the other types of photoneutron reactions. This has been done in order to throw some light on the absorption cross section above the giant resonance, although we cannot supplement, at present, this investigation with a knowledge of the photoproton emission.

A certain help to understand the (γ, np) process may certainly be obtained by getting some information about the photoneutron energy spectrum associated with the above process. For this purpose we have measured, in some cases, the total neutron yield not only by means of a moderated neutron detector, but also by means of a convenient threshold detector.

2. Experimental Procedure and Results

In this section we describe the experimental procedure used to measure the various photonuclear processes. As there are some differences in the specific experimental apparatus used in studying different elements and reactions, we shall describe the method employed separately for each element.

All samples ha vebeen irradiated in the X-ra ybeam of a 31 MeV betatron in the University of Turin. Doses were measured with an Al parallel plate ionization chamber; the roentgen units were converted to MeV/cm^2 using the calorimeter data given in ref. [4]). The activation curves were analyzed with the Penfold-Leiss method [5]), deriving the cross section curves from the best fit of the calculated integrated cross sections.

2.1. SULPHUR

The activation curve of the (γ, n) reaction in S^{32} has been obtained irradiating cubic samples of 150 g high purity fused sulphur. A $(2'' \times \frac{1}{2}'')$NaI(Tl) crystal, looked by a 6292 Du Mont photomultiplier, has been used to detect the annihilation γ rays from the 3 sec β^+ activity from S^{31}. The pulses conveniently amplified were fed into a one channel pulse height analyzer centered on the 0.51 MeV γ line. The decay was analyzed in time with a 7 channel mechanical time analyzer with a gate of 2 sec [6]).

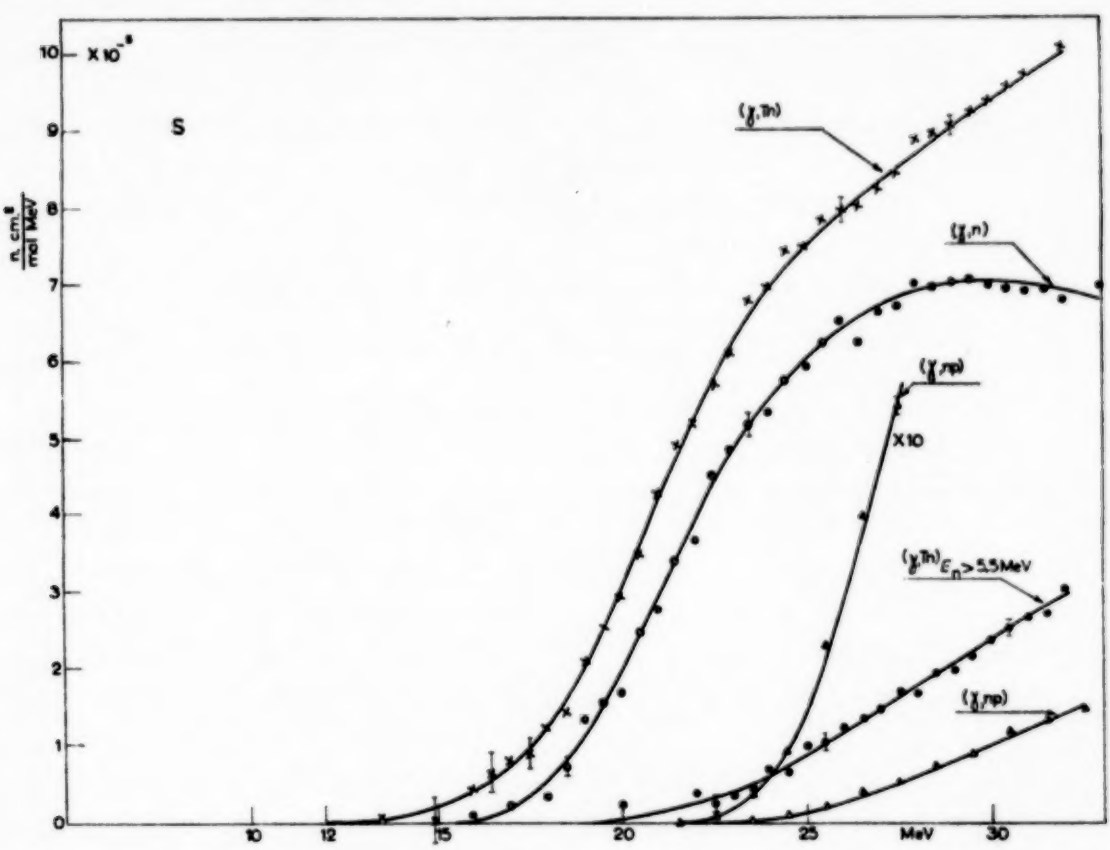

Fig. 1. (γ, n), (γ, Tn), $(\gamma, Tn)_{E_n \geq 5.5\,MeV}$ and (γ, np) excitation functions for S.

The absolute value of the (γ, n) yield has been obtained by comparison with copper at 30 MeV, using for the β^+ detection a coincidence technique (see appendix) and assuming for the $Cu^{63}(\gamma, n)Cu^{62}$ yield the data of Katz and Cameron [7]) extrapolated from 28 to 30 MeV.

The (γ, np) activation curve was obtained by detecting the β^+ activity from P^{30} ($T_{\frac{1}{2}} = 2.5$ min), employing the same technique as before, the only difference being the use of a well type crystal detector and cylindrical sulphur samples ($\approx$ 7g) that could be easily introduced in the well to get a very good counting efficiency. The absolute figure for the yield was obtained by comparison with the (γ, n) residual activity produced in the same sample. By threshold detector method and using the reaction $Si^{28}(n, p)Al^{28}$, the yield of the fast neutron

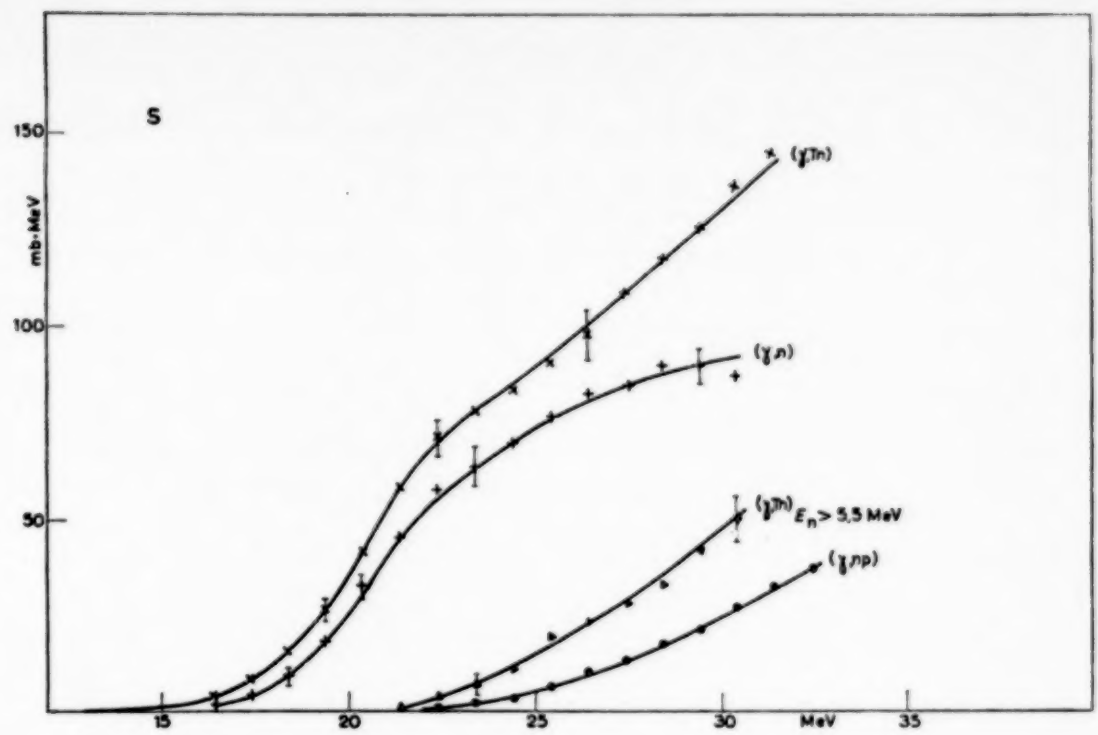

Fig. 2. Integrated cross sections deduced from the excitation functions of fig. 1.

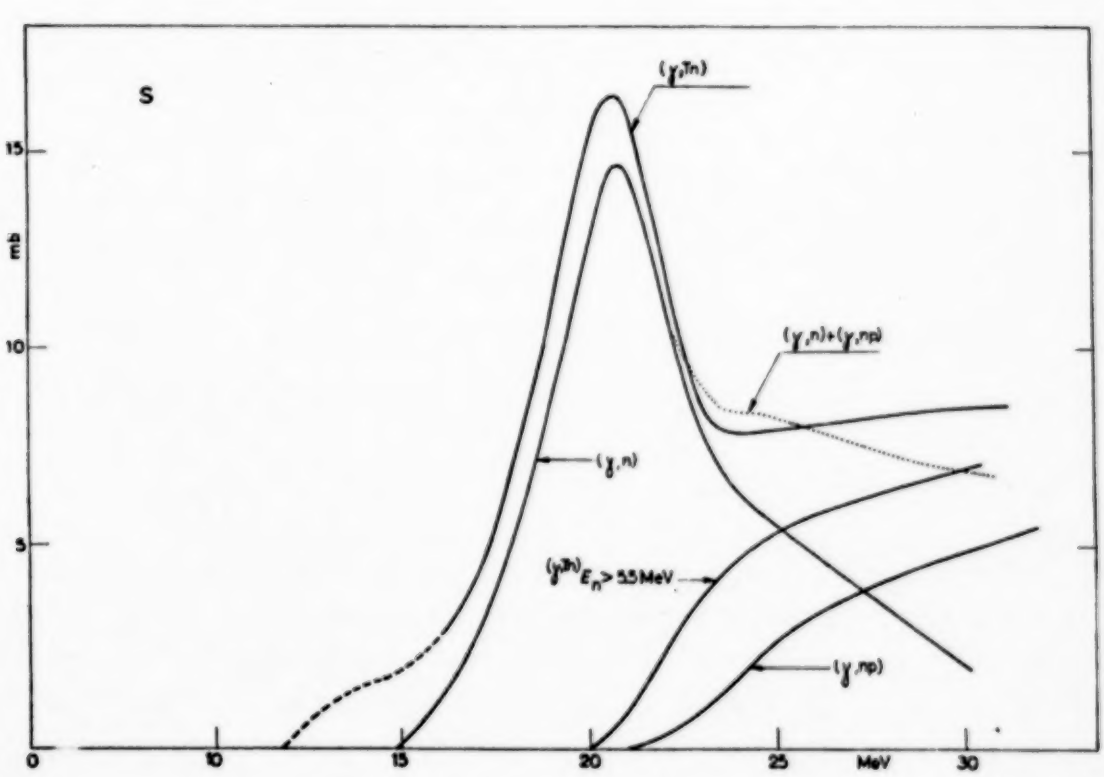

Fig. 3. Cross sections for the photonuclear processes of fig. 1.

component with energy $\geqq 5.5$ MeV, hereafter indicated with the subscript ($E_n \geqq 5.5$ MeV), has been measured and its absolute value obtained by comparison with Al at 30 MeV [6]).

Finally, the total photoneutron yield was measured by means of a moderated total neutron detector, consisting of a water tank (1m × 1m × 1m) in which three Geiger counters, surrounded with Rh powder, are conveniently placed. The device was calibrated with copper using the data of Montalbetti *et al.* [8]).

The activation curves, the integrated cross sections and the cross sections are plotted in figs. 1, 2 and 3 respectively.

2.2. CALCIUM

Rods of metallic calcium were used as samples for the following excitation functions: (γ, Tn) and $(\gamma, \mathrm{Tn})_{E_n \geqq 5.5\ \mathrm{MeV}}$. The detection method and the calibration procedure are the same as for S^{32}.

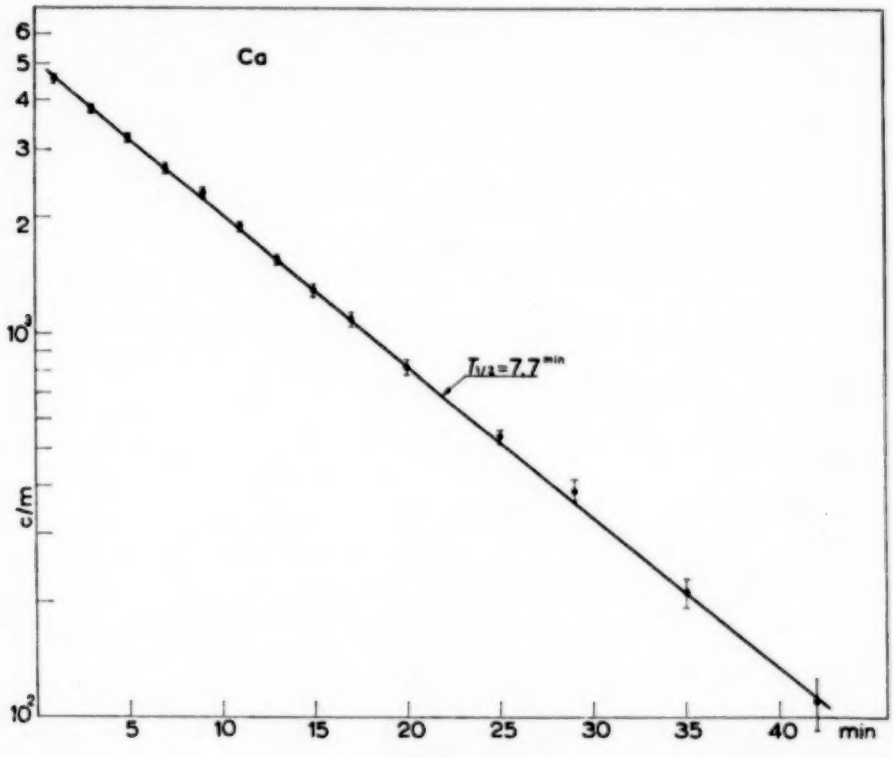

Fig. 4. The 7.7 min decaying activity of ($K^{38}_{g.s.} \xrightarrow{\beta^+} A^{38}$) produced by the (γ, np) reaction in Ca^{40}.

On the other hand, the yield curve for the (γ, np) process was determined by residual activity using samples of CaF_2 pressed powder in order to avoid the troubles due to calcium oxide, that is easily formed in metallic calcium rods. The radioactivity of the produced K^{38} was counted with a $(2'' \times 2'')$NaI(Tl) crystal and the pulse height discrimination was set in order to accept only the γ-ray pulses of energy > 1.2 MeV. This method was employed to detect the 2.18 MeV γ ray arising from the decay of the 2^+ level of A^{38}, following the

β^+ decay of $K^{38}(T_{\frac{1}{2}} = 7.7$ min, $E = 2.6$ MeV) [9]). The decay curve measured by this method was extremely pure, giving the correct half-life (fig. 4). Using instead the β^+ detection method and metallic calcium samples covered with a thin paraffin layer [10]), we were not able to get the correct decay curve. On the other hand CaF_2 samples gave rise to such an intense 1.8 h β^+ activity from the (γ, n) reaction in F^{19}, that it was very difficult to pick-up the contribution from the 7.7 min β^+ decay.

To get an absolute figure for the $Ca(\gamma, np)$ activity, we had to calibrate the scintillation counter. For this purpose we have made use of the yields of the (γ, n) processes in K^{39} and Cu^{63} in the following way. As we can see in ref. [9]) the 7.7 min activity feeds directly the 2.18 MeV γ ray in A^{38}. This implies that the ratio between the yields of the $Ca^{40}(\gamma, np)K^{38}$ and $K^{39}(\gamma, n)K^{38}$ reactions are the same either measured detecting the β^+ activity or the 2.18 MeV γ ray. The absolute value of the $K^{39}(\gamma, n)K^{38}$ process was calibrated in the usual way by comparison with Cu^{63}, detecting the β^+ activity in both elements with the coincidence technique. We have obtained in this way 6.35×10^{-5} dis $\cdot$ cm^2/mol $\cdot$ MeV for the above reaction at 30 MeV. Taking into account this figure we have obtained for $Ca^{40}(\gamma, np)K^{38}$ yield, at the same energy, 7.7×10^{-6} dis $\cdot$ cm^2/mol $\cdot$ MeV.

This crossing way for the absolute calibration was chosen to avoid the various difficulties connected with the residual activity measurement in Ca^{40} [10]). The actual yield of the (γ, np) process is certainly greater than the figure given above, because we have disregarded the formation of the isomeric state in K^{38}, which decay with 0.95 sec half-life β^+ activity to the ground state of A^{38} [9]). In order to give a tentative figure to the total yield of the above photoreaction, we shall make use of the branching ratio for the formation of the isomeric state in K^{38} according to the reaction

$$K^{39}(\gamma, n) \lessdot \begin{matrix} K^{38} \\ K^{38m}. \end{matrix}$$

We have measured, therefore, at 21 MeV, the yield of the above reactions both by total neutron counting and by residual activity. The ratio between these two quantities corresponds to the following expression:

$$\frac{(K^{39}(\gamma, n)K^{38}_{(g.s.)} + K^{39}(\gamma, n)K^{38}_{(i.s.)})}{K^{39}(\gamma, n)K^{38}_{(g.s.)}} = 2.2$$

where (g.s.) and (i.s.) means ground state and isomeric state respectively. The value 2.2 has been obtained at 21 MeV to avoid the contribution to the total neutron yield from multiple photoneutron processes in K^{39}.

Finally, assuming that the decay of K^{38} is independent from its mode of formation, we may use the above figure to calculate the total (γ, np) yield in Ca^{40}.

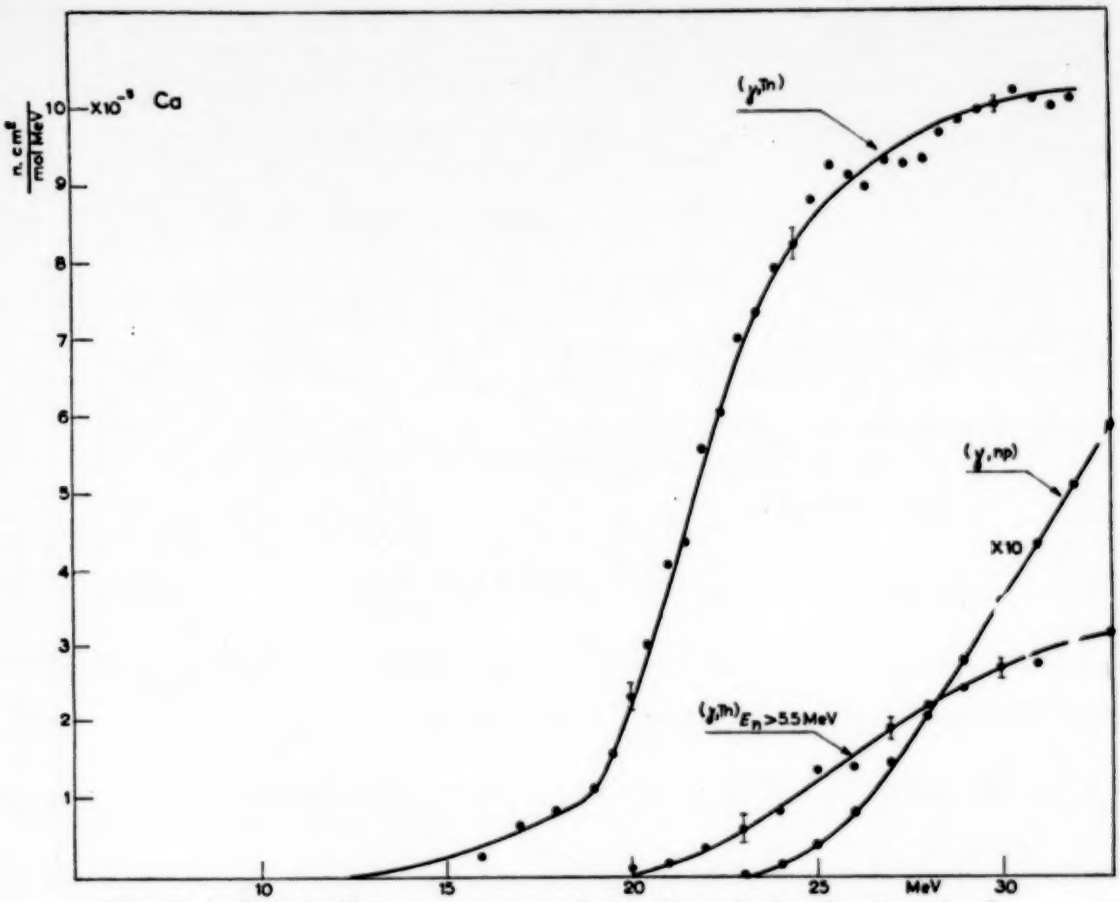

Fig. 5. (γ, Tn), (γ, Tn) $E_n \geq 5.5$ MeV and (γ, np) excitation functions for S.

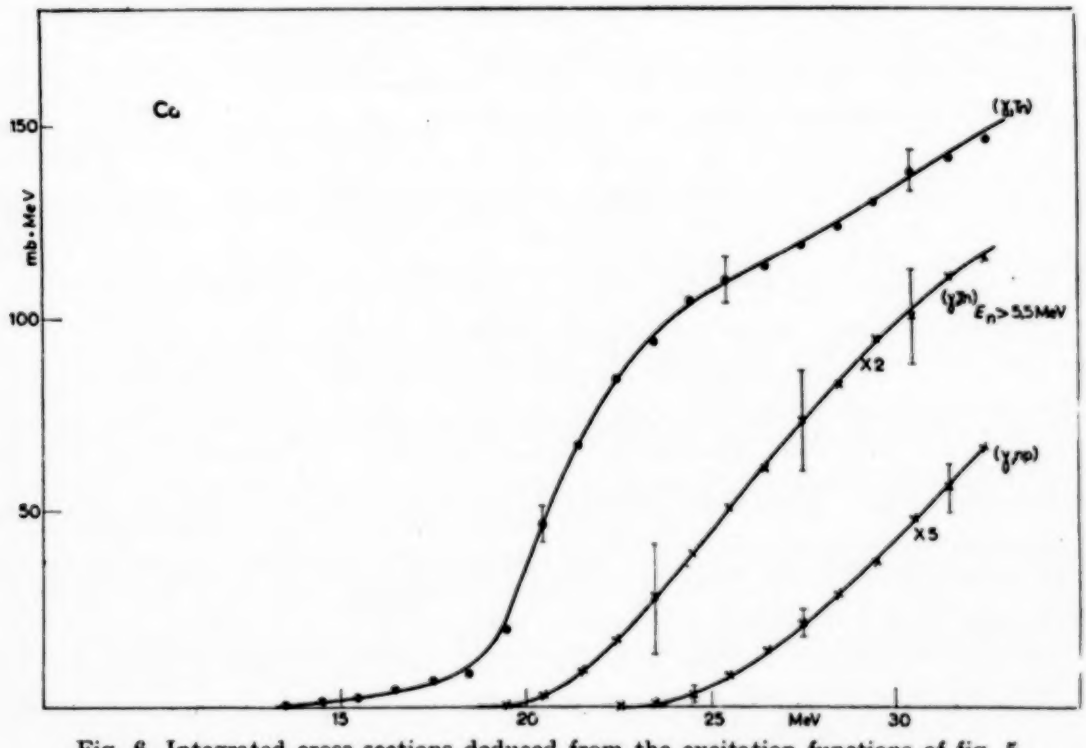

Fig. 6. Integrated cross sections deduced from the excitation functions of fig. 5.

Figs. 5, 6 and 7 contain the plots of the activation curves, of the integrated cross sections and of the cross sections, respectively.

2.3. GERMANIUM

Using natural powder Ge samples, the (γ, n) and (γ, np) yield curves in Ge^{70} were measured with the residual activity method, counting the β^+ activities from Ge^{69} and Ga^{68} by means of the coincidence technique. This detection method allows us to count only the β^+ activity, avoiding all troubles which can arise from the simultaneous activation of all Ge isotopes.

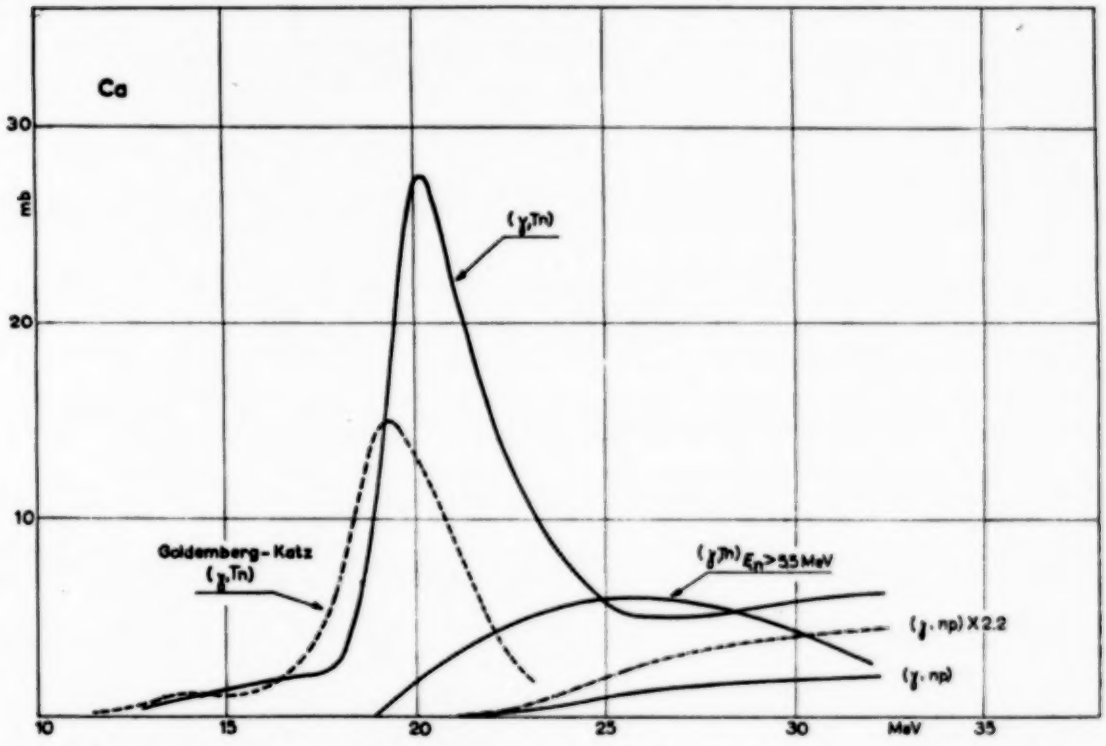

Fig. 7. Cross section for photonuclear processes of fig. 5. There are two curves which are related to the same (γ, np) processes. One (solid line) is deduced by analyzing the Ca^{40} $(\gamma, np)K^{38}_{g.s.}$ curve of fig. 5. The other (— · — · — line) is obtained by multiplying by 2.2 the preceding cross section, to take into account the photonuclear process which feeds the isomeric state of K^{38}.

The absolute value was obtained, as usual, by comparison with the (γ, n) yield in copper. The experimental results, i.e. the yield, the integrated cross sections and cross sections are plotted in figs. 8, 9 and 10.

2.4. REMARKS ON THE EXPERIMENTAL RESULTS

In some cases the measurement of the $(\gamma, {}^{np}_{d})$ processes by means of the residual activity method becames less indicative than one would expect, because the $(\gamma, 2n)$ reaction, which usually is followed by a β^+ activity, feeds the residual activity that is produced in the $(\gamma, {}^{np}_{d})$ reaction. If the latter process does not give rise to an activity much shorter than the former, the measured yield is a combination of the $(\gamma, {}^{np}_{d})$ and $(\gamma, 2n)$ yields. This is

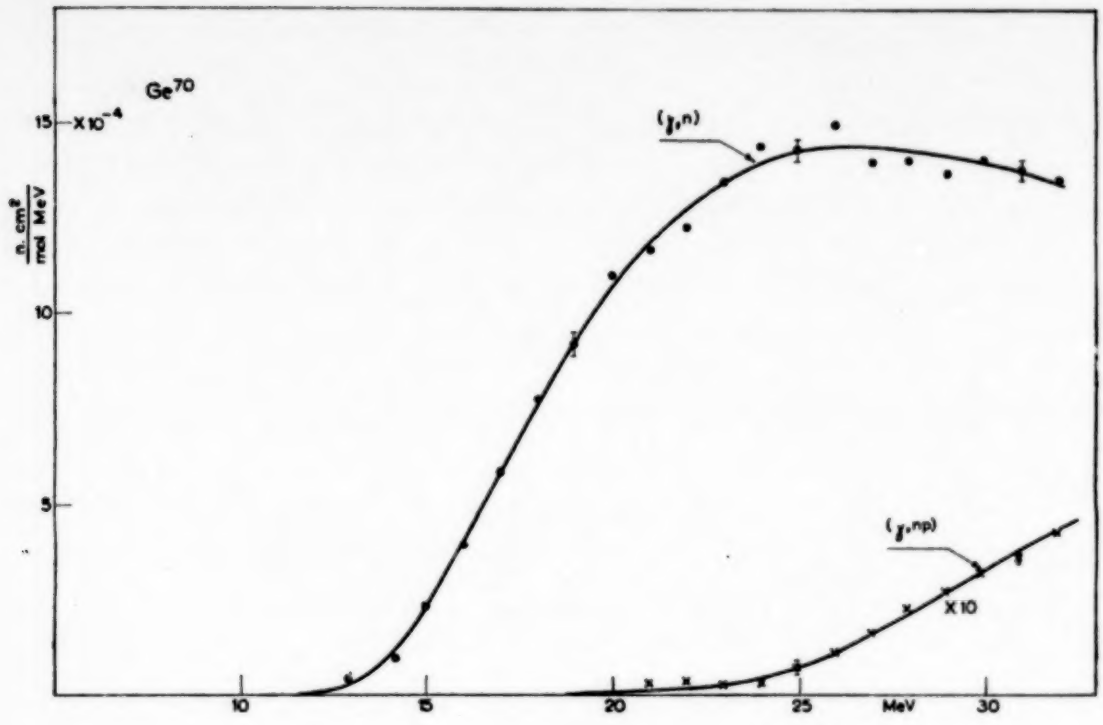

Fig. 8. (γ, n), (γ, np) excitation functions for Ge^{70}.

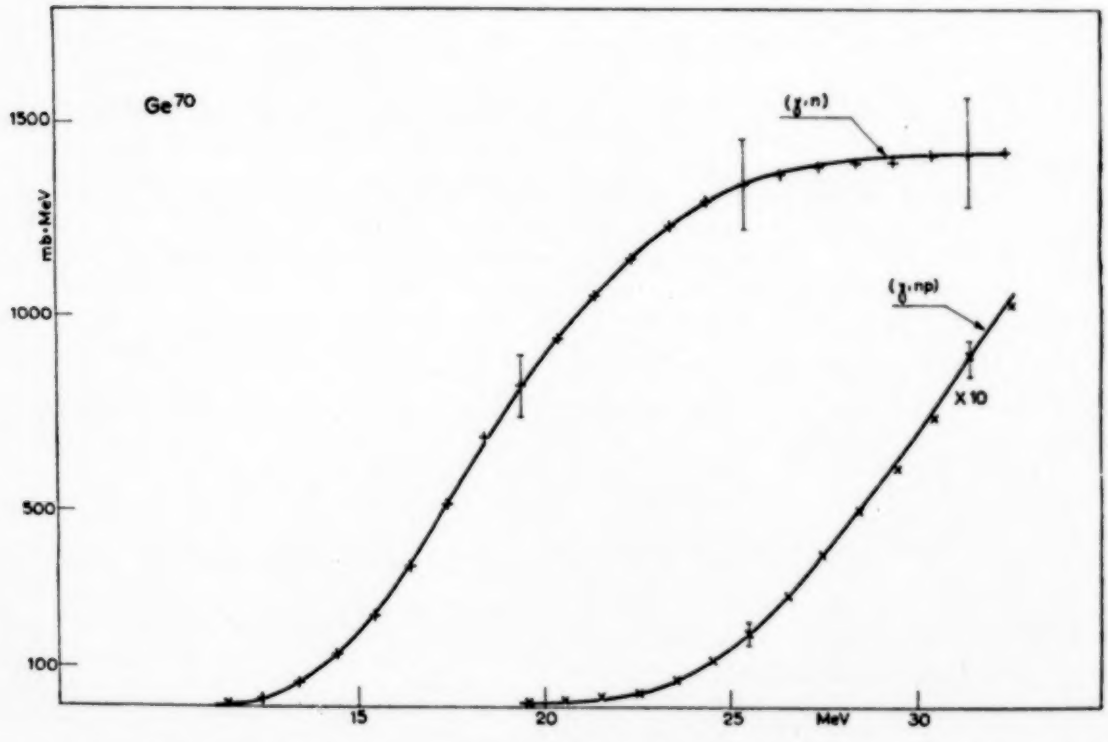

Fig. 9. Integrated cross section deduced from the excitation functions of fig. 8.

precisely the case for Ca^{40}, where the $(\gamma, 2n)$ activity has a half-life of only 0.66 sec that cannot be separated with certainty from either the 1 sec (γ, n) or the 0.95 sec $(\gamma, {}^{np}_{d})$ activities. No trouble arises, instead, in the case of Ge^{70}, where the $(\gamma, 2n)$ activity has a half-life of 250 d, to be compared with the 68 min (γ_d^{np}) activity.

Not so clear is the case of S^{32}. As a matter of fact S^{30} is still a white box in the Segrè chart. The semi-empirical mass formula would suggest, however, a smaller Q in the S^{30}—P^{30} than in the P^{30}—Si^{30} decay: consequently a longer half-life. Actually, from the total neutron yield, we can see that the $(\gamma, 2n)$

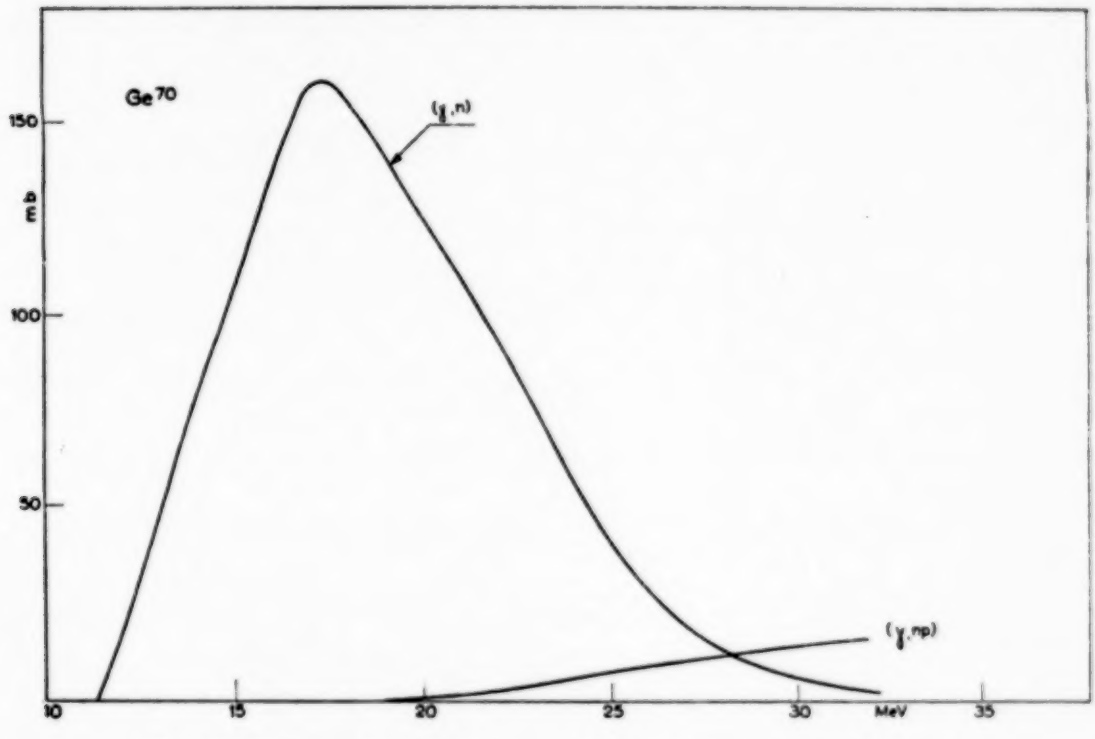

Fig. 10. Cross section for the two photonuclear processes of fig. 8.

cross section is certainly not very large at 30 MeV, not greater than 1 mb, or about $\frac{1}{4}$ of the (γ, np) cross section at the same energy (fig. 3).

Our results on the (γ_d^{np}) cross section in S^{32} are somewhat in disagreement with those of ref. [7]), previously obtained with a 22 MeV betatron. As a matter of fact, our experimental points are in very good agreement up to 25 MeV with the previous results, but we do not find a sharp peak at 26 MeV; on the contrary our cross section is still increasing slowly until 32 MeV (see fig. 3). We have tried to see if this experimental result could be explained by: α) saturation of the betatron core; β) insufficient knowledge of the sensitivity of our ionization chamber. As regards the first point, it can easily be shown that the core saturation could produce an electron energy, at the expansion time, lower than the value indicated by the measuring coils; the consequence would be a dis-

placement of any such peak to lower energy. The second doubt could be excluded because measurements done in our laboratory, measurements carried out at the N.B.S. [11]) and theory [12]) show that the sensitivity of the Al chamber does not change by more than 1 % between 20 and 30 MeV.

In the case of Ca both the maximum of the total neutron cross section and its integrated value are greater by a factor 1.8 than the results of ref. [13]), plotted for comparison in the same fig. 7 †. There is, indeed, a small difference in peak position not greater than 1 MeV, that could be attributed to a different calibration of the betatron energy scale and to the different method of yield curve analysis. On the contrary, the differences in the cross section absolute values are so great that they cannot be explained only in terms of a calibration error,

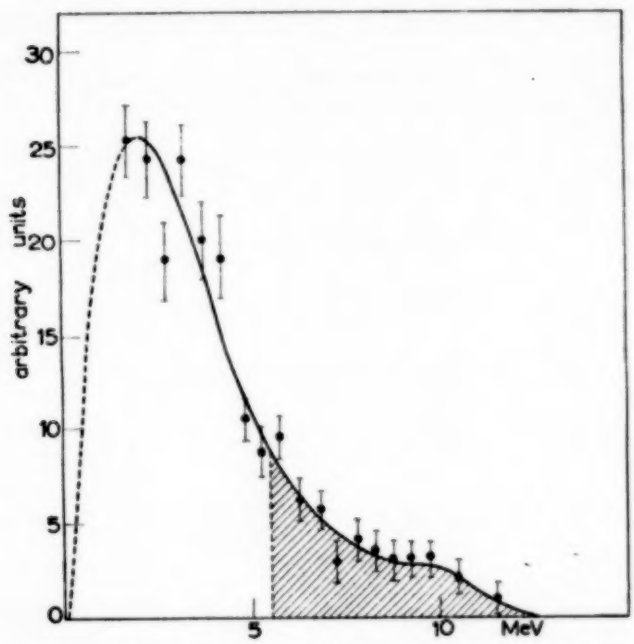

Fig. 11. Photoneutron spectrum of Ca at 30 MeV taken from ref. [14]).

taking also into account that the same calibration gives a (γ, Tn) cross section in S differing by no more than 10 % from the value given in ref. [8]). If, on the other hand, we decrease the total neutron cross section by a factor 1.8 we would obtain a value, at 25 MeV, lower than the fast neutron cross section.

In turn the ratio, at 30 MeV, between the fast neutron yield and the total neutron yield can be obtained also from the measurement [14]) on the photoneutron spectrum (fig. 11): actually this ratio (0.2) turns out to be still lower than our result (0.27). The peak in the fast neutron cross section at 25 MeV corresponds, taking into account the threshold value and the direct process of photoneutron emission, to the peak in the photoneutron spectrum.

† The fast decaying activities in calcium have also been measured, with the coincidence device at 30 MeV, obtaining 6.5×10^{-5} dis · cm²/mol · MeV. Using this figure and going back to 24 MeV, following the (γ, Tn) yield curve, we obtain 1.75×10^{5} dis./R · mol, in good agreement with ref. [14]).

3. Discussion

The continuum theory of nuclear reactions is usually the first method one can apply to interpret the experimental results, whatever be the particular reaction investigated.

Because the experimental data on sulphur are more complete than those on the other two elements, we shall limit the comparison with the statistical model to this element, sometimes supporting the conclusions with the results from the other elements investigated.

Following Heidmann and Bethe [16]) the statistical decay theory has been applied [17]) to calculate, at various excitation energies W, the following ratios:

$$\sigma(\gamma, \mathrm{np})/\sigma(\gamma, \mathrm{Tn}), \quad \sigma(\gamma, \mathrm{n})/\sigma(\gamma, \mathrm{Tn}), \quad \sigma(\gamma, \mathrm{Tp})/\sigma(\gamma, \mathrm{Tn}).$$

The level density has been chosen according to the well known relation

$$\omega(E) = a \exp(b\sqrt{E}),$$

where $b^2 = 0.14(A-12)\mathrm{MeV}^{-1}$ and $R = 1.4A^{\frac{1}{3}} \times 10^{-13}$ cm. The thresholds for the various processes are the following: (γ, n) 15 MeV; (γ, p) 9 MeV; (γ, np) 21 MeV; $(\gamma, 2\mathrm{n})$ 26 MeV; $(\gamma, 2\mathrm{p})$ 16 MeV and the proton Coulomb barrier is 5.2 MeV. In the above calculation the contributions from the (γ, α), $(\gamma, \mathrm{n}\alpha)$, (γ, d) and (γ, γ') reactions have been disregarded. There is a fairly good agreement for the first two ratios between the calculated and the experimental values, both in magnitude and behaviour versus excitation energy. The third ratio cannot be directly compared with the experiment because we know, at present, only the ratio between the total proton yield [18]) and the total neutron yield that turns out to be 1.4. Actually the theoretical value of the third ratio tells us that the photoproton number must be greater than the photoneutron number.

On the other hand, if we consider the data on the fast neutron cross section, we see that the statistical theory value of the fast neutron fraction associated with the (γ, np) process is ≈ 0.25 at 30 MeV, while the experimental value is very nearly 1. This last value has been obtained by subtracting directly from the $(\gamma, \mathrm{Tn})_{E_n \geq 5.5\ \mathrm{MeV}}$ cross section the (γ, n) cross section, the neutron associated to this last reaction being *certainly fast*, while the $(\gamma, 2\mathrm{n})$, $(\gamma, \mathrm{n}\alpha)$ reactions do not contribute to the fast neutron fraction †.

The disagreement is very peculiar and makes the (γ, np) reaction very different from other types of multiple processes. The fairly good agreement between the statistical decay theory and the experimental data completely loses its validity as soon as we take into account not only the cross sections but also the

† We must observe that the $(\gamma, \mathrm{np})_{E_n \geq 5.5\ \mathrm{MeV}}$ cross section is afffected by a large experimental error. The (γ, np) fast neutron fraction is, therefore, very uncertain, but its minimum value is still greater than 0.5.

spectrum of the emitted particles. Actually this fact is not peculiar to the present case but has been observed in other single particle photoreactions.

The fact that the (γ, np) reaction has so important a fast neutron fraction suggests that a direct process could be responsible for this situation. An explanation in this direction has been proposed by the Zürich group [10]). They observed that the dependence on Z of the (γ, np) cross section is more similar to the behaviour of the (γ, p) cross sections than to those of the (γ, n) reactions. For this reason they assumed that the (γ, np) reaction is essentially a (γ, p) process (partly direct and partly evaporative) followed by neutron evaporation. We think that, at least in the sulphur case, such an explanation would not work in view of the experimental results concerning the photoneutron spectrum associated to the (γ, np) reaction.

Actually the above statistical calculation indicates not only, that the (γ, pn) channel is less important than the (γ, np) one, but also that the fast neutron fraction at 30 MeV in the first channel is very nearly absent.

A direct process that can be taken in consideration is the extension to very low energies of the so called "quasi-deuteron model", suggested by Levinger [1]) to explain some features about photoprotons produced by very high energy photons. Some recent experiments of Whitehead *et al.* [19]) show that photoprotons from carbon are in agreement with the prediction of the quasi-deuteron model — in particular with the explicit calculations of Dedric [20]) — in the energy range between 50 and 100 MeV. The above evidence has suggested that a strong contribution to the (γ, np) cross section could come from this type of process also in our case. Although, at present, we cannot make a quantitative comparison because our data are not sufficient and the theory in its present state cannot be applied directly in this energy range. We may observe, however, that in all types of direct processes, in which neutrons and protons are treated on the same footing (as in the quasi-deuteron model), the spectrum of the emitted particles is symmetric between neutrons and protons: in the present case one would predict a fast neutron fraction smaller, than 50 %, the (γ, np) threshold being at 21 MeV, the detector threshold 5.5 MeV and the γ energy 30 MeV. To explain our data we have to assume, instead, that the neutron and proton spectrum is not symmetric around half the available energy.

As a matter of fact recent Wilson chamber experiments of a Russian group [21]) have shown that in the $He^4(\gamma, np)D$ reaction there is a rather important "dragging" effect of the proton on the deuteron recoil nucleus: that is, the angular correlation between deuteron and proton is not isotropic but peaks in the small angle region, causing therefore a conspicuous hardening of the associated neutron spectrum. From this point of view it would be particularly interesting to measure not only the neutron but also the proton spectrum associated with the (γ, np) reactions.

Independently from the above difficulty concerning the neutron spectrum, we may observe that a qualitative agreement between the quasi-deuteron model and the present results exists. Indeed:

a) the absolute value of the 30 MeV (γ, np) cross section is about one half of the theoretical prediction [22])

$$3.8\ (NZ/A)\sigma_{D},$$

which is plausible taking into account the nuclear reabsorption process and the Coulomb barrier;

b) the cross section shape is compatible with a large maximum located between 30 and 40 MeV;

c) integrating from 30 to 155 MeV the above quasi-deuteron cross section, a contribution to the integrated cross section of the right order of magnitude is obtained to complete the requirement of the E1 sum rule ($\approx$ 670 mb · MeV for S^{32}), while the absorption cross section [23]) integrated to 30 MeV does not yield more than $\approx$ 50 % of the above theoretical value.

Another direct interaction model which has been introduced by Sawicky to explain the large value of the $\sigma(\gamma, d)/\sigma(\gamma, p)$ ratio, considers the photodeuteron emission as a direct photonucleon excitation followed by a pick-up process. The model also predicts a knock-out process whose cross section should be of the same order of magnitude as the pick-up one [24]). The above photoprocess should have a very flat associated spectrum, therefore not in agreement with our experimental results. As a matter of fact, the shape of the measured (γ, np) cross section does not allow its interpretation as a sum of a (γ, d) and a (γ, np) reaction, as has been done in ref. [7]).

For the other two elements the discussion is severely limited because of the incompleteness of the experimental data. We may observe, however, that the absolute value of the (γ, np) cross section in Ca and Ge and the fast neutron fraction in calcium do not contradict the above tentative explanation.

In conclusion we can say that, at least in the measured elements, a large fraction of the (γ, np) cross section is due to a direct process, like in the quasi-deuteron model, rather than to a simple statistical decay. In order to put on a sounder basis the above statement, it is necessary, however, not only to perform more accurate and extensive experiments on the above elements, but to extend the investigation to many other elements in order to have a rather complete systematics of the (γ, np) reaction in the light element region at low energy. The experimental methods used in the present work are not convenient for this purpose and we have planned to proceed in this direction using the n—p coincidence method with large solid angle detectors.

Appendix

The coincidence experimental device consists of two NaI(Tl) (2″ × 2″) scintillators, looked by two 6292 Du Mont phototubes; the samples were placed

between the two opposite crystal detectors. The pulses, conveniently amplified, were received by a fast coincidence circuit; the output of one phototube was also analyzed with a single channel pulse height selector, centered on the 0.51 MeV γ ray. A slow coincidence circuit was fed by the output of the analyzer and the output of the fast coincidence. Usually the window of the pulse height selector was about 25 % of the base line; in this condition the analyzer and the slow coincidence output counting rates were in the ratio 2/1. The constancy of the coincidence apparatus was checked periodically with a small Na^{22} source.

For counting the fast decaying activities, like (γ, n) in S^{32} and Ca^{40}, the two phototubes and the samples were placed directly in the irradiation room with the two detectors perpendicular to the beam. The collimated X-ray beam had about the same diameter as the samples and to avoid a lowering in sensitivity of the phototubes, caused by a great light pulses occurring during the irradiation time, a negative voltage was applied to the shield of the phototube.

In order to have a complete β^+ conversion all the samples were enclosed in a thin cylindrical lead container; the axes of the containers were coincident with the phototube axis. In these conditions the equivalent volume of the samples becomes

$$[\pi(1+\tfrac{1}{2}\alpha^2 r^2)-(\tfrac{8}{3})\alpha r]r^2 d$$

where r is the radius of the cylindrical sample and α is the linear average attenuation coefficient for the bremsstrahlung γ rays. The absorption of the 0.51 γ rays, in this coincidence technique, turns out to be simply $\exp(-\delta d)$, where d is the height of the cylinder and δ the attenuation coefficient for 0.51 MeV γ rays.

References

1) J. S. Levinger, Phys. Rev. **84** (1951) 43
2) Y. M. Reid *et al.*, Congrès Int. Phys. Nucl. Paris 1958 (Dunod, 1959) p. 700; A. N. Gorbonnov and V. M. Spiridonov, *ibid.* p. 682
3) J. S. Levinger and H. A. Bethe, Phys. Rev. **78** (1950) 115
4) N. B. S. Handbook **55**, p. 33
5) A. S. Penfold and T. E. Leiss, Phys. Rev. **114** (1959) 1332; Phys. Res. Lab. University of Illinois (May 1958)
6) F. Ferrero *et al.*, Nuclear Physics **9** (1958/59) 32
7) L. Katz and G. W. Cameron, Can. J. Phys. **29** (1951) 518
8) R. Montalbetti, L. Katz and J. Goldemberg, Phys. Rev. **91** (1953) 659
9) J. E. Cline and P. R. Chagnon, Phys. Rev. **108** (1957) 1945
10) A. Hofmann and P. Stoll, Helv. Phys. Acta **31** (1958) 591
11) J. S. Pruitt and S. R. Domen, N.B.S. 6218
12) B. M. Flowers, J. O. Lawson and E. B. Fossey, Proc. Phys. Soc. B **65** (1952) 286
13) J. Goldemberg and L. Katz, Can. J. Phys. **32** (1954) 59
14) A. Agodi *et al.*, Congrès Int. Phys. Nucl. Paris 1958 (Dunod, 1958) p. 625
15) R. G. Summer Gill, R. N. H. Haslam and L. Katz, Can. J. Phys. **31** (1953) 70
16) J. Heidmann and H. A. Bethe, Phys. Rev. **84** (1951) 274
17) S. Costa, private communication

18) B. Cujec-Dobovisek, Congrès Int. Phys. Nucl. Paris 1958 (Dunod, 1958) p. 634
19) C. Whitehead *et al.*, Phys. Rev. **110** (1958) 941
20) K. G. Dedrick, Phys. Rev. **100** (1955) 58
21) A. N. Gorbulov and V. M. Spiridov J.E.T.P. **6** (1958) 16; **7** (1958) 596; **7** (1958) 600
22) A G. Odian, P. C. Stein, A. Wattaenberg, B. T. Feld and R. Weinstein Phys. Rev. **102** (1956) 837
23) J. Kockum and N. Starfelt, Nucl. Instr. **5** (1959) 37
24) J. Sawicki and W. Czyż, Nuclear Physics **4** (1956) 248

2.B

Nuclear Physics **15** (1960) 452—463; © *North-Holland Publishing Co., Amsterdam*

Not to be reproduced by photoprint or microfilm without written permission from the publisher

ENERGY AND ANGULAR DEPENDENCE OF THE LEFT-RIGHT ASYMMETRY OF D—D NEUTRONS SCATTERED BY CARBON

P. S. DUBBELDAM †, C. C. JONKER and H. J. BOERSMA

Natuurkundig Laboratorium der Vrije Universiteit, Amsterdam

Received 2 December 1959

Abstract: The left-right asymmetry in the intensity of neutrons from the D—D reaction, scattered by carbon, was measured for deuteron energies between 300 and 500 keV, at two angles $\vartheta_{\text{lab}} = 50°$ and 22° 30′, with a gold "drive-in" target. The polarization vector was turned by the magnetic field of a solenoid, and the detectors remained in a fixed position. From the comparison of the computed energy average of the effect with the experimental values it follows that the analysing properties of C^{12} derived from the phase analysis of Meier *et al.* [9]) give a much better agreement than those according to Wills *et al.* [18]). The experiments could not decide upon the possible existence of a sin $4\vartheta_1$ dependence of the differential polarization of the D—D neutrons. From the energy dependence of the differential polarization taken from other authors it follows that, within the limits of the description of the D—D reaction by Beiduk, Pruett and Konopinski, indeed other non-central forces besides the tensor force are present in the nucleon-nucleon interaction.

1. Introduction

The polarization of the neutrons originating from the D—D reaction can be measured by means of the left-right asymmetry in the intensity that results when one scatters the neutron by a spin-0 nucleide, usually He^4 or C^{12} [1–13]). The relative left-right asymmetry R is defined as

$$R(\varphi) = \frac{N(\varphi) - N(180° + \varphi)}{N(\varphi) + N(180° + \varphi)}; \tag{1}$$

$N(\varphi)$ and $N(180° + \varphi)$ are the numbers of neutrons counted by two detectors with equal efficiencies in diametral positions; φ is the azimuth, or the angle between reaction and scattering plane.

In the ideal case of a mono-energetic source, point scatterer, and point detectors the following formula applies, according to the theorem of Wolfenstein:

$$R_{\text{th}}(\varphi) = P_1 P_2 \cos \varphi; \tag{2}$$

P_1 is the magnitude of the polarization of the initial beam of neutrons, which is perpendicular to the reaction plane; P_2 is the magnitude of the polarization that would result if an unpolarized beam of neutrons were scattered by the same

† Present address: Phys. Dept. Un. of Wisconsin, Madison, Wisconsin.

nucleide; it is perpendicular to the scattering plane. P_1 is a function of the deuteron energy E_D and the angle ϑ_1 between deuteron and neutron beam; P_2 is a property of the scattering material and depends on the neutron energy E_n and the scattering angle ϑ_2.

In general one measures the asymmetry by rotating the neutron detector from one position to the diametral one. We have shown [3]) that it is advantageous to turn instead the polarization vector by means of a solenoid. The quoted reference gives the details of our method.

With our method we measured the left-right asymmetry at several energies E_D that are covered by our neutron generator. We used again a gold "drive-in" target; $\vartheta_{2\,\mathrm{lab}}$ was 42°. We performed these measurements at two angles $\vartheta_{1\,\mathrm{lab}} = 50°$ and 22°30′. These angles are such, that the influence of the third term in the formula of Fierz [14]) for the differential polarization † of D—D neutrons

$$\Pi(E_D, \vartheta_1) = \sigma_1(E_D) a \sin 2\vartheta_1 + \sqrt{\sigma_0 \sigma_2}\,\alpha \sin 2\vartheta_1 + \sigma_2(E_D)\beta \sin 2\vartheta_1 (3\cos^2\vartheta_1 - 1) \qquad (3)$$

would be most conspicuous (σ_0, σ_1, σ_2 are the approach cross sections defined in ref. [15])). In our energy region this term is zero for about $\vartheta_{1\,\mathrm{lab}} = 50°$, and maximum for about $\vartheta_{1\,\mathrm{lab}} = 22°30'$. This term is important, because its existence would prove, within the limits of the description of the D—D reaction by Beiduk, Pruett and Konopinski [15]), that other non-central forces besides the tensor force are present in the nucleon-nucleon interaction.

2. Measurements and Corrections

The values for R (i.e. $R(\varphi)$ for $\varphi = 0°$ or 180°) from the measurements are given in tables 1 and 2 for $\vartheta_{1\,\mathrm{lab}} = 50°$ and 22°30′, respectively, at several values of E_D, for the two detectors separately, and the average R for both detectors. The values of R have been corrected for the influence of the magnetic field of the solenoid on the photomultipliers (see ref. [3])). The values of R are shown in figures 1 and 2. The curves in these figures are discussed in section 3.

As to the geometrical corrections, only the finite size of the scatterer and detectors had to be taken into account. We computed their influence following the method of McCormac, Steuer, Bond and Hereford [7]). The factor with which the measured R should be multiplied is 1.03. We neglected this correction, in view of the obtained accuracy.

Because the size of our carbon scatterer is of the same order of magnitude (4 cm) as the scattering mean free path, plural scattering effects will occur. It is very difficult to compute this correction, because the differential scattering

† The differential polarization Π is defined by

$$P_1 = \frac{\Pi}{\sigma(\vartheta_1)},$$

where $\sigma(\vartheta_1)$ is the differential cross section.

cross section depends also on the azimuth, due to the polarization, and the P_2 in (2) for carbon varies strongly with the neutron energy (see below). We tried to find an upper limit for the correction along the following lines.

TABLE 1

Experimental values of R as a function of E_D at $\vartheta_{1\,lab} = 50°$

E_D (keV)	R in % Upper detector	R in % Lower detector	Weighed average of R
300	-3.1 ± 0.9	3.3 ± 1.1	$3.2\ \pm0.8$
350	-3.7 ± 0.6	1.9 ± 0.9	$3.1\ \pm0.5$
400	-1.9 ± 0.8	2.5 ± 1.1	$2.1\ \pm0.7$
450	-2.9 ± 0.6	2.6 ± 1.0	2.85 ± 0.5
500	-2.7 ± 0.9	3.4 ± 1.3	2.95 ± 0.7

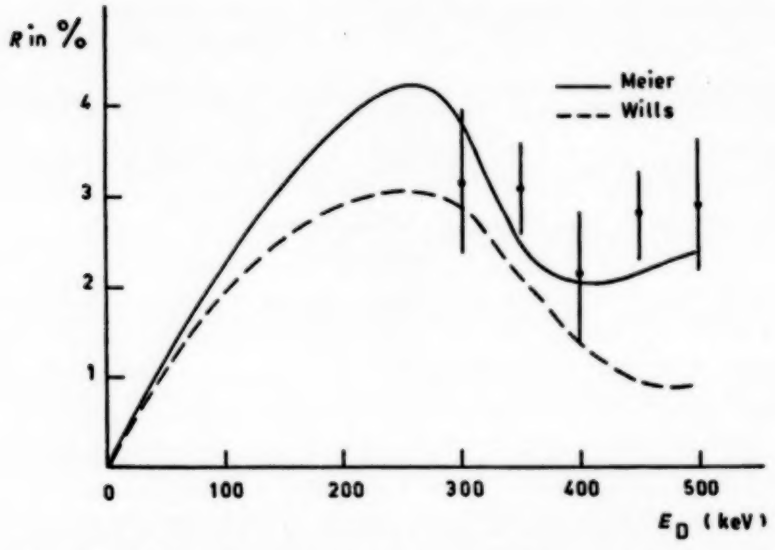

Fig. 1. R as a function of E_D at $\vartheta_{1\,lab} = 50°$. The curves are computed from other experimental data, taking into account the energy spread.

We computed the influence of the second scattering for unpolarized neutrons, following the method of Blok and Jonker [16]), taking into account the fact that our scatterer is finite in the direction perpendicular to the primary neutron beam. We determined the ratio of the number of once and twice scattered neutrons that reach the detector (I_1 and I_2) to the theoretically important number of neutrons that are scattered once into the direction of the detector (I_{th}). We found $I_1/I_{th} = 77$ % and $I_2/I_{th} = 12$ %. If we suppose that the ratio I_3/I_2 is about the same as I_2/I_1 etc., we can neglect the higher order scattering in view of our accuracy. Then the factor $(I_1+I_2)/I_{th} = 89$ % gives the amount by which the denominator of the definition (1) of R is too small in the measure-

ment. The contribution of the once scattered neutrons to the left-right difference in the numerator, divided by the theoretical value of the numerator, is 77 %.

We do not know the contribution of the twice scattered neutrons to the numerator, but it is not to be expected that it has the wrong sign, or is equal to

TABLE 2

Experimental values of R as a function of E_D at $\vartheta_{1\,lab} = 22° 30'$

E_D (keV)	R en % Upper detector	R in % Lower detector	Weighed average of R
300	-1.8 ± 0.5	1.0 ± 0.8	1.5 ± 0.4
350	-0.9 ± 0.45	2.1 ± 0.5	1.4 ± 0.3
400	-2.3 ± 0.4	2.7 ± 0.5	2.4 ± 0.3
450	-1.5 ± 0.7	2.8 ± 0.7	2.1 ± 0.5
500	-2.4 ± 0.5	1.6 ± 0.7	2.15 ± 0.4

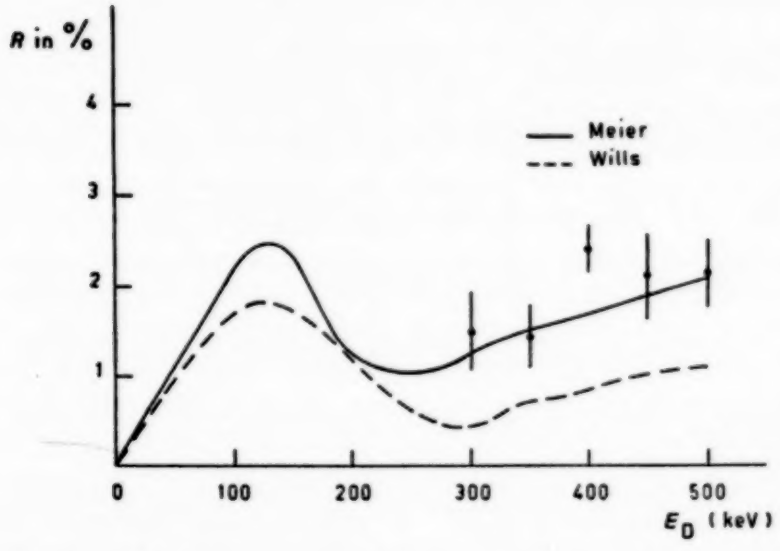

Fig. 2. R as a function of E_D at $\vartheta_{1\,lab} = 22° 30'$. The curves are computed from other experimental data, taking into account the energy spread.

zero, because, if e.g. the first scattering is preferably to the left, this will also be valid for the second scattering, as the density of the second scattering centres is larger in the left half than in the right half of the scatterer, and the screening effect for the left (twice) scattered neutrons accordingly smaller. Therefore, if we exclude the possibility that the second scattering would give a left-right difference of the opposite sign, the upper limit for the deviation of the numerator is found if we put the contribution of the second scattering zero, (i.e. complete symmetry). Then it is possible to say that the correction factor for the measured left-right asymmetry will not be larger than $\frac{77}{89}$ (= 87 %). The actual correction factor will be probably closer to 1. Because the upper limit of this correction,

a difference of 13 %, is smaller than the accuracy obtained, we feel justified not to make the complicated computations that are necessary to find a more accurate value for this correction.

3. Analysis and Discussion of the Results

3.1. ENERGY SPREAD OF THE NEUTRONS FROM A THICK TARGET

Because we used a thick target it is necessary to consider the influence of the energy spread on the measured left-right asymmetry, in order to compare our results with the published data. The spread in the neutron energy is small, relatively, but the polarization is a function of the deuteron energy, and this ranges from zero to the value of the energy of the deuterons in the beam.

The shape of the neutron spectrum, as a function of the deuteron energy, is given by

$$\mathrm{d}N(E_\mathrm{D}) = C\rho_\mathrm{D}(z)\sigma(E_\mathrm{D}, \vartheta_1)\left(\frac{\mathrm{d}E_\mathrm{D}}{\mathrm{d}z}\right)^{-1}\mathrm{d}E_\mathrm{D} \tag{5}$$

where $\rho_\mathrm{D}(z)$ is the density of the deuterons in the metal, at a depth z; $\sigma(E_\mathrm{D}, \vartheta_1)$ is the differential reaction cross section; $\mathrm{d}E_\mathrm{D}/\mathrm{d}z$ is the energy loss of the deuterons in the metal per unit length; E_D and z are connected by the range-energy relation for deuterons in the metal in question; C is a constant.

The density distribution ρ_D follows from the diffusion equation for the deuterons in the metal (Fiebiger [17])

$$J = -\alpha\frac{\mathrm{d}\rho_\mathrm{D}}{\mathrm{d}z}, \tag{6}$$

where J is the current of diffusing D-atoms and α the diffusion constant. The D-atoms are supposed to come from a plane source formed by the beam, with strength Q at a depth $z = R(E_\mathrm{D})$, where $R(E_\mathrm{D})$ is the range of the deuterons with energy E_D in the metal. The solution of (6) in the asymptotic case of saturation ($t \to \infty$), where $J = -Q$, and for α is a constant, is

$$\rho_\mathrm{D} = \frac{Q}{\alpha}z. \tag{7}$$

If one approximates $\sigma(E_\mathrm{D}, \vartheta_1)$ by a straight line, and takes $\mathrm{d}E_\mathrm{D}/\mathrm{d}z$ to be constant, the resulting spectrum has the form of a parabola, with two zeros at $E_\mathrm{D} = 0$ and $E_\mathrm{D} = E_{\mathrm{D\,max}}$, the energy of the deuterons in the beam. Computing the spectrum numerically with the experimental data for the mentioned factors we found a curve that indeed differed little from a parabola. Therefore we approximated the spectrum by a parabola in the averaging procedure described below.

In the solution of (6) we supposed that α is constant. Because α increases strongly with the temperature this is true only if the temperature does not change in time and with the place in the metal. If α were a constant the neutron yield should increase quadratically with the ion current at constant cross section of the beam. However, because of strong local heating of the metal, the temperature, and therefore α, will increase with the ion current. Thus it is understandable that in the experiment described in ref. [3]), where the beam was well focussed, we found a maximum in the yield-current dependence instead of a quadratic increase. Another effect occurs at high values of the beam current. Because the developed heat is mainly transported through the bulk of the target metal, a temperature gradient will exist along the track of the deuterons, and α will be a function of z. Then the density ρ_D will not be a linear function of z, but it will be appreciably smaller near the surface of the metal. Thus there will be less neutrons that are produced by deuterons with high energy. We shall then still approximate the spectrum by a parabola, but this has now its second zero at a value E_D^* that is lower than the energy $E_{D\,max}$ of the deuterons in the beam. We will call the place of the top of the parabola the effective deuteron energy $E_{D\,eff} = \frac{1}{2}E_D^*$.

This phenomenon of the shift in effective energy, due to the temperature conditions in the metal (in our case gold) can be used for the explanation of a discrepancy between the result for R given in ref. [3]), viz. $R = (4.6 \pm 0.2)$ % at $E_D = 450$ keV, with the present results, which give $R = (2.85 \pm 0.5)$ % at $E_D = 450$ keV. Apparently the strong heating of the gold in the former experiment, due to the well-focussed beam, caused a temperature gradient, and consequently a shift in the spectrum to lower energies. The solid curve in fig. 1, described below, shows that a shift of the second zero of the parabola, E_D^*, from 450 keV to 250 keV, and thus a shift in the effective energy from 225 keV to 125 keV could give a value for R that is very near to the value measured in the former experiment.

These conditions did not exist in the present experiment. For now the focussing of the beam was bad, due to a leak in the vacuum system, as could be seen by watching the beam when shooting with protons. As a consequence the local heating of the target was much less. This showed up in the fact that no maximum was reached in the yield-current dependence, and that one needed a finite time to reach the maximum in the yield when shooting on a fresh gold surface (the time needed to reach saturation of deuterons in a metal is inversely proportional to the diffusion constant). The agreement between the solid curves and the experimental points in figs. 1 and 2 indicate that now no apparent shift of the effective energy occurs.

3.2. THE ENERGY AVERAGE OF THE LEFT-RIGHT ASYMMETRY

The curves in figs. 1 and 2 are computed from published values for P_1 and P_2

by averaging R over the energy spectrum in the following way. As the expression for the differential cross section for the (n, C^{12}) scattering has the form

$$\sigma(\vartheta_2, \varphi) = \sigma_0(\vartheta_2)(1+P_1 P_2 \cos\varphi), \tag{5}$$

we could write for the average R

$$\bar{R} = \frac{\int_0^{E_{D\,max}} \sigma_0(E_n, \vartheta_2) P_1(E_D, \vartheta_1) P_2(E_n, \vartheta_2) \sin \frac{aI}{\sqrt{E_n}} N(E_D) dE_D}{\int_0^{E_{D\,max}} \sigma_0(\vartheta_2) N(E_D) dE_D}. \tag{6}$$

We derived the different factors as follows, for the case $\vartheta_{1\,lab} = 50°$: $\sigma_0(E_n, \vartheta_2)$

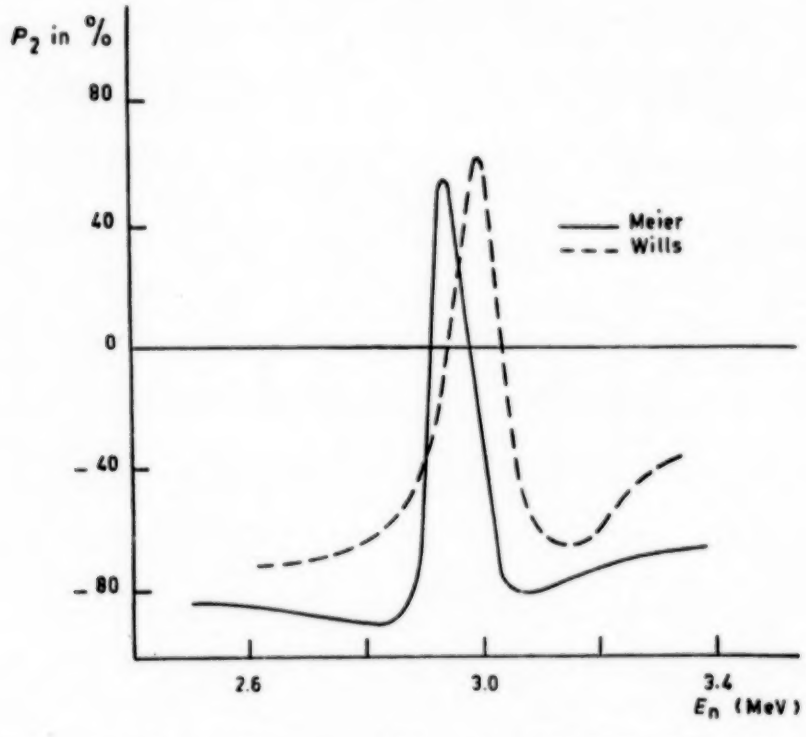

Fig. 3. P_2 as a function of E_n for C^{12}, computed from the coefficients of Meier [9]), and taken from the figure of Wills [18]), $\vartheta_{2\,lab} = 45°$.

from the graphs for the n—C^{12} differential cross section of Meier [9]); $P_1(E_D, \vartheta_1)$ from the low energy polarization experiments of Pasma [10]), approximated by $P_1(\text{in } \%) = \sqrt{0.18 E_D(\text{keV})}$; P_2 from the work of Meier [9]) and of Wills [18]), as shown in fig. 3. Thus we find two values for R to be compared with our experiments. $N(E_D)$ is approximated by a parabola, with its two zeros at $E_D = 0$ and at the energy $E_{D\,max}$ of the deuterons in the beam. The current through the solenoid, I, was so near to the optimum value, that the sine is practically 1.

To obtain the values for R in the case that $\vartheta_{1\,lab} = 22°30'$, we have to know $P_1(22°30')$. We suppose, to start with, that the differential polarization can be described by a sin 2ϑ angular dependence. Then we can compute $P_1(22°30')$

from the $P_1(50°)$ that is taken from experimental data, as discussed before, according to

$$P_1(E_D, \vartheta_{1\,\mathrm{lab}} = 22°30') = \frac{\sin 2\vartheta_1}{\sin 2\vartheta'_1} \frac{\sigma(E_D, \vartheta'_1)}{\sigma(E_D, \vartheta_1'')} P_1(E_D, \vartheta_{1\,\mathrm{lab}} = 50°); \quad (7)$$

ϑ'_1 and ϑ_1'' are the c.m.s. angles that correspond to the lab-angles 50° and 22°30′, respectively. We neglect here the transformation of the solid angle. We took the values of $\sigma(E_D, \vartheta)$ from the experiments of Chagnon and Owen [19]) combined with the experiments of Fuller, Dance and Ralph [20]). With this $P_1(22°30')$ the same averaging method was applied. The results are given as solid curves (Meier) and as dashed curves (Wills) in figs. 1 and 2. One sees that the positive peaks in fig. 3 result in dips in the R versus E_D curves. The dip shifts to a lower value for E_D at $\vartheta_{1\,\mathrm{lab}} = 22°30'$, because the same neutron energy is reached for a lower value of E_D. The curves, computed with the P_2 of Meier are in much better agreement with the experiments than those computed with the P_2 of Wills. Because the curves in figs. 1 and 2 that were computed on the base of a sin 2ϑ dependence of the differential polarization give a very satisfactory agreement of the computed R with the experimental points, there is no need within the accuracy of the experiment of adding a term with sin 4ϑ dependence to the expression of the differential polarization like in Fierz's formula (4). One cannot conclude from this that this term does not exist, because in the energy region in question D-waves are not yet very important, which is necessary for the occurrence of this term.

There is one paper in which the authors reach the conclusion that the phase analysis of Wills is preferable to that of Meier, contrary to our opinion: Steuer *et al.* [13]) report a value for the left-right asymmetry of $-(7.3\pm0.7)$ %, at $E_D = 750$ keV and $\vartheta_{2\,\mathrm{lab}} = 135°$. This is the mean value of the result of an experiment with a thick heavy ice target, using a coincidence technique, and of a result obtained in the same laboratory, with a "drive-in" target. One wonders, in the first place, whether it is allowed to average over two values obtained for two spectra that are probably very different. For, as we have seen, the neutron spectrum from a metal target as a function of the deuteron energy is approximately a parabola, because the density of the deuterons increases linearly with the depth from a value zero at the surface. In the same approximation we could represent the spectrum from a heavy ice target by a straight line passing through the origin, because the density of the deuterons is constant. Steuer says that P_2 computed for their energy distribution gives a value $P_1(53°) = -(8.4\pm0.8)$ %, when using the phase shifts of Meier, and a value $P_1(53°) = -(14.5\pm1.4)$ %, when using the phase shifts of Wills. The latter value then should be in better agreement with the results of Levintov *et al.* [6]) and Pasma [10]). We found the value for P_1 from the curve drawn by Pasma through his and others' results; at the energy in question ($E_D = 750$ keV) it is

12 %. We have computed the value for the average left-right asymmetry for a linear neutron spectrum at $\vartheta_{2\,\mathrm{lab}} = 135°$ and $E_D = 750$ keV with the method described before. We then find $\bar{R} = 1.2$ %, when using the P_2 of Wills and $\bar{R} = 5.2$ % when using the P_2 of Meier. Though neither value falls within the limits of Steuer's value for R, the last one is much nearer to it, and therefore it seems that also on the basis of this experiment the phase analysis of Meier is preferable.

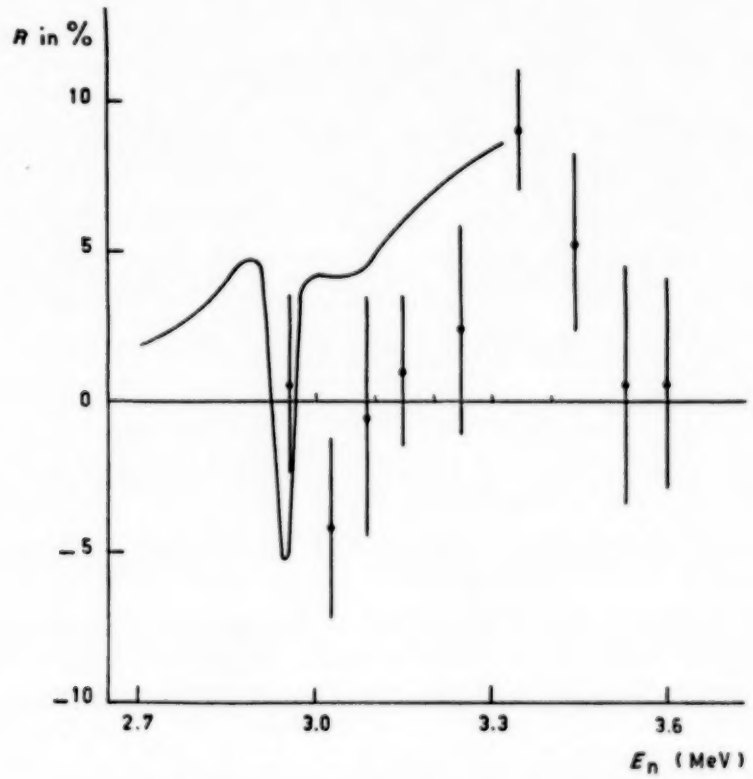

Fig. 4. Experimental values for R, according to Baumgartner, compared with the curve computed on the basis of Meier's phase analysis.

It seems that also the results of Baumgartner and Huber [1]) point towards the positive peak in the $P_2(E_n)$ curves. To check this we transformed the left-right ratio into the R and computed P_2 for $\vartheta_{2\,\mathrm{lab}} = 78°$ from the coefficients of Meier. (The corresponding values of Wills could not be computed, because he does not give the relevant coefficients.) We multiplied this P_2 with the corresponding P_1 to obtain the left-right asymmetry for a thin target that can be directly compared with the experimental points. This is shown in fig. 4. We see that indeed the computed curve represents very well the general behaviour of the experimental points. Only the energy scale for the computed curve is about 90 keV lower than the scale for the experimental points. There are several possible causes for this, as well on the experimental side, as in the

computation of P_2, which especially at angles near 90° is very sensitive to details in the phase shifts.

4. The Differential Polarization of D—D Neutrons

It was not possible to conclude from our experiments to the existence of the third term in the formula of Fierz for the differential polarization of D—D neutrons (4). We tried to find this term from the angular dependence of Π. This term has also an influence on the energy dependence of Π because the approach cross sections σ_1 and σ_2 behave quite differently as a function of the deuteron energy. The energy dependence of the second term is given by $\sqrt{\sigma_0\sigma_2}$ and this expression has about the same energy dependence as σ_1 at low energies. Therefore we computed Π from the published measurements of P_1 made with a thin target. The differential polarization follows from P_1 according to the formula (3).

TABLE 3

Values of P_1, $\sigma(\vartheta_1)$ and $\Pi = P_1\sigma(\vartheta_1)$ as a function of the deuteron energy for different angles, according to several authors

Reference	$\vartheta_{1\,\mathrm{lab}}$	E_D (keV)	$-P_1$ (%)	$\sigma(\vartheta_1)$ (mb)	$-\Pi$
Levintov *et al.* [6])	49°	900	13.7±0.4	5.76	0.79±0.02
		1200	13.8±1.4	9.3	1.28±0.08
		1500	15.8±0.9	10.2	1.61±0.09
		1800	16.8±1.0	10.9	1.83±0.11
Pasma [10])	47°	200	5.8±2.5	1.87	0.11±0.05
		300	9.0±2.3	2.78	0.25±0.06
		350	8.2±2.4	3.18	0.26±0.08
		400	8.7±1.1	3.55	0.31±0.04
		450	9.5±1.3	3.90	0.37±0.05
		500	9.1±0.8	4.22	0.38±0.03
Meier *et al.* [9])	49°	600	10.6±1.1	4.57	0.48±0.05
Baumgartner *et al.* [1]) and Budde *et al.* [2])	45°	600	18.0±7.0	4.99	0.90±0.35

In table 3 we give the values of P_1 for thin target measurements and add the values of $\sigma(\vartheta_1)$ obtained by combining the experiments of Chagnon and Owen[19]) with those of Fuller, Dance and Ralph [20]), and the values of Π found by multiplying P_1 and $\sigma(\vartheta_1)$. It is true that the values of P_1 are not all measured at precisely the same angle ϑ_1 but in our opinion this will not influence our conclusions. We wish to remark, however, that the angle is very near to the value

for which $(3\cos^2\vartheta_1 - 1)$ is zero, and thus not favourable for the evidence of this term. The values of Π as a function of E_D are shown in fig. 5. The solid curve in this figure is proportional to the first term of Fierz' formula, $\sigma_1 a \sin 2\vartheta_1$. Above $E_D = 1$ MeV the curve is dashed, because the analysis of Fierz is only valid to about this value. One sees that up to E_D about 500 keV there is good

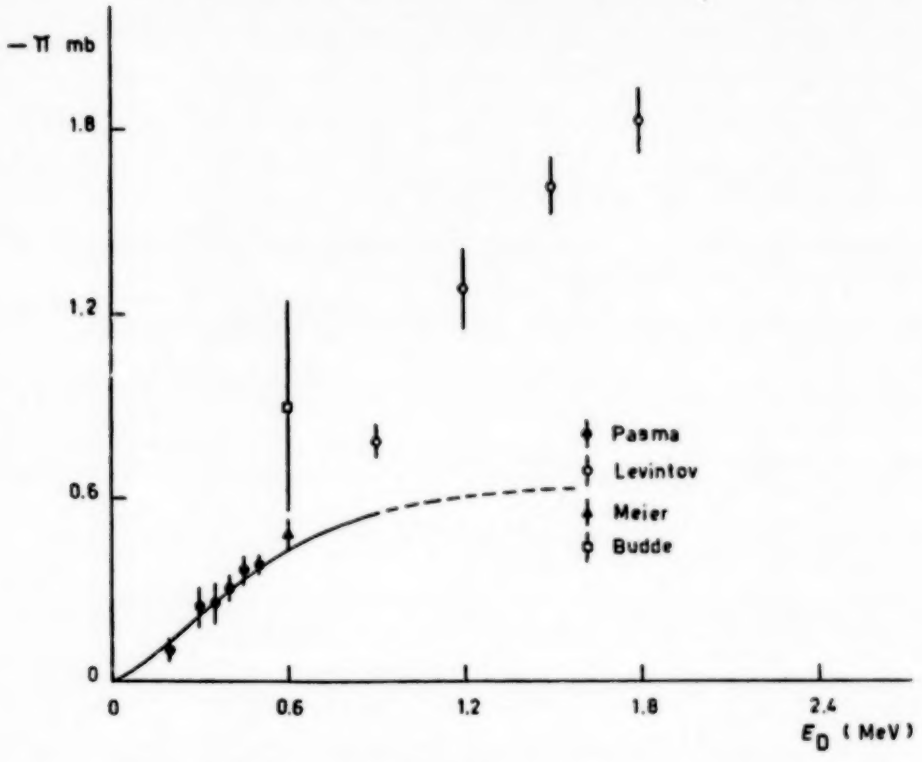

Fig. 5. Values of Π as a function of E_D. The solid curve represents $\sigma_1 a \sin 2\vartheta_1$ fitted to experimental points.

agreement with the experimental points. At higher energies it is impossible to make a fit to the points without introducing the next approach cross section σ_2. This can only supply a new term to the expression for Π if other than tensor forces are present. Therefore we conclude that, within the limits of BPK's description of the D—D reaction, it is necessary to assume that other non-central forces besides the tensor force are present in the nucleon-nucleon interaction. If one allows that the curve has an inflection point above 1 MeV, the points at higher energy cannot influence the curve at energies up to 1 MeV, where the analysis of Fierz is still valid. Then our conclusion is based only on the point of Levintov *et al.* at $E_D = 900$ keV. It will be useful to have more experimental data in this energy region. It is better, however, to have a series of values of Π at $\vartheta_{1\,\mathrm{lab}} = 22°30'$ where the relevant term has a maximum.

A more detailed description of this research is given in a thesis [21]). We wish to thank S. S. Klein for his help in performing the measurements and computa-

tions, one of us (H. J. B.) is indebted to the Foundation of Fundamental Research of Matter (Stichting F.O.M.) for a study grant.

References

1) E. Baumgartner and P. Huber, Helv. Phys. Acta **26** (1953) 545
2) R. Budde and P. Huber, Helv. Phys. Acta **28** (1955) 49
3) P. S. Dubbeldam, C. C. Jonker and F. J. Heemskerk, Nuclear Instruments **4** (1959) 234
4) P. P. Kane, Nuclear Physics **10** (1959) 429
5) I. I. Levintov, A. V. Miller and V. N. Shamshev, Nuclear Physics **3** (1957) 221
6) I. I. Levintov, A. V. Miller, E. Z. Tarumov, and V. N. Shamshev, Nuclear Physics **3** (1957) 237
7) B. M. McCormac, M. F. Steuer, C. D. Bond and F. L. Hereford, Phys. Rev. **104** (1956) 718
8) B. M. McCormac, M. F. Steuer, C. D. Bond and F. L. Hereford, Phys. Rev. **108** (1957) 116
9) R. W. Meier, P. Scherrer and G. Trumpy, Helv. Phys. Acta **27** (1954) 577
10) P. J. Pasma, Thesis, Groningen, 1958
11) P. J. Pasma, Nuclear Physics **6** (1958) 141
12) R. Ricamo, Nuovo Cimento **10** (1953) 1607
13) M. F. Steuer, W. P. Bucher and F. L. Hereford, Comptes Rendus du Congrès International de Physique Nucléaire, Dunod, Paris (1958) 545
14) M. Fierz, Helv. Phys. Acta **25** (1952) 629
15) F. M. Beiduk, J. R. Pruett and E. J. Konopinski, Phys. Rev. **77** (1950) 622
16) J. Blok and C. C. Jonker, Physica **18** (1952) 809
17) K. Fiebiger, Z. angew. Phys. **9** (1957) 213
18) J. E. Wills, J. K. Bair, H. O. Cohn and H. B. Willard, Phys. Rev. **109** (1958) 891
19) P. R. Chagnon and G. E. Owen, Phys. Rev. **101** (1956) 1798
20) J. C. Fuller, W. E. Dance and D. C. Ralph, Phys. Rev. **108** (1957) 91
21) P. S. Dubbeldam, Measurement of the polarization of D–D neutrons by a solenoid, Thesis Free University, Amsterdam, 1959.

2.G

Nuclear Physics **15** (1960) 464—468; © *North-Holland Publishing Co., Amsterdam*

Not to be reproduced by photoprint or microfilm without written permission from the publisher

ANGULAR DISTRIBUTION OF PROTONS FROM $Li^6(d, p)Li^7$ AND $Li^6(d, p)Li^{7*}$

G. O. ANDRÉ

The Norwegian Institute of Technology, Department of Physics, Trondheim, Norway

Received 27 November 1959

Abstract: The angular distribution of protons from $Li^6(d, p)Li^7$ and $Li^6(d, p)Li^{7*}$ has been measured, and the intermediate coupling parameter is calculated.

1. Experimental Arrangement and Procedure

The present paper is concerned with the (d, p) reaction on Li^6 at a deuteron energy of 1.57 MeV where the angular distribution of the protons has been studied. A considerable number of experiments have until now been done on this isotope both with low and high deuteron energies [1]). The energy of the deuterons was 1.57 MeV and the total charge on the target approximately 136 μC after 30 minutes exposure. The rather low beam intensity was desired so that the target should retain its uniformity during the sustained bombardment by the deuteron beam.

The lithium target material consisted of Li_2O, where the amount of Li was equivalent to a thickness of 30 $\mu g/cm^2$, supported on a 0.0002 inch thick Cu foil.

The scattering chamber (fig. 1) was a cylinder, 19.4 cm in diameter and 5.7 cm deep. The detector was Ilford C-2 emulsions placed with the central points circularly around the centre of the chamber, the emulsion surface of each plate making an angle of 15° with the income direction of the protons from the target. The plates are situated at angular intervals of 15° from 0° to 165°. The emulsions were shielded from the scattered deuterons by a 0.0001 cm Ni foil supported on a cylindric frame.

The target was placed in the middle of the scattering chamber with the surface making an angle of 30° with the direction of the deuteron beam. The thickness of the backing was chosen in such a way that the protons from the target should pass easily and the deuterons should stop. The advantage of this system was that only one exposure was needed for all the observed angles. Thus all the plates were exposed under almost the same conditions. The protons for the observation angles 0° to 60° has to pass both the Cu backing and the Ni foil and for angles 75° to 165° only the foil, indicating the significant difference in the conditions between the two sets of plates.

The emulsions were examined by a Zeiss Opton microscope with a magnification of 800. Since the protons are all coming in the same direction into the

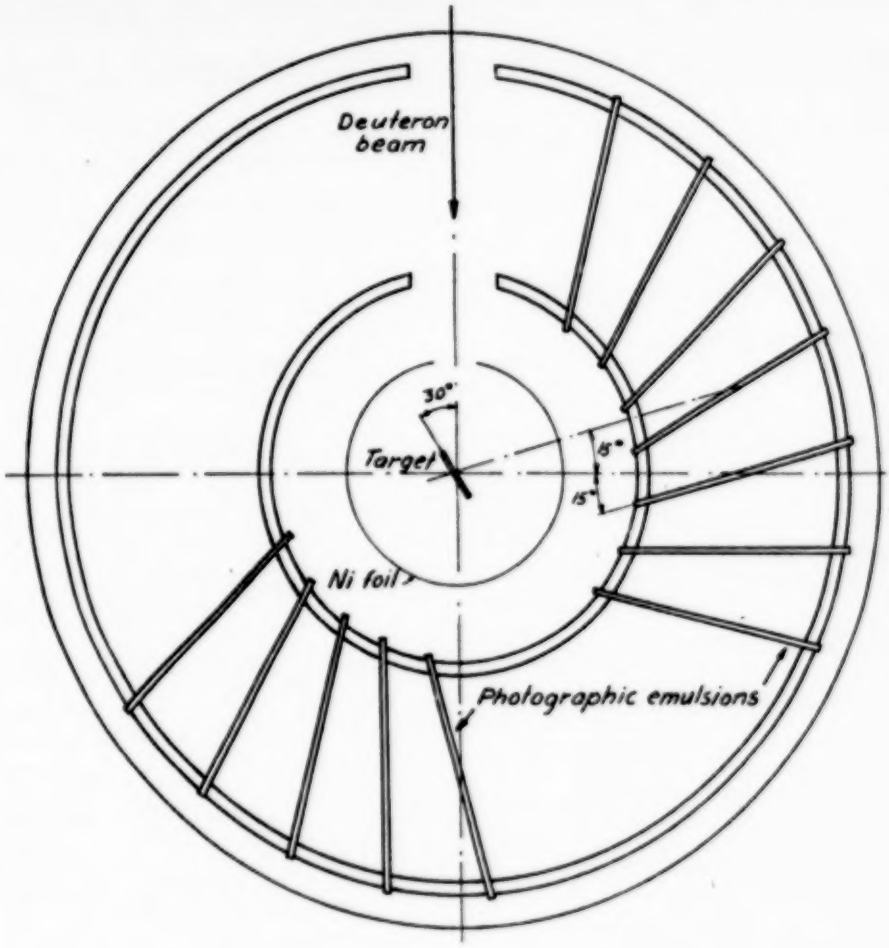

Fig. 1. The target chamber schematically.

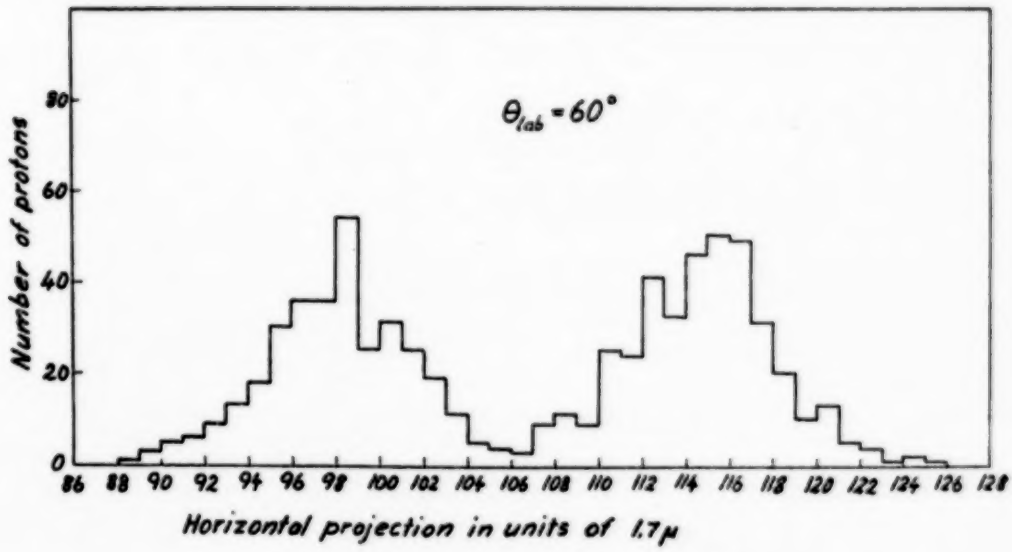

Fig. 2. Range spectrum for $\theta_{lab} = 60°$.

emulsion and the shrinkage-factor is approximately constant during an examination, only the horizontal projection was measured choosing the emulsion surface as horizontal plane. The solid angle in which the protons were examined was approximately 3×10^{-4} sr.

When the protons pass the foils and come to rest in the emulsion, large variations in their energy occur. Therefore a careful and complete analysis was made to solve the statistical problem in connection to the energy spread. It should be mentioned that the calculations of the middlepoints and the total spread of the peaks in the energy spectrum were in excellent agreement with the observed one.

As an example, fig. 2 shows the range spectrum of the protons corresponding to formation of Li^7 in the ground state and the first excited state for the observation angle 60°.

2. Results and Discussion

Calculations of the Q-values from the spectra for the ground state and the first excited state gave as result $Q_g = (4.988\pm0.035)$ MeV and

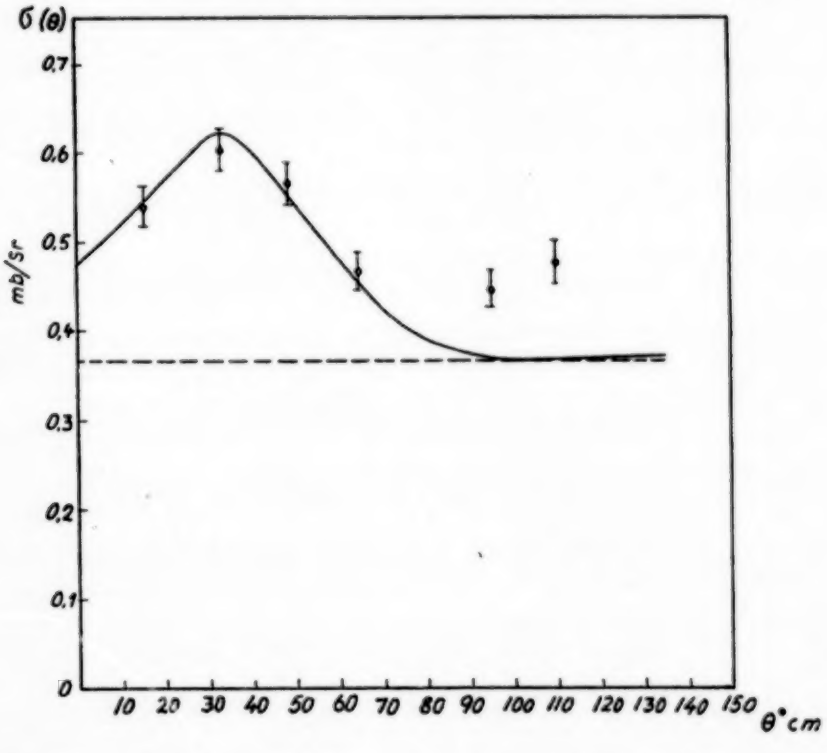

Fig. 3. Angular distribution of the protons corresponding to the ground state.

$Q_e = (4.505\pm0.036)$ MeV respectively. The quoted errors are the standard errors of the weighted mean of the Q's. Consequently the energy of the first excited state is (0.483 ± 0.050) MeV.

The angular distribution of the protons from the ground state and the first excited state of Li^7 are shown in figs. 3 and 4 respectively. The absolute differential cross sections are given for both states. The distributions show peaks in the forward direction suggesting possible stripping maxima. Earlier investigations [2, 3]) have shown that the angular momentum for the captured neutron for higher deuteron energies is $l_n = 1$ in both cases. Accordingly we have drawn the curve for $l_n = 1$ in the Butler-Born approximation [4]) with a radius para-

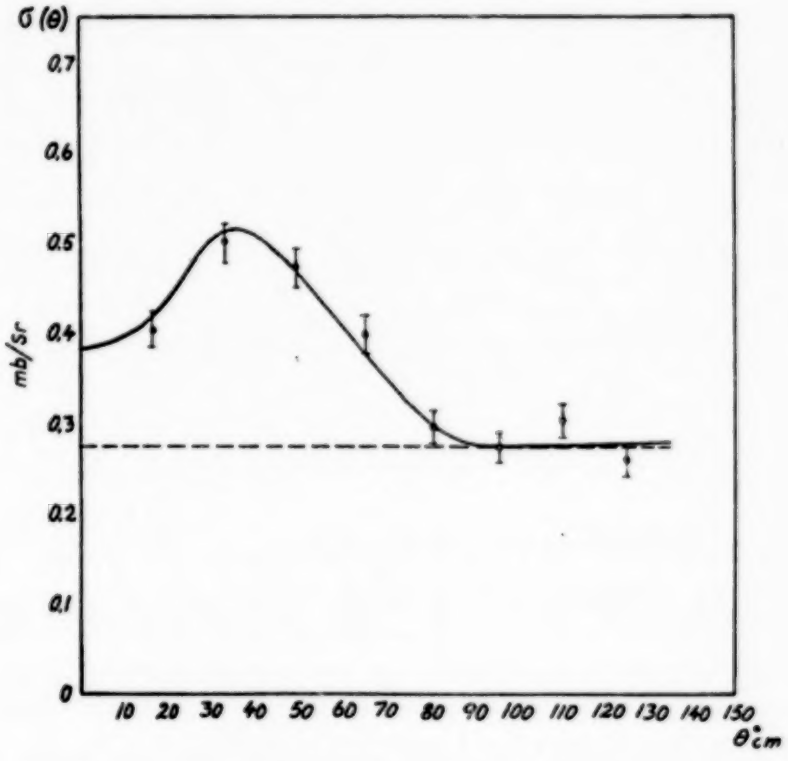

Fig. 4. Angular distribution of the protons corresponding to the first excited state.

meter $r_0 = 6.7 \times 10^{-13}$ cm. As figs. 3 and 4 show, there is good agreement with simple stripping theory for not too large angles even at this low deuteron energy. The broken line is an estimated isotropic contribution due to compound nucleus formation. The interference term between stripping and compound nucleus formation is not taken into account in the theoretical differential cross section. No resonances appear in the excitation curves in the region of our bombarding energy [5, 6]).

In the angular distribution curve for the ground state, fig. 3, there is a tendency of an increase of the cross section in the backward direction. According to Owen and Madansky [7]) this could be explained as a heavy particle stripping effect. This means that the stripped particle originally belonged to the target nucleus. The lower the separation energy of the last proton is, the larger is the chance that this kind of stripping should occur. In fact, the last proton in Li^6

is rather weakly bound, the binding energy is about 4.7 MeV as calculated from the known binding energies of isotopes [8]); but probably still our bombarding energy is too low. However, no attempt is made to calculate this contribution to the cross section.

From the absolute differential cross section we have calculated the ratio θ_g^2/θ_e^2 where θ_g^2 and θ_e^2 are the reduced neutron widths, both in units of the Wigner sum rule limit, of the ground state and first excited state respectively. For $30°_{cms}$ we found $\theta_g^2/\theta_e^2 = (0.53 \pm 0.06)$. The reduced width ratio 0.53 is slightly smaller than measured earlier [9]) for higher energies (about 0.68), but the agreement must be said to be satisfactory. We emphasize the very important fact that the reduced width ratio within experimental error is independent of the deuteron energies. The ratio 0.53 corresponds to a value of the intermediate coupling parameter $\xi = a/K$ as defined by Inglis [10]) of about 3.4 [11]), which is again in agreement with earlier experiments [9]). This value is in general larger that predicted by the simple nuclear model [12]), though values of $2 < \xi < 4$ have been found to be in agreement with theory [13]). In another calculation the best overall fit with the experimental energy level scheme was found to occur with ξ as low as 1.4 [14]). A simplified intermediate coupling procedure [15]) seems also to give a value of ξ in the region mentioned above and replaces the intermediate coupling interaction by a deformation of the potential field.

The author wishes to thank professor N. Hole for his kind interest in the present work. He is also grateful to the Royal Norwegian Council for Scientific and Industrial Research for financial support. The isotopic target of Li^6 was supplied from the Atomic Energy Research Establishment, Harwell, England.

References

1) F. Ajzenberg-Selove and T. Lauritsen, Nuclear Physics **11** (1959) 1
2) J. R. Holt and T. N. Marsham, Proc. Phys. Soc. A **66** (1953) 1032
3) S. H. Levine, R. S. Bender and J. N. McGruer, Phys. Rev. **97** (1955) 1249
4) C. R. Lubitz, Numerical Tables, Harrison M. Randall Laboratory of Physics, University of Michigan (1957)
5) W. Whaling and T. W. Bonner, Phys. Rev. **79** (1950) 258
6) W. E. Nickell, Phys. Rev. **95** (1954) 426
7) G. E. Owen and L. Madansky, Phys. Rev. **105** (1956) 1766
8) A. W. Wapstra, Physica **21** (1955) 367
9) J. B. Reynolds and K. G. Standing, Phys. Rev. **101** (1956) 158
10) D. R. Inglis, Revs. Mod. Phys. **25** (1953) 390
11) T. Auerbach and J. B. French, Phys. Rev. **98** (1955) 1276
12) J. B. French and A. Fujii, Phys. Rev. **105** (1957) 652
13) A. M. Lane, Proc. Phys. Soc. A **68** (1955) 189
14) J. M. Soper, Phil. Mag. 2 Ser. **8** (1957) 1219
15) D. Kurath and L. Pičman, Nuclear Physics **10** (1959) 313

7.A

Nuclear Physics **15** (1960) 469—479; ©*North-Holland Publishing Co., Amsterdam*

Not to be reproduced by photoprint or microfilm without written permission from the publisher

ON THE CONSTRUCTION OF THE *S* MATRIX FOR DRESSED PARTICLES

Yu. NOVOZHILOV

Physical Institute of Leningrad State University

Received 4 June 1959

Abstract: The problem of setting up the *S* matrix for dressed particles is considered by representing the unperturbed states of the dressed particles by means of asymptotic states and by assuming an exponential structure of the vacuum state. Auxiliary independent fields are introduced to describe dressed particles and the scattering theory is formulated in terms of operators and state vectors in the auxiliary field space. The energy operator in the auxiliary field space (effective Hamiltonian) is divided into two parts: the "free" Hamiltonian, whose eigenstates include states of non-interacting dressed particles, and the interaction operator which specifies the particle interaction (but not interaction between the fields).

1. Introduction

By an *S* matrix for dressed particles we mean an *S* matrix which is constructed on the basis of the conventional field theory formalism but does not involve the adiabatic hypothesis which is requisite in the Feynman-Dyson *S*-matrix theory. In contrast to the latter theory, that developed in the present paper assumes that one-particle and vacuum states cannot be derived by perturbation theory since a virtual particle cloud is always attached to the particles.

Correct account of the interaction between a particle and the field is important in view of the well known difficulties which present-day quantum field theory encounters, since there are many reasons for believing that at least part of these difficulties are due to unjustified use of perturbation theory.

Another reason why it should be important to develop a theory of dressed particles is that many attempts have been made to formulate a quantum field theory based only on general principles (covariance, causality, unitarity and spectrality) without taking recourse to the "bare" particle concept. The price one has to pay for trying to state the problem in such a general form is, as is well known, the absence of equations of motion for the field operators. In distinction to this approach, in the dressed particle theory equations of motion for field operators are assumed to exist, i.e., it is assumed that creation and absorption operators for physical particles can be set up by means of creation and absorption operators for bare particles.

An important advance in the development of the theory of dressed particles was made by Van Hove [1]) who employed the perturbation theory method

developed by himself to treat the asymptotic stationary states. The theory of scattering of dressed particles has been discussed by Ekstein [2]). Asymptotic dressed particle states constructed with the help of products of one-particle operators underlined the method for reducing two-nucleon matrix elements to single nucleon ones in a theory of dressed particle scattering in which vacuum polarization was neglected [3]). Some aspects of the scattering theory of dressed particles have also been considered with account of vacuum polarization [4]). Creation operators for dressed particles and the general theory were also investigated in model examples [5]). The relation between the dressed particle theory ("strong convergence method") and another method of description of physical particles ("weak convergence method") [6]) has been considered in an interesting paper by Haag [7]).

A new version of the theory of scattering of dressed particles is proposed in the present paper. The starting point is separation of interaction effects between dressed particles and "self-interaction" effects [4]). The problem of separating these effects is sometimes associated with the problem of dividing the total Hamiltonian into the free Hamiltonian (which includes "self-interaction" effects) and the interaction operator of dressed particles, or with the problem of constructing the creation and absorption operators for non-interacting dressed particles with the aid of bare particle operators. However, it seems very probable that the free Hamiltonian cannot be constructed for real theories. Therefore a different line of attack has been followed in the present work; use is made of the simplifying circumstance that for calculation of the S-matrix, eigenfunctions of the free Hamiltonian may be replaced by other functions possessing the same asymptotic values. As functions of this type we choose the asymptotic stationary states (in the Van Hove sense).

A short summary of scattering theory formulas is given in section 2; in this theory unperturbed motion of particles is described by asymptotic states. The main assumption made in the investigation is that concerning the exponential structure of the vacuum state as indicated by perturbation theory [8]).

Virtual particles belonging to clouds of different dressed particles are assumed to be identical in the asymptotic states. A set of orthonormal auxiliary vectors is introduced in sec. 3 for states in which virtual particles in the clouds of various dressed particles are assumed to be different ("state vectors of non-interacting dressed particles" [4]). In other words, for the description of each dressed particle a separate set of auxiliary independent fields is introduced. The fundamental relationships for state vectors and operators in auxiliary field space are also established in sec. 3. In particular, physical matrix elements in this space should be calculated with a metric operator.

The metric operator is eliminated from the scattering matrix formula in sec. 4. The rule for setting up the Hamiltonian in auxiliary field space is deduced and its explicit expression is presented in the same section.

2. Asymptotic States and the S Matrix

Consider the Schroedinger representation with a Hamiltonian $H(\alpha^+, \alpha)$ where for brevity α^+ and α denote the set of all creation operators $\alpha^+ \equiv (a^+, b^+, c^+)$ and absorption operators $\alpha \equiv (a, b, c)$. Operators a^+, b^+, a, b refer to the nucleon field and operators c^+, c to the meson field. The Hamiltonian H is the sum of the free field Hamiltonian and interaction Hamiltonian H_I. Eigenstates of H include stable states, e.g., the vacuum state Ψ_0, one particle states Ψ_N, $\Psi_{\bar{N}}$, Ψ_π and bound states Ψ_B. In this case $\hat{p}_N^2 = \hat{p}_{\bar{N}}^2 = -M_N^2$, $\hat{p}_\pi^2 = -m^2$, $\hat{p}_B^2 = -M_B^2$, where $\hat{p}_N$, $\hat{p}_\pi$, $\hat{p}_B$, M_N, m, M_B are the energy-momentum vector and observed nucleon, meson and bound state masses respectively. In the vacuum state Ψ_0 the energy and momentum are zero.

In the problem of scattering on a potential the wave functions describing the unperturbed motion are usually chosen to be the eigenfunctions of the free Hamiltonian. There is no free Hamiltonian in quantum field theory as the single interaction Hamiltonian H_I yields the particle interaction as well as the "self-action" effects. One must therefore turn to the concept of asymptotic stationary states $\Psi^{as}(t)$ [1,2]) defined as states independent of the initial conditions for $t \to \pm\infty$ and asymptotically satisfying at $t \to \pm\infty$ the Schroedinger equation with the total Hamiltonian H. If one assumes that for $t \to \pm\infty$ the particles are far removed from each other one can employ the $\Psi^{as}(t)$ states to describe the "unperturbed" particle motion. The scattering states $\Psi^{(\pm)}(t)$ will then be defined by the Schroedinger equation $(i\partial/\partial t - H)\Psi^{(\pm)}(t) = 0$ with the initial conditions $\Psi^{(\pm)}(t) = \Psi^{as}(t)$ for $t = \mp\infty$, the properties of $\Psi^{as}(t)$ ensure that the condition

$$||\Psi^{(\pm)}(t) - \Psi^{as}(t)|| \to 0, \quad t \to \mp\infty$$

is fulfilled. This condition can also be used to determine Ψ^{as} in terms of $\Psi^{(\pm)}$ [7]).

Asymptotic states for dressed particles can be constructed if the stable states are known. The fundamental assumption we now make is that the vacuum state Ψ_0 has an exponential structure

$$\Psi_0 = \hat{F}_0 \Lambda_0 = \exp[\hat{O}_0(\alpha^+) - \tfrac{1}{2}\tilde{G}_0] \cdot \Lambda_0, \tag{1}$$

where Λ_0 is the free field vacuum defined by the equalities $a\Lambda_0 = b\Lambda_0 = c\Lambda_0 = 0$; $\tilde{G}_0$ is a normalization constant assumed to be finite; the operator $\hat{O}_0$ depends only on the creation operators α^+ and can be expanded into a series in powers of α^+. A structure of this type for Ψ_0 has been obtained by means of perturbation theory [8]).

Because of the exponential structure of Ψ_0, when acting on Ψ_0 the absorption operator α is equivalent to the operator $[\alpha, \hat{O}_0]$ which contains the creation operators. Thus the operators A^+ defined by the formulas

$$\Psi_N = A_N{}^+\Psi_0, \quad \Psi_{\bar{N}} = A_{\bar{N}}{}^+\Psi_0, \quad \Psi_\pi = A_\pi{}^+\Psi_0, \quad \Psi_B = A_B{}^+\Psi_0 \tag{2}$$

may be considered to be independent of the absorption operators α.

Let $\Psi^{as}(t)$ be represented as

$$\Psi^{as}(t) = \int c(n)\Psi_n^{as} \exp(-iE_n t)\mathrm{d}n \tag{3}$$

($c(n)$ is a square integrable function), which for $t \to \pm\infty$ asymptotically goes over to a plane wave expansion of the wave packet of $\Psi^{as}(t)$ (Ψ_n^{as} is independent of time). The set of basis states Ψ_n^{as} consists of products of the operators A^+ acting on the vacuum state:

$$\Psi_n^{as} = A_N^+ \ldots A_{\overline{N}}^+ \ldots A_\pi^+ \ldots A_B^+ \ldots \Psi_0, \tag{4}$$

where n denotes the set of indices (N ... $\overline{\mathrm{N}}$ ... π ... B). From the condition of localizability of the particle clouds it is not difficult to show [9]) that for spatially separated particles $(i\partial/\partial t - H)\Psi^{as}(t) = 0$ if $\Psi^{as}(t)$ has the form (3), (4).

The states Ψ_n^{as} are non-orthogonal since the quantities

$$G_{nm} = (\Psi_n^{as}, \Psi_m^{as}) \tag{5}$$

approach δ_{nm} only asymptotically [1, 2, 7]):

$$\lim_{t \to \pm\infty} \int \mathrm{d}n\, c(n) G_{nm} \exp[i(E_n - E_m)t] = c(m).$$

When each of the indices runs over the values of N, $\overline{\mathrm{N}}$, π, B one gets $G_{nm} = \delta_{nm}$. Non-orthogonality of Ψ_n^{as} can be regarded as a consequence of the fact that the operator A^+ is represented in a form which does not contain the absorption operators α.

For dressed particles the scattering matrix can be represented by the formula [2])

$$S_{nm} = (\Psi_n^{(-)}, \Psi_m^{(+)}) \tag{6}$$

where $\Psi_n^{(+)}$ is expressed in terms of the asymptotic states

$$\Psi_n^{(\pm)} = \Psi_n^{as} - [H - E_n \mp i\varepsilon]^{-1}(H - E_n)\Psi_n^{as}. \tag{7}$$

Formulas (6) and (7) are the object of further transformation.

3. Introduction of Auxiliary Fields

The method by which particle interaction effects are separated from "self interaction" effects consists in the introduction of auxiliary independent fields for the description of dressed particles. The auxiliary set of meson and nucleon fields differing in the index j is defined by the following commutation relations between the creation and absorption operators:

$$\begin{aligned} a_{j\mathrm{N}} a^+_{j'\mathrm{N}'} + a^+_{j'\mathrm{N}'} a_{j\mathrm{N}} &= \delta_{jj'}\delta_{\mathrm{NN}'}, \\ b_{j\overline{\mathrm{N}}} b^+_{j'\overline{\mathrm{N}}'} + b^+_{j'\overline{\mathrm{N}}'} b_{j\overline{\mathrm{N}}} &= \delta_{jj'}\delta_{\overline{\mathrm{N}}\overline{\mathrm{N}}'}, \\ c_{j\pi} c^+_{j'\pi'} - c^+_{j'\pi'} c_{j\pi} &= \delta_{jj'}\delta_{\pi\pi'}, \end{aligned} \tag{8}$$

and by the conditions

$$a_j \Lambda_0 = b_j \Lambda_0 = c_j \Lambda_0 = 0,$$

where Λ_0 is the free field vacuum. The index j runs over positive integral values in accordance with the possible number of particles in the field. A separate set of fields is introduced for each dressed particle.

A set of eigenfunctions of the Hamiltonian $H_j = H(\alpha_j^+, \alpha_j)$ is constructed for each value of j. In other words, instead of Hilbert space D formed by the eigenvectors of operator $H(\alpha^\dagger, \alpha)$, a direct product of spaces is introduced:

$$\bar{D} = D_1 \times D_2 \times \ldots \times D_j \times \ldots$$

which is based on the eigenvectors φ_ν of the Hamiltonian

$$\bar{H}_0 = H_1 + H_2 + \ldots + H_j + \ldots \tag{9}$$

As the state space of non-interacting dressed particles one may then consider the subspace $\bar{D}_0$ constructed from the eigenvectors φ_n^0 of the Hamiltonian

$$\hat{H}_0 = \sum_j H_j P_j, \tag{10}$$

where the operator P_j acting in space D_j projects onto the subspace of one particle states Ψ_N, $\Psi_{\bar{N}}$, Ψ_π, of bound states Ψ_B and of vacuum Ψ_0. The vectors φ_n^0 have the form

$$\varphi_n^0 = A_N^+(\alpha_1^+) \ldots A_{\bar{N}}^+(\alpha_i^+) \ldots A_\pi^+(\alpha_l^+) \ldots A_B^+(\alpha_s^+) \ldots \bar{\Psi}_0, \tag{11}$$

$$\bar{\Psi}_0 = \prod_j \hat{F}_0(\alpha_j^+) \cdot \Lambda_0 \equiv \bar{\mathfrak{R}} \Lambda_0; \tag{12}$$

two operators A^+ which depend on operators α^+ with identical indices j are not encountered in φ_n^0. The vectors φ_n^0 are orthonormalized:

$$(\varphi_n^0, \varphi_m^0) = \delta_{(n)(m)}, \tag{13}$$

where $\delta_{(n)(m)}$ is neither symmetrized nor antisymmetrized in the indices $n \equiv (N \ldots \bar{N} \ldots \pi \ldots B \ldots)$ and $m \equiv (N' \ldots \bar{N}' \ldots \pi' \ldots B' \ldots)$ which enter δ_{nm}.

We now establish the rule for transition from a vector Ω in space D to its counterpart $\bar{\Omega}$ in auxiliary field space $\bar{D}$. The double line and bracket $||)$ will denote the operation of equating the indices of operators α_j^+ which are at the right of the double line:

$$||\mathfrak{L}(\alpha_1^+, \alpha_2^+, \ldots)\Lambda_0) = \mathfrak{L}(\alpha^+, \alpha^+, \ldots)\Lambda_0. \tag{14}$$

When operator $B(\alpha_1^+, \ldots; \alpha_1, \ldots)$ moreover depends on the absorption operators α_j the double line, such as in $||B(\alpha_1^+, \ldots; \alpha_1, \ldots)\Lambda_0)$, means that all absorption operators α_j should first be shifted to the right of Λ_0 (taking account of commutators) and it should then be assumed that $\alpha_1^+ = \alpha_2^+ = \ldots = \alpha^+$.

A vector Ω depending on creation operators α^+ can be derived from a vector $\tilde{\Omega}$ which depends on operators $\alpha_1^+, \alpha_2^+, \ldots \alpha_j^+$ by equating the indices in α_j^+:

$$\Omega = ||\tilde{\Omega}).$$

This relation can be formulated more precisely if we take into account that $\tilde{\Omega}$ can be expanded in a complete set of eigenfunctions φ_ν of the Hamiltonian $\overline{H}_0 = H_1 + H_2 + \ldots$ and if we compute the number of vacuum operators $\hat{F}_0$ contained in Ω and $\tilde{\Omega}$. The correspondence rule between vectors Ω and $\overline{\Omega}$ can then be written down as

$$\Omega = \hat{F}_0 || \overline{\mathscr{R}}^{-1} \overline{\Omega}). \tag{15}$$

It is evident that in accordance with formula (15) a set of vectors $\overline{\Omega}$ from space $\overline{D}$ can correspond to a single vector Ω. From the correspondence rule (15) it follows that "physical" matrix elements between some vectors $\overline{\Omega}$ and $\overline{\Omega}'$ in space $\overline{D}$ must be calculated with the metric operator $\hat{G}$:

$$(\Omega', \Omega) = (||\overline{\mathscr{R}}^{-1}\overline{\Omega}', \hat{F}_0^+ \hat{F}_0 || \overline{\mathscr{R}}^{-1}\overline{\Omega}) = (\overline{\Omega}', \hat{G}\overline{\Omega}), \tag{16}$$

and the value of $(\overline{\Omega}', \hat{G}\overline{\Omega})$ should not depend on the non-uniqueness of the transition from Ω to $\overline{\Omega}$ according to eq. (15).

The expression for operator $\hat{G}$ in terms of the creation and absorption operators α^+ and α can be obtained from (16) by introducing the weight operator [4])

$$\hat{\rho} = :\exp \sum_{i \neq j} \{ \sum_{N} a_{jN}^+ a_{iN} + \sum_{\overline{N}} b_{j\overline{N}}^+ b_{i\overline{N}} + \sum_{\pi} c_{j\pi}^+ c_{i\pi} \}: \tag{17}$$

where $:\mathscr{L}:$ designates the normal product of the field operators in $\mathscr{L}$. Then

$$\hat{G} = (\overline{\mathscr{R}}^{-1})^+ : \hat{\rho} V (\sum_j \alpha_j^+, \sum_i \alpha_i) : \overline{\mathscr{R}}^{-1}, \tag{18}$$

where $V(\alpha^+, \alpha)$ is the result of reduction of the operator $\hat{F}_0^+ \hat{F}_0$ to a sum of normal products. Formulas (17) and (18) for operator $\hat{G}$ are based only on the use of the commutation properties of operators α^+ and α on the one hand, and α_j^+ and α_j, $j = 1, 2k, \ldots$ on the other. The value of the scalar product on the right hand side of (16) therefore does not depend on the distribution of indices between operators α^+ in $\overline{\Omega}'$ and $\overline{\Omega}$. A different definition of operator $\hat{G}$ will be considered in section 4.

The matrix elements of operator $\hat{G}$ between states of non-interacting dressed particles φ_n^0 equal the quantities G_{nm} introduced by formula (5):

$$(\varphi_n^0, \hat{G}\varphi_m^0) = (\Psi_n^{as}, \Psi_m^{as}) = G_{nm}, \tag{19}$$

An operator of any physical quantity $\hat{\mathscr{L}}$ which acts on vectors $\overline{\Omega}$ must satisfy the self-conjugation condition in the form

$$\hat{G}\hat{\mathscr{L}} = \hat{\mathscr{L}}^+ \hat{G} \tag{20}$$

($\hat{\mathscr{L}}^+$ is Hermitian conjugate to $\hat{\mathscr{L}}$). The ambiguity in the correspondence between vectors Ω and $\overline{\Omega}$ in scattering problems can be practically removed by requiring that the state $\varphi_n{}^0$ correspond to the asymptotic states $\Psi_n{}^{as}$, namely,

$$\Psi_n{}^{as} = \hat{F}_0||\overline{\mathscr{R}}^{-1}\varphi_n{}^0). \tag{21}$$

Consider the vector

$$\Psi^{(+)}(t) = \hat{F}_0||\overline{\mathscr{R}}^{-1}\overline{\Psi}^{(+)}(t)), \tag{22}$$

which is a solution of the Schroedinger equation $(i\partial/\partial t - H)\Psi^{(+)}(t) = 0$ with the initial condition $\Psi^{(+)}(t) = \Psi^{as}(t)$ for $t = -\infty$. Since $\hat{F}_0$ is independent of time the Schroedinger equation for $\Psi^{(+)}(t)$ will be satisfied if $\overline{\Psi}^{(+)}(t)$ is a solution of the Schroedinger equation with an effective Hamiltonian $\hat{H}$, where $\hat{H}$ is defined by the formula

$$H\Psi = \hat{F}_0||\overline{\mathscr{R}}^{-1}\hat{H}\,\overline{\Psi}). \tag{23}$$

The initial condition for $\overline{\Psi}^{(+)}(t)$ has the form $\overline{\Psi}^{(+)}(t) = \varphi^0(t)$ for $t = -\infty$ where

$$\varphi^0(t) = \int \mathrm{d}n\, c(n)\varphi_n{}^0 \mathrm{e}^{-iE_n t}. \tag{24}$$

Thus, the scattering state $\overline{\Psi}_n{}^{(+)}$ corresponds to the state $\Psi_n{}^{(+)}$ with the same degree of ambiguity as the effective Hamiltonian $\hat{H}$ corresponds to Hamiltonian H. The construction of operator $\hat{H}$ on the basis of the Hamiltonian is considered in section 4.

The correspondence between operator $\mathscr{L}$ acting on vectors Ω and operator $\hat{\mathscr{L}}$ acting on vectors $\overline{\Omega}$ is specified by the formula

$$\mathscr{L}\Omega = \hat{F}_0||\overline{\mathscr{R}}^{-1}\hat{\mathscr{L}}\overline{\Omega}), \tag{23'}$$

which is a generalization of formula (23).

The rule for constructing operator $\hat{\mathscr{L}}(\alpha_1{}^+, \ldots; \alpha_1, \ldots)$ from a given operator $\mathscr{L}(\alpha^+, \alpha)$ is based on the following elementary identities:

$$\alpha||\overline{\Omega}) = ||\sum_j \alpha_j \overline{\Omega}), \tag{25}$$

$$\alpha^+||\overline{\Omega}) = ||\alpha_i{}^+ \overline{\Omega}), \tag{25b}$$

where the subscript i on the right of operator α^+ in (25b) may be arbitrary.

If the "unperturbed" Hamiltonian $\bar{H}_0$ is separated from the effective Hamiltonian

$$\hat{H} = \bar{H}_0 + \hat{U}, \tag{26}$$

it follows from (20) that the equality $\hat{U}^+ = \hat{U}$ cannot hold, for $[\hat{H}, \hat{G}] \neq 0$ in virtue of the hermiticity of $\bar{H}_0$. Since $[\bar{H}_0, \hat{G}] \neq 0$, the operators $\bar{H}_0$ and $\hat{U}$ are not related to any physical quantity. Only the total effective Hamiltonian $\hat{H}$ has the meaning of an energy operator in space $\bar{\mathfrak{D}}$. Operator $\hat{U}$ will be interpre-

ted as the interaction operator for dressed particles. From the properties of $\bar{H}_0$ and states Ψ_n^{as} and also from formula (23) it follows that $\hat{U}\varphi_m^0 = 0$ if m refers to a stable state. The many-particle states φ_m^0 are asymptotic states of $\hat{H}$ and therefore only asymptotically describe the real states of non-interacting particles.

The eigenfunctions $\overline{\Psi}_n^{(\pm)}$ of operator $\hat{H}$ can be represented in the form

$$\overline{\Psi}_n^{(\pm)} = \varphi_n^0 - [\hat{H} - E_n \mp i\varepsilon]^{-1}\hat{U}\varphi_n^0 \tag{27}$$

It follows from (16) and (20) and the condition $(\Psi_n^{(\pm)}, \Psi_m^{(\pm)}) = \delta_{nm}$ that

$$(\overline{\Psi}_n^{(\pm)}, \hat{G}\overline{\Psi}_m^{(\pm)}) = \delta_{nm}. \tag{28}$$

With the help of formulas (6) and (16) the following expression can be obtained for the scattering matrix:

$$S_{nm} = (\overline{\Psi}_n^{(-)}, \hat{G}\overline{\Psi}_m^{(+)}) = \delta_{nm}. \tag{29}$$

Unitarity of S-matrix (29) is ensured by formulas (20) and (28).

Formulas (23) and (26) solve, in principle, the problem of separating particle interaction effects (operator $\hat{U}$) from self-interaction effects. The number of independent fields α_j^+, α_j introduced depends on the number of particles in the initial and final scattering states (described by means of the vectors φ_n^0). For example, in the case of two-particle scattering, the introduction of two fields α_1^+, α_1 and α_2^+, α_2 is sufficient. However, for a unified treatment of all possible scattering processes the Hamiltonian should be the same in all cases. Since the number of particles may be infinite the index j should run over all positive integral values.

4. Effective Hamiltonian and the Metric Operator

According to formulas (27) and (29) the structure of the scattering matrix for dressed particles is specified by the interaction operator $\hat{U}$ and the metric operator. We shall show that the matrix elements of operator $\hat{G}$ can be found from the matrix elements of operator $\hat{U}$. This fact is also important in connection with the difficulties which arise in the determination of $\hat{G}$ by formula (18) for an infinite number of auxiliary fields [4]).

Operators $\hat{H}$ and $\hat{G}$ are connected by the self-conjugation relation for the effective Hamiltonian, $\hat{H}^+\hat{G} = \hat{G}\hat{H}$. Hence

$$(E_\nu - E_\mu)(\varphi_\nu, \hat{G}\varphi_\mu) = (\varphi_\nu, (\hat{U}^+\hat{G} - \hat{G}\hat{U})\varphi_\mu). \tag{30}$$

Let $\varphi_\nu = \varphi_n \equiv \varphi_n^0$; i.e. φ_ν refers to non-interacting dressed particles. The scalar product of asymptotic states G_{nm} can be represented in the form $G_{nm} = \delta_{nm} + g_{nm}$, where g_{nm} does not have any singularities for $E_n = E_m$ [1]).

Thus for non-vanishing g_{nm} and when going to the energy surface $E_n = E_m$ the right hand side of eq. (30) approches zero at least like $E_n - E_m$. Then,

$$G_{nm} = \delta_{nm} + \frac{1}{E_n - E_m}(\varphi_n^0, (\hat{U}^+\hat{G} - \hat{G}\hat{U})\varphi_m^0). \tag{31}$$

If φ_ν and φ_μ contain the scattering states of Hamiltonian H_j, $j = 1, 2 \ldots$ one should differentiate between $\varphi_\nu^{(+)}$ and $\varphi_\nu^{(-)}$ which contain correspondingly the outgoing and incoming waves. Then,

$$\begin{aligned} G_{\nu\mu}^{(\pm)} &\equiv (\varphi_\nu^{(\pm)}, \hat{G}\varphi_\mu^{(\pm)}) \\ &= \delta_{\mu\nu} + \frac{1}{E_\nu - E_\mu \mp i\varepsilon}(\varphi_\nu^{(\pm)}, (\hat{U}^+\hat{G} - \hat{G}\hat{U})\varphi_\mu^{(\pm)}), \end{aligned} \tag{32}$$

In virtue of (31) and (32) calculation of the S matrix reduces to calculation of matrix elements of the interaction operator $\hat{U}$.

We write the S-matrix in the form

$$S_{nm} = \delta_{nm} - 2\pi i\delta(E_n - E_m)\mathscr{R}_{nm}^{(-)}, \tag{33}$$

where, according to (27) and (28),

$$\mathscr{R}_{nm}^{(-)} = (\varphi_n^0, \hat{G}\hat{U}\varphi_m^0) - (\varphi_n^0, \hat{U}^+\hat{G}[\hat{H} - E_n - i\varepsilon]^{-1}\hat{U}\varphi_m^0). \tag{34}$$

The values of $G_{\nu\mu}$ from eqs. (31) and (32) now are inserted in (34). Then, expanding $[\hat{H} - E_n - i\varepsilon]^{-1}$ in $\hat{U}$ and using again eqs. (31) and (32), we get

$$\mathscr{R}_{nm}^{(-)} = (\varphi_n^0, \hat{U}\varphi_m^0) - (\varphi_n^0, \hat{U}[\hat{H} - E_n - i\varepsilon]^{-1}\hat{U}\varphi_m^0). \tag{35a}$$

The outward appearance of this formula is what one would expect if operators $\hat{H}_0$ and $\hat{U}$ were Hermitian. On the energy surface $\mathscr{R}_{nm}^{(-)} = \mathscr{R}_{nm}^{(+)}$, where $\mathscr{R}_{nm}^{(+)} = (\varphi_n^0, \hat{U}^+\hat{G}\overline{\Psi}_m^{(\pm)})$. This can easily be verified by means of formulas (28), (29), (31).

Besides formula (35a), the following formula is valid for $\mathscr{R}_{nm}^{(+)}$:

$$\mathscr{R}_{nm}^{(+)} = (\varphi_n^0, \hat{U}^+\varphi_m^0) - (\varphi_n^0, \hat{U}^+[\hat{H}^+ - E_n - i\varepsilon]^{-1}\hat{U}^+\varphi_m^0). \tag{35b}$$

We now deduce on the basis of formulas (23) and (25) an expression for operator $\hat{U}$. We have

$$H(\alpha^+, \alpha)\hat{F}_0||\overline{\mathscr{R}}^{-1}\overline{\Psi}) = \hat{F}_0 H(\alpha^+, \alpha + [\alpha, \hat{O}_0])||\overline{\mathscr{R}}^{-1}\overline{\Psi}). \tag{36}$$

Operators α^+ and α in operator $H(\alpha^+, \alpha + [\alpha, \hat{O}_0])$ can be ordered by reducing them to normal products. The result will be denoted by $H'(\alpha^+, \alpha)$. There are two types of terms in operator H'; those that contain the absorption operator α and those that do not. In virtue of the equation $H\Psi_0 = 0$ terms of the second type vanish. After carrying H' through the double line we find that the right

hand side of (36) is

$$\hat{F}_0||\overline{\mathscr{R}}^{-1}H'(\alpha_1^+, \alpha_2^+ \ldots; \beta_1, \beta_2 \ldots)\overline{\Psi}), \tag{37}$$

where $\beta = \alpha - [\alpha, \hat{O}_0]$ and the indices of operators α^+ are distributed in such a way as to separate out the term

$$\overline{H}_0 = \sum_j H'(\alpha_j^+, \beta_j) = \sum_j H(\alpha_j^+, \alpha_j).$$

Each term in the operator

$$U' = H'(\alpha^+, \sum\alpha_j) - \sum_j H'(\alpha_j^+, \alpha_j) \tag{38}$$

contains the product of at least two absorption operators, the indices of these operators being different. Thus, the structure of U' is determined by the interaction term H_1 in Hamiltonian H. According to (23) and (37) the operator

$$\hat{U}(\alpha_1^+, \alpha_2^+ \ldots; \alpha_1, \alpha_2 \ldots) = U'(\alpha_1^+, \alpha_2^+ \ldots; \beta_1, \beta_2 \ldots) \tag{39}$$

is the interaction operator which we are seeking in the effective Hamiltonian $\hat{H} = \overline{H}_0 + \hat{U}$.

Formula (39) yields the following expression for $\hat{U}$ when $H_1 = ig\int : \bar{\psi}\gamma\psi : \varphi \mathrm{d}^3x$:

$$\hat{U} = ig\sum_{i \neq j}\int \{\bar{\psi}_j\gamma\chi_i\xi_j + \varphi_j\bar{\chi}_i\gamma\chi_j - \gamma\psi_i\bar{\chi}_i\xi_j\}\mathrm{d}^3x + ig\sum'_{i,j,k}\int \bar{\chi}_k\gamma\chi_i\xi_j\mathrm{d}^3x \tag{40}$$

where the following notations have been employed:

$$\chi = \psi^{(+)} - [\psi, \hat{O}_0], \quad \bar{\chi} = \bar{\psi}^{(+)} - [\bar{\psi}, \hat{O}_0], \quad \xi = \varphi^{(+)} - [\varphi, \hat{O}_0] \tag{41}$$

and $\psi^{(+)}$, $\bar{\psi}^{(+)}$, $\varphi^{(+)}$ are the positive-frequency parts (those containing absorption operators) of the field operators ψ, $\bar{\psi}$ and φ. The prime in the summation symbol in the last term of (40) signifies that in the summation $i \neq j \neq k$, $i \neq k$. When the operators χ, $\bar{\chi}$ and ξ act on the vacuum Ψ_0, the result is zero:

$$\chi\Psi_0 = \bar{\chi}\Psi_0 = \xi\Psi_0 = 0.$$

Operator $\hat{U}$ yields a non-vanishing result only when it acts on a state vector $\varphi_n{}^0$ related to states involving two or more particles, and the last term in $\hat{U}$ when it acts on such $\varphi_n{}^0$ which refers to states with three or more particles. Besides formula (40), other expressions can be written down for operator $\hat{U}$; they differ from (40) in respect to arrangement of the creation operator indices in some terms of eq. (40). All formulas for $\hat{U}$ lead to the same scattering matrix since the scalar products of vectors in space $\bar{D}$, when taken with the metric operator $\hat{G}$, are independent of the distribution of the indices among operators α^+.

From formula (40) it follows that the simplest matrix elements $U^0_{nm} = (\varphi_n{}^0, \hat{U}\varphi_m{}^0)$ do not vanish for transitions $n \to m$ connected with scattering of particles and also for virtual transitions involving absorption of a pair or of mesons (e.g. nucleon + meson → nucleon). It also follows from formula (40)

that the matrix element $U_{\nu\mu} = (\varphi_\nu, \hat{U}\varphi_\mu)$ breaks up into the product of simpler matrix elements; each term in the first integral in (40) in this case is the product of two matrix elements, whereas the second integral in (40) can be expressed in terms of the product of three matrix elements. In the non-relativistic case this circumstance was used to reduce two-nucleon matrix elements to single nucleon ones [3]). Simplification of the matrix elements can be carried out until one of the states coincides with a one-particle state or a bound state. If the one-particle and bound states are known the remaining matrix elements can be evaluated.

Separation of the effective Hamiltonian into $\bar{H}_0$ and $\hat{U}$ can be employed to develop a method for approximate calculation of the scattering amplitudes $\mathscr{R}^{(\pm)}_{nm}$ (see formulas (35)) in which interaction between dressed particles $\hat{U}$ is assumed to be small. This type of approximate method is not identical to the expansion in the renormalized charge. In the non-relativistic case the expansion in $\hat{U}$ was applied to the problem of the potential between dressed particles [3, 10]). In this case the second approximation (restriction to terms with two operators $\hat{U}$) corresponds to account of all graphs which lead to exchange of two mesons. In the general case the approximations cannot be classified with respect to the number of operators $\hat{U}$ since for various processes the matrix elements are of different orders of magnitude. It is not difficult to go from the Schroedinger representation to the interaction representation or Heisenberg representation for dressed particles. In the interaction representation the operators $\psi_j^0(x) = e^{i\bar{H}_0 t}\psi_j(\mathbf{x})e^{-i\bar{H}_0 t}$ satisfy the equations of motion for Heisenberg operators and the state vector varies with time as a result of interaction between the particles: $\hat{U}(t) = e^{i\bar{H}_0 t}\hat{U}e^{-i\bar{H}_0 t}$. In the Heisenberg representation the operator $\hat{\psi}_j(x) = e^{i\hat{H}t}\psi_j(\mathbf{x})e^{-i\hat{H}t}$ satisfies an inhomogeneous equation, the right hand side of which depends on the field operators with indices $i \neq j$.

References

1) L. Van Hove, Physica **21** (1955) 901; **22** (1956) 343
2) H. Ekstein, Nuovo Cimento **3** (1956) 1017
3) Yu. V. Novozhilov, JETP **32** (1957) 1262; **33** (1957) 901; **35** (1958) 742
4) Yu. V. Novozhilov, Vestnik Leningrad Univ. No. 22 (1958) 93; No. 10 (1959) 5
5) O. W. Greenberg and S. S. Schweber, Nuovo Cimento **8** (1958) 378;
T. W. Ruijgrok, Physica **24** (1958) 185, 205;
R. E. Cutkovsky, Phys. Rev. **112** (1958) 1027;
R. T. Sharp, Nuovo Cimento **9** (1958) 23
6) N. N. Bogolyubov and D. V. Shirkov, An Introduction to Quantum Field Theory (Fizmatgiz 1957) § 46;
K. Nishijima, Prog. Theor. Phys. **17** (1956) 765; Phys. Rev. **111** (1958) 995;
H. Lehmann, K. Symanzik and W. Zimmermann, Nuovo Cimento **1** (1955) 205; **6** (1957) 319
7) R. Haag, Phys. Rev. **112** (1958) 669
8) N. Hugenholtz, Physica **23** (1957) 481;
W. Frazer and L. Van Hove, Physica **24** (1958) 137
9) Yu. V. Novozhilov, Vestnik Leningrad Univ. No. 16 (1958) 21
10) Yu. V. Novozhilov and I. A. Terentiev, JETP **36** (1959) 129;
Yu. V. Novozhilov and L. V. Prokhorov, Vestnik Leningrad Univ. No. 22 (1958) 80

8.B

Nuclear Physics **15** (1960) 480—485; © *North-Holland Publishing Co., Amsterdam*

Not to be reproduced by photoprint or microfilm without written permission from the publisher

THEORY OF K⁺-NUCLEON SCATTERING

I. R. GATLAND

Imperial College of Science and Technology, London †

Received 30 October 1959

Abstract: Dispersion relations for the K—N interaction show that the 'Born' term is dominant in K⁺—p scattering. Therefore we calculate the cross section and angular distribution for K⁺—p scattering by perturbation theory using the lowest order Feynman graphs and, given certain parities and coupling constants, this fits the experimental data. The theory does not give good results for K⁺—n scattering.

1. Introduction

It has been shown by Roy [1]) that the dispersion relations for the K—N interaction require the K meson to be pseudo-scalar, relative to the nucleon-hyperon system, if there is no resonance in K⁺—N scattering as is found experimentally. He then finds that at low energies the 'Born' term dominates over the integral in the dispersion relation for K⁺—p scattering (isospin 1). However the same is not necessarily true for the zero isospin state. This means that for the K⁺—p interaction the scattering is given mainly by the poles due to the "bound state" terms but that other effects may be important in K⁺—n scattering.

2. Theory

From this "pology" argument we see that we may calculate K⁺—p scattering by perturbation theory using the Feynman diagrams (fig. 1) which

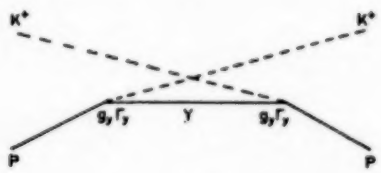

Fig. 1. Feynman graphs for K⁺—p scattering with an intermediate Λ or Σ particle.

have an intermediate Λ or Σ field (shown as a hyperon Y). Detailed calculations show that the Λ-Σ mass difference may be neglected so that the contributions from the two fields are similar except that the hyperons may have opposite parities with respect to the K—N system. Hence the scattering amplitude may be

† Work supported by the Department of Scientific and Industrial Research.

analysed into scalar and pseudo-scalar parts with coupling constants g_s and g_p. Then we find for the differential cross section

$$\frac{d\sigma}{d\Omega} = f(\theta)[a^2+2ab\cos\theta+b^2],$$

where

$$a = \frac{g_s^2}{4\pi}a_s + \frac{g_p^2 a_p}{4\pi},$$

$$b = \frac{g_s^2}{4\pi}b_s + \frac{g_p^2 b_p}{4\pi},$$

$$f(\theta) = [16(1+r^2\cos\theta)^2]^{-1};$$

a_s, a_p, b_s, b_p and r^2 are all functions of the total kinetic energy T in the C-M

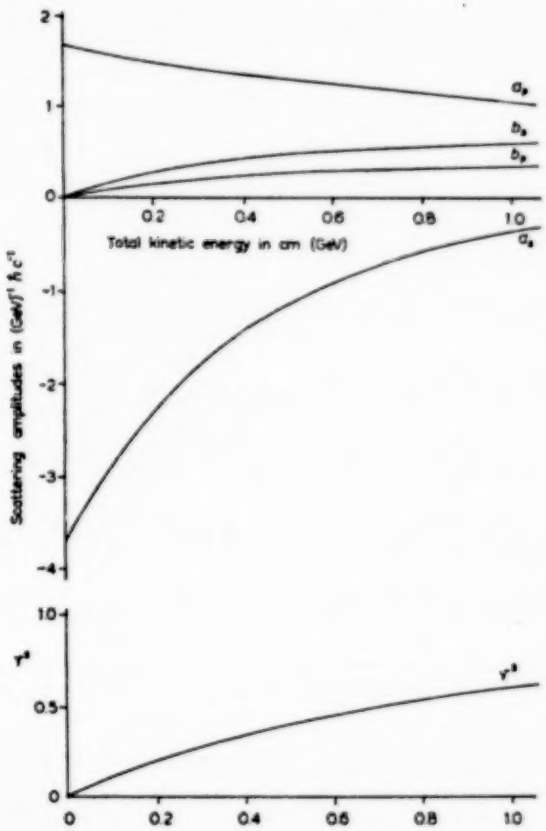

Fig. 2. Scalar and pseudo-scalar scattering amplitudes calculated from the Feynman graphs.

$$\langle|M|\rangle \approx \left\langle v' \left| a+b\frac{\boldsymbol{\sigma}\cdot\mathbf{p}'\boldsymbol{\sigma}\cdot\mathbf{p}}{\mathbf{p}^2} \right| v \right\rangle$$

frame and may be calculated from the Feynman graph. Their behaviour is shown in fig. 2. Since r^2 is small the total cross section is given by

$$\sigma = \frac{4\pi(a^2+b^2)}{16}\left[1+\left(r^2-\frac{2ab}{a^2+b^2}\right)\sum_{n=1}^{\infty}\frac{r^{4n-2}}{2n+1}\right].$$

Now, if we neglect particle production, we may compare this directly with the total cross section obtained experimentally by Burrows *et al.* [2]). From the behaviour of a_p we see that the high energy data may be reasonably fitted by a pure pseudo-scalar interaction but the predicted cross section at low energy will then be far too large. However, if we add a small contribution from the scalar interaction we see from the behaviour of a_s that this will have a negligible effect at high energies and interfere destructively at low energies so as to decrease the calculated cross section. This means of course that the Λ and Σ particles will have opposite parity though we cannot decide which is which. A good fit to the experimental data is given by the following values of the coupling constants:

$$\frac{g_p^2}{4\pi} = 6.6, \quad \frac{g_s^2}{4\pi} = 1.1.$$

This is shown graphically in fig. 3 (curve (1)).

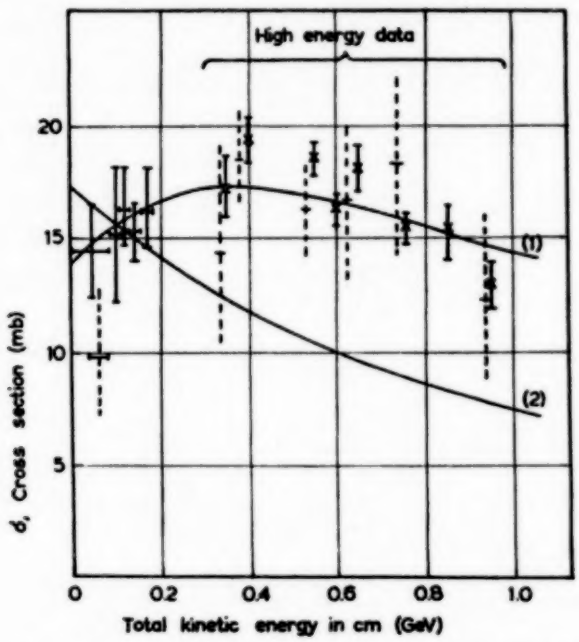

Fig. 3. The total cross sections given by the theory (i) for K^+-p alone, (ii) for K^+-p and K^+-n, together with the experimental results of Burrowes *et al.* [2]) and Kycia *et al.* [3]).

Experimental points	Theoretical curves
K^+-p	(1) $\frac{g_p^2}{4\pi} = 6.6, \quad \frac{g_s^2}{4\pi} = 1.1$
K^+-n	(2) $\frac{g_p^2}{4\pi} = 4.6, \quad \frac{g_s^2}{4\pi} = 0.$

3. Angular Distribution

Now that the only two parameters in the theory have been fixed the angular distribution may be calculated and compared with experiment. However, we must first add the Coulomb correction to the scattering amplitude, given by the

Feynman diagram shown in fig. 4, so that

$$a' = \frac{a}{4(1+r^2\cos\theta)} + \frac{\alpha}{1-\cos\theta}, \quad b' = \frac{b}{4(1+r^2\cos\theta)} + \frac{\beta}{1-\cos\theta}$$

and

$$\frac{d\sigma}{d\Omega} = a'^2 + 2a'b'\cos\theta + b'^2.$$

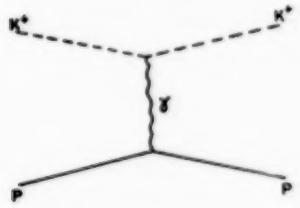

Fig. 4. Feynman graph for K⁺−p scattering through the photon field, giving α and β.

For an incident meson of energy 210 MeV in the laboratory frame the differential cross section is almost flat, except for the Coulomb effect at small angles, and the interference between the electromagnetic and mesic interactions is constructive (fig. 5).

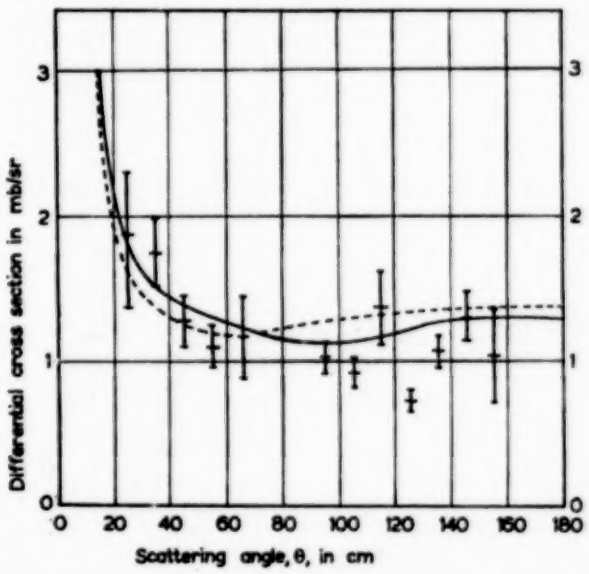

Fig. 5. Comparison of the angular distributions given by the theory and the experimental results of Kycia *et al.* [3]).

—— $\frac{g_p^2}{4\pi} = 6.6$, $\frac{g_s^2}{4\pi} = 1.1$; – – – $\frac{g_p^2}{4\pi} = 4.6$, $\frac{g_s^2}{4\pi} = 0$.

This angular distribution is to be compared with that obtained by Kycia *et al.* [3]) for an incident meson of 225 MeV. At this energy the total cross sections predicted by the theory and found experimentally are 16.1 mb and 15.2 ± 1.3 mb. These graphs giving the total and differential cross sections show that the scattering of K⁺-mesons on protons is in agreement with perturbation theory.

4. The K^+—n Interaction

Having satisfactorily fitted the K^+—p data we may now apply the theory to other related processes, though, for reasons previously considered, the results may be less encouraging. In particular, for K^+—n scattering we have two processes:

$$K^+ + n \to K^+ + n \quad \text{and} \quad K^+ + n \to K^0 + p.$$

The Feynman diagrams for these processes are the same as those for $K^+ + p \to K^+ + p$ except that the coupling constants will be altered by the isospin factors as follows:

for $K^+ + p \to K^+ + p$ the coupling constants are g_Λ^2 and g_Σ^2,
for $K^+ + n \to K^+ + n$ the coupling constants are 0 and $2g_\Sigma^2$,
for $K^+ + n \to K^0 + p$ the coupling constants are g_Λ^2 and g_Σ^2.

Now, if the Σ particle interaction dominates, the total cross section for K^+—n scattering is five times that for K^+—p scattering, but if the Λ interaction dominates, the cross sections are the same, and from the experiments of Burrows *et al.* [2]) we see that the latter case holds. Therefore we expect the ΛKN interaction to be pseudo-scalar and the ΣKN scalar. However, owing to the change of sign of g_Σ^2 for $K^+ + n \to K^0 + p$ the interference between the Λ and Σ fields will be constructive rather than destructive as in the K^+—p case so that the total cross section predicted for low energy K^+—n scattering is much too large. Thus the experimental data on K^+—p and K^+—n scattering cannot be reconciled by the theory in this form. On the other hand we have noted previously that it may be possible to fit the K^+—p scattering data using a pure pseudoscalar interaction if particle production is taken into account. Then both Λ and Σ particles may have the same parity (negative with respect to the K—N system) and for suitable choices of the coupling constants the K^+—p and K^+—n scattering amplitudes become similar as is indicated by the experimental results. The cross section for particle production both in K^+—p and K^+—n interactions would then appear to be about 6 mb throughout the high energy region (i.e. for the range of results given by Burrows *et al.* [2])). Unfortunately there is an energy gap of 350 MeV between the high and low energy data just above the one-pion production threshold. Other possibilities are that the K^+ and K^0 have opposite parities or that a systematic error exists which differentiates the high and low energy data.

5. Conclusion

Dispersion relations for the K—N interaction show that if there is no resonance in K^+—N scattering,

(1) the K-nucleon-hyperon interaction is predominantly pseudoscalar;

(2) the "bound state" terms in the dispersion relation for isospin 1 dominate over the integral;

(3) for zero isospin both the bound state terms and the integral can be important.

In virtue of (2) we calculate K⁺—p scattering using the lowest order Feynman diagrams and fit the theoretical elastic cross section to the experimental total cross section to obtain values of the effective scalar and pseudoscalar coupling constants. Then we find that

(4) the Λ ane Σ particles have opposite parity;

(5) the effective scalar and pseudoscalar coupling constants are

$$\frac{g_s^2}{4\pi} = 1.1, \quad \frac{g_p^2}{4\pi} = 6.6,$$

i.e. the pseudoscalar interaction dominates as required by (1);

(6) the theory is in good agreement with experiment both as regards the total cross section and the angular distribution; in particular the K⁺—p interaction is repulsive.

Applying the theory in this form to K⁺—n scattering does not give results in agreement with experiment, and it therefore appears that the integral in the zero isospin dispersion relation is important. It may be possible to reconcile K⁺—n and K⁺—p scattering, using perturbation theory, if we adopt a pure pseudoscalar interaction and, say, take particle production into account.

I wish to thank Professor A. Salam and Dr. J. Uretsky for discussions on this problem and Dr. P. T. Matthews and Dr. P. K. Roy for the results of the dispersion relation analysis.

References

1) P. K. Roy, Nuclear Physics (to be published)
2) H. C. Burrows, D. O. Caldwell, D. H. Frisch, D. A. Hill, D. M. Ritson and R. A. Schluter, Phys. Rev. Letters **2** (1959) 117
3) T. F. Kycia, L. T. Kerth and R. G. Baender, reported by L. W. Alvarez at the Kiev Conference 1959

7.C

Nuclear Physics **15** (1960) 486—494; © *North-Holland Publishing Co., Amsterdam*

Not to be reproduced by photoprint or microfilm without written permission from the publisher

NON-ELASTIC COLLISIONS OF FAST π MESONS WITH NUCLEONS AND PERIPHERAL ($\pi\pi$) INTERACTIONS

V. S. BARASHENKOV

Joint Institute of Nuclear Research, Laboratory of Theoretical Physics, Dubna, U.S.S.R.

Received 4 August 1959

Abstract: A model of central and peripheral pion-nucleon collisions is discussed on the basis of (π^-p)-collisions at $E = 5$ GeV. The asymmetry of angular distribution of produced particles observed in experiments may be explained on the assumption that the cross-section of peripheral collisions constitutes $\gtrsim 20$ % of the total cross-section of (π^-p) collisions. An estimate $\sigma_{\pi\pi} \approx \sigma_{\pi N}$ is obtained for the cross-section of ($\pi\pi$) interactions at $E \gtrsim 1$ GeV. Angular asymmetry of strange particles produced in (π^-p) collisions is discussed.

1. Introduction

The work in refs. [1,2]) has shown that the prong distribution in stars, the energy spectrum of charged π mesons and the energy spectrum of protons produced in (π^-p) collisions calculated in statistical theory of multiple production are in agreement with experiment. However, angular distributions of produced particles, isotropic according to the statistical theory of multiple production, prove to be anisotropic and asymmetric (relative to the angle $\theta = \frac{1}{2}\pi$) in experiments †.

The character of angular distributions may be explained by taking into account peripheral collisions of π mesons and nucleons. The numerical results of the calculations, however, depend on the so far insufficiently known details of nucleon and meson structure: the number of mesons on the periphery of a cloud, their energy etc. Therefore we may lay claims only to a qualitative interpretation of the experimental data.

The analysis of experimental data on the interaction of fast mesons and nucleons might conversely provide information concerning the structure of nucleon and π-meson. Unfortunately, the available experimental data are not yet sufficiently accurate to draw unique conclusions. Still, the relations obtained below might in future be used for such analysis of experimental data.

2. Analysis of Experimental Data

Let us consider inelastic (π^-p) collisions at energy $E = 5$ GeV. Table 1 lists values of angular asymmetry $A = \vec{n}/\overleftarrow{n}$ calculated on the basis of experimental

† Subsequently, unless specially stipulated, we shall consider colliding π^- meson and proton in the centre of mass system.

data of the work in ref. [4]). Here $\vec{n}$ is the number of particles emitted in the forward hemisphere and $\overleftarrow{n}$ is the number of particles emitted in the backward hemisphere (relative to the velocity vector of the primary π^- meson). It has

TABLE 1

Emitted particles	Version I	Version II	Average
p	0.37 ± 0.13	0	0.23 ± 0.11
n	0.38 ± 0.19	0.38 ± 0.19	0.38 ± 0.19
π^+	0.97 ± 0.34	1.71 ± 0.47	1.38 ± 0.42
π^-	1.54 ± 0.38	1.54 ± 0.38	1.54 ± 0.38
π^0	1.25 ± 0.59	1.25 ± 0.59	1.25 ± 0.59
p; π^+; π^- (All charged particles)	0.95 ± 0.16	1.19 ± 0.20	1.06 ± 0.18

been assumed that all unidentified positively charged particles are either protons (version I) or π^+ mesons (version II). The average was determined as

$$A = \left(\frac{\vec{n}_{\mathrm{I}}+\vec{n}_{\mathrm{II}}}{2}\right) \Big/ \left(\frac{\overleftarrow{n}_{\mathrm{I}}+\overleftarrow{n}_{\mathrm{II}}}{2}\right). \tag{1}$$

It is seen from the table that the angular asymmetry is determined with great statistical errors and, besides, considerably varies with the versions of identification. Here, as distinguished from the case of (pn) collisions (see refs. [5-6])), the charge asymmetry is absent (i.e. $A \approx 1$) within the limits of experimental errors, if one considers all charged particles.

3. Angular Asymmetry of Nucleons

Fig. 1 gives graphs of a central and of three possible versions of peripheral collisions. Central collisions (fig. I-a) were treated in detail in ref. [1]). Below we shall use the results of these calculations.

TABLE 2

Produced particles	Isobar model				Model without an isobar			
	Version A		Version B		Version A		Version B	
	$\vec{n}_1^{\,p}$	$\overleftarrow{n}_1^{\,p}$	$\vec{n}_1^{\,p}$	$\overleftarrow{n}_1^{\,p}$	$\vec{n}_1^{\,p}$	$\overleftarrow{n}_1^{\,p}$	$\vec{n}_1^{\,p}$	$\overleftarrow{n}_1^{\,p}$
p	0	0.78	0	0.78	0	0.33	0	0.33
n	0	0.22	0	0.22	0	0.67	0	0.67
π^+	1.15	0.79	1.35	0.79	1.0	0.34	1.15	0.34
π^-	1.0	0.39	1.2	0.39	1.0	0.34	1.15	0.34
π^0	0.95	0.59	1.25	0.59	0.86	0.34	1.15	0.34
p; π^+, π^- (All charged particles)	2.1	1.96	2.55	1.96	2.0	1.0	2.3	1.0

In order to calculate peripheral collisions corresponding to graphs I-b and I-c one should know the characteristics of $(\pi\pi)$ interactions. However, in the given energy range of the order of several GeV production of nucleons in $(\pi\pi)$ collisions is hardly probabie and the angular asymmetry of protons and neutrons in peripheral collisions of the I-b and I-c types does not depend on the $(\pi\pi)$ interaction assumptions.

Table 2 shows the calculated numbers of protons and neutrons produced in peripheral collisions of the I-b and I-c types and emitted into the forward ($\vec{n}^{\,p}_{1p}$, $\vec{n}^{\,p}_{1n}$) or backward ($\overleftarrow{n}^{\,p}_{1p}$, $\overleftarrow{n}^{\,p}_{1n}$) hemispheres. (Relative to the velocity vector of the primary π^- meson † in the coordinate system of colliding π^- meson and proton ††.) The A and B versions of calculation in table 2 correspond to different assumptions about $(\pi\pi)$ interaction (see below).

Contrary to the case of (pn) interactions when angular asymmetry of the produced particles cannot be explained without an isobar model [7, 8]) in the case of $(\pi^-\mathrm{p})$ interactions angular distributions of the produced particles in the $(\pi\mathrm{p})$ system are found to be asymmetric both in the model with an isobar and without it.

Peripheral collisions of the I-d type essentially depend on properties of the peripheral meson cloud produced in virtual dissociation of the incident π^- meson (for instance, $\pi \to \mathrm{N}+\tilde{\mathrm{N}}+2\pi$; $\pi \to 3\pi$). Calculation of such collisions is less unique than that of collisions of the 1-b and I-c types since very little is known at the present about the structure of mesons. However, if our consideration is restricted to the peripheral collisions with the impact parameter $b \gtrsim \hbar/2\mu c$ where μ is π meson mass, the average momentum transfer will be found to be comparatively small and the nucleon after colliding with peripheral π^* meson (see fig. I-d) will be emitted in the $(\pi\mathrm{p})$ system into the backward hemisphere due to the relativistic compression of angles which occurs when passing from the $(\pi^*\mathrm{p})$ system to the $(\pi\mathrm{p})$ system: $\vec{n}^{\,p}_{2p} \approx \vec{n}^{\,p}_{2n} \ll \overleftarrow{n}^{\,p}_{2p} \approx \overleftarrow{n}^{\,p}_{2n} \approx 0.5$ (for proton and neutron respectively).

Taking into account the central collisions, the angular asymmetry of the particles produced in $(\pi^-\mathrm{p})$ collisions is

$$A = \left\{\vec{n}^{\,c} + (\vec{n}_1{}^{p}\xi_1 + \vec{n}_2{}^{p}\xi_2)\frac{1}{1-\xi_1-\xi_2}\right\} \Big/ \left\{\overleftarrow{n}^{\,c} + (\overleftarrow{n}_1{}^{p}\xi_1 + \overleftarrow{n}_2{}^{p}\xi_2)\frac{1}{1-\xi_1-\xi_2}\right\}. \quad (2)$$

† Taking into account that the average momentum of nucleons produced in isobaric decay is $p \approx 0.23\ \mathrm{GeV}/c$ (in the system of rest of an isobar), one can easily see that all nucleons are emitted in the system of colliding π^--meson and proton at angles $\theta < 30°$ to $40°$ to the direction of the initial motion of an isobar (Cf. below similar calculations for the relativistic compression of angles for π mesons).

†† Subsequently, the centre-of-mass system of the colliding primary π^--meson and proton will be referred to as the $(\pi\mathrm{p})$ system, and that of the primary π^- meson and peripheral π meson, as the $(\pi\pi)$ system. In the same way the centre-of-mass system of the colliding peripheral π meson (emitted from the shell of the incident π^- meson) and proton will be designated as the $(\pi^*\mathrm{p})$-system.

Here

$$\xi_1 = \frac{\sigma_1^{\mathrm{p}}}{\sigma_{\pi\mathrm{N}}^{\mathrm{in}}} \approx n_{\mathrm{N}} \frac{\sigma_{\pi\pi}}{\sigma_{\pi\mathrm{N}}^{\mathrm{in}}}; \quad \xi_2 = \frac{\sigma_2^{\mathrm{p}}}{\sigma_{\pi\mathrm{N}}^{\mathrm{in}}} \approx n_{\pi} \frac{\sigma_{\pi\mathrm{N}}}{\sigma_{\pi\mathrm{N}}^{\mathrm{in}}}; \tag{3}$$

$\sigma_{\pi\pi}$ and $\sigma_{\pi\mathrm{N}}$ are the total cross-sections of $(\pi\pi)$ and $(\pi\mathrm{N})$ interactions; $\sigma_{\pi\mathrm{N}}^{\mathrm{in}}$ is the cross-section of all inelastic $(\pi\mathrm{N})$ interactions;

$$\begin{aligned} \sigma_1^{\mathrm{p}} &= \int \sigma_{\pi\pi}(\varepsilon) q_{\mathrm{N}}(\varepsilon) \mathrm{d}\varepsilon \approx \sigma_{\pi\pi} \times n_{\mathrm{N}}, \\ \sigma_2^{\mathrm{p}} &= \int \sigma_{\pi\mathrm{N}}(\varepsilon) q_{\pi}(\varepsilon) \mathrm{d}\varepsilon \approx \sigma_{\pi\mathrm{N}} \times n_{\pi} \end{aligned} \tag{4}$$

are the cross-sections of peripheral $(\pi\pi)$ and $(\pi\mathrm{p})$ interactions (see fig. 1).

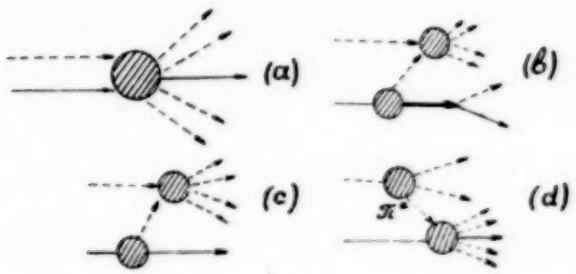

Fig. 1.

The number of peripheral mesons in the shell of a proton and an incident π^- meson is

$$n_{\mathrm{N}} = \int q_{\mathrm{N}}(\varepsilon) \mathrm{d}\varepsilon, \qquad n_{\pi} = \int q_{\pi}(\varepsilon) \mathrm{d}\varepsilon; \tag{5}$$

where $q_{\mathrm{N}}(\varepsilon)$ and $q_{\pi}(\varepsilon)$ are the energy spectra of these mesons; $\vec{n}^{\mathrm{c}} \approx \overleftarrow{n}^{\mathrm{c}} \approx \frac{1}{2} n^{\mathrm{c}}$ is the number of particles produced in a single inelastic $(\pi^- \mathrm{p})$ collision. In the particular case when the angular asymmetry of protons or neutrons is taken into consideration we have, respectively,

$$n^{\mathrm{c}} \equiv n_{\mathrm{p}}{}^{\mathrm{c}} \approx 0.4, \quad n^{\mathrm{c}} \equiv n_{\mathrm{n}}{}^{\mathrm{c}} \approx 0.6.$$

Assigning experimental values to the angular asymmetry A for protons and neutrons we shall obtain two equations for determining the ξ_1 and ξ_2 coefficients:

$$A_{\mathrm{p}} = A_{\mathrm{p}}(\xi_1; \xi_2), \quad A_{\mathrm{n}} = A_{\mathrm{n}}(\xi_1; \xi_2). \tag{6}$$

Since the experimental values A_{p} and A_{n} exhibit great errors (see table 1) a wide interval of values ξ_1 and ξ_2 will satisfy eq. (6). However, in all cases the total cross-section of peripheral collisions is

$$\sigma^{\mathrm{p}} \equiv (\xi_1 + \xi_2) \sigma_{\pi\mathrm{N}} \gtrsim 0.2 \times \sigma_{\pi\mathrm{N}}. \tag{7'}$$

If there is a notable probability of collisions of the I-b or I-c type (in other words, if the cross-section of $(\pi\pi)$ interaction is great), it is but natural to suppose that the virtual processes of peripheral shell formation of the incident π^-meson will also occur with great probability, i.e. the probability of the I-d collisions will also be notable and vice versa. Hence, it is to be expected that the values ξ_1 and ξ_2 should be of the same order. Under this condition the best agreement with experimental data can be obtained for both versions of peripheral collisions (with isobar and without it) if

$$\xi_1 \gtrsim 0.1, \quad \xi_2 \gtrsim 0.2. \tag{7''}$$

Physical consequences that follow from the thus determined values of ξ_1 and ξ_2 will be treated in sec. 5.

4. Angular Asymmetry of π Mesons

The average number of π mesons produced in peripheral $(\pi\pi)$ collision (see figs. I-b and I-c) is

$$\overleftrightarrow{n_1}^{\mathrm{p}} = (\overleftrightarrow{n_1}^{\mathrm{in}} \cdot \sigma_{\pi\pi}^{\mathrm{in}} + \overleftrightarrow{n_1}^{\mathrm{d}} \cdot \sigma_{\pi\pi}^{\mathrm{d}})/\sigma_{\pi\pi} + \overleftrightarrow{n}_{1\mathrm{s}}. \tag{8}$$

Here $\overleftrightarrow{n_1}^{\mathrm{in}}$ and $\overleftrightarrow{n_1}^{\mathrm{d}}$ are the numbers of mesons produced in inelastic and diffractional $(\pi\pi)$ interactions and emitted into the forward or backward hemispheres in the $(\pi\mathrm{p})$ system; $\sigma_{\pi\pi}^{\mathrm{in}}$ and $\sigma_{\pi\pi}^{\mathrm{d}}$ are the corresponding cross-sections; $\sigma_{\pi\pi} = \sigma_{\pi\pi}^{\mathrm{in}} + \sigma_{\pi\pi}^{\mathrm{d}}$; $\overleftrightarrow{n}_{1\mathrm{s}}$ is the corresponding number of π mesons produced in isobaric decay (in the model with isobar).

In the same way, the average number of π mesons produced in peripheral $(\pi\mathrm{p})$ collision (see fig. I-d) is

$$\overleftrightarrow{n_2}^{\mathrm{p}} = (\overleftrightarrow{n_2}^{\mathrm{in}} \sigma_{\pi\mathrm{N}}^{\mathrm{in}} + \overleftrightarrow{n_2}^{\mathrm{d}} \sigma_{\pi\mathrm{N}}^{\mathrm{d}})/\sigma_{\pi\mathrm{N}}. \tag{9}$$

In order to calculate n_1^{in} we shall transform to the $(\pi\pi)$ system. The total energy of the colliding mesons in this coordinate system is

$$W_{\pi\pi} = \sqrt{2\mu(\varepsilon+\mu)} \approx \sqrt{2\varepsilon\mu} \tag{10}$$

where μ is the π meson mass, $\varepsilon = ZE_{\mathrm{N}}$ the energy of peripheral meson, while $E_{\mathrm{N}} = M\varepsilon/\mu$ and $\beta \approx 1$ are the total energy and velocity of a proton in the system in which a primary π^- meson is at rest; M is the proton mass.

At $E = 5$ GeV, $\varepsilon/E_{\mathrm{N}}$ approximates on the average 30 % to 40 % (cf. ref.[8]). The corresponding value $W_{\pi\pi}$ in this case is close to the value of energy $W \approx 2M$ released in annihilation of a nucleon by a slow antinucleon. Therefore the average numbers of particles produced in these collisions must also be about the same. It follows from the statistical calculation of inelastic $(\pi\pi)$ collisions that

the number of emitted charged particles (for the most part $\pi^{\mp}$ mesons) is $n_1^{\text{in}} \approx 3$ while that of neutral (mainly π^0 mesons) is $n_1^{\text{in}} \approx 1.5$. These values are in fact close to the experimental ones obtained for $(N\bar{N})$ annihilation [9]).

The numbers of particles emitted in the $(\pi\pi)$ system isotropically and in the (πp) system into the forward or backward hemispheres, respectively, are

$$\vec{n}_1^{\text{in}} = n_1^{\text{in}}\Omega_1/4\pi, \quad \overleftarrow{n}_1^{\text{in}} = n_1^{\text{in}}\Omega_2/4\pi. \tag{11}$$

Here

$$\Omega_2 = 4\pi - \Omega_1; \quad \Omega_1 = 2\pi(1-\cos\theta^*) = 2\pi(1+\beta/v); \tag{12}$$

$v = p/\varepsilon$ is the average velocity of particles in the $(\pi\pi)$ system produced in an inelastic $(\pi\pi)$ collision †;

$$\varepsilon = W_{\pi\pi}/n_1^{\text{in}}, \quad p = \sqrt{\varepsilon^2-\mu^2} \tag{13}$$

are the average energy and momentum of particles produced in an inelastic $(\pi\pi)$ collision ††;

$$\beta = (\varepsilon_1^2-\varepsilon_2^2)/(\varepsilon_1^2+\varepsilon_2^2) \approx (1-Z)/(1+Z) \tag{14}$$

is the velocity of the $(\pi\pi)$ system relative to the (πp) system; ε_1 and ε_2 are correspondingly the total energies of the primary π^- meson in the (πp) and $(\pi\pi)$ systems †††:

$$\begin{aligned} \varepsilon_1 &= (\mu^2+ME)/\sqrt{\mu^2+M^2+2ME} \approx \sqrt{\tfrac{1}{2}ME}, \\ \varepsilon_2 &= \tfrac{1}{2}W_{\pi\pi} \approx \sqrt{Z}\cdot\varepsilon_1. \end{aligned} \tag{15}$$

In the specific case when $E=5$ GeV and $Z\approx 0.3$, one has $\Omega/4\pi = 0.8$, $\Omega_2/4\pi = 0.2$.

At the present time nothing whatsoever is known about diffractional $(\pi\pi)$ scattering; therefore the calculation will be carried out in two versions:

In version A we shall assume that in $(\pi\pi)$ collisions the cross section is $\sigma_{\pi\pi}^{\text{d}} = \frac{1}{3}\sigma_{\pi\pi}^{\text{in}}$ as for the case of (πN) and (NN) collisions at $E \gtrsim 1$ GeV.

In version B we shall neglect diffractional scattering altogether and shall assume that the total cross-section is $\sigma_{\pi\pi} = \sigma_{\pi\pi}^{\text{in}}$.

† At $\cos\theta^* = -\beta/v$ it is evident that $\operatorname{tg}\theta_1 = v\sqrt{1-\beta^2}\sin\theta/(\beta+v\cos\theta) = \infty$, i.e. all the particles emitted in the $(\pi\pi)$ system at angles $\theta > \theta^*$ are emitted in the (πp) system into the forward hemisphere $\theta_1 < \frac{1}{2}\pi$.

†† In passing over to the (πp) system we used only the average energy of mesons produced in $(\pi\pi)$ collisions. Strictly speaking, such a transformation should involve the entire enrgy spectrum $w = w(\varepsilon)$ of the produced mesons. However, this specification of the theory, while complicating formulas and numerical culculation, would not introduce considerable changes within the accuracy limits of the available experimental data.

††† Formula (14) is a consequence of the relations $\varepsilon_2 = \gamma(\varepsilon_1 - \beta p_1)$ and $\gamma^2 = 1/(1-\beta^2)$ under the condition that $p_1 \approx \varepsilon_1$.

Table 2 gives the values of $\overleftrightarrow{n_1}^p$ of the produced mesons for versions A and B †.

Calculations have been performed for two models of peripheral collisions corresponding to graphs b and c in fig. 1. As is seen the results of calculations reveal little quantitative difference. In both cases the predominant directions of emission of particles produced in collision correspond to those observed in experiment.

Variation in the cross-section of diffractional $(\pi\pi)$ scattering does not essentially affect the value of angular asymmetry.

Knowing the values $\overleftrightarrow{n}^p_{1\pi}$, ξ_1 and ξ_2 it becomes possible to determine in principle the average energy of virtual mesons in the shell of an incident π^- meson through experimental values of angular asymmetry of the produced π^+, π^- and π^0 mesons.

For this purpose we have to note that the statistical weights of the two possible dissociation channels of π^- meson are equal to

$$\pi^- \to 0.35(\pi^-\pi^0\pi^0)+0.65(\pi^-\pi^-\pi^+);$$

i.e. the relative probabilities of π^+, π^-, π^0 mesons collision with protons are respectively equal to 0.217, 0.55, 0.233. With a knowledge of these probabilities we shall be able to calculate $\overleftrightarrow{n}^p_{2\pi} = f(\varepsilon^*)$ for each value of energy ε^* of peripheral π^* meson (see fig. I-d) if we use experimental data on inelastic and diffractional (πp) $(\pi^+ p)$ and $(\pi^0 p)$ collisions at energy $E = \varepsilon^*$. When the experimental data are insufficient we may resort to theoretical calculations ††.

The number of particles emitted into the forward or backward hemispheres is then determined by relations (11) and (12), where ε is the energy of mesons after an inelastic or diffractional (πp) interaction (the value of this energy is taken from experimental data or is determined theoretically),

$$\beta = (\varepsilon_1^2-\varepsilon_2^2)/(\varepsilon_1^2+\varepsilon_2^2) \tag{16}$$

is the velocity of $(\pi^* p)$ system relative to the (πp) system; ε_1 is the energy of the incident π^- meson in the (πp) system (see eq. (15));

$$\varepsilon_2 = \varepsilon^*/\sqrt{1+2\varepsilon^*/M} \tag{17}$$

is the energy of this meson in the $(\pi^* p)$ system.

The calculations have shown that the experimental angular distributions of mesons produced in $(\pi^- p)$ collision at $E = 5$ GeV can be explained if a value of

† Since an overwhelming majority of particles in the $(\pi\pi)$ system after diffraction moves along the angles close to the angles 0 and π the greater part of the particles diffracted in the $(\pi\pi)$ system into the forward or backward hemispheres will be respectively emitted into the forward or backward hemispheres in the (πp) system as well.

†† We have used a statistical theory for inelastic reactions at $\varepsilon^* > 1$ GeV and an optical model for diffractional scattering.

the order of a nucleon mass is chosen for the energy of a peripheral meson. Great experimental errors in the angular asymmetry of π^+, π^-, π^0 mesons do not allow to draw more definite conclusions at the present.

5. Discussion

With the help of numerical values of (7′) and (7″) it is possible through relations (3) to estimate the cross-section of π meson interaction:

$$\sigma_{\pi\pi} \approx \sigma_{\pi N}^{\text{in}} \frac{\xi}{n_N} \approx \sigma_{\pi N} \frac{2\xi_1 \sigma_{\pi N}^{\text{in}}}{\sigma_{NN}^{p}} \approx \sigma_{\pi N}, \tag{18}$$

where $\sigma_{NN} \approx 2\sigma_{\pi N} n_N$ is the cross-section of peripheral collisions of nucleons; in the same way the number of mesons in a peripheral shell of π meson can also be estimated:

$$n_\pi \approx \tfrac{2}{3}\xi_2 \geqq 0.1. \tag{19}$$

Such great values of $\sigma_{\pi\pi}$ and n_π imply that the geometrical size of a pion is close to that of a nucleon †.

In our model of central and peripheral collisions of π mesons with nucleons in the energy range 1 GeV $\ll E \lesssim 10$ GeV, stars with hyperons can be formed only in central collisions, since in $(\pi\pi)$ collisions the energy $W_{\pi\pi}$ is not yet sufficient for effective pair formation of hyperons and antihyperons. The angular prong distribution in such stars should be symmetrical (in the (πN) system) relative to the angle $\theta = \frac{1}{2}\pi$. The analysis of $(\pi^- p)$ collisions at 7 GeV [11] however, point to a notable angular asymmetry of the produced Λ hyperons: $A_\Lambda = \vec{n}/\overleftarrow{n} < 1$. This experimental result can be understood if peripheral collisions of a primary π^- meson with a K-meson are considered to occur in the shell of a nucleon. In this case the Λ hyperon will be emitted into the backward hemisphere (cf. Sec. 3). Since alongside with dissociation of a proton into (ΛK) pair there is also a possibility of dissociation into (ΣK) pair, it is to be expected that Σ^+ and Σ^0 hyperons will have angular asymmetry $A_\Sigma < 1$. Of interest is on experimental check of this conclusion ††.

Measurements of angular asymmetry of hyperons and K-mesons may yield information on (πK) interactions.

† Since the total cross-sections of (πN) and (NN) interactions at $E > 1$ GeV are approximately equal, $\sigma_{\pi N} \approx \sigma_{NN}$, a rough estimate of $\sigma_{\pi\pi} \approx \sigma_{\pi N}$ can be obtained through simple geometrical considerations: the cross-sections $\sigma_{\pi N} = \pi(r_N + r_\pi)^2$ and $\sigma_{NN} = 4\pi r_N^2$ are equal only if the radii of nucleon and meson are approximately equal $r_N \approx r_\pi$, i.e. $\sigma_{\pi\pi} \approx 4\pi r_\pi^2 \approx \sigma_{\pi N}$. Earlier [10]) only a lower estimate $\sigma_{\pi\pi}^{\text{in}} \gtrsim 5$ mb was obtained since the π meson was considered as a combination of "stripped" nucleon and antinucleon.

†† It is to be reminded that our model is valid only at $E \gg 1$ GeV when the wave-lengths of the interacting particles are sufficiently small and we can distinguish between central and peripheral collisions. It is known that at $E \approx 1$ GeV, $A_\Sigma > 1$; but in this case a detailed consideration of matrix elements is required, as in explaining the angular distribution of π mesons at $E < 1$ GeV.

In conclusion the author wishes to use this opportunity and to thank Van Gan-Chiang, Din Da Tsao, V. Ivanov and K. Lebedev for the helpful discussion of π meson experiments.

References

1) V. S. Barashenkov and V. M. Maltsev, Acta Phys. Polonica **17** (1958) 177;
V. S. Barashenkov and V. M. Maltsev, JETP (in press);
V. S. Barashenkov, Nuovo Cimento (in press)
2) V. M. Maksimenko, JETP **35** (1958) 1302
3) R. C. Whitten and M. M. Block, Phys. Rev. **111** (1958) 1676
4) G. Maenchen, W. B. Fowler, W. M. Powell and R. W. Wright, Phys. Rev. **108** (1957) 850
5) N. P. Bogachev, S. A. Biunatov, I. M. Gramenitsky, V. B. Lubimov, Y. P. Merekov, M. I. Podgoretsky, V. M. Sidorov and D. Tuvdendorm, JETP (in press)
6) R. M. Kalbach, I. I. Lord and C. H. Tsao, Phys. Rev. **113** (1959) 330
7) I. E. Tamm (to be published)
8) V. S. Barashenkov, V. M. Maltsev and E. K. Mikhul, JETP **37** (1959) 1484; Nuclear Physics **13** (1959) 583
9) Horwitz, Miller, Murray and Tripp, reported by O. Piccioni at the 1958 Geneva High Energy Physics Conference
10) D. I. Blokhintsev, V. S. Barashenkov and V. M. Barbashov, Usp. Fiz. Nauk **68** (1959) 417; Nuovo Cimento **12** (1959) 602
11) Van Gan-Chiang, M. I. Solovyov *et al.* (to be published)

1.D.2.:
2.L

Nuclear Physics **15** (1960) 495—500; © *North-Holland Publishing Co., Amsterdam*
Not to be reproduced by photoprint or microfilm without written permission from the publisher

INELASTIC SCATTERING OF NUCLEONS BY ASYMMETRICALLY DEFORMED NUCLEI

A Comment on the Structure of Medium Weight Nuclei

HARUO UI

The Institute for Solid State Physics, University of Tokyo, Meguro-ku, Tokyo

Received 2 November 1959

Abstract: The inelastic scattering of nucleons by direct excitation of nuclear rotational states is investigated, in which the target nucleus is described by an asymmetric top wave function as recently proposed by Davydov and Filippov. Then, in even nuclei, not only the first rotation state, but also another 2^+ rotation state can be excited by the first order direct interaction. The cross sections to these two states are presented as functions of the deformation parameters β and γ of A. Bohr. Brief discussions are also added in connection with the vibration model.

It is pointed out that the measurement of these cross sections and angular correlations between emitted nucleons and γ-rays would provide means for determining the structure of medium weight nuclei.

1. Introduction

In a recent paper, Davydov and Filippov [1]) have treated the nucleus with ellipsoidal deformation, for which they calculated the nuclear low-lying levels and electric and magnetic transition rates between them, getting a fairly good agreement with experiment. Among their results, it seems particularly interesting that there appear two 2^+ excited states, both of which, in the range of not too small γ, appear at rather low excitation energies.

When the nuclear deformation has a symmetry axis, i.e. spheroidal shape, the states 2^+, 4^+, 6^+, ... occur as quantized rotation states about the axis perpendicular to the symmetry axis. The rotation about the symmetry axis has apparently infinite energy level distance from the ground state. If the nucleus has ellipsoidal shape, another 2^+ rotation state belonging to the latter axis † becomes lower until $\gamma = 30°$, where $E_2(2)/E_1(2)$ reaches the minimum value 2.0. Here $E_1(2)$ and $E_2(2)$ are the excitation energies of the first and second 2^+ states, respectively.

In even nuclei of medium weight, it is well-known [2]) that the first excited states are always 2^+ and the second excited states are 2^+ or 4^+ with a few exceptions. The second excited 2^+ state has been usually explained as one of

† Strictly speaking, the wave function is described by the superposition of wave functions belonging to the symmetrical tops in the former and latter axes. From group theory considerations, there are only two 2^+ states [1]).

the partners of the two-quanta surface vibration triplet state 0^+, 2^+, 4^+, the splitting of which has been treated by several authors. Scharf-Goldhaber and Weneser [3]) assumed the nucleus as composed of a spherical core and several outer particles, say $(1f_{\frac{7}{2}})$ [4]), allowing for the weak surface interaction between the outer particles and the core †. On the other hand, Wilets and Jean [4]) treated the same problem by the use of the strong coupling approximation of A. Bohr with a β- and γ-unstable potential. In view of the above situation, therefore, it seems to be of interest to have the possibility of selecting the most reliable model among them by a rather direct experimental method. In the present paper, we suggest that the inelastic scattering leading to the second 2^+ excited state is appropriate to this purpose.

The inelastic scattering to the low-lying excited states is usually well explained by simple direct interaction [5, 6, 7]), provided that [8]), firstly, the incident energy is sufficiently high so that the contribution from the compound nucleus be negligible, because there are so many open channels that the inelastically scattered nucleons evaporating from the compound nucleus are scarcely emitted in the relevant channel, and that, secondly, the energy spread of the incident beam be sufficiently broad so that many levels are contained in this energy range; fluctuation from statistical equilibrium is expected to be negligible. Moreover, in the case of not too strong interaction, we can safely adopt the first order Born approximation with the interaction localized near the nuclear surface. Such a condition may hold, in the region of medium weight nuclei, for $E > 10$ MeV [8]).

When the nucleus is described by the unified model of Bohr and Mottelson [9]), the states which can be most easily excited by direct interaction are rotational ones with the same internal structure as that of ground state [6, 8]). Only the first 2^+ state has a considerable cross section, while the second 4^+ state may show quite a small cross section, because it cannot be excited by the first order direct interaction in the simplified model in which the nucleus is treated as a whole with δ-function type surface interaction.

Vibration states can also be excited by the direct interaction. For the two-quanta triplet state (0^+, 2^+, 4^+), the cross sections may be small, because they cannot be excited by the first order interaction. Nevertheless, we can say that the absolute values of these cross sections are similar to each other; only the geometrical factor arising from the coupling of the two-quanta angular momenta plays a role. Angular distributions are almost the same for these three states, but different from the angular distribution leading to the first excited state. In the Scharf-Goldhaber and Weneser model, the essential feature of such circumstances will be unchanged.

On the other hand, in the Davydov and Filippov model, the angular distribu-

† Quite recently, there appeared a paper by Raz [14]), in which he used a model consisting of a core + $(1f_{\frac{7}{2}})^2$, with surface interaction and inter-particle force.

tion to the second 2^+ state is not similar to that of the neighbouring 4^+ and 0^+ states. Moreover, the angular distributions leading to the first 2^+ and the second 2^+ states have very similar shapes, though their absolute values are quite different, as will be shown in the present paper.

We hope, then, that the measurement of the cross sections to the low-lying 2^+ and 4^+ states in the medium weight nuclei would provide additional means for the better understanding of the nuclear structure, although accurate detection technique will be required owing to the smallness of the cross sections.

2. Cross Sections

The cross section for inelastic scattering between the initial state a and final state b may be written as follows [8]):

$$\frac{\mathrm{d}\sigma}{\mathrm{d}\Omega} = \left(\frac{M}{2\pi\hbar^2}\right)^2 \left(\frac{E_\mathrm{b}}{E_\mathrm{a}}\right)^{\frac{1}{2}} \sum_{\mathrm{Av}} |T_{\mathrm{ba}}|^2, \tag{1}$$

where M is the nucleon mass, E_a and E_b the kinetic energies of the incident and emitted nucleons, respectively. The symbol $\sum_{\mathrm{Av}}$ is used to represent a summation over final spin states and an average over initial spin states.

The transition matrix element T_{ba} between the states a and b is given, in the first order Born approximation, by

$$T_{\mathrm{ba}} = \int \mathrm{e}^{i\mathbf{q}\cdot\mathbf{r}} \psi_\mathrm{b}^*(\tau) V \psi_\mathrm{a}(\tau) \mathrm{d}\tau \mathrm{d}\mathbf{r}, \tag{2}$$

where

$$\mathbf{q} = \mathbf{k}_\mathrm{a} - \mathbf{k}_\mathrm{b}$$

represents the momentum transfer in the process, and V the interaction potential. According to A. Bohr [9]), The interaction V is assumed to be

$$V = -V_0 R\delta(r-R) \sum_\mu \alpha_\mu Y_{2\mu}(\theta, \varphi), \tag{3}$$

where (r, θ, φ) denotes the polar coordinates of an incident nucleon, R the average nuclear radius and the α_μ's are the parameters which determine the shape of nuclear deformation of order two.

It may be convenient to transform the parameters α_μ to body-fixed coordinates and the relevant Eulerian angles $(\theta_1, \theta_2, \theta_2) = \Theta$:

$$\begin{aligned} &\alpha_\mu = \sum a_\nu D^{2*}_{\mu\nu}(\Theta) \\ &a_0 = \beta \cos\gamma, \quad a_1 = a_{-1} = 0, \quad a_2 = a_{-2} = (\beta/\sqrt{2}) \sin\gamma; \end{aligned} \tag{4}$$

$D^2_{\mu\nu}$ are the transformation functions for the spherical harmonics of order two.

Next, the wave functions of target and residual nucleus, ψ_a and ψ_b, will be presented. For simplicity, we assume that the internal structure of nuclear

states is not changed during rotation. Therefore, it needs not be written explicitly here. Then,

$$\psi_0 = \frac{1}{\sqrt{4\pi^2}} D^0_{00}(\Theta) \qquad \text{for ground state,} \quad (5-1)$$

$$\psi_{21m} = \sqrt{\frac{5}{8\pi^2}} \left[A_1 D^2_{00}(\Theta) + B_1 \frac{D^2_{m2}(\Theta) + D^2_{m-2}(\Theta)}{\sqrt{2}} \right] \qquad \text{for first } 2^+ \text{ state,} \quad (5-2)$$

$$\psi_{22m} = \sqrt{\frac{5}{8\pi^2}} \left[A_2 D^2_{00}(\Theta) + B_2 \frac{D^2_{m2}(\Theta) + D^2_{m-2}(\Theta)}{\sqrt{2}} \right] \qquad \text{for second } 2^+ \text{ state.} \quad (5-3)$$

The explicit forms of A_1, B_1, A_2 and B_2 are given by Davydov and Filippov [1].

Inserting (3), (4), (5−1) and (5−2) [or (5−3)] into (2) and using the following properties of D-functions, viz.,

$$\int D^{J*}_{MN}(\Theta) D^{j}_{mn}(\Theta) \mathrm{d}\Theta = \delta_{Jj} \cdot \delta_{Mm} \delta_{Nn} \frac{8\pi^2}{2J+1},$$

$$\mathrm{d}\Theta = \sin\theta_2 \mathrm{d}\theta_2 \mathrm{d}\theta_1 \mathrm{d}\theta_3,$$

$$D^{J*}_{MN}(\Theta) = (-)^{M-N} D^{J}_{-M-N}(\Theta),$$

we get immediately

$$T_{21,0} = \sqrt{4\pi} V_0 R^3 \beta (A_1 \cos\gamma + B_1 \sin\gamma) j_2(qR), \qquad (6-1)$$

$$T_{22,0} = \sqrt{4\pi} V_0 R^3 \beta (A_2 \cos\gamma + B_2 \sin\gamma) j_2(q'R), \qquad (6-2)$$

in which $\exp i\mathbf{q}\cdot\mathbf{r}$ is expanded in spherical harmonics, the quantization axis of angular momentum being taken along the direction of the momentum transfer.

The cross section is, therefore, given by

$$\frac{\mathrm{d}\sigma}{\mathrm{d}\Omega} = \frac{1}{4\pi} \left(\frac{E_b}{E_a} \right)^{\frac{1}{2}} \left(\frac{2MV_0}{\hbar^2} \right)^2 R^6 \beta^2 P(\gamma) [j_2(qR)]^2, \qquad (7)$$

with

$$P_1(\gamma) = (A_1 \cos\gamma + B_1 \sin\gamma)^2 = \frac{1}{2} \left[1 + \frac{3 - 2\sin^2(3\gamma)}{\sqrt{9 - 8\sin^2(3\gamma)}} \right] \qquad (8-1)$$

for the transition from ground to first 2^+ state, and

$$P_2(\gamma) = (A_2 \cos\gamma + B_2 \sin\gamma)^2 = \frac{1}{2} \left[1 - \frac{3 - 2\sin^2(3\gamma)}{\sqrt{9 - 8\sin^2(3\gamma)}} \right] \qquad (8-2)$$

for the transition from ground to second 2^+ state.

It is to be noted that $P_1(\gamma)$ and $P_2(\gamma)$ are just proportional, respectively, to the E2 transition probability between the first 2^+ level and the ground state, and to that between the second 2^+ level and the ground state (the so-called

cross-over transition). This result is a straightforward consequence of the assumed type of interaction (3) and the use of first order Born approximation.

3. Results and Discussion

Assuming V_0 to be 40 MeV and $R = r_0 A^{\frac{1}{3}} \times 10^{-13}$ cm, we get

$$\frac{\mathrm{d}\sigma}{\mathrm{d}\Omega} = C \sqrt{\frac{E_b}{E_a}}\, P(\gamma)\beta^2 [j_2(qR)]^2,$$

with

$$C = \begin{cases} 8.90 \times A^2 \times 10^{-28}\ \mathrm{cm}^2 & (r_0 = 1.2), \\ 2.24 \times A^2 \times 10^{-27}\ \mathrm{cm}^2 & (r_0 = 1.4), \\ 4.49 \times A^2 \times 10^{-27}\ \mathrm{cm}^2 & (r_0 = 1.6). \end{cases}$$

The values of $P_1(\gamma)$ and $P_2(\gamma)$ are given as functions of γ in the table 1, in which the ratios $E_2(2)/E_1(2)$ are also listed †.

TABLE 1

γ	0° 60°	5° 55°	10° 50°	15° 45°	20° 40°	25° 35°	30° 30°
$P_1(\gamma)$	1.000	0.933	0.972	0.947	0.933	0.955	1.000
$P_2(\gamma)$	0	0.007	0.028	0.053	0.067	0.043	0
$E_2(\gamma)/E_1(\gamma)$	∞	64.2	15.9	6.85	3.73	2.41	2.00

† This table is the same as the table 1 of Davydov and Filippov, as noted in the preceding section. See also, eq. (1.2) of ref. [1]).

If the excitation energies and spins of nuclear low-lying states are known, γ is determined by the ratio $E_2(2)/E_1(2)$, as pointed out by Davydov and Filippov [1]), and β can be evaluated from the absolute value of $E_1(2)$ or the quadrupole moments of neighbouring nuclei with higher spin. Then, we can evaluate the cross sections by using the present result.

From the table, it is noted that for the maximum asymmetry, i.e. $\gamma = 30°$, the cross section leading to the second 2^+ state vanishes, which is a rather unfortunate situation for our purpose. However, it may be of interest to see whether the cross sections leading to the second 2^+ states show the γ-dependence of table 1 for the various nuclei for which the values of γ were assigned by Davydov and Filippov from the nuclear spectroscopic data.

Next, the angular correlation in (p, p'γ) will be discussed. It is easily shown that the angular correlations between emitted nucleon and γ-ray should be the same as that of the usual direct interaction theory [7, 10]) for both reactions

ground state (p, p′) first 2^+ state (γ_{10}) ground state

and

ground state (p, p′) second 2^+ state (γ_{20}) ground state

in the Davydov and Filippov model. The latter correlation, however, may be difficult to measure owing to the small cross section of the inelastic scattering and the very low intensity of the cross-over γ-transition. In this connection it is to be noted that the angular correlation for the second 2^+ state between the emitted nucleon and the first γ-ray in the cascade transition, i.e., the E2 transition from second 2^+ to first 2^+ state, may also be the same as that of Satchler [10]), whereas in the two-quanta vibration interpretation the correlation may not be so simple. Then, the measurement of such correlations might be an additional means for determining the structure of medium weight nuclei.

So far, the first order Born approximation has been adopted. The next approximation may be obtained by taking the first order perturbation with distorted waves, which will probably provide a sufficiently accurate result because of the rather small value of β and the greater value of the incident energy E_a [8]). In this case the cross section may differ from the result of the simple Born approximation presented in the previous sections, though it will be expected that the ratio of the cross sections

$$\frac{\mathrm{d}\sigma(\text{ground} \to \text{1st } 2^+)}{\mathrm{d}\Omega} \Big/ \frac{\mathrm{d}\sigma(\text{ground} \to \text{2nd } 2^+)}{\mathrm{d}\Omega}$$

will not be much altered, when $E_a \gg E_1(2),\ E_2(2)$.

The author wishes to express his sincere thanks to Professor T. Muto for reading the manuscript and valuable discussions.

References

1) A. S. Davydov and G. F. Filippov, Nuclear Physics **8** (1958) 237
2) G. Scharf-Goldhaber, Phys. Rev. **90** (1955) 587;
M. Nagasaki and T. Tamura, Prog. Theor. Phys. **12** (1954) 248;
F. K. McGowan, Coulomb Excitation (unpublished) (tabulation of recent data)
3) G. Scharf-Goldhaber and J. Weneser, Phys. Rev. **98** (1955) 212
4) L. Wilets and M. Jean, Phys. Rev. **102** (1956) 788
5) Austern, Butler and McManus, Phys. Rev. **92** (1956) 350;
S. T. Butler, Phys. Rev. **106** (1957) 272
6) S. Hayakawa and S. Yoshida, Prog. Theor. Phys. **14** (1955) 1;
D. M. Brink, Proc. Phys. Soc. A **68** (1955) 994;
S. Yoshida, Proc. Phys. Soc. A **69** (1956) 668; Prog. Theor. Phys. **19** (1958) 169;
Chase, Wilets and Edmonds, Phys. Rev. **110** (1958) 110
7) N. Austern, Fast Neutron Physics, Chapter 5, D (Direct Interaction Theories)
8) H. Ui, Prog. Theor. Phys. **18** (1957) 163
9) A. Bohr, Mat. Fys. Medd. Dan. Vid. Selsk. **26**, No. 14 (1952);
A. Bohr and B. Mottelson, Mat. Fys. Medd. Dan. Vid. Selsk. **27**, No. 16 (1953)
10) G. R. Satchler, Proc. Phys. Soc. A **68** (1955) 1037; see also ref. [7])
11) Raz, Phys. Rev. **114** (1959) 1116

7.B

Nuclear Physics **15** (1960) 501—509; © *North-Holland Publishing Co., Amsterdam*

Not to be reproduced by photoprint or microfilm without written permission from the publisher

ON THE CONSISTENCY OF QUANTIZATION IN QUANTUM ELECTRODYNAMICS

SHOJI OZAKI

Institute for Theoretical Physics, Kyushu University, Fukuoka, Japan

Received 9 September 1959

Abstract: It is shown that the new relativistically covariant quantization method of quantum electrodynamics in the Heisenberg representation leads to a self-consistent and definite formalism. If we divide the electromagnetic 4-potentials into a transverse part, a part related to Coulomb potential, and the remaining indefinite part, which is needed to satisfy identically the fundamental equations when the Lorentz condition is not imposed, the new relativistically covariant quantization determines the commutation relations of the indefinite potential. By transforming the formalism of quantum electrodynamics obtained by the method mentioned above in Heisenberg representation into the interaction representation and determining the interaction Hamiltonian by this procedure, the equivalence to the usual quantum electrodynamics can be proved without any indefiniteness.

1. Introduction

In a previous paper [1]), and almost at the same time by Dirac [2]), a formalism of quantum electrodynamics, was proposed which admits the generalized gauge transformation resulting when the Lorentz condition is not imposed on the electromagnetic potential. For the quantization of the electromagnetic potential, however, Dirac applied the usual canonical formalism, which gave rise to a subsidiary condition different from the Lorentz condition. This made necessary the use of a gauge invariant electron operator creating the Coulomb potential around the electron and complicated the formalism unnecessarily.

Here, the author proposes a new relativistically covariant quantization method of the electromagnetic potential in Heisenberg's representation, which does not make use of the canonical formalism, and, as in the previous paper, does not use the Lorentz condition. Therefore, after separating from the electromagnetic potential the relativistically covariant transverse wave and the term related to Coulomb potential, the remaining part satisfies identically an equation which has the same form as the original one, except for the source function. Then, the commutation relations between the electromagnetic 4-potentials determine the commutation relations between these remaining undetermined potentials.

However, it is very difficult to prove the equivalence of the formalism thus obtained with the usual one in the Heisenberg representation, because in this

representation the method of successive approximation developed by Yang-Feldman [3]) and Källén [4]) must be used. Therefore, as in the previous paper, we transform the formalism thus obtained in Heisenberg representation into the interaction representation by using Glauber's method [5]) (quite similar to that of Umezawa and Takahashi [6])), and adding the remaining quantized part absent in the previous case. Thus, by determining the interaction Hamiltonian by this procedure, the equivalence with the usual quantum electrodynamics is proved in a way which is relativistically covariant throughout.

2. Quantization of Electromagnetic Potentials in Heisenberg's Representation

The formalism of quantum electrodynamics without Lorentz condition in the Heisenberg representation is written down as follows:

$$(\gamma_\mu \partial_\mu - ie\gamma_\mu A_\mu(x) + \kappa)\psi(x) = 0, \tag{1}$$

$$\Box A_\mu(x) - \partial_\mu \partial_\nu A_\nu(x) = -j_\mu(x), \tag{2}$$

$$j_\mu(x) = \tfrac{1}{2} ie[\bar{\psi}(x), \gamma_\mu \psi(x)], \tag{3}$$

where $\psi(x)$ and $A_\mu(x)$ denote the electron field and the electromagnetic potential operators respectively. Here we impose the following anticommutator and commutator relations on $\psi(x)$ and $A_\mu(x)$:

$$\{\bar{\psi}_\alpha(x),\ \psi_\beta(x')\} = i(\gamma_\mu \partial_\mu - \kappa)_{\alpha\beta} \Delta(x, x'), \tag{4}$$

$$[A_\mu(x), A_\nu(x')] = i\delta_{\mu\nu} D(x, x'), \tag{5}$$

where

$$\Delta(x, x') = 0, \text{ for space-like } x, x' \tag{6}$$

$$\partial_4 \Delta(x, x')|_{t=t'} = \delta(\mathbf{x} - \mathbf{x}'), \tag{7}$$

$$D(x, x') = \Delta(x, x')|_{\kappa=0}, \tag{8}$$

other properties of the operator $\Delta(x, x')$ being unknown.

In the limit of vanishing-interaction it is assumed that $\Delta(x, x')$ tends to the form $\Delta(x - x')$. Here we must take care of the fact that the commutation relations for $A_\mu(x)$ are different from the usual ones, which are derived from the canonical formalism. Here, as in the previous paper, we divide $A_\mu(x)$ into the transverse $\mathfrak{A}_\mu(x)$, the term related to Coulomb potential, and the remaining undetermined part $\Lambda(x)$ which satisfies identically the following equation:

$$(\Box \delta_{\mu\nu} - \partial_\mu \partial_\nu) \partial_\nu \Lambda(x) = 0. \tag{9}$$

These equations are gauge-invariant. However, the general gauge transformation function must be a c-number in order to make invariant the anticommutator of electron field operators.

With the notation of the previous paper, we can express $\mathfrak{A}_\mu(x)$ as

$$\mathfrak{A}_\mu(x) = \mathfrak{A}_\mu(x, \sigma) + \int j_\nu(x'') d^1_{\nu\mu} D^\sigma(x, x'') dx'' - (n_\mu \partial + \partial_\mu)\partial^{-1}(\Box + \partial^2)^{-1} n_\lambda j_\lambda(x), \tag{10}$$

and the operator $\mathfrak{B}_\mu(x)$ as

$$\mathfrak{B}_\mu(x) = \partial_\mu \Lambda(x) + \partial_\mu \Lambda(x, \sigma) + n_\mu(\Box + \partial^2)^{-1} n_\lambda j_\lambda(x); \tag{11}$$

the commutators for $\mathfrak{A}_\mu(x)$ have been written as

$$[\mathfrak{A}_\mu(x), \mathfrak{A}_\nu(x')] = i d^1_{\nu\mu} D(x, x'). \tag{12}$$

More generally, $\mathfrak{B}_\mu(x)$ could be written as

$$\mathfrak{B}_\mu(x) = \partial_\mu \Lambda(x) + \partial_\mu \Lambda(x, \sigma) + (\alpha \partial_\mu \partial^{-1} + n_\mu)(\Box + \partial^2)^{-1} n_\lambda j_\lambda(x), \tag{13}$$

where α is an arbitrary constant. This means that $\mathfrak{B}_\mu$ can involve an arbitrary term related to Coulomb potential. But if we make use of the property $(n_\mu \partial + \partial_\mu)\mathscr{D}(x - x') = 0$, eq. (13) can be written as

$$\mathfrak{B}_\mu(x) = \partial_\mu \Lambda(x) + \partial_\mu \Lambda(x, \sigma) + (1 - \alpha) n_\mu(\Box + \partial^2)^{-1} n_\lambda j_\lambda(x), \tag{13'}$$

because

$$(\Box + \partial^2)^{-1} n_\lambda j_\lambda(x) = \int_\sigma d\sigma' \, n_\lambda j_\lambda(x') \partial \mathscr{D}(x - x'), \quad \text{if} \quad n_\mu(x_\mu - x'_\mu) = 0.$$

If we substitute (13') into the original equation to determine $\mathfrak{B}_\mu(x)$, (13') is satisfied only in the case of $\alpha = 0$. Therefore, so far as we adopt a hyperplane, satisfying $n_\mu(x_\mu - x'_\mu) = 0$, as the σ-surface, (11) is a unique expression.

Now, in order to determine the commutation relation for $\Lambda(x)$, we operate with $(\Box \delta_{\mu\lambda} - \partial_\lambda \partial_\mu)$ on eq. (5) from the left:

$$[j_\lambda(x), A_\nu(x')] = -i(\Box \delta_{\lambda\nu} - \partial_\lambda \partial_\nu) D(x, x'). \tag{14}$$

If we substitute

$$A_\nu(x') = \mathfrak{A}_\nu(x') + \partial'_\nu \Lambda(x') + (\alpha \partial'_\nu \partial'^{-1} + n_\nu)(\Box' + \partial'^2)^{-1} n_\lambda j_\lambda(x') \tag{15}$$

into (14), and make use of the relation $n_\nu \mathfrak{A}_\nu(x') = 0$, we get

$$[j_\lambda(x), \partial' \Lambda(x') + (\alpha - 1)(\Box' + \partial'^2)^{-1} n_\lambda j_\lambda(x')] = -i(\Box n_\lambda - \partial_\lambda \partial) D(x, x'). \tag{16}$$

Furthermore, we multiply (16) by n_λ, to obtain the following relation:

$$[n_\lambda j_\lambda(x), \partial' \Lambda(x') + (\alpha - 1)(\Box' + \partial'^2)^{-1} n_\lambda j_\lambda(x')] = i(\Box + \partial^2) D(x, x'). \tag{17}$$

Substituting (15) into (5) and multiplying it by n_μ and n_ν, we get

$$[\partial \Lambda(x) + (\alpha - 1)(\Box + \partial^2)^{-1} n_\lambda j_\lambda(x), \partial' \Lambda(x') + (\alpha - 1)(\Box' + \partial'^2)^{-1} n_\lambda j_\lambda(x')] = -i D(x, x'). \tag{18}$$

The left-hand side of (18) becomes

$$[\partial\Lambda(x), \partial'\Lambda(x')+(\alpha-1)(\Box'+\partial'^2)^{-1}n_\lambda j_\lambda(x')]$$
$$+(\alpha-1)(\Box+\partial^2)^{-1}[n_\lambda j_\lambda(x), \partial'\Lambda(x')+(\alpha-1)(\Box'+\partial'^2)^{-1}n_\lambda j_\lambda(x')]$$

and the use of the relation (17) gives

$$[\partial\Lambda(x), \partial'\Lambda(x')]+(\alpha-1)[\partial\Lambda(x), (\Box'+\partial'^2)^{-1}n_\lambda j_\lambda(x')]$$
$$-i(1-\alpha)D(x, x') = -iD(x, x').$$

We thus get

$$[\partial\Lambda(x), \partial'\Lambda(x')] = (1-\alpha)[\partial\Lambda(x), (\Box'+\partial'^2)^{-1}n_\lambda j_\lambda(x')]-i\alpha D(x, x'), \quad (19)$$

while from (17) the following relation is obtained:

$$[(\Box+\partial^2)^{-1}n_\lambda j_\lambda(x), \partial'\Lambda(x')]$$
$$= iD(x, x')-(\alpha-1)[(\Box+\partial^2)^{-1}n_\lambda j_\lambda(x), (\Box'+\partial'^2)^{-1}n_\lambda j_\lambda(x')].$$

Substituting this relation into (19), we get

$$[\partial\Lambda(x), \partial'\Lambda(x')] = -iD(x', x)+i\alpha\{D(x', x)-D(x, x')\}$$
$$-(1-\alpha)^2[(\Box+\partial^2)^{-1}n_\lambda j_\lambda(x), (\Box'+\partial'^2)^{-1}n_\lambda j_\lambda(x')]. \quad (20)$$

Operating with $(\Box'\delta_{\mu\nu}-\partial'_\mu\partial'_\nu)$ on (14) and furthermore multiplying it by n_λ and n_μ, the following relation is obtained:

$$[n_\lambda j_\lambda(x), n_\mu j_\mu(x')] = -i\Box'(\Box+\partial^2)D(x, x') = -i\Box(\Box'+\partial'^2)D(x, x'), \quad (21)$$

where the property that $D(x, x')$ is a function of $|x-x'|$ only is used.

By substituting (21) into (20), we get

$$[\partial\Lambda(x), \partial'\Lambda(x')] = -iD(x', x)+i(1-\alpha)^2(\Box+\partial^2)^{-1}\Box D(x, x')$$
$$= -iD(x', x)+i(1-\alpha)^2(\Box'+\partial'^2)^{-1}\Box' D(x, x'). \quad (22)$$

If we use the hyperplane satisfying the condition $n_\mu(x_\mu-x'_\mu) = 0$, the second term of (22) vanishes:

$$\Box(\Box+\partial^2)^{-1}D(x, x') = \Box\int_\sigma d\sigma'' D(x'', x')\partial''\mathscr{D}(x''-x) = 0,$$

and we finally get the commutation relation for $\Lambda(x)$:

$$[\partial\Lambda(x), \partial'\Lambda(x')] = -iD(x', x). \quad (23)$$

Here the vanishing of the third term of (20) can be also proved using the relations

$$[j_\mu(x), j_\nu(x')] = ie^2\{\bar\psi(x)\gamma_\mu S(x, x')\gamma_\nu\psi(x')-\bar\psi(x')\gamma_\nu S(x', x)\gamma_\mu\psi(x)\},$$
$$[(\Box+\partial^2)^{-1}n_\mu j_\mu(x), (\Box'+\partial'^2)^{-1}n_\lambda j_\lambda(x')]$$
$$= \iint_\sigma d\sigma''_\mu d\sigma'''_\nu \mathscr{D}(x-x'')\mathscr{D}(x'-x''')[j_\mu(x''), j_\nu(x''')]$$
$$= ie^2\iint_\sigma d\sigma''_\mu d\sigma'''_\nu \mathscr{D}(x-x'')\mathscr{D}(x'-x''')\{\bar\psi(x'')\gamma_\mu S(x'', x''')\gamma_\nu\psi(x''')$$
$$-\bar\psi(x''')\gamma_\nu S(x''', x'')\gamma_\mu\psi(x'')\},$$

while as $\Delta(x'', x''') = 0$, for space-like x'', x''', the right-hand side of the above formula becomes

$$= -e^2 \int\int_\sigma \mathrm{d}\sigma''_\mu \mathrm{d}\sigma'''_\nu \mathscr{D}(x-x'')\mathscr{D}(x'-x''')\{\bar{\psi}(x'')\gamma_\mu\gamma_4\partial''_4\Delta(x'', x''')\gamma_\nu\psi(x''') - \bar{\psi}(x''')\gamma_\nu\gamma_4\partial'''_4\Delta(x''', x'')\gamma_\mu\psi(x'')\};$$

taking a hyperplane as the σ-surface, we have

$$\partial''_4\Delta(x'', x''')|_{t''-t'''=0} = \delta(\mathbf{r}''-\mathbf{r}''');$$

the above expression can then be integrated and reduces to the following:

$$= -e^2 \int_\sigma \mathrm{d}\sigma''_\mu \mathscr{D}(x-x'')\mathscr{D}(x'-x'')\bar{\psi}(x'')\{\gamma_\mu\gamma_4\gamma_4-\gamma_4\gamma_4\gamma_\mu\}\psi(x'') = 0.$$

The solution of the quantized wave equation (1) is expressed as in the previous paper:

$$\psi(x) = \psi(x, \sigma) - ie\int S^\sigma(x, x'')\gamma_\mu\psi(x'')\{\mathfrak{A}_\mu(x'') + \partial''_\mu\Lambda(x'') + (\alpha\partial''_\mu\partial''^{-1} + n_\mu)(\Box'' + \partial''^2)^{-1}n_\lambda j_\lambda(x'')\}\,\mathrm{d}^4x''. \quad (24)$$

As is seen from (13) and (24), an arbitrary constant α cannot be determined in this formulation, so far as the hyperplane satisfying $n_\mu(x_\mu - x'_\mu) = 0$ is not adopted. But it is very difficult to prove the equivalence of this formalism with the usual one without using the hyperplane in the Heisenberg representation. Using this hyperplane, we can transform the above formalism in the Heisenberg representation into the interaction representation by Glauber's method [5]) (see also refs. [3]) and [6])) and determine the interaction Hamiltonian satisfying all requirements.

3. Proof of the Equivalence of the above Formalism with the usual Quantum Electrodynamics

As in the previous paper,

$$\begin{aligned} \psi(x)|_{x\subset\sigma} &= \psi(x/\sigma), \quad \mathfrak{A}_\mu(x)|_{x\subset\sigma} = \mathfrak{A}_\mu(x/\sigma), \\ \mathfrak{B}_\mu(x)|_{x\subset\sigma} &= \partial_\mu\Lambda(x)|_{x\subset\sigma} + \partial_\mu\Lambda(x/\sigma) + n_\mu(\Box+\partial^2)^{-1}n_\lambda j_\lambda(x/\sigma), \end{aligned} \quad (25)$$

$$\begin{aligned} \{\bar{\psi}_\alpha(x), \psi_\beta(x')\} &= iS_{\alpha\beta}(x-x'), \\ [\mathfrak{A}_\mu(x), \mathfrak{A}_\nu(x')] &= id^1_{\nu\mu}D(x-x'), \\ [\Lambda(x), \Lambda(x')] &= i\mathscr{D}(x-x'), \end{aligned} \quad (26)$$

where we assumed the existence of a unitary transformation matrix U such that $U\Delta(x, x')U^{-1}$ is the free $\Delta(x-x')$ function. The interaction Hamiltonian $H(x', n)$ can be determined by the commutation relations (26) and the following relations:

$$[\psi(x/\sigma),\ H(x', n)] = i\delta\psi(x/\sigma)/\delta\Omega(x'), \tag{27}$$

$$[\mathfrak{A}_\mu(x/\sigma),\ H(x', n)] = i\delta\mathfrak{A}_\mu(x/\sigma)/\delta\Omega(x'), \tag{28}$$

$$[\partial_\mu\Lambda(x/\sigma),\ H(x', n)] = i\delta\partial_\mu\Lambda(x/\sigma)/\delta\Omega(x'). \tag{29}$$

By differentiating functionally the equations (10), (13) and (24), we get

$$i\delta\mathfrak{A}_\mu(x/\sigma)/\delta\Omega(x') = -ij_\nu(x')d^1_{\nu\mu}D(x-x'), \tag{30}$$

$$i\delta\partial_\mu\Lambda(x/\sigma)/\delta\Omega(x') = in_\mu\partial'_\lambda(j_\lambda(x'/\sigma)\partial\mathscr{D}(x-x')) = in_\mu j_\lambda(x'/\sigma)\partial'_\lambda\partial\mathscr{D}(x-x'), \tag{31}$$

$$\begin{aligned} &i\frac{\delta\psi(x/\sigma)}{\delta\Omega(x')} \\ &= -eS(x-x')\gamma_\mu\psi(x'/\sigma)\{\mathfrak{A}_\mu(x'/\sigma)+\partial'_\mu\Lambda(x'/\sigma)+n_\mu\int_\sigma \mathrm{d}\sigma''_\lambda j_\lambda(x'')\partial'\mathscr{D}(x'-x'')\} \\ &-e\int \mathrm{d}^4x''\,S^\sigma(x, x'')\gamma_\mu\psi(x'')n_\mu\frac{\delta}{\delta\Omega(x')}\int^{\sigma(x')}\mathrm{d}^4x'''\,\partial'''_\lambda(j_\lambda(x''')\partial''\mathscr{D}(x''-x''')). \end{aligned} \tag{32}$$

The second term of (32) becomes

$$\begin{aligned} &-e\int \mathrm{d}^4x''\,S^\sigma(x, x'')\gamma_\mu\psi(x'')\partial'_\lambda(j_\lambda(x')n_\mu\partial''\mathscr{D}(x''-x')) \\ &\qquad = e(\gamma_\nu\partial_\nu-\kappa)\int \mathrm{d}^4x''\,\Delta^\sigma(x, x'')\gamma_\mu\psi(x'')\partial'_\lambda\partial''_\mu\mathscr{D}(x''-x')j_\lambda(x'); \end{aligned}$$

using the relations

$$\Delta^\sigma(x, x'') = \tfrac{1}{2}\{\varepsilon(\sigma, x'')-\varepsilon(x-x'')\}\Delta(x'-x''), \quad \partial'_\lambda\mathscr{D}(x''-x') = n_\lambda\partial''\mathscr{D}(x''-x'),$$

the above expression reduces to

$$\begin{aligned} &= -\tfrac{1}{2}e(\gamma_\nu\partial_\nu-\kappa)\left\{\int\varepsilon(\sigma, x'')\mathrm{d}^4x''-\int\varepsilon(x-x'')\mathrm{d}^4x''\right\} \\ &\Delta(x-x'')\gamma_\mu\psi(x'')\partial''_\mu\partial''\mathscr{D}(x''-x')n_\lambda j_\lambda(x') \\ &= -e(\gamma_\nu\partial_\nu-\kappa)\left\{\int_{-\infty}^{\sigma}-\int_{-\infty}^{x''}\right\}\mathrm{d}^4x''\,\Delta(x-x'')\gamma_\mu\psi(x'')\partial''_\mu\partial''\mathscr{D}(x''-x')n_\lambda j_\lambda(x') \\ &= -e\left\{\int_{-\infty}^{\sigma}-\int_{-\infty}^{x''}\right\}\mathrm{d}^4x''\,S(x-x'')\gamma_\mu\psi(x'')\partial''_\mu\partial''\mathscr{D}(x''-x')n_\lambda j_\lambda(x') \\ &= -e\left\{\int_{-\infty}^{\sigma}-\int_{-\infty}^{x''}\right\}\mathrm{d}^4x''\,\partial''_\mu[S(x-x'')\gamma_\mu\psi(x'')\partial''\mathscr{D}(x''-x')]n_\lambda j_\lambda(x') \end{aligned}$$

(where we used the relations

$$\partial''_\mu[S(x-x'')\gamma_\mu\psi(x'')] = 0, \quad \int_{-\infty}^{\infty}\mathrm{d}x''\,\varepsilon(\sigma, x'') = 2\int_{-\infty}^{\sigma}\mathrm{d}x'')$$

$$= -e\int_\sigma \mathrm{d}\sigma''_\mu\,S(x-x'')\gamma_\mu\psi(x'')\partial''\mathscr{D}(x''-x')n_\lambda j_\lambda(x'),$$

while the second integral vanishes:

$$\begin{aligned} &\int_{-\infty}^{x''}\mathrm{d}^4x''\,\partial''_\mu[S(x-x'')\gamma_\mu\psi(x'')\partial''\mathscr{D}(x''-x')] \\ &\qquad = \int_{-\infty}^{\infty}\mathrm{d}^3x''\,S(x-x'')\gamma_\mu\psi(x'')\partial''\mathscr{D}(x''-x')|^{x''}_{-\infty} = 0. \end{aligned}$$

Then (32) becomes

$$i\frac{\delta\psi(x/\sigma)}{\delta\Omega(x')} = -eS(x-x')\gamma_\mu\psi(x'/\sigma)\{\mathfrak{A}_\mu(x'/\sigma)+\partial'_\mu\Lambda(x'/\sigma) \tag{33}$$
$$+n_\mu\int_{\sigma'}\mathrm{d}\sigma''_\lambda j_\lambda(x'')\partial'\mathscr{D}(x'-x'')\}-e\int_\sigma\mathrm{d}\sigma''_\mu S(x-x'')\gamma_\mu\psi(x'')\partial''\mathscr{D}(x''-x')n_\lambda j_\lambda(x').$$

If we write the interaction Hamiltonian

$$H = -j_\mu(x)\mathfrak{A}_\mu(x)-n_\mu j_\mu(x)\int_\sigma\mathrm{d}\sigma'_\lambda j_\lambda(x')\partial\mathscr{D}(x-x')-j_\mu(x)\partial_\mu\Lambda(x), \tag{34}$$

the left-hand sides of (27), (28) and (29) are

$$[\psi(x), H(x')] = -eS(x-x')\gamma_\mu\psi(x')\left\{\mathfrak{A}_\mu(x')+\partial'_\mu\Lambda(x')+n_\mu\int_\sigma\mathrm{d}\sigma''_\lambda j_\lambda(x'')\partial'\mathscr{D}(x'-x'')\right\}$$
$$-en_\mu j_\mu(x')\int_\sigma\mathrm{d}\sigma''_\lambda S(x-x'')\gamma_\lambda\psi(x'')\partial''\mathscr{D}(x''-x'), \tag{35}$$

$$[\mathfrak{A}_\mu(x), H(x')] = -ij_\nu(x')d^1_{\nu\mu}D(x-x'), \tag{36}$$

$$[\partial_\mu\Lambda(x), H(x')] = -ij_\nu(x')\partial'_\nu\partial_\mu\mathscr{D}(x-x') = in_\mu j_\nu(x')\partial'_\nu\partial\mathscr{D}(x-x'). \tag{37}$$

The second terms of (33) and (35) differ from each other only with respect to the order of the factors, whose difference is related to the Coulomb static self-energy of electrons. In order to eliminate such a term, we must adopt the symmetrized expression $1/2\{A_\mu(x)\psi(x)+\psi(x)A_\mu(x)\}$ instead of $A_\mu(x)\psi(x)$ in (24). In fact, if we put

$$\psi(x) = \psi(x,\sigma)-\tfrac{1}{2}ie\int\{S^\sigma(x,x'')\gamma_\mu\psi(x'')A_\mu(x'')+A_\mu(x'')S^\sigma(x,x'')\gamma_\mu\psi(x'')\}\mathrm{d}x'', \tag{38}$$

eq. (33) becomes

$$i\frac{\delta\psi(x/\sigma)}{\delta\Omega(x')} = -eS(x-x')\gamma_\mu\psi(x'/\sigma)(\mathfrak{A}_\mu(x'/\sigma)+\partial'_\mu\Lambda(x'/\sigma))$$
$$-\tfrac{1}{2}e\left\{S(x-x')\gamma_\mu\psi(x'/\sigma)n_\mu\int_\sigma\mathrm{d}\sigma''_\lambda j_\lambda(x'')\partial'\mathscr{D}(x'-x'')\right.$$
$$\left.+n_\mu\int_\sigma\mathrm{d}\sigma''_\lambda j_\lambda(x'')\partial'\mathscr{D}(x'-x'')S(x-x')\gamma_\mu\psi(x'/\sigma)\right\} \tag{33'}$$
$$-\tfrac{1}{2}e\left\{n_\lambda j_\lambda(x'/\sigma)\int_\sigma\mathrm{d}\sigma''_\lambda S(x-x'')\gamma_\mu\psi(x''/\sigma)\partial''\mathscr{D}(x''-x')\right.$$
$$\left.+\int_\sigma\mathrm{d}\sigma''_\lambda S(x-x'')\gamma_\mu\psi(x''/\sigma)\partial''\mathscr{D}(x''-x')n_\lambda j_\lambda(x'/\sigma)\right\}.$$

Furthermore, if we take the symmetrized interaction Hamiltonian

$$H = -j_\mu(x)\mathfrak{A}_\mu(x)-\tfrac{1}{2}\left\{n_\mu j_\mu(x)\int_\sigma\mathrm{d}\sigma'_\lambda j_\lambda(x')\partial\mathscr{D}(x-x')\right.$$
$$\left.+\int_\sigma\mathrm{d}\sigma'_\lambda j_\lambda(x')\partial\mathscr{D}(x-x')n_\mu j_\mu(x)\right\}-j_\mu(x)\partial_\mu\Lambda(x) \tag{34'}$$

the left-hand side of (27) is

$$\begin{aligned}[\psi(x), H(x')] = &-eS(x-x')\gamma_\mu\psi(x'/\sigma)(\mathfrak{A}_\mu(x'/\sigma)+\partial'_\mu\Lambda(x'/\sigma))\\ &-\tfrac{1}{2}e\left\{S(x-x')\gamma_\mu\psi(x'/\sigma)n_\mu\int_\sigma d\sigma''_\lambda j_\lambda(x''/\sigma)\partial'\mathscr{D}(x'-x'')\right.\\ &\left.+n_\mu\int_\sigma d\sigma''_\lambda j_\lambda(x''/\sigma)\partial'\mathscr{D}(x'-x'')S(x-x')\gamma_\mu\psi(x'/\sigma)\right\} \qquad (35')\\ &-\tfrac{1}{2}e\left\{n_\lambda j_\lambda(x'/\sigma)\int_\sigma d\sigma''_\lambda S(x-x'')\gamma_\mu\psi(x''/\sigma)\partial''\mathscr{D}(x''-x')\right.\\ &\left.+n_\mu\int_\sigma d\sigma''_\lambda j_\lambda(x''/\sigma)\partial''\mathscr{D}(x''-x')n_\lambda j_\lambda(x'/\sigma)\right\}\end{aligned}$$

Then (33') and (35') coincide exactly. By this procedure, it can be proved that the Hamiltonian (34') satisfies all relations (27), (28) and (29).

Thus the equation of motion for the state vector $\Psi[\sigma]$ is given by

$$i\delta\Psi[\sigma]/\delta\Omega(x) = H(x)\Psi[\sigma], \qquad (39)$$

where

$$H(x) = -j_\mu(x)\mathfrak{A}_\mu(x)-n_\mu j_\mu(x)\int_\sigma d\sigma'_\lambda j_\lambda(x')\partial\mathscr{D}(x-x')-j_\mu(x)\partial_\mu\Lambda(x). \qquad (40)$$

We adopt (34) instead of (34') since the total Hamiltonians corresponding to (34) and (34') become the same.

In order to eliminate $\Lambda(x)$, we make use of the following unitary transformation of $\Psi[\sigma]$:

$$\Psi[\sigma] = \exp(-iG[\sigma])\Phi[\sigma], \quad G[\sigma] = \int_\sigma j_\mu(x')\Lambda(x')d\sigma'_\mu \qquad (41)$$

$$\begin{aligned}\exp(iG)\frac{\delta}{\delta\Omega(x)}\exp(-iG) &= -i\frac{\delta G}{\delta\Omega(x)}+\frac{1}{2!}\left[G,\frac{\delta G}{\delta\Omega(x)}\right]+\frac{i}{3!}\left[G,\left[G,\frac{\delta G}{\delta\Omega(x)}\right]\right]+\cdots\\ &= -ij_\mu(x)\mathfrak{A}_\mu(x)+\frac{1}{2!}\int_\sigma[j_\mu(x')\Lambda(x'), j_\nu(x)\partial_\nu\Lambda(x)]d\sigma'_\mu+\cdots\\ &= -ij_\mu(x)\mathfrak{A}_\mu(x)+\tfrac{1}{2}i\int_\sigma n_\mu j_\mu(x')n_\nu j_\nu(x)\partial\mathscr{D}(x-x')d\sigma'\end{aligned}$$

$$\begin{aligned}\exp(iG)H\exp(-iG) &= H(x)+i[G, H(x)]-\frac{1}{2!}[G,[G, H(x)]]+\cdots\\ &= H(x)-i\int_\sigma[j_\mu(x')\Lambda(x'), j_\nu(x)\partial_\nu\Lambda(x)]d\sigma'_\mu\\ &= H(x)+\int_\sigma n_\mu j_\mu(x')n_\nu j_\nu(x)\partial\mathscr{D}(x-x')d\sigma'.\end{aligned}$$

Therefore the final equation of motion for the state vector $\Phi[\sigma]$ becomes

$$i\frac{\delta\Phi[\sigma]}{\delta\Omega(x)} = \left\{-j_\mu(x)\mathfrak{A}_\mu(x)-\tfrac{1}{2}\int_\sigma n_\mu j_\mu(x)n_\nu j_\nu(x')\partial\mathscr{D}(x-x')d\sigma'\right\}\Phi[\sigma]. \qquad (42)$$

This formula is completely equivalent to the form of the ordinary quantum electrodynamics. But in this case no subsidiary conditions are needed

4. Conclusions

Quantum electrodynamics without Lorentz condition could be formulated by dividing the electromagnetic 4-potentials into a transverse part, a term related to Coulomb potential, and the remaining undetermined part in Heisenberg's representation. Here by setting up the new relativistically covariant commutation relations between electromagnetic potentials, the commutation relation for the undetermined part can be derived. This undetermined electromagnetic potential plays a role in defining the Coulomb potential. The commutation relation for the undetermined part could not be found if the canonical formalism were adopted and, although restricted by relativistic covariance, has a very wide scope. Of course, one should prove that the formalism presented here is equivalent to the usual one in Heisenberg representation, but the proof is very complicated and difficult, if the iteration method developed by Yang-Feldman and Källén is used. Furthermore, if the hyperplane is not used, an arbitrary term related to Coulomb potential remains in the electromagnetic potential $\mathfrak{B}_\mu$.

Therefore, using the hyperplane as a σ-surface, we transform the formalism obtained in Heisenberg's representation into the interaction representation by Glauber's method. Here we assume the existence of a unitary transformation matrix leading from the $\Delta(x, x')$ function to the free $\Delta(x-x')$ function. Then the equivalence of this formalism to the ordinary quantum electrodynamics is proved by symmetrizing the expression of the interaction between electromagnetic and electron fields in order to avoid the divergent term relating to the Coulomb static self-energy. Thus, by using the formalism presented here, the un-physical concept of the indefinite metric [7]), resulting from the Lorentz condition, can be avoided and the complications due to the canonical formalism used by Dirac [2]) and Goldberg [8]) vanish.

References

1) S. Ozaki, Prog. Theor. Phys. **14** (1955) 511
2) P. A. M. Dirac, Canadian Journal of Physics **33** (1955) 650;
See also P. A. M. Dirac, The Principles of Quantum Mechanics, 4th edition (1958) Ch. XII
3) C. N. Yang and D. Feldman, Phys. Rev. **79** (1950) 972
4) G. Källén, Arkiv för Fysik **2** Nr. 37 (1950) 371
5) R. J. Glauber in W. Pauli's Ausgewählte Kapitel aus der Feldquantisierung (H. Maag, Zürich, 1950/51) p. 91
6) Y. Takahashi and H. Umezawa, Prog. Theor. Phys. **9** (1953) 14
7) S. N. Gupta, Proc. Roy. Soc. **63** (1950) 681;
K. Bleuler, Helv. Phys. Acta **23** (1950) 567
8) I. Goldberg, Phys. Rev. **112** (1958) 1361

3.B

Nuclear Physics **15** (1960) 510—512; © *North-Holland Publishing Co., Amsterdam*

Not to be reproduced by photoprint or microfilm without written permission from the publisher

ON THE K-CONVERSION COEFFICIENT OF THE 279 keV GAMMA RAY IN THE DECAY OF Hg^{203}

M. K. RAMASWAMY and P. S. JASTRAM

Department of Physics, The Ohio State University, Columbus 10, *Ohio* †

Received 7 December 1959

Abstract: The K-conversion coefficient of the 279 keV gamma-ray following the beta-decay of Hg^{203} has been measured by comparing the X-ray and gamma-ray intensities in a scintillation spectrometer. The measured value of $\alpha_K = 0.195 \pm 0.014$ indicates that the transition is M1 with E2 mixed to the extent of 63 %. Our value is considerably higher than the magnetic beta spectrometer determinations, but is in agreement with the results of Johansson using the scintillation method.

1. Introduction

There have been several determinations of the K-conversion coefficient of the 279 keV gamma-ray following the beta-decay of Hg^{203} [1]). The beta spectrometer measurements give a value of about 0.15 for α_K whereas the only measurement using a scintillation spectrometer [2]) yielded a somewhat higher value of 0.21 with no errors assigned. Since the scintillation method can yield a fairly accurate estimate of α_K when the decay scheme is simple, as in the case of Hg^{203}, we have thought it desirable to remeasure the K-conversion coefficient of the 279 keV gamma-ray using this method.

The experiment consists in determining the relative number of K X-rays and gamma-rays; then if the K-fluorescence yield is known, α_K is given by

$$\alpha_K = \frac{1}{\omega_K} \frac{N_X}{N_\gamma}$$

where N_X = number of K X-rays, and N_γ = number of 279 keV gamma-rays.

2. Experimental Procedure

An Hg^{203} source obtained from Oak Ridge was deposited on a piece of Scotch tape. The source was enclosed in a Lucite well to absorb the beta-rays. The γ-ray spectrum from this source was measured in a $1'' \times 2''$ NaI(Tl) scintillation spectrometer. The source-to-detector distance was 6.3 cm. The spectrum is

† Supported by the U. S. Atomic Energy Commission.

shown in fig. 1. The iodine escape peak is partially resolved from the X-ray peak. In addition to the K X-ray and the 279 keV gamma-ray, there is an additional peak at 136 keV due to backscattering.

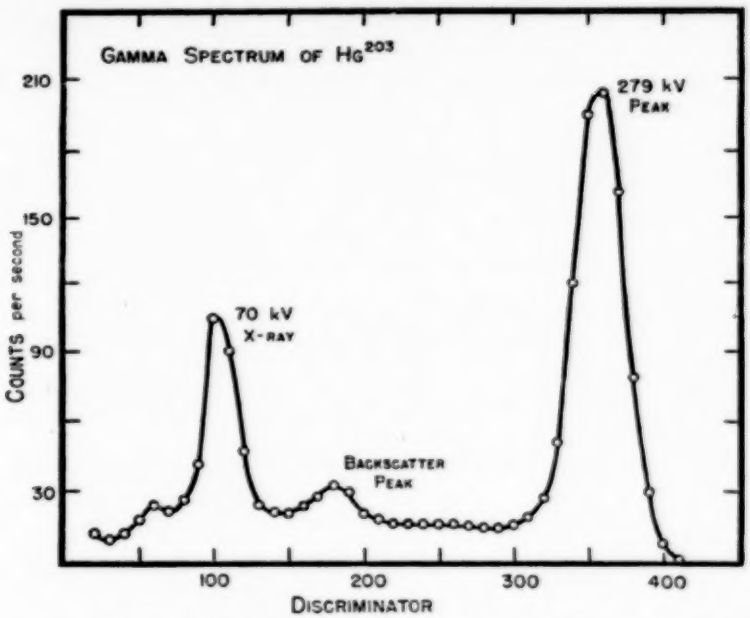

Fig. 1. Gamma-ray spectrum of Hg^{203} observed in a $1'' \times 2''$ NaI(Tl) spectrometer, source-to-detector distance = 6.3 cm.

3. Results

After subtraction of the Compton background under the K X-ray peak, the area under the K X-ray peak and iodine escape peak was estimated. The ratio of the areas under the escape peak and the X-ray peak was determined experimentally to be 0.104. This value was used to obtain the total area under the X-ray peak. The estimation of area in the 279 keV gamma-ray peak was straight forward. In order to estimate the true intensity the photopeak efficiences and peak-to-total ratio (0.84 for the 279 keV gamma-ray) were taken from Bell [3]). The X-ray and gamma-ray intensities were finally corrected for attenuation in the source, air, aluminium and aluminium oxide in the crystal mount. The attenuation factors were 0.776 for the 70 keV K X-ray and 0.887 for the 279 keV gamma-ray respectively. This gave $N_X = 152.1$ cps and $N_{279} = 816.2$ cps. Assuming a value of 0.954 [4]) for the K-shell fluorescence yield, the conversion coefficient α_K was computed to be 0.195 ± 0.014.

4. Discussion

The measured value of $\alpha_K = 0.195 \pm 0.014$ is consistent with a mixed M1—E2 transition, with a mixing ratio $|E2|/|M1|$ of 1.3. Our value is definitely

higher than the magnetic beta spectrometer measurements but agrees with the measurement of Johansson [2]) who also used a scintillation counter. We are unable to offer any explanation for this discrepancy.

References

1) A. H. Wapstra and G. J. Nijgh, Nuclear Physics **1** (1956) 245;
J. L. Wolfson, Can. J. Phys. **34** (1956) 256;
A. H. Wapstra, D. Maeder, G. J. Nijgh and L. T. M. Ornstein, Physica **20** (1954) 169;
S. Thulin and K. Nybö, Arkiv Fysik **7** (1954) 289;
N. Marty, Compt. Rend. **240** (1955) 291;
H. H. Wilson and S. C. Curran, Phil. Mag. **42** (1951) 762;
T. Azuma, Bull. Naniwa Univ. **3A** (1955) 237;
R. K. Doerner and A. H. Weber, Phys. Rev. **91** (1955) 424;
C. Nordling, K. Siegbahn, E. Sokolowski and A. H. Wapstra, Nuclear Physics **1** (1956) 326
2) S. A. E. Johansson, Arkiv Fysik **3** (1952) 533
3) P. R. Bell, in Beta and Gamma-Ray Spectroscopy, edited by K. Siegbahn (North-Holland Publishing Co, 1955) Chapter V
4) A. H. Wapstra, G. J. Nijgh and R. van Lieshout, Nuclear Spectroscopy Tables (North-Holland Publishing Co, 1959) p. 81

8.B

Nuclear Physics **15** (1960) 513—515; © *North-Holland Publishing Co., Amsterdam*

Not to be reproduced by photoprint or microfilm without written permission from the publisher

NOTE ON SYMMETRY OF STRONG INTERACTIONS

L. ŁUKASZUK

Institute of Theoretical Physics, University of Warsaw

Received 2 December 1959

In this note we discuss a certain form of strong interaction, in the frame of the theory of elementary particles given by W. Królikowski [1,2]. The interaction Hamiltonian contains only one arbitrary coupling constant, but one finds, that theoretical conclusions derived from it are not in contradiction with experimental data. It will be seen below, for example, that binding energies of hyperfragments and the baryon mass spectrum can be tentatively explained.

The interaction has the form

$$\mathscr{H}^{\mathrm{int}} = 2\mathring{g}\{\overline{\mathrm{B}}(i\gamma_5)\tfrac{1}{2}(\boldsymbol{\tau}+\xi_\alpha^*\boldsymbol{\tau}_{\alpha\beta}\xi_\beta)\mathrm{B}\cdot\boldsymbol{\pi}+[\overline{\mathrm{B}}(i\gamma_5)\tfrac{1}{2}(\xi_\alpha-\xi_\beta^*\xi_\alpha\xi_\beta)\mathrm{B}(\mathrm{CK})_\alpha+\mathrm{h.c.}]\}$$

where B is the field of baryons, and ξ_α is annihilation operator in isobaric space (see ref. [1])).

We see that $\frac{1}{2}(\boldsymbol{\tau}+\xi_\alpha^*\boldsymbol{\tau}_{\alpha\beta}\xi_\beta) = \mathbf{T}^{\mathrm{B}}$ is responsible for the π-interaction and that the K-interaction is connected with $\frac{1}{2}(N^{\mathrm{B}}-S^{\mathrm{B}}) = \frac{1}{2}(1-\xi_\beta^*\xi_\beta)$. For a more detailed discussion, see ref. [2]†, we only remind that $Q^{\mathrm{B}} = e[T_3{}^{\mathrm{B}} + \frac{1}{2}(N^{\mathrm{B}}-S^{\mathrm{B}})]$. After simple calculations we get

$$\mathscr{H}^{\mathrm{int}} = \mathring{g}\overline{\mathrm{B}}(i\gamma_5)\{2\boldsymbol{\pi}\cdot\mathbf{T}^{\mathrm{B}}+[(\mathrm{CK})_\alpha\xi_\alpha S^{\mathrm{B}}+\mathrm{h.c.}]\}\mathrm{B}.$$

Thus, isobaric spin and strangeness of the baryon field are responsible for different coupling constants in the π- and K-interactions. Writing components of the baryon field (cf. ref. [1])), we have

$$\mathscr{H}^{\mathrm{int}} = i\{\mathring{g}(\overline{\mathrm{N}}\gamma_5\boldsymbol{\tau}\mathrm{N}+\overline{\Xi}\gamma_5\boldsymbol{\tau}\Xi)-2i\mathring{g}\overline{\boldsymbol{\Sigma}}\gamma_5\times\boldsymbol{\Sigma}\}\cdot\boldsymbol{\pi}$$
$$+\left\{i\left[\frac{\mathring{g}}{\sqrt{2}}(\overline{\mathrm{N}}\gamma_5\Lambda^0+\overline{\mathrm{N}}\gamma_5\boldsymbol{\tau}\cdot\boldsymbol{\Sigma})+\mathring{g}\sqrt{2}(\bar{\Lambda}^0\gamma_5\Xi\mathrm{C}-\boldsymbol{\Sigma}\gamma_5\Xi\mathrm{C}\cdot\boldsymbol{\tau})\right]\mathrm{K}+\mathrm{h.c.}\right\}. \quad (1)$$

The large coupling constants $\mathring{g}^2_{\Sigma\mathrm{NK}} = \mathring{g}^2_{\Lambda\mathrm{NK}} = \frac{1}{2}\mathring{g}^2_{\mathrm{NN}\pi}$ resulting from the model are in agreement with K^+—p scattering: G. Białkowski and A. Jurewicz have in fact derived [3]) — using Tamm-Dancoff method with recoil — the K^+—p scattering cross-section in agreement with experiment up to 400 MeV

† There is a misprint in ref. [2]): one must replace $\mathbf{T}^{\mathrm{B}}$ by $2\mathbf{T}^{\mathrm{B}}$ in eq. (6). Besides, "h.c." refers to the K-interaction only.

(laboratory system). They must put $g^2_{\Sigma NK}+g^2_{\Lambda NK} \approx g^2_{NN\pi}$, exactly as in our Hamiltonian. (We neglect modifications of this symmetry caused by renormalization.)

The next characteristic feature of the Hamiltonian (1) is $\mathring{g}_{\Sigma\Lambda\pi} = 0$; the chief contribution to the Λ—N potential is thus given by the K-mesons. A detailed discussion of this type of potential has been made by D. B. Lichtenberg and M. Ross [4]), using a perturbation method. It follows from these authors' discussion that the V_K potential arising from one K-meson exchange only suffices to account for the binding energies of hyperfragments (in the case of PS coupling); besides, one finds that Λ—N has no bound state, but that there exist Σ^+—p and Σ^-—n bound states. The coupling constant necessary here, $g^2_{\Lambda NK} = \frac{1}{2}g^2_{NN\pi}$, is equal to that in the Hamiltonian (1).

In Lichtenberg and Ross's estimations, there are difficulties with the $V_{K\pi}$ potential, which is repulsive in ^{3}S states and exceeds V_K for $m_\pi r < 1$. On the other hand, the V_{KK} potential arising from two-K-meson exchange, which is attractive, is too weak to overcome $V_{K\pi}$. Note, however, that — according to Lichtenberg and Ross — difficulties arise only if all $g_K{}^2 < g^2_{NN\pi}$. In our case, because of the large $g^2_{\Sigma\Lambda K} = 2g^2_{NN\pi}$, we get $V_{KK}+V_{K\pi} < 0$ for $m_\pi r < 0.7$ and the potential $V = V_K+V_{K\pi}+V_{KK}$ is much more attractive than V_K alone. In the region $0.7 < m_\pi r < 1$, the potential $V = V_K+V_{K\pi}+V_{KK}$ is weaker than V_K itself, but this variation can be neglected in comparison with the variations in the region $m_\pi r < 0.7$. It follows that $V_{K\pi}$ and V_{KK} will not qualitatively spoil the results obtained from V_K. It is impossible to estimate quantitative effects of these potentials at present. We hope, however, that — if a hard core of the Λ—N potential exists — the influence of $V_{K\pi}$ and V_{KK} will not diminish the value necessary for $g_{\Lambda NK}$ too much.

Another effect caused by $\mathring{g}_{\Sigma\Lambda\pi} = 0$ is the non-existence of the virtual process $\Sigma \to \Lambda+\pi$ in the decay of Σ or Λ. D. Rogula [5]) remarked that the lack of a $\Sigma\Lambda\pi$ term diminishes corrections due to strong interactions to the decay process $\Lambda \to N+\pi$.

Finally, the Hamiltonian discussed above gives — with the additional phenomenological term $\mu\overline{B}S^B B$ ($\mu = 212m_e$ is the μ-meson mass) — a mass spectrum of baryons covering the experimental one [2]). The perturbation method in fixed-source theory was applied in computing this spectrum. The required cut-off, common for π- and K-interactions, $k_{max} = 3.5m_\pi = m_K$, is small in comparison with that of Chew and Low's theory. This fact may be understood as the influence of the term $\mu\overline{B}S^B B$, which causes k_{max} to be less than in the scattering problem. The term $\mu\overline{B}S^B B$ corresponds to the assumption that the μ-meson mass and the baryon "bare" mass spectra connected with different S^B have partly the same origin.

The author is indebted to Professor W. Królikowski for helpful advice.

References

1) W. Królikowski, Nuclear Physics **8** (1958) 461
2) L. Łukaszuk, Bull. Acad. Polon. Sci. **8** (1959) 515
3) G. Białkowski and A. Jurewicz, Phys. Rev. (to be published)
4) D. B. Lichtenberg and M. Ross, Phys. Rev. **109** (1958) 2163
5) D. Rogula, private communication

7.A

Nuclear Physics **15** (1960) 516—518; © *North-Holland Publishing Co., Amsterdam*

Not to be reproduced by photoprint or microfilm without written permission from the publisher

A NOTE ON DISPERSION RELATIONS

ALLADI RAMAKRISHNAN, N. R. RANGANATHAN † and R. VASUDEVAN ††

Department of Physics, University of Madras

and

S. K. SRINIVASAN

Department of Applied Mathematics, Indian Institute of Technology, Guindy, Madras

Received 26 October 1959

Abstract: Dispersion theory is examined on the basis of a reciprocal relationship between the real and imaginary part of the scattering amplitude and it is shown that the knowledge of the absorptive part over the unphysical region leads to a linear integral equation for the dispersive part.

The theory of dispersion relation arose in an attempt to meet the inadequacies of the perturbation theory. It is based upon the possibility of writing the real part of the scattering amplitude as an integral over the imaginary part as a consequence of the analytic properties of the matrix element. In a corresponding manner, the imaginary part can be related to the real part. If in the former relation we substitute the latter, we are naturally led to an identity which merely expresses the fact that one set of relations implies the other. However, we wish to point out that there are circumstances under which the substitution leads to a meaningful integral equation for the real or the imaginary part. Such a case arises if the imaginary part is known over a partial range. In our opinion, the principle used in this note is of general value. However, to demonstrate it, we confine ourselves to the special case of forward scattering of a charged pion by a nucleon.

The application of dispersion relations to pion-nucleon scattering phenomena becomes a little involved owing to the charge states of pions and nucleons (see for example, Goldberger [1])). From the forward scattering amplitudes F_+ and F_- of positive and negative pions by protons, which may be written

$$F_\pm(\omega) = D_\pm(\omega) + iA_\pm(\omega) \tag{1}$$

in the system in which the proton is at rest (ω denotes the energy of the pion), the following linear combinations can be formed:

$$F_E(\omega) = \tfrac{1}{2}\{F_-(\omega) + F_+(\omega)\}, \tag{2}$$

$$F_O(\omega) = \tfrac{1}{2}\{F_-(\omega) - F_+(\omega)\}. \tag{3}$$

† Indian Atomic Energy Commission Junior Research Fellow.

†† Government of India Senior Research Scholar. Now Assistant Research Physicist at the University of California, La Jolla.

From the general theory of scattering of a pseudoscalar boson by a nucleon, Goldberger [1]) has shown that

$$F_E^*(\omega) = F_E(-\omega), \tag{4}$$

$$F_O^*(\omega) = -F_O(-\omega). \tag{5}$$

It is easy to write down the dispersion relations by using equations (1) to (5) (see Goldberger *et al.* [2])):

$$D_E(\omega) - D_E(\mu) = \frac{2k^2}{\pi} \mathrm{P} \int_0^\infty \frac{\omega' A_E(\omega') \mathrm{d}\omega'}{k'^2(\omega'^2 - \omega^2)}, \tag{6}$$

$$D_O(\omega) = \frac{2\omega}{\pi} \mathrm{P} \int_0^\infty \frac{A_0(\omega') \mathrm{d}\omega'}{\omega'^2 - \omega^2}, \tag{7}$$

where μ is the meson mass and k its momentum. The absorptive parts A_E and A_O can be evaluated explicitly in the range $0 < \omega < \mu$ in the usual way. Thus (6) and (7) can be written in the form

$$D_E(\omega) - D_E(\mu) = \frac{f^2\omega^2}{M[\omega^2 - (1/2M)^2]} + \frac{2k^2}{\pi} \mathrm{P} \int_\mu^\infty \frac{\omega' A_E(\omega') \mathrm{d}\omega'}{k'^2(\omega'^2 - \omega^2)}, \tag{8}$$

$$D_O(\omega) = \frac{2f^2\omega}{\omega^2 - (1/2M)^2} + \frac{2\omega}{\pi} \mathrm{P} \int_\mu^\infty \frac{A_O(\omega')}{\omega'^2 - \omega^2} \mathrm{d}\omega'. \tag{9}$$

At this stage we observe that inverse relations can be written down expressing A_E or A_O as an integral over D_E or D_O, as the case may be. The arguments which have led to (5) and (6) yield

$$A_E(\omega) = -\frac{2\omega}{\pi} \mathrm{P} \int_0^\infty \frac{D_E(\omega')}{\omega'^2 - \omega^2} \mathrm{d}\omega', \tag{10}$$

$$A_O(\omega) = -\frac{2}{\pi} \mathrm{P} \int_0^\infty \frac{\omega' D_O(\omega') \mathrm{d}\omega'}{\omega'^2 - \omega^2}. \tag{11}$$

We have assumed that no subtraction is necessary for the absorptive parts.

We now observe that if (10) and (11) are fed into the right hand side of (8) and (9) respectively, we obtain integral equations for D_E and D_O:

$$D_E(\omega) - D_E(\mu) = \frac{f^2\omega^2}{M[\omega^2 - (1/2M)^2]} - \frac{4k^2}{\pi} \mathrm{P} \int_\mu^\infty \frac{\omega' \mathrm{d}\omega'}{k'^2(\omega'^2 - \omega^2)} \int_0^\infty \frac{D_E(\omega'') \mathrm{d}\omega''}{\omega''^2 - \omega'^2}, \tag{12}$$

$$D_O(\omega) = \frac{2f^2\omega}{\omega^2 - (1/2M)^2} - \frac{4\omega}{\pi^2} \int_\mu^\infty \frac{\mathrm{d}\omega'}{\omega'^2 - \omega^2} \int_0^\infty \frac{\omega'' D_O(\omega'')}{\omega''^2 - \omega'^2} \mathrm{d}\omega''. \tag{13}$$

We hope that this method of viewing the dispersive part as the solution of an integral equation might sometimes be helpful in understanding physical phenomena. Investigations based on (12) and (13) are in progress and will be reported in due course. The procedure adopted here amounts to using our knowledge of the functions over the range $(0, \mu)$ to obtain the functions in the residual range.

References

1) M. L. Goldberger, Phys. Rev. **99** (1955) 979
2) M. L. Goldberger, H. Miyazawa and R. Oehme, Phys. Rev. **99** (1955) 956

8.A

Nuclear Physics **15** (1960) 519—521; © *North-Holland Publishing Co., Amsterdam*

Not to be reproduced by photoprint or microfilm without written permission from the publisher

AN UNUSUAL DOUBLE STAR FROM A K⁻-CAPTURE IN EMULSION

M. NIKOLIČ †, W. KOCH, M. SCHNEEBERGER and H. WINZELER

Physikalisches Institut der Universität, Bern

Received 25 November 1959

In a systematic study of double stars produced by K⁻-interactions in flight and at rest an interesting event was found. The subject of the present paper is a discussion of the possible interpretations of the event in question.

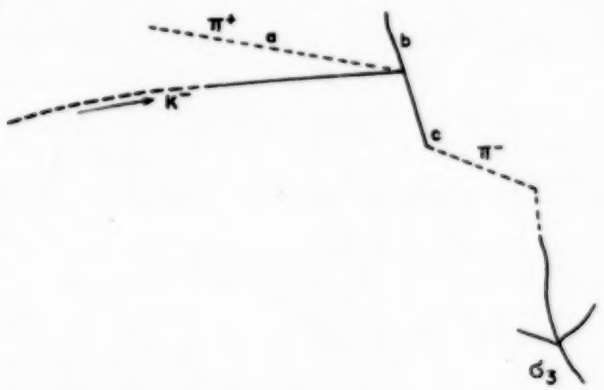

The event is illustrated in the figure. A K⁻-meson came to rest and produced a 3 prong star. Track a belongs to a π^+ meson of 62 MeV, tracks b and c have lengths of 14μ and 6μ respectively. At the end of track c a π^- is emitted with a total range of 9417μ and a corresponding energy of 22.2 MeV. The π^- undergoes an elastic deflection of 49°, 3612μ before coming to rest. The ionization was measured before and after the scattering. The change in ionization was $0 \pm 6.5\%$.

The space angle between the track c and the emitted π^- is about 63°. Track c being only 6μ long, it is impossible to conclude whether or not the corresponding particle came to rest. Neither a blob nor an electron was observed at its end. The event was also inspected from the glass side.

The emission of the π^+ from the K⁻-star provides certain evidence that the K⁻-meson was absorbed and that no K⁻ re-emission took place. As the charge exchange probability for pions is very small in this case [1]) the K⁻-absorption most probably gives rise to the reaction

$$K^- + p \rightarrow \Sigma^- + \pi^+.$$

† On leave of absence from the Institute of Nuclear Sciences, Boris Kidrich, Belgrade.

Therefore in the following we shall discuss various interpretation probabilities for the secondary event under the assumption that in the original event a Σ^- had been produced.

a) *Normal Σ-decay.* This assumption can be excluded by considering the kinematics of the decay. In order to emit a π^- with 22 MeV energy in any direction the Σ^- should have at least 145 MeV kinetic energy; which greatly exceeds the Q value of the primary one-nucleon reaction.

b) *Radiative Σ-decay.* The event we are dealing with could represent an example of Innerbremsstrahlung in the hyperon decay with a relatively high energy photon emission. The probability of this process has been calculated by Barshay and Behrends [2]).

In this connection we mention another event presented in an earlier paper [3]). No satisfactory explanation could be given there. However, if the small blob observed in that event is accidental, the event could be interpreted as a radiative Σ^+ decay.

c) *Λ^0 hyperfragment.* The Σ^- of the primary reaction can be reabsorbed forming a Λ^0 hyperfragment. The greatest difficulty in interpreting our event in this way is the absence of a visible recoil in the secondary event. A π^- decay of the Λ^0 hyperfragment would result in at least two positive charges among the decay products. A π^0 decay, with subsequent charge exchange scattering of the pion, would leave at least one positive charge in the recoil nucleus. In spite of the invisible recoil, the event in question could still be a Λ^0 hyperfragment under the assumption that the recoil coincides with the primary track (in this case it could not be longer than 7μ), or that the decay kinematics are such that the residual nucleus takes only very little momentum, or that it is very heavy.

In view of the observed low energy of the pion, mesic two-body decay of the hyperfragment is in this case consistent only with a heavier hyperfragment than has been identified to the present. However, the probability of the mesic decay mode decreases as Z increases.

Of the hyperfragments known up to now only three- or more-body decays of heavier hypernuclei and four- or more-body decays of light hypernuclei (both with neutron emission) can account for the low visible energy of the event without yielding an unreasonably high binding energy for the Λ^0.

It is hard to estimate the probability of these possible decay modes because no similar events have been recorded up to now. All we can say is that, in the case of a light hypernucleus, the probability of a four-body decay is low and becomes still lower under the condition that the recoil remains invisible or has to coincide with the primary track.

The assumption of the emission of 2 neutrons would also imply the decay of a heavier hypernucleus. However, the probability of the mesic decay mode of the latter is suppressed with increasing Z.

If we are dealing with a heavier hypernucleus one cannot completely exclude

the possibility that this event is the decay of a heavier Λ^0 hypernucleus with an undetected recoil and neutron emission.

d) (Σ^-nn) *compound.* The event in question can represent an example of a (Σ^-n) or (Σ^-nn) compound, the existence of which is possible according to theoretical considerations [4, 5]).

Baldo-Ceolin *et al.* [6]) found an event which was interpreted as a (Σ^+p) compound. Assuming charge symmetry, the (Σ^+p) and the (Σ^-n) compound are different from each other only with respect to the Coulomb potential.

In our case a (Σ^-nn) decay, in which the energy release is distributed among four particles, would correspond better to the observed low energy of the pion. Since a Σ^- compound would be absorbed immediately upon coming to rest (similarly to the Σ^- hyperon), the decay of the hypernucleus must have occurred in flight.

As may be seen from the above considerations, the event we are dealing with can represent either a radiative Σ^- decay or an example of the Σ^- compound; or if it is a Λ^0 hyperfragment, then it is probably heavier than any yet identified. So far we cannot say which of these interpretations is the most adequate.

This note was submitted to the Kiev Conference on High Energy Physics without the discussion of the possibility of a radiative Σ^- decay. An example of the (Σ^-n) compound, evidenced by precise mass measurements, was also communicated by Gandolfi, Heughebaert and Quereigh at that conference. This event has already been published in Nuovo Cimento [7]).

This work was supported in part by the Schweizerische Studienkommission für Atomenergie and the Kommission für Atomwissenschaften.

References

1) M. Nikolič, Y. Eisenberg, W. Koch, M. Schneeberger and H. Winzeler, preprint: Interactions of K⁻-Meson at Rest in Nuclear Emulsions. V. The Multi-Nucleon Capture Mode (Bern 1959) (to be submitted to Helv. Phys. Acta);
W. Koch, Y. Eisenberg, M. Nikolič, M. Schneeberger and H. Winzeler, preprint: Interactions of K⁻-Mesons at Rest in Nuclear Emulsions VI. The Single Nucleon Capture Mode (Bern, 1959) (to be submitted to Helv. Phys. Acta)
2) S. Barshay and R. E. Behrends, Phys. Rev. **114** (1959) 931
3) Y. Eisenberg, W. Koch, M. Nikolič, M. Schneeberger and H. Winzeler, Nuovo Cimento **9** (1958) 745
4) W. Holladay, quoted by Sachs, Phys. Rev. **99** (1955) 1573
5) R. N. Dalitz, Reports on Progress in Physics **20** (1957) 163
6) M. Baldo-Ceolin, W. F. Fry, W. D. B. Greening, H. Huzita and S. Limentani, Nuovo Cimento **6** (1957) 144
7) E. Gandolfi, J. Heughebaert and E. Quereigh, Nuovo Cimento **13** (1959) 864

1.D.2:
3.C

Nuclear Physics **15** (1960) 522—524; © *North-Holland Publishing Co., Amsterdam*
Not to be reproduced by photoprint or microfilm without written permission from the publisher

NUCLEAR SHAPE EFFECT ON ISOMERIC SHIFT

J. LARDINOIS

Aspirante au Fonds National de la Recherche Scientifique, Université Libre de Bruxelles

Received 16 November 1959

Abstract: The nuclear isomeric shift for $_{49}In^{115}$ III (odd-proton nucleus) and $_{80}Hg^{197}$ (odd-neutron nucleus) has been calculated taking account of a collective deformation of the core. Theoretical results agree with experimental data for Hg^{197}.

1. Introduction

The electrostatic charge distribution of a nucleus varies when it goes over from the isomeric m state to the fundamental f state. This variation perturbs the energy of the optical s electron, giving rise to an *isomeric shift*, that we shall calculate to the first order of perturbation. The problem has been treated by Weiner [1, 2]) who assumed that the optical nucleon is alone responsible for the isomeric transition and goes over from the individual state ψ_m to ψ_f, the remaining part of the nucleus being unaffected by the transition. It is seen immediately that, in such a model, the isomeric shift vanishes for odd neutron nuclei.

Let us first summarize the computation of the isomeric shift of $_{49}In^{115}$ III as it has been done in ref. [1]). The optical proton makes a transition from a $2p_{\frac{1}{2}}$ m state to the $1g_{\frac{9}{2}}$ f state and we take for the ψ's oscillator wave functions. The difference of electrostatic potential between m and f is given by

$$\varphi_m(r)-\varphi_f(r) = e\int \frac{\psi_m^*\psi_m-\psi_f^*\psi_f}{|\mathbf{r}-\mathbf{r}'|}\,d\mathbf{r}'.$$

When we limit ourselves to the monopole term it becomes

$$\varphi_m-\varphi_f = e\left[\frac{1}{r}\int_0^r r'^2(R_m^*R_m-R_f^*R_f)dr' + \int_r^\infty \frac{R_m^*R_m-R_f^*R_f}{r'}r'^2dr'\right],$$

which induces an energy shift of the optical s electron

$$\Delta E = -e\int(\varphi_m-\varphi_f)|\psi_e|^2 d\mathbf{r}'_e.$$

We take for $|\psi_e|^2$ in the neighbourhood of the origin

$$|\psi_e|^2 = \frac{2(1+\gamma)|\psi_e(0)|^2}{\Gamma^2(2\gamma+1)}\left(\frac{2Z}{a_0}\right)^{2\gamma-2} r^{2\gamma-2} = Ar^{2\gamma-2}, \quad \gamma = [1-(Z/137)^2]^{\frac{1}{2}};$$

from spectroscopic measurements, one derives [3])

$$\psi_e^2(0) = \frac{1}{\pi a_0^3} \frac{Z(1+z)}{n_{\text{eff}}^3}, \quad z = 2, \quad n_{\text{eff}} = 1.7.$$

Four our case, this gives $\psi^2(0) = 1.9 \times 10^{26}$ cm^{-3} and the other constants are given in ref. [1]): the radius of the nucleus is taken as $R_0 A^{\frac{1}{3}}$ with $R_0 = 1.2 \times 10^{-13}$ cm, the specific length of the oscillator $r_0 = [\hbar/\mu\omega]^{\frac{1}{2}} = 2.5 \times 10^{-13}$ cm. Then, the isomeric schift ΔE becomes -5×10^{-2} cm^{-1}, and seems thus to lie at the limit of optical measurability.

However, it results from the study of nuclear properties, and in particular of nuclear quadrupole moments, that the optical nucleon does not make a pure individual transition but remains coupled with the core; we shall take up again the calculation on the basis of a collective model, to test the limits of validity of Weiner's assumption.

We shall assume, on the analogy of Rainwater's model for the determination of quadrupole moments, that an odd-proton nucleus gives two contributions to the isomeric shift: the first, which was calculated by Weiner, comes from the optical proton transition, the other, which is due to the deformation of the core by attractive coupling with the optical nucleon, is of a collective nature. In a first study, we shall include the optical nucleon in the core, so as to find an upper limit to the collective term.

We shall study an odd-proton nucleus ($_{49}$In^{115} III) and an odd-neutron nucleus ($_{80}$Hg^{197}) for which recent measurements of isomeric shift have been made [4]).

2. Calculation of Isomeric Shift

In a collective model, the nucleus goes over from one state, characterized by the deformation parameter α_m, to another state α_f; α_m and α_f are supposed to be much smaller than 1 and are related to the equation of the nuclear surface by $R_s(\cos\theta) = R_0[1+\alpha P_2(\cos\theta)]$ where $P_2 = \frac{1}{2}(3\cos^2\theta - 1)$. We calculate here the isomeric shift as though it were due only to this change of shape. The electrostatic charge density is assumed to be uniform inside of the surface S and the volume included in the nuclear surface is assumed to remain constant during the deformation. The perturbation that appears in the optical electron level when the nucleus is deformed from the spherical shape to a shape that is characterized by α, has been calculated by Wilets, Hill and Ford [5]) in their study of shape effect on the isotope shift; it is equal to

$$\Delta_\alpha E = 4\pi Z e^2 A R^{2\gamma} \frac{3}{10} \frac{1}{2\gamma+1} \alpha^2.$$

The α parameter is known from experimental data on quadrupole moments. The uniform distribution of the Ze charge inside of R_s has a quadrupole mo-

ment [6]) $Q = \frac{3}{2} \cdot \frac{4}{5} Z R^2 \alpha$. For In we take arbitrarily for Q the highest of the two values given in ref. [7]): $Q_f = 1.14 \times 10^{-24}$ cm^2, and accordingly $\alpha_f = 0.06$. The quadrupole moment of the m state is equal to zero ($I = \frac{1}{2}$) and we do not know anything about the intrinsic deformation of this state; we suppose it to be smaller than α_f, since the optical proton in the $\frac{1}{2}$ state tends to reduce the deformation by attractive coupling with the core. We only ask for a qualitative result and therefore take $\alpha_m = 0$. We thus get

$$\Delta E = 4\pi Z e^2 A R^{2\gamma} \frac{3}{10} \frac{1}{2\gamma+1} (\alpha_m{}^2 - \alpha_f{}^2) = -5.5 \times 10^{-3} \text{ cm}^{-1}.$$

This result has the same sign as Weiner's result, but is ten times smaller.

For Hg, the quadrupole moment Q_m is given in ref. [4]): $Q_m = 1.5 \times 10^{-24}$ cm^2 ($I_m = \frac{13}{2}$), and we deduce $\alpha_m = 0.032$. Again Q_f is equal to zero ($I_f = \frac{1}{2}$) and we take $\alpha_f = 0$. We obtain for the 6s-electron which gives the 2537Å resonance line $6\,{}^1S_0 - 6\,{}^3P_1$, for which [8]) $n_{eff} = 1.56$, $z = 0$;

$$\Delta E = 21 \times 10^{-3} \text{ cm}^{-1}.$$

The isomeric shift of this line has been recently measured by Melissinos and Davis [4]), who find $\Delta E = 21 \times 10^{-3}$ cm^{-1}. The coincidence between theoretical and experimental results is of course fortuitous in view of the oversimplification of the theoretical treatment; but the collective model seems to provide a good estimate of the order of magnitude of the effect for this odd-neutron nucleus.

However, for the odd-proton In nucleus, the collective effect is ten times smaller than the individual one. This contrasts with the situation regarding quadrupole moments, for which the collective contribution is the most important one: this is due to the fact that the quadrupole moment is of the first order in α, whereas the isomeric shift is a monopole effect of the second order in α. In the case of In, the deformation is small and the modification of the optical nucleon wave function is important; therefore Weiner's model gives probably a better estimate of the effect.

I am indebted to Professor M. Demeur for helpful discussions on this problem. I wish to thank Dr. Melissinos for information about the isomeric shift in Hg^{197}.

References

1) R. Weiner, Nuovo Cimento **4** (1956) 1587
2) R. Weiner, Phys. Rev. **114** (1959) 256
3) F. Paschen and J. L. Campbell, Ann. d. Phys. **31** (1938) 29
4) A. C. Melissinos and S. P. Davis, Phys. Rev. **115** (1959) 130
5) L. Wilets, D. L. Hill and K. W. Ford, Phys. Rev. **91** (1953) 1488
6) M. G. Mayer and J. H. D. Jensen, Elementary theory of nuclear shell structure (J. Wiley, New York, 1955) p. 115
7) D. Strominger, J. M. Hollander and G. T. Seaborg, Revs. Mod. Phys. **30** (1958) 691
8) F. Paschen, Ann. d. Phys. **6** (1930) 49

4.E

Nuclear Physics **15** (1960) 525—526; © *North-Holland Publishing Co., Amsterdam*

Not to be reproduced by photoprint or microfilm without written permission from the publisher

THE HALF LIFE OF In^{116}

A. DUCAT † and R. H. THOMAS

Research Laboratory, Associated Electrical Industries, Aldermaston, Berks.

Received 30 November 1959

The half life of In^{116} has recently been reported as 14.5 ± 0.4 s by Capron and Stricht [1]), but previous determinations were of only moderate accuracy. Amaldi *et al.* [2]) and Cork and Lawson [3]) each gave values of 13 seconds but quoted no error, whilst Wilhelmi *et al.* [4]) obtained a value of 12.5 ± 2 s. We have been able to measure this half life to a higher accuracy than hitherto reported.

In the present measurement D—D neutrons were used to irradiate a type G20In indium activation counter set at the centre of a nine-inch diameter paraffin wax moderator. After irradiations of one minute the decay of activity was followed for nine successive periods of five seconds, using a time analyser of the type described by Churchill and Evans [5]). Approximately 80 % of the observed background rate was identified as being due to the 54 min meta-stable In^{116}, since the measured yield of the 54 min period activity agreed exactly with that calculated from the known thermal neutron absorption cross-sections. The experimental data were corrected for dead-time losses in the analyser, which was measured to within 10 % using the two source method and checked using a pulse generator. Channel dead-times were found to lie between 400 and 500 μs. Counts were taken over the region of the decay curve where the dead-time corrections were not excessive and the background count less than 10 % of the initial counting rate.

Six independent measurements were made and the half-life calculated by the method of least squares, the values obtained being

$$14.17 \pm 0.72 \qquad 13.97 \pm 0.45$$
$$13.40 \pm 0.95 \qquad 14.39 \pm 0.50$$
$$14.03 \pm 0.91 \qquad 13.82 \pm 0.74.$$

These give a weighted mean of

$$14.05 \pm 0.26 \text{ s.}$$

The errors quoted include a possible systematic error of ± 0.10 s from the uncertainty in the dead-time correction. Our value is in good agreement with

† Present address: Gonville and Caius College, Cambridge.

that obtained by Capron and Stricht, and within the limits of errors quoted by Wilhelmi *et al.*

Our thanks are due to Dr. T. E. Allibone, F.R.S., Director of the Laboratory, for permission to publish this note and to Dr. S. E. Hunt for his advice and interest in this work.

References

1) P. C. Capron and A. V. Stricht, Ann. Soc. Sci. Bruxelles **71** (1957) 20
2) E. Amaldi *et al.* Proc. Roy. Soc. A **149** (1935) 522
3) J. M. Cork and J. L. Lawson, Phys. Rev. **56** (1939) 291
4) Z. Wilhelmi, R. Brunsz and C. Dąbrowski, Bull. Akad. Polon. Sci. **1** (1953) 105
5) K. Churchill and W. W. Evans, Electronic Engineering, **27** (1955) 324

10.D *Nuclear Physics* **16** (1960) 527—532; © *North-Holland Publishing Co., Amsterdam*

BOOK REVIEWS

B. KOCKEL, W. MACKE, A. PAPAPETROU and W. FRANK, Editors, *Max-Planck-Festschrift* 1958 (VEB Deutscher Verlag der Wissenschaften, Berlin, 1959. 413 p. DM 54)

This commemorative volume,containing contributions by some thirty distinguished contributors, was issued to celebrate Max Planck's one-hundredth birthday. The contributions are in part original research papers, in part review or discussion articles. Broadly, they are classified as "classical", "relativistic", and "quantum-physical", with considerable overlap. The choice of contributors and topics was intended to reflect Planck's own attitude, his broad interests in all aspects of physics, coupled with his striving for organic unity of our science. The volume appears to be a truly important contribution to the scientific literature.

In view of the wide variety of contributions it is not feasible to comment on each article separately. Only one article appears to belong to the field of nuclear physics, and this paper, also, represents a borderline topic, "Collapsed Matter of Nuclear Density and Nuclear Goblins", by Fritz Zwicky, of the Mount Wilson and Palomar Observatories. In this paper, Zwicky suggests that under certain circumstances, particularly under very high pressure, matter may condense to the extent that it exhibits properties of nuclear matter in macroscopic amounts, including the stability of neutrons against beta-decay. Such a concentration of condensed matter Zwicky calls a goblin, and he speculates that goblins may exist in the interior of stars, and there perhaps in considerable numbers. If so, through random processes every now and then a goblin may escape into the star's exterior and there explode, giving rise to a flare star, or even to the eruption of a nova. Zwicky himself agrees that at present his hypothesis of goblins, and their connection with the explosive release of stellar energy, is speculative, but he considers the hypothesis a promising line of inquiry.

Particular attention should be called to the inclusion of several epistemological papers in this volume, by N. Bohr, V. Fock, L. de Broglie, L. Rosenfeld, and L. Janossy. These papers are concerned principally with the philosophical aspects of quantum theory and of statistical mechanics. There are also a few papers concerned with topics in quantum field theory, high-energy physics, the theory of elementary particles, and almost every other important area in contemporary theoretical physics. All in all, this book is a distinguished memorial to one of the very great spirits in modern physics.

Peter G. Bergmann

GEORG JOOS, *Lehrbuch der theoretischen Physik*, 10. Auflage (Akademische Verlagsgesellschaft, Frankfurt a/M, 1959. xxiii—842 pages. DM 38)

This edition of Joos' well-known textbook is the last to contain additions and improvements from his own hand: it appears as a memorial to a distinguished teacher who devoted many years to perfecting it and keeping it abreast of the new developments. The birth and growth of quantum theory was something of a *crux* to the teachers of theoretical physics of the older generation: how could the new-fangled stuff be introduced into a nicely poised curriculum without sacrificing the older subjects which had retained their full value, and yet without disturbing the balance of the whole by extending the duration of the theoretical course beyond the appointed period? None solved this challenging task better than Joos — no doubt because none had the courage to tackle it with such devotion: every detail in the treatise which became his life-work is the fruit of long thought and experience. Joos (as I learned from one of his old pupils) was a brilliant lecturer; he delighted in streamlined expositions clearly exhibiting the relations between the different parts and putting the right emphasis on essentials. These are precisely the qualities which distinguish the treatment given in this book, and thus convey to the reader something of the author's attractive personality.

L. R.

A. PIRIE *et al.*, *La menace radioactive. Danger des retombées radioactives provenant des explosions nucléaires*. Traduit par L. Chopard (Dunod, Paris, 1959. ix—127 pages. 9.50 n. f.)

French translation of an agitation pamphlet published by a group of distinguished British scientists, with a preface by Bertrand Russell. The aim of this booklet is to call the public's attention to the possible dangers of radioactive contamination as a result of nuclear-weapon tests. It contains a great deal of information, but this is unfortunately presented with some emotional bias, and without references to sources from which an independent judgment on the reliability of such information could be formed. The production of the French version is a hasty and careless piece of work (even the name of B. Russell as well as that of Dr. Burhop are misspelt on the title-page). The translation is sometimes obscure.

L. R.

I. SZABÓ, *Mathematische Formeln und Tafeln* (Wilhelm Ernst und Sohn, Berlin, 1959. xv—287 pages. DM 19.80)

The publishers of the famous engineer's handbook „Hütte" have had the excellent idea to make a separate issue of the part of this handbook devoted to mathematical tables and formulae. Thanks to unusually fine typography, it has been possible to compress in less than 300 pages of very legible type a formidable amount of mathematical information. Besides the usual logarithmical and arithmetical tables we find short tables of elliptical integrals, Bessel functions and Legendre polynomials: altogether 26 tables. Then comes a systematic and exhaustive survey of the whole field of mathematics, ranging from arithmetics to the theory of functions, followed by chapters on the theory of probabilities and on "practical mathematics" (i.e. methods of computation and evaluation in the widest sense). Series expansions and integrals, trigonometrical formulae, vector algebra, matrix calculus, analytical geometry, differential equations — there is no topic about which this universal repertory does not provide first aid in emergencies.

L. R.

O.E.E.C. (Editor), *The industrial challenge of nuclear energy III — Stresa Conference, part I* (European Nuclear Energy Agency of the O.E.E.C., 1959. 275 pages. 18s. 6d.)

The proceedings of the Stresa Conference (about which see this journal **14** (1959) 170) are being published in book form. The first volume covers the sessions devoted to surveying the European nuclear programmes, the economics of nuclear power, and financing the programmes. It includes two special ENEA studies, on *Estimates of Nuclear Energy Production in Europe* 1958—1965 and *Financing Nuclear Energy Programmes and Relations between State and Industry*, which were prepared for the Conference and have since then been revised in the light of the Conference findings. Three more volumes will follow, due to appear before the end of January 1960.

L. R.

GEORGE A. MODELSKI, *Atomic energy in the Communist bloc* (Melbourne University Press, Carlton, Victoria, 1959. 226 pages. 30 s.)

A. KRAMISCH, *Atomic energy in the Soviet Union* (Stanford University Press, 1959. x—232 pages. $ 4.75)

The subject treated in these books has given rise to a new literary genre, partaking of science fiction and the detective story. Dr. Kramisch has imagination, but is handicapped by the illusion that his ingenious constructions may have some connexion with reality. Mr. Modelski, by contrast, makes perhaps a bleak impression by his sober and scholarly approach, but his enquiry, bringing together a large amount of serious and well-ordered information, is at least not deprived of usefulness. He occasionally criticizes Kramisch's all-too-shrewd guesses, but even he has his unguarded moments: he assures us, for instance (p. 20), that the JETP reprinted excerpts from a certain speech "with evident satisfaction". Altogether, the kind of cramming of newspapers and documents in which our authors indulge appears as dusty a procedure as that of the armchair anthropologists of the Fraser school, and their conclusions have the same artificial flavour.

L. R.

NORMAN CLARKE, *Physics as a career*, second edition (Chapman and Hall, London, 1959. 79 pages. 8s. 6d. net)

All questions concerning the standard of education and training of physicists in Great Britain are an object of constant solicitude for the Institute of Physics, which is the foremost professional association of British physicists. The booklet under review, issued by the Institute, aims at acquainting young people with the prospects of physics as a profession, and at supplying students with the practical information they need in the course of their training for this professional acitivity. It is obviously the outcome of painstaking preparation and fulfils its purpose admirably. Although it is exclusively restricted to the British scene, it may also interest foreigners curious to compare the situation in Great Britain with that confronting them in their own country; they could not find a more handy source of first-hand information.

L. R.

ALBERT MESSIAH, *Mécanique quantique, Tome II* (Dunod, Paris, 1960. xv—542 pages. 48 n. f.)

This second volume brings to completion a text-book of quantum mechanics equally excelling in conception and execution. The first volume (reviewed in this journal **14** (1959) 172) was entirely devoted to an exposition of the foundations of the theory and their application to "simple" systems. Here we find a systematic treatment of symmetries and invariance, of the various methods of approximation, and of the well-established aspects of relativistic quantum theory (the theory of the electron and of the free electromagnetic field). The treatment is everywhere distinguished by the qualities traditionally cultivated by the French: rigour, clarity and elegance. The latest developments, some of which outside the main stream, but nonetheless important (e.g. the Foldy-Wouthuysen transformation), are cleverly incorporated into the text at their natural place. There are interesting problems at the end of each chapter, and the appendices on group theory and related techniques are probably the best available compendia of these subjects. The strikingly appropriate literary allusions spread as mottoes throughout the work provide an additional delight well worth mentioning.

L. R.

HENRY SEMAT and HARVEY E. WHITE, *Atomic age physics* (Rinehart and Company, New York, 1959, vii—230 pages. $ 2.00)

The scope of this slender volume, covering the main facts and ideas of modern atomic and nuclear physics, is surprisingly wide, and yet the authors, deservedly renowned for their didactic talent, have succeeded in maintaining a high standard of precision. They tell their story in a plain, matter-of-fact style, wisely considering (I presume) that it is sufficiently fascinating by itself to dispense with the usual kind of "popular" irrelevancies. The selection of the material is remarkable by a happy combination of the most up-to-date methods and most recent discoveries on the one hand with historically important and still valuable points of view on the other. Great care has been bestowed upon the illustration, which consists of very clear and neat diagrams, good portraits of the pioneers and beautiful photographs (mostly cloud-chamber pictures), some of them of historical fame. Unavoidably, the critical reader will detect here and there risky oversimplifications or slight inaccuracies, or find the very neatness of some drawings of atomic structures treacherous. But it is one of the very few books of this type which may be recommended to beginners and interested laymen.

L. R.

J. S. LOMONT, *Applications of finite groups* (Academic Press, New York, 1959. xi-346 pages. $ 11.00).

This severely mathematical treatise goes with great thoroughness through the traditional ground of those aspects of group theory which have found application in physics: although limited to finite groups for reasons of mathematical purity, it encroaches upon the field of continuous groups, and includes a lapidary, but nevertheless useful, appendix on the Lorentz group. Each successive development of the mathematical argument is illustrated by appropriate examples taken from the physics of atoms, molecules and crystals; there is also a short section on applications to nuclear physics. This physical part of the book is not intended to be systematic, but

does cover the ground fairly completely and contains, in particular, discussions of molecular and crystallographical problems which are omitted from most text books; of course, what is given is in each case the basic mathematical treatment with the help of group theory; physical consequences are not followed up in great detail. Copious lists of physical as well as mathematical literature are another useful feature of this valuable book.

L. R.

O. R. FRISCH (Editor), *Progress in nuclear physics, Vol.* 7 (Pergamon Press, London, 1959. vii—326 pages. 84s. net)

This year's crop of survey articles for the well-known "Progress" series edited by Professor Frisch is remarkably successful: there is a 50-page treatise on the bubble chamber; probably the first comprehensive discussion of resonance fluorescence in nuclei and the ingenious methods based on this process, which open such fascinating prospects; a monograph on spallation, a type of reaction interesting not only in itself, but also for the uncommon mathematical techniques involved in its analysis; a useful survey of the present status of the optical model for the interpretation of nuclear scattering; finally, an experimental article devoted to the helicity of γ-rays and leptons, and a theoretical discussion of weak interactions, both of them most helpful in fixing the picture which emerges from the momentous developments of the last three years.

L. R.

O. R. FRISCH, F. A. PANETH, F. LAVES, and P. ROSBAUD (Editors), *Beiträge zur Physik und Chemie des 20. Jahrhunderts. Lise Meitner, Otto Hahn, Max von Laue zum 80. Geburtstag* (Friedr. Vieweg und Sohn, Braunschweig, 1959. 285 pages. DM 29.50)

By a rare conjunction three great physicists celebrated their 80th birthday in 1959: three representatives of the German school of physics in its flourishing period. One of them was a victim of the wave of collective savagery which swept away this brilliant school, the other two are among the very few of their class who were honest and courageous enough to resist it. They are fittingly honoured together in this book, in which are collected essays specially written by eminent colleagues from many countries.

The editors of this *Festschrift* conceived their task in such a way, and found such an excellent response among the contributors they approached, that the volume they have produced will remain a memorial of lasting historical value. Several of the articles consist indeed of personal reminiscences or of sketches of the early developments in the fields which the jubilants have opened up. Other contributions, no less interesting, have the character of brief surveys, leading up to the latest progress; these are more technical, yet easily accessible — and therefore of great value — also to the non-specialist. It is certainly the most successful *Festschrift* I can recall; in fact, owing to the variety of its contents, it can be read from beginning to end with ever renewed interest and pleasure.

L. R.

J. V. JELLEY, *Čerenkov radiation and its applications* (Pergamon Press, London, 1958. x—304 pages. 65s. net).

This monograph on a phenomenon which has become a powerful auxiliary in nuclear research can be briefly characterized as a technical handbook. The discussion of the basic principles is too sketchy to be helpful; the theory, in particular, receives a treatment which can only be described as harsh even by British standards: there is hardly more of it in the book than an enumeration of uncommented papers and unexplained results. When it comes to the description of gadgets, the author warms up and becomes quite informative. He has also made a very complete survey of the physical investigations in which Čerenkov radiation plays a part. Numerous tables and diagrams enhance the practical usefulness of this competent, clear and handy manual.

L. R.

A. C. CROMBIE (Editor), *Turning points in physics* (North-Holland Publishing Co., Amsterdam, 1959. 192 pages. fl. 10.50).

In the University of Oxford, series of lectures are arranged every year on some general theme illustrating aspects of the history and philosophy of science. The book under review makes available to the public at large one of these series, in which are reviewed, as the title indicates, the fundamental features of the recent evolution of physical ideas — the field concept, the quantum of action, the statistical approach, relativity, complementarity and the symmetries and asymmetries of elementary particles. The lecturers, the editor informs us, are all "colleagues available in Oxford". He has sufficient self-restraint not to add that one of them is even a transfuge from another place. Without oxonian partiality, it must be said that all of them speak with authority, simplicity and grace: the collected texts of their lectures, which have retained their original vividness, form a most readable account, which can be throroughly recommended to the undergraduates of less fortunate universities. Congratulations are due to the editor, who took the excellent initiative of organizing these lectures, and to the publisher, who helps to their dissemination.

L. R.

MAX BORN and EMIL WOLF, *Principles of optics. Electromagnetic theory of propagation, interference and diffraction of light* (Pergamon Press, London, 1959. xxvi—803 pages. £ 6 net)

The long-awaited English version of Born's *Optik* presents itself as a completely new book, more restricted in scope than the original, but giving a more thorough and much modernized treatment of those topics which have been retained. It was a very wise decision to exclude molecular optics, i.e. the atomistic interpretation of the optical parameters, and too keep strictly within the bounds of macroscopic description; the presentation has thereby gained in homogeneity and harmony, and space has been left for the discussion of a large amount of new material, which is for the first time inserted at its natural place in a comprehensive picture of this vast and most beautiful branch of physical science. To some extent, the book has also become a collective undertaking, in the sense that quite a number of chapters have been written by specialized experts; but the broad vision and mastery of exposition which stamped the German work as a classic have been fully retained, and the substantial contributions of the junior author form a worthy complement to the old master's great work. Among the many points of interest I shall only mention the discussion of partial coherence (chapter 10), a topic of outstanding theoretical and practical importance. The treatment is everywhere very full and systematic, but the line of argument is so firmly drawn that it is never obscured by the abundance of details. This is therefore not some heavy encyclopedic handbook, but a very readable account of high aesthetic value. It will for many years remain the standard book of reference for all the fundamental questions of classical optics.

L. R.

B. VITALE, *A bibliography on heavy mesons and hyperons* (North-Holland Publishing Co., Amsterdam, 1960. vii—142 p. 9.50 fl.)

A bibliography which is not critical, but merely lists the titles of the papers on a given topic, is of limited use; at any rate it is better than nothing. In the present case, the author has attempted to be as helpful as possible by a judicious combination of chronological and systematic classification. The work is divided into two parts, covering the periods 1946—1956 and 1957—1958 respectively; this division corresponds to a change of outlook which occurred in 1957, when one began to characterize the particles by their modes of production rather than by their modes of decay. In each part there is a natural subdivision between heavy mesons and hyperons, and each of these sections is again subdivided into well-chosen groupings, which are rather more systematic in the second part than in the first. It is fortunate that a comparatively cheap offset process has made it possible for all interested research physicists to profit by a work which the author originally undertook for his own use.

L. R.

G. T. SEABORG, *The transuranium elements* (Addison-Wesley Publishing Co. and Yale University Press, 1958. xx—331 p. $ 7)

This very fine book owes its origin to a series of Silliman lectures given by the author at Yale

University in 1957. It was then incorporated in the series of 12 volumes presented by the U.S.A. at the Second Geneva Conference in September, 1958, and called for this reason "The Geneva Presentation Volumes". Neatly printed by the Yale University Press, it is distributed with the whole series in a uniform style of binding (also very neat) by the Addison-Wesley Co.

In the first place, as one would expect, we have here the authoritative monograph *par excellence* of an interesting family of elements, envisaged systematically and thoroughly under all chemical and physical aspects. Especially valuable are the numerous diagrams showing at a glance the remarkable regularities in nuclear and atomic structure which are most instructively illustrated by this numerous and varied group of nucleides. The relevant theoretical considerations are not presented in detail, but the main ideas and results are at least clearly outlined, with suitable references to the literature.

Besides this pragmatical aspect, if I may say so, there is, however, another feature in the book which considerably enhances its attractiveness: a third of it is devoted to the "Plutonium story", which is told in great detail with impressive photographic illustrations. The historical value of this first-hand account needs no emphasis. No less fascinating is the story of the discovery of Mendelevium which is also told and illustrated by a photograph of the decisive sheet on which spontaneous fission peaks of the Mv fraction were registered. The unusual designations of these peaks as "Hooray", "Double Hooray", "Triple Hooray" call to mind the sheet † full of the scribbled diagrams and calculations which led Huygens to the explanation of the double refraction of Iceland spar, and on which he wrote 'EYPHKA (this, I suppose, was his way of saying "hooray").

L. R.

† This sheet is reproduced in fac-simile in vol. 19 of the great edition of Huygens' *Oeuvres complètes*, p. 426.

J. HAMILTON, *The theory of elementary particles* (The Clarendon Press, Oxford, 1959. xii—482 pages. 75s. net).

This book is essentially devoted to a discussion of the methods of field theory, by which the various constituents of matter and their interactions are described; only two chapters out of nine are more particularly concerned with the properties commonly associated with what is called the "particle aspect" of these constituents. I take it that the author has nevertheless chosen to emphasize this aspect in the title in order to express his intention to insist on the physical reality which appears to us under either manifestation. If the title is equivocal, it is only because of the inadequacy of the current terminology: at the present stage it would be better, I think, to speak of the fundamental constituents of matter ("matter" being taken in its widest possible sense, and the problematic "elementary" being carefully avoided).

The book owes its existence to several courses of lectures, which have been remodelled and amalgamated; in the process, the lecture style has been partly sacrificed to an effort to present a survey verging on the encyclopedic; yet retained to the extent of confining the detailed discussion to the simpler points, and referring the reader to an abundant literature for the necessary refinements. The author's style of exposition is not always as direct as it could be: his habit of relegating minor points of an argument to footnotes does not make it easier to follow. The treatment is definitely oriented towards application to the analysis of experimental results, and difficulties of principle (which, as we know, abound in this domain) are mostly skipped (with due mention of their existence). In fact, in characteristic British fashion, the chapter on the foundations of field quantization is the last. It must be emphasized, however, that within these self-imposed limits the author has managed to cover a very wide ground, ranging from the usual elementary stuff to the most modern methods and conceptions, always keeping (to use the author's own phrase) "the physical concepts well in view". Especially valuable is the combination, carried through to a larger extent than in other treatises of similar scope, of the methods of field theory with those specifically developed to cope with the symmetries and invariance properties of the fundamental interactions.

L. R.

1.D.2:
1.E.1:
3.A

Nuclear Physics **15** (1960) 533—565; © *North-Holland Publishing Co., Amsterdam*

Not to be reproduced by photoprint or microfilm without written permission from the publisher

0+ LEVELS OF EVEN NUCLEI IN THE RARE-EARTH REGION

INGVAR MARKLUND, BOB VAN NOOIJEN † and ZBIGNIEW GRABOWSKI ††

Institute of Physics, Uppsala †††

Received 21 January 1960

Abstract: The quadrupole vibrations of beta type of deformed nuclei have been found in only a few cases in the heavy element region. We started a search in order to find such levels also in the rare-earth region. A 0+ level of beta vibrational type at 685.0 keV was found in the deformed nucleus Sm^{152} by measuring conversion coefficients. Its corresponding 0+ level of two-phonon type was observed in Gd^{152} at 615.3 keV. The strongly deformed nucleus Er^{166} has a 0+ level at 1460.4 keV now confirmed by angular correlation measurements. The 1087 keV level in Os^{188} and the 1267 keV level in the spherical nucleus Pt^{194} were also measured by angular correlation to have zero spins, indicating the same trend of the 0+ levels as theoretically expected. (A second excited 0+ level was found in Os^{188} at 1766 keV and in Pt^{194} at 1480 keV.) When the beta and gamma vibrational bands are known, the theoretical and experimental rotational-vibrational coefficients can be compared: $B^{\text{theory}} = kB^{\text{exp}}$. A k-value of 2—4 is found, indicating a weaker coupling than that theoretically expected. The experimental trend of levels in even nuclei with $A = 50$—250 is discussed, and some new spin assignments are proposed.

1. Introduction

Collective excitations of nuclei have been observed throughout the whole of the periodic system [1,4]). Even nuclei in the neighbourhood of closed shells have spherical equilibrium shape and the collective excitations of such nuclei are harmonic oscillations about this shape [2–4]). The one and two phonon quadrupole vibrations (positive parity) are usually lowest in frequency, giving a singlet (2+ level) and a triplet (0+, 2+, 4+ levels) respectively. Among the odd parity levels of these even nuclei the octupole vibrations have the lowest frequency.

Nuclei far from closed shells often have stable non-spherical equilibrium shape but usually keep cylinder symmetry [3,4]). The lowest collective excitations of such even nuclei are pure rotations about an axis perpendicular to the nuclear symmetry axis and vibrations of quadrupole or octupole type with superimposed rotation. See fig. 1. These nuclei may exhibit quadrupole vibrations about their cylindrical equalibrium configuration (gamma vibrations) or about their elliptical equalibrium (beta vibrations). A common octupole vibration here is the pear-shaped vibration (keeping cylinder symmetry).

† On leave from Lab. voor Technische Physica, Delft, Holland.

†† On leave from Instytut Badań, Jądrowych, Kraków, Poland.

††† This work is in part supported by the U. S. Air Research and Development Command.

Some possible low frenquency collective excitations of non-spherical nuclei are shown schematically in fig. 1, where z is the axis of symmetry. The resulting bands of excited states are each labelled with the associated total angular momentum quantum number I, its component along the axis of nuclear symmetry K, and the parity π. The gamma vibration band has the spin-parity sequence $K = 2$, $I = 2+, 3+, 4+ \ldots$, and the beta vibration band the sequence $K = 0$, $I = 0+, 2+, 4+ \ldots$. The $0+$ level is most characteristic in the

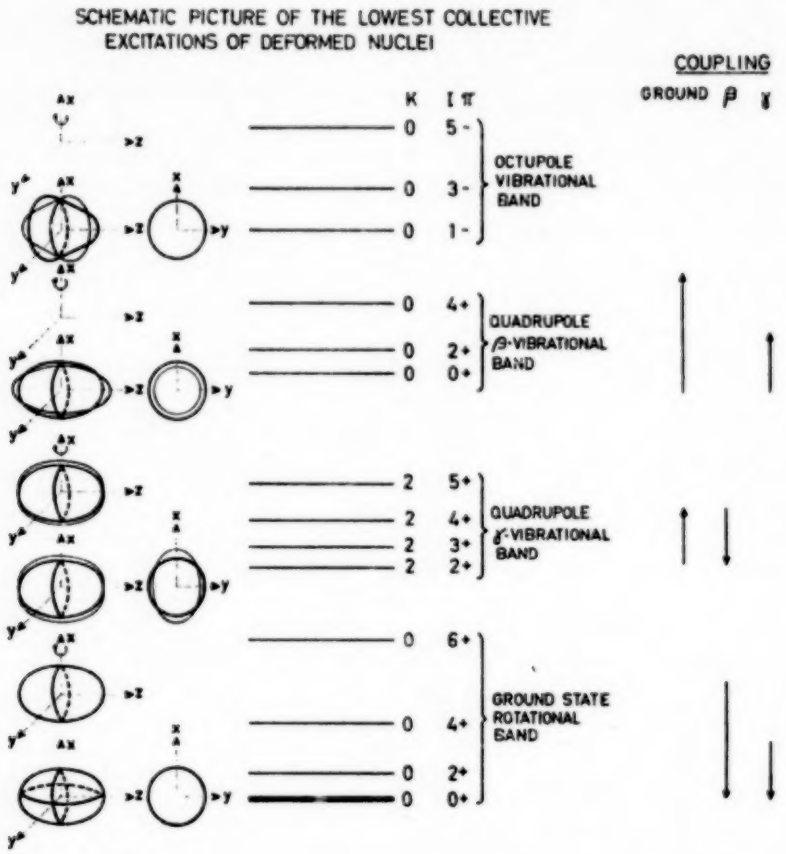

Fig. 1. Schematic picture of the lowest collective modes of excitations of non-spherical even nuclei and the resulting levels. The arrows to the right in the figure indicate the direction and strength of interaction between the different levels.

latter band. Furthermore, at about the double excitation energy as the one-phonon band, a two-phonon beta vibrational band is expected with $K = 0$, $I = 0+, 2+, 4+ \ldots$, as well as a two-phonon gamma vibration with bands $K = 0$, $I = 0+, 2+, 4+ \ldots$, and $K = 4$, $I = 4+, 5+, 6+ \ldots$. A band with $K = 0$, $I = 0+, 2+, 4+ \ldots$ is also expected, when two decoupled nucleons are lifted to an excited state. This pair excitation energy has recently been estimated theoretically [5]) to about 1200—1400 keV in the rare-earth and heavy element region. Bands with the same spin-parity sequences may be recognized by their decay branchings [6]).

The different bands will obey the rotational energy formula for axially symmetric nuclei [3])

$$E_I = E_0 + \frac{\hbar^2}{2\mathscr{I}} I(I+1) + BI^2(I+1)^2; \tag{1}$$

E_0 is a constant for each rotational band depending only on the intrinsic structure (occupied particle orbits and collective vibrations) and gives the position of the band head. The constant $A \equiv \hbar^2/2\mathscr{I}$ is inversely proportional to the effective moment of inertia $\mathscr{I}$ of the nucleus and depends on the nuclear deformation. The last term in eq. (1) accounts for the deviation of the rotational band from the strong coupling limit.

Two levels of the same spin and parity generally repel each other, and the strength of this interaction depends on the distance between the levels (or between their corresponding band heads, as long as the moments of inertia of the bands in question are about the same.) The perturbation of a band caused by the interaction of a level with energy E_j from other levels E_i of the same spin and parity may be written

$$B_j = \left(\frac{\hbar^2}{\mathscr{I}_j}\right)^3 \sum_i \frac{k_{ij}}{(E_i - E_j)^2}; \tag{2}$$

but k_{ij} may contain a factor $\mathscr{I}_j(E_i - E_j)$, depending upon the approximation used. The interactions between the levels in fig. 1 are indicated with arrows to the right in the figure. Thus, the 2+ gamma vibrational level is lifted by the action of the ground state rotational 2+ level, while the latter level is depressed by a force of the same strength, and the beta vibrational 2+ level will here depress both the above mentioned levels. The coefficient for the effective interaction between beta and gamma vibrational levels is still not known. But for the ground state rotational band the hydrodynamical approximation (second order perturbation theory) gives the rotational-vibrational coefficient [3])

$$B_{\mathrm{RV}} = \left(\frac{\hbar^2}{\mathscr{I}}\right)^3 \left(\frac{-3}{2(\hbar\omega_\beta)^2} - \frac{1}{2(\hbar\omega_\gamma)^2}\right), \tag{3}$$

where $\hbar\omega_\beta$ and $\hbar\omega_\gamma$ are the excitation energies of the beta and gamma vibrations. The rotation-vibration interaction also gives a positive term in eq. (1) proportional to $I(I+1)$, causing a somewhat larger effective moment of inertia of the ground state rotational band.

The general trend of the excitation energies of the respective positive parity levels as function of neutron number has been estimated by Bohr and Mottelson and is shown in fig. 2 [7]). The energies of the quadrupole vibrations of even nuclei near closed shells are relatively high and will decrease rapidly with addition of pairs of particles until the new nucleus formed has stable non-

spherical equilibrium shape. The energies of the ground state rotational levels of such nuclei also decrease with increasing neutron number until the shell in question is about half filled, while the quadrupole vibrations of these nuclei are expected to increase with addition of pairs of particles. (See fig. 2.) Approaching the next closed shell the positions of the levels change back through a similar scheme, as the only unoccupied particle orbits are those giving nuclei with less deformation.

The experimental data of the energy levels as function of neutron number are in general agreement with the theoretical predictions in fig. 2. But the whole

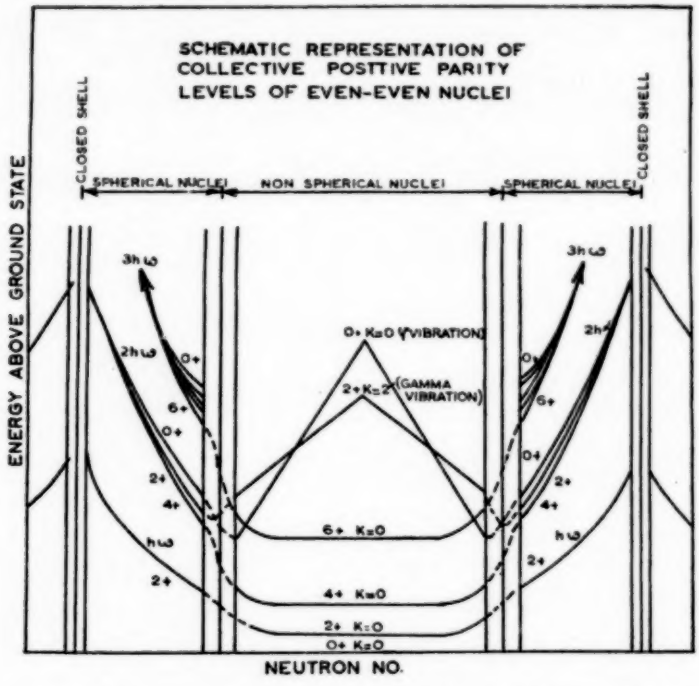

Fig. 2. Schematic representation of the expected trend of collective positive parity levels of even nuclei as a function of neutron number. This figure is taken from ref. [7]).

two-phonon triplet (0+, 2+, and 4+) was not observed with certainty in any spherical nucleus, and only one nucleus (Er^{166}) in the whole region of rare-earth nuclei was reported to have a 0+ level of probable beta vibrational character [1]), when this investigation started. One of our aims was to find some nuclei with energy levels with beta vibrational characteristics in the rare-earth region in order to test the rather weak theoretical predictions of the energy trend of beta vibrations as function of neutron number. Furthermore, the deviations of the positions of the ground state rotational levels from the strong coupling limit, $B = 0$ in eq. (1), have been accurately measured in many cases in recent years, giving many values of B^{exp}. And the excitation energies for gamma vibrations $\hbar\omega_\gamma$, are now also known for many nuclei. Thus, knowledge of the

beta vibrational energies $\hbar\omega_\beta$ will give a measure of the accuracy of the hydrodynamical approximation of the rotational-vibrational interaction, eq. (3), for nuclei in the rare-earth region. And if this approximation is good, unobserved beta or gamma vibrational levels may be calculated from eqs. (1) and (3).

2. Method of Measurements

In order to detect possible excited 0+ levels we made use of two properties of such states. The radiation to the ground state is fully converted and the cascade via the first excited state, $0 \to 2 \to 0$, gives the highest possible anisotropy of radiation. Thus a high resolution beta spectrometer is efficient in detecting the monopole transition, and a directional correlation apparatus will easily uniquely determine the zero spin of an excited level also in relatively complicated decay schemes.

We used a double focusing iron-yoke beta-spectrometer ($\rho = 50$ cm) with exact field measurement relative to that of an iron-free Helmholtz coil by the rotating coil method [8]). Sources for these measurements were produced by reactor irradiation at AB Atomenergi, Stockholm. The internal conversion sources were vacuum evaporated on 0.2—0.8 mg/cm² Al-backing with an estimated source thickness of 0.1—0.8 mg/cm² and a size of 2×20 mm and 4×20 mm. The momentum resolution was then 0.2—0.3 %. The external conversion sources were produced by irradiating Al capsules (wall thickness 0.15 mm) containing the oxide of the metal in question. This container was then put in a copper cylinder (wall thickness 2.5 mm) for absorption of the beta-rays. The rectangular converters used were 2×20 mm and 4×20 mm and their thickness 0.9—3.3 mg U_2O_3/cm². The resulting momentum resolution was 0.3—0.5 %. The spectrometer was always carefully demagnetized before each run and the measurements only performed in increasing magnet field. Reference lines from Co^{60}, Cs^{137}, Eu^{152m}(121.78 keV) [9]) and Bi^{207} sources were put in at their proper places. The method of Hultberg [24]) was used to determine the relative gamma intensities accurately [10]).

The directional correlation $W(\theta)$ between two successive gamma rays from a nucleus is a function of the spins I_1, I_2 and I_3 of the three levels of the cascade and of the multipolarities of the radiations [11, 12]):

$$W(\theta) = \sum_\nu A_\nu P_\nu(\cos\theta) = 1 + A_2 P_2(\cos\theta) + A_4 A_4(\cos\theta), \tag{4}$$

where $P_\nu(\cos\theta)$ are the Legendre polynomials. When a radiation is a mixture of two multipoles L and $L+1$, the mixing parameter δ is the ratio of respective matrix elements

$$\delta = \frac{\langle L+1 \rangle}{\langle L \rangle}, \tag{5}$$

and δ^2 is the intensity ratio of the two multipoles. If the cascade is denoted $I_1(L_1, L_1+1)I_2(L_2)I_3$ and only the upper transition is assumed to be mixed, the coefficients A_ν in eq. (4) are

$$A_\nu = \frac{1}{1+\delta^2}[F_\nu(L_1L_1I_1I_2)+2\delta\, F_\nu(L_1, L_1+1, I_1I_2) + \delta^2 F_\nu(L_1+1, L_1+1, I_1I_2)]F_\nu(L_2L_2I_2I_3). \quad (6)$$

The F_ν coefficients are tabulated in ref. [12]) for a great number of spins and multipolarities. The A_2 and A_4 coefficients in eq. (6) as a function function of δ are drawn in figs. 3 and 4 for the common spin sequences $I_1 \to 4 \to 2$ and $I_1 \to 2 \to 0$ with $I_1 = 6, 5, 4, 3, 2$ and 1. The experimental angular distribution of an investigated cascade must be corrected for isotropic accidental coincidences (caused by the finite time resolution of the coincidence unit), anisotropic true coincidences from other overlapping cascades, source decay and the finite solid angle of the counters [13]). (No correction was necessary for source extension as the source dimensions were always less than or equal to 2.0 mm in diameter and 10 mm in height, giving a correction [14]) of less than one percent on the A_2 and A_4 coefficients.) The thus corrected A_2 and A_4 values from, for example, an $I_1 \to 2 \to 0$ sequence are to be put in fig. 4 and combined to give δ-values of the same sign and magnitude. If the mixing ratio is not unique, combination with a measured conversion coefficient will often exclude all but one possibility. The cascade $0 \to 2 \to 0$ gives

$$A_2 = +0.357, \quad A_4 = +1.145. \quad (7)$$

These values are quite outside the possible values for all other spin sequences $I_1 \to 2 \to 0$. (See fig. 4).

The directional correlation measurements were performed with a scintillation coincidence spectrometer [13]) with an effective resolving time of 3×10^{-8} sec. Two NaI(Tl) crystals $1\frac{1}{2}$ in. in diameter by $1\frac{1}{2}$ in. in height were coupled to RCA 6342 photomultiplers. The source—crystal distances were 50 mm. Al-absorbers (and sometimes Pb-absorbers) were put in front of each crystal to stop all beta rays, (or intense low energy gamma rays) and the crystals were shielded laterally by a gradiated Pb-shield. The sources were always centered until the single counting rate in the movable detector as function of position was constant to about one percent. The apparatus was automatically shifting angle every 15th minute (90°, 135°, 180°, 225°, 225°, 180°, 135°, 90° . . .) and recording the coincidence and single counting rates in both the channels.

3. Levels in Gd^{152} and Sm^{152}

The search for excited 0+ levels was started in the transition region between spherical and deformed nuclei, where these levels were expected to be very low

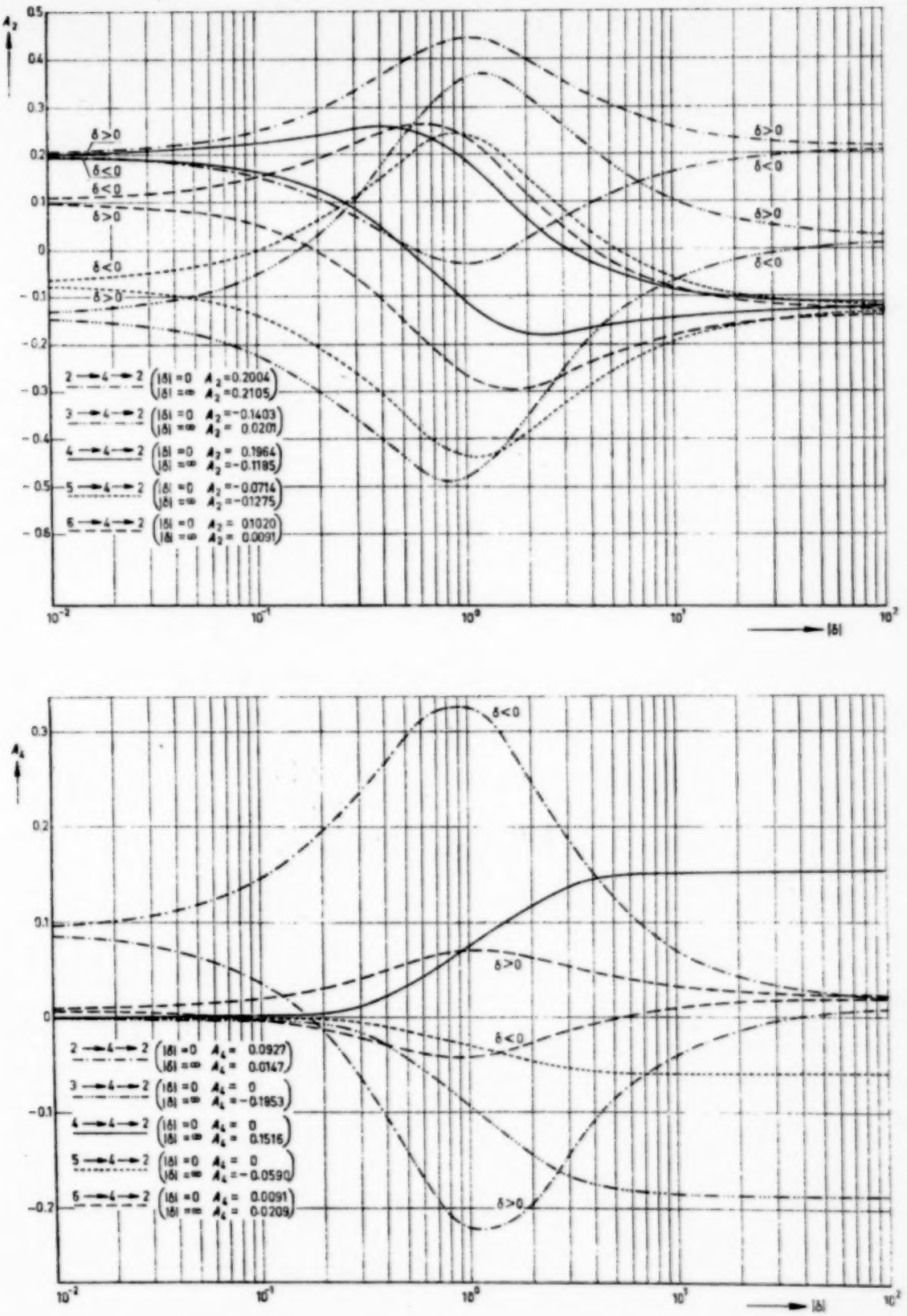

Fig. 3. The theoretical correlation coefficients A_2 and A_4 in eq. (4) as function of the amplitude mixing ratio δ for the spin sequence $I_1 \to 4 \to 2$ with $I_1 = 6$, 5, 4, 3 and 2.

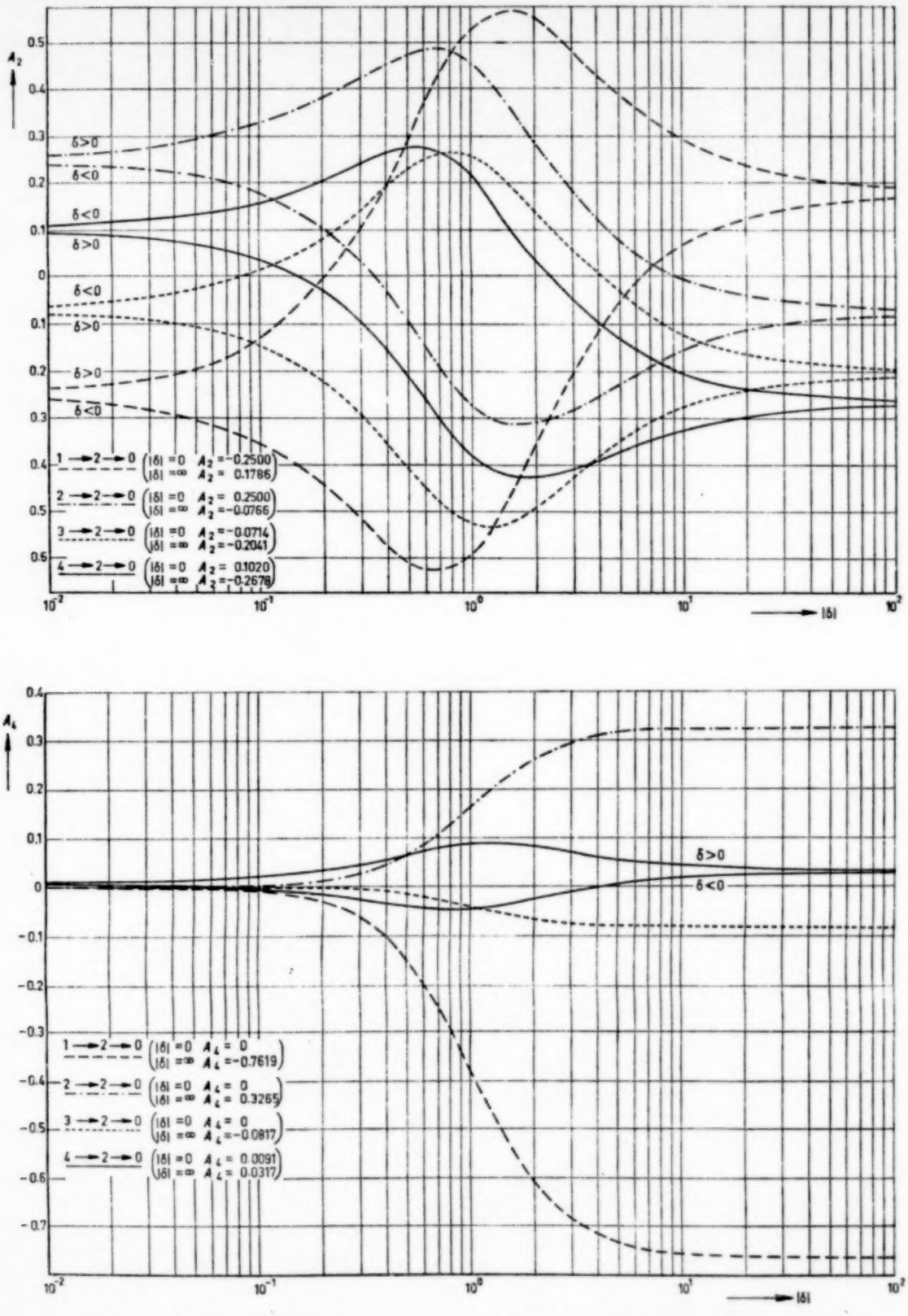

Fig. 4. The theoretical correlation coefficients A_2 and A_4 in eq. (4) versus δ for the spin sequence $I_1 \rightarrow 2 \rightarrow 0$ with $I_1 = 4$, 3, 2 and 1.

in energy. (See fig. 2). Marklund *et al.*[10]) investigated the decay of $Eu^{152m}(0-)$ (9.2h), a nucleus feeding both the almost spherical nucleus Gd^{152} and the strongly deformed nucleus Sm^{152}. A 615.0 keV level was found in Gd^{152} and a 685.3 keV level in Sm^{152} both with 0+ properties, identified by observed E0 transitions. A 2+ level at 811 keV in Sm^{152}, excited from the 12 year Eu^{152} activity (3−), is a probable first rotational member on the 685.3 keV level as observed by Nathan and Hultberg [15]). The results are collected in fig. 5. A second excited 0+ level in Gd^{152} is recently observed at 1047 keV by K. Toth *et al.*[38]) in the decay of Tb^{152}.

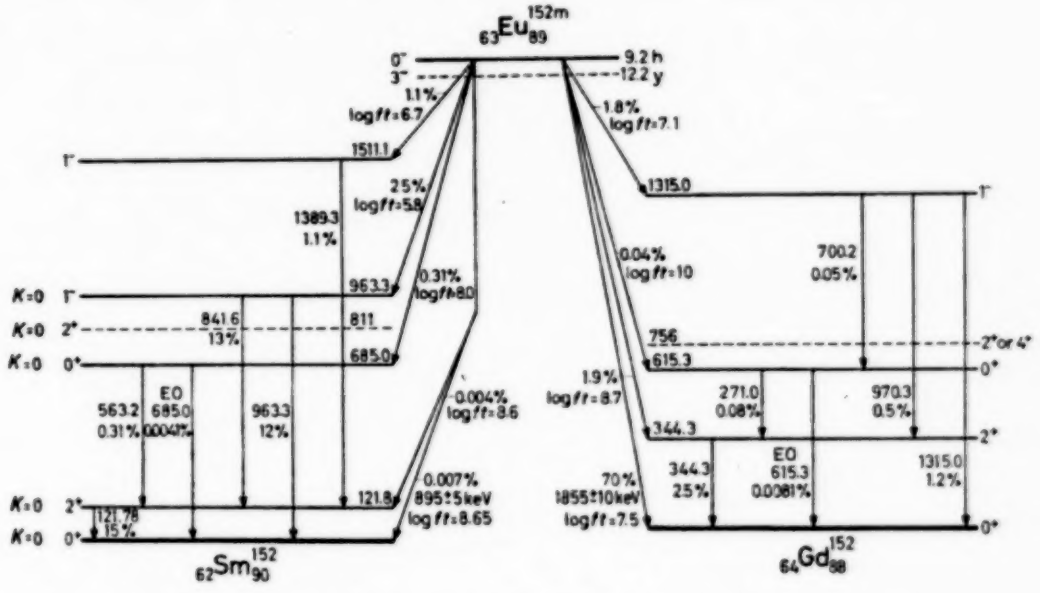

Fig. 5. Decay scheme of Eu^{152m} (9.2h). The dashed levels are excited from the 12.2 y Eu^{152} activity.

4. Levels in Er^{166}

The ground state of Ho^{166}(27h) has spin-parity 0− [20]), while the metastable state ($\geqq$ 30y) has a probable spin of 7− [17]). The odd proton and neutron in $_{67}Ho^{166}_{99}$ are then in the Nilsson [16]) orbits ($\pi\frac{7}{2}-|523|$) and ($\nu\frac{7}{2}+|633|$) with parallel and antiparallel spins. The Ho^{166} levels decay by negaton emission, exciting low and high spin states respectively in Er^{166}. And still more levels in Er^{166} are excited in the electron capture decay of Tm^{166}(7.7h) [26]), which has a probable spin-parity assignment of 2− or 3−. The odd nucleons are then in the Nilsson orbits ($\pi\frac{1}{2}+|411|$) and ($\nu\frac{5}{2}-|523|$).

Several investigations have been carried through on the decomposition of the beta continuum from the short-lived Ho^{166} activity [19–21]). But the succeeding gamma rays have only been observed in scintillation spectra, except the 80 keV ray. The results of these works are collected in table 1.

We have measured the internal conversion spectrum with the high resolution

TABLE 1

Energies and intensities of beta components and gamma rays in the decay of Ho^{166}(27h)

Ray no.	Mihelich and Church [18])		A. W. Sunyar [19])		Graham *et al.* [20])		Cork *et al.* [21])		Present investigation			Theory [23])
	E (keV)	I_{rel}	E (keV)	I %	E (keV)	I %	E (keV)	I %	E (keV)	I_{rel}	I %	
β_1			230	0.3			230	2	(181)		0.32	
β_2			400	1	393	0.76	412	5	(384)		0.90	
β_3							869	9			(<0.09)	
β_4			1760	74	1771	47.6	1756	37	(1763)		46.7	
β_5			1840	25	1854	51.6	1839	47	(1844)		52.0	
γ_1	80.7		80	85†	80.3		80.25		80.53±0.05[a]		47.8	
e^-_K		13†						44†		80† [b]		84†
$e^-_{L_1}$		<10†								8†		8†
$e^-_{L_2}$		71†						91†		97†		96†
$e^-_{L_3}$		100†						100†		100†		100†
γ_2							970	~(9)				
γ_3			1360	10†	1380	0.76	1380	(5)	1379.8 ±0.4		0.90	
γ_4			1440	<2†					1460		<0.005	
γ_5			1530	2†			1540	(2)	1582.4 ±0.4		0.21	
γ_6			1610	1†			1620		1663.0 ±0.5		0.11	

[a] In Coulomb excitation Chupp *et al.* [22]) recently have measured the first excited stated in Er^{166} to $E_\gamma = 80.57 \pm 0.02$ keV.

[b] The I_{eK} intensity is uncertain as corrected for absorption in the source and the detector window.

† Relative intensities.

double focusing spectrometer mentioned in section 2. After careful demagnetisation and determination of the influence of the earth magnetic field in the Helmholtz coil, the 80 keV K-line and L-group were studied. (See fig. 6.). Our results are included in table 1. Parts of the high energy region were also carefully scanned. The intensity of the 1379 keV e_K^--line was $(10\pm5)\times10^{-6}$ of the beta continuum, while the e_K^--line of the 1460 keV transition was more than 15 times weaker and not observed with certainty in spite of several serious attempts.

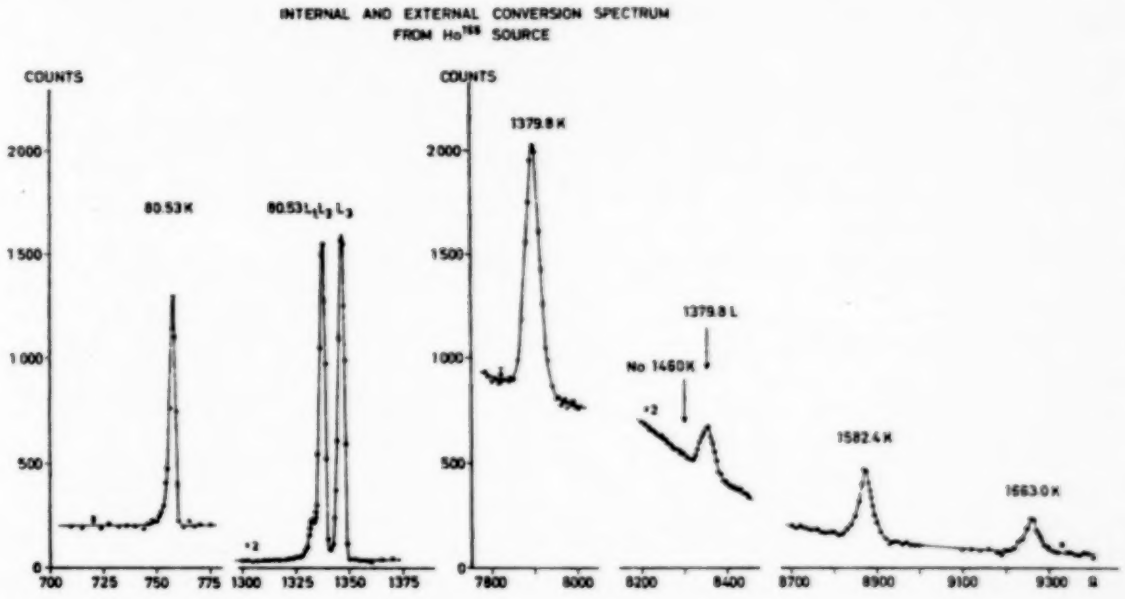

Fig. 6. Parts of internal and external conversion spectrum of the Ho^{166} decay to Er^{166}. A 3.3 mg U_3O_8 converter was used in external conversion. No indication of any 1460 keV transition was observed in the external spectrum.

The gamma emission in the decay of Ho^{166}(27h) is investigated both by scintillation technique with a $1\frac{1}{2}$ in. $\times$ $1\frac{1}{2}$in. NaI(Tl) crystal, fig. 7, and in external conversion, fig. 6, using the earliier mentioned beta spectrometer. Cork *et al.* [21]) report a 970 keV gamma ray, observed in their scintillation spectrum. They do not present any spectrum and give no value of the intensity of the 970 keV line but report a beta branch of 9 % to a 970 keV level. The small bump at 950 keV in fig. 7 may indicate a gamma ray of this energy. We have made a search for such a gamma ray with external conversion technique. No line was found at 970 keV, but a very weak transition of 945.0 keV was observed. Its intensity was one tenth of the 1379 keV gamma ray intensity, which means about 0.1 % absolute intensity. Because of the low intensity of the line and its position on a high Compton background from other gamma rays, no attempt was made to determine its half-life. The region around 1460 keV was also scan-

ned with great care, giving an upper limit of the 1460 keV gamma ray intensity less than 1/200 of the 1379.8 keV gamma intensity. (See fig. 6.)

The scintillation spectrum, fig. 7, gives a conversion coefficient for the 80 keV gamma ray $\alpha_{80K} = 1.76 \pm 0.15$ [the table of Rose [23]) gives $\alpha_K = 1.60$] after correction for absorption, escape peaks and fluorescent yield. This spectrum

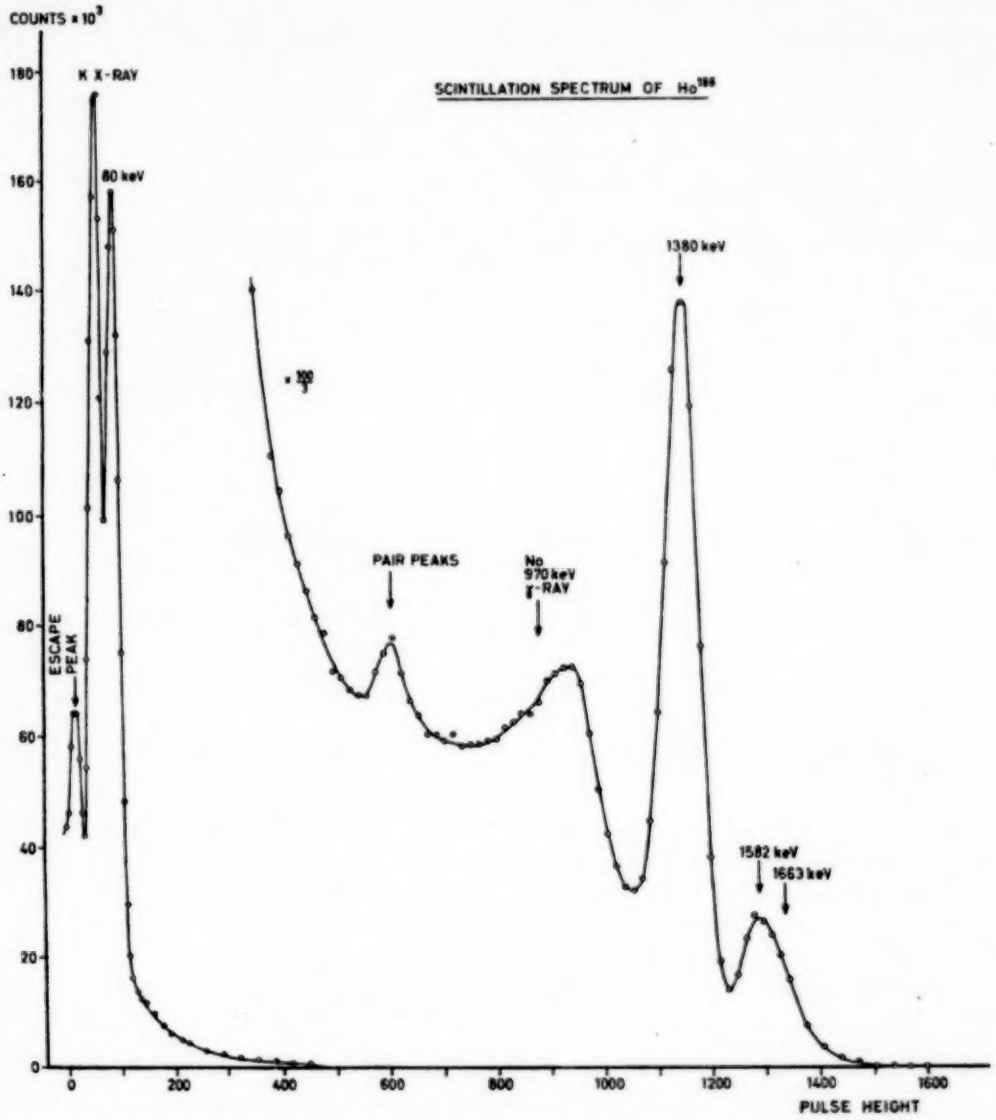

Fig. 7. Scintillation spectrum of Ho^{166} in a $1\frac{1}{2}$ in. $\times$ $1\frac{1}{2}$ in. NaI(Tl) crystal.

also gave an intensity ratio between the 80 keV ray and the high energy gamma rays, using an earlier determined photopeak efficiency curve of the crystal. The relative intensities between the gamma rays measured in external conversion could be accurately fixed, using the method of Hultberg [10, 24]). The values reported in table 1 are thus corrected for source and converter extension and for the angular distribution of the photoelectrons from the converter. The relative gamma intensities could then tentatively be converted into abso-

lute transition intensities by assuming the beta branch to the ground state to contain 52 % of the beta intensity. This value is reported by Graham *et al.* [20]) and seems to be the most dependable. As there are large deviations in the reported values of the beta components (table 1), the other beta branches and log *ft* values are calculated from our gamma measurements and included in the decay scheme, fig. 8. It is possible to explain the exceptional beta branchings to the ground and first excited states in Er^{166} by assuming a tensor matrix element of small magnitude [34]).

In order to give a unique and independent spin assignment of the 1663 and 1460 keV levels in Er^{166}, directional correlation measurements were carried through. The apparatus used is described in section 2. Spectroscopically pure Ho_2O_3 powder was neutron bombarded for about 80 hours in the Stockholm reactor at a flux of 2×10^{12} neutrons/cm$^2\cdot$ sec. We used aqueous solutions of holmium trichloride as sources for our correlation measurements. The 80—1380 keV cascade gave

$$W(\theta) = 1+(0.226\pm0.012)P_2(\cos\theta)+(0.783\pm0.029)P_4(\cos\theta).$$

These A_2 and A_4 values are far too high to be compatible with any other spin sequence $I \to 2 \to 0$ in fig. 4 than with $0 \to 2 \to 0$. But the intermediate level has a measured half-life $T_{\frac{1}{2}} = 1.7\times10^{-9}$ sec [1]), and the Er^{166} nucleus is strongly deformed. The quadrupole interaction in the intermediate state will thus have a strong smearing out effect on the correlation pattern. This effect accounts partly for the deviations between the theoretical, eq. (7), and experimental A_2 and A_4 coefficients. The attenuation factors

$$G_2 = \frac{A_2^{\text{exp}}}{A_2^{\text{theory}}} = 0.63\pm0.03, \quad G_4 = \frac{A_4^{\text{exp}}}{A_4^{\text{theory}}} = 0.69\pm0.03,$$

with a somewhat larger G_4 than G_2 value, are in agreement with theory [11]) and give a measure of the strength of the quadrupole interaction.

The cascade 80—1580 keV is also measured, giving

$$W(\theta) = 1+(0.165\pm0.019)P_2(\cos\theta)-(0.006\pm0.044)P_4(\cos\theta).$$

As the intermediate level is the same here as in the other cascade, we can use the G_2 and G_4 values measured there. The corrected values are

$$A_2 = \frac{A_2^{\text{exp}}}{G_2} = -(0.26\pm0.03), \quad A_4 = \frac{A_4^{\text{exp}}}{G_4} = -(0.01\pm0.06).$$

The only spin sequences in fig. 4 fitting these A_2 and A_4 values are $3 \to 2 \to 0$ and $1 \to 2 \to 0$. The former spin sequence is excluded as a strong 1663.0 keV cross-over transition is observed (table 1). The multipole amplitude mixture

in the 1580 keV transition is then

$$\delta = \frac{\langle L+1 \rangle}{\langle L \rangle} \leqq 3 \times 10^{-2},$$

and as the log *ft* value of the beta branch to the 1663 keV level, fig. 8, favours negative parity, we assign the 1663.0 keV level a spin-parity of 1−. The 1580 keV transition then contains more than 99.9 % E1.

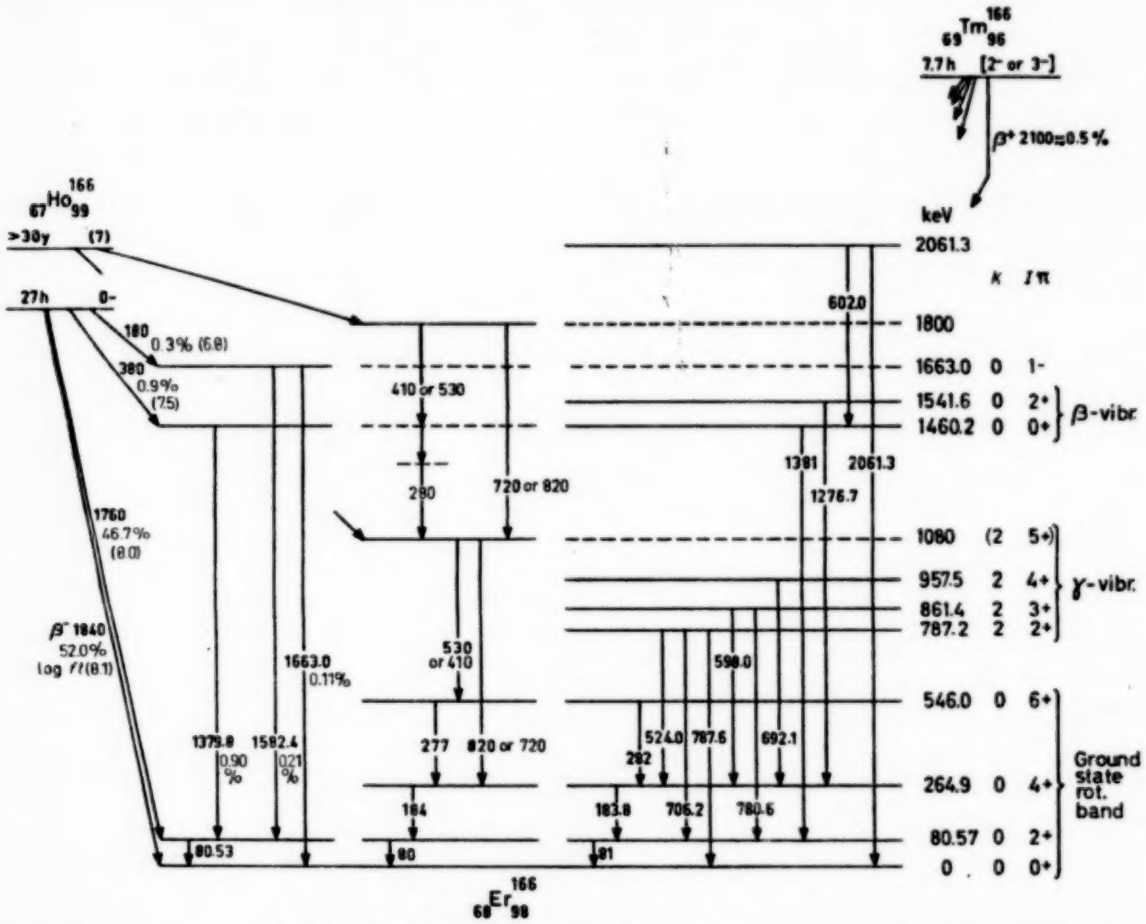

Fig. 8. Level scheme of Er^{166}. To the left is shown the result of the present investigation of the Ho^{166}(27h) decay with internal and external conversion and directional correlation. In the middle of the figure are the levels excited from Ho^{166}(≧ 30y) [17]), and to the right is the low energy part of the levels in the decay of Tm^{166} [26, 28]). The gamma vibrational band is constructed from gamma rays by Gromov *et al.* [26]). Two Dutch groups [51, 52]) have very recently published a study of the Er^{166} levels from the long-lived Ho^{166} decay and from Tm^{166}. They have placed the gamma band 100 keV too low in energy and arrive at a decay scheme of Ho^{166}(≧ 30y) in principle the alternative one to that given in the middle of fig. 8.

Fraser and Milton [25]) have also measured these two cascades, but they observed a severe attenuation, and in order to remove it partly they kept their source of $Ho(NO_3)_3$ above its melting point. Although their correlation coeffi-cients were much lower than ours, they could assign a spin zero to the 1460 keV

level. But from their results on the 1580—80 keV cascade they could not even exclude a spin 2 assignment of the 1660 keV level.

The long-lived Ho^{166} activity [1]) is most thoroughly studied by Grace *et al.* [17]) using scintillation coincidence technique. $Ho^{166}(\geqq 30y)$ decays to about 80 % via a high spin level at about 1800 keV in Er^{166} and from there cascading downwards, exciting a spin 5 level at 1080 keV (perhaps belonging to the gamma vibrational band) and several levels in the ground state rotational band. Some of the gamma rays were alternatively placed in their decay scheme as indicated in fig. 8.

The decay of the 7.7 h $Tm^{166}(2-$ or $3-)$ activity is studied carefully by Gromov *et al.* [26]). They publish accurate gamma energies and intensities and suggest a decay scheme. We have in fig. 8 placed several of the gamma rays not fitted in their decay scheme and altered the position of three others. We were then guided by the levels and spin-parities (but no gamma rays) in the decay of Tm^{166} to Er^{166} recently announced by Jacob *et al.* [28]). They suggest levels in Er^{166} at 80.7(2+), 265.4(4+), 545.8(6+), 787.4(2+), 861.0(3+) and 957.9(4+) keV. The level scheme of Er^{166} in fig. 8 shows to the left the decay of Ho^{166}(27h), containing only the results from our measurements, in the middle is the decay of $Ho^{166}(\geqq 30y)$ and to the right the low energy part of the scheme gained from the Tm^{166} decay. The energy values of the levels excited from Tm^{166} are mean values between the energy determinations by Gromov *et al.* and those by Jacob *et al.* and the gamma rays are from Gromov *et al.* In Er^{166} are thus excited three rotational levels in the ground state band, three (or four) members of the gamma vibrational band, two beta vibrational levels and a probable first member of an octupole band.

5. Levels in Os^{188} †

The nuclide Re^{188} decays to Os^{188} by negaton emission with a halflife of 17 hours. The decay of Re^{188} has been investigated by several authors [1, 30, 31]). Their results are summarized in the decay scheme presented in fig. 9.

The present investigation was originally undertaken in order to determine the position of the first member of the beta-vibrational band by means of gamma-gamma directional correlation measurements. It appeared worth while to extend these measurements to other cascades.

Sources were prepared in the AB Atomenergi pile in Stockholm by irradiation of enriched Re^{187} dissolved in nitric acid: $Re^{187}(n, \gamma)Re^{188}$. Liquid sources were used thoroughout the measurements as liquids generally yield unperturbed correlations. The experimental data were treated as depicted in section 2.

The directional correlation was measured between the 931 keV and 155 keV

† The results described in this section have already been reported at the Stockholm Conference, June 1959 [29]).

gamma rays using sources with small diameters (less than 1 mm) in order to minimize the effects of scattering and absorption of the 155 keV quanta in the source. The result after corrections for contributions from overlapping cascades was

$$W(\theta) = 1+(0.276\pm0.012)P_2(\cos\theta)+(0.930\pm0.025)P_4(\cos\theta).$$

The next step consisted in attacking the 828—633 keV and 673—633 keV cascades. The results obtained for these cascades did not agree with any

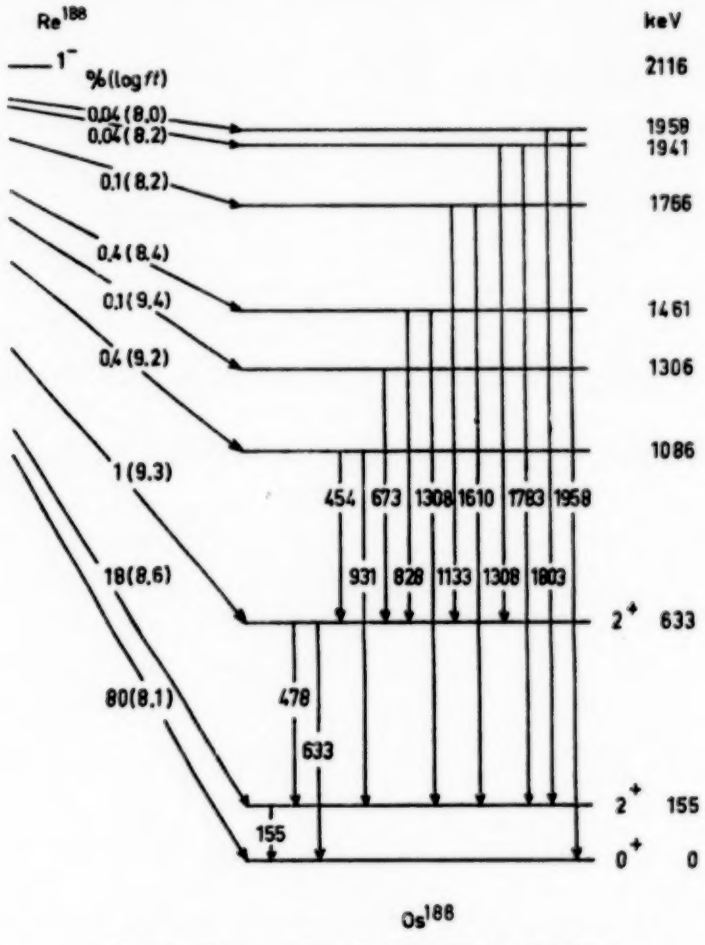

Fig. 9. Decay scheme of Re^{188} to Os^{188} [1]).

theoretical possibility. The contribution to the coincidence counting rate from the 1133—633 keV cascade was small ($\leqq 7\,\%$ and $16\,\%$ respectively) and could only account for the discrepancies if it would show an extremely large anisotropy. The existence of such a large anisotropy was proved by a measurement of the directional correlation between the 1133 keV and 633 keV gamma rays. The result was

$$W(\theta) = 1+(0.37\pm0.03)P_2(\cos\theta)+(0.92\pm0.07)P_4(\cos\theta).$$

No correction has been applied for the contribution from the 1308—633 keV

cascade, since the coincidence counting rate in the 1308—633 keV cascade appeared to be very low and did not show any strong anisotropy. Moreover, the 1308 keV line is double, and the intensity ratio of these coinciding lines is not accurately known, so that a reliable correction cannot be obtained.

Using the above result the measurements on the 828—633 keV cascade could be corrected for the contribution from the 1133—633 keV cascade. The result was

$$W(\theta) = 1+(0.295\pm0.009)P_2(\cos\theta)+(0.015\pm0.020)P_4(\cos\theta).$$

The result for the 673—633 keV cascade after subtraction of the 1133—633 keV and 828—633 keV contributions was

$$W(\theta) = 1(0.068\pm0.008)P_2(\cos\theta)+(0.017\pm0.018)P_4(\cos\theta).$$

The cascades which have been investigated are all of the type $I_1(L, L+1)2+(\mathrm{E2})0+$, where I_1 denotes the spin of the initial level. Fig. 4 shows theoretical curves of the anisotropy coefficients A_2 and A_4 versus the amplitude mixing ratio δ for possible values of I_1(except for $I_1 = 0$, since in this case the electromagnetic transitions involved are, of course, pure). Comparing the experimental coefficients with the theoretical ones the following conclusions are drawn.

THE 931—155 keV CASCADE.

The experimental coefficients A_2 and A_4 are only compatible with those for a $0 \rightarrow 2 \rightarrow 0$ cascade, so that the spin of the 1086 keV level is zero. The deviation from the theoretical coefficients might be due to an attenuation of the correlation function by extranuclear fields, as the half-life of the 155 keV level is 0.62×10^{-9} sec. [32]) The attenuation factors are $G_2 = 0.79\pm0.03$ and $G_4 = 0.81\pm0.03$.

THE 673—633 keV CASCADE.

It appears from figure 4 that the experimental results agree with the following spin assignments to the 1306 keV level:

$$I = 2 \text{ with } \delta = -(0.25\pm0.01),$$
$$I = 4 \text{ with } \delta = +(0.06\pm0.02).$$

It is impossible to make a choice between these cases on the basis if the directional correlation experiments alone. However, a spin of $I = 4$ can be ruled out if the 1306 keV level is directly fed from the Re^{188} ground state ($I = 1-$). Although the case $I = 3$ is just outside the limits of error, a spin of 3 cannot be rigorously excluded. Nevertheless preference has to be given to $I = 2$.

THE 828—633 keV CASCADE.

Only a spin of $I = 2$ for the 1461 keV level with $\delta = 0.05\pm0.01$ fits the experimental correlation function.

THE 1133–633 keV CASCADE.

The results are only consistent with a spin 0 for the 1766 keV level.

Even parity has to be attributed to the discussed Os^{188} levels if one considers the log *ft* values for the beta branches feeding these levels. The results of the directional correlation experiments are collected in table 2.

Fig. 10 shows again the Os^{188} level structure as found from the decay of Re^{188}.

TABLE 2

Energies of cascading gamma rays (keV)	A_2	A_0	Energy of initial level (keV)	Resulting spin of initial level	Multipole mixing on upper gamma transition
931—155	$+(0.276\pm0.012)$	$+(0.930\pm0.025)$	1086	0	
673—633	$+(0.068\pm0.008)$	$+(0.017\pm0.018)$	1306	2	94% dipole +6% quadrupole
828—633	$+(0.295\pm0.009)$	$+(0.15\pm0.20)$	1461	2	100% dipole
1133—633	$+(0.37\pm0.03)$	$+(0.92\pm0.07)$	1766	0	

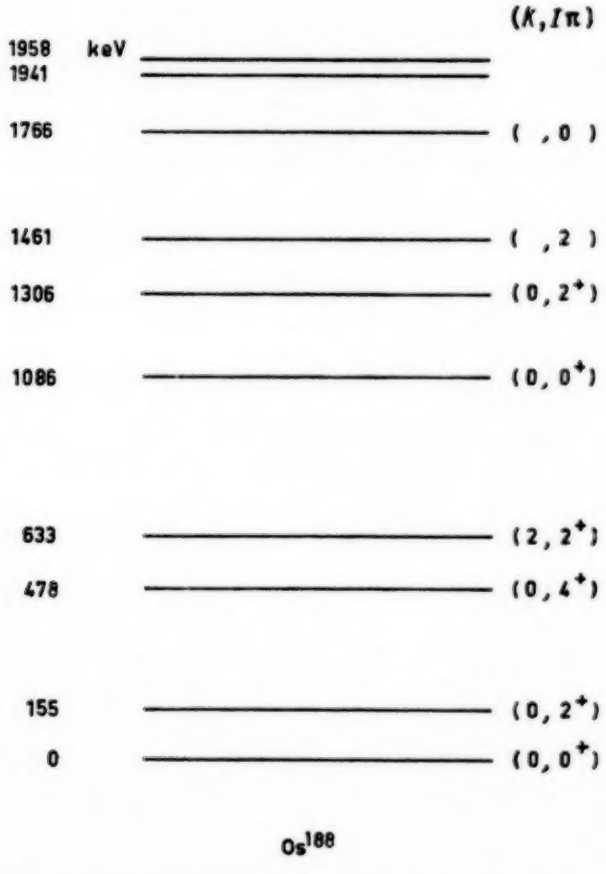

Fig. 10. Level scheme of Os^{188} as found from the decay of Re^{188} with the present results included. The 478 keV level is excited in the decay of Ir^{188} [37]).

The 478 keV level, which has been established from the decay of Ir^{188}, is included.

The three lowest levels in Os^{188} belong to the ground state rotational band with $(K, I\pi)$: (0, 0+), (0, 2+), and (0, 4+). It is believed that the 633 keV 2+ level forms the first member of the gamma-vibrational band with quantum numbers (2,2+). There is no rotational structure found on this level as the 1− ground state spin of Re^{188} probably excluces population of rotational levels built on this level †. The first member of a possible beta-vibrational band (0, 0+) is present at 1086 keV. The level at 1306 keV forms probably the second member (0, 2+). This latter assignment leads to a reasonable value for the moment of inertia of the nucleus. On the other hand, the 673 keV gamma transition between the (0, 2+) and (2, 2+) levels should have predominantly E2 character which is in contradiction to the experimental result. The violation of the K-selection rule indicates K-impurity in the 1306 keV level. The character of the 1461 keV level is not clear; this level also de-excites by almost pure dipole radiation. The 1766 keV level with spin zero will be discussed in section 7.

Shortly after the Stockholm conference (see footnote p. 547) King and Johns [33]) published their results of directional correlation measurements on Re^{188}. Although the experimental correlation functions for some cascades deviate considerably from those described in the present article, the conclusions King and Johns arrive at are strictly the same as ours.

6. Levels in Pt^{194}

The decay of $Ir^{194}(1-)(19h)$ to Pt^{194} has been investigated by many authors[1]). Johns and Nablo [35]) have used external conversion technique to establish their decay scheme, shown to the left in fig. 11. Many more levels of Pt^{194} are excited in the decay of $Au^{194}(1-)(39h)$ [1]). Bäckström *et al.* [36]) at this institute have recently carefully investigated the Au^{194} decay in internal conversion and also with e^-—e^- coincidences, and an external conversion measurement is in progress. Their level scheme is drawn to the right in fig. 11 (electron transitions). They suggest the 923 and 1267 keV levels to have spin parities (4+) and 0+, while a second 0+ level is observed at 2164 keV. The gamma rays in the middle of fig. 11 are taken from a very recently started investigation on the decay of Ir^{194} with external conversion by Bäckström and Kern [40]) at this institute. Their four gamma rays around 1170 keV are easily identified and placed using the information from the Au^{194} decay.

We have investigated the decay of Au^{194} as well as Ir^{194} with the directional correlation apparatus described in section 2 in order to find the possible excited 0+ levels in the spherical nucleus Pt^{194}. The Au^{194} sources were produced in the

† A 3+ gamma vibrational level at 827.5 keV is probably excited in the decay of Ir^{188}, as concluded from an investigation by O. A. Bruil and B. Jung.

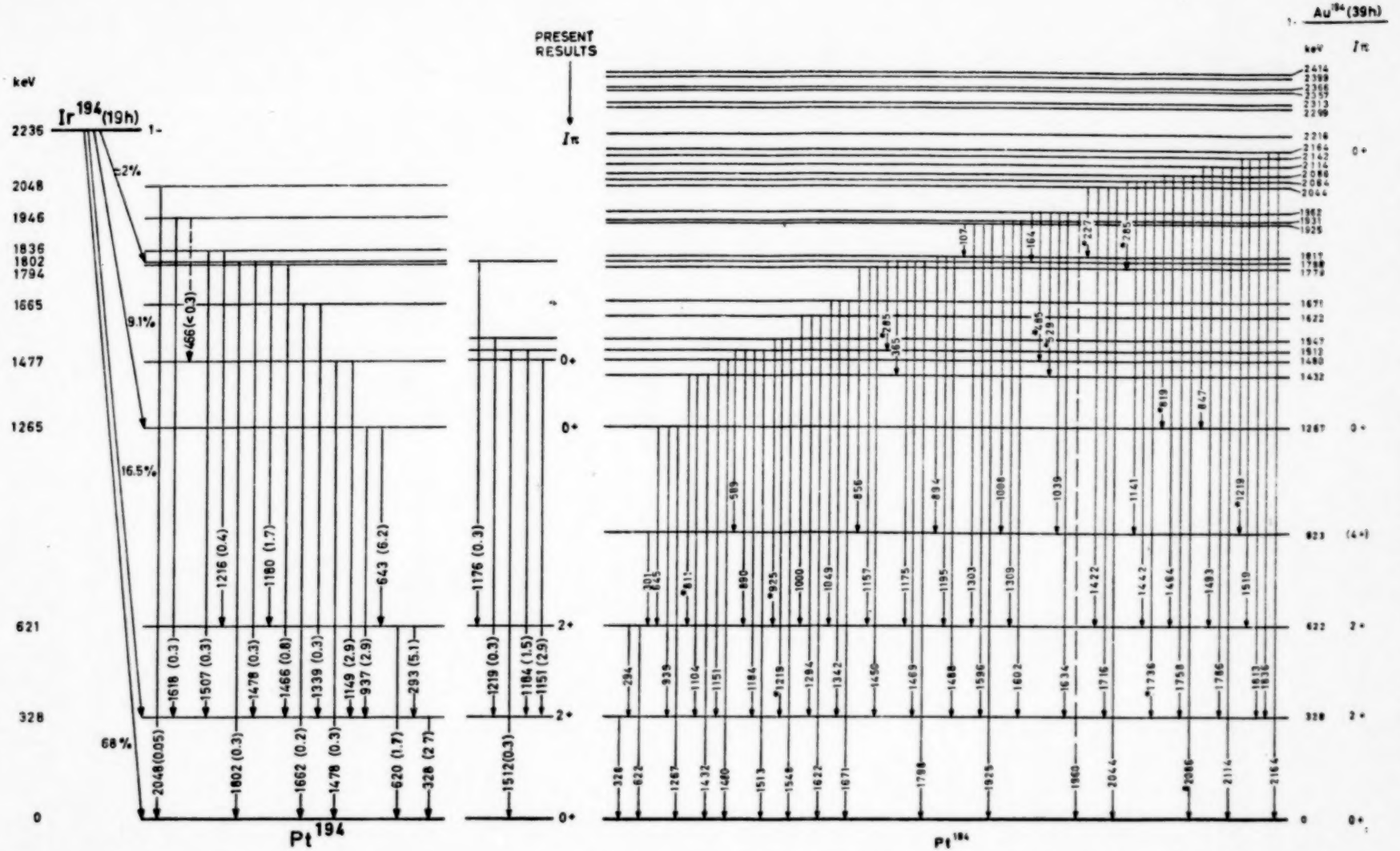

Fig. 11. Level scheme of Pt^{194} excited from Ir^{194} and Au^{194}, as determined by Johns and Nablo [35]) and by Bäckström *et al.* [36]) (Gamma intensities given in brackets.) The gamma rays in the middle of fig. 11 are taken from a very recent external conversion measurement on Ir^{194} by Bäckström and Kern [40]).

Uppsala cyclotron by proton bombardment of platium metal: $Pt^{194}(p, n)\ Au^{194}$. After chemical separation we used the source desolved in hydrochloric acid. The Ir^{194} sources were obtained by neutron irradiation of spectroscopically pure natural Ir sponge in a flux of 3×10^{12} n/cm^2 . sec at AB Atomenergi, Stockholm. Enriched Ir^{193} powder was used in the latter measurements in order to get rid of the Ir^{192} activity. The measurements were performed on Ir sources in powder form. Such a source condition was not thought to attenuate the correlation

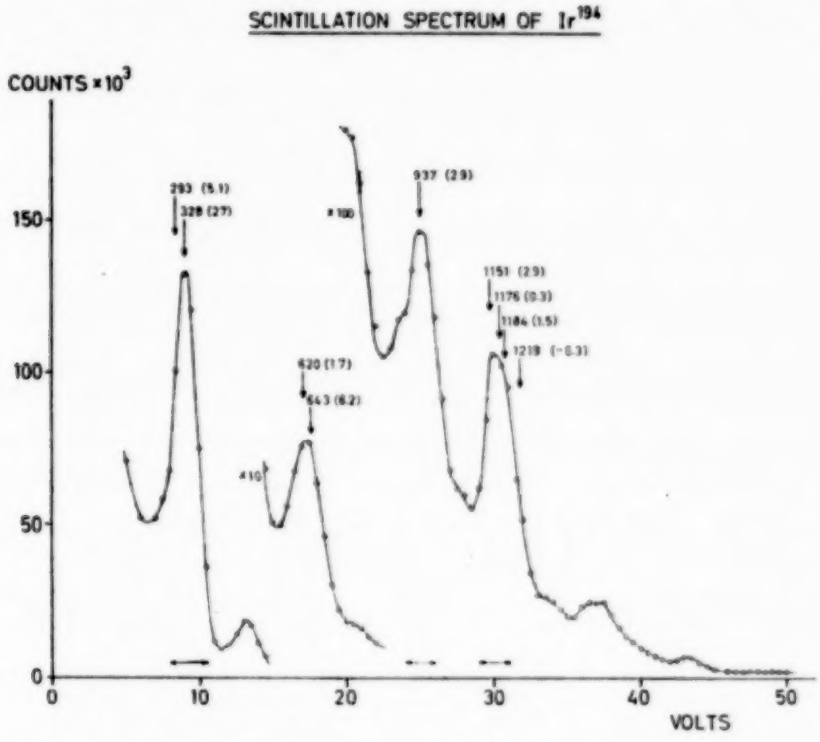

Fig. 12. Scintillation spectrum of Ir^{194} in a $1\frac{1}{2}$ in. $\times$ $1\frac{1}{2}$ in. NaI(Tl) crystal with indications of the selected channels.

appreciably, as the half-life of the first excited state is measured to $T_{\frac{1}{2}} = 3.9\times 10^{-11}$ sec [1]) in Coulomb excitation, and the half-life of the 622 keV level (also Coulomb excited [1])) is still shorter.

Our correlation measurements on the Au^{194} sources gave only qualitative results because of the complexity of the decay scheme. A large anisotropy was observed, when the 328 keV gamma ray was selected in one channel, and the other channel was focused in the region of 1000 keV.

In the investigation of the decay of Ir^{194} we used the same method as described in the earlier sections with careful determination of the correlation function of a certain photopeak, or parts of it, compared with the contributing „background" correlation function. A scintillation spectrum is presented in fig. 12 with indicated channel settings. Thus, when the 328 keV transition was selected, we found two gamma ray peaks with high anisotropy at 940 and 1200

keV. A coincidence spectrum at two different angles determined the energy of the strongly anisotropic gamma ray of higher energy to 1170±30 keV, while a correlation run with channel setting just above this energy (and the 328 keV peak in the other channel) gave an almost isotropic distribution. The coincidence rate with the 940 and 1170 keV rays dropped sharply, when the 622 keV gamma ray was selected instead of the 328 keV peak. The resulting corrected correlation functions are:

THE 937—328 keV CASCADE:

$$W(\theta) = 1+(0.234\pm0.017)P_2(\cos\theta)+(0.868\pm0.038)P_4(\cos\theta).$$

THE 1170—328 keV CASCADE:

$$W(\theta) = 1+(0.128\pm0.010)P_2(\cos\theta)+(0.850\pm0.037)P_4(\cos\theta).$$

These correlations are only compatible with $0 \rightarrow 2 \rightarrow 0$ pattern (although the errors given here are only statistical ones). From the first equation we can assign a zero spin to the 1267 keV level. The 1170—328 keV correlation must originate from an 1170 keV gamma ray in direct cascade with the 328 keV gamma ray. The 1184(1.5) and 1151(2.9) keV rays are thus possible candidates, while the 1219(0.3) keV ray has too high energy and is responsible for only 7 % of the peak intensity. Bäckström and Kern [11]) have observed a 1512 keV gamma ray but no 1480 keV gamma transition. We thus assign a zero spin to the 1480 keV level in Pt^{194}.

7. Levels in even nuclei with A = 50—250

All data of even nuclei with $A = 50$—250, published or from private communications [1, 27, 53]), are treated. The excitation energies of the levels below 4 and 2 MeV are plotted in fig. 13a and 13b as a function of neutron number N. Definite and probable levels (with spin and parity) are distinguished (by black and open marks) as well as known beta, gamma and octupole bands of deformed nuclei and corresponding levels of spherical nuclei (by squares, triangles and crosses). Corresponding levels are connected with whole lines between isotopes and dashed lines between nuclei with different number of protons. Straight dashed lines are also drawn between levels, separated by regions with lacking experimental data.

Comparison of the experimentally obtained trend of levels in fig. 13 with the theoretically predicted trend in fig. 2 at once gives a number of similarities. Thus the excitation energies of the one-phonon vibrations (2+) of spherical nuclei drop sharply with addition or subtraction of pairs of neutrons from closed shell nuclei. (The trend of low energy levels in the Hg and Pb isotopes is exceptional but expected from both shell model and collective model considerations [39])).

The two-phonon vibrations also show the same tendency and at the same time a splitting up into the predicted triplet. In most cases only one or two members of the 0+, 2+, 4+ triplet are excited in beta decay and high lying 0+ levels weakly fed, as the energy factor strongly favours the ground state feeding. But the nucleus Cd^{114} exhibits an established close triplet of 2+, 4+ and 0+ levels [41]). Fig. 13a also shows a strong influence from the closed proton shells at $Z = 50$ (and 28), causing the excitation energies of the first excited levels to increase rapidly, when approaching these numbers. The closure of the proton shell at $Z = 50$ in the middle between $N = 50$ and $N = 82$ is also probably responsible for the fact that nuclei in this region do not exhibit a stable non-spherical shape.

Nuclei in the middle of the rare-earth and actinide regions show clear rotational bands of deformed nuclei, similar to the spectrum discussed in fig. 1. Thus, the ground state rotational band 2+, 4+, 6+ ... is clearly shown. (Observed higher members of the ground state rotational band are excluded in fig. 13b for clarity.) Several members of the gamma vibrational band are also found. The general prediction (fig. 2) of the behaviour of the ground state rotational band to increase in energy while the gamma vibrational band is to decrease when approaching the transition regions between spherical and deformed nuclei is thus verified in fig. 13. The observed decrease of gamma vibrational energies from $N = 92$ to $N = 98$ is probably a proton effect as no drop in energy with increasing N-value is observed there within a definite proton number. See $Gd^{154, 156, 158}$ in fig. 13.

As mentioned earlier, one of our aims was to find the trend of the beta vibrational band in the rare earth region and the corresponding levels in spherical nuclei. The detected 0+ levels at 615 keV in the spherical Gd^{152} nucleus and at 685 keV, with accompaning first rotational level (2+) at 811 keV, in the deformed nucleus Sm^{152} (see section 3), were thus possible candidates. A 0+ and a 2+ level have recently been observed [42]) in Gd^{154} at about the same excitation energies as in Sm^{152}. The 1460 keV 0+ level in Er^{166} and accompanying first rotational level (2+) at 1542 keV show the properties expected for beta vibrational levels. (The theoretical branching rules [6]) thus predict the strongest feeding from the beta vibrational 2+ level to the 4+ ground state band, and this transition is the only one observed in the Tm^{166} decay. See section 4 and fig. 8.) In the other transition region Os^{188} was found to have a 0+ level at 1086 keV. This level may be a first member of the beta vibrational band in this nucleus. But the observed reduced transition probabilities are about equal for the decay of the 1086 keV level to the ground state 2+ rotational level and to the 633 keV 2+ gamma vibrational level, and the E0 feeding to the ground state is unknown, hidden in the strong beta continuum, so that no definite conclusion can be drawn from the branching ratios. Finally, a first excited 0+ level at 1265 keV in Pt^{194} was found (see section 6). We may thus conclude,

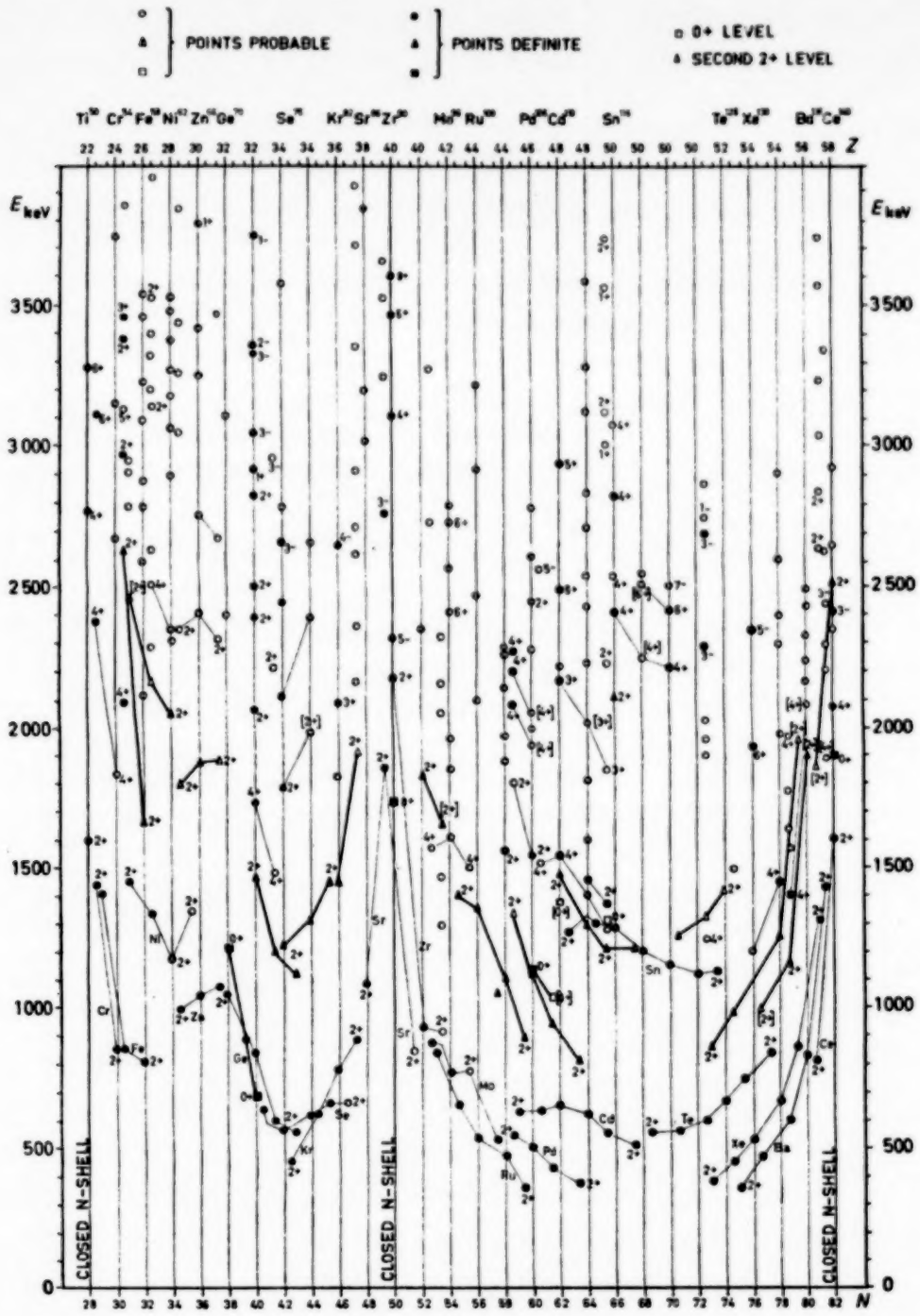

Fig. 13a. Excitation energies of observed levels belcw 4 and 2 MeV as a function of neutron number N. Nuclei with the same N but with different numbers of protons Z are displaced some what from the most stable (some exceptions) nucleus of a given N value. This performance is indicated on the upper axis Z. Spins in square brackets are predicted from level systematics. (The beta band in Gd^{154} is not definite.)

that the experimentally observed trend of excited 0+ levels of probable beta vibrational character is compatible with the trend predicted in fig. 2. The

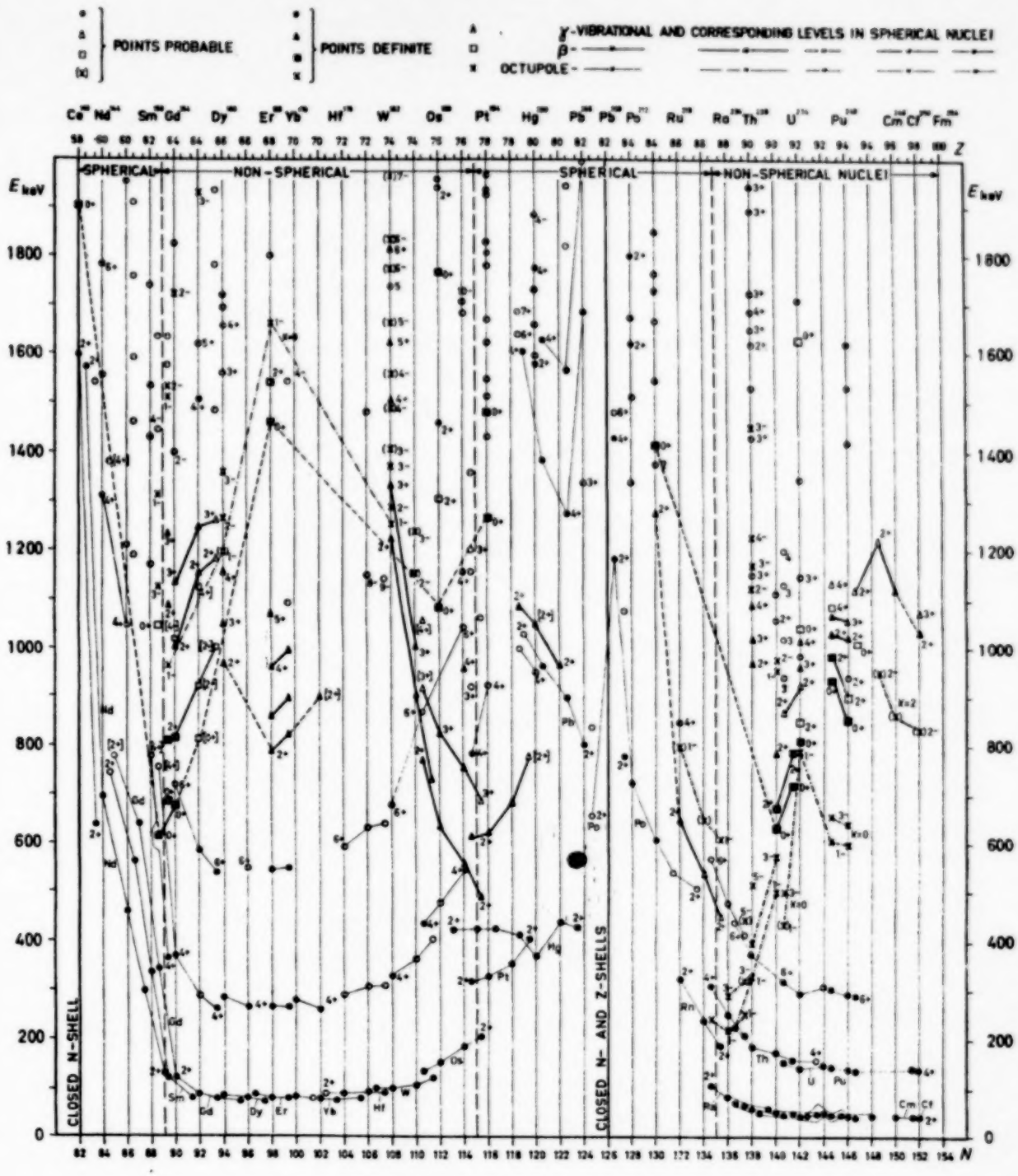

Fig. 13b. (See caption fig. 13a)

trend of the beta and gamma vibrational levels in the heavy element region is similar to that in the first part of the rare-earth region and thus gives additional strength to the conclusions made.

In the course of this work higher excited 0+ levels have also been observed. Thus, Toth *et al.* [38]) found a 0+ level in Gd^{152} at 1047 keV, we observed a

second excited 0+ level in Os^{188} at 1766 keV as well as one in Pt^{194} at 1480 keV, while Bäckström *et al.* [36]) found a third 0+ level in the latter nucleus at 2164 keV. In the actinide region Bjørnholm *et al.* [43]) have observed excited 0+ levels in U^{234} at 812, 1045 and possibly at 1624 keV. As mentioned earlier excited 0+ levels may have several different origins. The identification of the lowest 0+ levels in the spherical and non-spherical nuclei as two-phonon vibrational and beta vibrational levels respectively is to some extent arbitrary. But keeping to that assumption, the 1047 keV level in the spherical nucleus Gd^{152} may be identified as a three-phonon 0+ level from its de-excitation mainly to the 615 keV 0+ level and its energy being almost three times the 2+ one-phonon level energy of 344 keV. The 1766 keV 0+ level in Os^{188} seems to have a mixed character and may be described in terms of admixture of two rotational bands as has been done explicitly for Gd^{156} [44]). The 1480 and 2164 keV 0+ levels in Pt^{194} may be of particle excitation character. The 1624 keV 0+ level in the non-spherical nucleus U^{234} feeds strongly the 812 keV 0+ level and has just the double excitation energy. It may thus tentatively be identified as a two-phonon beta vibrational level. No prediction of the excitation energy of the octupole levels as a function of neutron number is available. But fig. 13b indicates an octupole band, $K = 0$, $I = 1-$, $3-$, $4-$, with about the same trend as the beta and gamma vibrational levels in both the regions of non-spherical nuclei.

The excitation energy of low-lying levels seems from fig. 13 to be a smooth function of the neutron number N for a certain Z value, and a similar trend is found for the level energy of neighbouring Z values. The level systematics in fig. 13 may thus be used in order to predict the character of new low energy levels and as a guide for construction of decay schemes. We have used the first mentioned method to predict probable spins and parities of some levels in fig. 13. (The assignments are put in square brackets.) As an example the 691 keV level in Os^{192} will be discussed. This level has been assigned spin-parity 3+ by some authors [45]) and identified as a 4+ ground state rotational level by others [46, 47]). But the level energy fits smoothly on the 3+ gamma vibrational curve in fig. 13b and is too high for the 4+ curve belonging to the ground state rotational band. Furthermore, under the 4+ assignment of the 691 keV level the rotational energy formula, eq. 1, gives a positive value of the rotational-vibrational interaction coefficient, $B = +16.7 \times 10^{-3}$, while no other nucleus has a positive B-value for the ground state band (table 3) and these values are increasingly negative, when approaching the transition regions between spherical and deformed nuclei. The 3+ assignment by Shiel *et al.* [45]) is thus concluded to be correct.

8. Moments of inertia and rotational-vibrational interaction

The moments of inertia of deformed nuclei may be determined from their rotational bands, see eq. (1). And the interaction between levels in such nuclei

TABLE 3

Empirical constants in the rotational energy formula

$$E_I = E_0 + AI(I+1) + B^{\text{exp}} I^2(I+1)^2, \quad A = \frac{\hbar^2}{2\mathcal{J}}, \quad B^{\text{theory}}_{\substack{\text{ground}\\\text{state}\\\text{band}}} = A^3\left[\frac{-12}{(\hbar\omega_\beta)^2} + \frac{-4}{(\hbar\omega_\gamma)^2}\right]$$

N	Nucleus	First excited state $E_{0,2+}$ (keV)	$6A = \frac{3\hbar^2}{\mathcal{J}}$ (keV)				$B^{\text{exp}} \times 10^3$ (keV)				$k = \frac{B^{\text{theory}}}{B^{\text{exp}}}$
			Ground state band	β	γ	Octupole	Ground state band	β	γ	Octupole	Ground state band
90	Sm^{152}	121.78	126.8	$(126)_0$ †	$(148)_0$		−141				2.02±0.02
	Gd^{154}	123.07	128.1	[153]	$(132)_0$		−139.6	−409			2.12±0.02
92	Gd^{156}	88.96	89.9	[112]	$(94)_0$		−29.9	[−179]			3.18±0.12
94	Gd^{158}	79.57	80.0		$(75)_0$		−11.8				
	Dy^{160}	86.9	87.6		81.8		−20		−37.5		
96	Dy^{162}	80.65	81.1				−11.9				
98	Er^{164}	80.57	81.0	$(81.4)_0$	77		−13.0		−25		2.45±0.20
100	Er^{166}	79.80	80.0		74.8		−5.7		−1		
	Yb^{170}	84.25	84.6				−10.8				
102	Yb^{172}	78.70	79.0				−7.6				
104	Hf^{176}	88.35	88.9				−14.4				
106	Hf^{178}	93.15	93.6				−13.1				
108	Hf^{180}	93.29	93.5				−6.0				
						$K=2-$				$K=2-$	
	W^{182}	100.09	100.6		108	20.6	−15.1		+20.3	+590	
110	W^{184}	111.13	112.0		$(102)_0$	$(83)_0$	−23.3				
	Os^{186}	137.2	140.2		196		−83		−455		
112	Os^{188}	155.05	160.0	$(219)_0$	$(194)_0$		−138				3.66±0.05
114	Os^{190}	186.7	196		250		−266		−540		
134	Ra^{222}	111.1	118				−200				
						$K=0-$					
136	Ra^{224}	84.45	88.3			$(43)_0$	−108				
	Th^{226}	72.13	74.0				−50			$K=0-$	
138	Ra^{226}	67.62	69.6			38.0	−55			+14.5	
	Th^{228}	57.5	58.2		54.5	41.3	−18		−14	−5.2	
140	Th^{230}	52.8	53.1	$(42)_0$		$(39)_0$	−7.8				3.4 ±0.5
	U^{232}	47.2	47.3			$(40)_0$	−3.6				
142	U^{234}	43.4	43.5	$(42)_0$	37.4		−4.9		+24		1.8 ±1.0
144	Pu^{238}	44.07	44.1	50.9	34.3	$(51)_0$	−3.3	−39	+70		2.1 ±0.3
146	Pu^{240}	42.87	43.0	$(42)_0$		$(40)_0$	−4.0				1.6 ±0.3

† Values within parentheses $(\quad)_0$ have been calculated with $B = 0$.

is reflected in the deviation of the rotational bands from the simple rotational pattern of a symmetric top, eq. (1) with $B = 0$. Accurate measurements of the energy of the rotational bands in many nuclei are now available. The resulting values of the moments of inertia and coefficients of interaction are presented in table 3.

The ground state rotational band gives a value of $6A = 3\hbar^2/\mathcal{I}$, inversely proportional to the moment of inertia, eq. (1), with about the same trend as function of neutron number as the energy of the first excited states. But the $6A$-curve is a little steeper in the transition regions than the excitation energy curve, as the latter is depressed there by strong interactions, table 3. Nuclei in excited states have about the same values of moment of inertia as in their ground states. The small deviations are plotted in fig. 14 as function of neutron number. Strongly deformed nuclei seem to have a somewhat larger moment of inertia in excited states than in their ground state, while the opposite effect is observed

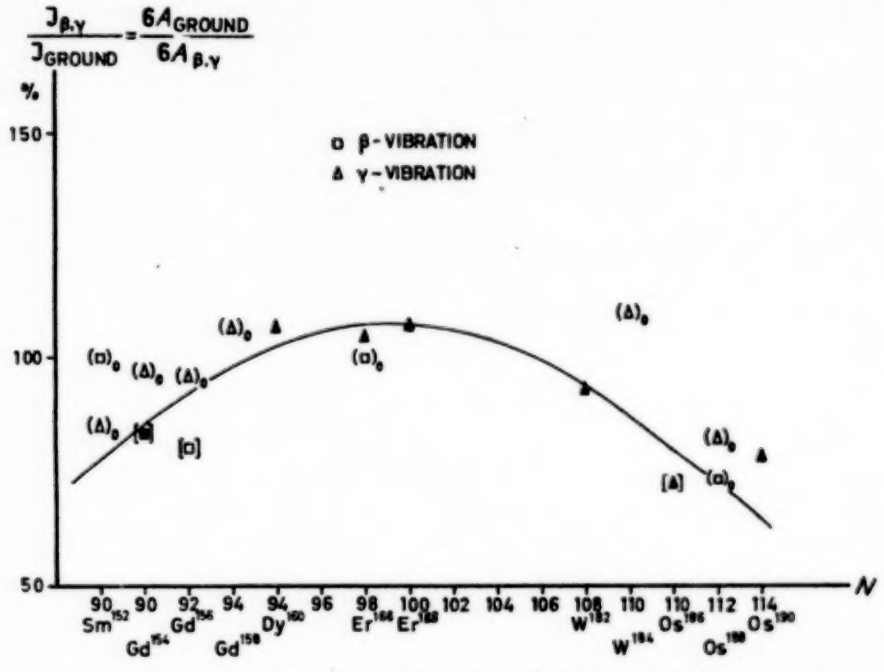

Fig. 14. The ratios of the moments of inertia of nuclei in vibrational states and ground states as function of neutron number. The points within parentheses are calculated assuming $B=0$ in eq. (1) and are thus most in error in the transition regions.

for nuclei in the neighbourhood of the transition regions. If the simple formula, $\mathcal{I} = 3B_1\beta^2$ is approximately valid, connecting a certain moment of inertia with a certain deformation β, the observed effect may be expressed by saying that strongly deformed nuclei are still more deformed in excited states and nuclei near the transition regions are less deformed in excited states than in their ground states.

Table 3 shows negative B^{exp} values for the ground state band in all nuclei, that is, the ground state rotational band is depressed by the interaction with other levels of the same spin and parity. This effect is most pronounced near the transition regions, where the beta and gamma vibrational levels are low in energy. The amount of depression of the ground state band from the beta and gamma bands is predicted in eq. (3). In nuclei with known positions of these

bands, the coefficient B^{theory} may be calculated. The ratio $k = B^{\text{theory}}/B^{\text{exp}}$ is tabulated in column 12 of table 3. A k-value of 2 to 4 is found, indicating a weaker coupling than the theoretically expected from eq. (3). (The coupling to additional levels will only make the deviation larger.) Furthermore, k does not seem to be constant. More accurate calculations of the rotational-vibrational interaction than the hydrodynamical approximation are thus needed to explain the experimental data, and such calculations are also planned by the Copenhagen group.

The observed gamma vibrational bands show negative B^{exp} values, with the exception of three cases (table 3). The depression from higher levels is thus more effective on the gamma vibrational band than the opposite effect from the ground state band and from the beta vibrational band, when this is situated below the gamma band. The positive B^{exp} values of the gamma bands of W^{182}, U^{234} and Pu^{238} are calculated from the 2+, 3+ and 4+ levels. (The only gamma levels observed in U^{234} and Pu^{238}). Beta vibrational bands are also found in these two nuclei. The B^{exp} value of this band in Pu^{238} is negative and comparatively large, while only two levels of the beta band are observed in U^{234}. The distance between the 2+ levels in the beta and gamma bands of these two nuclei is only 67 and 45 keV respectively, and the levels will, according to eq. (2), repel each other strongly, causing the observed depression of the beta band. For the same reason the gamma levels of even spins will be lifted, while the odd-spin levels remain undisturbed by the beta band. We thus expect a gamma band here with two close levels, 2+ and 3+, followed by a gap before the next two close levels, 4+ and 5+, and so on. Unfortunately, the decay schemes of U^{234} and Pu^{238} are not too well established and the higher members of the beta and gamma bands not yet observed. But W^{182} has recently been carefully reinvestigated by Gallagher and Rasmussen [48]). They have found a gamma vibrational band with five members, where the above-mentioned grouping of the gamma vibrational levels is clearly shown, fig. 13b. A number of other levels are also observed in the same energy region, but they have negative parity and do not disturb the gamma band. The calculated values of B^{exp} for the gamma bands in W^{182}, U^{234} and Pu^{238} are about equal. A beta vibrational band is thus expected in W^{182} with a 0+ level at about 1050 keV.

Some of the subjects in section 7 and 8 are also recently discussed by R. K. Sheline [49]) and by Birbair *et al.* [50]). The first author calculates the beta vibrational levels by assuming the ratio k between B^{theory} and B^{exp} to be a constant equal to 2.12. Birbair *et al.* estimate the interaction between the beta vibration and ground state bands. The difficulties encountered by these authors with a ten-fold decrease in the stability against beta vibrations between the isotopes W^{182} and W^{184} are solved, if the more accurate A and B values in table 3 are used, giving a reasonable ratio of 1.7 for the beta vibrational stabilities of W^{182} and W^{184}.

The authors are indebted to Professor Kai Siegbahn for excellent working conditions and stimulating interest. Theoretical discussions with Professor Ben Mottelson, Dr. Sven-Gösta Nilsson and Dr. Ove Nathan are appreciated. Two of us (I. M. and B. v. N.) are grateful to NORDITA and the Netherlands Organization for Pure Research, respectively, for financial support. Our thanks are also due to Mr. T. Petersén and Mr. Å. Svanheden for co-operating in carrying out the irradiations, to Mr. A. Tjeder for chemical Au separations, to Mr. S. Gustafsson and the spectrometer group for valuable assistance and to Mr. K. Sevier for correcting the English.

References

1) Strominger, Hollander and Seaborg, Revs. Mod. Phys. **30** (1958) 585
2) G. Scharff-Goldhaber and J. Weneser, Phys. Rev. **98** (1955) 212
3) A. Bohr and B. R. Mottelson, Mat. Fys. Medd. Dan. Vid. Selsk. **30** No 1 (1955)
4) Alder, Bohr, Huus, Mottelson and Winther, Revs. Mod. Phys. **28** (1956) 432
5) L. S. Kisslinger and B. R. Mottelson, private communication
6) Alaga, Alder, Bohr and Motterson, Mat. Fys. Medd. Dan. Vid Selsk. **29** No 9 (1955)
7) R. K. Sheline, Proc. of the University of Pittsburg Conference, June 1957, 479
8) G. Bäckström, Arkiv. f. Fysik **10** (1956) 387;
G. Bäckström, Nuclear Instruments **1** (1957) 253
9) Crystal spectrometer measurement, I. Marklund, Nuclear Physics **9** (1958/59) 83
10) Marklund, Nathan and Nielsen, Nuclear Physics **15** (1960) 199
11) H. Frauenfelder, in Beta and Gamma Ray Spectroscopy, K. Siegbahn, ed. (Amsterdam, 1955) 795
12) M. Ferentz and N. Rosenzweig, ANL-5324 (unpublished)
13) T. Lindqvist, Arkiv. f. Fysik **12** (1957) 495
14) A. M. Feingold and S. Frankel, Phys. Rev. **97** (1955) 1025
15) O. Nathan and S. Hultberg, Nuclear Physics **10** (1959) 118
16) B. R. Mottelson and S. G. Nilsson, Mat. Fys. Medd. Dan. Vid. Selsk. **1** No. 8 (1959)
17) Grace, Taylor and Treacy, Phil. Mag. **3** (1958) 90
18) J. W. Mihelich and E. L. Church, Phys. Rev. **85** (1952) 690
19) A. W. Sunyar, Phys. Rev. **93** (1954) 1345
20) Graham, Wolfson and Clark, Phys. Rev. **98** (1955) 1173A
21) Cork, Brice, Helmer and Woods Jr., Phys. Rev. **110** (1958) 526
22) Chupp, DuMond, Gordon, Jopson and Mark, Bull. Am. Phys. Soc. **2** (1958) 55
23) M. E. Rose, Table of Internal Conversion Coefficients (Amsterdam, 1958)
24) S. Hultberg and R. Stockendal, Arkiv f. Fysik **14** (1959) 565;
S. Hultberg, Arkiv f. Fysik **15** (1959) 307; Phys. Rev. Letters **3** (1959) 227
25) J. W. Fraser and J. C. D. Milton, Phys. Rev. **98** (1955) 1173
26) G. Gromov, B. Dželepow, B. Preobrazenskii, W. Morozov and L. Peker in ref. [27])
27) B. S. Dželepov and L. K. Peker, Decay schemes of radioactive nuclei (Moscow, 1958)
28) K. P. Jacob and J. W. Mihelich, Bull. Am. Phys. Soc. **2** (1958) 358
29) Stockholm Conference Report (June 1959) Arkiv f. Fysik **16** (1960)
30) K. O. Nilsen and O. B. Nielsen, Nuclear Physics **5** (1958) 319
31) T. Wiedling, Thesis, University of Stockholm (1957)
32) A. W. Synuar, Phys. Rev. **98** (1955) 653
33) W. J. King and M. W. Johns, Can. J. Phys. **37** (1959) 755
34) G. Alaga and B. Jakšič, Phys. Rev. **103** (1956) 1441
35) M. Johns and S. Nablo, Phys. Rev. **96** (1954) 1599
36) Bäckström, Bergman, Burde and Lindskog, Nuclear Physics **15** (1960) 566

37) P. S. Fisher and R. A. Nauman, Phys. Rev. **112** (1958) 1717;
R. M. Diamond and M. J. Hollander, Nuclear Physics **8** (1958) 150
38) O. B. Nielsen, private communication
39) S. Wahlborn, private communication;
B. R. Mottelsson, private communication
40) G. Bäckström and J. Kern (to be published)
41) H. T. Motz, Phys. Rev. **104** (1956) 1353;
ref. [55]);
T. Tamura and L. G. Komai, Phys. Rev. Letters **3** (1959) 344
42) O. Nathan, private communication
43) S. Bjørnholm, private communication
44) Hansen, Nielsen and Sheline, Nuclear Physics **12** (1959) 389
45) V. Shiel, L. D. Wyly and C. H. Braden, Phys. Rev. **105** (1957) 1521
46) R. M. Diamond and J. M. Hollander, Nuclear Physics **8** (1958) 150
47) Barloutaud, Levesque, Lehmann and Duidort, J. phys. radium **19** (1958) 60
48) C. J. Gallagher, Jr. and J. O. Rasmussen, Phys. Rev. **112** (1958) 1730
49) R. K. Sheline, Revs. Mod. Phys. (to be published)
50) Birbrair, Peker and Sliv, JETP **36** (9) (1959) 566
51) P. Boskma and H. de Waard, Nuclear Physics **12** (1959) 533
52) Postma, Miedemaand and Eversdijk, Physica **25** (1959) 671
53) Nuclear Data Sheets, National Academy of Sciences, National Research Council, Washington D.C.
54) R. K. Girgis, Thesis (University of Amsterdam, 1959)
55) F. K. McGowan and P. H. Stelson, BAPS **4** (1959) 232;
Congrés International de Physique Nucleaire (Paris, 1958) p. 765

References to fig. 13, 14 and table 3

Refs. [1, 27, 53]) are used generally
Abbreviations: PR = Phys. Rev.
PRL = Phys. Rev. Letters
NP = Nuclear Physics
BAPS = Bull. Am. Phys. Soc.

Ti^{50}	Morinago, Mutsoro, Sugawara	PR **114** (1959) 1146
Cr^{54}	Porter, v. Patter, Rothman, Mandeville,	PR **112** (1958) 468
Fe^{56}	C. Sharp Cook	NP **7** (1958) 480
	P. Kienle, R. E. Segel	PR **114** (1959) 1559
Ni^{62}	J. W. Butler, C. R. Gossett	PR **112** (1958) 1257
Zn^{64}	D. J. Horen	PR **113** (1959) 578
Zn^{66}	D. J. Horen and W. E. Meyerhof	PR **111** (1958) 560
	B. v. Nooijen	Thesis Amsterdam 1958
Zn^{68}	D. J. Horen	PR **113** (1959) 572
	M. K. Ramaswamy	NP **10** (1959) 205
Zn^{70}	[50])	
Ge^{72}	R. G. Arns, M. L. Wiedenbeck	PR **112** (1958) 229
Ge^{74}	[54]) [55])	
	Horen, Meyerhof, Kraushaar, Wells, Brun, Neighbor	PR **113** (1959) 875
Ge^{76}	[55])	
Se^{74}	Girgis, Ricci, v. Lieshout	NP **13** (1959) 461
	G. Bäckström and I. Marklund	Arkiv f. Fysik **17** (1960)
	Grabowski, Gustafsson, Marklund	Arkiv f. Fysik **17** (1960)
Se^{78}	[55])	
	Nemilov, Pisarevskii, Soshin	JETP **35** (8) (1959) 555
Se^{80}	[55])	
Se^{82}	[55])	

Sr^{90}	Johnson, O'Kelly, Eichler	BAPS **3** (1958) 207
Mo^{98}	P. H. Stelson, F. K. McGowan	PR **110** (1958) 489
Mo^{100}	P. H. Stelson, F. K. McGowan	PR **110** (1958) 489
Ru^{96}	P. H. Stelson, F. K. McGowan	PR **110** (1958) 495
Ru^{98}	[55])	
Ru^{100}	[55])	
	O'Kelly, Eichler, Johnson	BAPS **3** (1958) 62
Ru^{102}	[55])	
	K. Histake, J. D. Kurbatov	BAPS **3** (1958) 315
Pd^{104}	[54, 55])	
Pd^{106}	Robinson, McGowan, Smith	BAPS **4** (1959) 279
	D. J. Horen, H. E. Bosch	BAPS **4** (1959) 373
	W. L. Bendel	BAPS **4** (1959) 426
Pd^{108}	G. S. Goldhaber, Proc. of the University of Pittsburg Conference 1957, p. 447	
Cd^{110}	[55])	
	E. G. Funk, M. L. Wiedenbeck	PR **112** (1958) 1248
	H. W. Taylor, W. R. Frisken	**114** (1959) 127
	B. S. Dželepow, N. N. Zhukovsky	NP **6** (1958) 655
Cd^{112}	[54, 55])	
Cd^{114}	[55])	
Sn^{116}	[54])	
	Jensén, Nielsen and Skilbreid (to be published)	
Sn^{118}	C. L. McGinnis, D. N. Kundu	BAPS **3** (1958) 62
Sn^{120}	C. L. McGinnis	PR **109** (1958) 890
Te^{124}	[54])	
	B. S. Dželepow, N. H. Zhukovsky	NP **6** (1958) 655
	R. K. Girgis, R. v. Lieshout	Physica **25** (1959) 133
Te^{126}	H. E. Bosch	BAPS **4** (1959) 374
Xe^{130}	Smith, Stelson, McGowan	PRL **2** (1959) 486
Xe^{134}	G. Holm, H. Ryde	Arkiv f. Fysik **15** (1959) 387
Xe^{136}	Noak R. Johnson, G. D. O'Kelly	PR **114** (1959) 279
Ba^{134}	[54])	
	J. D. French, M. Goodrich	BAPS **4** (1959) 391
	R. K. Girgis, R. van Lieshout	NP **12** (1959) 682
Ba^{136}	[54])	
	R. K. Girgis, R. van Lieshout	NP **12** (1959) 204
Ce^{140}	Dželepow, Kholnov, Prikhodtseva	NP **9** (1959) 665
	S. Ofer, A. Schvarzschild	PRL **3** (1959) 451
Nd^{144}	Campion, Knowles, Bartholomew	BAPS **4** (1959) 247
	Funk, Mihelich, Schwerdtfeger	BAPS **4** (1959) 292
	S. Ofer	PR **113** (1959) 895
Nd^{146}	Funk, Mihelich, Schwerdtfeger	BAPS **4** (1959) 292
Sm^{146}	J. R. Grover	PRL **3** (1959) 454
Sm^{148}	Bhattacherjee, Sahai, Baba	NP **12** (1959) 356
Sm^{150}	V. K. Fischer, E. A. Remler	BAPS **3** (1958) 62
Sm^{152}	I. Marklund	NP **9** (1958/59) 83
	O. Nathan, S. Hultberg	NP **10** (1959) 118
	G. T. Wood	PRL **3** (1959) 589
	Marklund, Nathan, Nielsen	N.P. (to be published)
	P. Debrunner	(private communication)
Gd^{150}	Toth, Bjørnhom, Jørgensen, Nielsen, Skilbreid	PR **116** (1959) 118
Gd^{152}	Toth, Faler, Rasmussen	PR **115** (1959) 158
	[38]) see also Sm^{152}	
Gd^{154}	K. S. Toth, J. O. Rasmussen	PR **115** (1959) 150
	O. Nathan	(private communication)
	P. Debrunner	(private communication)

Gd^{156}	Boehm, Hatch	BAPS **1** (1956) 390
	J. T. Holloway, L. J. Laslett	PR **113** (1959) 1581
	S. Ofer	PR **115** (1959) 414
	Hansen, Nielsen, Sheline	NP **12** (1959) 389
	Knowles, Bartholomew, Champion	BAPS **4** (1959) 476
		NSA **11** No 6 B (1957) 37
	[44])	
Gd^{158}	Knowles, Bartholomew, Campion	BAPS **4** (1959) 246
	Knowles, Bartholomew, Campion	(privat communication)
Dy^{160}	S. Ofer	NP **5** (1958) 331
	Arns, Sund, Wiedenbeck	NP **11** (1959) 411
	Ewan, Graham, Geiger	BAPS **4** (1959) 292
	C. E. Johnson, D. A. Shirley	BAPS **4** (1959) 373
	K. S. Toth, J. O. Rasmussen	P.R. **115** (1959) 150
Dy^{162}	Chupp, DuMond, Gordon, Jopson, Mark	P.R. **112** (1958) 518
Er^{166}	[26, 28])	
Er^{168}	K. P. Jacob, J. W. Mihelich	BAPS **3** (1958) 358
	[28])	
Yb^{172}	Dillman, Henry, Gove, Becker	PR **113** (1959) 635
W^{182}	C. J. Gallagher, J. O. Rasmussen	PR **112** (1958) 1730
	[45])	
W^{184}	Gallagher, Strominger, Unik	PR **110** (1958) 725
	F. K. McGowan, P. H. Steelson	BAPS **3** (1958) 228
W^{186}	F. K. McGowan, P. H. Steelson	BAPS **3** (1958) 228
Os^{186}	K. O. Nielsen, O. B. Nielsen	NP **5** (1958) 326
	R. M. Diamond, J. M. Hollander	NP **8** (1958) 143
Os^{188}	[37])	
	F. K. McGowan, P. H. Steelson	BAPS **3** (1958) 228
	W. A. Bruil, B. Jung	(to be published)
Os^{190}	Nielsen, Poulsen, Sheline, Jenson	NP **10** (1953) 475
Os^{192}	F. K. McGowan, P. H. Steelson	BAPS **3** (1958) 228
Pt^{192}	G. Scharff-Goldhaber, M. McKeown	PRL **3** (1959) 47
Pt^{194}	[35, 36, 40])	
Pt^{196}	F. K. McGowan, P. H. Steelson	BAPS **3** (1958) 228
Hg^{192}	G. Andersson	(private communication)
Hg^{194}	B. Jung and G. Andersson	NP **15** (1960) 108
Hg^{200}	[54])	
	Z. Grabowski, B. van Nooijen	Arkiv f. Fysik (1960)
Hg^{202}	Born, Molenaar, Blok	Physica **25** (1959) 326
Pb^{204}	Novakov, Stockendal, Schwerak, Johansson	Arkiv f. Fysik **14** (1959) 82
Rn^{218}	J. O. Rasmussen	PR **113** (1959) 1593
Ra^{226}	J. O. Rasmussen	PR **113** (1959) 1593
Th^{226}	J. O. Rasmussen	PR **113** (1959) 1593
Th^{228}	Arbman, Bjørnholm, Nielsen	(to be published)
Th^{230}	Arbman, Bjørnholm, Nielsen	(to be published)
U^{234}	C. J. Gallagher, T. D. Thomas	NP **14** (1959) 1
	S. Bjørnholm, O. B. Nielsen	(private communication)
	[43])	
Pu^{238}	R. G. Albridge, J. M. Hollander	UCRL-**8034** (1957) (unpublished
	A. S. Davydov, A. A. Chaban	JETP **6** (1958) 428
Pu^{240}	J. O. Rasmussen	PR **113** (1959) 1956
	Bunker, Dropesky, Knight, Starner, Warren	PR **116** (1959) 143
Cm^{244}	[49])	
Cf^{250}	Vandenbosch, Diamond, Sjoblom, Fields	PR **115** (1959) 115

1.E.1:
3.B

Nuclear Physics **15** (1960) 566—608; © *North-Holland Publishing Co., Amsterdam*
Not to be reproduced by photoprint or microfilm without written permission from the publisher

THE DECAY OF Au^{194}

G. BÄCKSTRÖM, O. BERGMAN, J. BURDE† and J. LINDSKOG
Institute of Physics, Uppsala

Received 5 December 1959

Abstract: The decay of Au^{194} was investigated by the use of high resolution spectrometers for the measurements of the conversion spectrum and a double lens spectrometer for coincidence measurements. By careful analysis of the conversion spectrum, which was recorded at a resolution of ≈0.2%, it was possible to identify more than 100 transitions in Pt^{194}. The use of strong sources and a double counter operated in coincidence made possible the detection of lines of intensity only 10^{-5} times that of the strongest line. Multipolarities could be found from K/L ratios for a few low energy transitions and some information could also be extracted from a comparison with results of previous gamma ray work. Energies of the strongest lines were measured absolutely by means of an iron free double focusing instrument, and further energy determinations were made relatively to these lines. The standard error of the measurements was frequently as low as 2 parts in 10^4. A complete set of energy sums was computed in order to survey the possibilities of cascade-crossover combinations. The reliability of the numerical relationships was investigated statistically, and it was shown that a reasonably unique level scheme could be constructed on the basis of energies, although the positions of transitions remained to some extent ambiguous. The results of 79 coincidence experiments are reported, and when analyzed these data lead to a level scheme in agreement with the conclusions of the other approach. Furthermore, these experiments helped in deciding the location of transitions. Evidence for at least two 0^+ states was found. The discovery of a level at 923 keV, probably of 4^+ character, revealed a close analogy with the level scheme of Pt^{192}. The interpretation of this level as a three-phonon state is in agreement with theory.

1. Introduction

$_{79}Au^{194}$ (40 hours) decays by electron capture and positon emission to $_{78}Pt^{194}$. Thieme and Bleuler [1]) investigated this decay with various techniques. The conversion lines of energies higher than 1 MeV were measured by means of a magnetic lens spectrometer of 2.7 % resolution. Gamma ray intensities were measured by analysis of the scintillation spectrum, and gamma spectra in coincidence with the K conversion lines of the prominent 291 keV and 328 keV transitions were also obtained. The total positon spectrum, as well as the positon spectrum coincident with the 328 keV line, was recorded. Gamma-gamma coincidence experiments were also performed. These authors proposed a decay scheme which accommodated the 17 observed transitions and made use of auxiliary data [2]) from the decay of Ir^{194}.

The conversion line spectrum of Au^{194} has been studied further by Al-

† Present address: The Hebrew University, Jerusalem, Israel.

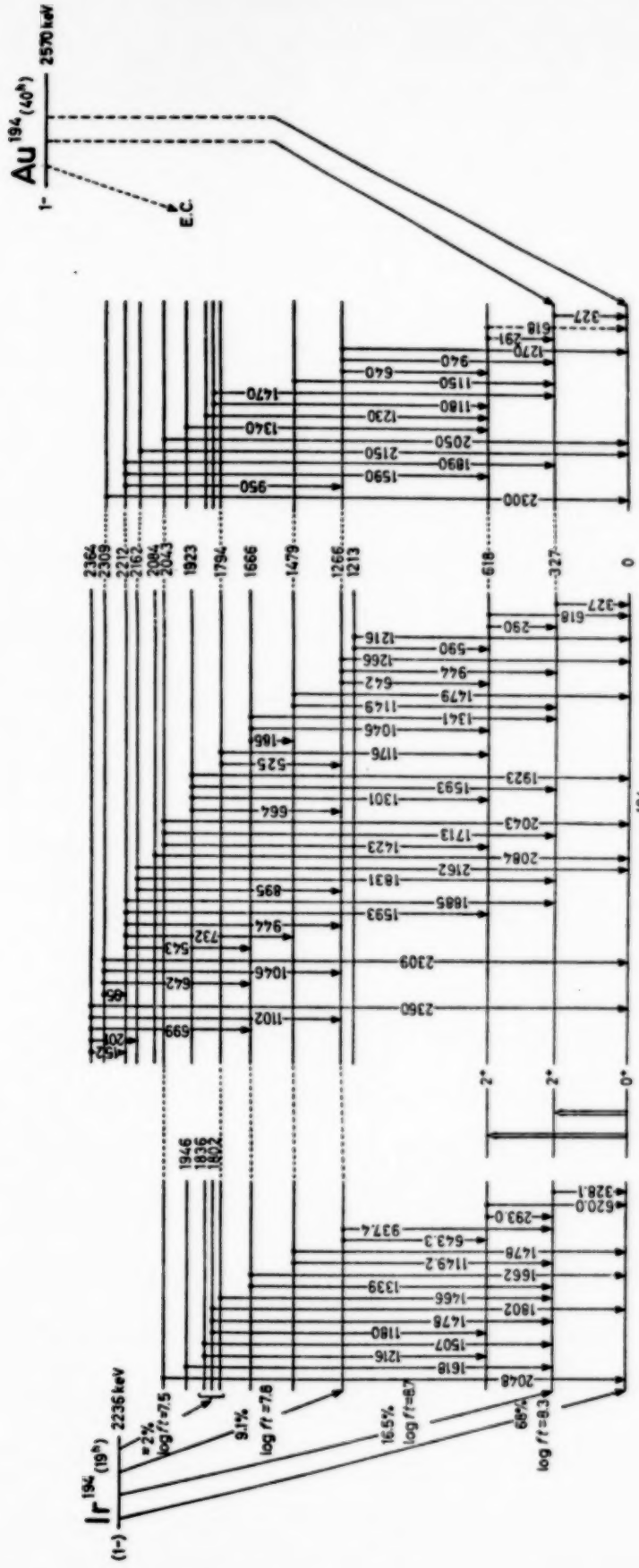

Fig. 1. Level schemes of $_{78}Pt^{194}$ according to previous investigations.

TABLE 1

Comparison of transition data for Pt^{194}. Notations: E_γ = transition energy, I_γ = photon intensity, I_K = K conversion line intensity. The intensities are on a relative scale, except for the Ir data of Johns and Nablo. The limits of error for E_γ are about $\pm 0.1\%$ in the work of Johns and Nablo, and $\pm 0.5\%$ in the work of Alburger. A full list of transitions found in the present investigation is given in table 3.

Johns, Nablo[2])		Alburger[3])		Thieme, Bleuler[1])		Present work	
E_γ	I_γ	E_γ	I_K	E_γ	I_γ	E_γ	I_K
keV	%	keV		keV		keV	
		95	–			–	–
		154	10			–	–
		185	7			–	–
		201	14			202.91	0.6
293.0	5.1	290	27	291.3	26	293.55	24
328.1	27	327	100	326.7	100	328.50	100
		525	2.6			528.95	1.8
		543	0.38			544.66	0.05
		590	1.5			593.72	0.57
620.0	1.7	618	1.2	640	20	622.05	0.77
643.3	6.2	642	1.3			645.32	0.90
		664	0.24			668.56	0.12
		699	0.61			–	–
		732	0.22			736.45	0.12
		895	0.23			–	–
937.4	2.9	–				938.87	0.22
		944	1.8	940	9	948.40	1.1
		1046	0.50			1048.72	0.35
		1102	0.29			1104.12	0.17
1149.2	2.9	1149	0.43	1120	6	1150.91	0.20
1180	1.7	1176	0.30	1160	6	1183.63	0.12
1216	0.4	1216	0.32	1230	<2	1219.01	0.16
	<0.2	1266	0.12	1270	2	1267.37	0.08
		1301	0.1			1302.55	0.05
1339	0.3	1341	0.54	1340	2	1342.44	0.32
		1423	0.09			1421.77	0.066
1466	0.8					1469.36	0.26
1478	0.2	1479	3.7	1470	8	1479.75	2.2
1507	0.3	–		1500	1	–	–
		1593	0.79	1590	6	1592.9	0.20
1618	0.3	–				1617.8	0.007
1662	0.2	–				–	–
		1713	0.11			1715.69	0.064
1802	0.3	–				1803.1	0.013
		1831	0.07			1830.12	0.028
		1885	0.52	1890	7	1886.80	0.28
		1923	0.30			1924.60	0.18
2048	0.05	2043	0.50	2050	5	2044.1	0.28
		2084	0.23			2085.8	0.13
		2162	0.73	2150	1	2164.1	0.38
		2309	0.012	2300	0.6	2312.7	0.008
		2360	0.014			2357.0	0.008

burger [3]) with an intermediate image spectrometer. A resolution of 0.74 % was obtained in the higher energy spectrum, but at low energies the source thickness caused appreciable broadening of the lines. In all, 36 transitions were identified and were fitted from energy considerations into a decay scheme. This scheme is shown in fig. 1 together with that of Thieme and Bleuler. The energy and intensity data are summarized in table 1.

The levels of Pt^{194} can also be studied through the negaton decay of Ir^{194} (19 hours). Johns and Nablo [2]) investigated the photoelectron spectrum by means of a double focusing spectrometer. Sixteen transitions and their gamma intensities were reported (table 1). Because of the presence of a longer lived isotope (192), the possibility that some transitions may have been masked cannot be excluded. The beta spectrum was accurately measured and analyzed. The decay scheme proposed by these workers is included in fig. 1.

Mandeville *et al.* [4]) produced Ir^{194} from a target enriched in Ir^{193} and investigated the coincidence relationship between the gamma rays observed in NaI(Tl) scintillators. They were able to present definite coincidence information about the transitions of 295, 325, 640, 930 and 1140 keV.

Finally, data on the Coulomb excitation of Pt^{194} have been obtained by Heydenburg and Temmer [5]) (α-particles) and McGowan and Stelson [6]) (protons).

A few well established facts concerning the energy levels of Pt^{194} will be summarized here. Coulomb excitation [5, 6]) data definitely indicate a 2^+ level at 328 keV. The existence of this level is strongly supported by the energies [2]) of the complex Ir^{194} beta spectrum, as well as by the shapes of the total and coincident positon spectra [1]) from the decay of Au^{194}. The strength of the 328 keV line also suggests such a level.

A second level, at 620 keV, has also been directly excited and has been shown [6]) to be deexcited by coincident photons of 328 keV and 293 keV. Also in Ir^{194} decay these two gamma rays were found to be in coincidence and gamma-gamma angular correlation [4]) data indicate a 2^+ assignment for this state in agreement with the Coulomb excitation results.

The negaton spectrum [2]) of Ir^{194} definitely exhibits branching to a level at 1265 keV. Gamma-gamma coincidence measurements [4]) further show that the 643 keV gamma ray precedes that of 293 keV, whereas the 937 keV gamma is coincident with the 328 keV line but not with the 293 keV line. The beta and gamma ray intensities [2]) also support the fact that the 1265 keV level is deexcited by the transitions of 643 keV. and 937 keV. It should be mentioned that all these coincidence relationships have been verified in the present work by electron coincidence experiments

The spin of Au^{194} has been determined [7]) to be 1 by atomic beam methods. Odd parity is strongly indicated both by the log *ft* value [1]) of the positon branch to the Pt^{194} ground state, and from shell model considerations.

The spin of Ir^{194} has not been directly measured, but again the log *ft* value

of the ground state beta branch together with the allowed shape of this branch suggests the character 1^-.

2. Source production

Au^{194} is difficult to produce free of other activities. The most favourable mode of production for conversion line measurements is the Ir(He^3, 2n) reaction, which yields a source practically free of negaton radiation (fig. 2). However, since no He^3 beam was available, deutron or proton bombardments were used for all these experiments. Au^{199}, whose beta spectrum was a severe obstacle in the low energy measurements of Au^{194} is produced by deutron irradiation of platinum but practically not at all by proton irradiation. It was noticed, however, that the Au^{194} yield of the deutron reaction was higher.

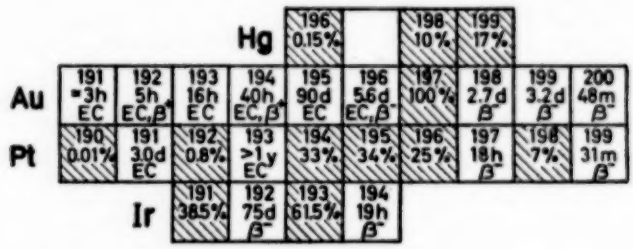

Fig. 2. Partial isotope chart, illustrating the possibilities of producing Au^{194}

Therefore this alternative was used to provide the strongest sources for the energy region higher than 500 keV. Bombardments of platinum foils were carried out in the cyclotrons of Oak Ridge, Birmingham and Stockholm and in the synchrocyclotrons of Uppsala and Amsterdam. The strongest source was produced by a 3-hour deutron irradiation with a beam current of $\simeq 200\,\mu$A. The beam energy was usually 20 MeV except in a few irradiations in which a higher energy was chosen in order to investigate the contribution of shorter lived isotopes to the conversion spectrum.

The platinum target was dissolved in hot aqua regia, a procedure which generally required several hours. The chemical separation was then carried out by the procedure described by Wilkinson and Hicks [8]).

The source was prepared by electroplation, either with or without external voltage. In the former case the source backing was a thin, vacuum deposited layer of platinum on a 1 mg/cm² mylar film or simply a platinum foil coated with "Araldite" on the rear side. From this film a suitably large source strip, usually 0.2 cm wide, was cut. The strip was stretched over the edge of a glass-spade and partially immersed into the active solution. A platinum foil served as the second electrode. Several trial experiments were made in order to find the optimum conditions for electroplation. The highest yield was obtained with

the activity in a 0.1 *N* solution of HCl and the electrode voltage set at 4 V. The resulting current, 30 mA, deposited 75 % of the activity in 2—3 hours. The strongest source prepared in this way gave a dose-rate of 1 r/h at a distance of 35 cm. This type of electroplation, however, sometimes results in a black deposit which noticeably distorts the line shapes at energies lower than about 500 keV. The deposit is most probably platinum but it is not known whether it originates from the target or from the platinum electrode.

For spectra below $\simeq$ 500 keV, the method of chemical deposition was used to provide the very thin sources necessary. In this case the most favourable backing was found to be a silver layer on mylar. However, the rate of deposition was relatively slow unless the glass-rod supporting the strip was rotated. Heating the active solution in water bath also accelerated the collection of activity. The silver film, however, slowly dissolved in the HCl solution, and it was generally not possible to use deposition times longer than thirty minutes. The yield varied from a few percent to 70 %. Low yield was always accompanied by a yellowish deposit, and it was concluded that the platinum target had contained a small amount of gold. With the most successful depositions no evidence of source thickness was found from the line shape at a resolution of 0.17 % even as low as 35 keV electron energy.

3. The conversion spectrum

3.1. INSTRUMENTS

A double-focusing spectrometer ($\rho_0 = 50$ cm, $\beta = \frac{3}{8}$), similar to that described by Hedgran *et al.* [9]) was used for almost all experiments on the internal conversion lines. The magnetic field was continuously measured by a system of rotating coils [10]). The momenta of adjacent lines could be compared with an accuracy better than $1:10^4$, and for lines differing by a factor of two in their momenta, the resulting accuracy was $\simeq 2:10^4$. The reason for the increasing relative error is that the field measurement is taken in a small probe volume in the unused sector of the magnet. Thus deviation from rotational symmetry of the iron yoke might produce some nonlinearity. In order to minimize this effect, the iron was demagnetized carefully before each run, and the current was steadily increased during the measurements.

With a 0.2×2 cm^2 source and a 0.2 cm detector slit a resolution of 0.2 % was obtained, which corresponded to an acceptance angle of 0.15 %. This geometry was used in most experiments.

The detector was a specially constructed twin Geiger tube. The tubes were separated by a 2 mg/cm^2 mylar film covered with a vacuum evaporated layer of aluminium in order to ensure conductivity and opaqueness. The front window, which was similarly prepared, had a thickness of 1.0 mg/cm^2. It was

found that the general background could be reduced by a factor of five by operating the two tubes in coincidence. The resulting loss in counting rate was negligible at energies higher than about 500 keV. In the region below 1 MeV, where most of the background was due to the beta spectrum only the front tube was used. For the MeV region, however, the coincidence arrangement considerably contributed to the success of the investigation. In addition, the size of the instrument permitted the placement of 30 cm of lead shielding between source and detector. Consequently the stray gamma background could be kept as low as 5 counts/min even with the strongest source. The intensity ratio between the strongest and the weakest lines detected was actually $\simeq 10^5$.

An iron-free double focusing spectrometer [11]) ($\rho_0 = 30$ cm, $\beta = \frac{3}{8}$) was used for a precision determination of the crucial gamma ray energies. With this instrument relative momentum measurements could be made with an accuracy of a few parts in 10^5.

The low energy region (10—100 keV) was scanned with an automatic double focusing spectrometer [12])† ($\rho_0 = 18$ cm, $\beta = \frac{1}{4}$) provided with a very thin Geiger tube window.

3.2. ENERGY AND INTENSITY MEASUREMENTS

In order to construct a decay scheme, it is sufficient to have relative values for the transition energies. However, since magnetic spectrometer measurements normally yield relative values of electron momenta, these momenta must be normalized to absolute values if crossover relations in the decay scheme are to hold accurately. To provide a reference line for the energy measurements on Au^{194}, the strongest conversion line (328 keV) was carefully measured on an absolute scale. Our results are compared with those of other workers in table 2. In the investigations of Ryde and Andersson [13]) and Beckman and Bergvall [14]) the source had consisted of reactor-activated iridium; however, in the present work the source was always Au^{194}. A comparison measurement with the F line of Th B [11]) was carried out with a composite source, with the ThB deposited on top of the Au^{194} activity. The measurements relative to Au^{198} and Au^{192} could conveniently be done, since both isotopes are present in a cyclotron-produced source. The energy of the 412 keV transition in the decay of Au^{198} has been accurately measured by two groups [15,16]), and the strong 316 keV transition in the decay of Ir^{192} has been measured with a curved crystal spectrometer [16]). In the measurements with the iron-free double focusing spectrometer, a source consisting of a perfect mixture of Au^{194} and Au^{199} was used. The lines of the latter isotope have previously been measured [17]) absolutely with the same instrument, and thus a measure-

† We are indebted to Dr. E. Arbman for the use of this instrument.

ment of the 328 keV K-line relative to the 146 keV L_{III} line of Au^{199} was sufficient to provide an absolute value †.

A K-binding energy for platinum of 78.391 keV has been used to compute the gamma ray energies from measured electron energies. As seen in table 2,

TABLE 2

Precision measurements of the energy of the 328 keV gamma ray in Pt^{194}

E_γ (keV)	Reference lines	Type of instrument	Authors
328.1 ±0.2	Ir ^{192}	Double focusing spectrometer	Johns and Nablo [3])
329.07±0.08	Au ^{198} (412 keV)	Curved crystal	Ryde and Andersson [13])
328.38±0.13	ThB (F)	Double focusing spectrometer	Present work
328.47±0.11	Au ^{198} (412 keV)	Double focusing spectrometer	
328.48±0.12	Au ^{192} (316 keV)	Double focusing spectrometer	
328.52±0.05	Au ^{199} (158 L_{III})	Iron free double focusing spectrometer	
328.49±0.05	X-ray lines	Curved crystal	Beckman and Bergvall [14])

Adopted mean value $\bar{E}_\gamma = 328.50$ keV.

the various energy measurements agree satisfactorily with the exception of that of Ryde and Andersson. A deviation of the same magnitude in another measurement (As^{76}) by these authors has been noticed [19]). Thus, the possibility of a systematic error in their measurements is suggested.

The measurements on the over-all conversion spectrum were performed in a number of experiments with the 50 cm radius spectrometer. This instrument was normally set at a resolution of 0.2 %. In fact almost all conversion lines

† In the investigation [17]) on Au^{199} the conversion line energies were determined on the basis of energies of the X-ray lines (K_α) of mercury. Since no very accurate measurement of these lines was available at the time, these energies were computed by interpolation of the data for neighbouring elements [18]). The recent X-ray energy measurements of Beckman and Bergvall show, however, that the data on which the interpolation was based [18]) were somewhat low. Most of the discrepancy comes from the choice of transformation constant (X units to keV), which in reference [18]) was taken to be lower than the best value now known. The energies found by Beckman and Bergvall [14]) for the Hg X-ray lines are $K_{\alpha_1} = 70.8196 \pm 0.002$ keV and $K_{\alpha_2} = 68.8952 \pm 0.002$ keV. If the data of ref. [17]) are recalculated with the new X-ray energies, we obtain $E_{\gamma_1} = 49.830$ keV, $E_{\gamma_2} = 158.396$ keV and $E_{\gamma_3} = 208.226$ keV for the gamma rays of $Au^{199} \rightarrow Hg^{199}$.

have been recorded with a resolution of 0.2 % or better. At this high resolution it was not practical to cover more than a limited energy region in each experiment. With the strongest source used, for instance, it was not found worthwhile to extend the measurement over more than the region 500 keV—1800 keV. Part of the conversion spectrum is shown in fig. 3.

In the calculation of energies the line positions were defined as the line centre at half maximum. By use of the known momentum of the 328 keV line, the energies of other transitions were computed. The following cross-over relationships appeared to hold (fig. 2) within the limits of error expected for survey runs (a few parts in 10^4)

$$E_\gamma(294) + E_\gamma(328) = E_\gamma(622)$$
$$E_\gamma(645) + E_\gamma(622) = E_\gamma(1267)$$
$$E_\gamma(294) + E_\gamma(645) = E_\gamma(939)$$
$$E_\gamma(1303) + E_\gamma(622) = E_\gamma(1925).$$

This is also in agreement with existing coincidence information.

Since it was desirable to have at least one reference line within the energy span of each measurement, use was made of the above cross-over relationships to achieve approximate energy doublings. The basis of this calibration procedure was the energy value $E_\gamma = 328.50 \pm 0.05$ keV, taken from table 2, and the value $E_\gamma = 293.55 \pm 0.05$ keV, a result from the determinations with the ironfree instrument. The energy of the cross-over transition thus becomes $E_\gamma = 622.05$ keV. With this line as a reference, we could accurately measure the energy of the 645 keV line. The procedure was successively applied to higher transitions. As a result the following transition energies were obtained; 938.87 keV, 1267.37 keV, 1302.55 keV, and 1924.60 keV. The measurements leading to these energy values involve many steps, and the accumulated statistical error could be expected to be large. However, each step of the measurements was repeated many times, and excellent agreement was found between the results of the various measurements.

Areas were measured of a number of strong conversion lines throughout the spectrum, and the intensities were computed from the areas. For weaker lines the intensity was simply assumed to be proportional to the height compared with that of a neighbouring line of measured area. The standard error of these intensities is believed to be $\simeq 10$ % for well-defined lines.

3.3. INTERPRETATION OF THE CONVERSION SPECTRA

Since the platinum used for the targets was very pure (although not of a spectroscopic grade) and the chemical procedure known to be strongly selective, the only activities present in the source were almost certainly gold isotopes and their decay products. For experiments devoted to a search for electron

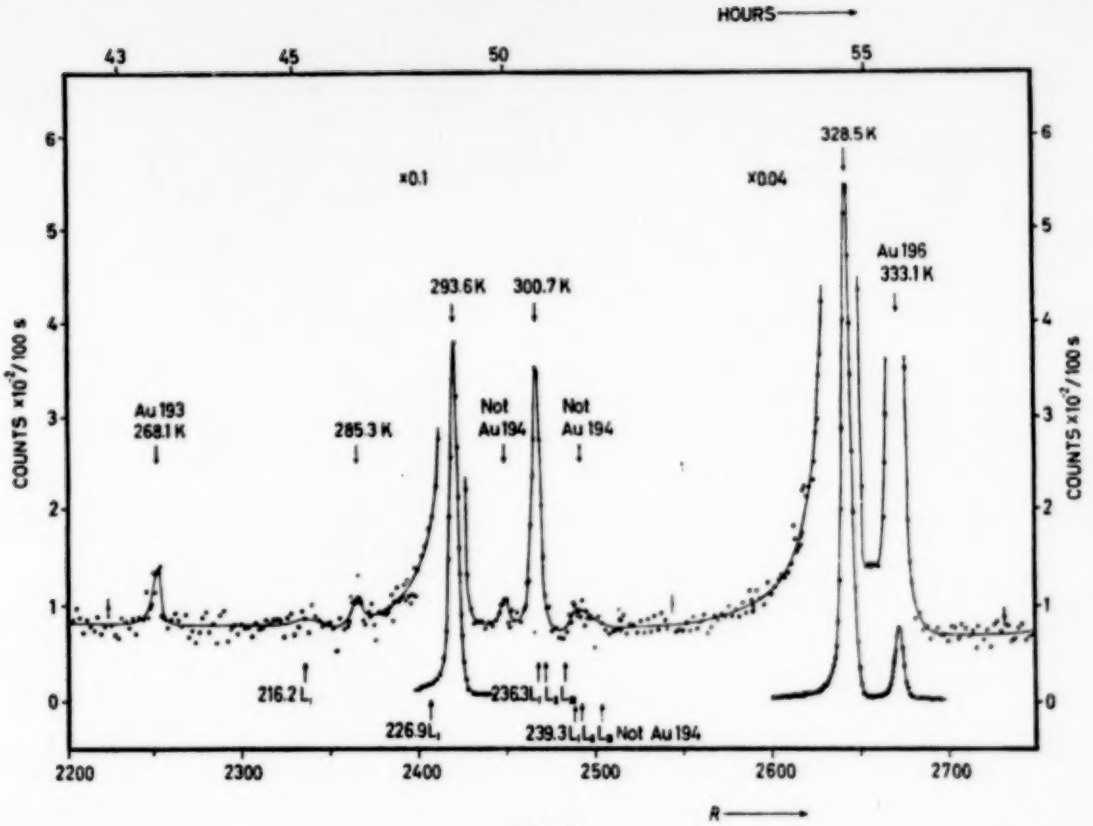

Fig. 3a

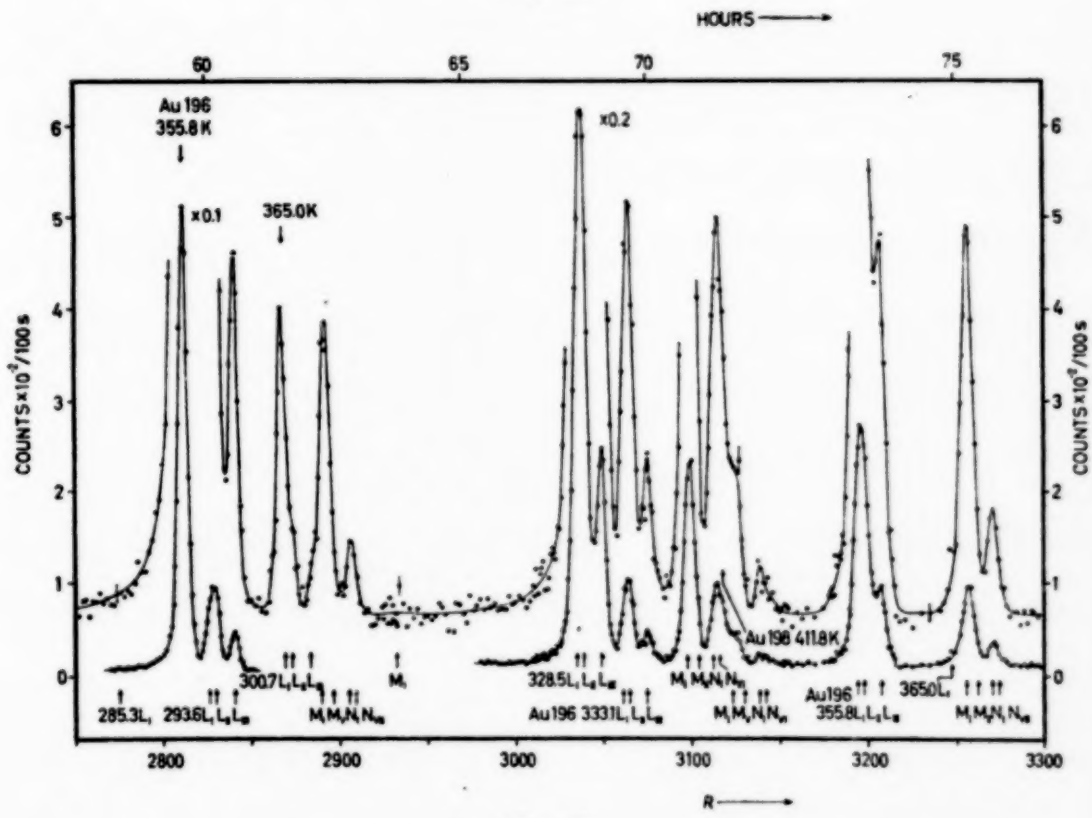

Fig. 3b

Fig. 3a—3i. Examples of high resolution spectra recorded with the double focusing spectrometer. These figures comprise almost all the lines of interest.

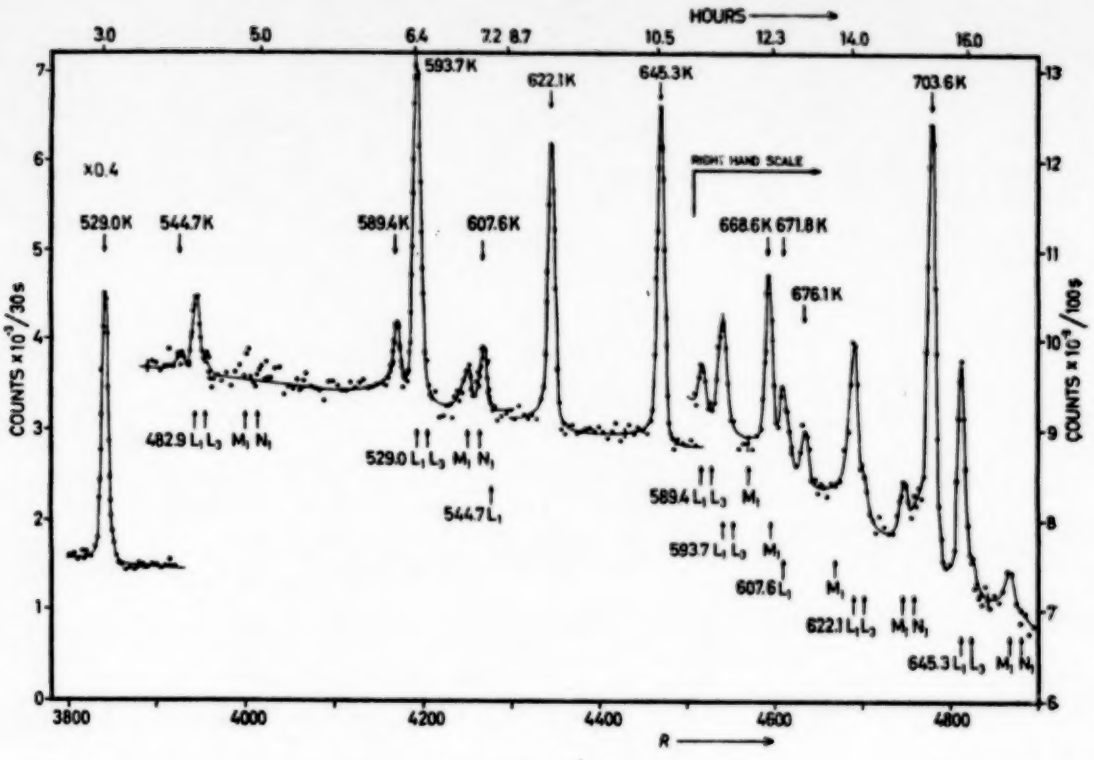
HOURS
3.0
5.0
6.4
7.2
8.7
10.5
12.3
14.0
16.0
593.7K
622.1K
645.3K
703.6K
RIGHT HAND SCALE
×0.4
529.0K
544.7K
589.4K
607.6K
668.6K
671.8K
676.1K
482.9 L1 L3 M1 N1
529.0 L1 L3 M1 N1
544.7 L1
589.4 L1 L3 M1
593.7 L1 L3 M1
607.6 L1
M1
622.1 L1 L3
M1 N1
645.3 L1 L3 M1 N1
COUNTS ×10³/30s
COUNTS ×10³/100s
3800
4000
4200
4400
4600
4800
R

Fig. 3c

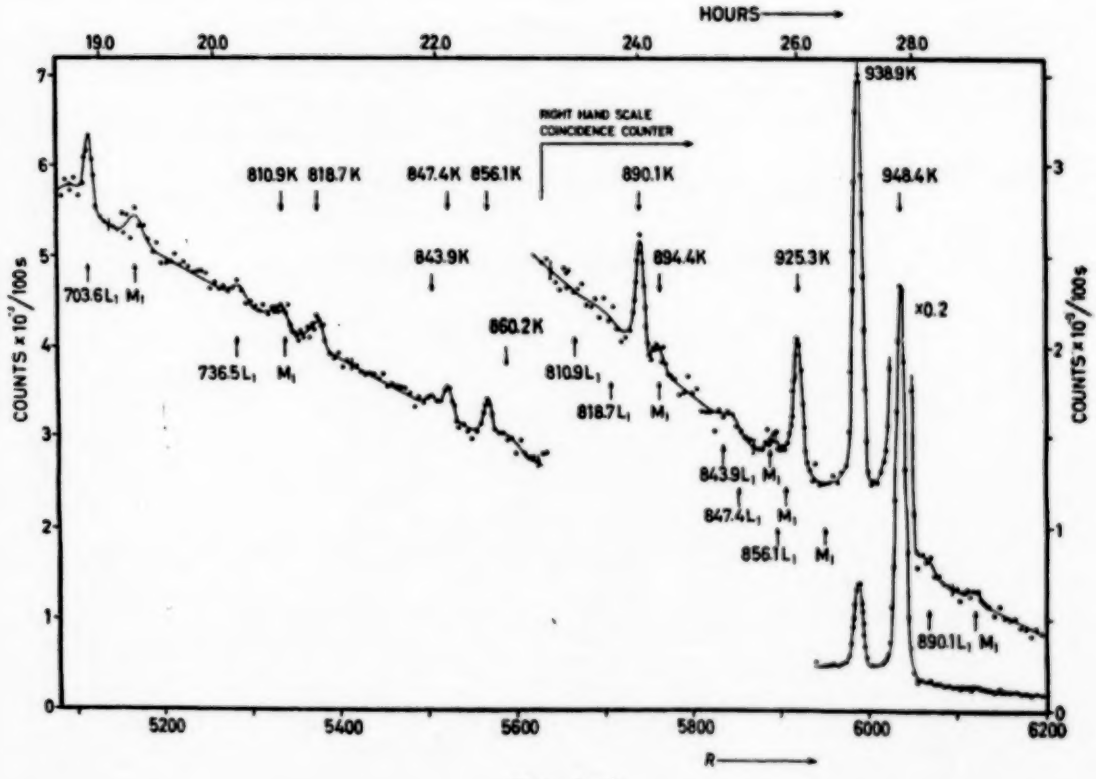
HOURS
19.0
20.0
22.0
24.0
26.0
28.0
938.9K
RIGHT HAND SCALE
COINCIDENCE COUNTER
810.9K
818.7K
847.4K
856.1K
890.1K
948.4K
843.9K
894.4K
925.3K
×0.2
860.2K
703.6 L1 M1
736.5 L1 M1
810.9 L1
818.7 L1 M1
843.9 L1 M1
847.4 L1 M1
856.1 L1 M1
890.1 L1 M1
COUNTS ×10⁻²/100s
COUNTS ×10³/100s
5200
5400
5600
5800
6000
6200
R

Fig. 3d

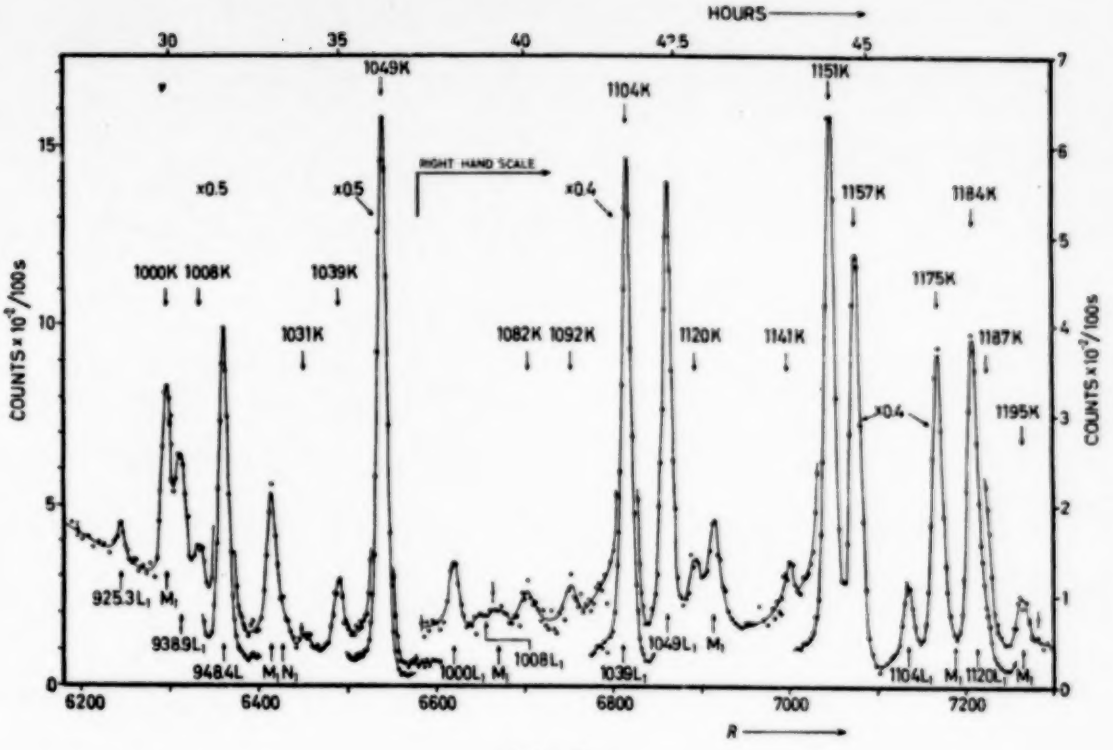
HOURS
30
35
40
42.5
45
1049K
1104K
1151K
RIGHT HAND SCALE
x0.5
x0.5
x0.4
1157K
1184K
1000K
1008K
1039K
1175K
1031K
1082K
1092K
1120K
1141K
1187K
x0.4
1195K
925.3L1 M1
938.9L1
948.4L
M1 N1
1000L1 M1
1008L1
1039L1
1049L1 M1
1104L1 M1
1120L1 M1
COUNTS x 10²/100s
6200
6400
6600
6800
7000
7200
R

Fig. 3e

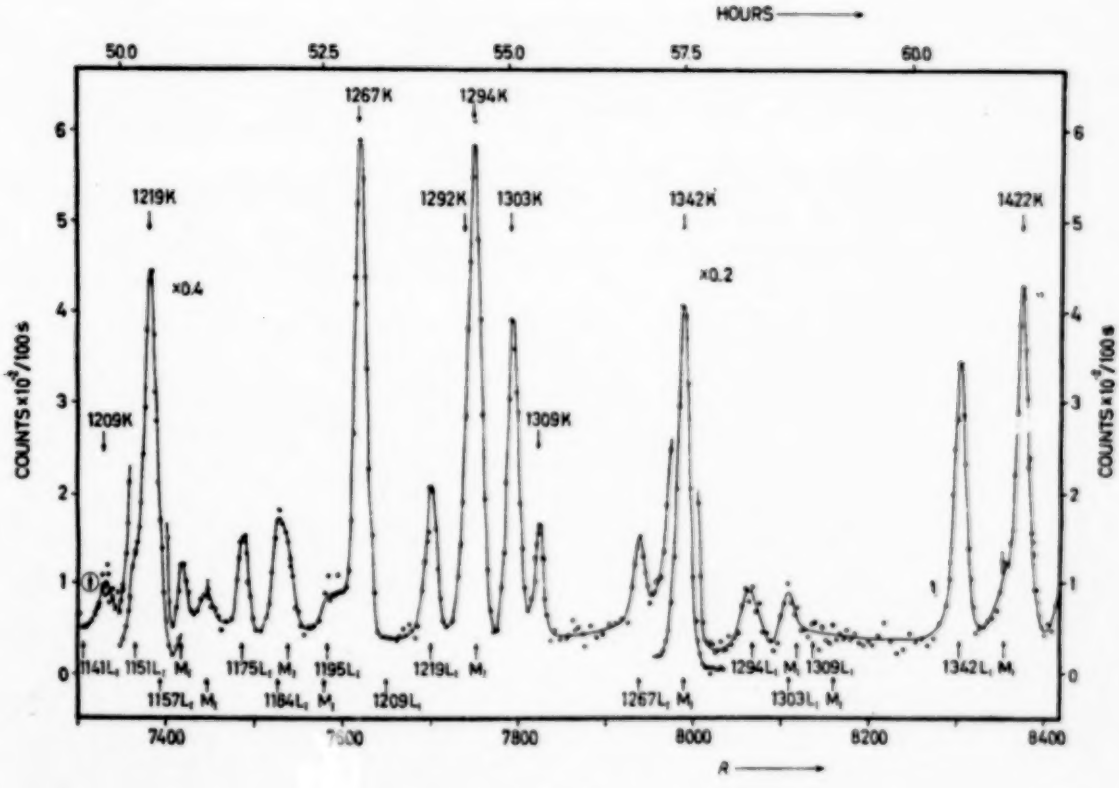
HOURS
50.0
52.5
55.0
57.5
60.0
1267K
1294K
1219K
1292K
1303K
1342K
1422K
x0.4
x0.2
1209K
1309K
1141L1
1151L1 M1
1157L1 M1
1175L1 M1
1184L1 M1
1195L1
1209L1
1219L1 M1
1267L1 M1
1294L1 M1
1303L1 M1
1309L1
1342L1 M1
COUNTS x 10³/100s
7400
7600
7800
8000
8200
8400
R

Fig. 3f

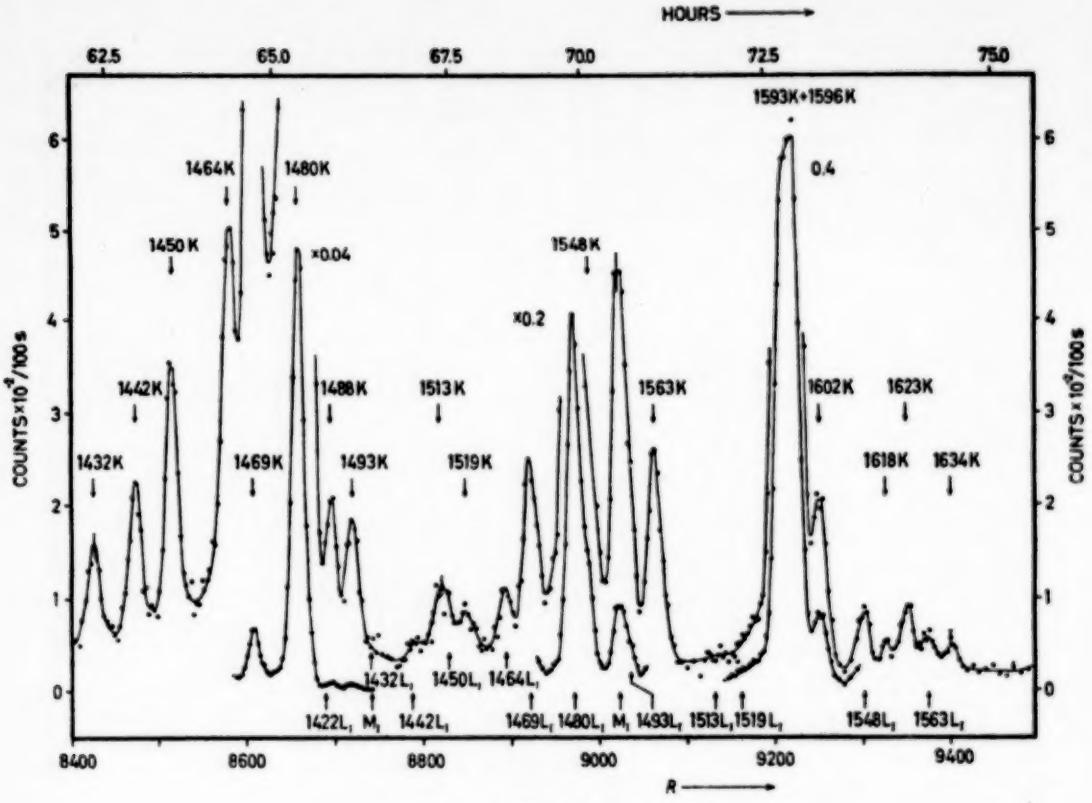
HOURS
62.5
65.0
67.5
70.0
72.5
75.0
1593K+1596K
1464K
1480K
0.4
1450K
×0.04
1548K
×0.2
1442K
1488K
1513K
1563K
1602K
1623K
1432K
1469K
1493K
1519K
1618K
1634K
1432L1
1450L1
1464L1
1422L1 M1
1442L1
1469L1
1480L1 M1
1493L1
1513L1
1519L1
1548L1
1563L1
COUNTS×10⁴/100s
COUNTS×10³/100s
8400
8600
8800
9000
9200
9400
R

Fig. 3g

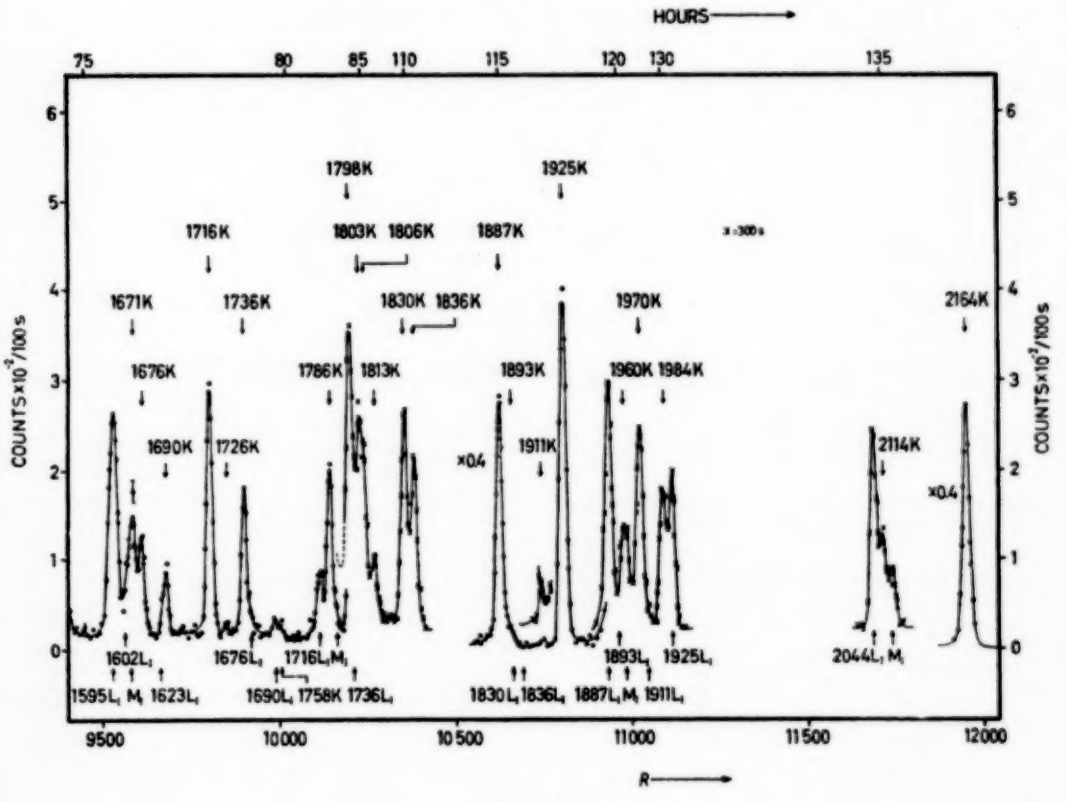
HOURS
75
80
85
110
115
120
130
135
1798K
1925K
1716K
1803K
1806K
1887K
1671K
1736K
1830K
1836K
1970K
2164K
1676K
1786K
1813K
1893K
1960K
1984K
1690K
1726K
×0.4
1911K
2114K
×0.4
1602L1
1676L1
1716L1 M1
1893L1
1925L1
2044L1 M1
1595L1 M1
1623L1
1690L1
1758K
1736L1
1830L1
1836L1
1887L1 M1
1911L1
COUNTS×10²/100s
COUNTS×10³/100s
9500
10000
10500
11000
11500
12000
R

Fig. 3h

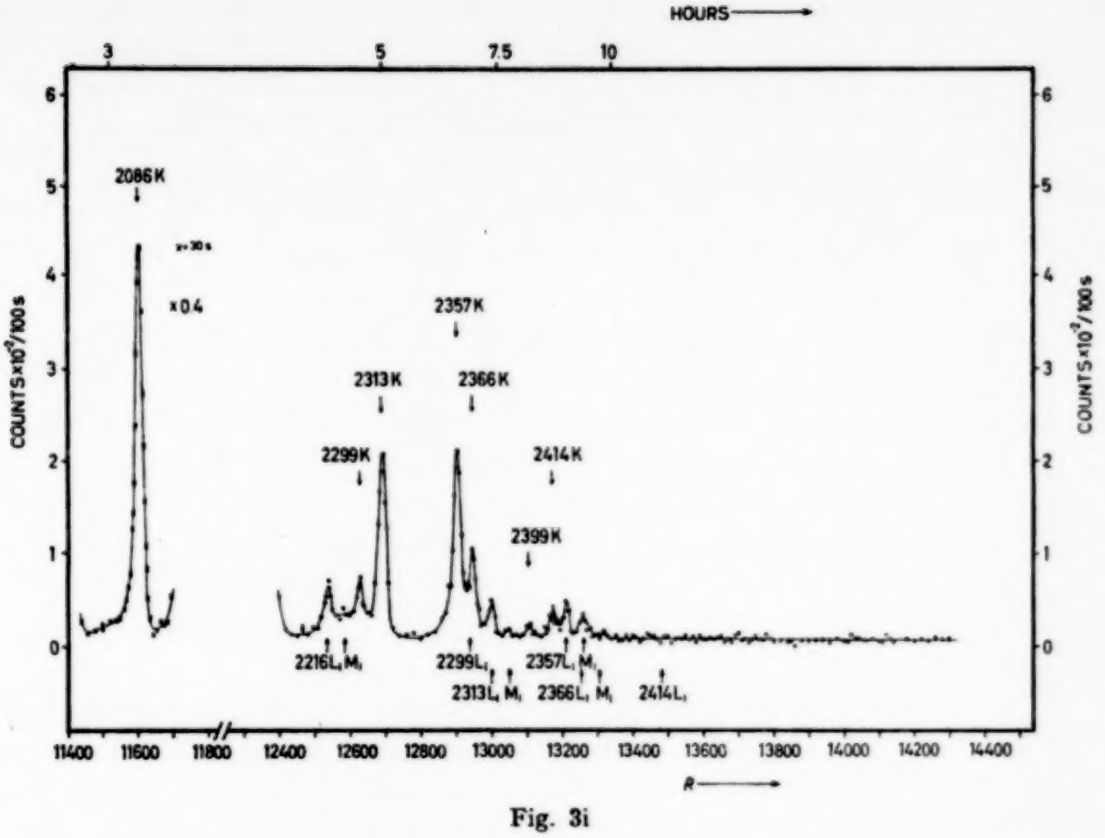

Fig. 3i

lines, the bombardments were made at a particle energy of $\simeq$ 20 MeV, and 2—3 days elapsed between irradiation and chemical separation. None of the known lines [20, 21]) from $Au^{192} \rightarrow Pt^{192}$ was observed, and no line was found that could be attributed to the decay of Au^{191} or its daughter Pt^{191} (3.0d). However, lines from the decay of Au^{193} were observed, which means that Pt^{193} was also present. This decay, however, is known [22]) to produce no gamma rays. No other daughter activities can be expected to enter into the conversion spectra.

In all, there are six gold isotopes, with mass numbers ranging from 193 to 199, definitely contributing to the electron spectra. The decay of Au^{199} exhibits only three gamma rays [17, 23]), and the Q-value is 460 keV. The radiations from Au^{198} have been studied carefully by many workers [3, 16]). This gamma ray spectrum consists of three transitions; 412 keV, 676 keV, and 1088 keV, the last two being very weak. The Q-value is 1370 keV. The decay of Au^{196} to Hg^{196} ($Q = 700$ keV) excites one level at 426 keV [24]). The competing decay by electron capture [25]) to Pt^{196} yields two transitions (333 keV and 356 keV) with a possible cross-over transition [3]). Au^{195} decays by electron capture ($Q = 270$ keV) with three low energy gamma rays [26]) (31 keV, 99 keV, and 130 keV). The electron capture of Au^{193} is followed by the emission of a complicated gamma ray spectrum, extending to an energy of about 500 keV. This spectrum has recently been investigated in detail by Ewan [27]) with

sources free of Au^{194}. By the use of his published values of the conversion line energies and intensities, we could determine which lines in our spectra were due to this isotope. Conversely it was sometimes possible to conclude that a certain line did not come from Au^{193} because it had not been observed by Ewan. Finally, none of the transitions reported by Huq [28]) as belonging to the decays of Au^{191} and Au^{192} were observed with this type of source.

The main basis for the assignment of electron lines to the decay of Au^{194} was the observed half-lives, obtained by recording each part of the spectrum twice. Naturally it was not possible, within a reasonable length of time, to determine the half-lives of the very weakest lines. However, an indirect check of the isotopic assignments of lines was obtained from measurements made with different sources. These sources, which were not equally old nor always produced under the same conditions, should have yielded different relative intensities for lines not belonging to Au^{194}. Some lines, however, have been observed only once with an especially strong source. Those lines falling above 500 keV were uniquely assigned to Au^{194} on the argument that they could not have been produced by any other isotope present. This is further justified by the fact that no deviation from a 40 h half-life was ever observed in this energy region, although this was not the case below 500 keV. It was felt that greater caution was necessary for assignments in this region, and a few weak lines were actually left unassigned.

Lines that were not fully resolved by the spectrometer were separated graphically by the use of the known shape of a monoenergetic line. Because of electron straggling and some remanence effect of the magnet, this line shape showed a slight variation with energy. A large number of sufficiently isolated lines in the spectrum itself yielded, however, the necessary information about the line shapes in the various energy regions.

The first step in the analysis of spectra was to decide which lines were K-lines. This is very easy to do at energies higher than 500 keV since the $K/\sum L$ ratios are known [29]) to be larger than unity for any reasonably expected multipolarity. The transition energies were generally computed from the energies of the K-lines. Energies of the corresponding L sub-lines and of M and N lines were calculated and their positions indicated on the plot. The L sub-lines were then reconstructed at these calculated positions. In a few cases this procedure disclosed the existence of a superimposed K-line in such an L group. Such conclusions were ventured when the shape of the group was in definite disagreement with theoretical expectations for multipole orders lower than five. The empirical thumb-rule for higher shells, $L/(M+N) \simeq 3$, was also used as a guide in the search for hidden transitions. It was thus possible to arrive at a very good understanding of all observed conversion lines (totalling 300) except for a few below 300 keV. Supporting arguments for each individual transition are summarized in table 3.

TABLE 3

Conversion lines from the decay of Au^{194}. The errors given are estimated standard deviations on a relative scale. The K line intensities are referred to 328 K whose intensity has been arbitrarily set at 100. The figures in brackets indicate powers of 10. The symbol $T_{\frac{1}{2}}$ should be taken to mean that the half-life has been measured with sufficient accuracy to exclude an interpretation involving other Au isotopes. Where this information is missing other support for the assignment is given. It was thus not attempted to give a complete presentation of the data underlying the assignments. Graphical separation of lines was often carried out but no remark about this is made in the table for cases where there is a clear valley between the lines. Such a comment has further only been given for the weaker line (-s) of the group. A doubtful transition is indicated by "?".

E_γ (keV)	Conversion line intensity I(K)	Conversion lines observed. Remarks
107.24±0.06	$I(L_I)$ 2.4	(K)L_IMN. $T_{\frac{1}{2}}$. Indication of K observed in automatically recorded spectrum. L_{II} and L_{III} masked by 99 M from Au^{195}. M not fully resolved from other activity.
163.94±0.05	4.2	KL_I. $T_{\frac{1}{2}}$. K coincides with 99 L_{II} from Au^{195} and was resolved by following its decay. M masked by other activity.
202.91±0.06	6 (−1)	K? Observed with different sources. Cannot be identified as 208 K from Au^{199} for intensity reasons. L may have too low intensity to be observed.
216.15±0.05	7.3 (−1)	KL. $T_{\frac{1}{2}}$.
226.94±0.10	3 (−1)	K?. $T_{\frac{1}{2}}$. Observed with different sources. Shell assignment doubtful but most probable.
236.29±0.10	5 (−1)	K? Observed with different sources. Shell assignment doubtful but most probable.
285.34±0.05	2.4 (−1)	K? Observed with different sources. L falls too near 356 K from Au 196 to be observed. Shell assignment doubtful but most probable.
293.55±0.04	24	$KL_I L_{II} L_{III}$MN. $T_{\frac{1}{2}}$.
300.71±0.05	1.8	$KL_I L_{II} L_{III}$M. $T_{\frac{1}{2}}$.
328.50±0.03	100	$KL_I L_{II} L_{III}$MN. $T_{\frac{1}{2}}$.
364.97±0.06	2.5	KLM. Observed with different sources. M noticeable as a deformation of 356 M from Au^{196}.
482.88±0.10	9.5 (−1)	KLM. $T_{\frac{1}{2}}$.
528.95±0.10	1.8	K(L)MN. $T_{\frac{1}{2}}$. L almost coincides with 594 K.
544.66±0.20	5 (−2)	K. Could not be produced by any other Au isotope. L had too low intensity to be observed.
589.39±0.10	1.8 (−1)	KL. $T_{\frac{1}{2}}$. MN too weak to be seen.
593.72±0.11	5.7 (−1)	(K)L. $T_{\frac{1}{2}}$. K coincides with 529 L, but L/(M+N) for 529 would be too high without the assumption of 594 K. MN masked by 668 K and 608 L.
607.61±0.08	1.5 (−1)	KLM. K observed with different sources.
622.05±0.06	7.7 (−1)	KLM. $T_{\frac{1}{2}}$.
645.32±0.08	9.0 (−1)	KLM. $T_{\frac{1}{2}}$.
668.56±0.10	1.2 (−1)	KL. $T_{\frac{1}{2}}$. L well resolved from 607 L. K coincides with 594 M but the contribution of this line is small. M had too low intensity to be observed.

TABLE 3 (continued)

E_γ (keV)	Conversion line intensity I(K)	Conversion lines observed. Remarks
671.8 ±0.6	2 (−2)	K? K was inferred from the fact that 608 L was too high and not quite in the right position. No other Au isotope could have produced this line.
676.11±0.30	4.5 (−2)	KL. K observed with different sources.
703.61±0.10	4.0 (−1)	KLM. $T_{\frac{1}{2}}$.
736.45±0.15	1.2 (−1)	KL(M). $T_{\frac{1}{2}}$.
810.9 ±0.5	1.5 (−2)	K. Inferred from the fact that 736 M was slightly shifted and too high. No other isotope of Au could have produced this line.
818.70±0.30	2.4 (−2)	KL. $T_{\frac{1}{2}}$. M falls under 894 K.
843.89±0.30	1.5 (−2)	KL? No other Au isotope could have produced these lines.
847.42±0.20	3.0 (−2)	KL. $T_{\frac{1}{2}}$.
856.08±0.20	3.4 (−2)	KL(M). $T_{\frac{1}{2}}$. A somewhat too high intensity of L is explained by superposition of 844 M and 847 M.
860.2 ±0.8	8 (−3)	K?
890.09±0.15	5.3 (−2)	KLM. $T_{\frac{1}{2}}$.
894.4 ±0.4	1.0 (−2)	K. $T_{\frac{1}{2}}$. No other isotope of Au could have produced this line.
925.28±0.12	6.8 (−2)	KL. $T_{\frac{1}{2}}$. M masked by 1000 K.
938.87±0.10	2.2 (−1)	KL. $T_{\frac{1}{2}}$. M masked by 948 L.
948.40±0.12	1.1	KLMN. $T_{\frac{1}{2}}$.
1000.17±0.18	5.7 (−2)	KLM. $T_{\frac{1}{2}}$.
1007.51±0.30	1.5 (−2)	KLM. $T_{\frac{1}{2}}$.
1030.9 ±0.4	5.1 (−3)	K. Observed with different sources.
1038.80±0.20	1.9 (−2)	K. $T_{\frac{1}{2}}$. L masked by 1104 K and M masked by 1049 L.
1048.72±0.15	3.5 (−1)	KLM. $T_{\frac{1}{2}}$.
1081.64±0.35	5 (−3)	K? Observed with different sources. Could possibly be interpreted as 1088 K from Au^{198}.
1091.6 ±0.5	4 (−3)	K. L is masked by 1157 K.
1104.12±0.20	1.7 (−1)	KL(M). $T_{\frac{1}{2}}$. M just noticeable between 1175 K and 1184 K.
1119.73±0.35	1.1 (−2)	K. Observed with different sources. L masked by 1184 K.
1141.04±0.35	1.0 (−2)	K. Observed with different sources.
1150.91±0.20	2.0 (−1)	KL. $T_{\frac{1}{2}}$. L observed as a deformation on the low energy side of 1219 K.
1156.59±0.20	1.5 (−1)	KLM. $T_{\frac{1}{2}}$. L observed as a deformation on the high energy side of 1219 K.
1175.46±0.20	1.2 (−1)	KLM. $T_{\frac{1}{2}}$. M not resolved from 1184 L.
1183.63±0.20	1.2 (−1)	KLM. $T_{\frac{1}{2}}$.
1187.1 ±0.4	1.3 (−2)	K. Observed with different sources. K graphically resolved from 1184 K. L could not be resolved from 1184 L.
1195.09±0.35	6.6 (−3)	K. Coincides with 1120 M, but this line contributes negligibly to the intensity.
1208.47±0.35	6.4 (−3)	K. Observed with different sources.

TABLE 3 (continued)

E_γ (keV)	Conversion line intensity I(K)	Conversion lines observed. Remarks
1219.01±0.20	1.6 (−1)	KL. $T_{\frac{1}{2}}$. K is deformed by the presence of the weaker 1151 L and 1157 L. M is masked by 1294 K.
1267.37±0.15	8.0 (−2)	KL. $T_{\frac{1}{2}}$. M masked by 1342 K.
1291.8 ±1.0	2 (−2)	K? Observed as a broadening of 1294 K, not explainable as 1219 M.
1293.9 ±0.5	7.3 (−2)	KL. $T_{\frac{1}{2}}$. Energy uncertain because of broadening from 1292 K.
1302.55±0.15	5.1 (−2)	KL(M). $T_{\frac{1}{2}}$.
1308.59±0.20	1.9 (−2)	KL.
1342.44±0.20	3.2 (−1)	KLM. $T_{\frac{1}{2}}$.
1421.77±0.20	6.6 (−2)	KL. $T_{\frac{1}{2}}$. L graphically resolved from 1488 K.
1432.29±0.30	1.8 (−2)	KL. Observed with different sources.
1442.03±0.30	2.5 (−2)	KL. Observed with different sources.
1450.48±0.20	5.1 (−2)	KL(M). $T_{\frac{1}{2}}$.
1463.69±0.25	6.4 (−2)	KL. Observed with different sources.
1469.36±0.25	2.6 (−1)	KL. $T_{\frac{1}{2}}$.
1479.75±0.25	2.2	KLMN. $T_{\frac{1}{2}}$.
1487.9 ±0.5	2.2 (−2)	K. Observed with different sources. Graphically resolved from the weaker 1422 L. L masked by 1480 M.
1492.7 ±0.5	2.9 (−2)	K. $T_{\frac{1}{2}}$. L masked by 1480 M.
1512.8 ±0.6	1.4 (−2)	K(L). Graphically resolved from 1450 L.
1518.9 ±0.6	9.0 (−3)	K(L). Graphically resolved from 1450 L. Observed with different sources.
1547.9 ±0.4	8.1 (−2)	KL. $T_{\frac{1}{2}}$. M masked by 1623 K.
1563.4 ±0.4	4.4 (−2)	KL. $T_{\frac{1}{2}}$.
1592.9 ±0.4	2.0 (−1)	KL(M). $T_{\frac{1}{2}}$. K graphically resolved from 1596 K.
1596.2 ±0.4	2.9 (−1)	KL(M). $T_{\frac{1}{2}}$. K graphically resolved from 1593 K.
1602.0 ±0.5	3.6 (−2)	K(L). Observed with different sources.
1617.8 ±0.6	7.3 (−3)	KL. Observed with different sources.
1622.6 ±0.5	1.3 (−2)	KL. Observed with different sources. 1623 K and 1634 K cannot be L and M lines respectively.
1633.5 ±0.5	7 (−3)	K? L had too low intensity to be seen.
1670.9 ±0.6	1.8 (−2)	K? Remains after subtraction of 1595 M and 1602 L.
1675.9 ±0.5	2.2 (−2)	KL. Observed with different sources.
1690.2 ±0.4	1.8 (−2)	KL. K observed with different sources.
1715.69±0.30	6.4 (−2)	KLM. Observed with different sources.
1735.83±0.30	3.4 (−2)	K. $T_{\frac{1}{2}}$. L masked by 1798 K and 1806 K.
1757.6 ±1.5	2 (−3)	K? Noticed as a deformation on 1690 L.
1786.3 ±0.4	4.4 (−2)	KL. Observed with different sources.
1798.0 ±0.4	2.6 (−2)	KL. Observed with different sources.
1803.1 ±0.8	1.3 (−2)	K. Graphically resolved from 1806 K. Group observed with different sources.
1805.9 ±0.8	1.2 (−2)	K. Graphically resolved from 1803 K. L observed for the group.
1812.8 ±0.6	5 (−3)	K. Observed with different sources.
1830.12±0.30	2.8 (−2)	K. Observed with different sources. L masked by 1893 K.

TABLE 3 (continued)

E_γ (keV)	Conversion line intensity I(K)	Conversion lines observed. Remarks
1835.9 ±0.4	2.4 (−2)	K. Observed with different sources.
1886.80±0.30	2.8 (−1)	KLM. $T_{\frac{1}{2}}$.
1893.1 ±0.4	1.8 (−2)	K. L masked by 1960 K.
1911.1 ±0.5	3.5 (−3)	KL. Observed with different sources.
1924.60±0.20	1.8 (−1)	KLM. $T_{\frac{1}{2}}$.
1959.7 ±0.6	1.2 (−2)	KL. Observed with different sources.
1970.08±0.30	3.4 (−2)	KL. Observed with different sources.
1983.9 ±0.4	3.0 (−2)	K. Observed with different sources.
2044.1 ±0.4	2.8 (−1)	KLM. $T_{\frac{1}{2}}$.
2085.8 ±0.4	1.3 (−1)	KL. $T_{\frac{1}{2}}$.
2114.0 ±0.4	1.9 (−2)	KL. Observed with different sources.
2164.1 ±0.4	3.8 (−1)	KLM. $T_{\frac{1}{2}}$.
2215.6 ±0.7	1.3 (−2)	KLM. Observed with different sources.
2298.7 ±1.0	2 (−3)	KL. Observed with different sources.
2312.7 ±0.8	8 (−3)	KLM. Observed with different sources.
2357.0 ±0.8	8 (−3)	KL. Observed with different sources.
2366.1 ±0.8	3 (−3)	KL. Observed with different sources.
2398.9 ±1.0	7 (−4)	K. Observed with different sources.
2413.5 ±1.0	1.2 (−3)	K. Observed with different sources.

4. Disintegration Energy

It is of interest to have a precise Q-value for the disintegration, since this helps to decide which of the transitions leads to the ground state. It is known [1]) that there is a positon branch to the ground state and thus it is sufficient to determine the end point of this distribution. A run was taken with a source of intermediate strength and with the spectrometer set at a resolution of 0.8 %. From the data an allowed Fermi plot was constructed (fig. 4). In agreement with the assignment of 1^- to the parent nucleus the plot follows very accurately a straight line from the end point down to 1100 keV, where an indication of the second branch is noticeable. The result of the end point determination is $E_{max} = 1487 \pm 15$ keV and our value for the disintegration energy thus becomes 2509 ± 15 keV.

5. Multipolarities

The present conversion electron study in principle yields ratios for conversion intensities in different shells and subshells and it should be possible to draw conclusions from them about the multipole orders of the transitions. The sensitivity of $K/\sum L$ ratios to multipolarity, however, decreases with increasing energy so that at energies higher than 1 MeV it becomes difficult experimentally to distinguish between the common cases E1, M1, and E2 on this basis. L subshell ratios retain their sensitivity better in this region,

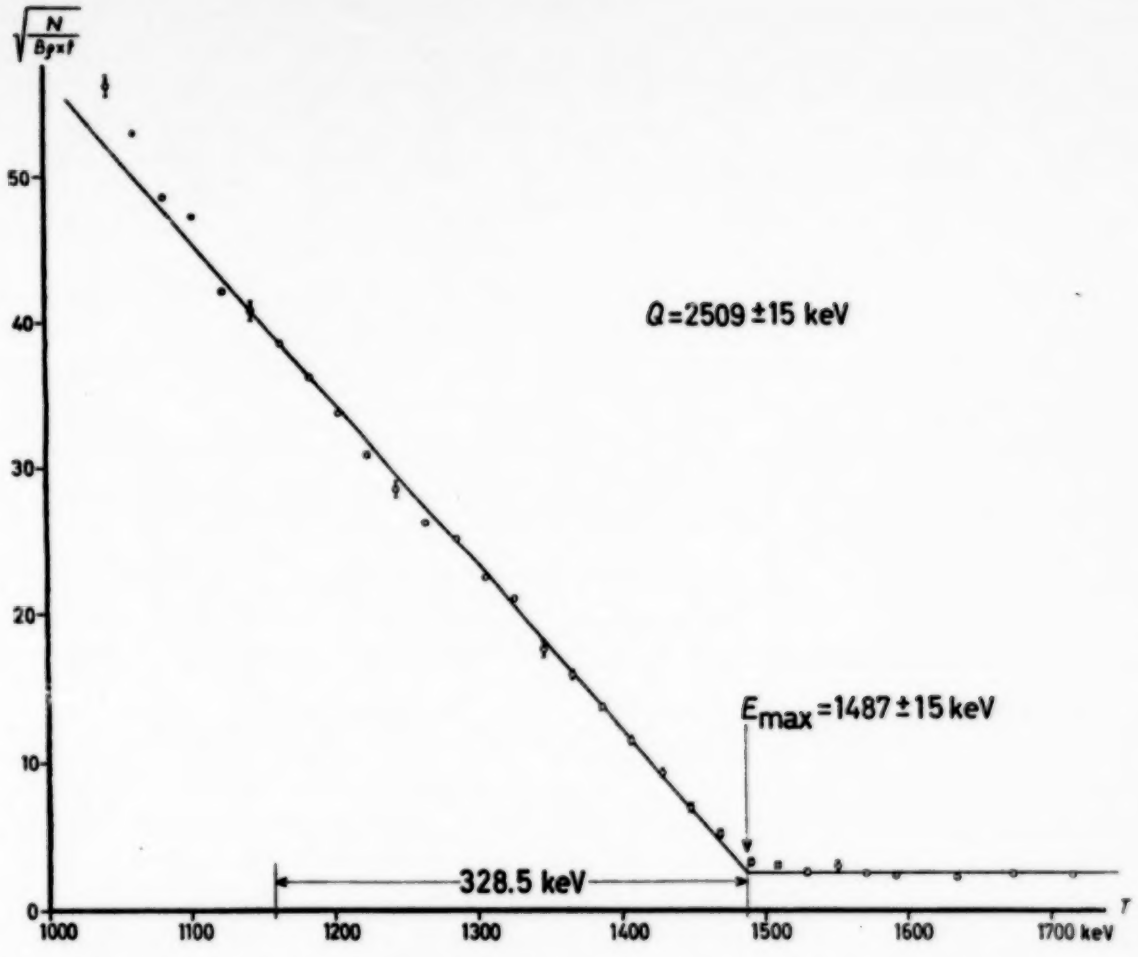

Fig. 4. Fermi plot of the positon spectrum. The experimental points follow a straight line from the maximum energy down to about 1100 keV, where the onset of the second branch is noticeable. The small departure from theoretical shape near the end point is caused by the finite resolution of the instrument.

TABLE 4

Multipolarity information derived from conversion spectra

Transition (keV)	Basis of assignment	Multipolarity
164	$K/\Sigma L = 4.6 \pm 1$ $\quad L_I/L_{III} > 14$	M1, M2
216	$K/\Sigma L > 5.2$	E1, M1, (M2)
294	$K/\Sigma L = 1.89 \pm 0.20$	E2 (< 3% M1)
301	$K/L_{II} = 3.5 \pm 1$; $\quad K/L_{III} > 8$	E2
483	$K/\Sigma L = 4.9 \pm 0.8$; $\frac{L_I + L_{II}}{L_{III}} = 6$	(E1, E2)
622	$K/\Sigma L = 4.2 \pm 0.8$	E2
645	$K/\Sigma L = 4.7 \pm 0.5$; $\frac{L_I + L_{II}}{L_{III}} = 7$	E2

but the determination of these quantities instead sets unreasonable demands on the resolving power of the instrument. A special difficulty that was encountered in this investigation was the great line density, which usually impaired the intensity measurement of either the K-line or the L-lines. Often the L-group could not even be detected against the background. Table 4 summarizes the information on multipolarity which could be obtained in this way. The most accurate conclusion concerns the 294 transition of which the $K/\sum L$ ratio has been measured in two instruments. Also one may have confidence in this result since the statistics permitted an accurate measurement of the L sublines. Although this did not directly contribute to the accuracy of the M1 admixture, the agreement with theoretical data can be taken as proof of the purity of the L-group. A similar study of the 328 transition, which is well known to be E2, did show agreement with the theoretical $K/\sum L$ value to within 10 %.

If absolute conversion coefficients could be measured, this would allow the determination of multipolarities with fair accuracy even as high as 2 MeV. Since strong sources of Au^{194} may be produced, the necessary gamma intensities may conveniently be determined by means of photo-electrons. Such studies of this isotope are now in progress. Meanwhile the conversion electron intensities reported here may be supplemented by the gamma intensities published by Thieme and Bleuler. These data were obtained by scintillation techniques, however, and the results must be considered very uncertain considering the complexity of the decay. Furthermore, each scintillation peak extends over a region of several gamma rays and thus only reflects an average intensity. A reasonably strict analysis may be carried out in terms of upper and lower limits of conversion coefficients. The gamma intensities are normalized to fit the theoretical conversion coefficient of the 328 keV E2 transition. Any of the intensities obtained in this way then constitutes an upper limit for each transition that is included in the corresponding scintillation peak. The ratio of conversion line to gamma intensity thus gives a lower limit for the conversion coefficients. As is seen from table 5, which presents the results of these considerations, a few non-trivial conclusion indeed become possible. It would seem feasible to obtain a lower limit for the gamma intensity, and thus an upper limit to the conversion coefficient, by subtracting the contributions from neighbouring lines to the gamma intensity, where for these transitions the lowest conversion coefficient compatible with the results of table 5 is taken. Such calculations were carried out but were found to yield only very uncertain or trivial conclusions in this case.

The gamma intensities given by Johns and Nablo in the decay of Ir^{194} are also pertinent to the decay of Au^{194} insofar as the gamma ray branching from a given level should be the same. In applying this to the 1267 keV level, it was noticed that, while the lines of 645 keV and 939 keV are observed in

both types of decay, the ground state transition has only been observed from Au^{194}. If the 645 keV line is taken to be E2, as has been found, and the conversion line and gamma ray intensities are combined to yield the conversion coefficient of the 939 keV line, it appears that the latter transition would have

TABLE 5

Lower limits of conversion coefficients

Transition (keV)	I_K (Present work)	I_γ (Ref. [1]))	Lower limit of α_K	Theoretical conversion coefficients (Sliv) for the excluded multipolarities
948	1.1	9	6 (−3)	E1:2.0 (−3)
1219	0.16	2	4.0 (−3)	E1:1.3 (−3)
1342	0.32	2	8 (−3)	E1:1.1 (−3) E2:2.6 (−3)
1469	0.26	8	1.6 (−3)	E1:9 (−4)
1480	2.2	8	1.4 (−2)	E1:9 (−4) E2:2.1 (−3) M1, E3:4.2 (−3)
1593	0.20	6	1.7 (−3)	E1:8 (−4)
1596	0.29	6	2.4 (−3)	E1:8 (−4)
1887	0.28	7	2.0 (−3)	E1:6 (−4)
2044	0.28	5	2.8 (−3)	E1:5 (−4) E2: 1.2 (−3)
2086	0.13	5	1.3 (−3)	E1:5 (−4)
2164	0.38	1	1.9 (−2)	E1:5 (−4) E2: 1:1 (−3) etc. M5:1.4 (−2)

the same multipolarity. Further, the assumption that the ground state transition has the same multipolarity as the other de-exciting lines, implies that its gamma intensity would be about 2 on the scale of Johns and Nablo. From their published spectrum it is estimated that this line would have been visible even with an intensity of 0.4. The conversion coefficient of the 1267 keV transition thus has to be at least a factor of five higher and, since the 645 keV line seems to be E2 from its $K/\sum L$ ratio, an E0 assignment to the 1267 keV line is the only reasonable one †.

6. Utilization of the Transition Energies for the Construction of the Decay Scheme

The most definitive type of information that is obtained from transition energies alone is: $E_1+E_2 \neq E_3$ which expresses the impossibility of a cross-over relationship. On the other hand, if one were given a sufficiently accurate equality

$$E_1+E_2 = E_3 \qquad (1)$$

† Angular correlation experiments have since been performed by Marklund *et al.* [34]), for the cascades leading from the 1267 keV state to the ground state. A source of Ir^{194} was used in this measurement. The results are only compatible with a 0^+ assignment to this level.

it could be concluded with reasonable certainty that the transitions involved form a closed circuit in the decay scheme. The way a given transition occurs in several sum relationships indicates how these circuits are coupled to each other to generate the decay scheme. In practical cases where many lines are involved, the possibility of accidental fulfilment of relationship (1), within the experimental errors has to be taken into account. It is desirable in any case, however, to know the complete set of such relationships when a decay scheme is to be constructed. Each transition energy was added to each of the others and the results arranged in matrix form in the usual way. Since no sums higher than 2414 keV had to be considered, it was sufficient to calculate 2700 sums. Each of these energy sums was compared to the transition energies, and values that coincided to within ± 0.1 % were marked (underlined) to form the material for a detailed analysis. This 0.1 % error was the highest one to be expected.

The number of random sum relationships may easily be calculated. The probability that an energy value ε coincides with the energy of a gamma ray, within its limits of error $\pm \Delta\varepsilon$, is: $\rho(\varepsilon) \times 2\Delta\varepsilon$, where $\rho(\varepsilon)$ is the line density (number of lines per keV). The density of energy sums $\rho_s(\varepsilon)$ may be taken directly from the matrix. The total number N_{ch} of random relationships contained in the matrix then becomes

$$N_{ch} = \sum \rho(\varepsilon) 2\Delta\varepsilon \, \rho_s(\varepsilon) \delta\varepsilon \qquad (2)$$

where the sum is taken over all energies and the energy span is subdivided into intervals of length $\delta\varepsilon$. With a deviation of ± 0.1 % and for a suitable subdivision, the total number of random cross-over relationships was calculated to be 420 whereas the number actually found from the matrix was 526. This implies that only about 20 % of these sum relationships may be expected to be true. To tell exactly which are real would probably not be feasible if it were not for the following factors: (i) The accuracy of the measurements is expected to be better on the average than assumed above. (ii) Closed circuits, formed in a random way from transition energies, are not likely to connect with each other to generate a consistent decay scheme. (iii) It may be expected that some transitions, E_1, show a higher tendency to relationships of the type (1), simply because of their location in the level scheme, and such transitions would show a more favourable statistics. For example, a transition which is the only observable depopulation of a level, as shown in fig. 5a, would not exhibit any true sum relationship. On the other hand, the 294 keV transition (fig. 5b), which has a low location and connects levels of the same spin, should show many such relationships since higher levels are expected to populate both levels to a comparable degree. The number of chance relationships pertaining to a certain transition E_1 is given by

$$N_{ch}(E_1) = \sum \rho(\varepsilon) 2\Delta\varepsilon \, \rho(\varepsilon - E_1) \delta\varepsilon \qquad (3)$$

where the sum is taken the same way as before. The value obtained for N_{ch} (E_1) depends to some extent on the subdivision $(\delta\varepsilon)$. For E_1 in the region of 300 keV and with the error $\Delta\varepsilon = \pm 10^{-3}\varepsilon$, a value of $N_{ch} = 12\pm 1$ was obtained from different modes of calculation. The actual number of sums in the case of the

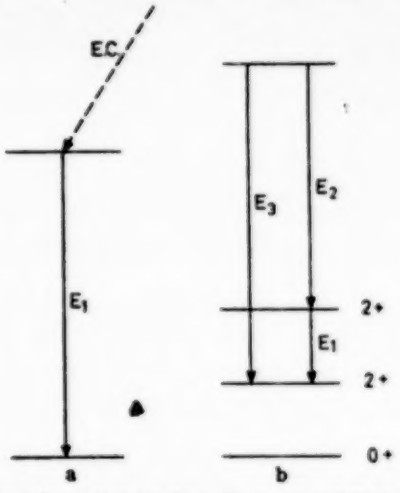

Fig. 5. Instances of decay scheme where transition E_1 may exhibit (b) one or several sum relationships and (a) none. The former example (b) is taken from the presented decay scheme, with E_1 corresponding to the 294 keV transition.

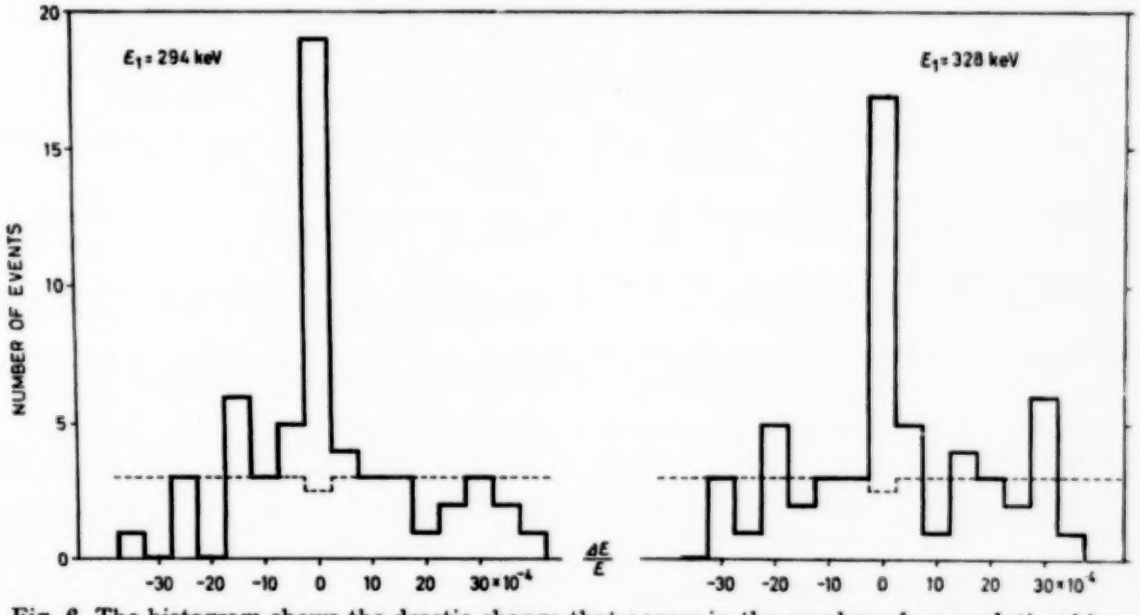

Fig. 6. The histogram shows the drastic change that occurs in the number of sum relationships, involving a given transition E_1, when an error ΔE is added to the measured energies E_3. The dashed line represents the calculated level of accidental relationships.

294 keV transition was 28 and for the 328 keV transition, 26. Consequently the number of true relationships N_t should be $N_t(294) = 16\pm\sqrt{12}$ and $N_t(328) = 14\pm\sqrt{12}$ respectively. Since the number N_t here is appreciable compared to the number of choices of E_2, which is about a hundred, one should correct N_{ch} accordingly. There are only 85 sums (E_1+E_2) out of a

hundred which could coincide by accident with a value of E_3, and thus $N_{ch} = 10$ is a more accurate value.

For a value E_1 which does not correspond to any transition, one could generally expect only random relationships (1), and this suggests an alternative method of determining $N_{ch}(E_1)$. Such a statistical investigation was carried out for the transitions of 294 keV and 328 keV. A histogram was constructed for the distribution of $\Delta E_3/E_3$ from the equation $E_1+E_2=E_3+\Delta E_3$. This diagram (fig. 6) shows how the number of relationships for a given E_1 varies as the transitions E_3 are changed out of position. Apparently there is fair agreement between the level of random relationships as obtained from the histogram and as calculated above for the same relative error ($\pm 2.5\times 10^{-4}$). It may also be inferred that, within these limits of error, $N_t(294) = 16.5\pm\sqrt{3}$ and $N_t(328) = 14.5\pm\sqrt{3}$. Furthermore, since these numbers are nearly the same as obtained for the limits of error $\pm 10^{-3}$ and since the diagrams in fig. 4 show little positive effect outside the central interval, it is clear that the combined error of the true relationships is generally less than 2.5 parts in 10^4. This lends independent support to the validity of the calibration procedure described in a previous section.

When the best cross-over relationships with the lines of 294 keV and 328 keV were examined, fourteen cases were found in which pairs of relationships had a common member. The obvious interpretation is a set of levels which decay with comparable probabilities to the ground state and to the levels at 328 and 622 keV (table 6). It is interesting to note that this number of levels agrees reasonably well with the number predicted from fig. 5. A level which is located on the basis of three lines, one to the ground state and one each to two well known levels, must be considered as well established. In fact, it is easy to estimate the number of such energy combinations that may occur by accident. Within the limits of error ($\pm 2.5\times 10^{-4}$), there are about three accidental sum relationships for each of the lines 294 keV and 328 keV. Since there are approximately a hundred choices for the common member (transition E_3 in fig. 4b), the chance for a particular circuit to connect with one of the others is $\simeq 3/100$, and thus the probable number of random configurations becomes 3×0.03. Other modes of approach yield the same result. Consequently it is unlikely that any of these levels should be of random origin. As a further support, a few of these levels decay to a level at 1267 keV, which in turn is defined by three depopulating transitions and which has been definitely observed in the decay of Ir^{194}.

If it is assumed that no level exists between the ground state and the 328 keV state, which is quite reasonable from a systematical point of view, there are seven lines (2216 keV and higher) which, from consideration of the Q-value, must be ground state transitions. Some of these lines had already received a ground state assignment for reasons previously discussed.

It is noted that the high intensity and the large number of cross-over relationships reflect the receiving character of the 294 keV and 328 keV lines. Another line, of 301 keV, shows analogous features with 22 relationships (with $\Delta\varepsilon = \pm 10^{-3}\varepsilon$). Among those with the best energy fit, seven cross-

TABLE 6

Summary of energy support for levels.

The table is concerned with the transitions leading to the ground state and to the three lowest excited states. The first column gives the level energy, obtained as a weighted average of the energies of the depopulating cascades. The second column contains the deviation i.e. the level energy minus the energy of the cascade considered, and the third one gives the estimated standard error of the cascade. The other columns have a corresponding meaning.

Level energy (keV)	Transition to ground state		Transition to 328-keV level		Transition to 622-keV level		Transition to 923-keV level	
	Deviation (keV)	Error (keV)	Deviation (keV)	Error (keV)	Deviation (keV)	Error (keV)	Deviation (keV)	Error (keV)
1432.48	+0.19	0.30	−0.14	0.20	−0.47	0.5		
1479.60	−0.15	0.25	+0.19	0.20				
1512.19	−0.61	0.6	+0.06	0.20	+0.05	0.15	+0.04	0.10
1547.44	−0.46	0.4	+0.03	0.20	+0.11	0.12		
1622.33	−0.27	0.5	−0.07	0.5	+0.11	0.18		
1670.85	−0.05	0.6	−0.09	0.20	+0.08	0.15		
1778.85			−0.13	0.20	+0.21	0.20	+0.01	0.20
1797.76	−0.24	0.4	−0.10	0.25	+0.25	0.20		
1816.92			+0.52	0.5	−0.22	0.35	−0.24	0.4
1924.61	+0.01	0.20	−0.09	0.4	+0.01	0.15		
1930.58			+0.08	0.5	−0.06	0.20	+0.31	0.30
1961.64			−0.36	0.5			+0.08	0.22
2044.00	−0.10	0.4	−0.19	0.3	+0.18	0.20		
2064.14			−0.19	0.3	+0.06	0.30	+0.34	0.35
2085.77	−0.03	0.4	+0.67	1.5	+0.03	0.25		
2114.40	+0.40	0.4	−0.40	0.4	−0.35	0.5		
2141.59			+0.29	0.6	+0.64	0.6	−0.18	0.20
2164.23	+0.13	0.4	−0.17	0.4				
2215.24	−0.36	0.7	−0.06	0.3	+0.29	0.4	+0.68	1.0
2298.39	−0.31	1.0	−0.19	0.3	+0.44	0.5		
2312.40	−0.30	0.8	0.00	0.4	+0.15	0.4		
2357.70	+0.70	0.8			−0.18	0.30		
2414.1	+0.59	1.0	−0.21	0.4				

overs were found to involve lines which had been found to feed the state at 622 keV. Two of them depopulated well established levels of the type just discussed; the remaining five formed sum relationships with the 294 keV line. This evidence strongly suggested a level at 923 keV, which decays exclusively by the 301 keV line. The 594 keV transition can not be interpreted as leading to the 328 keV state since the energy deviation would be intolerably large (0.5 keV). One may attempt to calculate the statistical significance of a state

at 923 keV. If the transition energies are added to this level energy, the sums may accidentally coincide with the energy of some of the 25 levels that are known to exist above 923 keV. On the assumption of an error of ± 5 parts in 10^4 (referred to the energy of the levels), the probable number of random lines which feed the 923 keV state becomes 2.0. In the present case there are two transitions from known levels and five transitions from levels supported by cross-over relationships which should be true in roughly 16 cases out of 19. Hence there would seem to be six feeding transitions in total, and it is calculated from the Poisson formula that the probability of obtaining six or more random transitions is $\simeq 10^{-3}$. Although some positive as well as negative corrections have been neglected in this estimate, it shows convincingly enough that the 923 keV level cannot very likely be the result of a numerical accident. A similar consideration shows that the 1267 keV level is very well established even from this point of view.

Since the level at 923 keV is known to be depopulated by the 301 keV transition only, it would be of interest to investigate the balance of feeding and decay of this state. Although gamma intensities have not yet been obtained for the lines involved, the 301 keV line is known to be of multipolarity E2, and it may be asked whether the conversion intensities can be explained in terms of reasonable multipolarities. In fact, the feeding becomes approximately correct if an "average" multipolarity of E2 is assumed for the lines leading to this state. Multipolarities M1 and E1 may also be present.

After a large number of transitions have been located in the manner outlined above, the density of lines not yet located has decreased appreciably so that a higher significance may be attached to the energy relationships between the remaining transitions. It thus becomes possible to arrange most lines plausibly into a partial decay scheme in which, however, some alternative configurations occur. The location of these transitions is discussed in the coincidence section.

When a set of levels has been established, it is found that certain transitions fit energetically between pairs of these levels, sometimes even in alternative positions. It is in a sense justifiable to locate transitions on such grounds, because transitions between any two levels do take place. The partition of the available intensity between the alternative locations naturally cannot be decided on energy arguments alone. Where definite coincidence information was not available, the transitions have been allowed to occupy more than one position in the decay scheme.

It is tempting to generalize the statistical treatment of transition energies in the following way. The number of relationships $N(\varepsilon)$ of the type $\varepsilon + E_2 = E_3 + \Delta E_3$ is recorded as a function of ε, where E_2 and E_3 are transition energies as before. The function $N(\varepsilon)$ may be considered as a transform of the original gamma spectrum. The peak heights would correspond, however, to

the tendency of the various gamma rays to combine energetically with others. Peaks could also be expected to occur in the function $N(\varepsilon)$ at energies where no gamma ray has been observed. Such evidence would thus indicate a forbidden transition, such as 594.26 keV in the present decay scheme. This statistical spectrum predicts how many relationships (1) are expected for each transition. Restrictions are thus imposed on the possible ways of combining the line energies into a set of level energies, and it seems that by constructing the level scheme such that it accommodates roughly the predicted number of transition circuits, one makes the optimal use of the information inherent in the energy data. Combinations of the types $E_1+E_2 = E'_1+E'_2$ and $E_1+E_2+E_3 = E_4$ are, of course, partly neglected in this treatment, but the percentage of random relationships should be much larger in these cases.

It might be questioned whether a statistical treatment of nuclear transitions really is adequate. Admittedly, the transition energies cannot be expected to obey statistical laws, since they form differences between a set of level energies and hence are not numerically independent. However, it is exactly this deviation from normal statistical behaviour that must be detected to gain knowledge of the connection between various transitions, and from this point of view our treatment is fully justified. On the other hand, the level energies might, by mechanisms yet unknown, exhibit numerical properties such that relationships of type (1) occur even if the transitions involved do not form a closed circuit in the decay scheme. Such "false" relationships would be counted as "true" in the above analysis, but the evidence of such an effect would simply be the impossibility of accounting for all true sum relationships in terms of closed circuits. Further, the occurrence of simple numerical relationships between level energies has not been reported and is a remote possibility.

In conclusion, the possibilities of utilizing transition energy data for the construction of a complicated decay scheme are more favourable than expected, since evidently there are factors which counteract the large number of lines. In particular, it is noted that the difficulties should increase with the number of existing levels rather than the number of lines. The more depopulating lines that are observed for a given level, the higher is the statistical significance of the level assignment. With high precision iron-free spectrometers now coming into use it should be possible to reach an average accuracy that is a factor of five higher than in the present work. The resulting increase in the ratio of true to random relationships is marked particularly for higher order combinations, such as where three transitions depopulate a certain level, in which case the number of accidental relationships becomes proportional to the square of the energy error.

7. Coincidence Measurements

The analysis of the single spectrum yielded more than a hundred different

transitions. With such high density of lines, conversion-gamma or gamma-gamma coincidence measurements would contribute only very limited information concerning the structure of the decay scheme. Such measurements were performed by various investigators, as reviewed in the introduction.

In order to gain further information, a large number of coincidences between pairs of conversion lines were investigated with a double lens coincidence spectrometer [30]). The transmission in each spectrometer was adjusted to 3 % and with sources of 3 to 4 mm in diameter the momentum resolution was also about 3 %. Helical baffles were introduced in both channels to stop the positons. At first the coincidence set-up was a conventional fast-slow arrangement with resolving time of $2\tau = 3\times10^{-7}$ sec. Later on, to allow for stronger sources, R.C.A. 6810 photomultipliers were introduced, utilizing a Bell unit adjusted to a resolving time of $2\tau = 1\times10^{-8}$ sec.

The chance coincidences were measured by introducing in one channel a time delay long compared with the resolving time of the proper coincidence unit.

The genuine coincidence counts N_c were obtained in each case by subtracting the accidental from the total coincidences. A simplified formula might be used here in connection with the interpretation of the coincidence measurements: $N_c = N_1\omega_2\kappa_2\delta_{12} = N_2\omega_1\kappa_1\delta_{21}$. Where the indices 1 and 2 refer to the different spectrometer channels and also to the transitions focused in them. N_1 and N_2 are the singles counting rates, ω_1 and ω_2 are the transmission factors, and κ_1, κ_2 are the conversion probabilities ($\kappa = \alpha(\text{line})/[1+\alpha(\text{total})]$) δ_{12} is the fraction of transition 1 which is in coincidence with transition 2, and δ_{21} has a corresponding meaning. The formulae are valid on the assumption that the efficiencies of the detectors are independent of the electron energy and that the effect of angular correlation is negligible.

The transmission ω_2 was obtained by performing coincidence measurements between the 294 keV conversion line and the 328 keV line. The 294 keV transition is known from previous work to be deexcited to the ground state only via the 328 keV transition. The δ_{12} value is therefore unity and the ratio of N_c/N_1 furnishes the value $\omega_2\kappa_2$. The 328 keV transition having E2 multipolarity, the κ_2 value can be taken from tables. In this way the transmission was generally found with a precision of about 5 % for each source, the transmission being rather sensitive to centering and dimensions of the source. The value found for the transmission in this way was compatible with the value obtained from previous work with the same spectrometer under similar experimental conditions. The last observation supports the known fact that the 294 keV transition is in 100 % coincidence with the 328 keV line.

Except for a few cases, every focused line contained fractions of neighbouring transitions and their contribution to the coincidences had to be taken into account when interpreting the experimental results. The K conversion

line of the 483 keV transition, for instance, could be resolved completely from the adjoining lines of Au^{194} but it included the L conversion line of the 411 keV line due to Au^{198}. This last transition is in coincidence with the continuous β^- spectrum having an end point at 960 keV. This fact rendered the coincidence measurements with the K 483 keV line difficult when the second line was focused below the end point of β^-. To overcome this difficulty the K 483 keV line was focused in one channel and the second spectrometer scanned the 294 and 328 lines, the contribution due to the 483 keV transition being inferred from the peaks over the background.

The effect on the coincidence counting rate of interfering lines in spectrometer 2 is taken into account by summing over these lines:

$$N_c = N_1 \sum_\nu \delta_{1\nu}\kappa_\nu\omega_\nu,$$

where ω_ν is now energy dependent and has a lower value for off-focus lines. When spectrometer 2 focuses the 328 keV line there is no nearby line of sufficient intensity to contribute noticeably to the coincidences. When the 294 keV line is focused, however, there is a contribution from the tails of the 301 keV line and the 328 keV line. Since the conversion probability κ is known for these lines, an upper limit for their coincidence contribution can be obtained by putting $\delta_{1\nu} = 1$, if the branching ratio should not be known from other experiments.

Spectrometer 1 was usually set to focus a line of rather high energy and as a consequence often accepted appreciable contributions from other lines. It is seen directly from the formula that the various lines entering in channel 1 contribute to the coincidence counting rate in proportion to their contribution to the singles counting rate in this channel and to the value of δ_{12}. Thus the magnitude of the disturbing effect can be calculated, or estimated in terms of an upper limit. With many experiments, the intensity of the disturbing line was such that the correction had to be known accurately. The calculation of this correction required knowledge of the location of lines in the level scheme, and when such information was drawn from energy relationships, a comment about this is given in table 7.

There is not much ambiguity in the interpretation of coincidence measurements between the 294 keV or the 328 keV line and other lines. There is a second class of measurements, however, where there is no strong predominance of the focused line over the neighbouring ones in any of the two channels, and where the multipolarity of the lines concerned is not known. In such cases an off-focus line might contribute appreciably to the coincidences if it has a conversion probability much higher than that of the focused line. Although it is felt that such events should be very rare accidents in the present decay, this type of coincidence experiments are considered to be less conclusive.

TABLE 7

Results of electron coincidence experiments. The data have been numbered in column 1. Columns 2 and 3 give the lines at which the spectrometers were focused. Unless otherwise stated the. K conversion line is referred to. Column 4 contains the experimental branching ratio δ_{12} for the transitions studied. In certain cases, only the product $\delta_{12}\kappa_2$ is given. The succeeding column indicates the value of δ_{12} according to the positions the lines finally received in the decay scheme. The branching ratio for transitions going into the levels at 328 keV, 622 keV and 1267 keV can be calculated from known gamma intensities. In other cases, only an indication of the coincidence relationship is given (0 or >0).

No.	Conversion line focused in		δ_{12} measured	δ_{12} according to decay scheme
	Spectrometer 1	Spectrometer 2		
1	622	294	0.1 ± 0.1	0
2	622	328	0.3 ± 0.25	0
3	645 [1]	622	0.16 ± 0.06	0.15
4	645	294	0.93 ± 0.1	0.85
5	645	328	1.0 ± 0.2	0.85
6	948 [1]	645	0.47 ± 0.1	
			$\delta_{12}\kappa_2 = (5.0 \pm 1) \times 10^{-3}$	0.68
7	948 [1]	939	0.54 ± 0.22	
			$\delta_{12}\kappa_2 = (2.7 \pm 1.1) \times 10^{-3}$	0.32
8	948	294	0.88 ± 0.22	>0
9	948	328	1.1 ± 0.4	>0
10	1267 [1]	294	-0.1 ± 0.3	0
11	1267 [1]	328	0.1 ± 0.4	0
12	301	294	1.6 ± 0.4	0.85
13	1480	294	-0.01 ± 0.1	0
14	1480	328	0.23 ± 0.2	0
15	736 [1]	1480	$\delta_{12}\kappa_2 = (4.4 \pm 3) \times 10^{-2}$	>0 [2]
16	1342	294	0.16 ± 0.2	0
17	1342	328	2.5 ± 1.4	1
18	1049	294	0.80 ± 0.15	0.85
19	1049	328	0.78 ± 0.2	0.85
20	1925	294	0.08 ± 0.12	0
21	1925	328	-0.1 ± 0.2	0
22	1593 [1] +1596	328	0.95 ± 0.4	0.94
23	1593 [1] +1596	294	0.36 ± 0.12	0.35
24	1303 [1]	294	1.7 ± 0.5	0.85
25	2044	328	0.28 ± 0.3	0
26	1716 [1]	328	0.74 ± 0.5	1
27	1422 [1]	294	2 ± 0.8	0.85
28	1786 [1]	294	0.12 ± 0.2	0
29	1786 [1]	328	0.6 ± 0.4	1
30	2164	328	-0.1 ± 0.2	0
31	1836 [1] +1830	294	0.06 ± 0.23	
32	1836 [1] +1830	328	1.4 ± 0.6	
33	1887	294	-0.14 ± 0.2	0
34	1887	328	1.1 ± 0.2	1
35	1294 [1]	294	-0.05 ± 0.4	0

[1]) In order to evaluate the corrections to the coincidence counting rate, it was necessary to assume that the location of interfering lines is as proposed in the present decay scheme.

[2]) $\delta(E0) = (4.4 \pm 3) \times 10^{-2}$ shows that the transitions are probably in coincidence, because assuming the 1151 keV transition to be of E2 character (from the 0+ assignment of the level), one obtains an expected value of $\delta = 3 \times 10^{-3}$.

No.	Conversion line focused in		δ_{12} measured	δ_{12} according to decay scheme
	Spectrometer 1	Spectrometer 2		
36	1294 [1]	328	2.5 ± 0.8	1
37	594 [1]	1000	$\delta_{12}\kappa_2 = (1.6 \pm 0.9) \times 10^{-3}$	>0
38	594 [1]	948	$\delta_{12}\kappa_2 = (-1.9 \pm 2.3) \times 10^{-3}$	0
39	594	294	0.55 ± 0.2	>0
40	594	328	1.1 ± 0.3	>0
41	2086	328	0.4 ± 0.3	(4)
42	1736 [1]	294	0.33 ± 0.4	(4)
43	1736 [1]	328	1.0 ± 0.7	0.85−1
44	1219	294	-0.3 ± 0.4	0
45	1219	328	3 ± 1.7	1
46	1104	294	0.18 ± 0.15	0
47	1104	328	0.92 ± 0.27	1
48	1469 [1]	294	0.05 ± 0.8	0
49	1469 [1]	328	1.2 ± 1	1
50	1676 [1]	294	0.6 ± 0.8	0.85
51	1676 [1]	328	0.85 ± 1	0.85
52	1984 +1970	328	0.54 ± 0.5	1
53	529	294	0.2 ± 0.05	>0
54	529	328	1.2 ± 0.4	>0
55	164 [1]	1104	$\delta_{12}\kappa_2 = (1 \pm 0.4) \times 10^{-3}$	>0
56	164 [1]	1049	$\delta_{12}\kappa_2 = (6.7 \pm 4) \times 10^{-4}$	0
57	483	294	0.23 ± 0.14	>0
58	L, M 483	294	0.43 ± 0.2	>0
59	483	328	1.3 ± 0.3	0.95
60	L, M 483	328	0.95 ± 0.4	0.95
61	483 [1]	1104	$\delta_{12}\kappa_2 = (2.2 \pm 1.5) \times 10^{-3}$	0
62	483 [1]	1184	$\delta_{12}\kappa_2 = (0 \pm 8) \times 10^{-4}$	0
63	483 [1]	1887	$\delta_{12}\kappa_2 = (3.5 \pm 4.8) \times 10^{-4}$	0
64	365 [1]	K, L 1104	$\delta_{12}\kappa_2 = (1.5 \pm 2.8) \times 10^{-3}$	>0
65	365 [1]	L 1104	$\delta_{12}\kappa_2 = (0.65 \pm 2.7) \times 10^{-3}$	>0
66	365 [1]	K, L 1104	$\delta_{12}\kappa_2 = (4.5 \pm 2.8) \times 10^{-3}$	>0
67	1151 [1] +1157	294	0.7 ± 0.3	0.35
68	1151 [1] +1157	328	1.9 ± 0.8	0.94
69	1175 [1] +1184	294	0.7 ± 0.3	0.42
70	1175 [1] +1184	328	1.7 ± 1.0	0.92
71	164 [1]	L 1798	$\delta_{12}\kappa_2 = (2 \pm 1.5) \times 10^{-4}$	>0
72	365	294	1 ± 0.4	>0
73	365	328	2.5 ± 0.7	>0
74	365 [1]	1480	$\delta_{12}\kappa_2 = (-1.5 \pm 3.6) \times 10^{-3}$	0 [3]
75	704	294	1.1 ± 0.5	>0
76	704	328	1.1 ± 0.7	>0
77	704 [1]	1184	$\delta_{12}\kappa_2 = (2.8 \pm 3.3) \times 10^{-3}$	>0
78	1806 [1] +1803	294	0.2 ± 0.4	
79	1806 [1] +1803	328	1.0 ± 1	

[3]) $\delta(E0) = (-1.5 \pm 3.6) \times 10^{-3}$ must be interpreted as a negative result, on the argument given under footnote [2]) of this table.

[4]) The transition energies indicate two alternative locations of this line. In the case of the 1736 keV transition the alternatives correspond to $\delta = 0$ and $\delta = 0.85$, and in the case of the 2086 keV transition the δ-values are 0 and 1.

Contributions to the coincidence counting rate from interfering lines have been calculated on basis of conversion intensities, and the data are not completely independent, in so far as use has been made of the coincidence relationships between lines according to the decay scheme constructed on energy arguments.

8. Interpretation of the Coincidence Information

The approach in constructing the decay scheme from coincidence data tried to be independent as far as possible of the results of previous works. However, the two lowest excited levels, both with 2^+ assignment, that were produced by Coulomb excitation, were assumed to exist from the outset. In the coincidence measurements, the aim was to arrive at an independent support for the validity of the excited levels and to find the true position of the transitions in the decay scheme.

As already mentioned in a previous section, the 294 keV transition is in 100 % coincidence with the 328 keV line. The negative results of the coincidences between the 622 keV transition and the 294 keV (no. 1), 328 keV (no. 2) lines indicate that the 622 keV line is a cross-over of the 294 keV and the 328 keV transitions. These facts once again establishes the 622 keV level.

Coincidences no. 3, 4, and 5 show that the 645 keV transition is de-excited via the 622 keV level, and coincidences no. 6, 7, establish the levels at 1267 keV and 2216 keV. Coincidences no. 8, 9, serve as additional support, and no. 10, 11, indicate that the 1267 keV transition leads directly to the ground state.

The strong coincidence effect between the 301 keV and the 294 keV transitions (no. 12), indicates the existence of a level at 923 keV, also supported by the presence of 8 feeding transitions from upper levels.

The 1480 keV level is based on negative results of coincidence measurements no. 13 and 14. Furthermore, a slight coincidence effect was observed between the 736 keV and 1480 keV lines (no. 15) and if this cascade were terminating at the first excited state or higher, the Q-value would be violated.

The 1342 keV transition is coincident with the 328 keV line and not with the 294 line (no. 16 and 17), whereas the 1049 keV transition is de-excited through the 622 keV level (no. 18 and 19). These facts establish the 1671 keV level, for which an energetically possible ground state transition has also been observed.

The 1925 keV transition proceeds to the ground state as shown by the negative coincidence measurements with the 294 keV and 328 keV lines (no. 20 and 21). These measurements suffice to establish the 1925 keV level. Additional support for this level results from experiments 22, 23 and 24.

The 2044 keV level is established by the negative result of experiment 25. In addition, measurements no. 26 and 27 show that the transitions of 1716 keV and 1422 keV probably originate in this level.

Coincidences no. 28 and 29 indicate that the 1786 keV transition proceeds to the 328 keV level, and this helps to establish a level at 2114 keV.

The negative result of experiment 30 establishes the 2164 keV level. Furthermore, no. 31 and 32 suggest that the 1836 keV transition might depopulate this state by way of the 328 keV level.

Coincidences no. 33 and 34 show clearly that the 1887 keV transition should be placed in cascade with the 328 keV transition so as to yield a state at 2216 keV, and according to no. 23 this state is also de-excited by the 1593 keV line.

Coincidences no. 35 and 36 indicate that the 1294 keV transition is in cascade with the 328 keV transition, but not with the 622 keV transition, thereby providing a 1623 keV level. The existence of this level is further supported by coincidence no. 37. Measurement no. 38 was taken in order to estimate the contribution of interfering lines in experiment 37. No. 39 and 40 suggest that the 1623 keV level is chiefly depopulated through the two first excited states, which seems to be corroborated by the conversion line intensities of depopulating transitions.

The 2086 keV transition is not completely coincident with the 328 keV line, as is seen from measurement no. 41. The line cannot be placed in a higher position, because the Q-value would then be exceeded. A plausible interpretation of these facts is that the 2086 keV transition consists of two unresolved components, one of which goes to the ground state and the other to the first excited state. This evidently implies new levels at 2086 keV and at 2414 keV. A similar situation seems to exist in the case of the 1736 keV line, according to experiments no. 42 and 43. The δ-values can be explained in terms of a 1736 keV doublet, which may be taken as evidence for at least one of the levels 2357 keV or 2064 keV. Indeed, both of these levels were established on energy arguments.

Coincidences no. 44 and 45 reflect the fact that the 1219 keV transition is de-excited through the 328 keV level and not through the 622 keV level, thereby establishing the 1548 keV level.

Measurements no. 46 and 47 show that the 1104 keV transition proceeds to the 328 keV level, because if it were located above the 1267 keV or the 923 keV levels experiment 46 would result in a higher value of δ.

The existence of a 1798 keV level may be inferred from coincidence results no. 48 and 49, although the estimated errors are rather high.

The coincidences no. 50 and 51, although not conclusive because of the high uncertainty, suggest that the 1676 keV line feeds the 622 keV level. The 1970 keV line to the 328 keV state is compatible with no. 52, which also supports the existence of the 2299 keV level.

The proposed 1962 keV level is de-excited by 1634, 1039, 529 and 164 keV transitions. The transition to the ground state is a very weak, unresolved line

with relatively uncertain determination of its energy. The coincidences between the 529 keV line and 294, 328 keV transitions (no. 53 and 54) seem compatible with the assumed position of 529 keV line. In addition, measurement no. 55 between the 164 keV and 1104 keV lines indicates a positive effect. Experiment no. 56 indicates that the counting rate in no. 55 cannot be attributed to coincidences with the L 1049 line. These results are in accord with the assumption that the 164 keV transition is feeding the 1432 keV level via the 365 keV transition, and this is further corroborated by experiments 71—74. The results no. 57—63 are compatible with two assumed position of the 483 keV transition.

Experiments 64, 65, and 66 may be taken to imply that the 365 keV and 1104 keV transitions are indeed coincident, in agreement with the proposed positions in the decay scheme.

The lines of 1151 keV and 1157 keV were not resolved in the lens spectrometer. Results no. 67 and 68 on the combination of these lines are, however, in agreement with the assigned positions. The same may be said about the transitions of 1175 keV and 1184 keV.

The assigned position of the 704 keV transition is fairly well supported by no. 75—77.

Experiments 78 and 79 indicate that at least one of the transitions at 1803 keV and 1806 keV is coincident with the 328 keV transition.

9. Discussion

Fig. 7 combines into a decay scheme the knowledge of levels and transitions presented in the preceding sections. This decay scheme comprises 93 transitions, which together depopulate 29 levels. Coincidence support was found for 25 of these levels, while the remaining four levels (at 1817, 1931, 1962, and 2142 keV) were derived from certain energy combinations which must be considered to be of high statistical significance. The results of the two independent modes of approach to the assignments of levels are evidently in such excellent agreement that one may have good confidence in the decay scheme as a whole.

The 14 transitions for which a location could not be found are all relatively weak, and three of them are even reported as doubtful. Four transitions may possibly be combined in the way shown to the right of the decay scheme proper, but this necessitates the inclusion of two new energy states.

The general pattern of transitions in the present decay is rather easily understood. Since the parent nucleus has spin and parity 1^-, it may decay by allowed or once forbidden transitions to levels with spin values 0, 1, or 2 and by generally slower first forbidden unique transitions to levels of character 3^+. From levels of spin-parity 0^+, $1^\pm$ and 2^+, transitions to the three

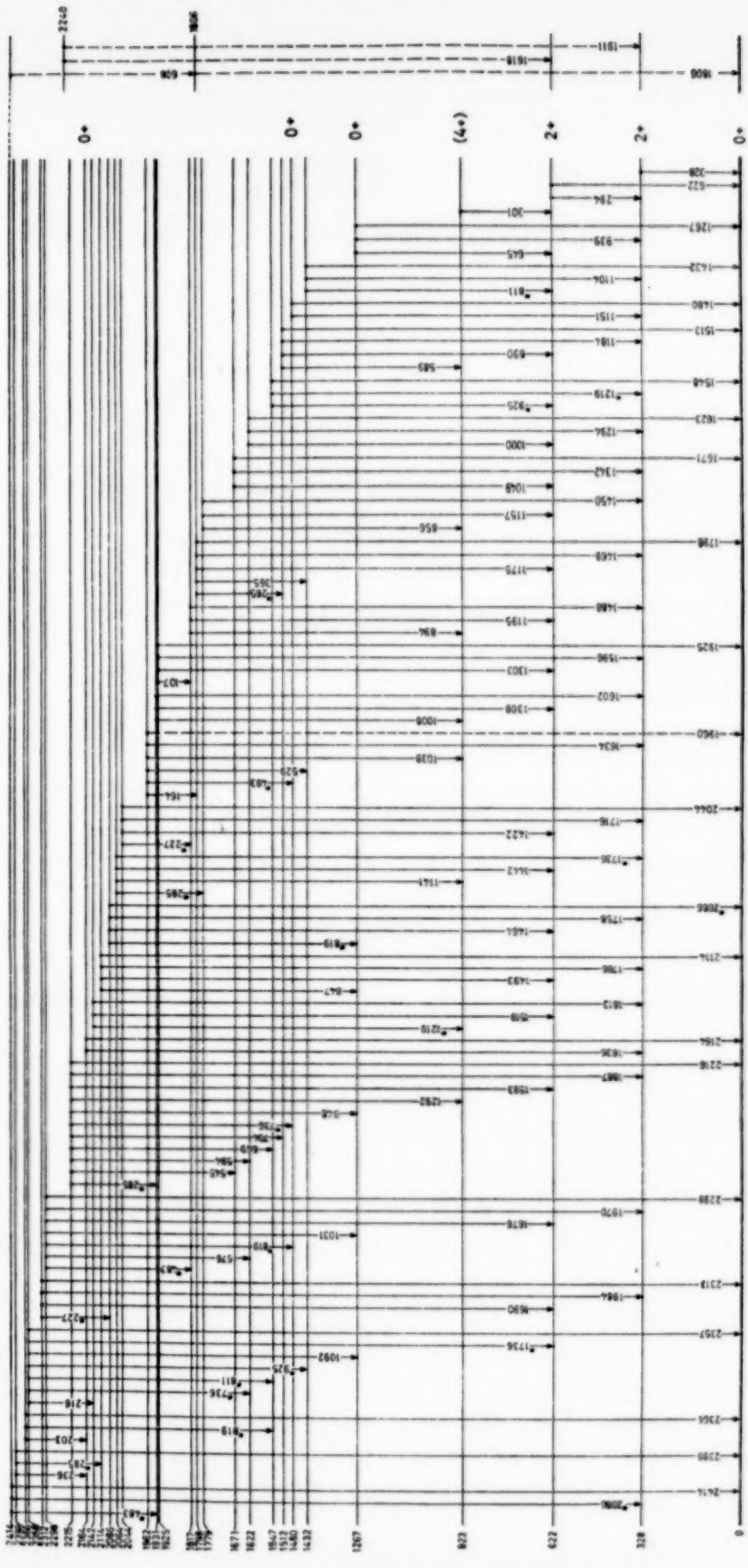

Fig. 7. The level scheme of Pt^{194} obtained from the study of Au^{194}. A plausible way of accounting for some additional transitions is shown to the right. Asterisks have been used to indicate that the intensity of a transition probably is shared between alternative locations in the level scheme.

lowest states (0^+, 2^+ and 2^+) may be expected to be observed with comparable intensities judging from existing knowledge on transition probabilities. In the cases of 0^- and 3^+, only the transitions to the 2^+ states should be seen, whereas for a 2^- state the ground state transition (M2) might be observed in competition with the E1 line to the 2^+ levels, because of the higher conversion coefficient of M2 and to the frequently observed retardation of low energy E1 transitions. Finally, levels of higher spin may of course be populated by two-step processes through high energy states.

It is already concluded from the statistical evidence of the preceding section that, in general, wherever two of the three lowest states are populated from a given level the third one is also populated. More exactly, there are some more relationships with the 294 keV transition than with 328 keV, and this suggests that a few levels should not have direct ground state transitions.

The 923 keV level decays exclusively to the 622 keV state with the emission of an E2 gamma ray. In order to account for the absence ($I_K < 5\times10^{-3}$) of a ground state transition, a spin of 3 or 4 has to be assumed. This assumption is strengthened by the observation that the 923 keV is fed from levels which also show no ground state transition and that feeding from levels possessing ground state transitions has been observed only in two cases. Furthermore, no beta-branch to the 923 keV level has been observed in the Ir^{194} decay, and in the decay of Au^{194} the conversion intensities may be explained without the assumption of direct feeding to this state. From these points of view, an assignment of 4^+ is the most probable one. The spin of the higher levels which lack ground state lines must also be expected to be high (3 or more) and the question of the manner in which they are populated arises. Direct population is of course possible in the case of 2^- or 3^+ levels. It is interesting to note, however, that the lines of 216, 227, and 483 keV fit as feeding transitions to the levels at 1817, 1931, and 2142 keV and that the rates of population and depopulation may well be equal.

As discussed in the multipolarity section the 1267 keV level should have spin parity 0^+, and this assignment is also reasonable in the light of the beta branching from Ir^{194} to this level as found by Johns and Nablo [2]). These authors report the value $\log f_0 t = 7.8$ which is approximately as expected for a transition from Ir^{194} (1^-) to a 0^+ level, whereas 3^+ is definitely ruled out.

When attempting to make a spin and parity assignment for the 1480 keV level, one is faced with conflicting evidence. The coincidence result as well as the lower limit of the conversion coefficient (table 5) indicate that the lowest multipole order possible for the 1480 keV line is M2 and that probably the conversion coefficient is even higher. The same level is also depopulated by the 1151 keV transition, and if one forms the ratio of conversion coefficients α (1480)/α (1151) by means of the gamma intensities of ref. [2]) and the present conversion line intensities, the result becomes 1.6×10^2, a value which is

incompatible with any spin assignment. It must therefore be concluded that the transitions of 1480 keV and 1151 keV found in this work may not both be identified with transitions reported in ref. [2]). The gamma intensity of the 1480 keV transition observed in the iridium decay is quite low, however, and the line may have been of other origin. Under this assumption, the data are in agreement with a 0^+ assignment for the level †. This conclusion would also agree with the fact that the log *ft*-value for the Ir decay to this level is the same as for the branch to the 0^+ state at 1267 keV.

Generally, the negaton decay and the electron capture decay to Pt^{194} should populate the same levels, although a negaton decay populates higher levels to a less extent and also, with Ir^{194}, the Q-value is lower. Bearing this in mind, one finds satisfactory agreement between the spectra from the present work with that from the decay of Ir^{194}. In fact, to each line reported by Johns and Nablo there is a corresponding strong conversion line in our spectrum. Conversely, however, there is no correspondence in the decay of Ir^{194} to the following prominent transitions reported here (keV): 948, 1049, 1104, 1593, 1596, 1887, and 1925. From the location that has been given to these lines in the present decay scheme, it is evident why the transitions of 948, 1543 and 1887 keV do not appear in the decay of Ir^{194}. The decay energy simply becomes too low for appreciable population of the 2216 keV state from which these transitions emerge. A similar explanation could also apply to the 1596 and 1925 keV transitions, while for the lines 1049 and 1104 it is more difficult to understand why they do not occur in the Ir spectrum.

The conclusion of Thieme and Bleuler that the 2164 transition is of M4 character must be modified. In view of the fact that the scintillation peak observed by these authors may have been due to the 2114 keV line, one now has to consider the alternative possibility of an E0 assignment. If the level at 2164 keV would have a spin of four or more, its direct population would be strictly excluded, and since no feeding transitions of sufficient intensity have been detected, an interpretation in terms of another 0^+ state seems necessary.

Pt^{194} with its 78 protons and 116 neutrons is not sufficiently far from closed shells to possess appreciable static deformation. The first two excited states have spin-parity 2^+ in conformity with the whole class of nuclei systematized by Scharff-Goldhaber and Wenezer [31, 32]). The theory of collective vibrations of spherical nuclei predicts a sequence of equidistant levels, on the assumption that the restoring force is of the simple harmonic type. Transitions between members of the vibrational band should have lifetimes short compared to the single particle estimate and be of the electric quadrupole character. Furthermore, such transitions are restricted by the selection rules $\Delta n = \pm 1$, where n is the phonon number. The first excited state of an even-even nucleus should

† The E0 character of the 1480 keV transition has since been proved in a photoelectron experiment [33]).

be of 2^+ character, while a second phonon may couple to the first one to produce the spin values 0, 2, 4. Similarly, a state composed of three phonons may have an angular momentum of up to 6 units. On the same assumptions as before, the level energies are simply the sum of the phonon energies and are independent of the total angular momenta.

In the present case, the level spacing is 328 keV and 294 keV respectively. Coulomb excitation data show that the 328 keV transition is indeed enhanced, and data from this and other works show that the 622 keV transition ($\Delta n = -2$) is hindered by a factor of 250 in comparison with the competing 294 keV transition ($\Delta n = -1$). Also, as seen from table 4, the 294 keV transition has a rather pure (> 97 %) E2 multipolarity. Agreement in these respects with the theory of collective motion has actually been reported in many cases [32]).

The 923 keV level, which is most likely of 4^+ character, is also quite probably of collective nature. Considering the selection rules, a quadrupole phonon number of 3 units is the only possible assignment, because the level decays strongly to a state with $n = 2$ but has not been observed to decay to the first excited state ($n = 1$), although a transition to this state may be masked by the 594 keV line. However, even when taking the intensity of the masking line as an upper limit for a hidden transition, one obtains the result that the E2 matrix element is at least 20 times lower for $\Delta n = 2$ than for $\Delta n = 1$ (391 keV). Finally, it is noted that the spin-parity is a possible one for a 3-phonon state and that the energy spacing has a quite reasonable value. Furthermore, the occurrence of states of this character may well be a general feature of undeformed nuclei, since other spherical nuclei which have been investigated at sufficiently high excitation energies, exhibit levels that could be classified analogously. The level sequence [33]) of Pt^{192} is 317 keV (2^+), 613 keV (2^+), and 921 keV, the last level being almost certainly of 4^+ character. According to the published gamma intensities, there exists in this case a corresponding inhibition of the transition from 921 keV to 317 keV in comparison to the transition to the 613 keV state, the ratio of the reduced lifetimes being 80. Considering that there is a difference of only two neutrons between these platinum isotopes, the remarkable similarity of level energies and branching ratios may possibly be explained as effects of single particle character. However, in another region of the periodic table one encounters the same features in the nucleus Te^{124}, where the corresponding level energies are 603 keV, 1326 keV, and 1972 keV [34]), and the inhibition factor is 100. The obvious obstacle to the interpretation of the third excited state as a 3-phonon state is the absence of levels of other possible spin values compatible with $n = 3$ and this applies of course also to the second excited state. It is for instance difficult to understand why no 0^+ level appears at approximately 622 keV, since such a state could be populated both directly and via higher states. An exact degeneracy does

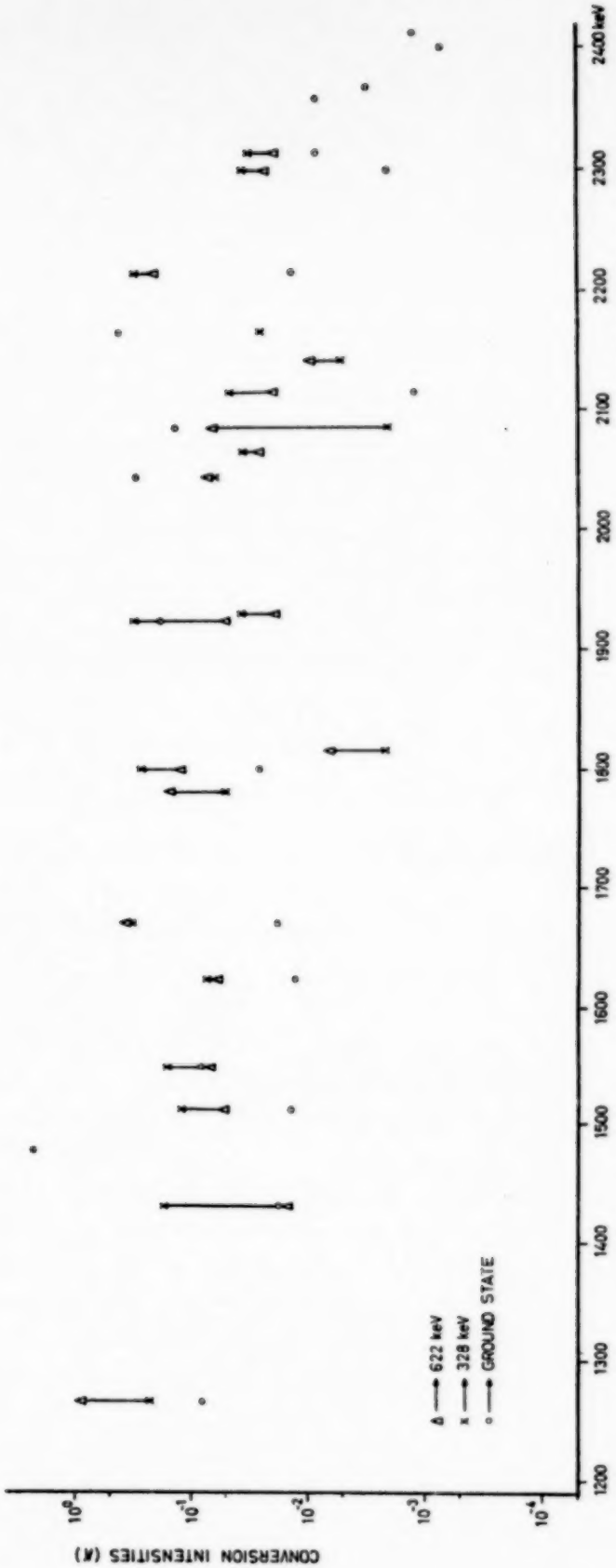

Fig. 8. Conversion intensities (K) for transitions to the lowest states from each level. Points corresponding to transitions to the 2+ states have been joined by vertical lines.

not seem possible for the reason that no evidence of a 0^+, 2^+, 0^+ sequence has been reported from angular correlation measurements on the 294-328 keV cascade.

The energy spacing between the 923 keV level and the next one at 1267 keV (0^+) is not far from the value of the phonon energy. However, an interpretation of this 0^+ level in terms of vibrational excitation meets with difficulties. If, for instance, the level is given the assignment $n = 4$, the transitions to the ground state and to the two lowest excited states all become forbidden, and theory predicts nothing about their intensity ratios. The explanation that this be a level of $n = 3$, shifted to higher energies, is unsatisfactory, since the inhibition of the two-phonon transition is relatively small, and on similar grounds $n = 2$ is of course excluded. On the other hand this level may be the result of a two-particle excitation. In view of the many possibilities of formation of 0^+ states, it seems aimless to discuss, at present, the origin of the higher levels of this type. It will only be pointed out that the transition branching to the two lowest states (0 and 328 keV) is very different for the 0^+ levels of 1267 keV and 1480 keV.

On the assumption that the nucleus retains its spherical shape in a state of intrinsic excitation, shape vibration may still take place with approximately the same phonon energy as with the ground state vibrations. The higher states could thus in principle be classified by their oscillator quantum numbers. At the present stage, with little multipolarity data available, such a classification can only be made on the basis of the selection rules, which are the same as before within the vibrational bands but which require $\Delta n = 0$ for inter-band transitions. Since the K-conversion intensities were expected to reflect rather well the gamma intensities, a plot was prepared for the conversion intensities to the ground state band versus level energy (fig. 8). It is seen that the intensities of lines to the $n = 1$ and $n = 2$ states are frequently the same within a factor of three. Moreover, four of the exceptions from this rule may be explained in terms of masked lines in the spectrum or of alternative positions of lines. Intensity ratios of an order of magnitude exist, however, for the levels of 1432 keV, 1925 keV, and 2086 keV. The even distribution of intensities to the 2^+ states may possibly be accounted for as a result of strong coupling between the intrinsic motion and the vibration, which is expected to lead to an admixture of oscillator states. Furthermore, some states of intrinsic excitation which according to the theory of vibrations should decay exclusively to the ground state, may have been overlooked in the present work, because of the special method used in arriving at the levels.

The authors take great pleasure in expressing their gratitude to Professor Kai Siegbahn for his stimulating interest in the present investigation. One of us is also indebted to Professor A. Bohr, Copenhagen, for a discussion on

the collective model. We further thank Miss I. B. Svensson and Mr. W. Parker for their essential contribution of performing the numerous chemical separations, and also Mr. A. Bäcklin for his frequent assistance in taking data. For one of us, J. B., the stay at the institute was made possible by a UNESCO fellowship. This work was financially supported by the Air Research and Development Command, USAF.

Note added in proof: A recently completed work on the decay of Ir^{194} (G. Bäckström and J. Kern, to be published) has disclosed the existence of many additional transitions, which necessitates essential modifications of the previous decay scheme, due to Johns and Nablo. The puzzling gamma ray of 1478 keV, which seemed to connect two states of 0^+ character, has now been shown to be identical with the transition of 1488 keV reported in this paper. The conversion line corresponding to the E0 transition of 1480 keV has also been found to exist in the iridium decay.

The 301 keV transition was found in the decay of Ir^{194} as well, and the possibility of a direct population cannot be excluded at present. It should be pointed out that the theory of Davydov and Filippov, although not strictly applicable to this nucleus because of the energy ratio of the 2^+ states, does predict a 3^+ level at 951 keV, and that the gamma ray branching for our 923 keV level may be in agreement with this theory.

The new results on the iridium decay generally support the level scheme proposed here.

References

1) M. T. Thieme and E. Bleuler, Phys. Rev. **102** (1956) 195
2) M. W. Johns and S. V. Nablo, Phys. Rev. **96** (1954) 1599
3) D. E. Alburger, Phys. Rev. **108** (1957) 812
4) C. E. Mandeville, J. Varma and B. Saraf, Phys. Rev. **98** (1955) 94
5) N. P. Heydenburg and G M. Temmer, Phys. Rev. **93** (1954) 906
6) F. K. McGowan and P. H. Stelson, Phys. Rev. **106** (1957) 522
7) Reynolds, Christensen, Hooke, Hamilton, Stroke, Ewbank, Nierenberg, Shugart and Silsbee, Bull. Am. Phys. Soc. **2** (1957) 317
8) Wilkinson and Hicks, ed. W. Meinke, Chemical Procedures used in Bombardment Work at Berkeley UCRL - 432
9) A. Hedgram, K. Siegbahn and N. Svartholm, Proc. Phys. Soc. A **63** (1950) 960
10) G. Bäckström, Nuclear Instruments **1** (1957) 253
11) K. Siegbahn and K. Edvarson, Nuclear Physics **1** (1956) 137
12) E. Arbman and N. Svartholm, Arkiv Fysik **10** (1956) 1
13) N. Ryde and B. Andersson, Proc. Phys. Soc. B **68** (1955) 1117
14) O. Beckman and P. Bergvall, Arkiv Fysik (in course of publication)
15) D. A. Lind and A. Hedgran, Arkiv Fysik **5** (1952) 29
16) D. E. Muller, H. C. Hoyt, D. J. Klein and J. W. Du Mond, Phys. Rev. **88** (1952) 775
17) G. Bäckström, O. Bergman and J. Burde, Nuclear Physics **7** (1958) 263
18) S. Fine and C. F. Hendee, Nucleonics **13** (1955) 36
19) G. Bäckström, to be published
20) L. L. Baggerly, P. Marmier, F. Boehm and J. W. M. Du Mond, Phys. Rev. **100** (1955) 1364

21) G. T. Ewan and A. L. Thompson, Proc. Roy. Soc. Canada **47** (1953) 126
22) R. A. Naumann, Bull. Am. Phys. Soc. **1** (1956) 42
23) S. K. Haynes and W. T. Achor, J. Phys. Radium **16** (1955) 635
24) P. Staehelin, Phys. Rev. **87** (1952) 374
25) R. M. Steffen, O. Huber and F. Humbel, Helv. Phys. Acta **22** (1949) 167
26) P. J. Cressman and R. G. Wilkinson, Phys. Rev. **109** (1958) 872
27) G. T. Ewan, Can. J. Phys. **35** (1957) 672
28) M. S. Huq, Nuovo Cimento **5** (1957) 1456
29) M. E. Rose, Internal Conversion Coefficients (North Holland Publishing Company, Amsterdam, 1958)
30) T. R. Gerholm, Rev. Sci. Instr. **26** (1955) 1069
31) G. Scharff-Goldhaber and J. Weneser, Phys. Rev. **98** (1955) 212
32) G. Goldhaber, ed. S. Meshkov, Proc. of the Univ. of Pittsburgh Conference 1957, p. 447
33) Bäckström and Bergman, to be published
34) I. Marklund, B. van Nooijen and Z. Grabowski, Nuclear Physics **15** (1960) 533

1.B:2.B

Nuclear Physics **15** (1960) 609—625; © *North-Holland Publishing Co., Amsterdam*

Not to be reproduced by photoprint or microfilm without written permission from the publisher

POLARIZATION IN PROTON-PROTON SCATTERING NEAR 3.3 MeV

I. ALEXEFF and W. HAEBERLI

University of Wisconsin, Madison, Wisconsin †

Received 27 November 1959

Abstract: The polarization in proton-proton scattering was measured for energies near 3.3 MeV and scattering angles of $\theta_{c.m.} = 30°$, 45°, and 53°. The purpose of the experiment was to remove some of the ambiguities in the proton-proton scattering phase shifts at low energies. Protons were first scattered from gaseous hydrogen. The scattered protons were then scattered from helium, and the right-left asymmetry was measured by means of two counter telescopes. The gas density of the helium target was increased locally by cooling with liquid air. Corrections on the observed polarization of up to 0.6 % were applied to compensate for a number of experimental effects. The following values for the polarization were found: $\theta_{c.m.} = 30°$, $P = (0.07 \pm 0.16)$ %; $\theta_{c.m.} = 45°$, $P = (0.25 \pm 0.16)$ %; $\theta_{c.m.} = 53°$, $P = (0.58 \pm 0.24)$%. These values are averages of measurements at slightly different proton energies. The errors are standard deviations and include all known uncertainties.

1. Introduction

The study of the proton-proton interaction is one of the fundamental problems in nuclear physics. From accurate measurements of the differential scattering cross section one knows that for energies of a few MeV only S-wave scattering is important. Above 10 MeV P- and D-wave scattering becomes apparent [1]). It is well known, however, that differential cross-section measurements do not allow the individual P-wave phase shifts $^3P_0$, $^3P_1$, $^3P_2$ to be determined. As long as the P-wave phase shifts are small, only a certain linear combination of the three P-wave phase shifts, the "effective P-wave phase shift", can be determined. Although for proton energies of a few MeV the effective P-wave phase shift is known to be essentially zero, there is no *a priori* reason to assume that there is no P-wave scattering present. Hull and Shapiro [2]) and MacGregor [1]) have shown that P-wave phase shifts of up to a few degrees are possible without contradicting the observed angular distributions. Even larger P-phase shifts are possible if a small amount of D-wave scattering is also included. These phase shift solutions imply the presence of spin-orbit coupling in the P-state and should therefore produce polarization in proton-proton scattering. The purpose of the present experiment was to measure this polarization. While polarizations of several percent are possible with some sets of phase shifts, the polarization is generally expected to be rather smaller than

† Work supported by the U. S. Atomic Energy Commission and by the Graduate School from funds supplied by the Wisconsin Alumni Research Foundation.

that. Consequently the experiment was designed to detect a polarization of a fraction of one percent.

For proton energies below 100 MeV two other polarization experiments have been reported. For protons of 17.7 MeV scattered by hydrogen through a centre-of-mass angle of 60° Brockman [3]) found a polarization of (1.2 ± 2) % †. Palmieri *et al.* [4]) reported measurements for proton energies of 46 MeV and above. The polarization was found to rise smoothly from (1.3 ± 1.3) % at 46 MeV to about 13 % at 100 MeV.

2. Apparatus

2.1. GENERAL DESCRIPTION

The familiar double-scattering arrangement is used. The polarization of protons scattered by protons is found from the left-right asymmetry which

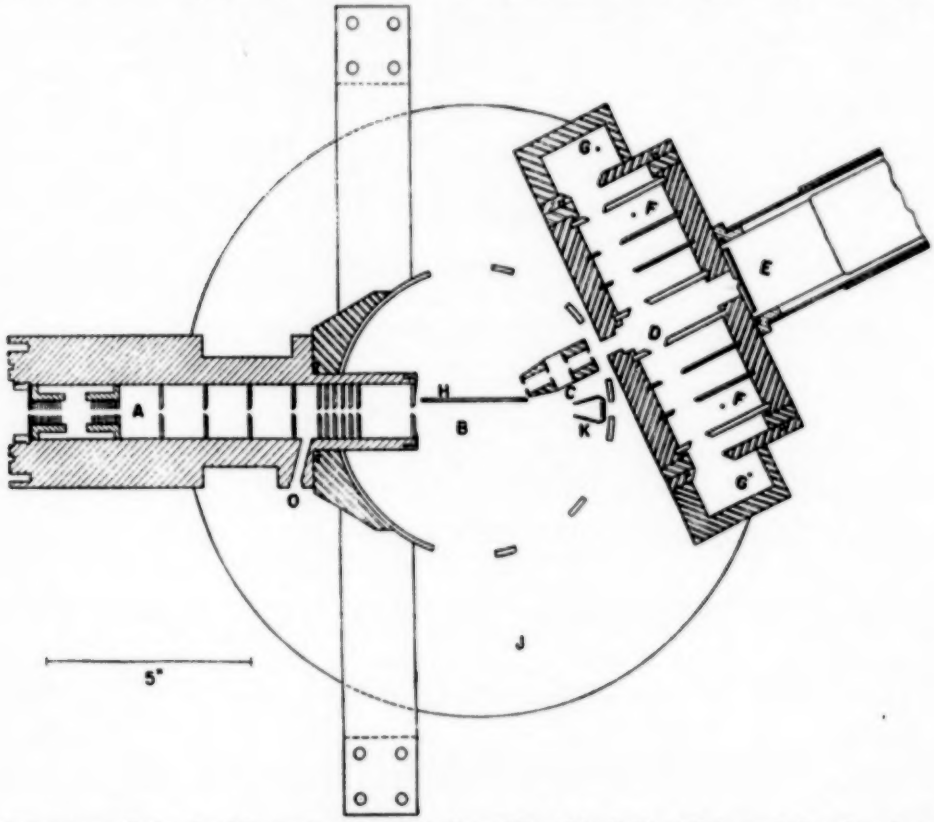

Fig. 1. Top view of the double-scattering chamber. The thin foils which seal the chambers are not shown.

A. Differential pumping system
B. First scattering region
C. Slits for first scattering
D. Second scattering region
E. CsI(Tl) scintillation counter
F. Inner proportional counters
G. Outer proportional counters
H. Auxiliary shield
J. Turntable carrying second chamber
K. Retractable collector cup.

† In this paper the positive direction of polarization is chosen in the direction of the vector $\mathbf{k}_0 \times \mathbf{k}$, where $\mathbf{k}_0$ and $\mathbf{k}$ are the propagation vectors of the incident and outgoing beam, respectively. This is opposite to the convention used in ref. [3]).

results when the scattered protons are scattered from helium. For proton energies near 2.2 MeV and scattering through a laboratory angle of 90°, helium is an almost perfect polarization analyser.

Drawings of the double-scattering equipment are shown in figs. 1 and 2. The proton beam enters the first scattering chamber through the differential pumping column A. The first scattering occurs in the hydrogen at point B. The proton-proton scattering angle is selected by the slits C. Scattered protons

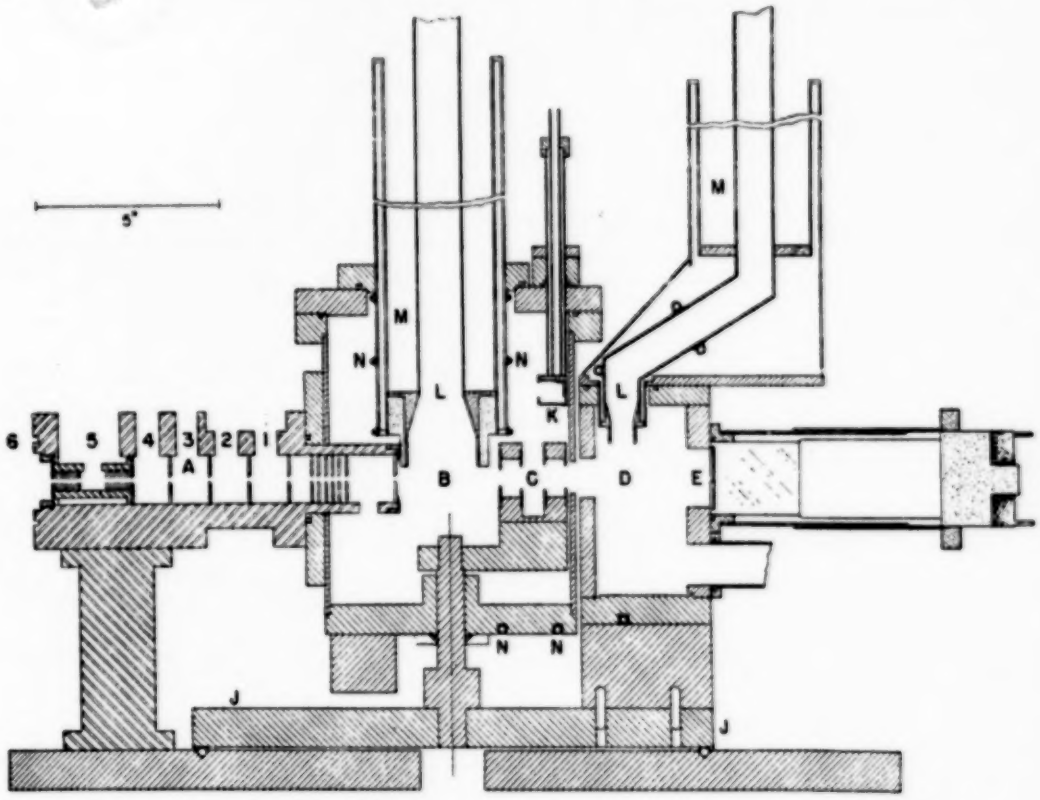

Fig. 2. Side view of the double-scattering chamber. The second scattering chamber is in the zero-degree position. The collector cup K is retracted from its normal position; L are the nozzles through which cold target gas falls; M are volumes filled with liquid air; N are water lines. The other symbols are the same as those of fig. 1.

after passing through these slits go through a thin Mylar† window, cross a small air gap, and enter the second scattering chamber through another thin Mylar window. The slits C are rigidly connected to the axle of the turntable J. The second scattering chamber is bolted to the edge of this turntable. Thus the polarizer slits and the chamber always move together.

The second scattering chamber is filled with helium. Scattering occurs at point D. Protons scattered to either the left or the right through 90° are counted by the adjacent counters F and G in coincidence. Protons not scattered in the second scattering chamber enter the scintillation counter E. It serves to meas-

† Mylar foils supplied by E. I. DuPont de Nemours and Co., Wilmington, Delaware.

ure the proton energy at the helium scatterer and to check the contamination in the hydrogen gas. These procedures are described in section 3.

Both chambers are kept at atmospheric pressure. This pressure represents a compromise between high counting rate and high energy loss of the protons in the gas. The counting rate can be increased without appreciably increasing the energy loss by cooling the target volume to liquid-air temperature, keeping the rest of the scattering chamber at room temperature. The dewars M in fig. 2 serve for this purpose. Cold gas streams continually into the scattering chambers through the nozzles L and falls smoothly under gravity. The counting rate of double-scattered protons was about eight times higher with the cool targets than with the targets at room temperature.

2.2. DIFFERENTIAL PUMPING COLUMN

The high-vacuum system of the electrostatic accelerator is separated from the hydrogen in the first scattering chamber by the differential pumping system. The apertures consist of tantalum discs with circular holes of 1 mm diameter. To reduce scattering of the incident beam all aperture edges exposed to the beam were made only 0.1 mm thick. The last aperture has a diameter of 2 mm. This aperture prevents protons scattered from the preceding beam-defining aperture from entering the slit system C (fig. 1).

Six pumps are used to drop the pressure from one atmosphere in the chamber to 10^{-5} mm Hg at the far left of fig. 2. For stages 1 through 4 (fig. 2) mechanical pumps were used with free air displacements of 7.2, 7.2, 3.3 and 3.3 l/sec, respectively. Stages 5 and 6 were pumped on with 20 l/sec diffusion pumps. Stages 4 and 5, and stages 5 and 6 were separated from each other by 12 apertures in series. In the rest of the pumping column only one aperture per stage was used, since experiments showed that in the high pressure region (*i.e.*, where the mean free path is short compared to the dimensions of the apertures) the impedance of several apertures in series is primarily that of the last aperture of the group.

The system thus far described consumed gas at a rate of about 2 m^3 per hour. To reduce the gas consumption to a more convenient level the pumped gas was recirculated. Since in the scattering chamber high gas purity must be maintained, the exhaust of the first-stage pump was fed not into the chamber itself but rather into a point (0 in fig. 1) intermediate between the chamber and the first pump. This point is separated from the chamber by six apertures, which makes it unlikely that hydrogen contaminated with pump oil diffuses back into the chamber. No such difficulties were experienced. To prevent the differential pumping apertures from becoming excessively contaminated with oil, a number of oil-removing filters were installed in the feedback line. Recirculation of the pumped gas reduced gas consumption by a factor of 7.

2.3. FIRST SCATTERING CHAMBER

The first scattering chamber contains the slits C which are made of Stellite †. The front and rear slits which define the angle of acceptance form rectangular apertures 3.5 mm wide and 12.7 mm high. The beam stop K is a hollow tantalum box which can be retracted vertically to allow the slit system to rotate through zero degrees. The beam is stopped in a gold target. The temperature of a thermocouple spot-welded to the target gives a measure of the proton beam intensity. The scattered protons leave the first scattering chamber through a 0.006-mm thick Mylar window, cross a 3-mm air gap and enter the second chamber through a similar window. The Mylar films are not shown in figs. 1 and 2.

2.4. SECOND SCATTERING CHAMBER

The second scattering chamber is shown in fig. 1. The gas in the scattering region D is cooled by a cold gas column. To minimize thermal contraction of the slits they are made of Invar. The slits next to D and the slits between the counters F and G are the defining apertures. The rear aperture is 1 cm wide and 6 cm high. The slits in the first scattering chamber rather than those in the second determine the height of the target volume D.

The proportional counters which detect double-scattered protons consist of 0.05-mm tungsten wires placed to one side of the scattered proton beam. Although the counting volumes are not separated by foils or grids it was found that there is no interaction between them. To improve the counting characteristics of the helium gas, 3 % of hydrogen was added.

The monitor counter which is attached to the rear wall of the second chamber (fig. 2) is a CsI(Tl) scintillator, about 0.1 mm thick, attached to a phototube through a light pipe. The active part of the scintillator was defined by an aperture with a 1-mm hole placed over the crystal.

2.5. COLD GAS COLUMN

The cold gas columns which are used to increase the density of the target gas consist essentially of vertical pipes which are cooled on the outside with liquid air. Target gas enters at the top of the pipe and emerges as a laminar flow of cold gas through an opening L at the bottom (fig. 2). The shape of the opening is chosen to conform to the desired target dimensions. Tests with a Schlieren optical system showed that the boundaries of the cold region are sharp and stationary for several centimeters below the end of the nozzle. The cold gas simply falls under gravity in the surrounding volume of warmer gas.

The bottom of the dewar on the first scattering chamber is insulated with Styrofoam ††. Protons scattered from the lower end of the copper pipe are

† An alloy of cobalt, chromium, and tungsten. Alloy 98—M2 supplied by Hayes Stellite Company, Kokomo, Ind., U.S.A.

†† Foamed polystyrene.

prevented from entering the slits C by the auxiliary shield H (fig. 1). When some nitrogen was added to the hydrogen of the first scattering chamber the proton beam produced easily visible fluorescence of the gas, which showed that the cold gas column in the first scattering chamber functioned properly in the presence of the beam. The cold target gas was visible as a uniformly bright region against the less intense light in the warm part of the chamber.

The helium cold gas column of the second scattering chamber is similar to the one of the first chamber. An acoustic pump [5]) draws the helium from the port at the rear of the chamber and returns it to the top of the cold gas column. Density profiles in the cold helium scattering volume were measured with a thermocouple probe. With the acoustic pump in operation the density profiles were flatter and more reproducible than without it. Both scattering chambers were prevented from getting cold by appropriately placed water lines.

Each cold gas column increased the counting rate of double-scattered protons by a factor of 2.8. The hydrogen target was cooled only in the first measurements. Sufficient counting rates were obtained without it and its omission reduced the energy loss of the incident proton beam by almost 100 keV, so that the accelerator could be operated at a somewhat lower voltage.

2.6. ACCURACY OF ALIGNMENT

The alignment of the chamber was checked after construction and some trial runs with the following results:

1. Slit size and slit separation of left- and right-hand counters were identical to better than 1 percent. The scattering angle of each of the two counters was equal to 90° within 0.3°. Asymmetries of these counters are cancelled by averaging measurements at θ and $-\theta$ as discussed in section 5.

2. The angle θ_1 which the centre line of the first slit system C made with the axis of the beam collimator was known to within 0.1 degree.

3. The axis about which slits and second scattering chamber rotate is supposed to intersect the axis of the beam collimator. This requirement was satisfied to better than 0.15 mm.

4. The centre line of the slit system C is supposed to pass through the axis of rotation of the slits. This requirement was satisfied to better than 0.1 mm.

Only the more important features of chamber alignment are mentioned here. The effect of misalignment on the results is discussed in section 5.

3. Measurements

3.1. INCIDENT BEAM ENERGY

Over the past decade the beam deflection system which was used with the Wisconsin electrostatic generator consisted of a combination of magnetic and electrostatic deflections. Normally the beam is first deflected magnetically by

15°, and passes then in turn through a pair of "energy control slits", which supply a feedback signal to the accelerator to keep its energy constant, and through a 90° cylindrical electrostatic analyzer. In the present experiment, however, the beam was not passed through the electrostatic analyzer. Rather the beam entered the scattering chamber directly after having passed through the energy control slits. Since the beam now by-passed the electrostatic analyzer, its energy had to be measured separately. To this end the electrostatic analyzer was used essentially as a reaction product spectrograph. A thick tantalum target was so positioned in the beam that protons scattered by the target through 120° could pass through the analyzer and be detected by a counter. The energy of the proton beam incident on the target was then derived from the voltage on the analyzer which just still allowed scattered protons to reach the scintillation counter. The accuracy of the beam energy measurement was ± 0.1 %.

The energy of the protons at the centre of the first scattering chamber differs from the energy of the incident beam by the energy loss which the beam suffers in passing through the differential pumping system and through part of the hydrogen in the scattering chamber. To measure this energy loss the resonance which occurs in the $O^{16}(p, p)O^{16}$ cross section at 2.66 MeV [6]) was used. A small amount of oxygen in the form of water vapor was added to the hydrogen and the apparent shift of the resonance energy was observed. The energy loss was found to be 230 ± 10 keV, which agrees with the value computed from the known stopping power [7]) of hydrogen. For other incident proton energies the energy loss was computed from the known variation of stopping power [7]) with proton energy.

3.2. GAS PURITY

The polarization of protons scattered by protons is expected to be quite small. Since protons scattered from impurities in the hydrogen gas could possibly be strongly polarized, high purity of the hydrogen gas was important in this experiment. Mass spectrographic analysis of a number of tanks of commercial electrolytic grade hydrogen showed that the only impurities are oxygen, water, and nitrogen. By passing the hydrogen through several "Deoxo" catalytic purifiers † oxygen combines with hydrogen to form water which is then removed by liquid air traps. The remaining nitrogen contamination varied appreciably between different tanks. By selecting the better ones, hydrogen with a maximum contamination of 1 part of nitrogen to 10^4 parts of hydrogen was obtained.

During the polarization measurements the gas purity was monitored at frequent intervals with the monitor counter. Protons scattered from nitrogen

† "Deoxo" catalytic purifier, 5 C.H.F., 50 psi, manufactured by Baker and Co., Inc., 113 Astor St., Newark, New Jersey, U.S.A.

are more energetic than those scattered by hydrogen and can be counted separately. Fig. 3 shows a typical pulse height spectrum of the monitor counter output. It was obtained during measurements at a scattering angle of 22.5° and a proton energy of 3.28 MeV. To show the contamination peak more clearly its scale was expanded by a factor of 64. The relative areas under the two peaks of

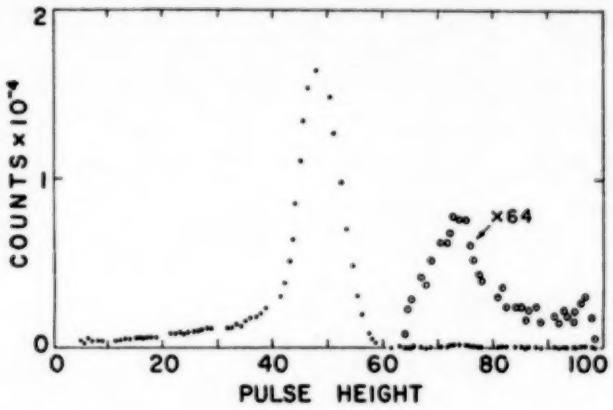

Fig. 3. Pulse height spectrum of protons in the second scattering volume, observed with a CsI(Tl) scintillator. The peak near 50 pulse height units is due to protons which in the first scattering chamber were scattered by hydrogen. The peak near 70 pulse height units is caused by protons scattered by heavier gas impurities (nitrogen) in the first scattering chamber. The scale of the second peak is expanded by a factor of 64.

the pulse-height spectrum is a measure of the number of protons scattered from contaminants relative to the number scattered from hydrogen.

3.3. PROTON ENERGY IN SECOND SCATTERING CHAMBER

The energy of the protons leaving the first scattering chamber depends on both the accelerator energy and the proton-proton scattering angle. The energy of protons in the helium scattering volume was kept constant throughout the experiment by placing appropriate combinations of Mylar foils in the air gap between first and second scattering chambers. The energy of the protons at the centre of the helium scattering volume was chosen to be 2.2 MeV.

The thickness of Mylar foil necessary to obtain the desired proton energy was determined experimentally by means of the monitor counter which was repeatedly calibrated with protons of known energy. In three of the runs no foil was used. They are those runs of table 1 for which at a given scattering angle the incident proton energy is the lowest. In these cases the incident proton energy was adjusted to give the desired energy in the helium scatterer.

To find from the energy of the protons at the scintillator the proton energy at the centre of the helium target, one must compute the proton energy loss in the helium between these two points. This computation is somewhat uncertain because the cold gas column produces a temperature distribution in the helium

gas which in some parts of the gas volume is not known accurately. Taking into account all uncertainties the energy at the centre of the helium volume was 2.20 ± 0.08 MeV.

3.4. COUNTS DUE TO NEUTRONS

Neutrons appeared to originate in the differential pumping system. To test for counts in the proportional counters caused by neutrons alone, a shutter was placed between first and second scattering chambers to stop protons. About one coincidence count per minute was observed, compared to a single neutron counting rate in each proportional counter of about 60 per minute. This coincidence rate is much too large to be explained by accidental coincidences. Rather the counts must be interpreted as being true coincidences caused by recoils penetrating the two adjacent proportional counters Since the neutron background increased with increasing proton bombarding energy, in the later part of the experiment the counter wires of counters F (fig. 1) were moved one baffle space further from counters G. This reduced the neutron coincidence rate by a factor of 4.

In the actual experiment an additional possible source of neutron-induced counts arises from accidental coincidences between neutron pulses in the outer counters, G, and proton pulses in the inner counters, F. This source has to be considered, because a large fraction of the pulses in the inner counters are caused by protons which do not reach the outer counters, and thus are not true coincidence counts. The single counting rate in the inner counters was particularly high after they had been moved closer to the helium target volume D. However, tests showed that even in this case accidental coincidences caused an error in the measured polarization of less than 0.01 %.

3.5. POLARIZATION MEASUREMENTS

For each measurement somewhat more than 10^5 double-scattered protons had to be detected in each set of counters. The data were taken in short runs, each comprising about 5000 counts. These runs were alternated between the proton-proton scattering angles of θ and $-\theta$. With a proton beam of 3 microamperes, the counting rate varied between about 300 and 600 per minute.

Each pair of proportional counters F and G was connected to a simple dual-diode coincidence circuit which had the property of passing the lower of the two pulses entering it. Hence, the output of each coincidence circuit gave a crude idea of the proton pulse height distribution in one of the counters. The coincidence circuits were connected to scalers which were equipped with pulse height discriminators. To insure that a scaler failure would be quickly detected, each coincidence circuit fed two scalers in parallel. In addition the coincidence pulse height spectrum was displayed on a 100-channel pulse height analyzer. Pulses from a pulse generator were superimposed on the spectrum to mark the minimum

pulse height accepted by the scalers. A sample spectrum is shown in fig. 4. It illustrates that double-scattered protons produce a clear, although fairly

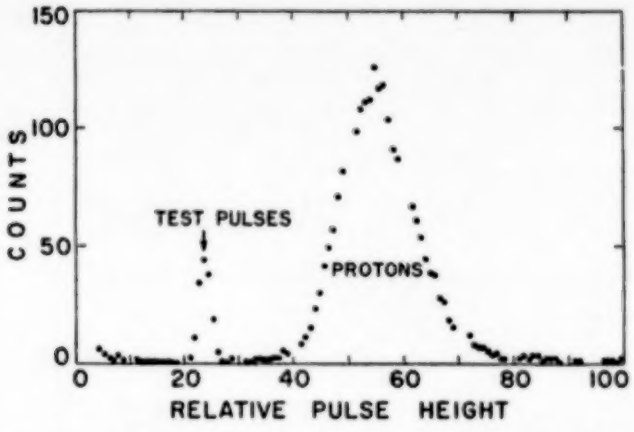

Fig. 4. Pulse height spectrum of double-scattered protons. The peak labelled "test pulses" marks the pulse height to which the threshold of the scalers was set.

broad, peak with few pulses above and below the peak. Thus the setting of the scaler threshold is not critical, particularly since runs at scattering angles $+\theta_1$ and $-\theta_1$ are alternated.

4. Reduction of Data

4.1. UNCORRECTED ASYMMETRY

The counting rate of double-scattered protons in the two counters is related to the polarization by

$$P_1 P_2 = e = \frac{N_R - N_L}{N_R + N_L} = \frac{r-1}{r+1}. \tag{1}$$

The subscript R refers to the counter which detects protons deflected twice in the same sense, L to the detector of protons which have been scattered first in one sense and then in the other. The relative counting rate

$$r = N_R/N_L \tag{2}$$

will be called the right-left ratio while e will be referred to as the asymmetry. The quantity P_1 is the polarization of protons after the first scattering, P_2 is the polarization in p—α scattering. Of course, both P_1 and P_2 depend on scattering angle and on energy.

Eq. (1) assumes that both counters have identical solid angles of acceptance and identical counting efficiency. The asymmetry of the counters cancels if the left-right ratio r is taken as the geometrical mean of the left-right ratios r' and r'' measured for first scattering angles $+\theta_1$ and $-\theta_1$:

$$r = N_R/N_L = (r'r'')^{\frac{1}{2}}. \tag{3}$$

Also the relative solid angle of acceptance K of the two counters may be determined from $K = (r'/r'')^2$. In this experiment K was found to be equal to 1.005 ± 0.0016, which indicates that the two counters were almost identical.

The asymmetries obtained from the measurements by eqs. (1) and (3) for different bombarding energies and scattering angles are given in column 4 of table 1. The errors shown are standard deviations due to the statistical uncertainty.

In the remainder of this section corrections will be discussed. Since all corrections are small, cross terms between them can be neglected. Therefore the corrections due to various effects will be computed separately, and added individually to the uncorrected asymmetry.

4.2. CORRECTIONS FOR GAS CONTAMINATION AND NEUTRONS

A certain fraction of protons reaching the detectors are protons which in the first scattering chamber were scattered from gas contaminants rather than from hydrogen. Therefore the measured asymmetry $e' = (N'_R - N'_L)/(N'_R + N'_L)$ differs somewhat from $P_1 P_2$. A correction for this can be applied if each measurement is repeated with hydrogen gas the contamination of which is artificially increased by a known factor. Since the only detectable gas impurity was nitrogen, each measurement was repeated with the nitrogen concentration increased by a factor of ten to a few hundred, which corresponds to nitrogen concentrations in the order of one-tenth percent.

In order to evaluate this correction the actual number of detector counts N'_R, N'_L is represented as the sum of counts due to protons scattered from hydrogen N_R, N_L and counts due to scattering from contaminants n_R, n_L. One finds that the correction α which is to be added to the observed asymmetry e' may be expressed as

$$\alpha = (e' - e'') \frac{n_R + n_L}{N_R + N_L}, \tag{4}$$

where e'' is the asymmetry observed with the artificially increased gas contamination. In the above equation it is assumed that the contamination is increased by a factor $f \gg 1$. The contamination correction is listed in table 1. The ratios $(n_R + n_L)/(N_R + N_L)$ were approximately 0.01. They were deduced from the monitor counter pulse height spectra (fig. 3).

The number of neutron counts can be measured directly and can simply be subtracted from the total number of counts. The neutron correction of table 1 indicates the amount by which the asymmetry is increased by the subtraction of neutron counts. The ratio of neutron to proton counts was always less than 0.02. The neutron corrections are generally less than 0.1 percent.

4.3. GEOMETRICAL CORRECTION

In addition to the asymmetry caused by polarization, a left-right asymmetry arises from the finite size of the beam apertures. The asymmetry stems from the fact that the intensity and the energy of protons in the second scatterer is different for elements of the scatterer close to one counter from elements of the scatterer close to the other counter. In order to evaluate the magnitude of this asymmetry, the double-scattered flux entering the counters was expressed as an integral over first- and second-scattering volume and counter apertures. To carry out the integration the integrand was expanded in terms of slit widths over slit separations, taking into account terms up to third order. The cross sections in first and second scattering, σ_1 and σ_2, as a function of scattering angle and proton energy were expressed as a Taylor series which included terms up to second order. Details of this calculation will be published separately [8]). One then obtains an expression for the asymmetry which, besides the apparatus dimensions and the scattering angles, contains derivatives of the cross sections with respect to angle and proton energy: $(\partial\sigma_1/\partial\theta_1)$; $(\partial\sigma_2/\partial\theta_2)$; $(\partial^2\sigma_2/\partial\theta_2\partial E_2)$, $\partial\sigma_2/\partial E_2$. The variation of the incident proton energy in the hydrogen target with position was found to be negligible. Consequently no derivative of σ_1 with respect to energy appears in the correction. Similarly the change of proton energy E_2 in the second scatterer due to varying distance traversed in the gas was neglected. However, the differentiation of σ_2 with respect to energy still appears because the proton energy in the second scatterer depends sensitively on the first scattering angle θ_1. The reason that the change of E_2 with θ_1 is more important than the change of E_2 with distance is that the former produces a left-right asymmetry of proton energies in the second scatterer while the latter does not. Also neglected in the correction is the finite diameter of the beam from the accelerator. Since the beam is scattered very little in the hydrogen gas the beam diameter is only slightly larger than 0.1 cm.

The derivative of the proton-proton cross section σ_1 with respect to angle was obtained by numerical differentiation of published p—p cross sections [9, 10]). For the computation of the derivatives of the proton-helium cross section σ_2 with respect to energy and angle an expression was derived for these derivatives in terms of the scattering phase shifts and the rate of change of the phase shifts with energy. Numerical results were obtained by using the p—α phase shifts of Critchfield and Dodder [11]). It should be pointed out that, as long as the phase shifts accurately describe the experimental cross sections, this procedure does not assume that the phase shifts themselves are the correct nuclear phase shifts. Rather the phase shift expansion is only being used as a means of interpolating between measured cross sections.

The geometrical corrections so obtained vary between 0.41 and 0.64 percent (table 1). The corrections are largest for $\theta_1 = 15°$, due to the large rate of

change of σ_1 with θ_1. For the other two scattering angles the largest contribution to the correction comes from the term which contains $(\partial^2\sigma_2/\partial\theta_2\partial E)_2$.

Since the corrections are relatively large, it is important to estimate their uncertainty. The quantities in terms of which the correction was expanded are ratios of slit widths over slit separation. The correction is due to a second order term in these variables. All odd terms vanish. We did not attempt to compute the fourth order term. The assumption that the fourth order term is small compared to the statistical uncertainty of ± 0.2 % is probably justified since the ratios of slit width over slit separation which enter have a maximum value of 0.09.

Errors in the correction may also be caused by errors in the cross section derivatives. Some of these are hard to estimate, but they probably do not cause errors of more than 10 % of the correction. The largest known error of the correction is due to the uncertainty in the proton energy at the centre of the helium target (section 3.3). The uncertainty of the geometrical correction given in table 1 is based on an energy uncertainty of ± 110 keV, which is a conservative estimate. The values were obtained by recalculating the geometrical corrections for a different proton energy in the helium volume.

5. Results and Errors

The results are summarised in table 1. The first three columns list the run number, the energy at the centre of the hydrogen target, and the angle at which the proton-proton scattering occurred. It is apparent from the table that

TABLE 1

Summary of results and corrections †

Run number	Energy (MeV)	θ_{lab}	Uncorrected asymmetry in percent	Corrections in percent			Polarization in percent
				Contamination	Neutron	Geometry	
1	3.11 ± 0.06	15°	-0.86 ± 0.25	-0.03 ± 0.06	$+0.01\pm0.01$	$+0.64\pm0.14$	-0.25 ± 0.32
2	3.28 ± 0.02	22.5°	-0.02 ± 0.19	-0.03 ± 0.04	$+0.04\pm0.03$	$+0.41\pm0.06$	$+0.43\pm0.22$
3	3.28 ± 0.02	15°	-0.68 ± 0.22	$+0.01\pm0.05$	$+0.01\pm0.01$	$+0.63\pm0.13$	-0.03 ± 0.28
4	3.52 ± 0.02	26.5°	-0.25 ± 0.17	$+0.05\pm0.03$	$+0.25\pm0.12$	$+0.49\pm0.07$	$+0.58\pm0.24$
5	3.52 ± 0.02	15°	-0.38 ± 0.18	0.00 ± 0.00	$+0.04\pm0.03$	$+0.64\pm0.12$	$+0.32\pm0.23$
6	3.52 ± 0.02	22.5°	-0.45 ± 0.20	$+0.04\pm0.01$	$+0.01\pm0.02$	$+0.46\pm0.07$	$+0.06\pm0.23$

† Errors shown are rms errors (standard deviations).

the angular interval which can be investigated increases with increasing bombarding energy. The energy uncertainty is larger in the first run than in others because in this run the hydrogen target was cooled. The energy spread in the hydrogen target was 0.07 MeV in the first run and about 0.02 MeV in the others.

Column 4 lists the values of the uncorrected asymmetries. Their magnitude

is in all cases less than 1 %. Each value was obtained from a total of about 120 000 counts in each counter which results in a standard deviation of about ± 0.2 %. This contributes the largest error to the final results.

The corrections for gas contaminants and for neutrons are listed in the following two columns. They were obtained in the manner described in section 4. The errors are statistical. In all cases except one the magnitude of these two corrections is less than 0.1 %. For the last run the modification mentioned in section 3 produced a low neutron correction in spite of the rapid increase of neutron background with bombarding energy and with scattering angle.

The geometrical correction of column 7 is large compared to the other corrections and significantly larger than the statistical error of the uncorrected polarization. The source of this correction and the manner in which the uncertainty was assigned is discussed in section 4.

In order to find from the corrected asymmetry the values of the proton-proton polarization P_1, the effective p—α polarization P_2 has to be known. Using the phase shifts of Critchfield and Dodder [11]) and recent results by Scott [12]) one finds a value of P_2 averaged over the acceptance angle of the slits of $+0.94 \pm 0.05$. A very accurate value of P_2 is not needed since the relative error in $P_1 P_2$ is large.

The final results for the polarization in proton-proton scattering are contained in the last column of table 1. The uncertainties are the rms values of the uncertainties in the uncorrected space asymmetries and all corrections. The uncertainty of the proton-helium polarization P_2 is of no importance. However, since we are concerned with rather small effects other possible sources of error must also be considered.

One additional error source is due to the possibility of misalignment in the scattering chambers. Small displacements of the slits in the direction normal to the scattering planes is not important. The only serious effects are those which make asymmetric the first scattering angles θ_1 and $-\theta_1$, or make unequal the second scattering angle θ_2 for the two counters R and L. By considering only the centre rays through the different slits, it can easily be seen that either one of these misalignments alone causes in first approximation no error. If the measurements are averaged between slightly asymmetric first scattering angles $(\theta_1 + \Delta\theta)$ and $-\theta_1$, the polarization P_1 applies to the mean between these two angles, as long as θ_2 is symmetric. If θ_1 is symmetric, asymmetries in θ_2 cancel when the average between runs at $+\theta_1$ and $-\theta_2$ is taken. However, if both misalignments occur at the same time the effects do not cancel because the cross section of the second target is a function of angle θ_2 *and* of energy, and the energy of protons will be slightly different for first scattering angles $(\theta_1 + \Delta\theta)$, and $-\theta_1$. This error was investigated assuming the maximum alignment errors given in section 2. It was found that the effect on the measured polarization is negligible. In addition we investigated the effect of misalignment on the

geometrical corrections. This error is less than 0.01 %.

Scattering of protons from the edges of the apertures which define incident and scattered beams was considered as another possible source of error. The number of protons which in the first scattering chamber are scattered from slit edges rather than from hydrogen can be estimated from the pulse height spectrum of the monitor counter. The final polarization results are altered by slit-edge scattering by no more than 0.01 %.

6. Discussion

The results are represented graphically in fig. 5. For a centre-of-mass scattering angle of $\theta_{1,\text{c.m.}} = 30°$ the weighted mean of the measurements at energies

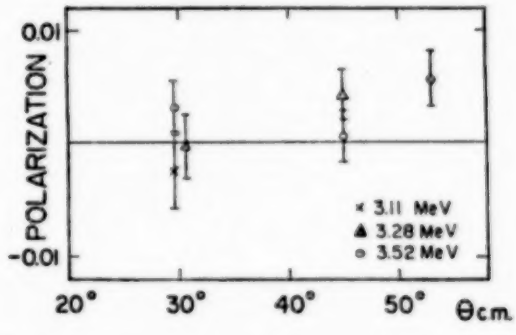

Fig. 5. Polarization in proton-proton scattering for laboratory energies of 3.11, 3.28 and 3.52 MeV and centre-of-mass scattering angles of 30°, 45°, and 53°.

3.11, 3.28, and 3.52 MeV is (0.07 ± 0.16) %. At $\theta_{1,\text{c.m.}} = 45°$ the mean of the two measurements, $P_1 = (0.25 \pm 0.16)$ %, is consistent with zero polarization, but favors slightly positive values. For $\theta_{1,\text{c.m.}} = 53°$ the value found is positive and differs from zero polarization by 2.4 standard deviations. As can be seen from table 1 for this particular measurement the neutron correction is unusually large and tends to make the polarization more positive. Also the correction for gas contamination makes a small positive contribution. However, both of these corrections are well understood and there is no reason to assume that they are in error by more than is indicated in table 1.

We may conclude that for proton energies of about 3.3 MeV the polarization in proton-proton scattering is less than 1 % at scattering angles between 30° and 53°. At 30° the polarization is less than 0.5 % and probably zero, while at 53° the polarization is probably positive. The probability that the polarization is negative is about 1 in 120. The sign of the polarization agrees with that found at higher proton energies ($E \geqq 56$ MeV). The small amount of polarization found in this experiment indicates that those p—p scattering phase shift solutions [2]) which have P-wave phase shifts in the order of 10° and D-wave phase shifts of more than 0.3° are to be excluded.

MacGregor [1]) recently published the results of an extensive phase shift

analysis of proton-proton angular distributions at 4.2 MeV and at higher energies in terms of S-, P- and D-waves. He finds that (within certain limits) for each chosen pair of S- and D-wave phase shifts there are four different sets of P-wave phase shifts which satisfactorily explain the data. At 4.2 MeV, three of the four sets give negative polarization for scattering through $\theta_{c.m.} = 50°$. Only solution I (see tables IV and XI of ref. [1])) gives a positive polarization of a fraction of one percent. From the results of the present experiment it seems therefore likely that this particular solution is the correct one. However, since in MacGregor's paper the polarization is given only for some representative pairs of S- and D-wave phase shifts, there remains the possibility that one of the other solutions also produces positive polarization.

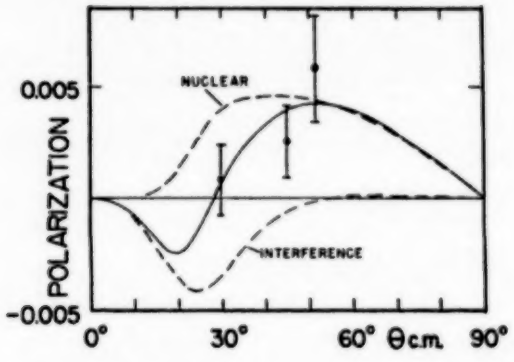

Fig. 6. Angular dependence of nuclear- and interference-polarization, and of their sum. The curves have only qualitative meaning (see text).

Hull and Shapiro expressed the polarization in p—p scattering as the sum of two parts. One part is due to interference between nuclear and coulomb amplitudes, the other contains only nuclear phase shifts. The angular dependence of nuclear- and interference-polarization and of their sum is shown in fig. 6. The amplitude of the nuclear polarization is proportional to $d = \delta_2[9\delta_1(\delta_1-\delta_2)+6\delta_0/(\delta_0-\delta_2)]$, where δ_0, δ_1, δ_2 are the triplet P phase shifts for $J = 0, 1, 2$, respectively. The curves have only qualitative meaning, since they were computed for a proton energy of 4.2 MeV and for simplicity the interference term neglects the part which contains the square of the P phase shifts. This assumption is not justified for a large number of the phase-shift solutions of refs. [1, 2]). With this assumption the amplitude of the interference polarization is proportional to $\Delta = -2\delta_0-3\delta_1+5\delta_2$. The curves of fig. 6 are drawn for $\Delta = 0.2$, $d = 5\times10^{-3}$. Although the experimental results are not accurate enough to determine the amplitudes of the nuclear and interference polarization, it appears likely from fig. 6 that the nuclear polarization is positive, the interference polarization negative or zero. This conclusion remains unaltered if the term containing the square of the phase shifts is included in the interference polarization.

We should like to thank Professor R. G. Herb for many valuable discussions. The assistance of Mr. R. I. Brown, Mr. R. A. Lux, and Mr. S. J. Moss in preparing the equipment and operating the accelerator was most helpful. Mr. L. O. Scharnke is to be thanked for the precise work he did in constructing the scattering chamber.

References

1) M. H. MacGregor, Phys. Rev. **113** (1959) 1559
2) M. H. Hull and J. Shapiro, Phys. Rev. **109** (1958) 846
3) K. W. Brockman, Jr., Phys. Rev. **110** (1958) 163
4) J. N. Palmieri, A. Cormack, N. F. Ramsey and R. Wilson, Ann. Phys. (N.Y.) **5** (1958) 299
5) T. M. Dauphinee, Rev. Sci. Instr. **28** (1957) 452
6) F. J. Eppling, Ph. D. Thesis, University of Wisconsin **1953** (unpublished); see also R. A. Laubenstein, M. J. W. Laubenstein, L. J. Koester and R. C. Mobley, Phys. Rev. **84** (1951) 12
7) W. A. Aron, B. G. Hoffman and F. C. Williams, AEC Publication AECU-663 (UCRL-121), second edition 1949. Available from AEC Depository Libraries
8) I. Alexeff, to be published
9) J. M. Blair, G. Freier, E. E. Lampi, W. Sleator, Jr. and J. H. Williams, Phys. Rev. **74** (1948) 553
10) H. R. Worthington, J. N. McGruer and D. E. Findley, Phys. Rev. **90** (1953) 899
11) C. L. Critchfield and D. C. Dodder, Phys. Rev. **76** (1949) 602
12) M. J. Scott, Phys. Rev. **110** (1958) 1398

2.C

Nuclear Physics **15** (1960) 626—635; © *North-Holland Publishing Co., Amsterdam*

Not to be reproduced by photoprint or microfilm without written permission from the publisher

ALPHA SPECTRA FROM THE DECAYS OF Li^8 AND B^8

B. J. FARMER † and C. M. CLASS

The Rice Institute, Houston, Texas ††

Received 7 December 1959

Abstract: The spectra of alpha particles accompanying the dissociation of Be^8, following the beta decays of Li^8 and B^8, have been measured. The spectra were found to be essentially identical, confirming the expected symmetry in the decay schemes of Li^8 and B^8. The spectrum associated with the decay of Li^8 has been compared with that given by the modified single level of Wheeler. The spectrum is not adequately accounted for by this formula if current values of the parameters are used to describe the 2^+ and 4^+ levels at 2.9 and 11.7 MeV in Be^8 which are assumed to be participating. An alternative description of the alpha spectrum, involving only the 2^+ levels in Be^8 at 2.9 and 16.7 MeV, has been given recently by Biedenharn and Griffy. Their expressions are found to be in agreement with the data over an energy range of more than 10 MeV, and hence may be taken as the preferred description of the process.

1. Introduction

The ground states of the mirror nuclei Li^8 and B^8 are the $T_z = \pm 1$ members of the isobaric spin triad of mass number eight, and are expected to decay symmetrically to the same final states in Be^8. The evidence available hitherto from the beta decay of Li^8 has indicated that less than 1 % of the transitions go to the ground state of Be^8, that about 90 % of the transitions occur to the broad 2^+, $T = 0$ level located at 2.9 MeV, and the remainder are to unidentified levels at an excitation energy in Be^8 of 10 MeV or more [1]).

The broad level in Be^8 at 2.9 MeV is particularly interesting since it dissociates into alpha particles which are distributed in energy up to about 7 MeV [2]). The efforts to account theoretically for the shape of this continuous alpha spectrum have not met with very much success [3]), although, to be sure, a plausible empirical modification of the expression of Wheeler reproduces the trends in the data for alpha energies up to about 3 MeV reasonably well. At higher energies, however, the expression accounts for only a fraction of the observed yield. In the past, conclusions regarding the adequacy of the modified Wheeler formula over the entire range of energy could not be drawn because of the uncertainty as to the number and location of higher lying states in Be^8,

† Now with the Chance-Vought Aircraft Company, Dallas, Texas.

†† Supported in part by the U. S. Atomic Energy Commission.

which might be contributing to the alpha yield. This uncertainty has been removed by recent investigations on the basis of which it is known that only one level occurs in the relevant region of the Be^8 spectrum at 11.7 MeV having a spin of 4^+ [4]). With this in mind, how to account for the higher energy portion of the alpha distribution in terms of the Wheeler formulation becomes quite perplexing, since beta transitions to the 4^+ state are second forbidden [4]) so that few, if any, alpha particles should be contributed by this state. Recently the problem of the continuous alpha spectrum has been re-examined by Griffy and Biedenharn [5]). They have obtained an expression for the alpha distribution by making use of the d-wave phase shifts, obtained from alpha-alpha scattering, to more precisely characterize the 2^+ level at 2.9 MeV. On the basis of this semi-empirical approach, an essentially satisfactory fit to the data over the entire energy range is achieved, which requires only an additional minor contribution of alpha particles from the 2^+, $T = 1$ state at 16.7 MeV to be exact. This agreement will be illustrated in the following discussion with data obtained in the present work. For comparison, an analysis based on the formula of Wheeler will also be shown.

It is a common feature of all theories for the continuous spectrum that the alpha intensity is proportional to $(Q-2E_\alpha)^5$ where Q is the total disintegration energy and E_α is the energy of the alpha particle. Since the Q values differ in the cases of Li^8 and B^8 by almost 1 MeV, the two spectra will be expected to have somewhat different trends with energy. The possibility of an additional difference between the two spectra arises from the fact that B^8 is energetically allowed to decay to the mirror $T = 1$ level in Be^8 at 16.7 MeV. Even though this transition is strongly unfavoured because of the small energy difference ($\approx$ 300 keV) and the break-up of the state into two alphas is inhibited by the isobaric spin selection rule, a small contribution to the yield of alphas might still be expected, because of the large matrix element for a super-allowed beta transition.

To investigate these questions, the alpha spectra from both decays were obtained over as wide an energy range as possible. While the measurement of the continuous alpha spectrum is a classic problem, repeatedly investigated when associated with the beta decay of Li^8, the spectrum accompanying the positon decay of B^8 has been measured only once [6]), no doubt owing to the inability to make B^8 conveniently. This situation was remedied recently when He^3 became commonly available, since B^8 is readily made by means of the He^3 (Li^6, n) reaction at bombarding energies of 3 MeV or more. With the availability of B^8, it is now possible to compare the alpha spectra from the two modes of decay with much improved accuracy. From the experimental point of view, this comparison is greatly aided by the use of a scintillation counter together with a multi-channel analyzer which enable all parts of the spectrum to be recorded simultaneously under identical conditions.

2. Experimental Methods

The alpha spectra were obtained with a crystal scintillation spectrometer consisting of a 5 mil thick CsI(Tl) crystal detector attached to a DuMont 6363 photomultiplier tube used in conjunction with a 256-channel pulse-height analyzer. The spectrometer was inserted into a port in the target chamber so as to view the target at 90° with respect to the direction of the beam. In order to avoid the interference from competing reactions, advantage was taken of the approximately 0.8 second half lives of B^8 and Li^8 to observe the alpha particles with the beam off the target. To accomplish this both the counter and the beam from the accelerator were pulsed at the convenient frequency of 5 cycles per second. The pulsing was controlled by a variable frequency oscillator which drove two square wave-forming circuits. One square wave output switched the voltage applied across a set of beam deflection plates between 2 and 6 kV. The former voltage deflected the charged part of the beam onto the target in order to eliminate the small neutral portion of the beam as a possible source of background. The latter voltage deflected the beam off the target and onto a tantalum beam stop for the counting portion of the cycle.

The second square wave output was used to control a gate circuit for the photomultiplier tube. This gate was phased with respect to the deflection of the beam such that counting commenced approximately 10 milliseconds after the beam was off the target and ended approximately 10 milliseconds before it was deflected back on. The photomultiplier tube switching was accomplished by reversing the voltage on the focus electrode with respect to the photo-cathode. This method, which has been discussed in the literature [7]), served not only to inhibit counting during the beam-on portion of the cycle but also to prevent 'fatiguing' of the photo-cathode and dynodes resulting from the high intensity of particles, incident on the crystal during the 'beam-on' period.

The background caused by delayed beta and gamma activity in the target, was reduced by the use of a thin CsI(Tl) crystal. The remaining background was significant only for pulse heights corresponding to alpha particle energies of less than 1.5 MeV and was allowed for by subtracting from the gross spectrum the yield obtained when the alphas were screened out by a thin foil of Ni interposed between the counter and crystal. In the case of the B^8 spectrum, due to the relatively lower yield of alphas, the background subtraction was more sensitive to the running conditions and not as reliable as in the case of Li^8.

The response of a CsI(Tl) crystal is not a linear function of alpha particle energy so that it was necessary to obtain a calibration curve. The points for this curve, giving pulse height as a function of alpha energy as shown in fig. 1, were obtained at 5 MeV and less by elastically scattering alpha particles from a thin layer of gold evaporated on a VYNS film [8]). The points at 6.05 and 8.78 MeV were obtained with a Th(B+C+C'') source. When the calibration curve

was used subsequently to assign energies to the alphas from Be^8, the pulse height scale was normalized to the check points obtained with the thorium source measured with the counter operating in the pulsed mode. Two additional check points at 3.92 and 7.21 MeV were obtained by placing a 3.4 mg/cm² aluminium foil between the source and the crystal [9]).

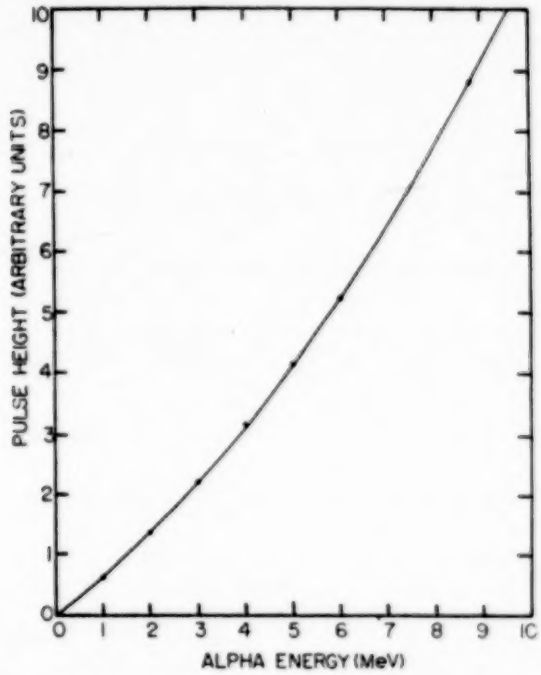

Fig. 1. The relative pulse height as a function of energy for alpha particles incident on a 5 mil thick CsI(Tl) crystal.

The reactions used to produce the B^8 and Li^8 nuclei were $Li^6(He^3, n)$ and $Li^7(d, p)$, respectively. The target material for the former reaction was metallic lithium enriched to 96 % in Li^6 and that for the latter reaction was natural lithium metal. The targets were prepared in identical fashion by evaporating the metal onto thin ($\approx$ 200 μg/cm²) carbon foils while in place in the reaction chamber. Under the conditions of the evaporation, the lithium layers deposited were partially oxidized. The thicknesses of the targets were measured with the aid of the scintillation spectrometer by means of deuterons elastically scattered from the carbon backing. The position of the well resolved elastic peak was determined before evaporation with the target oriented at 45° to the direction of the beam. After evaporating the lithium, the target again was positioned at 45° to the beam but so arranged that the lithium was on the back side of the foil with respect to the beam and facing the scintillation crystal. Then the scattering was repeated and from the shift of the peak due to the absorption of energy by the lithium and/or lithium oxide layer, it was possible to calculate the thickness of this layer using the experimentally determined stopping

power for deuterons [10]). To check the result from this measurement, the thickness was also estimated from the yield of deuterons elastically scattered from the lithium, assuming the Rutherford scattering cross-section and making use of the known solid angle of the detector. The values of the thicknesses obtained in this manner agreed satisfactorily with those obtained with the above method when the uncertainties in the scattering cross-section and the target composition were taken into account. The target thicknesses used when observing the alpha spectra ranged from 300 to 500 $(\pm 50)\mu g/cm^2$.

3. Results

The spectra of alpha particles accompanying the decays of B^8 and Li^8 are displayed in fig. 2. The distribution associated with the Li^8 decay contains on

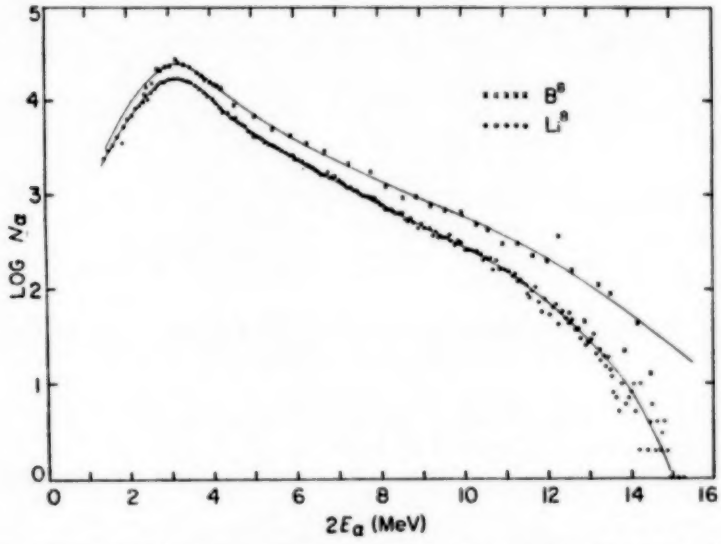

Fig. 2. The energy spectra of alpha particles from the $Li^8(\beta^-)Be^8(\alpha)\alpha$ and $B^8(\beta^+)Be^8(\alpha)\alpha$ decays. Note that the intensity scale is logarithmic. The upper curve, to which the B^8 data has been normalized at 3 MeV, was calculated from the best fit to the Li^8 data with the aid of eq. (4).

the order of 2×10^5 alpha particle counts while that associated with the B^8 decay contains about 2×10^4 counts. Both distributions have been observed several times with substantially the same results. The smaller number of counts in the B^8 alpha spectrum is due partly to the small cross section of the (He^3, n) reaction at convenient bombarding energies, and partly to the loss of many alpha particles because the parent B^8 nuclei were ejected from the target due to the large recoil momenta imparted by incident He^3 beam. The spectra have been corrected for small distortions which result from (1) the finite target thickness, (2) the dissociation of the Be^8 nucleus in flight, the motion here

resulting from the recoil momentum imparted by the beta and neutrino in the preceding decay, and (3) the effect of counter resolution.

The correction to the spectrum arising from the finite target thickness takes two effects into account: (a) a shift in the observed energy to compensate for the energy loss of the alpha particles emerging from some average depth within the target and (b) the spread in energy about the mean value due to alphas originating at various depths within the target. The corrections for both of these effects were relatively small except at the lower energies because in the counting arrangement used the alphas needed to traverse only the thin lithium target layer. Indeed, the effective thickness of the layer to the alphas was further reduced in accord with the dynamics of the recoiling nuclei, which required that these nuclei either come to rest in a surface layer or be ejected from the target altogether. By taking into account the measured thicknesses of the targets, the average recoil energies of the Li^8 and B^8 nuclei, and available range-energy data for lithium nuclei [11]), it was estimated that the alphas in both the spectra penetrated on the average about 150 μg of material. The corresponding energy losses for various energy alpha particles are given in table 1.

TABLE 1

Corrections to alpha spectra

E_α (MeV)	1.5	3.5	6.0
Target correction			
Energy shift (MeV)	0.16	0.13	0.10
Energy broadening (MeV)	0.13	0.10	0.08
Beta-neutrino broadening (MeV)	0.14	0.14	0.10
Counter broadening (MeV)	0.13	0.20	0.27
ΔE (R.M.S. energy broadening in MeV)	0.23	0.22	0.30
Change in ordinate, eq. (2)	+1.6%	−0.5%	−0.9%

These losses have been determined from an experimental stopping power curve extrapolated to low energies on the basis of other complete curves [10]). The inaccuracy of the stopping power obtained in this way for the lower energy alphas causes about a 15 % uncertainty in the energy for a 1 MeV alpha. The spread in the energy of the alphas due to production at different depths in the target layer was also estimated in the same manner. This spread effectively reduced the intrinsic counter resolution and was applied with the counter resolution correction. The magnitude of this effect is also indicated in table 1 for various alpha particle energies.

The Li^8 and B^8 nuclei are at rest when their beta decays occur; however, the recoil momentum of the beta and neutrino sets the residual Be^8 nucleus in motion. Due to the extremely short life-times of the states in Be^8, the dissociation of the nucleus occurs while it is in flight causing a slight shift in the

energies of the alphas. The resulting distortion to the spectrum has been calculated by Frost and Hanna [2]) and may be described in terms of a loss of energy resolution. It was thus possible to include this effect also in the counter resolution correction. The magnitude of this energy broadening is given in table 1 for several energies.

The true counter resolution was determined from the calibration data. The resolution at the 8.78 MeV was 3.7 % and was found to follow closely the familiar $E^{-\frac{1}{2}}$ energy dependence observed with such crystal spectrometers. The magnitude of this energy broadening is included in table 1 for several energies. Also included in the table are the root-mean-square values of all three broadening effects. The resolution correction was applied by a method which involves the fitting of the experimental curve by analytical expressions [12]). The expression for the true undistorted spectrum $T(E_\alpha)$ is related to the experimental curve $S(E_\alpha)$ by the following integral equation

$$S(E'_\alpha) = \int_0^\infty T(E_\alpha) R(E_\alpha, E'_\alpha) \mathrm{d}E_\alpha \tag{1}$$

where $R(E_\alpha, E'_\alpha)$ is the resolution function. If the resolution function is assumed to be Gaussian, the undistorted spectrum is given by

$$T(E_\alpha) = S(E'_\alpha) - \frac{E'_\alpha \Delta E'_\alpha}{4} \left[\frac{\pi}{4 \ln 2}\right]^{\frac{1}{2}} \frac{\mathrm{d}^2 S(E'_\alpha)}{\mathrm{d}E'^2_\alpha} \tag{2}$$

where $\Delta E'_\alpha$ is the width of the resolution function at half maximum. Although the uncertainties were considerable in estimating the magnitudes of the individual contributions to the energy broadening, the resulting correction to

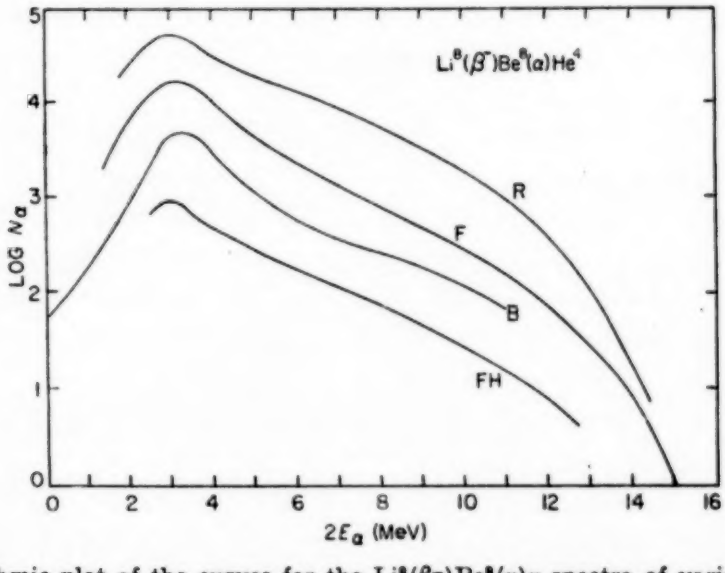

Fig. 3. Logarithmic plot of the curves for the $Li^8(\beta^-)Be^8(\alpha)\alpha$ spectra of various authors: R = Rumbaugh, Roberts, and Hafstad; F = present authors; B = Bonner *et al.*; and FH = Frost and Hanna. The curves have been shifted vertically for convenience of display.

the spectrum shape was small, as is indicated in table 1. The corrected spectra from both the Li^8 and B^8 decays are shown in fig. 2. Fig. 3 shows the results of the present work on Li^8, denoted by F, compared to those of Bonner *et al.* (B), Frost and Hanna (FH), and Rumbaugh *et al.* (R) [2]).

4. Discussion

Under the assumption that the beta decay and alpha dissociation are two very close but separate events as opposed to a four-body dissociation of two alphas, a beta, and a neutrino, the alpha spectrum resulting from the population of a single level in Be^8 has been given by Wheeler [3]) and modified by Bonner *et al.* [2]) through the inclusion of a penetrability factor. The resulting expression for the number of alphas N_α as a function of dissociation energy $2E_\alpha$ is

$$N_\alpha dE_\alpha = \frac{(Q-2E_\alpha)^5}{[(2E_\alpha-E_{gs})-E_0]^2+\frac{1}{4}\Gamma^2} P_l dE_\alpha \tag{3}$$

where Q is the relevant disintegration energy, E_0 is the energy of the level in Be^8, E_{gs} is the excitation energy of the ground state of Be^8(94 keV), Γ is the width of the level in Be^8, and P_l is the penetrability of one alpha in the field of another.

The first step in the analysis of the spectra was a test of the $(Q-2E_\alpha)^5$ dependence †. Since the parameters in the denominator of eq. (3) and P_l concern only Be^8, they will be the same for both the Li^8 and B^8 decay schemes, giving for the intensity ratio of the spectra

$$\frac{N_{B^8}}{N_{Li^8}} = \left[\frac{Q_{B^8}-2E_\alpha}{Q_{Li^8}-2E_\alpha}\right]^5. \tag{4}$$

The test of this expression is displayed with the data in fig. 2. The line through the Li^8 data represents the best fit while the line through the B^8 data was obtained by multiplying the ordinates of the lower curve by the ratio given in eq. (4). It is seen that the calculated upper curve agrees well with the data except possibly at the high energy end where the counting statistics are poor. The adequacy of the fit tends to confirm the expectation that apart from an energy dependent factor the alpha spectra obtained from the decays of B^8 and Li^8 should be identical.

Equation (3) was next evaluated for the Li^8 decay assuming only the first excited state in Be^8 to be participating and using for values of the level para-

† As mentioned above, any expression describing the distribution in energy of the alphas must contain a factor $(Q-2E_\alpha)^5$ to take into account the density of electron-neutrino states in the final system as required by the theory of beta decay. The discussion in this paragraph is, then, independent of the particular form of the expression for $N_\alpha dE_\alpha$.

meters those obtained from alpha-alpha scattering experiments [4]). The result of this calculation is shown in fig. 4, along with the data for comparison. It is evident that the agreement is poor. Some improvement can be achieved in the higher energy region if eq. (3) is used to describe an additional contribution to the spectrum arising from the now well established broad, 4^+, second excited state at 11.7 MeV. However, even a contribution from this state of 10 % of the total alpha intensity [1, 4]) does not lead to a satisfactory fit. It must also be kept in mind that what agreement is achieved is done so by overlooking the second forbidden character of the beta transition to the 4^+ state.

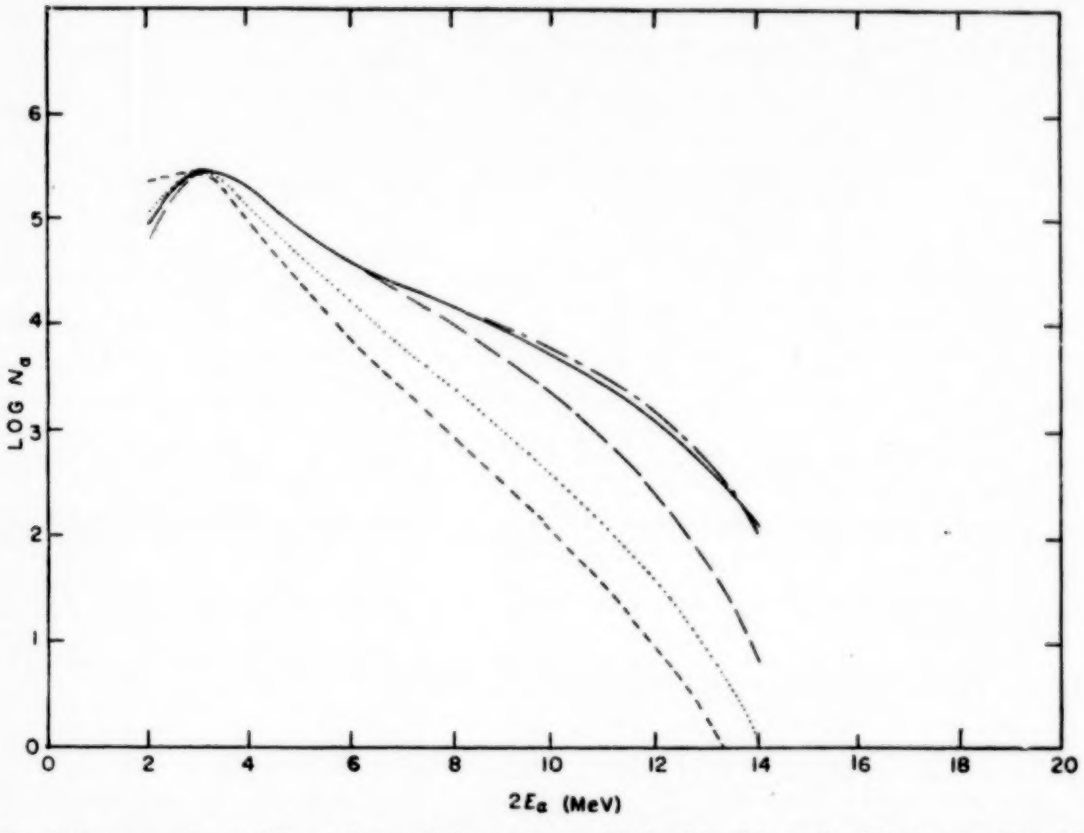

Fig. 4. A comparison of the alpha particle spectrum obtained in this work with that predicted by Wheeler [3]), Bonner *et al.* [2]), and Griffy and Biedenharn [5]).
——— Present experiment — — — — Wheeler's Theory ..... Bonner's modification
——— ——— ——— Griffy and Biedenharn ——— — ——— — Griffy and Biedenharn including transitions to the $T = 1$ state.

As mentioned earlier, an alternative description of the alpha spectrum has been provided in the recent work of Griffy and Biedenharn [5]), which makes use of the d-wave phase shifts available from alpha-alpha scattering. Their expression for the spectrum is

$$N_\alpha \mathrm{d}E_\alpha = k(Q-2E_\alpha)^5 \frac{\sin^2 \delta^{2+}}{P_2} \qquad (5)$$

where k is an arbitrary normalization constant, δ^{2+} is the d-wave phase shift taken from alpha-alpha scattering data, and P_2 is the penetrability factor for $l = 2$ alpha particles. In fig. 4 this formula is shown for comparison with the data. It is seen that the agreement is much improved in comparison to the foregoing analysis over an energy interval of nearly 8 MeV. Griffy and Biedenharn have also shown that the agreement may be extended to the high energy limit of the spectrum by adding a term to eq. (5) to account for a contribution from the first $T = 1$, 2^+ level in Be^8 at 16.7 MeV, which is sufficiently broad to influence the upper portion of the spectrum. The calculated distribution, when corrected in this manner, agrees quite well with the experimental data, as shown in fig. 4. The remaining discrepancy between the calculated and observed distributions is within the experimental error but appears exaggerated when the curves are shown on a logarithmic scale. In the high energy region in particular, the differences between the distributions in terms of the actual numbers of counts is exceedingly small.

References

1) W. Hornyak and T. Lauritsen, Phys. Rev. **77** (1950) 160
2) See for example: W. A. Fowler and C. C. Lauritsen, Phys. Rev. **51** (1937) 1103;
Rumbaugh, Roberts and Hafstad, Phys. Rev. **54** (1938) 657;
C. L. Smith and W. Y. Chang, Proc. Roy. Soc. A **166** (1938) 415;
Bonner, Evans, Malich and Risser, Phys. Rev. **73** (1948) 885;
C. W. Li and W. Whaling, Phys. Rev. **81** (1951) 661;
Frye, Armstrong and Rosen, Phys. Rev. **98** (1955) 241(A);
T. Frost and S. S. Hanna, Phys. Rev. **99** (1955) 8
3) C. Kittel, Phys. Rev. **55** (1939) 55;
J. A. Wheeler, Phys. Rev. **59** (1941) 27.
4) F. Ajzenberg-Selove and T. Lauritsen, Nuclear Physics **11** (1959) 1
5) T. A. Griffy and L. C. Biedenharn, Nuclear Physics **15** (1960) 636
6) F. C. Gilbert, Phys. Rev. **93** (1954) 499
7) U. Farinelli and R. Malvano, Rev. Sci. Inst. **29** (1958) 699
8) B. D. Pate and L. Yaffe, Can. J. Chem. **33** (1955) 15
9) Aron, Hoffman and Williams, A.E.C.U.-663 (1951)
10) W. Whaling in Encyclopedia of Physics, Vol. 34 (Springer Verlag, Berlin, 1958)
11) Neuendorffer, Inglis and Hanna, Phys. Rev. **82** (1951) 75
12) K. Liden and N. Starfelt, Arkiv für Fysik **7** (1954) 427

2.C

Nuclear Physics **15** (1960) 636—645; © *North-Holland Publishing Co., Amsterdam*

Not to be reproduced by photoprint or microfilm without written permission from the publisher

BETA DECAY INVOLVING THE $Be^{8*}(2^+)$ STATE

T. A. GRIFFY † and L. C. BIEDENHARN

The Rice Institute, Houston, Texas ††

Received 7 December 1959

Abstract: The shape of the alpha and beta spectra in the $Li^8(\beta^-, \alpha)\alpha$ and $B^8(\beta^+, \alpha)\alpha$ decay is calculated directly from alpha-alpha scattering phase shifts, using methods developed in section 2 for this purpose, and the assumption that the decays involve only Be^{8*} in a (2^+) intermediate state. Recent experimental results are in good agreement with the calculated spectra.

1. Introduction and Summary

The beta decays of Li^8 and B^8 are almost unique in nuclear physics, not only for their very large energy ($\approx$ 16 MeV end point), but also because the 'final' states for the beta decay are all unstable to particle emission. The unusual features of these decays have been extensively studied — chiefly experimentally — over the past two decades. We shall in the following, for brevity, explicitly discuss the Li^8 decay, but it is to be understood that exactly similar remarks will apply to the analogous B^8 decay.

The most recent experimental studies of the Li^8 beta spectrum are those of Vedder [1]), Farmer and Class [2]), and the earlier experiment of Hornyak and Lauritsen [3]); the most recent measurement of the alpha spectrum resulting from the beta decay of Li^8 is that of Farmer and Class [2])*. In refs. [1]) and [3]) the Li^8 beta spectrum is analyzed and this analysis ††† (in particular that of ref. [1]) indicates that < 1 % of the transitions are to the (0^+) ground state in Be^8; that ≈ 90 % are to the $(2^+, T = 0)$ state; and that ≈ 10 % are to the (4^+) state. We reproduce in fig. 1 the relevant information in an energy level diagram for Be^8, taken from the recent summary of Ajzenberg and Lauritsen [4]).

The recent measurement of Lauritsen *et al.* [5]), which indicates that the spin and parity of the Li^8 ground state is (2^+), poses something of a puzzle for the analyses just mentioned. For if one assumes that the 0^+, 2^+, and 4^+ states of Be^8 are those of a rotator (with essentially the same intrinsic state), a view consistent with the precision measurements of alpha-alpha scattering just complet-

† National Science Foundation Fellow in Physics.

†† Supported in part by the U. S. Atomic Energy Commission and The Research Corporation.

††† It should be noted that the standard Kurie plot analysis does not apply to the cases at hand. In refs. [1]) and [3]) this is largely, but not completely consistently, taken into account by using the observed alpha spectrum. The results presented in section 2 furnish the desired techniques.

* The β-spectrum of Li^8 will be published separately.

ed [6]), then the transitions to the (4^+) and (0^+) states should be roughly equally forbidden, and the observed transition rates are then clearly inconsistent. (Vedder [1]), to avoid this difficulty, took the spin and parity of the ground state of Li^8 to be (3^+); his analysis, of course, preceded the results of ref. [5])).

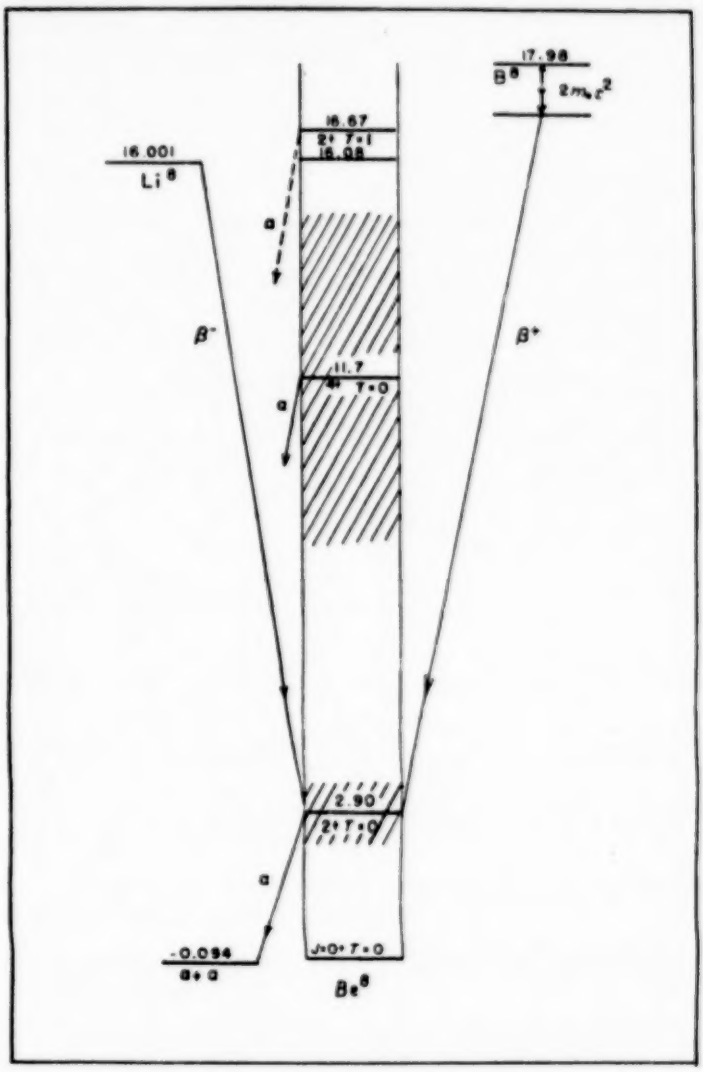

Fig. 1. Energy level diagram of Be^8 (from ref. [4])).

It is the purpose of the present note to demonstrate that all the experimental data are consistent — within the limitations imposed by the data — with the view that the beta decay goes entirely to the (2^+) excited system of Be^8. The key point in the present work is the direct introduction of the alpha-alpha scattering data into an approximate treatment of the beta decay process. The technique for this is developed in section 2, and a discussion of its essential features is given briefly. The usefulness of this procedure — which is basically an attempt to approximate cascade reactions as a sequence of two-body processes — is apparently not restricted to the particular and unusual nature of the

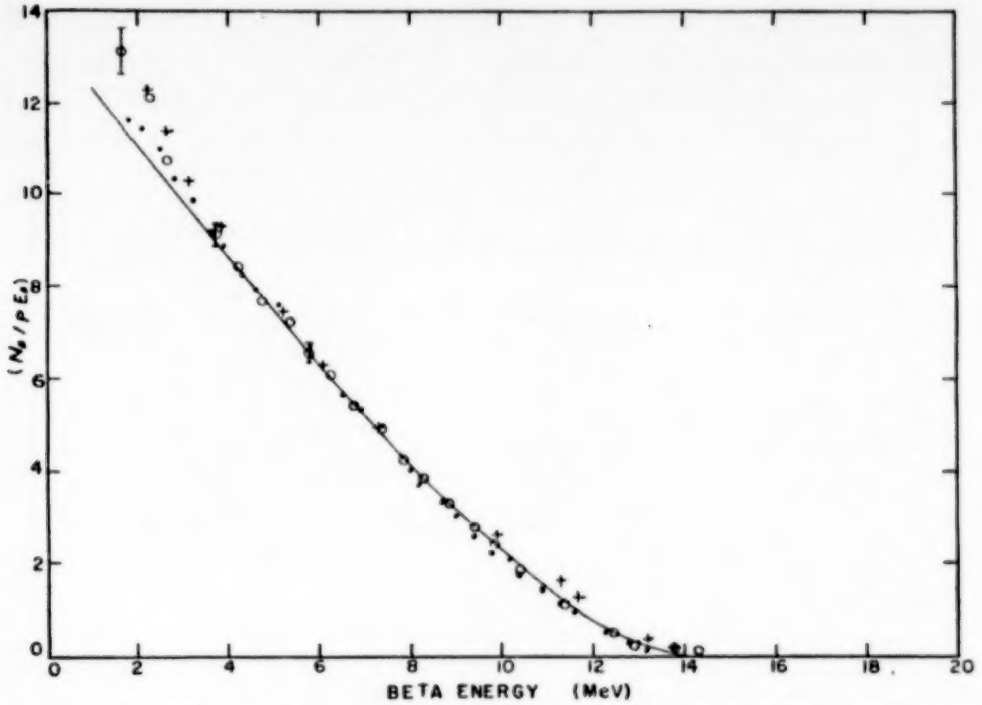

Fig. 2. Kurie plot of Li^8 beta decay. The circles represent the experimental points of Vedder [1]), the dots show the experimental points of Farmer and Class [2]), and the crosses are the experimental results of Hornyak and Lauritsen [3]). The solid line shows the theoretically predicted spectrum, normalized at 6 MeV.

o Vedder • Farmer and Class + Hornyak and Lauritsen

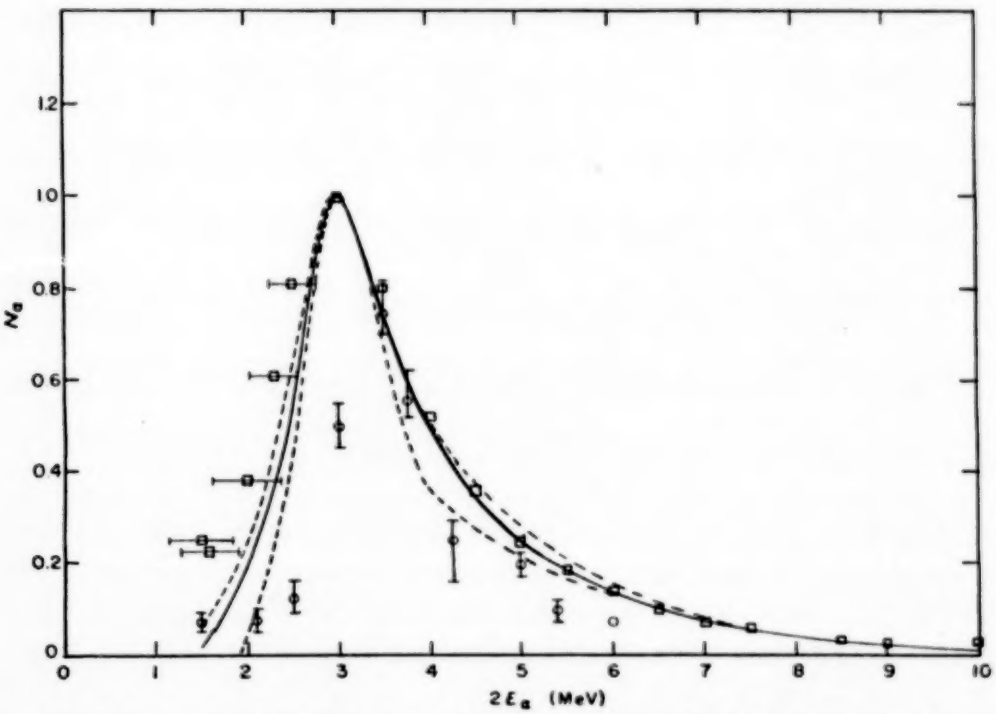

Fig. 3. Energy distribution of alpha particles from the $Li^8(\beta^-)Be^{8*}(\alpha)\alpha$ decay. The squares are representative experimental points of Farmer and Class [2]) and the circles show the experimental results of Bonner *et al.* [11]). The solid line shows the spectrum predicted by the present theory and the dashed curves show the effect of the uncertainty in the alpha-alpha scattering phase shifts on the theoretical prediction.

□ Farmer and Class o Bonner *et al.*

present decays and further application will be discussed in a later paper [7]).

Section 3 details the application to the experimental data, in particular, to the recent data of Farmer and Class [2]). Figs. 2 and 3 illustrate the results obtained. A concluding section discusses the limitations of the present analysis of the data.

2. Method of Analysis

In order to see the method most easily, consider a hypothetical excited nuclear state that involves two channels, denoted by α and β (though only later will these actually have the significance of alpha and beta processes). It follows from the spectral form of Wigner's nuclear reaction theory [8]), that processes through *only* this state *factor* into parts involving the excited nuclear state, the incident and exit channels separately. Explicitly one has

$$\sigma_{\alpha\to\beta} = \pi\lambda_\alpha^2(2J+1)(\sin^2\delta^{J\pi})(U_\alpha^{J\pi})^2(U_\beta^{J\pi})^2. \tag{1}$$

Apart from the essentially geometrical factor $\pi\lambda_\alpha^2(2J+1)$ the content of eq. (1) is the statement that only the $J\pi$ eigenstate of the intermediate nuclear system enters in the reaction $\alpha \to \beta$, and this eigenstate enters through the factors: (a) $\sin^2\delta^{J\pi}$ (where $\delta^{J\pi}$ is the *eigenphaseshift* of the excited state) and (b) the factors $(U_\alpha{}^{J\pi})^2$ and $(U_\beta{}^{J\pi})^2$, where $\mathbf{U}^{J\pi}$ is the normalized *eigenvector* of the state $J\pi$, and $U_{\alpha,\beta}^{J\pi}$ the components of this eigenvector in the channels α, β. Under the assumption that the influence of the beta channel is small, we may approximate the alpha component $U_\alpha{}^{J\pi}$ of the eigenvector by unity.

Eq. (1) describes a two-step *reaction* process. In order to apply this result to a two-step *cascade* process we observe that: (a) $U_\beta{}^{J\pi}$ may be obtained for the beta channel using perturbation theory and that (b) the same *formal* results obtain if absorption is replaced by emission. The first point shows that

$$U_\beta{}^{J\pi} \propto \frac{\langle J_f||H_\beta||J_i\rangle}{P_\alpha{}^{\frac{1}{2}}} \tag{2}$$

where we have used the one-level approximation to the eigenvector [9]). (Here the numerator is a reduced matrix element — or more properly the width — for channel beta using perturbation theory; P_α is the penetration factor for channel alpha — this enters from the requirement that the eigenvectors are normalized, i.e. $\sum_c(U_c{}^{J\pi})^2 = 1$.) While strictly speaking this application of the Wigner theory is largely heuristic, the applicability of perturbation theory to the beta channel allows one to have some confidence in the result.

It follows that the beta-alpha cascade is described by

$$dN_{\alpha\beta} = \text{constant} \cdot [E_\beta(E_\beta{}^2 - m^2c^4)^{\frac{1}{2}}(Q - E_\beta - \bar{E}_\alpha)^2] \cdot [(\sin\delta^{2+})^2/P_2] \cdot d\bar{E}_\alpha dE_\beta. \tag{3}$$

Here E_β is the energy of the beta particle; $\bar{E}_\alpha = 2E_\alpha$ (denoting by E_α the energy

of one of the alphas); δ^{2+} is the eigenphaseshift of the (2^+) Be^{8*} level; Q is the total energy available for the cascade; and m is the electron mass. We have explicitly assumed in eq. (3) that the beta decay is an allowed transition, (and have neglected Coulomb effects specific to the beta particles).

One may view eq. (3) alternatively as a variant form of the conventional perturbation result that the transition probability is the square of a reduced matrix element (here taken as a constant) multiplied by a density of states, $\rho(E)$. Eq. (3) states that in addition to the density of lepton states the "density of the (2^+) state" is approximated by $\sin^2\delta^{2+}/P_2$. Such a factor is essential for treating very broad states in the continuum †.

Further Discussion of the Approximation

The results obtained in the above paragraphs are clearly of an approximate nature. The trouble lies not so much with the assumption of perturbation theory for the first transition (and also the attendant weak effect on the properties of the intermediate state) but in the inherent differences between cascade and reaction processes, also neglected by the perturbation argument. For example, in a cascade the two emissions exist coherently in the final state, (and not as reaction alternatives) and interactions in the continuum can possibly be of much more importance than in the reaction process. Such interactions are neglected in the treatment above (and the neglect is probably justified for the beta decay channel). Much more important than this is the very essential difference that in a cascade the energy of the intermediate state is *not* sharp, unlike the situation for reactions. By treating the intermediate state (here $Be^{8*}(2^+)$) as if the energy were 'quasi-sharp' we are thereby neglecting the possibility of processes through virtual states of the Be^{8*} system. The validity of this approximation might be indicated by the reasonably well defined levels in Be^8; more likely one would argue that the success of the approximation is its real justification.

There are further difficulties that can be found in a closer analysis of our procedure. For example, one might reasonably argue that all that is really measured about the reaction is that a beta particle and two alpha particles emerge. Why not consider them a cascade of, say, $Li^8 \rightarrow \alpha + {}_1H^{4*}$ and then ${}_1H^{4*} \rightarrow \beta^- + \alpha$? Such a process might very well occur — even though it appears unlikely — but (assuming the intermediate state is not virtual) the two break-up processes should be distinguishable, and therefore incoherent. In actual fact our reason for not considering this, and other competing processes, is that it appeared unnecessary.

A final difficulty concerns the precise meaning of the eigenphaseshift used in eq. (3). Were the Coulomb field not involved, the meaning of this phase shift would be clear. But for the Coulomb field case, two quite different phase shifts might be employed, either the total phase shift, δ^T, experienced by the $J\pi$ eigenvector, or the phase $\delta = \delta^T - \sigma$, where σ is the Coulomb phase shift caused by the long range interaction. Since the phase shift σ is diagonal, either phase shift may be employed for reactions. *Both phase shifts will lead to the same result*, for the meaning of the mixing phase ε (defined as $\tan\varepsilon = U_\beta{}^{J\pi}/U_\alpha{}^{J\pi}$ for the two-channel case) will be changed accordingly. Approximations based upon a simple energy dependence for the $\sin\varepsilon$ factor will, however, depend strongly upon which phase shift is employed. In ref. [7]), it is shown (using perturbation theory and the method of eigendifferentials for continuum wave functions) that yet another choice of phase-shift is possible, $\delta^T + \xi - \sigma$, where ξ is the (diagonal) Coulomb hard sphere phaseshift. *The present analysis definitely shows that in order to achieve a fit over the entire energy range the customary scattering phase $\delta^T - \sigma$ must be employed.* Further discussion of this question will be found in ref. [7]).

We regard eq. (3) as essentially correct, within the accuracy of our basic assumption of a two-step process, neglecting continuum interactions and involving a single state. On the other hand, the approximation involved in

† We are indebted to Professor Christy for calling our attention to the work of Cook *et al.* [15]), where a similar view has been utilized in discussing the alpha spectrum of B^{12}.

estimating sin ε is rather crude, and *uses penetration factors alone to obtain the relevant energy dependence.*

Formulas which represent various specializations of eq. (3) have appeared previously in the literature. Wheeler in his pioneer discussion [10]) used the Breit-Wigner dispersion approximation to eq. (3) (but neglected penetration effects, which were introduced later by Bonner *et al.*[11]). (The use of a dispersion shape also stems from earlier work on line widths in atomic spectra.) Watson [12]) gave a result similar to eq. (3) † in discussing meson production in nuclear collisions, (omitting Coulomb effects, which did not enter this problem).

3. Application

To obtain the beta spectrum one integrates eq. (3) over all allowed alpha energies; i.e.

$$\frac{dN_\beta}{dE_\beta} = \text{constant} \cdot E_\beta(E_\beta^2 - m^2c^4)^{\frac{1}{2}} \int_0^{Q-E_\beta} d\bar{E}_\alpha (Q - E_\beta - \bar{E}_\alpha)^2 [(\sin \delta^{2+})^2 / P_2]. \quad (4)$$

For the alpha spectrum, one obtains the result

$$\frac{dN_\alpha}{d\bar{E}_\alpha} = \text{constant} \cdot (Q - \bar{E}_\alpha)^5 [(\sin \delta^{2+})^2 / P_2]. \quad (5)$$

(An additional approximation which has been made in eq. (5) involves replacing the electron mass by zero; this yields the factor $(Q - \bar{E}_\alpha)^5$. The error involved is minor; however, in the calculations plotted in the figures, the exact expression was used.)

We have evaluated eqs. (4) and (5) numerically using the parameter $Q = 16.10$ MeV and taking the phase shift δ^{2+} from a smooth curve through the data points of ref. [6]), augmented by the data of Burcham [13]).

The nuclear radius — which enters in the penetration factor — has been taken as a parameter in our calculations and adjusted for best fit. The value used was $R = 6 \times 10^{-13}$ cm, which is about the same as that found by Phillips [6]) ($R = 5.5 \times 10^{-13}$ cm).

A further interesting, though minor, point arises in treating these unusual beta decays. As customarily applied, the Fermi theory of beta decay leads to a function f such that the ft value is a measure of the size of the matrix element. Although an ft value can be obtained for the $Li^8 \rightarrow Be^8$ and $B^8 \rightarrow Be^8$ decays, the application, strictly speaking, to determining the size of the matrix element is no longer permitted, since this concept depends on the states being sharp (aside from the beta decay). In practice the difference is rather slight; the analogous Fermi function f^*, which can be defined from eq. (4) above, differs from f by a factor ≈ 2 — which is insignificant for present day applications.

† Watson and Gell-Mann refer to this result in their review [14]) and discuss a related problem in an appendix.

(To obtain this value, the arbitrary definition that f^* is normalized to $\pi\Gamma$ was used. In the limit of vanishing width, $f^* \to f$.)

The predicted spectra from this analysis are shown in fig. 2 (Kurie plots of the beta spectra) and figs. 3 and 4 (the alpha spectra). In fig. 2 the data points are taken from refs. [1, 2, 3]) and the predicted curve is normalized to fit at 6 MeV. In fig. 3 we have compared the predicted alpha spectrum with the results of refs. [2, 11]). The solid line shows the predicted spectra and the dotted curves show the effect of the experimental error in the alpha-alpha scattering phase shifts on the predictions.

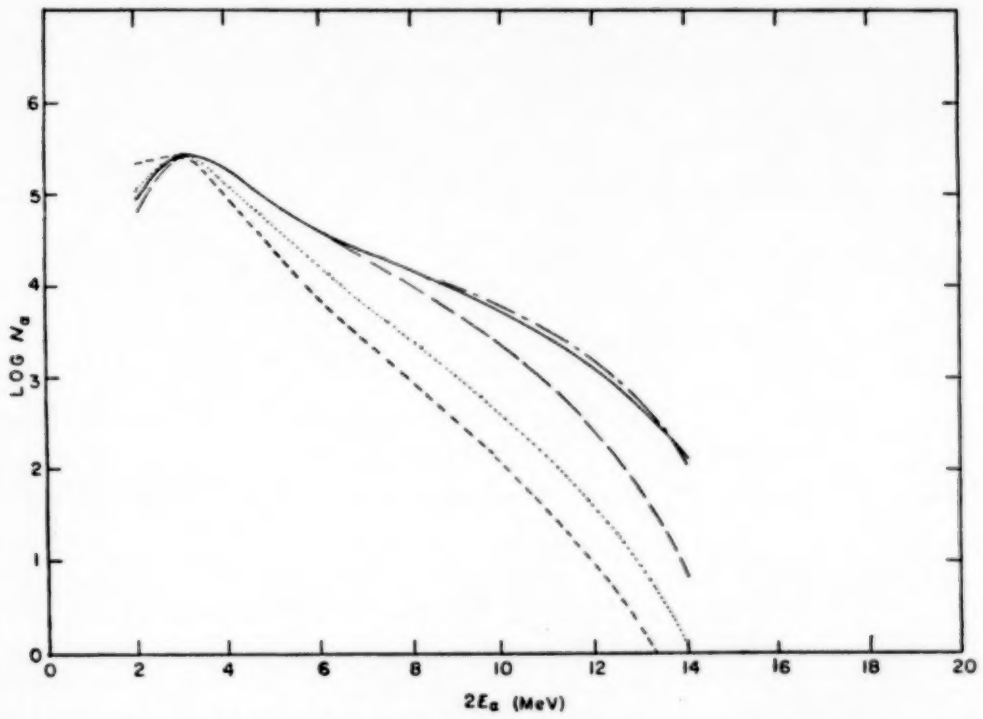

Fig. 4. Comparison of the alpha particle spectrum predicted by the present theory with that predicted by Wheeler [10]) and by Bonner *et al.* [11]). The effect of transitions to the 2^+, $T = 1$ state in Be^{8*} is also shown.

——— Experiment of Farmer and Class — — Present theory - - - - Wheeler's theory
····· ····· Bonner's modification — - — Present theory including transitions to $T = 1$ state

To calculate the effect of the uncertainty in the experimental alpha-alpha scattering phase shifts, the upper and lower limits of the phase shifts, taken from ref. [6]), were used. It is seen from fig. 3 that the predicted spectrum is especially sensitive to changes in the phase shift below the maximum.

Figure 4 shows a comparison of the present theory with the previous work of Wheeler [10]) and of Bonner *et al.* [11]). The parameters used in calculations of the spectrum predicted by Wheeler and by Bonner *et al.* were $E_0 = 3$ MeV, $\Gamma = 2$ MeV, and $R = 6 \times 10^{-13}$ cm. We have also used $L = 2$ in calculating the

Bonner curve. We also show in fig. 4 the spectrum obtained if transitions to the 2^+, $T = 1$, state are included as discussed in section 4 below.

Calculations of the $B^8(\beta^+)Be^{8*}(\alpha)\alpha$ decay have also been performed with similar results.

In view of the good agreement, refinements such as Coulomb effects (in the beta decay), were felt to be inessential to the present discussion. Similarly, other interesting, though minor effects, as virtual Coulomb excitation, are neglected.

4. Discussion

4.1. ALPHA SPECTRUM

The fit is very good over the region of the maximum to, say, 10 MeV, and is, in fact, a marked improvement over previous fits in this region. Below the

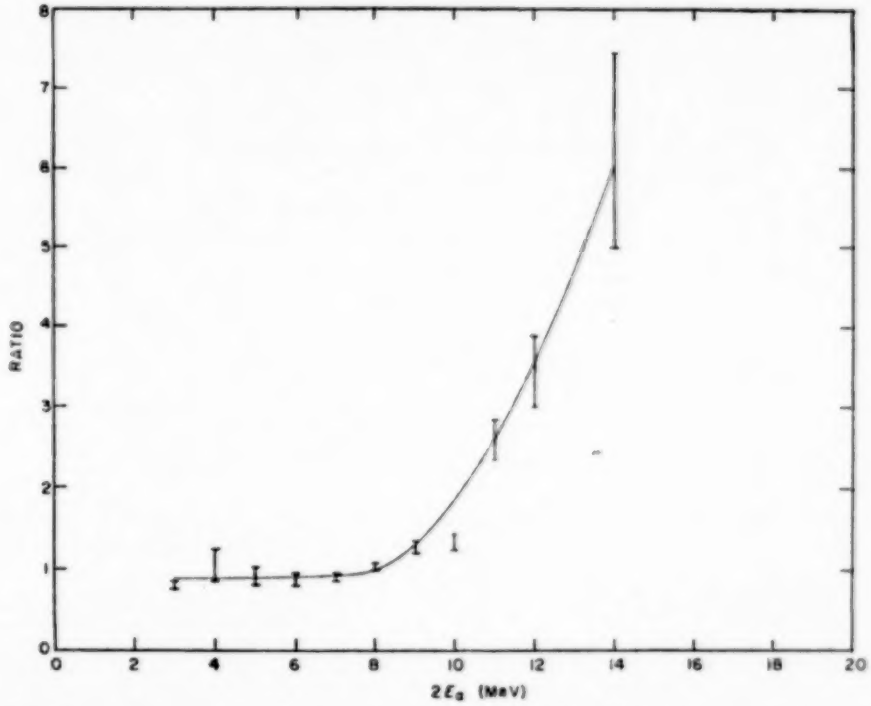

Fig. 5. Ratio of the experimental α-spectrum from the $Li^8(\beta^-)Be^{8*}(\alpha)\alpha$ decay to the theoretical prediction of the present theory. The error bars show the effect of the statistical error in the experimental spectrum and the uncertainty in the theoretical prediction due to the error in the δ^{2+} phase shifts.

maximum, the agreement between experiment and the present analysis is not unsatisfactory. This is a difficult region experimentally, because of the uncertainty which arises in correcting for energy loss in the target (which can easily amount to 15 % at low energies). Moreover, this region was not the principal concern of the experiment of Farmer and Class †.

† This region, however, might be of interest because of its extreme sensitivity to the δ^{2+} phase shift.

For the region above 10 MeV, the results predicted by eq. (5) lie consistently below the experimental data. The principal experimental error in this region is statistical, for the number of counts diminishes very rapidly with energy. Despite the large errors in this region, we feel that the indicated discrepancy might nevertheless be significant. In order to present our reason for this view, we have plotted in fig. 5, as a function of the alpha energy, the ratios of the experimental results to the theoretical results given by eq. (5). This figure shows that the deviation increases rapidly and systematically beyond 10 MeV.

A possible explanation for the discrepancy indicated by fig. 5, can be found in the existence of a second 2^+ state for Be^8, of $T = 1$, at 16.67 MeV, whose width is approximately 0.2 MeV. This state lies *above* the ground state of Li^8 but *below* the ground state of B^8. Nonetheless, the discrepancy observed in the alpha spectra of both the Li^8 and B^8 decays are essentially the same. We believe that in both cases the anomalous rise shown in fig. 5 is due to the tail of the $T = 1$, 2^+ resonance. (The contributions of the 4^+ and 0^+ states have the wrong shape to be an explanation for this discrepancy.)

To estimate the size of the effect of the $T = 1$, 2^+ state we assume that the beta decay via the $T = 1$ mode is coupled by means of isobaric spin mixing to the $T = 0$ mode, of the intermediate 2^+ system (as is necessary since the alpha channel has $T = 0$). The 2^+ intermediate system thus has four channels in this approximation: $T = 0, 1$, and (α, β). Omitting details, this leads to the approximate result

$$\frac{\sin^2\delta}{P_2} \to \frac{\sin^2\delta}{P_2}\left|1+\left(\frac{\varepsilon_1 \nu}{\varepsilon_0}\right) e^{i(\delta_1-\delta_0)} \frac{\sin\delta_1}{\sin\delta_0}\right|^2 \equiv \frac{\sin^2\delta}{P_2}\Delta^2.$$

Here ν is a measure of the isobaric spin mixing and ε_1 and ε_0 are the channel mixing phases for the $T = 1$ and $T = 0$ states respectively. The correction factor

$$\Delta^2 \approx \left|1+\frac{\varepsilon_1 \nu}{\varepsilon_0} e^{i\delta_1} \frac{\sin\delta_1}{i}\right|^2$$

in the region $E_\alpha = 10$ MeV, since $\delta_0{}^{2+} \approx \frac{1}{2}\pi$. We use the f^*t value and the fact that the beta decay of a $T = 1$ to $T = 1$ supermultiplet has a matrix element of the order unity to infer that $\varepsilon_1/\varepsilon_0 \approx 300$. The experimental rise then implies that the isobaric spin mixing is roughly 2 %, which is a reasonable order of magnitude.

We conclude that the discrepancy at the high energy end of the alpha spectrum, if indeed genuine, is probably the influence of the tail of the $T = 1$, 2^+ resonance. More accurate data in this experimentally difficult region would be of interest; quantitatively, however, the discrepancy involves very few counts.

Despite our lengthy attention to the discrepancy discussed above, it is rather surprising — from another point of view — that one can indeed fit the data so well over an interval of 10 MeV with the crude assumption that the beta decay matrix element in the initial transition is, aside from penetration factors, simply a *constant*.

4.2. BETA DECAY

The fit seems reasonably satisfactory, except, perhaps, at the low energy end,

where the experiments also disagree. This rise is *not* connected with the discrepancy in the number of high energy alphas, and remains even if the experimental alpha spectrum is used to calculate the beta spectrum, using the method of Bayley and Crane [14]).

5. Conclusion

The above analysis shows that it is not necessary to assume any contribution to the beta decay of Li^8 or B^8 involving the 0^+ and 4^+ states in Be^{8*}. Rather, both the alpha spectrum and the beta spectrum are consistent with the assumption that the decay goes entirely to the 2^+, $T = 0$ state. We further conclude that the discrepancy at the high energy end of the alpha spectrum above 10 MeV that occurs in such an analysis, if indeed real, is probably due to decays involving the 2^+, $T = 1$ state in Be^{8*}.

We are especially indebted to Professor C. M. Class, who drew our attention to the problem posed by the recent data, and to Professor G. C. Phillips, who suggested the basic viewpoint for the present work. We would also like to thank Professor Christy for a helpful discussion on a preliminary version of the manuscript.

References

1) J. F. Vedder, UCRL (8324) (June 1958)
2) B. J. Farmer and C. M. Class, Nuclear Physics **15** (1960) 626
3) W. F. Hornyak and T. Lauritsen, Phys. Rev. **77** (1950) 160
4) F. A. Ajzenberg and T. Lauritsen, Nuclear Physics **11** (1959) 45
5) Lauritsen, Barnes, Fowler and Lauritsen, Phys. Rev. Letters **1** (1958) 326
6) Phillips, Jones, and Miller, to be published
7) G. C. Phillips and L. C. Biedenharn, in preparation
8) J. M. Blatt and L. C. Biedenharn, Revs. Mod. Phys. **24** (1952) 258
9) L. C. Biedenharn and H. B. Willard, Proc. Phys. Soc. **72** (1958) 874
10) J. A. Wheeler, Phys. Rev. **59** (1941) 27
11) Bonner, Evans, Malich and Risser, Phys. Rev. **73** (1948) 885
12) K. Watson, Phys. Rev. **88** (1952) 1163
13) W. E. Burcham, Congrès International de Physique Nucléaire, Paris (1958) (Dunod, Paris, 1959)
14) D. S. Bayley and H. F. Crane, Phys. Rev. **52** (1937) 604
15) Cook, Fowler, Lauritsen and Lauritsen, Phys. Rev. **111** (1958) 569
16) K. Watson and M. Gell-Mann, Annual Rev. of Nucl. Sc. **4** (1954) 219

2.B:2.L

Nuclear Physics **15** (1960) 646—652; © *North-Holland Publishing Co., Amsterdam*
Not to be reproduced by photoprint or microfilm without written permission from the publisher

POLARIZATION IN C^{12}(pp) SCATTERING

J. E. EVANS and M. A. GRACE †

Atomic Energy Research Establishment, Harwell, Berks.

Received 30 December 1959

Abstract: Measurements have been made of polarization in C^{12}(pp) scattering at 60° (lab.) in the energy range 2.3—4.3 MeV. The results are significantly different from those derived from a phase-shift analysis and this can be explained by the extreme sensitivity of the polarization to small changes in the phase shifts. The experimental values then indicate a correction for the d-wave splitting.

1. Introduction

A solid target such as carbon has several advantages over helium when used as an analyser to measure polarization of protons, or as an agency to produce a polarized beam of protons. These advantages are:

1. The greater density of scattering nuclei makes for better geometry;
2. No containing windows are needed;
3. Less energy is lost in the recoil.

In the important energy range 2.5 MeV to 5 MeV very little experimental work has been done on the polarization, although its value has been predicted [1]) from phase shift data deduced from scattering experiments [2]). If carbon is to be used in this energy range, these phase shift predictions should be tested directly. Furthermore, because polarization can be very sensitive [1]) to changes in some of the phase shifts of the proton partial waves, its measurement can reveal small inaccuracies in the phase shift analysis of the elastic scattering.

We have determined this polarization in proton elastic scattering from carbon using the left-right asymmetry in helium as a polarization analyser. Because of the discrepancy between the experimental results and the theoretical predictions a measurement was also made using carbon both as polarizer and analyser to provide a check on the helium analysis.

2. Experimental Equipment

The arrangement for the experiment is shown in fig. 1. The proton beam from the A.E.R.E. Van de Graaff generator entered the first scattering chamber through a $\frac{1}{4}''$ gold stop and was scattered at 60° (lab.) by a natural carbon target (2mg/cm²). The scattered beam was then scattered again in helium at

† Clarendon Laboratory, Oxford.

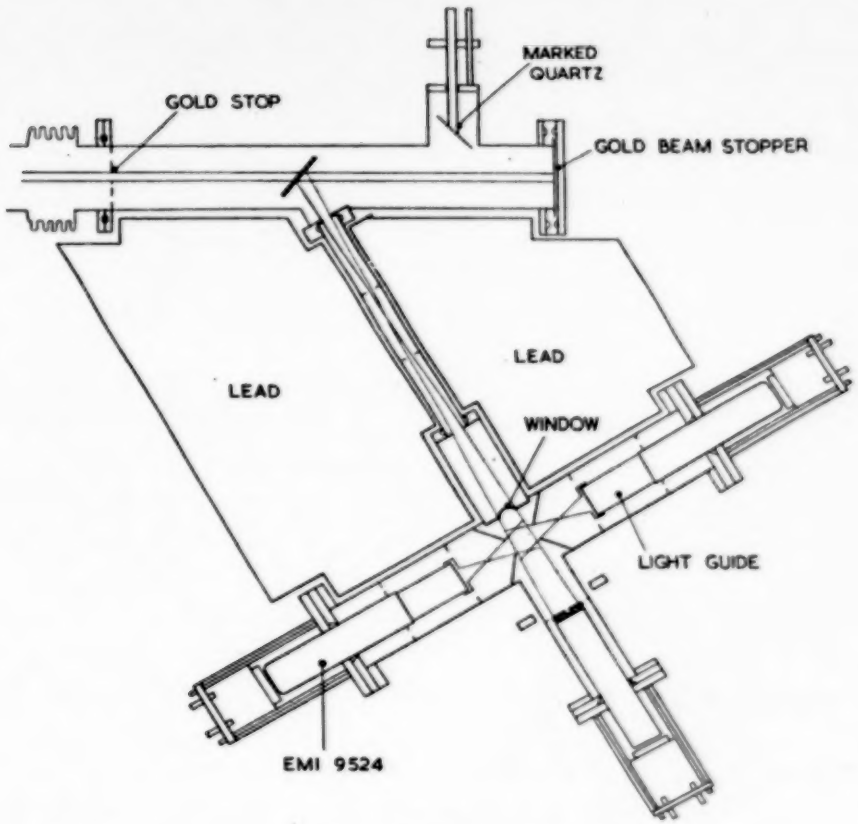

Fig. 1. The first scattering chamber and the helium polarimeter.

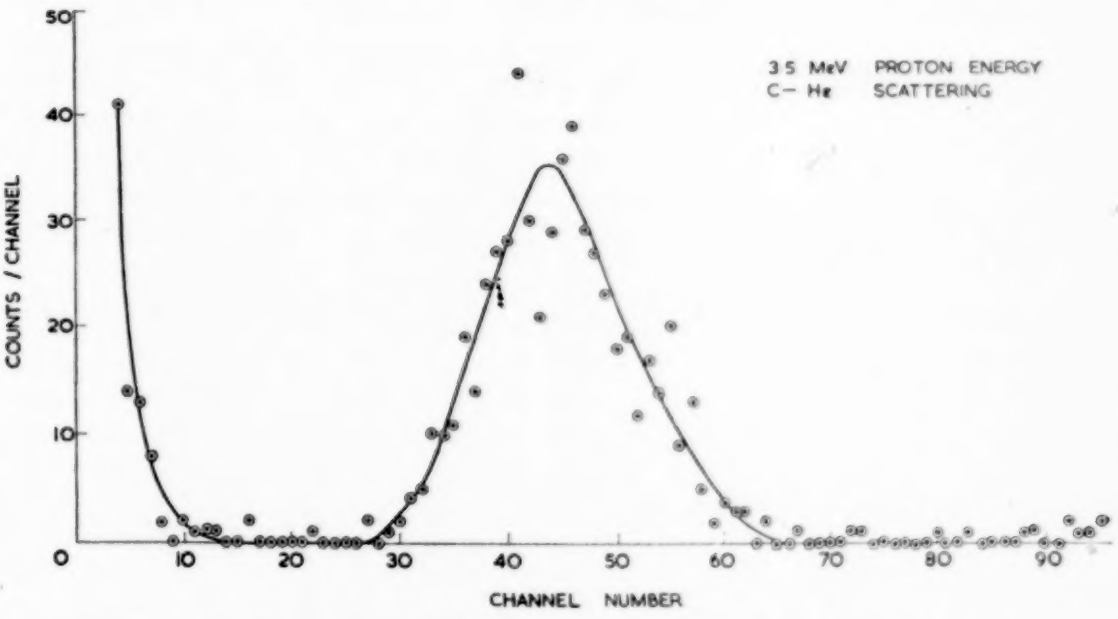

Fig. 2. The pulse height spectrum of protons after double scattering from carbon and helium. The initial energy was 3.5 MeV.

90° (lab.) and the protons were detected by scintillation counters fitted with thin (0.0025)" CsI(Tl) crystals covered with thin aluminium foil.

It is convenient if the carbon foil is self-supporting and uniformly thick. The target used was made by spraying Alcohol-Dag † on a glass slide and floating off in water. The result was a very flexible foil which chemical analysis showed to be 94 % carbon. About 1 % consisted of heavier elements, principally iron and the remaining 5 % was probably organic bonding agent which was likely to be reduced quickly to carbon under the heating due to the beam. No evidence for hydrogen in the foil could be seen in the spectrum of scattered protons.

The tantalum support for the carbon foil also held a gold foil which could be moved up to replace the carbon when desired. The quartz plate shown could be moved in to intercept the beam and it was marked to show any deviation from the required angle of 60° between the beam and the polarimeter axis.

The helium used in the polarimeter was 99.8 % pure. It was contained by a Melanex †† window 0.0003" thick which was sealed with Araldite ††† over the $\frac{1}{2}$" diameter entrance aperture.

The pulse height spectrum in the detectors (fig. 2) showed a background without structure which decreased quickly with increasing pulse height and which was attributed to γ-radiation. This arose largely from the carbon foil. Negligible background originated in the gold beam stopper. This background was minimized by the lead shielding and by reducing the thickness of the CsI(Tl) crystals to little more than the range of the detected protons. This reduction was achieved on a milling machine, the crystal being held by vacuum. Fine holes were drilled through the top of a brass drum over an area slightly less than the crystal size and the drum was clamped to the milling machine table. A first cut was taken over the surface, the crystal laid on and the drum evacuated. The machining was then carried out until the crystal was 0.0025" thick.

Light guides were found to be necessary with the thin crystals in order to distribute the light over the photo-cathode. The pulses were amplified and recorded in two 100 channel pulse height analysers, each monitored by a scaler in parallel. The counting rate for the protons was of the order of 100 counts per hour with a beam current of 2μA.

The helium polarimeter could be rotated about the axis of the scattered beam in order to reveal any intrinsic asymmetry in the apparatus. The whole was carefully aligned to ensure that the intersection of the beam and the foil lay on the polarimeter axis and remained there during a rotation of 180°.

† Alcohol-Dag: a suspension of colloidal graphite in alcohol.

†† Melanex — a plastic produced by the Imperial Chemical Industries Ltd. The equivalent in the U.S.A. is Mylar.

††† Araldite — a cold-setting 2-component epoxy-resin.

Fig. 3 shows the carbon polarimeter which was used to check the results obtained with helium. The geometry of the polarimeters was the same except for the change in scattering angle and the fact that the scattering volume was much smaller for the carbon foil.

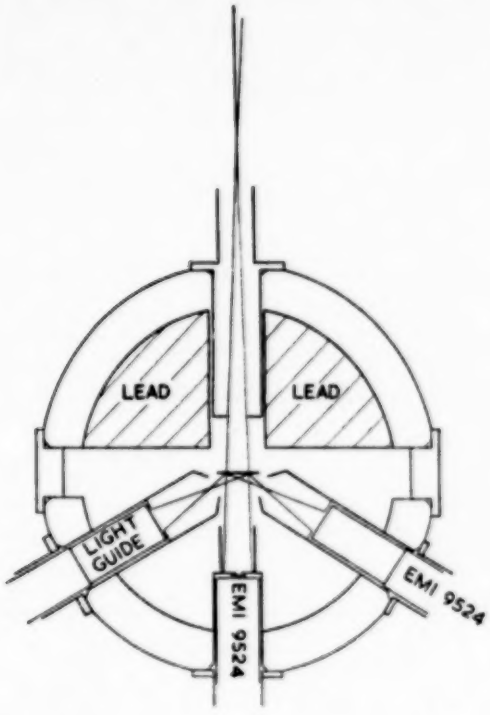

Fig. 3. The carbon polarimeter.

Two carbon analysing foils were used. One was made from Alcohol-Dag and the other from pure natural carbon. This latter was built up from 40 layers of vacuum-deposited foil by Dr. G. Dearnaley and Mr. M. Nobes. No difference was found between the results obtained with the two foils.

3. Analysis of Results

In principle the ratio (R/L) of the counting rates in the right-hand and left-hand detectors gives the product of the polarizations at the first and second scatterings, through the formula

$$\frac{R}{L} = \frac{1 + P_1 P_2}{1 - P_1 P_2}.$$

The experimental ratios have to be corrected for asymmetries in the apparatus, and these were investigated using the gold foil at the first scattering. At the energies used, the scattering from gold is not expected to be polarized because of the large Rutherford contribution. This has been confirmed experimentally at

10 MeV [3]) and, in fact, the ratio R/L with gold was never found to be significantly different from unity. To compensate for any small asymmetry, however, the ratio R/L for the experiment was taken as the mean of two equal runs, the polarimeter being rotated through 180° between runs. The ratio was not found to have changed significantly after the rotation.

Because of the finite geometry of the experiment a spread in differential scattering cross section $\sigma(E, \theta)$ and polarization $P(E, \theta)$ was introduced. It is easy to show that if the first scattering takes place with perfect geometry, then

$$\frac{R}{L} = \frac{1 + P_1 \bar{P}_2}{1 - P_1 \bar{P}_2},$$

where $\bar{P}_2$ is a mean polarization defined by

$$\bar{P}_2 = \frac{\int \sigma P_2 \phi \mathrm{d}\theta}{\int \sigma \phi \mathrm{d}\theta}.$$

Here $\phi(\theta)$ is a geometrical factor associated with the apparatus. Numerical integration showed that $\bar{P}_{\mathrm{He}}$ was not significantly different from P_{He} at the mean scattering angle of 90°. As shown in fig. 1 the geometry of the first scattering is very much better than that of the second, and the quantities P_1 and P_2 were accordingly always taken to correspond to the mean scattering angle.

The appropriate values for the helium polarization have been calculated by Dr. M. J. Scott from the results of a phase-shift analysis [4]) and agreement obtained experimentally at three points [5]).

Our results for C^{12}(pp) polarization at 60° (lab.) are shown in fig. 4. The sign of the polarization is defined by the vector $\mathbf{n} = \mathbf{K}_{\mathrm{out}} \times \mathbf{K}_{\mathrm{in}} / |\mathbf{K}_{\mathrm{out}} \times \mathbf{K}_{\mathrm{in}}|$. The horizontal bars on the experimental points indicate the energy spread arising from target thickness while the vertical bars represent the errors from counting statistics. It is seen that the experimental points lie close to a smooth curve which is markedly higher than the predicted [1]) polarization at all energies greater than about 2.5 MeV. The polarization at 60° (c.m.) has been measured up to 2.5 MeV by Sorokin and Taranov [6]) and all three results are in reasonable agreement in the region of overlap.

The greatest discrepancy occurs at about 4 MeV where our result is more than twice the predicted value. Accordingly the double scattering from carbon was carried out in this neighbourhood. The result was a product of two values for the carbon polarization at 60° (lab.), at different energies because of the energy loss in the scatterings. This product was measured as 0.13 ± 0.022. The results using the helium analyser give 0.107 ± 0.015 but use of the polarization predicted by the phase shift analysis leads to a value of only 0.02.

It is clear that the carbon and helium analyser results are self consistent but both are in disagreement with the phase shift analysis.

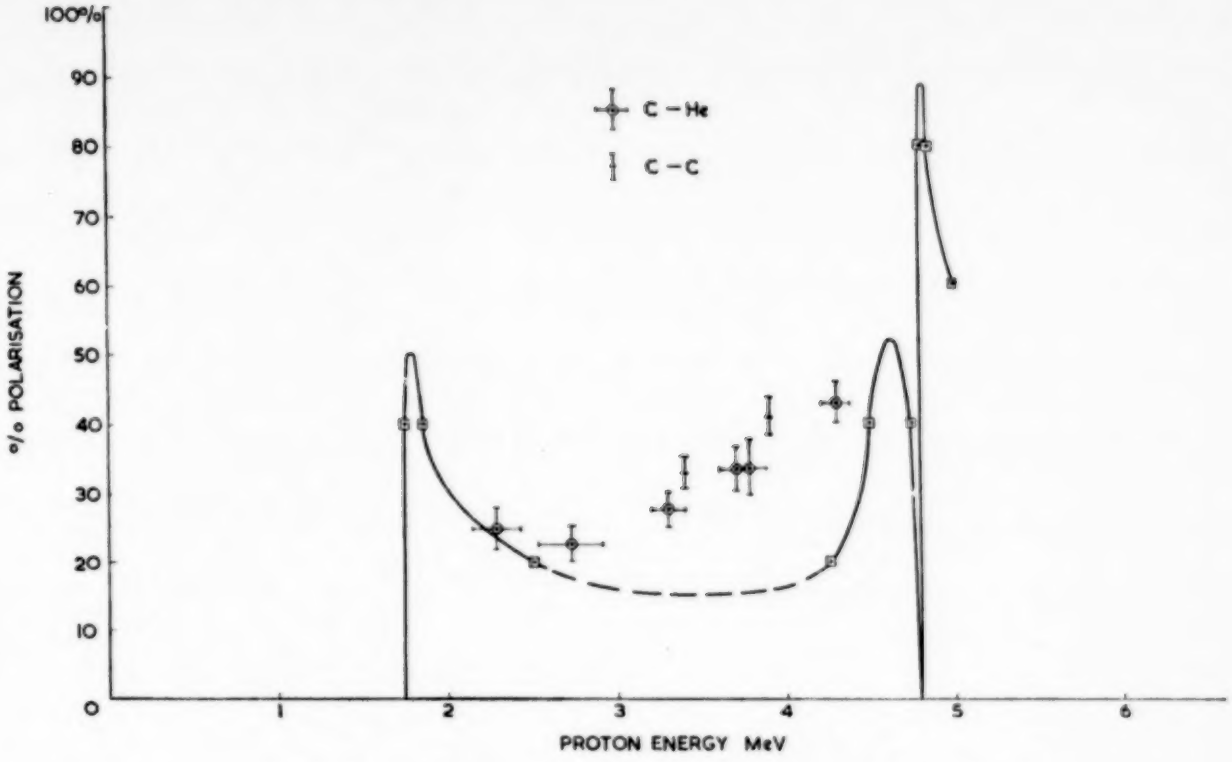

Fig. 4. Experimental results for C^{12}(pp) polarization at 60° (lab.) with the polarization predicted from the phase shift analysis.

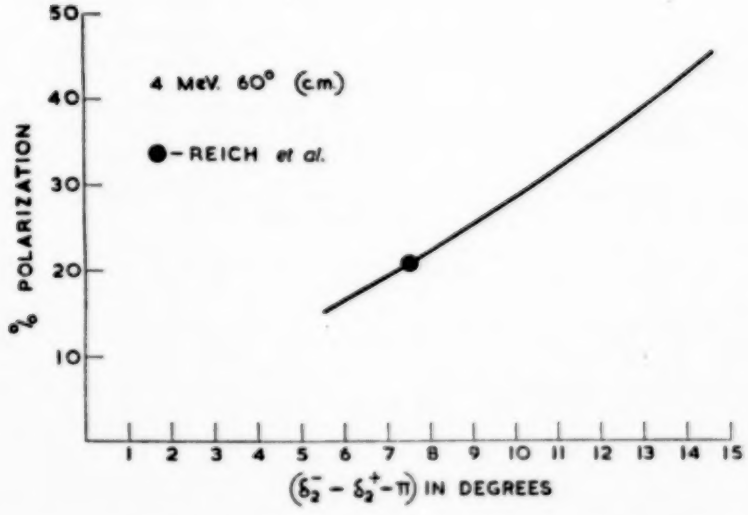

Fig. 5. C^{12}(pp) polarization at 4 MeV and 60° (c.m.) as calculated from the phase shifts of Reich *et al.* [2]) with the d-wave splitting varied.

A possible explanation for the discrepancy lies in the extreme sensitivity of the polarization to small changes in the two d wave phase shifts, δ_2^+ and δ_2^-. The presence of such effects in the off-resonance region was noted by Phillips and Miller [1]). Values for these two phase shifts were derived by Reich *et al.* [2]) from measurement of the differential scattering cross section at 54°44′ and 125°16′, these angles being zeros of the second-order Legendre polynomial, chosen to simplify the analysis. We find that if the derived values are separated by a further 6°, the polarization at 4 MeV agrees with our results (see fig. 5). The change in cross section produced by the new phase shifts is +3 % at 54°44′ and +5 % at 125°16′, and this is of the order of accuracy quoted for the cross section measurement [2]). The polarization at 4 MeV is much less sensitive to changes in the s-wave and p-wave phase shifts.

We are indebted to Dr. E. B. Paul for suggesting this work and to other members of the Van de Graaff group for helpful discussions. The A.E.R.E. workshops carried out the milling of the CsI(Tl) crystals.

References

1) G. C. Phillips and P. D. Miller, Proceedings of the International Conference on Nuclear Physics, Paris July 1958 (Dunod, 1959) p. 522
2) C. W. Reich, G. C. Phillips and J. L. Russell, Jr., Phys. Rev. **104** (1956) 143
3) L. Rosen and J. E. Brolley, Jr., Paper 668, Second United National International Conference on the Peaceful Uses of Atomic Energy, Geneva 1958
4) C. L. Critchfield and D. C. Dodder, Phys. Rev. **76** (1949) 602
5) M. J. Scott, Phys. Rev. **110** (1958) 1398
6) P. V. Sorokin and A. I. Taranov, Doklady **111** (1956) 82

1.E.1:
3.B

Nuclear Physics **15** (1960) 653—656; © *North-Holland Publishing Co., Amsterdam*
Not to be reproduced by photoprint or microfilm without written permission from the publisher

GAMMA RAYS FOLLOWING THE DECAY OF Nd^{147} AND Sm^{153}

T. J. WALTERS †, J. H. WEBBER †, N. C. RASMUSSEN and HANS MARK

Department of Nuclear Engineering and Department of Physics, Massachusetts Institute of Technology, Cambridge 39, *Massachusetts* ††

Received 28 December 1959

Abstract: A two meter radius bent quartz crystal spectrograph has been used to study gamma rays following the β^--decay of Nd^{147} and Sm^{153}. A gamma ray of 91.05 ± 0.04 keV was observed following the decay of Nd^{147}. This gamma ray corresponds to the transition between the first excited level and the ground state of the isotope Pm^{147}. Three gamma rays are observed in the decay of Sm^{153}. Two strong lines at 103.17 ± 0.04 keV and 69.66 ± 0.02 keV correspond to short-lived isomeric levels in Eu^{153}. These have been observed previously. In addition, a weak line at 97.42 ± 0.04 keV is present. A line at approximately this energy has been observed in the electron capture decay of Gd^{153} to Eu^{153}. The intensity ratio of the 103.17 keV transition to the 97.42 keV line is greater than 20 to 1.

1. Introduction and Experimental Methods

The availability of very strong radioactive sources has revived interest in using bent quartz crystal spectrometry to measure nuclear gamma ray energies. Several groups have been pursuing studies of this type in recent years. There are two methods for using the bent quartz crystal to measure gamma ray wave lengths. One is the technique developed by DuMond [1]) and his co-workers with the Mark I spectrometer. In this instrument, a line source is placed on the focal circle of the crystal and a counter on the convex side of the crystal is used to observe the gamma rays. The most accurate wave length measurements of many nuclear gamma ray lines to date have been made with the Mark I instrument. Another way of using the bent crystal is to place an extended source on the convex side of the crystal and to use a photographic emulsion on the focal circle of the spectrograph to record the gamma ray lines. This method was introduced by Y. Cauchois [2]) and has been developed for the study of nuclear gamma rays by the Livermore group [3]).

In the present series of experiments, a two meter radius spectrograph is used in the Cauchois geometry to measure gamma rays following the β^--decay of various rare earth isotopes. Since it is very difficult to make accurate absolute measurements of gamma ray wave lengths using the Cauchois geometry, it is necessary to calibrate the photographic plates with gamma rays of accurately

† Submitted in Partial Fulfillment of the Requirements for the degree of Master of Science at MIT.

†† This work was supported by a grant from the National Science Foundation.

known wave lengths. As in the past [3]), the wave lengths of gamma rays and X-rays observed in the decay of Ta^{182} are used for this purpose. The values of the wave lengths used are shown in table 1.

TABLE 1

Wave lengths of calibration lines

Element	Line	Wave length in Siegbahn X-units
Tantalum	$K\alpha_1$ X-ray	215.050±0.010 [a])
Tungsten	$K\alpha_2$ X-ray $K\alpha_1$ X-ray	213.383±0.010 [a]) 208.571±0.010 [a])
Tungsten gamma rays from W^{122}	68 keV 100 keV	182.638±0.018 [b]) 123.599±0.014 [b])

[a]) E. Inglestam, Nova Acta Regiae, Soc. Sci. Upaliensis **4**, No. 5 (1936)
[b]) Murray, Boehm, Marmier and DuMond, Phys. Rev. **97** (1955) 1007

The methods used to determine the unknown wave lengths are precisely the same as those described in ref. [3]). The wave length scale of the plate is determined by making a least squares fit using the calibration lines of known wave length. The instrument parameter determined in this manner is then used to compute the unknown wave lengths. The errors in the wave lengths are determined using only the statistical theory of errors since systematic errors in the system are small. Wave length in the 100 mÅ region can be determined with a precision of about one part in two thousand.

TABLE 2

Gamma rays following the decay of Yb^{169}
(from energy levels in Tm^{169})

Energy in keV (Present work)	Energy in keV (DuMond group)
63.11±0.02	63.12±0.01
109.77±0.04	109.78±0.02
130.53±0.06	130.53±0.03
177.27±0.10	177.24±0.05
197.99±0.13	197.97±0.06

The wave lengths of the DuMond group gamma rays are taken from: Hatch, Boehm, Marmier and DuMond, Phys. Rev. **104** (1956) 745

The initial measurements made with the two meter crystal spectrograph were conducted to check the reliability of the instrument. A Yb^{169} source was made at the MIT Reactor and the low energy gamma rays emitted by the source

were studied. The energies obtained are shown in table 2 and are compared to the energies obtained by DuMond and his co-workers using the Mark I spectrometer.

2. Results

2.1. Nd^{147}

A sample of Nd_2O_3 was irradiated in the MIT Reactor. The only isotope made in appreciable quantities is 11.1 day Nd^{147} which results from neutron capture in 17.2 % abundant Nd^{146}. The source strength obtained was roughly 0.3 curie. This isotope decays by β^- emission to Pm^{147}. Many gamma rays have been observed [6]) following this decay which correspond to the energy levels in the daughter nucleus. Seventy-nine percent of the β-decay goes to the first excited level of Pm^{147}. A gamma ray of 91.05 ± 0.04 keV was observed after a source exposure of approximately 20 curie-hours. This energy corresponds to the energy of the lowest observed level. Unfortunately, none of the other gamma rays emitted by this isotope were intense enough to be visible on the plate.

2.2. Sm^{153}

A sample of Sm_2O_3 was irradiated in the reactor. The isotope Sm^{153} is made by neutron capture on 26.6 % abundant Sm^{152}. Sm^{153} decays by β^- emission to Eu^{153} with a half life of 47 hours. The β^--decay is accompanied by gamma rays corresponding to energy levels in Eu^{153}. The level structure of Eu^{153} is quite complex. It has been studied by observing the β^--decay [7]) of Sm^{153}, the electron capture decay [8]) of Gd^{153} and by coulomb excitation [9]) of stable Eu^{153}. Neither β-decay apparently populates the rotational levels observed in the coulomb excitation experiments. Two short-lived isomeric states at 173 keV and 103 keV are populated in the β-decay of Sm^{153}. Two gamma rays at 103.17 ± 0.04 keV and 69.66 ± 0.02 keV are observed on the plate. The former corresponds to the 103 keV level to the ground state and the latter is the cascade transition between the 173 and the 103 keV levels.

In addition to the two strong gamma rays mentioned above, a very weak line at 97.42 ± 0.04 keV was also observed. A gamma ray of this energy is observed in the electron capture decay [8]) of Gd^{153}. It corresponds to a transition between a level at 97.42 keV and the ground state in Eu^{153}. This level has also been observed by A. W. Sunyar [10]) using an electron-conversion spectrometer. The possibility that the observed gamma ray could arise from a gadolinium impurity in the Sm_2O_3 sample can be ruled out on several grounds. The principal one is that the electron capture has a half life of 236 days whereas the activity of the sample used in these experiments was substantially gone after a few 47-hour half-periods. The source strength of the isotope was estimated at one curie and a total exposure of the order of 100 curie-hours was made. From the lines on the

plate it is estimated that the 103 keV gamma ray is at least 20 times as intense as the 97 keV gamma ray.

TABLE 3

Experimental results

Isotope	Gamma ray wave length in X units	Gamma ray energy in keV	Previous measurements of gamma ray
Pm^{147}	135.88±0.05	91.05±0.04	91.3 [a])
Eu^{153}	117.60±0.05 127.00±0.05 119.92±0.05	69.66±0.02 97.42±0.04 103.17±0.04	69.66 [b]) 97.3 [c]) 103.18±0.04 [b]) 103.27±0.02 [d])

[a]) J. M. Cork. M. K. Brice, R. G. Helmer, and R. M. Woods, Jr., Bull. Am. Phys. Soc. **3** (1958)64
[b]) O. Beckman, Nuclear Instruments **3** (1958) 27
[c]) E. L. Church and M. Goldhaber, Phys. Rev. **95** (1954) 626A
[d]) B. Anderssen, Proc. Phys. Soc. A **69** (1956) 415

The wave lengths and energies of all the gamma rays measured in the present work are shown in table 3.

The authors would like to thank Dr. John Garfield of Brookhaven National Laboratory for processing the emulsions. Thanks are also due to the MIT reactor staff and to Professor T. J. Thompson for their help and encouragement.

References

1) J. W. M. DuMond, in Beta and Gamma Ray Spectroscopy, Ed. K. Siegbahn (North-Holland Publishing Co, Amsterdam, 1955) Ch. IV
2) Y. Cauchois, Comptes Rendus **199** (1934) 857
3) Chupp, DuMond, Gordon, Jopson and Mark, Phys. Rev. **112** (1958) 518
4) Murray, Boehm, Marmier and DuMond, Phys. Rev. **97** (1955) 1007
5) T. S. Walters and H. J. Webber, Measurements of Some Rare Earth Gamma Rays Using a Two Meter Bent-Crystal Spectrograph, S. M. Thesis, MIT, 1959 (unpublished)
6) Strominger, Hollander and Seaborg, Revs. Mod. Phys. **30** (1958) 585
7) Dubey, Mandeville and Rothman, Phys. Rev. **103** (1957) 1430
8) E. L. Church, Private communication quoted in ref. [6])
9) H. Mark and G. T. Paulissen, Phys. Rev. **100** (1955) 813
10) A. W. Sunyar, private communication

7.A

Nuclear Physics **15** (1960) 657—663; © *North-Holland Publishing Co., Amsterdam*

Not to be reproduced by photoprint or microfilm without written permission from the publisher

ON THE REDUCTION FORMULAE FOR THE *S*-MATRIX ELEMENTS

J. HILGEVOORD

Institute for Theoretical Physics, University of Amsterdam

Received 18 November 1959

Abstract: Reduction formulae for the *S*-matrix elements, given by Lehmann, Symanzik and Zimmermann, are derived with particular emphasis on a proper use of the asymtotic condition and on the order of integration which is not always irrelevant. It is also stressed that local commutativity is not needed for the derivation of most of these formulae.

1. Introduction

Some years ago, Lehmann, Symanzik and Zimmermann [1]) have given so-called reduction formulae, in which a general element of the *S*-matrix of field theory is expressed in terms of the interacting operator field. In their derivation, they make only use of the general postulates for a relativistic quantum field theory and of an asymptotic condition which relates the field asymptotically to the free fields describing the ingoing and outgoing particles. The interaction need not be specified. Such formulae have been the starting point for a rigorous derivation of dispersion relations, which may be considered as special consequences, for the *S*-matrix elements, of the postulate of local commutativity. This postulate states that any two field operators, taken at points x and y such that $(x-y)$ is space-like, commute (or anticommute).

The reduction formulae are not unique. In fact, several forms are possible, which in some cases seems almost paradoxical. It is the purpose of this note to derive, for the special case of the *S*-matrix element between two-particle states, some alternative forms, in a little more careful manner than usual, and to make clear that they are not contradictory. It is also stressed that the postulate of local commutativity is not needed for a derivation of the reduction formulae of L.S.Z. In a recent paper, F. Kaschluhn [2]) has raised some doubts with respect to this point. He bases himself on a comparison of L.S.Z.'s and of Bogoliubov's formulation of the theory. We shall show that the expression for the *S*-matrix element, used by him, is not equivalent to one of the forms of L.S.Z. and can be derived from them only if local commutativity is assumed.

2. Derivation of Reduction Formulae

For convenience, we summarize the formulation of a relativistic quantum theory of a real, scalar field, given by Lehmann, Symanzik and Zimmermann [1]) as far as is needed for the following. Two fields, $A_{\text{in}}(x)$ and $A_{\text{out}}(x)$ are introduced, satisfying the free field equations

$$(\Box - m^2)A_{\text{in}}(x) = 0, \quad (\Box - m^2)A_{\text{out}}(x) = 0, \tag{1}$$

and the commutation relations

$$[A_{\substack{\text{in}\\\text{out}}}(x),\ A_{\substack{\text{in}\\\text{out}}}(y)]_- = i\Delta(x-y).$$

These fields describe the asymptotically free ingoing and outgoing particles. We assume that no bound states exist. Let $f_\alpha(x)$ represent a complete set of positive frequency solutions of the Klein-Gordon equation (1), orthonormal with respect to the Klein-Gordon in-product

$$(f_\alpha, f_\beta) = i\int \left\{ f_\alpha^* \frac{\partial f_\beta}{\partial t} - \frac{\partial f_\alpha^*}{\partial t} f_\beta \right\} \mathrm{d}_3 x = \delta_{\alpha\beta}.$$

Then the operators

$$A_{\text{in}}^\alpha = (f_\alpha, A_{\text{in}}(x)) \quad \text{and} \quad A_{\text{out}}^\alpha = (f_\alpha, A_{\text{out}}(x)), \tag{2}$$

which on account of equation (1) do not depend on time, create ingoing and outgoing particles, respectively, in the state f_α. With the help of these operators, two complete sets of states in our Hilbert space may be constructed:

$$\Phi_{\text{in}}^{\alpha_1\cdots\alpha_n} = A_{\text{in}}^{\alpha_1}\cdots A_{\text{in}}^{\alpha_n}|0\rangle, \quad \Phi_{\text{out}}^{\alpha_1\cdots\alpha_n} = A_{\text{out}}^{\alpha_1}\cdots A_{\text{out}}^{\alpha_n}|0\rangle.$$

The scattering operator is defined as the unitary operator that connects these two sets

$$\Phi_{\text{in}}^{\alpha_1\cdots\alpha_n} = S\Phi_{\text{out}}^{\alpha_1\cdots\alpha_n},$$

or also

$$A_{\text{out}} = S^\dagger A_{\text{in}} S.$$

The dynamical aspect of the theory is now introduced by the assumption that there exists an invariant field $A(x)$, called the interpolating field, which connects the in- and outgoing fields according to the following asymptotic conditions:

$$\begin{aligned} \lim_{t\to-\infty} \langle\Phi|A^\alpha(t)|\Psi\rangle &= \langle\Phi|A_{\text{in}}^\alpha|\Psi\rangle, \\ \lim_{t\to+\infty} \langle\Phi|A^\alpha(t)|\Psi\rangle &= \langle\Phi|A_{\text{out}}^\alpha|\Psi\rangle \end{aligned} \tag{3}$$

for all pairs of normalized states Φ and Ψ.

The field $A^\alpha(t)$ is defined analogously to (2), and will in general depend on

time. Here we obviously assume that the operators $A^{\alpha}(t)$ are defined, i.e. that they lead to states with a finite norm, which is not required of the operators $A(x)$. It is essential to have normalized states when applying the asymptotic condition (3).

Lehmann, Symanzik and Zimmermann now show how one can derive from these assumptions so-called reduction formulae, by which the elements of the S-matrix are expressed in terms of the interpolating field. We here derive again these formulae, in the special case of the S-matrix elements between two incoming states, each containing two particles, in a slightly more careful manner, making only use of the asymptotic condition between states with finite norm. We shall find that several forms of the final result are possible, and that one has to be careful when interchanging orders of integration, in order to avoid paradoxical results.

Consider the S-matrix element

$$\langle \Phi_{\text{in}}^{\beta_1\beta_2}|S|\Phi_{\text{in}}^{\alpha_1\alpha_2}\rangle = \langle \Phi_{\text{out}}^{\beta_1\beta_2}|\Phi_{\text{in}}^{\alpha_1\alpha_2}\rangle. \tag{4}$$

According to the asymptotic condition we may write this

$$\begin{aligned}\langle \Phi_{\text{out}}^{\beta_1\beta_2}|\Phi_{\text{in}}^{\alpha_1\alpha_2}\rangle &= \langle \Phi_{\text{out}}^{\beta_2}|A_{\text{out}}^{\beta_1*}A_{\text{in}}^{\alpha_1}|\Phi_{\text{in}}^{\alpha_2}\rangle \\ &= \lim_{t_x\to-\infty}\lim_{t_y\to+\infty}\langle \Phi_{\text{out}}^{\beta_2}|A^{\beta_1*}(t_y)A^{\alpha_1}(t_x)|\Phi_{\text{in}}^{\alpha_2}\rangle,\end{aligned} \tag{5}$$

where the order in which the limits are taken is irrelevant. Now, introduce two kinds of time-ordered products

$$\mathrm{T}_{\pm}A(x)A(y) = \theta(x-y)A(x)A(y) \pm \theta(y-x)A(y)A(x),$$

where $\theta(x) = 1$ if $t > 0$, and $= 0$ if $t < 0$. For equal times we suppose $\mathrm{T}_{\pm}$ to be defined in some way, which we do not specify here because it will turn out to be not important for our present purpose. Expression (5) may then be replaced by

$$\lim_{t_x\to-\infty}\lim_{t_y\to+\infty}\langle \Phi_{\text{out}}^{\beta_2}|\mathrm{T}_{\pm}A^{\beta_1*}(t_y)A^{\alpha_1}(t_x)|\Phi_{\text{in}}^{\alpha_2}\rangle \tag{6}$$

where both kinds of T-product are allowed. Now, due to the time-ordering

$$\lim_{t_y\to-\infty}\langle \Phi_{\text{out}}^{\beta_2}|\mathrm{T}_{\pm}A^{\beta_1*}(t_y)A^{\alpha_1}(t_x)|\Phi_{\text{in}}^{\alpha_2}\rangle = 0,$$

if $(f_{\beta_1}, f_{\alpha_2}) = 0$, e.g. From now on, we suppose that both f_{α_1} and f_{α_2} are orthogonal with respect to both f_{β_1} and f_{β_2}. Thus, (6) may be written

$$\lim_{t_x\to-\infty}\int_{-\infty}^{\infty}\mathrm{d}t_y\,\partial_{t_y}\langle \Phi_{\text{out}}^{\beta_2}|\mathrm{T}_{\pm}A^{\beta_1*}(t_y)A^{\alpha_1}(t_x)|\Phi_{\text{in}}^{\alpha_2}\rangle.$$

On the other hand, by performing the steps in the opposite direction,

$$\begin{aligned}&\lim_{t_x\to+\infty}\int \mathrm{d}t_y\,\partial_{t_y}\langle \Phi_{\text{out}}^{\beta_2}|\mathrm{T}_{\pm}A^{\beta_1*}(t_y)A^{\alpha_1}(t_x)|\Phi_{\text{in}}^{\alpha_2}\rangle \\ &\qquad = \lim_{t_x\to+\infty}\lim_{t_y\to+\infty}\langle \Phi_{\text{out}}^{\beta_2}|A^{\beta_1*}(t_y)A^{\alpha_1}(t_x)|\Phi_{\text{in}}^{\alpha_2}\rangle = \langle \Phi_{\text{out}}^{\beta_1\beta_2}|\Phi_{\text{out}}^{\alpha_1\alpha_2}\rangle = 0.\end{aligned}$$

Here we used the fact that for one-particle states $\Phi^{\alpha}_{\text{in}} = \Phi^{\alpha}_{\text{out}}$, and the orthogonality of the in- and out-states as assumed above. We get

$$\langle \Phi^{\beta_1\beta_2}_{\text{out}} | \Phi^{\alpha_1\alpha_2}_{\text{in}} \rangle = -\int \mathrm{d}t_x \partial_{t_x} \int \mathrm{d}t_y \partial_{t_y} \langle \Phi^{\beta_2}_{\text{out}} | \mathrm{T}_{\pm} A^{\beta_1 *}(t_y) A^{\alpha_1}(t_x) | \Phi^{\alpha_2}_{\text{in}} \rangle. \tag{7}$$

In this expression, the order in which the integrations are performed is irrelevant; the origin of this lies in the fact that in (6) the limits may be interchanged, irrespective of the presence of the time-ordering.

We can now perform the well-known transformation to integrals over space-time, by substituting the definition (2) of the operators and using the fact that the f_{α} are normalized solutions of the Klein-Gordon equation. Treating $A^{\beta_1 *}(t_y)$ first, we get

$$i \int \mathrm{d}t_x \partial_{t_x} \int \mathrm{d}y \, f^*_{\beta_1}(y) (\Box_y - m^2) \langle \Phi^{\beta_2}_{\text{out}} | \mathrm{T}_{\pm} A(y) A^{\alpha_1}(t_x) | \Phi^{\alpha_2}_{\text{in}} \rangle. \tag{8}$$

The Klein-Gordon operator in this expression also acts on the time-dependence contained in the time-ordering. We notice that an extra term,

$$\int \mathrm{d}t_x \partial_{t_x} \int \mathrm{d}y \, \partial_{t_y} \left\{ f^*_{\beta_1}(y) \langle \Phi^{\beta_2}_{\text{out}} | \dot{\mathrm{T}}_{\pm} A(y) A^{\alpha_1}(t_x) | \Phi^{\alpha_2}_{\text{in}} \rangle \right\},$$

appearing when going from expression (7) to (8), is zero, because for fixed t_x the expression in curly brackets vanishes at the boundaries of the t_y-integration. The operator $\dot{\mathrm{T}}_{\pm} A(y) A^{\alpha_1}(t_x)$ denotes all the terms of the derivative of the T-product that contain derivatives of the θ-function. Treating next $A^{\alpha_1}(t_x)$ in the same way, we obtain

$$-\int\int \mathrm{d}x \, \mathrm{d}y \, f_{\alpha_1}(x) f^*_{\beta_1}(y) (\Box_x - m^2)(\Box_y - m^2) \langle \Phi^{\beta_2}_{\text{out}} | \mathrm{T}_{\pm} A(y) A(x) | \Phi^{\alpha_2}_{\text{in}} \rangle$$
$$-\int\int \mathrm{d}x \, \mathrm{d}y \, f^*_{\beta_1}(y) (\Box_y - m^2) \partial_{t_x} \{ f_{\alpha_1}(x) \langle \Phi^{\beta_2}_{\text{out}} | \dot{\mathrm{T}}_{\pm} A(y) A(x) | \Phi^{\alpha_2}_{\text{in}} \rangle \}.$$

The second term vanishes again. We remark, however, that to conclude this, it is not necessary to interchange the time integrations: the term on which the Klein-Gordon operator acts, vanishes for fixed t_x at the boundaries of the t_y-integration, so we may integrate over y by parts, whereby all boundary terms, both of space (on account of the normalized character of $f^*_{\beta_1}(y)$) and of time vanish. The result is then zero because $f^*_{\beta_1}(y)$ satisfies the Klein-Gordon equation. The final result, in accordance with ref. [1]) is therefore,

$$\langle \Phi^{\beta_1\beta_2}_{\text{out}} | \Phi^{\alpha_1\alpha_2}_{\text{in}} \rangle$$
$$= -\int\int \mathrm{d}x \, \mathrm{d}y \, f_{\alpha_1}(x) f^*_{\beta_1}(y) (\Box_x - m^2)(\Box_y - m^2) \langle \Phi^{\beta_2}_{\text{out}} | \mathrm{T}_{\pm} A(y) A(x) | \Phi^{\alpha_2}_{\text{in}} \rangle, \tag{9}$$

where the order of integration is irrelevant, although we did not use this fact in our derivation.

A completely analogous result may be derived by using the retarded commu-

tator or anticommutator instead of the $T_\pm$ products. Define

$$R_\pm A(x)A(y) = -i\theta(x-y)[A(x)A(y)]_\pm.$$

Then

$$\langle \Phi^{\beta_1\beta_2}_{\text{out}}|\Phi^{\alpha_1\alpha_2}_{\text{in}}\rangle = \langle \Phi^{\beta_2}_{\text{out}}|A^{\beta_1 *}_{\text{out}} A^{\alpha_1}_{\text{in}}|\Phi^{\alpha_2}_{\text{in}}\rangle = \langle \Phi^{\beta_2}_{\text{out}}|[A^{\beta_1 *}_{\text{out}} A^{\alpha_1}_{\text{in}}]_\pm|\Phi^{\alpha_2}_{\text{in}}\rangle$$
$$= \lim_{t_x\to-\infty} \lim_{t_y\to+\infty} \langle \Phi^{\beta_2}_{\text{out}}|iR_\pm A^{\beta_1 *}(t_y)A^{\alpha_1}(t_x)\Phi^{\alpha_2}_{\text{in}}\rangle.$$

The extra term, introduced in the second step, is zero e.g. on account of $(f_{\beta_1}, f_{\alpha_2}) = 0$. The order of the limits is irrelevant. By going through the same steps as in the former derivation we now get

$$\langle \Phi^{\beta_1\beta_2}_{\text{out}}|\Phi^{\alpha_1\alpha_2}_{\text{in}}\rangle$$
$$= i\int\int dx\, dy\, f_{\alpha_1}(x) f^*_{\beta_1}(y)(\Box_x - m^2)(\Box_y - m^2)\langle \Phi^{\beta_2}_{\text{out}}|R_\pm A(y)A(x)|\Phi^{\alpha_2}_{\text{in}}\rangle. \quad (10)$$

We have thus obtained four equivalent expressions for the matrix element (4), with the two kinds of T-product and the retarded commutator and anticommutator respectively, irrespective of the boson or fermion character of the field; if we had started from a fermion field, we should have got similar results. That several answers may come out is not surprising, because in the procedure of obtaining these formulae, boundary values of integrals have been replaced by complete integrals, which is of course not a unique procedure. This arbitrariness may give rise, however, to an apparent contradiction, if we take out the two in-particles, instead of one in- and one out-particle. This leads, via

$$\langle \Phi^{\beta_1\beta_2}_{\text{out}}|\Phi^{\alpha_1\alpha_2}_{\text{in}}\rangle = \langle \Phi^{\beta_1\beta_2}_{\text{out}}|A^{\alpha_1}_{\text{in}} A^{\alpha_2}_{\text{in}}|0\rangle$$
$$= \lim_{t_x\to-\infty} \lim_{t_y\to-\infty} \langle \Phi^{\beta_1\beta_2}_{\text{out}}|T_\pm A^{\alpha_1}(t_x)A^{\alpha_2}(t_y)|0\rangle, \quad (11)$$

to the result

$$\langle \Phi^{\beta_1\beta_2}_{\text{out}}|\Phi^{\alpha_1\alpha_2}_{\text{in}}\rangle$$
$$= -\int\int dx\, dy\, f_{\alpha_1}(x) f_{\alpha_2}(y)(\Box_x - m^2)(\Box_y - m^2)\langle \Phi^{\beta_1\beta_2}_{\text{out}}|T_\pm A(x)A(y)|0\rangle, \quad (12)$$

which seemingly leads to the contradiction that it is symmetric or antisymmetric in α_1 and α_2, according to our choice of T_+ or T_-. Such a conclusion is not allowed, however, for in this case the order of integration *is* relevant. This may be seen from (11), where an interchange of the limits results in an interchange of the two in-particles. Consequently, because in our case we have bosons, the order of integration in (12) may be interchanged if we choose T_+, but may not if we choose T_-. If we have fermions, just the opposite is true.

The above derivation of formulae (9) and (12) may be directly generalized if an arbitrary number of particles are present in the ingoing and outgoing states. We get expressions where an arbitrary number of $A(x)$ operators is taken out

from both sides. Integrals which correspond to particles from different sides can be freely interchanged. Integrals which correspond to particles from the same side can be interchanged if the choice of the sign in $T_\pm$ agrees with the statistics of the asymptotic particles; in the other case, a change of sign is introduced, which is equal to the sign of the permutation involved. The form (10) does not permit such a generalization without the introduction of extra terms.

Still another version of (9) and (10) is obtained if we shift one of the Klein-Gordon operators to the right of the time ordering or retardation. Introducing $j(x) = (\Box_x - m^2)A(x)$, we obtain

$$\langle \Phi^{\beta_1\beta_2}_{\text{out}} | \Phi^{\alpha_1\alpha_2}_{\text{in}} \rangle = -\int\int \mathrm{d}x\, \mathrm{d}y\, f_{\alpha_1}(x) f^*_{\beta_1}(y)(\Box_y - m^2)\langle \Phi^{\beta_2}_{\text{out}} | \mathrm{T}_\pm A(y) j(x) | \Phi^{\alpha_2}_{\text{in}} \rangle, \quad (9')$$

$$\langle \Phi^{\beta_1\beta_2}_{\text{out}} | \Phi^{\alpha_1\alpha_2}_{\text{in}} \rangle = i\int\int \mathrm{d}x\, \mathrm{d}y\, f_{\alpha_1}(x) f^*_{\beta_1}(y)(\Box_y - m^2)\langle \Phi^{\beta_2}_{\text{out}} | \mathrm{R}_\pm A(y) j(x) | \Phi^{\alpha_2}_{\text{in}} \rangle. \quad (10')$$

These are indeed equivalent to expressions (9) and (10), although the integrands differ; but this difference contains the function $f^*_{\beta_1}(y)$ together with the operator $(\Box_y - m^2)$ operating on a function with support only at $t_y = t_x$. Therefore, a partial integration with respect to space and time is allowed and yields zero because $(\Box_y - m^2) f^*_{\beta_1}(y) = 0$.

We conclude this section by remarking once more that in this derivation of the reduction formulae we assumed the interpolating field $A(x)$ to be such that operators like $A^\alpha(t)$ give rise to states with finite norm. As far as I know, it is not clear at the moment whether this assumption leads to a wide enough framework for a field theory. Less restrictive schemes have been formulated, in which one only assumes that averages of the field over space-time of the form $\int A(x) f(x) \mathrm{d}x$, $f(x)$ being a test function, give rise to well-defined operators [3]), It is not difficult to give a modified formulation of the asymptotic condition in this scheme; the main difference consists in the replacement of our operators by time-averaged operators. However, I do not see how one can derive the above reduction formulae in this case; the concept of time ordering does not seem to fit well into a scheme where one considers time averages of the fields only.

3. Comparison to an other Result

Finally, we want to compare the above results with still another from of the S-matrix element, given by Bogoliubov, Medvedev and Polivanov [4]), and used by them in their proof of dispersion relations:

$$\langle \Phi^{\beta_1\beta_2}_{\text{out}} | \Phi^{\alpha_1\alpha_2}_{\text{in}} \rangle = \int\int \mathrm{d}x\, \mathrm{d}y\, f_{\alpha_1}(x) f^*_{\beta_1}(y) \langle \Phi^{\beta_2}_{\text{out}} | \frac{\delta^2 S}{\delta A_{\text{in}}(y) \delta A_{\text{in}}(x)} S^\dagger | \Phi^{\alpha_2}_{\text{in}} \rangle. \quad (13)$$

It can be shown that, for all points $x \neq y$,

$$\frac{\delta^2 S}{\delta A_{\text{in}}(y)\delta A_{\text{in}}(x)} S^\dagger = -\mathrm{T}_+ j(y)j(x), \tag{14}$$

where

$$j(x) = i \frac{\delta S}{\delta A_{\text{in}}(x)} S^\dagger,$$

if we assume the causality condition as stated by Bogoliubov, namely

$$\frac{\delta j(x)}{\delta A_{\text{in}}(y)} = 0, \tag{15}$$

if y is earlier than x, or if $(x-y)$ is space-like. The definition of $j(x)$ given here can be shown to be equivalent to that of the preceding section. The condition (15) implies local commutativity for the operators $j(x)$, but is in fact stronger [2]).

To obtain a comparable result, we start from (9′) with the T_+-product and take the Klein-Gordon operator to the right of the time ordering. This, however, introduces an extra term which is not zero. Formally we get

$$\begin{aligned}\langle \Phi_{\text{out}}^{\beta_1\beta_2} | \Phi_{\text{in}}^{\alpha_1\alpha_2} \rangle = &- \int\int \mathrm{d}x\, \mathrm{d}y\, f_{\alpha_1}(x) f^*_{\beta_1}(y) \langle \Phi_{\text{out}}^{\beta_2} | \mathrm{T}_+ j(y)j(x) | \Phi_{\text{in}}^{\alpha_2} \rangle \\ &+ \int\int \mathrm{d}x\, dy\, f_{\alpha_1}(x) f^*_{\beta_1}(y) \{\dot{\delta}(t_y - t_x)[A(y), j(x)]_- - 2\delta(t_y - t_x)[\dot{A}(y), j(x)]_-\}.\end{aligned} \tag{16}$$

In contrast to section 2, we now meet a situation where the definition of the time ordered product at $x = y$ becomes important. We see that, if local commutativity is assumed for all operators, the extra term in (16) vanishes, except for a possible contribution from the points $x = y$. Therefore, for a formula like (16) (without the extra term) to hold †, local commutativity is required, while this is not the case for the expressions of section 2. The result then agrees with (13), (14), up to contributions from the integrand at $x = y$. A fuller comparison of both results requires a knowledge of the definition of the quantities appearing in (14), at $x = y$.

† This formula has been used by Kaschluhn, ref. [2]).

References

1) H. Lehmann, K. Symanzik and W. Zimmermann, Nuovo Cimento **1** (1955) 205; **6** (1957) 319
2) F. Kaschluhn, Nuovo Cimento **12** (1959) 541
3) See e.g. A. S. Wightman, Quelques problèmes mathématiques de la théorie quantique relativiste, Lille Conference 1957
4) N. N. Bogoliubov, B. V. Medvedev and M. K. Polivanov, Problems in the theory of dispersion relations (Fizmatgiz, Moscow, 1958); German translation in Fortschritte der Physik **6** (1958) 169

1.D.2:
1.E.1:
4.E

Nuclear Physics **15** (1960) 664—677; © *North-Holland Publishing Co., Amsterdam*
Not to be reproduced by photoprint or microfilm without written permission from the publisher

PROTACTINIUM-237

K. TAKAHASHI† and H. MORINAGA†
Department of Physics, Tôhoku University, Sendai, Japan

Received 1 December 1959

Abstract: Protactinium-237 was produced from the reaction $U^{238}(\gamma, p)Pa^{237}$ by the 25-MeV bremsstrahlung. The activity produced was chemically separated with the aid of a recoil method from fission products. The half-life of this new isotope was found to be $T_{\frac{1}{2}} = 39 \pm 3$ min. The radiations were measured with a scintillation spectrometer. Three beta components were identified with the end-points of 2.30 ± 0.05 MeV, 1.35 MeV, and about 0.8 MeV. Many gamma rays were also found. A decay scheme was constructed with the aid of Nilsson's unified model.

1. Introduction

The isotope protactinium-237 was first reported by Crane and Iddings [1]) in 1954, from the reaction U^{238}(d, 2pn)Pa^{237} by the 190-MeV deuterons from a synchro-cyclotron. The half-life of the beta decay of this new isotope was determined to be about 11 min. No detailed investigation about the characteristics of this nucleide has been made since then. Usually, in the case of such a high energy reaction of fissile elements, it is likely that the reactions become very much complicated. Moreover, Pa^{237} is not the most abundant isotope among protactinium isotopes produced in high energy spallation reactions.

On the other hand, in the case of photoreaction with the 25-MeV bremsstrahlung, there are only four competing reactions, viz., the (γ, n), the $(\gamma, 2n)$, the (γ, p) and the (γ, f) reactions on fissile elements. Pa^{237}, therefore, is the major protactinium isotope produced by low energy photoreactions on natural uranium. Difficulty, however, is that the cross sections of the (γ, p) reactions in the region of uranium are about the order of some hundredth of those of the (γ, n) or the (γ, f) reactions. The products of the latter reactions, having many species of activities with various half-lives and various chemical behaviours, will complicate any separation procedure for protactinium.

In order to remove this difficulty, a physical separation technique of spallation products from fission products was employed, in addition to the specific chemical procedure to separate protactinium. Recently, Nakai and Yajima [2]) showed that UO_2 powder of about 8 microns in grain size embedded in oxalic acid powder with the mixing ratio 1 : 70, loses fission products into bedding material almost completely when it is activated by pile neutrons. They also showed that almost complete separation is achieved in the case of

† Now at Department of Physics, University of Tôkyo, Bunkyôku, Tôkyo, Japan.

$UO_2(NO_3)_2 \cdot 6H_2O$ powder of about the same grain size embedded in amorphous graphite powder with the same mixing ratio, as in the case of UO_2—$C_2H_2O_4 \cdot 2H_2O$ mixture.

The spallation products such as (γ, n), (γ, p), (γ, 2n) products however, have extremely low recoil energies, of the order of 10 keV, or extremely short ranges when produced in the photoreactions. Therefore, they can not get out from the phase of fissile material in such a mixture and will remain in the same phase making it possible to separate themselves from fission products. We have tried to employ this principle using the above two recipes for eliminating the disturbing fission product activities before finally separating the protactinium activity, by usual chemical separation methods.

Of late years, methods for isolation of protactinium have been studied by many investigators and several standard procedures have well been established [3]). In the present work, two types of these methods were employed after the physical separation of fission products from UO_2 powder: one is the codeposition technique with manganese dioxide precipitates from the nitric acidic solution of UO_2 and the other is the solvent extraction with methyl-isobutylketone (Hexon) from the nitric acidic aqueous solution of UO_2.

2. Experimental Procedure

In most of this work, a mixture of UO_2 powder of small grains (diameter 8μ) mixed with oxalic acid powder of about the same grain size with the ratio of 1 : 40 in weight was used. The total weight of each sample was about 41 g. Some of irradiations were carried out with uranyl nitrate-graphite mixture in which the former is 1 : 40 in weight ratio to the latter, the amorphous graphite. They were bombarded with the 25-MeV bremsstrahlung from the Tôhoku University betatron at the position of approximately 500 r/min for about 40 minutes.

After each irradiation, in the case of UO_2-oxalic acid mixture, the sample was dissolved into hot water and the residue, the UO_2 powder, was centrifuged. This residue was then washed once or twice with a hot diluted oxalic acidic solution in order to avoid the C^{11} activity to contaminate the final Pa activity, and also to minimize the fission product activities which could adsorb onto the surface of the fine UO_2 powder. The UO_2 was then dissolved into 8*N* HNO_3 solution.

In the case of uranyl nitrate-graphite mixture, the irradiated sample was dissolved into hot diluted nitric acidic solution and the graphite was filtered out. The filtrate was boiled and dried in order to remove the N^{13} activity. The assay was then dissolved into the diluted solution of lithium carbonate. This step was added so that the C^{11} produced from graphite and mixed into the uranyl nitrate phase could be driven out at the next step when the solution was again made acidic. Then the solution was again made 8*N* nitric acidic.

Two independent methods were employed in order to separate protactinium from such nitric acidic solution. One was the codeposition technique with manganese dioxide precipitate from nitric acidic solution of UO_2 [4]).

To the nitric acidic solution, a saturated solution of $Mn(NO_3)_2$ was added and then 0.1*N* $KMnO_4$ solution was dropped so that it was just enough for making the precipitation of MnO_2. This MnO_2 was centrifuged and then filtered and dried onto a filter paper. It took about 15 minutes to complete this procedure.

Another method used was the solvent extraction of protactinium with methyl-isobutylketone (Hexon) from the nitric acidic aqueous solution of UO_2[3, 5]). After dissolving the UO_2 into 8*N* HNO_3 solution, it was shaken with equal volume of hexon. Before starting to count the activity of this solution it did not take more than a few minutes. For long counting the hexon wad dried. This extraction method was used only for the samples of UO_2 mixed with oxalic acid.

The measurement of the half-life was made with a G-M counter and from the change of beta and gamma spectra with time measured by a scintillation spectrometer.

The beta ray end-point energy was measured with a beta scintillation spectrometer; the detector was a plastic scintillator of 1 inch thickness and 2 inches in diameter with a 7 μ aluminium window.

For the observation of gamma rays, a conventional multi-channel NaI(Tl) scintillation spectrometer was used. The sizes of the sodium iodide cyrstal used were $1\frac{1}{2}$ inches in thickness and $1\frac{1}{2}$ inches in diameter for most of the measurements, and $4'' \times 4''$ for the detection of high energy gamma rays.

Gamma-gamma coincidence measurements were also carried out for some intense gamma rays, such as 145, 205, 275, 330 and 460 keV, using a slow coincidence circuits ($2\tau = 5$ μsec). Conventional single channel pulse height analyser was used for energy discrimination of gamma ray pulses from one of the detectors. Output pulses from the analyser controlled the coincidence gate of the multi-channel pulse height analyser, which received gamma pulses from another detector. The performance of this coincidence circuit system was checked for the 330-keV gamma ray from Au^{196} ($T_{\frac{1}{2}} = 5.6$ d) which has the 356-keV coincident gamma ray.

3. Experimental Results

Fig. 1 shows the decay curve of the activities obtained according to the above recipe from a sample of uranium nitrate mixed with graphite powder. Quite similar results were obtained from samples of UO_2—$C_2H_2O_4$ mixture. In fig. 1, the long-lived activity is due to the beta decay of Th^{234} ($T_{\frac{1}{2}} = 24.1$ d) which mixed into the MnO_2 precipitates by a very small amount (about 0.3 percent). The 6.66-h activity comes from Pa^{234} which is in the radioactive

equilibrium in natural uranium. Referring to the amount of this Pa^{234} activity, the chemical yield of protactinium throughout this chemical procedure was estimated to be approximately 30 percent. After the subtraction of these well known activities, an appreciable amount of activity with a half-life of 39 ± 3 min was observed. This activity must be either due to Pa^{237}, or to some fission products which followed this chemical procedure, or may be due to

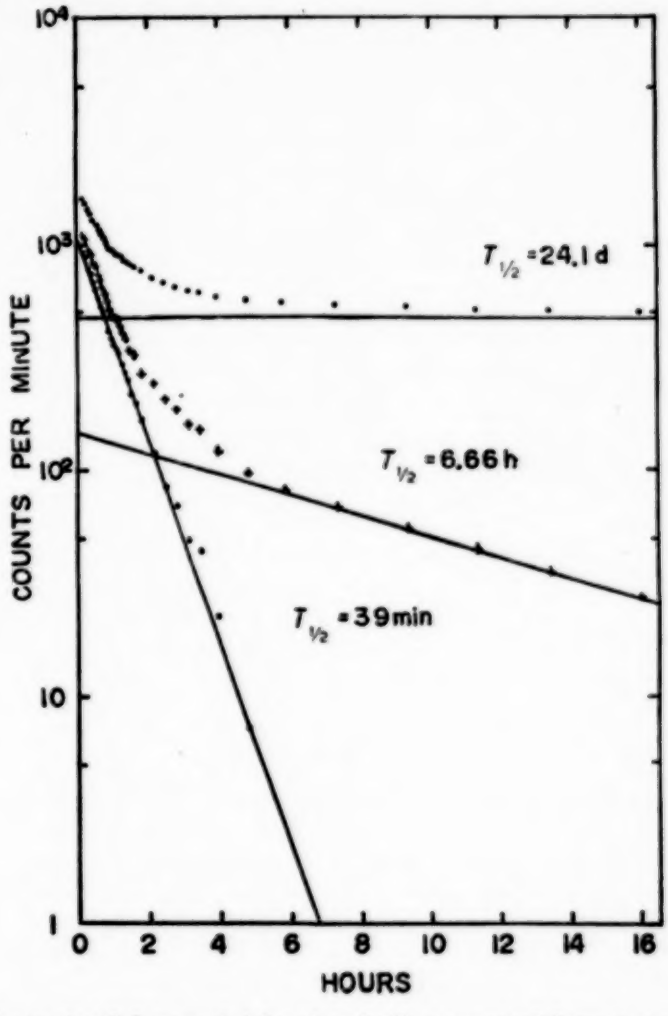

Fig. 1. Decay of the protactinium activities chemically separated from a sample of the uranium nitrate-graphite mixture bombarded with the 25-MeV bremsstrahlung.

other impurities. There is, however, no fission product activity which has only such a half-life. It is also difficult to attribute this 39-min activity to any conceivable impurity. Therefore, it is suspected that this activity is assigned to Pa^{237}. No 11-min activity [1]) was observed with an intensity expected from the (γ, p) yield systematics.

The beta ray end-point energy of this new activity was measured with a plastic phosphor. Following the decay of the beta spectrum, similar value of half-life was obtained after the subtraction of long-lived activities. The Kurie

plot for the 39-min component is shown in fig. 2(a). The end-point energy of the highest energy beta ray was determined to be 2.30 ± 0.05 MeV. This value agrees well with the value estimated by Seaborg *et al.* [6]) for Pa^{237} from the energy systematics of the alpha and beta decays of heavy elements. Here, no correction for the finite resolution of the phosphor was applied. Since the Kurie plot is linear in rather large portion of the spectra, the extrapolation of the

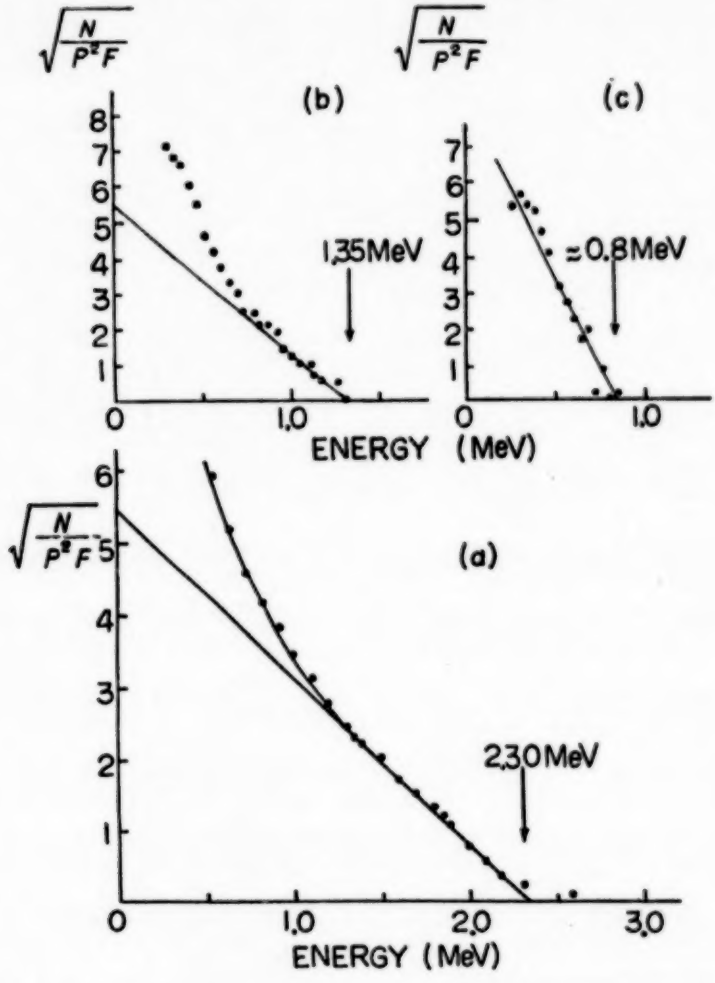

Fig. 2. Kurie plots of Pa^{237} beta spectrum: (a) total, (b) after the subtraction of the 2.30-MeV component, (c) after the subtraction of the 2.30-MeV and 1.35-MeV components.

linear part was used for determining the end-points. The Kurie plot of the beta spectrum begins to deviate upwards from the straight line at the vicinity of 1.3 MeV. In order to check the linearity of the Kurie plots of beta spectra, an examination of the performance of our spectrometer was made with the beta rays from In^{114} which has almost simple allowed spectrum. The result is shown in fig. 3. Comparing this to the spectra of the 39-min activity, it is concluded that other lower energy components should be included in the decay of Pa^{237}. After the Kurie plot analysis, two more branches of lower energies

were detected. The Kurie plots of these components are also shown in fig. 2(b) and (c), respectively: the higher energy one having $E_{\beta\,\max}$ at 1.35 MeV and, the lowest one at approximately 0.8 MeV. The branching ratios of these three components are roughly 60 : 30 : 10. For the lowest component, the value of

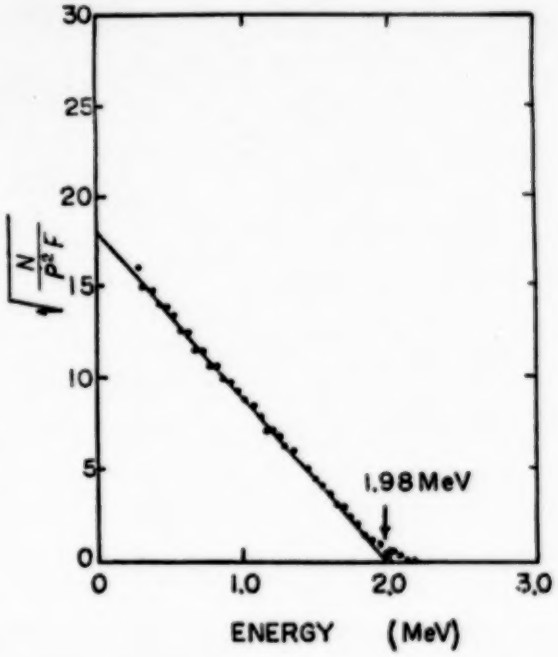

Fig. 3. Kurie plot of the beta spectrum of In^{111}.

its end-point energy and its branching should have rather large uncertainties because of the poor resolution and difficulty of the subtraction of the higher energy components. Results of the beta ray measurements with considerations of gamma ray spectra and the results of other experiments, are listed in table 1.

TABLE 1

Summary of the beta decay of Pa^{237}.

E_0 (MeV)	Intensity (%)	Log ft	Classification
2.30	60	7.2	1.u
1.35	23	7.3	1.u
	7	7.4	a.h
≈0.8	≲10	≳6.5	a.h

The gamma ray spectrum was measured with a conventional scintillation spectrometer. The decay of the spectrum was followed for several hours and almost all the peaks were found to decay with a half-life of about 39 min. Small fractions of the long component activity coming from Pa^{234} were also

observed. Therefore, those gamma rays are assigned to the new isotope Pa^{237}. After the subtraction of the long component gamma ray spectrum and the background spectrum, the gamma ray spectrum for Pa^{237} was obtained. This is shown in fig. 4. Because of the low counting efficiencies for high energy gamma rays, some of high energy gamma rays might have been missed. The intense 90-keV line is considered to be mainly due to the K X-ray from U^{237}.

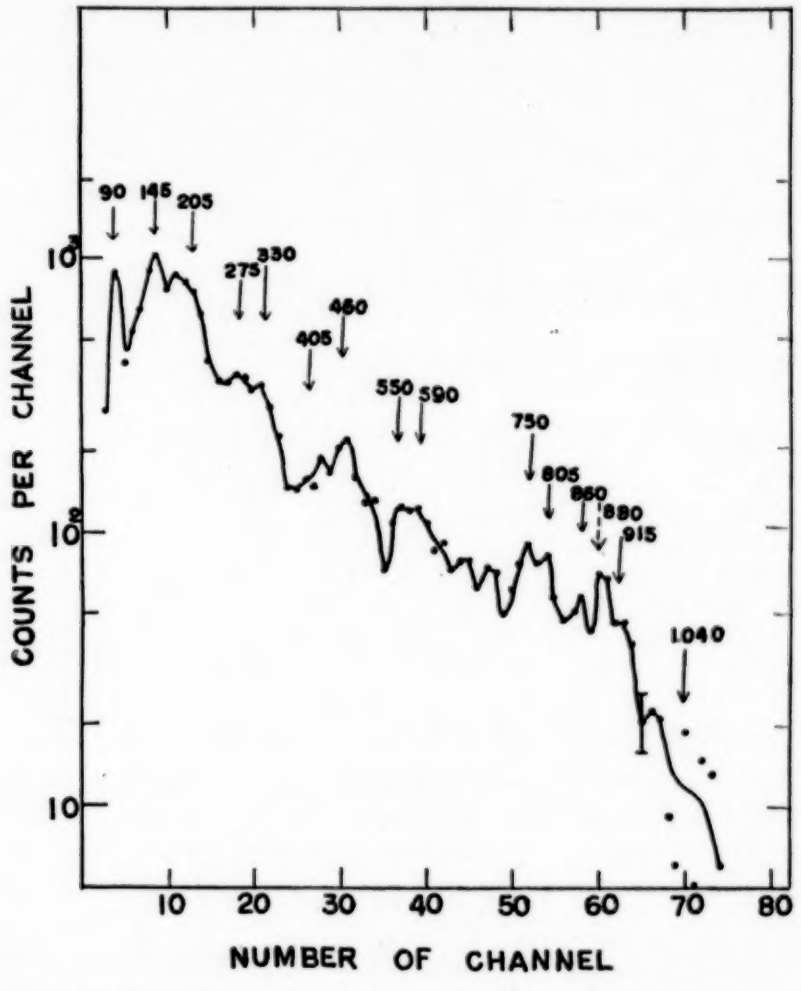

Fig. 4. Scintillation spectrum of the gamma rays from Pa^{237} observed with a $1\frac{1}{2}'' \times 1\frac{1}{2}''$ NaI(Tl) crystal. Gamma ray energies are given in keV.

For the observation of high energy gamma rays, a $4'' \times 4''$ NaI(Tl) was used. In order to cut off the low energy gamma rays, a $\frac{1}{4}''$-thick lead shield was placed at the face of the crystal. Fig. 5 shows the observed spectrum.

The analysis of the gamma ray spectra was carried out using, as a guide, the spectral shapes obtained in the same geometry from In^{114}, Hg^{203}, Na^{22}, Cs^{137} and Zn^{65} sources. After the subtraction of the back-scattering and the Compton peaks of higher energy components, relative heights of the photopeaks were obtained. Therefore, relative intensities of lower energy components may

have considerable uncertainties. Because of the rather large number of gamma rays quite a few peaks may actually be double or triple lines. Especially at lower energies the separation of peaks could have bad ambiguities. The intensity ratios of the observed gamma rays were determined using photopeak efficien-

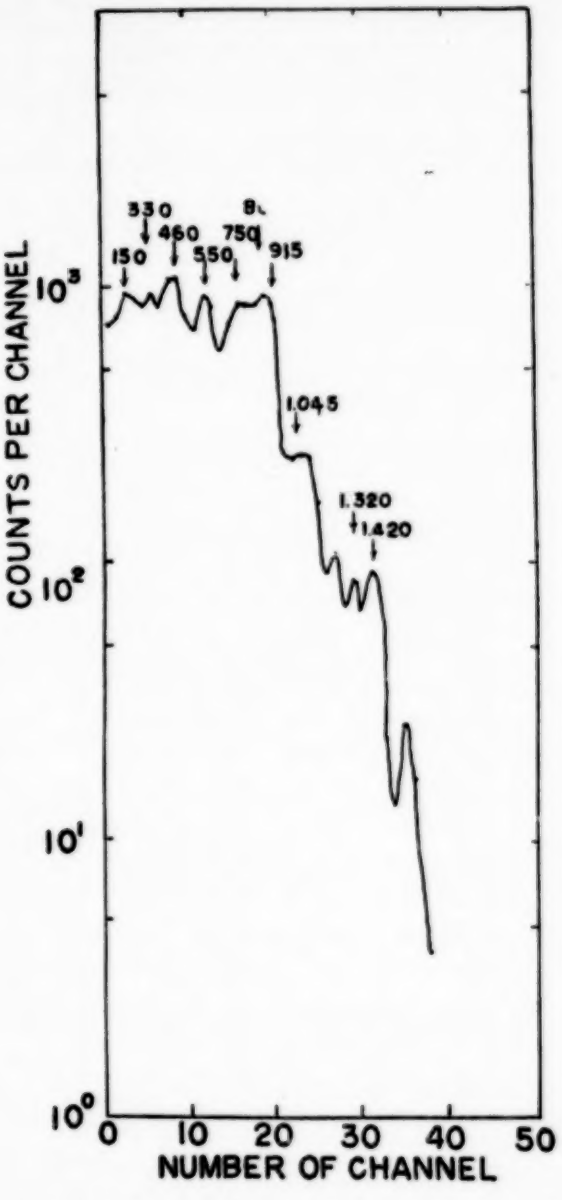

Fig. 5. Scintillation spectrum of the gamma rays from Pa^{237} observd with a 4″×4″ NaI(Tl) crystal. Gamma ray energies are given in keV.

cies of the present geometry of the spectrometers. They are listed in table 2.

Since the activity produced was weak and its half-life is short, gamma-gamma coincidence measurements may give only qualitative results. The 145-keV gamma ray was observed coincident with many other gamma rays as listed in table 2. The 205- and 275-keV gamma rays were also found to be in

coincidence with the 90-, 145- and 460-keV gamma rays. Similar results were observed for the 330-keV gamma ray but were not conclusive. A measurement with the 460-keV gamma ray gave a consistent result with the above data.

It is interesting to know the yield ratio of the reaction $U^{238}(\gamma, p)\ Pa^{237}$ relative to the reaction $U^{238}(\gamma, n)U^{237}$ at the 25-MeV bremsstrahlung energy. The chemical yield of Pa^{237} was estimated with reference to that of Pa^{234}

TABLE 2.

Intensities of the gamma rays from Pa^{237}

Energy (keV)	Relative intensity	Relative intensity coincident with the 145-keV γ-ray
90	50	5
145	45	3
205	55	3
275	20	2.5
330	40	1.5
405	30	(5) †
460	100	3.5
550	30	—
590	25	(5) †
750	50	2.5
805	45	—
860	100	—
880		—
915	100	—
1045	35	—
1320	10	—
1420	15	—

† Figures in parentheses may not be entirely due to Pa^{237}, since such coincidences may arise from the decay of Pa^{234}.

which was present in natural uranium in a condition of radioactive equilibrium. Then, we can calculate the yield of $U^{238}(\gamma, p)Pa^{237}$ using the C^{11} activity which was produced in the sample of the mixture as the monitor of the beam intensity. The measured value of the yield ratio was one five-hundredth relative to the (γ, n) reaction of U^{238}. This value of yield ratio is in good agreement in the order of magnitude with the value expected from the (γ, p) yield systematics. This further supports that this 39-min activity is due to Pa^{237}.

4. Discussion

As it is well known, $A = 237$ is in the strongly deformed region. Through recent studies [7, 8]), it has been established that the description of nuclear states

by the unified model is quantitatively successful. Here, we try to analyze our experimental results in the light of such theories.

The Kurie plot analysis of beta ray spectrum of Pa^{237} shows that the beta branching to the ground state (and its vicinity) of U^{237} is about 60 percent of the total disintegration and that the end-point energy of this ground state transition is 2.30 MeV. Since the measured value of the half-life is about 39 min, the log *ft* value of this ground state transition turns out to be about 7.2.

The ground state spin and parity of Pa^{237} is $\frac{3}{2}-$ from the systematics of the ground state properties of several known Pa isotopes. According to the analysis using Nilsson diagram, this is the first rotational state belonging to the $\frac{1}{2}-[530]$ intrinsic state [8]). It seems to be unreasonable that $\frac{1}{2}-$ comes lower at $A = 237$ since the decoupling factor does not change so much with the neutron number. On the other hand, the ground state of U^{237} has been found to be a $\frac{1}{2}+$ state and has been assigned to the $\frac{1}{2}+[631]$ intrinsic state from the investigations of the alpha decay of Pu^{241} [9]). Therefore, the beta transition from Pa^{237} to the ground state and its vicinity of U^{237} is classified as first forbidden and unhindered (abbreviated as 1.u.) transition. This is quite consistent with the log *ft* value of 7.2 obtained above, in the view of the recent studies on the systematics of the selection rules for beta transitions [7]).

The second beta group has an end-point energy of 1.35 MeV and its branching was about 30 percent (cf. fig. 2 and table 1). Since the log *ft* value of this group was estimated to be about 7, the transition must be classified as either 1.u. or allowed but hindered (abbreviated as a.h.).

From the theoretical examinations of the Nilsson diagram for neutron levels near $N = 145$ and the analysis of the level schemes of $U^{233}(N = 141)$, we can expect an intrinsic hole-state of $\frac{3}{2}+[631]$ in U^{233} among low energy states. This state appears at about 313 keV in U^{233}. In U^{233}, the $\frac{1}{2}+[631]$ state is also observed, but as an excited particle-state at about 400 keV. This means that for U^{233} the separation of $\frac{1}{2}+[631]$ and $\frac{3}{2}+[631]$ state is about 700 keV. Since the energy dependence of the states on deformations is very similar for these two states, the separation of the corresponding states in U^{237} should be close to 700 keV. Since the $\frac{3}{2}+[631]$ state can be reached by the 1.u. transition from Pa^{237} ground state, one may suspect that the 1.35-MeV beta branching includes such a 1.u. transition.

As shown in table 2, four gamma rays that have energies of 750, 805, 860 and 915 keV, were observed with large intensities. If the $\frac{3}{2}+[631]$ level exists at about 910 keV, the direct transitions to the ground state and its vicinity would occur from this level. Such transitions are the unhindered M1 transitions. From these facts we can tentatively assign the 910-keV level as the $\frac{3}{2}+[631]$ Nilsson level.

Recent investigations of the alpha decay of Pu^{241} show that in U^{237} the $\frac{5}{2}+[622]$ state appears at 145 keV. The first member of the rotational band of

this $\frac{5}{2}+[622]$ level has also been observed at 200 keV having a spin of $\frac{7}{2}$. In analogy to Pu^{239}, the ground-state rotational band should be observed between the ground state and the $\frac{5}{2}+[622]$ level. In the observed gamma ray spectra, however, the photopeak of the 915-keV line is wider than the energy resolution of our spectrometer (fig. 4): this suggests that more higher energy

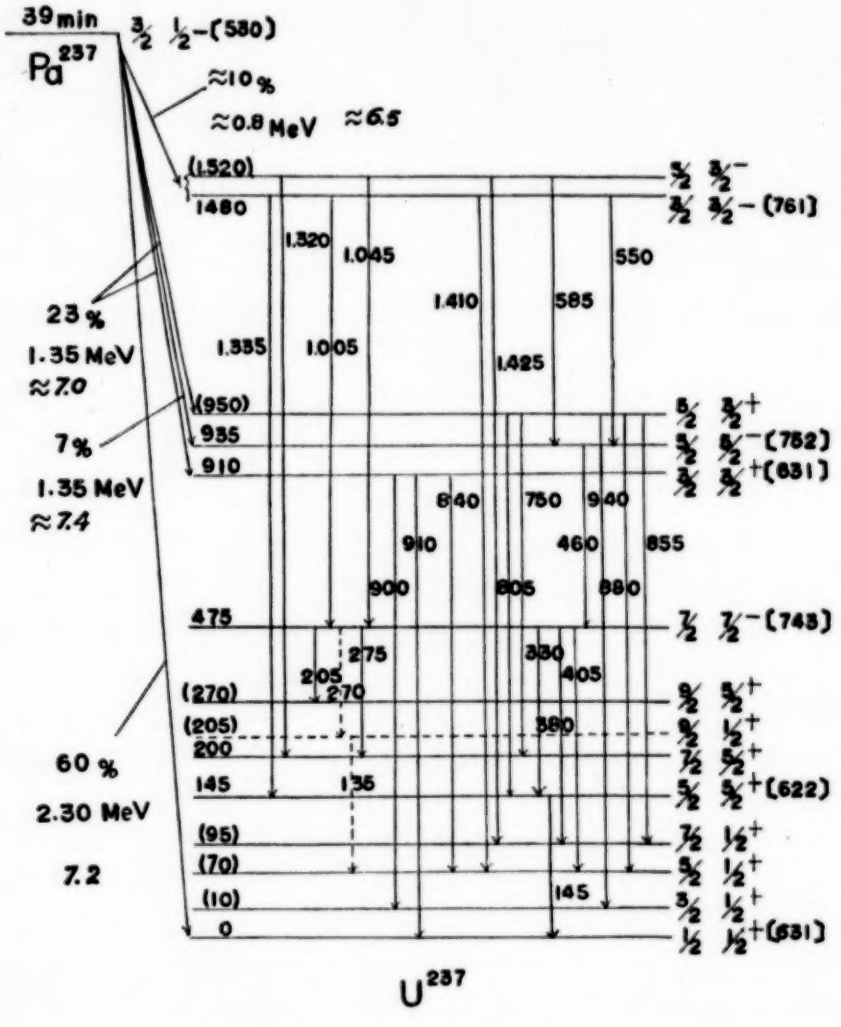

Fig. 6. Tentative decay scheme of Pa^{237}.

components may be included in this 915-keV line. This component may probably be the M1 transition to the $\frac{3}{2}+$ rotational level of the ground state from the level a little above the 910-keV level of $\frac{3}{2}+[631]$. Therefore, we can expect a possible state of $\frac{5}{2}$ belonging to the rotational family of $\frac{3}{2}+[631]$ at an energy of about 950 keV. Thus, it might be inferred that the transitions to these rotational members of $\frac{1}{2}+[631]$ and $\frac{5}{2}+[622]$, occur from the ground $\frac{3}{2}$ and the rotational $\frac{5}{2}$ states of the $\frac{3}{2}+[631]$ level in the unhindered M1 transitions. The above-mentioned gamma rays of 750, 805, 860, and 915 keV (actually two lines) are considered to correspond to these transitions.

Taking account of the beta and gamma counting efficiencies and the photopeak efficiencies of our spectrometer, we can calculate the intensity of the 1.35-MeV beta branching on the assumption that the above-described M1 transitions are the only transitions to take place. Since such M1 transitions are expected to be the fastest ones, this assumption is plausible. The total intensity of the 1.u. beta transitions to the $\frac{3}{2}+[631]$ level and its $\frac{5}{2}$ rotational member was thus estimated to be about 23 percent. The log *ft* value is about 7.0. Approximately a half of the 23 percent branching seems to decay to the $\frac{3}{2}+$ state and the rest decays to the $\frac{5}{2}+$ state. In this case, the log *ft* value turns out to be 7.3 for each transition. This value is consistent with the systematics of the beta decay selection rules for the 1.u. transition.

As shown in table 2, another intense gamma ray was observed at 460 keV. In gamma-gamma coincidence experiments, this gamma ray was observed in coincidence with the gamma rays of the energies of 145, 205, 275 and 330 keV. Very little information is available, because the weakness of the source intensity of Pa^{237} made it difficult to get enough statistics.

However, we have observed that both the 275- and 330-keV gamma rays were coincident with the 145-keV gamma ray. We may therefore postulate two new intrinsic states, the $\frac{7}{2}-[743]$ Nilsson level at about 475 keV and the $\frac{5}{2}-[752]$ state at about 935 keV, from which an intense M1 gamma transition of 460 keV decays to the former state. Analyses of the Nilsson diagram for neutron levels near $N = 145$ and of the level schemes of Pu^{239}, Pu^{237}, U^{235} and U^{233} would seem to support these assignments of energies and the intrinsic states.

The ground state of $Pu^{237}(N = 143)$ has been almost surely assigned $\frac{7}{2}-[743]$ and a state at 145 keV is considered to be $\frac{1}{2}+[631]$. On the other hand, Pu^{239} $(N = 145)$ has the ground state of $\frac{1}{2}+[631]$, and has the $\frac{7}{2}-[743]$ state at 392 keV. The energy difference between these two intrinsic states changes fairly rapidly with the change of neutron number. Such a tendency is also observed in the level structures of $U^{235}(N = 143)$ and $U^{233}(N = 141)$. The ground state of $\frac{7}{2}-[743]$ occurs in U^{235}, as in the case of Pu^{237}, but the state of $\frac{1}{2}+[631]$ appears very close to the ground state. In U^{233}, however, these two states appear as the excited states: the $\frac{1}{2}$ state appears at 400 keV and the $\frac{7}{2}$ state is observed at about 295 keV. The energy difference between these states is about 100 keV.

In the case of the $\frac{7}{2}-[743]$ state in $U^{237}(N = 145)$, it will be expected from the above discussions that this level would be observed between 300 keV and 550 keV. Thus the $\frac{7}{2}-[743]$ orbital can reasonably be assigned to a state at about 475 keV, as expected before. Therefore, the intense 460-keV transition to the $\frac{7}{2}-[743]$ state can reasonably be explained to occur from the $\frac{5}{2}-[752]$ state at about 935 keV in the M1 transition as expected before. Since the level postulated at 953 keV is $\frac{5}{2}-[752]$, the a.h. transition of the beta ray from the

$\frac{3}{2}-$ ground state of Pa^{237} is expected to occur. Actually such a beta branching must be assumed to exist being mixed in the spectrum of the 1.35-MeV mentioned above. According to the estimation from the intensity ratios of the 460-keV gamma ray and of the 1.35-MeV beta rays, and the beta and gamma counting efficiencies, this transition is expected to correspond to the remaining 7 percent branching of 1.35 MeV. The experimental log *ft* value was calculated to be about 7.4 for this branching. The value is indeed what is expected for the a.h. transition of the beta ray.

Thus, it may be concluded that the $\frac{5}{2}-[752]$ state decays to the $\frac{7}{2}-[743]$ state at about 475 keV with the emission of the 460-keV gamma ray in M1. From this level, many gamma rays of such energies as 205, 275, 330 and 405 keV lead to the lower states; they are the $\frac{9}{2}+$ state at about 270 keV, the $\frac{7}{2}+$ state at 200 keV, the $\frac{5}{2}+$ state at 145 keV and the $\frac{5}{2}+$ state at about 70 keV. The first three states are probably the members of the rotational band of the $\frac{5}{2}+[622]$ Nilsson level at 145 keV and the last one is the rotational member of the $\frac{1}{2}+[631]$ orbital.

Results of high energy gamma ray measurements show that the 1420-, 1320-, 1045- and 1010-keV gamma rays lead to the lower states, and suggest that another intrinsic state and its rotational members appear in the vicinity of 1500 keV. Therefore, the beta branching whose energy is about 0.8 MeV can be attributed to the decay to these highly excited states of U^{237}. The experimental log *ft* value of the 0.8-MeV beta branching was estimated to be about 6.5 and this value implies that the transition should be classified as either a.h. or 1.u. from the systematics. Referring again to the Nilsson diagram, we can tentatively assign the states as the $\frac{3}{2}-[761]$ state and the first member of its rotational band at around 1500 keV. The intensity ratios of such gamma rays emitted from these levels as those of 1420, 1320, 1045, 1010, 590 and 550 keV, can be explained quite consistently, if one assumes that the $\frac{3}{2}-[761]$ ground and its first rotational states appear at 1480 and 1530 keV.

According to the above discussion, we can construct a very tentative decay scheme of Pa^{237}. The proposed decay scheme is shown in fig. 6, where the log *ft* values are given in italics and the gamma ray transition energies are in keV. The energy assignments of the excited states which have ambiguities are shown in parentheses.

It is interesting to see such a large number of intrinsic states having been observed in the decay of a radioisotope. This is due to its high disintegration energy. Because of the intrinsically poor resolution of the scintillation spectrometer it was difficult, in general, to resolve gamma rays to or from levels in the same intrinsic structure. They are separated usually by several tens of keV. Therefore, our assignments of rotational members may not be so certain. As for the intrinsic states, the assignments seem to be more certain. It will be very interesting to make more elaborate analysis of this decay scheme using stronger source of Pa^{237}.

The authors wish to express their appreciations to Professor S. Kachi and Dr. S. Yajima for their helpful suggestions and advices concerning the chemical procedures.

References

1) W. W. T. Crane and G. M. Iddings, Phys. Rev. **95** (1954) 1702
2) T. Nakai and S. Yajima, J. Chem. Soc. Japan (Pure Chemistry) **79** (1958) 1267
3) J. J. Katz and G. T. Seaborg, The Chemistry of the Actinide Elements (John Wiley and Sons, New York, 1957) Chap. IV
4) J. Golden and A. G. Maddock, J. Inorg. and Nuclear Chem. **2** (1956) 47
5) G. H. Morrison and H. Freiser, Solvent Extraction in Analytical Chemistry (John Wiley and Sons, New York, 1957) p. 140
6) B. M. Foreman Jr., and G. T. Seaborg, J. Inorg. and Nuclear Chem. **7** (1958) 305.
7) B. R. Mottelson and S. G. Nilsson, Mat. Fys. Skr. Dan. Vid. Selsk. **1** No. 8 (1959)
8) F. S. Stephens, F. Asaro and I. Perlman, Phys. Rev. **113** (1959) 212
9) M. S. Freedman, F. Wagner, Jr., and G. W. Engelkemeir, Phys. Rev. **88** (1952) 1155

2.F

Nuclear Physics **15** (1960) 678—682; © *North-Holland Publishing Co., Amsterdam*

Not to be reproduced by photoprint or microfilm without written permission from the publisher

THE INELASTIC SCATTERING OF DEUTERONS FROM ^{12}C

W. M. FAIRBAIRN

Mathematics Department, The College of Science and Technology, Manchester

Received 23 November 1959

Abstract: The angular distribution of deuterons scattered inelastically from ^{12}C is determined using a direct interaction theory which assumes the excitation of a single one-particle level in the intermediate state. Comparison is made with the experimental data for two bombarding energies. The agreement is good and the method could be extended to other nuclei to obtain information about nuclear structure.

1. Introduction

There are three derivations of the differential cross-section for the inelastic scattering of deuterons under the assumption that only one of the constituent nucleons of the deuteron interacts with the bombarded nucleus (Huby and Newns [1]), Fairbairn [2]), Sawicki [3])). Sawicki has claimed that the inelastic scattering from ^{24}Mg considered by Huby and Newns and by the present author should be analysed using his formula which assumes excitation of the collective rotational levels of the bombarded nucleus. Since ^{24}Mg is an even nucleus which shows rotational level structure this claim is justified. The purpose of the present paper is to consider a reaction which is more likely to proceed by the excitation of single particle states and to analyse the experimental data using the formula derived previously by the author.

2. The One-Level Formula

The formula (ref. [2]), eq. (5.4)) for the differential cross-section when deuterons are scattered inelastically assumes that the reaction proceeds through intermediate states in which only one of the nucleons of the deuteron reacts with the bombarded nucleus to form a compound nucleus. Such one-particle excitation of the nucleus implies that in those reactions the structure of the final excited level must differ from that of the ground level only by the state of one of its constituent nucleons. Both the ground state and the excited state of the bombarded nucleus must be possible "parent states" for the intermediate compound nucleus state formed by the addition of one nucleon. This requirement restricts the number of allowed intermediate states.

If the actual nuclear states were shell model states, then for many reactions only one intermediate state would be allowed. The actual wave functions for

these states contain admixtures of other shell model configurations even when the shell model is a good approximation, but we consider the case in which the shell model wave functions form the major portion of the actual wave functions and in which there is only one possible intermediate state for these shell model states.

In the formula cited above † we require that, given $(j_0, 0)$ and (j_t, t), the product

$$u_{J_s I^* j_0 0 l_n^*}(k^s_{n0}, r_0) u_{J_s I j_t t l_n}(k^s_{nt}, r_0)$$

is appreciable for only one (J_s, s) with corresponding fixed values of (I, I^*, l_n, l_n^*). Under these conditions the integration over k_p will give a contribution only at the zero $k_p = k_{ps}$ of $b_{JI^* j_0 0 l_n^*}(k_p)$ which corresponds to the state (J_s, s). The resulting expression for the differential cross-section is

$$\sigma_t(\theta_d) = \frac{3\pi^4(2J_s+1)^2\alpha^2 K_t k_{ps}^2}{(2j_0+1)K_0} |u_{J_s I j_t t l_n}(k^s_{nt}, r_0) u_{J_s I^* j_0 0 l_n^*}(k^s_{n0}, r_0)|^2$$

$$\sum_{LSPQ} \left(\frac{2L+1}{2P+1}\right) W^2(1\tfrac{1}{2}\,1\tfrac{1}{2};\tfrac{1}{2}S) W^2(I j_t I^* j_0; J_s L) \chi^2(l_n^* \tfrac{1}{2} l_n \tfrac{1}{2}; I^* I; PS; L)$$

$$\left| \int \frac{r_0 \left(\frac{\partial}{\partial r_0} - f^{s0}_{l_n^*}\right) j_{l_n^*}(|\mathbf{K}_0 - \mathbf{k}_{ps}| r_0)}{|\tfrac{1}{2}\mathbf{K}_0 - \mathbf{k}_{ps}|^2 + \alpha^2} \cdot \frac{r_0 \left(\frac{\partial}{\partial r_0} - f^{st}_{l_n}\right) j_{l_n}(|\mathbf{K}_t - \mathbf{k}_{ps}| r_0)}{|\tfrac{1}{2}\mathbf{K}_t - \mathbf{k}_{ps}|^2 + \alpha^2} \right. \tag{1}$$

$$\left. \sum_{m_n m_n^*} C^{PQ}_{l_n^* m_n^* l_n m_n} Y_{l_n^* m_n^*}(\mathbf{K}_0 - \mathbf{k}_{ps}) Y_{l_n m_n}(\mathbf{K}_t - \mathbf{k}_{ps})\, d\Omega_{ps} \right|^2 .$$

The above formula is obtained using j-j coupling. A similar expression can be found when L-S coupling is used. The factors inside the modulus signs are unaltered: the difference occurs in the Racah W-functions and χ-function which show how the various spins and angular momenta are coupled. However, these terms only give a numerical factor in the differential cross-section and the angular distribution is determined by the energies involved and by the values of l_n^*, l_n and P. For a particular intermediate state and given energy of incident deuterons the quantum numbers l_n, l_n^* and the energies are fixed. The equations

$$\mathbf{P} = \mathbf{l_n} + \mathbf{l_n}^*, \quad \mathbf{P} = \mathbf{S} + \mathbf{L} = \tfrac{1}{2} + \tfrac{1}{2} + \mathbf{j_0} + \mathbf{j_t}$$

determine the allowed values of P, and thus the angular distribution of the inelastically scattered deuterons can be calculated from eq. (1).

† The notation is the same as that used in ref. [2]): the suffix 0 and the starred quantum numbers refer to the ground state and the suffix t to the excited state of the bombarded nucleus; the suffix s is associated with the particular intermediate compound state contributing to the reaction.

3. Results

A convenient reaction to analyse is $^{12}C(d, d')^{12}C^*$ with Q-value -4.43 MeV. This reaction leaves the ^{12}C nucleus in its excited state at 4.43 MeV which is known to be a $2+$ state: the ground state of ^{12}C is a $0+$ state. The angular distribution has been determined at two energies of bombardment; at 15.0 MeV by Haffner [4]) and at 19.1 MeV by Freemantle *et al.* [5]). Both energies are in the laboratory system.

In L-S coupling the ground state of ^{12}C is $^1S[4,4]$ and the excited state is $^1D[4, 4]$: the only possible intermediate state is $^2P[4, 4, 1]$ which corresponds to the ground state of ^{13}C or ^{13}N. The corresponding states in j-j coupling are $(p_{\frac{3}{2}})^8$, $(p_{\frac{3}{2}})^7\,(p_{\frac{1}{2}})$, $(p_{\frac{3}{2}})^8\,(p_{\frac{1}{2}})$. Using the known properties of these nuclear levels (their energies, spins and parities) the angular distribution can be calculated by eq. (1). We have $j_0 = 0$, $j_t = 2$, $J_s = \frac{1}{2}$, $l_n = l_n^* = 1$, $I = \frac{3}{2}$, $I^* = \frac{1}{2}$; these give $L = 2$ and $P = 1$ or 2. The value $r_0 = 4.47 \times 10^{-13}$ cm has been chosen as in the corresponding (d, p) reaction.

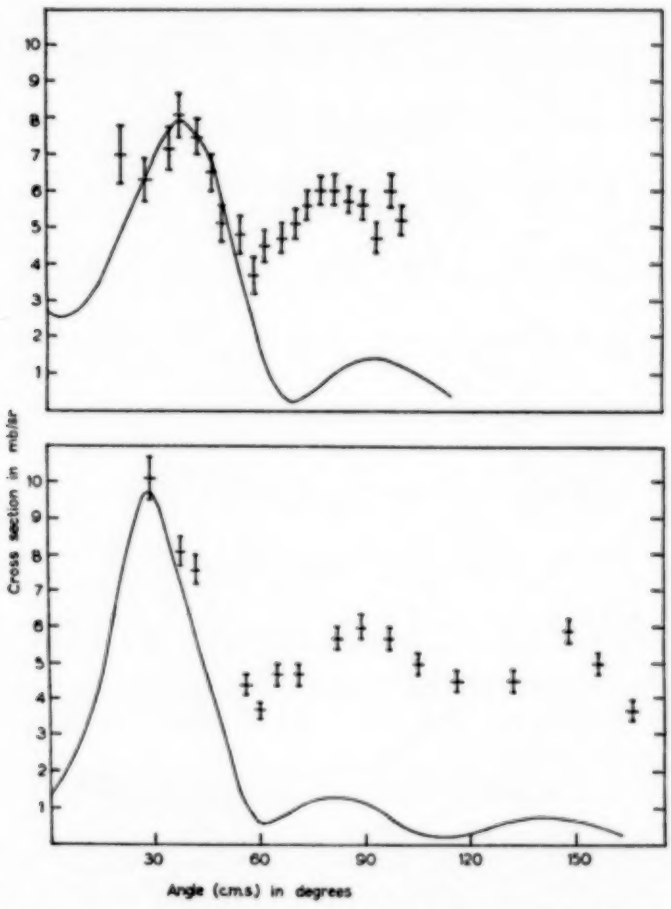

Fig. 1. Experimental and calculated angular distributions.

Since the calculation involves the evaluation of a double integral for each value of the scattering angle it was not convenient to perform it by hand and

the calculation was performed on the Mercury computer at Manchester University. The experimental and the calculated angular distributions are shown in figure 1.

4. Discussion

The model used to determine the angular distribution of the inelastically scattered deuterons has been the shell model with either L-S or j-j coupling. It has been shown by Almqvist *et al.* [6]) that the intermediate coupling shell model gives a very good representation of the properties of the low lying levels in ^{12}C, and thus the two states which are the initial and the final states in the reaction belong principally to the $(1s)^4(2p)^8$ configuration. Because the coupling is intermediate the ground state of ^{13}C (or ^{13}N) may not be the only level of the compound nucleus which contributes as an intermediate state in this (d, d′) reaction, but since the predicted maxima and minima of the angular distribution are in good agreement with the experimental ones it seems that it provides the major portion of the direct interaction cross-section and that any other levels which contribute can be treated as background.

At both energies the predicted magnitude for the cross-section is too large by a factor five. This is in accordance with previous results on (d, p) stripping reactions, and if the Coulomb interaction and the proton-nucleus interaction were taken into account the theoretical cross-section should be reduced. It is unlikely that this would alter appreciably the form of the angular distribution because the Butler stripping amplitude is a very good approximation to the correct one and it is the angular dependence of the stripping amplitude which determines the angular distribution in the inelastic scattering reaction.

Haffner [4]) has shown that the formula obtained by Huby and Newns [1]) using Born approximation gives a reasonable fit to the experimental data at 15.0 MeV. At 19.1 MeV there is similar agreement. The expression obtained by Sawicki [3]) would replace the zeros of the Born approximation formula by non-zero minima as eq. (1) does. Thus all three formulae predict angular distributions which are in good agreement with the data on the ^{12}C(d, d′)$^{12}C^*$ reaction. It would be helpful if measurements could be made more nearly in the forward direction as the present data are inconclusive as to whether or not the angular distributions fall off towards zero scattering angle. For the present reaction all the direct interaction theories predict a forward minimum whereas the electric interaction theory predicts a forward maximum (Mullin and Guth[7])).

It is intended to extend the programme which was used to evaluate the double integral in formula (1) so that other (d, d′) reactions can be investigated. In this way it should be possible to obtain information about the structure of nuclear levels in general and of the lower excited states of the p-shell nuclei in particular.

References

1) R. Huby and H. C. Newns, Phil. Mag. **42** (1951) 1442
2) W. M. Fairbairn, Proc. Roy. Soc. A **238** (1957) 448
3) J. Sawicki, Nuclear Physics **6** (1958) 613
4) J. W. Haffner, Phys. Rev. **103** (1956) 1398
5) R. G. Freemantle, W. M. Gibson and J. Rotblat, Phil. Mag. **45** (1954) 1200
6) E. Almqvist, D. A. Bromley, A. J. Ferguson, H. E. Gove and A. E. Litherland, Phys. Rev. **114** (1959) 1040
7) C. G. Mullin and E. Guth, Phys. Rev. **82** (1951) 141

8.A

Nuclear Physics **15** (1960) 683—686; © *North-Holland Publishing Co., Amsterdam*

Not to be reproduced by photoprint or microfilm without written permission from the publisher

THE CIRCULAR POLARIZATION OF THE GAMMA RAYS FOLLOWING THE β DECAY OF Fe-59

H. H. FORSTER and N. L. SANDERS

University of Southern California, Los Angeles †

Received 4 November 1959

Abstract: The circular polarization of the gamma rays emitted in the beta decay of Fe^{59} has been measured using the method of forward scattering from a magnetized Armco iron cylinder. A method is described to separate the effects due to the two dominant decay modes. For the 461 keV β — 1.099 MeV γ cascade an asymmetry coefficient $A = -0.46 \pm 0.08$ was determined; for the 271 keV β — 1.20 MeV γ transition the asymmetry coefficient was $A = -0.04 \pm 0.11$.

1. Introduction

As a consequence of the non-conservation of parity in beta decay the gamma rays emitted in the de-excitation of the nucleus following a beta transition are circularly polarized. The angular distribution of the gamma rays relative to the

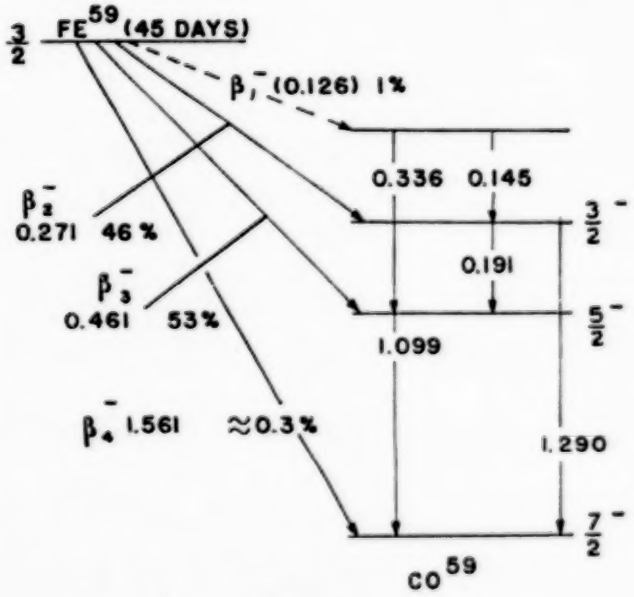

Fig. 1. Decay scheme of Fe^{59}.

direction of electron emission is given by $W(\vartheta, \tau) = 1 + \tau A (v/c) \cos \vartheta$ [1]) where $\tau = \pm 1$ depending on whether the photons are right or left circularly polarized. The asymmetry parameter A depends on the spin of the states

† Work supported in part by an AAUW fellowship grant.

involved in the transition, on the coupling constants, and on the matrix elements describing the beta decay. Thus, from an experimental determination of the asymmetry parameter A, information concerning these quantities can be obtained.

An experiment has been performed in this laboratory to determine the asymmetry coefficient in the beta-gamma circular polarization correlation for the two main transitions in the decay of Fe^{59}. The decay scheme of Fe^{59} is illustrated in fig. 1 [2,3]). As can be seen from the diagram, the two principal modes of decay are through the 271 keV β—1.29 MeV γ and through the 461 keV β—1.099 MeV γ cascades, respectively. The probability for either beta transition is $\approx 50\,\%$; the probability of de-excitation of the 1.29 MeV level through the 191 keV—1.099 MeV gamma cascade is only 6 % of the probability of de-excitation through the 1.29 MeV gamma ray.

2. Experimental Procedure and Results

High specific activity Fe^{59} in the form of $FeCl_3$ in HCl solution was obtained from the Oak Ridge National Laboratory. Thin sources were prepared by the insulin mounting technique, using tygon films as backing. Fig. 2 shows the experimental arrangement. The experimental apparatus was similar to that described by Schopper [4]), and Boehm and Wapstra [1]), and was based on the fact that the scattering cross section of circularly polarized gamma rays scattered from magnetized iron depends on the relative directions of the spins of the aligned electrons and the spins of the incident photons. The scattering magnet consisted of a hollow Armco iron cylinder magnetized to saturation by a concentric coil. The detector for the beta particles was a $\frac{1}{6}$ cm $\times$ 2.5 cm diameter anthracene crystal, that of the gamma rays a 5 cm $\times$ 5 cm thallium activated sodium iodide crystal. The average angle between the beta and gamma rays was $\approx 154°$. Beta-gamma coincidences were detected by the fast-slow method, the coincidence circuit having a resolving time of 16 ns. Care was taken to prevent changes in gain in the photomultiplier tubes on reversal of the magnetic field; the percent difference in single counting rates upon field reversal was less than 0.05 % for both betas and gammas. As many as 500 runs of 256 sec each were taken for each experiment and the fractional difference in coincidence counting rate upon field reversal computed for each run and corrected for chance coincidences and magnetic field effect. From the fractional difference in counting rate the anisotropy coefficient A was computed by the method described by Schopper [5]). This included corrections for: the unoriented electrons in the scattering magnet, finite geometry, change in polarization on absorption in the scattering iron, and the dependence of the gamma crystal efficiency on the position of the scattering point.

As a check on the performance of the instrument, the asymmetry coefficient

of Co^{60} was determined, yielding a value $A = -0.36 \pm 0.06$, in good agreement with the results of other experiments [6]).

For the investigation of the 461 keV β—1.099 MeV γ cascade in Fe^{59}, the discriminator in the beta channel was set above the endpoint energy of the 271 keV β group in order to exclude coincidences due to this beta transition. The percent difference in coincidence counting rate on field reversal was found to be (2.42 ± 0.38) % leading to an asymmetry coefficient $A = -0.46 \pm 0.08$.

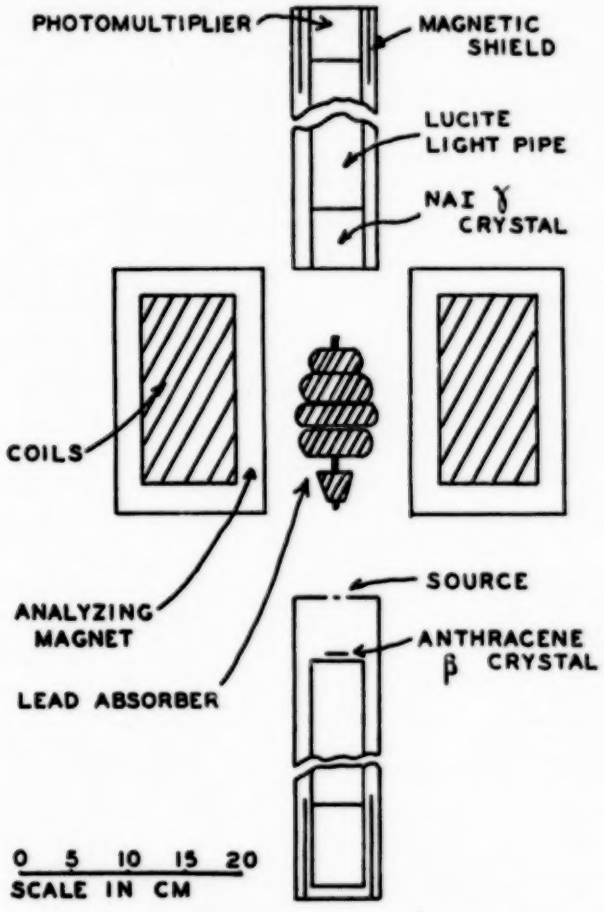

Fig. 2. Experimental arrangement.

This result is compatible with a theoretical value $A = -0.500$ computed [7]) on the assumption of a pure Gamow-Teller beta transition followed by a pure M1 gamma ray.

An attempt was made to determine the asymmetry coefficient for the 271 keV β—1.290 MeV γ cascade. Since in this case, complete separation of the beta groups could not be obtained in the beta channel, the experiment was performed as follows:

The upper level discriminator in the beta channel was set at the endpoint of the low energy beta group; the lower energy level discriminator was set so as to limit the total number of betas reaching the counter. Since calculation

showed that the difference between the maximum energies of the Compton scattered gamma rays was 66 keV, it was clear that one could not completely exclude the 1.099 MeV gamma ray by a lower energy level gamma discriminator. Nevertheless, a discriminator was set at the calculated position (e.g., above the maximum energy of the scattered 1.099 MeV photons) and an estimate of the contribution from the 461 keV β—1.099 MeV gamma cascade to the coincidence counting rate was made in the following manner: The coincidence rate was determined with the gamma ray discriminator and the beta window set as described above, and then remeasured with the gamma discriminator left unchanged but the beta window set above the endpoint of the 271 keV beta group. The ratio of the coincidence counting rates after correction for the relative contributions from the 461 keV β group (estimated by comparing the appropriate areas under the partial beta spectrum) indicated that $\approx 14\,\%$ of the coincidence counting rate was due to leakage from the 461 keV β group.

The percent difference in coincidence counting rate on field reversal for the $\frac{3}{2}^- \beta \rightarrow \frac{3}{2}^- \gamma \rightarrow \frac{7}{2}^-$ transition was found to be $(0.48 \pm 0.42)\,\%$ leading to an asymmetry coefficient $A = -0.04 \pm 0.11$. For an allowed beta transition followed by a pure E2 gamma ray the theoretical value of A for these spin assignments is given by [1,7])

$$A = (-0.133X^2 \pm 0.516X)/(1+X^2)$$

where

$$|X| = |C_{GT}||M_{GT}|/|C_F||M_F|,$$

assuming the validity of the two-component neutrino theory with time reversal invariance. Taking the value [8]) of $|C_{GT}|^2/|C_F|^2 = 1.3$, our result indicates that for this transition either

$$|M_{GT}|/|M_F| > 2 \quad \text{or} \quad |M_{GT}|/|M_F| < 0.3.$$

It may be of interest to point out that if no correction for leakage had been applied the value of the anisotropy coefficient A would have been $A = -0.13 \pm 0.12$. This, of course, would lead to a different ratio of the magnitudes of the Fermi and Gamow Teller matrix elements.

References

1) F. Boehm and A. H. Wapstra, Phys. Rev. **109** (1958) 459
2) L. Slack and K. Way, Radiation from radioactive atoms in frequent use (United States Government Printing Office, Washington, D.C., 1959) p. 23
3) F. R. Metzger, Phys. Rev. **88** (1952) 1360
4) H. Schopper, Phil. Mag. **2** (1957) 710
5) H. Schopper, Nuclear Instruments **3** (1958) 168
6) L. W. Fagg and S. S. Hanna, Rev. Mod. Phys. **3** (1959) 751
7) Alder, Stech and Winther, Phys. Rev. **107** (1951) 728
8) O. Kofoed-Hansen and A. Winther, Mat. Fys. Medd. Dan. Vid. Selsk, **30** No. 20 (1956)

2.D:2.L

Nuclear Physics **15** (1960) 687—693; © *North-Holland Publishing Co., Amsterdam*

Not to be reproduced by photoprint or microfilm without written permission from the publisher

THE ELASTIC SCATTERING OF ^{3}He BY MEDIUM WEIGHT NUCLEI

G. W. GREENLEES and P. C. ROWE

Physics Department, University of Birmingham

Received 11 December 1959

Abstract: Absolute differential cross-sections have been measured for the elastic scattering of ^{3}He from Ni, Pd, Cd, Sn, Au. Energy distributions for Ni, Cd and Au in the region 30—18 MeV and angular distributions for Ni, Pd, Cd, Sn in the range 15°—60° (C.M.) were found. The results show that an approximately exponential fall-off in cross-section occurs in both the energy and angular variations. Interaction radii have been derived from the experimental curves by using the sharp cut-off theory of Blair.

By comparison with recent alpha-particle results the difference in the ^{3}He and ^{4}He interaction radii was found to be $(0.11 \pm 0.01) \times 10^{-13}$ cm.

1. Introduction

The elastic scattering of alpha-particles in the medium energy region has been studied extensively in recent years by several authors [1]) with particular attention to the variation of differential cross-section with both energy and angle. The main feature of the results is a decrease of the observed cross-section, relative to that expected on the basis of Rutherford scattering, as the angle of observation, or the energy, is increased. Attempts to fit these results with a nuclear model have met with considerable success; in particular the sharp cut-off model [2]) and the optical model [3]) have given a good description of the data. The optical model calculation represents the data in detail but involves a number of adjustable parameters and the choice of these for the best fit with experiment is not unique.

The sharp cut-off model of Blair [2]) postulates a strongly absorbing nucleus of definite radius. The incident beam is described in terms of partial waves each corresponding to an angular momentum l and those partial waves with angular momentum less than some value l^1, dependent on the incident energy, are totally absorbed; an increase in the incident energy results in an increase in l^1. Further, the scattered particle is considered as following a classical trajectory corresponding to a particular value of angular momentum l_{cl}, and it has been shown that $l^1 = l_{cl}$ when the total scattered amplitude has fallen to half that of the incident wave. The appropriate value of l^1 is associated with the interaction radius for the collision, l_{cl} is related to the classical

apsidal distance and the interaction radius is given by

$$R = \frac{Z_1 Z_2 e^2}{2E}(1 + \operatorname{cosec} \tfrac{1}{2}\phi),$$

where Z_1 and Z_2 are the atomic numbers of the target and incident nuclei and E and ϕ are the energy and angle at which the scattered amplitude is one half of the incident, i.e. when the ratio of observed to Rutherford cross-sections is 0.25. In a later paper Kerlee *et al.* [4]) showed that the ratio appropriate for radius calculations was a slowly varying function of angle and calculated the appropriate value for all angles. Kerlee *et al.* [4]) measured the variation of cross-section with energy for alpha-particle elastic scattering by a series of 28 elements and interaction radii D were found from the experimental angular distributions. These radii were represented by the relation $D = R_0 A^{\frac{1}{3}} + a$, where a is a measure of the alpha-particle radius.

The calculation of alpha-particle scattering distributions suggest that these particles have a short mean free path in a target nucleus. If this is ascribed to a high probability of compound nucleus formation, or to direct nuclear reactions, incident ^{3}He particles would be expected to show similar behaviour and "black nucleus" calculations should have a similar validity. The present experiments with ^{3}He were undertaken to verify this prediction and to determine the interaction radius for the ^{3}He nucleus.

2. Method and Apparatus

A doubly charged ^{3}He beam was accelerated in, and extracted from, the Nuffield 60" cyclotron [5]). The cyclotron was operated with a magnetic field reduced to 0.75 of the field normally used for accelerating deuterons and the final ^{3}He energy was 29.4 MeV.

The extracted beam passed through a bending magnet and entered a 12" scattering chamber [6]) situated behind a screening wall. This chamber is fitted with a scintillation counter which can be rotated through an angular range of 15°—165° about a central target. The acceptance angle in the present experiment was about 1° and the counter could be set to within 0.2°. The energy of the incident beam was varied by introducing aluminium absorbers in front of the beam defining collimator. A 3 mm CsI(Tl) crystal and Dumont 6292 photomultiplier were used to detect the scattered particles and the pulse height spectrum was recorded on a 100 channel pulse height analyser; the energy resolution obtained was 3 %. The targets were in all cases in the form of thin foils and the beam traversing the target was collected in a Faraday-cup and integrated electronically.

3. Results

Absolute differential cross-sections for elastic scattering were calculated directly from the observed spectra. From figs. 1 and 2, which represent typical

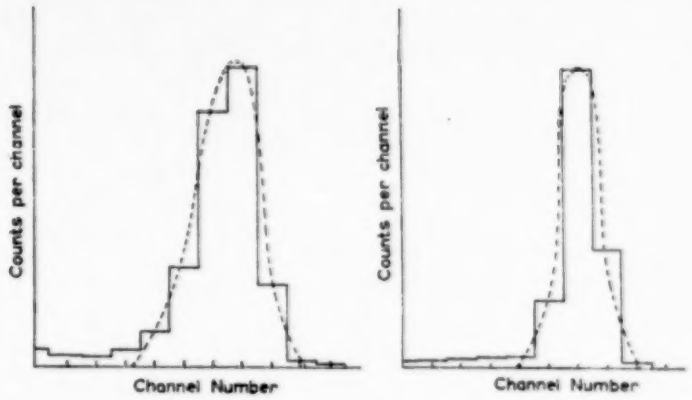

Figs. 1 and 2. Typical pulse height spectra. Fig. 1: Sn target, incident energy 29.1 MeV, angle 47° (C.M.). Fig. 2: Ni target, incident energy 28.3 MeV, angle 30° (C.M.).

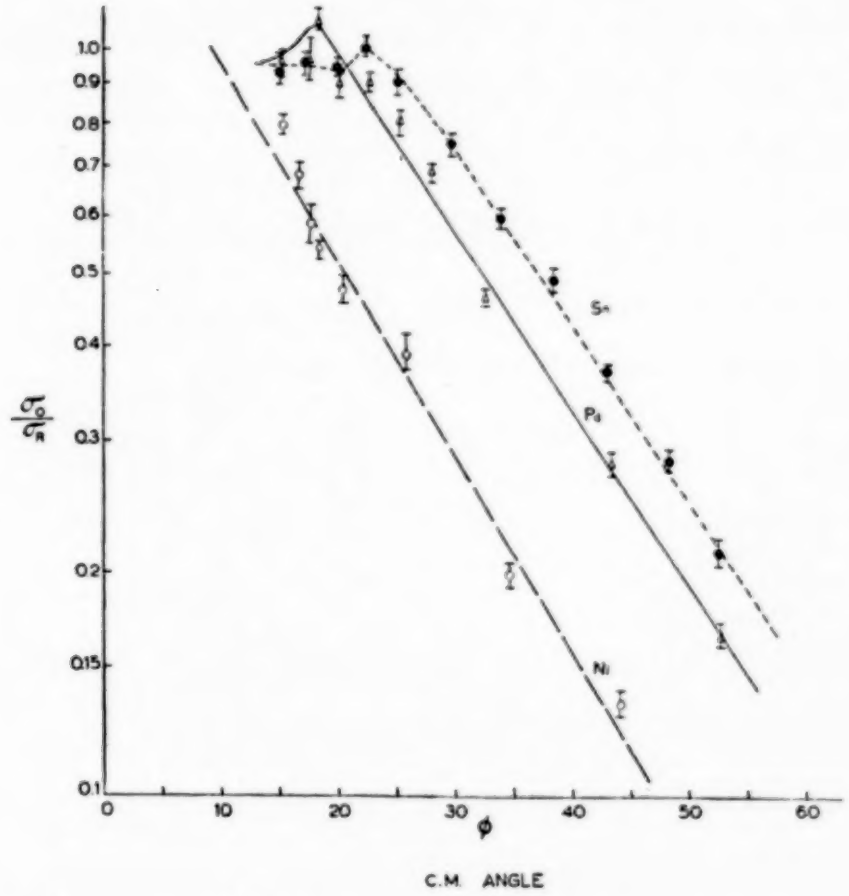

Fig. 3. Centre of mass angular distribution of 29.1 MeV ^{3}He scattered elastically from Sn, Pd, and Ni.

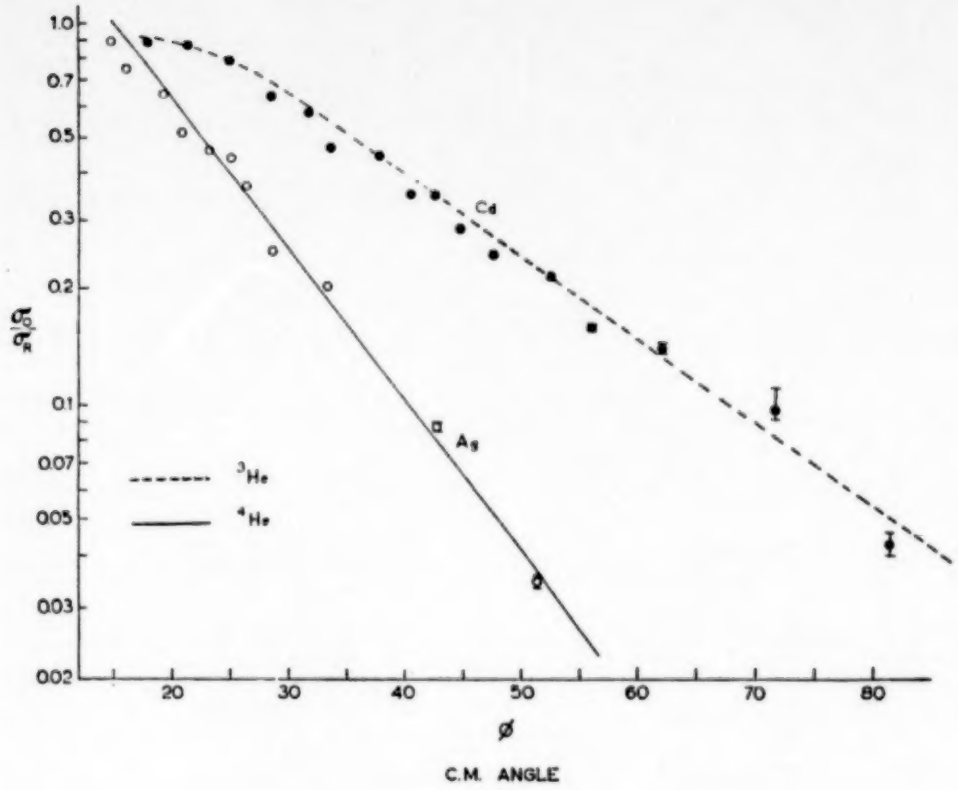

Fig. 4. Centre of mass angular distributions for 29.1 MeV ^{3}He scattered elastically from Cd and for 38.8 MeV ^{4}He scattered elastically from Ag.

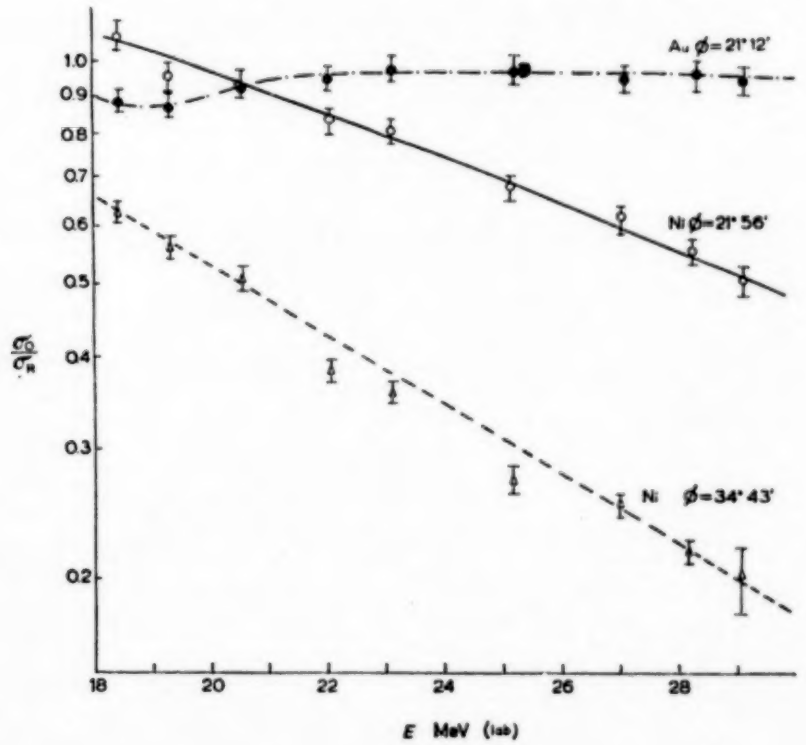

Fig. 5. The variation of σ_0/σ_R with incident ^{3}He energy for elastic scattering from Au and Ni.

spectra, it can be seen that very little background correction was required; the inelastic cross-section was small in all the elements studied and had little effect on the size of the elastic peaks. The ratio of the absolute elastic differential cross-section to the Coulomb cross-section was plotted against either energy or angle. Angular distributions of the ratio were obtained for Ni, Pd, Cd and Sn at full energy (figs. 3 and 4). The yield of scattered particles as a function of incident energy was measured for Ni, Cd and Au at a number of angles (figs. 5 and 6). The range of energy and angle available was limited

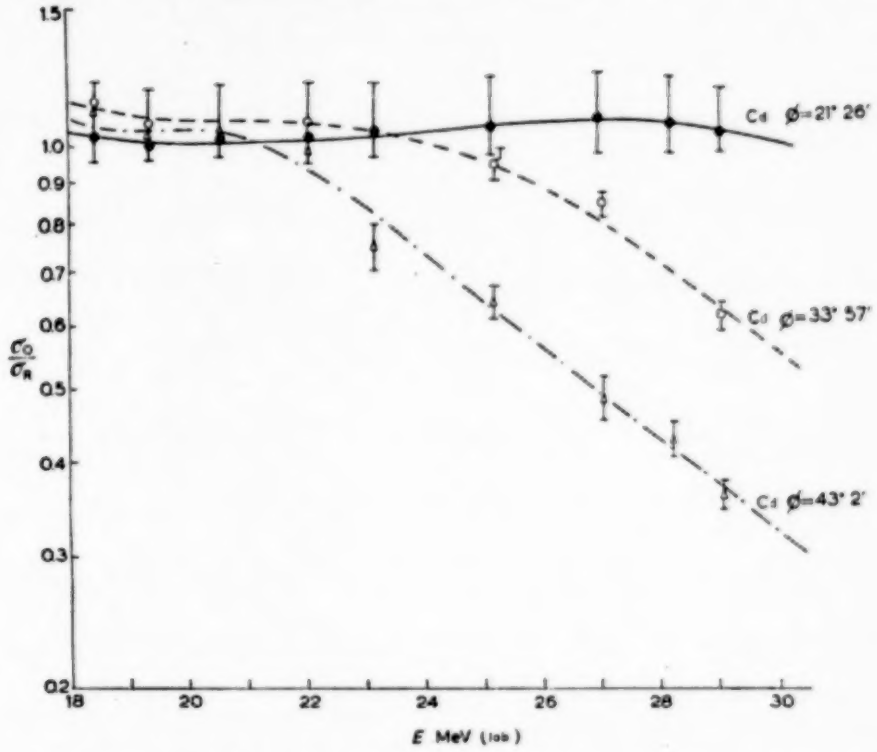

Fig. 6. A comparison of the effects of charging scattering angle in the variation of σ_0/σ_R with incident ^{3}He energy for elastic scattering from Cd.

by the beam intensity on the target; this was approximately 0.5 nA at full energy (29.4 MeV) but fell considerably with the introduction of absorber foils. The target nuclei chosen were such that the expected fall-off would occur at an energy and scattering angle which were experimentally accessible.

Two checks were made to ensure that the method of measurement did not involve any large systematic errors. The cross-section ratio σ_0/σ_R for gold should be unity over the range of energies used because of the high Coulomb barrier, and this was tested experimentally (fig. 5). Secondly a measurement of an angular distribution for silver was obtained (fig. 4), using alpha-particles of 40 MeV incident energy and compared with the results of Kerlee *et al.* [4]). These checks indicated the absence of any appreciable systematic errors in the present experiments. Relative errors are estimated at 3 % and absolute errors 6 %; errors are shown on all the experimental points in the figures.

4. Discussion

The curves in figs. 3—6 show the expected fall-off in cross-section, in agreement with the alpha-particle results [1]). The comparable angular distributions for alpha-particle scattering often show a marked rise in the cross-section ratio to a value just above unity before the fall-off begins. Kerlee *et al.* [4]) made a quantitative study of this rise and associated it with the closing of nuclear shells; it can be seen that there is evidence for the rise in the Pd and Cd ^{3}He results. The present work is not sufficiently precise to show the

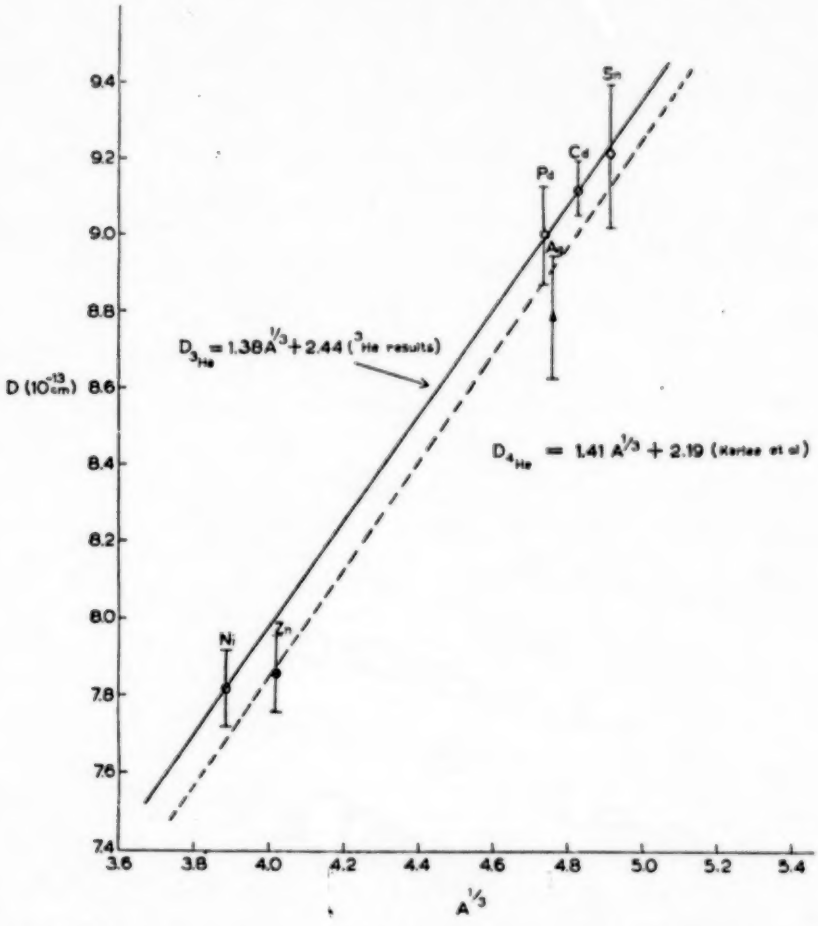

Fig. 7. Plot of the corrected interaction radius, D (according to Kerlee *et al.*) against $A^{\frac{1}{3}}$. The ^{3}He points represent means of values taken from the present data and the full straight line is a least squares fit through these points.

The dashed line is taken from Kerlee *et al.* and is a least squares fit of 28 points obtained from ^{4}He elastic scattering data; only the point for Zn is given. The point for Ag is the result obtained in the present experiments.

diffraction oscillations in the angular distributions such as are found superimposed on an exponential fall-off in alpha-particle scattering from light to medium weight elements.

Using the method outlined earlier for alpha-particles, interaction radii were

calculated for the present ^{3}He results; a comparison of these with the alpha-particle data is shown in fig. 7, the ^{3}He points are the weighted means of several values of the interaction radii and the full straight line is a least squares fit to the points obtained for the four elements studied. The radius obtained in the present work from the ^{4}He scattering by silver is shown in fig. 7 and is seen to be close to be alpha-particle line (dashed) given by Kerlee *et al.* [4]). Typical errors obtained in the latter results are shown on the point for Zn.

The interaction radii for ^{3}He are found to be very similar to those of the alpha particle. The differences in the two sets of radii are found by subtracting the ordinates of the ^{3}He points and the alpha curve of figure 7. The mean value obtained is

$$D_{^3\mathrm{He}} - D_{^4\mathrm{He}} = (0.11 \pm 0.01) \times 10^{-13} \text{ cm}.$$

The accuracy of the present work is not thought sufficient to justify a detailed fit of the cross-section curves to the Blair model. Such an analysis might lead, through the determination of critical angular momenta, to slightly different values for the interaction radii, as discussed by Blair [1]) for the alpha-particle results. It may be of interest to analyse comparable ^{3}He and ^{4}He elastic scattering experiments in terms of the optical model. Comparison of the results might then show the effect of spin orbit forces in the scattering of ^{3}He.

The authors wish to express their thanks to Prof. W. E. Burcham for suggesting the experiments and for his subsequent assistance and advice. Members of the Cyclotron Scattering Group are to be thanked for help in recording experimental data and the authors would also like to thank Mr. W. Hardy and the Cyclotron Staff for obtaining the ^{3}He beams.

References

1) J. S. Blair, Phys. Rev. **108** (1957) 827
2) J. S. Blair, Phys. Rev. **95** (1954) 1218
3) G. Igo and R. M. Thaler, Phys. Rev. **106** (1957) 126
4) D. D. Kerlee, J. S. Blair and G. W. Farwell, Phys. Rev. **107** (1957) 1343
5) J. H. Fremlin, W. Hardy and H. R. Shaylor, J. Sci. Instr. **36** (1959) 390
6) G. W. Greenlees, B. C. Haywood, L. G. Kuo and M. Petravic, Proc. Phys. Soc. A **70** (1957) 331

6.C NOTE ON UNITS AND NOMENCLATURE

1. Use of British units

It has been pointed out to the Editor that there is no reason (except perhaps in very exceptional cases) to tolerate (as has hitherto been done) the use of British units in the description of apparatus and experimental arrangements. Contributors are accordingly requested to give all measurements exclusively in metrical units; in manuscripts disregarding this request, the necessary changes will be made by the editorial staff; in case of doubt, the manuscript will be returned to the authors for emendation.

2. Nomenclature of nuclear species

From occasional reactions of colleagues the Editor has got the impression that there is still widespread confusion on this point. This confusion arises from the fact that, in order to designate the nuclear species characterized by the double dichotomy

$$A \text{ even} \begin{cases} Z \text{ even}, N \text{ even} \\ Z \text{ odd}, N \text{ odd} \end{cases}$$

$$A \text{ odd} \begin{cases} Z \text{ even}, N \text{ odd} \\ Z \text{ odd}, N \text{ even}, \end{cases}$$

two systems of nomenclature are used concurrently:

System 1		*System* 2	
even nuclei	even-even	even-A nuclei	even-even
	odd-odd		odd-odd
odd nuclei	even-odd	odd-A nuclei	odd-N
	odd-even		odd-Z.

There should be little hesitation in admitting that System 2 is far superior to System 1, and *it is therefore this System 2 which is adopted in this journal*, with modifications of pure form which do not in the least alter its structure:

(a) The use of (undefined) symbols A, N, Z is an unnecessary clumsiness, since there are plain words fulfilling the same function: odd-mass nucleus, odd-neutron nucleus convey the same idea as odd-A, odd-N nucleus in a more immediate way.

(b) The repetition involved in even-even, odd-odd is obviously superfluous, and to drop it can cause no confusion (within the framework of System 2).

One thus arrives at the nomenclature consistently used in this journal:

even-mass nuclei	even
	odd
odd-mass nuclei	odd-neutron
	odd-proton.

It must be stressed once more that this nomenclature is *not* an innovation, but is *essentially identical* with the widely used System 2. People accustomed to the repetitive names even-even, odd-odd may, if they wish, regard the simple forms even, odd as abbreviations, or read them through a piece of Iceland spar: it will not change their meaning. No ambiguity can arise from the use of the simple form odd, in the meaning of odd-odd, *if there is general agreement to use only System* 2. Since the elimination of System 1 would seem to be desirable also for other reasons (the alternation even-odd, odd-even is utterly confusing), it should not be too difficult (one would hope) to reach such an agreement.

10.E ERRATUM

J. R. Bird, M. C. Moxon and F. W. K. Firk, Gamma ray spectra and parameters of neutron resonances in mercury (Nuclear Physics **13** (1959) 525).

On p. 538, line 15 from bottom, instead of 'odd isotopes' read 'odd-mass isotopes'.

10.D *Nuclear Physics* **15** (1960) 695—697; © *North-Holland Publishing Co., Amsterdam*

BOOK REVIEWS

I. W. CLEGG and D. D. FOLEY, editors, *Uranium Ore Processing* [The Geneva Presentation Volumes, presented by the U.S.A. at the Second International Conference on the Peaceful Uses of Atomic Energy, Geneva, September 1958] (Addison-Wesley Publishing Co. 436 p. $ 8.50)

This book is the result of the collaboration of 32 authors and in one volume it covers the entire field of uranium winning, starting with the minerals in the ground and following the material through all stages until a concentrate has been obtained.

The first four chapters: (1) Uranium Occurrence and Sources, (2) Uranium Exploration and Mining, (3) Sampling and Analysis of Ores, (4) Mineralogy of Uranium, do not impart much to the professional man and they are not easily read by others.

To make up for it the next six chapters: (5) Preliminary Ore Treatment, (6) Acid Leaching of Uranium Ores, (7) Carbonate Leaching of Uranium Ores, (8) Liquid-Solids Separations, (9) Uranium Recovery by Ion Exchange, (10) Uranium Recovery by Solvent Extraction, are substantial and illustrated with excellent graphs and flowsheets. Especially the chapter on ion exchange calls attention by its lucid and thorough account.

Chapter 11 describes six typical plants. Chapter 12 deals with marginal sources such as phosphate rock and lignite shale. Chapter 13 finally covers health and safety in mining and milling.

The style appears somewhat inhomogeneous, probably owing to the number of authors. Also it seems that not all of the topics are suitable for the condensed form. Nevertheless the large amount of information compiled here makes the volume a valuable reference source for workers in the field.

Emil Sørensen

PAUL I. RICHARDS, *Manual of mathematical physics* (Pergamon Press, London, 1959. xi—486 pages. £5 10s. net)

At first sight, this volume looks just like a compilation of the main facts and formulae which form the arsenal of the theoretical physicist; and it is indeed such a compilation. But on closer inspection it is soon apparent that it is also something more and better; the author has given his task a great deal of searching thought, and his ambition has been to present his material in such a way that the conceptual framework of the great doctrines of theoretical physics can be easily grasped in its full harmony. The result of this endeavour is a surprisingly complete survey of the vast field, which is not only of great practical utility, but also aesthetically satisfying to a remarkable degree. The author has been guided, more consciously than is usual nowadays, by philosophical criteria, which are explicitly formulated, with studied concision, at the appropriate places, but which are also reflected, throughout the book, by the selection of the topics, the relative emphasis put on each of them and the method of presentation. The author's attitude in all these respects, while not strikingly original, is at any rate perfectly sound. In particular, while studious of logical rigour and formal elegance, he is immune to the pest of axiomatics.

The scope of the book is limited to "established" theoretical physics, which covers the whole of classical physics and quantum mechanics including the relativistic treatment of the free fermion and electromagnetic fields. Besides giving the fundamentals, the treatment leads up to the principal applications, selected from a very modern point of view (e.g. about 20 pages, out of 250, are devoted to circuit theory and communication theory). The second half of the book contains a brilliant survey of the whole field of mathematics under some 15 headings (one of which, for instance, is probability and game theory).

Apart from its obvious usefulness as a vade-mecum for trained physicists, this book may render a precious service to students, by helping them to acquire a synthetic view of the inter-relations between the various branches of physics, which are usually taught to them in separate, and often disconnected, courses.

L. R.

F. L. CUTHBERT, *Thorium Production Technology* [The Geneva Presentation Volumes 1958] (Addison-Wesley Publishing Co. 303 p. $ 5.50)

After reading this book one is inclined to believe that it contains practically all the information currently available on the subject, as is also asserted by the publisher.

The opening chapter is a historical survey followed by a section on the physical and chemical properties of thorium.

Next is given a well arranged description of thorium bearing ores and their treatment leading to a thorium concentrate.

The purification of the concentrate and the preparation of reducible thorium salts are accounted for with considerable detail. The reduction, melting and casting procedures are very well illustrated with photographs of apparatus and products from commercially working plants.

In the chapter on thorium fabrication much attention has been paid to recrystallisation. Hardness dependence on time, temperature and carbon content is shown in numerous graphs.

The special health and safety aspects connected with thorium production are carefully considered. A comparison with uranium is made.

The last chapter outlines the testing procedures, chemical as well as metallurgical, suitable for production scale work.

Each chapter is accompanied by a reference list.

Emil Sørensen

C. F. POWELL, P. H. FOWLER and D. H. PERKINS, *The study of elementary particles by the photographic method* (Pergamon Press, 1959. xvi–669 p. £12 10s.)

When Professor Powell was lecturing to the Colston Society in Bristol about the discovery of the π-meson, he did not fail to impress the audience by producing a small cardboard box containing some photographic plates and explaining in the most casual tone that this was all the equipment he needed. He readily admitted, afterwards, that it was perhaps not quite fair to suggest that the emulsion method, with its imposing background of patient and painstaking research in colloid technology, was as cheap as that. Anyhow, he has now composed, with his distinguished collaborators, a very expensive book about this method.

The original intention was to collect an atlas of typical photographs, which would supplement the existing ones for the cloud chamber method; but the final outcome is an encyclopedic record of almost all phenomena which have been discovered or studied by the traces they leave in the photographic emulsion; the technical aspects of the method itself are also fully treated and illustrated. In spite of the abundance of details and references, the presentation is so lucid and masterly that it provides even for the non-specialist a most readable introduction into every part of the vast subject. The theoretical implications are, with very few omissions, clearly indicated. Neither has the historical aspect been neglected: we find even a brief account (perhaps a bit too condensed to be really useful) of the discovery of photography; but more interesting are the neat summaries, at the appropriate places throughout the book, of the historical development of the various problems.

The physicists who have followed the spectacular sequence of discoveries in the field of cosmic radiation since its inception until the latest period, in which the competition from the big accelerators has set in, will be glad to recognize all the famous plates, and (no less important) the well-devised diagrams showing the statistical distribution of the results, which remain the landmarks in this development. Many plates, however, drawn from the Bristol stock, are published here for the first time.

The typographical execution, entrusted to a German firm, is in every respect worthy of this monumental record of one of the most fascinating chapters in the history of modern science.

L. R.

B. R. T. Frost and M. B. Waldron, *Nuclear Reactor Materials* (Temple Press, London 1959. vii—79 p. 12s. 6d.)

The present volume in the series of Nuclear Engineering Monographs gives in 73 pages first a description of fundamental and nuclear metallurgy and then of the reactor materials in general use. The material is divided into six chapters with titles as follows: I. Theoretical Metallurgy — II. Structural Materials — III. Fuel Materials — IV. Liquid Metals — V. Ceramics and Metal-Ceramic Mixtures as reactor Materials — VI. Corrosion.

The first chapter and part of the sixth are an introduction to the terminology of metallurgy, — "to understand the properties of materials it is first necessary to understand the language of the metallurgist", — which occupies approx. 40 % of the total number of pages. The remainder falls fairly evenly into three groups: Fuel, Structural Materials, Other Materials and Reactor Corrosion. The first two subjects are — the small space considered — treated rather thoroughly. However, for uranium alloys the mentioning of low-alloyed uranium is lacking completely, as only the possibility for stabilization of the gamma-phase in high-alloyed uranium is mentioned. In the third group liquid metals occupy disproportionately much space (10 pages), on the other hand a more detailed description of other coolants, for instance organic liquids, is missing.

Further, it would have served the purpose better if the outline of the book was laid according to the *application* of the materials only, and not — as is the case — to a certain extent also according to their character. Especially so as the book is written "to explain to engineers and chemical engineers associated with the Nuclear Power Industry the properties of the materials which they will be called upon to use". The present outline is possibly due to the fact that the book has been written by *four* authors (all from Harwell).

Conclusion: It is impossible with the available space to give non-metallurgists a general background for the selection of reactor materials. Therefore, the book should have been written for metallurgists only, and the introductory chapters should only treat the general aspects of *reactor* metallurgy and more thoroughly so. Further, the chapters on the special subjects would improve by a better defined outline.

Per Knudsen

P. A. Petrow, *Kernenergieanlagen* (VEB, Verlag Technik, Berlin 1959. 279 p.)

The book is an introduction to reactor engineering. The first four chapters deal with reactor physics, the remaining with shielding, cooling, materials, existing reactors, design of power stations including the economy and, finally, the calculation of some typical parameters for a definite reactor.

As mentioned in the preface, the book is intended for teaching in institutes of technology. It is written on the basis of a series of lectures given by the author at an institute for thermology in Moscow. It is evident from the book that consequently the author mainly takes an interest in the cooling problems. The reactor physics part is not entirely satisfactory if the book is intended for physics engineers mainly. However, from a general educational point of view, the book has its good points, although sometimes it seems a little too cursory. The final illustrative calculations are definitely a good idea.

Taking into account that it seems an impossible job to write a good introduction to this tremendous subject, one might say that the book is no better and no worse than other books with the same scope.

S. J. Christensen.

AUTHOR INDEX

ALEXEFF, I. and W. HAEBERLI, Polarization in proton-proton scattering near 3.3 MeV 609
ANDERSSON, G., *see* B. JUNG
ANDRÉ, G. O., Angular distribution of protons from Li^6(d, p)Li^7 and Li^6(d, p)Li^{7*} 464
ARNS, R. G., R. D. RIGGS and M. L. WIEDENBECK, Decay of Re^{188} . . . 125
BÄCKSTRÖM, G., O. BERGMAN, J. BURDE and J. LINDSKOG, The decay of Au^{194} 566
BADRINATHAN, C. *see* E. KONDAIAH
BARASHENKOV, V. S., Non-elastic collisions of fast π mesons with nucleons and peripheral ($\pi\pi$) interactions 486
BAYMAN, B. F., A derivation of the pairing-correlation method 33
BERGMAN, O., *see* G. BÄCKSTRÖM
BERKES, I. and I. DEMETER, Small angle scattering of electrons 421
BIEDENHARN, L. C., *see* T. A. GRIFFY
BISI, A., A. FASANA and L. ZAPPA, Circular polarization of external bremsstrahlung from γ-rays in magnetized targets 231
BODENSTEDT, E., E. MATTHIAS, H. J. KÖRNER, E. GERDAU, F. FRISIUS, and D. HOVESTADT, The nuclear g-factor of the 111 keV rotational level and other angular correlation measurements on W^{184} 239
BOERSMA, H. J., *see* P. S. DUBBELDAM
BREIT, G. and M. H. HULL, Jr., Note on one pion exchange potential . . 216
BURDE, J., *see* G. BÄCKSTRÖM
CLASS, C. M., *see* B. J. FARMER
COHEN, S. G., and R. WIENER, Search for pseudoscalar interaction in beta-decay 79
COOPER, Jr., PAUL F. and RICHARD WILSON, Cross section and asymmetry in the deuteron pickup reaction C^{12}(p, d)C^{11} at 145 MeV 373
CROSS, W. G. and R. G. JARVIS, Scattering of 14.6 MeV neutrons by Mg, Ca, Cd, Ta and Bi 155
DEMETER, I., *see* I. BERKES
DUBBELDAM, P. S., C. C. JONKER and H. J. BOERSMA, Energy and angular dependence of the left-right asymmetry of D-D neutrons scattered by carbon 452
DUCAT, A. and R. H. THOMAS, The half-life of I^{116} 525
ELBEK, B., *see* M. C. OLESEN
EVANS, J. E. and M. A. GRACE, Polarization in C^{12}(pp) scattering 646
EVERLING, F., L. A. KÖNIG, J. H. E. MATTAUCH and A. H. WAPSTRA,

Atomic masses of nuclides for $A \leqq 70$ 342
FAIRBAIRN, W. M., The inelastic scattering of deuterons from ^{12}C . . . 678
FALL'EROS, S., R. A. FERRELL and M. K. PAL, Excitation of the nuclear giant-dipole resonance by inelastic electron scattering 363
FARMER, B. J. and C. M. CLASS, Alpha spectra from the decays of Li^8 and B^8 626
FASANA, A., *see* A. BISI
FERRELL, R. A., *see* S. FALLIEROS
FERRERO, F., S. FERRONI, R. MALVANO, S. MENARDI and E. SILVA $(\gamma, {}^{np}_{d})$ reactions in S^{32}, Ca^{40}, Ge^{70} 436
FERRONI, S., *see* F. FERRERO
FINK, R. W., *see* I. KUMABE
FINK, R. W., *see* I. L. PREISS
FORSTER, H. H. and N. L. SANDERS, The circular polarization of the gamma rays following the β decay of Fe-59. 683
FRANTZ, LEE M., and ROBERT L. MILLS, Many-body basis for the optical model 16
FRENCH, J. B., Symplectic symmetry in the nuclear shell model . . . 393
FRISIUS, F., *see* E. BODENSTEDT
GATLAND, I. R., Theory of K^+-nucleon scattering 480
GAUDIN, MICHEL, Une démonstration simplifiée du théorème de Wick en mécanique statistique 89
GERDAU, E., *see* E. BODENSTEDT
GOTTFRIED, K., Dispersive effects in elastic electron scattering by complex nuclei 92
GRABOWSKI, ZBIGNIEW, *see* INGVAR MARKLUND
GRACE, M. A., *see* J. E. EVANS
GREENLEES, G. W. and P. C. ROWE, The elastic scattering of ^3He by medium weight nuclei. 687
GRIFFY, T. A. and L. C. BIEDENHARN, Beta decay involving the $Be^{8*}(2^+)$ state. 636
HAGEDOORN, H. L. and A. H. WAPSTRA, Measurements of the fluorescent yield of the K-shell with a proportional counter 146
HAEBERLI, W., *see* I. ALEXEFF
HEBBARD, D. F., Proton capture by N^{15} 289
HEERDEN, I. J. VAN, and D. J. PROWSE, The scattering of 38 MeV alpha particles by C^{12} 356
HELMHOLZ, A. C., The Nobel prize in physics for 1959 387
HILGEVOORD, J., On the reduction formulae for the S-matrix elements 657
HORI, SHOICHI, On the spin of the Σ-hyperon 56
HOVESTADT, D., *see* E. BODENSTEDT
HULL, Jr., M. H., *see* B. BREIT

JARVIS, R. G., *see* W. G. CROSS
JASTRAM, P. S., *see* M. K. RAMASWAMY
JIN, Y. S., Proof of dispersion relations for pion-hyperon scattering . . . 102
JONKER, C. C., *see* P. S. DUBBELDAM
JUNG, B., and G. ANDERSSON, Low mass odd-odd isomers of thallium . 108
KAVANAGH, RALPH W., Proton capture in Be^7. 411
KHANNA, F. C. and Y. C. TANG, Neutron strength functions in a surface absorption optical model. 337
KOCH, W., *see* M. NIKOLIČ
KONDAIAH, E. and C. BADRINATHAN, Spin of the first excited state of B^{12} 254
KÖNIG, L. A., *see* F. EVERLING
KÖRNER, H. J., *see* E. BODENSTEDT
KRAMER, GUSTAV, Deuteron photodisintegration and P-wave phase shifts in the medium energy range. 60
KUMABE, I. and R. W. FINK, The angular and energy distribution of protons from Ni^{58} reactions induced by 14.8 MeV neutrons 316
LANE, A. M. and E. D. PENDLEBURY, On the existence of octupole vibrations in nuclei 39
LARDINOIS, J., Nuclear shape effect on isomeric shift 522
LINDSKOG, J., *see* G. BÄCKSTRÖM
ŁUKASZUK, L., Note on symmetry of strong interactions 513
MALVANO, R., *see* F. FERRERO
MANNING, G. and J. D. ROGERS, Measurement of g-factors of several short lived nuclear states in odd-mass nuclei 166
MARK, HANS, *see* T. J. WALTERS
MARKLUND, I., O. NATHAN and O. B. NIELSEN, 0+ states of Sm^{152} and Gd^{152} 199
MARKLUND, INGVAR, BOB VAN NOOIJEN and ZBIGNIEW GRABOWSKI, 0+ levels of even nuclei in the rare-earth region 533
MATTAUCH, J. H. E., *see* F. EVERLING
MATTHIAS, E., *see* E. BODENSTEDT
MENARDI, S., *see* F. FERRERO
MILLS, ROBERT L., *see* LEE M. FRANTZ
MORINAGA, H., *see* K. TAKAHASHI
NATHAN, O., *see* I. MARKLUND
NIELSEN, O. B., *see* I. MARKLUND
NIKOLIČ, M., W. KOCH, M. SCHNEEBERGER and H. WINZELER, An unusual double star from a K^--capture in emulsion 519
NOVOZHILOV, YU., On the construction of the S matrix for dressed particles 469
OKUN, L. B. and A. P. RUDIK, On a method of finding singularities of Feynman graphs 261

OLESEN, M. C. and B. ELBEK, Inelastic scattering from odd-mass rare earths 134
OZAKI, SHOJI, On the consistency of quantization in quantum electrodynamics. 501
PAL, M. K., *see* S. FALLIEROS
PENDLEBURY, E. D., *see* A. M. LANE
PREISS, I. L. and R. W. FINK, New isotopes of cobalt; activation cross-sections of nickel, cobalt and zinc from 14.8 MeV neutrons 326
PROWSE, D. J., *see* I. J. VAN HEERDEN
RAMAKRISHNAN, ALLADI, N. R. RANGANATHAN, R. VASUDEVAN and S. K. SRINIVASAN. A note on dispersion relations 516
RAMASWAMY, M. K., and P. S. JASTRAM, On the K-conversion coefficient of the 279 keV gamma ray in the decay of Hg^{203} 510
RANGANATHAN, N. R., *see* ALLADI RAMAKRISHNAN
RASMUSSEN, N. C., *see* T. J. WALTERS
RIEZLER, WOLFGANG, Eine Kernreaktion vom Typ $(\alpha, \alpha+3n)$ 143
RIGGS, R. D., *see* R. G. ARNS
RODBERG, LEONARD S., Relation between angular distribution and polarization in the optical model 72
ROGERS, J. D., *see* G. MANNING
ROWE, P. C., *see* G. W. GREENLEES
RUDIK, A. P. *see* L. B. OKUN
SANDERS, N. L., *see* H. H. FORSTER
SCHNEEBERGER, M., *see* M. NIKOLIČ
SHIROKOV, YU. M., Space and time reflections in relativistic theory . . 1
SHIROKOV, YU. M., Types of symmetry of elementary particles 13
SILVA, E., *see* F. FERRERO
SRINIVASAN, S. K., *see* ALLADI RAMAKRISHNAN
TAKAHASHI, K. and H. MORINAGA, Protactinium-237 664
TANG, Y. C., *see* F. C. KHANNA
THOMAS, R. H., *see* A. DUCAT
TYRÉN, H., *see* U. L. VALLINDER
UI, HARUO, Inelastic scattering of nucleons by asymmetrically deformed nuclei. A comment on the structure of medium weight nuclei 495
VALADARES, M., Salomon Rosenblum (1896—1959). 189
VALLINDER, U. L. and H. TYRÉN, Angular distribution of fragments from fission of uranium induced by 185-MeV protons 152
VAN HEERDEN, I. J., *see* HEERDEN VAN, I. J.
VAN NOOIJEN, BOB, *see* INGVAR MARKLUND
VASUDEVAN, R., *see* ALLADI RAMAKRISHNAN
WALTERS, T. J., J. H. WEBBER, N. C. RASMUSSEN and HANS MARK, Gamma rays following the decay of Nd^{147} and Sm^{153} 653

WAPSTRA, A. H., *see* F. EVERLING
WAPSTRA, A. H., *see* H. L. HAGEDOORN
WEBBER, J. H., *see* T. J. WALTERS
WIEDENBECK, M. L., *see* R. G. ARNS
WIENER, R., *see* S. G. COHEN
WILSON, RICHARD, *see* PAUL F. COPPER JR.
WINZELER, H., *see* M. NIKOLIČ
ZAPPA, L., *see* A. BISI

SUBJECT INDEX

1. Nuclear Structure

1.B *Two- and three-body problems*

Deuteron photodisintegration and P-wave phase shifts in the medium energy range, Gustav Kramer 60
Note on one pion exchange potential, G. Breit and M. H. Hull, Jr. 216
Polarization in proton-proton scattering near 3.3 MeV, I. Alexeff and W. Haeberli. 609

1.C *Many-particle systems*

A derivation of the pairing-correlation method, B. F. Bayman 33
Une démonstration simplifiée du théorème de Wick en mécanique statistique, Michel Gaudin 89

1.D *Nuclear models*

1.D.1 *Shell model*

Symplectic symmetry in the nuclear shell model, J. B. French 393

1.D.2 *Collective model*

On the existence of octupole vibrations in nuclei, A. M. Lane and E. D. Pendlebury 39
Decay of Re^{188}, R. G. Arns, R. D. Riggs and M. L. Wiedenbeck . . . 125
Inelastic scattering from odd-mass rare earths, M. C. Olesen and B. Elbek 134
Measurement of *g*-factors of several short lived nuclear states in odd-mass nuclei, G. Manning and J. D. Rogers. 166
0+ states of Sm^{152} and Gd^{152}, I. Marklund, O. Nathan and O. B. Nielsen 199
The nuclear *g*-factor of the 111 keV rotational level and other angular correlation measurements on W^{184}, E. Bodenstedt, E. Matthias, H. J. Körner, E. Gerdau, F. Frisius and D. Hovestadt 239
Inelastic scattering of nucleons by asymmetrically deformed nuclei, A comment on the structure of medium weight nuclei, Haruo Ui . . . 495
Nuclear shape effect on isomeric shift, J. Lardinois 522
0+ levels of even nuclei in the rare-earth region, Ingvar Marklund, Bob van Nooijen and Zbigniew Grabowski 533
Protactinium-237, K. Takahashi and H. Morinaga 664

1.D.3 *Other models*

Eine Kernreaktion vom Typ (α, α+3n), Wolfgang Riezler 143

1.E. *Properties of nuclei*

1.E.1 *Energy levels*

Low mass odd-odd isomers of thallium, B. Jung and G. Andersson . . 108
Decay of Re^{188}, R. G. Arns, R. D. Riggs and M. L. Wiedenbeck 125
0+ states of Sm^{152} and Gd^{152}, I. Marklund, O. Nathan and O. B. Nielsen 199
Spin of the first excited state of B^{12}, E. Kondaiah and C. Badrinathan . 254
0+ levels of even nuclei in the rare-earth region, Ingvar Marklund, Bob van Nooijen and Zbigniew Grabowski 533
The decay of Au^{194}, G. Bäckström, O. Bergman, J. Burde and J. Lindskog 566
Gamma rays following the decay of Nd^{147} and Sm^{153}, T. J. Walters, J. H. Webber, N. C. Rasmussen and Hans Mark 653
Protactinium-237, K. Takahashi and H. Morinaga 664

1.E.2 *Binding energies; masses*

Atomic masses of nuclides for $A \leqq 70$, F. Everling, L. A. König, J. H. E. Mattauch and A. H. Wapstra 342

1.E.3 *Electric and magnetic moments*

Measurement of g-factors of several short lived nuclear states in odd-mass nuclei, G. Manning and J. D. Rogers 166
The nuclear g-factor of the 111 keV rotational level and other angular correlation measurements on W^{184}, E. Bodenstedt, E. Matthias, H. J. Körner, E. Gerdau, F. Frisius and D. Hovestadt 239

1.E.4 *Transition probabilities; cross sections*

Inelastic scattering from odd-mass rare earths, M. C. Olesen and B. Elbek 134
The nuclear g-factor of the 111 keV rotational level and other angular correlation measurements on W^{184}, E. Bodenstedt, E. Matthias, H. J. Körner, E. Gerdau, F. Frisius and D. Hovestadt 239

1.E.5 *Nuclear radii; matter distributions*

Dispersive effects in elastic electron scattering by complex nuclei, K. Gottfried 92

2. Nuclear Reactions

2.A *General properties*

2.A.1 *Cross-sections, energy relations*

New isotopes of cobalt; activation cross-sections of nickel, cobalt and zinc from 14.8 MeV neutrons, I. L. Preiss and R. W. Fink 326
Proton capture in Be^{7}, Ralph W. Kavanagh 411

2.B *Angular distributions; correlations; polarization*

Relation between angular distribution and polarization in the optical model, Leonard S. Rodberg 72
The angular and energy distribution of protons from Ni^{58} reactions induced by 14.8 MeV neutrons, I. Kumabe and R. W. Fink 316
Energy and angular dependence of the left-right asymmetry of D-D neutrons scattered by carbon, P. S. Dubbeldam, C. C. Jonker and H. J. Boersma . . 452
Polarization in proton-proton scattering near 3.3 MeV, I. Alexeff and W. Haeberli. 609
Polarization in C^{12}(pp) scattering, J. E. Evans and M. A. Grace. 646

2.C *Resonance reactions; R-matrix theory*

Proton capture by N^{15}, D. F. Hebbard 289
Alpha spectra from the decays of Li^8 and B^8, B. J. Farmer and C. M. Class . . 626
Beta decay involving the $Be^{8*}(2^+)$ state, T. A. Griffy and L. C. Biedenharn . 636

2.D *Statistical model*

The angular and energy distribution of protons from Ni^{58} reactions induced by 14.8 MeV neutrons, I. Kumabe and R. W. Fink 316
New isotopes of cobalt; activation cross-sections of nickel, cobalt and zinc from 14.8 MeV neutrons, I. L. Preiss and R. W. Fink 326
The elastic scattering of ^3He by medium weight nuclei, G. W. Greenlees and P. C. Rowe 687

2.E *Optical model*

Many-body basis for the optical model, Lee M. Frantz and Robert L. Mills . . 16
Relation between angular distribution and polarization in the optical model, Leonard S. Rodberg 72
Scattering of 14.6 MeV neutrons by Mg, Ca, Cd, Ta and Bi, W. G. Cross and R. G. Jarvis. 155
Neutron strength functions in a surface absorption optical model, F. C. Khanna and Y. C. Tang 337

2.F *Direct interaction (other than stripping)*

Eine Kernreaction vom Typ $(\alpha, \alpha+3n)$, Wolfgang Riezler 143
The inelastic scattering of deuterons from ^{12}C, W. M. Fairbairn 678

2.G *Stripping and pick-up*

Spin of the first excited state of B^{12}, E. Kondaiah and C. Badrinathan 254
Cross section and asymmetry in the deuteron pickup reaction $C^{12}(p, d)C^{11}$ at 145 MeV, Paul F. Cooper Jr. and Richard Wilson 373
Angular distribution of protons from $Li^6(d, p)Li^7$ and $Li^6(d, p)Li^{7*}$, G. O. André 464

2.H *Coulomb excitation*

Inelastic scattering from odd-mass rare earths, M. C. Olesen and B. Elbek . . 134

2.I *Photonuclear processes*

Excitation of the nuclear giant-dipole resonance by inelastic electron scattering, S. Fallieros, R. A. Ferrell and M. K. Pal 363
$(\gamma, {}^{np}_{d})$ reactions in S^{32}, Ca^{40}, Ge^{70}, F. Ferrero, S. Ferroni, R. Malvano, S. Menardi and E. Silva. 436

2.J *Fission and spallation*

Angular distribution of fragments from fission of uranium induced by 185-MeV protons, U. L. Vallinder and H. Tyrén 152

2.L *Scattering processes (except two-nucleon system and meson scattering)*

Dispersive effects in elastic electron scattering by complex nuclei, K. Gottfried 92
Scattering of 14.6 MeV neutrons by Mg, Ca, Cd, Ta and Bi, W. G. Cross and R. G. Jarvis. 155

The scattering of 38 MeV alpha particles by C^{12}, I. J. van Heerden and D. J. Prowse 356
Small angle scattering of electrons, I. Berkes and I. Demeter 421
Inelastic scattering of nucleons by asymmetrically deformed nuclei. A comment on the structure of medium weight nuclei, Haruo Ui 495
Polarization in C^{12}(pp) scattering, J. E. Evans and M. A. Grace 646
The elastic scattering of ^{3}He by medium weight nuclei, G. W. Greenlees and P. C. Rowe 687

3. Electromagnetic Radiation

3.A *Gamma radiation*

Decay of Re^{188}, R. G. Arns, R. D. Riggs and M. L. Wiedenbeck 125
Spin of the first excited state of B^{12}, E. Kondaiah and C. Badrinathan 254
New isotopes of cobalt; activation cross-sections of nickel, cobalt and zinc from 14.8 MeV neutrons, I. L. Preiss and R. W. Fink 326
0+ levels of even nuclei in the rare-earth region, Ingvar Marklund, Bob van Nooijen and Zbigniew Grabowski 533

3.B *Internal conversion*

0+ states of Sm^{152} and Gd^{152}, I. Marklund, O. Nathan and O. B. Nielsen . . . 199
On the K-conversion coefficient of the 279 keV gamma ray in the decay of Hg^{203}, M. K. Ramaswamy and P. S. Jastram 510
The decay of Au^{194}, G. Bäckström, O. Bergman, J. Burde and J. Lindskog . . . 566
Gamma rays following the decay of Nd^{147} and Sm^{153}, T. J. Walters, J. H. Webber, N. C. Rasmussen and Hans Mark 653

3.C *Extranuclear effects*

Measurements of the fluorescent yield of the K-shell with a proportional counter, H. L. Hagedoorn and A. H. Wapstra 146
Circular polarization of external bremsstrahlung from γ-rays in magnetized targets, A. Bisi, A. Fasana and L. Zappa 231
Nuclear shape effect on isomeric shift, J. Lardinois, ... 522

4. Beta Decay; Parity

4.A *General theory*

Search for pseudoscalar interaction in beta-decay, S. G. Cohen and R. Wiener 79

4.E *Analysis of data*

Low mass odd-odd isomers of thallium, B. Jung und G. Andersson. 108
The half life of In^{116}, A. Ducat and R. H. Thomas 525
Protactinium-237, K. Takahashi and H. Morinaga. 664

6. Methods and Instruments

6.C *Constants, standards and units*

Note on units and nomenclature 694

6.D *Tables and computational aids*

Atomic masses of nuclides for $A \leqq 70$, F. Everling, L. A. König, J. H. E. Mattauch and A. H. Wapstra 342

7. Quantum Field Theory

7.A *General*

Proof of dispersion relations for pion-hyperon scattering Y. S. Jin 102
On a method of finding singularities of Feynman graphs, L. B. Okun and A. P. Rudik 261
On the construction of the S matrix for dressed particles, Yu. Novozhilov . . . 469
A note on dispersion relations, Alladi Ramakrishnan, N. R. Ranganathan, R. Vasudevan and S. K. Srinivasan 516
On the reduction formulae for the S-matrix elements, J. Hilgevoord 657

7.B *Quantum electrodynamics*

On the consistency of quantization in quantum electrodynamics, Shoji Ozaki . 501

7.C *π-meson field (scattering and nuclear forces)*

Note on one pion exchange potential, G. Breit and M. H. Hull, Jr 216
Non-elastic collisions of fast π mesons with nucleons and peripheral ($\pi\pi$) interactions, V. S. Barashenkov 486

8. Elementary Particles

8.A *Experimental*

An unusual double star from a K^--capture in emulsion, M. Nikolič, W. Koch, M. Schneeberger and H. Winzeler 519
The circular polarization of the gamma rays following the β decay of Fe-59, H. H. Forster and N. L. Sanders 683

8.B *Theory, interactions, transformation properties*

Space and time reflections in relativistic theory, Yu. M. Shirokov 1
Types of symmetry of elementary particles, Yu. M. Shirokov 13
On the spin of the Σ-hyperon, Shoichi Hori 56
Proof of dispersion relations for pion-hyperon scattering Y. S. Jin 102
Theory of K^+-nucleon scattering, I. R. Gatland 480
Note on symmetry of strong interactions, L. Łukaszuk 513

10. News Items

10.A *News Items*

CERN budget for 1960 187
The Nobel prize in physics for 1959, A. C. Helmholz 387
Conference on solid state microwave amplifiers (6—8 April 1960) 390
First annual report of NORDITA. 390

10.C *Obituaries*

Salomon Rosenblum (1896–1959), M. Valadares 189

10.D *Book Reviews*

FLÜGGE, S. V., editor, Handbuch der Physik — Encyclopedia of Physics, vol. 41/1, Nuclear reactions II: Theory; vol. 44, Nuclear instrumention I; vol. 38/2 neutrons and related gamma ray problems 188

BRUIJN, N. G. DE, Asymtotic methods in analysis 392
FLINT, RICHARD FORSTER and EDWARD S. DEEVEY, Jr. (Editors), American Journal of Science, Radiocarbon Supplement Vol. 1 392
KOCKEL, B., W. MACKE, A. PAPAPETROU and W. FRANK, Editors, Max-Planck-Festschrift 1958 (Peter G. Bergmann) 527
JOOS, GEORG, Lehrbuch der theoretischen physik (L. R.) 527
PIRIE, A. *et al.*, La menace radioactive. Danger des retombées radioactives provenant des explosions nucléaires (L. R.) 528
SZABÓ, I., Mathematische Formeln und Tafeln, (L. R.) 528
O.E.E.C. (Editor), The industrial challenge of nuclear energy III-Stresa Conference, part I (L. R.) 528
MODELSKI, GEORGE A., Atomic energy in the communist bloc (L. R.) 528
KRAMISCH, A., Atomic energy in the Sovjet Union (L. R.) 528
CLARK, NORMAN, Physics as a career (L. R.) 529
MESSIAH, ALBERT, Mécanique quantitique, Tome II (L. R.) 529
SEMAT, HENRY and HARVEY E. WHITE, Atomic age physics 529
LOMONT, J. S., Applications of finite groups (L. R.) 530
FRISCH, O. R. (Editor), Progress in nuclear physics, Vol. 7 530
FRISCH, O. R., F. A. PANETH, F. LAVES and P. ROSBAUD, (Editors), Beiträge zur Physik und Chemie des 20. Jahrhunderts (L. R.) 530
JELLEY, J. V., Čerenkov radiation and its applications, (L. R.) 530
CROMBIE, A. C. (Editor), Turning points in physics (L. R.) 531
BARN, MAX and EMIL WOLF, Principles of optics. Electromagnetic theory of propagation, interference and diffraction of light (L. R.) 531
VITALE, B., A Bibliography on heavy mesons and hyperons 531
SEABORG, G. T., The transuranium elements 531
HAMILTON, J., The theory of elementary particles 532
CLEGG, I. W. and D. D. FOLEY, Editors, Uranium Ore Processing (Emil Sørensen) 695
RICHARDS, PAUL I.. Manual of mathematical physics (L. R.) 695
CUTHBERT, F. L., Thorium Production Technslogy (Emil Sørensen) . . . 696
POWELL, C. F., P. H. FOWLER and D. H. PERKINS, The study of elementary particles by the photographic method (L. R.). 696
FROST, B. R. T. and M. B. WALDRON, Nulear Reactor Materials (Per Knusden) 697
PETROW, P. A., Kernenergieanlagen (S. J. Christensen) 697